Providing the underlying principles of digital communication and the design techniques of real-world systems, this textbook prepares senior undergraduate and graduate students for the engineering practices required in industry. Covering the core concepts, including link analysis, modulation, demodulation, spread spectrum, equalization, channel fading effects, and channel coding, it provides step-by-step mathematical derivations to aid understanding of background material. In addition to describing the basic theory, the principles of system and subsystem design are introduced, enabling students to visualize the intricate connections between subsystems and understand how each aspect of the design supports the overall goal of achieving reliable communications. Throughout the book, theories are linked to practical applications with over 250 real-world examples, whilst 370 varied homework problems in three levels of difficulty enhance and extend the text material. With this textbook, students can understand how digital communication systems operate in the real world, learn how to design subsystems, and evaluate end-to-end performance with ease and confidence.

Tri T. Ha is a Professor in the Department of Electrical and Computer Engineering at the Naval Postgraduate School (NPS), Monterey, California, a position he has held since 1989. Prior to joining NPS he worked at Fairchild Industries and GTE, and he was an Associate Professor at Virginia Tech for four years. He is an IEEE Fellow who has written two previous textbooks, and his current research interests are in wireless communications and cyber warfare.

• Detailed solutions manual for instructors

HA

THEORY AND DESIGN OF DIGITAL COMMUNICATION SYSTEMS

Cover designed by Zoe Naylor

CAMBRIDGE
UNIVERSITY PRESS
www.cambridge.org

ISBN 978-0-521-76174-1

CAMBRIDGE

THEORY AND DESIGN OF DIGITAL COMMUNICATION SYSTEMS

TRI T. HA

CAMBRIDGE

Theory and Design of Digital Communication Systems

Providing the underlying principles of digital communication and the design techniques of real-world systems, this textbook prepares senior undergraduate and graduate students for the engineering practices required in industry. Covering the core concepts, including link analysis, modulation, demodulation, spread spectrum, equalization, channel fading effects, and channel coding, it provides step-by-step mathematical derivations to aid understanding of background material. In addition to describing the basic theory, the principles of system and subsystem design are introduced, enabling students to visualize the intricate connections between subsystems and understand how each aspect of the design supports the overall goal of achieving reliable communications. Throughout the book, theories are linked to practical applications with over 250 real-world examples, whilst 370 varied homework problems in three levels of difficulty enhance and extend the text material. With this textbook, students can understand how digital communication systems operate in the real world, learn how to design subsystems, and evaluate end-to-end performance with ease and confidence.

Tri T. Ha is a Professor in the Department of Electrical and Computer Engineering at the Naval Postgraduate School (NPS), Monterey, California, a position he has held since 1989. Prior to joining NPS he worked at Fairchild Industries and GTE, and was an Associate Professor at Virginia Tech for four years. He is an IEEE Fellow who has written two previous textbooks, and his current research interests are in wireless communications and cyber warfare.

Theory and Design of Digital Communication Systems

TRI T. HA

Naval Postgraduate School, Monterey, California

CAMBRIDGE UNIVERSITY PRESS
Cambridge, New York, Melbourne, Madrid, Cape Town, Singapore,
São Paulo, Delhi, Dubai, Tokyo, Mexico City

Cambridge University Press
The Edinburgh Building, Cambridge CB2 8RU, UK

Published in the United States of America by Cambridge University Press, New York

www.cambridge.org
Information on this title: www.cambridge.org/9780521761741

First published 2011

Printed in the United Kingdom at the University Press, Cambridge

A catalog record for this publication is available from the British Library

Library of Congress Cataloging in Publication data
Ha, Tri T., 1949–
Theory and design of digital communication systems / Tri T. Ha.
p. cm.
ISBN 978-0-521-76174-1 (hardback)
1. Digital communications. I. Title.
TK5103.7.H35 2011
384–dc22
2010024374

ISBN 978-0-521-76174-1 Hardback

Additional resources for this publication at www.cambridge.org/9780521761741

World peace must develop from inner peace. Peace is not the absence of violence. Peace is the manifestation of human compassion.

14th Dalai Lama of Tibet (Inscription on United States Congressional Medal)

Contents

Preface

This book was written with two goals in mind: to provide the underlying principles of digital communication and to study design techniques integrated with real world systems. The ultimate aim of a communication system is to provide reliable transmission of information to the user(s). This fundamental foundation was established in 1948 by Claude Shannon, the founding father of information theory, and led eventually to the development of modern digital communication. Analog communication is near extinction or at the very gate of it. The full spectrum dominance of digital communication has arrived and new frontiers are being established every decade; from cellular systems to wireless LAN and MAN, the bit rates are being pushed ever higher for ubiquitous mobile applications.

Knowing the limit of digital transmission is vital to the design of future communication systems, particularly mobile wireless systems, where both spectrum and power are precious resources, and design techniques can be used to manipulate these two main resources to fit real world applications. No single technique can cover all the requirements of a modern communication system, which makes it necessary for students to understand the intricate web between subsystems, each designed to support others to achieve the common goal of reliable communication.

The book contains more than 250 examples to help students achieve a firmer understanding of the subject. The problems at the end of each chapter follow closely the order of the sections. They are designed for three levels: level one covers the straightforward application of equations; level two requires patience and deep thinking; whilst level three requires some research of the literature to assist in finding a solution. A solutions manual for the instructor accompanies the book.

The book was written for both senior undergraduate and graduate students studying communications at universities and colleges. The entire book is suitable for two-semester courses in digital communications. The first course is typically a one-semester senior course in digital communication, which may be taken by students new to studying communications (the conventional wisdom is that students should learn analog communication before learning digital communications) or after completing an introductory course in communication systems (one that is heavy in analog communication systems such as AM and FM). The second course is a one-semester course for graduate students who already have a firm background in random variables and processes. The practical material included in this book (much of it focused on commercial and military systems) will be helpful for practitioners and professionals in the digital communication field.

As in the learning of any subject, some prerequisites are required for the reading of this book. A first course in probability theory is necessary and exposures to random processes

would be helpful. Readers should also be familiar with linear system analysis. A knowledge of analog communication is helpful but not required. For readers who do not have the patience to go through all the design techniques but would appreciate the beauty of the underlying principles, we recommend our favorite book, *Principles of Digital Communication*, authored by the legendary Robert G. Gallager.

Acknowledgements

I would like to express my thanks to Dr. Phil Meyler of Cambridge University Press for his enthusiastic support and for suggesting the title of the book to closely reflect its coverage. I would like to thank the anonymous reviewers for their valuable comments that helped in improving the book. I am grateful for the support of my friends Nathan Beltz, Professor Vicente Garcia, Professor Jeff Knorr, Professor Frank Kragh, Donna Miller, Rita Painter, Professor Clark Robertson, Professor Wei Su, Dr. Jan Tighe, and Dr. Charlie Victory. I also would like to thank my students over the years for their valuable suggestions to improve the original notes. I am grateful to my parents for providing me the opportunity to go to the United States for higher education, and to Thuy, Khanh, Tuan, Huong and Dennis, Thu, and Hien for their help and support over the years. This book is dedicated to the people who work tirelessly for world peace.

Symbols

A	amplitude, smallest signal amplitude in MQAM, azimuth angle
$\mathbf{A}$	matrix $\mathbf{A}$
$\|\|\mathbf{A}\|\|^2$	squared Frobenius norm of matrix $\mathbf{A}$
$\mathbf{A}^*$	conjugate and transpose of a matrix $\mathbf{A}$
A_d	number of paths of Hamming weight d that merge with the all-zero paths
A_e	effective aperture area of the receiver antenna
$A \cap B, AB$	intersection of set A and set B, A and B
$A \cup B, A + B$	union of set A and set B, A or B
a	Gaussian filter parameter
$a(h_R)$	correction factor in Hata model
a_f	frequency sensitivity
a_k	Fourier series coefficients
B	bandwidth
B_d	information weight (number of information bit errors) of all paths of Hamming weight d
$\boldsymbol{B}_{d_{free}}$	information weight (number of information bit errors) of all paths of Euclidean distance d_{free} of TCM
C	channel capacity in coded bits/input symbol, correlation
$\mathbf{C}$	channel capacity in coded bits/second
C_o	outage capacity
$c(\boldsymbol{D}_K)$	correlation metric in MLSD
C_N	correlation metric in CPM
$C_X(t_1, t_2)$	autocovariance of the random process $x(t)$
$C(z)$	transfer function of causal ZF-LE, z-transform of the sequence $c(k)$
$Cov(N_j N_k)$	covariance of two noise samples
$\boldsymbol{c}$	code word, PN sequence
c_i	a coded bit, a differentially coded bit
$c(t)$	PN function of N chips
$\boldsymbol{c}(t)$	complex PN function
$c_I(t)$	PN function of I-channel
$c_Q(t)$	PN function of Q-channel
$c(\boldsymbol{x}\|\boldsymbol{H_i})$	metric for CPM demodulation
D_i	ith symbol in the symbol stream

d	distance
$\boldsymbol{d}$	data sequence
dB	decibel
d_{free}	free distance of a convolutional code
$\boldsymbol{d}_{free}$	Euclidean free distance of TCM
d_i, $d(i)$	normalized bit or symbol amplitude, $d_i \in \{-1, +1)$, $d_i \in \{0, 1)$
$\{d_i\}$, $\{d(i)\}$	data sequence
d_{min}	minimum Hamming distance, minimum Euclidean distance
$d(u,v)$	Hamming distance between two code words
$d(\boldsymbol{x}, \boldsymbol{s}_i)$	Euclidean distance between two vectors
E	energy (with or without a subscript), smallest symbol energy in MQAM or MASK, electric-field wave, elevation angle
E_b	bit energy
$\boldsymbol{\mathcal{E}}_b$	diversity bit energy
$E(d,t)$	free space E-field at distance d from transmitter and time t
E_h	hop energy
$EIRP$	effective isotropic radiated power
E_0	free space E-field at distance d_0 from transmitter
E_s	symbol energy
$\boldsymbol{\mathcal{E}}_s$	diversity symbol energy
$\mathbf{E}(X)$	expected value (mean value) of X
$\mathbf{E}(X^2)$	mean-square value of X^2
e	2.718
$\boldsymbol{e}$	error word
$e(k)$	error sequence of MSE-LE
$e(t)$	error process
F	noise figure
$F\{x(t)\}$	Fourier transform of $x(t)$
$F(z)$	minimum-phase transfer function, transfer function of a synthetic channel, z-transform of the sequence $f(k)$
$F^*(1/z^*)$	maximum-phase function
$F^{-1}\{X(f)\}$	inverse Fourier transform of $X(f)$
${}_2F_1$	Gauss hypergeometric function
$F^{(-1)}_{\lvert h\rvert^2}(p_o)SNR$	outage signal-to-noise ratio
$F_X(x)$	distribution function of X
$F_{XY}(x,y)$	joint distribution function of X and Y
$f_{\lvert h\rvert}(x)$	density function of the channel tap magnitude $\lvert h\rvert$
$f_{XY}(x,y)$	joint density function of X and Y
$f_{X\lvert Y}(x\lvert y)$	conditional density function of X given Y
f	frequency, Doppler shift

f_c	carrier frequency
f_D	Doppler spread
f_j	instantaneous carrier frequency of FH
$f_{L,i}$	instantaneous local carrier frequency of a frequency synthesizer
f_m	maximum Doppler shift
f_s	sampling frequency
$f_X(x)$	density function of X
$f_{\boldsymbol{X}}(\boldsymbol{x})$	density function of vector $\boldsymbol{X}$
G	amplifier gain, gain of a two-port network
$\mathbf{G}$	generator matrix, space-time block code matrix
$\boldsymbol{G}$	TCM asymptotic coding gain
G_{DC}	gain of a downconverter
G_{LNA}	gain of a low-noise amplifier
G_R	receiver antenna gain
G_R/T_s	antenna gain-to-noise temperature ratio of the earth station
G_S/T_{sat}	antenna gain-to-noise temperature ratio of the satellite
G_T	transmitter antenna gain
g	parity
$g(t)$	pulse
$g_n(t)$	orthonormal pulse shapes in OFDM
$g(x)$	code generator polynomial
$\mathbf{H}$	Hadamard matrix (with or without a subscript), parity check matrix, channel tap matrix
H	source entropy in bits/second
H_i	hypothesis
$H(f)$	transfer function or frequency response
$H_{FE}(f)$	transfer function of the front-end filter of the receiver
$\lvert H(f)\rvert$	magnitude response (amplitude response)
$H_T(f)$	transfer function of transmit filter
$H_R(f)$	transfer function of receive filter
$H(k)$	N-point DFT of the sequence $h(n)$
$H(X)$	entropy of the discrete random variable (discrete source) X
h	Planck constant, digital modulation index, complex channel tap
$\mathbf{h}$	row vector of a Hadamard matrix
$\hat{\boldsymbol{h}}$	MMSE of the vector $\boldsymbol{h}$
$h_i,\ h(i)$	ith channel tap
$\tilde{h}(i)$	complex channel tap
$h_L(t)$	complex envelope of the impulse response $h(t)$
$h(n)$	sequence used in OFDM
h_R	receive antenna height

h_T	transmit antenna height
$h(t)$	impulse response
$h(\boldsymbol{X})$	differential entropy of a continuous random variable X
$h(X\|Y)$	conditional differential entropy of a continuous random variable X
$h(\boldsymbol{X})$	differential entropy of a continuous n-dimensional random vector $\boldsymbol{X}$
$h(x)$	monic binary irreducible primitive polynomial, PN code polynomial
I	interference power, photodiode current
I_m	interchannel interference
I	MUI variable
$I(X)$	self-information of the discrete random variable (discrete source) X
$I(u_i, v_j)$	pair-wise mutual information
$I(U, V)$	mutual information
$I_0(\bullet)$	modified Bessel function of the first kind of zero order
$I_n(\bullet)$	modified Bessel function of the first kind of nth order
J	jamming variable
J_0, $J_0(\bullet)$	jamming spectral density, Bessel function of zero order
K	number of simultaneous users in CDMA, Kelvin
$\mathbf{K}$	covariance matrix
k	integer, Boltzmann constant, number of information bits in a block code, number of inputs of a convolutional encoder
k_0	free space wave number
k/n	code rate
L_C	path loss
L	diversity order, loss of a two-port network
$L(f)$	transfer function of an equalizer
L_r	receive antenna diversity
L_s	number of symbol times for m transmitted symbols in transmit diversity
L_{TL}	loss of a transmission line
L_t	transmit antenna diversity
L_{dB}	mean value in decibels of the log-normal density variable
$L(\lambda, P_1, ..., P_n)$	Lagrangian
l	length of a code word
$\bar{l}$	average length of a code word
ln	natural logarithm
$\ln \Lambda(X\|y)$	conditional ln-likelihood ratio
log	base-10 logarithm
$\log_2$	base-2 logarithm
M	number of distinct M-ary symbols
$\mathbf{M}(\boldsymbol{r} \mid \boldsymbol{c})$	path metric in Viterbi algorithm or log-likelihood function
m	mean value of a random variable, Nakagami-m parameter

$m_A(X^{-1})$	arithmetic mean of $1/X(f)$
$m_G(X)$	geometric mean of $X(f)$
m_n	metric for OFDM timing synchronization
$m(t)$	message signal
$\mathbf{m}_{ij}^{(l)}$	message sent by the bit node i to check node j at the lth iteration
$\hat{\mathbf{m}}_{ji}^{(l)}$	message sent by the check node j to bit node i at the lth iteration
m_l^2	sum of the squares of the means
$m_X(t)$	mean value of the random process $x(t)$
N	noise variable, available noise power, number of OFDM subcarriers, period of a PN sequence
$\boldsymbol{N}$	noise vector, complex noise
$\mathcal{N}$	noise variable at detector input
N	noise variable
$\mathfrak{N}$	complex noise variable, complex noise vector
$N(f)$	power spectral density of the equivalent lowpass noise $n(t)$
N_D	number of branches in a frequency bin determinator
N_H	number of hop bins
N_i	system noise power
N_n	average number of nearest neighbors of a signal vector
$N(0,\sigma^2)$	Gaussian random variable with zero mean and variance σ^2
$\boldsymbol{N}(0,\sigma^2)$	Gaussian vector with iid components of zero mean and variance σ^2
N_k	noise sample
$N_0/2$	power spectral density of noise
$\mathcal{N}_V$	average number of level crossings
n	code word length, path loss exponent
$n_I,\ N_I$	in-phase noise variables
$n_Q,\ N_Q$	quadrature noise variables
(n,k)	block code of k information bits and code word length n
$n(t)$	noise
$n_L(t)$	complex envelope of bandpass noise
$n_0(t)$	output noise of a matched filter
P	power
$P_{c,h}$	probability of correctly identifying the frequency bin
$P(d)$	pair-wise error probability ($\Pr(\boldsymbol{c} \to \boldsymbol{c}')$)
P_e	error probability (bit, symbol, code word)
$P(f)$	energy spectrum, Fourier transform of pulse shape $p(t)$
P_j	power of a jamming signal
P_p	peak power
$\Pr(A)$	probability of A
$\Pr(A,B)$	joint probability of A and B

$\Pr(A\|B)$	conditional probability of A given B
$\Pr(\boldsymbol{c} \rightarrow \boldsymbol{c}')$	pair-wise error probability
$\Pr(\boldsymbol{c} \mid \boldsymbol{r})$	a posteriori probability
$\Pr(\boldsymbol{r} \mid \boldsymbol{c})$	likelihood of the transmitted code vector $\boldsymbol{c}$
P_T	transmit power
$P(z)$	linear predictor in MSE-DFE
p	crossover probability of a BSC, probability of a binary symbol
p_{out}	outage probability
$p_{UV}(u_i, v_j)$	joint distribution of u_i, v_j
$p(v_j\|u_i)$	transition probability of a discrete channel
$p_X(x_i)$	distribution of the discrete random variable X, $i = 1, 2, \ldots, n$
$p(t)$	pulse shape
$\boldsymbol{Q}(a, b)$	Marcum $\boldsymbol{Q}$-function
$Q(x)$	Gaussian integral Q-function of argument x
$Q(z)$	transfer function of the composite channel in suboptimum MSE-LE
q	optimum number of jamming tones
R	resistance, Rayleigh random variable, source rate in symbols/second
R_b	bit rate
R_c	chip rate
$\boldsymbol{\mathcal{R}}$	responsivity
R_e	Earth's radius (6378 km)
$R_h(\tau, \boldsymbol{t}')$	multipath autocorrelation profile
$R_{h_i}(\boldsymbol{t}')$	ith path autocorrelation
$R(i-j)$	autocorrelation of the data sequence $\{d_i\}$
R_s	symbol rate
$R(t)$	envelope of a bandpass process
$\boldsymbol{\mathcal{R}}_V$	level crossing rate
R_w	Walsh chip rate
$R_x(\tau)$	autocorrelation of WSS random process $x(t)$
$R_X(t_1, t_2)$	autocorrelation of the random process $x(t)$
r	value assumed by a random variable R, code rate, spectral efficiency
$\boldsymbol{r}$	received word
r^2	signal-to-intertone interference ratio
r_e	extinction ratio
S	input variable of a Gaussian channel
$\boldsymbol{S}$	input vector of a Gaussian channel
$\boldsymbol{S}$	sample space
$S(f)$	power spectral density (with or without a subscript)
$S_h(\tau, \boldsymbol{f}')$	multipath Doppler profile
$S_{h_i}(\boldsymbol{f}')$	ith path Doppler power spectrum

$\boldsymbol{s}$	syndrome vector, orthogonal covering symbol
sgn (x)	signum function
sign$[x]$	sign of x
$s(t)$	digital signal
$\{s_i(t)\}$	set of M digital signals, $i = 1, 2, \ldots, M$
$\{\boldsymbol{s}_i\}$	set of M signal vectors in the signal space, $i = 1, 2, \ldots, M$
$\|\boldsymbol{s}_i\|$	norm of signal vector $\boldsymbol{s}_i$
s_{ik}	coefficients of the Gram–Schmidt orthogonal expansion, I–Q values of a two-dimensional signal vector
$s_L(n)$	time samples of an OFDM signal
$s_L(t)$	complex envelope a bandpass signal $s(t)$
$s_0(t)$	output signal of a matched filter
s_p	pilot symbol
T	time interval, period, sampling period
$\mathbf{T}$	phase error rotation matrix
T_A	antenna noise temperature
T_b	bit time
T_c	chip time, channel coherence time
T_d	time delay, multipath delay spread
T_{DC}	effective noise temperature of a downconverter
T_{DM}	effective noise temperature of a demodulator
T_e	effective noise temperature
T_h	hop time
T_{LNA}	effective noise temperature of a low-noise amplifier
T_n	physical temperature of the resistor
T_0	reference temperature, time interval, period
T_p	pulse width
$Tr(\mathbf{A})$	trace of matrix $\mathbf{A}$
T_s	symbol time, system noise temperature
t	time, error-correcting capability of a block code
U	set of M input symbols of a discrete channel
$\bigcup_{i=1}^{M} A_i$	union of A_i set
$u(t)$	unit step function
$\boldsymbol{u}$	message vector
V	voltage, set of Q output symbols of a discrete channel
$\mathrm{Var}(X)$	variance of X
V_{rms}	root mean-square voltage
V_T	threshold voltage
v	radial velocity
$v(t)$	voltage signal

W	bandwidth, watt
$\{w_n(t)\}$	set of Walsh functions, $n = 1, 2, \ldots, M$
X	random variable, discrete source, output variable of a Gaussian channel or a matched filter
$\boldsymbol{X}$	random vector, output vector of a Gaussian channel
$\overline{X}$	mean value (expected value) of X
$\overline{X^2}$	mean-square value of X^2
$X\left(e^{j2\pi f'}\right)$	discrete-time Fourier transform of the sequence $x(k)$
$\left\|X(f)^2\right\|$	energy spectral density of the energy signal $x(t)$
$X(f)$	Fourier transform of $x(t)$, folded spectrum
$X(k)$	N-point DFT of the sequence $x(n)$
X^n	nth extension of the discrete source X
$X_T(f)$	Fourier transform of $x_T(t)$, $2T$-truncation of $x(t)$, $-T \leq t \leq T$
$X(z)$	z-transform of the sequence $x(k)$, transfer function of the composite channel in optimum MSE-LE
x	value assumed by a random variable X
$\boldsymbol{x}$	value assumed by a random vector $\boldsymbol{X}$
$\lfloor x \rfloor$	integer part of x
$x(n)$	discrete-time signal, sequence used in OFDM
$x(t)$	continuous-time signal (with or without a subscript)
$x_I(t)$	in-phase component of the bandpass signal $x(t)$
$\{x_k(t)\}$	set of L orthonormal basis functions, $k = 1, 2, \ldots, L$
$\{\mathbf{x}_k\}$	set of L orthonormal basis vectors, $k = 1, 2, \ldots, L$
$x_L(t)$	complex envelope (equivalent lowpass signal) of the bandpass signal $x(t)$
$x_p(t)$	periodic signal
$x_Q(t)$	quadrature component of the bandpass signal $x(t)$
$x_s(t)$	sampled function
$x_T(t)$	$2T$-truncation of $x(t)$, $-T \leq t \leq T$
$Y(k)$	N-point DFT of the sequence $y(n)$
$y(n)$	sequence
$y(t)$	continuous-time function
$\boldsymbol{Z}$	pre-mapped vector at the input of the combiner
$Z(k)$	frequency samples of an OFDM signal (the I–Q values of symbols of OFDM subcarriers)
Z_0	amplifier transimpedance
$z_k(t)$	complex envelope of the kth OFDM subcarrier
$*$	linear convolution
$\otimes$	circular convolution
$(\ )^*$	complex conjugate
α	arbitrary constant

α_n	normalized signal amplitude in MQAM
α_p	complex Doppler factor
$\lvert\alpha_p\rvert$	Doppler loss factor
β	proportionality constant, roll-off factor of a raised-cosine filter
γ	threshold
$\gamma_{k,m}$	complex Doppler loss factor
γ_n	MSK data stream
Γ	ground reflection coefficient, gamma function
ΔF	frequency offset in OFDM
Δf	peak frequency deviation
$\Delta\varepsilon_l$	differential Doppler phase error
$\Delta\hat{\varepsilon}_{l-1}$	post-estimated differential Doppler phase error
$\Delta\varepsilon_l - \Delta\hat{\varepsilon}_{l-1}$	double-differential Doppler phase error
δ	jamming pulse duty cycle, fraction of FH bandwidth being jammed, fraction of a hop being jammed
δ_{ij}	0 for $i \neq j$ and 1 for $i = j$
$\delta(t)$	unit impulse function
ε	phase error
ε_l	Doppler phase error
θ	phase
θ_k	azimuth angle of the kth wave
θ_L	Earth station longitude
θ_ℓ	Earth station latitude
θ_S	GEO satellite longitude
$\theta(t)$	phase function
λ	wavelength, Lagrange multiplier
μ	conditional mean value
$\Lambda(\mathrm{X}\lvert\boldsymbol{y})$	conditional likelihood ratio
Π	product, fractional coverage area
ρ	spatial correlation coefficient
$\rho_X(\boldsymbol{\tau})$	normalized autocovariance of the random process $x(t)$
σ^2	variance of noise
σ_{dB}	standard deviation of the log-normal density variable in decibels
σ_X^2	variance of the random variable X
σ_s^2	power of the diffuse paths
τ	time delay variable, average fade duration
$\tau_i(t)$	path delay
φ	phase state in CPM
φ_k	polar angle of the kth wave
ϕ	impossible event, null set, phase in MFSK and CPM, phase shift

$\Phi_0(f)$	power spectral density of the equalizer output noise
$\{\phi_k(t)\}$	set of orthonormal eigenfunctions of the noise autocorrelation
χ	voice activity factor or data duty cycle
χ^2	chi-square
ψ	angle of mobile direction with respect to the x-axis, Doppler phase error
$\Psi(f)$	power spectral density of sampled noise
$\Psi_0(f)$	power spectral density of output noise of ZF-LE
$\Psi(t)$	phase of a bandpass process
Ω	mean-square value of the envelope of the Nakagami-m process

Abbreviations

2G	second generation
3G	third generation
A/D	analog/digital conversion
AGN	additive Gaussian noise
AMPS	advanced mobile phone system
APD	avalanche photodiode
ASK	amplitude shift keying
AWGN	additive white Gaussian noise
BCH	Bose–Chaudhuri–Hocquenghem code
BEC	binary erasure channel
BPA	belief propagation algorithm
BSC	binary symmetric channel
CDM	code division multiplexing
CDMA	code division multiple access
CDMA 2000	3G CDMA
CP	cyclic prefix
CPM	continuous phase modulation
CP-MFSK	continuous phase M-ary frequency shift keying
CRC	cyclic redundancy check
CSI	channel side information
CSIR	channel side information at the receiver
CSK	code shift keying
D/A	digital/analog conversion
DD-DF	double-differential decision-feedback algorithm
D-DF	differential decision-feedback algorithm
DEMUX	demultiplexer
DFS	decision-feedback selection
DFT	discrete Fourier transform
DMC	discrete memoryless channel
DMPSK	differential M-ary phase shift keying
DMQAM	differential quadrature amplitude modulation
DPSK	differential phase shift keying
DQPSK	differential quadrature phase shift keying

DSB-AM	double sideband–amplitude modulation
DS	direct sequence
DS-CSK	direct sequence–code shift keying
DS-PSK	direct sequence–phase shift keying
DS-SS	direct sequence spread spectrum
DTFT	discrete-time Fourier transform
EGC	equal gain combining
EIRP	effective isotropic radiated power
ESN	electronic serial number
ETACS	extended total access cellular system
FCC	Federal Communications Commission
FDM	frequency division multiplexing
FDMA	frequency division multiple access
FFH	fast frequency hop
FFT	fast Fourier transform
FH	frequency hop
FIR	finite impulse response
FM	frequency modulation
FSE	fractionally spaced equalizer
FSK	frequency shift keying (binary frequency shift keying)
fT	frequency–time product
GEO	geostationary orbit
GMSK	Gaussian minimum shift keying
GPS	global positioning system
GSM	global system for mobile communication
$\|h\|^2 SNR$	instantaneous SNR
ICI	intercarrier interference
ICI	interchannel interference
IDFT	inverse discrete Fourier transform
IEEE	Institute of Electrical and Electronics Engineers
IFFT	inverse fast Fourier transform
iid	independent and identically distributed
IIR	infinite impulse response
IPI	intrapath interference
IS	interim standard
ISI	intersymbol interference
$\mathcal{ISI}$	intersample interference
JDC	Japanese digital cellular system
JTACS	Japanese total access communication system
LDPC	low-density parity-check code

LFSR	linear feedback shift-register
LLR	ln-likelihood ratio
LR	likelihood ratio
L-REC	rectangular pulse of duration L symbols
L-RC	raised cosine pulse shape of duration L symbols
LSB	lower sideband
LTI	linear time-invariant
MAP	maximum a posteriori
MASK	M-ary amplitude shift keying
MFSK	M-ary frequency shift keying
MIMO	multiple-input multiple-output
MIN	mobile identification number
MIP	multipath intensity profile
MISO	multiple-input single-output
ML	maximum likelihood
MLSD	maximum likelihood sequence detection
MMSE	minimum mean-square error
MPA	message passing algorithm
MPSK	M-ary phase shift keying
MQAM	quadrature amplitude modulation
MRC	maximal ratio combining
MSC	mobile switching center
MSE-DFE	mean-square error decision-feedback equalizer
MSE-LE	mean-square error linear equalizer
MSK	minimum shift keying
MUI	multi-user interference
MUX	multiplexer
NAMPS	narrowband advanced mobile phone system
NRZ	non-return-to-zero
NTACS	narrowband total access communication systems
OFDM	orthogonal frequency division multiplexing
OOK	on–off keying
OQPSK	offset quadrature phase shift keying
PCS	personal communication system
PD	pin photodiode
PDC	Pacific (or personal) digital cellular system
PDF	probability distribution function
pdf	probability density function
$\pi/4$-DQPSK	$\pi/4$ shift differential quadrature phase shift keying
PLL	phase-locked loop

PN	pseudo-noise
PSK	phase shift keying (binary phase shift keying)
PSTN	public switched telephone network
QPSK	quadrature phase shift keying
RS	Reed–Solomon code
SC	selection combining
SCM	station class mark
SFH	slow frequency hop
SIMO	single-input multiple-output
$SINR$	signal-to-interference and noise ratio
$\boldsymbol{SINR}$	path signal-to-interference-and-noise ratio
$SINR_0$	output signal-to-interference plus noise ratio
SIR	signal-to-interference ratio
SIR_i	input signal-to-interference ratio
SIR_0	output signal-to-interference ratio
$SJNR_0$	output signal-to-jamming-plus-noise ratio
SJR_i	input signal-to-jamming ratio
$SJR_{i,\,p}$	input signal-to-pulse jamming ratio
SJR_0	output signal-to-jamming ratio
$SJR_{0,\,p}$	output signal-to-pulse jamming ratio
SNR	signal-to-noise ratio
$\boldsymbol{SNR}$	diversity symbol signal-to-noise ratio
SNR_0	output signal-to-noise ratio
SPA	sum product algorithm
TCM	trellis coded modulation
TDMA	time division multiple access
TIA/EIA	Telecommunication Industry Association/Electronic Industry Association
USB	upper sideband
USDC	US digital cellular
VCO	voltage-controlled oscillator
WCDMA	wideband CDMA (3G CDMA)
WLAN	wireless local area network
WMAN	wireless metropolitan area network
WSCS	wide-sense cyclostationary
WSS	wide-sense stationary
ZF-DFE	zero-forcing decision-feedback equalizer
ZF-LE	zero-forcing linear equalizer

1 Introduction

If the mind is in tranquility, time and space cease to exist.

Essence of Buddhism

1.1 Brief overview

This book provides the principles of digital communication and studies techniques to design and analyze digital communication systems for point-to-point and point-to-multipoint transmission and reception. Other than for radio broadcasting, modern communication systems are going digital, and in the USA the conversion of analog TV broadcasting into digital HDTV broadcasting at the beginning of 2009 signified the coming end of analog communications. Communications between living beings began with the voice, and the three biggest voice systems in the world are the telephone, and the cellular and radio broadcasting systems.

The dissemination of visual activities then propelled the development of TV broadcasting systems. The pioneer telephone network and radio broadcasting systems employed analog communication techniques, such as AM and FM, for transmission of analog voice, as did the analog TV broadcasting systems, which employed VSB-AM for picture transmission. The quality of the message, such as voice and images, at the analog receiver depends on how well the waveform that carries the message over the physical channel (twisted-pair telephone wires, coaxial and fiber-optic cables, space, and water) can be reproduced. In addition, the fidelity of the received message depends on the signal-to-noise ratio at the receiver input. For good analog communications, the signal-to-noise ratio must be large, and this requires high-power transmitters, such as are used in AM radio and TV broadcasting. For FM radio broadcasting a large frequency spectrum is used, such as 200 kHz for radio broadcasting, which shows that analog communications do not utilize power and bandwidth efficiently. Furthermore, the advent of the Internet requires audio, video, imagery, and text messages to be integrated for transmission over a common channel and this in effect rules out analog communications such as AM and FM.

In analog communications, the message signal requires an *infinite set of continuous-time waveforms* for transmission over a physical channel. This is because the message itself, such as audio or video, must first be converted into a *voltage baseband waveform* with a *continuous range* in amplitude that has countless possible values. When the baseband voltage waveform is used to modulate an RF carrier for transmission, such as in AM or FM, the modulated RF signal transmitted over the physical channel also has countless possible values in both its amplitude and frequency ranges. The only way to recover the

message signal is to faithfully reproduce the baseband waveform from the modulated signal. This can be done easily in the case of no noise and no equipment imperfections, but otherwise the fidelity of the message signal may be reduced. Digital communication does not involve the faithful reproduction of the baseband waveform in the presence of noise and equipment imperfections. Digital communication operates instead with a *finite set of continuous-time modulation waveforms* for transmission over a physical channel. This implies that the message signal must be represented by a *finite set of voltage baseband waveforms*. Mathematically, a finite set of waveforms can only represent a finite set of alphabets, commonly referred to as *symbols*. A symbol consists of a fixed number of binary digits or *bits*. For example, the set of four distinct symbols {00, 01, 10, 11} can be represented by four distinct waveforms $\{\pm A\cos 2\pi f_c t, \pm A\sin 2\pi f_c t\}$. The time separation of consecutive waveforms that represent a symbol stream is called the *symbol time*, which is the inverse of the *symbol rate*. If the waveforms are of finite duration then this duration is the symbol time. This begs the question of how to obtain the bits or symbols that represent the message. The process of converting a voltage baseband waveform that represents an audio or video message into bits is referred to as the *analog-to-digital conversion* (or A/D). Text messages generated by computers are inherently in bits, so with A/D conversion, audio, video, text, and imagery can all be integrated into a single digital stream of bits. The process of A/D, bit-symbol mapping, baseband waveform shaping, and modulation is referred to as digital transmission. The process of demodulating the modulated signal, detecting the symbol, symbol–bit mapping, and *digital-to-analog conversion* (or D/A) is called digital reception.

Digital communication makes no attempts to reproduce the finite set of voltage baseband waveforms. Instead, the receiver detects the energy content of each baseband waveform in the presence of noise and equipment imperfections, and then makes a best estimate of which transmitted symbol was received. If the *signal-to noise ratio per symbol* is reasonably large, a symbol will most likely be detected correctly with high probability. If not, a symbol error may occur. This is the essence of digital communication. For a given signal-to-noise ratio, an analog communication receiver attempts to reproduce the voltage baseband waveform with certain *subjective* fidelity. On the other hand, for a given signal-to-noise ratio per symbol, a digital communication receiver produces symbols with a *quantitative* error rate. It is important to know in advance the *lower bound* of the signal-to-noise ratio per symbol for a specified error rate irrespective of the type and size of the set of modulation waveforms. In 1948 Claude Shannon established this lower bound and also provided the channel capacity for reliable transmission [1]. Shannon's work gives the designers of digital communication systems the freedom to choose the set of modulation waveforms that achieve either the best power or bandwidth efficiency, or a trade-off combination of both. As long as the transmission rate is below the channel capacity and the signal-to-noise ratio per symbol is above the *Shannon limit*, reliable communication is possible with an arbitrarily small error rate. Guided by the *Shannon channel capacity theorem* (*main theorem*), the designer can further integrate error-correction codes with modulation techniques to lower the signal-to-noise ratio per symbol to achieve a specified error rate. The first error-correction code, the *Hamming code*, was discovered by Richard W. Hamming in 1950, two years after Shannon published his landmark work [2]. In addition to the main theorem, the *Shannon first theorem*

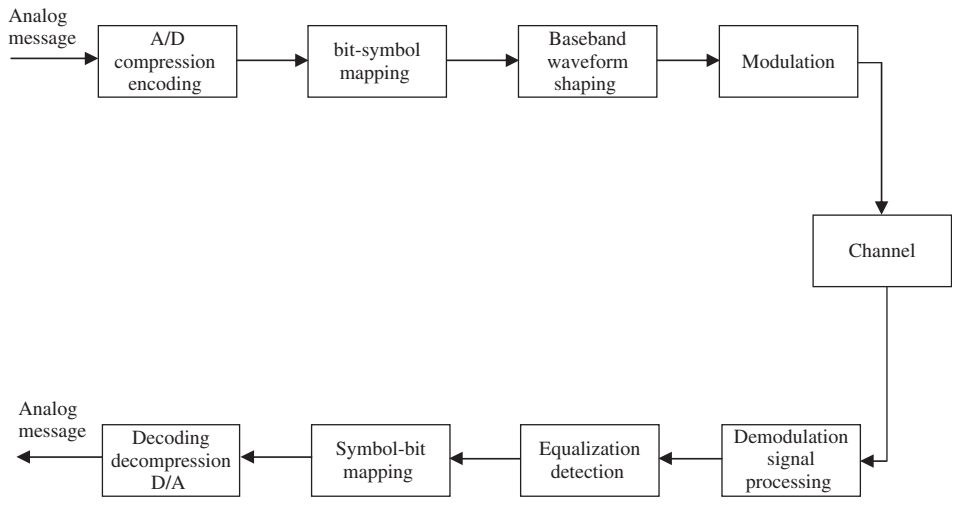

Figure 1.1 Conceptual block diagram of a digital communication system.

provided the framework for encoding a discrete source of a finite set of symbols to minimize the bit rate at the source encoder output. This allows the compression of the A/D samples of the message signal to remove redundancy and any insignificant information not perceptible by the human eye or ear.

The most common compression algorithms in use today are MP3 for music, JPEG for pictures, and MPEG for video. Figure 1.1 shows the conceptual block diagram of a digital communication system. The material in the book is organized to cover the transmitter, receiver, and channel.

1.2 Scope

Chapter 2 provides a general study of deterministic signals that can be analyzed with Fourier transform and Fourier series. Simple classification of signals and the concept of power and energy are reviewed. One important class of signal, namely orthogonal signals, such as the Walsh functions employed in IS-95, CDMA 2000, and WCDMA, is discussed in detail. The majority of continuous-time and finite-energy signals in practice can be conveniently analyzed via their signal spaces. These signal spaces are displays of the signal vectors in their respective constellations. The signal vectors which can be viewed as the A/D versions of a signal set contain all the information about the signal set. Practical communication systems are inherently linear time-invariant systems operating in the small-signal range. They can be analyzed by Fourier series and Fourier transform to provide a frequency-domain snapshot of the signal bandwidth. The concept of autocorrelation and its relationship with energy or power spectral density are discussed for linear time-invariant systems. The sampling theorem that governs the A/D conversion of an analog signal and the

Nyquist–Shannon interpolation for reconstruction of the analog signal are presented. Finally, the representations of a bandpass signal, that is, the signal sent over a physical channel, are discussed. The complex envelope (equivalent lowpass signal) of a bandpass signal that can be employed to simplify the analysis of a communication system is also included.

Chapter 3 studies random signals and their statistics. Although a finite set of deterministic signals is employed to represent a finite set of information symbols, the transmitted symbols are truly random, with each one in the set occuring with a fixed probability. Therefore, the infinite series of signals transmitted over the channel is indeed a random process with finite power. The study of random processes allows the establishment of the Fourier transform relationship between the autocorrelation of the random process and its power spectral density via the *Einstein–Wiener–Khinchine theorem*. The emphasis here is on cyclostationary processes, which encompass all digitally modulated signals. The Gaussian process that is used to represent channel noise is discussed in sufficient detail. Sampling of bandlimited white Gaussian process, sufficient statistics for white Gaussian samples, the *Karhunen–Loeve theorem*, and whitening filter are studied. To study the performance of wireless communication via a fading channel we look at a variety of processes derived from the Gaussian process, such as the Rayleigh, Rice, Nakagami-m, χ^2, and log-normal processes.

Chapter 4 provides a general study of information theory developed by Shannon, and addresses both source and channel coding. The concept of source entropy and prefix code is discussed. *Shannon–Fano* and *Huffman* prefix codes are used as examples. The *Shannon first theorem* is presented with a proof, and the concept of mutual information is presented together with the *Shannon main theorem* for a discrete channel. The concept of differential entropy for a Gaussian channel is introduced, and leads to mutual information and Shannon channel capacity. Vector Gaussian channels and the water filling strategy are presented to highlight the concept of channel coding, which is also interpreted via the sphere packing bound. The channel capacity of a bandlimited Gaussian channel and the channel capacity of a Gaussian channel with discrete inputs are derived. The latter provides a snapshot of how efficient digitally modulated signals perform as compared to the *Shannon capacity*. Channel coding can be done with error-correction codes such as block codes and convolutional codes. Performance of coded digital signals is presented for both block codes and convolutional codes, with the emphasis on low-density parity-check codes (LDPC) and convolutional codes. The decoding of LDPC codes is implemented via the *message passing algorithm*. The decoding of convolutional codes is carried out via the *Viterbi algorithm*, which includes hard decoding, and quantized or unquantized soft decoding.

Chapter 5 examines methods for establishing a communication link between the transmitter and receiver, commonly referred to as link analysis. The link budget involves the allocation of power to the transmitter and noise temperature (or noise figure) to the receiver so that a signal-to-noise ratio is established at the receiver to match a specified error rate range. Given the transmitter power and the channel attenuation, the power of the received signal can then be established. The channel attenuation is unique for each physical medium. The chapter begins with the concept of the noise temperature of a two-port network, which leads to the concept of the *system noise temperature* of a cascade of two-port

networks modeling a receiver. The system noise temperature allows the evaluation of noise power in the receiver bandwidth, and hence the *system signal-to-noise ratio*. The physical channels investigated in this chapter are the cellular and satellite channels. For the cellular channel, we adopt the well-known *Hata* model to estimate the median path loss between the transmitter and receiver. The presence of co-channel interference between cells is also taken into account. Both narrowband cellular systems (IS-136, GSM) and wideband CDMA cellular systems (IS-95, CDMA-2000, WCDMA) are covered. For a satellite channel, the communication link is a point-to-point link, consisting of up- and downlinks. The *Friis* formula for free-space attenuation is employed to establish the uplink or downlink attenuation.

Chapter 6 presents modulation techniques for transmitting information over the physical channel. The chapter essentially has two parts, namely binary modulation and M-ary modulation. The structure of each modulation technique is studied via the signal waveform, the power spectral density, and the modulator. For binary modulation we investigate phase shift keying (PSK), differential phase shift keying (DPSK), amplitude shift keying (ASK) (commonly referred to as intensity-modulated on–off keying (OOK), a technique used in fiber optic communication), frequency shift keying (FSK), minimum shift keying (MSK), and Gaussian MSK employed by the GSM cellular standard. Many practical applications require either the higher spectral efficiency or higher power efficiency that binary modulation techniques can provide; M-ary modulation can accommodate both. The second part of this chapter covers M-ary amplitude shift keying (MASK), M-ary phase shift keying (MPSK), offset quadrature phase shift keying (OQPSK), differential M-ary phase shift keying (DMPSK), $\pi/4$ shifted differential quadrature phase shift keying ($\pi/4$-DQPSK), M-ary quadrature amplitude modulation (MQAM), code shift keying (CSK), M-ary frequency shift keying (MFSK), and continuous phase modulation (CPM). The chapter continues with a treatment of the dominant multiplexing-modulation technique, namely *orthogonal frequency division multiplexing* (OFDM), which is used in many wireless standards. The chapter ends with a look at *trellis coded modulation* (TCM) for bandlimited channels. Both Ungerboeck and pragmatic TCM are investigated.

Chapter 7 provides a treatment of digital demodulation. A generic digital demodulator consists of two major subsystems, namely the signal processor and the detector. There are four types of signal processor: the matched filter, the correlator, the noncoherent matched filter, and the noncoherent correlator. The first two types are employed in coherent demodulation while the last two types are used in noncoherent demodulation. For binary demodulation the two fundamental detectors are threshold and maximum detectors. For M-ary demodulation the two fundamental detectors are the minimum Euclidean distance detector and the M-ary maximum detector. Combining the signal processor(s) and the detector in that order produces an L-path demodulator for the set of digital signals with L orthonormal basis functions and an M-path demodulator for the set of M orthogonal signals. The bit error probability analysis is carried out for binary modulation techniques such as coherent PSK, coherent DPSK, direct-detection ASK (for fiber optic communication), coherent FSK, coherent MSK, precoded MSK and GMSK, noncoherent FSK and MSK, and noncoherent DPSK. For M-ary demodulation, the bit error probability analysis is carried out for coherent MASK, coherent MPSK, coherent DMPSK, noncoherent DMPSK,

coherent MQAM and DMQAM, coherent CSK and MFSK, noncoherent CSK and MFSK, coherent CPM with sequence detection, coherent CPM with symbol-by-symbol detection, and noncoherent CPM. The chapter continues with OFDM demodulation, with emphasis on the IEEE 802.11a,g standards. Finally, the demodulation and decoding of TCM are studied and performance analysis is investigated. The Viterbi algorithm is again used to illustrate the decoding process.

Chapter 8 investigates two major spread spectrum communication techniques for both commercial and military applications: direct sequence (DS) and frequency hop (FH). The chapter begins with a presentation of the pseudo-noise (PN) sequences needed for spreading the modulated signal. Next the concept of quadrature orthogonal covering using Walsh functions of the same length for multiplexing DS signals with an identical symbol rate is discussed. This concept is then extended to variable-length orthogonal covering for variable symbol rates. IS-95 is used as a real life example for the study of the direct sequence spread spectrum. The demodulation of DS signals in the presence of tone jamming, broadband jamming, and pulse jamming is analyzed. Demodulation of quadrature orthogonal covering (IS-95 forward link) as well as noncoherent DS-CSK (IS-95 reverse link) is presented. The analysis of code division multiple access (CDMA) with random spreading sequences is presented together with a closed form expression and a tight upper bound for bit error probability. For frequency hop signals, three jamming strategies are studied: partial-band jamming, multi-tone jamming, and follower jamming. Both slow and fast hops are considered for follower jamming.

Chapter 9 deals with intersymbol interference (ISI) in a bandlimited channel. The Nyquist criterion for zero ISI is stated together with the corresponding pulse shapes that satisfy it. The design of an optimum demodulator for a bandlimited channel with Gaussian noise is carried out. The optimum demodulator relies on the signal pulse shape implemented at the modulator. The channel is converted to an ideal channel via an equalizer implemented at the modulator (the equalizer is a filter with a transfer function equal to the inverse transfer function of the channel). At the demodulator, a matched filter matched to the signal pulse shape simultaneously achieves both the maximum signal-to-noise ratio and zero ISI as long as the pulse shape at the matched filter output satisfies the Nyquist criterion of zero ISI. In practice, because the channel transfer function is not known or varies with time, ISI removal is instead implemented at the demodulator. The equalizer implemented at the demodulator can be classified into two types: linear and nonlinear. The treatment of linear equalizers covers zero-forcing and mean-square error equalizers. The latter alleviates the noise enhancement effect that severely degrades the former in channels with deep attenuation in the passband. Nonlinear equalizers such as zero-forcing decision-feedback and mean-square error decision-feedback can avoid the noise enhancement effect altogether, although in channels with severe distortion the error propagation due to decision feedback could worsen the performance. To obtain optimum performance, maximum likelihood sequence detection may be employed to mitigate the ISI. The motivation behind sequence detection is to use the symbol energy that resides in the ISI portion of the symbol to aid the detection instead of throwing it away. The Viterbi algorithm is employed in practice for sequence detection. Finally, a fractionally spaced equalizer that can mitigate timing error is presented.

Chapter 10 studies the transmission and reception of a digitally modulated signal over a fading channel. Unlike the AWGN channel, where noise is the only problem, a fading channel is a greater challenge, as it may cause signal envelope variations, phase errors, and intersymbol interference, all of which are detrimental to the performance of the signal. Thus, it is necessary to understand the mechanism that causes these unwanted effects and find ways to mitigate them. A fading channel arises from the movement of the transmitter and receiver, commonly referred to as the time-varying effect or Doppler effect. This may cause random amplitude attenuation and random phase rotation of the signal space. In underwater acoustic communication, the medium also changes over time, further compounding the problem. A fading channel also exhibits a space-varying effect, where the locations of the transmitter and receiver and the physical structures in the environment dictate the paths that the signal may travel. A transmitted signal representing an arbitrary symbol may arrive at the receiver via multiple paths. Depending on the time delay between paths, signal echoes of a symbol may overlap the next several symbols causing intersymbol interference. Both time-varying and space-varying effects can be classified into four fading characteristics: *slow fading* with random amplitude attenuation and negligible phase error, *fast fading* with random amplitude attenuation and large phase error, *flat fading* with random amplitude attenuation and negligible intersymbol interference, and *frequency-selective fading* with random amplitude attenuation and intersymbol interference. A mobile wireless channel may have two of these four characteristics where the random amplitude attenuation is described by a special distribution (Rayleigh, Rice, and Nakagami-m). For analysis, it is convenient to model a fading channel with a channel impulse response that includes both time- and space-varying effects. From the channel impulse response, the multipath autocorrelation and Doppler profiles are derived, which lead to the concept of the Doppler power spectrum. Clarke–Doppler and Aulin–Doppler spectra are studied as examples. Using a mathematical model, the performance of a modulated signal in a fading channel is analysed. First, *ideal* coherent demodulation (assuming the carrier phase is always available for symbol-by-symbol detection) is investigated and the fading channel is assumed to produce only random amplitude attenuation. Channel tap estimation as well as the channel tap error effect is studied to reflect real world situations.

Next, the slow fading channel with random amplitude attenuation is investigated for *pilot symbol-aided* demodulation (the pilot symbols are periodically transmitted in the symbol stream; this represents a less desirable situation than ideal coherent demodulation but remains in line with practical applications). These investigations are extended to OFDM (the major waveform that was adopted by IEEE 802.11a-g, 802.16 to name a few) where a slow and frequency-selective fading channel is assumed. The fundamentals of coherent demodulation are extended to noncoherent demodulation, where the Doppler tracking of orthogonal signals is investigated. The next discussion centers on another major waveform that was adopted by IS-95, CDMA 2000, and WCDMA (for use either in the forward channel or reverse channel or both) for their respective cellular systems, namely, orthogonal covering and spread spectrum signals. Complex spreading and despreading as well as Doppler analysis and tracking are presented. For completeness the demodulation of the signal used in the reverse channel of IS-95 is also presented. Once the Doppler phase error resulting from either slow or fast fading is corrected via Doppler tracking, and the ISI

resulting from frequency-selective fading is mitigated via OFDM and equalization, only random amplitude attenuation remains to be dealt with. This particular effect can be effectively alleviated via the use of time, frequency, antenna, or multipath delay diversity. Diversity is a signal combining method that makes use of uncorrelated signal redundancy for both transmission and reception to enhance symbol detection in the presence of a deep fade which may destroy a non-diversity symbol. Diversity can be achieved via redundant symbol interleaving for time diversity, or via uncorrelated subcarrier combining in OFDM for frequency diversity. It can also be achieved via multiple transmit antennas for transmit antenna diversity, and via multiple receive antennas for receive antenna diversity or using a Rake receiver for multipath delay diversity. Combinations of these methods are also possible. Three main signal combining methods are studied: maximal ratio combining (MRC), selection combining (SC), and equal gain combining (EGC). MRC is the optimum combining scheme for coherent or pilot symbol-aided demodulation in AWGN and is the most commonly used method for wireless LAN, MAN, WAN, and cellular systems. It is superior to SC and EGC, although it cannot be used for noncoherent demodulation, unlike the other two schemes. Wireless communication in a fading channel favors the use of multiple transmit antennas for performance enhancement. This type of antenna diversity employs orthogonal space-time block codes with rates of ½, ¾, and 1 with MRC at the receiver. The Alamouti code with unity rate was recommended for the IEEE 802.16 family. Integrating both transmit and receive antenna diversity provides the receiver with a powerful method to combat random amplitude attenuation.

The remaining parts of this chapter investigate the capacity of a fading channel. Since a fade causes an outage that may drive the instantaneous channel capacity to zero, the average channel capacity defined for an AWGN channel does not exist for a slow fading channel. Therefore, the outage channel capacity is defined instead. The evaluation of outage capacity for a slow fading channel, as well as slow fading channels with receive antenna diversity (SIMO), transmit antenna diversity (MISO), both receive and transmit antenna diversity (MIMO), and OFDM are presented. For a fast fading channel, the average channel capacity is well defined since symbols fade independently and there exists a coding system that ensures a maximum reliable rate, which is the ensemble average rate. Fast fading is less detrimental than slow fading from the capacity point of view but requires more complex channel coding to deal with both Doppler phase error (virtually eliminated via Doppler tracking in slow fading) and random amplitude attenuation.

1.3 Summary

The structure of the book can be summarized as follows:

- **Acquiring** the prerequisite knowledge of communication signals: Chapters 2 and 3.
- **Packaging** the message and introducing the concept of signal-to-noise ratio and bandwidth: Chapter 4.

- **Measuring and establishing** the required signal-to-noise ratio for a given communication coverage: Chapter 5.
- **Sending** the message based on the required signal-to-noise ratio and bandwidth: Chapter 6.
- **Receiving** the message and **providing** the best detection: Chapter 7.
- **Enhancing** the survivability of narrowband modulation in the presence of interference via bandwidth spreading, i.e., spread spectrum modulation: Chapter 8.
- **Pulse shaping and equalizing** the effect of a bandlimited channel for modulated signals: Chapter 9.
- **Dealing** with sending and receiving signals over a mobile channel for previously discussed modulation techniques: Chapter 10.

Bibliography

1. C. E. Shannon, "A mathematical theory of communication," *Bell Syst. Tech. J.*, Vol. **27**, pp. 379–423, pp. 623–56, 1948. Also available at http://cm.bell-labs.com/cm/ms/what/shannonday/paper.html.
2. R. W. Hamming, "Error detecting and error correcting codes," *Bell Syst. Tech. J.*, Vol. **29**, pp. 147–60, 1950.
3. R. W. Hamming, *Coding and Information Theory*, 2nd edition, Hemel Hempstead: Prentice-Hall, 1986.
4. R. G. Gallager, *Principles of Digital Communications*, Cambridge: Cambridge University Press, 2008.

2 Deterministic signal analysis

Introduction

In this chapter we lay the foundation for the analysis and design of communication systems, and digital communication systems in particular. We employ *deterministic signals* to carry information from the transmitter to the receiver. These deterministic signals contain certain *a priori* features sufficiently adequate for the receiver to retrieve the information. Note that the information always appears random to the receiver, that is, it does not know which data it will receive; otherwise, communications would not be needed. Deterministic signals form a very broad class of signals; therefore, the first step is to categorize them so that their characterization can be fully exploited. The categorization leads to the labels *continuous-time*, *discrete-time*, *periodic*, *aperiodic*, *analog*, *digital*, *energy*, and *power signals*. Further study leads us to *orthogonal signals* and the use of *signal space* to represent digital signals as vectors. We also review *linear time-invariant* (LTI) systems and the important *convolution* operation that relates the inputs and outputs of an LTI system.

We then investigate *Fourier series* representation of continuous-time periodic signals, and *Fourier transform* of continuous-time aperiodic signals. The Fourier transform is indispensable in the analysis and design of LTI systems. The *energy spectral density* of an energy signal and the *power spectral density* of a power signal are studied. From here the *autocorrelation* functions of both energy and power signals are examined.

The process of representing a continuous-time signal by its samples is then studied using the *sampling theorem*. We also discuss the process of recovering a continuous-time signal from its samples. Finally, we study various representations of *bandpass signals*, which are commonly used in the analysis of communication systems.

2.1 General description of deterministic signals

A deterministic signal is completely specified at any instant of time t. There is no uncertainty about its value at t. The transmitter employs deterministic signals to carry random information. When the receiver receives a transmitted signal that has been corrupted by noise (a random signal), it attempts to detect the information by stripping away the deterministic signals. A deterministic signal can fall into a number of categories, which are described below.

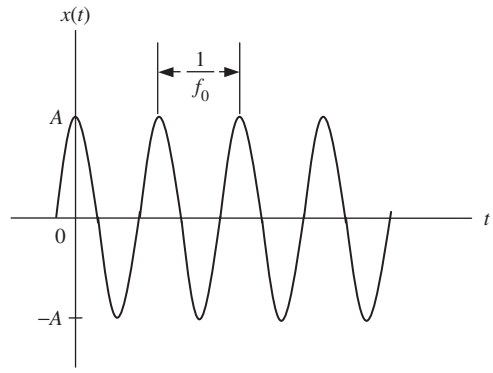

Figure 2.1 Sinusoidal signal.

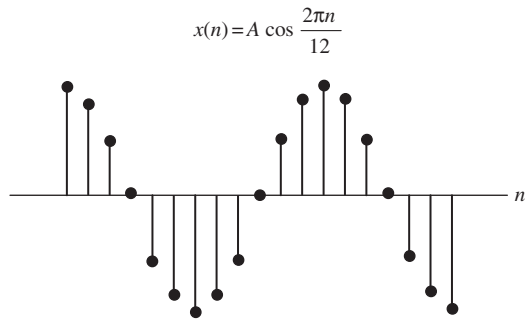

Figure 2.2 Discrete-time sinusoidal signal.

Continuous-time signals

A *continuous-time* signal $x(t)$ is a signal of the real variable t. For example, the sinusoidal signal

$$x(t) = A \cos 2\pi f_0 t \tag{2.1}$$

shown in Figure 2.1 is a function of the time variable t, with amplitude A and frequency f_0.

Discrete-time signals

A *discrete-time* signal $x(n)$ is a sequence where the values of the index n are integers. For example, the discrete-time sinusoidal signal

$$x(n) = A \cos 2\pi f_0 n \tag{2.2}$$

with $f_0 = 1/12$ is shown in Figure 2.2.

Often a discrete-time signal is obtained from a continuous-time signal $x(t)$ by sampling at the time instants separated by a *sampling interval* T. Thus, $x(n) = x(nT)$. For example, if $x(t) = \cos 2\pi f_0 t$, then $x(n) = x(nT) = \cos 2\pi f_0 nT$. Specifically, $f_0 T = 1/12$ for Figure 2.2.

Periodic and aperiodic signals

A *periodic* signal $x(t)$ satisfies the following condition:

$$x(t) = x(t + T_0) \tag{2.3}$$

for all time t, where T_0 is the *period*. A signal $x(t)$ that is not periodic is referred to as an *aperiodic* or *nonperiodic* signal.

Example 2.1 Continuous-time sinusoid
The signal $x(t) = A \cos 2\pi f_0 t$ shown in Figure 2.1 is a continuous-time periodic signal with period $T_0 = 1/f_0$. Note that

$$\begin{aligned} x(t + T_0) &= A\cos[2\pi f_0(t + T_0)] = A\cos(2\pi f_0 t + 2\pi f_0 T_0) \\ &= A\cos[2\pi f_0 t + 2\pi] = A\cos 2\pi f_0 t = x(t) \end{aligned} \tag{2.4}$$

■

Periodic signals are defined analogously in discrete time. Specifically, a discrete-time periodic signal $x(n)$ satisfies the following condition:

$$x(n) = x(n + N_0) \tag{2.5}$$

for all integers n, where the positive integer N_0 is the period.

Example 2.2 Discrete-time sinusoid
The signal $x(n) = A \cos 2\pi f_0 n$ is periodic if

$$\begin{aligned} A\cos 2\pi f_0 n &= A\cos 2\pi f_0(n + N_0) \\ &= A\cos(2\pi f_0 n + 2\pi f_0 N_0) \end{aligned} \tag{2.6}$$

This implies that $2\pi f_0 N_0$ must be a multiple of 2π. Thus, for an arbitrary integer m

$$2\pi f_0 N_0 = 2\pi m \tag{2.7}$$

or equivalently

$$f_0 = m/N_0 \tag{2.8}$$

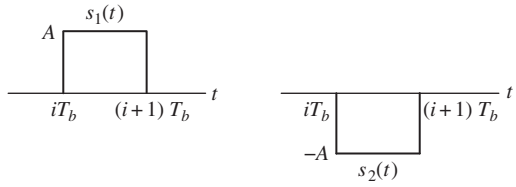

Figure 2.3 Antipodal signals.

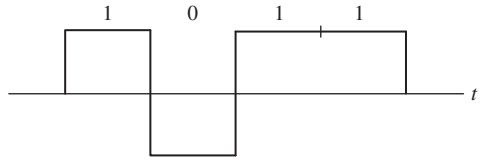

Figure 2.4 Representation of the bit sequence {1, 0, 1, 1}.

Thus $x(n)$ is periodic only if f_0 is a *rational number*. Obviously, the *fundamental frequency* is $f_0 = 1/N_0$, assuming that m and N_0 do not have a common factor. The sequence $x(n) = A\cos(2\pi n/12)$ is periodic with period $N_0 = 1/f_0 = 12$.

■

Analog and digital signals

An *analog* signal is a signal with a continuous range of amplitudes. For example, the signal $x(t) = A\cos 2\pi f_0 t$, $-\infty < t < \infty$, is an analog signal.

A digital signal is a member of a set of M unique analog signals that represent M data symbols.

Example 2.3 Antipodal signals

The binary digital signals $s_1(t) = A$, $iT_b \le t < (i{+}1)T_b$ and $s_2(t) = -A$, $iT_b \le t < (i{+}1)\,T_b$ shown in Figure 2.3 represent bit 1 and bit 0, respectively. The parameter T_b is the duration of $s_1(t)$ or $s_2(t)$, and it is called the *bit time* (bit interval, bit duration). The time index i is an integer. The amplitude is A. This signaling technique is called *antipodal signaling* (also referred to as bipolar, non-return-to-zero (NRZ), or polar NRZ in the literature).

The digital signals $s_1(t)$ and $s_2(t)$ can be employed to represent the sequence of bits {1, 0, 1, 1}, as shown in Figure 2.4.

■

Example 2.4 Phase shift keying

The set of two digital signals $s_1(t) = A\cos 2\pi f_c t$, $iT_b \le t < (i+1)T_b$ and $s_2(t) = -A\cos 2\pi f_c t = A\cos(2\pi f_c t + \pi)$, $iT_b \le t < (i{+}1)\,T_b$ shown in Figure 2.5 can be

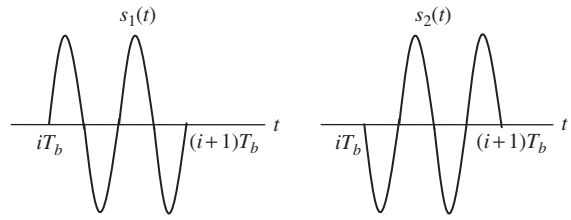

Figure 2.5 Binary digital signals.

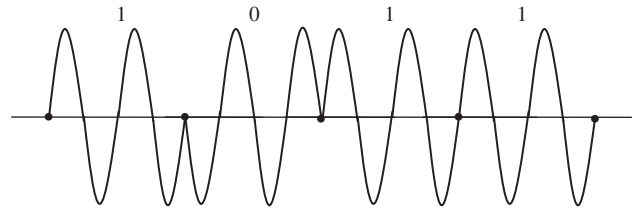

Figure 2.6 Representation of bit sequence {1, 0, 1, 1}

employed to represent bit 1 and bit 0, respectively. The frequency f_c is normally greater than $1/T_b$. The parameter $R_b = 1/T_b$ is referred to as the *bit rate*. Note that there is a phase shift of π radians between bits 1 and 0. This signaling or modulation technique is called *binary phase shift keying* or simply PSK (also referred to as BPSK or 2PSK in the literature).

The sequence of bits {1, 0, 1, 1} represented by $s_1(t)$ and $s_2(t)$ is shown in Figure 2.6.

■

A generalization of PSK is *M-ary phase shift keying* (MPSK) where M data symbols are represented by M signals with distinct phase shifts. Each symbol has k bits, hence, $M = 2^k$. The *symbol time* (symbol interval, symbol duration) is T_s. The parameter $R_s = 1/T_s$ is referred to as the *symbol rate*. Note that a symbol has k bits; therefore, a symbol time consists of k bit times, that is, $T_s = kT_b$. Thus, the symbol rate is $1/k$ times the bit rate, that is, $R_s = R_b/k = 1/kT_b$.

The MPSK signals can be written in an arbitrary symbol interval $iT_s \leq t < (i+1)T_s$, where i is an integer, as follows:

$$s_n(t) = A\cos\left(2\pi f_c t + (2n-1)\frac{\pi}{M}\right), \quad n = 1, 2, ..., M \tag{2.9}$$

where the frequency $f_c > 1/T_s$.

Example 2.5 Quadrature phase shift keying

For the case $M = 4$, there are four signals representing four distinct symbols 00, 01, 10, 11. In this case, each symbol has $k = 2$ bits and the signals are given as

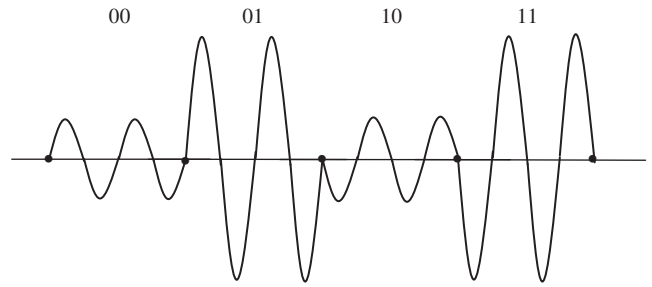

Figure 2.7 4ASK for the sequence {00, 01, 10, 11}

$$s_1(t) = A\cos\left(2\pi f_c t + \frac{\pi}{4}\right) \text{ for } 00$$
$$s_2(t) = A\cos\left(2\pi f_c t + \frac{3\pi}{4}\right) \text{ for } 01$$
$$s_3(t) = A\cos\left(2\pi f_c t + \frac{5\pi}{4}\right) \text{ for } 11$$
$$s_4(t) = A\cos\left(2\pi f_c t + \frac{7\pi}{4}\right) \text{ for } 10$$

This signaling or modulation technique is called *quadrature phase shift keying* or simply QPSK (also referred to as 4PSK in the literature).

■

Example 2.6 4-ary amplitude shift keying

Consider the set of $M = 4$ symbols {00, 01, 10, 11}. The following four digital signals represent the above symbols in an arbitrary symbol interval $iT_s \leq t < (i+1)\ T_s$:

$$s_1(t) = A\ \cos 2\pi f_c t \text{ for } 00$$
$$s_2(t) = 3A\ \cos 2\pi f_c t \text{ for } 01$$
$$s_3(t) = -A\ \cos 2\pi f_c t \text{ for } 10$$
$$s_4(t) = -3A\ \cos 2\pi f_c t \text{ for } 11$$

Figure 2.7 shows the sequence {00, 01, 10, 11} as represented by $s_1(t), s_2(t), s_3(t)$, and $s_4(t)$ in time. This signaling or modulation technique is called *4-ary amplitude shift keying* or simply 4ASK.

■

In the next section we will investigate two special types of deterministic signals, namely, power and energy signals, and their relationship.

2.2 Power and energy

The *average power* in watts delivered by a voltage signal $v(t)$ in volts to a resistive load R in ohms is given by

$$P = \frac{V_{rms}^2}{R} \tag{2.10}$$

where V_{rms} is the *root mean-square* (rms) value of $v(t)$, defined as

$$V_{rms} = \left[\lim_{T\to\infty} \frac{1}{2T} \int_{-T}^{T} v^2(t)\,\mathrm{d}t\right]^{1/2} \tag{2.11}$$

In communications, the value of the resistive load is normally assumed to be

$$R = 1\,\Omega \tag{2.12}$$

Thus the average (normalized) power in watts is given by

$$P = \lim_{T\to\infty} \frac{1}{2T} \int_{-T}^{T} v^2(t)\,\mathrm{d}t \tag{2.13}$$

A signal $v(t)$ is called a *power* signal if and only if the average power is non-zero and finite, that is,

$$0 < P < \infty \tag{2.14}$$

Example 2.7 Power of a sinusoid

Let a voltage signal $v(t) = A\cos 2\pi f_0 t$ volts be applied across a resistive load $R = 1\,\Omega$. The average (normalized) power in watts delivered to the load is

$$\begin{aligned} P &= \lim_{T\to\infty} \frac{1}{2T} \int_{-T}^{T} (A\cos 2\pi f_0 t)^2 \mathrm{d}t \\ &= \lim_{T\to\infty} \frac{A^2}{4T} \int_{-T}^{T} (1+\cos 4\pi f_0 t)\mathrm{d}t \\ &= \frac{A^2}{2} + \lim_{T\to\infty} \frac{A^2}{4T}\left(\frac{\sin 4\pi f_0 T}{4\pi f_0} + \frac{\sin 4\pi f_0 T}{4\pi f_0}\right) \\ &= \frac{A^2}{2} + \frac{A^2}{2} \lim_{T\to\infty} \frac{\sin 4\pi f_0 T}{4\pi f_0 T} = \frac{A^2}{2} \end{aligned} \tag{2.15}$$

Therefore, $v(t) = A\cos 2\pi f_0 t$ is a power signal.

■

The energy in joules of a voltage signal $v(t)$ in volts is given by

$$E = \int_{-\infty}^{\infty} |v(t)|^2 \mathrm{d}t \tag{2.16}$$

A signal $v(t)$ is called an *energy* signal if and only if its energy is non-zero and finite, that is,

$$0 < E < \infty \tag{2.17}$$

Example 2.8 Energy of a sinusoid
The power signal in Example 2.7 has infinite energy, as proved below:

$$\begin{aligned} E &= \int_{-\infty}^{\infty} (A\cos 2\pi f_0 t)^2 \mathrm{d}t \\ &= \int_{-\infty}^{\infty} \frac{A^2}{2}(1+\cos 4\pi f_0 t)\ \mathrm{d}t = \infty \end{aligned} \tag{2.18}$$

■

The above two examples show that a power signal has infinite energy. In the next two examples we investigate some additional energy signals.

Example 2.9 Energy and power of antipodal signals
Consider the digital signals $s_1(t) = A$, $iT_b \le t \le (i+1)T_b$, and $s_2(t) = -A$, $iT_b \le t < (i+1)T_b$, as given in Example 2.3. The energy E_b of these two signals, commonly referred to as the *bit energy*, can be calculated as follows:

$$E_b = \int_{-\infty}^{\infty} (\pm A)^2 \mathrm{d}t = \int_{iT_b}^{(i+1)T_b} A^2 \mathrm{d}t = A^2 T_b \tag{2.19}$$

The energy of $s_1(t)$ and the energy of $s_2(t)$ satisfy (2.17), hence both signals are energy signals. However, the average power of these two signals is zero, as shown below:

$$\begin{aligned} P &= \lim_{T\to\infty} \frac{1}{2T} \int_{-T}^{T} (\pm A)^2 \mathrm{d}t = \lim_{T\to\infty} \frac{1}{2T} \int_{iT_b}^{(i+1)T_b} A^2 \mathrm{d}t \\ &= \lim_{T\to\infty} \frac{1}{2T} A^2 T_b = 0 \end{aligned} \tag{2.20}$$

■

Example 2.10 Energy and power of PSK signals

Consider the PSK signals $s_1(t) = A\ \cos 2\pi f_c t, iT_b \le t < (i+1)T_b$ and $s_2(t) = -A\ \cos 2\pi f_c t, iT_b \le t < (i+1)T_b$ shown in Example 2.4. Again, we can calculate the energy E_b of $s_1(t)$ or $s_2(t)$ as follows:

$$\begin{aligned} E_b &= \int_{-\infty}^{\infty} (\pm A \cos 2\pi f_c t)^2 \mathrm{d}t \\ &= \int_{iT_b}^{(i+1)T_b} \left(\frac{A^2}{2} + \frac{A^2}{2}\cos 4\pi f_c t\right) \mathrm{d}t \\ &= \frac{A^2 T_b}{2} + \frac{A^2 T_b}{2}\left[\frac{\sin 4\pi f_c (i+1)T_b}{4\pi f_c T_b} - \frac{\sin 4\pi f_c i T_b}{4\pi f_c T_b}\right] \end{aligned} \tag{2.21}$$

In practice, the frequency f_c is normally chosen to be much greater than $1/T_b$. Thus, the second term on the right-hand side of (2.21) is very small compared to the first term, and E_b is approximately equal to

$$E_b \approx \frac{A^2 T_b}{2} \tag{2.22}$$

When f_c is selected to be an integer multiple of $1/T_b$, that is,

$$f_c = \frac{k}{T_b} \tag{2.23}$$

where k is a positive integer, then, the second term on the right-hand side of (2.21) is zero and

$$E_b = \frac{A^2 T_b}{2} \tag{2.24}$$

It is noted that E_b in (2.21) satisfies (2.17), hence $s_1(t)$ and $s_2(t)$ are both energy signals. It can be shown that the average power of both $s_1(t)$ and $s_2(t)$ is zero.

■

From the above examples we observe that a power signal has infinite energy and an energy signal has zero average power. This is true for practical signals employed in both digital and analog communication systems. It is quite obvious that any transmitted signal must be a power signal because the transmitter can only have finite power. But, over an infinite time, such a power signal must have infinite energy since energy is a product of power and time.

In a digital communication system, data bits or symbols represented by associated digital signals are transmitted sequentially in time. The sequence of digital signals must therefore be a power signal due to the finite transmitted power. Although a single digital signal must have zero average power, an infinite sequence of signals turns out to have finite power. The next example discusses the energy–power relationship.

Example 2.11 Power of an infinite sequence of PSK signals

Consider an infinite sequence of digital signals that represents a set of integers. Let $s_1(t) = x(t - iT_b) = A\ \cos\ 2\pi f_c t,\ iT_b \le t < (i+1)T_b$ for even i, represents even integers

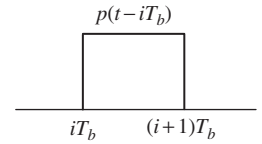

Figure 2.8 Unit amplitude pulse of duration T_b.

and $s_2(t) = x(t - iT_b) = -A\cos 2\pi f_c t = A\cos(2\pi f_c t + \pi)$, $iT_b \leq t < (i+1)T_b$ for odd i, represents odd integers. We can write the sequence as one composite signal as follows:

$$\begin{aligned} s(t) &= \sum_{i=-\infty}^{\infty} x(t - iT_b) \\ &= A\sum_{i=-\infty}^{\infty} (-1)^i p(t - iT_b)\cos 2\pi f_c t \end{aligned} \tag{2.25}$$

where $p(t - iT_b)$ is a pulse of unit amplitude and duration T_b, as shown in Figure 2.8

$$p(t - iT_b) = \begin{cases} 1, & iT_b \leq t < (i+1)T_b \\ 0, & \text{otherwise} \end{cases} \tag{2.26}$$

The average power of $s(t)$ is given by (2.13):

$$\begin{aligned} P &= \lim_{T\to\infty} \frac{1}{2T}\int_{-T}^{T} s^2(t)\,\mathrm{d}t \\ &= \lim_{T\to\infty} \frac{1}{2T}\int_{-T}^{T} A^2\left[\sum_{i=-\infty}^{\infty} (-1)^i p(t - iT_b)\cos 2\pi f_c t\right]^2 \mathrm{d}t \end{aligned} \tag{2.27}$$

Since the pulses $p(t-hT_b)$ and $p(t-iT_b)$ do not overlap for $i \neq h$, the cross-terms that involve the product $p(t-hT_b)\,p(t-iT_b)$ are all zeros, and (2.27) reduces to

$$\begin{aligned} P &= \lim_{T\to\infty} \frac{A^2}{2T}\int_{-T}^{T}\left[\sum_{i=-\infty}^{\infty} p^2(t - iT)\cos^2 2\pi f_c t\right]\mathrm{d}t \\ &= \lim_{T\to\infty} \frac{A^2}{2T}\int_{-T}^{T} \cos^2 2\pi f_c t\;\mathrm{d}t \\ &= \lim_{T\to\infty} \frac{A^2}{4T}\int_{-T}^{T} (1 + \cos\;4\pi f_c t)\,\mathrm{d}t \\ &= \frac{A^2}{2} \end{aligned} \tag{2.28}$$

The last two lines of (2.28) follow (2.15). From (2.22) and (2.24), we have the following relationship between the energy of the digital signals $s_1(t)$ and $s_2(t)$ and their associated sequence $s(t)$ in (2.25):

$$E_b \approx PT_b \tag{2.29}$$

or

$$E_b = PT_b \tag{2.30}$$

when the product nf_cT_b is a positive integer.

■

Example 2.11 shows that although the infinite sequence $s(t)$ of digital signals has finite average power, its component digital signal must have zero average power. If its component digital signal has finite power, an infinite number of them would result in a sequence $s(t)$ possessing infinite power. The concept can be made simpler by the following example.

Example 2.12 Power of a finite sequence of PSK signals

Instead of using the power averaged over infinite time, we can employ the power averaged over *finite time*. Let $P(T)$ be the power of a voltage signal $v(t)$ averaged over the finite time T:

$$P(T) = \frac{1}{2T}\int_{-T}^{T} v^2(t)\mathrm{d}t \tag{2.31}$$

Now consider the sequence $s(t)$ in (2.25). For simplicity let $f_c = k/T_b$, where k is a positive integer. By using the definition of power in (2.31) and choosing $T = nT_b$, where n is a positive integer, we can calculate the power of $s(t)$ as follows:

$$\begin{aligned} P(T) &= \frac{A^2}{2} + \frac{A^2}{2}\left(\frac{\sin 4\pi f_c T}{4\pi f_c T}\right) = \frac{A^2}{2} + \frac{A^2}{2}\left(\frac{\sin 4\pi nk}{4\pi nk}\right) \\ &= \frac{A^2}{2} \end{aligned} \tag{2.32}$$

Similarly, the power of the digital signal $s_1(t) = Ap(t - iT_b)\cos 2\pi f_c t$ or $s_2(t) = -Ap(t - iT_b)\cos 2\pi f_c t$ averaged over $2T = 2nT_b > 4(i+1)T_b$ is

$$\begin{aligned} P_s(T) &= \frac{1}{2T}\int_{-T}^{T} A^2\left[p^2(t - iT_b)\cos^2 2\pi f_c t\right]\,\mathrm{d}t \\ &= \frac{A^2}{4T}\int_{iT_b}^{(i+1)T_b} (1 + \cos 4\pi f_c t)\,\mathrm{d}t \\ &= \frac{A^2 T_b}{4T} \end{aligned} \tag{2.33}$$

Substituting $T = nT_b$ into (2.33) we get

$$P_s(T) = \frac{A^2}{4n} \tag{2.34}$$

Since there are $2n$ non-overlapping signals $s_1(t)$ and $s_2(t)$ in the interval $2T$, it is obvious that

$$P(T) = 2nP_s(T) \tag{2.35}$$

In practice, (2.31) is used in laboratory instruments to measure power averaged over a *finite time*. This is also true for other average quantities, such as *dc value* and *rms value*. ■

2.3 Orthogonal signals

Orthogonal signals are employed in many modern communication systems. Two signals $x(t)$ and $y(t)$ are said to be *orthogonal* over the interval (a, b) if their *inner product* is zero, that is,

$$\int_a^b x(t)y^*(t)\ \mathrm{d}t = 0 \tag{2.36}$$

where $y^*(t)$ is the complex conjugate of $y(t)$. If, in addition, the energy of each signal defined over the interval (a, b) is unity, that is,

$$E_x = \int_a^b |x(t)|^2 \mathrm{d}t\ =\ 1,\ E_y\ =\ \int_a^b |y(t)|^2 \mathrm{d}t\ =1 \tag{2.37}$$

then the two signals are said to be *orthonormal.* A set of signals $\{x_i\,(t)\}$ is said to be orthogonal (orthonormal) if each pair of signals in the set is orthogonal (orthonormal). Conditions (2.36) and (2.37) can be relaxed to include *quasi-orthogonal* (*quasi-orthonormal*) signals. Two signals $x(t)$ and $y(t)$ are said to be quasi-orthogonal over the interval (a, b) if their *inner product* is much less than the energy of each signal, that is,

$$\int_a^b x(t)y^*(t)\ \mathrm{d}t\ \ll\ E_x\ \approx\ E_y \tag{2.38}$$

In addition, if

$$E_x\ \approx\ E_y\ \approx\ 1 \tag{2.39}$$

then the two signals are said to be quasi-orthonormal. A set of signals $\{x_i\,(t)\}$ is said to be quasi-orthogonal (quasi-orthonormal) if each pair of signals in the set is quasi-orthogonal (quasi-orthonormal).

Example 2.13 Orthonormal sinusoids with identical frequency
Consider two sinusoidal signals $x(t) = \sqrt{2/T_0}\cos 2\pi n f_0 t$ and $y(t) = \sqrt{2/T_0}\sin 2\pi n f_0 t$, where $n = 1, 2, \ldots$, and $T_0 = 1/f_0$. Substituting $x(t)$ and $y(t)$ into (2.36) with $a = 0$ and $b = T_0$ we have

$$\int_0^{T_0} \frac{2}{T_0} \cos 2\pi n f_0 t \sin 2\pi n f_0 t \, \mathrm{d}t = \frac{1}{T_0} \int_0^{T_0} \sin 4\pi n f_0 t \, \mathrm{d}t$$
$$= \frac{1}{T_0} \left(-\frac{\cos 4\pi n f_0 t}{4\pi n f_0} \right)_0^{T_0} = 0 \tag{2.40}$$

Furthermore, applying (2.37) we obtain the energy of $x(t)$ and $y(t)$, defined over $(0, T_0)$ as follows:

$$\begin{aligned} E &= \int_0^{T_0} \frac{2}{T_0} \cos^2 2\pi n f_0 t \, \mathrm{d}t = \int_0^{T_0} \frac{2}{T_0} \sin^2 2\pi n f_0 t \, \mathrm{d}t \\ &= \frac{1}{T_0} \int_0^{T_0} (1 + \cos \ 4\pi n f_0 t) \, \mathrm{d}t = \frac{1}{T_0} \int_0^{T_0} (1 - \cos \ 4\pi n f_0 t) \, \mathrm{d}t \\ &= 1 \end{aligned} \tag{2.41}$$

Thus, the two signals $x(t)$ and $y(t)$ are orthonormal over $(0, T_0)$.

■

The above example shows that two sinusoidal signals with a relative phase difference of $\pi/2$ radians are orthogonal over an integer multiple of their period $1/nf_0 = T_0/n$. In practice, the frequency of the sinusoidal signals might not be an integer multiple of $1/T_0$. In other words, n is not a positive integer but a positive real number. In this case the energy E_x of $x(t)$ and the energy E_y of $y(t)$ as calculated in (2.41) become

$$E_x = 1 + \frac{\sin \ 4\pi n}{4\pi n} \approx 1 \tag{2.42a}$$

$$E_y = 1 - \frac{\sin \ 4\pi n}{4\pi n} \approx 1 \tag{2.42b}$$

for a large n. Also from (2.40) we have for a large n:

$$\int_0^{T_0} \frac{2}{T_0} \cos 2\pi n f_0 t \sin 2\pi n f_0 t \, \mathrm{d}t = \frac{1}{T_0} \int_0^{T_0} \sin 4\pi n f_0 t \, \mathrm{d}t$$
$$= \frac{1}{T_0} \left(-\frac{\cos 4\pi n f_0 t}{4\pi n f_0} \right)_0^{T_0}$$
$$= \frac{1 \ - \ \cos 4\pi n}{4\pi n} \ll 1 \tag{2.43}$$

Thus, the two signals $x(t)$ and $y(t)$ have near unity energy and their inner product is much smaller than unity. In this case they are quasi-orthonormal.

Example 2.14 Orthonormal sinusoids with different frequencies

Consider the set of sinusoidal signals $\{x_n(t)\}$, $n = 1, 2, ...$, where $x_n(t)$ is given by

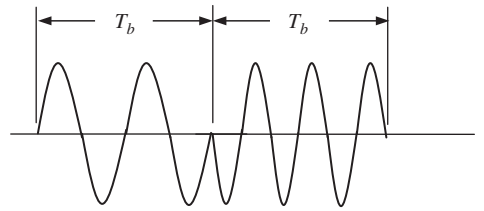

Figure 2.9 FSK representation of two consecutive and different bits.

$$x_n(t) = \sqrt{\frac{2}{T_0}}\cos(2\pi n f_0 t + \theta_n), \qquad T_0 = \frac{1}{f_0} \tag{2.44}$$

Substituting a pair of signals $x_k(t)$ and $x_m(t)$ with $k \neq m$ into (2.36) and setting $a = 0$ and $b = T_0$ yields

$$\begin{aligned}\int_0^{T_0} x_k(t)x_m(t)\,\mathrm{d}t &= \int_0^{T_0} \frac{2}{T_0}\cos(2\pi k f_0 t + \theta_k)\cos(2\pi m f_0 t + \theta_m)\,\mathrm{d}t \\ &= \frac{1}{T_0}\int_0^{T_0} \{\cos[2\pi(k-m)f_0 t + \theta_k - \theta_m] \\ &\qquad + \cos[2\pi(k+m)f_0 t + \theta_k + \theta_m]\}\mathrm{d}t \\ &= 0\end{aligned} \tag{2.45}$$

Furthermore, it can be seen that the energy of each signal $x_k(t)$ and $x_m(t)$ is unity by applying (2.37). Thus, the set of sinusoidal signals $\{x_n(t)\}$ is orthonormal over $(0, T_0)$.

■

The signals in (2.45) are often employed to represent data bits or symbols. For example, two adjacent signals $x_n(t)$ and $x_{n+1}(t)$ can be used to represent bit 0 and bit 1, respectively. The parameter T_0 is set to be the bit time T_b. Note that the frequencies of the two signals are separated by $f_0 = 1/T_0 = 1/T_b$, which is also the bit rate. This is the *minimum frequency spacing* between $x_n(t)$ and $x_{n+1}(t)$. This modulation technique is referred to as *binary frequency shift keying* or simply FSK (also referred to as BFSK or 2FSK in the literature). In another example, $M = 2^k$ adjacent signals, $x_n(t)$, $x_{n+1}(t)$, $\ldots$, $x_{n+M}(t)$, can be used to represent M symbols. In this case the parameter T_0 is set to be the symbol time T_s. The adjacent frequencies are separated by the *minimum frequency spacing* $f_0 = 1/T_0 = 1/T_s$, which is also the symbol rate. This is called *M-ary frequency shift keying* or simply MFSK. Figure 2.9 illustrates an FSK representation of two consecutive bits 0 and 1.

Example 2.15 Continuous-phase orthonormal sinusoids with minimum frequency spacing
Consider two sinusoidal signals $x_{n,i}(t)$ and $x_{n+1,i}(t)$ defined over the interval $(iT_0, (i+1)T_0)$ as follows:

$$x_{n,i}(t) = \sqrt{\frac{2}{T_0}}\cos\left[\pi n f_0(t - iT_0) + \theta_{n,i}\right] \tag{2.46}$$

$$x_{n+1,i}(t) = \sqrt{\frac{2}{T_0}}\cos[\,(\pi(n+1)f_0(t - iT_0) + \theta_{n+1,i}] \tag{2.47}$$

where $n = 2, 3, ..., T_0 = 1/f_0$, and $\theta_{n,i}$ and $\theta_{n+1,i}$ are the initial phases of $x_{n,i}(t)$ and $x_{n+1,i}(t)$ at time $t = iT_0$, respectively. Note that the minimum frequency spacing between these two signals is $f_0/2$. Applying these two signals to (2.36) over the interval $(iT_0, (i+1)T_0)$ we get

$$\begin{aligned}
&\int_{iT_0}^{(i+1)T_0} x_{n,i}(t)x_{n+1,i}(t)\,\mathrm{d}t \\
&\quad= \frac{1}{T_0}\int_{iT_0}^{(i+1)T_0} \{\cos(\pi f_0 t + \pi i + \theta_{n+1,i} - \theta_{n,i}) \\
&\qquad\qquad + \cos[\pi(2n+1)\,f_0(t - iT_0) + \theta_{n,i} + \theta_{n+1,i}]\}\mathrm{d}t \\
&\quad= \frac{1}{T_0}\left[\frac{\sin(\pi f_0 t + \pi i + \theta_{n+1,i} - \theta_{n,i})}{\pi f_0}\right. \\
&\qquad\left. + \frac{\sin[\pi(2n+1)\,f_0(t - iT_0) + \theta_{n,i} + \theta_{n+1,i}]}{\pi(2n+1)f_0}\right]_{iT_0}^{(i+1)T_0} \\
&\quad= \frac{1}{T_0}\left(\frac{\sin(2\pi\, i + \pi + \theta_{n+1,i} - \theta_{n,i}) - \sin(2\pi\, i + \theta_{n+1,i} - \theta_{n,i})}{\pi f_0}\right. \\
&\qquad\left. + \frac{\sin((2n+1)\pi + \theta_{n,i} + \theta_{n+1,i}) - \sin(\theta_{n,i} + \theta_{n+1,i})}{\pi(2n+1)f_0}\right)
\end{aligned} \tag{2.48}$$

The result in (2.48) shows that the two signals are not orthogonal unless the following conditions are satisfied:

$$\theta_{n+1,i} - \theta_{n.i} = k\pi \tag{2.49a}$$

$$\theta_{n+1,i} + \theta_{n.i} = m\pi \tag{2.49b}$$

where k and m are integers. This implies that $\theta_{n,i}$ and $\theta_{n+1,i}$ must be an integer multiple of π radians. In practice, it is difficult to force the phases of two sinusoidal signals at different frequencies to satisfy (2.49). It can be seen that the second term of the last equation in (2.48) is much smaller than the first term. Thus, when only (2.49a) is required to be satisfied, then the first term reduces zero. Furthermore, for a large n, the second term is much smaller than unity. Condition (2.49a) can be implemented in practice since it requires only the phase difference to be an integer multiple of π radians. It is easy to verify that the energy of the signals is unity via (2.37). In this case, the signals $x_{n,i}(t)$ and $x_{n+1,i}(t)$ are said to be *quasi-orthonormal* over the interval $(iT_0, (i+1)T_0)$.

Now consider two signals $x_{n,i-1}(t)$ and $x_{n+1,i}(t)$ in two consecutive intervals $((i-1)T_0, iT_0)$ and $(iT_0, (i+1)T_0)$. At time $t = iT_0$ the phase of $x_{n,i-1}(t)$ is $\pi n + \theta_{n,i-1}$, and the phase of $x_{n+1,i}(t)$ is $\theta_{n+1,i}$. It is seen that if the phases of the two signals are forced to be continuous at the transition time $t = iT_0$, that is, $\pi n + \theta_{n,i-1} = \theta_{n+1,i}$, then the phase difference $\theta_{n+1,i} - \theta_{n,i-1}$ must be an integer multiple of π radians. This is the same condition as (2.49a). The same result holds if the roles of the signals are reversed.

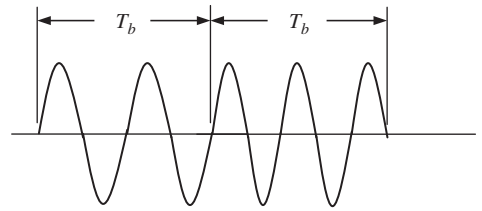

Figure 2.10 MSK representation of two consecutive and different bits.

Equations (2.46) and (2.47) can be used to represent binary data by selecting T_0 to be the bit interval T_b and $\theta_{n,i} = \theta_{n+1,i}$. This signaling or modulation technique is called *minimum shift keying* or simply MSK. It has the *minimum frequency spacing* of $f_0/2 = 1/2T_b$, which is half the bit rate. Furthermore, the phase at the bit transition time is continuous and the signals are orthonormal. Figure 2.10 shows the MSK representation of two consecutive bits 0 and 1.

■

In the three examples above, orthogonal sinusoids were investigated. In the following discussion other orthogonals signals called *Walsh functions* will be studied. The Walsh functions can be obtained from the *Hadamard matrix*, which can be generated by means of the following recursive procedure:

$$\mathbf{H}_1 = 1 \quad \mathbf{H}_2 = \begin{bmatrix} 1 & 1 \\ 1 & -1 \end{bmatrix} \quad \mathbf{H}_M = \begin{bmatrix} \mathrm{H}_{M/2} & \mathrm{H}_{M/2} \\ \mathrm{H}_{M/2} & -\mathrm{H}_{M/2} \end{bmatrix} \tag{2.50}$$

where M is a power of two. For example, the Hadamard matrix of order 4 is

$$\mathbf{H}_4 = \begin{bmatrix} 1 & 1 & 1 & 1 \\ 1 & -1 & 1 & -1 \\ 1 & 1 & -1 & -1 \\ 1 & -1 & -1 & 1 \end{bmatrix} \tag{2.51}$$

Note that the row vectors of the Hadamard matrix are mutually orthogonal, that is, $\mathbf{h}_i \mathbf{h}_j^t = 0$ where $\mathbf{h}_i$ is the ith row vector and $\mathbf{h}_j^t$ is the jth column vector of $\mathbf{H}_M$.

The Walsh functions of M chips are given as follows:

$$w_n(t) = \sum_{i=1}^{M} h_{ni}\, p(t - (i-1)T_c), \quad n = 1, 2, ..., M \tag{2.52}$$

where T_c is the *chip time*, $p(t - (i-1)T_c)$ is a pulse of unit amplitude and duration T_c, $(i-1)T_c \leq t < iT_c$, and h_{ni} is the element (n, i) of $\mathbf{H}_M$. Since Walsh functions are formed from the orthogonal row vectors of the Hadamard matrix, they are also mutually orthogonal. A normalization constant $1/\sqrt{MT_c}$ can be used in the Walsh functions to form an orthonormal set. The orthonormality of Walsh functions can be verified by using (2.36) and (2.37).

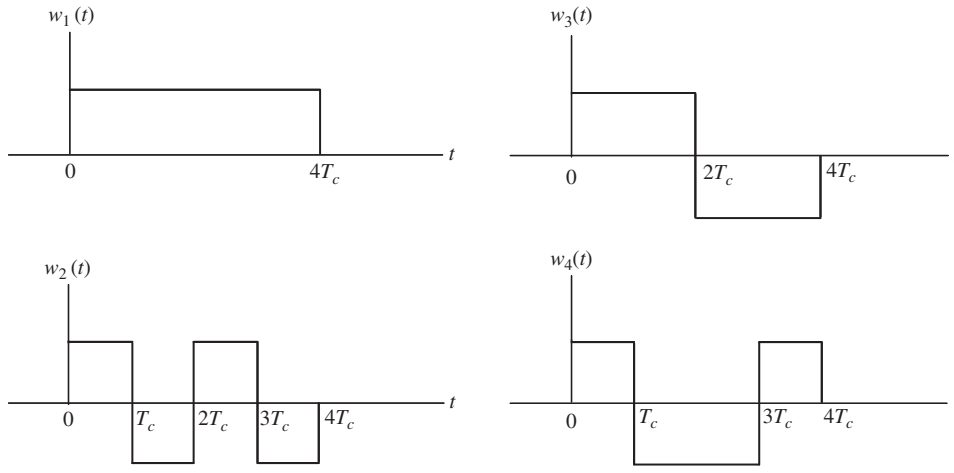

Figure 2.11 4-ary Walsh functions of four chips.

Example 2.16 4-ary Walsh functions

If we let $M = 4$ in (2.52), we obtain the set of four Walsh functions, each function having four chips, as follows:

$$w_n(t) = \sum_{i=1}^{4} h_{ni} p(t - (i-1)T_c), \quad n = 1, 2, 3, 4 \tag{2.53}$$

Figure 2.11 shows these four Walsh functions.

■

Another extension of the Walsh functions referred to as the *sinusoidal Walsh functions* is defined as follows:

$$w_n(t) = \sum_{i=1}^{M} h_{ni} p(t - (i-1)T_c) \cos 2\pi f_c t, \quad n = 1, 2, ..., 2n \tag{2.54}$$

where $f_c = m/T_c$ and m is a positive integer. It can be verified that the sinusoidal Walsh functions form an orthogonal set by using (2.36). A normalization constant $1/\sqrt{MT_c/2}$ can be used in the sinusoidal Walsh functions to form an orthonormal set.

The Walsh functions and the sinusoidal Walsh functions can be used to represent $M = 2^k$ k-bit symbols. The cellular standard IS-95 employs 64-chip Walsh functions in both forward (base station-to-mobile) and reverse (mobile-to-base station) channels.

Example 2.17 4-ary sinusoidal Walsh functions

If we let $M = 4$ in (2.54), we obtain four sinusoidal Walsh functions, each with four chips. Figure 2.12 shows these functions with $f_c = 2/T_c$. Note the phase change of π radians at the chip transition time.

■

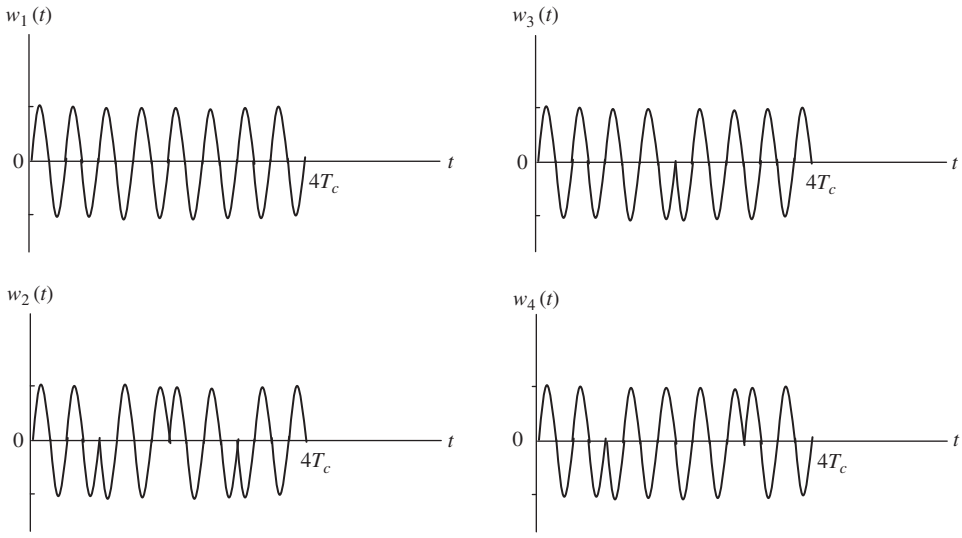

Figure 2.12 4-ary sinusoidal Walsh functions with four-chip duration.

2.4 Signal space

In the analysis of digital communication systems it is often convenient to represent a set of *finite-energy* digital signals by a corresponding set of *vectors*. Each vector represents a digital signal; thus the time dependency can be removed. These vectors define a *signal space*. To obtain the signal vectors, each digital signal must be represented by an orthogonal series in terms of the *basis functions*. This *orthogonalization* process can be achieved by means of the *Gram–Schmidt* procedure.

Gram–Schmidt procedure

Let $s_i(t)$, $i = 1, 2, \ldots, M$ be a set of real-valued signals with corresponding finite energies E_i. In terms of representation, each signal in the set can be expressed as a linear combination of L *orthonormal basis functions* $x_k(t)$, $k = 1, 2, \ldots, L$, where $L \leq M$. When the signals $s_i(t)$, $i = 1, 2, \ldots, M$ form a linearly independent set, then $L = M$. We have

$$s_i(t) = \sum_{k=1}^{L} s_{ik} x_k(t) \tag{2.55}$$

where the coefficients of the series expansion are defined by

$$s_{ik} = \int_{-\infty}^{\infty} s_i(t) x_k(t)\, \mathrm{d}t \tag{2.56}$$

The orthonormal basis functions can be obtained by means of the following recursive procedure:

$$x_1(t) = \frac{s_1(t)}{\sqrt{\int_{-\infty}^{\infty} s_1^2(t)\,\mathrm{d}t}} = \frac{s_1(t)}{\sqrt{E_1}} \tag{2.57}$$

$$x_2(t) = \frac{f_2(t)}{\sqrt{\int_{-\infty}^{\infty} f_2^2(t)\mathrm{d}t}}, \qquad f_2(t) = s_2(t) - s_{21}x_1(t) \tag{2.58}$$

$$x_k(t) = \frac{f_k(t)}{\sqrt{\int_{-\infty}^{\infty} f_k^2(t)\mathrm{d}t}}, \qquad f_k(t) = s_k(t) - \sum_{m=1}^{k-1} s_{km}x_m(t), \qquad k \leq L \tag{2.59}$$

Signal vectors

From the Gram–Schmidt procedure we observe that for each orthonormal basis function $x_k(t)$ there is a corresponding *orthonormal basis vector* $\mathbf{x}_k$:

$$\mathbf{x}_1 = \begin{bmatrix} 1 \\ 0 \\ . \\ . \\ . \\ 0 \end{bmatrix}, \quad \mathbf{x}_2 = \begin{bmatrix} 0 \\ 1 \\ 0 \\ . \\ . \\ 0 \end{bmatrix}, \quad \ldots, \quad \mathbf{x}_L = \begin{bmatrix} 0 \\ 0 \\ . \\ . \\ . \\ 1 \end{bmatrix} \tag{2.60}$$

The set of orthonormal basis vectors $\mathbf{x}_k$ spans an L-dimentional Euclidean signal space. In this signal space we observe that each signal $s_i(t)$ is completely determined by the signal vector $\mathbf{s}_i$:

$$\boldsymbol{s}_i = \begin{bmatrix} s_{i1} \\ s_{i2} \\ . \\ . \\ . \\ s_{iL} \end{bmatrix} = \sum_{k=1}^{L} s_{ik}\mathbf{x}_k, \qquad i = 1, 2, \ldots, M \tag{2.61}$$

We may visualize the set of M signal vectors as defining a set of M points in the signal space with L mutually perpendicular axes labeled $\mathbf{x}_1, \mathbf{x}_2, \ldots, \mathbf{x}_L$. The signal vector contains all the information such as *energy* and relative *phase shift* or *orthogonality* needed to analyze the performance of the signal.

The energy of a signal turns out to be the *squared length* or *squared norm* of its signal vector as shown below. First consider the *length* or *norm* of a signal vector $\boldsymbol{s}_i$ of the signal $s_i(t)$, defined as

$$\|\boldsymbol{s}_i\| = \sqrt{\sum_{k=1}^{L} s_{ik}^2} \tag{2.62}$$

Now consider the signal energy E_i, evaluated with the help of (2.55):

$$\begin{aligned} E_i &= \int_{-\infty}^{\infty} s_i^2(t)\,\mathrm{d}t = \int_{-\infty}^{\infty} \sum_{k=1}^{L}\sum_{m=1}^{L} s_{ik}s_{im}x_k(t)x_m(t)\,\mathrm{d}t \\ &= \sum_{k=1}^{L}\sum_{m=1}^{L} s_{ik}s_{im}\int_{-\infty}^{\infty} x_k(t)x_m(t)\mathrm{d}t = \sum_{k=1}^{L} s_{ik}^2 \end{aligned} \tag{2.63}$$

The last expression on the right-hand side of (2.63) results from the fact that $x_k(t)$ and $x_m(t)$ form a pair of orthonormal functions, and therefore

$$\int_{-\infty}^{\infty} x_k(t)x_m(t)\mathrm{d}t = \begin{cases} 1, & k = m \\ 0, & k \neq m \end{cases} \tag{2.64}$$

Comparing (2.63) and (2.62) we obtain

$$E_i = \|\boldsymbol{s}_i\|^2 \tag{2.65}$$

Another useful quantity for signal analysis is the *Euclidean distance* between the two signal vectors:

$$\|\boldsymbol{s}_i - \boldsymbol{s}_j\| = \sqrt{\sum_{k=1}^{L}(s_{ik} - s_{jk})^2} \tag{2.66}$$

The Euclidean distance indicates the *degree of separation* between two signals in the signal space.

Example 2.18 Signal space of antipodal signals

Consider the set of two antipodal signals $s_1(t) = Ap(t - iT_b)$ and $s_2(t) = -Ap(t - iT_b)$, where $p(t - iT_b)$ is defined in (2.26). The signal energy is $E_1 = E_2 = E_b = A^2T_b$. From the Gram–Schmidt procedure we obtain

$$x_1(t) = \frac{A}{\sqrt{E_1}}p(t - iT_b) = \frac{A}{\sqrt{A^2T_b}}p(t - iT_b) = \frac{1}{\sqrt{T_b}}p(t - iT_b) \tag{2.67}$$

Furthermore,

$$\begin{aligned} s_{11} &= \int_{-\infty}^{\infty} s_1(t)x_1(t)\mathrm{d}t = \int_{-\infty}^{\infty} [Ap(t - iT_b)]\left[\frac{1}{\sqrt{T_b}}p(t - iT_b)\right]\mathrm{d}t \\ &= A\sqrt{T_b} \end{aligned} \tag{2.68}$$

$$\begin{aligned} s_{21} &= \int_{-\infty}^{\infty} s_2(t)x_1(t)\mathrm{d}t = \int_{-\infty}^{\infty} [-Ap(t - iT_b)]\left[\frac{1}{\sqrt{T_b}}p(t - iT_b)\right]\mathrm{d}t \\ &= -A\sqrt{T_b} \end{aligned} \tag{2.69}$$

Substituting (2.67) and (2.69) into (2.58) we have

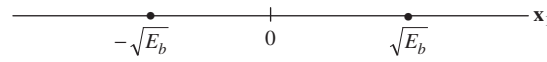

Figure 2.13 Signal space of antipodal signals.

$$x_2(t) = -Ap(t - iT_b) - \frac{-A\sqrt{T_b}}{\sqrt{T_b}}p(t - iT_b) = 0 \tag{2.70}$$

In addition, we also get $s_{12} = s_{22} = 0$. Thus, the signal space is a *one-dimensional* space. The signal vectors are given by

$$\boldsymbol{s}_1 = [A\sqrt{T_b}] = [\sqrt{E_b}] = \sqrt{E_b}\,\mathbf{x}_1 \tag{2.71}$$

$$\boldsymbol{s}_2 = [-A\sqrt{T_b}] = [-\sqrt{E_b}] = -\sqrt{E_b}\,\mathbf{x}_1 \tag{2.72}$$

It is seen that the signal energy is equal to the squared length of the signal vector. The Euclidean distance between the two signal vectors is given by

$$\|\boldsymbol{s}_1 - \boldsymbol{s}_2\| = 2\sqrt{E_b} \tag{2.73}$$

The signal space for the set of antipodal signals is given in Figure 2.13.

■

Example 2.19 Signal space of PSK signals

Consider the set of PSK signals $s_1(t) = A\cos 2\pi f_c t$ and $s_2(t) = -A\cos 2\pi f_c t$ defined over the bit time $(iT_b, (i+1)T_b)$, where i is an arbitrary integer and the frequency f_c is an integer multiple of the bit rate $1/T_b$. The signal energy is $E_1 = E_2 = E_b = A^2T_b/2$. From (2.57) and (2.58) we obtain

$$x_1(t) = \sqrt{\frac{2}{T_b}}\cos 2\pi f_c t \tag{2.74}$$

$$x_2(t) = 0 \tag{2.75}$$

By using (2.56) the coefficients of the signal vector can be calculated as follows:

$$s_{11} = A\sqrt{\frac{T_b}{2}}\ , \quad s_{12} = 0\ , \quad s_{21} = -A\sqrt{\frac{T_b}{2}}\ , \quad s_{22} = 0 \tag{2.76}$$

Thus the signal space is a *one-dimensional* space. The signal vectors are given by

$$\boldsymbol{s}_1 = [A\sqrt{T_b/2}] = [\sqrt{E_b}] = \sqrt{E_b}\,\mathbf{x}_1 \tag{2.77}$$

$$\boldsymbol{s}_2 = [-A\sqrt{T_b/2}] = [-\sqrt{E_b}] = -\sqrt{E_b}\,\mathbf{x}_1 \tag{2.78}$$

It is seen that the signal energy is equal to the squared length of the signal vector. The Euclidean distance between the two signal vectors is given by

$$\|\boldsymbol{s}_1 - \boldsymbol{s}_2\| = 2\sqrt{E_b} \tag{2.79}$$

The signal space of PSK signals is therefore identical with that of the antipodal signals given in Figure 2.13, although their waveforms differ.

■

For many digital signal sets, the orthonormal basis functions and the signal vectors can be found by inspection without going through the Gram–Schmidt procedure. The following example illustrates this.

Example 2.20 Signal space of FSK signals

Consider the set of two FSK signals $s_1(t) = A\cos 2\pi f_1 t$ and $s_2(t) = A\cos 2\pi f_2 t$ defined over the bit time $(iT_b, (i+1)T_b)$, where i is an arbitrary integer and the frequencies f_1 and f_2 are integer multiples of the bit rate $1/T_b$. The minimum frequency spacing is equal to the bit rate $|f_1 - f_2| = 1/T_b$. Thus, from the result in Example 2.14, the signals $s_1(t)$ and $s_2(t)$ are orthogonal. We can write them as follows:

$$s_1(t) = A\sqrt{\frac{T_b}{2}}\left[\sqrt{\frac{2}{T_b}}\cos 2\pi f_1 t\right] = A\sqrt{\frac{T_b}{2}}x_1(t) = \sqrt{E_b}\,x_1(t) \tag{2.80}$$

$$s_2(t) = A\sqrt{\frac{T_b}{2}}\left[\sqrt{\frac{2}{T_b}}\cos 2\pi f_2 t\right] = A\sqrt{\frac{T_b}{2}}x_2(t) = \sqrt{E_b}\,x_2(t) \tag{2.81}$$

where $E_b = A^2 T_b/2$ is the signal energy, and the two functions $x_1(t) = \sqrt{2/T_b}\cos 2\pi f_1 t$ and $x_2(t) = \sqrt{2/T_b}\cos 2\pi f_2 t$ form a set of orthonormal functions over the interval $(iT_b, (i+1)T_b)$. The signal vectors are displayed in Figure 2.14 and given as follows:

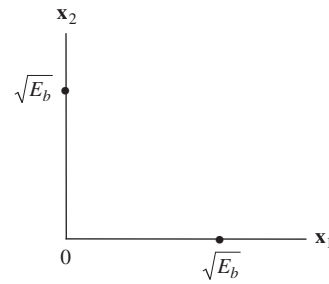

Figure 2.14 FSK signal space.

$$\boldsymbol{s}_1 = \begin{bmatrix} \sqrt{E_b} \\ 0 \end{bmatrix} = \sqrt{E_b}\,\mathbf{x}_1 \tag{2.82}$$

$$\boldsymbol{s}_2 = \begin{bmatrix} 0 \\ \sqrt{E_b} \end{bmatrix} = \sqrt{E_b}\,\mathbf{x}_2 \tag{2.83}$$

The Euclidean distance between the two signal vectors is given by

$$\|\mathbf{s}_1 - \mathbf{s}_2\| = \sqrt{2E_b} \tag{2.84}$$

■

Example 2.21 Signal space of MPSK signals

Consider the set of MPSK signals given in (2.9) for $M > 2$. The signals are defined over the symbol time $(iT_s, (i+1)T_s)$:

$$s_n(t) = A\,\cos\Big(2\pi f_c t + (2n-1)\frac{\pi}{M}\Big), \quad n = 1, 2, ..., M \tag{2.85}$$

The frequency f_c is assumed to be an integer multiple of the symbol rate $1/T_s$. Expanding (2.85) we obtain

$$s_n(t) = A\cos\Big[(2n-1)\frac{\pi}{M}\Big]\ \cos\ 2\pi f_c t\ -\ A\sin\Big[(2n-1)\frac{\pi}{M}\Big]\ \sin\ 2\pi f_c t \tag{2.86}$$

$$\begin{aligned} s_n(t) &= A\sqrt{\frac{T_s}{2}}\cos\Big[(2n-1)\frac{\pi}{M}\Big]\ \Big[\sqrt{\frac{2}{T_s}}\cos\ 2\pi f_c t\Big] \\ &\quad -\ A\sqrt{\frac{T_s}{2}}\sin\Big[(2n-1)\frac{\pi}{M}\Big]\ \Big[\sqrt{\frac{2}{T_s}}\sin\ 2\pi f_c t\Big] \\ &= \sqrt{E_s}\cos\Big[(2n-1)\frac{\pi}{M}\Big]\,x_1(t) + \sqrt{E_s}\sin\Big[(2n-1)\frac{\pi}{M}\Big]\,x_2(t) \end{aligned} \tag{2.87}$$

where $E_s = A^2 T_s/2$ is the signal energy, and the two functions $x_1(t) = \sqrt{2/T_s}\,\cos\,2\pi f_c t$ and $x_2(t) = -\sqrt{2/T_s}\,\sin\,2\pi f_c t$ form a set of orthonormal functions over the symbol time $(iT_s, (i+1)T_s)$. The signal vectors are given as follows:

$$\begin{aligned} \boldsymbol{s}_n &= \begin{bmatrix} \sqrt{E_s}\,\cos\Big[(2n-1)\frac{\pi}{M}\Big] \\ \sqrt{E_s}\,\sin\Big[(2n-1)\frac{\pi}{M}\Big] \end{bmatrix} \\ &= \sqrt{E_s}\,\cos\Big[(2n-1)\frac{\pi}{M}\Big]\,\mathbf{x}_1 + \sqrt{E_s}\,\sin\Big[(2n-1)\frac{\pi}{M}\Big]\,\mathbf{x}_2 \end{aligned} \tag{2.88}$$

Thus the MPSK signal space is a *two-dimensional* space. The Euclidean distance between the two adjacent MPSK signals is given by

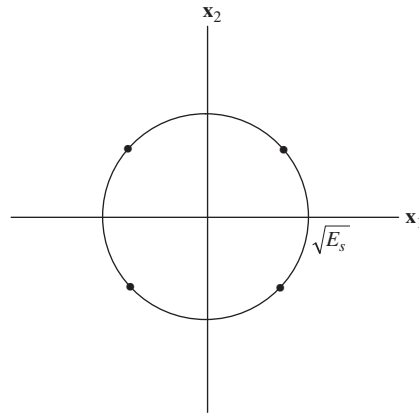

Figure 2.15 QPSK signal space.

$$\begin{aligned}\|\boldsymbol{s}_k - \boldsymbol{s}_m\| &= \left(\left[\sqrt{E_s}\cos\left[(2k-1)\frac{\pi}{M}\right] - \sqrt{E_s}\cos\left[(2m-1)\frac{\pi}{M}\right]\right]^2\right. \\ &\quad \left.+\left[\sqrt{E_s}\sin\left[(2k-1)\frac{\pi}{M}\right] - \sqrt{E_s}\sin\left[(2m-1)\frac{\pi}{M}\right]\right]^2\right)^{1/2} \\ &= \left(2E_s - 2E_s\left[\cos\left[(2k-1)\frac{\pi}{M}\right]\cos\left[(2m-1)\frac{\pi}{M}\right]\right.\right. \\ &\quad \left.\left.+\sin\left[(2k-1)\frac{\pi}{M}\right]\sin\left[(2m-1)\frac{\pi}{M}\right]\right]\right)^{1/2}\end{aligned} \tag{2.89}$$

Consequently,

$$\|\boldsymbol{s}_k - \boldsymbol{s}_m\| = \sqrt{2E_s\left[1-\cos(k-m)\frac{2\pi}{M}\right]} \tag{2.90}$$

The Euclidean distance between two adjacent MPSK signal vectors corresponds to the case of $|k-m|=1$, that is,

$$\|\boldsymbol{s}_k - \boldsymbol{s}_{k-1}\| = \|\boldsymbol{s}_k - \boldsymbol{s}_{k+1}\| = \sqrt{2E_s\left(1-\cos\frac{2\pi}{M}\right)} = 2\sqrt{E_s}\sin\frac{\pi}{M} \tag{2.91}$$

Figures 2.15 and 2.16 show the signal spaces of QPSK and 8PSK, respectively.

■

From Examples 2.18 and 2.19 we observe that antipodal signals and PSK signals have the identical signal space. Therefore, these two sets of signals must have the same noise performance. From Examples 2.19 and 2.20 it is seen that PSK has a larger Euclidean distance than FSK. It turns out that a larger Euclidean distance corresponds to a better noise performance. A PSK signal is less likely to be mistaken by the other PSK signal in noise than its FSK counterpart.

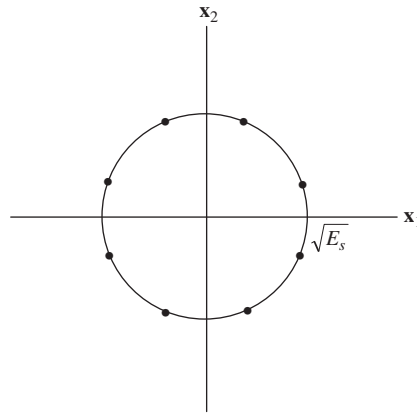

Figure 2.16 8PSK signal space.

2.5 Linear time-invariant systems

Many physical communication systems are *linear time-invariant* (LTI) and can be easily analyzed in detail. A system is time-invariant if a time shift in the input signal causes the same time shift in the output signal. Specifically, if $y(t)$ is the output of a continuous-time LTI system when $x(t)$ is the input, then $y(t - t_0)$ is the output when $x(t - t_0)$ is the input. In a discrete-time LTI system with $y(n)$ the output when $x(n)$ is the input, then $y(n - n_0)$ is the output when $x(n - n_0)$ is the input.

Example 2.22 Time-invariant system
Consider the output voltage $v(t)$ at time t across a resistor with resistance R and input current $i(t)$. The output voltage $v(t)$ is given by

$$v(t) = Ri(t) \tag{2.92}$$

Now consider a second input obtained by shifting $i(t)$ by t_0, that is, $i(t - t_0)$. The corresponding output $v_1(t)$ is

$$v_1(t) = Ri(t - t_0) = v(t - t_0) \tag{2.93}$$

Hence the system is time-invariant.
■

Example 2.23 Time-varying system
(a) Consider the discrete-time system

$$y(n) = x(n) - x(n - 1) \tag{2.94}$$

It is seen that by applying the shifted input $x(n-n_0)-x((n-n_0)-1)$ we get the output $\hat{y}(n)$ as

$$\begin{aligned}\hat{y}(n) &= x(n-n_0)-x((n-n_0)-1)\\ &= y(n-n_0)\end{aligned} \tag{2.95}$$

Thus this is a linear time-invariant system.
(b) Now consider the discrete-time system

$$y(n) = n\,x(n) \tag{2.96}$$

By applying the shifted input $x(n-n_0)$ we get

$$\hat{y}(n) = nx(n-n_0) \tag{2.97}$$

On the other hand,

$$y(n-n_0) = (n-n_0)\,x(n-n_0) \tag{2.98}$$

Thus

$$\hat{y}(n) \neq y(n-n_0) \tag{2.99}$$

Hence this system is *time-varying.*

■

A system is *linear* if the response to the input

$$x = \sum_k a_k x_k = a_1 x_1 + a_2 x_2 + \cdots \tag{2.100}$$

is

$$y = \sum_k a_k y_k = a_1 y_1 + a_2 y_2 + \cdots \tag{2.101}$$

where $y_k, k=1,2,\ldots$, is the response to $x_k, k=1,2,\ldots$. Equations (2.100) and (2.101) hold for both continuous-time and discrete-time systems.

2.6 Convolution

The output of a continuous-time LTI system can be expressed in terms of the input $x(t)$ and the impulse response $h(t)$ as a *convolution* integral:

$$\begin{aligned}y(t) = x(t) * h(t) &= \int_{-\infty}^{\infty} x(\tau)\,h(t-\tau)\,\mathrm{d}\tau\\ &= \int_{-\infty}^{\infty} h(\tau)\,x(t-\tau)\mathrm{d}\tau = h(t) * x(t)\end{aligned} \tag{2.102}$$

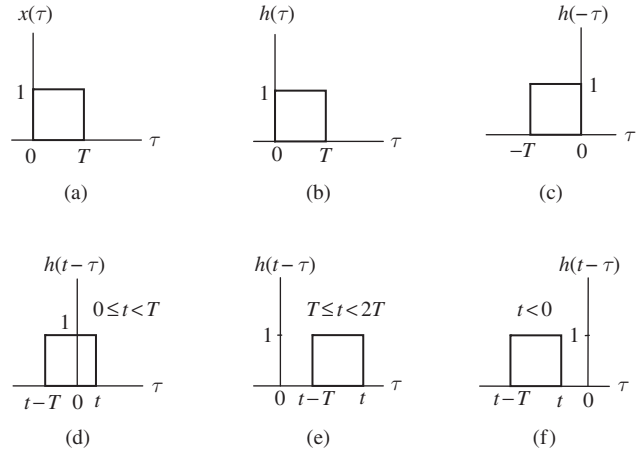

Figure 2.17 $x(\tau)$ and $h(t-\tau)$ for different values of t.

For a discrete-time system, the convolution integral in (2.102) becomes the convolution sum

$$y(n) = x(n) * h(n) = \sum_{k=-\infty}^{\infty} x(k)h(n-k) = \sum_{k=-\infty}^{\infty} h(k)x(n-k) \tag{2.103}$$

Example 2.24 Convolution

Let us verify (2.102) by means of a substitution of variables. If we let $\lambda = t - \tau$ or, equivalently, $\tau = t - \lambda$, (2.102) becomes

$$y(t) = \int_{-\infty}^{\infty} x(t-\lambda)\, h(\lambda)\, \mathrm{d}\lambda \;\; = h(t) * x(t) \tag{2.104}$$

■

Example 2.25 Convolution of two squared pulses

Let $x(t)$ be the input to an LTI system with impulse response $h(t)$, where $x(t)$ and $h(t)$ are both unit amplitude squared pulses of duration T defined in (2.26):

$$x(t) = h(t) = \begin{cases} 1, & 0 \le t < T \\ 0, & \text{otherwise} \end{cases} \tag{2.105}$$

Figure 2.17 depicts the evaluation of the output $y(t)$ as a convolution of $x(t)$ and $h(t)$. It is seen that the product of $x(\tau)$ and $h(t-\tau)$ is zero for $t < 0$, and for $t > 2T$. For $0 \le t < T$ the value of the product is 1 in $0 \le \tau \le t$:

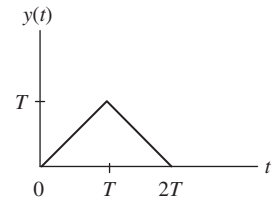

Figure 2.18 Response $y(t)$.

$$y(t) = \int_0^t x(\tau)\, h(t-\tau)\, \mathrm{d}\tau = \int_0^t \mathrm{d}\tau = t, \qquad 0 \le t < T \tag{2.106}$$

For $T \le t < 2T$ the value of the product is 1 in $t - T \le \tau \le T$:

$$y(t) = \int_{t-T}^{T} \mathrm{d}\tau = 2T - t, \qquad T \le t < 2T \tag{2.107}$$

The function $y(t)$ is shown in Figure 2.18.

■

2.7 Fourier series of continuous-time periodic signals

In the analysis of signals and LTI systems, it is often useful to represent an input signal as a linear combination of *basis functions*, as in (2.100). One famous representation is the *Fourier series*, which employs periodic *complex exponentials* as basis functions to represent *periodic* signals. The periodic fundamental complex exponential is

$$x_1(t) = \mathrm{e}^{\mathrm{j}2\pi f_0 t} \tag{2.108}$$

It is easy to see that $x_1(t + T_0) = x_1(t)$, where $T_0 = 1/f_0$, as shown below:

$$\begin{aligned} x_1(t+T_0) &= \mathrm{e}^{\mathrm{j}2\pi f_0 (t+T_0)} = \mathrm{e}^{\mathrm{j}2\pi f_0 t + j2\pi} \\ &= \mathrm{e}^{\mathrm{j}2\pi f_0 t} = x_1(t) \end{aligned} \tag{2.109}$$

The period of $x_1(t)$ is T_0. Associated with $x_1(t)$ is an infinite set of periodic harmonic components:

$$x_k(t) = \mathrm{e}^{\mathrm{j}2\pi k f_0 t}, \qquad k = 0, \pm 1, \pm 2, \ldots \tag{2.110}$$

The period of the kth harmonic $x_k(t)$ is T_0/k and its frequency is kf_0. It is obvious that $x_k(t)$ is also periodic with period T_0, as seen below:

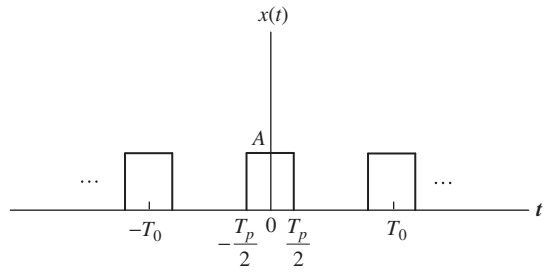

Figure 2.19 Periodic pulse signal.

$$\begin{aligned} x_k(t+T_0) &= \mathrm{e}^{\mathrm{j}2\pi k f_0(t+T_0)} = \mathrm{e}^{\mathrm{j}2\pi k f_0 t + j2\pi k} \\ &= \mathrm{e}^{\mathrm{j}2\pi k f_0 t} = x_k(t) \end{aligned} \tag{2.111}$$

Furthermore, a linear combination $x(t)$ of the harmonics $x_k(t)$ is also periodic with period T_0:

$$x(t) = \sum_{k=-\infty}^{\infty} a_k \mathrm{e}^{\mathrm{j}2\pi k f_0 t} \tag{2.112}$$

$$a_k = \frac{1}{T_0}\int_0^{T_0} x(t)\mathrm{e}^{-\mathrm{j}2\pi k f_0 t}\mathrm{d}t \tag{2.113}$$

The representation of a periodic signal $x(t)$ in the form of (2.112) is termed the *Fourier series* representation. By multiplying both sides of (2.112) by $\mathrm{e}^{-\mathrm{j}2\pi k f_0 t}$ and integrating from 0 to T_0 we obtain the *complex Fourier series coefficient* a_k in (2.113).

We note that the coefficient a_0 is given by

$$a_0 = \frac{1}{T_0}\int_0^{T_0} x(t)\mathrm{d}t \tag{2.114}$$

Thus, a_0 represents the *average value* (dc value) of $x(t)$ averaged over one period T_0. The other a_k coefficients represent the portion of $x(t)$ in each harmonic component. Specifically, the magnitude $|a_k|$ of the complex Fourier series coefficient a_k is the *amplitude* of the kth harmonic component of $x(t)$.

Example 2.26 Periodic pulse signal

Consider the periodic pulse signal $x(t)$ with period $T_0 = 1/f_0$ and pulse width $T_p < T_0$, as shown in Figure 2.19.

Using (2.13) we can evaluate the complex Fourier series coefficient a_k as follows:

$$a_0 = \frac{1}{T_0}\int_0^{T_0} A\,\mathrm{d}t = \frac{1}{T_0}\int_{-T_0/2}^{T_0/2} A\,\mathrm{d}t = \frac{1}{T_0}\int_{-T_p/2}^{T_p/2} A\,\mathrm{d}t = \frac{AT_p}{T_0} \tag{2.115}$$

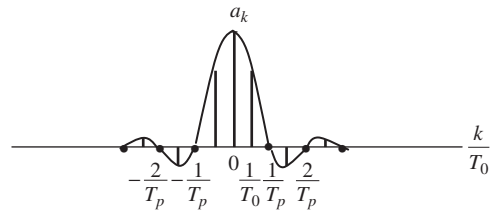

Figure 2.20 Fourier series coefficients and their envelope, for $T_0 = 2T_P$.

$$a_k = \frac{1}{T_0}\int_{-T_0/2}^{T_0/2} A\,\mathrm{e}^{-\mathrm{j}2\pi kt/T_0}\,\mathrm{d}t = \frac{1}{T_0}\int_{-T_p/2}^{T_p/2} A\,\mathrm{e}^{-\mathrm{j}2\pi kt/T_0}\,\mathrm{d}t = \frac{-A}{j2\pi k}\left[\mathrm{e}^{-\mathrm{j}\pi kT_p/T_0} - \mathrm{e}^{\mathrm{j}\pi kT_p/T_0}\right]$$

$$= A\frac{\sin(\pi kT_p/T_0)}{\pi k} = \frac{AT_p}{T_0}\left(\frac{\sin(\pi kT_p/T_0)}{\pi kT_p/T_0}\right), \qquad k \neq 0 \tag{2.116}$$

The Fourier series coefficients in this case are real and assume the form of the well-known function $(\sin u)/u$. Figure 2.20 shows a plot of a_k as a function of the *discrete-frequency* $kf_0 = k/T_0$, together with their envelope, for $T_0 = 2T_p$.

■

Parseval relation for periodic signals

The *Parsevals relation* states that the average power in a periodic signal equals the sum of the average power in all of its harmonic components. The relation can be proved by using the definition of average power in (2.13) and letting the time interval T be an integer multiple of the period T_0, that is, $T = nT_0$:

$$P = \lim_{n\to\infty}\frac{1}{nT_0}\int_{-nT_0/2}^{nT_0/2}|x(t)|^2\,\mathrm{d}t = \lim_{n\to\infty}\frac{n}{nT_0}\int_{-T_0/2}^{T_0/2}|x(t)|^2\,\mathrm{d}t = \frac{1}{T_0}\int_{-T_0/2}^{T_0/2}|x(t)|^2\,\mathrm{d}t$$

$$= \frac{1}{T_0}\int_0^{T_0} x(t)x^*(t)\,\mathrm{d}t = \frac{1}{T_0}\int_0^{T_0} x(t)\sum_{k=-\infty}^{\infty} a_k^*\mathrm{e}^{-\mathrm{j}2\pi kf_0t}\,\mathrm{d}t = \sum_{k=-\infty}^{\infty} a_k^*\frac{1}{T_0}\int_0^{T_0} x(t)\mathrm{e}^{-\mathrm{j}2\pi kf_0t}\,\mathrm{d}t$$

$$= \sum_{k=-\infty}^{\infty} a_k^*a_k = \sum_{k=-\infty}^{\infty}|a_k|^2 \tag{2.117}$$

Note that $|a_k|^2$ is the average power in the kth harmonic component $a_k\mathrm{e}^{\mathrm{j}2\pi kf_0t}$ of $x(t)$.

Unit step and unit impulse functions

Two functions that play important roles in signal analysis are the *unit step* and the *unit impulse* functions. The unit step function is defined as

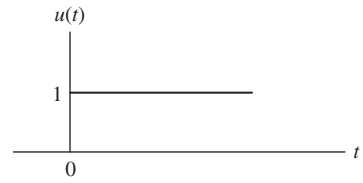

Figure 2.21 The unit step function.

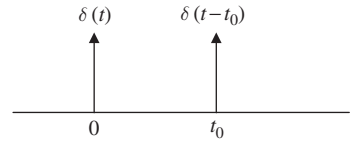

Figure 2.22 The unit impulse function.

$$u(t) = \begin{cases} 0, & t<0 \\ 1, & t>0 \end{cases} \tag{2.118}$$

and is shown in Figure 2.21.

The unit impulse function is defined as

$$\delta(z) = \begin{cases} \infty, & z = 0 \\ 0, & z \neq 0 \end{cases} \tag{2.119}$$

and

$$\int_{-\infty}^{\infty} \delta(z)\ \mathrm{d}z = 1 \tag{2.120}$$

The variable z can be time or frequency depending on the application. The unit impulse function has the following properties:

$$\int_{-\infty}^{\infty} x(z)\delta(z)\ \mathrm{d}z = x(0) \tag{2.121}$$

$$\int_{-\infty}^{\infty} x(z)\delta(z - z_0)\ \mathrm{d}z = x(z_0) \tag{2.122}$$

$$x(z)\delta(z - z_0) = x(z_0)\delta(z - z_0) \tag{2.123}$$

$$\delta(t) = \frac{\mathrm{d}\,u(t)}{\mathrm{d}t} \tag{2.124}$$

$$u(t) = \int_{-\infty}^{t} \delta(z)\,\mathrm{d}z \tag{2.125}$$

Figure 2.22 shows the unit impulse as a function of time at location $t = 0$ and $t = t_0$.

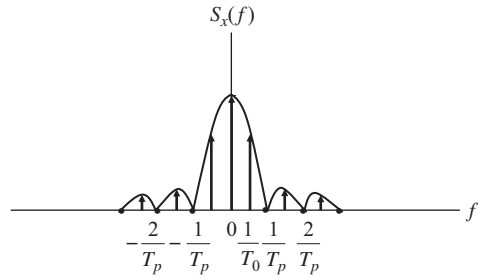

Figure 2.23 Power spectral density and corresponding envelope.

Power spectral density

From (2.117) we may define the *power spectral density* or *power spectrum* $S_x(f)$ of a periodic signal $x(t)$ as a function of the frequency f, the total area under the graph of which yields the average power of the signal, that is,

$$P = \int_{-\infty}^{\infty} S_x(f)\,\mathrm{d}f \tag{2.126}$$

Combining (2.117) and (2.126) we obtain the power spectral density as an infinite series of impulses occurring at the harmonically related frequencies, and for which the area of the impulse at the kth harmonic frequency kf_0 is $|a_k|^2$:

$$S_x(f) = \sum_{k=-\infty}^{\infty} |a_k|^2 \delta(f - kf_0) = \sum_{k=-\infty}^{\infty} |a_k|^2 \delta\left(f - \frac{k}{T_0}\right) \tag{2.127}$$

Figure 2.23 shows the power spectral density $S_x(f)$, and its envelope, of the periodic pulse signal in Example 2.26.

From (2.127) we observe that the power spectral density of a real-valued periodic signal is a nonnegative real-valued and even function of frequency, that is,

$$S_x(f) > 0, \qquad \text{for all } f \tag{2.128}$$

$$S_x(-f) = S_x(f) \tag{2.129}$$

A signal with a power spectral density concentrated around the zero frequency is referred to as a *baseband* or *lowpass* signal. This definition applies to power signals that include periodic signals. The periodic pulse signal in Example 2.26 is a baseband signal.

Bandwidth

The power spectral density allows us to determine the frequency range that contains most of the power of the signal. The *positive* part of this frequency range denoted as B is loosely defined as the *bandwidth* of the signal. For example, the frequency range $-B \leq f \leq B$ that

contains most of the power of the periodic pulse signal shown in Figure 2.23 is the main lobe. This is called the *first-null* bandwidth, and is equal to $B = 1/T_p$. It is seen that a narrower pulse width T_p results in a wider first-null bandwidth.

Frequency shifting property

This property plays an important role in the analysis of signals with dominant higher harmonic components. Let $x(t)$ be a periodic signal with period $T_0 = 1/f_0$, and $y(t)$ be defined as

$$y(t) = x(t)\,\mathrm{e}^{\mathrm{j}2\pi f_c t} = x(t)\,\mathrm{e}^{\mathrm{j}2\pi n f_0 t} \tag{2.130}$$

where the shifting frequency $f_c = nf_0$, and n is a positive integer. We observe that

$$\begin{aligned} y(t+T_0) &= x(t+T_0)\,\mathrm{e}^{\mathrm{j}2\pi n f_0 (t+T_0)} \\ &= x(t)\,\mathrm{e}^{\mathrm{j}2\pi n f_0 t} = y(t) \end{aligned} \tag{2.131}$$

Therefore, $y(t)$ is also periodic with period T_0. The Fourier series representation of $y(t)$ is given by

$$y(t) = \sum_{k=-\infty}^{\infty} b_k \mathrm{e}^{\mathrm{j}2\pi k f_0 t} \tag{2.132}$$

$$b_k = \frac{1}{T_0}\int_0^{T_0} y(t)\mathrm{e}^{-\mathrm{j}2\pi k f_0 t}\mathrm{d}t \tag{2.133}$$

Substituting (2.130) into (2.133) we have

$$b_k = \frac{1}{T_0}\int_0^{T_0} x(t)\,\mathrm{e}^{-\mathrm{j}2\pi(k-n)f_0 t}\,\mathrm{d}t \tag{2.134}$$

The right-hand side of (2.134) is just a_{k-n} as viewed from (2.113). Thus

$$b_k = a_{k-n} \tag{2.135}$$

In other words, $b_{n-1} = a_{-1}$, $b_{n+1} = a_1$, $b_n = a_0$, and so on. Hence, the harmonic components of $y(t)$ are simply the harmonic components of $x(t)$ shifted in frequency by $f_c = nf_0$.

Similarly, the Fourier series coefficients of the signal

$$y(t) = x(t)\,\mathrm{e}^{-\mathrm{j}2\pi f_c t} = x(t)\,\mathrm{e}^{-\mathrm{j}2\pi n f_0 t} \tag{2.136}$$

is given by

$$b_k = a_{k+n} \tag{2.137}$$

Example 2.27 Periodic sinusoidal pulse signals

Consider the periodic sinusoidal pulse sequence $y(t)$ shown in Figure 2.24. The pulse repetition period is $T_0 = 1/f_0$ and the pulse width is $T_p < T_0$. The oscillating frequency of the sinusoidal pulse is $f_c = nf_0$, where n is a positive integer.

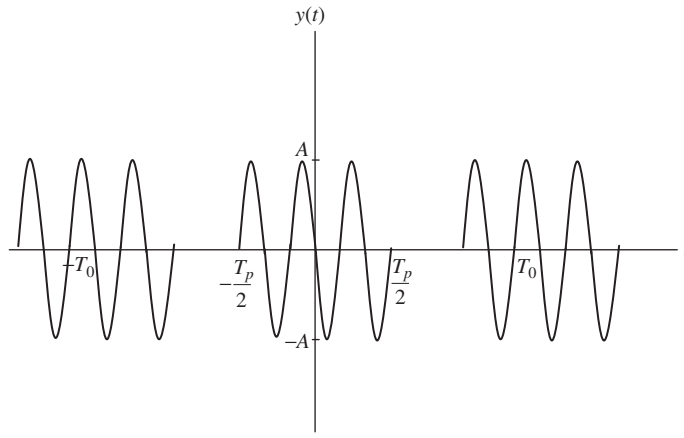

Figure 2.24 Periodic sinusoidal pulse signals.

The periodic signal $y(t)$ is simply the product of the periodic signal $x(t)$ in Figure 2.19 and $\cos 2\pi f_c t$. We have

$$\begin{aligned} y(t) &= x(t)\cos 2\pi f_c t \\ &= \frac{1}{2}x(t)\left(e^{j2\pi f_c t} + e^{-j2\pi f_c t}\right) \\ &= \frac{1}{2}x(t)\left(e^{j2\pi n f_0 t} + e^{-j2\pi n f_0 t}\right) \end{aligned} \tag{2.138}$$

It is seen that $y(t)$ is periodic with period T_0. The Fourier series representation of $y(t)$ is given by (2.132) and (2.133) with the following coefficients:

$$b_k = \frac{1}{2}(a_{k-n} + a_{k+n}) \tag{2.139}$$

Using (2.116) we have

$$b_k = \frac{AT_p}{2T_0}\left(\frac{\sin(\pi(k-n)f_0T_p)}{\pi(k-n)f_0T_p} + \frac{\sin(\pi(k+n)f_0T_p)}{\pi(k+n)f_0T_p}\right) \tag{2.140}$$

A plot of b_k as a function of kf_0 for $T_0 = 2T_p$ is shown in Figure 2.25.

Note that $b_n = (a_0 + a_{2n})/2$, $b_{-n} = (a_{-2n} + a_0)/2$, $b_{n-1} = (a_{-1} + a_{2n-1})/2$, $b_{n+1} = (a_1 + a_{2n+1})/2$, $b_{-n-1} = (a_{-2n-1} + a_{-1})/2$, $b_{-n+1} = (a_{-2n+1} + a_1)/2$, and so on. For $f_c \gg 1/T_p$, we have the following approximations: $b_n \approx a_0/2$; $b_{-n} \approx a_0/2$; $b_{n-1} \approx a_{-1}/2$; $b_{n-1} \approx a_1/2$; $b_{-n-1} \approx a_{-1}/2$; $b_{-n+1} \approx a_1/2$; and so on.

■

Example 2.28 Power spectral density of periodic sinusoidal pulse signals

Consider the periodic sinusoidal pulse signals $y(t)$ in Example 2.27. From the Parseval relation, the power of $y(t)$ is given by

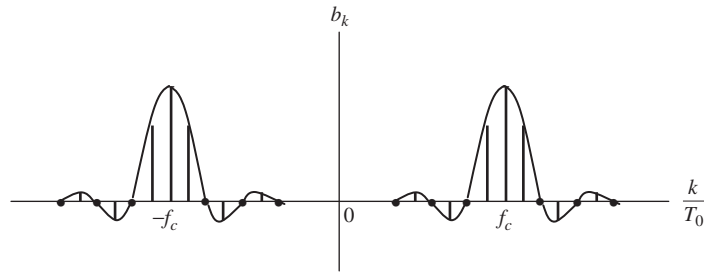

Figure 2.25 The Fourier series coefficients of periodic sinusoidal pulse signals.

$$P = \sum_{k=-\infty}^{\infty} |b_k|^2 \tag{2.141}$$

Consequently, the power spectral density of $y(t)$ is

$$S_y(f) = \sum_{k=-\infty}^{\infty} |b_k|^2 \delta(f - kf_0) \tag{2.142}$$

Substituting (2.139) into (2.142) we obtain

$$\begin{aligned}
S_y(f) &= \frac{1}{4}\sum_{k=-\infty}^{\infty} |a_{k-n} + a_{k+n}|^2 \delta(f - kf_0) \\
&= \frac{1}{4}\sum_{k=-\infty}^{\infty} \left[|a_{k-n}|^2 + \mathrm{Re}(a_{k-n}a_{k+n}^*)\right] \delta(f - kf_0) \\
&\quad + \frac{1}{4}\sum_{k=-\infty}^{\infty} \left[|a_{k+n}|^2 + \mathrm{Re}(a_{k-n}a_{k+n}^*)\right] \delta(f - kf_0) \\
&= \frac{1}{4}\sum_{i=-\infty}^{\infty} \left[|a_i|^2 + \mathrm{Re}(a_i a_{i+2n}^*)\right] \delta(f - (i+n)f_0) \\
&\quad + \frac{1}{4}\sum_{m=-\infty}^{\infty} \left[|a_m|^2 + \mathrm{Re}(a_{m-2n}a_m^*)\right] \delta(f - (m-n)f_0) \\
&= \frac{1}{4}\sum_{i=-\infty}^{\infty} \left[|a_i|^2 + \mathrm{Re}(a_i a_{i+2n}^*)\right] \delta(f - f_c - if_0) \\
&\quad + \frac{1}{4}\sum_{m=-\infty}^{\infty} \left[|a_m|^2 + \mathrm{Re}(a_{m-2n}a_m^*)\right] \delta(f + f_c - mf_0)
\end{aligned} \tag{2.143}$$

When $f_c \gg 1/T_p$ we have $\mathrm{Re}\,(a_i a_{i+2n}^*) \ll |a_i|^2$ and $\mathrm{Re}\,(a_{m-2n}a_m^*) \ll |a_m|^2$; hence $S_y(f)$ can be approximated as

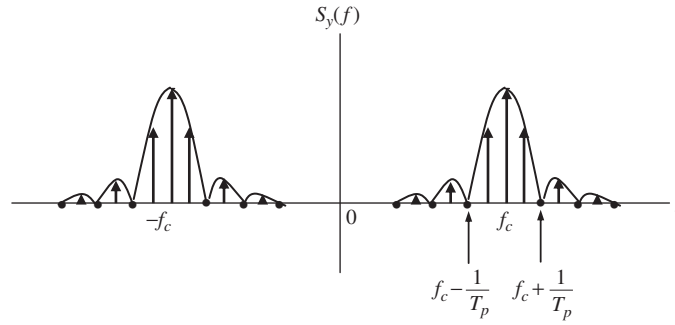

Figure 2.26 Power spectral density of periodic sinusoidal pulse signals.

$$\begin{aligned} S_y(f) &\approx \frac{1}{4}\sum_{i=-\infty}^{\infty} |a_i|^2\,\delta(f - f_c - if_0) + \frac{1}{4}\sum_{m=-\infty}^{\infty} |a_m|^2\,\delta(f + f_c - mf_0) \\ &\approx \frac{1}{4}[S_x(f - f_c) + S_x(f + f_c)] \end{aligned} \tag{2.144}$$

The power spectral density of $y(t)$ is shown in Figure 2.26 for $T_0 = 2T_p$.

The bandwidth of $y(t)$ is defined loosely as the positive frequency range around f_c that contains most of the power of $y(t)$. The *null-to-null* bandwidth B is the frequency range from $f_c - 1/T_p$ to $f_c + 1/T_p$, that is, $B = 2/T_p$. The signal $y(t)$ is referred to as a *bandpass* or *passband* signal. It is seen that the power spectral density of $y(t)$ is one-fourth the power spectral density of $x(t)$ shifted to the positive frequency range by f_c and one-fourth the power spectral density of $x(t)$ shifted to the negative frequency range by $-f_c$ for $f_c \gg 1/T_p$. The periodic signal $x(t)$ is referred to as the equivalent *baseband* or *lowpass* signal of $y(t)$.

■

The above study shows that Fourier series representation is an indispensable tool for analyzing periodic signals in the frequency domain via their harmonic components or their power spectral density. The frequency domain approach allows us to determine the frequency range that contains most of the signal power. This frequency range is defined loosely as the bandwidth of the signal. In the next section we will investigate the response of an LTI system to a periodic input signal.

Response of an LTI system to a periodic signal

The output response $y(t)$ of an LTI system, with impulse response $h(t)$ when a signal $x(t)$ is applied to its input, is determined by the convolution operation in (2.102):

$$y(t) = x(t) \;*\; h(t) = \int_{-\infty}^{\infty} x(\tau)\,h(t-\tau)\,\mathrm{d}\tau = \int_{-\infty}^{\infty} h(\tau)\,x(t-\tau)\mathrm{d}\tau \tag{2.145}$$

Let $x(t)$ be a periodic signal with the Fourier series representation given in (2.112). Substituting (2.112) into (2.145) we obtain

$$\begin{aligned} y(t) &= \int_{-\infty}^{\infty} h(\tau) \sum_{k=-\infty}^{\infty} a_k \mathrm{e}^{\mathrm{j}2\pi k f_0 (t-\tau)} \, \mathrm{d}\tau \\ &= \sum_{k=-\infty}^{\infty} a_k \mathrm{e}^{\mathrm{j}2\pi k f_0 t} \int_{-\infty}^{\infty} h(\tau) \, \mathrm{e}^{-\mathrm{j}2\pi k f_0 \tau} \, \mathrm{d}\tau \end{aligned} \tag{2.146}$$

The transfer function of the LTI system is defined as follows:

$$H(f) = \int_{-\infty}^{\infty} h(t) \, \mathrm{e}^{-\mathrm{j}2\pi f t} \, \mathrm{d}t \tag{2.147}$$

Note that the transfer function is a function of the frequency f. By using (2.147) in (2.146) we get

$$y(t) = \sum_{k=-\infty}^{\infty} H(kf_0) \, a_k \mathrm{e}^{\mathrm{j}2\pi k f_0 t} \tag{2.148}$$

From (2.148) we note that the Fourier series coefficients of $y(t)$ are the Fourier coefficients of $x(t)$ weighted by the values of the transfer function at the harmonic frequencies. Consequently, the power spectral density function of $y(t)$ is given by

$$S_y(f) = \sum_{k=-\infty}^{\infty} |H(kf_0)|^2 |a_k|^2 \delta(f - kf_0) \tag{2.149}$$

Substituting (2.127) into (2.149), and with the help of (2.123), we obtain the following relation between the power spectral density $S_y(f)$ of the output signal $y(t)$ of an LTI system and the power spectral density $S_x(f)$ of the periodic input signal $x(t)$:

$$S_y(f) = |H(f)|^2 S_x(f) \tag{2.150}$$

The result in (2.150) is very important because it enables the design of LTI filters to pass certain desirable harmonic components and to eliminate undesirable ones.

Example 2.29 Periodic pulse signals and the ideal lowpass filter

Let the periodic pulse signal $x(t)$ in Example 2.26 be the input to an ideal lowpass filter with the following transfer function:

$$H(f) = \begin{cases} 1, & -\frac{1}{T_p} \le f \le \frac{1}{T_p} \\ 0, & \text{otherwise} \end{cases} \tag{2.151}$$

A plot of $H(f)$ is shown in Figure 2.27(a). The ideal lowpass filter passes all the harmonic components of $x(t)$ within the main lobe. Figure 2.27(b) shows the power spectral density of $y(t)$ and its envelope, for $T_0 = 2T_p$.

■

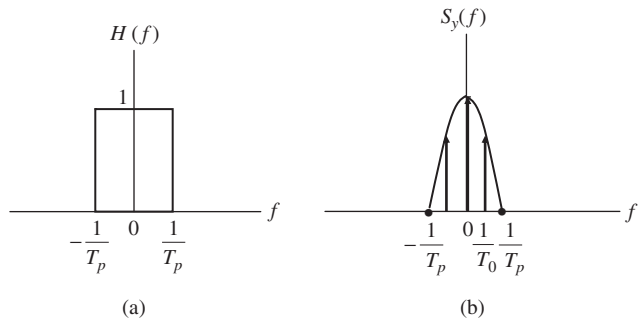

Figure 2.27 (a) Ideal lowpass filter; (b) power spectral density of output signal.

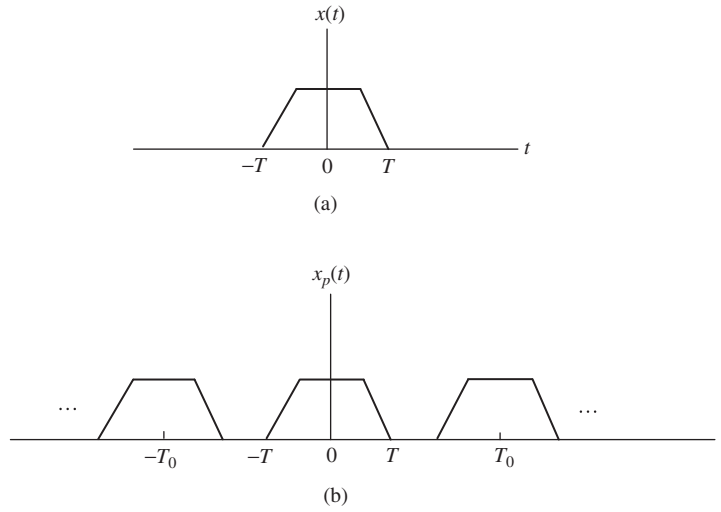

Figure 2.28 (a) Aperiodic signal $x(t)$; (b) periodic signal $x_P(t)$, constructed to be equal to $x(t)$ over one period T_0.

2.8 Fourier transform of continuous-time signals

The previous section dealt with the Fourier series representation of continuous-time periodic signals. In this section, we extend this concept to cover *aperiodic* signals, which includes all finite-energy signals used in communications. We can view an aperiodic signal as a periodic signal with an arbitrarily large period T_0 and we can examine the limiting behavior of the Fourier series representation of this signal. For simplicity, assume that the aperiodic signal $x(t)$ is of finite duration. Let us construct the periodic signal $x_p(t)$ for which $x(t)$ is one period. As the period $T_0 \to \infty$, $x_p(t)$ is equal to $x(t)$ for any finite value of t. Figure 2.28 illustrates this process.

The periodic signal $x_p(t)$ can be represented by the Fourier series as follows:

$$x_p(t) = \sum_{k=-\infty}^{\infty} a_k e^{j2\pi k f_0 t} \tag{2.152}$$

$$a_k = \frac{1}{T_0}\int_{-T_0/2}^{T_0/2} x_p(t)\, e^{-j2\pi k f_0 t} dt \tag{2.153}$$

Define the following quantity:

$$X(kf_0) = T_0 a_k = \int_{-T_0/2}^{T_0/2} x_p(t)\, e^{-j2\pi k f_0 t}\, dt \tag{2.154}$$

Rewriting (2.152) in terms of $X(kf_0)$ we obtain

$$x_p(t) = \sum_{k=-\infty}^{\infty} X(kf_0) e^{j2\pi k f_0 t} f_0 \tag{2.155}$$

As $T_0 \to \infty$, $x_p(t)$ approaches $x(t)$ and consequently (2.155) becomes a representation of $x(t)$. The summation becomes an integral, and the term inside the summation becomes the integrand $X(f)e^{j2\pi ft}$, with f_0 becoming df. Thus, (2.155) and (2.154) become

$$x(t) = \int_{-\infty}^{\infty} X(f) e^{j2\pi ft} df \tag{2.156}$$

$$X(f) = \int_{-\infty}^{\infty} x(t) e^{-j2\pi ft} dt \tag{2.157}$$

The above two equations are referred to as the *Fourier transform pair*. The function $X(f)$ is called the *Fourier transform* of the signal $x(t)$, and $x(t)$ is the *inverse Fourier transform* of $X(f)$. The following notations are often used:

$$x(t) \longleftrightarrow X(f) \tag{2.158}$$

$$X(f) = F\{x(t)\} \tag{2.159}$$

$$x(t) = F^{-1}\{X(f)\} \tag{2.160}$$

A signal $x(t)$ has a Fourier transform if it satisfies the following Dirichlet conditions:

1. $x(t)$ is absolutely integrable, that is,

$$\int_{-\infty}^{\infty} |x(t)|\, dt < \infty.$$

2. $x(t)$ has a finite number of maxima and minima within any finite interval.
3. $x(t)$ has a finite number of finite discontinuities within any finite interval.

Another sufficient condition for the existence of the Fourier transform is that the signal $x(t)$ is a finite energy signal, that is, it is square integrable, so that

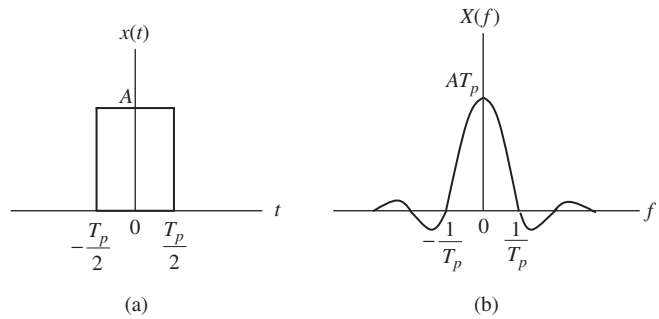

Figure 2.29 (a) Pulse signal; (b) its Fourier transform.

$$\int_{-\infty}^{\infty} |x(t)|^2 \mathrm{d}t < \infty.$$

Example 2.30 Fourier transform of a pulse signal
Consider the pulse signal

$$x(t) = \begin{cases} A, & -\frac{T_p}{2} \le t \le \frac{T_p}{2} \\ 0, & \text{otherwise} \end{cases} \tag{2.161}$$

as shown in Figure 2.29(a). Applying (2.157) we obtain the Fourier transform of $x(t)$ as

$$\begin{aligned} X(f) &= \int_{-T_p/2}^{T_p/2} A\mathrm{e}^{-\mathrm{j}2\pi ft}\,\mathrm{d}t = A\frac{\mathrm{e}^{-\mathrm{j}\pi fT_p} - \mathrm{e}^{\mathrm{j}\pi fT_p}}{-\mathrm{j}2\pi f} \\ &= AT_p\frac{\sin \pi fT_p}{\pi fT_p} \end{aligned} \tag{2.162}$$

The plot of $X(f)$ is shown in Figure 2.29(b). Note that $T_0X(f)$ is exactly the envelope of the Fourier series coefficients of the periodic pulse signal $x(t)$ shown in Example 2.26.

■

Example 2.31 Inverse Fourier transform
Consider the following signal $x(t)$, whose Fourier transform $X(f)$ is shown in Figure 2.30(a):

$$X(f) = \begin{cases} 1, & -B \le f \le B \\ 0, & \text{otherwise} \end{cases} \tag{2.163}$$

Applying the inverse Fourier transform in (2.156) we obtain

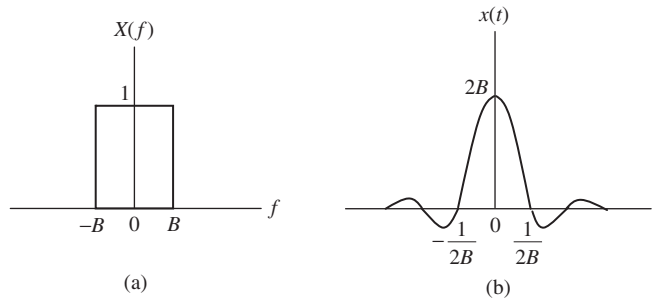

Figure 2.30 (a) Fourier transform of $x(t)$; (b) the signal $x(t)$.

$$\begin{aligned} x(t) &= \int_{-B}^{B} \mathrm{e}^{\mathrm{j}2\pi ft}\,\mathrm{d}f = \frac{\mathrm{e}^{\mathrm{j}2\pi Bt} - \mathrm{e}^{-\mathrm{j}2\pi Bt}}{\mathrm{j}2\pi t} \\ &= 2B\frac{\sin 2\pi Bt}{2\pi Bt} \end{aligned} \tag{2.164}$$

The pulse $x(t)$ is shown in Figure 2.30(b).

■

Frequency shifting property

As in the case of periodic signals, the frequency shifting property plays an important role in the frequency domain analysis of aperiodic signals. Let $x(t)$ be a signal with Fourier transform $X(f)$. Define the signal $y(t)$ as follows:

$$y(t) = x(t)\,\mathrm{e}^{\mathrm{j}2\pi f_c t} \tag{2.165}$$

Applying the Fourier transform to $y(t)$ we have

$$\begin{aligned} Y(f) &= \int_{-\infty}^{\infty} y(t)\,\mathrm{e}^{-\mathrm{j}2\pi ft}\mathrm{d}t \\ &= \int_{-\infty}^{\infty} x(t)\,\mathrm{e}^{-\mathrm{j}2\pi(f-f_c)t}\mathrm{d}t \\ &= X(f - f_c) \end{aligned} \tag{2.166}$$

Similarly, the Fourier transform of the signal

$$y(t) = x(t)\,\mathrm{e}^{-\mathrm{j}2\pi f_c t} \tag{2.167}$$

is given by

$$Y(f) = X(f + f_c) \tag{2.168}$$

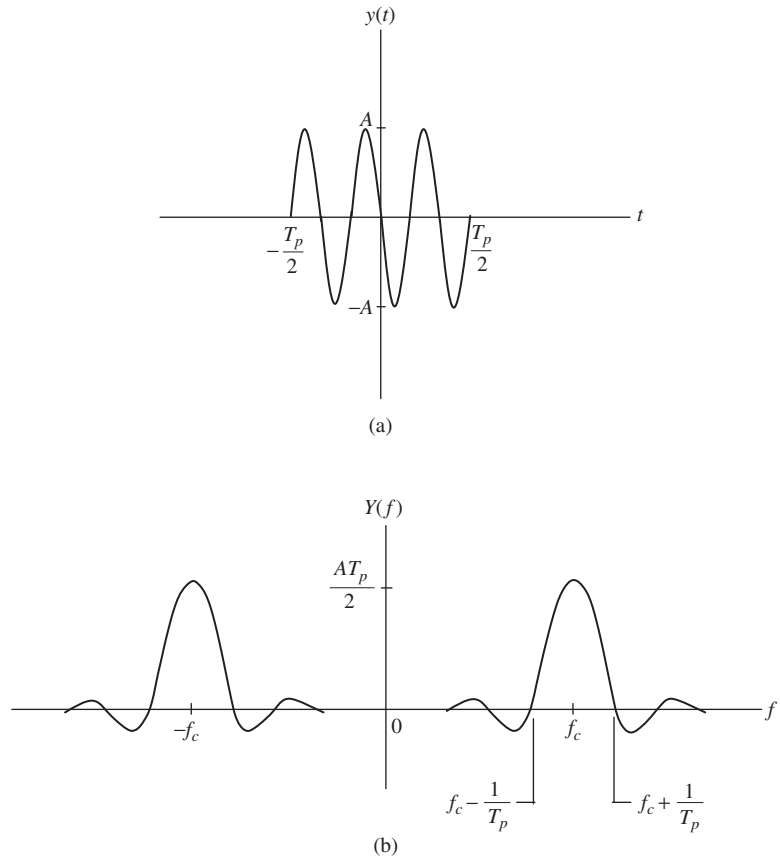

Figure 2.31 (a) Sinusoidal pulse signal; (b) its Fourier transform.

Example 2.32 Sinusoidal pulse signal
Consider the sinusoidal pulse signal

$$y(t) = \begin{cases} A\cos 2\pi f_c t, & -\frac{T_p}{2} \le t \le \frac{T_p}{2} \\ 0, & \text{otherwise} \end{cases} \tag{2.169}$$

as shown in Figure 2.31(a). We note that $y(t)$ is simply the product of $x(t)$ in (2.161) and $\cos 2\pi f_c t$, that is,

$$y(t) = x(t)\cos 2\pi f_c t = \frac{1}{2}\left[x(t)\,\mathrm{e}^{\mathrm{j}2\pi f_c t} + x(t)\,\mathrm{e}^{-\mathrm{j}2\pi f_c t}\right] \tag{2.170}$$

The Fourier transform of $y(t)$ as sketched in Figure 2.31(b) can be obtained from (2.166) and (2.168) as

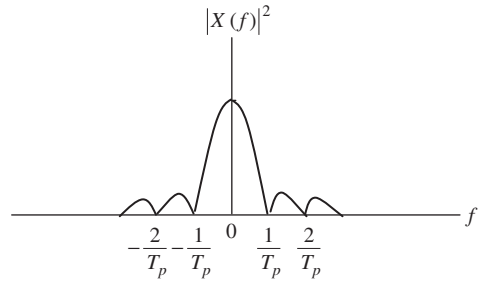

Figure 2.32 Energy spectral density of the pulse signal.

$$Y(f) = \frac{1}{2}[X(f - f_c) + X(f + f_c)] \tag{2.171}$$

where $X(f)$ is given in (2.162).

■

Parseval relation

For aperiodic signals such as energy signals, the *Parseval relation* is the direct counterpart of the Parseval relation for periodic signals. It expresses the signal energy in terms of the Fourier transform of the signal. If we consider an energy signal $x(t)$, its energy is given by

$$\begin{aligned} E &= \int_{-\infty}^{\infty} |x(t)|^2 \, \mathrm{d}t = \int_{-\infty}^{\infty} x(t)x^*(t) \, \mathrm{d}t \\ &= \int_{-\infty}^{\infty} x(t) \left[\int_{-\infty}^{\infty} X^*(f) \mathrm{e}^{-\mathrm{j}2\pi ft} \, \mathrm{d}f \right] \mathrm{d}t \\ &= \int_{-\infty}^{\infty} X^*(f) \left[\int_{-\infty}^{\infty} x(t) \mathrm{e}^{-\mathrm{j}2\pi ft} \, \mathrm{d}t \right] \mathrm{d}f \end{aligned} \tag{2.172}$$

The bracketed term in the last line is the Fourier transform of $x(t)$, thus

$$E = \int_{-\infty}^{\infty} |x(t)|^2 \, \mathrm{d}t = \int_{-\infty}^{\infty} |X(f)|^2 \, \mathrm{d}f \tag{2.173}$$

The quantity $|X(f)|^2$ is referred to as the *energy spectral density* or *energy spectrum* of the signal $x(t)$, and displays the distribution of the energy in the frequency domain. The energy spectral density of the pulse signal $x(t)$ in Example 2.30 is shown in Figure 2.32. This is a *baseband* signal with the *first-null bandwidth* equal to $1/T_p$.

The energy spectral density of the sinusoidal pulse signal in Example 2.32 is obtained from (2.171) as follows:

$$\begin{aligned} |Y(f)|^2 &= \frac{1}{4}|X(f - f_c) + X(f + f_c)|^2 \\ &\approx \frac{1}{4}[|X(f - f_c)|^2 + |X(f + f_c)|^2] \end{aligned} \tag{2.174}$$

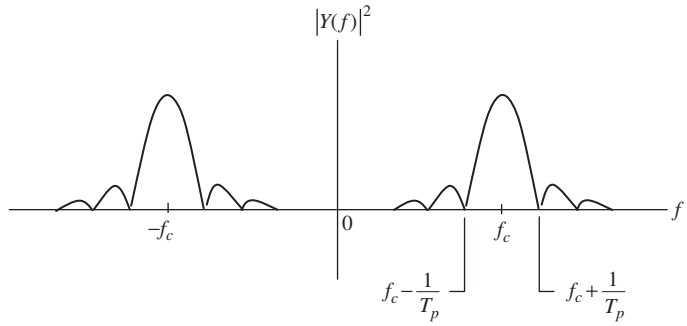

Figure 2.33 Energy spectral density of the sinusoidal pulse signal.

The approximation results from the fact that the term $2\,\mathrm{Re}\{X(f-f_c)X^*(f+f_c)\}$ is very small compared to either $|X(f-f_c)|^2$ or $|X(f+f_c)|^2$, because these two energy spectral densities are almost *non-overlapping* for f_c much larger than $1/T_p$. Figure 2.33 shows the energy spectral density of the sinusoidal pulse signal.

Fourier transform of periodic signals

Consider a periodic signal $x(t)$ with the Fourier representation in (2.112). Applying the Fourier transform in (2.156) we have

$$\begin{aligned} X(f) &= \int_{-\infty}^{\infty} \sum_{k=-\infty}^{\infty} a_k \mathrm{e}^{\mathrm{j}2\pi k f_0 t}\, \mathrm{e}^{-\mathrm{j}2\pi f t}\mathrm{d}t \\ &= \sum_{k=-\infty}^{\infty} a_k \int_{-\infty}^{\infty} \mathrm{e}^{\mathrm{j}2\pi k f_0 t}\, \mathrm{e}^{-\mathrm{j}2\pi f t}\mathrm{d}t \end{aligned} \tag{2.175}$$

Using the property of impulse function in (2.122) we obtain

$$\int_{-\infty}^{\infty} \delta(f - kf_0)\, \mathrm{e}^{\mathrm{j}2\pi f t}\, \mathrm{d}f = \mathrm{e}^{\mathrm{j}2\pi k f_0 t} \tag{2.176}$$

Note that the left-hand side of (2.176) is simply the inverse Fourier transform of $\delta(f - kf_0)$, therefore we conclude that the integral inside the summation on the right side of (2.175) is just the Fourier transform of $\mathrm{e}^{\mathrm{j}2\pi k f_0 t}$, which is precisely $\delta(f - kf_0)$. Thus

$$X(f) = \sum_{k=-\infty}^{\infty} a_k \delta(f - kf_0) \tag{2.177}$$

Response of LTI systems

The Fourier transform provides a very convenient way to analyze LTI systems. Consider an LTI system with impulse response $h(t)$ and input $x(t)$. The output $y(t)$ is given by the convolution operation

$$y(t) = \int_{-\infty}^{\infty} x(\tau)h(t-\tau)\,\mathrm{d}\tau \tag{2.178}$$

Taking the Fourier transform of both sides of (2.178) we get

$$\begin{aligned} Y(f) &= \int_{-\infty}^{\infty} \left[\int_{-\infty}^{\infty} x(\tau)h(t-\tau)\,\mathrm{d}\tau\right] \mathrm{e}^{-\mathrm{j}2\pi ft}\,\mathrm{d}t \\ &= \int_{-\infty}^{\infty} x(\tau)\left[\int_{-\infty}^{\infty} h(t-\tau)\,\mathrm{e}^{-\mathrm{j}2\pi ft}\,\mathrm{d}t\right]\mathrm{d}\tau \\ &= \int_{-\infty}^{\infty} x(\tau)\left[\int_{-\infty}^{\infty} h(t')\,\mathrm{e}^{-\mathrm{j}2\pi f(t'+\tau)}\,\mathrm{d}t'\right]\mathrm{d}\tau \\ &= \int_{-\infty}^{\infty} x(\tau)\,\mathrm{e}^{-\mathrm{j}2\pi f\tau}\left[\int_{-\infty}^{\infty} h(t')\,\mathrm{e}^{-\mathrm{j}2\pi ft'}\,\mathrm{d}t'\right]\mathrm{d}\tau \\ &= \int_{-\infty}^{\infty} h(t')\,\mathrm{e}^{-\mathrm{j}2\pi ft'}\,\mathrm{d}t' \int_{-\infty}^{\infty} x(\tau)\,\mathrm{e}^{-\mathrm{j}2\pi f\tau}\,\mathrm{d}\tau \end{aligned} \tag{2.179}$$

The above integrals are just the Fourier transforms $H(f)$ and $X(f)$ of $h(t)$ and $x(t)$, respectively. Note that $H(f)$ is simply the transfer function of the LTI system as defined in (2.147). Thus

$$Y(f) = H(f)X(f) \tag{2.180}$$

is the Fourier transform of

$$y(t) = h(t) * x(t) \tag{2.181}$$

Equation (2.180) provides a convenient means to evaluate the frequency response of an LTI system. It also allows the design of LTI filters to shape the output signal.

Example 2.33 Pulse signals and ideal lowpass filter

Consider an ideal lowpass filter with the transfer function $H(f)$ in (2.151) and shown in Figure 2.27(a). Let the input to the filter be the pulse signal $x(t)$ in (2.161). The Fourier transform $Y(f)$ of the output signal $y(t)$ is shown in Figure 2.34, which is the *mainlobe* of $X(f)$ in Figure 2.29(b).

■

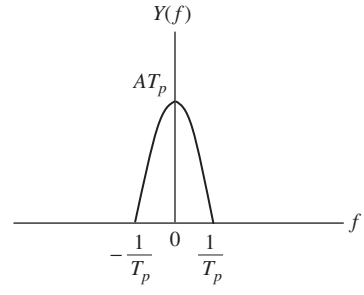

Figure 2.34 Fourier transform of the output signal of an ideal lowpass filter with a pulse signal input.

Example 2.34 Response to a periodic input signal

Consider an LTI system with a periodic input signal $x(t)$ whose Fourier transform is given in (2.177). Applying (2.180) we obtain the Fourier transform of the output signal as follows:

$$\begin{aligned} Y(f) &= H(f) \sum_{k=-\infty}^{\infty} a_k \delta(f - kf_0) \\ &= \sum_{k=-\infty}^{\infty} H(f) a_k \delta(f - kf_0) \end{aligned} \tag{2.182}$$

Using property (2.123) of the unit impulse function we have

$$Y(f) = \sum_{k=-\infty}^{\infty} H(kf_0) a_k \delta(f - kf_0) \tag{2.183}$$

Now taking the inverse Fourier transform of both sides of the above equation and noting that the inverse Fourier transform of $\delta(f - kf_0)$ is $\mathrm{e}^{\mathrm{j}2\pi kf_0 t}$ as given in (2.176) we obtain

$$y(t) = \sum_{k=-\infty}^{\infty} H(kf_0) a_k \mathrm{e}^{\mathrm{j}2\pi kf_0 t} \tag{2.184}$$

This is exactly the same expression for $y(t)$ given in (2.148) by the convolution operation. ■

Example 2.35 Distortionless transmission

Consider an LTI system with transfer function $H(f)$ and input $x(t)$ with Fourier transform $X(f)$. For the input signal $x(t)$ to pass through the LTI system undistorted, the output signal $y(t)$ must be a *delayed version* of $x(t)$, that is,

$$y(t) = Ax(t - t_0) \tag{2.185}$$

where t_0 is the time delay through the system and A is an arbitrary constant. Taking the Fourier transform of (2.185) we obtain

$$\begin{aligned} Y(f) &= \int_{-\infty}^{\infty} Ax(t - t_0)\, \mathrm{e}^{-\mathrm{j}2\pi ft}\, \mathrm{d}t = \int_{-\infty}^{\infty} Ax(\tau)\, \mathrm{e}^{-\mathrm{j}2\pi f(\tau + t_0)}\, \mathrm{d}\tau \\ &= A\, \mathrm{e}^{-\mathrm{j}2\pi ft_0} \int_{-\infty}^{\infty} x(\tau)\, \mathrm{e}^{-\mathrm{j}2\pi f\tau}\, \mathrm{d}\tau = A\, \mathrm{e}^{-\mathrm{j}2\pi ft_0} X(f) \end{aligned} \tag{2.186}$$

Comparing (2.180) and (2.186) we observe that a *distortionless* transmission occurs if and only if

$$H(f) = |H(f)|\, \mathrm{e}^{\mathrm{j}\theta(f)} = A\, \mathrm{e}^{-\mathrm{j}2\pi ft_0} \tag{2.187}$$

Table 2.1 Properties of the Fourier transform

Property	Signal	Fourier transform
Conjugate symmetry	$x(t)$ real	$X(f) = X^*(-f)$
Linearity	$ax(t) + by(t)$	$aX(f) + bY(f)$
Time scaling	$x(at)$	$\frac{1}{\lvert a\rvert}X\left(\frac{f}{a}\right)$
Time reversal	$x(-t)$	$X(-f)$
Conjugation	$x^*(t)$	$X^*(-f)$
Time shifting	$x(t - t_0)$	$X(f)\mathrm{e}^{-\mathrm{j}2\pi f t_0}$
Frequency shifting	$x(t)\mathrm{e}^{\pm\mathrm{j}2\pi f_c t}$	$X(f \mp f_c)$
Modulation	$x(t)\ \cos 2\pi f_c t$	$\frac{1}{2}(X(f - f_c) + X(f + f_c))$
Convolution	$x(t) * h(t)$	$X(f)H(f)$
Multiplication	$x(t)y(t)$	$X(f) * Y(f)$
Duality	$X(t)$	$x(-f)$
Differentiation	$\frac{\mathrm{d}^n x(t)}{\mathrm{d}t^n}$	$(\mathrm{j}2\pi f)^n X(f)$
Differentiation in frequency	$t^n x(t)$	$(-\mathrm{j}2\pi)^{-n}\frac{\mathrm{d}^n X(f)}{\mathrm{d}f^n}$
Integration	$\int_{-\infty}^{t} x(t)\,\mathrm{d}t$	$\frac{X(f)}{\mathrm{j}2\pi f} + \frac{1}{2}X(0)\delta(f)$

where $|H(f)|$ and $\theta(f)$ are the magnitude and phase of the transfer function $H(f)$, respectively. Equation (2.187) indicates that the transfer function magnitude must be a *constant*, and the transfer function phase must be a *linear function of frequency*, that is,

$$|H(f)| = A \tag{2.188}$$

$$\theta(f) = -2\pi t_0 f \tag{2.189}$$

Such a distortionless LTI system is referred to as an ideal linear phase filter.

■

Tables of Fourier properties and Fourier transform pairs

The Fourier transform possesses many important properties that are useful for signal analysis. These properties are listed in Table 2.1. The Fourier transforms of signals commonly used in communication are listed in Table 2.2.

2.9 Autocorrelation

We have seen the important role of energy spectral density and power spectral density in determining the bandwidth of energy signals and power signals, respectively. In this section we investigate the counterparts of these functions in the time domain.

Table 2.2 Fourier transform pairs

Signal		Fourier transform
Unit impulse	$\delta(t)$	1
Unit step	$u(t)$	$\frac{1}{\mathrm{j}2\pi f}+\frac{1}{2}\delta(f)$
Unit impulse at $t=t_0$	$\delta(t-t_0)$	$\mathrm{e}^{-\mathrm{j}2\pi f t_0}$
Constant	1	$\delta(f)$
Signum	$\operatorname{sgn}(t)=\begin{cases}1, & t>0\\ -1, & t<0\end{cases}$	$\frac{1}{\mathrm{j}\pi f}$
Hilbert transformer	$\frac{1}{\pi t}$	$-\mathrm{j}\operatorname{sgn}(f)$
Impulse train	$\sum_{k=-\infty}^{\infty}\delta(t-kT)$	$\frac{1}{T}\sum_{k=-\infty}^{\infty}\delta\left(f-\frac{k}{T}\right)$
Periodic signal	$\sum_{k=-\infty}^{\infty}a_k\mathrm{e}^{\mathrm{j}2\pi k f_0 t}$	$\sum_{k=-\infty}^{\infty}a_k\delta(f-kf_0)$
Complex exponential	$\mathrm{e}^{\mathrm{j}2\pi f_0 t}$	$\delta(f-f_0)$
Cosine	$\cos 2\pi f_c t$	$\frac{1}{2\mathrm{j}}[\delta(f-f_c)+\delta(f+f_c)]$
Sine	$\sin 2\pi f_c t$	$\frac{1}{2\mathrm{j}}[\delta(f-f_c)-\delta(f+f_c)]$
Gaussian pulse	$\mathrm{e}^{-\pi(t/T)^2}$	$T\,\mathrm{e}^{-\pi(fT)^2}$
Rectangular pulse	$x(t)=\begin{cases}A, & -\frac{T_p}{2}\le t\le\frac{T_p}{2}\\ 0, & \text{otherwise}\end{cases}$	$AT_p\dfrac{\sin\pi fT_p}{\pi fT_p}$
(sinz)/z pulse	$2B\dfrac{\sin 2\pi Bt}{2\pi Bt}$	$X(f)=\begin{cases}1, & -B\le f\le B\\ 0, & \text{otherwise}\end{cases}$
One-sided exponential	$\mathrm{e}^{-at}u(t),\quad a>0$	$\frac{1}{a+\mathrm{j}2\pi f}$
Two-sided exponential	$\mathrm{e}^{-a\lvert t\rvert}u(t),\quad a>0$	$\frac{2a}{a^2+(2\pi f)^2}$
	$\frac{t^{k-1}}{(k-1)!}\mathrm{e}^{-at}u(t),\quad a>0$	$\frac{1}{(a+\mathrm{j}2\pi f)^k}$
Parseval formula:	$\int_{-\infty}^{\infty}x(t)y^*(t)\,\mathrm{d}t=\int_{-\infty}^{\infty}X(f)Y^*(f)\,\mathrm{d}f$	
Poisson sum formula	$x(t)=\sum_{n=-\infty}^{\infty}m(t-nT)=\frac{1}{T}\sum_{k=-\infty}^{\infty}M(k/T)\mathrm{e}^{\mathrm{j}2\pi kt/T}$	

Autocorrelation and energy spectral density

Let $|X(f)|^2$ be the *energy spectral density* of a real-valued signal $x(t)$ with a corresponding Fourier transform $X(f)$. We are interested in the inverse Fourier transform $R_x(\tau)$ of $|X(f)|^2$. By convention, the time variable τ is used to distinguish it from the time variable t of the signal $x(t)$. We have

$$\begin{aligned}R_x(\tau)&=F^{-1}\left\{|X(f)|^2\right\}=\int_{-\infty}^{\infty}|X(f)|^2\mathrm{e}^{\mathrm{j}2\pi f\tau}\,\mathrm{d}f=\int_{-\infty}^{\infty}X(f)X^*(f)\;\mathrm{e}^{\mathrm{j}2\pi f\tau}\,\mathrm{d}f\\&=\int_{-\infty}^{\infty}X(f)X(-f)\;\mathrm{e}^{\mathrm{j}2\pi f\tau}\,\mathrm{d}f=\int_{-\infty}^{\infty}X(f)\left[\int_{-\infty}^{\infty}x(t)\,\mathrm{e}^{\mathrm{j}2\pi ft}\,\mathrm{d}t\right]\mathrm{e}^{\mathrm{j}2\pi f\tau}\,\mathrm{d}f\\&=\int_{-\infty}^{\infty}x(t)\left[\int_{-\infty}^{\infty}X(f)\,\mathrm{e}^{\mathrm{j}2\pi f(t+\tau)}\,\mathrm{d}f\right]\mathrm{d}t\end{aligned}\tag{2.190}$$

or

$$R_x(\tau)=\int_{-\infty}^{\infty}x(t)x(t+\tau)\,\mathrm{d}t\tag{2.191}$$

The function $R_x(\tau)$ is referred to as the *autocorrelation* of the *energy signal* $x(t)$. It provides a measure of the similarity between the signal and its delayed version. An important property of the autocorrelation is that the energy E of the signal $x(t)$ is equal to the value of $R_x(\tau)$ at the delay time $\tau = 0$:

$$E = \int_{-\infty}^{\infty} x^2(t)\,\mathrm{d}t = R_x(0) \tag{2.192}$$

From (2.191) let $t' = t + \tau$, then we can formulate the autocorrelation as follows:

$$R_x(\tau) = \int_{-\infty}^{\infty} x(t')x(t'-\tau)\,\mathrm{d}t' = x(\tau) * x(-\tau) \tag{2.193}$$

Thus, the autocorrelation of a real-valued energy signal is a real-valued even function, that is,

$$R_x(\tau) = R_x(-\tau) \tag{2.194}$$

Furthermore, the maximum value of the autocorrelation occurs at the origin, that is,

$$|R_x(\tau)| \le R_x(0) \text{ for all } \tau \tag{2.195}$$

The inequality in (2.195) holds because the similarity between the signal $x(t)$ and its delayed version $x(t+\tau)$ is reduced as τ is increased. We can prove (2.195) by considering the following inequality:

$$\int_{-\infty}^{\infty} [x(t) - x(t+\tau)]^2 \mathrm{d}t \ge 0 \qquad \text{for all } \tau \tag{2.196}$$

Equivalently, we have

$$\begin{aligned} \int_{-\infty}^{\infty} x^2(t)\,\mathrm{d}t + \int_{-\infty}^{\infty} x^2(t+\tau)\,\mathrm{d}t &\ge 2\int_{-\infty}^{\infty} x(t)x(t+\tau)\,\mathrm{d}t \\ &\ge 2\left|\int_{-\infty}^{\infty} x(t)x(t+\tau)\,\mathrm{d}t\right| \quad \text{for all } \tau \end{aligned} \tag{2.197}$$

The left-hand side of (2.197) is simply the sum of $R_x(0)$ and $R_x(0)$ and the right-hand side is just $2|R_x(\tau)|$. This proves (2.195).

Now consider an LTI system with input $x(t)$, transfer function $H(f)$, and corresponding real-valued impulse response $h(t)$. We are interested in the energy spectral density of the output signal $y(t)$ whose Fourier transform is $Y(f)$. Let the input signal $x(t)$ be an energy signal with the Fourier transform $X(f)$. From (2.180) we obtain

$$|Y(f)|^2 = |H(f)|^2|X(f)|^2 \tag{2.198}$$

Taking the inverse Fourier transform of both sides of (2.198), and noting that $|H(f)|^2 = H^*(f)H(f)$, we have

$$R_y(\tau) = h(-\tau) * h(\tau) * R_x(\tau) \tag{2.199}$$

where $R_y(\tau)$ and $R_x(\tau)$ are the autocorrelation functions of $y(t)$ and $x(t)$, respectively.

Autocorrelation and power spectral density

In this section we derive the inverse Fourier transform of the power spectral density. First we consider periodic signals that are special cases of power signals. For a periodic signal $x(t)$ with a Fourier representation in (2.112), the power spectral density is given by (2.127) and repeated here for convenience:

$$S_x(f) = \sum_{k=-\infty}^{\infty} |a_k|^2 \delta(f - kf_0) \tag{2.200}$$

Denoting $R_x(\tau)$ as the inverse Fourier transform of $S_x(x)$, and applying (2.156) to (2.200) we obtain

$$R_x(\tau) = F^{-1}\{S_x(f)\} = \sum_{k=-\infty}^{\infty} |a_k|^2 \mathrm{e}^{\mathrm{j}2\pi k f_0 \tau} \tag{2.201}$$

We observe that the power P of the periodic signal $x(t)$ is equal to $R_x(0)$ via (2.117), that is,

$$P = R_x(0) = \sum_{k=-\infty}^{\infty} |a_k|^2 \tag{2.202}$$

For a real-valued signal $x(t)$ that is not periodic, the power spectral density must be derived separately. From (2.13) the average power of $x(t)$ is given by

$$P = \lim_{T\to\infty} \frac{1}{2T} \int_{-T}^{T} x^2(t)\,\mathrm{d}t = \lim_{T\to\infty} \frac{1}{2T} \int_{-\infty}^{\infty} x_T^2(t)\,\mathrm{d}t \tag{2.203}$$

where $x_T(t)$ is a truncated version of $x(t)$:

$$x_T(t) = \begin{cases} x(t), & -T \le t \le T \\ 0, & \text{otherwise} \end{cases} \tag{2.204}$$

Although the power signal $x(t)$ might not have a Fourier transform because its energy is infinite, its truncated version $x_T(t)$ has finite energy and hence possesses a Fourier transform $X_T(f)$. By using the Parseval relation for (2.203) we have

$$P = \lim_{T\to\infty} \frac{1}{2T} \int_{-\infty}^{\infty} |X_T(f)|^2\,\mathrm{d}f \tag{2.205}$$

Since the average power P is finite, we can exchange the order in which the limit and the integration are performed:

$$P = \int_{-\infty}^{\infty} \lim_{T\to\infty} \frac{1}{2T} |X_T(f)|^2\,\mathrm{d}f \tag{2.206}$$

If we let $S_x(f)$ be the *power spectral density* of the power signal $x(t)$, by definition we have

$$P = \int_{-\infty}^{\infty} S_x(f)\,\mathrm{d}f = \int_{-\infty}^{\infty} \lim_{T\to\infty} \frac{1}{2T} |X_T(f)|^2\,\mathrm{d}f \tag{2.207}$$

Hence, the power spectral density of a power signal is defined as

$$S_x(f) = \lim_{T\to\infty} \frac{1}{2T} |X_T(f)|^2 \tag{2.208}$$

The function $|X_T(f)|^2/2T$ is commonly referred to by statisticians as the *periodogram* of the power signal.

If we denote the *inverse Fourier transform* of $S_x(f)$ as $R_x(\tau)$, we have

$$\begin{aligned} R_x(\tau) = F^{-1}\{S_x(f)\} &= \int_{-\infty}^{\infty} \left[\lim_{T\to\infty} \frac{1}{2T} |X_T(f)|^2\right] e^{j2\pi f\tau} df \\ &= \lim_{T\to\infty} \frac{1}{2T} \int_{-\infty}^{\infty} |X_T(f)|^2 e^{j2\pi f\tau} df \end{aligned} \tag{2.209}$$

Using the relation that leads to (2.190) we obtain

$$R_x(\tau) = \lim_{T\to\infty} \frac{1}{2T} \int_{-\infty}^{\infty} x_T(t) x_T(t+\tau)\, dt \tag{2.210}$$

Substituting (2.204) into (2.210) we obtain

$$R_x(\tau) = \lim_{T\to\infty} \frac{1}{2T} \int_{-T}^{T} x(t) x(t+\tau)\, dt \tag{2.211}$$

The function $R_x(\tau)$ in (2.211) is referred to as the *autocorrelation* of the power signal $x(t)$. Note that the autocorrelation of the periodic signal given in (2.201) is a special case of (2.211). In fact, (2.201) can be obtained by substituting (2.112) directly into (2.211). We also observe that the average power P of the power signal $x(t)$ is equal to $R_x(0)$ by virtue of (2.203) and (2.211). Thus, the average power of the power signal $x(t)$ is equal to the autocorrelation at the origin, that is,

$$P = R_x(0) \tag{2.212}$$

Furthermore, the autocorrelation of a power signal also satisfies (2.194) and (2.195).

The autocorrelation reflects the degree of coupling between a signal and its delayed version. If the signal $x(t)$ varies slowly, the signal's delayed version $x(t+\tau)$ looks almost like the signal as the delayed interval τ gets larger. In the extreme case of a dc (constant) signal, the autocorrelation is a constant, meaning that the power spectral density is an impulse function at zero frequency. This is expected since all power must be concentrated at zero frequency. When $x(t)$ varies rapidly then its delayed version $x(t+\tau)$ can be very much different to $x(t)$ within a short delayed interval τ, and the autocorrelation can go down to zero. In this case the signal may contain many harmonics at various frequencies. The high-frequency harmonics are the rapidly time-varying signals and may contain a large amount of power. In this case, the power spectral density may have high weighting at the high frequencies, which means that the signal has a large bandwidth. In the extreme case, the signal varies so rapidly that its autocorrelation is an impulse function at time zero. This implies that the power spectral density is a constant, and the signal has infinite bandwidth and infinite power.

Output autocorrelation and power spectral density

In this section we investigate the autocorrelation and power spectral density of the output signal $y(t)$ of an LTI system with an input power signal $x(t)$. As usual, let $h(t)$ be the real-valued impulse response of the LTI system. The corresponding transfer function $H(f)$ is simply the Fourier transform of $h(t)$. The autocorrelation of $y(t)$ is given by

$$R_y(\tau) = \lim_{T\to\infty} \frac{1}{2T} \int_{-T}^{T} y(t)y(t+\tau)\,\mathrm{d}t \tag{2.213}$$

Noting that $y(t) = h(t) * x(t)$, we can express (2.213) as

$$R_y(\tau) = \lim_{T\to\infty} \frac{1}{2T} \int_{-T}^{T} \int_{-\infty}^{\infty} h(u)x(t-u)\,\mathrm{d}u \int_{-\infty}^{\infty} h(v)x(t+\tau-v)\,\mathrm{d}v\,\mathrm{d}t \tag{2.214}$$

Making the following change of variable, $\lambda = t - u$, we can write (2.214) as

$$R_y(\tau) = \int_{-\infty}^{\infty} \int_{-\infty}^{\infty} h(u)\,h(v) \left[\lim_{T\to\infty} \frac{1}{2T} \int_{-T}^{T} x(\lambda)\,x(\lambda + (u+\tau-v))\,\mathrm{d}\lambda \right] \mathrm{d}u\,\mathrm{d}v \tag{2.215}$$

Note that the term in the bracket is simply the autocorrelation of $x(t)$ with the argument $u + \tau - v$, that is, $R_x(u+\tau-v)$, thus (2.215) can be expressed as

$$\begin{aligned} R_y(\tau) &= \int_{-\infty}^{\infty} \int_{-\infty}^{\infty} h(u)\,h(v)\,R_x(u+\tau-v)\mathrm{d}u\,\mathrm{d}v \\ &= \int_{-\infty}^{\infty} h(u) \left[\int_{-\infty}^{\infty} h(v)\,R_x((u+\tau)-v)\,\mathrm{d}v \right] \mathrm{d}u \\ &= \int_{-\infty}^{\infty} h(u)[h(u+\tau) * R_x(u+\tau)]\,\mathrm{d}u \end{aligned} \tag{2.216}$$

Again, making a change of variable, $z = u + \tau$, we obtain

$$R_y(\tau) = \int_{-\infty}^{\infty} h(z-\tau)[h(z) * R_x(z)]\,\mathrm{d}z \tag{2.217}$$

The right-hand side of (2.217) is just the convolution operation of $h(-\tau)$ and $h(\tau) * R_x(\tau)$, therefore

$$R_y(\tau) = h(-\tau) * h(\tau) * R_x(\tau) \tag{2.218}$$

The power spectral density of the output signal $y(t)$ can be obtained from (2.218) by taking the Fourier transform of $R_y(\tau)$. Using the convolution, conjugate symmetry, and real signal properties in Table 2.2 we have

$$S_y(f) = H^*(f)H(f)S_x(f) \tag{2.219}$$

or, equivalently,

$$S_y(f) = |H(f)|^2 S_x(f) \tag{2.220}$$

This is exactly the same expression that we derived for periodic signals in (2.150).

2.10 Sampling

Sampling is the first step in the process of converting a continuous-time analog signal into a set of digital signals that represent bits or symbols. Sampling produces values or samples of the continuous-time signal at points equally spaced in time. Sampling is useful only when the continuous-time signal can be reconstructed from its samples. In general, many signals can generate a given set of samples. Therefore, the samples can *uniquely* specify the signal if and only if additional conditions are obeyed. These conditions are stated in a well-known theorem called the *sampling theorem.*

Sampling theorem

Let $x(t)$ be a *bandlimited* signal with a Fourier transform $X(f)$ such that $X(f) = 0$ for $|f| > B$, where B is the *absolute* signal bandwidth (highest frequency of the signal). Then, $x(t)$ is *uniquely* specified by its samples $x(kT)$, $k = 0, \pm 1, \pm 2, \ldots$, equally spaced in time $T = 1/f_s$. The parameter T is referred to as the *sampling period*, and the *sampling frequency* f_s must be *greater* than *twice* the absolute signal bandwidth B, that is,

$$f_s > 2B \tag{2.221}$$

The sampling rate $f_N = 2B$ is referred to as the *Nyquist sampling rate*.

The samples can be generated by impulse-train sampling in which the signal $x(t)$ is multiplied by a periodic unit impulse train of period T. This operation produces impulses at locations kT with amplitudes $x(kT)$, $k = 0, \pm 1, \pm 2, \ldots$. The signal $x(t)$ can be reconstructed by passing the sampled signal through an ideal lowpass filter with gain T and bandwidth W that satisfies the following condition:

$$B < W < f_s - B \tag{2.222}$$

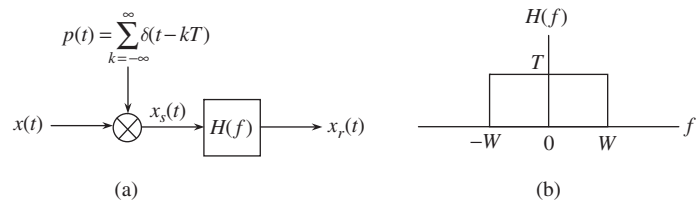

Figure 2.35 (a) Sampling and reconstruction; (b) ideal lowpass filter.

The sampling theorem is summarized in Figure 2.35, where $p(t)$ is the unit impulse-train, $x_s(t)$ is the sampled signal, $x_r(t)$ is the reconstructed signal, and $H(f)$ is the transfer function of the ideal lowpass filter, given by

$$H(f) = \begin{cases} T, & |f| \le W \\ 0, & \text{otherwise} \end{cases} \tag{2.223}$$

Impulse-train sampling

The sampled signal $x_s(t)$ is generated by multiplying the continuous-time signal $x(t)$ with a unit impulse train $p(t)$:

$$x_s(t) = x(t)p(t) \tag{2.224}$$

where

$$p(t) = \sum_{k=-\infty}^{\infty} \delta(t - kT) \tag{2.225}$$

Thus,

$$x_s(t) = x(t) \sum_{k=-\infty}^{\infty} \delta(t - kT) = \sum_{k=-\infty}^{\infty} x(t)\delta(t - kT) \tag{2.226}$$

Using (2.123) in (2.226) we obtain

$$x_s(t) = \sum_{k=-\infty}^{\infty} x(kT)\delta(t - kT) \tag{2.227}$$

Example 2.36 Sampling of a $(\sin x)/x$ pulse

Consider the pulse signal $x(t)$ and its Fourier transform $X(f)$ shown in Figure 2.30 of Example 2.31 and repeated here for convenience in Figure 2.36. It is obvious that the signal

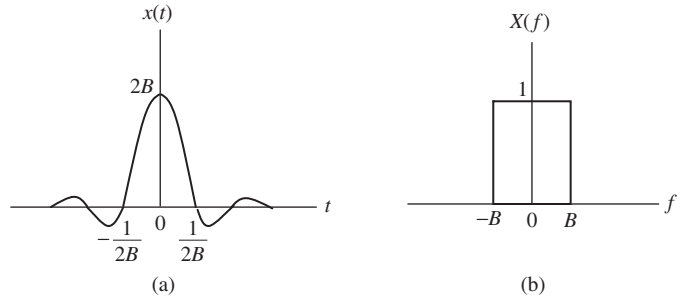

Figure 2.36 (a) $x(t) = 2B[(\sin 2\pi Bt)/2\pi Bt]$ pulse; (b) its Fourier transform.

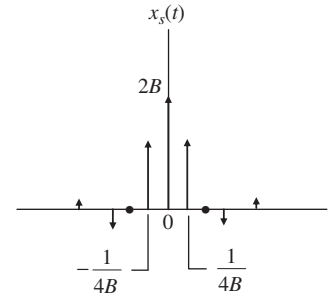

Figure 2.37 The sampled signal produced by impulse-train sampling.

$x(t)$ is bandlimited to a bandwidth B. Assume that we want to sample the signal at a sampling frequency equal to four times the bandwidth, that is,

$$f_s = 4B \tag{2.228}$$

The sampling period is then given by

$$T = \frac{1}{f_s} = \frac{1}{4B} \tag{2.229}$$

Consequently, the sampled signal $x_s(t)$ shown in Figure 2.37 is given by

$$x_s(t) = \sum_{k=-\infty}^{\infty} x\left(\frac{k}{4B}\right)\delta\left(t - \frac{k}{4B}\right) \tag{2.230}$$

$$= \sum_{k=-\infty}^{\infty} 2B\frac{\sin(k\pi/2)}{k\pi/2}\delta\left(t - \frac{k}{4B}\right) \tag{2.231}$$

■

Reconstruction with an ideal lowpass filter

We now look at the sampled signal $x_s(t)$ in the frequency domain via its Fourier transform $X_s(f)$, which can be obtained from (2.224). Using the multiplication property in Table 2.1 we have

$$X_s(f) = X(f) * P(f) \tag{2.232}$$

where $X(f)$ and $P(f)$ are the Fourier transforms of $x(t)$ and $p(t)$, respectively. Using the Fourier transform of the impulse train in Table 2.2 we obtain the Fourier transform $P(f)$ of $p(t)$ as follows:

$$P(f) = \frac{1}{T}\sum_{k=-\infty}^{\infty} \delta(f - kf_s) \tag{2.233}$$

Substituting (2.233) into (2.232) and performing the convolution operation we get

$$\begin{aligned} X_s(f) &= \int_{-\infty}^{\infty} P(u)X(f-u)\,\mathrm{d}u \\ &= \frac{1}{T}\int_{-\infty}^{\infty} \sum_{\mathrm{k}=-\infty}^{\infty} \delta(u-kf_s)X(f-u)\mathrm{d}u \\ &= \frac{1}{T}\sum_{k=-\infty}^{\infty} \int_{-\infty}^{\infty} \delta(u-kf_s)X(f-u)\,\mathrm{d}u \end{aligned} \tag{2.234}$$

Applying (2.122) to (2.234) we arrive at the following expression for the Fourier transform of the sampled signal:

$$X_s(f) = \frac{1}{T}\sum_{k=-\infty}^{\infty} X(f-kf_s) \tag{2.235}$$

It can be seen that the Fourier transform of the sampled signal is the sum of *shifted replicas* of $X(f)$ scaled by the factor $1/T$. Furthermore, $X_s(f)$ is a *periodic* function of frequency f with period f_s. When the sampling frequency $f_s > 2B$, the adjacent shifted replicas of $X(f)$ do not overlap. By passing the sampled signal through an ideal lowpass filter, with a transfer function given in (2.223) that satisfies the constraint in (2.222), we can recover the original signal $x(t)$. The recovered signal $x_r(t)$ can be described in the frequency domain by its Fourier transform $X_r(f)$ as follows:

$$\begin{aligned} X_r(f) &= H(f)X_s(f) \\ &= \begin{cases} \displaystyle\sum_{k=-\infty}^{\infty} X(f-kf_s), & |f| \le W \\ 0, & |f| > W \end{cases} \\ &= X(f) \end{aligned} \tag{2.236}$$

Thus, the original signal $x(t)$ is completely recovered. The next example illustrates the reconstruction process.

Example 2.37 Reconstruction of sampled $(\sin x)/x$ pulse

The Fourier transform of the sampled signal of the pulse given in Figure 2.36 is sketched in Figure 2.38. The sampling frequency is $f_s = 3B$. It is obvious that any ideal lowpass filter with gain T and bandwidth W such that $B < W < 2B$ can recover $X(f)$ and reject all shifted replicas of $X(f)$, as shown in the same figure. Thus, the reconstructed signal $x_r(t)$ is exactly the same as the original signal $x(t)$.

■

So far we have investigated the reconstruction process in the frequency domain. An equivalent time domain approach is also feasible. Let $h(t)$ be the impulse response of the

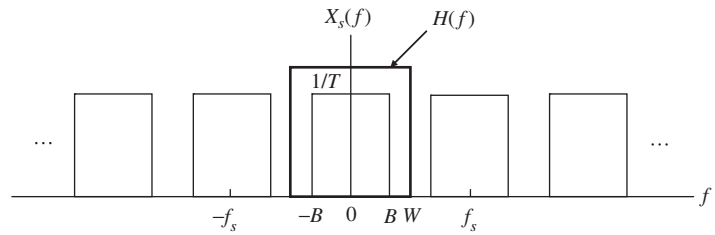

Figure 2.38 Fourier transform of the sampled signal of the pulse in Figure 2.36.

ideal lowpass filter. Thus $h(t)$ is the inverse Fourier transform of $H(f)$. We can write the reconstructed signal $x_r(t)$ as follows:

$$\begin{aligned} x_r(t) &= x_s(t) * h(t) \\ &= \int_{-\infty}^{\infty} x_s(\tau) h(t-\tau)\, \mathrm{d}\tau \end{aligned} \tag{2.237}$$

Substituting (2.227) into (2.237) we obtain

$$\begin{aligned} x_r(t) &= \int_{-\infty}^{\infty} \sum_{k=-\infty}^{\infty} x(kT)\delta(\tau - kT)\, h(t-\tau)\, \mathrm{d}\tau \\ &= \sum_{k=-\infty}^{\infty} x(kT) h(t-kT) \end{aligned} \tag{2.238}$$

Given $H(f)$ in Figure 2.35(b) the corresponding $h(t)$ can be obtained from Table 2.2 as

$$h(t) = 2WT \frac{\sin 2\pi Wt}{2\pi Wt} \tag{2.239}$$

Combining (2.238) and (2.239) we can write the reconstructed signal as follows:

$$x_r(t) = \sum_{k=-\infty}^{\infty} x(kT) \left[2WT \frac{\sin 2\pi W(t-kT)}{2\pi W(t-kT)} \right] \tag{2.240}$$

The left-hand side of (2.240) is just the inverse Fourier transform of the left-hand side of (2.236), which is exactly $x(t)$. Equation (2.240) provides a convenient way of representing a bandlimited signal as a series of *time-shifted* $(\sin x)/x$ pulses. The coefficients of the series are the samples of the signal. It turns out that the above series is also an orthogonal series when $2WT = 1$ or $2W = 1/T = f_s$: this is proven below in Example 2.38.

Example 2.38 Orthogonal $(\sin x)/x$ functions

Consider the infinite set of time-shifted pulses defined as follows:

$$x_k(t) = \frac{\sin \pi f_s(t-kT)}{\pi f_s(t-kT)}, \quad \text{where } k \text{ is an integer} \tag{2.241}$$

where $f_s = 1/T$. We need to show that this is a set of orthogonal functions. We first establish the inner product of two distinct functions $x_k(t)$ and $x_m(t)$ as indicated by (2.36) and make use of the Parseval relation in Table 2.2:

$$\int_{-\infty}^{\infty} x_k(t)x_m^*(t)\,\mathrm{d}t = \int_{-\infty}^{\infty} X_k(f)X_m^*(f)\,\mathrm{d}f \tag{2.242}$$

where $X_k(f)$ and $X_m(f)$ are the Fourier transforms of $x_k(t)$ and $x_m(t)$, respectively. Note that $x_k(t) = x_0(t - kT)$ and $x_m(t) = x_0(t - mT)$. Hence, by applying the time shifting property in Table 2.1 we get

$$X_k(f) = X_0(f)\,\mathrm{e}^{-\mathrm{j}2\pi kTf} \tag{2.243}$$

$$X_m(f) = X_0(f)\,\mathrm{e}^{-\mathrm{j}2\pi mTf} \tag{2.244}$$

where $X_0(f)$ is the Fourier transform of $x_0(t)$. Substituting (2.243) and (2.244) into (2.242) we obtain

$$\int_{-\infty}^{\infty} x_k(t)x_m(t)\,\mathrm{d}t = \int_{-\infty}^{\infty} |X_0(f)|^2\mathrm{e}^{-\mathrm{j}2\pi(k-m)Tf}\,\mathrm{d}f \tag{2.245}$$

Note that $X_0(f)$ is given in Figure 2.36(b) with f_s replacing $2B$, and its amplitude is $1/f_s$. Equation (2.245) can now be rewritten as

$$\int_{-\infty}^{\infty} x_k(t)x_m(t)\,\mathrm{d}t = \int_{-f_s/2}^{f_s/2} \frac{1}{f_s^2}\mathrm{e}^{-\mathrm{j}2\pi(k-m)Tf}\,\mathrm{d}f = 0 \tag{2.246}$$

Thus, the set of functions in (2.241) is an orthogonal set. This example shows that a continuous-time finite-energy signal $x(t)$, bandlimited to a bandwidth B, can be represented by an orthogonal series of the form

$$x(t) = \sum_{k=-\infty}^{\infty} x(kT)\left[\frac{\sin\,\pi f_s(t - kT)}{\pi f_s(t - kT)}\right] \tag{2.247}$$

where $f_s = 1/T = 2B$. The above expression is referred to as the *Nyquist–Shannon interpolation formula*.

■

Example 2.39 Aliasing

We have shown that impulse sampling produces a sampled signal with a periodic Fourier transform consisting of scaled replicas of the Fourier transform of the original signal equally spaced in frequency by the sampling frequency f_s. The sampling frequency must be greater than twice the absolute bandwidth or highest frequency of the original signal. When this condition is not satisfied, the Fourier transform of the sampled signal no longer consists of replicas of the original signal. Hence, the Fourier transform of the original

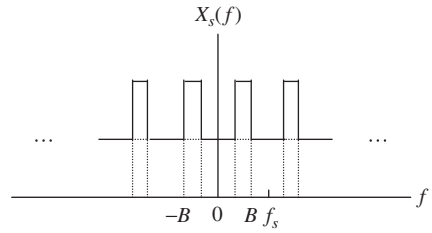

Figure 2.39 Aliasing effect of undersampling.

signal cannot be recovered by lowpass filtering. This happens because the periodic components of the Fourier transform of the sampled signal overlap. This effect is referred to as *aliasing.*

The Fourier transform of the sampled signal of the pulse given in Figure 2.36 is sketched in Figure 2.39. The sampling frequency is $f_s = 3B/2$. It is seen that lowpass filtering cannot reconstruct the Fourier transform of the original signal shown in Figure 2.36. Therefore, the recovered signal after lowpass filtering will be distorted.

■

2.11 Bandpass signals

Most practical communication systems are bandpass systems, and signals that they transmit and receive are therefore bandpass signals. The sinusoidal pulse signal shown in Figure 2.31(a) is a classical example of a bandpass signal. In general, the spectral density of a bandpass signal concentrates around a carrier frequency f_c as shown in Figure 2.31(b) for the sinusoidal pulse signal. The positive and negative parts of the spectral density do not overlap for all practical purposes, since their values around the zero frequency are very small compared to their peak values. Also, the bandwidth of the bandpass signal, which is defined loosely as the frequency range around f_c that contains most of the energy or power of the signal, is normally small compared to the carrier frequency f_c.

Representations

A bandpass signal can be described mainly by three representations: *envelope-phase*, *in-phase and quadrature* or I-Q, and *complex envelope*. In the envelope-phase representation, a bandpass signal $x(t)$ can be expressed as

$$x(t) = A(t)\cos[2\pi f_c t + \theta(t)] \tag{2.248}$$

where f_c is the carrier frequency, $A(t)$ is the time-varying amplitude, and $\theta(t)$ is the time-varying phase. When a bandpass signal is employed to carry information, the amplitude $A(t)$

and/or the phase $\theta(t)$ may vary according to the information, resulting in various types of modulation techniques.

In the I-Q representation, the bandpass signal $x(t)$ can be expressed as follows:

$$x(t) = x_I(t)\cos 2\pi f_c t - x_Q(t)\sin 2\pi f_c t \tag{2.249}$$

The components $x_I(t)$ and $x_Q(t)$ are referred to as the in-phase and quadrature components of $x(t)$, respectively. The term quadrature results from the fact that $\sin 2\pi f_c t$ is in phase-quadrature with respect to $\cos 2\pi f_c t$, that is, $\pi/2$ radians or 90° out-of-phase.

For the complex envelope representation, the bandpass signal $x(t)$ can be written as

$$x(t) = \mathrm{Re}\{x_L(t)\,\mathrm{e}^{\mathrm{j}2\pi f_c t}\} \tag{2.250}$$

where the complex envelope $x_L(t)$ of $x(t)$ is often referred to as the *equivalent lowpass signal*. The three representations of a bandpass signal are equivalent and their relations are shown below:

$$A(t) = \sqrt{x_I^2(t) + x_Q^2(t)} = |x_L(t)| \tag{2.251}$$

$$x_L(t) = x_I(t) + \mathrm{j}x_Q(t) = A(t)\,\mathrm{e}^{\mathrm{j}\theta(t)} \tag{2.252}$$

$$\theta(t) = \tan^{-1}\left[\frac{x_Q(t)}{x_I(t)}\right] \tag{2.253}$$

$$x_I(t) = \mathrm{Re}\{x_L(t)\} = A(t)\cos\theta(t) \tag{2.254}$$

$$x_Q(t) = \mathrm{Im}\{x_L(t)\} = A(t)\sin\theta(t) \tag{2.255}$$

Example 2.40 Fourier transform of the complex envelope representation

Considering the Fourier transform $X(f)$ of the complex envelope representation of the bandpass signal $x(t)$ in (2.250), we get

$$\begin{aligned} X(f) &= \int_{-\infty}^{\infty} \mathrm{Re}\left\{x_L(t)\,\mathrm{e}^{\mathrm{j}2\pi f_c t}\right\}\mathrm{e}^{-\mathrm{j}2\pi f t}\,\mathrm{d}t \\ &= \int_{-\infty}^{\infty} \frac{1}{2}\left[x_L(t)\,\mathrm{e}^{\mathrm{j}2\pi f_c t} + x_L^*(t)\,\mathrm{e}^{-\mathrm{j}2\pi f_c t}\right]\mathrm{e}^{-\mathrm{j}2\pi f t}\,\mathrm{d}t \end{aligned} \tag{2.256}$$

Applying the conjugation and frequency shifting properties in Table 2.1 we obtain

$$X(f) = \frac{1}{2}\left[X_L(f - f_c) + X_L^*(-f - f_c)\right] \tag{2.257}$$

where $X_L(f)$ is the Fourier transform of the equivalent lowpass signal $x_L(t)$ of $x(t)$. Thus, the characteristics of $X(f)$ are all contained in $X_L(f)$.

■

Example 2.41 Equivalent lowpass signal
Consider the following sinusoidal pulse signal with duration $0 \le t < T$:

$$x(t) = p(t)\,\cos\left(2\pi f_c t + \frac{\pi}{4}\right) \tag{2.258}$$

where the function $p(t)$ is defined in (2.26). The envelope $A(t)$ and the phase $\theta(t)$ are given by

$$A(t) = p(t) \tag{2.259}$$

$$\theta(t) = \frac{\pi}{4} \tag{2.260}$$

By expanding $x(t)$ we can write (2.258) as follows:

$$\begin{aligned} x(t) &= \left[p(t)\,\cos\frac{\pi}{4}\right]\,\cos\,2\pi f_c t - \left[p(t)\,\sin\frac{\pi}{4}\right]\,\sin\,2\pi f_c t \\ &= \left[\frac{\sqrt{2}}{2}p(t)\right]\,\cos\,2\pi f_c t - \left[\frac{\sqrt{2}}{2}p(t)\right]\,\sin\,2\pi f_c t \end{aligned} \tag{2.261}$$

Therefore, the in-phase and quadrature components are

$$x_I(t) = \frac{\sqrt{2}}{2}p(t) \tag{2.262}$$

$$x_Q(t) = \frac{\sqrt{2}}{2}p(t) \tag{2.263}$$

Finally, the complex envelope or equivalent lowpass signal $x_L(t)$ is given by

$$x_L(t) = \frac{\sqrt{2}}{2}p(t) + \mathrm{j}\frac{\sqrt{2}}{2}p(t) \tag{2.264}$$

■

Response of an LTI bandpass system

An LTI bandpass system is designed to pass and/or shape a bandpass signal. Its transfer function normally centers around the carrier frequency f_c of the bandpass signal and is almost zero at the zero frequency. The impulse response $h(t)$ of an LTI bandpass system can be expressed by the complex envelope representation as follows:

$$h(t) = \mathrm{Re}\left[h_L(t)\,\mathrm{e}^{\mathrm{j}2\pi f_c t}\right] \tag{2.265}$$

where the complex envelope $h_L(t)$ is called the impulse response of the equivalent lowpass system. Following the derivation of (2.257) we arrive at the Fourier transform $H(f)$ of $h(t)$ as

$$H(f) = \frac{1}{2}\left[H_L(f - f_c) + H_L^*(-f - f_c)\right] \tag{2.266}$$

where $H_L(f)$ is the Fourier transform of $h_L(t)$. Now assume that the input signal $x(t)$ has a Fourier transform $X(f)$, the output signal $y(t)$ of the bandpass system is

$$y(t) = h(t) * x(t) \tag{2.267}$$

or equivalently, the Fourier transform $Y(f)$ of $y(t)$ is given by

$$Y(f) = H(f)X(f) \tag{2.268}$$

Substituting (2.257) and (2.266) into (2.268) we have

$$\begin{aligned} Y(f) &= \frac{1}{4}\left[H_L(f - f_c) + H_L^*(-f - f_c)\right]\ \left[X_L(f - f_c) + X_L^*(-f - f_c)\right] \\ &= \frac{1}{4}\left[H_L(f - f_c)X_L(f - f_c) + H_L^*(-f - f_c)X_L^*(-f - f_c)\right] \end{aligned} \tag{2.269}$$

We arrive at the above equation with the assumption that $H_L(f - f_c)$ and $X_L^*(-f - f_c)$ do not overlap, and neither do $H_L^*(-f - f_c)$ and $X_L(f - f_c)$. Thus, we have the relations $H_L(f - f_c)X_L^*(-f - f_c) = 0$ and $H_L^*(-f - f_c)X_L(f - f_c) = 0$. Define the following parameter

$$Y_L(f) = \frac{1}{2}H_L(f)X_L(f) \tag{2.270}$$

Then, we have

$$Y(f) = \frac{1}{2}\left[Y_L(f - f_c) + Y_L^*(-f - f_c)\right] \tag{2.271}$$

Taking the inverse Fourier transform of $Y(f)$ yields the output response $y(t)$:

$$\begin{aligned} y(t) &= \frac{1}{2}\left[y_L(t)\,\mathrm{e}^{\mathrm{j}2\pi f_c t} + y_L^*(t)\,\mathrm{e}^{-\mathrm{j}2\pi f_c t}\right] \\ &= \mathrm{Re}\{y_L(t)\,\mathrm{e}^{\mathrm{j}2\pi f_c t}\} \end{aligned} \tag{2.272}$$

where the complex envelope $y_L(t)$ of $y(t)$ is the inverse Fourier transform of $Y_L(f)$ in (2.270) and is given by

$$y_L(t) = \frac{1}{2}h_L(t) * x_L(t) \tag{2.273}$$

In summary, when the bandwidths of both bandpass signal and bandpass system are much smaller than the carrier frequency such that the assumption leading to (2.269) holds, we can obtain the response $y(t)$ via (2.267) or via the equivalent lowpass operation given in (2.272) and (2.273).

2.12 Summary

In this chapter we have provided a fairly detailed study of deterministic signals. We have placed the emphasis on continuous-time signals that are often employed in practical communications systems. The concept of continuous-time digital signals was introduced via examples such as PSK and ASK.

We then introduced the concept of power and energy signals. We showed that a power signal has infinite energy and an energy signal has zero average power. It was noted that the digital signals employed in practice are energy signals and an infinite sequence of them forms a power signal.

The study of energy signals has led to a special class of important digital signals, namely, orthogonal signals, that are widely used in commercial and military systems. The most well-known pair of orthogonal signals are the cosine and sine functions with identical frequency. We also studied the well-known orthogonal Walsh functions, which are derived from the Hadamard matrix. The Walsh functions are employed in the cellular standard IS-95.

Further study of finite-energy signals has led to the concept of signal space. The Gram–Schmidt procedure enables us to express continuous-time finite-energy signals as vectors in the signal space, thus simplifying the analysis.

A review of linear time-invariant systems was provided together with the important convolution operation. It is worth mentioning that the majority of communication systems are LTI systems. Even nonlinear communication systems contain many subsystems that are linear time-invariant.

Two great techniques that are indispensable in the analysis of communications systems were presented. They are Fourier series for periodic signals and Fourier transform for aperiodic signals.

The study of Fourier series has revealed a number of important properties. The Parseval relation states that the average power in a periodic signal equals the sum of the average power in all of its harmonics components. The power in a harmonic component is equal to the squared magnitude of the corresponding Fourier series coefficient. This relation leads to the study of power spectral density, which consists of an infinite series of weighted impulses at harmonic frequencies. As the signal propagates through an LTI system, its power spectral density is shaped by the transfer function of the system. The output power spectral density function is equal to the product of the squared magnitude of the system's transfer function and the input power spectral density.

The study of Fourier transform of aperiodic finite energy signals has provided a number of interesting results. The energy of a signal is equal to the total area under the energy spectral density function, which is simply the squared magnitude of the Fourier transform of the signal. This is the Parseval relation for an energy signal. One surprising result is that a continuous-time periodic signal has a Fourier transform that is an infinite series of impulses at harmonic frequencies. The coefficients of the impulses are simply the Fourier series coefficients. As an energy signal propagates through an LTI system, its Fourier transform is shaped by the transfer function of the system. The Fourier transform of the output signal is simply the product of the system's transfer function and the Fourier transform of the input signal.

It was shown that the autocorrelation and the energy spectral density of an energy signal form a Fourier transform pair. For a power signal, the autocorrelation and the power spectral density also form a Fourier transform pair. The spectral density of the output signal of an LTI system is equal to the product of the squared

magnitude of the system's transfer function and the spectral density of the input signal. This applies to both energy and power signals.

Again using the Fourier transform we have studied the sampling of a bandlimited signal. It was shown that the original signal can be recovered from the sampled signal by means of an ideal lowpass filter provided that the sampling rate exceeds the Nyquist rate The Nyquist rate is exactly twice the absolute bandwidth or highest frequency of the original signal. If the sampling rate is smaller than the Nyquist rate, then aliasing results, and the original signal cannot be recovered from the sampling signal.

In the last section we have investigated the representations of bandpass signals which are employed in practical communication systems. Three representations were considered, namely, envelope-phase, in-phase and quadrature (I-Q), and complex envelope representations. The relationship between a bandpass signal and its equivalent lowpass signal was studied. The equivalent lowpass signal is simply the complex envelope of the bandpass signal.

Problems

1. Examine whether the following signals are periodic: $s(t) = \sin 6\pi t + \cos 7\pi t$, $s(t) = 5\cos(14\pi t + \theta) + 7\sin(42\pi t + 6\theta)$. Specify the smallest period.
2. Write the expression for the PSK waveform $s(t)$ that represents four consecutive bits 1011, assuming that the leftmost bit starts at time $t = 0$ and the carrier frequency is an integer multiple of $1/T_b$, where T_b is the bit time.
3. Write the expression for the QPSK waveform $s(t)$ that represents four consecutive symbols 10 01 11 00, assuming that the leftmost symbol starts at time $t = 0$ and the carrier frequency is an integer multiple of $1/T_s$, where T_s is the symbol time.
4. Write the expression for the 4ASK waveform $s(t)$ that represents four consecutive symbols 00 01 10 11, assuming that the leftmost symbol starts at time $t = 0$ and the carrier frequency is an integer multiple of $1/T_s$, where T_s is the symbol time.
5. Find the energy and power of the following signals: $s(t)=10\sin 6\pi t+3\cos 7\pi t\,(\mathrm{V})$, $s(t)=\sin(5\pi t+\theta)+2\cos(7\pi t+\phi)\,(\mathrm{mV})$, and $s(t)=20\cos(15\pi t+\theta)\cos(25\pi t+\phi)\,(\mathrm{V})$.
6. Find the energy of the unit impulse function. Is it a power signal?
7. Find the energy and power of the unit step function.
8. Find the energy of the signal $s(t) = 2B\frac{\sin 2\pi Bt}{2\pi Bt}$.
9. Find the PSK signal energy assuming the bit time $T_b = 10^{-4}$ s and the amplitude $A = 100$ mV. Find the QPSK signal energy assuming the symbol time $T_s = 2 \times 10^{-4}$ s and the amplitude $A = 100$ mV.
10. Consider the following two signals for $0 \le t < T_b$:

$$s_1(t) = A\cos(2\pi f_1 t + \theta_1)$$
$$s_2(t) = A\cos(2\pi f_2 t + \theta_2)$$

where for a positive integer $\ell > 1$ and $f_c = \ell/T_b$ we have

$$f_1 = f_c - \frac{1}{2T_b}$$
$$f_2 = f_c + \frac{1}{2T_b}$$

Show that the two signals are orthogonal.

11. Consider the following two signals for $0 \leq t < T_b$:

$$s_1(t) = A\cos\left[2\pi\left(f_c + \frac{1}{4T_b}\right)t + \theta_n\right]$$
$$s_2(t) = A\cos\left[2\pi\left(f_c - \frac{1}{4T_b}\right)t + \theta_n\right]$$

where $\theta_n \in \{0, \pi\}(\text{mod } 2\pi)$. Show that the two signals are quasi-orthogonal assuming that the frequency f_c is an integer multiple of $1/T_b$.

12. Consider the following two signals in the interval $0 \leq t < T_b$:

$$s_1(t) = A\cos(2\pi ft + \theta)$$
$$s_2(t) = A\cos(2\pi[f + \Delta f]t + \theta)$$

where $f \gg \Delta f$. The requirement for both signals to be quasi-orthogonal is their inner product must be less than 0.01 of the energy of $s_1(t)$ or $s_2(t)$. What would be the range of Δf?

13. Consider the cascade of two identical 4-ary Walsh functions representing the third row of the Hadamard matrix $\mathbf{H}_4$. Find all 8-ary Walsh functions with the same period that are orthogonal with it.
14. Show that the Hadamard matrix of order $M = 2^n$ divided by $\sqrt{M}$ is a unitary matrix.
15. Use the Gram–Schmidt procedure to find the orthonormal basis functions for the following set of four quadrature phase shift keying signals: $s_n(t) = \cos[(2\pi/T)t + (n-1)\pi/2],\ \ n = 1, 2, 3, 4;\ \ 0 \leq t < T$ starting with signal $s_1(t)$. Express $s_n(t)$ in terms of the basis functions and find the corresponding signal vectors. Calculate the Euclidean distance between two adjacent signal vectors.
16. Consider the following set of signals:

$$s_n(t) = \{\pm A\cos 2\pi f_c t,\ \pm 3A\cos 2\pi f_c t,\ 0 \leq t < T_s\}$$

Let E be the smallest signal energy. Find the basis function and express each signal in the set in terms of the basis function and E. Plot the signal space.

17. Determine if the following systems are LTI:
    (a) $y(t) = \frac{\mathrm{d}}{\mathrm{d}t}[3x(t) - x(t-7)]$
    (b) $y(t) = \int_0^{7t} x(\tau)\mathrm{d}\tau$
    (c) $y(t) = x(t)\sin 300\pi t$
    (d) $y(t) = x^2(t)$
    (e) $y(n) = 2n + 3x(n) + x(n+3)$
18. Find the convolution of the waveform $x(t) = p(t) - p(t-T) + p(t+T)$ with $p(t)$, where $p(t)$ is a unit amplitude pulse of duration T.

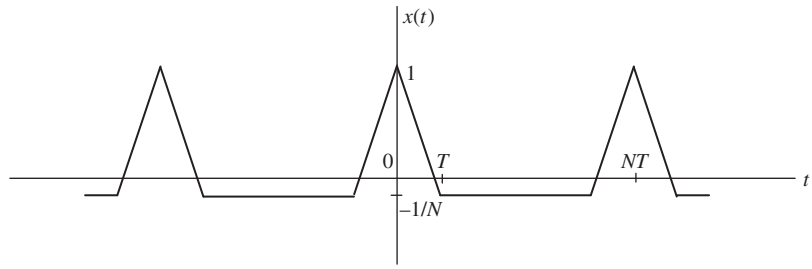

Figure 2.40 The periodic signal $x(t)$ with period NT.

19. Find the convolution of $p(t)$ and $h(t) = tp_{2T}(t)$, where $p(t)$ is a unit amplitude pulse of duration T, and $p_{2T}(t)$ is a unit amplitude pulse of duration $2T$.
20. Find the Fourier series coefficients of $x(t) = \sum_{k=-\infty}^{\infty} \delta(t - kT)$.
21. Consider the periodic signal $x(t) = \sum_{k=-\infty}^{\infty} w_n(t - kT)$ with period T, where $w_n(t)$ is the nth Walsh function corresponding to the $M \times M$ Hadamard matrix. Express the signal $x(t)$ as a Fourier series for (a) $M = 2$ and $n = 2$ (second row of the Hadamard matrix); and (b) $M = 4$ and $n = 3$ (third row of the Hadamard matrix).
22. Find the Fourier series of the periodic signal $y(t) = x(nt - t_0)$, where $x(t)$ is a periodic signal with period T, t_0 is an arbitrary time, and n is an integer.
23. Consider the periodic signal $x(t) = \cos 20\pi t + \cos 60\pi t + \cos 100\pi t$. Construct a circuit to recover the third harmonic.
24. Consider a periodic signal $x(t)$ with period T. Find the Fourier coefficients of the following signal in terms of those of $x(t)$: $y(t) = \mathrm{d}^2x(7t - 3)/\mathrm{d}t^2$.
25. Find the Fourier transform of the periodic signal shown in Figure 2.40.
26. A periodic signal with period T can be expressed in the summation form $x(t) = \sum_{k=-\infty}^{\infty} m(t - kT)$.
    (a) Show that the Fourier series coefficients of $x(t)$ are given by

$$a_k = \frac{1}{T}\int_{-\infty}^{\infty} m(t)\, \mathrm{e}^{-\mathrm{j}2\pi kt/T}\, \mathrm{d}t = \frac{1}{T}M(k/T)$$

    where $M(k/T)$ is the Fourier transform of $m(t)$ evaluated at $f = k/T$.
    (b) Show that $x(t) = \frac{1}{T}\sum_{k=-\infty}^{\infty} M(k/T)\mathrm{e}^{\mathrm{j}2\pi kt/T}$.
27. Consider a *Hilbert* transformer with impulse response $h(t) = 1/\pi t$. Let $x(t)$ be the input signal. Write the expression for the output signal $y(t) = h(t) * x(t)$, that is, the Hilbert transform of $x(t)$. Find $y(t)$ when $x(t) = \sin nt$.
28. Given the signal $x(t) = \frac{A}{2}[m(t)\cos 2\pi f_c t - \hat{m}(t)\sin 2\pi f_c t]$, where $\hat{m}(t) = m(t) * 1/\pi t$ is the Hilbert transform of $m(t)$, find the Fourier transform of $x(t)$.
29. Consider the inner product of two following signals $x_1(t) = p(t)\cos 2\pi f_c t$ and $x_2(t) = p(t)\sin 2\pi f_c t$ given the Fourier transform $P(f)$ of $p(t)$. We have

$$\langle x_1, x_2 \rangle = \int_{-\infty}^{\infty} x_1(t)x_2^*(t)\, \mathrm{d}t$$

    Find the sufficient conditions for $x_1(t)$ and $x_2(t)$ to be orthogonal in terms of $P(f)$.

30. An *upconverter* shifts the carrier frequency f_0 of a modulated signal $x(t) = R(t)\cos[2\pi f_0 t + \psi(t)]$ to a higher frequency $f_c \gg f_0$ for transmission in a designated spectrum without affecting the envelope $R(t)$ and the phase $\psi(t)$. The reason is that it is much less expensive to design a modulator at the low intermediate frequency (IF) f_0 than to design it at the high radio frequency (RF) f_c. Given a local reference sinusoidal signal at frequency f_{lo}, design an upconverter to accomplish the frequency shifting.
31. A *downconverter* shifts the carrier frequency f_c of a modulated signal $y(t) = R(t)\cos[2\pi f_c t + \psi(t)]$ to a lower frequency $f_0 \ll f_c$ for demodulation without affecting the envelope $R(t)$ and the phase $\psi(t)$. The reason is that it is much less expensive to design a demodulator at the low intermediate frequency (IF) f_0 than to design it at the high radio frequency (RF) f_c. Given a local reference sinusoidal signal at frequency f_{lo}, design a downconverter to accomplish the frequency shifting.
32. Find the autocorrelation of the following function $x(t) = 7\cos 2000\pi t$. What is its power spectral density function? Calculate the power of $x(t)$ via two methods.
33. Determine the impulse response $h(t)$ of a LTI system whose input is $x(t)$ so that the output $y(t)$ is the autocorrelation of $x(t)$.
34. Given the power signal $x(t)$ with autocorrelation $R_x(\tau)$, determine the autocorrelation $R_y(\tau)$ of $y(t) = x(t)\cos 2\pi f_c t$.
35. Given the power signals $x(t)$ and $\hat{x}(t)$ with autocorrelation $R_x(\tau)$ and $R_{\hat{x}}(\tau)$, respectively, determine the autocorrelation $R_y(\tau)$ of $y(t) = x(t)\cos 2\pi f_c t - \hat{x}(t)\sin 2\pi f_c t$.
36. The following signal $x(t) = \cos 20\pi t$ is sampled at rate $f_s = 8$ Hz. Plot the Fourier transform of the sampled signal. Can an ideal lowpass filter with a bandwidth of 11 Hz be able to extract $x(t)$?
37. The signal $x(t) = \sin(2\pi f_0 t + \theta)$ is sampled at a rate $f_s = 2f_0$. Can an ideal lowpass filter with a cut-off frequency f_0 recover the signal $x(t)$?
38. Consider the bandpass signal $y(t) = x(t)\sin 2\pi f_c t$, where $x(t)$ is a bandlimited lowpass signal given as $x(t) = 2B(\sin 2\pi Bt/2\pi Bt)$. The frequency f_c is much larger than B. What is the Nyquist sampling frequency? Plot the Fourier transform of the sampling signal. Find the smallest f_c so that the signal $y(t)$ can be recovered without aliasing.
39. Consider the bandpass signal $x(t) = x_I(t)\cos 2\pi f_c t - x_Q(t)\sin 2\pi f_c t$, where both lowpass signals $x_I(t)$ and $x_Q(t)$ are bandlimited to B (Hz).
    (a) First, perform frequency shifting and lowpass filtering of $x(t)$ to produce $x_I(t)$. Next, perform frequency shifting and lowpass filtering of $x(t)$ to produce $x_Q(t)$.
    (b) Sample both $x_I(t)$ and $x_Q(t)$ at Nyquist rate. Write the expressions for both $x_I(t)$ and $x_Q(t)$ in terms of their samples.
    (c) Write the expression for the samples of $x(t)$ in terms of the samples of $x_I(t)$ and $x_Q(t)$.
    (d) Write the expression for $x(t)$ in terms of its samples.
40. Consider the bandpass signal $x(t) = x_I(t)\cos 2\pi f_c t - x_Q(t)\sin 2\pi f_c t$, where both lowpass signals $x_I(t)$ and $x_Q(t)$ are bandlimited to B (Hz).
    (a) Multiply $x(t)$ with $e^{-j2\pi f_c t}$. Write the expression for the resulting signal $x(t)e^{-j2\pi f_c t}$.
    (b) Filter $x(t)e^{-j2\pi f_c t}$ with an ideal complex-valued lowpass filter with cutoff frequency equal to B. Write the expression for the output signal $y(t)$.

41. Design an *upconverter* to shift the carrier frequency f_0 of the bandpass signal $x(t) = \mathrm{Re}\{x_L(t)\, e^{j2\pi f_0 t}\}$ to the new carrier frequency f_c, where $f_c \gg f_0$, using the complex local reference signal $e^{j2\pi f_{lo} t}$ at frequency $f_{lo} \gg f_0$. Identify the signals at the output of every device employed in the upconverter.
42. Design a *downconverter* to shift the carrier frequency f_c of the bandpass signal $x(t) = \mathrm{Re}\{x_L(t)\, e^{j2\pi f_c t}\}$ to the new carrier frequency f_0, where $f_0 \ll f_c$, using the complex local reference signal $e^{-j2\pi f_{lo} t}$ at frequency $f_{lo} \gg f_0$. Identify the signals at the outputs of all devices employed in the downconverter.

Further reading

For a thorough analysis of Fourier series, Fourier transforms, discrete-time Fourier transforms, and z-transforms we recommend Oppenheim, Willsky, and Nawab [1]. Advanced materials in signal analysis can be found in Bracewell [2].

Bibliography

1. A. V. Oppenheim and A. S. Willsky, with S. Hamid Nawab, *Signals and Systems*, 2nd edition, Upper Saddle River, NJ: Prentice Hall, 1997.
2. R. N. Bracewell, *The Fourier Transform and its Applications*, 2nd edition, revised, New York: McGraw-Hill, 1986.
3. L. W. Couch II, *Digital and Analog Communication Systems*, 7th edition, Harlow: Prentice Hall, 2007.
4. S. Haykin, *Communication Systems*, 3rd edition, Chichester: John Wiley & Sons, 1994.
5. R. E. Ziemer and W. H. Tranter, *Principles of Communications*, 4th edition, Chichester: John Wiley & Sons, 1995.
6. J. G. Proakis and M. Salehi, *Fundamentals of Communication Systems*, Hallow: Pearson Prentice Hall, 2005.
7. A. Bruce Carlson, P. B. Crilly, and J. C. Rutledge, *Communication Systems*, 4th edition, New York: McGraw-Hill, 2002.

3 Random signal analysis

Introduction

So far we have studied deterministic signals that are used to carry information. As far as the receiver is concerned, the stream of transmitted digital waveforms that carries information symbols is a random signal because the information is random. Also, as the transmitted signal travels through the channel, it is modified by noise, which is a *random signal* and is often referred to as a *random process*. Therefore, the receiver receives the transmitted signal plus noise. Such a channel is called an *additive noise* channel. Furthermore, wireless signals such as cellular signals and wireless LAN and MAN signals always travel through a *time-varying multipath fading* channel, which causes the *signal envelopes* to vary randomly. The *time-varying* phenomenon arises from *Doppler shift*, which is the result of the motion of the transmitters and/or receivers. The *multipath fading* is the result of the destructive interference of signal rays that travel via *randomly delayed and attenuated paths.* Therefore, the received signal itself becomes a random signal. To analyze random signals in communication receivers we need to know their statistics. In this section we explore some tools necessary for such a task. We divide the discussion into reviews of probability theory and random variables, and study of random processes and their applicability to communication theory.

3.1 Review of probability theory

Let $\boldsymbol{S}$ denote the *sample space*. The elements of $\boldsymbol{S}$ are called *experimental outcomes*, and its subsets are called *events*. The sample space $\boldsymbol{S}$ is a *certain event*, and the empty set ϕ is the impossible event. The *union* of two events A and B is denoted as $A \cup B$ and their intersection as AB (also $A \cap B$). For an event A we assign a number $\Pr(A)$ called *probability of event A* that satisfies the following *axioms*:

I. $\Pr(A) \geq 0$
II. $\Pr(\boldsymbol{S}) = 1$
III. If $AB = \phi$ then $\Pr(A \cup B) = \Pr(A) + \Pr(B)$

The following two theorems are widely used in the performance analysis of digital communications systems.

Total probability theorem

Let $\{A_1, A_2, \ldots, A_n\}$ be the partition of the sample space S and let B be an event in S. The total probability theorem states the following result:

$$\Pr(B) = \sum_{i=1}^{n} \Pr(B|A_i) \Pr(A_i) \tag{3.1}$$

where $\Pr(B|A_i)$ is the conditional probability of the event B given that the event A_i occurred.

Bayes theorem

The a-posteriori probability $\Pr(A_i|B)$ is expressed in terms of the a-priori probability $\Pr(A_i)$, the conditional probability $\Pr(B|A_i)$, and the total probability $\Pr(B)$ as follows:

$$\Pr(A_i|B) = \frac{\Pr(B|A_i) \Pr(A_i)}{\sum_{i=1}^{n} \Pr(B|A_i) \Pr(A_i)} = \frac{\Pr(B, A_i)}{\sum_{i=1}^{n} \Pr(B|A_i) \Pr(A_i)} \tag{3.2}$$

Here $\Pr(B, A_i)$ is the joint probability of B and A_i.

Independence

The concept of independence plays an important role in signal analysis. Two events A and B are *independent* if

$$\Pr(AB) = \Pr(A) \Pr(B) \tag{3.3}$$

Union bound

Let $\bigcup_{i=1}^{n} A_i$ be the union of n events A_i, then, we have the following union bound:

$$\Pr\left(\bigcup_{i=1}^{n} A_i\right) \leq \sum_{i=1}^{n} \Pr(A_i) \tag{3.4}$$

In the following discussion we study *random variables* that are essential to signal analysis where they represent *decision voltage samples* at the receiver

3.2 Random variables

In a digital communication system the received signal representing a symbol is a random signal due to noise and other factors such as fading. It is processed to achieve the maximum

signal-to-noise ratio and then sampled to obtain a decision sample for the detector to decide which symbol had been transmitted. The decision sample is referred to mathematically as a *random variable*.

A random variable is a function defined on the sample space. We use a capital letter such as X for a random variable and the lower-case letter x for the value it assumes. Depending on the experiment, the random variable X can be *discrete* or *continuous.* Let X be a discrete random variable and let x_i, $i = 1, 2, \ldots, n$, be the values that X assumes. For each event $\{X = x_i\}$ and its probability $\Pr\{X = x_i\}$ the function

$$p_X(x_i) = \Pr\{X = x_i\} \qquad i = 1, 2, \ldots, n \tag{3.5}$$

is called the (*probability*) *distribution function* of X which satisfies $p_X(x_i) \geq 0$ and $\sum_{i=1}^{n} p_X(x_i) = 1$. Now let X be a continuous random variable. The *distribution function* of X is then defined as

$$F_X(x) = \Pr(X \leq x) \qquad -\infty < x < \infty \tag{3.6}$$

It satisfies the properties $F_X(-\infty) = 0$, $F_X(+\infty) = 1$, and $F_X(x_2) - F_X(x_1) = \Pr(x_1 < X \leq x_2)$. The *density function* of X is the *derivative* of the distribution function $F_X(x)$ and is given as

$$f_X(x) = \frac{\mathrm{d}F_X(x)}{\mathrm{d}x} \tag{3.7}$$

This yields the following equivalent relationship:

$$F_X(x) = \Pr(X \leq x) = \int_{-\infty}^{x} f_X(y)\,\mathrm{d}y \tag{3.8}$$

The density function satisfies the following properties:

$$f_x(x) \geq 0 \qquad \int_{-\infty}^{\infty} f_X(x)\,\mathrm{d}x = 1 \qquad \Pr(x_1 < x \leq x_2) = \int_{x_1}^{x_2} f_X(x)\,\mathrm{d}x \tag{3.9}$$

The *joint distribution function* of two random variables X and Y is defined as

$$F_{XY}(x, y) = \Pr(X \leq x, Y \leq y) \tag{3.10}$$

and the corresponding *joint density function* is

$$f_{XY}(x, y) = \frac{\partial^2 F_{XY}(x, y)}{\partial x\,\partial y} \tag{3.11}$$

Thus, the density function of either X or Y can be found by integrating its joint density function with respect to the other variable. We have

$$f_X(x) = \int_{-\infty}^{\infty} f_{XY}(x, y)\,\mathrm{d}y \tag{3.12}$$

Bayes theorem and total probability revisited

For continuous random variables, Bayes theorem is expressed as follows:

$$f_{X|Y}(x|y) = \frac{f_{Y|X}(y|x)f_X(x)}{f_Y(y)} = \frac{f_{Y|X}(y|x)f_X(x)}{\int f_{XY}(x,y)\,\mathrm{d}x} = \frac{f_{Y|X}(y|x)f_X(x)}{\int f_{Y|X}(y|x)f_X(x)\mathrm{d}x} = \frac{f_{XY}(x,y)}{\int f_{Y|X}(y|x)f_X(x)\mathrm{d}x} \tag{3.13}$$

where $f_{X|Y}(x|\ y)$ is the conditional density function of X given Y and the joint density is given by

$$f_{XY}(x,y) = f_{Y|X}(y|x)f_X(x) = f_{X|Y}(x|y)f_Y(y) \tag{3.14}$$

If X and Y are *independent* random variables, then the following relationship holds:

$$f_X(x,y)\ = f_X(x)f_Y(y) \tag{3.15}$$

The *total probability* theorem is expressed explicitly above as

$$f_Y(y) = \int f_{Y|X}(y|x)f_X(x)\,\mathrm{d}x \tag{3.16}$$

In random signal analysis it is sometimes necessary to get a snapshot of a random variable, such as a decision sample at the receiver. This can be done via the *statistical averages* of the random variable, such as the *mean value* or *expected value* $\overline{X} = \mathbf{E}(X)$, the *mean-square value* $\overline{X^2} = \mathbf{E}(X^2)$, and the *variance* $\sigma_X^2 = \mathrm{Var}(X) = \mathbf{E}\{(X - \overline{X})^2\}$. These quantities are defined for both discrete and continuous random variables as follows:

$$\overline{X} = \mathbf{E}(X) = \sum_i x_i p_X(x_i) \qquad \overline{X} = \mathbf{E}(X) = \int_{-\infty}^{\infty} x f_X(x)\,\mathrm{d}x \tag{3.17}$$

$$\overline{X^2} = \mathbf{E}(X^2) = \sum_i x_i^2 p_X(x_i) \qquad \overline{X^2} = \mathbf{E}(X^2) = \int_{-\infty}^{\infty} x^2 f_X(x)\,\mathrm{d}x \tag{3.18}$$

$$\sigma_X^2 = \mathrm{Var}(X) = \mathbf{E}\{(X - \overline{X})^2\} = \mathbf{E}(X^2) - \overline{X}^2 \tag{3.19}$$

The quantity σ_X is called the *standard deviation* of the random variable X. The mean and mean-square values of a random variable are also referred to as its *first* and *second moments.* The nth moment of the random variable X is defined as

$$\overline{X^n} = \mathbf{E}(X^n) = \sum_i x_i^n p_X(x_i) \qquad \overline{X^n} = \mathbf{E}(X^n) = \int_{-\infty}^{\infty} x^n f_X(x)\,\mathrm{d}x \tag{3.20}$$

The above results can be generalized to a function $g(X)$. For example, the expected value of $g(X)$ is given by

$$\mathbf{E}\{g(X)\} = \sum_i g(x_i)p_X(x_i) \qquad \mathbf{E}\{g(X)\} = \int_{-\infty}^{\infty} g(x)f_X(x)\,\mathrm{d}x \tag{3.21}$$

In the following discussion we present the application of probability theory and random variables to the analysis of digital communication signals from the standpoint of random processes.

3.3 Random processes

In a communication system the received signal is always a random signal due to the fact that the transmitted signal is subjected to channel distortion and, moreover, because it is contaminated by noise and possibly unintended or intended interference. Therefore, the performance analysis of a communication signal cannot be based solely on the theory developed for deterministic signals. For example, the Gaussian channel required the knowledge of the noise variance (noise power) together with the signal power to establish the signal-to-noise ratio at the receiver. In order to calculate the noise variance, the statistics of noise at the receiver must be known a priori. Furthermore, filters employed at the receiver for signal processing can affect the noise statistics. For example, if Gaussian noise is processed by a linear filter, will the noise at the filter output still be Gaussian? In this section we study random processes to provide the background for applying random signal analysis to communication systems. We use the term *random process* as customarily cited in the literature to include noise and other random signals of interest to communication theorists. We will use a time function to represent a sample of a random process. We consider real-valued processes unless stated otherwise.

Definition 3.1 A random process is an indexed sequence (ensemble, family) of random variables. The index can be a real variable t for a continuous-time random process $X(t)$ or an integer i for a discrete-time random process X_i.

The definitions of *mean value*, *mean-square value*, and *variance* of a random variable also apply to a random process. The mean value $\mathbf{E}\{X(t)\}$ of a noise voltage $X(t)$ across a 1 Ω resistor represents its dc-component, its mean-square value $\mathbf{E}\{X^2(t)\}$ is the power, and its variance $\mathbf{E}\{[X(t) - \mathbf{E}\{X(t)\}]^2\}$ is the ac-power.

Autocorrelation and autocovariance

The most important parameter of a random process is its *autocorrelation*, which is defined as follows:

$$R_X(t_1, t_2) = \mathbf{E}\{X(t_1)X(t_2)\} \tag{3.22}$$

The *autocovariance* is simply the autocorrelation of a random process minus its mean value, that is,

$$C_X(t_1, t_2) = \mathbf{E}\{[X(t_1) - \mathbf{E}\{X(t_1)\}][X(t_2) - \mathbf{E}\{X(t_2)\}]\} \tag{3.23}$$

Therefore, the autocorrelation and autocovariance are related by the following expression:

$$C_X(t_1, t_2) = R_X(t_1, t_2) - \mathbf{E}\{X(t_1)\}\mathbf{E}\{X(t_2)\} \tag{3.24}$$

It is seen that the autocovariance is zero, that is, $C_X(t_1, t_2) = 0$ if and only if $R_X(t_1, t_2) = \mathbf{E}\{X(t_1)\}\mathbf{E}\{X(t_2)\}$. In this case the two random variables $X(t_1)$ and $X(t_2)$ are *uncorrelated*. Obviously, if they are *independent* then the autocovariance is also zero. Also $R_X(t, t) = \mathbf{E}\{X^2(t)\}$ is the average power of the random process and $C_X(t, t) = R_X(t, t) - [\mathbf{E}\{X(t)\}]^2 = \mathbf{E}\{X^2(t)\} - [\mathbf{E}\{X(t)\}]^2 = \mathrm{Var}\{X(t)\}$ is its ac-power.

Example 3.1 Autocorrelation of a sequence of antipodal signals

Consider an antipodal signal sequence $X(t) = \sum_{i=-\infty}^{\infty} d_i p(t - iT_b)$ that represents *independent and equally likely* bits $\{0, 1\}$, where $p(t)$ is the squared pulse shape of unit amplitude and duration T_l, which is a bit time, and $d_i \in \{1, -1\}$ represents the normalized signal amplitudes. The mapping $0 \rightarrow 1$ *and* $1 \rightarrow -1$ maps bit 0 to amplitude 1 and bit 1 to amplitude -1 (the mapping $0 \rightarrow -1$ *and* $1 \rightarrow 1$ maps bit 0 to amplitude -1 and bit 1 to amplitude 1 would give the same result). Since the amplitudes are equally likely, the mean value of this random process is zero. Consider the times $t_1 = t$ *and* $t_2 = t + \tau$, where τ is an arbitrary time interval. We have

$$R_X(t,\ t+\tau) = \mathbf{E}\{X(t)X(t+\tau)\} = \mathbf{E}\{X(t)\}\mathbf{E}\{X(t+\tau)\} = 0,\ |\tau| > T_b \tag{3.25}$$

since the process has *zero mean* and the bits are *independent*. For $|\tau| < T_b$, and with an arbitrary time index $i = 0$, let us assume that the time origin t of the zeroth bit is *uniformly distributed* in the bit interval T_b (without any knowledge about the location of the time origin the uniform distribution is the worst-case assumption), we have

$$\begin{aligned} R_X(t,\ t+\tau) &= \mathbf{E}\{X(t)X(t+\tau)\}, \quad 0 < t+\tau \le T_b \\ &= \begin{cases} \int_0^{T_b-\tau} (\pm 1)^2 \frac{1}{T_b}\,\mathrm{d}t = \frac{T_b-\tau}{T_b} = 1 - \frac{\tau}{T_b}, & 0 \le \tau \le T_b \\ \int_{-\tau}^{T_b} (\pm 1)^2 \frac{1}{T_b}\,\mathrm{d}t = \frac{T_b+\tau}{T_b} = 1 + \frac{\tau}{T_b}, & -T_b \le \tau \le 0 \end{cases} \\ &= 1 - \frac{|\tau|}{T_b},\ |\tau| \le T_b = R_X(\tau) \end{aligned} \tag{3.26}$$

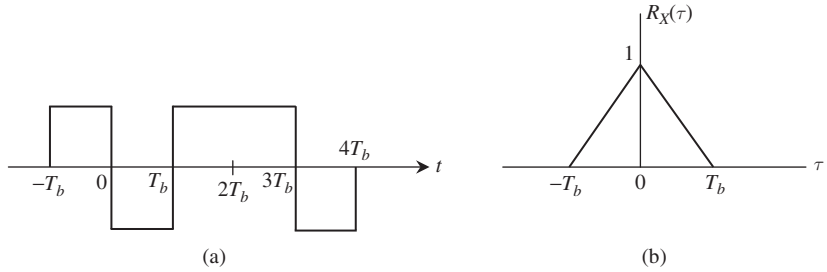

Figure 3.1 (a) Antipodal signal; (b) corresponding autocorrelation.

Thus, the random sequence of antipodal signals with a *uniform time origin* has a triangular autocorrelation, which depends only on the *time difference* $|\tau| = |t_2 - t_1|$, that is, $R_X(t,\ t+\tau) = R_X(\tau)$. Note that $R_X(0) = 1$ as expected. Figure 3.1 shows the representative antipodal signal sequence and its autocorrelation.

In the above analysis we assume that the time origin of the zeroth bit is *uniformly distributed* in the bit time T_b. This is equivalent to *shifting* the process $X(t)$ by a time delay Δ uniformly distributed in a bit time and independent of $X(t)$.

■

Example 3.2 Autocorrelation of a sequence of on–off keying (OOK) signals

Consider an OOK signal sequence $X(t) = \sum_{i=-\infty}^{\infty} d_i\, p(t - iT_b)$ that represents *independent* and *equally likely* bits $\{0,1\}$, where $p(t)$ is the squared pulse shape of unit amplitude and duration T_b, which is a bit time, and $d_i \in \{1, 0\}$ represents the normalized signal amplitudes. The mapping $0 \rightarrow 1$ *and* $1 \rightarrow 0$ maps bit 0 to amplitude 1 and bit 1 to amplitude 0 (the mapping $0 \rightarrow 0$ *and* $1 \rightarrow 1$ maps bit 0 to amplitude 0 and bit 1 to amplitude 1 would give the same result). We assume that the time origin is *uniform* in a bit time T_b. The mean value of this random process is

$$\begin{aligned} \mathbf{E}\{X(t)\} &= \sum_{i=-\infty}^{\infty} \mathbf{E}\{d_i\}\, \mathbf{E}\{p(t - iT_b)\} \\ &= 0.5 \sum_{i=-\infty}^{\infty} \int_{iT_b}^{iT_b+T_b} (1)\, \frac{1}{T_b}\, \mathrm{d}t = 0.5 \end{aligned} \tag{3.27}$$

The process $Y(t) = X(t) - 0.5$ therefore represents an antipodal signal sequence of amplitudes 0.5 and -0.5. Since $X(t) = Y(t) + 0.5$ the autocorrelation of $X(t)$ can be obtained from that of $Y(t)$, which has been derived in the previous example. Consider the times $t_1 = t$ *and* $t_2 = t + \tau$, where τ is an arbitrary time interval. We have

$$\begin{aligned} R_Y(t,\ t+\tau) &= \mathbf{E}\{Y(t)Y(t+\tau)\}, \quad 0 < t+\tau \le T_b \\ &= \frac{1}{4}\left(1 - \frac{|\tau|}{T_b}\right), \qquad |\tau| \le T_b \end{aligned} \tag{3.28}$$

And consequently the autocorrelation of the OOK signal sequence with a *uniform time origin* is given as

$$\begin{aligned} R_X(t,\ t+\tau) &= R_Y(t,\ t+\tau) + 0.5^2 \\ &= \begin{cases} \frac{1}{4}\left(1 - \frac{|\tau|}{T_b}\right) + \frac{1}{4}, & |\tau| \le T_b \\ \frac{1}{4}, & |\tau| > T_b \end{cases} \\ &= R_X(\tau) \end{aligned} \tag{3.29}$$

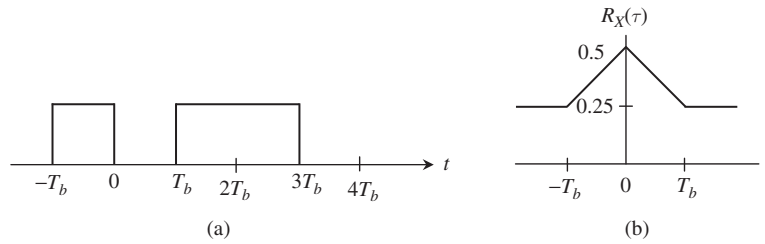

Figure 3.2 (a) OOK sequence; (b) corresponding autocorrelation.

Thus, this autocorrelation depends only on the time difference $|\tau| = |t_2 - t_1|$, that is, $R_X(t,\ t+\tau) = R_X(\tau)$. Figure 3.2 shows the representative OOK sequence and its autocorrelation.

■

Types of random processes

Definition 3.2 A random process is *stationary* (or *strict-sense stationary*) if the joint distribution of any set of samples is invariant with a shift of the time origin. In other words, the statistical properties are unchanged if the random process is shifted in time.

Stationarity is a strong property and not easily verifiable in practice. Instead communication theorists rely on a milder property called *wide-sense stationarity.*

Definition 3.3 A random process is *wide-sense stationary* (WSS) if its mean value is constant and its autocorrelation is a function of the time difference, that is, $R_X(t_1, t_2) = R_X(t_2 - t_1)$, or, for notational convenience, $R_X(t,\ t+\tau) = R_X(\tau)$.

A stationary process is obviously wide-sense stationary but not necessarily vice versa. The antipodal signal and OOK signal sequences with uniform time origin are both WSS processes. For a WSS process we have

$$R_X(0) = \mathbf{E}\{X^2(t)\}, R_X(\tau) = R_X(-\tau), |R_X(\tau)| \leq R_X(0) \tag{3.30}$$

Definition 3.4 A random process is *cyclostationary* (or *strict-sense cyclostationary*) with period T if the joint distribution of any set of samples is invariant to a shift of the time origin by integer multiples of T. In other words, the statistical properties are unchanged if the random process is shifted periodically in time.

Cyclostationarity is a weaker form of stationarity and many physical processes possess this property.

Definition 3.5 A random process is *wide-sense cyclostationary* (WSCS) if its mean value and its autocorrelation are periodic in time t with some period T, that is, they are invariant to

a shift of the time origin by integer multiples of T. In other words, we have $m_X(t) = m_X(t + iT)$, where $m_X(t) = \mathbf{E}\{X(t)\}$, and $R_X(t_1 + iT, t_2 + iT) = R_X(t_1, t_2)$.

The antipodal signal and OOK signal sequences are both WSCS random processes given a *fixed time origin*. But if we assume the time origin is *uniform* over $(0, T_b)$ and average out the mean and autocorrelation we obtain a constant mean value and an autocorrelation of the time difference.

Example 3.3 Wide-sense cyclostationary process

Consider a signal sequence $X(t) = \sum_{i=-\infty}^{\infty} d_i p(t - iT_b)$ that represents *independent* and *equally likely* bits [0,1] where $d_i \in \{1, -1\}$ represents the normalized signal amplitudes. The mapping $0 \rightarrow 1$ *and* $1 \rightarrow -1$ maps bit 0 to amplitude 1 and bit 1 to amplitude -1 (the mapping $0 \rightarrow -1$ *and* $1 \rightarrow 1$ maps bit 0 to amplitude -1 and bit 1 to amplitude 1 would give the same result). Also, $p(t)$ is the half-squared pulse shape of unit amplitude and duration T_b, which is a bit time, and is defined as $p(t) = 1,\ 0 \le t < T_b/2$ and $p(t) = 0,\ T_b/2 \le t < T_b$. A sample function of this signal sequence is shown in Figure 3.3.

We wish to evaluate the mean value and autocorrelation at different *fixed time origins t*. We consider two cases with a common time delay $\tau = T_b/4$ and two time origins $t = 0$ and $t = 3T_b/4$ as follows:

$$\begin{aligned} \mathbf{E}\{X(0)\} &= 0 \\ \mathbf{E}\{X(3T_b/4)\} &= 0 \end{aligned} \tag{3.31}$$

$$\begin{aligned} R_X(0, T_b/4) &= \mathbf{E}\{X(0)X(T_b/4)\} = 1 \\ R_X(3T_b/4, T_b) &= \mathbf{E}\{X(3T_b/4)X(T_b)\} = 0 \end{aligned} \tag{3.32}$$

Since the autocorrelation depends on the time origin the process is *not WSS*. Let us examine the mean value and autocorrelation of this random process in general. We have

$$\begin{aligned} \mathbf{E}\{X(t)\} &= \mathbf{E}\left\{\sum_{i=-\infty}^{\infty} d_i p(t - iT_b)\right\} = \sum_i \mathbf{E}(d_i) p(t - iT_b) \\ &= \mathbf{E}(d_i) \sum_i p(t - iT_b) \end{aligned} \tag{3.33}$$

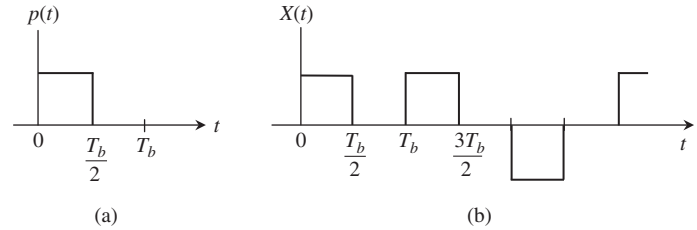

Figure 3.3 (a) Half-squared pulse shape; (b) sequence of half-squared pulse shapes.

$$R_X(t,\ t+\tau) = \mathbf{E}\{X(t)X(t+\tau)\} = \mathbf{E}\left\{\sum_{i=-\infty}^{\infty} d_i\, p(t-iT_b) \sum_{j=-\infty}^{\infty} d_j\, p(t+\tau-jT_b)\right\}$$
$$= \sum_i \sum_j \mathbf{E}(d_i d_j) p(t-iT_b) p(t+\tau-jT_b) \tag{3.34}$$

Using the fact that $\mathbf{E}(d_i) = 0$, and $\mathbf{E}(d_i d_j) = 1,\ i = j$ *and* $\mathbf{E}(d_i d_j) = 0,\ i \neq j$, we obtain $\mathbf{E}\{X(t)\} = 0$, and $R_X(t,\ t+\tau) = \sum p(t-iT_b)p(t+\tau-iT_b)$ is *time-varying* but *periodic* with period T_b. Thus, for a *fixed time origin*, this random process is a WSCS process.

■

Digital signal sequences that are often found in practice are wide-sense cyclostationary processes in nature. This property implies that the sequence's mean value and autocorrelation are periodic in T (bit or symbol time). Therefore, these statistical averages possess Fourier series with a harmonic at frequency $1/T$, the data clock rate. This provides a means for designing timing recovery circuits to extract the data clock signal, for the purpose of sampling the received signal to obtain a decision sample for bit or symbol detection to recover the transmitted information. The following theorem shows how a WSS process can be derived from a WSCS process.

Theorem 3.6 (*Conversion of a WSCS process into a WSS process*) *If $X(t)$ is a WSCS process with periodic mean value $m_X(t)$ and autocorrelation $R_X(t,\ t+\tau)$ of period T, then the shifted process $Y(t) = X(t-\Delta)$, where Δ is a uniform random variable in $(0, T)$ and independent of $X(t)$, is a WSS process with constant mean and t-invariant autocorrelation given by*

$$m_Y = \frac{1}{T}\int_0^T m_X(t)\,\mathrm{d}t$$
$$R_Y(\tau) = \frac{1}{T}\int_0^T R_X(t,\ t+\tau)\,\mathrm{d}t \tag{3.35}$$

Proof With the time delay Δ independent of the process $X(t)$ and $m_X(t)$ periodic with period T, the mean value of $Y(t)$ is given by

$$m_Y = \mathbf{E}\{X(t-\Delta)\} = \mathbf{E}\{\mathbf{E}[X(t-\Delta)|\Delta]\} = \mathbf{E}\{m_X(t-\Delta)\}$$
$$= \frac{1}{T}\int_0^T m_X(t-\Delta)\,\mathrm{d}\Delta = \frac{1}{T}\int_0^T m_X(t)\,\mathrm{d}t \tag{3.36}$$

Also, with $R_X(t,\ t+\tau)$ periodic with period T, we have

$$R_Y(\tau) = \mathbf{E}\{X(t-\Delta)X(t+\tau-\Delta)\} = \mathbf{E}\{\mathbf{E}[X(t-\Delta)X(t+\tau-\Delta)|\Delta]\}$$
$$= \mathbf{E}\{R_X(t-\Delta,\ t+\tau-\Delta)\}$$
$$= \frac{1}{T}\int_0^T R_X(t-\Delta,\ t+\tau-\Delta)\,\mathrm{d}\Delta = \frac{1}{T}\int_0^T R_X(t,\ t+\tau)\,\mathrm{d}t \tag{3.37}$$

■

The above theorem enables us to calculate the *time-averages* of the mean value and autocorrelation of a WSCS process. This will prove to be very useful in dealing with the power spectral density of the process, which will be covered later. In fact, since the autocorrelation function of a WSCS process is a function of both t and τ, its power spectral density is not defined. By doing time-averaging we can convert a WSCS process into a WSS process so that its power spectral density can be calculated.

So far we have presented examples of WSCS and WSS processes that are of *lowpass* or *baseband* types, such as the antipodal and OOK signal sequences. The waveform that represents a bit is a lowpass waveform (such as the squared pulse shape) whose *amplitude spectrum* (the magnitude of its Fourier transform) centers on the zero frequency. In the following examples we present two cases of digital signals that are of *bandpass* or *modulated* types, used to carry information over *high-frequency* channels.

Example 3.4 Sequence of phase shift keying signals

If we multiply an antipodal signal sequence with a carrier $\cos\ 2\pi f_c t$ at carrier frequency f_c we obtain a PSK signal sequence $X(t) = \sum_{i=-\infty}^{\infty} d_i\, p(t - iT_b) \cos\ 2\pi f_c t$. By convention we assume the carrier frequency is integer multiples of the bit rate $1/T_b$. The mean and autocorrelation of this bandpass process are given by

$$\begin{aligned}\mathbf{E}\{X(t)\} &= \mathbf{E}\left\{\sum_{i=-\infty}^{\infty} d_i\, p(t - iT_b) \cos\ 2\pi f_c t\right\} = \sum_i \mathbf{E}(d_i) p(t - iT_b) \cos\ 2\pi f_c t \\ &= \mathbf{E}(d_i) \sum_i p(t - iT_b) \cos\ 2\pi f_c t\end{aligned} \tag{3.38}$$

and

$$\begin{aligned}R_X(t,\ t+\tau) &= \mathbf{E}\{X(t)X(t+\tau)\} \\ &= \mathbf{E}\left\{\sum_{i=-\infty}^{\infty} d_i\, p(t - iT_b) \cos\ 2\pi f_c t \sum_{j=-\infty}^{\infty} d_j\, p(t + \tau - jT_b) \cos\ 2\pi f_c (t+\tau)\right\} \\ &= \frac{1}{2} \sum_i \sum_j \mathbf{E}(d_i d_j) p(t - iT_b) p(t + \tau - jT_b)\, [\cos\ 2\pi f_c \tau\ +\ \cos\,(4\pi f_c t + 2\pi f_c \tau)]\end{aligned} \tag{3.39}$$

Using the fact that $\mathbf{E}(d_i) = 0$, and $\mathbf{E}(d_i d_j) = 1,\ i = j$ *and* $\mathbf{E}(d_i d_j) = 0,\ i \neq j$, the mean value of the process is zero, that is, $\mathbf{E}\{X(t)\} = 0$, and the autocorrelation $R_X(t,\ t+\tau) = \frac{1}{2}\sum_i p(t - iT_b) p(t + \tau - iT_b)[\cos\ 2\pi f_c \tau + \cos\,(4\pi f_c t + 2\pi f_c \tau)]$ is *time-varying* but *periodic* with period T_b. Thus for a *fixed time origin*, this random process is a WSCS process. To convert this WSCS process into a WSS we need to time-average the autocorrelation function using the same procedure as used in the case of the antipodal signal sequence. By introducing a uniform time shift into the data sequence but not the carrier we obtain a WSS PSK signal sequence. Therefore, the time-averaged autocorrelation function is given as follows:

$$R_X(\tau) = \frac{1}{2}\left(\frac{T_b - |\tau|}{T_b}\right)\cos 2\pi f_c\tau = \frac{1}{2}\left(1 - \frac{|\tau|}{T_b}\right)\cos 2\pi f_c\tau, \ |\tau| \le T_b$$
$$= 0, \quad |\tau| > T_b \tag{3.40}$$

■

Example 3.5 Sequence of quadrature phase shift keying signals

The QPSK signaling requires two carriers, namely, an in-phase carrier $\cos 2\pi f_c t$ (I-carrier) and a quadrature carrier $\sin 2\pi f_c t$ (Q-carrier). The iid data bits {0,1} are grouped in pairs to form four distinct symbols [00,01,10,11]. The four symbols are mapped into the amplitude pair (I, Q) as shown in Table 3.1. Note that the amplitudes I and Q are independent and have zero mean.

Thus the QPSK signal sequence can be represented as follows:

$$X(t) = \sum_{i=-\infty}^{\infty} [I_i p(t - iT_s)\cos 2\pi f_c t - Q_i p(t - iT_s)\sin 2\pi f_c t] \tag{3.41}$$

where T_s is the symbol time, which is twice the bit time, and the carrier frequency is taken to be integer multiples of the symbol rate $1/T_s$. We observe that the QPSK signal sequence is the *sum of two orthogonal PSK signal sequences at the symbol rate*, and that both are WSCS processes. Thus, the QPSK signal sequence is itself a WSCS process. If we convert this WCCS process into a WSS process by assuming a uniform time origin over $(0, T_s)$, we obtain a *mean value of zero* and a *time-averaged autocorrelation* identical to the sum of the autocorrelations of two orthogonal PSK signal sequences with T_b replaced by T_s and amplitude ± 1 replaced by $\pm\sqrt{2}/2$, as follows:

$$R_X(\tau) = \frac{1}{2}\left(1 - \frac{|\tau|}{T_s}\right)\cos 2\pi f_c\tau, \quad |\tau| \le T_s$$
$$= 0, \quad |\tau| > T_s \tag{3.42}$$

The QPSK signal sequence can be represented in complex notation as

$$X(t) = X_I(t)\cos 2\pi f_c t - X_Q(t)\sin 2\pi f_c t$$
$$= \mathrm{Re}\{X_L(t)\, e^{j2\pi f_c t}\} \tag{3.43}$$

Table 3.1 QPSK symbol mapping

Symbol number	Input bits	I	Q
1	1 1	$+\sqrt{2}/2$	$+\sqrt{2}/2$
2	0 1	$-\sqrt{2}/2$	$+\sqrt{2}/2$
3	0 0	$-\sqrt{2}/2$	$-\sqrt{2}/2$
4	1 0	$+\sqrt{2}/2$	$-\sqrt{2}/2$

where $X_L(t)$ is the complex envelope (equivalent lowpass process, or baseband process) of the bandpass process $X(t)$ and is given by

$$\begin{aligned} X_L(t) &= X_I(t) + jX_Q(t) \\ X_I(t) = \sum_{i=-\infty}^{\infty} I_i p(t - iT_s), &\quad X_Q(t) = \sum_{i=-\infty}^{\infty} Q_i p(t - iT_s) \end{aligned} \tag{3.44}$$

The autocorrelation of the complex envelope is defined as

$$R_{X_L}(t, t+\tau) = \mathbf{E}\{X_L(t)X_L^*(t+\tau)\} = R_{X_I}(t, t+\tau) + R_{X_Q}(t, t+\tau) \tag{3.45}$$

Because the amplitudes I_i and Q_i are iid, the in-phase process $X_I(t)$ and the quadrature process $X_Q(t)$, both with zero mean, are independent and therefore their cross-correlations $R_{X_IX_Q}(\tau) = \mathbf{E}\{X_I(t)X_Q(t+\tau)\}$ and $R_{X_QX_I}(\tau) = \mathbf{E}\{X_Q(t)X_I(t+\tau)\}$ are both *zero*. Note that the *time-averaged autocorrelations* of $X_I(t)$ and $X_Q(t)$ are identical and are given by

$$\begin{aligned} R_{X_I}(\tau) = R_{X_Q}(\tau) &= \frac{1}{2}\left(1 - \frac{|\tau|}{T_s}\right), \qquad |\tau| \le T_s \\ &= 0, \qquad\qquad\quad |\tau| > T_s \end{aligned} \tag{3.46}$$

The *time-averaged autocorrelation* of the complex envelope $X_L(t)$ is simply the sum of two *time-averaged autocorrelations* $R_{X_I}(\tau)$ and $R_{X_Q}(\tau)$, thus, $R_{X_L}(\tau) = R_{X_I}(\tau) + R_{X_Q}(\tau)$. On the other hand, the *time-averaged autocorrelation* of the bandpass process $X(t)$ is given by $R_X(\tau) = \frac{1}{2}[R_{X_I}(\tau) + R_{X_Q}(\tau)]\cos 2\pi f_c\tau = R_{X_I}(\tau)\cos 2\pi f_c\tau = \frac{1}{2}R_{X_L}(\tau)\cos 2\pi f_c\tau$.

■

Definition 3.7 A bandpass signal $X(t) = X_I(t)\cos 2\pi f_c t - X_Q(t)\sin 2\pi f_c t$ belongs to a class of *jointly wide-sense stationary* processes if and only if it possesses the following properties:

1. The in-phase process $X_I(t)$ and quadrature process $X_Q(t)$ are *jointly WSS* and have zero mean.
2. $R_{X_I}(\tau) = R_{X_Q}(\tau)$.
3. $R_{X_IX_Q}(\tau) = \mathbf{E}\{X_I(t)X_Q(t+\tau)\} = -R_{X_QX_I}(\tau) = -\mathbf{E}\{X_Q(t)X_I(t+\tau)\}$.

The *time-averaged autocorrelation* of the WSS bandpass process $X(t)$ is given as

$$\begin{aligned} R_X(\tau) &= \tfrac{1}{2}[R_{X_I}(\tau) + R_{X_Q}(\tau)]\cos 2\pi f_c\tau - \tfrac{1}{2}[R_{X_IX_Q}(\tau) - R_{X_QX_I}(\tau)]\sin 2\pi f_c\tau \\ &= R_{X_I}(\tau)\cos 2\pi f_c\tau - R_{X_IX_Q}(\tau)\sin 2\pi f_c\tau \end{aligned} \tag{3.47}$$

If, in addition, the in-phase and quadrature processes are *uncorrelated*, that is, $R_{X_IX_Q}(\tau) = \mathbf{E}\{X_I(t)\}\mathbf{E}\{X_Q(t+\tau)\} = 0$ for all τ (this also implies that they are *orthogonal*), then the *time-averaged autocorrelation* of $X(t)$ is reduced to the following expression:

$$R_X(\tau) = R_{X_I}(\tau)\cos 2\pi f_c\tau = \frac{1}{2}R_{X_L}(\tau)\cos 2\pi f_c\tau \tag{3.48}$$

where $X_L(t) = X_I(t) + jX_Q(t)$ is the equivalent lowpass process of $X(t)$ and its autocorrelation is $R_{X_L}(\tau) = \mathbf{E}\{X_L(t)\}\mathbf{E}\{X_L^*(t+\tau)\}$.

So far we have dealt with ensemble averages (statistical averages) of a random process. This can be achieved if a large number of sample functions (realizations) of the random process are available. In practice, we perform measurements on a *single sample* of a random process to obtain time averages instead. This results in the *estimation* of the ensemble averages if the length of the available sample is very long. In that case, we expect the sample function to be typical of all realizations of the random process. This property is referred to as *ergodicity*. The following theorems establish the criteria for a random process to be ergodic.

Theorem 3.8 (Slutsky theorem) *A WSS process X(t) is said to be* mean-ergodic, *that is*,

$$\frac{1}{2T}\int_{-T}^{T} X(t)\,\mathrm{d}t \underset{T\to\infty}{\to} \mathbf{E}\{X(t)\} \tag{3.49}$$

if and only if

$$\frac{1}{T}\int_{0}^{T} C_X(\tau)\,\mathrm{d}\tau \underset{T\to\infty}{\to} 0 \tag{3.50}$$

■

Theorem 3.9 *A WSS process X(t) is said to be* autocovariance-ergodic, *that is*,

$$\frac{1}{2T}\int_{-T}^{T} [X(t) - \boldsymbol{E}\{X(t)\}][X(t+\tau) - \boldsymbol{E}\{X(t)\}]\}\,\mathrm{d}t \underset{T\to\infty}{\to} C_X(\tau) \tag{3.51}$$

if and only if

$$\frac{1}{T}\int_{0}^{T} C_Y(\tau)\,\mathrm{d}\tau \underset{T\to\infty}{\to} 0 \tag{3.52}$$

where $Y(t) = X(t)X(t+\Delta)$ and $C_Y(\tau)$ *is its autocovariance, given by*

$$C_Y(\tau) = E\{X(t)X(t+\Delta)X(t+\tau)X(t+\Delta+\tau)\} - C_X^2(\Delta) \tag{3.53}$$

The result also applies to autocorrelation-ergodic *processes if we replace the autocovariance with autocorrelation. Also the process is* variance-ergodic *if we set* $\Delta = 0$ *in the autocovariance* $C_Y(\tau)$.

■

Example 3.6 Sequence of quadrature phase shift keying signals revisited
The QPSK signal sequence with uniform time origin is a WSS process with zero mean and autocorrelation (and hence covariance) given in (3.48). So the time average of the autocorrelation is

$$\begin{aligned}\frac{1}{T}\int_0^T C_X(\tau)\,\mathrm{d}\tau &= \frac{1}{2T}\int_0^T \left(1-\frac{|\tau|}{T_s}\right)\cos 2\pi f_c\tau\,\mathrm{d}\tau, \quad |\tau| \le T_s \\ &= 0, \text{ elsewhere}\end{aligned} \tag{3.54}$$

The integral approaches zero as $T \to \infty$, and when f_c is integer multiples of T_s the integral is zero independent of T. Therefore the sequence is mean-ergodic.
■

Definition 3.10 The *normalized autocovariance* of a WSS process is defined as

$$\rho_X(\tau) = \frac{C_X(\tau)}{C_X(0)} \tag{3.55}$$

We note that as the delay time τ increases the process decorrelates, that is, it loses its correlation. Thus, it makes sense to define a *delay spread* to reflect this characteristic of the process.

Definition 3.11 The *delay spread* τ_d of a WSS process is the delay time beyond which the normalized autocovariance remains below 0.1, that is,

$$|\rho_X(\tau)| \le 0.1 \text{ for all } \tau > \tau_d \tag{3.56}$$

The normalized autocovariance of the QPSK signal sequence with uniform origin is a scaled version of its time-averaged autocorrelation. The *delay spread* is $\tau_d \approx 0.9T_s$. By observation we see that the autocorrelation is zero for $|\tau| > T_s$, that is, the sequence looses its correlation after one symbol time. Hence the delay spread gives a fairly accurate prediction of the *decorrelation*. We note that the inequality (3.56) is purely *empirical* and can be adjusted to fit any decorrelation requirement.

Power spectral density

In the previous chapter we established a relation between the autocorrelation of a deterministic signal and its power spectral density, that is, they form a Fourier transform pair. This same relation holds for a WSS process and for convenience we restate it here.

Definition 3.12 The power spectral density $S_X(f)$ and the autocorrelation $R_X(\tau)$ of a WSS process $X(t)$ form a Fourier transform pair known as the *Einstein–Wiener–Khinchine* relation:

$$S_X(f) = \int_{-\infty}^{\infty} R_X(\tau)\,\mathrm{e}^{-\mathrm{j}2\pi f\tau}\,\mathrm{d}\tau = F[R_X(\tau)] \tag{3.57}$$

$$R_X(\tau) = \int_{-\infty}^{\infty} S_X(f)\, \mathrm{e}^{\mathrm{j}2\pi f\tau}\, \mathrm{d}f = F^{-1}[S_X(f)] \tag{3.58}$$

Theorem 3.13 (Einstein–Wiener–Khinchine theorem) *The power spectral density of a WSS process is given by*

$$S_X(f) = \lim_{T\to\infty} \frac{1}{2T} \mathrm{E}\left\{ |F[X_T(t)]|^2 \right\} = \int_{-\infty}^{\infty} R_X(\tau)\, \mathrm{e}^{-\mathrm{j}2\pi f\tau}\, \mathrm{d}\tau \tag{3.59}$$

if the following condition holds:

$$\int_{-\infty}^{\infty} |\tau R_X(\tau)|\, \mathrm{d}\tau < \infty \tag{3.60}$$

where $X_T(t)$ is a 2T-truncation *of a single sample of the random process $X(t)$ and $F[X_T(t)]$ is its Fourier transform.*

Proof We consider the truncated version of a sample function for the reason that it is not an energy signal and may not have a Fourier transform. We have

$$F[X_T(t)] = \int_{-\infty}^{\infty} X_T(t)\, \mathrm{e}^{-\mathrm{j}2\pi ft}\, \mathrm{d}t = \int_{-T}^{T} X(t)\, \mathrm{e}^{-\mathrm{j}2\pi ft}\, \mathrm{d}t \tag{3.61}$$

Therefore,

$$\begin{aligned} \frac{1}{2T}\mathbf{E}\left\{ |F[X_T(t)]|^2 \right\} &= \frac{1}{2T}\mathbf{E}\left\{ \int_{-T}^{T} X(t_1)\, \mathrm{e}^{-\mathrm{j}2\pi ft_1}\, \mathrm{d}t_1 \int_{-T}^{T} X(t_2) \mathrm{e}^{\mathrm{j}2\pi ft_2}\, \mathrm{d}t_2 \right\} \\ &= \frac{1}{2T}\int_{-T}^{T}\int_{-T}^{T} \mathbf{E}\{\, X(t_1)\, X(t_2)\,\} \mathrm{e}^{-\mathrm{j}2\pi f(t_1-t_2)}\, \mathrm{d}t_1\, \mathrm{d}t_2 \\ &= \frac{1}{2T}\int_{-T}^{T}\int_{-T}^{T} R_X(t_1-t_2)\, \mathrm{e}^{-\mathrm{j}2\pi f(t_1-t_2)}\, \mathrm{d}t_1\, \mathrm{d}t_2 \end{aligned} \tag{3.62}$$

Making the change of integration variable as $\tau = t_1 - t_2$, we have

$$\begin{aligned} \frac{1}{2T}\mathbf{E}\left\{ |F[X_T(t)]|^2 \right\} &= \frac{1}{2T}\int_{-T}^{T}\int_{-T-t_2}^{T-t_2} R_X(\tau)\, \mathrm{e}^{-\mathrm{j}2\pi f\tau} \mathrm{d}\tau\, \mathrm{d}t_2 \\ &= \frac{1}{2T}\int_{-2T}^{0}\int_{-T-\tau}^{T} R_X(\tau)\, \mathrm{e}^{-\mathrm{j}2\pi f\tau}\, \mathrm{d}t_2\, \mathrm{d}\tau + \frac{1}{2T}\int_{0}^{2T}\int_{-T}^{T-\tau} R_X(\tau)\, \mathrm{e}^{-\mathrm{j}2\pi f\tau}\, \mathrm{d}t_2\, \mathrm{d}\tau \\ &= \frac{1}{2T}\int_{-2T}^{0} (2T+\tau) R_X(\tau) \mathrm{e}^{-\mathrm{j}2\pi f\tau}\, \mathrm{d}\tau + \frac{1}{2T}\int_{0}^{2T} (2T-\tau) R_X(\tau) \mathrm{e}^{-\mathrm{j}2\pi f\tau}\, \mathrm{d}\tau \\ &= \frac{1}{2T}\int_{-2T}^{2T} (2T-|\tau|) R_X(\tau) \mathrm{e}^{-\mathrm{j}2\pi f\tau}\, \mathrm{d}\tau = \int_{-2T}^{2T} \left(1 - \frac{|\tau|}{2T}\right) R_X(\tau) \mathrm{e}^{-\mathrm{j}2\pi f\tau}\, \mathrm{d}\tau \end{aligned} \tag{3.63}$$

In the limit as $T \to \infty$ the *periodogram* $\mathbf{E}\left\{|F[X_T(t)]|^2\right\}/2T$ becomes the power spectral density.

■

The periodogram is a nonnegative function for all frequencies, consequently, the power spectral density is also a nonnegative function for all frequencies, that is,

$$S_X(f) \geq 0 \text{ for all } f \tag{3.64}$$

Furthermore, since the autocorrelation is real and even, the power spectral density is an even function, hence

$$S_X(f) = S_X(-f) \tag{3.65}$$

The power of the WSS process is given by

$$P = \mathbf{E}\{X^2(t)\} = R_X(0) = \int_{-\infty}^{\infty} S_X(f)\, \mathrm{d}f \tag{3.66}$$

Example 3.7 Power spectral densities of digital signal sequences with squared pulse shape
The power spectral density of a digital signal sequence of uniform time origin is the Fourier transform of its autocorrelations. We have added the amplitude $\pm A$ to the original sequence, which also has the amplitude ± 1 to make the results more general.

$$\text{Antipodal: } S_X(f) = A^2 T_b \left(\frac{\sin \pi f T_b}{\pi f T_b}\right)^2 \tag{3.67}$$

$$\text{OOK: } S_X(f) = \frac{1}{4} A^2 T_b \left(\frac{\sin \pi f T_b}{\pi f T_b}\right)^2 + \frac{1}{4} A^2 \delta(f) \tag{3.68}$$

$$\text{PSK: } S_X(f) = \frac{A^2 T_b}{4} \left[\left(\frac{\sin \pi (f - f_c) T_b}{\pi (f - f_c) T_b}\right)^2 + \left(\frac{\sin \pi (f + f_c) T_b}{\pi (f + f_c) T_b}\right)^2\right] \tag{3.69}$$

$$\text{QPSK: } S_X(f) = \frac{A^2 T_s}{4} \left[\left(\frac{\sin \pi (f - f_c) T_s}{\pi (f - f_c) T_s}\right)^2 + \left(\frac{\sin \pi (f + f_c) T_s}{\pi (f + f_c) T_s}\right)^2\right] \tag{3.70}$$

Jointly WSS process with uncorrelated in-phase $X_I(t)$ and quadrature $X_Q(t)$ data sequences and complex envelope, $X_L(t) = X_I(t) + jX_Q(t)$:

$$S_X(f) = \frac{1}{2}[S_{X_I}(f - f_c) + S_{X_I}(f + f_c)] = \frac{1}{4}[S_{X_L}(f - f_c) + S_{X_L}(f + f_c)] \tag{3.71}$$

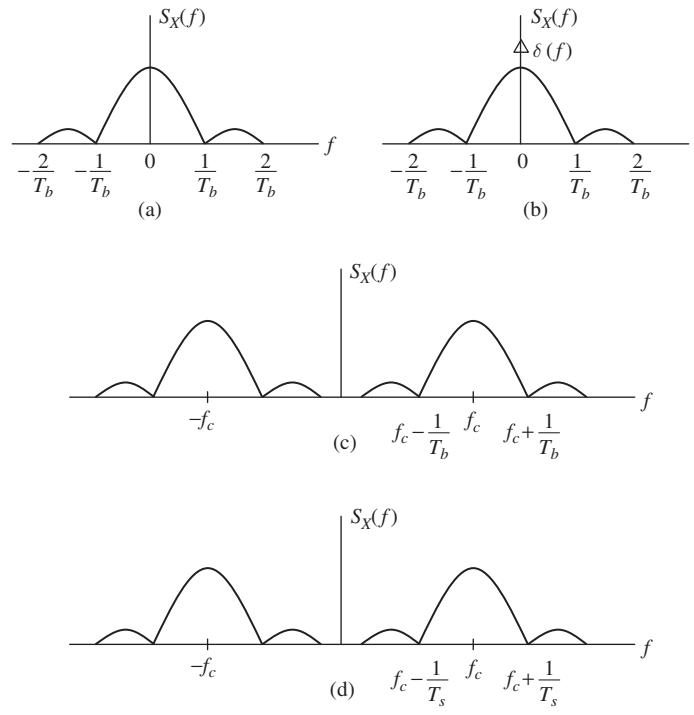

Figure 3.4 Power spectral densities of various random processes: (a) antipodal; (b) OOK; (c) PSK; (d) QPSK.

Figure 3.4 shows the power spectral densities of the antipodal, OOK, PSK, and QPSK signals.

■

Linear filters are used in communication systems for signal processing purposes, such as limiting noise within a prescribed bandwidth, shaping a signal spectrum to meet the FCC requirement, rejecting the out-of-band interference, and so forth. Therefore, it is necessary to know the response of linear filters to random processes. We will consider a linear time-variant filter with impulse response $h(t)$ and corresponding Fourier transform $H(f)$.

Theorem 3.14 *Let the input $X(t)$ of a linear time-invariant filter with impulse response $h(t)$ and corresponding Fourier transform $H(f)$ be a WSS process with power spectral density $S_X(f)$ and autocorrelation $R_X(\tau)$. The output $Y(t)$ of the filter is also a WSS process with power spectral density $S_Y(f)$ and autocorrelation $R_Y(\tau)$ given by*

$$S_Y(f) = |H(f)|^2 S_X(f) \tag{3.72}$$

$$R_Y(\tau) = h(\tau) * h^*(-\tau) * R_X(\tau) \tag{3.73}$$

Proof Let $X_T(t)$ be a $2T$-*truncation* of a single sample of the random process $X(t)$ and $F[X_T(t)]$ be its Fourier transform. Also let $Y_T(t)$ be the response of the filter to the input $X_T(t)$. We have

$$\begin{aligned}\frac{1}{2T}\mathbf{E}\left\{|F[Y_T(t)]|^2\right\} &= \frac{1}{2T}\mathbf{E}\left\{|H(f)F[X_T(t)]|^2\right\} \\ &= |H(f)|^2\left(\frac{1}{2T}\mathbf{E}\left\{|F[X_T(t)]|^2\right\}\right)\end{aligned} \tag{3.74}$$

Taking the limit as $T \to \infty$ we obtain

$$\begin{aligned}S_Y(f) &= \lim_{T\to\infty}\frac{1}{2T}\mathbf{E}\left\{|F[Y_T(t)]|^2\right\} = |H(f)|^2\lim_{T\to\infty}\frac{1}{2T}\mathbf{E}\left\{|F[X_T(t)]|^2\right\} \\ &= |H(f)|^2 S_X(f)\end{aligned} \tag{3.75}$$

We also have

$$S_Y(f) = H(f)H^*(f)S_X(f) \tag{3.76}$$

Taking the inverse Fourier transform of $S_Y(f)$ and realizing that the inverse Fourier transform of $H^*(f)$ is $h^*(-\tau)$ we obtain

$$R_Y(\tau) = h(\tau) * h^*(-\tau) * R_X(\tau) \tag{3.77}$$

■

Example 3.8 Power spectral density of a digital signal sequence with arbitrary pulse shape
In Example 3.7 we calculated the power spectral densities of digital signal sequences employing a squared pulse shape. This particular pulse shape yields a $(\sin x/x)^2$ power spectral density that requires an infinite bandwidth, although about 90% of the sequence power is contained within the null-to-null bandwidth. In practice, other pulse shapes that yield finite bandwidth may be used such as the *raised-cosine* pulse shape. We wish to derive the general expression for power spectral density for an arbitrary pulse shape in this example. We consider a WSCS digital signal sequence $X(t) = \sum_{i=-\infty}^{\infty} d_i\, p(t - iT)$ and convert it into a WSS process by assuming a uniform time origin over (0, T), where T is a bit time or a symbol time depending on the type of digital signal. The data d_i can be real or complex. If it is complex, the process represents the envelope of another bandpass process. The pulse shape $p(t)$ is assumed to have a Fourier transform $P(f)$. The autocorrelation of the sequence is

$$\begin{aligned}R_X(t,\ t+\tau) &= \mathbf{E}\{X^*(t)X(t+\tau)\} = \mathbf{E}\left\{\sum_{i=-\infty}^{\infty} d_i^*\, p^*(t - iT)\sum_{j=-\infty}^{\infty} d_j\, p(t+\tau - jT)\right\} \\ &= \sum_i\sum_j \mathbf{E}(d_i^* d_j)\mathbf{E}[p^*(t - iT)p(t+\tau - jT)]\end{aligned} \tag{3.78}$$

The term $\mathbf{E}(d_i d_j^*)$ is the autocorrelation of the data and is denoted as $R_d(i-j)$. Hence

$$\begin{aligned} R_X(t,\ t+\tau) &= \frac{1}{T}\sum_i \sum_j R_d(i-j) \int_0^T p^*(t-iT)p(t+\tau-jT)\,\mathrm{d}t \\ &= \frac{1}{T}\sum_m R_d(m) \sum_i \int_{-iT}^{-iT+T} p^*(\lambda)p(\lambda+\tau-mT)\,\mathrm{d}\lambda \\ &= \frac{1}{T}\sum_m R_d(m) \int_{-\infty}^{\infty} p^*(\lambda)p(\lambda+\tau-mT)\,\mathrm{d}\lambda \\ &= \frac{1}{T}\sum_m R_d(m)[p(\tau-mT) * p^*(-\tau)] \\ &= R_X(\tau) \end{aligned} \tag{3.79}$$

Taking the Fourier transform of the autocorrelation we obtain

$$\begin{aligned} S_X(f) &= \frac{1}{T}\sum_m R_d(m)[P(f)\,\mathrm{e}^{-\mathrm{j}2\pi mfT}P^*(f)] \\ &= \frac{1}{T}|P(f)|^2 \sum_m R_d(m)\,\mathrm{e}^{-\mathrm{j}2\pi mfT} \\ &= \frac{1}{T}|P(f)|^2 S_d(\mathrm{e}^{\mathrm{j}2\pi fT}) \end{aligned} \tag{3.80}$$

The term $S_d(\mathrm{e}^{\mathrm{j}2\pi fT}) = \sum_m R_d(m)\,\mathrm{e}^{-\mathrm{j}2\pi mfT} = \mathrm{DTFT}[R_d(m)]$ is the *discrete-time Fourier transform* of the autocorrelation of the data sequence.

White data

The data sequence $\{d_i\}$ is said to be *white* if its autocorrelation $R_d(m)$ and its discrete-time Fourier transform $S_d(\mathrm{e}^{\mathrm{j}2\pi fT})$ are given by

$$S_d(\mathrm{e}^{\mathrm{j}2\pi fT}) = 1, \quad R_d(m) = \begin{cases} 1, m = 0 \\ 0, m \neq 0 \end{cases} \tag{3.81}$$

Thus, for *white data* that is encountered in practice, the power spectral density is simply $|P(f)|^2/T$. In the case of the antipodal signal sequence with squared pulse shape of duration T, its Fourier transform is given by $P(f) = T(\sin \pi fT/\pi fT)$ and we get the previously derived result.

■

Definition 3.15 The *coherence bandwidth* B_c of a WSS lowpass process is defined as one-half the inverse of its *delay spread* τ_d:

$$\text{Lowpass:} \qquad B_c = \frac{1}{2\tau_d} \tag{3.82}$$

Furthermore, the coherence bandwidth of a WSS bandpass process is the inverse of the *delay spread* of its in-phase or quadrature process:

$$\text{Bandpass:} \qquad B_c = \frac{1}{\tau_d} \tag{3.83}$$

The coherence bandwidth of a WSS antipodal signal sequence is $B_c = 1/2\tau_d \approx 1/(2 \times 0.9T_b) = 0.55/T_b$. This is about 55% of its *first-null bandwidth*.

The coherence bandwidth of a WSS QPSK signal sequence is $B_c = 1/\tau_d \approx 1/0.9T_s = 1.11/T_s$. This is about 55% of the *null-to-null bandwidth*.

In communications the channel noise is composed of thermal noise generated by electronics components in the receiver and cosmic noise from the sky. These noise processes have a constant spectrum that extends to very high frequencies beyond the frequency band of all communication signals. Therefore, they are commonly modeled as noise with ideal constant power spectral densities that extend to infinite frequency.

Definition 3.16 The WSS process $n(t)$ is called *white noise* if it has the following power spectral density and autocorrelation:

$$S_n(f) = \frac{N_0}{2} \qquad R_n(\tau) = \frac{N_0}{2}\delta(\tau) \tag{3.84}$$

where N_0 is a constant to be discussed in Chapter 5.

The term white noise is employed in analogy with *white light*, which is light that contains all frequencies.

More properties of WSS bandpass processes

In the following discussion we present some more properties of a WSS process that are helpful in the analysis of random signals, especially noise. As usual, we consider the jointly WSS bandpass process

$$X(t) = X_I(t)\cos 2\pi f_c t - X_Q(t)\sin 2\pi f_c t \tag{3.85}$$

By direct substitution, the lowpass in-phase and quadrature processes can be expressed in terms of the bandpass process and its Hilbert transform $\hat{X}(t) = 1/\pi t * X(t)$ as follows [1,2]:

$$\begin{aligned} X_I(t) &= X(t)\cos 2\pi f_c t + \hat{X}(t)\sin 2\pi f_c t \\ X_Q(t) &= \hat{X}(t)\cos 2\pi f_c t - X(t)\sin 2\pi f_c t \end{aligned} \tag{3.86}$$

Furthermore, it can be shown that the autocorrelations of both $X_I(t)$ and $X_Q(t)$ are given by

$$R_{X_I}(\tau) = R_{X_Q}(\tau) = R_X(\tau)\cos 2\pi f_c \tau + \hat{R}_X(\tau)\sin 2\pi f_c \tau \tag{3.87}$$

where $\hat{R}_X(t) = 1/\pi t * R_X(t)$ is the Hilbert transform of $R_X(\tau)$. In addition we get

$$R_{X_I X_Q}(\tau) = -R_{X_Q X_I}(\tau) = R_X(\tau)\sin 2\pi f_c \tau - \hat{R}_X(\tau)\cos 2\pi f_c \tau \tag{3.88}$$

Note that the Fourier transform of $\hat{R}_X(t) = 1/\pi t * R_X(t)$ is $-\text{jsgn}(f)S_X(f)$. Therefore, taking the Fourier transform of both sides of (3.87) we obtain

$$S_{X_I}(f) = S_{X_Q}(f) = \frac{1}{2}[1 - \text{sgn}(f - f_c)]S_X(f - f_c) + \frac{1}{2}[1 + \text{sgn}(f + f_c)]S_X(f + f_c) \tag{3.89}$$

The Fourier transforms of the crosscorrelations $R_{X_I X_Q}(\tau)$ and $R_{X_Q X_I}(\tau)$ are referred to as their *cross-spectral densities*. From (3.88) we have

$$S_{X_I X_Q}(f) = -S_{X_Q X_I}(f) = -\frac{\mathrm{j}}{2}[1 - \mathrm{sgn}(f - f_c)]\, S_X(f - f_c) + \frac{\mathrm{j}}{2}[1 + \mathrm{sgn}(f + f_c)]\, S_X(f + f_c) \tag{3.90}$$

Bandlimited WSS bandpass processes

When the power spectral density of the bandpass process $X(t)$ is strictly limited to a frequency band $f_c - B \leq |f| \leq f_c + B$, where $f_c > B$, then the power spectral densities of both in-phase and quadrature processes simplify to the following expression

$$\begin{aligned} S_{X_I}(f) = S_{X_Q}(f) &= S_X(f - f_c) + S_X(f + f_c), \quad |f| \leq B \\ &= 0, \quad |f| > B \end{aligned} \tag{3.91}$$

In addition the cross-spectral densities of the in-phase and quadrature processes become

$$\begin{aligned} S_{X_I X_Q}(f) = -S_{X_Q X_I}(f) &= \mathrm{j}[S_X(f + f_c) - S_X(f - f_c)], \quad |f| \leq B \\ &= 0, \quad |f| > B \end{aligned} \tag{3.92}$$

When the power spectral density of the WSS bandpass process is *symmetric* around the carrier frequency $\pm f_c$ then

$$S_X(f + f_c) = S_X(f - f_c), \quad |f| \leq B \tag{3.93}$$

Consequently,

$$S_{X_I X_Q}(f) = -S_{X_Q X_I}(f) = 0 \quad \rightarrow R_{X_I X_Q}(\tau) = -R_{X_Q X_I}(\tau) = 0 \tag{3.94}$$

And the in-phase and quadrature processes are *uncorrelated*. Figure 3.5 illustrates the power spectral densities of *strictly bandlimited white noise* $n(t)$.

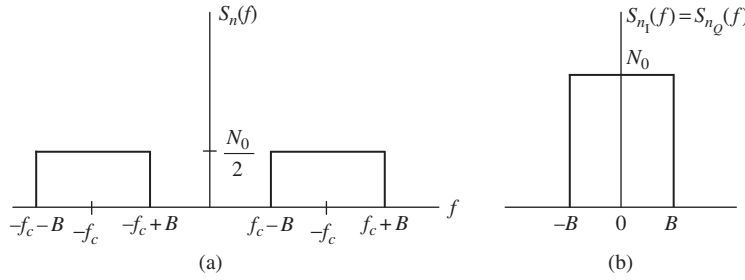

Figure 3.5 (a) Power spectral density of bandlimited white noise process. (b) Power spectral density of in-phase and quadrature noise processes.

3.4 Gaussian process

The Gaussian process plays an important role in communication theory. Noise in a communication channel is modeled as a Gaussian process and the detection theory of signals in noise is developed based on this assumption, and can be accurately verified by measurements. In this section we discuss some basic properties of the Gaussian process and its applications to communication theory

Definition 3.17 The *Gaussian process* $X(t)$ is characterized by a set of *n jointly Gaussian random variables* $X_1 = X(t_1), \ldots, X_n = X(t_n)$ for all n and t_n. The joint density function of the random variables is given by

$$f_{\boldsymbol{X}}(x) = \frac{\mathrm{e}^{-(x-\overline{\boldsymbol{X}})^t \mathbf{K}^{-1}(x-\overline{\boldsymbol{X}})/2}}{(2\pi)^{n/2}|\mathbf{K}|^{1/2}} \tag{3.95}$$

where $\boldsymbol{X} = (X_1\ X_2\ \ldots\ X_n)^t$, $\overline{\boldsymbol{X}}$ is the mean of $\boldsymbol{X}$, and $\mathbf{K}$ is the $n \times n$ covariance matrix defined as $\mathbf{K} = [C_X(t_i, t_j)]$, where $C_X(t_i, t_j) = \mathbf{E}\{(X_i - \overline{X_i})(X_j - \overline{X_j})\}$. The symbol $|\mathbf{K}|$ denotes the determinant of $\mathbf{K}$ as usual.

Example 3.9 Independent and identically distributed Gaussian random variables
Consider a discrete-time Gaussian sequence of n iid random variables of mean m and variance σ^2. The covariance matrix is $\mathbf{K} = \sigma^2\mathbf{I}_n$ and $\mathbf{I}_n$ is the $n \times n$ identity matrix. The corresponding density function is given by the product of n Gaussian density functions,

$$f_{\boldsymbol{X}}(x) = \frac{1}{(\sqrt{2\pi}\sigma)^n}\mathrm{e}^{-\sum_{i=1}^{n}(x_i-m)^2/2\sigma^2} \tag{3.96}$$

We note that if the n Gaussian random variables are *uncorrelated*, that is, $C_X(t_i, t_j) = 0,\ \ i \neq j$, then they are automatically *independent*.
■

Linear transformation

In a communication system Gaussian noise is processed by linear filters of various kinds such as the *matched filter* and *integrator* for signal processing. Linear filtering does not change the Gaussian nature of noise as we will subsequently show. The following theorem shows that a linear transformation of a sequence of jointly Gaussian random variables preserves the Gaussian property.

Theorem 3.18 *The linear transformation of a jointly Gaussian vector is another jointly Gaussian vector.*

Proof Consider a jointly Gaussian vector $\boldsymbol{X} = (X_1\ X_2\ \cdots\ X_n)^t$ with mean $\overline{\boldsymbol{X}}$ and covariance matrix $\mathbf{K}$. We now consider the following linear transformation:

$$\boldsymbol{Y} = \mathbf{A}\boldsymbol{X} \tag{3.97}$$

where $\boldsymbol{Y}$ is the linear transformation of $\boldsymbol{X}$, and $\mathbf{A}$ is an $n \times n$ nonsingular matrix. We wish to find the density function of the random vector $\boldsymbol{Y}$, which can be calculated by the following general expression:

$$f_{\boldsymbol{Y}}(\boldsymbol{y}) = f_{\boldsymbol{X}}(\boldsymbol{x})/|J(\boldsymbol{y}, \boldsymbol{x})| \tag{3.98}$$

The parameter J is the *Jacobian* of the transformation and is given by $J(\boldsymbol{y}, \boldsymbol{x}) = |\partial \boldsymbol{y}/\partial \boldsymbol{x}| = |[\partial y_i/\partial x_j]|$. For the linear transformation we get $J(\boldsymbol{y}, \boldsymbol{x}) = |\mathbf{A}|$. Substituting $\boldsymbol{X} = \mathbf{A}^{-1}\boldsymbol{Y}$ we obtain the density of $\boldsymbol{Y}$:

$$\begin{aligned} f_{\boldsymbol{Y}}(\boldsymbol{y}) &= \frac{\mathrm{e}^{-(\mathbf{A}^{-1}\boldsymbol{y} - \mathbf{A}^{-1}\overline{\boldsymbol{Y}})^t \mathbf{K}^{-1} (\mathbf{A}^{-1}\boldsymbol{y} - \mathbf{A}^{-1}\overline{\boldsymbol{Y}})/2}}{(2\pi)^{n/2}|\mathbf{K}|^{1/2}|\mathbf{A}|} \\ &= \frac{\mathrm{e}^{-(\boldsymbol{y} - \overline{\boldsymbol{Y}})^t (\mathbf{A}^{-1})^t \mathbf{K}^{-1} \mathbf{A}^{-1} (\boldsymbol{y} - \overline{\boldsymbol{Y}})/2}}{(2\pi)^{n/2}|\mathbf{K}|^{1/2}|\mathbf{A}|} \end{aligned} \tag{3.99}$$

which is a jointly Gaussian density function. By integrating on $(n-1)$ variables y_i from $-\infty$ to ∞ the remaining variable is shown to be a Gaussian density function. Thus, we conclude that a linear combination of n jointly Gaussian random variables is a new Gaussian random variable.

■

Example 3.10 Integral of a Gaussian process

The integral of a Gaussian process occurs in signal detection in noise. Therefore, it is necessary to examine the output $Y(t)$ of an integrator when the input process $X(t)$ is Gaussian and characterized by a joint density function. We have

$$Y(t) = \int_0^t X(\tau)\, \mathrm{d}\tau \tag{3.100}$$

This integral can be approximated by a sum of n terms as

$$Y(t) \approx \sum_{j=1}^{n} X(\tau_j(t))\, \Delta\tau_j(t) \tag{3.101}$$

which converges to the exact value as $n \to \infty$ and $\Delta\tau_j(t) \to 0$. This is a linear combination of n jointly Gaussian random variables. Hence, for a given t, $Y(t)$ is a Gaussian random variable.

■

Example 3.11 Response of a linear filter to a Gaussian process
The integrator treated in the above example is the special case of a linear filter. We wish to generalize the above result to any linear filter with impulse response $h(t)$. Again, considering a Gaussian process $X(t)$ at the input of the filter, the output process $Y(t)$ is given by the convolution operation as

$$Y(t) = \int_{-\infty}^{\infty} h(t-\tau)\, x(\tau)\, \mathrm{d}\tau \tag{3.102}$$

We can approximate this integral by a sum of n terms as

$$Y(t) \approx \sum_{j=1}^{n} h(t-\tau_j)\, x(\tau_j)\, \Delta\tau_j \tag{3.103}$$

which converges to the exact value as $n \to \infty$ and $\Delta\tau_j \to 0$. This is a linear combination of n jointly Gaussian random variables. This holds for any t, hence $Y(t)$ is a Gaussian process.

■

The above examples show that the Gaussian process is *closed* under a linear operation. That is, *any linear operation on a Gaussian process produces another Gaussian process*. This forms the basic foundation for detection of random signals in Gaussian noise that are processed by a linear system. Only the impulse response of the system, the mean, and autocorrelation of the input process are required to completely characterize the density function of the output process and hence the calculation of the probability of detection or error of any output sample.

Theorem 3.19 *The response of a linear system to an input Gaussian process is also a Gaussian process*.

■

Sampling

The *sampling theorem* plays an important role in the processing of deterministic signals. In the following discussion we show that the same sampling theorem can be applied to a strictly bandlimited white Gaussian process to produce independent Gaussian samples. This provides an alternative means of analyzing a continuous-time signal as a discrete-time sequence and the derivation of the information capacity of a strictly bandlimited white Gaussian channel.

Theorem 3.20 (Sampling Theorem) *The samples of a strictly bandlimited zero mean white Gaussian process taken at* the Nyquist *rate are independent Gaussian random variables*.

Proof Let us consider the *white* noise process $n(t)$ with the following power spectral density

$$\begin{aligned} S_n(f) &= \frac{N_0}{2}, \quad |f| \leq B \\ &= 0, \qquad \text{otherwise} \end{aligned} \tag{3.104}$$

The corresponding autocorrelation is the inverse Fourier transform of the power spectral density and is given as

$$R_n(\tau) = N_0 B\left(\frac{\sin 2\pi B\tau}{2\pi B\tau}\right) \tag{3.105}$$

Consider two Nyquist samples taken at time $t_1 = iT$ and $t_2 = jT$ for integers i and j, where $T = 1/2B$. Since the mean of the process is zero, the autocovariance is the same as the autocorrelation, hence

$$C_n(t_1, t_2) = R_n(t_1, t_2) = R_n[(j-i)T] = N_0 B\left(\frac{\sin 2\pi B(j-i)T}{2\pi B(j-i)T}\right) \tag{3.106}$$

which is zero when $i \neq j$ for any i and j. This proves that the Gaussian samples are *uncorrelated* and hence *independent*.

■

Sufficient statistics for signal processing in white Gaussian noise

In the following discussion we consider the case of *signal processing* in white Gaussian noise. We are particularly interested in obtaining the *statistics* of a transmitted signal that has been contaminated by noise for the purpose of detection. The detection of signal in noise will be studied in Chapter 7. Such a communication channel is often referred to as an *additive white Gaussian noise* (AWGN) channel. Suppose we consider a set of M digital signals $s_i(t),\ i = 1, 2, \ldots, M$, as described in Chapter 2, and that each of them can be represented by a linear combination of *orthonormal* basis functions $x_k(t)\,,\ k = 1, 2, \ldots, L$, via the *Gram–Schmidt* orthogonalizing procedure. We have

$$s_i(t) \ = \ \sum_{k=1}^{L} s_{ik} x_k(t) \tag{3.107}$$

where, for each i and k,

$$s_{ik} \ = \ \int_{-\infty}^{\infty} s_i(t) x_k(t)\, \mathrm{d}t \tag{3.108}$$

The coefficients s_{ik} contain all the information about the transmitted signal $s_i(t)$. Now consider an AWGN channel with noise $n(t)$ having power spectral density $N_0/2$. There is no constraint on the bandwidth of noise so that its autocorrelation is $R_n(\tau) = (N_0/2)\,\delta(\tau)$.

The *signal plus noise* at the receiver input is modeled as the sum of a transmitted signal $s_i(t)$ and noise $n(t)$ as

$$X(t) = s_i(t) + n(t) \tag{3.109}$$

How do we extract the information in the transmitted signal? By using (3.108) we simply multiply the received signal $X(t)$ with the known orthonormal basis functions $x_1(t), \ldots, x_L(t)$ to obtain the set of L samples

$$X_k = s_{ik} + N_k \quad k = 1, 2, \ldots, L \tag{3.110}$$

where the noise samples N_k are the *projection* of noise $n(t)$ onto the orthonormal basis functions and are given by

$$N_k = \int_{-\infty}^{\infty} n(t) x_k(t)\, \mathrm{d}t \quad k = 1, 2, \ldots, L \tag{3.111}$$

Note that these noise samples are zero mean Gaussian random variables with covariance given by

$$\begin{aligned}
\mathrm{Cov}(N_j N_k) &= \mathbf{E}(N_j N_k) \\
&= \mathbf{E}\left[\int_{-\infty}^{\infty}\int_{-\infty}^{\infty} n(t)n(\tau)x_j(t)x_k(\tau)\,\mathrm{d}t\,\mathrm{d}\tau\right] = \int_{-\infty}^{\infty}\int_{-\infty}^{\infty} \mathbf{E}[n(t)n(\tau)]x_j(t)x_k(\tau)\,\mathrm{d}t\,\mathrm{d}\tau \\
&= \int_{-\infty}^{\infty}\int_{-\infty}^{\infty} R_n(t-\tau)x_j(t)x_k(\tau)\,\mathrm{d}t\,\mathrm{d}\tau = \int_{-\infty}^{\infty}\int_{-\infty}^{\infty} \frac{N_0}{2}\delta(t-\tau)\,x_j(t)x_k(\tau)\,\mathrm{d}t\,\mathrm{d}\tau \\
&= \frac{N_0}{2}\int_{-\infty}^{\infty} x_j(t)x_k(t)\,\mathrm{d}t \\
&= \begin{cases} N_0/2, & j = k \\ 0, & j \neq k \end{cases}
\end{aligned} \tag{3.112}$$

Thus the noise samples are *uncorrelated* for $j \neq k$ and since they are Gaussian they are also *independent*.

The received signal can be represented by

$$X(t) = \sum_{k=1}^{L} X_k x_k(t) + e(t) \tag{3.113}$$

where the process $e(t)$ is defined by

$$\begin{aligned}
e(t) &= X(t) - \sum_k X_k x_k(t) = s_i(t) + n(t) - \sum_k s_{ik} x_k(t) - \sum_k N_k x_k(t) \\
&= n(t) - \sum_k N_k x_k(t)
\end{aligned} \tag{3.114}$$

This process depends only on the noise, not on the signal, and it is also a zero mean Gaussian process. Furthermore, the following derivation shows that the Gaussian process $e(t)$ is *independent* of the received samples $X_k = s_{ik} + N_k,\ k = 1, 2, \ldots, L$ and hence irrelevant in the detection of $X(t)$:

$$\begin{aligned}\mathbf{E}[e(t)X_j] &= \mathbf{E}\left\{[n(t) - \sum_k N_k x_k(t)](s_{ij} + N_j)\right\} \\ &= \mathbf{E}\left\{n(t)\int_{-\infty}^{\infty} n(\tau)x_j(\tau)\,\mathrm{d}\tau\right\} - \sum_k \mathbf{E}(N_k N_j)x_k(t) \\ &= \frac{N_0}{2}x_j(t) - \frac{N_0}{2}x_j(t) = 0\end{aligned} \tag{3.115}$$

Thus only L samples $X_k = s_{ik} + N_k,\ k = 1, 2, \ldots, L$ are needed to completely characterize the received signal $X(t)$. They represent *sufficient statistics* for any decision making on $X(t)$. Note that the joint density of the X_ks is the product of L Gaussian density functions, each of mean s_{ik} and variance $N_0/2$. The AWGN channel is thus a *memoryless* channel.

When the Gaussian noise is non-white, that is, it has an arbitrary power spectral density, then the noise samples are no longer independent. For applications that require an independent set of random variables another kind of series expansion called the *Karhunen–Loeve* expansion can be employed.

Karhunen–Loeve expansion

Again we consider a zero mean Gaussian noise process $n(t)$ with autocorrelation $R_n(\tau)$ that accompanies a transmitted signal $s_i(t),\ 0 \le t < T$, for arbitrary T. The following theorem verifies the existence of a set of *orthonormal eigenfunctions* $\phi_k(t)$ of the noise autocorrelation. This set represents the noise process $n(t)$ as a series expansion with coefficients n_k forming a set of independent Gaussian random variables with zero mean and variance equal to the *eigenvalues* of the noise autocorrelation function. In other words we have

$$n(t) = \sum_{k=-\infty}^{\infty} n_k \phi_k(t) \tag{3.116}$$

where, for all values of i and j,

$$\int_0^T \phi_i(t)\phi_j(t)\,\mathrm{d}t = \begin{cases} 1 & i = j \\ 0 & i \ne j \end{cases} \tag{3.117}$$

such that the series coefficients are uncorrelated, that is,

$$\mathbf{E}(n_i n_j) = 0 \quad i \ne j \tag{3.118}$$

where

$$n_k = \int_0^T \phi_k(t)n(t)\,\mathrm{d}t \tag{3.119}$$

Theorem 3.21 (Karhunen–Loeve theorem) *Let* $\phi_k(t)$ *and* λ_k *represent the* orthonormal eigenfunctions *and* eigenvalues, *respectively, of the* integral equation

$$\int_0^T R_n(t-\tau)\phi_k(\tau)\,\mathrm{d}\tau = \lambda_k \phi_k(t) \tag{3.120}$$

where $R_n(\tau)$ is the autocorrelation of the zero mean random process $n(t)$. Then the expansion coefficients n_k of the series $n(t) = \sum_{k=-\infty}^{\infty} n_k \phi_k(t)$ are uncorrelated and have variances $\lambda_k = E(n_k^2)$. Furthermore, if $n(t)$ is Gaussian, then the coefficients n_k are independent Gaussian random variables.

Proof We establish the following relation to show that the series coefficients are uncorrelated:

$$\begin{aligned} E(n_i n_j) &= E\left[\int_0^T n(t)\phi_i(t)\,\mathrm{d}t \int_0^T n(\tau)\phi_j(\tau)\,\mathrm{d}\tau\right] \\ &= \int_0^T \phi_i(t) \int_0^T E[n(t)n(\tau)]\phi_j(\tau)\,\mathrm{d}\tau\mathrm{d}t \\ &= \int_0^T \phi_i(t) \int_0^T R_n(t-\tau)\phi_j(\tau)\,\mathrm{d}\tau\mathrm{d}t \\ &= \lambda_j \int_0^T \phi_i(t)\,\phi_j(t)\,\mathrm{d}t \\ &= \begin{cases} \lambda_j & i = j \\ 0 & i \neq j \end{cases} \end{aligned} \tag{3.121}$$

Since the random variables n_k are both Gaussian and uncorrelated, they are also independent. ■

The *eigenfunctions* $\phi_k(t)$ form a complete set of orthonormal basis functions for the finite-energy signals $s_i(t),\ 0 \le t < T$, when the noise autocorrelation is a positive-definite function. The signals can then be represented by the series

$$s_i(t) = \sum_k s_{ik}\phi_k(t) \quad i = 1, 2, \ldots, M \tag{3.122}$$

where

$$s_{ik} = \int_{-\infty}^{\infty} s_i(t)\phi_k(t)\,\mathrm{d}t \tag{3.123}$$

The receiver for this type of channel will not be practical since the samples of noise and signal form a countable set and are hence infinitely dimensional. In the next section we discuss a method to transform non-white noise into white noise so that the result of the previous section applies.

Whitening filter

The power spectral density of noise at the receiver is shaped by the receiver transfer function $H(f)$ whose corresponding impulse response is $h(t)$. For example, if the input noise is white

and has power spectral density $N_0/2$, then as the noise propagates through the receiver the noise at the detector ends up with a new power spectral density $S_n(f) = |H(f)|^2 N_0/2$ and becomes non-white. In another scenario, the noise at the input of the receiver could already be non-white with arbitrary power spectral density $S_n(f)$, and the receiver is wide-band such that its transfer function can be considered constant over a bandwidth of the signal. In either case we can *whiten* the input noise by using a filter whose transfer function satisfies $|G(f)| = 1/\sqrt{S_n(f)}$. Such a filter reproduces white noise at its output. In the first scenario the signals $y_i(t),\ i = 1, 2, \ldots, M,$ at the output of the *whitening filter* are $y_i(t) = s_i(t) * h(t) * g(t)$, where $s_i(t),\ i = 1, 2, \ldots, M$, are the original transmitted signals, and $g(t)$ is the inverse Fourier transform of $G(f)$. In the second scenario the output of the whitening filter is $y_i(t) = s_i(t) * g(t)$.

Example 3.12 Spectral factorization

When the power spectral density of non-white noise is rational, that is, the ratio of two polynomials in f^2, we can design a *stable and causal* filter $G(f)$ called a *minimum-phase* filter from $S_n(f)$ via *spectral factorization*. Let us consider the following non-white noise rational power spectral density:

$$S_n(f) = \frac{A(f^2)}{B(f^2)} \tag{3.124}$$

Let $s = \mathrm{j}2\pi f$ to obtain the transfer function $S_n(s)$ as follows:

$$S_n(s) = \frac{A(-s^2)}{B(-s^2)} \tag{3.125}$$

The roots of $S_n(s)$ which are either zeros or poles must be either real or complex conjugate. Furthermore, if z_k is a root, then $-z_k$ is also a root. Therefore, we can factor $S_n(s)$ into products of polynomials with roots in the *left-half s-plane* $(\mathrm{Re}\ s < 0)$ and roots in the *right-half s-plane* $(\mathrm{Re}\ s > 0)$:

$$S_n(s) = \frac{C(s)C(-s)}{D(s)D(-s)} \tag{3.126}$$

The minimum-phase factor $G(\mathrm{s})$ is the ratio of two polynomials formed with roots in the *left-half s-plane*:

$$G(s) = \frac{C(s)}{D(s)} \tag{3.127}$$

Consider the following rational noise power spectral density:

$$S_n(f) = \frac{a}{b^2 + (2\pi f)^2} \tag{3.128}$$

We have

$$S_n(s) = \frac{a}{b^2 - s^2} = \frac{a}{(b+s)(b-s)} \tag{3.129}$$

Thus the whitening filter has the following transfer function:

$$G(s) = \frac{\sqrt{a}}{b+s} \rightarrow G(f) = \frac{\sqrt{a}}{b + \mathrm{j}2\pi f} \tag{3.130}$$

■

We now conclude the study of Gaussian processes with the following important theorem.

The central limit theorem

Consider n independent continuous random variables X_i with means $\overline{X_i}$ and variances σ_i^2. We form their sum $X = \sum_{i=1}^{n} X_i$ with mean $\overline{X} = \sum_{i=1}^{n} \overline{X_i}$ and variance $\sigma^2 = \sum_{i=1}^{n} \sigma_i^2$. The *central limit theorem* states that as n increases the probability density function of X approaches a Gaussian density function:

$$f_X(x) \overset{n\to\infty}{\longrightarrow} \frac{1}{\sqrt{2\pi}\sigma} \mathrm{e}^{-(x-\overline{X})^2/2\sigma^2} \tag{3.131}$$

3.5 Gaussian-derived processes

Besides the Gaussian process, communication theorists often encounter other important random processes that influence their design. These random processes may arise from the method of signal detection in Gaussian noise or from the type of channel through which the signal passes, such as a multipath fading channel in mobile communication systems. Two well-known Gaussian-derived processes are the Rayleigh and Rice processes. They play an important role in the analysis of communication systems that focus on the detection of the *signal envelopes* of digital waveforms, such as orthogonal signals (FSK, Walsh, OOK).

Rayleigh and Rice processes

Let us consider a simple example of detecting the envelope of a bandpass OOK signal $s(t) = Ap(t)\cos(2\pi f_c t + \theta)$ (bit 0) and $s(t) = 0$ (bit 1), where $p(t)$ is the squared pulse shape of unit amplitude and bit time T_b. The zero mean Gaussian noise is a WSS bandpass process represented by $n(t) = n_I(t)\cos 2\pi f_c t - n_Q(t)\sin 2\pi f_c t$. Practical communication systems are bandlimited so we assume $n(t)$ is also bandlimited. When bit 1 is transmitted the *signal is not present* and the received signal is just noise $n(t)$. When bit 0 is transmitted the *signal is present* and the received signal is the sum of both signal and noise. In the first case the receiver detects the *envelope of noise*, and in the second case the *envelope of the signal plus noise*. Let us consider the first case where we write the bandpass noise $n(t)$ via the envelope-phase representation

$$n(t) = R(t)\cos[2\pi f_c t + \Psi(t)] \tag{3.132}$$

The *envelope* $R(t)$ and *phase* $\Psi(t)$ of the noise process are related to the *in-phase* noise $n_I(t)$ and *quadrature* noise $n_Q(t)$ as follows:

$$R(t) = [n_I^2(t) + n_Q^2(t)]^{1/2} \qquad \Psi(t) = \tan^{-1}\left(\frac{n_Q(t)}{n_I(t)}\right) \tag{3.133}$$

$$n_I(t) = R(t)\cos\Psi(t) \qquad n_Q(t) = R(t)\sin\Psi(t) \tag{3.134}$$

Both in-phase and quadrature noise components of $n(t)$ are uncorrelated. Since they are Gaussian processes, they are also independent. Let us consider a sample of a realization of the envelope $R(t)$ at a *fixed time* t. We represent this sample via the random variable R. Similarly, we obtain a sample of the phase process at time t, which can be represented by the random variable Ψ. At the fixed time t, we also obtain the in-phase and quadrature noise samples n_I and n_Q, which are independent zero mean Gaussian random variables of the same variance as the variance of $n(t)$, that is, $\mathrm{Var}(n_I) = \mathrm{Var}(n_Q) = \mathrm{Var}(n) = \mathbf{E}(n^2) = \sigma^2$.

Applying the theory of transformation of random variables we obtain the probability density functions of both random variables R and Ψ:

$$f_R(r) = \frac{r}{\sigma^2}\mathrm{e}^{-r^2/2\sigma^2} \quad r \geq 0 \tag{3.135}$$

$$f_\Psi(\psi) = \frac{1}{2\pi} \quad 0 \leq \psi \leq 2\pi \tag{3.136}$$

Note that the probability density function of R is independent of Ψ, hence, these two random variables are independent *when they are taken at the same time*. This does not mean that the two random processes $R(t)$ and $\Psi(t)$ are independent. The density function of the noise envelope is the well-known *Rayleigh density function*. The density function of the phase is the *uniform density function*. Note that $\mathbf{E}(R^2) = 2\sigma^2$.

Example 3.13 Complex envelope representation of noise

We can use the complex envelope representation of the noise $n(t)$ to get its envelope and phase. We have

$$n(t) = \mathrm{Re}\{n_L(t)\mathrm{e}^{\mathrm{j}2\pi f_c t}\} \tag{3.137}$$

where the complex envelope is $n_L(t) = n_I(t) + jn_Q(t)$. The envelope is simply the absolute value of $n_L(t)$, which is $R(t) = [n_I^2(t) + n_Q^2(t)]^{1/2}$.

■

Now let us return to the second case where we attempt to detect the *envelope of the signal plus noise*. The received signal for bit 0 plus noise can be written as

$$\begin{aligned} X(t) &= A\cos(2\pi f_c t + \theta) + n(t) \\ &= [A\cos\theta + n_I(t)]\cos 2\pi f_c t - [A\sin\theta + n_Q(t)]\sin 2\pi f_c t \end{aligned} \tag{3.138}$$

The process $X(t)$ has an envelope-phase representation as follows:

$$X(t) = R(t)\cos[2\pi f_c t + \Psi(t)] \tag{3.139}$$

$$\begin{aligned} R(t) &= \{[A\cos\theta + n_I(t)]^2 + [A\sin\theta + n_Q(t)]^2\}^{1/2} \\ \Psi(t) &= \tan^{-1}\left(\frac{A\sin\theta + n_Q(t)}{A\cos\theta + n_I(t)}\right) \end{aligned} \tag{3.140}$$

The Gaussian processes $n_I'(t) = A\cos\theta + n_I(t)$ and $n_Q'(t) = A\sin\theta + n_Q(t)$ are independent with mean $A\cos\theta$ and $A\sin\theta$, respectively, and variance σ^2, the variance of $n(t)$. Applying the theory of transformation of random variables we obtain the following well-known *Rice density function* for the envelope

$$f_R(r) = \frac{r}{\sigma^2}\mathrm{e}^{-(r^2+A^2)/2\sigma^2} I_0\left(\frac{Ar}{\sigma^2}\right) \quad r \geq 0 \tag{3.141}$$

The function $I_0(x)$ is the *modified Bessel function of the first kind of zero order*. When there is no signal, that is, $A = 0$ and $I_0(0) = 1$, the Rice density function reduces to the Rayleigh density function. Note that $\mathbf{E}(R^2) = A^2 + 2\sigma^2$. The ratio $A^2/2\sigma^2$ is the familiar *signal-to-noise ratio*.

Example 3.14 Complex envelope representation of signal and noise

The sum process of signal plus noise $X(t)$ can be represented in its complex envelope form as follows:

$$X(t) = \mathrm{Re}\{X_L(t)\mathrm{e}^{\mathrm{j}2\pi f_c t}\} \tag{3.142}$$

where the complex envelope is

$$X_L(t) = [A\cos\theta + n_I(t)] + j[A\sin\theta + n_Q(t)] \tag{3.143}$$

The envelope of $X(t)$ is the absolute value of $X_L(t)$, which is $R(t)$ given the above.

■

Example 3.15 Envelope of signal in a multipath fading channel

In a multipath fading channel, such as the one encountered by cellular systems, local area networks, metropolitan area networks, and home networks, the transmitted signal arrives at the receiver via multiple paths. Signal rays can arrive via a direct path plus paths resulting from *reflection* from large objects, *scattering* from small objects, and *diffraction* via ray bending around structures. These signal rays add at the receiver to form a received signal that can be quite different from the transmitted signal. We are interested in the envelope of such a multipath fading signal. We assume that the signal travels via independent paths and arrives at the receiver with *independent attenuations*, *paths delays*, and *phase shifts*. Let us consider bandpass digital signals that can be represented by the process

$X(t) = X_I(t)\cos 2\pi f_c t - X_Q(t)\sin 2\pi f_c t$, where both in-phase and quadrature processes are independent. The received signal is a sum of attenuated and delayed-shifted and phase-shifted versions of $X(t)$. For n independent paths we have

$$\begin{aligned} Y(t) &= \sum_{k=1}^{n} X_{I,k}(t)\cos 2\pi f_c t - \sum_{k=1}^{n} X_{Q,k}(t)\sin 2\pi f_c t \\ &= Y_I(t)\cos 2\pi f_c t - Y_Q(t)\sin 2\pi f_c t \end{aligned} \tag{3.144}$$

The in-phase component of the received signal $Y(t)$ is $Y_I(t) = \sum_{k=1}^{n} X_{I,k}(t)$ and the quadrature component is $Y_Q(t) = \sum_{k=1}^{n} X_{Q,k}(t)$. The complex envelope of $Y(t)$ is

$$Y_L(t) = Y_I(t) + kY_Q(t) \tag{3.145}$$

The path components $X_{I,k}(t)$ and $X_{Q,k}(t)$ are functions of path attenuations, path delays, and path phase-shifts. We are interested in the envelope $R(t)$ of the received multipath fading signal $Y(t)$ at a *fixed time t*. We observe that as the number of paths n approaches infinity, the *central limit theorem* dictates that both $Y_I(t)$ and $Y_Q(t)$ approach independent Gaussian random variables with common variance σ_s^2, which is also the variance of $Y(t)$. If there is *no direct path* then the mean of these in-phase and quadrature components is zero and the density function of the envelope $R(t)$ of $Y(t)$ at a fixed time t is a Rayleigh density function. Note that $\mathbf{E}(R^2) = 2\sigma_s^2$ is the power of all non-direct (diffuse) paths. If there is a *direct path* with amplitude A then the density function of the envelope $R(t)$ of $Y(t)$ at a fixed time t is a Rice density function. Note that $\mathbf{E}(R^2) = A^2 + 2\sigma_s^2$ is the power of the direct path and all diffuse paths. The ratio $A^2/2\sigma_s^2$ is referred to as the *direct signal-to-diffuse signal ratio*.

■

Squared envelope

The detection of the envelope of signal plus noise is the same as the detection of its *squared envelope* since both quantities are nonnegative. For some applications it is more mathematically tractable to deal with the squared envelope. The density function of the *squared envelope of noise* $Z(t) = R^2(t)$ at a fixed time t is the *exponential density function* given by

$$f_Z(z) = \frac{1}{2\sigma^2}\mathrm{e}^{-z/2\sigma^2} \quad z \geq 0 \tag{3.146}$$

On the other hand, the density function of the *squared envelope of signal plus noise* at a fixed time t is

$$f_Z(z) = \frac{1}{2\sigma^2}\mathrm{e}^{-(A^2+z)/2\sigma^2} I_0\left(\frac{A\sqrt{z}}{\sigma^2}\right) \qquad z \geq 0 \tag{3.147}$$

Sum of squared Gaussian processes

In many wireless communication systems the use of *diversity* to improve the performance of a digital signal is necessary to combat the multipath fading effect. This effect can cause losses in the signal-to-noise ratio, especially in a Rayleigh channel. Diversity can be achieved via *independent multiple channel reception of the same signal*. *Frequency diversity* employs multiple channels of different frequencies. The same signal is transmitted simultaneously on these frequencies and their energies are combined at the receiver. If each channel fades independently, then the average error rate will improve. The same principle applies to *time diversity*, which transmits the same signal serially in consecutive time slots. The fading in each time slot is assumed to be independent. The signal energies in these time slots are then combined at the receiver to improve the average error rate. The third type of diversity is *antenna diversity*, where multiple antennas are employed to receive the transmitted signal that arrives at the receiver via independent paths. The signal energies from these paths are combined to improve the average error rate. When diversity is used the squared envelopes of the signals plus the noise in each path are combined to yield the following sum:

$$\begin{aligned} U(t) &= \sum_{k=1}^{L} |Y_{L,k}(t)+n_{L,k}(t)|^2 = \sum_{k=1}^{L} |[Y_{I,k}(t) + n_{I,k}(t)] + \mathrm{j}[Y_{Q,k}(t) + n_{Q,k}(t)]|^2 \\ &= \sum_{k=1}^{L} \{[Y_{I,k}(t) + n_{I,k}(t)]^2 + [Y_{Q,k}(t) + n_{Q,k}(t)]^2\} \end{aligned} \tag{3.148}$$

where L is the diversity order, and $Y_{L,k}(t)$ and $n_{L,k}(t)$ are the complex envelopes of the signal and noise in the kth *diversity channel*, respectively. We are interested in the density function of $U(t)$.

Case 1: Signal is not present

$$U(t) = \sum_{k=1}^{L} [n_{I,k}^2(t) + n_{Q,k}^2(t)] \tag{3.149}$$

In this case we have the *sum of* $2L$ *squared Gaussian processes*. These Gaussian processes are mutually *independent* and each has *zero mean* and *common variance* σ^2. The density function of $U(t)$ at a fixed time t is commonly referred to as the χ^2*-density function* (English pronunciation: *chi-squared*; Greek pronunciation: *hee-squared*) *with n degrees of freedom*, given by

$$f_U(u) = \frac{1}{(2\sigma^2)^L (L-1)!} u^{L-1} \mathrm{e}^{-u/2\sigma^2} \quad u \geq 0 \tag{3.150}$$

Case 2: Diffuse signal is present

In this case the received signal in the kth *diversity channel* is a multipath fading signal consisting of the diffuse (non-direct) paths only and we have

$$U(t) = \sum_{k=1}^{L} \{[Y_{I,k}(t) + n_{I,k}(t)]^2 + [Y_{Q,k}(t) + n_{Q,k}(t)]^2\} \tag{3.151}$$

At a fixed time t, the Gaussian random variables $U_{I,k}(t) = Y_{I,k}(t) + n_{I,k}(t)$ and the Gaussian random variables $U_{Q,k}(t) = Y_{Q,k}(t) + n_{Q,k}(t)$ are independent and have zero mean and common variance $\sigma_k^2 = \sigma_s^2 + \sigma^2$, where σ_s^2 is the power of the diffuse paths. The density function of $U(t)$ is the *χ^2-density function with $2L$ degrees of freedom*, given by

$$f_U(u) = \frac{1}{(2\sigma_k^2)^L (L-1)!} u^{L-1} \mathrm{e}^{-u/2\sigma_k^2} \quad u \geq 0 \tag{3.152}$$

Case 3: Direct and diffuse signals are present

In this case the received signal in the kth *diversity channel* is a multipath fading signal consisting of a direct path and the diffuse (non-direct) paths. Therefore, we have

$$U(t) = \sum_{k=1}^{L} \{[Y_{I,k}(t) + n_{I,k}(t)]^2 + [Y_{Q,k}(t) + n_{Q,k}(t)]^2\} \tag{3.153}$$

At a fixed time t, the Gaussian random variables $U_{I,k}(t) = Y_{I,k}(t) + n_{I,k}(t)$ and the Gaussian random variables $U_{Q,k}(t) = Y_{Q,k}(t) + n_{Q,k}(t)$ are independent and have non-zero mean $A_k \cos\theta_k$ and $A_k \sin\theta_k$, respectively, and common variance $\sigma_k^2 = \sigma_s^2 + \sigma^2$. The density function of $U(t)$ is the *non-central χ^2-density function with $2L$ degrees of freedom*, given by

$$f_U(u) = \frac{1}{2\sigma_k^2} \left(\frac{u}{A^2}\right)^{(L-1)/2} \mathrm{e}^{-(A^2+u)/2\sigma_k^2} I_{L-1}\left(\frac{A\sqrt{u}}{\sigma_k^2}\right) \quad u \geq 0 \tag{3.154}$$

where the non-central parameter A^2 is defined as

$$A^2 = \sum_{k=1}^{L} [A_k^2 \cos^2\theta_k + A_k^2 \sin^2\theta_k] = \sum_{k=1}^{L} A_k^2 \tag{3.155}$$

We also have $A_k^2/2\sigma_k^2 = A_k^2/(2\sigma_s^2 + 2\sigma^2) = 1/[(A_k^2/2\sigma_s^2)^{-1} + (A_k^2/2\sigma^2)^{-1}]$. Note that $A_k^2/2\sigma_s^2$ is the *direct signal-to-diffuse signal ratio* and $A_k^2/2\sigma^2$ is the *direct signal-to-noise ratio* of the kth *diversity channel*.

Nakagami-m density function

The Rayleigh and Rice density functions are *particular solutions* of the random amplitude-phase problem

$$|R(t)| = |Y_I(t) + \mathrm{j}Y_Q(t)| = \left|\sum_{k=1}^{n} X_{I,k}(t) + \mathrm{j}\sum_{k=1}^{n} X_{Q,k}(t)\right| = \left|\sum_{k=1}^{n} R_k(t)\mathrm{e}^{\mathrm{j}\Psi_k(t)}\right| \tag{3.156}$$

The *Nakagami-m density function* is a *general but approximate solution* and is given by

$$f_R(r) = \frac{2m^m r^{2m-1}}{\Gamma(m)\Omega^m} e^{-mr^2/\Omega} \tag{3.157}$$

where

$$\Omega = \mathbf{E}(R^2) \qquad m = \frac{\Omega^2}{\mathbf{E}[(R^2 - \Omega)^2]} \geq \frac{1}{2} \tag{3.158}$$

$$\begin{aligned} &\Gamma(m) = \int_0^\infty x^{m-1} e^{-x}\, dx, \quad m > 0 \\ &\Gamma(m) = (m-1)!, \quad m = \text{positive integer} \\ &\Gamma(\tfrac{1}{2}) = \sqrt{\pi}, \ \Gamma(\tfrac{3}{2}) = \tfrac{1}{2}\sqrt{\pi} \end{aligned} \tag{3.159}$$

The Rayleigh density function is a special case of the Nakagami-m density function where $m = 1$ and $\Omega = 2\sigma^2$. The Nakagami-m density function only approximates the exact density function of the envelope of the sum of random vectors whose amplitudes and phases vary according to certain statistical laws. However, the approximation is sufficiently good for many engineering applications. This fact has been verified experimentally in the *ionospheric* and *troposheric* propagations.

Log-normal density function

In wireless communications the path losses between mobile receivers at various locations but at the same distance from the transmitter may vary due to different terrains. This effect is often referred to as *shadowing*. The uncertainty in the path loss around its mean value is commonly expressed in terms of a Gaussian random variable X with mean L_{dB} and variance σ_{dB}^2 since path loss is calculated in decibels (dB). The density function of X is referred to as the *log-normal density function* and is given by

$$f_X(x) = \frac{1}{\sqrt{2\pi}\sigma_{dB}} e^{-(x-L_{dB})^2/2\sigma_{dB}^2} \tag{3.160}$$

We can transform the log-normal random variable X with decibel unit to ratio via the following relation:

$$Y = 10^{X/10} \leftrightarrow X = 10 \log Y \tag{3.161}$$

Thus the density function of Y is

$$f_Y(y) = \frac{10/\ln 10}{\sqrt{2\pi}\sigma_{dB} y} e^{-(10 \log y - L_{dB})^2/2\sigma_{dB}^2}, \quad y > 0 \tag{3.162}$$

Example 3.16 Outage probability

Consider a cell with radius R and a mobile at a distance r from the base station located at the center of the cell. The path loss is modeled as a log-normal random variable X with mean $L_{dB}(r)$ and variance σ_{dB}^2. The received power of the mobile in dBW (1 W = 0 dBW) is given

as $P(r) = P_T - X$, where P_T (dBW) is the transmit power of the base station. If we designate $\overline{P(r)} = P_T - L_{dB}(r)$ as the mean value of the received power of the mobile, then $P(r)$ is a log-normal random variable with mean $\overline{P(r)}$ and variance σ_{dB}^2. The probability that the received power exceeds a given *threshold signal power* γ (dBW) can be calculated from the density function in (3.160) as

$$\Pr[P(r) > \gamma] = Q\left(\frac{\gamma - \overline{P(r)}}{\sigma_{dB}}\right) \tag{3.163}$$

where $Q(\cdot)$ is the *Gaussian integral function* defined by

$$Q(a) = \frac{1}{\sqrt{2\pi}} \int_a^{\infty} \mathrm{e}^{-x^2/2} \mathrm{d}x \tag{3.164}$$

The *outage probability* is defined as the probability that the received power falls below the threshold γ. We have

$$p_{\text{out}}(r) = \Pr[P(r) \leq \gamma] = Q\left(\frac{\overline{P(r)} - \gamma}{\sigma_{dB}}\right) \tag{3.165}$$

For numerical illustration let us fix the outage probability as $p_{\text{out}}(r) = 0.01$. The argument of the Q-function is given by $[\overline{P(r)} - \gamma]/\sigma_{dB} = 2.32$. Thus, we get $\overline{P(r)} = \gamma + 2.32\sigma_{dB}$. For example, with $\sigma_{dB} = 10$ dB the mean value of the received power of the mobile has to be 23.2 dB above the threshold value to achieve this outage probability. Normally one would like to achieve this benchmark at the cell boundary, where $r = R$. In practice, the threshold γ can be calculated given a *threshold signal-to-noise ratio SNR* (dB) at the cell boundary. If the noise power N (dBW) is known as described in Chapter 5, the threshold signal power γ at the cell boundary can be calculated as $\gamma = SNR + N$. For the above numerical example we can then calculate the received power of the mobile at the cell boundary as $\overline{P(R)} = \gamma + 2.32\sigma_{dB} = SNR + N + 2.32\sigma_{dB}$. Since $\overline{P(R)} = P_T - L_{dB}(R)$ the base station can adjust the transmit power P_T to meet the required threshold *SNR* if the path loss is known either by *measurements* or by using an empirical model such as the *Hata model* (see Chapter 5). The Hata model estimates the *median path loss* (dB) given the carrier frequency, the transmit and receive antenna heights, the path loss exponent, and the distance between base station and mobile for various environments. For the log-normal shadowing path loss (dB), the median is the same as the mean value (the mean value of the Gaussian random variable is also its median).

■

Example 3.17 Coverage area

In cellular communication the coverage area of a cell with radius R is defined as the fraction of the cell area in which the received signal power exceeds a threshold signal power. Let us consider a differential area ΔA_i at distance r_i from the base station located at the cell center. Let $P(r_i)$ be the received power in ΔA_i. Using the *total probability theorem*, the

probability that the received signal exceeds the threshold γ (the fractional coverage area) is given by

$$\Pi = \sum_i \Pr[P(r_i) > \gamma | \Delta A_i] \Pr(\Delta A_i) \tag{3.166}$$

Furthermore, we have $\Pr(\Delta A_i) = \Delta A_i / \pi R^2$. Therefore,

$$\Pi = \frac{1}{\pi R^2} \sum_i \Pr[P(r_i) > \gamma | \Delta A_i] \Delta A_i \tag{3.167}$$

In the limit the above expression becomes the integral over the cell area. We have

$$\begin{aligned} \Pi &= \frac{1}{\pi R^2} \int_{Area} \Pr[P(r) > \gamma] \ \mathrm{d}A \\ &= \frac{1}{\pi R^2} \int_0^{2\pi} \int_0^R \Pr[P(r) > \gamma] \ r \, \mathrm{d}r \, \mathrm{d}\theta \end{aligned} \tag{3.168}$$

Substituting (3.163) into (3.168) we obtain the *fractional coverage area*, as follows:

$$\Pi = \frac{1}{\pi R^2} \int_0^{2\pi} \int_0^R Q\left(\frac{\gamma - \overline{P(r)}}{\sigma_{dB}} \right) r \, \mathrm{d}r \, \mathrm{d}\theta \tag{3.169}$$

Since $\overline{P(r)} = P_T - L_{dB}(r)$ we can evaluate the path loss at distance r based on measurements or on the Hata model.

1. **Measurement model**: the path loss is given by $L_{dB}(r) = L_{dB}(r_0) + 10n \log(r/r_0)$, where r_0 is a reference distance close to the base station but in the *far-field* or *Fraunhofer region* of its antenna (the far-field distance is $r_f = 2D^2/\lambda$, where D is the largest physical dimension of the antenna and λ is the signal wavelength). The reference path loss $L_{dB}(r_0)$ can be obtained via measurement or it can be calculated using the *Friis formula* for *free space loss* $L_{dB}(r_0) = 10 \log(4\pi r_0/\lambda)^2$. The *path loss exponent* n is obtained from measurements. Note that in *ratio form* the path loss is expressed as the *power-law* $L(r) = L(r_0)(r/r_0)^n$. For free space (n = 2), the power-law expression becomes the Friis formula that applies for any distance r.
2. **Hata model**: the path loss in the Hata model is the median path loss and is given by $L_{dB}(r) = \alpha + 10n \log r$, where the path loss exponent n is given explicitly as a function of the base station antenna height h_T, $n = 4.49 - 0.655 \log h_T$, $30\,\mathrm{m} \le h_T \le 200\,\mathrm{m}$ (see Chapter 5). The constant α depends on the carrier frequency, and the base station and mobile antenna heights.

In both cases the path loss can be expressed in general as $L_{dB}(r) = \beta + 10n \log(r/R)$, where $\beta = L_{dB}(r_0) + 10n \log(R/r_0)$ for the measurement model and $\beta = \alpha + 10n \log R$ for the Hata model. The received power is $\overline{P(r)} = P_T - L_{dB}(r) = P_T - \beta - 10n \log(r/R)$. Let

$$a = \frac{\gamma - P_T + \beta}{\sigma_{dB}} = \frac{\gamma - \overline{P(R)}}{\sigma_{dB}}, \qquad b = \frac{10n}{\sigma_{dB}} \tag{3.170}$$

Then we have the following expression for the fractional coverage area:

$$\Pi = \frac{2}{R^2}\int_0^R Q\left(a + b\,\log\frac{r}{R}\right) r\,\mathrm{d}r \tag{3.171}$$

The above integral can be evaluated as follows:

$$\Pi = Q(a) + \exp\left(\frac{2-2ab}{b^2}\right) Q\left(\frac{2-ab}{b}\right) \tag{3.172}$$

In (3.172) we note that $Q(a) = 1 - Q(-a) = 1 - p_{out}(R)$, where $p_{out}(R) = Q(-a)$ is the *outage probability at the cell boundary*. For numerical illustration, let us consider the case of $\sigma_{dB} = 10$ dB, $n = 4$, and a specified outage probability at the cell boundary of 0.01. Then $a = -2.32$, $b = 4$, and, consequently, $\Pi = 0.9986$, or 99.86% of the cell is covered with an outage probability inside the cell of less than 0.01.

■

3.6 Summary

In this chapter we have presented a fairly detailed study of the random signals often encountered in communications. These signals belong to two broad classes of random processes, namely, wide-sense cyclostationary (WSCS) and wide-sense stationary (WSS). The sequence of digital signals that carries random information symbols is itself a WSCS process. Noise that contaminates the signals is a WSS process. Furthermore, in a multipath fading channel, the envelope of the signal can be represented by special Rayleigh and Rice processes. A WSS process is characterized by a constant mean and an autocorrelation that is a function of the time difference. On the other hand, a WSCS process is characterized by periodic mean and autocorrelation.

A WSS process possesses a power spectral density function that is the Fourier transform of its autocorrelation. A WSCS process with a uniform time shift becomes a WSS process. This procedure allows the calculation of the power spectral densities of digital signal sequences. White noise has constant power spectral density. The most important process in communication theory is the Gaussian process. We learned that the processing of a Gaussian process by a linear filter also produces a Gaussian process. Noise that is encountered in communications is modeled as white Gaussian noise. Signal processing in an additive white Gaussian noise channel using a complete set of L orthonormal basis functions has sufficient statistics to be represented by exactly L samples for detection. If the noise is non-white, a whitening filter can be employed at the receiver to obtain white noise for subsequent signal processing. There are important Gaussian-derived processes that play an important role in noncoherent demodulation of digital signals in noise and in analyzing their performance in a multipath fading environment. They are the Rayleigh and Rice processes, which represent the envelope of noise and that of signal plus noise in noncoherent demodulation. In a fading channel both processes represent the envelope of the sum of diffuse signal vectors and that of the sum of direct and diffuse signal vectors, respectively. We also present the Nakagami-m density function of the envelope of the sum of random signal vectors and the log-normal density function for signals that encounter the shadowing effect.

Problems

1. The *complementary distribution function* of a Gaussian random variable X with zero mean and unit variance is given by the following Gaussian integral:

$$Q(x) = 1 - F_X(x) = \Pr(X > x) = \frac{1}{\sqrt{2\pi}} \int_x^\infty \mathrm{e}^{-y^2/2} \mathrm{d}y$$

Using integration by parts show that $Q(x)$ is upper bounded by $Q(x) < \mathrm{e}^{-x^2/2}/\sqrt{2\pi}x$

2. The *characteristic function* $\Phi_X(\omega) = \mathbf{E}\left(\mathrm{e}^{\mathrm{j}\omega X}\right)$ of the random variable X is defined as

$$\Phi_X(\omega) = \int_{-\infty}^{\infty} f_X(x) \mathrm{e}^{\mathrm{j}\omega x} \mathrm{d}x$$

Similarly, the *moment generating function* $\Phi_X(s) = \mathbf{E}(\mathrm{e}^{sX})$ of the random variable X is obtained by changing $\mathrm{j}\omega$ to s:

$$\Phi_X(s) = \int_{-\infty}^{\infty} f_X(x) \mathrm{e}^{sx} \mathrm{d}x$$

(a) Find $\Phi_X(s)$ of a Gaussian random variable X with zero mean and unit variance.
(b) Find $\Phi_X(s)$ of a Gaussian random variable X with mean m and variance σ^2

3. The *Chernoff bound* is useful in establishing the upper bound for the distribution function of a random variable X with corresponding moment generating function $\Phi_X(s) = \mathbf{E}(\mathrm{e}^{sX})$. We have the following three forms of the Chernoff bound for real s:

$$1 - F_X(x) = \Pr(X > x) \leq \mathrm{e}^{-sx}\Phi(s), \quad s > 0$$

$$F_X(x) = \Pr(X \leq x) \leq \mathrm{e}^{sx}\Phi(-s), \quad s > 0$$

$$\Pr\left(\mathrm{e}^{sX} > a\right) \leq \frac{\Phi_X(s)}{a}, \quad a > 0$$

(a) Verify all three forms of the Chernoff bound.
(b) For a zero mean, unit variance Gaussian random variable, find the Chernoff bound for the complimentary distribution function, that is, $Q(x) \leq \mathrm{e}^{-x^2/2}$.
(c) For a random variable $X > 0$ show that $\mathbf{E}\left[Q\left(\sqrt{X}\right)\right]$ has the upper bound $\mathbf{E}\left[Q\left(\sqrt{X}\right)\right] < \Phi_X(-1/2)$, where

$$Q(x) = \frac{1}{\sqrt{2\pi}} \int_x^\infty \mathrm{e}^{-y^2/2} \mathrm{d}y$$

4. Consider the complex Gaussian random variable $X = X_1 + \mathrm{j}X_2$, where X_1 and X_2 are independent Gaussian random variables with zero mean and identical variance σ^2. The mean value and variance of X are

$$\overline{X} = \mathbf{E}(X) = \mathbf{E}(X_1) + \mathrm{j}\mathbf{E}(X_2)$$

$$\mathrm{Var}(X) = \mathbf{E}\left[\left|X - \overline{X}\right|^2\right]$$

We have $\overline{X} = 0$ and $\mathrm{Var}(X) = \mathbf{E}\left[\left|X - \overline{X}\right|^2\right] = \mathbf{E}\left[|X|^2\right] = 2\sigma^2$. Now consider the random variable $Y = \mathrm{e}^{\mathrm{j}\theta}X$ for arbitrary θ. Show that both Gaussian random variables Y and X have the same mean and variance. (This property is called *circular symmetry*.)

5. A complex Gaussian random variable $X = X_1 + \mathrm{j}X_2$, where X_1 and X_2 are independent Gaussian random variables with zero mean and identical variance σ^2, can be represented in vector form as $\boldsymbol{X} = [X_1 \quad X_2]^t$. The mean value of $\boldsymbol{X}$ is $\overline{\boldsymbol{X}} = 0$, and the variance is $\mathbf{E}(\boldsymbol{X}^t\boldsymbol{X}) = 2\sigma^2$. Express the complex random variable $Y = \mathrm{e}^{\mathrm{j}\theta}X$ for arbitrary θ in vector form $\boldsymbol{Y}$ and calculate the covariance matrix $\mathbf{K}$ of $\boldsymbol{Y}$.
6. Consider the process $X(t) = A\sin(2\pi ft + \Theta)$, where A is a constant and Θ is a random variable. Is $X(t)$ wide-sense stationary? Find the conditions for which the process is wide-sense stationary.
7. Consider the process $X(t) = A\sin(2\pi ft + \Theta)$, where Θ is a discrete random variable with probability distribution $\Pr(\Theta = 0) = 1/2,\ \Pr(\Theta = \pi) = 1/2$. Shows that $X(t)$ is not stationary by demonstrating that two random variables $X(0)$ and $X(a)$ for a selected time $t = a$ have different distributions. Is it wide-sense stationary?
8. Find the autocorrelation of the process $X(t) = A\cos(2\pi ft + \Theta)$, where Θ is uniformly distributed on $[0, 2\pi]$ and A is a Gaussian random variable with zero mean and unit variance and is independent of Θ.
9. Find the autocorrelation of the process $Y(t) = X(t)\cos(2\pi ft + \Theta)$, where Θ is uniformly distributed on $[0, 2\pi]$ and $X(t)$ is a wide-sense stationary process.
10. Consider a Gaussian vector $\boldsymbol{X} = (X_1\ X_2\ \cdots\ X_n)$ whose independent elements have zero mean and identical variance σ^2. Find the moment generating function of the random variable $Y = \boldsymbol{X}\boldsymbol{X}^t$
11. Derive the general expression for the autocorrelation of the random process $X(t) = \sum_{i=-\infty}^{\infty} d_i\, p(t - iT - \Delta)$ with arbitrary pulse shape $p(t)$ and independent bits d_i; assuming that the time delay Δ is *uniformly distributed in* $(0, T)$ and independent of d_i, where T is the pulse time. Show that the power spectral density of the process $X(t)$ is given by

$$S_X(f) = \frac{|P(f)|^2}{T} S_d(\mathrm{e}^{\mathrm{j}2\pi fT}), \quad S_d(\mathrm{e}^{\mathrm{j}2\pi fT}) = \sum_k R_d(k)\mathrm{e}^{-\mathrm{j}2\pi fkT}$$

where $R_d(k)$ is the discrete autocorrelation of the data symbols d_i.

12. Consider the process $X(t) = A\sin(2\pi ft + \Theta)$, where A is a constant and Θ is a uniform random variable in $[-\pi, \pi]$. Is $X(t)$ ergodic in the autocorrelation function?
13. Consider an OOK signal sequence $X(t) = \sum_{i=-\infty}^{\infty} d_i\, p(t - iT_b)$ that represents *independent* and *equally likely* bits [0,1], where $p(t)$ is the *half-squared* pulse shape of unit amplitude and duration T_b, which is a bit time (Figure 3.3(a)), and $d_i \in \{1, 0\}$ represents the normalized signal amplitudes. The mapping $0 \rightarrow 1$ *and* $1 \rightarrow 0$ maps bit 0 to amplitude 1 and bit 1 to amplitude 0 (the mapping $0 \rightarrow 0$ *and* $1 \rightarrow 1$

maps bit 0 to amplitude 0 and bit 1 to amplitude 1 would give the same result). Assuming the time origin is *uniform* in a bit time T_b, find the power spectral density function of $X(t)$.

14. Consider the *alternative mark inversion* (AMI) signaling, where bit 1 is represented by alternate positive and negative half-squared pulses and bit 0 is represented by a zero voltage level. Assuming the time origin is *uniform* in a bit time T_b, find the power spectral density function of $X(t)$.
15. Consider the *Manchester* signaling, where bit 1 is represented by a positive half-squared pulse followed by a negative half-squared pulse and bit 0 is represented by a negative half-squared pulse followed by a positive half-squared pulse. Assuming the time origin is *uniform* in a bit time T_b, find the power spectral density function of $X(t)$.
16. Let $X(t)$ be a WSS process and $Y(t) = X(t+T) - X(t-T)$. Find the autocorrelation and power spectral density function of $Y(t)$.
17. Let $g(t)$ be a deterministic periodic function and $X(t)$ is a zero mean ergodic process. Find the autocorrelation and power spectral density of $Y(t) = g(t) + X(t)$
18. Consider the process $X(t) = \sum_{i=-\infty}^{\infty} d_i p(t - iT_b)$ with uncorrelated and equally likely bits $d_i \in \{-1, 1\}$. The bit time is T_b. Form the process $Y(t) = X(t)X(t - T_b/2)$
    (a) Is $Y(t)$ WSCS?
    (b) Find the deterministic periodic component of $Y(t)$ which is also the bit clock.
    (c) Design a circuit to extract the bit clock.
19. Consider an RC circuit with frequency response $H(f) = 1/(1 + \mathrm{j}2\pi fRC)$. The input to this circuit is white noise with power spectral density function $N_0/2$.
    (a) Derive the expression for the output noise power spectral density.
    (b) Derive the expression for the output noise autocorrelation.
20. The integrate-and-dump filter is a linear system with output $Y(t) = \int_{t-T}^{t} X(\tau)\mathrm{d}\tau$ when $X(t)$ is applied to its input. Derive the expression for the power spectral density of $Y(t)$.
21. Consider the process $X(t) = A\sin(2\pi ft + \Theta)$ where A is a constant, Θ is a uniform random variable in $[-\pi, \pi]$, and f is a random variable with a density function satisfying the relationship $p_F(f) = p_F(-f)$. Find the power spectral density of $X(t)$.
22. Consider non-white noise of power spectral density $S_n(f) = (\omega^2 + 1)/(\omega^4 + 64)$. Design a minimum-phase whitening filter.
23. Consider an integrator over (0, T) driven by zero mean white Gaussian noise of power spectral density $N_0/2$. Find the variance of the output noise.
24. A *Gauss–Markov* process $X(t)$ with variance σ^2 and time constant $1/\beta$ is a stationary Gaussian process with an exponential autocorrelation of the form $R_X(\tau) = \sigma^2 \mathrm{e}^{-\beta|\tau|}$.
    (a) Evaluate the power spectral density function of $X(t)$.
    (b) Apply $X(t)$ to the input of an integrator, find the power spectral density of the output process.
25. Consider the random variable $X = \log_2(1 + R^2\gamma)$. where R is Rayleigh distributed with $E(R^2) = 1$ and γ is a nonnegative constant. Find $\Pr(X \leq x)$.
26. Consider the case of log-normal shadowing with $\sigma_{dB} = 10$ dB, $n = 4$, and a specified outage probability at the cell boundary of 0.1. Find the fractional coverage area.

27. Consider a log-normal shadowing model with a standard deviation $\sigma = 12$ dB and a single circular cell. The receiver at the cell boundary has a noise power of -146.9 dBW. The cell has a path loss exponent $n = 4$. The percentage of coverage area is determined to be 95%. The received signal threshold (which is set at a smaller value than the mean received signal) is fixed at -129 dBW. What is the mean received signal-to-noise ratio?

Further reading

For a thorough review of probability theory, random variables, and random processes, we recommend Papoulis [3], Helstrom [4], and Leon-Garcia [5]. Advanced materials can be found in Feller [6]. More materials on cyclostationary processes can be found in Gardner [7].

Bibliography

1. R. N. McDonough and A. D. Whalen, *Detection of Signals in Noise*, 2nd edition, London: Academic Press, 1995.
2. S. Haykin, *Communications Systems*, 2nd edition, Chichester: John Wiley & Sons, 1983.
3. A. Papoulis, *Probability, Random Variables, and Stochastic Processes*, 3rd edition, New York: McGraw-Hill, 1991.
4. C. W. Helstrom, *Probability and Stochastic Processes for Engineers*, 2nd edition, New York: Macmillan, 1991.
5. A. Leon-Garcia, *Probability and Random Processes for Electrical Engineering*, 2nd edition, Reading, MA: Addison-Wesley, 1994.
6. W. Feller, *An Introduction to Probability Theory and its Applications*, Vol. **I** (3rd edition), Vol. II (2nd edition), Chichester: John Wiley & Sons, 1968, 1971.
7. W. A. Gardner, *Introduction to Random Processes*, 2nd edition, New York: McGraw-Hill, 1990.
8. J. R. Cogdell, *Modeling Random Systems*, Harlow: Pearson Prentice-Hall, 2004.
9. M. Nakagami, "The m-distribution-A general formula of intensity distribution of rapid fading," in *Statistical Methods of Radio Wave Propagation*, edited by W. C. Hoffman, Oxford: Pergamon Press, pp. 3–36, 1960.
10. P. Z. Peebles, Jr., *Probability, Random Variables, and Random Signal Principles*, 3rd edition, New York: McGraw-Hill, 1993.
11. S. O. Rice, "Mathematical analysis of random noise," *Bell Syst. Tech. J.*, Vol. **23**, pp. 282–332, 1944, Vol. **24**, pp. 46–156, 1945.
12. J. B. Thomas, *An Introduction to Statistical Communication Theory*, Chichester: John Wiley & Sons, 1969.

4 Information theory and channel coding

Introduction

In this chapter we present the applicability of probability theory and random variables to the formulation of *information theory* pioneered by Claude Shannon in the late 1940s [1,2]. Information theory introduces the general idea of *source coding* and *channel coding*. The purpose of source coding is to minimize the bit rate required to represent the source (represented mathematically by a discrete random variable) with a specified efficiency at the output of the source coder. On the other hand, the goal of channel coding is to maximize the bit rate at the input of the channel encoder so that code words can be transmitted through the channel with a specified reliability. Both source coding and channel coding can be achieved with the knowledge of the statistics of both the source and channel.

4.1 Entropy of a discrete source

Information comes from observing the outcome of an event. Common events occur frequently (high probability) and therefore carry little information. On the other hand, rare events occur infrequently (low probability) and hence carry much more information. In 1928 R. V. L. Hartley proposed a logarithmic measure of information that illustrates this observation [3]. Let us consider a *discrete source* that is represented mathematically by the discrete random variable X. The source emits M symbols x_i, $i = 1,2, \ldots, M$, which are characterized by the probability distribution function $p_X(x_i)$. The *self-information* of the source is the function $I(X)$ that assumes the values $I(x_i)$, defined as follows:

$$I(x_i) = -\log_2 p_X(x_i) \tag{4.1}$$

It is seen that the smaller the probability of the outcome x_i, the larger its self-information. Thus, a *certain event* has zero self-information and an *impossible event* has infinite self-information. The average information in the source X with a given distribution is the expected value of $I(X)$ and is formally denoted as the *entropy* of X with the designated notation $H(X)$. Using (3.17) we have

$$H(X) = E\{I(X)\} = -\sum_{i=1}^{M} p_X(x_i)\, \log_2 p_X(x_i) \tag{4.2}$$

The use of the *base-two logarithm* indicates that the unit of entropy is the *bit*.

Example 4.1 Binary source
Consider a discrete source that emits binary symbols 0 and 1 with probability distribution $p_X(0) = p$ and $p_X(1) = 1 - p$. The entropy of this binary source is given by

$$H(X) = -p \log_2 p \; - \; (1-p) \log_2 (1-p) \tag{4.3}$$

Let $p = 0.1$, then $H(X) = 0.47$ bits. This is the average number of bits needed per source symbol. The entropy is maximum, that is, $\max_p \; H(X) = 1$ bit, when $p = 0.5$. This indicates that the entropy is at maximum when the distribution is *uniform* or *equally likely*. Since the average symbol length is 1 bit and the source is binary, the source coder transmits the symbol unaltered.

■

Theorem 4.1 *Consider a discrete source X with a given probability distribution* $p_X(x_i)$, $i = 1,2, \ldots, M$. *Then its entropy satisfies the following inequality*

$$H(X) \leq \log_2 M \tag{4.4}$$

The equality *is achieved when the distribution is uniform (equally likely symbols), that is*, $p_X(x_i) = 1/M$ *for all i.*

Proof We make use of the identities $\sum_{i=1}^{M} p_X(x_i) = 1$ and $\ln a \leq a - 1$ in the following expression:

$$\begin{aligned} H(X) - \log_2 M &= -\sum_i p_X(x_i) \; \log_2 p_X(x_i) \; - \; \log_2 M \sum_i p_X(x_i) \\ &= -\sum_i p_X(x_i) \; \log_2 \{M p_X(x_i)\} = \sum_i p_X(x_i) \; \log_2 \frac{1}{M p_X(x_i)} \\ &= \sum_i p_X(x_i) \; \frac{\ln \frac{1}{M p_X(x_i)}}{\ln 2} \\ &\leq \frac{1}{\ln 2} \sum_i p_X(x_i) \left[\frac{1}{M p_X(x_i)} - 1 \right] \end{aligned} \tag{4.5}$$

Therefore,

$$\begin{aligned} H(X) - \log_2 M \; &\leq \frac{1}{\ln 2} \sum_i \left[\frac{1}{M} - p_X(x_i) \right] \\ &\leq \frac{1}{\ln 2} \left[\sum_i \frac{1}{M} - \sum_i p_X(x_i) \right] \\ &\leq \frac{1}{\ln 2} (1 - 1) \\ &\leq 0 \end{aligned} \tag{4.6}$$

When $p_X(x_i) = 1/M$ for all i, that is, the distribution is uniform, we have $H(X) = -\sum_i (1/M)\log_2(1/M) = -(1/M)\log_2(1/M)\sum_i 1 = \log_2 M$.
■

The next discussion centers around source encoding, that is, what kind of code should one use to represent source symbols with a given distribution such that the bit rate at the source coder output is minimized? Intuitively one would think about a code with the average code word length (each source symbol is represented by a code word whose length is in bits) equal to the source entropy. After all, the source entropy, which is the average self-information of the source, is its best snapshot. We will present the best code that can approach the prescribed goal. Furthermore, the average code word length is of interest because if we transmit a long string of n symbols with a total length L_n bits, then the *law of large numbers* dictates that the number of bits per symbols L_n/n approaches the average code word length with a probability close to one.

4.2 Source coding

From the above study we observe that when the source symbols are *equally likely* the best code is simply the *block code* or *fixed-length code* in which all the code words have $\log_2 M$ bits (the source entropy). For source symbols that are not equally likely, a *variable-length code* must be used to approach the source entropy. Intuitively, we assign a long code word to a less frequent symbol and a short code word to a more frequent symbol. This is the idea behind *Morse code*, with the most frequently used letter E given the code word "dot." There is a problem with decoding a variable-length code at the receiver, that is, recognizing the end of one code word and the beginning of the next. This problem can be solved if no code word is the *prefix* of another code word. A source code that possesses such a property is called a *prefix code* or *instantaneous code*. Thus, a string of prefix code words is *self-punctuating*, as illustrated for a source of four symbols and their corresponding prefix code words below:

$$x_1 = 0, \quad x_2 = 10, \quad x_3 = 110, \quad x_4 = 111 \tag{4.7}$$

$$0011110110 \ \rightarrow 0, 0, 111, 10, 110 \ \rightarrow x_1, x_1, x_4, x_2, x_3 \tag{4.8}$$

Thus, in a prefix code each symbol can be decoded without looking to the right of it. The prefix codes are examples of *uniquely decodable codes* whose code words can be unambiguously reconstructed from the bit sequence. Here, it is assumed that synchronization is established before decoding starts. The existence of a prefix code can be verified by the *Kraft inequality*, as stated in the following theorem.

Theorem 4.2 (*Kraft inequality*) *The necessary and sufficient condition for the existence of a prefix code of M symbols with code words of length* l_m, $m = 1, 2, ..., M$, *is*

$$\sum_{m=1}^{M} \frac{1}{2^{l_m}} \ \leq \ 1 \tag{4.9}$$

The code in (4.7) satisfies the Kraft inequality with an equals sign. The following theorem shows a relationship between the average code word length and the entropy.

Theorem 4.3 *Consider a discrete source X with a given distribution* $p_X(x_i)$, $i = 1,2, \ldots, M$. *Each symbol* x_i *is encoded by a code word of length* l_i *of a prefix code. Then, the average code word length* $\bar{l} = \sum_i p_X(x_i) l_i$ *of the prefix code satisfies the following relationship*:

$$H(X) \leq \bar{l} \tag{4.10}$$

Proof The first step is to establish the expression $H(X) - \bar{l}$ and show that it is less than or equal to zero. We use the following identities:

$$\log_2 x = (\log_2 \mathrm{e}) \ln x, \quad \ln x \leq x - 1$$

$$\begin{aligned} H(X) - \bar{l} &= -\sum_i p_X(x_i) \log_2 p_X(x_i) - \sum_i p_X(x_i) l_i \\ &= \sum_i p_X(x_i) \left(\log_2 \frac{1}{p_X(x_i)} + \log_2 2^{-l_i} \right) = \sum_i p_X(x_i) \left(\log_2 \frac{2^{-l_i}}{p_X(x_i)} \right) \\ &= \log_2 \mathrm{e} \sum_i p_X(x_i) \left(\ln \frac{2^{-l_i}}{p_X(x_i)} \right) \\ &\leq \log_2 \mathrm{e} \sum_i p_X(x_i) \left(\frac{2^{-l_i}}{p_X(x_i)} - 1 \right) \\ &\leq \log_2 \mathrm{e} \left(\sum_i 2^{-l_i} - \sum_i p_X(x_i) \right) \leq \log_2 \mathrm{e} \ (1 - 1) \leq 0 \end{aligned} \tag{4.11}$$

The last line follows the Kraft inequality.

■

Theorem 4.4 *Consider a discrete source X with a given distribution* $p_X(x_i)$, $i = 1, 2, \ldots, M$. *Each symbol* x_i *is encoded by a* Shannon–Fano prefix code, *whose code word of length* l_i *is selected according to the relationship*

$$-\log_2 p_X(x_i) \leq l_i \leq -\log_2 p_X(x_i) + 1 \tag{4.12}$$

Then, the average code word length satisfies the following inequalities:

$$H(X) \leq \bar{l} \leq H(X) + 1 \tag{4.13}$$

Proof The left-hand side of (4.12) yields $2^{-l_i} \leq p_X(x_i)$ and hence $\sum_i 2^{-l_i} \leq \sum_i p_X(x_i) = 1$. Since the Kraft inequality is satisfied there exists a prefix code with the above selected lengths such that the left-hand side of (4.13) is satisfied per Theorem 4.3. From the right-hand side of (4.12) we have

$$\bar{l} = \sum_i p_X(x_i) l_i \leq -\sum_i p_X(x_i) \log_2 p_X(x_i) + \sum_i p_X(x_i) \leq H(X) + 1 \tag{4.14}$$

■

Example 4.2 Shannon–Fano code
Consider a discrete source with distribution

$$p_X(x_1) = p_X(x_2) = 0.1, \quad p_X(x_3) = p_X(x_4) = 0.2, \quad p_X(x_5) = 0.4 \tag{4.15}$$

The Shannon–Fano code words have the following length in bits:

$$l_1 = l_2 = 4, \quad l_3 = l_4 = 3, \quad l_5 = 2 \tag{4.16}$$

The average code word length in bits is

$$\bar{l} = \sum_{i=1}^{5} p_X(x_i)\, l_i \;=\; 2.8 \;>\; H(X) = -\sum_{i=1}^{5} p_X(x_i)\, \log_2 p_X(x_i) \;=\; 2.12 \tag{4.17}$$

■

The above theorem shows that one can do no worse than $H(X) + 1$ with Shannon–Fano codes. The question is, can one do better? In the following discussion we present the *Huffman codes*, which are optimum in the sense that they are the prefix codes that approach the entropy in average lengths. Furthermore, no other prefix codes have smaller average code word lengths.

Huffman codes

A Huffman code is constructed as follows:

1. The source symbols are listed in order of decreasing probability.
2. A tree is constructed to the right with the two source symbols of the smallest probabilities combined to yield a new symbol with the probability equal to the sum of the two previous probabilities.
3. The final tree is labeled with 0 on the lower branch (upper branch) and 1 on the upper branch (lower branch).

Example 4.3 Huffman code
Consider a discrete source with distribution

$$p_X(x_1) = p_X(x_2) = 0.1, \quad p_X(x_3) = p_X(x_4) = 0.2, \quad p_X(x_5) = 0.4 \tag{4.18}$$

We construct the two trees shown in Figure 4.1. Both Huffman codes have the following average length in bits:

$$\begin{aligned} \bar{l} &= 0.1(4) + 0.1(4) + 0.2(3) + 0.2(2) + 0.4(1) = 2.2 \\ \bar{l} &= 0.1(3) + 0.1(3) + 0.2(2) + 0.2(2) + 0.4(2) = 2.2 \end{aligned} \tag{4.19}$$

The source entropy is $H(X) = 2.12$. If we compare the Huffman code with the Shannon–Fano code in the previous example we conclude that the former is more efficient.

■

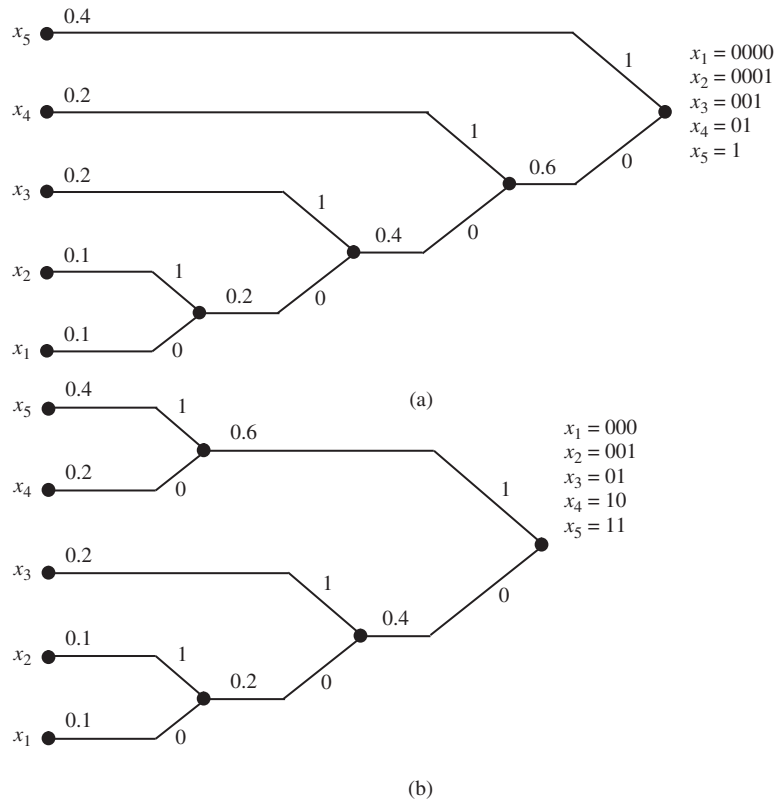

Figure 4.1 Huffman codes.

Shannon noiseless source coding theorem (first theorem)

Consider a discrete source X of M symbols with a given distribution. The average code word length can be made to approach the source entropy as close as required, so that

$$H(X) \leq \bar{l} < H(X) + \varepsilon \tag{4.20}$$

where $\varepsilon < 1$ is an arbitrary positive constant.

Proof Let us consider the nth extension of the source X called X^n, which consists of M^n *extended symbols*. Each extended symbol consists of n concatenated original source symbols and has a probability equal to the product of n probabilities. Since the log of the product equals the sum of logs, the entropy of the extended source is n times the entropy of the original source, that is,

$$H(X^n) = nH(X) \tag{4.21}$$

Applying the result of Theorem 4.4 to the extended source we obtain the following bounds on $\bar{L}$, the average code word length of X^n:

$$H(X^n) \leq \overline{L} \leq H(X^n) + 1 \tag{4.22}$$

Substituting (4.21) into (4.22) and dividing by n, we have

$$H(X) \leq \frac{\overline{L}}{n} \leq H(X) + \frac{1}{n} \tag{4.23}$$

Note that $\bar{l}$, the average code word length of the original source X, is equal to $\overline{L}/n$ since the extended symbol has n original symbols. Therefore,

$$H(X) \leq \bar{l} \leq H(X) + \frac{1}{n} \tag{4.24}$$

Choose $\varepsilon \geq 1/n$, and we obtain the result in (4.20).

■

In the subsequent discussion we introduce the concept of *channel coding* to maximize the rate of reliable transmission over a noisy channel. This necessitates the evaluation of the *Shannon channel capacity*, which cannot be exceeded if reliable transmission is to be accomplished. We investigate information capacities of *discrete* and *Gaussian channels*.

4.3 Discrete channel

All communication channels are noisy and therefore the symbols at the channel output are not always the same as the input symbols. Thus, we ask ourselves the question, "How much information can we reliably transmit through a noisy channel?" Or, equivalently, "What is the maximum data rate for arbitrary small error probability?" The answer had been provided by Claude Shannon in 1948 [1,2]. In this section we present the Shannon channel capacity for a discrete channel characterized by a set U of M input symbols u_i, a set V of Q *output symbols* v_j and their *conditional probabilities* $p(v_j|u_i)$, called *transition probabilities*. The sizes of M and Q are not necessarily the same. We assume that the channel noise corrupts the input symbols independently, therefore the channel is said to be *memoryless*. Figure 4.2 illustrates the discrete channel concept. The discrete channel is a synthetic channel that can be derived from the physical channel, as illustrated in Figure 4.3 for a wireless communication system. In this case, the channel transition probability can be evaluated from the knowledge of the modulated waveform, the received signal-to-noise-ratio via the link analysis and the demodulation technique. The input m_i to the channel encoder is one of M message blocks (*source code words*) obtained from the *source coder* output. For example, consider a binary source with equally likely symbols x_1, x_2. Using k-symbol source block

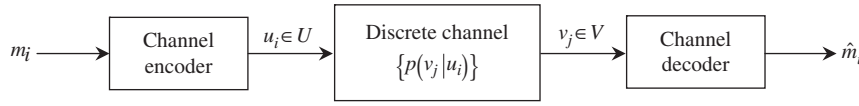

Figure 4.2 Discrete channel model.

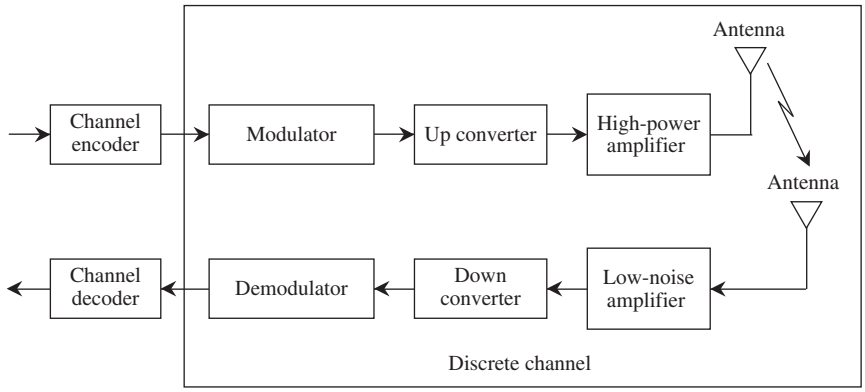

Figure 4.3 A physical channel.

code the message block consists of any k source symbols, and hence there are $M = 2^k$ distinct message blocks. The channel encoder may encode each message block into an n-bit input symbol (*channel code word*) u_i, where $n > k$. Thus, there are a total of $M = 2^k$ input symbols. Given the n-bit input symbol $u_i = (u_{i1}, ..., u_{in})$ the probability of observing the n-bit output symbol $v_j = (v_{j1}, ..., v_{jn})$ is the following transition probability:

$$p(v_j|u_i) = \prod_{l=1}^{n} p(v_{jl}|u_{il}) \tag{4.25}$$

Thus throughout our discussion we assume that the channel is characterized by the conditional probabilities $p(v_{jl}|u_{il}),\ i \in U, j \in V$, and hence $p(v_j|u_i)$.

Mutual information

The concept of mutual information is intuitive. Suppose a symbol u_i was sent by the channel encoder with probability $p_U(u_i)$. This is often called the *a-priori probability* of the input symbol u_i. The probability that u_i was the sent symbol after the observation of the output symbol v_j becomes $p(u_i|v_j)$. This is often referred to as the *a-posteriori probability* of u_i . If the channel is noiseless then after receiving v_j one would know exactly that u_i was sent and the a-posteriori probability is 1. Now consider the case of a very noisy channel. The reception of v_j will not help at all in determining what input symbol in the set U was sent. This means that the a-posteriori probability is the same as the a-priori probability. If the channel is somewhere between these two extreme cases, then the a-posteriori probability is larger than the a-priori probability. Hence, one obtains an *information gain* from the reception of the output symbol. This can be expressed quantitatively as the difference between the self-information of u_i and the self-information of u_i after v_j was observed, and is called the *pair-wise mutual information*:

$$\begin{aligned} I(u_i, v_j) &= \log_2 \frac{1}{p_U(u_i)} - \log_2 \frac{1}{p_U(u_i|v_j)} \\ &= \log_2 \frac{p_U(u_i|v_j)}{p_U(u_i)} = \log_2 \frac{p_V(v_j|u_i)}{p_V(v_j)} \end{aligned} \tag{4.26}$$

since $p_U(u_i|v_j)p_V(v_j) = p_V(v_j|u_i)p_U(u_i) = p_{UV}(u_i, v_j)$, where $p_{UV}(u_i, v_j)$ is the joint distribution of u_i, v_j.

The *mutual information* is the average of $I(u_i, v_j)$ over the input symbol set U and output symbol set V and is given by

$$\begin{aligned} I(U,V) &= \sum_i \sum_j p_{UV}(u_i, v_j) I(u_i, v_j) \\ &= \sum_i \sum_j p_{UV}(u_i, v_j) \log_2 \frac{p_U(u_i|v_j)}{p_U(u_i)} \\ &= \sum_i \sum_j p_{UV}(u_i, v_j) \log_2 \frac{p_V(v_j|u_i)}{p_V(v_j)} \end{aligned} \tag{4.27}$$

Expanding the log term we have

$$\begin{aligned} I(U,V) &= -\sum_i \sum_j p_{UV}(u_i, v_j) \log_2 p_U(u_i) + \sum_i \sum_j p_{UV}(u_i, v_j) \log_2 p_U(u_i|v_j) \\ &= -\sum_i p_U(u_i) \log_2 p_U(u_i) - \left(-\sum_i \sum_j p_{UV}(u_i, v_j) \log p_U(u_i|v_j) \right) \\ &= H(U) - H(U|V) \end{aligned} \tag{4.28}$$

where the entropy $H(U)$ and the conditional entropy $H(U|V)$ are given by

$$H(U) = -\sum_i p_U(u_i) \log_2 p_U(u_i) \tag{4.29}$$

$$\begin{aligned} H(U|V) &= \sum_j p_V(v_j) H(U|v_j) = -\sum_j \sum_i p_V(v_j) p_U(u_i|v_j) \log_2 p_U(u_i|v_j) \\ &= -\sum_i \sum_j p_{UV}(u_i, v_j) \log_2 p_U(u_i|v_j) \end{aligned} \tag{4.30}$$

By symmetry we also obtain the following expression:

$$I(U,V) = H(V) - H(V|U) \tag{4.31}$$

where the entropy $H(V)$ and the conditional entropy $H(V|U)$ are given by

$$H(V) = -\sum_j p_V(v_j) \log_2 p_V(v_j) \tag{4.32}$$

$$\begin{aligned} H(V|U) &= \sum_i p_U(u_i) H(V|u_i) = -\sum_j \sum_i p_U(u_i) p_V(v_j|u_i) \log_2 p_V(v_j|u_i) \\ &= -\sum_i \sum_j p_{UV}(u_i, v_j) \log_2 p_V(v_j|u_i) \end{aligned} \tag{4.33}$$

Theorem 4.5 *The mutual information obeys the following relationship*:

1. $I(U,V) \geq 0$.
2. $I(U,V) = 0$ *if and only if* U *and* V *are independent*.
3. $I(U,V) = I(V,U)$

■

Channel capacity

The *information channel capacity* is the *maximum* of the mutual information over all possible input symbol distributions

$$C = \max_{p_U(u_i)} I(U,V) \tag{4.34}$$

To see why the maximum is carried out over $p_U(u_i)$ only, we need to examine (4.32) and (4.33). Applying the total probability theorem we have $p_V(v_j) = \sum_i p_V(v_j|u_i)p_U(u_i)$. Furthermore, $p_{UV}(u_i, v_j) = p_V(v_j|u_i)p_U(u_i)$, thus $I(U,V)$ is a function of $p_U(u_i)$ and $p_V(v_j|u_i)$. The *channel transition probabilities* $p_V(v_j|u_i)$ which completely describe the channel are fixed once the channel model is specified. This leaves the designer with only the choice of finding a suitable $p_U(u_i)$ to maximize the mutual information. Thus, *the channel capacity depends only on the channel transition probabilities.* In practice, finding a suitable input symbol (code word) distribution is equivalent to finding a *suitable channel code* to approach the channel capacity defined in (4.34). A suitable code must apparently have code words that contain long message blocks to be efficient and the code must be able to correct as many errors as possible in the message blocks given the channel model, that is, its transition probabilities. The smaller the specified bit error probability, the larger the size of the code words in order to *average out* the channel errors (by the law of large numbers). In other words, there exist codes that allow one to arbitrarily approach channel capacity via the optimization in (4.34) and at the same time arbitrarily approach a specified error rate via the law of large numbers. This is the essence of *Shannon noisy channel coding*. If the information rate exceeds the Shannon channel capacity, then the error rate cannot be kept arbitrarily small.

The channel capacity unit is *coded bits/input symbol* since this is the unit of entropy. If the unit is in *coded bits/second*, then we need to multiply the channel capacity in coded bits/input symbol by the input symbol rate in *input symbols/second* to have the channel capacity in *coded bits/second*. We can restate the Shannon channel capacity in an alternate way using the *Shannon main theorem*, described next.

Shannon noisy channel coding theorem (main theorem)

Let **C** be the capacity of a discrete channel, and **H** be the entropy per second of a discrete source. If $\mathbf{H} \leq \mathbf{C}$, there exists a coding system such that the output of the source can be transmitted over the channel with an arbitrarily small frequency of errors.

The meaning of the *Shannon main theorem* can be interpreted in the following manner. Let X be a discrete source with M source symbols and entropy $H(X)$ in bits/source symbol. The source symbols are encoded into M channel input symbols (code words). For example, if the source symbol (message block) has k bits and the input symbol (code word) has $n > k$ coded bits, then the *code rate* is $r = k/n$. Assume that the source transmits R source symbols/second, then the source entropy in bits/second is $\mathbf{H} = RH(X)$ bits/second. The channel capacity C is given in coded bits/input symbol. The channel capacity is $\mathbf{C} = RC/r$ coded bits/second. If $\mathbf{H} \leq \mathbf{C}$ then we have $RH(X) \leq RC/r$. This implies $r \leq C/H(X)$. The key to designing a good communication system is to find a code with rate r close to $C/H(X)$ that can meet a specified error rate.

■

The converse of the *Shannon noisy channel coding theorem* is if $\mathbf{H} > \mathbf{C}$ it is not possible to transmit the output of the source over the channel with an arbitrarily small frequency of errors.

With the publication of his work [1,2], Shannon opened the field of coding theory and set the course for coding theorists to discover many types of efficient codes [4,5] capable of achieving what Shannon stated in his famous main theorem.

Example 4.4 Binary symmetric channel

The binary symmetric channel (BSC) in Figure 4.4 is a simple but widely used model for binary communication systems. In this channel model the binary source is equally likely with distribution 0.5 for bit 0 and 0.5 for bit 1. Hence, the *source entropy is* 1 *bit*. The source transmits the bits unaltered (no channel coding) and the channel transition probabilities are given by

$$p(0|1) = p(1|0) = p,\ p(0|0) = p(1|1) = 1 - p \tag{4.35}$$

Using (4.31) and (4.34) we obtain the *capacity* of the binary symmetric channel as follows:

$$C = 1 + p\log_2 p + (1-p)\log_2(1-p) \tag{4.36}$$

It is 1 bit when $p = 0$ or 1, and 0 when $p = 0.5$.

■

Example 4.5 Repetition code

Let us consider a BSC with $p = 10^{-2}$. From Example 4.4, we obtain the channel capacity $C = 0.919$ bits. Suppose we want to send information bits over this channel with arbitrarily

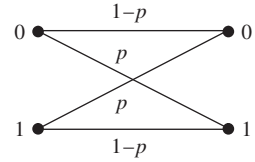

Figure 4.4 Binary symmetric channel.

small error probability, then according to the *Shannon main theorem* there exist codes with rate $r \leq C/H(X) = 0.919/1 = 0.919$ that can accomplish this task. For simplicity we consider the *repetition code* $(n,1)$ with code rate $r = 1/n$, where an information bit is encoded by repetition into a code word (channel input symbol) of n identical bits. For example, in a (3,1) repetition code the following encoding is carried out: $0 \rightarrow (000),\ 1 \rightarrow (111)$. In practice, the code word length n is commonly chosen to be an odd integer. Thus, if a received code word has more 0s than 1s, the decoded bit is bit 0. Otherwise, the decoded bit is bit 1. An error occurs when $\lfloor (n-1)/2 \rfloor$ or more coded bits out of n bits are received incorrectly, where $\lfloor (n-1)/2 \rfloor$ is the largest integer no greater than $(n-1)/2$. Thus a $(n,1)$ repetition code can correct $t = \lfloor (n-1)/2 \rfloor$ errors in a code word. The *bit error probability*, which is the same as the *code word error probability* (a code word carries only one information bit), for the coded system is given by

$$P_e = \sum_{i=t+1}^{n} \binom{n}{i} p^i (1-p)^{n-i} \tag{4.37}$$

Numerically we have $r = 1/3$ yields $P_e = 3 \times 10^{-4}$ and $r = 1/5$ yields $P_e = 10^{-6}$. Thus we can achieve arbitrarily small error probability by using longer codes. For the same transmission rate a repetition code decreases the channel throughput by a factor n. This also implies that the transmission rate over the channel will be n times larger for a constant throughput, and hence the physical channel must have a larger bandwidth to accommodate this higher transmission rate. In the next example we introduce a more efficient code to reduce the transmission rate as compared with the repetition code.

■

Example 4.6 Hamming code

The historic (n,k) *Hamming codes* with code rate $r = k/n$ were first discovered by Richard W. Hamming in 1950 [6]. For a positive integer $m \geq 3$ the code structure is summarized as follows:

Code word length	$n = 2^m - 1$
Message block	$k = 2^m - 1 - m$
Parity-check block	$n - k = m$
Error-correcting capability	$t = 1$
Minimum Hamming distance	$d_{min} = 3$

The message block is the number of information bits; the parity-check block is unique to the code and is a linear sum of the information bits. The *Hamming distance* between two different code words is the number of positions in which they differ. The error-correcting capability t is related to the minimum Hamming distance as $t = \lfloor (d_{min} - 1)/2 \rfloor$. In other words, we also have $d_{min} \geq 2t + 1$. Note that this relationship holds for repetition code $(n,1)$ for any n (even or odd). To prove this relationship, which is true for any linear block code, let t be a positive integer such that the following inequalities hold:

Table 4.1 The (7,4) Hamming code

Message block	Code word	Message block	Code word
0000	0000000	1000	1101000
0001	1010001	1001	0111001
0010	1110010	1010	0011010
0011	0100011	1011	1001011
0100	0110100	1100	1011100
0101	1100101	1101	0001101
0110	1000110	1110	0101110
0111	0010111	1111	1111111

$$2t + 1 \leq d_{min} \leq 2t + 2 \tag{4.38}$$

Let u, v, and w be the transmitted code word, the received word, and an arbitrary code word in the code. Applying the *triangle inequality* to the Hamming distances among u, v, and w, we obtain

$$d(u, v) + d(w, v) \geq d(u, w) \tag{4.39}$$

Note that $d(u, w) \geq d_{min} \geq 2t + 1$, therefore any *error pattern which has less than or equal to t errors*, that is, $d(u, v) \leq t$, results in the following inequality for an arbitrary w:

$$d(w, v) \geq 2t + 1 - t = t + 1 \tag{4.40}$$

The decoder selects u over all w's in the code since u is closer in Hamming distance to v.

Table 4.1 shows the 16 code words of the (7,4) Hamming code together with the corresponding message block. The first three bits are the parity-check bits and the last four bits are the message bits.

The *code word error probability* is given in (4.37). Using the approximation that for an error pattern of $i > t$ errors, at most $i + t$ errors can occur if all i channel errors occur in the information bits and t correct bits are changed by the decoder. Thus, there is a fraction $(i + t)/n$ of k information bits to be decoded erroneously, and hence the *bit error probability* of the coded system is given by [5]

$$P_e \approx \sum_{i=t+1}^{n} \frac{i+t}{n} \binom{n}{i} p^i (1-p)^{n-i} \tag{4.41}$$

For a BSC with $p = 10^{-2}$ we obtain the bit error probability $P_e \approx 6 \times 10^{-4}$. Therefore, the (7,4) Hamming code increases the transmission rate by a factor 7/4.

■

4.4 Gaussian channel

The *Gaussian channel* is the most important channel in communication. In practice, it models most physical channels, including both wired and wireless channels. Theoretically, the Gaussian channel is depicted in Figure 4.5(a) with the *continuous output random*

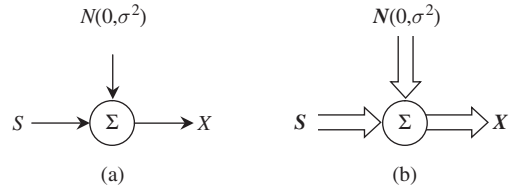

Figure 4.5 (a) Gaussian channel. (b) Vector Gaussian channel.

variable X being the *sum* of the *input random variable S* and the *independent continuous channel noise variable N*:

$$X = S + N \tag{4.42}$$

The noise variable N is a Gaussian random variable with zero mean and variance σ^2. It is a common practice to write the Gaussian noise variable as $N(0, \sigma^2)$. The probability density function of $N(0, \sigma^2)$ is given by

$$f_N(\eta) = \frac{1}{\sqrt{2\pi}\sigma} \mathrm{e}^{-\eta^2/2\sigma^2} \tag{4.43}$$

This channel model is usually referred to as an *additive Gaussian noise* (AGN) channel. If the noise has a constant power spectral density function (called *white noise*) then the channel is referred to as an *additive white Gaussian noise* (AWGN) channel. Figure 4.5(b) depicts the case of a *multiple input-multiple output* Gaussian channel (vector Gaussian channel), where the *continuous output random vector* $\boldsymbol{X}$ is the *sum* of the *input random vector* $\boldsymbol{S}$ and the *independent continuous channel noise vector* $\boldsymbol{N}$:

$$\boldsymbol{X} = \boldsymbol{S} + \boldsymbol{N} \tag{4.44}$$

The components of $\boldsymbol{N}$ are *independent and identically distributed* (iid) Gaussian random variables, each with zero mean and common variance σ^2. For the vector Gaussian channel, the probability density function of the noise vector $\boldsymbol{N}(0, \sigma^2)$ is simply the joint density of its n independent components and is given by

$$f_{\boldsymbol{N}}(\boldsymbol{\eta}) = \frac{1}{(\sqrt{2\pi}\sigma)^n} \mathrm{e}^{-\sum_{i=1}^{n} \eta_i^2/2\sigma^2} \tag{4.45}$$

Figure 4.6 illustrates the Gaussian channel model of a coded communication system. The mapping $u_i \rightarrow \boldsymbol{S}_i$ represents the equivalent lowpass model of the modulator. It maps the *code word* u_i into the *voltage vector* $\boldsymbol{S}_i$. For example, the code word u_i = (010) is mapped into $\boldsymbol{S}_i = (\sqrt{E_b}, -\sqrt{E_b}, \sqrt{E_b})$, which is the equivalent lowpass vector of the set of three PSK signals $(A \cos 2\pi f_c t,\ -A \cos 2\pi f_c t,\ A \cos 2\pi f_c t)$, each defined in their time interval. The mapping $\boldsymbol{X} \rightarrow v_j$ represents the equivalent lowpass model of the demodulator. It maps the *received voltage vector* $\boldsymbol{X}$ into the *received word* v_j. The two mappings and the Gaussian channel model constitute the discrete channel shown in Figure 4.2.

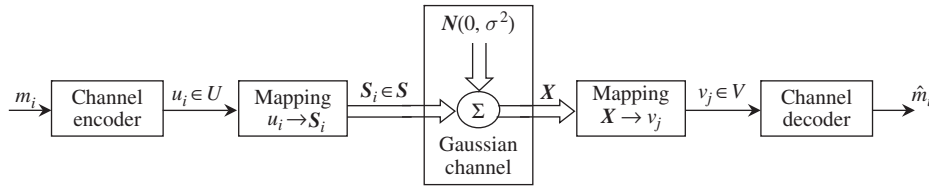

Figure 4.6 A coded Gaussian channel.

Since the Gaussian random variable is a continuous random variable, the definition of entropy for a discrete random variable does not apply in a straightforward manner. To illustrate this case let us approximate the probability density function $f_X(x)$ by a probability distribution function p_i, where $p_i = f_X(x_i)\,\Delta x$ is the area under $f_X(x)$ in the ith interval of width Δx. Note that in the limit we have

$$\sum_i p_i = \sum_i f_X(x_i)\Delta x \xrightarrow{\Delta x \to 0} \int_{-\infty}^{\infty} f_x(x)\mathrm{d}x = 1 \tag{4.46}$$

The entropy of the approximating distribution is given by

$$\begin{aligned} H &= -\sum_i p_i \log_2 p_i \\ &= -\sum_i f_X(x_i)\,\Delta x\, \log_2[f_X(x_i)\,\Delta x] \\ &= -\sum_i f_X(x_i) \log_2 f_X(x_i)\,\Delta x\, - \log_2 \Delta x \sum_i f_X(x_i)\Delta x \\ &= -\sum_i f_X(x_i) \log_2 f_X(x_i)\,\Delta x\, - \log_2 \Delta x \end{aligned} \tag{4.47}$$

In the limit as $\Delta x \to 0$ the second term becomes infinite and renders the entropy of a continuous random variable *infinite*. But since the second term of H is common to any two density functions $f_X(x)$ and $g_X(x)$, the difference in their entropies is equal to the difference of the first terms and is finite as long as their first terms are. The first term of H is commonly referred to as the *differential entropy*.

Differential entropy

Definition 4.6 The *differential entropy* $h(X)$ of a continuous random variable X with a given density function $f_X(x)$ is defined as

$$h(X) = -\int_{-\infty}^{\infty} f_X(x) \log_2 f_X(x)\,\mathrm{d}x \tag{4.48}$$

Definition 4.7 The *differential entropy* $h(\boldsymbol{X})$ of a continuous n-dimensional random vector $\boldsymbol{X}$ with a given density function $f_{\boldsymbol{X}}(\boldsymbol{x})$ is defined as

$$h(\boldsymbol{X}) = -\int f_{\boldsymbol{X}}(\boldsymbol{x}) \log_2 f_{\boldsymbol{X}}(\boldsymbol{x})\, \mathrm{d}\boldsymbol{x} \tag{4.49}$$

where the integral symbol represents n-fold integration.

Example 4.7 Differential entropy of a Gaussian random variable
Let X be a Gaussian random variable with mean $\overline{X}$and variance σ^2. Calculating the differential entropy in *bits* we get

$$\begin{aligned} h(X) &= -\int_{-\infty}^{\infty} f_X(x)\, \log_2\left[\frac{1}{\sqrt{2\pi}\sigma} \mathrm{e}^{-(x-\overline{X})^2/2\sigma^2}\right] \mathrm{d}x \\ &= \int_{-\infty}^{\infty} f_X(x)\left[\log_2(\sqrt{2\pi}\sigma) + \frac{(x-\overline{X})^2}{2\sigma^2}\log_2 \mathrm{e}\right] \mathrm{d}x \\ &= \log_2(\sqrt{2\pi}\sigma) + \frac{\log_2 \mathrm{e}}{2\sigma^2}\mathbf{E}\{(X-\overline{X})^2\} \\ &= \frac{1}{2}\log_2 2\pi\sigma^2 + \frac{1}{2}\log_2 \mathrm{e} \\ &= \frac{1}{2}\log_2 2\pi\mathrm{e}\sigma^2 \end{aligned} \tag{4.50}$$

Therefore, the differential entropy of a Gaussian random variable is independent of the mean.

■

Example 4.8 Differential entropy of a Gaussian random vector
Let $\boldsymbol{X}$ be an n-dimensional Gaussian random vector with iid components, each with zero mean and variance σ^2. Because entropy adds for independent random variables, the differential entropy of $\boldsymbol{X}$ is given by the sum of differential entropies of its components, and we obtain

$$h(\boldsymbol{X}) = \frac{n}{2}\log_2 2\pi\mathrm{e}\sigma^2 \tag{4.51}$$

■

Theorem 4.8 (Maximum differential entropy) *The Gaussian random variable X with arbitrary mean $\overline{X}$ and variance σ^2 has the largest differential entropy of all random variables of the same mean and variance.*

Proof By applying the *Jensen inequality* to a concave function $u(X)$ of a random variable X (a function is concave if it always lies above any chord; $\log x$ and $\sqrt{x}$ for $x > 0$ are examples of concave functions) which states that

$$\mathbf{E}\{u(X)\} \leq u\{\mathbf{E}(X)\} \tag{4.52}$$

we obtain, for arbitrary density functions $f_X(x)$ and $g(x)$ with the same mean $\overline{X}$ and variance σ^2,

$$\begin{aligned}\mathbf{E}\left(\log_2 \frac{g(X)}{f_X(X)}\right) &= \int_{-\infty}^{\infty} f_X(x) \log_2 \frac{g(x)}{f_X(x)} \mathrm{d}x \\ &\leq \log_2 \mathbf{E}\left(\frac{g(X)}{f_X(X)}\right) = \log_2 \int_{-\infty}^{\infty} f_X(x) \frac{g(x)}{f_X(x)} \mathrm{d}x \\ &\leq \log_2 \int_{-\infty}^{\infty} g(x)\, \mathrm{d}x = \log_2 1 = 0\end{aligned} \tag{4.53}$$

Hence, the upper bound of the differential entropy $h(X)$ of the random variable X with arbitrary density function $f_X(x)$ is given by

$$h(X) = -\int_{-\infty}^{\infty} f_X(x) \log_2 f_X(x)\, \mathrm{d}x \leq -\int_{-\infty}^{\infty} f_X(x) \log_2 g(x)\, \mathrm{d}x \tag{4.54}$$

Since the density function $g(x)$ is arbitrary we can choose it to be a Gaussian density function with mean $\overline{X}$ and variance σ^2 as those of $f_X(x)$. Therefore, using (4.50) we have

$$\begin{aligned}h(X) &\leq -\int_{-\infty}^{\infty} f_X(x) \log_2 \left[\frac{1}{\sqrt{2\pi}\sigma} \mathrm{e}^{-(x-\overline{X})^2/2\sigma^2}\right] \mathrm{d}x \\ &\leq \frac{1}{2} \log_2 2\pi \mathrm{e}\sigma^2\end{aligned} \tag{4.55}$$

The right-hand side of the above inequality is the differential entropy of a Gaussian random variable with variance σ^2. Thus the Gaussian random variable attains the largest differential entropy. In summary we have

$$\max_{\mathbf{E}\{(X-\overline{X})^2\}=\sigma^2} h(X) = \frac{1}{2} \log_2 2\pi \mathrm{e}\sigma^2 \tag{4.56}$$

The above result can be generalized to the case of a random vector $\boldsymbol{X}$ with iid components as follows:

$$\max_{\mathbf{K}} h(\boldsymbol{X}) = \frac{n}{2} \log_2 2\pi \mathrm{e}\sigma^2 \tag{4.57}$$

where $\mathbf{K} = \mathbf{E}\{(\boldsymbol{X} - \overline{\boldsymbol{X}})^t (\boldsymbol{X} - \overline{\boldsymbol{X}})\} = \sigma^2 \mathbf{I}_n$ is the covariance matrix of $\boldsymbol{X}$, and $\mathbf{I}_n$ is the $n \times n$ identity matrix.

■

Mutual information and channel capacity

Using the concept of differential entropy we can extend the definition of *mutual information* between two discrete random variables to two continuous random variables.

Definition 4.9 The mutual information $I(X,Y)$ between two continuous random variables X and Y with a given joint density function $f_{XY}(x,y) = f_{Y|X}(y|x)f_X(x) = f_{X|Y}(x|y)f_Y(y)$, is defined as

$$\begin{aligned} I(X,Y) &= \int_{-\infty}^{\infty}\int_{-\infty}^{\infty} f_{XY}(x,y)\log_2\frac{f_{XY}(x,y)}{f_X(x)f_Y(y)}\,\mathrm{d}x\,\mathrm{d}y \\ &= \int_{-\infty}^{\infty}\int_{-\infty}^{\infty} f_{XY}(x,y)\log_2\frac{f_{Y|X}(y|x)}{f_Y(y)}\,\mathrm{d}x\,\mathrm{d}y \\ &= \int_{-\infty}^{\infty}\int_{-\infty}^{\infty} f_{XY}(x,y)\log_2\frac{f_{X|Y}(x|y)}{f_X(x)}\,\mathrm{d}x\,\mathrm{d}y \end{aligned} \tag{4.58}$$

Definition 4.10 Let X and Y be two continuous random variables with the joint density function $f_{XY}(x,y)$. The *conditional differential entropies* $h(X|Y)$ and $h(Y|X)$ are defined as

$$\begin{aligned} h(X|Y) &= -\int_{-\infty}^{\infty} f_Y(y)\int_{-\infty}^{\infty} f_{X|Y}(x|y)\log_2 f_{X|Y}(x|y)\,\mathrm{d}x\,\mathrm{d}y \\ &= -\int_{-\infty}^{\infty}\int_{-\infty}^{\infty} f_{XY}(x,y)\log_2 f_{X|Y}(x|y)\,\mathrm{d}x\,\mathrm{d}y \end{aligned} \tag{4.59}$$

and

$$\begin{aligned} h(Y|X) &= -\int_{-\infty}^{\infty} f_X(x)\int_{-\infty}^{\infty} f_{Y|X}(y|x)\log_2 f_{Y|X}(y|x)\,\mathrm{d}x\,\mathrm{d}y \\ &= -\int_{-\infty}^{\infty}\int_{-\infty}^{\infty} f_{XY}(x,y)\log_2 f_{Y|X}(y|x)\,\mathrm{d}x\,\mathrm{d}y \end{aligned} \tag{4.60}$$

From the above definitions we obtain the mutual information in terms of the differential entropies as follows:

$$I(X,Y) = h(X) - h(X|Y) = h(Y) - h(Y|X) \tag{4.61}$$

Definition 4.11 The *information capacity of a Gaussian channel* $X = S + N$ with $\overline{S} = 0$ and power constraint $\mathbf{E}(S^2) \le P$ and independent noise $N(0,\sigma^2)$ in *bits/transmission* (bits/channel use) is defined as

$$C = \max_{\mathbf{E}(S^2)\le P} I(S,X) = \frac{1}{2}\log_2(1+SNR) \tag{4.62}$$

where $SNR = P/\sigma^2$ is the *signal-to-noise ratio*.

Similarly, the *information capacity of a vector Gaussian channel* $\boldsymbol{X} = \boldsymbol{S} + \boldsymbol{N}$, where $\boldsymbol{S}$ is an n-dimensional random vector with independent zero mean components, and variance $E(S_i^2) = P_i$, $i = 1,2,\ \ldots,\ n$, such that $\sum_{i=1}^{n} P_i = \boldsymbol{\mathcal{P}}$, and noise vector $\boldsymbol{N}$ whose components

are independent zero mean Gaussian random variables, and variance σ_i^2, $i = 1,2, \ldots, n$, is given in *bits/vector transmission* (bits/vector channel use) as

$$C = \max_{\mathbf{E}(\boldsymbol{SS}^t)\leq \boldsymbol{\mathcal{P}}} I(\boldsymbol{S}, \boldsymbol{X}) = \max_{\mathbf{E}(\boldsymbol{SS}^t)\leq \boldsymbol{\mathcal{P}}} \sum_{i=1}^{n} \frac{1}{2}\log_2(1 + SNR_i) \tag{4.63}$$

where $SNR_i = P_i/\sigma_i^2$ and $\sum_{i=1}^{n} P_i = \boldsymbol{\mathcal{P}}$.

The calculation of the channel capacity follows directly from the definition of mutual information. We have

$$\begin{aligned} I(S,X) &= h(X) - h(X|S) \\ &= h(X) - h(S+N|S) \\ &= h(X) - h(N|S) \\ &= h(X) - h(N) \\ &= h(X) - \frac{1}{2}\log_2 2\pi e\sigma^2 \end{aligned} \tag{4.64}$$

Furthermore, $\mathbf{E}(X^2) = \mathbf{E}\{(S+N)^2\} = \mathbf{E}(S^2 + 2SN + N^2) \leq P + \sigma^2$ and hence the entropy of X is upper bounded by the entropy of a Gaussian random variable with variance $P + \sigma^2$, which is $\frac{1}{2}\log_2 2\pi e(P + \sigma^2)$. Therefore, we obtain

$$I(S,X) \leq \frac{1}{2}\log_2\left(1 + \frac{P}{\sigma^2}\right) = \frac{1}{2}\log_2(1 + SNR) \tag{4.65}$$

The information capacity of the Gaussian channel is the maximum of $I(S, X)$ and is achieved when *input S* is a *Gaussian random variable* with zero mean and variance *P*.

The result for a vector Gaussian channel can be investigated via the constraint optimization problem, which for this case can be solved using *Lagrange multipliers*. Consider the *Lagrangian*

$$\boldsymbol{\mathcal{L}}(\lambda, P_1, ..., P_n) = \sum_{i=1}^{n} \frac{1}{2}\log_2\left(1 + \frac{P_i}{\sigma_i^2}\right) - \lambda \sum_{i=1}^{n} P_i \tag{4.66}$$

where λ is the Lagrange multiplier. The *Kuhn–Tucker* condition for the optimality of a power allocation is given by

$$\frac{\partial \boldsymbol{\mathcal{L}}}{\partial P_i} \begin{cases} = 0 \text{ if } P_i > 0 \\ \leq 0 \text{ if } P_i = 0 \end{cases} \tag{4.67}$$

And hence the power constraint optimization problem yields the following power allocation:

$$P_i = \max\left(0, \frac{1}{2\lambda} - \sigma_i^2\right) \tag{4.68}$$

where the Lagrange multiplier is selected such that $\sum_{i=1}^{n} P_i = \boldsymbol{\mathcal{P}}$.

In the special case where the noise vector has iid components with zero mean and common variance σ^2, the power allocation strategy allocates equal signal power P to each subchannel, that is, $P = \mathcal{P}/n$. Therefore,

$$C = \max_{\mathbf{E}(\boldsymbol{S}\boldsymbol{S}^t) \leq \mathcal{P}} I(\boldsymbol{S}, \boldsymbol{X}) = \frac{n}{2}\log_2(1 + SNR) \tag{4.69}$$

where $SNR = \mathcal{P}/n\sigma^2 = P/\sigma^2$ is the subchannel signal-to-noise ratio. As expected, the information capacity of a vector Gaussian channel with iid noise is n times its subchannel capacity. The analysis of a vector Gaussian channel in this case is identical to that of a scalar Gaussian channel.

Example 4.9 Vector Gaussian channel and water-filling strategy

Let us consider the case of a vector Gaussian channel consisting of n parallel Gaussian subchannels. One example of this is *orthogonal frequency division multiplexing* (OFDM), which is employed in the popular IEEE 802.11a,g and 802.16e standards. OFDM employs n orthogonal subcarriers separated by the subcarrier symbol rate. In this case a symbol transmitted by a subcarrier can be represented by a component of the input Gaussian vector $\boldsymbol{S}$. Figure 4.7 plots the noise power for each subchannel to illustrate the power allocation strategy to achieve the channel capacity. The total signal power and noise power in each subchannel is set at $1/2\lambda$. Starting with the subchannel with the lowest noise power, allocate the signal power to reach this level, and move on to the subchannel with the next lowest noise power until all subchannels are allocated with power from $\mathcal{P}$. If the noise power is above $1/2\lambda$ allocate no signal power. Thus, strong subchannels are allocated more signal power than weaker subchannels to take advantage of better subchannel conditions, with none for very poor subchannels since they convey almost no information. This power allocation is similar to filling a vessel with water and is referred to as the *water-filling* strategy. The water level is $1/2\lambda$ and the depth of the water in a subchannel is its signal power.

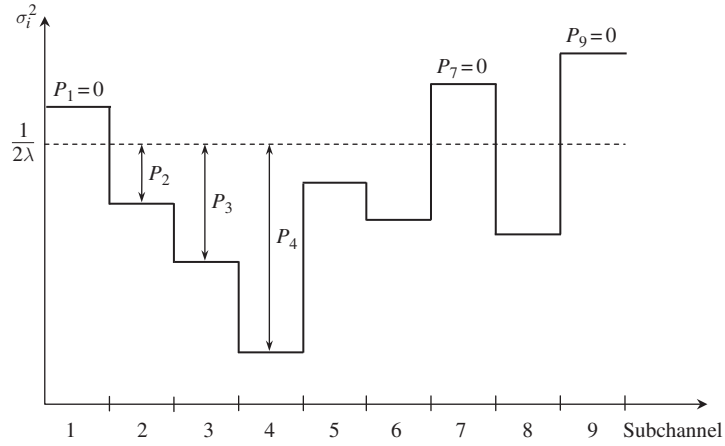

Figure 4.7 Water filling strategy.

For numerical illustration consider the case of three subchannels with noise powers $\sigma_1^2 = 5,\ \sigma_2^2 = 1,\ \sigma_3^2 = 8$ power units. The total signal power for allocating to the three subchannels is $\mathscr{P} = 10$ power units. We have

$$\begin{aligned} P_1 &= \max\left(0,\ \frac{1}{2\lambda} - \sigma_1^2\right) = \max\left(0,\ \frac{1}{2\lambda} - 5\right) \\ P_2 &= \max\left(0,\ \frac{1}{2\lambda} - \sigma_2^2\right) = \max\left(0,\ \frac{1}{2\lambda} - 1\right) \\ P_3 &= \max\left(0,\ \frac{1}{2\lambda} - \sigma_3^2\right) = \max\left(0,\ \frac{1}{2\lambda} - 8\right) \end{aligned} \tag{4.70}$$

subject to $\sum_{i=1}^{n} P_i = \mathscr{P} = 10$. Solving for the subchannel signal power we obtain $P_1 = 3,\ P_2 = 7$, and $P_3 = 0$ with $1/2\lambda = 8$.

Using the above background fundamentals we arrive at the following information capacity theorem for a Gaussian channel with a power constraint.

■

Theorem 4.12 ***(Gaussian channel capacity theorem)*** *The information capacity of a Gaussian channel with independent noise $N(0, \sigma^2)$ and power constraint P in bits/transmission is*

$$C = \frac{1}{2}\log_2\left(1 + \frac{P}{\sigma^2}\right) = \frac{1}{2}\log_2(1 + SNR) \tag{4.71}$$

For a rate less than C, there exists a coding system such that the code words can be transmitted over the channel with an arbitrarily small frequency of errors.

■

Example 4.10 Sphere packing bound

The *sphere packing bound* is a simple method to calculate the information capacity of a Gaussian channel with independent noise $N(0, \sigma^2)$ and power constraint P. Consider a code with equally likely code words long enough to average out the errors. Each code word is represented by an *n-dimensional* vector $\boldsymbol{S}$ whose components have a common mean-square value P. Each reception represented by a component of a received vector $\boldsymbol{X}$ has a mean-square value $P + \sigma^2$. All received vectors $\boldsymbol{X}$ have a mean-square value $n(P + \sigma^2)$ and lie within an *n-dimensional* sphere of radius $\sqrt{n(P + \sigma^2)}$. Each received vector is distributed around its mean $\boldsymbol{S}$ and variance equal to the variance of the noise vector $\boldsymbol{N}$, which is $n\sigma^2$. The *decoding spheres* of all received vectors $\boldsymbol{X}$ have a radius equal to $\sqrt{n\sigma^2}$. If a received vector $\boldsymbol{X}$ falls within its decoding sphere centered on the transmitted vector $\boldsymbol{S}$ there would be no error, and this happens with high probability with long code words. Otherwise, if the received vector falls outside its decoding sphere, there would be an error, and this happens with low probability.

The question is how many decoding spheres can be packed within a sphere of radius $\sqrt{n(P + \sigma^2)}$. Since *each decoding sphere is associated with a code word*, the more

decoding spheres that can be packed within the larger sphere, the more code words that can be sent and the higher the channel capacity. The volume of an *n-dimensional sphere* is proportional to the *n*th power of its radius. Thus, the *maximum number of decoding spheres* that can be packed into the receiving sphere is at most equal to

$$\frac{[n(P+\sigma^2)]^{n/2}}{[n\sigma^2]^{n/2}} = \left[1+\frac{P}{\sigma^2}\right]^{n/2} = 2^{\frac{n}{2}\log_2\left(1+P/\sigma^2\right)} \tag{4.72}$$

This number is also the maximum number of code words that can be sent. Hence, the number of bits that can be reliably sent over the Gaussian channel per code word is at most $\frac{n}{2}\log_2(1+P/\sigma^2)$, and the number of bits per transmission is $\frac{1}{2}\log_2(1+P/\sigma^2)$.

■

Example 4.11 Conversion of a Gaussian channel to a discrete channel

A Gaussian channel with arbitrary discrete input S can be converted into a discrete channel if the mappings are known (Figure 4.6). Consider the case of a Gaussian channel where PSK signaling is employed with bits 0 and 1 represented by two physical waveforms $A\cos 2\pi f_c t$ *and* $-A\cos 2\pi f_c t$, respectively. The mappings of bits 0 and 1 to the input scalar random variable S are

$$0 : A\cos 2\pi f_c t,\ 0 \le t < T \ \rightarrow\ S = \sqrt{P}, \text{ and}$$
$$1 : -A\cos 2\pi f_c t,\ 0 \le t < T \ \rightarrow\ S = -\sqrt{P}.$$

Here T represents the transmission time of a PSK waveform (bit time) and $\mathbf{E}(S^2) = P$. The bit error probability for optimum detection of PSK signals is given in Chapter 7 as $p = Q(\sqrt{2SNR})$, where $Q(\cdot)$ is the *Gaussian integral function* defined in (3.164) and repeated here for convenience:

$$Q(a) = \frac{1}{\sqrt{2\pi}}\int_a^\infty \mathrm{e}^{-x^2/2}\mathrm{d}x \tag{4.73}$$

Thus, we can convert the Gaussian channel with PSK signaling into a *binary symmetric channel* with crossover probability p and capacity $C = 1 + p\log_2 p + (1-p)\log_2(1-p)$. The maximum transmission rate of a PSK signaling is 1 bit per transmission and this happens when $p = 0$ (noiseless channel or infinite *SNR*). For numerical illustration consider the case of *SNR* = 2.7 or 4.3 dB, which results in $p = 10^{-2}$. The capacity of the BSC is $C =$ 0.919 bits. For the same *SNR* the information capacity of a Gaussian channel with Gaussian input is given by $C = \frac{1}{2}\log_2(1+SNR) = \frac{1}{2}\log_2(1+2.7) = 0.94$ bits. Thus, at $p = 10^{-2}$, the capacity of a BSC is about 3% below that of a Gaussian channel with Gaussian input.

Now let us consider the case of *SNR* = 9.1 or 9.6 dB. This results in a PSK bit error probability of $p = 10^{-5}$. The information capacity of the BSC is very close to 1 bit/transmission. On the other hand, to achieve the information capacity of 1 bit/transmission, the Gaussian channel with Gaussian input requires *SNR* = 3 or 4.8 dB. Thus, there is a potential power gain of 9.5−4.8 = 4.7 dB for communication over the BSC at 1 bit/transmission at a bit error rate of 10^{-5}.

■

Bandlimited Gaussian channel capacity

So far the study of the information capacity of both discrete and Gaussian channels makes no mention of the channel bandwidth. In the physical world all channels are *almost bandlimited* and therefore the transmission of physical waveforms over such channels must comply with this spectrum constraint. Note that a waveform that is strictly bandlimited cannot be time-limited, although most of them are almost time-limited; that is, most of its energy is confined within a finite duration of time good enough for practical applications.

Suppose the channel is bandlimited to a bandwidth designated as B (with units in Hz). According to the *sampling theorem*, any physical waveform that complies with this bandwidth constraint can be uniquely represented in any time interval T seconds by no more than $2BT$ samples taken every $1/2B$ seconds apart. This is the case because the *Nyquist* sampling rate for a bandlimited waveform is $2B$ samples/second. Furthermore, if the Gaussian noise has constant power spectral density (*white noise*), the noise samples that accompany the waveform samples are iid Gaussian samples. The information capacity for a bandlimited Gaussian channel is therefore given by

$$C = \frac{1}{2}\log_2\left(1+\frac{P}{\sigma^2}\right) = \frac{1}{2}\log_2(1+SNR) \quad \text{bits/sample} \tag{4.74}$$

Since there are $2B$ samples each second, the capacity can be expressed in *bits/second* as follows:

$$C = B\log_2\left(1+\frac{P}{\sigma^2}\right) = B\log_2(1+SNR) \quad \text{bits/second} \tag{4.75}$$

Gaussian channel with discrete inputs

The information capacity of a Gaussian channel was achieved with Gaussian inputs. Suppose we restrict the channel inputs to a finite set. This is the case of digital signaling where a set of M distinct waveforms represents a set of M symbols. The channel outputs are still continuous random variables because noise is Gaussian. Obviously, the channel capacity is reduced by putting a restriction on the channel inputs. But if the reduction is small then the choice is justifiable especially when the coding scheme is less complex. For digital signals such as those discussed in Chapters 2 and 6, the signal points in their signal space represent the channel discrete inputs. Let the set of *L-dimensional* signal vectors be $\{\mathbf{s}_i = (s_{i1}, s_{i2}, ..., s_{iL}), i = 1, 2, ..., M\}$ and let their distribution be $p_i,\ i = 1, 2, ..., M$. By using a modified version of (4.58), the capacity of a vector Gaussian channel $\boldsymbol{X} = \boldsymbol{s}_i + \boldsymbol{N}$ where $\boldsymbol{N} = \boldsymbol{N}(0, \sigma^2)$, with the above restriction of the channel inputs, is given by

$$\begin{aligned} C &= \max_{p_i} \sum_{i=1}^{M} p_i \int f_{\boldsymbol{X}|\boldsymbol{s}_i}(\boldsymbol{x}|\boldsymbol{s}_i)\log_2\frac{f_{\boldsymbol{X}|\mathbf{s}_i}(\boldsymbol{x}|\boldsymbol{s}_i)}{f_{\boldsymbol{X}}(\boldsymbol{x})}\mathbf{d}\boldsymbol{x} \\ &= \max_{p_i} \sum_{i=1}^{M} p_i \int f_{\boldsymbol{X}|\boldsymbol{s}_i}(\boldsymbol{x}|\boldsymbol{s}_i)\log_2\frac{f_{\boldsymbol{X}|\mathbf{s}_i}(\boldsymbol{x}|\boldsymbol{s}_i)}{\sum_{j=1}^{M} p_j f_{\boldsymbol{X}|\mathbf{s}_j}(\boldsymbol{x}|\boldsymbol{s}_j)}\mathbf{d}\boldsymbol{x} \end{aligned} \tag{4.76}$$

where the integral is an L-fold integral and the L-dimensional Gaussian density function $f_{\boldsymbol{X}|\boldsymbol{s}_i}(\boldsymbol{x}|\boldsymbol{s}_i)$ is

$$\begin{aligned} f_{\boldsymbol{X}|\boldsymbol{s}_i}(\boldsymbol{x}|\boldsymbol{s}_i) &= \frac{1}{\left(\sqrt{2\pi}\sigma\right)^L} \mathrm{e}^{-\frac{1}{2\sigma^2}\sum_{k=1}^{L}(x_k - s_{ik})^2} \\ &= \frac{1}{\left(\sqrt{2\pi}\sigma\right)^L} \mathrm{e}^{-\|\boldsymbol{x}-\boldsymbol{s}_i\|^2/2\sigma^2} \end{aligned} \tag{4.77}$$

For digital communications all symbols are *equally likely*, therefore the signal vector distribution $p_i,\ i = 1, 2, ..., M$, is constrained to $p_i = 1/M,\ i = 1, 2, ..., M$. Thus the channel capacity given a set of $\boldsymbol{s}_i,\ i = 1.2, ..., M$ is

$$\begin{aligned} C &= \sum_{i=1}^{M} \frac{1}{M} \int f_{\boldsymbol{X}|\mathbf{s}_i}(\boldsymbol{x}|\boldsymbol{s}_i) \log_2 \frac{f_{\boldsymbol{X}|\mathbf{s}_i}(\boldsymbol{x}|\mathbf{s}_i)}{\sum_{j=1}^{M} p_j f_{\boldsymbol{X}|\mathbf{s}_j}(\boldsymbol{x}|\boldsymbol{s}_j)} \, \mathbf{d}\boldsymbol{x} \\ &= \sum_{i=1}^{M} \frac{1}{M} \int \frac{1}{\left(\sqrt{2\pi}\sigma\right)^L} \mathrm{e}^{-\|\boldsymbol{x}-\boldsymbol{s}_i\|^2/2\sigma^2} \log_2 \frac{\mathrm{e}^{-\|\boldsymbol{x}-\boldsymbol{s}_i\|^2/2\sigma^2}}{M^{-1}\sum_{j=1}^{M} e^{-\|\boldsymbol{x}-\boldsymbol{s}_j\|^2/2\sigma^2}} \, \mathbf{d}\boldsymbol{x} \end{aligned} \tag{4.78}$$

To simplify the integration we make the following transformation of integration variables. Letting $\boldsymbol{v}_i = \boldsymbol{s}_i/\sigma$ and $\boldsymbol{y} = (\boldsymbol{x} - \boldsymbol{s}_i)/\sigma$, we have

$$\begin{aligned} C &= \sum_{i=1}^{M} \frac{1}{M} \int \frac{1}{\left(\sqrt{2\pi}\right)^L} \mathrm{e}^{-\|\boldsymbol{y}\|^2/2} \log_2 \frac{\mathrm{e}^{-\|\boldsymbol{y}\|^2/2}}{M^{-1}\sum_{j=1}^{M} \mathrm{e}^{-\|\boldsymbol{y}+\boldsymbol{v}_i-\boldsymbol{v}_j\|^2/2}} \, \mathbf{d}\boldsymbol{y} \\ &= \log_2 M - \sum_{i=1}^{M} \frac{1}{M} \int \frac{1}{\left(\sqrt{2\pi}\right)^L} \mathrm{e}^{-\|\boldsymbol{y}\|^2/2} \log_2 \sum_{j=1}^{M} \mathrm{e}^{-\|\boldsymbol{y}+\boldsymbol{v}_i-\boldsymbol{v}_j\|^2/2} e^{\|\boldsymbol{y}\|^2/2} \, \mathbf{d}\boldsymbol{y} \end{aligned} \tag{4.79}$$

Since $\left\|\boldsymbol{y} + \boldsymbol{v}_i - \boldsymbol{v}_j\right\|^2 = \left\|\boldsymbol{v}_i - \boldsymbol{v}_j\right\|^2 + 2\left[\boldsymbol{v}_i - \boldsymbol{v}_j\right]^t \boldsymbol{y} + \|\boldsymbol{y}\|^2$, we obtain

$$\begin{aligned} C &= \log_2 M - \sum_{i=1}^{M} \frac{1}{M} \int \frac{1}{\left(\sqrt{2\pi}\right)^L} \mathrm{e}^{-\|\boldsymbol{y}\|^2/2} \log_2 \sum_{j=1}^{M} \mathrm{e}^{-\|\boldsymbol{y}+\boldsymbol{v}_i-\boldsymbol{v}_j\|^2/2} \mathrm{e}^{\|\boldsymbol{y}\|^2/2} \, \mathbf{d}\boldsymbol{y} \\ &= \log_2 M - \sum_{i=1}^{M} \frac{1}{M} \int \frac{1}{\left(\sqrt{2\pi}\right)^L} \mathrm{e}^{-\|\boldsymbol{y}\|^2/2} \log_2 \sum_{j=1}^{M} \mathrm{e}^{-\|\boldsymbol{v}_i-\boldsymbol{v}_j\|^2/2 \, - \, (\boldsymbol{v}_i-\boldsymbol{v}_j)^t y} \, \mathbf{d}\boldsymbol{y} \end{aligned} \tag{4.80}$$

For one-dimensional ($L = 1$) signal vectors such as PSK and ASK and two-dimensional ($L = 2$) signal vectors such as MPSK and MQAM (Chapter 6) we note that the *average energy per dimension* is $(1/LM)\sum_{i=1}^{M} \|\boldsymbol{s}_i\|^2$, and the *noise variance per dimension* is σ^2, therefore the *average signal-to-noise ratio per dimension* is $SNR = (1/LM)\sum_{i=1}^{M} \|\boldsymbol{s}_i/\sigma\|^2 = (1/LM)\sum_{i=1}^{M} \|\boldsymbol{v}_i\|^2$. Thus, the channel capacity for these digital signals can be calculated as a function of the average *signal-to-noise ratio per dimension*. For a white Gaussian noise

channel with power spectral density $N_0/2$, the variance of a component of the noise vector $\boldsymbol{N}$ is $\sigma^2 = N_0/2$ (Chapter 7). The squared length (squared norm) of the signal vector $\boldsymbol{s}_i$ is the signal energy E_i, that is, $E_i = \|\boldsymbol{s}_i\|^2$. This is the result that arises from the use of *orthonormal basis functions* to obtain the signal vectors (Chapters 2 and 6). Furthermore, the noise vector provides sufficient statistics for the detection of signal vectors (Chapter 3). Hence, the *average signal-to-noise ratio per dimension* is $SNR = 2E_s/LN_0$, where the *average signal (symbol) energy* is E_s and is given by $E_s = (1/M)\sum_{i=1}^{M} E_i$. Since $\boldsymbol{v}_i = \boldsymbol{s}_i/\sigma$, we get $\|\boldsymbol{v}_i\|^2 = 2E_i/N_0$. The normalized signal vector $\boldsymbol{v}_i$ can therefore be expressed in term of the *average symbol energy-to-noise density ratio* E_s/N_0 as $\boldsymbol{v}_i = \sqrt{E_s/N_0}\boldsymbol{c}_i$, where $\boldsymbol{c}_i$ is a fixed constant vector characterizing a given signal set. The channel capacity can then be calculated as a function of E_s/N_0 and is shown in Figure 4.8 for some digital modulation techniques [12,14,28]. These are two-dimensional ($L = 2$) signaling techniques, therefore the integral in (4.80) is a double-integral. The capacity of the *vector Gaussian channel* is $C = (L/2)\log_2(1 + SNR) = \log_2(1 + SNR)$ bits/symbol. The *average signal-to-noise ratio per dimension* is $SNR = E_s/N_0$. The potential *coding gain* (reduction in *SNR* at the same bit error probability) is about 7.5–8.5 dB if channel coding is employed. For example, QPSK requires 13.5 dB in *SNR* to achieve a bit error probability of 10^{-6} and a capacity of 2 bits/symbol. On the other hand, the channel capacity theorem says that the required *SNR* is only 5 dB for communication at 2 bits/symbol. Furthermore, channel coding does not need to increase the bandwidth as with repetition codes or Hamming code. Instead,

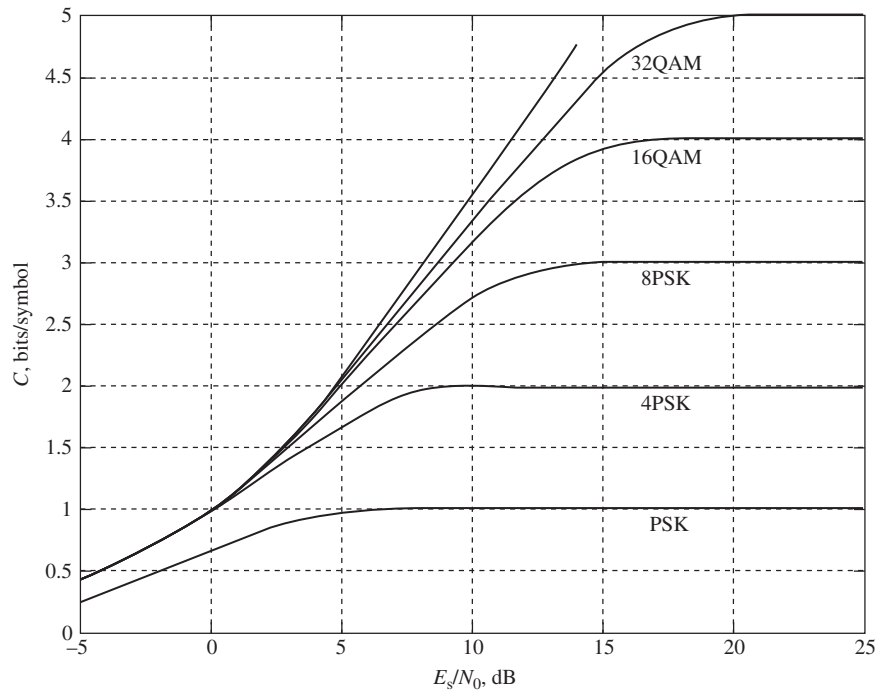

Figure 4.8 Capacity of digital modulation techniques versus the Shannon limit $\log_2(1 + SNR)$, where $SNR = E_s/N_0$.

one can employ an expand signal space, for example, from 16QAM to 64QAM, to compensate for the increase in the channel bit rate due to the redundancy of the code. The use of 64QAM (capacity is 6 bits/symbol) reduces the bandwidth by a factor of 6/4 as compared to 16QAM (capacity is 4 bits/symbol). This fact permits the use of codes with rate 4/6 with 64QAM to achieve the same bandwidth as uncoded 16QAM (thus, both uncoded 16QAM and coded 64QAM signals provide a capacity of 4 bits/symbol). Furthermore, at 4 bits/symbol, 64QAM requires about 8 dB less in *SNR* as compared to 16QAM, thus a potential coding gain of 8 dB can be achieved with codes of rate 4/6.

4.5 Channel coding with block codes

Many types of error-correcting codes have been discovered to realize the coding gain promised by the Shannon channel capacity. In this section we provide the general description of some popular linear block codes. The famous historic Hamming code has been discussed previously. An (n, k) linear block code with k information bits and $n-k$ parity-check bits has k linearly independent code words, and the remaining $2^k - k$ code words are linear combinations of these k code words. A code word can be generated by the $k \times n$ *generator matrix* $\mathbf{G}$ and the $1 \times k$ message vector $\boldsymbol{i}$ via the following operation:

$$\boldsymbol{c} = \boldsymbol{i}\mathbf{G} \tag{4.81}$$

The generator matrix $\mathbf{G}$ can be put into the following forms which produce linear *systematic* block codes:

$$\mathbf{G} = [\mathbf{I}_k \quad \mathbf{P}] \text{ or } \mathbf{G} = [\mathbf{P} \quad \mathbf{I}_k] \tag{4.82}$$

The matrix $\mathbf{I}_k$ is the $k \times k$ *identity matrix*. For example, the following generator matrices can produce the set of 16 Hamming code words:

$$\mathbf{G} = \begin{bmatrix} 1 & 0 & 0 & 0 & 1 & 0 & 1 \\ 0 & 1 & 0 & 0 & 1 & 1 & 1 \\ 0 & 0 & 1 & 0 & 1 & 1 & 0 \\ 0 & 0 & 0 & 1 & 0 & 1 & 1 \end{bmatrix} \text{ and } \mathbf{G} = \begin{bmatrix} 1 & 1 & 0 & 1 & 0 & 0 & 0 \\ 0 & 1 & 1 & 0 & 1 & 0 & 0 \\ 1 & 1 & 1 & 0 & 0 & 1 & 0 \\ 1 & 0 & 1 & 0 & 0 & 0 & 1 \end{bmatrix} \tag{4.83}$$

Note that for systematic codes generated by $\mathbf{G} = [\mathbf{P} \quad \mathbf{I}_k]$ the last k bits of the code words are identical to the information bits. On the other hand, if $\mathbf{G} = [\mathbf{I}_k \quad \mathbf{P}]$ is used, the first k bits of the code words are identical to the information bits. Note that the rows of $\mathbf{G}$ are linearly independent.

Associated with a generator matrix is an $(n-k) \times n$ *parity check matrix* $\mathbf{H}$ that satisfies the relationship

$$\mathbf{H}\mathbf{G}^t = \mathbf{0} \text{ or } \mathbf{G}\mathbf{H}^t = \mathbf{0} \tag{4.84}$$

where $\mathbf{0}$ is a *null matrix*. For a systematic code the parity-check matrix assumes the following forms

$$\mathbf{H} = \begin{bmatrix} \mathbf{P}^t & \mathbf{I}_{n-k} \end{bmatrix} \text{ or } \mathbf{H} = \begin{bmatrix} \mathbf{I}_{n-k} & \mathbf{P}^t \end{bmatrix} \tag{4.85}$$

It is seen that $\boldsymbol{c}$ is a code word if and only if the following relationship holds:

$$\boldsymbol{c}\mathbf{H}^t = \mathbf{0} \tag{4.86}$$

The parity-check matrices for the above generator matrices are given by

$$\mathbf{H} = \begin{bmatrix} 1 & 1 & 1 & 0 & 1 & 0 & 0 \\ 0 & 1 & 1 & 1 & 0 & 1 & 0 \\ 1 & 1 & 0 & 1 & 0 & 0 & 1 \end{bmatrix} \text{ and } \mathbf{H} = \begin{bmatrix} 1 & 0 & 0 & 1 & 0 & 1 & 1 \\ 0 & 1 & 0 & 1 & 1 & 1 & 0 \\ 0 & 0 & 1 & 0 & 1 & 1 & 1 \end{bmatrix} \tag{4.87}$$

The symmetry relationship in (4.84) shows that $\mathbf{H}$ can be used as a generator matrix for an $(n, n-k)$ linear block code and $\mathbf{G}$ as a parity-check matrix. The rows of $\mathbf{H}$ are linearly independent. The parity-check matrix therefore performs $n-k$ parity checks on n bits of the received word.

The decoding of simple block codes can be carried out via *syndrome decoding*. Let the code word $\boldsymbol{c}$ be transmitted over a noisy channel, and hence the received word $\boldsymbol{r}$ may contain errors as follows:

$$\boldsymbol{r} = \boldsymbol{c} + \boldsymbol{e} \tag{4.88}$$

where $\boldsymbol{e}$ is the *error word* or *error pattern*, which is the zero vector when there is no error. The syndrome vector $\boldsymbol{s}$ is defined as

$$\begin{aligned} \boldsymbol{s} &= \boldsymbol{r}\mathbf{H}^t \\ &= (\boldsymbol{c} + \boldsymbol{e})\mathbf{H}^t \\ &= \boldsymbol{e}\mathbf{H}^t \end{aligned} \tag{4.89}$$

When there is no error, the syndrome is a zero vector. For block codes that can correct a single error in the code words like Hamming codes, the syndrome is the column of $\mathbf{H}$ that corresponds to the error position in the error vector $\boldsymbol{e}$. Because all columns of $\mathbf{H}$ are distinct, it is simple to locate the column of $\mathbf{H}$ that is identical to the syndrome $\boldsymbol{s}$ and correct the error.

Example 4.12 Syndrome decoding of (7,4) Hamming code

Let $\boldsymbol{c} = (0001011)$ be the transmitted code word (first $\mathbf{G}$ of (4.83)) and $\boldsymbol{r} = (0101011)$ be the received word. The syndrome is given by (using the first $\mathbf{H}$ of (4.87))

$$\boldsymbol{s} = (0101011) \begin{bmatrix} 1 & 0 & 1 \\ 1 & 1 & 1 \\ 1 & 1 & 0 \\ 0 & 1 & 1 \\ 1 & 0 & 0 \\ 0 & 1 & 0 \\ 0 & 0 & 1 \end{bmatrix} = (111) \tag{4.90}$$

This syndrome matches the second column of **H** and indicates an error in the second element of the vector ***r***, which is 1 and can be corrected to 0.

■

In general, syndrome decoding is not effective for long linear block codes with multiple errors correcting capability. In the following discussion we present some important linear block codes.

Cyclic codes

A linear block code is cyclic if a cyclic shift of a code word is also a code word. For example, if $(c_0, c_1, ..., c_{n-1})$ is a code word, then $(c_{n-1}, c_0, ..., c_{n-2}), \ldots, (c_1, c_2, ..., c_{n-1}, c_0)$ are also code words. A cyclic linear block code (n, k) is characterized by its *generator polynomial* $g(x) = 1 + g_1 X + \cdots + g_{n-k-1} X^{n-k-1} + X^{n-k}$, which yields the following generator matrix:

$$\mathbf{G} = \begin{bmatrix} 1 & g_1 & g_2 & ... & g_{n-k-1} & 1 & 0 & 0 & 0 & ... & 0 \\ 0 & 1 & g_1 & g_2 & ... & g_{n-k-1} & 1 & 0 & 0 & ... & 0 \\ 0 & 0 & 1 & g_1 & g_2 & ... & g_{n-k-1} & 1 & 0 & ... & 0 \\ \vdots & \vdots & \vdots & \vdots & \vdots & \vdots & \vdots & \vdots & \vdots & \vdots & \vdots \\ 0 & 0 & ... & 0 & 1 & g_1 & g_2 & ... & g_{n-k-2} & g_{n-k-1} & 1 \end{bmatrix} \tag{4.91}$$

Note that the generator matrix of a cyclic code is not in systematic form. For example, the (7,4) cyclic Hamming code with the generator polynomial $g(x) = 1 + X + X^3$ is given by

$$\mathbf{G} = \begin{bmatrix} 1 & 1 & 0 & 1 & 0 & 0 & 0 \\ 0 & 1 & 1 & 0 & 1 & 0 & 0 \\ 0 & 0 & 1 & 1 & 0 & 1 & 0 \\ 0 & 0 & 0 & 1 & 1 & 0 & 1 \end{bmatrix} \tag{4.92}$$

Another generator polynomial for the (7,4) cyclic Hamming code is $g(x) = 1 + X^2 + X^3$.

Golay codes

The Golay code is a (23,12) cyclic code with an error-correcting capability of $t = 3$ and a minimum Hamming distance $d_{min} = 7$. The two generator polynomials for Golay codes are $g(x) = 1 + X^2 + X^4 + X^5 + X^6 + X^{10} + X^{11}$, and $g(x) = 1 + X + X^5 + X^6 + X^7 + X^9 + X^{11}$.

Bose–Chaudhuri–Hocquenghem (BCH) codes

The BCH codes, a generalization of the Hamming code, are cyclic codes with the following description. For positive integers $m \geq 3$ and $t < 2^{m-1}$ the code structure is summarized as follows:

Code word length	$n = 2^m - 1$
Parity-check block	$n - k \leq mt$
Error-correcting capability	t
Minimum Hamming distance	$d_{min} \geq 2t + 1$

Reed–Solomon (RS) codes

The RS codes are non-binary BCH codes. The encoding is performed on symbols in GF(2^m) instead of bits. There are m bits per symbol. An (n,k) RS code word has k information symbols in a block of n symbols. Thus a code word has a total of mn coded bits. A t-error-correcting RS code is characterized in symbols as follows:

Code word length	$n = 2^m - 1$
Parity-check block	$n - k = 2t$
Error-correcting capability	t
Minimum Hamming distance	$d_{min} = 2t + 1$

Since RS codes can correct random symbol errors which are equivalent to random bursts of m bit errors, RS codes are suitable for wireless applications in fading channels. The IEEE 802.16e employs RS (255,239) code with 8 bits/symbol in GF(2^8). The bit error probability of an RS code is given by a modified form of (4.41) as follows:

$$P_e \approx \frac{2^{m-1}}{2^m - 1} \sum_{i=t+1}^{n} \frac{i+t}{n} \binom{n}{i} p_s^i (1 - p_s)^{n-i} \tag{4.93}$$

where p_s is the symbol error probability at the decoder input and $2^{m-1}/(2^m - 1)$ is the average number of bit errors per symbol error.

Example 4.13 Golay code for BSC

We wish to compare the bit error probabilities of uncoded and coded systems for BSC. For illustrative purposes we use PSK as the transmitted signal (Chapter 7) and the corresponding bit error probability for an AWGN channel is $Q(\sqrt{2\,SNR})$, where SNR is the received signal-to-noise ratio per bit. Assume that both uncoded and coded systems transmit with the same power, the signal-to-noise ratio per bit for the coded system is reduced by the code rate $r = k/n$ relative to that of the uncoded system. This happens because the coded bit rate is $1/r$ times the bit rate of the uncoded system. The transition probabilities of the BSC are taken to be $p = p(0|1) = p(1|0) = Q(\sqrt{2rSNR})$. For Golay code we have $r = 12/23$. At $SNR = 9.6$ dB, the bit error of the uncoded system is $P_b = Q(\sqrt{18.24}) = 10^{-5}$. The transition probabilities of the BSC are given by $p = p(0|1) = p(1|0) = Q(\sqrt{2rSNR}) = 10^{-3}$. Applying (4.41) we obtain the bit error probability of the coded system as

$$P_{b,coded} \approx \sum_{i=4}^{23} \frac{i+3}{23} \binom{23}{i} (10^{-3})^i (1 - 10^{-3})^{23-i} = 3 \times 10^{-9} \tag{4.94}$$

At this bit error probability an uncoded PSK system would require $SNR = 12.3$ dB. Thus a *coding gain* of 12.3 – 9.6 = 2.7 dB is realized. Note that this coding gain is achieved at the expense of bandwidth, which increases by a factor $1/r = 23/12 = 1.92$.

■

Low-density parity-check (LDPC) codes

An LDPC code is a linear block code whose parity-check matrix $\mathbf{H}$ is a *sparse* matrix. LDPC codes were first proposed by Robert G. Gallager and documented in [7,8]. Long LDPC codes can approach the Shannon limit within a few tenths of a dB. A *regular* LDPC code with block length n is defined by a parity-check matrix that has exactly w_r ones in each row and exactly w_c ones in each column, where $w_c < w_r < n$. An *irregular* LDPC code does not have the constant row and column weights. The rows of $\mathbf{H}$ are not necessarily linearly independent and the code dimension is determined by the rank of $\mathbf{H}$. A detailed investigation of LDPC codes will continue in Section 4.6.

Concatenated codes

To achieve the large error-correcting capability of a code with long block length, two shorter codes connected in concatenation can be employed. The first code is the *outer code* (n_o, k_o) with code rate $r_o = k_o/n_o$ and the second code is the *inner code* (n_i, k_i) with code rate $r_i = k_i/n_i$. For example, the outer code can be an RS code with k_i-bit symbols. Each RS code symbol is then encoded by the inner code to form an inner code word of length n_i. The overall code rate is $r = r_o r_i$. The bit error probability of concatenated codes can be evaluated by first calculating the bit error probability of the inner code using (4.41), for example, then finding the bit error probability of the outer code using (4.93).

Example 4.14 Concatenated RS and Hamming codes

Consider the case where the inner code is the (7,4) Hamming code with $t_i = 1$ error-correcting capability. With $k_i = 4$ we can select the RS code with block length $n_o = 2^m - 1 = 2^{k_i} - 1 = 15$. The information block for the RS code is $k_o = n_o - 2t_o$, where t_o is the error-correcting capability. For $t_o = 3$, we get the (15,9) RS code. Let us consider a BSC whose transition probabilities are taken to be $p = p(0|1) = p(1|0) = Q(\sqrt{2rSNR})$, where SNR is the received signal-to-noise ratio per bit. Assume that both uncoded and coded systems transmit with the same power, the signal-to-noise ratio per bit for the coded system is reduced by the code rate $r = r_o r_i = k_o k_i / n_o n_i = 0.34$ relative to that of the uncoded system. At $SNR = 9.6$ dB, the bit error of the uncoded system is $P_b = Q(\sqrt{18.24}) = 10^{-5}$. The transition probabilities of the BSC are given by $p = Q(\sqrt{2rSNR}) = 6 \times 10^{-3}$. First we calculate the bit error probability of the inner Hamming code from (4.41). We have

$$P_{b,H} \approx \sum_{i=2}^{7} \frac{i+1}{7} \binom{7}{i} p^i (1-p)^{7-i} = 3.2 \times 10^{-4} \tag{4.95}$$

The symbol error probability at the input of outer RS decoder is given by $p_s = 1 - (1 - P_{b.H})^{k_i} = 1.3 \times 10^{-3}$. Applying (4.93) we obtain the coded bit error probability as follows:

$$P_e \approx \frac{2^{4-1}}{2^4 - 1} \sum_{i=4}^{15} \frac{i+3}{15} \binom{15}{i} p_s^i (1 - p_s)^{15-i} = 9 \times 10^{-10} \tag{4.96}$$

At this bit error probability an uncoded PSK system would require SNR = 12.6 dB. Thus a *coding gain* of 12.6 – 9.6 = 3 dB is realized. Note that this coding gain is achieved at the expense of bandwidth, which increases by a factor $1/r = 2.92$. The advantage is the ability of the RS outer code to correct an error burst of up to 4 consecutive bits.

■

4.6 Low-density parity-check codes (LDPC)

After being dormant for some three decades LDPC codes were revived and found use in several applications in digital video broadcasting via satellites (DVB-S). To achieve large coding gains, codes with long block lengths are used. For example, block length of 16,200 bits and 64,800 bits were proposed for the second generation DVB-S2 (European Telecommunications Standards Institute (ETSI)) with rates varying from ¼ to ⁹⁄₁₀. The low-density property requires the parity-check matrix **H** to be sparse. For example, given even n, the parity-check matrix **H** of dimension ½ $n \times n$ may have three 1s per column ($w_c = 3$) and six 1s per row ($w_r = 6$). The parity-check matrix **H** can be chosen at random [18] conditioned on these constraints to ensure, in the probabilistic sense, a good code. Also the sparseness of **H** enables efficient decoding.

Example 4.14 Parity-check matrix of regular (10,5) LDPC code
The parity-check matrix of a regular LDPC code of length 10 is given below:

$$\mathbf{H} = \begin{bmatrix} 1 & 1 & 1 & 1 & 0 & 0 & 0 & 0 & 0 & 0 \\ 1 & 0 & 0 & 0 & 1 & 1 & 1 & 0 & 0 & 0 \\ 0 & 0 & 1 & 0 & 0 & 0 & 1 & 0 & 1 & 1 \\ 0 & 1 & 0 & 0 & 0 & 1 & 0 & 1 & 0 & 1 \\ 0 & 0 & 0 & 1 & 1 & 0 & 0 & 1 & 1 & 0 \end{bmatrix} \tag{4.97}$$

■

Example 4.16 Parity-check matrix of regular (12,6) LDPC code
The parity-check matrix of a regular LDPC code of length 12 is given below:

$$\mathbf{H} = \begin{bmatrix} 1 & 1 & 1 & 0 & 0 & 1 & 1 & 0 & 0 & 0 & 1 & 0 \\ 1 & 1 & 1 & 1 & 1 & 0 & 0 & 0 & 0 & 0 & 0 & 1 \\ 0 & 0 & 0 & 0 & 0 & 1 & 1 & 1 & 0 & 1 & 1 & 1 \\ 1 & 0 & 0 & 1 & 0 & 0 & 0 & 1 & 1 & 1 & 0 & 1 \\ 0 & 1 & 0 & 1 & 1 & 0 & 1 & 1 & 1 & 0 & 0 & 0 \\ 0 & 0 & 1 & 0 & 1 & 1 & 0 & 0 & 1 & 1 & 1 & 0 \end{bmatrix} \tag{4.98}$$

■

Tanner graph

The Tanner graph [27] visually describes a block code via its parity-check matrix. Since the parity-check matrix performs $n - k$ parity checks on n bits of the received word, one can represent the parity-check operation by two separate sets of nodes. The left set of nodes consists of *n bit nodes* (circle), one node for each bit in the code word, with no direct connection between any two bit nodes. The right set of nodes consists of *n – k check nodes* (square), one node for each parity check, with no direct connection between any two check nodes. The check nodes are connected to the bit nodes they check via branches, that is, the check node i is connected to the bit node j if and only if $h_{ij} = 1$. Thus, the $n - k$ rows of **H** specify the check nodes connections and the n columns of **H** specify the bit nodes connections. The Tanner graph is a *bipartite graph* whose nodes are separated into two distinct types with connections only between nodes of different types. Figure 4.9 shows the Tanner graph of the regular LDPC code of (4.98).

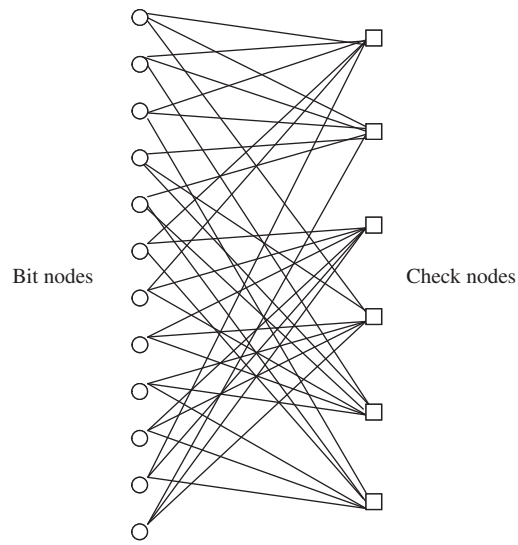

Figure 4.9 Tanner graph of (12,6) LDPC Code.

The cycle in a Tanner graph is a path that closes on itself. The *shortest cycle* of the Tanner graph has *four branches*. Cycles degrade the performance of decoding algorithms that are based on iterative techniques. The Tanner graph in Figure 4.9 has the shortest cycle.

Message passing algorithm (MPA)

The decoding of LDPC is carried out by a general class of iterative algorithms commonly referred to as *message passing algorithms* (MPA). The *belief propagation algorithm* (BPA) proposed by Gallager [7,8] is a subclass of MPA. Another name used for MPA is the *sum product algorithm* (SPA). The name MPA will be used in the subsequent discussion. For each iteration of the algorithm, the messages (probability, likelihood ratio (LR), or ln-likelihood ratio (LLR); all are also referred to as beliefs, but it is more practical to work with LLR) are passed along the branches from bit nodes to check nodes and from check nodes back to bit nodes. The message sent by a bit node i to a check node j is the belief that i has a certain value given the observed value of i from the channel and all incoming observables available to i from check nodes *other* than j. Thus, the message is *extrinsic information* and is computed for each bit node/check node connection at each half-iteration. On the other half-iteration, the message sent from a check node j to a message node i is the belief that i has a certain value given all messages sent to j in the previous iteration from bit nodes other than i. If at each iteration the incoming messages are independent (this is true if the Tanner graph has no cycles) then the update beliefs can be correctly calculated. Otherwise, the independence assumption is only true for up to the mth iteration, where m is half the length of the shortest cycle. After that, messages circulate back on themselves in other cycles. Simulations have shown that MPA is effective for LDPC with no length-4 cycles. In the following discussion we provide the definitions and calculations of messages for the bit nodes.

Example 4.17 Conditional a-posteriori probability, likelihood ratio, and ln-likelihood ratio of equiprobable binary random variable

The *conditional a-posteriori probabilities* of an equiprobable binary random variable X given the observed vector $\boldsymbol{y} = (y_1\ y_2\ \cdots\ y_n)$ of another random vector $\boldsymbol{Y}$ are denoted as $\Pr(X = 0|\boldsymbol{y})$ and $\Pr(X = 1|\boldsymbol{y})$. The *conditional likelihood ratio* (LR) $\Lambda(X|\boldsymbol{y})$ of X is defined via *Bayes rule*, $\Pr(X = i|\boldsymbol{y}) = f_{\boldsymbol{Y}|X}(\boldsymbol{y}|X = i)\Pr(X = i)/f_{\boldsymbol{Y}}(\boldsymbol{y}),\ i = 0, 1$, as

$$\Lambda(X|\boldsymbol{y}) = \frac{\Pr(X = 0|\boldsymbol{y})}{\Pr(X = 1|\boldsymbol{y})} = \frac{f_{\boldsymbol{Y}|X}(\boldsymbol{y}|X = 0)}{f_{\boldsymbol{Y}|X}(\boldsymbol{y}|X = 1)} \tag{4.99}$$

Similarly, the *conditional ln-likelihood ratio* (LLR) $\ln\Lambda(X|\boldsymbol{y})$ of X is defined as

$$\ln\Lambda(X|\boldsymbol{y}) = \ln\frac{\Pr(X = 0|\boldsymbol{y})}{\Pr(X = 1|\boldsymbol{y})} \tag{4.100}$$

For binary communications, the binary random variable X is equiprobable. Furthermore, if the components of the random vector $\boldsymbol{Y}$ are independent then we also have

$$\begin{aligned}\ln \Lambda(X|\boldsymbol{y}) &= \ln \frac{\Pr(X=0|\boldsymbol{y})}{\Pr(X=1|\boldsymbol{y})} \\ &= \ln \frac{\prod_{k=1}^{n} \Pr(X=0|y_k)}{\prod_{k=1}^{n} \Pr(X=1|y_k)} \\ &= \sum_{k=1}^{n} \ln \Lambda(X|y_k)\end{aligned} \tag{4.101}$$

■

Example 4.18 Binary symmetric channel

Consider a BSC with $X \in \{0,1\}$ and $Y \in \{0,1\}$. The BSC transition probabilities are p and $1-p$. The conditional probabilities are $\Pr(X=0|Y=0) = \Pr(X=1|Y=1) = 1-p$ and $\Pr(X=0|Y=1) = \Pr(X=1|Y=0) = p$. Therefore, the conditional LRs are

$$\begin{aligned}\Lambda(0|0) &= \frac{1-p}{p} \\ \Lambda(0|1) &= \frac{p}{1-p}\end{aligned} \tag{4.102}$$

Similarly, the conditional LLRs are given by

$$\ln \Lambda(0|0) = -\ln \Lambda(0|1) = \ln(1-p) - \ln p \tag{4.103}$$

■

Example 4.19 Binary erasure channel

Consider a BEC with $X \in \{0,1\}$ and $Y \in \{0,1,E\}$. The transition probabilities of the BEC are given by $\Pr(Y=0|X=0) = \Pr(Y=1|X=1) = 1-p$, and $\Pr(Y=E|X=0) = \Pr(Y=E|X=1) = p$. Therefore, the conditional probabilities are $\Pr(X=0|Y=0) = \Pr(X=1|Y=1) = 1$, $\Pr(X=0|Y=1) = \Pr(X=1|Y=0) = 0$, and $\Pr(X=0|Y=E) = \Pr(X=1|Y=E) = 0.5$. Therefore, the conditional LRs are

$$\Lambda(0|0) = \infty,\ \Lambda(0|1) = 0,\ \Lambda(0|E) = 1 \tag{4.104}$$

Similarly, the conditional LLRs are given by

$$\ln \Lambda(0|0) = \infty,\ \ln \Lambda(0|1) = -\infty,\ \ln \Lambda(0|E) = 0 \tag{4.105}$$

■

Example 4.20 AWGN channel

Consider an AWGN channel with equiprobable input $X \in \{-A, A\}$, which is obtained from the binary input [0,1] via the mapping $0 \rightarrow A$ and $1 \rightarrow -A$, and the Gaussian output $Y = X + N$, where N represents the Gaussian noise variable $N(0, \sigma^2)$. The conditional probability of X is given by

$$\Pr(X = x|y) = \frac{f_{Y|X}(y|x)\Pr(X = x)}{f_Y(y)} \tag{4.106}$$

The conditional Gaussian density function $f_{Y|X}(y|x)$ of the received variable Y can be expressed as follows:

$$f_{Y|X}(y|x) = \frac{1}{\sqrt{2\pi}\sigma} \mathrm{e}^{-(y-x)^2/2\sigma^2} \tag{4.107}$$

Therefore, the LR is given by

$$\Lambda(X|y) = \frac{\Pr(X = A|y)}{\Pr(X = -A|y)} = \frac{f_{Y|X}(y|A)}{f_{Y|X}(y|-A)} = \frac{\mathrm{e}^{-(y-A)^2/2\sigma^2}}{\mathrm{e}^{-(y+A)^2/2\sigma^2}} = \mathrm{e}^{2Ay/\sigma^2} \tag{4.108}$$

and consequently, we obtain the following LLR:

$$\ln \Lambda(X|y) = \frac{2Ay}{\sigma^2} \tag{4.109}$$

■

The messages for the check nodes are defined and calculated according to the parity-check equation $\boldsymbol{c}\mathbf{H}^{\mathbf{t}} = \mathbf{0}$. Each check node sums (modulo-2 addition) the bits from adjacent bit nodes via the parity

$$g = \boldsymbol{c}\boldsymbol{h}_j^t = \sum_{i=1}^{n} c_i h_{ji} = \sum_{i=1}^{n} x_i \tag{4.110}$$

where $x_i = c_i h_{ji}$ for a given column j of $\mathbf{H}^{\mathbf{t}}$. Obviously, the parity $g = 0, j = 1,2, \ldots, n-k$ if and only if $\boldsymbol{c}$ is a code word. The message sent by a check node is the conditional LLR of g, $\ln \Lambda(g|\boldsymbol{y})$, given the observed vector $\boldsymbol{y}$. Let the conditional LR of bit x_i be defined as

$$\Lambda(x_i|y_i) = \frac{\Pr(x_i = 0|y_i)}{\Pr(x_i = 1|y_i)} = \frac{\Pr(x_i = 0|y_i)}{1 - \Pr(x_i = 0|y_i)} \tag{4.111}$$

Therefore, the conditional probability $\Pr(x_i = 0|y_i)$ can be evaluated as follows:

$$\Pr(x_i = 0|y_i) = \frac{\Lambda(x_i|y_i)}{\Lambda(x_i|y_i) + 1} \tag{4.112}$$

Consequently we have

$$\begin{aligned} 2\Pr(x_i = 0|y_i) - 1 &= \frac{\Lambda(x_i|y_i) - 1}{\Lambda(x_i|y_i) + 1} \\ &= \tanh\left(\frac{1}{2}\ln\Lambda(x_i|y_i)\right) \end{aligned} \tag{4.113}$$

Furthermore, from (4.110) it is seen that the parity-check g is 0 when the number of ones in the set of bits $\{x_i\}$ is even and the parity-check g is 1 when the number of ones in $\{x_i\}$ is odd. If all bits x_i are *independent* and occur with conditional probabilities $\Pr(x_i = 0|y_i)$ and $\Pr(x_i = 1|y_i)$, then the conditional probability $\Pr(g = 0|\boldsymbol{y})$ that the set of bits $\{x_i\}$ contains an even number of ones is given by [8]

$$\Pr(g = 0|\boldsymbol{y}) = \frac{1}{2} + \frac{1}{2}\prod_{i=1}^{n}[2\Pr(x_i = 0|y_i) - 1] \tag{4.114}$$

The right-hand side of (4.114) can be verified via the following proof.

Proof Let $2\Pr(x_i = 0|y_i) - 1 = p_i$, $i = 1, 2$, then $\Pr(x_i = 0|y_i) = (1 + p_i)/2$ and $\Pr(x_i = 1|y_i) = (1 - p_i)/2$. We have

$$\begin{aligned} 2\Pr(x_1 + x_2 = 0|y_1, y_2) - 1 &= 2\Pr[(x_1 = 0, x_2 = 0|y_1, y_2) \\ &\quad \cup (x_1 = 1, x_2 = 1|y_1, y_2)] - 1 \\ &= 2[\Pr(x_1 = 0, x_2 = 0|y_1, y_2) \\ &\quad + \Pr(x_1 = 1, x_2 = 1|y_1, y_2)] - 1 \\ &= 2\Pr(x_1 = 0|y_1)\Pr(x_2 = 0|y_2) \\ &\quad + 2\Pr(x_1 = 1|y_1)\Pr(x_2 = 1|y_2) - 1 \\ &= \frac{1}{2}(1 + p_1)(1 + p_2) + \frac{1}{2}(1 - p_1)(1 - p_2) - 1 = p_1 p_2 \\ &= \prod_{i=1}^{2}[2\Pr(x_i = 0|y_i) - 1] \end{aligned} \tag{4.115}$$

Similarly,

$$\begin{aligned} 2\Pr(x_1 + x_2 + x_3 = 0|y_1, y_2, y_3) - 1 &= 2\Pr[(x_1 + x_2) + x_3 = 0|y_1, y_2, y_3] - 1 \\ &= [2\Pr(x_1 + x_2 = 0|y_1, y_2) - 1] \\ &\quad \times [2\Pr(x_3 = 0|y_3) - 1] \\ &= \prod_{i=1}^{3}[2\Pr(x_i = 0|y_i) - 1] \end{aligned} \tag{4.116}$$

Equation (4.114) is proved by the repeated application of this result.

Substituting (4.113) into (4.114) we obtain

$$\begin{aligned} 2\Pr(g=0|y)-1 &= \prod_{i=1}^{n}\left[2\Pr(x_i=0|y_i)-1\right] \\ &= \prod_{i=1}^{n}\tanh\left(\frac{1}{2}\ln\Lambda(x_i|y_i)\right) \end{aligned} \tag{4.117}$$

The LR and LLR of the parity-check g are given respectively by

$$\begin{aligned} \Lambda(g|\boldsymbol{y}) &= \frac{\Pr(g=0|\boldsymbol{y})}{\Pr(g=1|\boldsymbol{y})} \\ &= \frac{1+\prod_{i=1}^{n}\tanh\left(\frac{1}{2}\ln\Lambda(x_i|y_i)\right)}{1-\prod_{i=1}^{n}\tanh\left(\frac{1}{2}\ln\Lambda(x_i|y_i)\right)} \end{aligned} \tag{4.118}$$

and

$$\ln\Lambda(g|\boldsymbol{y}) = \ln\left[\frac{1+\prod_{i=1}^{n}\tanh\left(\frac{1}{2}\ln\Lambda(x_i|y_i)\right)}{1-\prod_{i=1}^{n}\tanh\left(\frac{1}{2}\ln\Lambda(x_i|y_i)\right)}\right] \tag{4.119}$$

The implementation of MPA is based on the recursive calculations of (4.101) for the bit node LLR message and (4.119) for the check node LLR message. Denote $\mathbf{m}_{ij}^{(l)}$ as the message sent by the bit node i to check node j at the l^{th} iteration, and $\hat{\mathbf{m}}_{ji}^{(l)}$ as the message sent by the check node j to bit node i at the l^{th} iteration. Note that for iteration $l=0$, that is, the initialization, the message $\mathbf{m}_{ij}^{(l)}$ is independent of all the check nodes and is denoted as $\mathbf{m}_i^{(0)}$. For example, $\mathbf{m}_i^{(0)} = 2Ay_i/\sigma^2$, $i = 1,2, \ldots, n$ for an AWGN channel and $\mathbf{m}_i^{(0)} = \ln(1-p) - \ln p$, $i = 1,2, \ldots, n$ for a BSC. The MPA is summarized as follows:

1. **Initialization**
   - $\hat{\mathbf{m}}_{ji}^{(0)} = 0$ for all i and j.
   - $\mathbf{m}_{ij}^{(0)} = \mathbf{m}_i^{(0)}$ for all i.
2. **Iteration** ($l = 1, 2, ..., l_{\max}$)
   - Check node update via (4.119)

$$\hat{\mathbf{m}}_{ji}^{(l)} = \ln\left[\frac{1+\prod_{k\in B_j\backslash i}\tanh\left(\mathbf{m}_{kj}^{(l-1)}/2\right)}{1-\prod_{k\in B_j\backslash i}\tanh\left(\mathbf{m}_{kj}^{(l-1)}/2\right)}\right] \tag{4.120}$$

     where B_j is the set of bit nodes adjacent to check node j and $B_j\backslash i$ is the set of bit nodes adjacent to check node j excluding bit node i.
   - Bit node update via (4.101)

$$\mathbf{m}_{ij}^{(l)} = \mathbf{m}_i^{(0)} + \sum\nolimits_{k\in C_i\backslash j}\hat{\mathbf{m}}_{ki}^{(l)} \tag{4.121}$$

where C_i is the set of check nodes adjacent to bit node i and $C_i \backslash j$ is the set of check nodes adjacent to bit node i excluding check node j.

- For $i = 1,2, \ldots, n$ set $\hat{c}_i = \begin{cases} 0 \text{ if } \mathbf{m}_{ij}^{(l)} \geq 0 \\ 1 \text{ if } \mathbf{m}_{ij}^{(l)} < 0 \end{cases}$
- Stop when $\hat{\boldsymbol{c}}\mathbf{H}^t = \mathbf{0}$ or $l = l_{\max}$.

The check node message requires the calculation of a product of tanh-terms. From the implementation point of view addition is preferable to multiplication. Therefore, it would be advantageous to simplify the LLR of a check node. Returning to (4.118) and solving for the product of tanh-terms we get

$$\begin{aligned} \prod_{i=1}^{n} \tanh\left(\frac{1}{2}\ln\Lambda(x_i|y_i)\right) &= \frac{\Lambda(g|\boldsymbol{y})-1}{\Lambda(g|\boldsymbol{y})+1} \\ &= \frac{e^{\ln\Lambda(g|\boldsymbol{y})}-1}{e^{\ln\Lambda(g|\boldsymbol{y})}+1} \\ &= \tanh\left(\frac{1}{2}\ln\Lambda(g|\boldsymbol{y})\right) \end{aligned} \tag{4.122}$$

Consequently we have

$$\ln\Lambda(g|\boldsymbol{y}) = 2\tanh^{-1}\prod_{i=1}^{n}\tanh\left(\frac{1}{2}\ln\Lambda(x_i|y_i)\right) \tag{4.123}$$

Consider the following identity:

$$\begin{aligned} \tanh\left(\frac{1}{2}\ln\Lambda(x_i|y_i)\right) &= [\text{sign}[\ln\Lambda(x_i|y_i)]]\frac{e^{|\ln\Lambda(x_i|y_i)|}-1}{e^{|\ln\Lambda(x_i|y_i)|}+1} \\ &= [\text{sign}[\ln\Lambda(x_i|y_i)]]\tanh\left(\frac{1}{2}|\ln\Lambda(x_i|y_i)|\right) \end{aligned} \tag{4.124}$$

This identity allows (4.123) to be written as follows:

$$\begin{aligned} \ln\Lambda(g|\boldsymbol{y}) &= 2\tanh^{-1}\left\{\left[\prod_{i=1}^{n}\text{sign}[\ln\Lambda(x_i|y_i)]\right]\left[\prod_{i=1}^{n}\tanh\left(\frac{1}{2}|\ln\Lambda(x_i|y_i)|\right)\right]\right\} \\ &= \left[\prod_{i=1}^{n}\text{sign}[\ln\Lambda(x_i|y_i)]\right]\left[2\tanh^{-1}\ln^{-1}\ln\prod_{i=1}^{n}\tanh\left(\frac{1}{2}|\ln\Lambda(x_i|y_i)|\right)\right] \\ &= \left[\prod_{i=1}^{n}\text{sign}[\ln\Lambda(x_i|y_i)]\right]\left[2\tanh^{-1}\ln^{-1}\sum_{i=1}^{n}\ln\left[\tanh\left(\frac{1}{2}|\ln\Lambda(x_i|y_i)|\right)\right]\right] \end{aligned} \tag{4.125}$$

Example 4.21 A self-inverse function

Consider the function $f(z) = -\ln[\tanh(z/2)]$. For $z > 0$, $f(z)$ is positive and monotonically decreasing and $f(z)$ is its own inverse, that is, $f[f(z)] = z$. This can be verified as follows:

$$f(z) = -\ln[\tanh(z/2)] = -\ln\left(\frac{e^z - 1}{e^z + 1}\right) = \ln\left(\frac{e^z + 1}{e^z - 1}\right) \tag{4.126}$$

Solving for z in terms of f we get

$$\begin{aligned} z &= 2\tanh^{-1}\left[\ln^{-1}[-f(z)]\right] \\ &= \ln\left[\frac{e^{f(z)} + 1}{e^{f(z)} - 1}\right] \\ &= f[f(z)] \end{aligned} \tag{4.127}$$

■

Using the above result in (4.125) we obtain

$$\ln \Lambda(g|\boldsymbol{y}) = \left[\prod_{i=1}^{n} \text{sign}[\ln \Lambda(x_i|y_i)]\right]\left[f\left(\sum_{i=1}^{n} f(|\ln \Lambda(x_i|y_i)|)\right)\right] \tag{4.128}$$

Applying this result to (4.120) gives an alternative method of updating the check node message, as follows:

$$\hat{\mathbf{m}}_{ji}^{(l)} = \left[\prod_{k\in B_j\setminus i} \text{sign}\left[\mathbf{m}_{kj}^{(l-1)}\right]\right]\left[f\left(\sum_{k\in B_j\setminus i} f\left(\left|\mathbf{m}_{kj}^{(l-1)}\right|\right)\right)\right] \tag{4.129}$$

Syndrome decoding discussed in Section 4.5 is the first iteration of MPA. By recursively updating the LLRs, the decoder improves the detection probability of a code word. MPA is a soft decoding technique and achieves a higher *coding gain* (about 2 dB) at low bit error probability than predicted by (4.41) for a hard decoder.

4.7 Channel coding with convolutional codes

Convolutional codes are linear trellis codes whose code words can be described by a labeled trellis and whose encoders are finite-state machines. The encoder of a rate $r = k/n$ convolutional code produces n output coded bits from k input information bits. A state depends only on a finite number of past information bits. For a code with 2^v states the number of past information bits that determine a present state are between v and kv bits. The parameter $K = v + 1$ is called the *constraint length* of the convolutional code. Typical code rates are between 1/3 and 7/8 and constraint lengths between 2 and 8. The terminology "convolutional" refers to the fact that the output coded bits are obtained by the convolution of the input information bits with the encoder *generator sequences* (impulse responses). For illustration let us consider the rate ½ convolutional encoder in Figure 4.10. Given the input sequence $\boldsymbol{i} = (100\ldots)$, the output sequences are the following generator sequences $g_1 = (10100...)$ and $g_2 = (11100...)$. The encoding operations are $\boldsymbol{c}_1 = \boldsymbol{i} * \boldsymbol{g}_1$ and $\boldsymbol{c}_2 = \boldsymbol{i} * \boldsymbol{g}_2$ to yield the coded bits $c_{1,l} = i_l + i_{l-2}$ and $c_{2,l} = i_l + i_{l-1} + i_{l-2}$. The two output sequences are multiplexed (parallel-to-serial conversion) into a single sequence $c = (c_{1,0}\ c_{2,0}\ c_{1,1}\ c_{2,1}\ c_{1,2}\ c_{2,2}...)$ for transmission.

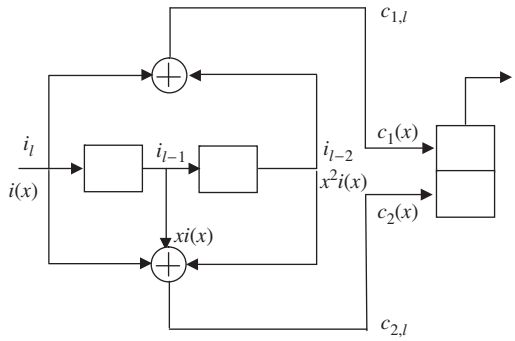

Figure 4.10 Rate ½ convolutional code with constraint length $K = 3$.

The convolutional encoder can also be described by its *generator polynomials* that represent the connection between the shift registers (SR) and the modulo-2 adders. For example, the two generator polynomials for the convolutional code in Figure 4.10 are $g_1(x) = x^2 + 1$ and $g_2(x) = x^2 + x + 1$. They represent the upper and lower connections, respectively, where the lowest-order coefficients represent the connection to the leftmost SR stage, and the highest-order coefficients represent the connection to the rightmost SR stage. Given an input sequence represented by the polynomial $i(x)$, the two output code sequences are $c_1(x) = i(x)g_1(x)$ and $c_2(x) = i(x)g_2(x)$, where the polynomial multiplication is carried out in GF(2).

The number of states of the rate k/n convolutional encoder is 2^v, where v is given by $v = \sum_{i=1}^{k} \max_j[\text{degree } g_{ij}(x)], j = 1, 2, \ldots, n$, and $g_{ij}(x)$ are the generator polynomials. The constraint length is $K = v + 1$. The code polynomial vector is $\boldsymbol{c}(x) = \boldsymbol{i}(x)\boldsymbol{G}(x)$, where $\boldsymbol{c}(x) = [c_1(x)\ c_2(x)\ \cdots\ c_n(x)]$, $\boldsymbol{i}(x) = [i_1(x)\ i_2(x)\ \cdots\ i_k(x)]$, and $\boldsymbol{G}(x) = [g_{ij}(x)]$ is the $k \times n$ *generator polynomial matrix*.

Example 4.22 Rate ½ convolutional code with constraint length $K = 7$

The IEEE 802.11a-g employs a rate ½ convolutional code with $2^v = 64$ states. The constraint length is $K = v + 1 = 7$. The generator polynomials are given by $g_1(x) = x^6 + x^5 + x^3 + x^2 + 1$ and $g_2(x) = x^6 + x^3 + x^2 + x + 1$. Figure 4.11 shows the encoder with six SR stages.

The IEEE 802.11a-g employs three different code rates, namely, rate ½, ¾, and ⅔. To facilitate decoding at the receiver, rates ¾, and ⅔ are obtained from rate ½ by *puncturing*. Puncturing is a procedure for omitting some encoded bits at the encoder output to reduce the number of transmitted bits and increase the code rate. At the receiver dummy bits are inserted in place of the omitted bits. To obtain rate ¾ code from rate ½ code, bits 4 and 5 are omitted for every six encoded bits (bits 1, 2, 3, and 6 are transmitted). Thus, for every three information bits, there are four transmitted coded bits. To obtain rate ⅔ code from rate ½ code, bit 4 is omitted for every four encoded bits (bits 1, 2, and 3 are transmitted). Thus, for every two information bits, there are three transmitted coded bits.

■

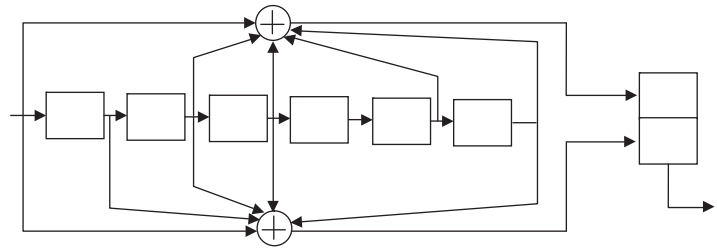

Figure 4.11 Rate ½ convolutional encoder with constraint length $K = 7$.

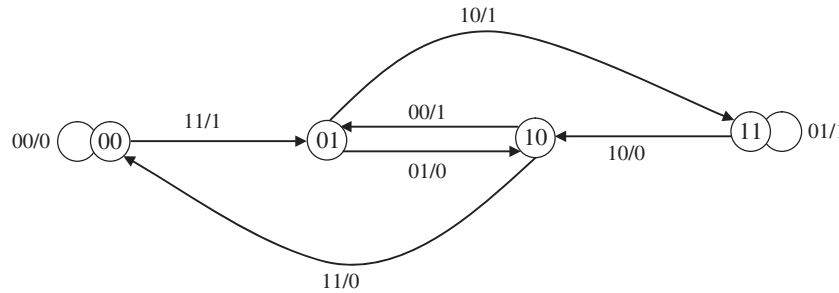

Figure 4.12 State diagram of rate ½ convolutional code with $K = 3$.

Example 4.23 Catastrophic convolutional code

A catastrophic convolutional code produces an infinite number of errors at the decoder output for a finite-channel error pattern. Consider the convolutional code with generator polynomials $g_1(x) = x^2 + 1$ and $g_2(x) = x + 1$. For the all-one input information sequence $i = (1, 1, 1, ...)$, the corresponding polynomial is $i(x) = 1 + x + x^2 + \cdots = 1/(1 + x)$. Thus, the code polynomials are $c_1(x) = i(x)g_1(x) = (x^2 + 1)/(x + 1) = (x + 1)$, and $c_2(x) = i(x)g_2(x) = 1$. The corresponding output sequences before multiplexing are $c_1 = (1, 1, 0, 0, 0, ...)$ and $c_2 = (1, 0, 0, 0, 0, ...)$. The transmitted code sequence after multiplexing $\boldsymbol{c}_1$ and $\boldsymbol{c}_2$ is $\boldsymbol{c} = (1, 1, 1, 0, 0, ...)$. Therefore, if the channel causes three errors in the first three bits of the transmitted code sequence $\boldsymbol{c}$, the receiver would receive the all-zero sequence. Since the information sequence is an all-one sequence, there are infinite errors. In particular a rate $1/n$ convolutional code is catastrophic if and only if its generator polynomials have a common polynomial factor. For rate k/n catastrophic convolutional codes, the determinants of all distinct $k \times k$ submatrices of the generator polynomial matrix do not have a common polynomial factor.

■

The convolutional encoder is a finite-state machine, and therefore can be described by a *state diagram* depicting all 2^v states and the corresponding transitions between states. Figure 4.12 shows the state diagram for the convolutional encoder in Figure 4.10, where the label *yz*/*x*

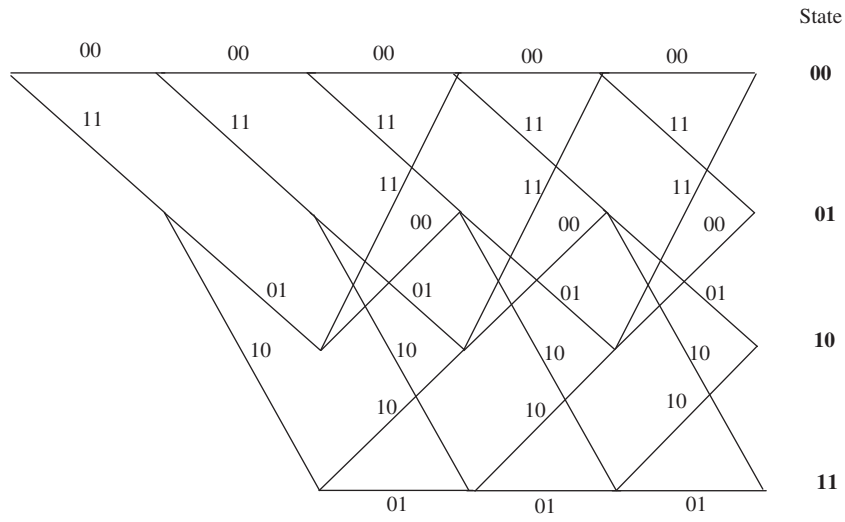

Figure 4.13 Trellis of rate ½ convolutional code with $K = 3$.

indicates the transition associated with the input information bit x and the output encoded bits yz. The encoder's corresponding *trellis* is shown in Figure 4.13, where the initial state is 00 and the length of time is five information bits (or ten coded bits); the *upper branch* corresponds to input information bit 0 and the *lower branch* corresponds to input information bit 1. The trellis is just a concatenation of successive state diagrams in time. Each input sequence and its corresponding code sequence are associated with a particular *path* through the trellis.

Hard decoding–BSC

The error-correcting capability of a convolutional code is characterized by its *free distance* d_{free}, which is the smallest *Hamming distance* between any two distinct code sequences. Since convolutional codes are linear codes, the all-zero code sequence is a legitimate code sequence. Thus, d_{free} is the *Hamming weight* (the total number of 1s) of the minimum-weight path through the trellis that originates from the all-zero state and ends in the all-zero state after a finite time. For the trellis in Figure 4.13, the minimum-weight path includes the set of states {00, 01, 10, 00} and corresponds to the code sequence (11, 01, 11), which has the Hamming weight of 5, hence $d_{free} = 5$.

The decoding at the receiver can be performed on the trellis via the well-known *Viterbi algorithm*, which efficiently implements the *maximum likelihood* (ML) sequence decoding scheme. In practice the rate k/n encoder takes a finite-length input sequence of kL bits and produces a finite-length output code sequence of nL bits. The decoding is carried out on each received code sequence independently. To implement this scheme, the encoder inserts *tail bits* at the end of each input sequence. If the constraint length of the code is K, the number of tail bits is $k(K-1)$. The tail bits return the encoder to the initial state, which is normally the all-zero state. This enables the decoder to reset the Viterbi algorithm to the all-zero state for the next code sequence decoding. Hence, in practice the input sequence to the encoder can

be represented by a $k(L + K - 1)$-vector $\boldsymbol{i}$ and the output code sequence by a $n(L + K - 1)$-vector $\boldsymbol{c}$. Let us consider a *discrete memoryless channel* (DMC) with binary input and Q-ary output that presents the decoder a vector $\boldsymbol{r}$, which is the transmitted code vector $\boldsymbol{c}$ that may contain errors in its components. Using Bayes theorem we have

$$\Pr(\boldsymbol{c}|\boldsymbol{r}) = \frac{\Pr(\boldsymbol{r}|\boldsymbol{c})\Pr(\boldsymbol{c})}{\Pr(\boldsymbol{r})} \tag{4.130}$$

Since convolutional codes are linear, all code vectors of the same length are equally likely; therefore, $\Pr(\boldsymbol{c})$ is identical for all possible values of $\boldsymbol{c}$. Furthermore, $\Pr(\boldsymbol{r}) = \sum \Pr(\boldsymbol{r}|\boldsymbol{c})\Pr(\boldsymbol{c})$ is independent of whichever code vector was transmitted. The decoder that maximizes the *a-posteriori probability* $\Pr(\boldsymbol{c}|\boldsymbol{r})$, that is, maximizing the probability of selecting the code vector correctly given the received vector $\boldsymbol{r}$, is called an ML decoder. Consequently, the ML decoder also maximizes the probability $\Pr(\boldsymbol{r}|\boldsymbol{c})$, the *likelihood* of the transmitted code vector $\boldsymbol{c}$. Since $\log x$ is a monotonically increasing function of x, the maximization of $\Pr(\boldsymbol{r}|\boldsymbol{c})$ is equivalent to the maximization of the *log-likelihood function* $\mathbf{M}(\boldsymbol{r}|\boldsymbol{c}) = \log \Pr(\boldsymbol{r}|\boldsymbol{c})$, commonly referred to as the *path metric* in the Viterbi algorithm.

Example 4.24 Path metric for BSC

Consider the BSC with transition probability p. The path metric is given by

$$\begin{aligned}\mathbf{M}(\boldsymbol{r}|\boldsymbol{c}) &= \log \Pr(\boldsymbol{r}|\boldsymbol{c}) = \log\left[\prod_{i=1}^{n_c} \Pr(r_i|c_i)\right] \\ &= \sum_{i=1}^{n_c} \log \Pr(r_i|c_i) = \sum_{i=1}^{n_c} \mathbf{M}(r_i|c_i)\end{aligned} \tag{4.131}$$

where n_c is the length of the binary vectors $\boldsymbol{r}$ and $\boldsymbol{c}$, and $\mathbf{M}(r_i|c_i) = \log \Pr(r_i|c_i)$ represents the *bit metric*. For a BSC we have

$$\Pr(r_i|c_i) = \begin{cases} p, & r_i \neq c_i \\ 1 - p, & r_i = c_i \end{cases} \tag{4.132}$$

Let $d = d(\boldsymbol{r}, \boldsymbol{c})$ be the *Hamming distance* between the two binary vectors $\boldsymbol{r}$ and $\boldsymbol{c}$, we obtain $\Pr(\boldsymbol{r}|\boldsymbol{c}) = p^d(1 - p)^{n_c - d}$ and consequently

$$\begin{aligned}\mathbf{M}(\boldsymbol{r}|\boldsymbol{c}) &= d \log p + (n_c - d)\log(1 - p) \\ &= d \log\left(\frac{p}{1 - p}\right) + n_c \log(1 - p)\end{aligned} \tag{4.133}$$

The term $n_c \log(1 - p)$ is common for all code vectors $\boldsymbol{c}$. Furthermore, we have $\log[p/(1 - p)] < 0$ for $p < 0.5$. Therefore, the Viterbi algorithm chooses a path in the trellis that maximizes $\mathbf{M}(\boldsymbol{r}|\boldsymbol{c}) = \log \Pr(\boldsymbol{r}|\boldsymbol{c})$ or, equivalently, chooses a code vector that *minimizes* the Hamming distance $d = d(\boldsymbol{r}, \boldsymbol{c})$. This also means choosing a code vector that differs from the received vector in the *fewest* places. The decoder that implements the Viterbi algorithm for a BSC is commonly referred to as a *hard decoder*.

■

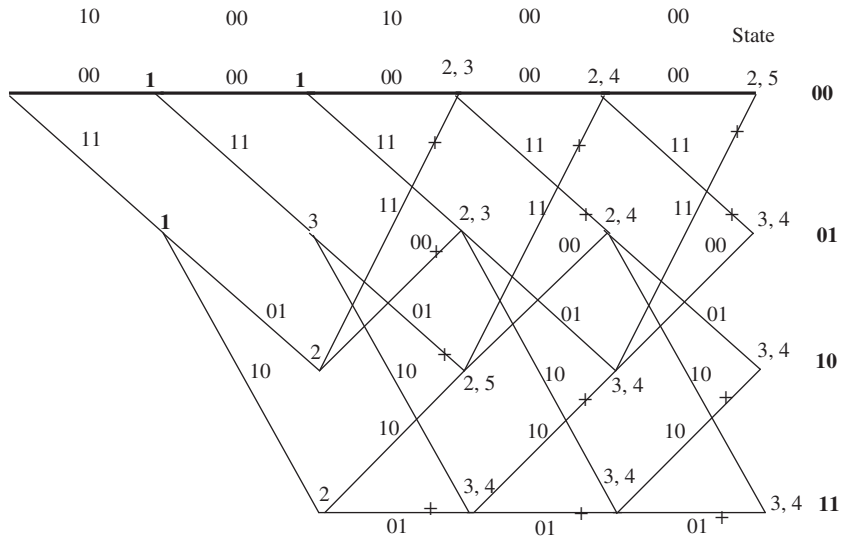

Figure 4.14 Hard Viterbi algorithm for rate ½ convolutional code with $K = 3$.

Example 4.25 Viterbi algorithm for a hard decoder

The Viterbi algorithm for each received vector $\boldsymbol{r}$ starts with an initial state which is commonly the all-zero state. The encoder always returns to this initial state via the use of tail bits. At each state in the trellis, the Viterbi algorithm chooses a branch that belongs to a path with the *smallest* Hamming distance. This retained path is called the *survivor path*. All other paths at each state with higher Hamming distances are not retained. In the case of a tie, a survivor path might be chosen randomly. At the end of the decoding window, the survivor path with the smallest Hamming distance is selected and the associated code vector is chosen as the transmitted code vector. For illustration, the transmitted code vector is $\boldsymbol{c}$ = (00,00,00,00,00). The channel causes two errors and the received vector is $\boldsymbol{r}$ = ($\underline{1}$0,00,$\underline{1}$0,00,00), as shown in Figure 4.14. The path that associates with the code sequence 00,00,00,00,00 has the minimum Hamming distance of 2 and hence is selected as the decoding path. The two errors are corrected.

■

Soft decoding–DMC

When the components of the received vector $\boldsymbol{r}$ are voltages, such as the sample values at the output of the matched filter in the receiver (Chapter 7), the metric can no longer be expressed in terms of the Hamming distance. In practice, the received components of $\boldsymbol{r}$ are *quantized* to Q-levels (16 to 64 levels are sufficient in practice) to form Q-ary outputs with a set of transition probabilities $\Pr[r_i(j)|c_i]$. Thus, $\Pr[r_i(j)|c_i]$ is the probability that the output

Table 4.2 The bit metric $\mathbf{M}[r_i(j)|c_i)] = \log \Pr[r_i(j)|c_i]$ for a 4-ary channel

	$r_i(0) = 0_0$	$r_i(1) = 0_1$	$r_i(2) = 1_1$	$r_i(3) = 1_0$
$\mathbf{M}[r_i(j)\|0)]$	–0.4	–0.5	–0.7	–1
$\mathbf{M}[r_i(j)\|1)]$	–1	–0.7	–0.5	–0.4

Table 4.3 The positive bit metric $\mathbf{M}[r_i(j)|c_i)] = -17.3 - 17.3 \log \Pr[r_i(j)|c_i]$ for a 4-ary channel

	$r_i(0) = 0_0$	$r_i(1) = 0_1$	$r_i(2) = 1_1$	$r_i(3) = 1_0$
$\mathbf{M}[r_i(j)\|0)]$	10	8	5	0
$\mathbf{M}[r_i(j)\|1)]$	0	5	8	10

Table 4.4 The uniform branch metric $\mathbf{M}[r_i(j)|1)] = j$ and $\mathbf{M}[r_i(j)|0)] = 3 - j$, $0 \leq j \leq 3$, for a 4-ary channel

	$r_i(0) = 0_0$	$r_i(1) = 0_1$	$r_i(2) = 1_1$	$r_i(3) = 1_0$
$\mathbf{M}[r_i(j)\|0)]$	3	2	1	0
$\mathbf{M}[r_i(j)\|1)]$	0	1	2	3

voltage of the ith bit falls in the jth quantized level given the transmitted coded bit c_i. For example, with $Q = 4$, we have the following assignments: $r_i(0) = 0_0$, $r_i(1) = 0_1$, $r_i(2) = 1_1$, $r_i(3) = 1_0$. The quantized levels $0_0, 0_1, 1_1$, and 1_0 refer to strong zero, weak zero, weak one, and strong one, respectively. The transition probabilities depend on the knowledge of the received signal-to-noise ratio. A common practice is to set the branch or bit metric in some convenient positive range without affecting the performance of the Viterbi algorithm by using the following expression:

$$\mathbf{M}[r_i(j)|c_i] = -A - B \log \Pr[r_i(j)|c_i] \tag{4.134}$$

where the constants A and B are chosen accordingly. Table 4.2 shows the branch metrics $\mathbf{M}[r_i(j)|c_i)] = \log \Pr[r_i(j)|c_i]$ for 4-ary channels and Table 4.3 shows the corresponding positive branch metrics. The knowledge of the transition probabilities is required for the computation of the metric. Furthermore, as the signal-to-noise varies in a wireless fading channel, the metrics must be adjusted accordingly. Therefore, a fixed set of metrics that can be easily specified and represents a good compromise over a large range of signal-to-noise ratios is desirable. For Q-level quantization, the branch metrics are $\mathbf{M}[r_i(j)|1)] = j$ and $\mathbf{M}[r_i(j)|0)] = Q - 1 - j$, $0 \leq j \leq Q - 1$. Table 4.4 shows the uniform branch metric assignment. Simulation shows a small degradation in performance over a broad range of signal-to-noise ratios. The decoder that implements the Viterbi algorithm for a DMC is commonly referred to as *soft decoder*.

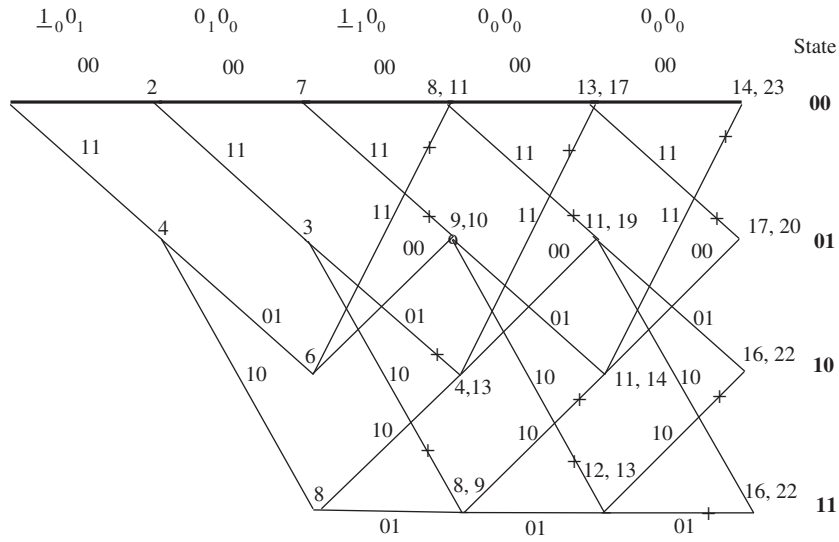

Figure 4.15 Soft Viterbi algorithm for rate ½ convolutional code with $K = 3$.

Example 4.26 Viterbi algorithm for a soft decoder

As in the case of hard decoding, the Viterbi algorithm for each received vector $\boldsymbol{r}$ starts with an initial state which is commonly the all-zero state. The encoder always returns to this initial state via the use of tail bits. At each state in the trellis, the Viterbi algorithm chooses a branch that belongs to a path with the *largest path metric*. This retained path is called the *survivor path*. All other paths at each state with smaller path metrics are not retained. In the case of a tie, a survivor path might be chosen randomly. At the end of the decoding window, the survivor path with the largest path metric is selected and the associated code vector is chosen as the transmitted code vector. For illustration the transmitted code vector is $\boldsymbol{c}$ = (00,00,00,00,00). The received quantized vector is $\boldsymbol{r} = (\underline{1}_0 0_1, 0_1 0_0, \underline{1}_1 0_0, 0_0 0_0, 0_0 0_0)$ with two errors underlined as shown in Figure 4.15. The path that associates with the code vector (00,00,00,00,00) has the maximum path metric of 23 and hence is selected as the decoding path. The two errors are corrected.

■

Soft decoding–Gaussian input vector

When the received vector $\boldsymbol{r}$ is a Gaussian voltage vector, we can express $\boldsymbol{r}$ as $\boldsymbol{r} = \boldsymbol{s} + \boldsymbol{N}$, where $\boldsymbol{s}$ is the voltage vector that represents the transmitted code vector $\boldsymbol{c}$, and $\boldsymbol{N}$ is the Gaussian noise vector whose components are independent Gaussian random variables with zero mean and variance σ^2. Using Bayes theorem we have

$$\Pr(\boldsymbol{c}|\boldsymbol{r}) = \frac{f_{\boldsymbol{R}}(\boldsymbol{r}|\boldsymbol{c})\Pr(\boldsymbol{c})}{f_{\boldsymbol{R}}(\boldsymbol{r})} \tag{4.135}$$

The conditional Gaussian density function $f_{\boldsymbol{R}}(\boldsymbol{r}|\boldsymbol{c})$ of the received vector $\boldsymbol{r}$ can be expressed as follows:

$$\begin{aligned} f_{\boldsymbol{R}}(\boldsymbol{r}|\boldsymbol{c}) &= \prod_k \frac{1}{\sqrt{2\pi}\sigma} \mathrm{e}^{-(r_k - s_k)^2/2\sigma^2} \\ &= \frac{1}{\left(\sqrt{2\pi}\sigma\right)^n} \mathrm{e}^{-\|\boldsymbol{r}-\boldsymbol{s}\|^2/2\sigma^2} \end{aligned} \tag{4.136}$$

Since convolutional codes are linear, all code vectors of the same length are equally likely; therefore, $\Pr(\boldsymbol{c})$ is identical for all possible values of $\boldsymbol{c}$. Furthermore, $f_{\boldsymbol{R}}(\boldsymbol{r}) = \sum f_{\boldsymbol{R}}(\boldsymbol{r}|\boldsymbol{c}) \Pr(\boldsymbol{c})$ is independent of whichever code vector was transmitted. The decoder that maximizes the *a-posteriori probability* $\Pr(\boldsymbol{c}|\boldsymbol{r})$, that is, maximizes the probability of selecting the transmitted code vector correctly given the received vector $\boldsymbol{r}$, is the ML decoder. Consequently, the ML decoder also maximizes the *likelihood* $f_{\boldsymbol{R}}(\boldsymbol{r}|\boldsymbol{c})$ of the transmitted code vector $\boldsymbol{c}$. Since $\log x$ is a monotonically increasing function of x, the maximization of $f_{\boldsymbol{R}}(\boldsymbol{r}|\boldsymbol{c})$ is equivalent to the maximization of the *ln-likelihood function* $\mathbf{M}(\boldsymbol{r}|\boldsymbol{c}) = \ln f_{\boldsymbol{R}}(\boldsymbol{r}|\boldsymbol{c}) = -\|\boldsymbol{r} - \boldsymbol{s}\|^2/2\sigma^2 - n\ln(\sqrt{2\pi}\sigma)$, or the *path metric* in the Viterbi algorithm. This in turn is equivalent to minimizing the *squared Euclidean distance* $d^2 = \|\boldsymbol{r} - \boldsymbol{s}\|^2$ (or simply the Euclidean distance) between the received vector $\boldsymbol{r}$ and the voltage vector $\boldsymbol{s}$ that represents the transmitted code vector $\boldsymbol{c}$. Therefore, the Viterbi algorithm chooses a path in the trellis that maximizes $\mathbf{M}(\boldsymbol{r}|\boldsymbol{c}) = \ln f_{\boldsymbol{R}}(\boldsymbol{r}|\boldsymbol{c})$, or equivalently, chooses a code vector that has the smallest squared Euclidean distance to the received vector. The decoder that implements the Viterbi algorithm for a Gaussian channel is referred to as the *unquantized soft decoder*. If the received Gaussian vector $\boldsymbol{r}$ is quantized to Q levels, then the Gaussian channel becomes a DMC.

Example 4.27 Viterbi algorithm for an unquantized soft decoder

As in the case of hard decoding, the Viterbi algorithm for each received vector $\boldsymbol{r}$ starts with an initial state which is commonly the all-zero state. The encoder always returns to this initial state via the use of tail bits. At each node in the trellis, the Viterbi algorithm chooses a branch that belongs to a path with the *smallest path squared Euclidean distance*. This retained path is called the *survivor path*. All other paths at each node with higher squared Euclidean distances are not retained. In the case of a tie, a survivor path might be chosen randomly. At the end of the decoding window, the survivor path with the smallest path squared Euclidean distance is selected and the associated code vector is chosen as the transmitted code vector. For illustration, let the transmitted code vector be $\boldsymbol{c}$ = (00,00,00,00,00). The corresponding transmitted voltage vector $\boldsymbol{s}$ is obtained by the mapping $0 \to \sqrt{rE_b}$ and $1 \to -\sqrt{rE_b}$, where r is the code rate and E_b is the *energy of the information bit*. The product rE_b represents the *energy of the coded bit*. Thus we have $\boldsymbol{s} = \left(\sqrt{rE_b}, \sqrt{rE_b}; \sqrt{rE_b}, \sqrt{rE_b}; \sqrt{rE_b}, \sqrt{rE_b}; \sqrt{rE_b}, \sqrt{rE_b}; \sqrt{rE_b}, \sqrt{rE_b}\right)$. The received unquantized vector is assumed to be the vector $\boldsymbol{r} = \left(-\underline{\sqrt{rE_b}}, \sqrt{rE_b}; 0.5\sqrt{rE_b}, \sqrt{rE_b}; -0.5\underline{\sqrt{rE_b}}, \sqrt{rE_b}; \sqrt{rE_b}, \sqrt{rE_b}; \sqrt{rE_b}, \sqrt{rE_b}\right)$ with two errors underlined. In Figure 4.16 the components of $\boldsymbol{r}$ are normalized to $\sqrt{rE_b}$. Each branch on the trellis is represented by one of the following voltage vectors: $00 \to \left(\sqrt{rE_b}, \sqrt{rE_b}\right)$, $01 \to \left(\sqrt{rE_b}, -\sqrt{rE_b}\right)$, $11 \to$

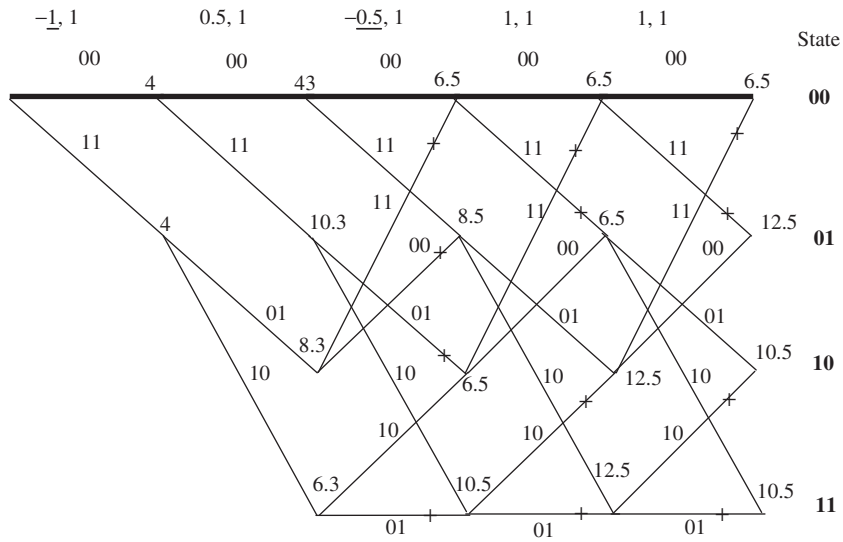

Figure 4.16 Unquantized soft Viterbi algorithm for rate ½ convolutional code with $K = 3$.

$\left(-\sqrt{rE_b}, -\sqrt{rE_b}\right), 10 \rightarrow \left(-\sqrt{rE_b},\ \sqrt{rE_b}\right)$. The path that associates with the code vector (00,00,00,00,00) has a normalized minimum squared Euclidean distance of 6.5 and hence is selected as the decoding path. The two errors are corrected.

■

Convolutional codes with large constraint length are very powerful. Furthermore, the concatenated *outer RS code-inner convolutional code* (adopted by IEEE 802.16e) can provide a very large coding gain that may come within 2 dB of the Shannon limit. This is perhaps the reason why LDPC codes were forgotten for three decades.

4.8 Summary

We have provided an introductory study of *information theory* pioneered by Shannon that centers on source coding and channel coding. We studied the *Shannon noiseless source coding theorem* and the famous *Huffman code*, which is the optimum prefix code (no other prefix codes have smaller average code word lengths). We stated without proof the *Shannon noisy channel coding theorem* and derived the information capacities of both discrete and Gaussian channels. For Gaussian channels, we considered those with no constraint on bandwidth and inputs, those with bandwidth constraints, and those with input constraints, especially equiprobable discrete inputs. The channel coding is carried out by error-correcting codes such as block codes and convolutional codes. The latter are widely used in IEEE 802.11 and 802.16 standards and in 2G and 3G cellular communications.

Problems

1. Given a source $X = \{0, 1, 2, 3)$ with distribution $p_X(0) = 1/2,\ p_X(1) = 1/4,\ p_X(2) = 1/8,\ p_X(3) = 1/8$, find the source entropy.
2. Consider the binomial random variable $X = \{0, 1, ...n\}$ with distribution $p_X(x_i) = \binom{n}{i} p^i (1-p)^{n-i}$ for a given probability p.
   (a) Plot $H(X)$ as a function of p with n as a parameter.
   (b) Find $H(X)$ for $p = 0.5$ and $n = 5, 10, 16$.
3. Consider a Gaussian source Z with zero mean and unit variance. The source is sampled and quantized to produce the output X, as shown in Figure 4.17. Find $H(X)$. (Hint: Find the distribution of the random variable X.)

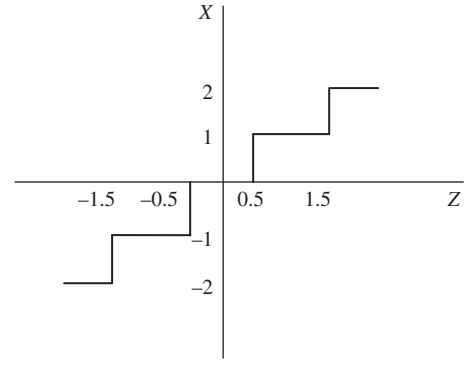

Figure 4.17 Quantizer

4. Consider a geometric random variable $X = \{0, 1, 2, ...\}$ with distribution $p_X(i) = p(1-p)^i$.
   (a) Find the source entropy $H(X)$ in term of the entropy of a binary source.
   (b) Find $H(X)$ for $p = 1/2$.
5. Find the entropy of a continuous random variable.
6. Let X be a discrete random variable and $g(X)$ be a function of X.
   (a) Given $\mathbf{E}\{g(X)\}$ find the probability distribution function of X that maximizes the entropy.
   (b) Consider the random variable $X = \{0, 1, 2, ...\}$. Given $\mathbf{E}(X) = \overline{X}$ find the probability distribution function of X that maximizes the entropy.
7. Consider the code [0, 01, 011]. Is this code uniquely decodable? Decode the bit sequence 0110010100001101.
8. Consider the code [0, 10, 110, 1110, 11110]. What unique property does this code have and is the code uniquely decodable? Decode the bit sequence 011001010000110.
9. Consider the code [1, 01, 001, 0001, 0000]. Cite two unique properties and decode the bit sequence 00101111001011100010100... .
10. Let X and Y be two independent discrete random variables. Calculate the entropy of XY.

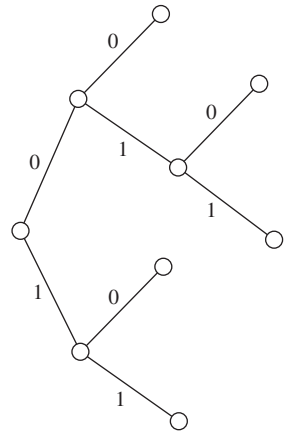

Figure 4.18 Binary tree for prefix codes.

11. The code {0, 11, 110, 111} is not a prefix code. Does it satisfy the Kraft inequality?
12. Show that the prefix codes have the binary tree shown in Figure 4.18.
    (a) If we let $l > \max l_m$, how many nodes exist at level l?
    (b) When a code word of length l_m is chosen, how many nodes on level l are blocked off?
    (c) Show that a prefix code satisfies the Kraft inequality.
13. The Kraft inequality determines whether there is a corresponding prefix code for a given set of code word lengths. Find a non-prefix code whose code word lengths [1, 2, 3, 3] satisfy the Kraft inequality.
14. In this problem we wish to show that the Kraft inequality applies not just to prefix codes but to all uniquely decodable codes. Show the inequality

$$\left(\sum_{m=1}^{M} \frac{1}{2^{l_m}}\right)^n \leq nl$$

    where n is an arbitrary positive integer and l is the longest code word length. From this inequality show that Kraft inequality applies to all uniquely decodable codes.
15. Given a discrete source X with distribution $p_X(x_i)$, show that a prefix code for this source whose average code word length is minimum has the following properties:
    (a) If $p_X(x_i) > p_X(x_j)$, then $l_i \leq l_j$.
    (b) Two symbols with smallest probabilities have code words of equal length.
    (c) If there are two or more code words of equal length, then two of these code words agree in all places except the last place.
16. Construct a Huffman code for the random variable X with the distribution {1/16, 3/16, 3/4}. Compare the average code word length to the entropy of X.
17. Construct a Huffman code for the random variable X with the distribution {1/32, 1/32, 1/16, 1/8, 3/16, 3/16, 3/8}. Compare the average code word length to the entropy of X.

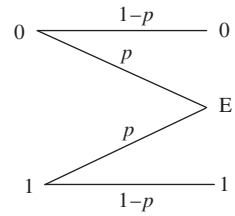

Figure 4.19 Binary erasure channel.

18. Consider a discrete source of three symbols $\{A, B, C\}$ with the distribution {1/16, 3/16, 3/4}. Construct a Huffman code for the extended source $\{AA, AB, AC, BA, BB, BC, CA, CB, CC\}$. Compare the code rate to the entropy of the original source. Calculate the variance of the code.
19. Show that the entropy of the extended source is n times the entropy of the original source as described in (4.21).
20. Consider a binary erasure channel (BEC) with two equiprobable inputs 0 and 1 and three outputs 0, 1, and E, where a fraction p of the bits is erased rather than corrupted. The receiver is supposed to know which bits are erased. The BEC is shown in Figure 4.19. Find the channel capacity.
21. Verify the BSC capacity in (4.36).
22. Find the mutual information $I(0,V)$ and $I(1,V)$ of a BSC. Calculate the channel capacity using these results.
23. Find the mutual information $I(0,V)$ and $I(1,V)$ of the BEC in Problem 20. Calculate the channel capacity using these results.
24. Consider a BSC with $p = 0.5$, that is, $C = 0$. Show that there are no repetition codes that can meet a specified bit error rate less than 0.5.
25. Find the channel capacity of a series connection of n identical BSCs.
26. Consider a BSC with error probability $p = 0.14$.
    (a) What is the BSC capacity?
    (b) Is there a code that can be used to achieve a specified error rate? What is the code rate?
    (c) Assume that Hamming code is used to achieve a bit error probability equal to 0.1. Can the goal be achieved? Provide two solutions.
27. Find the differential entropy of the random variable $Y = X + c$, where X is an arbitrary continuous random variable and c is a real constant.
28. Find the differential entropy of $Y = cX$, where X is an arbitrary continuous random variable and c is a real constant.
29. Consider a random variable X uniformly distributed over (a, b). Find the differential entropy of X. Can the differential entropy be negative?
30. Derive (4.54) using the inequality $\ln z \leq z - 1$ instead of the Jansen inequality.
31. Consider the water-filling strategy for a vector Gaussian channel with four subchannels. The noise variances of the subchannels are $\sigma_1^2 = 2,\ \sigma_2^2 = 4,\ \sigma_3^2 = 1,\ \sigma_4^2 = 8$. The total power for allocating to the subchannels is nine power units. Calculate the power allocated to each subchannel.

32. Consider the water-filling strategy for a vector Gaussian channel with five subchannels. The noise variances of the subchannels are $\sigma_1^2 = 1,\ \sigma_2^2 = 5,\ \sigma_3^2 = 3,\ \sigma_4^2 = 9,\ \sigma_5^2 = 8$. The total power for allocating to the subchannels is 20 power units.
    (a) Calculate the power allocated to each subchannel.
    (b) Suppose the total power is increased to 30 power units, calculate the power allocated to each subchannel.
33. Consider the conversion of a Gaussian channel with PSK signaling into a BSC channel with a crossover probability of $p = 10^{-6}$.
    (a) Calculate the BSC capacity.
    (b) Calculate the required *SNR* for a Gaussian channel with Gaussian inputs to have the same capacity as the BSC.
    (c) Calculate the potential coding gain.
34. Consider a (8,4) block code whose generator matrix is given by

$$\mathbf{G} = \begin{bmatrix} 1 & 0 & 0 & 0 & 0 & 1 & 1 & 1 \\ 0 & 1 & 0 & 0 & 1 & 1 & 1 & 0 \\ 0 & 0 & 1 & 0 & 1 & 1 & 0 & 1 \\ 0 & 0 & 0 & 1 & 1 & 0 & 1 & 1 \end{bmatrix}$$

    (a) Find the code word for the input sequence (1011).
    (b) Is the word (10111101) a valid code word?
    (c) Use the syndrome decoding to decode the received word (11100101) with one error in it.
35. Consider a sphere of radius t around a code word $\boldsymbol{c}$ of length n and rate $r = k/n$. This sphere contains the set of all code words of Hamming distance less than or equal to t from the code word $\boldsymbol{c}$.
    (a) Calculate the number of code words in the sphere.
    (b) Calculate the number of code words in all legitimate spheres of radius t.
    (c) Show the following bound:

$$1 - r \geq \frac{1}{n}\log_2\left[\sum_{i=0}^{t}\binom{n}{i}\right]$$

36. Verify (4.99).
37. Consider two independent binary random variables x_1 and x_2 with corresponding probabilities $\Pr(x_1 = 0) = p_1$, $\Pr(x_1 = 1) = 1 - p_1$, $\Pr(x_2 = 0) = p_2$, and $\Pr(x_2 = 1) = 1 - p_2$.
    (a) Evaluate the probabilities of $x_1 + x_2$.
    (b) Evaluate the LLR of $x_1 + x_2$ in terms of the LLRs of x_1 and x_2.
    (c) Generalize the result to n independent binary random variables.
38. Plot the function $f(z) = -\ln[\tanh(z/2)]$ and show that the smallest value of z dominates. This means that the check node LLR is dominated by a bit that is least certain, that is, likely to be zero or one. In this case the parity is also likely to be either zero or one irrespective of other bits. Modify the check node LLR to reflect this observation for less complex calculation.

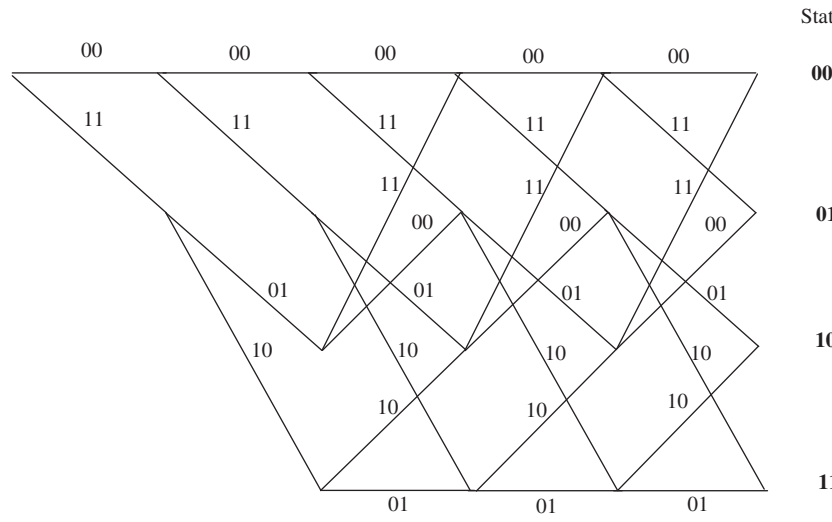

Figure 4.20 Trellis of rate ½ convolutional code with $K = 3$.

39. Implement the MPA for the Hamming code (7,4) and plot the bit error probability versus E_b/N_0 (dB).
40. Consider a rate $2/3$ convolutional code with the following generator matrix:

$$G(x) = \begin{bmatrix} 1+x & 1+x & 1 \\ 0 & x & 1+x \end{bmatrix}$$

    (a) Design the encoder.
    (b) Calculate the constraint length.
41. Consider the convolutional encoder specified by the generator polynomials $g_1(x) = 1 + x^3$ and $g_2(x) = x + x^2 + x^3$.
    (a) Draw the encoder.
    (b) For the input sequence (10111), add the smallest number of tail bits and find the output sequence.
    (c) Draw the state diagram.
42. Perform the Viterbi algorithm for the convolutional code with the trellis shown in Figure 4.20, assuming the received vector $\boldsymbol{r} = (0101011111)$.
43. Perform the Viterbi algorithm for the convolutional code with the trellis shown in Figure 4.20, assuming the received vector $\boldsymbol{r} = (1000100001)$.
44. Perform the Viterbi algorithm for the convolutional code with the trellis shown in Figure 4.20, assuming the received vector $\boldsymbol{r} = (0_1 0_1 1_0 0_0 0_0 1_1 0_0 1_1 1_1 0_0)$.
45. Perform the Viterbi algorithm for the convolutional code with the trellis shown in Figure 4.20, assuming the received vector $\boldsymbol{r} = (1_1 0_1 1_0 0_0 1_1 1_1 0_0 1_0 1_1 0_1)$.
46. Perform the Viterbi algorithm for the convolutional code with the trellis shown in Figure 4.20, assuming the received vector $\boldsymbol{r} = (-0.8, -0.6, 1, -0.7, 0.7, 0.6, 0.5, -0.9, -0.8, -0.6)$.

47. Perform the Viterbi algorithm for the convolutional code with the trellis shown in Figure 4.20, assuming the received vector $\boldsymbol{r} = (0.7, 0.9, -1, 0.7, 0.7, -0.6, -0.5, -0.9, 0.8, -0.6)$

Further reading

The foundation of information theory was laid out by Shannon in [1,2]. For an introduction to information theory and coding we recommend Hamming [6,9]. The serious reader can explore [4,10–16] for advanced materials.

Bibliography

1. C. E. Shannon, "A mathematical theory of communication," *Bell Syst. Tech. J.*, Vol. **27**, pp. 379–423, pp. 623–656, 1948.
2. C. E. Shannon, "Communication in the presence of noise," *Proc. IRE*, Vol. **37**, pp. 10–21, 1949.
3. R. V. L. Hartley, "The transmission of information," *Bell Syst. Tech. J.*, Vol. **7**, pp. 535–563, 1928.
4. S. Lin and D. J. Costello, Jr., *Error Control Coding*, 2nd edition, Englewood Cliffs, NJ: Pearson Prentice-Hall, 2004.
5. G. C. Clark, Jr. and J. B. Cain, *Error-Correction Coding for Digital Communications*, New York: Plenum Press, 1981.
6. R. W. Hamming, "Error detecting and error correcting codes," *Bell Syst. Tech. J.*, Vol. **29**, pp. 147–160, 1950.
7. R. Gallager, "Low-density parity-check codes," *IRE Trans. Inform. Theory*, pp. 21–28, January 1962.
8. R. Gallager, *Low-Density Parity-Check Codes*, Cambridge, MA: MIT Press, 1963.
9. R. W. Hamming, *Coding and Information Theory*, 2nd edition, London: Prentice-Hall, 1986.
10. N. Abramson, *Information Theory and Coding*, New York: McGraw-Hill, 1963.
11. R. G. Gallager, *Information Theory and Reliable Communication*, New York: Wiley, 1968.
12. R. E. Blahut, *Principles and Practice of Information Theory*, Reading, MA: Addison-Wesley, 1987.
13. T. M. Cover and J. A. Thomas, *Elements of Information Theory*, 2nd edition, Chichester: John Wiley & Sons, 2006.
14. J. R. Barry, E. A. Lee, and D. G. Messerschmitt, *Digital Communication,* 3rd edition, Amsterdam: Kluwer Academic Publishers, 2004.
15. R. G. Gallager, *Principles of Digital Communications*, Cambridge: Cambridge University Press, 2008.

16. A. Lapidoth, *A Foundation in Digital Communication*, Cambridge: Cambridge University Press, 2009.
17. D. MacKay, "Good error correcting codes based on very sparse matrix," *IEEE Trans. Inform. Theory*, pp. 399–431, 1999.
18. T. J. Richardson and R. Urbanke, "Efficient encoding of low-density parity-check codes," *IEEE Trans. Inform. Theory*, Vol. **47**, No. 2, pp. 638–656, 2001.
19. C. E. Shannon, "Communication theory of secrecy systems," *Bell Syst. Tech. J.*, Vol. **28**, pp. 656–715, 1949.
20. C. E. Shannon, "Prediction and entropy of printed English," *Bell Syst. Tech. J.*, Vol. **30**, pp. 50–64, 1951.
21. C. E. Shannon, "The zero error capacity of a noisy channel," *IRE Trans. Inform. Theory*, Vol. **IT-2**, pp. 8–19, 1956.
22. C. E. Shannon, "Certain results in coding theory for noisy channels," *Inform. Contr.*, Vol. **1**, pp. 6–25, 1957.
23. C. E. Shannon, "Channels with side information at the transmitter," *IBM J. Res. Develop.*, Vol. **2**, pp. 289–293, 1958.
24. C. E. Shannon, "Coding theorems for a discrete source with a fidelity criterion," *IRE Nat. Conv. Rec.*, Part 4, Vol. **2**, pp. 142–143, 1959.
25. C. E. Shannon, "Probability of error for optimal codes in a Gaussian channel," *Bell Syst. Tech. J*, Part 4, Vol. **38**, pp. 611–656, 1959.
26. C. E. Shannon, R. G. Gallager, and E. R. Berlekamp, "Lower bounds to error probability for coding on discrete memoryless channels, I and II," *Inform. Contr.*, Vol. **10**, pp. 65–103, pp. 527–552, 1967.
27. R. M. Tanner, "A recursive approach to low complexity codes," *IEEE Trans. Inform. Theory*, Vol. **IT-27**, pp. 533–547, 1981.
28. S. G. Wilson, *Digital Modulation and Coding*, Englewood Cliffs, NJ: Prentice-Hall, 1996.

5 Communication link analysis

Introduction

In this chapter, we provide the foundation for analyzing a wireless communication link. The purpose is to evaluate the *signal-to-noise ratio* at the receiver to assess the link performance. Evaluation of the signal power and noise power requires the path loss and receiver system noise temperature, respectively. The receiver consists of an antenna, a low-noise amplifier, a downconverter, and a demodulator. The concept of the thermal noise source and its noise temperature, as well as the antenna noise temperature, is discussed. We also introduce the *effective noise temperature* and *noise figure* of a two-port network such as the low-noise amplifier, downconverter, or demodulator. The effective noise temperature and noise figure of a cascade or series connection of two-port networks are derived. This leads to the evaluation of the receiver *system noise temperature.*

For free space links, such as satellite communications links, we introduce the *Friis* equation to calculate the path loss. For cellular communications links, we present the well-known *Hata* model. Many important aspects of cellular systems are also discussed, such as the frequency spectrum, standards, and the co-channel interference.

5.1 Basic wireless communication link

In wireless communications, the point-to-point link is the simplest connection between a transmitter and a receiver. In this basic link, the transmitted signal travels the line-of-sight path to the receiver and the channel is the free space. A typical wireless communication system is shown in Figure 5.1.

The transmitter consists of a modulator, an upconverter, a high-power amplifier, and a transmitter antenna. The receiver consists of a receiver antenna, a low-noise amplifier, a downconverter, and a demodulator. The upconverter translates the IF carrier frequency of the modulated signal to the RF carrier frequency for transmission. The downconverter translates the RF carrier frequency of the received signal to the IF carrier frequency for demodulation.

Each subsystem in the transmitter and receiver processes the information signal and adds thermal noise to it. The thermal noise is generated by the electronic components of the subsystem. At the transmitter, the signal power is much larger than the composite thermal

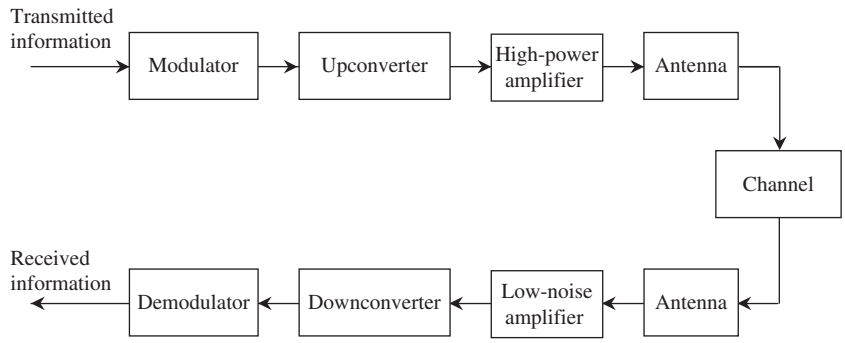

Figure 5.1 Typical wireless communication system.

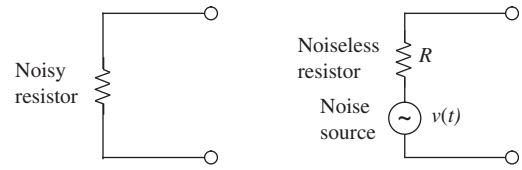

Figure 5.2 Thermal noise source.

noise power generated by the transmitter's subsystems; therefore, the effect of the thermal noise is negligible. The signal is attenuated as it travels through the channel. When the signal arrives at the receiver, its power can diminish to a level so that the effect of noise becomes relevant. The receiver antenna receives the signal contaminated by sky noise. At each subsystem of the receiver, the signal is processed and thermal noise is added to the signal.

The purpose of link analysis is to obtain the signal-to-noise ratio at the receiver that can provide a qualitative assessment of the performance of the entire communication system. Two quantities need to be evaluated, namely, the receiver noise power and the received signal power. We first study the effect of thermal noise in the receiver.

Thermal noise

Thermal noise is generated by random motion of electrons in a resistor whose temperature is above absolute zero kelvin. A noise voltage is generated across the terminal of the resistor, which can be modeled as a noiseless resistor with resistance R ohms in series with a noise voltage source $v(t)$ as in Figure 5.2.

The power spectral density of the thermal noise source $v(t)$, which is normalized to $R = 1\,\Omega$, is given in W/Hz as follows:

$$S_v(f) = 2\left[\frac{h|f|}{2} + \frac{h|f|}{e^{h|f|/kT_n} - 1}\right] \text{ W/Hz} \tag{5.1}$$

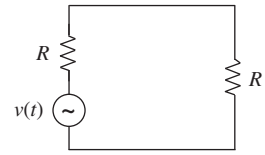

Figure 5.3 Thermal noise source with a matched load.

where $h = 6.6 \times 10^{-34}$ Js is the *Planck constant*, $k = 1.38 \times 10^{-23}$ J/K is the *Boltzmann constant*, T_n is the physical temperature of the resistor (also referred to as the noise temperature of the source) in kelvin, and f is the frequency in Hz.

For frequency $f < 1000$ GHz, the *power spectral density* of a thermal noise source can be very well approximated by the following constant:

$$S_v(f) = 2kT_n \tag{5.2}$$

Noise with a constant power spectral density is called *white noise*. In a communication system, all subsystems are designed to have matched impedances at both input and output. For example, the output impedance of the antenna is matched with the input impedance of the low-noise amplifier. In practice, these input and output impedances are 50 Ω. In our discussion, we assume a normalized impedance of $R = 1\,\Omega$. Matched impedances are employed to provide the *maximum power transfer* from one subsystem to the next one. Unfortunately, this also allows the maximum power transfer of noise.

When a matched load is connected across the thermal noise source as shown in Figure 5.3, the *available power spectral density* in W/Hz across the load is

$$S(f) = |H(f)|^2 S_v(f) \tag{5.3}$$

where $H(f)$ is the transfer function of the resistor divider network and is given by

$$H(f) = \frac{R}{R+R} = \frac{1}{2} \tag{5.4}$$

Substituting (5.2) and (5.4) into (5.3), we obtain

$$S(f) = \frac{kT_n}{2} \tag{5.5}$$

Note that the available power spectral density of a thermal noise source is independent of the value of R.

The *available noise power*, in watts, delivered by the thermal noise source $v(t)$ to the matched load in a bandwidth of B Hz is therefore given by

$$N = \int_{-B}^{B} S(f)\,\mathrm{d}f = \int_{-B}^{B} \frac{kT_n}{2}\,\mathrm{d}f = kBT_n \tag{5.6}$$

Figure 5.4 illustrates the evaluation of the available noise power.

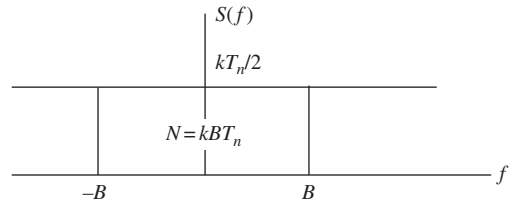

Figure 5.4 Available noise power.

Example 5.1 Available noise power

Consider a thermal noise source with noise temperature $T_n = 290\,\text{K}$. The available power spectral density is given as

$$S(f) = \frac{kT_n}{2} = 2 \times 10^{-21}\ \text{W/Hz}$$

Assuming that the operating bandwidth is $B = 1\,\text{MHz}$, the available noise power is

$$N = kBT_n = 4 \times 10^{-15}\ \text{W}$$

■

In summary, a thermal noise source is specified by its noise temperature T_n, which is also its physical temperature. Returning to Figure 5.1, we observe that the receiver antenna receives the signal plus *sky noise*. The term sky noise is used to include noise signals from emitting–absorbing objects in space. High-temperature-emitting objects such as the stars and the Sun produce electromagnetic radiation with a white noise power spectral density in the practical frequency range that wireless communications operate in. The antenna also receives noise signals from absorbing objects, such as the Earth and the Moon. A blackbody that absorbs electromagnetic radiation also acts as a resistor above absolute zero kelvin and hence also radiates noise. The composite noise signal received by the receiver antenna can be modeled as a white noise source of temperature T_A called the antenna noise temperature. This equivalent noise source delivers an available noise power of kT_AB. In other words, the noise that the antenna receives can be taken into account by assigning a noise temperature T_A to the antenna radiation resistance. The antenna noise temperature is a function of frequency and antenna beam angle, and includes contributions from sources of radiation in the main beam as well as sources of radiation in all directions in proportion to the antenna pattern.

Example 5.2 Antenna noise temperature

An antenna is pointing at the sky with a temperature of 10 K. This temperature consists of the sky background temperature of 3 K (the residual temperature of the Big Bang that created the universe) and 7 K due to atmospherical absorption. Assuming the non-ideal case where 90% of the beam is directed at the sky and 10% at the ground at a temperature of 290 K, the antenna noise temperature can be calculated as follows:

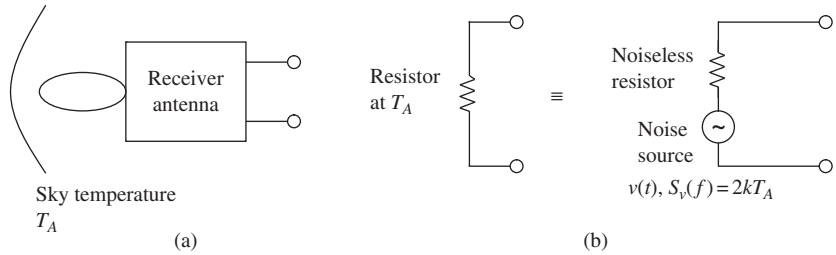

Figure 5.5 (a) Antenna with entire pattern sees the sky at temperature T_A; (b) resistor at temperature T_A. The same noise power spectral density is available at the output terminals in both cases.

$$\text{Sky contribution :} \quad 0.9 \times 10\,\text{K} = 9\,\text{K}$$
$$\text{Ground contribution :} \quad 0.1 \times 290\,\text{K} = 29\,\text{K}$$

Thus,

$$T_A = 9\,\text{K} + 29\,\text{K} = 38\,\text{K}$$

The noise power spectral density available at the antenna output is given by (5.5) as

$$S(f) = \frac{kT_A}{2} = 2.6 \times 10^{-22}\ \text{W/Hz}$$

■

In summary, the noise that the antenna receives can be taken into account by assigning a noise temperature T_A to the antenna radiation resistance. Thus, if the antenna is replaced by a resistor of the same radiation resistance at temperature T_A, the noise power spectral density available at the output terminals is unchanged, and so is the noise power available within a bandwidth B. Figure 5.5 illustrates the modeling of the noise received by the receiver antenna.

Returning to Figure 5.1, the signal and sky noise received by the receiver antenna are delivered to the low-noise amplifier. The low-noise amplifier amplifies both signal and sky noise and also adds its own thermal noise to the signal. More thermal noise is added as the signal is downconverted from the carrier frequency to an intermediate frequency by the downconverter and, finally, the demodulator adds more noise as it detects the information from the modulated signal.

We assume that the gains of both the low-noise amplifier and downconverter are constant over the operating frequency range. This is the case in practice to avoid frequency-selective distortion of the signal spectrum, which in return can cause intersymbol interference and/or loss of the signal-to-noise ratio.

Effective noise temperature

To account for the effect of the internal thermal noise generated by a two-port network such as the low-noise amplifier, downconverter, or demodulator, we consider a noisy two-port network

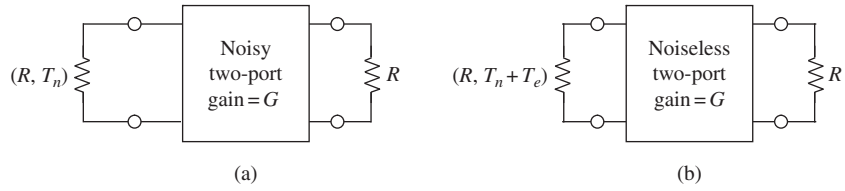

Figure 5.6 (a) Noisy two-port network with input noise source at temperature T_n; (b) model with the effect of noise temperature T_e added to noise source temperature.

as shown in Figure 5.6(a). The input and output of the network are matched to R ohms. The network has a constant gain G and is driven by a thermal noise source at temperature T_n.

The noise power available in a bandwidth B at the input of the network is kBT_n as indicated by (5.6). The noise power available in B at the output of the network due to the input noise source is simply $kBGT_n$. Let N_I denote the noise power available in the bandwidth B at the output port due to the internal noise sources of the network. Then, the total available noise power at the output port is given by

$$\begin{aligned} N &= kBGT_n + N_I \\ &= kBG\left(T_n + \frac{N_I}{kBG}\right) \\ &= kBG(T_n + T_e) \end{aligned} \tag{5.7}$$

where

$$T_e = \frac{N_I}{kBG} \tag{5.8}$$

is defined as the *effective noise temperature* of the two-port network and is incorporated in the model shown in Figure 5.6(b). In this model, the noisy two-port network is replaced by a noiseless two-port network with the same gain G, and the input noise source temperature is changed from T_n to $T_n + T_e$. Note that the noise power available at the input of the noiseless two-port network is $kB(T_n + T_e)$, as compared to kBT_n at the input of the noisy two-port network. Nevertheless, they both yield the same available output noise power given in (5.7).

In summary, the effective noise temperature of a noisy two-port network is the additional temperature that a noise source requires to produce the same available noise power at the output of the equivalent noiseless two-port network (the noisy two-port network with the internal noise removed).

Definition 5.1 The *system noise temperature* of a noisy two-port network is defined by

$$T_s = T_n + T_e \tag{5.9}$$

Definition 5.2 The *system noise power* is defined by

$$N_i = kBT_s \tag{5.10}$$

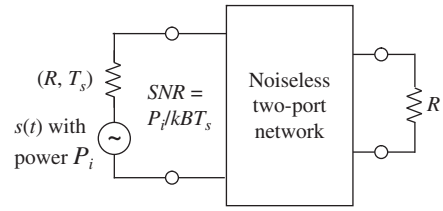

Figure 5.7 System signal-to-noise ratio where the input signal $s(t)$ has power P_i, and the system noise $n(t)$ has power kBT_s.

Definition 5.3 The *available output noise power* of a two-port network is defined by

$$N = kBGT_s \tag{5.11}$$

Definition 5.4 The *system signal-to-noise ratio* of a noisy two-port network of effective noise temperature T_e, driven by an input noise source of temperature T_n and an input signal source of power P_i , is defined by

$$SNR = \frac{P_i}{N_i} = \frac{P_i}{kBT_s} \tag{5.12}$$

and is illustrated in Figure 5.7.

We remark that the quantity P_i/kBT_n is *not* the *system signal-to-noise ratio*, because it does not account for the internal noise of the two-port network.

Another measure employed to characterize a noisy two-port network driven by an input noise source of reference temperature T_0 is the *noise figure*, which is defined as the *ratio* of the *available output noise power* to the *available output noise power produced by the input noise source at reference temperature only* (that is, without the addition of the internal noise). Thus, using (5.6) and (5.7), we obtain the noise figure F as follows:

$$\begin{aligned} F &= \frac{kBG(T_0 + T_e)}{kBGT_0} \\ &= 1 + \frac{T_e}{T_0} \end{aligned} \tag{5.13}$$

It is seen that the noise figure is defined for a reference noise source temperature T_0. The reference room temperature adopted by the IEEE is $T_0 = 290$ K, which yields

$$F = 1 + \frac{T_e}{290} \tag{5.14}$$

Therefore, the effective noise temperature in kelvin of the noisy two-port network can be related to its noise figure as

$$T_e = 290(F - 1) \tag{5.15}$$

Example 5.3 Noisy two-port network

Consider a noisy two-port network with an effective noise temperature $T_e = 120\,\text{K}$, a gain $G = 50\,\text{dB}$, and a bandwidth $B = 1\,\text{MHz}$. The input noise source is at temperature $T_n = 60\,\text{K}$ and the input signal source has a power $P_i = 10^{-12}\,\text{W}$. Calculate the noise figure of the two-port network, the system noise temperature, the system signal-to-noise ratio, and the available output noise power.

From (5.14), the noise figure is given by

$$F = 1 + \frac{120}{290} = 1.41 = 1.5\ \text{dB}$$

The system noise temperature can be calculated from (5.9) as

$$T_s = 120 + 60 = 180\,\text{K}$$

From (5.12), we obtain the system signal-to-noise ratio as

$$SNR = \frac{10^{-12}}{(1.38 \times 10^{-23})(10^6)(180)} = 402.6 = 26\,\text{dB}$$

From (5.11), the available output noise power is given by

$$\begin{aligned} N &= \left(1.38 \times 10^{-23}\right)\left(10^6\right)\left(10^5\right)(180) \\ &= 2.5 \times 10^{-10}\,\text{W} \end{aligned}$$

■

Returning to Figure 5.1, we note that the antenna output might be connected to the low-noise amplifier via a transmission line, such as a waveguide. To account for the loss of the transmission line, we return to Figure 5.6 and consider the transmission line as a reciprocal two-port network with loss L, or equivalently with gain

$$G = \frac{1}{L} \tag{5.16}$$

Let the characteristic impedance of the transmission line be R ohms, so that both input and output are matched to R ohms. Also, let T_0 be the physical temperature of the transmission line. Thus, looking into the output of the transmission line, the load sees a resistor R at temperature T_0. Therefore, the available output noise power at the load in a bandwidth of B Hz is kBT_0. But this is also equal to the quantity on the right-hand side of (5.7), that is,

$$kBG(T_0 + T_e) = kBT_0 \tag{5.17}$$

This yields the *effective noise temperature* of the transmission line as follows:

$$T_e = T_0(L - 1) \tag{5.18}$$

If T_0 is chosen to be 290 K, then

$$T_e = 290(L - 1) \tag{5.19}$$

Comparing (5.15) and (5.19), we obtain the *noise figure* of the transmission line of loss L as

$$F = L \tag{5.20}$$

From the link analysis point of view, the effective noise temperature of the transmission line can be evaluated by (5.18) knowing its loss L and its physical temperature T_0. Note that the loss $L = 1$ or gain $G = 1$ corresponds to a lossless transmission line with $T_e = 0$.

Example 5.4 Transmission line

Consider a lossy transmission line with $L = 0.1$ dB. Calculate the effective noise temperatures, assuming the transmission line physical temperatures are 290 K and 273 K, respectively. First convert dB into a ratio: we get $L = 0.1$ dB $= 1.023$. Using (5.18) we obtain, for $T_0 = 290$ K,

$$T_e = 290(1.023 - 1) = 6.755 \text{ K}$$

and, for $T_0 = 273$ K,

$$T_e = 273(1.023 - 1) = 6.359 \text{ K}$$

We note that a change of 13 K in the physical temperature results in only a change of 0.396 K in the effective noise temperature.

■

Returning to Figure 5.1, we also need to account for the internal noise generated by the downconverter and the demodulator. These two systems are connected in series with the low-noise amplifier. To account for their noise effects, we consider the model shown in Figure 5.8, which consists of two noisy two-port networks. Each two-port network has an effective noise temperature T_{ek} and a gain G_k, $k = 1, 2$. The input noise source has a temperature T_n. We assume that the two-port networks are matched to R ohms at their inputs and outputs. Our purpose is to evaluate the *effective noise temperature of the series connection*, which obviously has a gain G_1G_2.

We note that by using (5.9) and (5.11), we obtain the available noise power at the output of the first two-port network as

$$N_1 = kBG_1(T_n + T_{e1}) \tag{5.21}$$

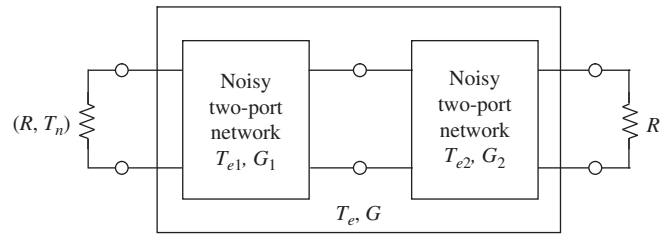

Figure 5.8 Two networks connected in series.

The available noise power N at the output of the second two-port network consists of G_2N_1 and the power delivered by the internal noise sources of the second two-port network. Using (5.8) we have

$$\begin{aligned} N &= G_2N_1 + kBG_2T_{e2} \\ &= kBG_1G_2(T_n + T_{e1}) + kBG_2T_{e2} \\ &= kBG_1G_2\left(T_n + T_{e1} + \frac{T_{e2}}{G_1}\right) \end{aligned} \tag{5.22}$$

From (5.9) and (5.11), we conclude that the *effective noise temperature* T_e of the series connection is $T_{e1} + T_{e2}/G_1$. Now, if we connect a third two-port network with effective noise temperature T_{e3} and gain G_3 in series with the second two-port network, we end up with a series connection of two networks, one with $T_{e1} + T_{e2}/G_1$ and G_1G_2 and one with T_{e3} and G_3. Applying (5.22) with T_{e1} replaced by $T_{e1} + T_{e2}/G_1$, where T_{e2} is replaced by T_{e3} and G_1 is replaced by G_1G_2, the effective noise temperature of the series connection of three two-port networks is $T_{e1} + T_{e2}/G_1 + T_{e3}/G_1G_2$ and its gain is $G_1G_2G_3$. Continuing this way, we can generalize the result to a series connection of n two-port networks with gain $G = G_1G_2 \cdots G_n$ and effective noise temperature T_e given by

$$T_e = T_{e1} + \frac{T_{e2}}{G_1} + \frac{T_{e3}}{G_1G_2} + \cdots + \frac{T_{en}}{G_1G_2\cdots G_{n-1}} \tag{5.23}$$

Applying (5.15) to (5.23) yields the noise figure F of a series connection of n two-port networks, each with noise figure F_i, $i = 1, 2, \ldots, n$:

$$F = F_1 + \frac{F_2 - 1}{G_1} + \frac{F_3 - 1}{G_1G_2} + \cdots + \frac{F_n - 1}{G_1G_2\cdots G_{n-1}} \tag{5.24}$$

Observing (5.23), we come to the following conclusion. If the *gain* G_1 of the *first* two-port network is *large*, then the noise contribution of subsequent two-port networks becomes negligible.

Example 5.5 Series connection

Consider the series connection of a low-noise amplifier with $T_{e1} = 120\,\text{K}$, $G_1 = 50\,\text{dB}$, a downconverter with $T_{e2} = 2 \times 10^4\,\text{K}$, $G_2 = 20\,\text{dB}$, and a demodulator with $T_{e3} = 10^5\,\text{K}$. Calculate the effective noise temperature T_e of the series connection. If $G_1 = 30\,\text{dB}$, evaluate the impact on T_e.

Using (5.23), we obtain

$$\begin{aligned} T_e &= 120 + \frac{2 \times 10^4}{10^5} + \frac{10^5}{(10^5)(10^2)} \\ &= 120 + 0.2 + 0.01 = 120.21\text{K} \end{aligned}$$

Thus, with a large amplifier gain, the effective noise temperature of the low-noise amplifier solely determines the effective noise temperature of the series system.

Now, with $G_1 = 30$ dB, we have

$$T_e = 120 + \frac{2 \times 10^4}{10^3} + \frac{10^5}{(10^3)(10^2)}$$
$$= 120 + 20 + 1 = 141 \text{ K}$$

The impact on T_e is significant, as it is increased by 21 K. In practice, the larger gain is much easier and less costly to achieve than the lower noise temperature. Therefore, it is appropriate to choose $T_{e1} = 120$ K and $G_1 = 50$ dB than $T_{e1} = 99$ K and $G_1 = 30$ dB to achieve $T_e = 120$ K.

■

Receiver noise model

Returning to Figure 5.1, we can model the receiver noise effect using Figure 5.9. The antenna is modeled as a noise source of temperature equal to the antenna noise temperature T_A. The transmission line that connects the antenna to the LNA has a loss L_{TL} and a physical temperature T_0. The low-noise amplifier has a gain G_{LNA} and an effective noise temperature T_{LNA}. The downconverter has a gain G_{DC} and an effective noise temperature T_{DC}. The effective noise temperature of the demodulator is T_{DM}.

Example 5.6 System noise temperature at the input of the transmission line

To evaluate the system noise temperature at the input of the transmission line, we employ (5.9) and the model shown in Figure 5.6. We note that $T_n = T_A$. The effective noise temperature T_e of the series connection of the transmission line, the low-noise amplifier, the downconverter, and the demodulator is calculated via (5.18) and (5.23) and is given as follows:

$$T_e = T_0(L_{TL} - 1) + L_{TL}T_{LNA} + \frac{L_{TL}T_{DC}}{G_{LNA}} + \frac{L_{TL}T_{DM}}{G_{LNA}G_{DC}} \tag{5.25}$$

Using (5.9), the *system noise temperature* is obtained as

$$T_s = T_n + T_e \tag{5.26}$$

$$T_s = T_A + T_0(L_{TL} - 1) + L_{TL}T_{LNA} + \frac{L_{TL}T_{DC}}{G_{LNA}} + \frac{L_{TL}T_{DM}}{G_{LNA}G_{DC}} \tag{5.27}$$

■

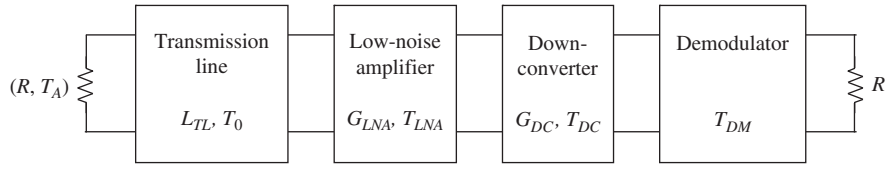

Figure 5.9 Receiver noise model.

Example 5.7 System noise temperature at the input of the low-noise amplifier
We can model the antenna and the transmission line as a combined noise source at temperature T_n'. First we evaluate the available noise power N' at the output of the transmission line via (5.7) and (5.18):

$$N' = \frac{kB}{L_{TL}}[T_A + T_0(L_{TL} - 1)] \tag{5.28}$$

Since N' must also be equal to kBT_n', we obtain

$$T_n' = \frac{1}{L_{TL}}[T_A + T_0(L_{TL} - 1)] \tag{5.29}$$

The effective noise temperature T_e' of the series connection of the low-noise amplifier, the downconverter, and the demodulator is calculated via (5.23) as

$$T_e' = T_{LNA} + \frac{T_{DC}}{G_{LNA}} + \frac{T_{DM}}{G_{LNA}G_{DC}} \tag{5.30}$$

From (5.9), the *system noise temperature* is given by

$$\begin{aligned} T_s' &= T_n' + T_e' \\ &= \frac{1}{L_{TL}}[T_A + T_0(L_{TL} - 1)] + T_{LNA} + \frac{T_{DC}}{G_{LNA}} + \frac{T_{DM}}{G_{LNA}G_{DC}} \end{aligned} \tag{5.31}$$

By comparing (5.31) with (5.27), we have

$$T_s' = \frac{T_s}{L_{TL}} \tag{5.32}$$

■

Example 5.8 System noise temperature at the input of the downconverter
We first model the antenna, the transmission line, and the low-noise amplifier as a combined noise source at temperature T_n''. The transmission line and the low-noise amplifier can be modeled as a two-port network with gain G_{LNA}/L_{TL} and effective noise temperature $T_0(L_{TL} - 1) + L_{TL}T_{LNA}$. The available noise power at the low-noise amplifier output can be calculated via (5.7) as

$$N'' = \frac{kBG_{LNA}}{L_{TL}}[T_A + T_0(L_{TL} - 1) + L_{TL}T_{LNA}] \tag{5.33}$$

Since N'' must also be equal to kBT_n'' we get

$$T_n'' = \frac{G_{LNA}}{L_{TL}}[T_A + T_0(L_{TL} - 1) + L_{TL}T_{LNA}] \tag{5.34}$$

The effective noise temperature T_e'' of the series connection of the downconverter and the demodulator can be calculated via (5.23) as

$$T_e'' = T_{DC} + \frac{T_{DM}}{G_{DC}} \tag{5.35}$$

From (5.9), the *system noise temperature* is given by

$$\begin{aligned} T_s'' &= T_n'' + T_e'' \\ &= \frac{G_{LNA}}{L_{TL}}[T_A + T_0(L_{TL} - 1) + L_{TL}T_{LNA}] + T_{DC} + \frac{T_{DM}}{G_{DC}} \end{aligned} \tag{5.36}$$

By comparing (5.36) with (5.31) and (5.32), we have

$$T_s'' = G_{LNA}T_s' = \frac{G_{LNA}T_s}{L_{TL}} \tag{5.37}$$

■

Example 5.9 System noise temperature at the input of the demodulator

At this reference input, the antenna, the transmission line, the low-noise amplifier, and the downconverter combine to act as a combined noise source at temperature T_n'''. The transmission line, the low-noise amplifier, and the downconverter can be modeled as a two-port network with gain $G_{LNA}G_{DC}/L_{TL}$ and effective noise temperature $T_0(L_{TL} - 1) + L_{TL}T_{LNA} + L_{TL}T_{DC}/G_{LNA}$. The available noise power at the downconverter output is given by (5.7) as

$$N''' = \frac{kBG_{LNA}G_{DC}}{L_{TL}}\left[T_A + T_0(L_{TL} - 1) + L_{TL}T_{LNA} + \frac{L_{TL}T_{DC}}{G_{LNA}}\right] \tag{5.38}$$

Setting $N''' = kBT_n'''$ to obtain the effective noise temperature of the combined noise source, we get

$$T_n''' = \frac{G_{LNA}G_{DC}}{L_{TL}}\left[T_A + T_0(L_{TL} - 1) + L_{TL}T_{LNA} + \frac{L_{TL}T_{DC}}{G_{LNA}}\right] \tag{5.39}$$

Using (5.9), we obtain the system noise temperature as follows:

$$\begin{aligned} T_s''' &= T_n''' + T_{DM} \\ &= \frac{G_{LNA}G_{DC}}{L_{TL}}\left[T_A + T_0(L_{TL} - 1) + L_{TL}T_{LNA} + \frac{L_{TL}T_{DC}}{G_{LNA}}\right] + T_{DM} \end{aligned} \tag{5.40}$$

From (5.40) and (5.36), we conclude that

$$T_s''' = G_{DC}T_s'' = G_{LNA}G_{DC}T_s' = \frac{G_{LNA}G_{DC}T_s}{L_{TL}} \tag{5.41}$$

■

System signal-to-noise ratio

The purpose of the link analysis is to obtain the system signal-to-noise ratio defined in (5.12) for performance assessment. It requires the knowledge of the system noise temperature discussed in the previous section, and the input signal power at the receiver. Returning to Figure 5.1, let P_T, G_T, G_R, and L_C be the power of the high-power amplifier, the transmitter antenna gain, the receiver antenna gain, and the channel loss, respectively. We can calculate the input signal power at any reference input of the receiver. Let P_R, P_R', P_R'', and P_R''' be the received signal powers at the input of the transmission line, the low-noise amplifier, the downconverter, and the demodulator, respectively. Then

$$P_R = L_{TL}P_R' = \frac{L_{TL}P_R''}{G_{LNA}} = \frac{L_{TL}P_R'''}{G_{LNA}G_{DC}} = \frac{P_T G_T G_R}{L_C} \tag{5.42}$$

Using (5.42), (5.32), (5.37), and (5.41), we obtain the *system signal-to-noise ratio* (*SNR*) as follows:

$$SNR = \frac{P_R}{kBT_s} = \frac{P_R'}{kBT_s'} = \frac{P_R''}{kBT_s''} = \frac{P_R'''}{kBT_s'''} \tag{5.43}$$

It is seen that the system signal-to-noise ratio is *invariant* with respect to any reference input and is given by

$$SNR = \frac{P_T G_T G_R}{L_C kBT_s} \tag{5.44}$$

where T_s is given in (5.27). The product $P_T G_T$ is called the *effective isotropic radiated power* (EIRP) of the transmitter, and the ratio G_R/T_s is called the receiver *figure-of-merit*.

Example 5.10 System signal-to-noise ratio

Consider a line-of-sight communication link with a transmitter *EIRP* = 30 dBW. The receiver antenna has a gain G_R = 20 dB and a noise temperature T_A = 200 K. The low-noise amplifier has a gain G_{LNA} = 40 dB and an effective noise temperature T_{LNA} = 120 K. The rest of the receiver has an effective noise temperature of $T_e = 10^4$ K. Calculate the distance between the transmitter and receiver to achieve a system signal-to-noise ratio of 20 dB, assuming a receiver noise bandwidth of 10 MHz, and a carrier frequency of 4 GHz.

The system noise temperature at the low-noise amplifier input is

$$T_s = T_A + T_{LNA} + \frac{T_e}{G_{LNA}} = 200 + 120 + \frac{10^4}{10^4} = 321 \text{ K}$$

The gain of the low-noise amplifier is large; therefore, the contribution of noise from the rest of the receiver is only 1 K. From (5.44), we obtain the *channel loss* L_C as

$$L_C = \frac{(EIRP)G_R}{kBT_s(SNR)}$$
$$= \frac{10^3 \times 10^2}{(1.38 \times 10^{-23})10^7 \times 321 \times 10^2} = 2.26 \times 10^{16}$$

The free space loss is given by the Friis equation as

$$L_C = \left(\frac{4\pi d}{\lambda}\right)^2 \tag{5.45}$$

where d is the distance between the transmitter and receiver and λ is the signal wavelength given by

$$\lambda = \frac{c}{f} = \frac{3 \times 10^8 \text{ m/s}}{f} \tag{5.46}$$

Using $f = 4$ GHz, we get

$$d = 896.7 \text{ km}$$

■

5.2 Cellular communication link

Cellular communication was invented to serve mobile users. It was based on the concept of *frequency reuse*, that is, the entire frequency spectrum is reused at many locations separated by large distances to avoid interference. This is necessary because there are simply not enough voice channels in the mobile frequency spectrum to serve a large population of mobile users. In a cellular system, the coverage area is divided into *M clusters*. Each cluster consists of a fixed number of *cells N*. Each cell uses a separate portion of the frequency spectrum and, hence, there is no interference between cells in the same cluster. On the other hand, all clusters reuse the same frequency spectrum and, therefore, the coverage area is served M times by the same frequency spectrum. Because of frequency reuse, cells in adjacent clusters that employ the same portion of the frequency spectrum (*co-channel* cells) produce interference to each other. To keep the interference within a tolerable limit, co-channel cells must be separated far enough. Figure 5.10 illustrates a cellular system, which consists of *base stations*, *mobiles*, and a *mobile switching center* (MSC). The MSC is connected to the public switched telephone network (PSTN).

All mobiles in a cell communicate with the cell's base station. A call is handed off to another base station as the mobile moves out of its cell. The base stations connect all the mobiles to the MSC via coaxial cable, fiber optic cable, or microwave links. The MSC is responsible for connecting all mobiles to the PSTN.

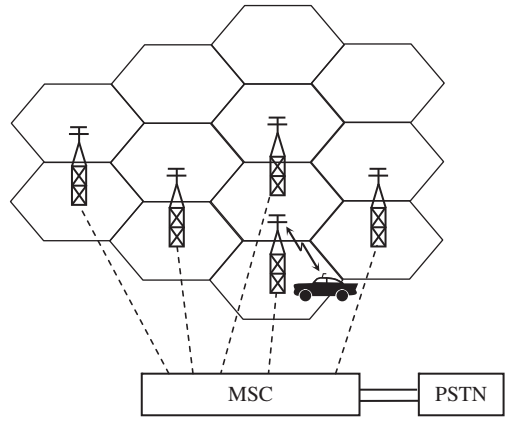

Figure 5.10 Cellular system with towers representing base stations.

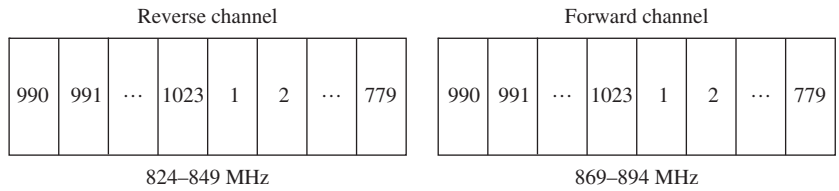

Figure 5.11 Frequency spectrum for the US cellular band.

Frequency spectrum

In the United States, the *Federal Communications Commission* (FCC) allocated a frequency spectrum of 50 MHz to cellular communication in the 800 MHz band as shown in Figure 5.11. The frequency spectrum consists of two bands. The *forward channel* band of 25 MHz (869–894 MHz) is used for *base station-to-mobile* communication. The *reverse channel* band of 25 MHz (824–849 MHz) is used for *mobile-to-base station* communication. Each band consists of 832 channels (channel 990 is not used) and each channel has a bandwidth of 30 kHz. Two channels of the same number, one in each band, form a 60 kHz *full duplex* channel, which allows simultaneous two-way communication between the base station and the mobile. To encourage competition, the Federal Communications Commission licensed the frequency spectrum to two competing service providers in each geographical area. *Block A* channels were licensed to a non-wireline company, which does not provide a telephone service. *Block B* channels were licensed to a wireline company that provides a telephone service. Table 5.1 shows the channel allocation for both providers A and B, and Table 5.2 shows the center frequency of the channel.

Major cellular standards

The *first generation* (1G) cellular system employs *frequency modulation* (FM) and hence is an analog system. In North America, these use the *advanced mobile phone system*

Table 5.1 Channel allocation for providers A and B

Provider	Bandwidth (MHz)	Number of channels	Channel number
Not used		1	990
A	1	33	991 to 1023
	10	333	1 to 333
	1.5	50	667 to 716
B	10	333	334 to 666
	2.5	83	717 to 799

Table 5.2 Channel number and center frequency

Type	Channel number	Center frequency (MHz)
Forward channel	$1 \leq N \leq 799$	$0.03\,N + 825$
	$990 \leq N \leq 1023$	$0.03\,(N - 1023) + 825$
Reverse channel	$1 \leq N \leq 799$	$0.03\,N + 870$
	$990 \leq N \leq 1023$	$0.03\,(N - 1023) + 870$

(AMPS), established in 1983, and the *narrowband advanced mobile phone system* (NAMPS), established in 1992 [1]. Each AMPS provider has 416 duplex channels (416 reverse channels and 416 forward channels). Each FM channel (reverse or forward) has a channel bandwidth of 30 kHz and a peak frequency deviation of 12 kHz. Out of 416 channels, there are 395 voice channels and 21 control channels (channels 313 to 333 for provider A and channels 334 to 354 for provider B).

As the number of mobile users increased, more channels were needed to meet the demand. NAMPS was designed to provide three times as many channels as AMPS and at the same time be backward compatible with it. An FM channel of NAMPS (reverse or forward) has a bandwidth of 10 kHz and a peak frequency deviation of 5 kHz. Thus, a provider can gradually replace an AMPS channel with three NAMPS channels to phase in a new system. The frequency spectrum of 50 MHz can accommodate 2496 duplex NAMPS channels. Both AMPS and NAMPS employ *frequency division multiple access* (FDMA) to provide duplex channels to mobiles. In FDMA, the frequency spectrum is divided into channels that occupy distinct frequency bands. Users are assigned separate channels for access to the frequency spectrum.

The first generation analog cellular system in Europe was deployed in 1985 and was named the *extended total access cellular system* (ETACS). ETACS employs a frequency spectrum of 62 MHz (917–933 MHz and 935–960 MHz for forward channels; 872–888 MHz and 890–915 MHz for reverse channels), which can accommodate 1000 full-duplex FM channels. Each FM channel (reverse or forward) has a bandwidth of 25 kHz and a peak frequency deviation of 9.5 kHz.

The *Japanese total access communication system* (JTACS) was deployed in 1988 in the 800 MHz band. JTACS provides full-duplex FM channels. Each channel has a 25 kHz

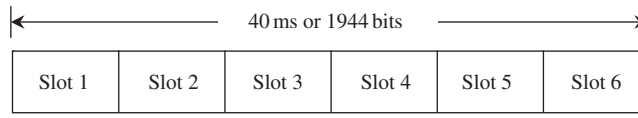

Figure 5.12 IS-136 TDMA frame.

bandwidth with a peak frequency deviation of 9.5 kHz. In 1993, Japan introduced *narrowband total access communication systems* (NTACS) to double the capacity of JTACS. An NTACS FM channel has a bandwidth of 12.5 kHz and a peak frequency deviation of 5 kHz. The total number of duplex channels is 1040. Both JTACS and ETACS employ FDMA to provide access for mobiles.

The *second generation* (2G) cellular system was digital and was developed to provide a larger capacity than the first generation systems. Two major digital standards were deployed in the United States: the *Telecommunication Industry Association/Electronic Industry Association* (TIA/EIA) *Interim Standard IS-54* [2], later became *IS-136*, also known as *US digital cellular* (USDC) in 1990, and the TIA/EIA *Interim Standard IS-95* in 1993 [3]. IS-136 operates in the same frequency spectrum as AMPS. Also, each IS-136 channel has a bandwidth of 30 kHz, but can support three mobiles using *full-rate* speech coding of 7.95 kbps or six mobiles using *half-rate* via *time division multiple access* (TDMA), as shown in Figure 5.12.

The base station or the mobile transmits a π/4-DQPSK signal, which carries data at a *TDMA burst rate* of 48.6 kbps. The π/4-DQPSK signal occupies a bandwidth of 30 kHz (one AMPS forward or reverse channel). When full-rate speech (high quality voice) is employed, the channel can accommodate three mobiles simultaneously in each TDMA frame as follows: time slots 1 and 4 for mobile 1, time slots 2 and 5 for mobile 2, and time slots 3 and 6 for mobile 3. For half-rate speech, the channel can accommodate six mobiles simultaneously with one time slot for each mobile per TDMA frame. By allowing mobiles to access the 30 kHz channel sequentially on a time division basis, IS-136 can provide *three times* the capacity of AMPS with full-rate speech or *six times* with half-rate speech. Note that a 30 kHz AMPS channel allows access to only one user. Since IS-136 employs the same frequency reuse plan as AMPS, the backward compatibility with AMPS allows providers to gradually replace one AMPS channel by three or six IS-136 channels to meet the growing demand for capacity. IS-136 can provide 2496 full duplex TDMA channels with full-rate speech or 4992 full-duplex TDMA channels with half-rate speech in a bandwidth of 50 MHz.

AMPS, NAMPS, and IS-136 employ a frequency reuse plan of seven cells per cluster. Therefore, each AMPS cell has about $416/7 \approx 59$ full-duplex channels, while an NAMPS cell can have 178 full-duplex channels and an IS-136 cell can have 178 full-duplex TDMA channels for full-rate speech or 356 full-duplex TDMA channels for half-rate speech.

In 1993, the IS-95 system was deployed as a competing digital cellular system. IS-95 employs *code division multiple access* (CDMA) to provide mobile access to a spread spectrum channel of 1.25 MHz. All mobiles in a spread spectrum channel employ distinct *quasi-orthogonal pseudo-noise* (PN) codes to separate themselves from each other and to

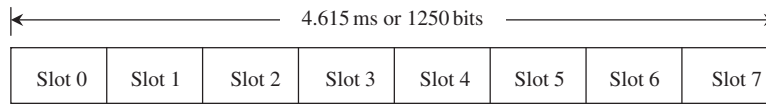

Figure 5.13 GSM TDMA frame.

reduce *multi-user interference*. There is no separation in frequency as AMPS or NAMPS using FDMA or in time as IS-136 using TDMA. IS-95 can operate in the frequency spectrum of AMPS or in the higher *personal communication system* (PCS) band (1930–1990 MHz forward channel and 1850–1910 MHz reverse channel), which will be used to deploy the *third generation* (3G) of cellular systems. An IS-95 spread spectrum channel can accommodate about 59 *half-duplex* 9.6 kbps channels. In a spectrum of 25 MHz allocated to a service provider, there are 20 IS-95 spread spectrum channels that can accommodate 700 half-duplex 9.6 kbps channels or 350 full-duplex 9.6 kbps channels. Since IS-95 employs CDMA, it does not rely on a frequency reuse plan of seven cells per cluster as AMPS, NAMPS, or IS-136. Each cell uses the same frequency spectrum of 25 MHz and, therefore, each service provider can offer 350 full-duplex channels per cell, which is about the same capacity as IS-136 with half-rate speech.

In 1990, Europe deployed the second generation (2G) cellular system, called *global system for mobile communication* (GSM) [1]. GSM is a digital system that employs TDMA to provide channel access to mobiles. The forward channel occupies the 935–960 MHz band and the reverse channel occupies the 890–915 MHz band. A 200 kHz TDMA channel has a TDMA burst rate of 270.833 kbps and can accommodate *eight* users employing GMSK as the modulation technique. Mobile users have *full-rate* speech of 13.4 kbps. The GSM TDMA frame is shown in Figure 5.13. The total number of traffic channels in a bandwidth of 25 MHz is 1000 (forward channel or reverse channel). Thus, there are 1000 full duplex channels in a 50 MHz spectrum.

The Japanese digital cellular system (JDC), which was later called the *Pacific digital cellular system* (PDC), was deployed in 1993. PDC is a TDMA system with the forward channel occupying the 940–956 MHz, 1477–1489 MHz, and 1501–1513 MHz bands, and the reverse channel occupying the 810–826 MHz, 1429–1441 MHz, and 1453–1465 MHz bands. The 20 ms TDMA frame accommodates three time slots for three users with a TDMA burst rate of 43 kbps in a channel bandwidth of 25 kHz. The modulation technique is $\pi/4$-DQPSK.

To support demands for true mobile multimedia with applications, such as full Internet access as well as mobile video teleconferencing, two *third generation* (3G) cellular systems are being deployed. The third generation systems are *wideband CDMA* (WCDMA) and *CDMA 2000* [4]. These two systems provide data rates as high as 2.4 Mbps for local-area coverage and 384 kbps for full-area coverage.

Cell connection

In a cellular system, a number of channels are designated as control channels that are employed specifically for transmission of information concerning call setup, call request,

call initiation, and other control purposes. In AMPS, there are 21 forward control channels out of 416 channels on the forward link, and the same number on the reverse link.

When a mobile initiates a call, it sends a request on the reverse control channel to the cell base station. Along with the request, the mobile submits its telephone number, called *mobile identification number* (MIN), its *electronic serial number* (ESN), and the telephone number of the called party. A *station class mark* (SCM) indicating the nominal EIRP of the mobile is also transmitted to the base station. The cell base station receives this information and passes it to the MSC, which verifies the valid MIN and ESN. The ESN of a stolen phone will be rejected by the MSC, and the call request is invalidated. The MSC instructs the cell base station to notify the mobile via the forward control channel to tune to a full-duplex voice channel. If the called party is also another mobile, the MSC then instructs all base stations to broadcast a paging message for the called mobile over all forward control channels throughout the home area. The called mobile receives the paging message from the forward control channel of the base station that it monitors, and acknowledges over the reverse control channel with its MIN, ESN, and SCM. The base station passes the data to the MSC to validate the ESN. Then, the MSC instructs the base station to notify the called mobile via the forward control channel to tune to a full-duplex channel and to ring the phone. If the called party is a landline subscriber, the connection is established by the MSC via the PSTN. The connection is similar when a landline subscriber initiates a call via the PSTN to the MSC.

When a mobile moves to another cell during a call, the MSC performs a handoff to transfer the call to a new full-duplex channel of the new cell. The handoff is initiated when the received power at the present base station falls below a prefixed threshold for a predetermined dwell time, but still above a minimum usable level. Handoff is made to a new base station once the dwell time expires and must be done before the received power at the present base station drops below the minimum usable level.

To provide services to mobiles that travel to a new coverage area, all cellular systems require roaming registration. The roaming mobile monitors a forward control channel and reports its MIN and ESN over the reverse control channel upon receiving a command issued periodically by the MSC. Unregistered mobiles are not allowed to receive or initiate calls from the new area. Billing for roaming mobiles is forwarded to the home provider.

Path loss: two-ray ground reflection model

In free space communication, where there is a single path between the transmitter and the receiver, the path loss is given by the *Friis* equation (5.45). In cellular communication, the transmitted signal arrives at the receiver via multiple paths due to reflection, diffraction, and scattering by the terrain. These multipath components are time-delayed (hence, phase-shifted) and amplitude-attenuated versions of the transmitted signal. They add vectorially at the receiver to produce a composite signal whose power is attenuated far more than is predicted by the Friis equation. Consider a simple two-ray model for path loss with ground reflection as shown in Figure 5.14.

In this simple model, the Earth is assumed to be flat and the transmitter and receiver antenna heights h_T and h_R are small compared to their separation distance d. The received electric-field wave has two components: a direct wave E_1 and a ground reflected wave E_2.

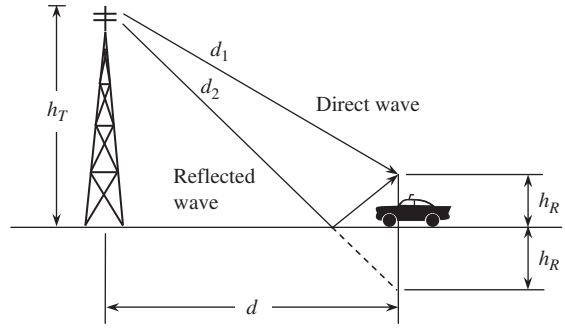

Figure 5.14 Two-ray model with ground reflection.

Let Γ be the ground reflection coefficient and θ be the relative phase shift between E_1 and E_2. Then, with phasor notation we have

$$E_2 = \Gamma E_1 e^{j\theta} \tag{5.47}$$

Thus, the received wave is given by

$$\begin{aligned} E &= E_1 + E_2 \\ &= \left(1 + \Gamma e^{j\theta}\right) E_1 \end{aligned} \tag{5.48}$$

The phase shift θ can be related to the differential distance between the direct wave distance d_1 and the ground reflected wave d_2 as

$$\theta = \frac{2\pi}{\lambda}(d_2 - d_1) \tag{5.49}$$

where λ is the signal wavelength. For the mobile environment, the phase shift θ is much smaller than one radian, and assuming perfect ground reflection, that is, $\Gamma = -1$, we obtain

$$E \approx -j\theta E_1 \tag{5.50}$$

The total receiver power P_R at the antenna output is proportional to the square of the field strength, that is,

$$\begin{aligned} P_R &= \frac{A_e}{120\pi}|E|^2 \\ &= |\theta|^2 \left(\frac{A_e}{120\pi}|E_1|^2\right) \end{aligned} \tag{5.51}$$

where A_e is the effective aperture area of the receiver antenna, and the intrinsic impedance of the free space is 120π ohms. But $(A_e/120\pi)|E_1|^2$ is simply the received power due to the direct wave and can be calculated via (5.42) and (5.45) as

$$\frac{A_e}{120\pi}|E_1|^2 = P_T G_T G_R \left(\frac{\lambda}{4\pi d_1}\right)^2 \tag{5.52}$$

where P_T is the transmitter power, G_T is the transmitter antenna gain, and G_R is the receiver antenna gain. Substituting (5.52) into (5.51) yields the received power as

$$P_R = |\theta|^2 P_T G_T G_R \left(\frac{\lambda}{4\pi d_1}\right)^2 \tag{5.53}$$

To calculate P_R in (5.53), we need to evaluate $|\theta|^2$. We note that

$$d_1 = \sqrt{(h_T - h_R)^2 + d^2} = d\sqrt{1 + \frac{(h_T - h_R)^2}{d^2}} \tag{5.54}$$

and

$$d_2 = \sqrt{(h_T + h_R)^2 + d^2} = d\sqrt{1 + \frac{(h_T + h_R)^2}{d^2}} \tag{5.55}$$

Using the fact that in a mobile environment $h_T + h_R \ll d$, we thus have $(h_T + h_R)^2/d^2 \ll 1$ and $(h_T - h_R)^2/d^2 \ll 1$. Applying the following series expansion:

$$\sqrt{1+x} = 1 + \frac{1}{2}x - \frac{1}{2\cdot 4}x^2 + \frac{1\cdot 3}{2\cdot 4\cdot 6}x^3 - \cdots, \quad -1 < x \le 1 \tag{5.56}$$

to (5.54) and (5.55) we obtain

$$d_1 = d\left[1 + \frac{1}{2}\frac{(h_T - h_R)^2}{d^2} - \cdots\right] \approx d + \frac{1}{2}\frac{(h_T - h_R)^2}{d} \tag{5.57}$$

$$d_2 = d\left[1 + \frac{1}{2}\frac{(h_T + h_R)^2}{d^2} - \cdots\right] \approx d + \frac{1}{2}\frac{(h_T + h_R)^2}{d} \tag{5.58}$$

Substituting (5.57) and (5.58) into (5.49) yields

$$\theta \approx \frac{4\pi h_T h_R}{\lambda d} \tag{5.59}$$

Combining (5.51), (5.52), and (5.59) we obtain the received power at the receiver antenna output as follows:

$$P_R \approx \frac{P_T G_T G_R h_T^2 h_R^2}{d_1^2 d^2} \approx \frac{P_T G_T G_R h_T^2 h_R^2}{d^4} \tag{5.60}$$

Thus, the path loss L_C of the two-ray model is

$$L_C \approx \frac{d^4}{h_T^2 h_R^2} \tag{5.61}$$

Note that the role of h_T and h_R in (5.61) can be interchanged. Therefore, the path loss calculation applies to both forward and reverse channels. Equations (5.60) and (5.61) show

that, at *large distance*, the received power is *inversely proportional* to the *fourth power* of *distance* for a two-ray model. The resulting path loss is much larger than the free space loss. Furthermore, it becomes (nearly) independent of the signal frequency. The two-ray model is applicable to an open area with flat ground.

Example 5.11 Two-ray model

Consider a cell in an open rural area with flat ground. The base station antenna has a height of 200 m, and the mobile antenna height is 2 m. The cell has a radius of 10 km. Assume that the received signal-to-noise ratio at the mobile station must be 25 dB for the forward link and that the system noise temperature of the mobile station receiver is 500 K. Calculate the received power at the mobile station and the required transmitted power per channel for the base station at the cell boundary assuming that the channel bandwidth is 30 kHz. Both base station and mobile employ omni-directional antennas with 0 dB gain.

Let P_R be the received power at the mobile station, then according to (5.43), we have

$$\begin{aligned} P_R &= kBT_s(SNR) \\ &= \left(1.38 \times 10^{-23}\,\text{J/K}\right)\left(30 \times 10^3\,\text{Hz}\right)(500\,\text{K})(316.23) \\ &= 6.54 \times 10^{-14}\,\text{W} \end{aligned}$$

Let G_T be the base station transmitter antenna gain and G_R be the mobile station receiver antenna gain. The base station transmitted power P_T per channel can be evaluated by (5.43) and (5.44) as follows:

$$P_T = \frac{P_R L_C}{G_T G_R} \tag{5.62}$$

where the channel path loss L_C is given in (5.61). We have

$$\begin{aligned} P_T &= \frac{(6.54 \times 10^{-14})(10^4)^4/(2^2 \times 200^2)}{(1)(1)} \\ &= 4.1 \times 10^{-3}\,\text{W} \end{aligned}$$

■

Hata model

The two-ray ground reflection model is too simple to represent propagation mechanisms in urban areas, where signals arrive at the receiver via reflection, diffraction, and scattering. Empirical formulas of the path loss for different environments have been developed. A popular model is the Hata model, which is valid from 150 MHz to 1500 MHz [5]. The median (50 percentile) path loss in urban areas is given in dB by

$$L_C(\text{urban}) = 69.55 + 26.16\log f_c - 13.82\log h_T - a(h_R) + (44.9 - 6.55\log h_T)\log d\,(\text{dB}) \tag{5.63}$$

where f_c is the carrier frequency in MHz, h_T is the effective base station antenna height in meters ($30\,\text{m} \le h_T \le 200\,\text{m}$), h_R is the effective mobile antenna height in meters ($1\,\text{m} \le h_R \le 10\,\text{m}$), d is the base station–mobile separation distance in km, and $a(h_R)$ is the correction factor for h_R and is a function of the coverage area. For a small to medium-sized city:

$$a(h_R) = (1.1\log f_c - 0.7)h_R - (1.56\log f_c - 0.8)\ \text{dB} \tag{5.64}$$

For a large city:

$$a(h_R) = 8.29(\log 1.54h_R)^2 - 1.1\,\text{dB}, \quad f \le 300\,\text{MHz} \tag{5.65}$$

$$a(h_R) = 3.2(\log 11.75h_R)^2 - 4.97\,\text{dB}, \quad f \ge 300\,\text{MHz} \tag{5.66}$$

The median path loss in suburban areas is given by

$$L_C(\text{suburban}) = L_C(\text{urban}) - 2\left[\log\left(\frac{f_c}{28}\right)\right]^2 - 5.4\,\text{dB} \tag{5.67}$$

For open rural areas, the median path loss is

$$L_C(\text{open area}) = L_C(\text{urban}) - 4.78(\log f_c)^2 + 18.33\log f_c - 40.94\,\text{dB} \tag{5.68}$$

Example 5.12 Hata model for open rural areas
Consider a cell in an open area with the following parameters:

$$h_T = 200\,\text{m}, \quad h_R = 2\,\text{m}, \quad d = 10\,\text{km}, \quad f_c = 894\,\text{MHz}$$
$$G_T = 0\,\text{dB}, \quad G_R = 0\,\text{dB}$$

Mobile station:

$$SNR = 25\,\text{dB}, \quad T_s = 500\,\text{K}, \quad B = 30\,\text{kHz}$$

Calculate the median path loss using the Hata model and the required transmitted power per channel for the base station.

From (5.66) and (5.63), we get

$$a(h_R) = 3.2[\log(11.75 \times 2)]^2 - 4.97 = 1.05\,\text{dB}$$

$$\begin{aligned} L_C(\text{urban}) &= 69.55 + 26.16\log(894) - 13.82\log(200) - 1.05 \\ &\quad + (44.9 - 6.55\log 200)\log(10) \\ &= 143.74\,\text{dB} \end{aligned}$$

Applying (5.68), we obtain the median path loss for the open area as follows:

$$\begin{aligned} L_C(\text{open area}) &= 143.74 - 4.78[\log(894)]^2 \\ &\quad + 18.33\log(894) - 40.94 \\ &= 115.26\,\text{dB} \end{aligned}$$

If we use (5.64) instead of (5.66), we get

$$\begin{aligned} a(h_R) &= [1.1\ \log(894) - 0.7](2) - [1.56\log(894) - 0.8] \\ &= 1.29\,\text{dB} \end{aligned}$$

We will use $a(h_R) = 1.05$ dB for a more conservative estimate of the path loss. Substituting $G_T = 1$, $G_R = 1$, L_C (open area) $= 3.36 \times 10^{11}$, and $P_R = 6.54 \times 10^{-14}$ W as calculated in Example 5.11 into (5.62), we obtain the transmitted power for the base station per channel as

$$P_T = \left(6.54 \times 10^{-14}\right)\left(3.36 \times 10^{11}\right) = 22 \times 10^{-3}\,\text{W}$$

■

Example 5.13 Hata model for large cities (150–1500 MHz)
Consider a cell in a large city with the following parameters:

$$h_T = 200\,\text{m}, \quad h_R = 2\,\text{m}, \quad f_c = 894\,\text{MHz}, \quad G_T = 0\,\text{dB}, \quad G_R = 0\,\text{dB}$$

Mobile station:

$$SNR = 25\,\text{dB}, \quad T_s = 500\,\text{K}, \quad B = 30\,\text{kHz}$$

Base station:

$$\text{maximum transmitted power per channel } P_T = 4\,\text{W}$$

Calculate the base station–mobile separation distance d.

Using $P_R = 6.54 \times 10^{-14}$ W as calculated in Example 5.11, $P_T = 4$ W, and $G_T = G_R = 1$ in (5.62), we obtain the corresponding median path loss as follows:

$$\begin{aligned} L_C(\text{urban}) &= \frac{P_T G_T G_R}{P_R} = \frac{4}{6.54 \times 10^{-14}} = 6.1 \times 10^{13} \\ &= 137.9\,\text{dB} \end{aligned}$$

The distance d can be evaluated using (5.63) and (5.66). We have

$$a(h_R) = 3.2[\log(11.75 \times 2)]^2 - 4.97 = 1.05\,\text{dB}$$

Also,

$$\begin{aligned} L_C(\text{urban}) &= 69.55 + 26.16\log(894) - 13.82\log(200) - 1.05 \\ &\quad + (44.9 - 6.55\log 200)\log d \\ &= 137.9\,\text{dB} \end{aligned}$$

Solving for d, we get

$$d = 6.35\,\text{km}$$

■

Modified Hata model

The Hata model has been modified for the frequency band 1500 MHz to 2000 MHz. The median path loss in dB for urban areas is given by

$$\begin{aligned} L_C(\text{urban}) = {} & 46.3 + 33.9\log f_c - 13.82\log h_T - a(h_R) \\ & + (44.9 - 6.55\log h_T)\log d + CF\,(\text{dB}) \end{aligned} \tag{5.69}$$

where $a(h_R)$ is given in (5.64)–(5.66), and the correction factor CF is

$$\begin{aligned} &CF = 3\,\text{dB for metropolitan centers} \\ &CF = 0\,\text{dB for medium-sized city and suburban areas} \end{aligned}$$

Also,

$$\begin{aligned} &1500\,\text{MHz} \le f_c \le 2000\,\text{MHz} \\ &30\,\text{m} \le h_T \le 200\,\text{m} \\ &1\,\text{m} \le h_R \le 10\,\text{m} \\ &1\,\text{km} \le d \le 20\,\text{km} \end{aligned}$$

Example 5.14 Modified Hata model for large cities (1500–2000 MHz)
Consider a cell situated in a large city with the following parameters:

$$h_T = 200\,\text{m}, \quad h_R = 2\,\text{m}, \quad f_c = 1950\,\text{MHz}, \quad G_T = 0\,\text{dB}, \quad G_R = 0\,\text{dB}$$

Mobile station:

$$SNR = 15\,\text{dB}, \quad T_s = 500\,\text{K}, \quad B = 200\,\text{kHz}$$

Base station:

$$\text{maximum transmit power per } 200\,\text{kHz channel } P_T = 4\,\text{W}$$

Calculate the base station–mobile separation distance d.

The received power P_R at the mobile station can be obtained from (5.43) as

$$\begin{aligned} P_R &= kBT_s(SNR) \\ &= \left(1.38 \times 10^{-23}\,\text{J/K}\right)\left(200 \times 10^3\,\text{Hz}\right)(500\,\text{K})(31.62) \\ &= 4.36 \times 10^{-14}\,\text{W} \end{aligned}$$

The corresponding median path loss is given by (5.62) as follows:

$$L_C(\text{urban}) = \frac{P_T G_T G_R}{P_R} = \frac{4}{4.36 \times 10^{-14}} = 0.92 \times 10^{14}$$
$$= 139.6\,\text{dB}$$

The distance d can be evaluated via (5.69) and (5.66). We have

$$a(h_R) = 1.05\,\text{dB}$$

$$L_C(\text{urban}) = 46.3 + 33.9 \log 1950 - 13.82 \log 200$$
$$- 1.05 + (44.9 - 6.55 \log 200) \log d + 3$$
$$= 139.6\,\text{dB}$$

Solving for d we get

$$d = 2.45\,\text{km}$$

■

In summary, the cellular link analysis enables us to determine the cell size given a specific signal-to-noise ratio, receiver system noise temperature, and transmitter power. In the next section, we will discuss the limitation imposed on a link by the cell architecture.

Reciprocity and the reverse link

The reciprocity principle implies that the paths traveled by a signal in the forward link are identical to the paths traveled by a signal in the reverse link provided that the antenna location, frequency, and time are identical. Thus, the path loss method employed above for the forward link also applies to the reverse link. The path loss of the reverse link is simply the path loss of the forward link with the frequency of the forward link replaced by the frequency of the reverse link.

5.3 Co-channel interference in a narrowband cellular system

A cellular coverage consists of many clusters, and each cluster has a fixed number of cells. Because of frequency reuse, co-channel cells in adjacent clusters that employ the same portion of the frequency spectrum cause interference to each other. The co-channel interference dictates the cell architecture. Let us consider a seven-cell per cluster configuration as shown in Figure 5.15.

The first-tier co-channel cells are labeled A through F and are shown as the center cells of their parent clusters. The second-tier co-channel cells are labeled AA through LL and are also the center cells in their respective clusters. The reference cell is labeled O and the mobile is shown in the worst-case location. We will analyze the co-channel interference on

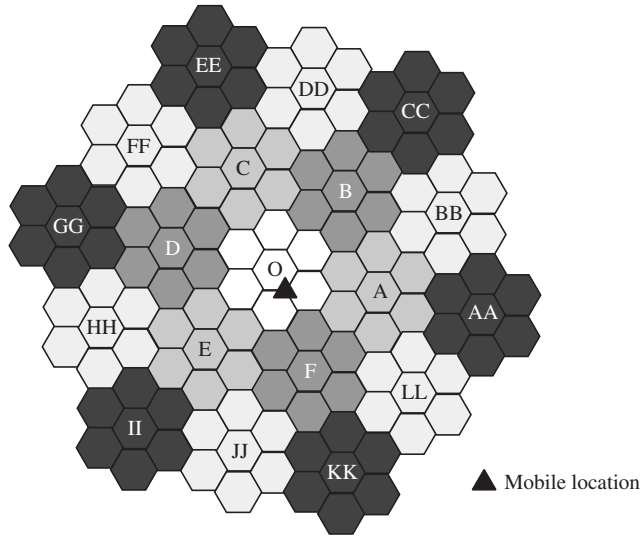

Figure 5.15 First- and second-tier co-channel cells for a seven-cell per cluster system with omni-directional antennas.

the forward link (base station-to-mobile) since this is the link that dictates the design of cellular architecture.

Consider the *forward link* from the base station at the center of the reference cell O to the mobile located at the corner of the hexagonal cell. The received signal power at the mobile is given by (5.42) as

$$P_R = \frac{P_T G_T G_R}{L_O} \tag{5.70}$$

where P_T and G_T are the transmitter power and the antenna gain of the base station O, respectively, and G_R is the mobile receiver antenna gain. The parameter L_O represents the path loss between the base station O and the mobile. Assume that all base stations have identical transmitter power and antenna gain, and all mobiles have identical receiver antenna gain. Then, the total co-channel interference power I, received by the mobile due to the first-tier base stations A, B, C, D, E, and F is

$$I = P_T G_T G_R \left(\frac{1}{L_A} + \frac{1}{L_B} + \frac{1}{L_C} + \frac{1}{L_D} + \frac{1}{L_E} + \frac{1}{L_F} \right) \tag{5.71}$$

where L_i, $i = A, B, C, D, E, F$ represents the path loss between the base station i and the mobile. The co-channel interference generated by the second-tier co-channel cells is small compared to that of the first-tier cells due to much larger path losses and can therefore be ignored.

The signal-to-interference ratio at the mobile is given by

$$SIR = \frac{P_R}{I} = \frac{L_O^{-1}}{L_A^{-1} + L_B^{-1} + L_C^{-1} + L_D^{-1} + L_E^{-1} + L_F^{-1}} \tag{5.72}$$

We know via the Friis equation that the free-space path loss is proportional to the squared distance. For non-free-space environments, we modify the Friis equation to have a channel path loss L_c as

$$L_c = \beta d^n \tag{5.73}$$

where d is the distance between the transmitter and receiver, n is the *path loss exponent*, and β is a proportionality constant that is a function of the antenna heights of both transmitter and receiver and the carrier frequency. Note that the median path loss, in dB, given by the Hata model in (5.63), (5.67)–(5.69) can be put in the dimensionless form of (5.73).

Let the cell radius R be the distance from the center of the cell to any of the six vertices of the cell. Applying (5.73) to (5.72), we obtain

$$SIR = \frac{\beta_0^{-1} R^{-n_o}}{\begin{aligned}&\beta_A^{-1}(4R)^{-n_A} + \beta_B^{-1}(5R)^{-n_B} + \beta_c^{-1}\left(\sqrt{31}R\right)^{-n_c} + \beta_D^{-1}\left(\sqrt{28}R\right)^{-n_D} \\ &+ \beta_E^{-1}\left(\sqrt{19}R\right)^{-n_E} + \beta_F^{-1}\left(\sqrt{13}R\right)^{-n_F}\end{aligned}} \tag{5.74}$$

where n_i and β_i, $i = 0, A, B, C, D, E, F$, are the path loss exponent and proportionality constant between the base station i and the mobile, respectively. If all values of n_i are identical and all values of β_i are also identical, (5.74) reduces to the following equation:

$$SIR = \frac{1}{(4)^{-n} + (5)^{-n} + \left(\sqrt{31}\right)^{-n} + \left(\sqrt{28}\right)^{-n} + \left(\sqrt{19}\right)^{-n} + \left(\sqrt{13}\right)^{-n}} \tag{5.75}$$

where n is the common path loss exponent for all seven clusters under consideration. Table 5.3 shows the signal-to-interference ratio for a seven-cell per cluster cellular system for various path loss exponents n. The result in Table 5.3 shows that the signal-to-interference ratio increases as the path loss exponent rises. This happens because the co-channel interference signals suffer more path loss in an environment with a larger path loss exponent. This explains why, in the case of free space loss with $n = 2$, the *SIR* is very low. In this situation, there are six direct line-of-sight co-channel signals that add up to a very strong interference.

From the Hata model, the path loss exponent n can be obtained from (5.63) or (5.69) as follows:

Table 5.3 Signal-to-interference ratio

Path loss exponent n	*SIR* (dB)
2	5.2
3	11.6
3.5	14.7
4	17.8
4.5	20.9
5	25

$$\begin{aligned} n &= 0.1(44.9 - 6.55\log h_T) \\ &= 4.49 - 0.655\log h_T, \quad (30\,\text{m} \le h_T \le 200\,\text{m}) \end{aligned} \tag{5.76}$$

Here h_T is the effective antenna height of the base station, and ranges from 30 m to 200 m. According to the Hata model, the path loss exponent for a cellular environment seems to fall between 3 and 3.5 depending on the antenna heights. Therefore, according to Table 5.3, the signal-to-interference ratio ranges from 11.6 dB for h_T = 200 m to 14.7 dB for h_T = 30 m. From the above results, we conclude that a higher base station antenna actually reduces the signal-to-interference ratio because of stronger co-channel interference. But, also according to the Hata model, a higher base station antenna reduces the path loss and thus increases the signal-to-noise ratio. Therefore, a compromise in the base station antenna height to achieve both the specified signal-to-interference ratio and the signal-to-noise ratio should be carried out in any design.

For the *reverse link*, *SIR* can be calculated in a similar way by considering the worst case of a mobile station located at the corner of the center cell of a seven-cell cluster. There are six interfering mobile stations from the corresponding first-tier co-channel cells. We have

$$SIR \approx \frac{1}{6(4)^{-n}} \tag{5.77}$$

For example, letting n = 4, we obtain *SIR* = 16.3 dB. This is slightly smaller than *SIR* = 17.8 dB of the forward channel.

Combined signal-to-interference and noise ratio

The effect of both co-channel interference and thermal noise must be combined to assess the performance of a cellular signal. Based upon the above analysis, we can establish the *signal-to-interference and noise ratio* as follows:

$$SINR = \frac{P_R}{I + N} \tag{5.78}$$

where P_R is the received signal power, I is the received co-channel power, and N is the received noise power. Furthermore,

$$SINR = \frac{1}{(P_R/I)^{-1} + (P_R/N)^{-1}} \tag{5.79}$$

or, equivalently,

$$SINR = \left(\frac{1}{SIR} + \frac{1}{SNR}\right)^{-1} \tag{5.80}$$

where $SIR = P_R/I$ is the signal-to-interference ratio and $SNR = P_R/N$ is the signal-to-noise ratio.

Example 5.15 Signal-to-interference and noise ratio for a seven-cell per cluster system
Consider a system in a large city that employs a frequency reuse plan of seven-cells per cluster. The system has the following parameters:

$$h_R = 2\,\text{m}, \quad f_c = 894\,\text{MHz}, \quad G_T = 0\,\text{dB}, \quad G_R = 0\,\text{dB}, \quad B = 30\,\text{kHz}, \quad d = 6.35\,\text{km}$$

Base station:

$$\text{transmitted power per channel} = 4\,\text{W}$$

Mobile:

$$\text{system noise temperature} = 500\,\text{K}$$

Calculate the signal-to-interference and noise ratio in (5.80) using the Hata model for large cities for two base station antenna heights $h_T = 200\,\text{m}$ and $100\,\text{m}$.

(a) $h_T = 200\,\text{m}$

Using (5.63) and (5.66) we have the following path loss:

$$\begin{aligned} L_C(\text{urban}) &= 69.55 + 26.16\log 894 - 13.82\log 200 - 1.05 \\ &\quad + (44.9 - 6.55\log 200)\log 6.35 = 137.9\,\text{dB} \end{aligned}$$

The received power at the mobile is given by

$$P_R = \frac{P_T G_T G_R}{L_C(\text{urban})} = \frac{(4)(1)(1)}{10^{13.79}} = 6.54 \times 10^{-14}\,\text{W}$$

From (5.43), we obtain the signal-to-noise ratio as

$$SNR = \frac{P_R}{kTB} = \frac{6.54 \times 10^{-14}\,\text{W}}{(1.38 \times 10^{-23}\,\text{J/K})(500\,\text{K})(30 \times 10^3\,\text{Hz})} = 316 = 25\,\text{dB}$$

From (5.76), the path loss exponent is $n = 3$. Using Table 5.3, the signal-to-interference ratio SIR for $h_T = 200\,\text{m}$ is $11.6\,\text{dB}$. Applying (5.80), we obtain the *signal-to-interference and noise ratio* as

$$SINR = \left(\frac{1}{10^{1.16}} + \frac{1}{10^{2.5}}\right)^{-1} = 13.76 = 11.4\,\text{dB}$$

The above result shows that $SINR \approx SIR$, that is, the link is interference-limited, and thermal noise has negligible effect.

(b) $h_T = 100\,\text{m}$

Again, using (5.63) and (5.66), we get the following path loss:

$$\begin{aligned} L_C(\text{urban}) &= 69.55 + 26.16\log 894 - 13.82\log 100 - 1.05 \\ &\quad + (44.9 - 6.55\log 100)\log(6.35) = 143.6\,\text{dB} \end{aligned}$$

Thus, the received power at the mobile is given by

$$P_R = \frac{P_T G_T G_R}{L_C(\text{urban})} = \frac{(4)(1)(1)}{10^{14.36}} = 1.75 \times 10^{-14}\,\text{W}$$

Again, from (5.43), we obtain the signal-to-noise ratio as follows

$$SNR = \frac{P_R}{kT_sB} = \frac{1.75 \times 10^{-14}\,\text{W}}{(1.38 \times 10^{-23}\,\text{J/K})(500\,\text{K})(30 \times 10^3\,\text{Hz})} = 84.35$$
$$= 19.3\,\text{dB}$$

From (5.76), the path loss exponent is $n = 3.18$. Substituting $n = 3.18$ into (5.75), we have $SIR = 18.65 = 12.7$ dB. Using (5.80) we obtain the *signal-to-interference and noise ratio* as follows:

$$SINR = \left(\frac{1}{18.65} + \frac{1}{84.35}\right)^{-1} = 15.27 = 11.84\,\text{dB}$$

■

The above results show that in a cellular environment, taller base station antennas do not necessarily provide a better signal-to-interference and noise ratio. For narrowband cellular systems, fairly good voice quality can be provided with a signal-to-interference and noise ratio of about 14 dB. This requirement cannot be met with a cell radius $R = 6.67$ km, at least from the worst-case point of view. One could use lower base station antenna heights to reduce the co-channel interference, that is, to increase *SIR*; for example, $h_T = 30$ m would yield $SIR = 14.7$ dB. Also, to increase *SNR*, the radius of the cell should be made smaller. From Example 5.15, a cell radius $R = 3$ km would yield a worst-case path loss for a mobile at a distance $d = R = 3$ km to be L_C (urban) = 141.5.1 dB for $h_T = 30$ m and a corresponding $SNR = 21.34$ dB. This would yield a signal-to-interference and noise ratio $SINR = 13.85$ dB, which meets the worst-case performance. This method increases the number of clusters per coverage area, and hence provides a larger capacity at the expense of more base stations. Another option is to increase the number of cells per cluster to reduce *SIR* while keeping the cell radius fixed. This method reduces the number of clusters per coverage area and hence decreases the system capacity.

Sectoring

Another popular method to reduce co-channel interference is sectoring. Sectoring is the replacement of the base station omni-directional antenna with several directional antennas, each transmitting to a certain sector of the cell. Sectoring patterns are normally implemented with three 120° antennas or six 60° antennas. In sectoring, the total number of channels per cell is divided equally among sectors. Thus, an idle channel in one sector cannot be assigned to a mobile in another sector of the same cell, hence sectoring increases the call blocking probability. Note that, in a conventional system, an idle channel in a cell can be assigned to any mobile in that cell. Therefore, sectoring reduces the capacity of a cellular system since

Table 5.4 *SIR* for 120°-sectoring

Path loss exponent n	*SIR* (dB)
2	8.7
3	15.3
3.5	18.6
4	21.8
4.5	25.1
5	28.3

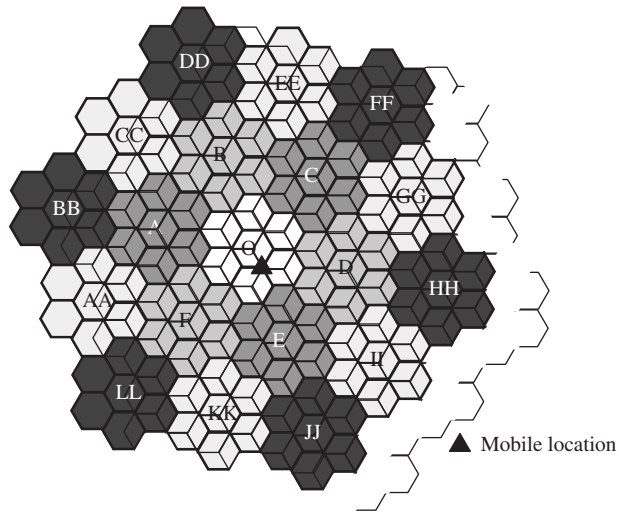

Figure 5.16 First- and second-tier co-channel cells for a seven-cell per cluster system and 120° sectoring.

the channels in a cell cannot be pooled together and assigned to mobiles on demand. This trunking efficiency reduction increases with the number of sectors per cell. Another disadvantage of sectoring is the frequent handoffs when a mobile moves from one sector to another sector. Modern base stations are normally equipped to handle sectoring handoffs without requiring the assistance of the MSC, and therefore this is not a major concern.

Let us consider first the *forward link*. Figure 5.16 shows a seven-cell per cluster system with 120°-sectoring. The worst-case mobile location is at the right-hand lower corner of cell O. The mobile is interfered by the three left-looking sectors of cells B, C, and D. The signal-to-interference ratio can be calculated as

$$SIR = \frac{1}{5^{-n} + \left(\sqrt{31}\right)^{-n} + 4^{-n}} \tag{5.81}$$

Table 5.4 tabulates the signal-to-interference ratio for various path loss exponents. A look at Table 5.4 reveals that *SIR*s improve by almost 4 dB for n in the range of 3 to 3.5.

For 60°-sectoring the signal-to-interference ratio is given by the following expression:

$$SIR = \frac{1}{5^{-n} + \left(\sqrt{31}\right)^{-n}} \tag{5.82}$$

Example 5.16 Signal-to-interference and noise ratio for a seven-cell per cluster system with 120°-sectoring

Consider the system in Example 5.15 with base station antenna height $h_T = 100$ m. The path loss exponent obtained from the Hata model is $n = 3.18$, which yields $SIR = 16.5$ dB. For a hexagon cell with radius $R = 6.67$ km, the worst case mobile location $d = R = 6.67$ km yields a $SNR = 19.2$ dB assuming the same antenna gain. The combined signal-to-interference and noise ratio is $SINR = 14.6$ dB as compared to 11.82 dB in the no-sectoring case. In practice, the sectoring antenna gain is larger than the omni-directional antenna gain and $SINR$ could be better. For example, if $G_T = 2$, then $SNR = 22.2$ dB and $SINR = 15.5$ dB.

■

For the *reverse link*, with the mobile station at the corner of the cell, the signal-to-interference ratio for the 120°-sectoring is given by

$$SIR = \frac{1}{5^{-n} + \left(\sqrt{19}\right)^{-n} + 4^{-n}} \tag{5.83}$$

For 60°-sectoring we have

$$SIR = \frac{1}{5^{-n} + \left(\sqrt{19}\right)^{-n}} \tag{5.84}$$

Microcell-zoning

Sectoring requires the allocation of a fixed set of channels to each sector. Thus, when the mobile moves from one sector to another sector in the same cell, handoff must be performed to a new channel in the new sector. Microcell-zoning, as illustrated in Figure 5.17, can be used to avoid too many handoffs in the same cell. The cell is divided into three micro-zones

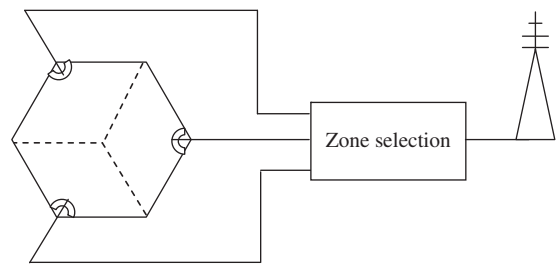

Figure 5.17 Microcell-zoning with three micro-zones.

with directional antennas aiming toward the center of the cell. The three antennas are connected via terrestrial lines to a zone-selection switch, which in turn is connected to the base station of the cell. The mobile station signal is received by all three zone antennas, and the switch selects the strongest signal. The base station communicates with the mobile via the corresponding zone antenna that produces the strongest signal. In this manner, the mobile station can move all over the cell without handoffs. For a seven-cell per cluster system, the signal-to-interference ratio for the forward link assuming the mobile station is at the zone center is given by the following expression:

$$SIR = \frac{1}{\left(\sqrt{112}\right)^{-n}+\left(\sqrt{109}\right)^{-n}+\left(\sqrt{103}\right)^{-n}+\left(\sqrt{64}\right)^{-n}+\left(\sqrt{79}\right)^{-n}+\left(\sqrt{91}\right)^{-n}} \tag{5.85}$$

5.4 CDMA cellular link analysis

CDMA cellular systems such as IS-95, CDMA 2000, and WCDMA are markedly different from narrowband cellular systems, such as IS-136 and GSM. Therefore, the previous link analysis does not apply to these wideband systems, especially from the co-channel interference point of view on both forward and reverse links, and from the point of view of multi-user interference (MUI) on the reverse link. In a CDMA cellular system, a cell uses the entire frequency spectrum. No frequency plan is necessary as in a narrowband system to coordinate the allocation of channels for cells in a cluster (each provider has a frequency spectrum of 416 30 kHz channels in the US cellular band, 59 channels for each cell in a seven-cells-per-cluster frequency reuse). The most important part of CDMA link analysis is the assessment of co-channel interference for both forward and reverse links. As in the narrowband case, we start first with the *forward link*.

Forward link

Consider seven hexagonal cells in Figure 5.18 arranged with the interested cell at the center surrounded by six adjacent co-channel cells. The base stations have *omni-directional* antennas and are located at cell centers. The worst case *signal-to-interference ratio* occurs

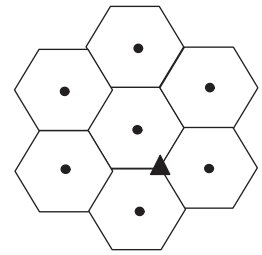

Figure 5.18 CDMA cells with base stations at cell centers and omni-directional antennas.

when the mobile station is located at the corner of the cell boundary. We make use of the results derived for CDMA in Chapter 8 for the following link analysis. The *spread factor* of the *orthogonal covering* forward channel is denoted as N. To be modulation-independent and PN sequence-independent, we use a conservative approach by accepting the interference power in the despread signal bandwidth as P_I/N, where P_I is the power of the interference signal. Assuming each base station transmits the *same power* and their forward links contain identical number of user channels, K, where $K \leq N$, we obtain the following worst case *despread* ***input*** *signal-to-interference ratio*:

$$SIR = \frac{N/\chi K}{2\left(\sqrt{7}\right)^{-n} + 2(2)^{-n} + 2} \tag{5.86}$$

where n is the path loss exponent (assuming to be identical for all cells), and χ is the voice activity factor or data duty cycle. The *despread* ***input*** *signal-to-interference-and-noise ratio* is $SINR = \left[(SIR)^{-1} + (SNR)^{-1}\right]^{-1}$.

Example 5.17 Modified Hata model for large cities

Consider a CDMA cell situated in a large city with the following parameters:

$$h_T = 200\,\text{m},\ \ h_R = 2\,\text{m},\ \ f_c = 1950\,\text{MHz},\ \ G_T = 0\,\text{dB},\ \ G_R = 0\,\text{dB},$$
$$B_{CDMA} = 1250\,\text{kHz},\ \ N = 64$$

Mobile station:

$$SNR = 15\,\text{dB},\ T_s = 500\,\text{K}$$

Base station:

$$\text{maximum transmit power per user channel } P_T = 4\,\text{W}$$

Calculate the base station to mobile separation distance d.

The despread information signal at the mobile station has a bandwidth equal to $B = B_{CDMA}/N = 1250\,\text{kHz}/64 = 19.53\,\text{kHz}$. The received power P_R at the mobile station is given by

$$\begin{aligned} P_R &= kBT_s(SNR) \\ &= \left(1.38 \times 10^{-23}\,\text{J/K}\right)\left(19.53 \times 10^{3}\,\text{Hz}\right)(500\,\text{K})(31.62) \\ &= 4.26 \times 10^{-15}\,\text{W} \end{aligned}$$

The corresponding median path loss is given as follows:

$$\begin{aligned} L_C(\text{urban}) &= \frac{P_T G_T G_R}{P_R} = \frac{4}{4.26 \times 10^{-15}} = 9.4 \times 10^{14} \\ &= 149.7\,\text{dB} \end{aligned}$$

The distance d can be evaluated via the modified Hata model. We have

$$a(h_R) = 1.05\,\text{dB}$$

$$\begin{aligned} L_C(\text{urban}) &= 46.3 + 33.9\log 1950 - 13.82\log 200 \\ &\quad - 1.05 + (44.9 - 6.55\log 200)\log d + 3 \\ &= 149.7\,\text{dB} \end{aligned}$$

Solving for d we get $d = 5.35$ km.

Now consider the co-channel interference for this forward link. Let us assume that the path loss exponent $n = 4$, the voice activity factor $\chi = 0.4$, and a required despread ***input*** signal-to-interference ratio $SIR = 7$ dB. Then, the number of transmitted user channels per base station is $K = 15$. This is the *maximum* number of user channels plus overhead channels (pilot channel for example) that the forward link can carry at any instant of time. It is smaller than the total number of user channels, which is 64 for IS-95. Using the ***input*** signal-to-noise ratio $SNR = 15$ dB, we get $SINR = 6.4$ dB.

■

In narrowband cellular systems, sectoring is employed to reduce the co-channel interference in order to improve link reliability. The allocated channels in a sector cannot be used in other sectors since the frequency plan is fixed. On the other hand, CDMA cellular systems operate with the entire allocated frequency spectrum for each cell. Therefore, a CDMA forward link is used for the entire cell irrespective of the sectors. This is called sector frequency reuse and it increases the cell capacity by the number of sectors. Thus, a mobile station, at the cell corner as shown in Figure 5.19, experiences all six CCI forward links with the same frequency. Hence, the *SINR* of sectoring CDMA remains the same as in the case of no sectoring, as is the number of user channels per sector. But the number of total user channels is now $3K$ for 120°-sectoring and $6K$ for 60°-sectoring. From Example 5.17, the maximum number of user channels that can be accommodated by a forward link is 45 with 120°-sectoring, and 64 with 60°-sectoring. For the US cellular band, the allocated frequency spectrum for the forward channel is 12.5 MHz, which accommodates *ten* 1.25 MHz-CDMA carriers. Thus, a CDMA cell can have $10K$ user channels for no sectoring, $30K$ user channels for 120°-sectoring, and max[$60K$, $10N$] user channels for 60°-sectoring.

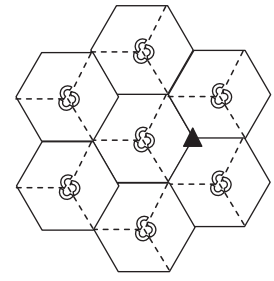

Figure 5.19 CDMA cells with base stations at cell centers and 120°-sectoring antennas.

Reverse link

The reverse link of a CDMA cellular system is a multiple access channel with mobile stations in the cell asynchronously transmitting to the base station using the same carrier frequency but with different PN sequences. The user rates may be identical or they may be different (integer multiple of the basic rate). With power control, all mobile station signals arrive at the base station with the same power. Both MUI and CCI must be accounted for. The despread ***input*** signal-to-interference-and-noise ratio *SINR* of the user channel consists of the despread ***input*** signal-to-MUI ratio, the despread ***input*** signal-to-CCI ratio, and the despread ***input*** signal-to-noise ratio. Therefore, we have $SINR = \left[(SIR)_{MUI}^{-1} + (SIR)_{CCI}^{-1} + (SNR)^{-1}\right]^{-1}$. With power control we have $(SIR)_{MUI} = N/\chi K$, where K is the number of multi-access users and χ is the voice activity factor or data duty cycle. The CCI depends on the distribution of mobile stations in the adjacent cells. In each adjacent cell, only a small fraction of interfering mobile stations, which are closer to the base station in the center cell, contributes to CCI. For example, assuming hexagonal cells and a path loss exponent $n = 4$, the interfering mobile station signals at the distance of 1.5 times the cell radius from the receiving base station in the center cell are attenuated by 7 dB. If the distance is increased to twice the cell radius, the attenuation is 12 dB. Thus, for no sectoring, it is reasonable to model the CCI of all *six adjacent cells* by $(SIR)_{CCI} = \eta N/\chi K$, where η is a factor that reflects the real world situation. For 120°-sectoring, only *two adjacent cells* facing the intended sector contribute to CCI, hence, we have $(SIR)_{CCI}^{120^\circ} = 3\eta N/\chi K$. The number of simultaneous users per sector is K; the number of simultaneous users for a 120°-sectoring cell is $3K$ per CDMA carrier. For 60°-sectoring, only *one adjacent cell* facing the intended sector contributes to CCI; hence, we have $(SIR)_{CCI}^{60^\circ} = 6\eta N/\chi K$. The number of simultaneous users per sector is K; the number of simultaneous users for a 60°-sectoring cell is $6K$ per CDMA carrier. For the US cellular band, the allocated frequency spectrum for the reverse channel is 12.5 MHz, which accommodates *ten* 1.25 MHz-CDMA carriers. Thus, a CDMA cell can have $10K$ user channels for no sectoring, $30K$ user channels for 120°-sectoring, and max[$60K$, $10N$] user channels for 60°-sectoring.

Example 5.18 *SINR* of 1.25 MHz reverse link

Consider the non-sectoring case and let *SINR* = 6.4 dB, $N = 64$, $K = 15$ users, $\chi = 0.4$, and *SNR* = 15 dB. We have $(SIR)_{MUI} = N/\chi K = 10.67$ (10.3 dB), and consequently, the required despread ***input*** signal-to-CCI ratio is $(SIR)_{CCI} = \eta N/\chi K = 9.6$ (9.8 dB). This implies that $\eta = 0.9$ and the CCI power is $1/\eta$ (111%) of the MUI power. The total number of simultaneous users for the cell is 150 assuming the allocated frequency spectrum is 12.5 MHz.

Now consider the case of 120°-sectoring with the same *SNR* = 15 dB as in the non-sectoring case and set $(SIR)_{MUI}^{120^\circ} = N/\chi K$ for $K = 15$ simultaneous user per sector, we have $(SIR)_{MUI}^{120^\circ} = 10.67$ (10.3 dB). Furthermore, set $(SIR)_{CCI}^{120^\circ} = 3\eta N/\chi K = 28.8$ (14.6 dB) with $\eta = 0.9$. Thus, *SINR* = 7.9 (9 dB) as compared to 6.4 dB for the non-sectoring case.

This is possible because the CCI power is greatly reduced. The number of users per CDMA carrier is 45 or 450 for the entire cell. For 60°-sectoring, the number of users per CDMA carrier is 64 or 640 for the entire cell.

■

5.5 Satellite communication link

One major invention of the twentieth century is the communication satellite, and most of them are placed in the *geostationary orbit* (GEO). This is an equatorial orbit with a radius of 42 164 km and an altitude of 35 786 km. The orbital period is the same as the Earth; therefore, a GEO satellite appears to be stationary to an observer on Earth. Thus, an Earth station can communicate with a GEO satellite by simply pointing the antenna toward the satellite location specified by the satellite longitude. Two angles are used to determine the pointing direction of the antenna: the *azimuth angle A* and the *elevation angle E* [5].

The azimuth angle A is given by:

1. Northern hemisphere:
   Earth station west of satellite: $A = 180^\circ - A'$
   Earth station east of satellite: $A = 180^\circ + A'$
2. Southern hemisphere:
   Earth station west of satellite: $A = A'$
   Earth station east of satellite: $A = 360^\circ - A'$

where A' is evaluated according to the following expression:

$$A' = \tan^{-1}\left(\frac{\tan|\theta_S - \theta_L|}{\sin\theta_\ell}\right) \tag{5.87}$$

Here θ_S is the GEO satellite longitude, and θ_L and θ_ℓ are the Earth station longitude and latitude, respectively.

The elevation angle E can be calculated as follows:

$$E = \tan^{-1}\left(\frac{r - R_e\cos\theta_\ell\cos|\theta_S - \theta_L|}{R_e\sin[\cos^{-1}(\cos\theta_\ell\cos|\theta_S - \theta_L|)]}\right) - \cos^{-1}(\cos\theta_\ell\cos|\theta_S - \theta_L|) \tag{5.88}$$

where $r = 42\,164$ km and $R_e = 6378$ km is the Earth radius.

The distance between the Earth station and the GEO satellite, called the slant range, is given by

$$d = \sqrt{r^2 + R_e^2 - 2R_e r\sin\left[E + \sin^{-1}\left(\frac{R_e}{r}\cos E\right)\right]} \tag{5.89}$$

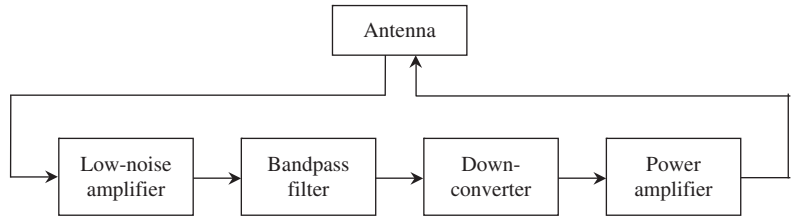

Figure 5.20 Repeater transponder.

The satellite path loss is given by the Friis equation

$$L_C = \left(\frac{4\pi d}{\lambda}\right)^2 \tag{5.90}$$

where $\lambda = c/f$ is the signal wavelength, $c = 3 \times 10^8$ m/s is the speed of light, and f is the carrier frequency.

Commercial GEO satellites operate mainly in the C-band (uplink: 6 GHz, downlink: 4 GHz) and the Ku-band (uplink: 14 GHz, downlink: 12 GHz). In each band, the higher frequency is used for the uplink (Earth station to satellite) and the lower frequency is used for the downlink (satellite to Earth station). The available bandwidth for the uplink or downlink of each band is about 500 MHz. A GEO satellite carries many transponders. Each transponder consists of a transreceiver that receives the uplink signal (6 or 14 GHz) in a particular bandwidth, then downconverts it to the downlink frequency (4 or 12 GHz), amplifies the signal and retransmits it back to Earth. This type of transponder is called a repeater and is shown schematically in Figure 5.20.

Example 5.19 Azimuth angle, elevation angle, and slant range

Consider an Earth station located at longitude $\theta_L = 80°$ W and latitude $\theta_\ell = 40°$ N, and a GEO satellite at longitude $\theta_S = 120°$ W. Evaluate the azimuth and elevation angles, and the slant range.

Because the Earth station is located in the Northern Hemisphere and east of the satellite, the azimuth angle is given by

$$A = 180° + A' = 180° + 52.5° = 232.5°$$

From (5.88), the elevation angle is

$$E = 28.3°$$

The slant range can be evaluated via (5.89) as

$$d = 38\,764.6 \text{ km}$$

■

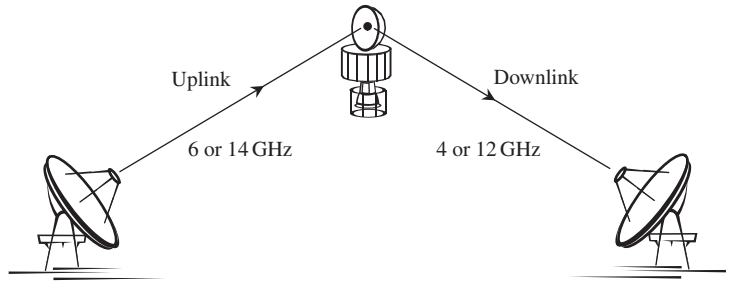

Figure 5.21 Satellite link.

A satellite link consists of both uplink and downlink, as shown in Figure 5.21. The uplink signal power at the satellite receiver input is

$$P_u = \frac{P_T G_T G_S}{L_u} \tag{5.91}$$

where:

P_T = transmitter power of the uplink Earth station
G_T = antenna gain of uplink Earth station
G_S = antenna gain of satellite receiver
L_u = uplink path loss

The noise power in the satellite receiver is

$$N_u = kT_{sat}B \tag{5.92}$$

where T_{sat} is the *satellite system noise temperature*, B is the *channel bandwidth*, and k is *Boltzmann constant*.

The Earth station on the downlink receives the satellite signal and accompanied noise with respective powers

$$P_d = \frac{P_u G G_R}{L_d} \tag{5.93}$$

$$N = \frac{N_u G G_R}{L_d} \tag{5.94}$$

where:

G = total transponder gain, which includes satellite transmit antenna gain
G_R = antenna gain of downlink Earth station
L_d = downlink path loss

The noise power in the downlink Earth station receiver is

$$N_d = kT_s B \tag{5.95}$$

Here T_s is the downlink Earth station's *system noise temperature*. The combined signal-to-noise ratio at the input of the downlink Earth station's receiver is given by

$$SNR = \frac{P_d}{N + N_d} = \frac{1}{\left(\frac{P_d}{N}\right)^{-1} + \left(\frac{P_d}{N_d}\right)^{-1}} = \frac{1}{\left(\frac{P_u}{N_u}\right)^{-1} + \left(\frac{P_d}{N_d}\right)^{-1}} = \frac{1}{\left(SNR_u^{-1}\right) + \left(SNR_d^{-1}\right)} \quad (5.96)$$

The ratio $SNR_u = P_u/N_u$ is the *uplink signal-to-noise ratio* and the ratio $SNR_d = P_d/N_d$ is the *downlink signal-to-noise ratio*. They are given by

$$SNR_u = \frac{P_u}{N_u} = \frac{P_T G_T G_S}{L_u k T_{sat} B} = \frac{(EIRP) G_S}{L_u k T_{sat} B} \quad (5.97)$$

and

$$SNR_d = \frac{P_d}{N_d} = \frac{P_u G G_R}{L_d k T_s B} = \frac{(EIRP_S) G_R}{L_d k T_s B} \quad (5.98)$$

The quantities $EIRP = P_T G_T$ and $EIRP_S = P_u G$ are called the *effective isotropic radiated powers* of the uplink Earth station and satellite, respectively. The quantities G_S/T_{sat} and G_R/T_s are called the *antenna gain-to-noise temperature ratios* of the satellite and downlink Earth station, respectively.

Example 5.20 Ku-band satellite link

Uplink frequency: 14 GHz	Downlink frequency: 12 GHz
Bandwidth $B = 36$ MHz $= 75.6$ dB-Hz	$EIRP = 10^8$ W $= 80$ dBW
$EIRP_S = 10^{4.4}$ W $= 44$ dBW	$G_S/T_{sat} = 1.6$ dB/K
$G_R/T_s = 34.3$ dB/K	$k = 1.38 \times 10^{-23}$ J/K $= -228.6$ dBW/K-Hz
Uplink slant range = 37 506 km	Downlink slant range = 37 506 km
Uplink path loss = 206.9 dB	Downlink path loss = 205.5 dB

Applying (5.96) and (5.97) in dB forms, we obtain

$$\begin{aligned} SNR_u(\text{dB}) &= \left(\frac{P_u}{N_u}\right)_{\text{dB}} = 80\,\text{dBW} + 1.6\,\text{dB/K} - 206.9\,\text{dB} \\ &\quad + 228.6\,\text{dBW/K-Hz} - 75.6\,\text{dB-Hz} \\ &= 27.7\,\text{dB} \\ SNR_d(\text{dB}) &= \left(\frac{P_d}{N_d}\right)_{\text{dB}} = 44\,\text{dBW} + 34.3\,\text{dB/K} - 205.5\,\text{dB} \\ &\quad + 228.6\,\text{dBW/K-Hz} - 75.6\,\text{dB-Hz} \\ &= 25.8\,\text{dB} \end{aligned}$$

Using (5.95), we obtain the combined signal-to-noise ratio for the satellite link as

$$\begin{aligned} SNR &= \frac{1}{10^{-2.77} + 10^{-2.58}} = 231 \\ &= 23.6\,\text{dB} \end{aligned}$$

■

5.6 Summary

In this chapter we have provided a detailed study of wireless communication links in free space and in cellular environments. The purpose of a link analysis is to find the *system signal-to-noise ratio* at the receiver.

The noise power is determined by the receiver *system noise temperature*, which is a function of the *antenna noise temperature* and the *effective noise temperatures* of various subsystems in the receiver, such as the low-noise amplifier, the downconverter, and the demodulator. We have shown that if the gain of the low-noise amplifier is large, then the noise contribution of the rest of the receiver can be made negligible.

The signal power in free space is a function of the path loss and can be evaluated by the Friis equation. We have also shown that the system signal-to-noise ratio is invariant with respect to the reference inputs at the receiver.

We have introduced the concept of *frequency reuse* in cellular communications. Each coverage area is divided into *clusters*; each cluster has a fixed number of *cells*. Each cell in a cluster employs a separate portion of the frequency spectrum to avoid inter-cell interference. Each cluster reuses the same frequency spectrum. If the number of cells per cluster is large, the *co-channel* interference between co-channel cells in adjacent clusters can be kept low.

A review of major cellular standards, such as AMPS, NAMPS, IS-136, IS-95, and GSM, was provided together with a discussion of call connection and handoff.

The study of the *two-ray ground reflection* path loss model in a cellular environment has shown that the path loss is proportional to the *fourth power* of the distance as compared to the *square* of the distance in free space loss.

The well-known empirical *Hata model* was introduced. This model can calculate the median path loss in small, medium-sized, and large cities as well as suburban and rural areas. The model covers the 150–2000 MHz frequency band. The Hata model was employed in the cellular link analysis, for example, to determine the cell size given a specified signal-to-noise ratio, receiver system noise temperature, and transmitter power.

The co-channel interference imposed on a cellular link was shown to be architecture-specific. Practical narrowband cellular systems, such as AMPS, GSM, and IS-136, normally employ seven cells per cluster. The *signal-to-interference ratio* for the worst-case mobile location was presented. Wideband cellular systems, such as IS-95, CDMA 2000, and WCDMA, employ one cell per cluster and rely on spread spectrum processing gain to reduce the interference effect.

The *link analysis* and *co-channel interference analysis* were then integrated to calculate the *combined signal-to-interference and noise ratio*. In order to reduce the co-channel interference and improve performance, cellular systems normally use *sectoring* at the base station. Sectoring patterns are commonly implemented with three 120°-sectoring antennas or six 60°-sectoring antennas.

Finally, the communication link for a geostationary *satellite* was studied. The *azimuth* and *elevation* angles are needed to point the Earth station antenna toward the satellite for both uplink transmission and downlink reception. The *slant range* between an Earth station and a geostationary satellite was shown to be a function of the elevation angle. The satellite path loss can be calculated via the Friis equation. The uplink and downlink signal-to-noise ratios were combined to form the total link signal-to-noise ratio.

Problems

1. Consider an Earth station receiver that can be modeled as a series connection of an antenna, a waveguide, a low-noise amplifier, a downconverter, and a demodulator. Find the system noise temperature at the input of the low-noise amplifier using the following parameters: waveguide loss = 0.1 dB, $G_{LNA} = 55$ dB, $T_{LNA} = 40$ K. The combined effective noise temperature of both downconverter and demodulator is 213 600 K. The ambient temperature is $T_0 = 290$ K. The antenna noise temperature contributors are: main beam: 25.6 K; sub-reflector spillover: 3.3 K; main-reflector spillover: 0.7 K; blockage: 9.8 K; surface tolerance: 1.5 K; and feed loss: 13.9 K.
2. Consider a noisy two-port network with gain $G = 50$ dB and bandwidth $B = 500$ MHz. The input of the two-port network is a noise signal with power spectral density 3×10^{-22} W/Hz and a signal with power P_i. Find the available noise power delivered to the network. The two-port has an effective noise temperature of 200 K. Find the system noise temperature, and the available output noise power. It is required that the system signal-to-noise ratio be at least 20 dB. What is the minimum received signal power P_i?
3. A communication system has the following parameters:

$$P_T = 10\,\text{W},\ G_T = 2\,\text{dB},\ L_C = 150\,\text{dB},\ G_R = 1\,\text{dB},\ T_A = 250\,\text{K},$$
$$G_{LNA} = 30\,\text{dB},\ T_{LNA} = 200\,\text{K},\ G_{DC} = 30\,\text{dB},\ T_{DC} = 10^4\,\text{K},$$
$$T_{DEM} = 10^4\,\text{K},\ B = 40\,\text{KHz}$$

   (a) Calculate the signal power at the demodulator input.
   (b) Calculate the system noise temperature at the demodulator input.
   (c) Calculate *SNR* of the receiver.
4. Consider a series connection of a low-noise amplifier, a downconverter, and a demodulator. Use the following specifications to calculate the effective noise temperature T_e of the series connection: $G_1 = 40$ dB, $T_{e1} = 120$ K, $G_2 = 30$ dB, $T_{e2} = 7 \times 10^4$ K, $T_{e3} = 2 \times 10^5$ K. If $G_1 = 50$ dB, evaluate the impact on T_e.
5. Consider a cascade two-port network, which is a series connection of a low-noise amplifier (LNA), a downconverter (DC), and a demodulator (DM), with the following specifications:

$$G_{LNA}, T_{LNA} = 200\,\text{K};\ G_{DC} = 20\,\text{dB}, T_{DC} = 2 \times 10^4\,\text{K}; T_{DM} = 2 \times 10^5\,\text{K}$$

   The input of the cascade two-port network is connected to a noise source with available power spectral density 10^{-21} W/Hz. The signal power at the input of the two-port is 3×10^{-11} W. The bandwidth of the two-port is $B = 500$ MHz.
   (a) Calculate the temperature T_n of the noise source.
   (b) Calculate the available noise power delivered by the noise source to the two-port.
   (c) Calculate the required minimum gain G_{LNA} of the LNA, so that the *system signal-to-noise ratio* at the input of the two-port (which is also the input of the LNA) is at least 10 dB.

6. Show that the median path loss, in dB, given by the Hata model in (5.63), (5.67)–(5.69) can be put into the dimensionless form of (5.73) with the path loss exponent given by (5.76).
7. Consider a cell in an open rural area. The base station antenna has a height of 200 m, and the mobile antenna height is 2 m. The base station antenna gain is 3 dB and the mobile employs an omni-directional antenna with 0 dB gain. A forward channel has a bandwidth of 200 kHz. The cell has a radius of 10 km. Assume that the received signal-to-noise ratio at the mobile station must be at least 15 dB for the forward link and that the system noise temperature of the mobile station receiver is 700 K. Calculate the received power at the mobile station and the required transmitted power for 60 channels at the base station assuming all mobiles are located at the cell boundary. Use the two-ray ground reflection model for open rural areas.
8. Consider a cell in an open rural area. The base station antenna has a height of 200 m, and the mobile antenna height is 2 m. The base station antenna gain is 3 dB and the mobile employs an omni-directional antenna with 0 dB gain. A forward channel has a bandwidth of 200 kHz. The cell has a radius of 10 km. Assume that the received signal-to-noise ratio at the mobile station must be at least 15 dB for the forward link and that the system noise temperature of the mobile station receiver is 700 K. Calculate the received power at the mobile station and the required transmitted power for 60 channels at the base station assuming all mobiles are located at the cell boundary. Assume that the nominal carrier frequency is 894 MHz. Use the Hata model for open rural areas.
9. Consider a cell in a large city that is allocated 60 GSM channels. The base station antenna has a height of 200 m, and the mobile antenna height is 2 m. The base station antenna gain is 3 dB and the mobile employs an omni-directional antenna with 0 dB gain. A forward GSM channel has a bandwidth of 200 kHz. Assume that the received signal-to-interference and noise ratio at the mobile station must be at least 9 dB for the forward link and that the system noise temperature of the mobile station receiver is 700 K. The maximum transmitted power for the base station is 240 W. Assume that the nominal carrier frequency is 894 MHz. Calculate the maximum radius of the cell with the Hata model for large cities and include co-channel interference.
10. Repeat Problem 9 for a cell in a large city with nominal carrier frequency of 1950 MHz and receiver noise temperature of 500 K.
11. Repeat Problem 9 with 120°-sectoring and 60°-sectoring.
12. Repeat Problem 10 with 120°-sectoring and 60°-sectoring.
13. For a three-cell per cluster system using microcell-zoning, derive the signal-to-interference ratio for the forward link, assuming that the mobile station is at the zone center.
14. Consider a forward CDMA link situated in a large city with the following parameters:

$$h_T = 100\,\text{m},\ h_R = 2\,\text{m},\ f_c = 1950\,\text{MHz},\ G_T = 0\,\text{dB},\ G_R = 0\,\text{dB},$$
$$B_{CDMA} = 1250\,\text{kHz},\ N = 64.$$

Mobile station:

$$T_s = 500\,\text{K}$$

Base station:

$$\text{maximum transmit power per Walsh channel } P_T = 4\,\text{W}$$

Assume that the path loss exponent $n = 4$, and the voice activity factor $\chi = 0.4$. The required despread input signal-to-interference-and-noise ratio is 8 dB. Given a cell radius of 5 km, calculate *maximum* number of user channels plus overhead channels (pilot channel for example) that the forward link can carry at any instant of time:

(a) without sectoring;
(b) with 120°-sectoring;
(c) with 60°-sectoring.

15. Ten forward CDMA links carry four types of users with bit rates kR_b, $k = 1, 2, 3, 4$. The percentage of users with bit rate R_b is 40%, the percentage of users with bit rate $2R_b$ is 25%, the percentage of users with bit rate $3R_b$ is 20%, and the percentage of users with bit rate $4R_b$ is 15%. A forward link carries a maximum of 60 user channels with basic bit rate R_b. Calculate the number of users for each type for the following cases:
(a) without sectoring;
(b) with 120°-sectoring;
(c) with 60°-sectoring.

16. Consider a reverse CDMA link situated in a large city with the following parameters:

$$h_T = 100\,\text{m},\ h_R = 2\,\text{m},\ f_c = 1850\,\text{MHz},\ G_T = 0\,\text{dB},\ G_R = 0\,\text{dB},$$
$$B_{CDMA} = 1250\,\text{kHz}, N = 64$$

Base station:

$$T_s = 500\,\text{K}$$

Mobile station:

$$\text{maximum transmit power per user channel } P_T = 4\,\text{W}$$

Assume that the path loss exponent $n = 4$, and the voice activity factor $\chi = 0.4$. The required despread input signal-to-interference-and-noise ratio is 8 dB. Given a cell radius of 5 km, calculate *maximum* number of user channels plus overhead channels (pilot channel for example) that the reverse link can carry at any instant of time:

(a) without sectoring;
(b) with 120°-sectoring;
(c) with 60°-sectoring.

17. Consider a 1.25 MHz reverse CDMA link with a required $SINR = 8$ dB. Given $N = 64$, $\chi = 0.5$, and $SNR = 20$ dB. The maximum despread input signal-to-CCI ratio without sectoring is $SIR_{CCI} = 10$ dB. The allocated spectrum is 12.5 MHz.
(a) Find the total number of simultaneous users in the cell without sectoring.
(b) Find the total number of simultaneous users in the cell with 120°-sectoring.
(c) Find the total number of simultaneous users in the cell with 60°-sectoring.

18. Consider a forward CDMA link with two types of users of bit rates R_b and $2R_b$. The users with the highest bit rate (30% of all users) have a spread factor of N and the users with the lowest bit rate (70% of all users) have a spread factor of $2N$. Thus, all

transmitted user signals have the same bandwidth. The available power for the link is P. Find the power allocated to a user of each type, so that the *SINR* is the same.

19. Consider a C-band satellite link (uplink frequency: 6 GHz, downlink frequency: 4 GHz). The *required* signal-to-noise ratio for the *combined link* must be at least 25 dB. The following parameters are given for the satellite system:

Satellite: $EIRP_S = 40$ dBW, $G_S/T_{sat} = 5\,\text{dB/K}$, bandwidth $B = 36$ MHz.

Transmit Earth station: uplink slant range $d_u = 37\,300$ km.

Receive Earth station: downlink slant range $d_d = 37\,000$ km, $G_R/T_s = 32\,\text{dB/K}$.

(a) Calculate the downlink signal wavelength λ_d and the uplink signal wavelength λ_u.
(b) Calculate the downlink path loss L_d(dB) and the uplink path loss L_u(dB).
(c) Calculate the *downlink* signal-to-noise ratio.
(d) Calculate the *required uplink* signal-to-noise ratio.
(e) Calculate the minimum *EIRP* of the transmit Earth station.

20. Consider a Ku-band (14/12 GHz) satellite link with the following parameters: bandwidth = 36 MHz, satellite antenna gain-to-noise temperature ratio = 1.6 dB/K, satellite EIRP = 44 dBW, transmit Earth station antenna gain = 57.6 dB, signal power from transmit Earth station = 174 W, receive Earth station antenna gain = 56.3 dB, receive Earth station system noise temperature = 160 K, uplink slant range = downlink slant range = 37 506 km, tracking loss = 1.2 dB (uplink) and 0.9 dB (downlink). Calculate the combined *SNR* (dB) of the entire satellite link.

21. The power flux density at the satellite induced by a transmitted signal with a given EIRP is defined as $\Omega = EIRP/4\pi d_u^2$, where d_u is the uplink slant range. Express the uplink signal-to-noise ratio as a function of Ω, satellite antenna gain-to-noise temperature ratio, uplink frequency f_u, and other suitable parameters, such as Boltzmann constant k, signal bandwidth B, and speed of light c.

22. Consider a C-band (6/4 GHz) satellite transponder that accommodates 200 distinct carriers with identical bandwidth. The carrier bandwidth is 40 kHz. The satellite antenna gain-to-noise temperature ratio is -7 dB/K, and its transponder EIRP is 36 dBW. To operate the transponder in a linear mode, the transponder amplifier output power is backed off by 6 dB. The power flux density at the satellite induced by all 200 carriers is $-91\,\text{dBW/m}^2$. The receive Earth station has an antenna gain-to-noise temperature ratio of 22 dB/K. The downlink slant range is 37 506 km. Calculate the combined *SNR* (dB) of the entire satellite link

23. A point-to-point communication system has the following parameters:

$$P_T = 0.5\,\text{W},\ G_T = 10\,\text{dB},\ L_C = 150\,\text{dB},\ G_R = 10\,\text{dB},\ T_A = 160\,\text{K},$$
$$G_{LNA} = 40\,\text{dB},\ T_{LNA} = 200\,\text{K}, G_{DC} = 10\,\text{dB},\ T_{DC} = 5000\,\text{K},$$
$$T_{DEM} = 4000\,\text{K},\ B = 50\,\text{KHz}$$

(a) Find the system noise temperature.
(b) Find the system *SNR* at the LNA input.
(c) Find the noise power at the demodulator input in dBW.

Further reading

For anyone who wants to study more about cellular systems we recommend the indispensable book by Rappaport [1]. The material on WCDMA and CDMA-2000 is readily available on the Internet, or the reader could consult the book by Garg [4]. For a detailed study of satellite communication, we recommend the book by Ha [6].

Bibliography

1. T. S. Rappaport, *Wireless Communications*, 2nd edition, Englewood Cliffs, NJ: Prentice-Hall, 2002.
2. EIA/TIA Interim Standard, "Cellular system dual mode mobile station–land station compatibility specifications," IS-54, Electronic Industries Association, May 1990.
3. TIA/EIA Interim Standard-95, "Mobile station–base station compatibility standard for dual mode wideband spread spectrum cellular system," July 1993.
4. V. K. Garg, *Wireless Network Evolution: 2G to 3G*, Englewood Cliffs, NJ: Prentice Hall, 2002.
5. M. Hata, "Empirical formula for propagation loss in land mobile radio services," *IEEE Trans. Vehicular Technol*., Vol. **VT-29**, No. 3, pp. 317–325, 1980.
6. T. T. Ha, *Digital Satellite Communications*, 2nd edition, New York: McGraw-Hill, 1990.

6 Modulation

Introduction

The purpose of digital modulation is to transmit information symbols via the amplitude and/or phase and/or frequency of a sinusoidal carrier. The symbol is transmitted over a symbol time which is the inverse of the symbol rate. For binary modulation, a bit is the same as the symbol. For higher order *M-ary* modulation ($M = 2^k$), a symbol consists of $k = \log_2 M$ bits. For binary modulation we investigate *phase shift keying* (PSK), *differential phase shift keying* (DPSK), *amplitude shift keying* (ASK), *frequency shift keying* (FSK), *minimum shift keying* (MSK), and *Gaussian minimum shift keying* (GMSK). For *M-ary* modulation we provide a detailed study of *M-ary amplitude shift keying* (MASK), *M-ary phase shift keying* (MPSK), *offset quadrature phase shift keying* (OQPSK), *differential M-ary phase shift keying* (DMPSK), *M-ary quadrature amplitude modulation* (MQAM), differential *M-ary quadrature amplitude modulation* (DMQAM), *code shift keying* (CSK), *M-ary frequency shift keying* (MFSK), *continuous phase modulation* (CPM), and *orthogonal frequency division multiplexing* (OFDM). For each modulation technique we will provide the signal space, power spectral density, and modulator.

6.1 Review of double sideband-amplitude modulation (DSB-AM)

Many digital modulation techniques are DSB-AM with a digital message signal. Therefore, it is appropriate to review this basic analog modulation. DSB-AM is the simplest form of amplitude modulation. The message signal $m(t)$ is multiplied with a high frequency carrier $A\cos 2\pi f_c t$, where A is the carrier amplitude and f_c is the carrier frequency, to provide a DSB-AM signal $s(t)$ as follows:

$$s(t) = Am(t)\cos 2\pi f_c t \tag{6.1}$$

Note that the amplitude of $s(t)$ is $Am(t)$, which varies according to the message signal $m(t)$, hence, the name amplitude modulation. In other words, the message signal is now being carried in the amplitude of the DSB-AM signal. The generation of $s(t)$ is achieved by the modulator shown in Figure 6.1

The voltage multiplier shown in Figure 6.1 is commonly referred to as the *mixer*.

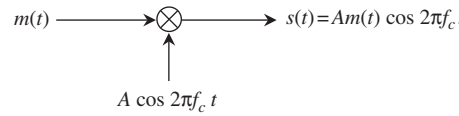

Figure 6.1 DSB-AM modulator.

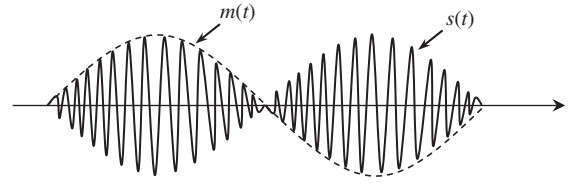

Figure 6.2 DSB-AM with a sinusoidal message signal.

Example 6.1 $m(t) = \cos 2\pi f_0 t$

The message signal is a sinusoid at frequency $f_0 \ll f_c$. Thus, the DSB-AM signal is given by (6.1) as

$$\begin{aligned} s(t) &= Am(t)\cos 2\pi f_c t \\ &= A\cos 2\pi f_0 t \cos 2\pi f_c t \\ &= \frac{A}{2}\cos 2\pi(f_c - f_0)t + \frac{A}{2}\cos 2\pi(f_c + f_0)t \end{aligned} \tag{6.2}$$

A plot of $s(t)$ in (6.2) is shown in Figure 6.2. Note that a phase reversal occurs at the point where $m(t)$ goes negative.

■

Example 6.2 $m(t) = p(t) + 3p(t-T) - p(t-2T) - 3p(t-3T)$

The message signal $m(t)$ is shown in Figure 6.3(a), which consists of four pulses of different amplitudes but with the same duration T. The DSB-AM signal is shown in Figure 6.3(b).

■

When the message signal $m(t)$ is deterministic and has the Fourier transform $M(f)$, then the Fourier transform $S(f)$ of the DSB-AM signal $s(t)$ in (6.1) can be evaluated using the modulation property in Table 2.1:

$$S(f) = \frac{A}{2}[M(f - f_c) + M(f + f_c)] \tag{6.3}$$

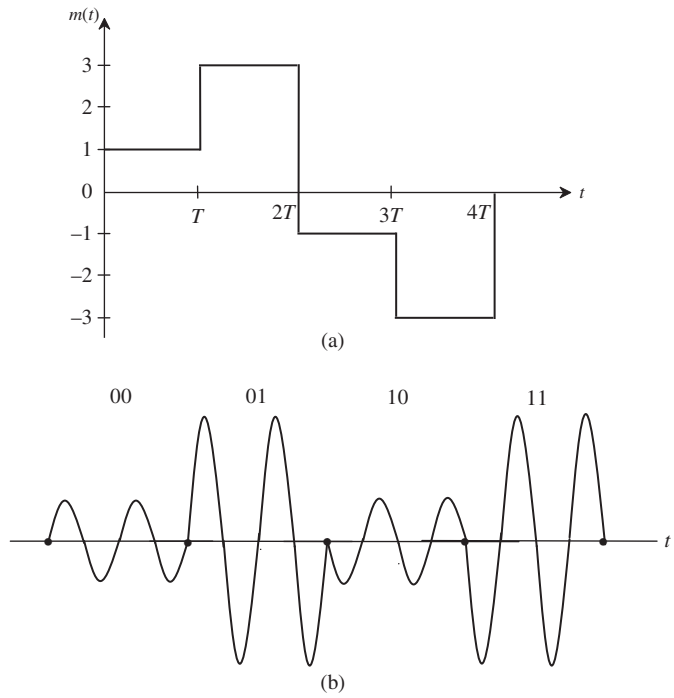

Figure 6.3 (a) Message signal; (b) DSB-AM signal.

Figure 6.4 illustrates the concept of DSB-AM in the frequency domain, and shows that $M(f)$ is shifted to $\pm f_c$.

Note that $S(f)$ consists of two sidebands: the upper sideband (USB) and the lower sideband (LSB). The bandwidth of a DSB-AM signal is $2B$, which is twice that of the message signal.

Example 6.3 Fourier transform of DSB-AM with $m(t) = \cos 2\pi f_0 t$

Taking the Fourier transform of $s(t)$ in (6.2) using Table 2.2 for cosine waveforms, we have

$$\begin{aligned} S(f) = &\frac{A}{4}[\delta(f-(f_c-f_0))+\delta(f+(f_c-f_0))] \\ &+\frac{A}{4}[\delta(f-(f_c+f_0))+\delta(f+(f_c+f_0))] \end{aligned} \tag{6.4}$$

which is shown in Figure 6.5. The USB consists of two impulse functions at f_c+f_0 and $-f_c-f_0$, and the LSB consists of two impulse function at f_c-f_0 and $-f_c+f_0$.

■

When $m(t)$ is a random signal (hence, its Fourier transform does not exist) we can look at the distribution of its power as a function of frequency via the power spectral density $S_m(f)$.

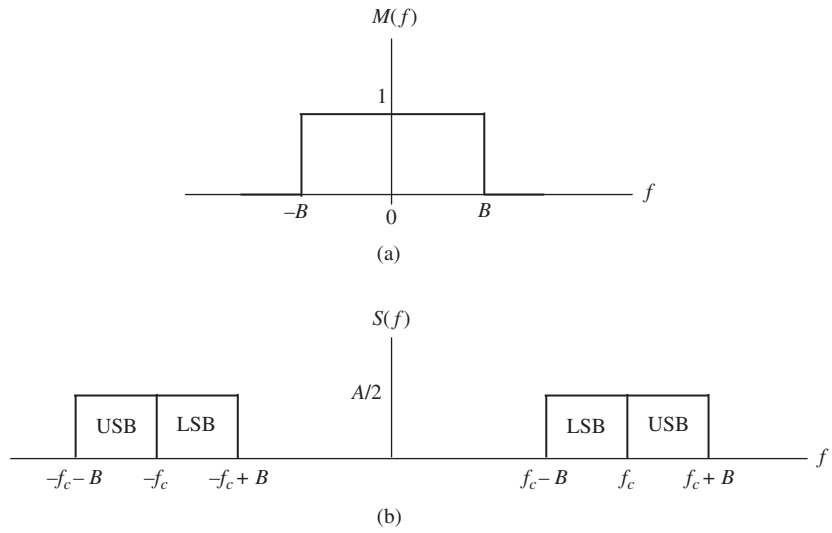

Figure 6.4 (a) Fourier transform of a message signal $m(t)$; (b) Fourier transform of DSB-AM signal $s(t)$.

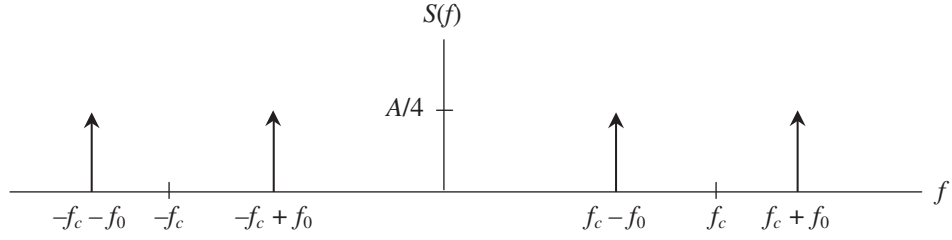

Figure 6.5 Fourier transform of a DSB-AM signal $s(t)$ with a sinusoidal message signal $m(t)$.

Consequently, the power spectral density $S_s(f)$ of the DSB-AM signal $s(t)$ in (6.1) can be evaluated via (3.71) as follows:

$$S_s(f) = \frac{A^2}{4}[S_m(f - f_c) + S_m(f + f_c)] \tag{6.5}$$

Example 6.4 Binary antipodal signaling message

The binary antipodal signaling is a line code that transmits a positive squared pulse to send a "0" bit and a negative squared pulse to send a "1" bit (or vice versa). If we assume unit amplitude pulses, then the power spectral density $S_m(f)$ of a binary antipodal signaling message $m(t)$ is given by (3.67) as

$$S_m(f) = T_b\left(\frac{\sin \pi f T_b}{\pi f T_b}\right)^2 \tag{6.6}$$

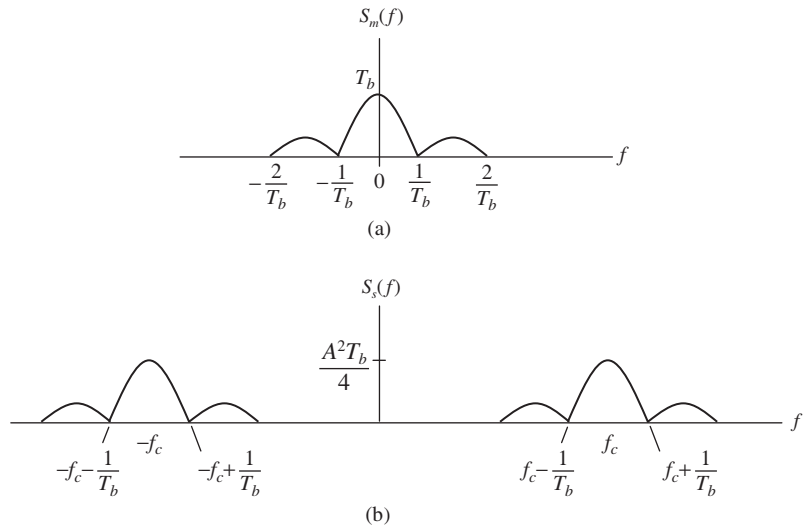

Figure 6.6 (a) PSD of an antipodal signaling message; (b) PSD of a DSB-AM signal.

where T_b is the pulse duration (or bit time). Using (6.5), the power spectral density of the DSB-AM signal $s(t)$ is

$$S_s(f) = \frac{A^2T_b}{4}\left[\left(\frac{\sin\pi(f-f_c)T_b}{\pi(f-f_c)T_b}\right)^2 + \left(\frac{\sin\pi(f+f_c)T_b}{\pi(f+f_c)T_b}\right)^2\right] \tag{6.7}$$

Both $S_m(f)$ and $S_s(f)$ are shown in Figure 6.6.

■

From Figure 6.4 or Figure 6.5, we observe that the message signal $m(t)$ can be extracted from the DSB-AM signal by simply retranslating its spectrum to the zero frequency.

6.2 Digital modulation

The need to transmit digital information in bits dictates the use of digital modulation instead of analog modulation. Generally speaking, a digital modulation technique requires the analog message signal to be converted first into bits, then bits into a baseband digital signal, which is used to modulate a carrier to produce a digitally modulated signal. Because the basic unit of the message is the bit, digital modulation does not distinguish whether the bits come from an audio signal, a video signal, or computer data. This feature makes digital modulation universally suited to all types of messages. Furthermore, bits can be represented by various types of baseband digital signals to shape the spectrum of the modulated signal, for example, to meet the channel bandwidth requirement. Bits can also be encoded at the transmitter and decoded at the receiver to correct errors due to channel noise and interference.

Transmission security is also a distinct feature of digital modulation. It is much easier to protect the integrity of the message signal carried by a digitally modulated signal.

The amount of information in bits per second, or channel capacity that can be achieved over a noisy channel via digital modulation is governed by the *Shannon channel capacity*. Given an ideal bandlimited channel of bandwidth B (Hz), AWGN having a constant power spectral density $N_0/2$ (W/Hz), and a received power P (W), the *channel capacity* C (bits/s) is given by

$$C = B\log_2\left(1 + \frac{P}{BN_0}\right) \tag{6.8}$$

The quantity BN_0 is the noise power in the bandwidth B (channel spectrum of $2B$), and hence P/BN_0 is the received signal-to-noise ratio. The Shannon channel capacity states that the data rate R (bits/s) through the channel must be smaller than C to achieve reliable transmission. In other words, a specified bit error rate can always be obtained via appropriate coding of the data. If $R > C$, reliable transmission is unattainable regardless of coding. Thus, it is necessary that

$$r = \frac{R}{B} < \frac{C}{B} = \log_2\left(1 + \frac{RE_b}{BN_0}\right) \tag{6.9}$$

where $E_b = P/R$ is the bit energy (J). From (6.9), the required *bit energy-to-noise density ratio* E_b/N_0, commonly referred to as the *signal-to-noise ratio per bit*, for reliable transmission is constrained by

$$\frac{E_b}{N_0} > \frac{2^r - 1}{r}, \quad r = R/B \tag{6.10}$$

An interesting observation on (6.9) reveals that, in the case of infinite bandwidth, the quantity $r = R/B$ in bits/s/Hz, commonly referred to as the *spectral efficiency*, approaches zero. On the other hand, the limit of E_b/N_0 can be found by L'Hôpital's rule as

$$\frac{E_b}{N_0} > \lim_{r\to 0}\frac{2^r - 1}{r} = \lim_{r\to 0}\frac{(\mathrm{d}/\mathrm{d}r)(2^r - 1)}{(\mathrm{d}/\mathrm{d}r)r} = \lim_{r\to 0} 2^r \ln 2 = \ln 2 = 0.693 \tag{6.11}$$

Or, in dB,

$$\frac{E_b}{N_0} > -1.59\,\mathrm{dB} \quad \text{(Shannon limit)} \tag{6.12}$$

It is seen that the ratio E_b/N_0 cannot be less than –1.59 dB, even with infinite bandwidth, for reliable transmission. A plot of r versus E_b/N_0 is shown in Figure 6.7.

The Shannon theorem provides a trade-off between the signal-to-noise ratio per bit E_b/N_0, which dictates the power efficiency of a digital modulation, and the spectral efficiency r, which dictates the bandwidth efficiency. Note that the Shannon theorem says nothing about the degree of reliability of the transmission, that is, about the bit error rate of a digitally modulated signal. Given an E_b/N_0 that is larger than –1.59 dB, and a spectral efficiency r such that the data rate is less than the channel capacity, one can always find a digital modulation and a channel coding scheme to achieve a desired bit error rate. A low error rate certainly requires a higher system complexity.

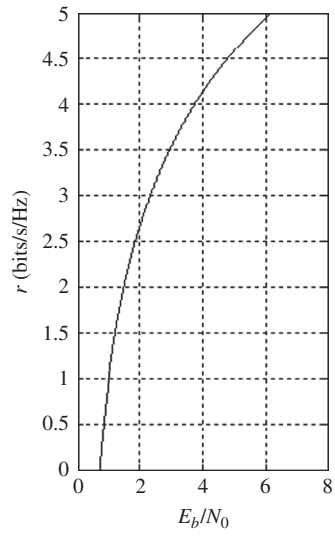

Figure 6.7 The Shannon limit for a Gaussian channel.

The rest of this chaper will be devoted to the study of various digital modulation techniques, which can be specifically classified into two broad groups, namely, binary modulation and M-ary modulation. The former is simple to implement and can achieve moderate power and spectral efficiencies. On the other hand, M-ary modulation transmits symbols (groups of $k = \log_2 M$ bits) instead of bits and can achieve high spectral efficiency with low power efficiency, or low to moderate spectral efficiency with high power efficiency. This flexibility makes M-ary modulation the choice in many real world applications.

6.3 Phase shift keying (PSK)

Phase shift keying (PSK) is perhaps the most popular binary modulation. It is used in many practical applications in satellite communications, cellular communications, and wireless local area networks. Certain aspects of PSK have been discussed in Chapter 2, such as signal space and bit energy (signal energy). The following discussion will further expand its scope. Two finite energy signals $s_1(t)$ and $s_2(t)$ that are π radians (or 180°) out of phase are employed to represent bit 1 and bit 0, respectively, over an arbitrary bit time T_b:

$$s(t) = \begin{cases} s_1(t) = Ap(t)\cos 2\pi f_c t: & \text{bit 1} \\ s_2(t) = Ap(t)\cos(2\pi f_c t + \pi): & \text{bit 0} \\ \quad = -Ap(t)\cos 2\pi f_c t & \end{cases} \tag{6.13}$$

where A is the signal amplitude, $p(t)$ is the bit pulse shape, and $\cos 2\pi f_c t$ is the carrier. As discussed in Chapter 2, the carrier frequency-bit duration product $f_c T_b$ is assumed to be a positive integer. Obviously, f_c is therefore an integer multiple of the bit rate $1/T_b$. The pulse

shape $p(t)$ can be a pulse of unit amplitude and duration T_b per (2.26), or a raised cosine pulse, which is commonly used in practice to shape the PSK spectrum to a required bandwidth and to eliminate intersymbol interference. Note that $s_1(t)$ and $s_2(t)$ in (6.13) can be combined into one for an infinite sequence of bits as follows:

$$s(t) = A\left[\sum_{i=-\infty}^{\infty} (2d_i - 1)\, p(t - iT_b)\right] \cos 2\pi f_c t \tag{6.14}$$

where $d_i \in \{0, 1\}$ represents the ith data bit. The complex envelope or equivalent lowpass signal of $s(t)$ is given by

$$m(t) = \sum_{i=-\infty}^{\infty} (2d_i - 1)\, p(t - iT_b) \tag{6.15}$$

Thus, PSK is simply a DSB-AM signal with the message signal $m(t)$. Note that $m(t)$ is the antipodal signal described in Example 2.3, where $p(t)$ is a unit amplitude squared pulse. Figures 2.4 and 2.6 show the complex envelope and the PSK signal itself for the sequence of bits {1 0 1 1} with squared pulse shape.

Example 6.17 PSK with squared pulse shape

The squared pulse shape is employed in practice when the bandwidth constraint is not a requirement. Figure 6.8 shows the complex envelope and the PSK signal for a squared pulse shape.

■

Example 6.18 Bit energy

The bit energy is the energy of the signal given in (6.13). Obviously, the energy of bit 1 is the same as the energy of bit 0 since $s_1(t) = -s_2(t)$

$$\begin{aligned} E_b &= \int_{-\infty}^{\infty} s_1^2(t)\, \mathrm{d}t = \int_{-\infty}^{\infty} s_2^2(t)\, \mathrm{d}t \\ &= \int_{-\infty}^{\infty} [Ap(t) \cos 2\pi f_c t]^2\, \mathrm{d}t \end{aligned} \tag{6.16}$$

For a squared pulse, we have $E_b = A^2 T_b/2$ as given in (2.24). In this example, we wish to calculate E_b for a raised-cosine pulse shape whose energy spectrum $P(f)$ is given as follows:

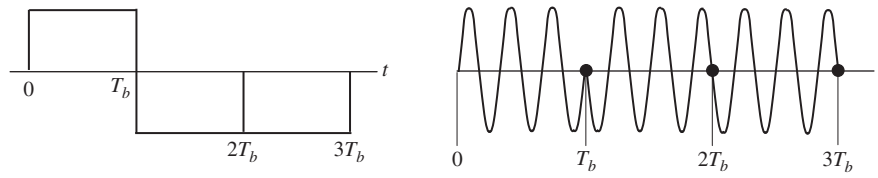

Figure 6.8 (a) Complex envelope; (b) PSK signal.

$$P(f)=\begin{cases} T_b, & 0\le |f|<\dfrac{1-\beta}{2T_b} \\ \dfrac{T_b}{2}\left\{1+\cos\left[\dfrac{\pi T_b}{\beta}\left(|f|-\dfrac{1-\beta}{2T_b}\right)\right]\right\}, & \dfrac{1-\beta}{2T_b}\le |f|\le \dfrac{1+\beta}{2T_b} \\ 0, & |f|>\dfrac{1+\beta}{2T_b} \end{cases} \tag{6.17}$$

where β is the filter roll-off factor. Applying the Parseval formula in Table 2.2 to (6.16), we have

$$E_b=\int_{-\infty}^{\infty} S_1^2(f)\,\mathrm{d}f=\int_{-\infty}^{\infty} S_2^2(f)\,\mathrm{d}f \tag{6.18}$$

where $S_1(f)$ and $S_2(f)$ are the energy spectra of $s_1(t)$ and $s_2(t)$ in (6.13), respectively. Using the frequency shifting property in Table 2.1 on (6.13), we get

$$S_1(f)=S_2(f)=\frac{A}{2}[P(f-f_c)+P(f+f_c)] \tag{6.19}$$

In practice, $f_c \gg 1/T_b$, thus $P(f-f_c)$ and $P(f+f_c)$ are non-overlapping. The symmetry property of $P(f)$ in (6.17) allows E_b to be calculated as follows:

$$E_b=A^2\int_0^{\infty} P^2(f)\,\mathrm{d}f \tag{6.20}$$

Hence,

$$\begin{aligned} E_b &= A^2\int_0^{(1-\beta)/(2T_b)} T_b^2\mathrm{d}f + A^2\int_{(1-\beta)/2T_b}^{(1+\beta)/(2T_b)} \frac{T_b^2}{4}\left(1+\cos\left[\frac{\pi T_b}{\beta}\left(f-\frac{1-\beta}{2T_b}\right)\right]\right)^2\mathrm{d}f \\ &= \frac{A^2T_b}{2}(1-\beta)+\frac{A^2T_b^2}{4}\int_{(1-\beta)/(2T_b)}^{(1+\beta)/(2T_b)}\left(1+2\cos\left[\frac{\pi T_b}{\beta}\left(f-\frac{1-\beta}{2T_b}\right)\right]+\cos^2\left[\frac{\pi T_b}{\beta}\left(f-\frac{1-\beta}{2T_b}\right)\right]\right)\mathrm{d}f \\ &= \frac{A^2T_b}{2}(1-\beta)+\frac{A^2T_b^2}{4}\left(\frac{\beta}{T_b}+\frac{\beta}{2T_b}\right)=\frac{A^2T_b}{2}\left(1-\frac{\beta}{4}\right) \end{aligned} \tag{6.21}$$

■

Example 6.19 Power spectral density

The power spectral density of a PSK signal $s(t)$ in (6.14) is that of a DSB-AM signal with the message $m(t)$ in (6.15). When $m(t)$ is an antipodal signal, the power spectral density of $s(t)$ is given in (6.7) and Figure 6.6. Given a general pulse shape $p(t)$, the power spectral density $S_s(f)$ is given by (6.5) where $S_m(f)$ is the power spectral density of $m(t)$ in (6.15). For the raised-cosine pulse shape, we have (Chapter 3)

$$S_m(f)=\frac{|P(f)|^2}{T_b} \tag{6.22}$$

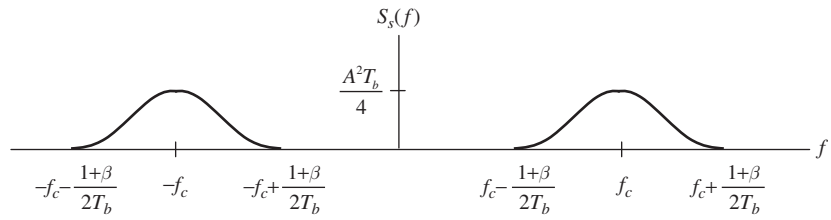

Figure 6.9 PSK power spectral density with raised-cosine pulse shape.

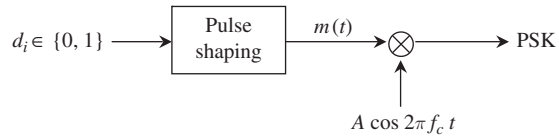

Figure 6.10 PSK modulator.

Note that the raised-cosine pulse shape limits the bandwidth to $(1+\beta)/T_b$, which is between $1/T_b$ and $2/T_b$ as shown in Figure 6.9. On the other hand, the squared pulse shape produces a power spectral density with an infinite bandwidth, although most of the PSK signal power is contained in the null-to-null bandwidth of $2/T_b$ as shown in Figure 6.6. The spectral efficiency of PSK is in the range 0.5–1 bits/s/Hz.

The power of the PSK signal in (6.15) with a raised-cosine pulse shape is given by

$$\begin{aligned} P &= \int_{-\infty}^{\infty} S_s(f)\,\mathrm{d}f = A^2 \int_0^{\infty} S_m(f)\,\mathrm{d}f \\ &= A^2 \int_0^{\infty} \frac{P^2(f)}{T_b}\,\mathrm{d}f = \frac{A^2}{T_b}\int_0^{\infty} P^2(f)\,\mathrm{d}f = \frac{A^2}{2}\left(1-\frac{\beta}{4}\right) \end{aligned} \tag{6.23}$$

Note that the bit energy E_b is equal to PT_b as expected.

■

The PSK signal in (6.13) or (6.14) can be generated by the modulator shown in Figure 6.10.

The PSK signal space is the same as that of the antipodal signal and is shown in Figure 2.13. Note that the basis function for the signal set in (6.13) is $x_1(t) = (A/\sqrt{E_b})p(t)\cos 2\pi f_c t$, where E_b is given in (6.16). Thus, the signal vectors are still given by (2.77) and (2.78) as $\boldsymbol{s}_1 = \sqrt{E_b}\mathbf{x}_1$ and $\boldsymbol{s}_2 = -\sqrt{E_b}\mathbf{x}_1$, where $\mathbf{x}_1 = [1]$.

6.4 Differential phase shift keying (DPSK)

Differential phase shift keying (DPSK) is a variation of PSK. In this modulation, the encoding of bits 1 and 0 is done via the phase difference between two successive bits. The DPSK signal $s_i(t)$ over an arbitrary bit time T_b, and the recursive phase encoding rule are given by

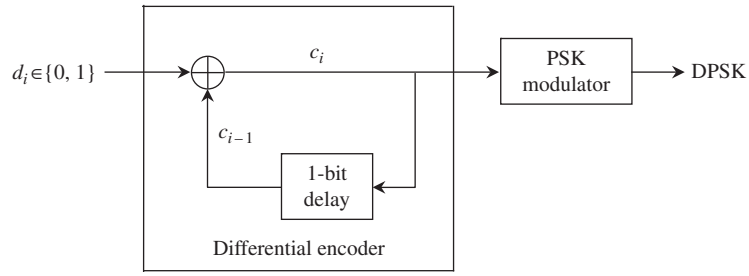

Figure 6.11 DPSK modulator.

$$s_i(t) = Ap(t)\cos(2\pi f_c t + \theta_i) \tag{6.24}$$

$$\theta_i = \theta_{i-1} + \pi d_i (\mathrm{mod}\, 2\pi) \tag{6.25}$$

where $p(t)$ is the pulse shape, $d_i \in \{0, 1\}$ represents the ith data bit, and θ_i and θ_{i-1} are the phases of the ith bit and the previous $(i-1)$th bit, respectively. The recursive phase encoding rule can be stated as follows:

(a) $d_i = 0$, $\theta_i = \theta_{i-1}$: no phase change between two successive waveforms when the current data bit is 0.
(b) $d_i = 1$, $\theta_i = \theta_{i-1} + \pi$: a phase change of π radians from the previous waveform to the current waveform when the current data bit is 1.

Thus, in DPSK the previous data bit serves as a reference for the current data bit. The recursive phase encoding rule in (6.25) can be implemented via a differential encoder shown in Figure 6.11 as part of the DPSK modulator.

The data bit d_i is modulo-2 added to the previously differentially encoded bit c_{i-1} to provide the current differentially encoded bit c_i, which is then PSK modulated. Hence,

$$c_i = d_i \oplus c_{i-1} \tag{6.26}$$

The operations in (6.25) and (6.26) are equivalent, that is, they produce the same DPSK signal for a given data bit d_i, as seen in the following example.

Example 6.20 Generation of DPSK signals

i	θ_i	d_i	c_i	$s_i(t)$
0	0	1	1	$Ap(t)\cos 2\pi f_c t$
1	0	0	1	$Ap(t)\cos 2\pi f_c t$
2	π	1	0	$-Ap(t)\cos 2\pi f_c t$
3	2π	1	1	$Ap(t)\cos 2\pi f_c t$
4	2π	0	1	$Ap(t)\cos 2\pi f_c t$
5	3π	1	0	$-Ap(t)\cos 2\pi f_c t$
6	3π	0	0	$-Ap(t)\cos 2\pi f_c t$

Note that bit $c_0 = d_0$ at the time index $i = 0$ is used as the initial reference bit.

■

The DPSK signal for an infinite sequence of bits can be written as

$$\begin{aligned} s(t) &= A\left[\sum_{i=-\infty}^{\infty}(2c_i - 1)p(t - iT_b)\right]\cos 2\pi f_c t \\ &= A\left[\sum_{i=-\infty}^{\infty}(2(d_i \oplus c_{i-1}) - 1)p(t - iT_b)\right]\cos 2\pi f_c t \end{aligned} \tag{6.27}$$

It is seen that DPSK is essentially PSK with the data bits d_i replaced by the differentially encoded bits c_i. Therefore, the power spectral density of a DPSK signal is the same as that of the corresponding PSK signal.

A natural question arises concerning the use of differential encoding in PSK. In practice, coherent detection of PSK requires the demodulator to extract the carrier from the PSK signal. This process is done via a carrier recovery circuit that inherently introduces a phase ambiguity of π radians (180°). That is, the recovered carrier is either $\cos 2\pi f_c t$ or $\cos(2\pi f_c t + \pi) = -\cos 2\pi f_c t$. If data are demodulated with $-\cos 2\pi f_c t$, bit 0 becomes 1, and vice versa. The use of differential encoding can resolve this phase ambiguity. Inverted data bits can be corrected via a differential decoder at the output of the demodulator. In addition to phase ambiguity resolution, differential encoding also allows DPSK to be demodulated noncoherently without a reference carrier, a feature that is attractive in applications where coherent demodulation is not feasible. Both phase ambiguity resolution and noncoherent demodulation of DPSK will be examined in the next chapter.

6.5 Amplitude shift keying (ASK)

Amplitude shift keying (ASK), commonly referred to as *on–off keying* (OOK), found its use mostly in fiber optic communications because it is more easily implemented than PSK. In this scheme the light intensity of the light source, either a light-emitting diode (LED) or a laser diode, is modulated linearly with respect to the input electrical signal [1]. Thus, the light source is turned on during bit 1 and turned off during bit 0. Figure 6.12 shows the block diagram of an optical ASK modulator using the intensity modulation technique. For example, the electrical signal is the pump current that drives the laser diode. The pump

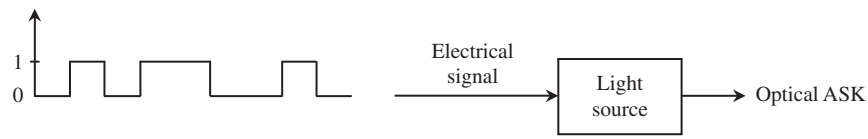

Figure 6.12 Intensity-modulated ASK modulator.

current is biased to be near the threshold value for bit 0 to nearly turn off the emitted light, and significantly above the threshold for bit 1. It is customary not to bias the laser diode so that the light during bit 0 is completely turned off to avoid the effect called transient chirp that can appear as crosstalk to adjacent channels in a multi-channel system. The ratio of the light energy for bit 0 to that for bit 1 is called the *extinction ratio* r_e. Note that $0 \le r_e < 1$.

The ASK signal that represents bit 1 or bit 0 over an arbitrary bit time T_b is given by

$$s(t) = \begin{cases} s_1(t) = \dfrac{1}{\sqrt{1+r_e}} Ap(t)\cos 2\pi f_c t: & \text{bit 1} \\ s_2(t) = \sqrt{\dfrac{r_e}{1+r_e}} Ap(t)\cos 2\pi f_c t: & \text{bit 0} \end{cases} \tag{6.28}$$

where $p(t)$ is the pulse shape. For an infinite sequence of bits, the ASK signal can be written as

$$s(t) = A\left[\sum_{i=-\infty}^{\infty} \frac{d_i\left(1-\sqrt{r_e}\right)+\sqrt{r_e}}{\sqrt{1+r_e}} p(t-iT_b)\right]\cos 2\pi f_c t \tag{6.29}$$

where $d_i \in \{0, 1\}$ represents the ith data bit. The complex envelope or equivalent lowpass signal for the ASK signal is

$$m(t) = \sum_{i=-\infty}^{\infty} \frac{d_i\left(1-\sqrt{r_e}\right)+\sqrt{r_e}}{\sqrt{1+r_e}} p(t-iT_b) \tag{6.30}$$

For the case of zero extinction ratio and squared pulse shape, the power spectral density of $m(t)$ is that of the unipolar signaling given by (3.68) as

$$S_m(f) = \frac{T_b}{4}\left(\frac{\sin \pi f T_b}{\pi f T_b}\right)^2 \left(1+\frac{\delta(f)}{T_b}\right) \tag{6.31}$$

The power spectral density of the ASK signal can be obtained by substituting (6.31) into (6.5). Again, note that the ASK signal is simply a DSB-AM signal with the message $m(t)$ in (6.30). The null-to-null bandwidth of the ASK signal with squared pulse is $2/T_b$. A spectral line represented by the $\delta(f)$ function in (6.31) indicated that a dc component exists at the carrier frequency f_c in its power spectral density.

Example 6.21 Average bit energy

Let us first consider a squared pulse shape. The energies of bit 1 and bit 0 are given by (6.28) as

$$E_1 = \int_0^{T_b} s_1^2 \mathrm{d}t = \frac{A^2 T_b}{2}\left(\frac{1}{1+r_e}\right) \tag{6.32}$$

$$E_2 = \int_0^{T_b} s_2^2 \mathrm{d}t = \frac{A^2 T_b}{2}\left(\frac{r_e}{1+r_e}\right) \tag{6.33}$$

Figure 6.13 ASK signal space.

The average bit energy E_b is given by the following relation, assuming bits 1 and 0 are equally probable:

$$\begin{aligned} E_b &= E_1 \Pr(\text{bit } 1) + E_2 \Pr(\text{bit } 0) \\ &= \frac{1}{2}E_1 + \frac{1}{2}E_2 = \frac{A^2 T_b}{4} \end{aligned} \tag{6.34}$$

For a raised-cosine pulse shape, using (6.21) we get

$$E_b = \frac{A^2 T_b}{4}\left(1 - \frac{\beta}{4}\right) \tag{6.35}$$

Note that $r_e = E_2/E_1$ by definition, as expected.

■

The ASK signal space is shown in Figure 6.13. The basis function for the signal set in (6.28) is $x_1(t) = \left(A/\sqrt{2E_b}\right)p(t)\cos 2\pi f_c t$. Note that $E_2 = 2E_b/(1 + r_e)$, and $E_1 = 2E_b(r_e/(1 + r_e))$.

6.6 Frequency shift keying (FSK)

Frequency shift keying (FSK) is a special form of frequency modulation (FM) [2–6] in which the message signal is a baseband digital signal. In this modulation, bits 1 and 0 are represented by a pair of orthogonal signals as follows:

$$\begin{aligned} s_1(t) &= A\cos(2\pi f_1 t + \theta_1): \quad \text{bit } 1 \\ s_2(t) &= A\cos(2\pi f_2 t + \theta_2): \quad \text{bit } 0 \end{aligned} \tag{6.36}$$

where for a positive integer $\ell > 1$, and $f_c = \ell/T_b$, we have

$$\begin{aligned} f_1 &= f_c - \frac{1}{2T_b} \\ f_2 &= f_c + \frac{1}{2T_b} \end{aligned} \tag{6.37}$$

Both frequencies f_1 and f_2 are selected to be an integer multiple of the bit rate $1/T_b$, and the minimum frequency spacing of $1/T_b$ is required to preserve orthogonality between $s_1(t)$ and $s_2(t)$. The peak frequency deviation is $\Delta f = 1/2T_b$.

Pulse shapes other than the squared pulse can be chosen to shape the power spectral density but care must be exercised to ensure orthogonality between the two signals $s_1(t)$ and

$s_2(t)$. From (6.36) and (6.37), the FSK signals for bits 1 and 0 can be combined into one equation for an infinite sequence of bits up to the nth bit as

$$s(t) = A\cos\left[2\pi f_c t + 2\pi\left(\frac{1}{2T_b}\right)\int_{-\infty}^{t}\sum_{i=-\infty}^{n}(2d_i - 1)\,p(\tau - iT_b)\mathrm{d}\tau\right] \tag{6.38}$$

where $d_i \in \{0,\ 1\}$ represents the ith data bit and $p(t - iT_b)$ is the squared pulse shape of the ith bit given in (2.26). The phase at the bit transition is required to be continuous, that is, at the bit transition the phase of the present bit is required to be the same as that of the previous bit. FSK is a special form of FM with the message signal $m(t)$ given by

$$m(t) = \sum_{i=-\infty}^{n}(2d_i - 1)\,p(t - iT_b) \tag{6.39}$$

The corresponding frequency sensitivity is $a_f = 1/2T_b$ [2–6]. Note that $\max|m(t)| = 1$ since $(2d_i - 1) \in \{-1,\ 1\}$ and the amplitude of $p(t)$ is one. Thus, the peak frequency deviation of $s(t)$ is [2–6]

$$\Delta f = a_f \max|m(t)| = \frac{1}{2T_b} \tag{6.40}$$

Note that the message signal $m(t)$ is an antipodal signal with an infinite bandwidth. Therefore, it is not appropriate to use Carson's rule bandwidth or the FM modulation index [2–6] unless we define a bandwidth B for $m(t)$ that contains, say over 90% of the power. This yields $B = 1/T_b$, which is the first null bandwidth.

Carson's rule bandwidth can then be estimated as follows:

$$B_C \approx 2\left(\Delta f + \frac{1}{T_b}\right) = 2\left(\frac{1}{2T_b} + \frac{1}{T_b}\right) = \frac{3}{T_b} \tag{6.41}$$

The modulation index of the FSK signal can be evaluated as $\beta = \Delta f/B = \Delta f/(1/T_b) = 0.5$. A *digital modulation index* $h = 2T_b\Delta f = 1$ is commonly used because it is independent of the bandwidth of $m(t)$.

Figures 6.14 and 6.15 show the FSK modulators for both discontinuous phase and continuous phase at the bit transitions.

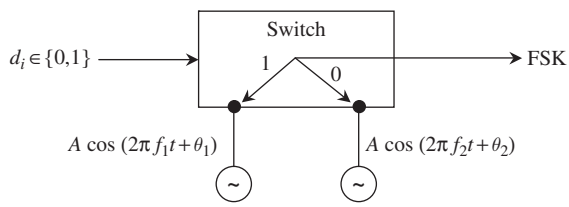

Figure 6.14 Modulator for discontinuous phase FSK.

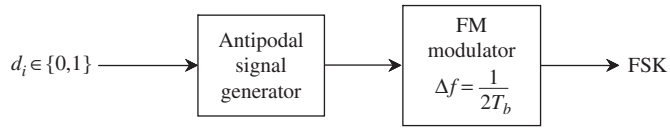

Figure 6.15 Modulator for continuous phase FSK with a frequency spacing equal to the data rate.

Power spectral density

For the antipodal message signal $m(t)$ given in (6.39), the power spectral density of the continuous phase FSK signal with the frequency spacing of $1/T_b$ can be evaluated analytically. Equation (6.38) can be simplified as follows:

$$\begin{aligned} s(t) &= A\cos\left[2\pi f_c t + \pi\sum_{i=-\infty}^{n-1}(2d_i - 1) + \frac{\pi}{T_b}\int_{nT_b}^{t}(2d_n - 1)\,p(\tau - nT_b)\mathrm{d}\tau\right] \\ &= A\cos\left[2\pi f_c t + (2d_n - 1)\frac{\pi t}{T_b} + \theta_n\right] \end{aligned} \tag{6.42}$$

where θ_n is the phase of $s(t)$ defined as

$$\theta_n = \pi\sum_{i=-\infty}^{n-1}(2d_i - 1) - (2d_n - 1)n\pi \tag{6.43}$$

The requirement for continuous phase at the nth bit transition $t = nT_b$ dictates that

$$2\pi f_c nT_b + (2d_n - 1)\pi n + \theta_n = 2\pi f_c nT_b + (2d_{n-1} - 1)\pi n + \theta_{n-1} \tag{6.44}$$

In other words,

$$\begin{aligned} \theta_n &= \theta_{n-1} + 2(d_{n-1} - d_n)\pi n \\ &= \theta_{n-1}\,(\mathrm{mod}\,2\pi) \end{aligned} \tag{6.45}$$

The above recursive relation also dictates that $\theta_n = \theta_{n-1} = \cdots = \theta_{-\infty}(\mathrm{mod}\,2\pi)$, where $\theta_{-\infty}$ is the initial phase at time $t = -\infty$. This proves that θ_n is independent of the data bits, and hence, without loss of generality, we set $\theta_{-\infty} = 0$ to yield $\theta_n = 0\,(\mathrm{mod}\,2\pi)$. Using this result in (6.42) we obtain, for $nT_b \le t < (n+1)T_b$,

$$\begin{aligned} s(t) &= A\cos\left[2\pi f_c t + (2d_n - 1)\frac{\pi t}{T_b}\right] \\ &= A\cos\left[(2d_n - 1)\frac{\pi t}{T_b}\right]\cos 2\pi f_c t - A\sin\left[(2d_n - 1)\frac{\pi t}{T_b}\right]\sin 2\pi f_c t \end{aligned} \tag{6.46}$$

Since $d_n \in \{0, 1\}$, hence $(2d_n - 1) \in \{-1,\ 1\}$, and (6.46) reduces to

$$\begin{aligned} s(t) &= A\cos\left(\frac{\pi t}{T_b}\right)\cos 2\pi f_c t - A(2d_n - 1)\sin\left(\frac{\pi t}{T_b}\right)\sin 2\pi f_c t \\ &= A\,\mathrm{Re}\left\{s_L(t)\mathrm{e}^{\mathrm{j}2\pi f_c t}\right\} \end{aligned} \tag{6.47}$$

where $s_L(t)$ is the complex envelope of $s(t)$ and is given by, for $nT_b \le t < (n+1)T_b$,

$$s_L(t) = \cos\left(\frac{\pi t}{T_b}\right) + \mathrm{j}(2d_n - 1)\sin\left(\frac{\pi t}{T_b}\right) \tag{6.48}$$

The power spectral density $S(f)$ of $s(t)$ can be evaluated as follows:

$$S(f) = \frac{A^2}{4}[S_L(f - f_c) + S_L(f + f_c)] \tag{6.49}$$

where $S_L(f)$ is the power spectral density of $s_L(t)$. Note that the in-phase (real) and quadrature (imaginary) components of $s(t)$ are independent, so $S_L(f)$ is the sum of the power spectral densities of $\cos(\pi t/T_b)$ and $(2d_n - 1)\sin(\pi t/T_b)$, respectively. Note that $\cos(\pi t/T_b)$ is a periodic signal for $-\infty < t < (n+1)T_b$ since it is independent of the data bit, while $(2d_n - 1)\sin(\pi t/T_b)$ is an antipodal signal with a pulse shape $\sin(\pi t/T_b)$ of duration T_b. The power spectrum of a periodic signal expressed in (2.112) is given in (2.127). Thus, for the periodic in-phase signal $\cos(\pi t/T_b)$ with frequency $1/2T_b$, the power spectral density is

$$S_{L,I}(f) = \frac{1}{4}\left[\delta\left(f - \frac{1}{2T_b}\right) + \delta\left(f + \frac{1}{2T_b}\right)\right] \tag{6.50}$$

The power spectral density of the antipodal quadrature signal $(2d_n - 1)\sin(\pi t/T_b)$ is given by

$$S_{L,Q}(f) = \frac{1}{T_b}\left|F\left\{\sin\left(\frac{\pi t}{T_b}\right)p(t - nT_b)\right\}\right|^2 \tag{6.51}$$

where $p(t - nT_b)$ is a unit amplitude pulse with duration T_b from nT_b to $(n+1)T_b$.

Example 6.22 Evaluating $|F\{\sin(\pi t/T_b)p(t - nT_b)\}|^2$

Recall from Table 2.1 that multiplication in the time domain becomes convolution in the frequency domain. Furthermore, the pulse $\sin(\pi t/T_b)p(t - nT_b)$ is simply the pulse $\cos(\pi t/T_b)p(t + T_b/2)$ shifted in time by $(n + 1/2)T_b$ seconds, where

$$p\left(t + \frac{T_b}{2}\right) = \begin{cases} 1, & -\dfrac{T_b}{2} \le t < \dfrac{T_b}{2} \\ 0, & \text{otherwise} \end{cases} \tag{6.52}$$

Therefore, from Table 2.2, we get

$$\begin{aligned}\left|F\left\{\cos\left(\frac{\pi t}{T_b}\right)p\left(t + \frac{T_b}{2}\right)\right\}\right|^2 &= \left|\frac{1}{2}\left[\delta\left(f - \frac{1}{2T_b}\right) + \delta\left(f + \frac{1}{2T_b}\right)\right] * T_b\frac{\sin \pi T_b f}{\pi T_b f}\right|^2 \\ &= \left|\frac{T_b}{2}\left[\frac{\sin \pi T_b(f - 1/2T_b)}{\pi T_b(f - 1/2T_b)} + \frac{\sin \pi T_b(f + 1/2T_b)}{\pi T_b(f + 1/2T_b)}\right]\right|^2 \\ &= \left|\frac{2T_b}{\pi}\left[\frac{\cos \pi T_b f}{(2T_b f)^2 - 1}\right]\right|^2\end{aligned} \tag{6.53}$$

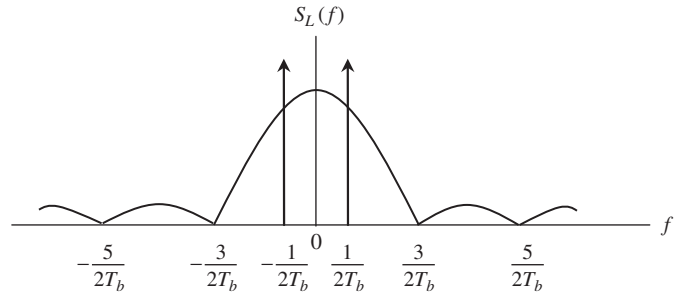

Figure 6.16 Power spectral density of the complex envelope of FSK.

Using the time-shifting property in Table 2.1, we obtain

$$\left|F\left\{\sin\left(\frac{\pi t}{T_b}\right)p(t-nT_b)\right\}\right|^2 = \left|\frac{2T_b}{\pi}\left[\frac{\cos\pi T_b f}{(2T_b f)^2-1}\right]e^{-j2\pi f(n+1/2)T_b}\right|^2 \tag{6.54}$$

■

By substituting (6.54) into (6.51), the power spectral density $S_{L,Q}(f)$ is given by

$$S_{L,Q}(f) = \frac{4T_b}{\pi^2}\left[\frac{\cos\pi T_b f}{(2T_b f)^2-1}\right]^2 \tag{6.55}$$

From (6.50) and (6.51), we obtain the power spectral density of the complex envelope $s_L(t)$ of the continuous phase FSK signal $s(t)$, as follows:

$$S_L(f) = \frac{1}{4}\left[\delta\left(f-\frac{1}{2T_b}\right)+\delta\left(f+\frac{1}{2T_b}\right)\right]+\frac{4T_b}{\pi^2}\left[\frac{\cos\pi T_b f}{(2T_b f)^2-1}\right]^2 \tag{6.56}$$

A plot of $S_L(f)$ is shown in Figure 6.16 where the first null bandwidth is equal to $1.5/T_b$. The null-to-null bandwidth of a FSK signal is therefore equal to $3/T_b$. This is the same as Carson's rule bandwidth in (6.41). In practice, the bandwidth is normally chosen to be between $1.25/T_b$, which contains about 90% of the total power, and $2.1/T_b$, which contains about 99% of the signal power. The spectral efficiency of FSK is, therefore, about 0.5–0.8 bits/s/Hz.

The FSK signal space is illustrated in Figure 2.14. Note that the Euclidean distance between the two signals is $\sqrt{2E_b}$ as compared to $2\sqrt{E_b}$ for PSK. The shorter Euclidean distance results in an inferior performance in noise than PSK, as will be studied in Chapter 7.

6.7 Minimum shift keying (MSK)

We have seen a preliminary description of minimum shift keying (MSK) in Example 2.15. It is a continuous phase FSK with a minimum frequency spacing of $1/2T_b$ and a peak

frequency deviation of $\Delta f = 1/4T_b$. The digital modulation index of MSK is $h = 2T_b\Delta f = 0.5$. The MSK signal for an infinite sequence of data bits $d_i \in \{0, 1\}$ up to the nth bit can be modified from (6.38) to account for $\Delta f = 1/2T_b$, as follows:

$$\begin{aligned} s(t) &= A\cos\left[2\pi f_c t + 2\pi\left(\frac{1}{4T_b}\right)\int_{-\infty}^{t}\sum_{i=-\infty}^{n}(2d_i - 1)\,p(\tau - iT_b)\mathrm{d}\tau\right] \\ &= A\cos\left[2\pi f_c t + \frac{\pi}{2}\sum_{i=-\infty}^{n-1}(2d_i - 1) + \frac{\pi}{2T_b}\int_{nT_b}^{t}(2d_i - 1)p(\tau - nT_b)\mathrm{d}\tau\right] \\ &= A\cos\left[2\pi f_c t + (2d_n - 1)\frac{\pi t}{2T_b} + \theta_n\right] \end{aligned} \tag{6.57}$$

where $p(t)$ is a squared pulse shape of unit amplitude and duration T_b, and θ_n is given by

$$\theta_n = \left[\frac{\pi}{2}\sum_{i=-\infty}^{n-1}(2d_i - 1)\right] - (2d_n - 1)\frac{n\pi}{2} \tag{6.58}$$

For the phase to be continuous at the nth bit's transition $t = nT_b$, we must have

$$2\pi f_c nT_b + (2d_n - 1)\frac{\pi n}{2} + \theta_n = 2\pi f_c nT_b + (2d_{n-1} - 1)\frac{\pi n}{2} + \theta_{n-1}$$

or

$$\theta_n = \theta_{n-1} + (d_{n-1} - d_n)\pi n \tag{6.59}$$

Thus, we get $\theta_n = \theta_{n-1}(\mathrm{mod}\,2\pi)$ for $d_n = d_{n-1}$, and $\theta_n = \theta_{n-1} \pm \pi n(\mathrm{mod}\,2\pi)$ for $d_n \neq d_{n-1}$. Without loss of generality, we assume the initial phase at time $t = -\infty$ is 0, that is, $\theta_{-\infty} = 0$. Then, $\theta_n \in \{0, \pi\}(\mathrm{mod}\,2\pi)$. By observing (6.57), we can represent the data bit $d_n \in \{0, 1\}$ as follows:

$$\begin{aligned} s_1(t) &= A\cos\left[2\pi\left(f_c + \frac{1}{4T_b}\right)t + \theta_n\right]; \quad d_n = 1 \\ s_2(t) &= A\cos\left[2\pi\left(f_c - \frac{1}{4T_b}\right)t + \theta_n\right]; \quad d_n = 0 \end{aligned} \tag{6.60}$$

It is obvious that the peak frequency deviation is $\Delta f = 1/4T_b$, which is half that of FSK. This explains the name minimum shift keying. The *digital modulation index* is $k = 2T_b\Delta f = 0.5$. Note that $s_1(t)$ and $s_2(t)$ are *orthogonal* if f_c is an integer multiple of $1/T_b$ as indicated by (2.49), and they are *quasi-orthogonal* if $f_c \gg 1/T_b$.

Power spectral density

Expanding $s(t)$ in (6.57) into quadrature form, and using the fact that $\sin\theta_n = 0$, we get, for $nT_b \leq t < (n+1)T_b$,

$$\begin{aligned} s(t) &= A\cos\theta_n\cos\left[(2d_n - 1)\frac{\pi t}{2T_b}\right]\cos 2\pi f_c t - A\cos\theta_n\sin\left[(2d_n - 1)\frac{\pi t}{2T_b}\right]\sin 2\pi f_c t \\ &= A\,\mathrm{Re}\left\{s_L(t)\mathrm{e}^{\mathrm{j}2\pi f_c t}\right\} \end{aligned} \tag{6.61}$$

where $\cos\theta_n \in \{-1, 1\}$, and $s_L(t)$ is the complex envelope of $s(t)$ defined for $nT_b \leq t < (n+1)T_b$ as

$$\begin{aligned} s_L(t) &= \cos\theta_n \cos\left[(2d_n - 1)\frac{\pi t}{2T_b}\right] + \mathrm{j}\cos\theta_n \sin\left[(2d_n - 1)\frac{\pi t}{2T_b}\right] \\ &= \cos\theta_n \cos\left(\frac{\pi t}{2T_b}\right) + \mathrm{j}(2d_n - 1)\cos\theta_n \sin\left(\frac{\pi t}{2T_b}\right) \end{aligned} \tag{6.62}$$

It is obvious that $\cos\theta_n$ and $(2d_n - 1)\cos\theta_n$ represent the data for the in-phase (real) and quadrature (imaginary) parts of $s_L(t)$, respectively. From (6.59), we observe that

$$\cos\theta_n = \cos\theta_{n-1}, \quad d_n = d_{n-1} \tag{6.63}$$

$$\cos\theta_n = \begin{cases} \cos\theta_{n-1}, & \text{even } n \\ -\cos\theta_{n-1}, & \text{odd } n \end{cases}, \quad d_n \neq d_{n-1} \tag{6.64}$$

Thus, $\cos\theta_n$ remains constant over a two-bit interval of $2T_b$ and can only change sign when n is odd. Also,

$$\begin{aligned} (2d_n - 1)\cos\theta_n &= (2d_{n-1} - 1)\cos\theta_{n-1}, \quad d_n = d_{n-1} \\ (2d_n - 1)\cos\theta_n &= \begin{cases} -(2d_{n-1} - 1)\cos\theta_{n-1}: & \text{even } n \\ (2d_{n-1} - 1)\cos\theta_{n-1}: & \text{odd } n \end{cases}, \quad d_n \neq d_{n-1} \end{aligned} \tag{6.65}$$

Thus $(2d_n - 1)\cos\theta_n$ remains constant over a two-bit interval of $2T_b$ and can only change sign when n is even.

The in-phase data $\cos\theta_n$ and quadrature data $(2d_n - 1)\cos\theta_n$, for all n, therefore represent two antipodal data streams of period $2T_b$; one is offset from the other by T_b duration.

Example 6.23 In-phase and quadrature data

n	d_n	$\theta_n (\mathrm{mod}\, 2\pi)$	$\cos\theta_n$	$(2d_n - 1)\cos\theta_n$
0	1	0	1	1
1	0	π	–1	1
2	0	π	–1	1
3	1	0	1	1
4	0	0	1	–1
5	1	π	–1	–1
6	0	π	–1	1
7	1	0	1	1
8	0	0	1	–1

For convenience, the initial phase θ_0 is assumed to be 0. Note that the in-phase data stream $\cos\theta_n$ is always constant during a $2T_b$ interval starting with odd n = 1, 3, 5, 7. On the

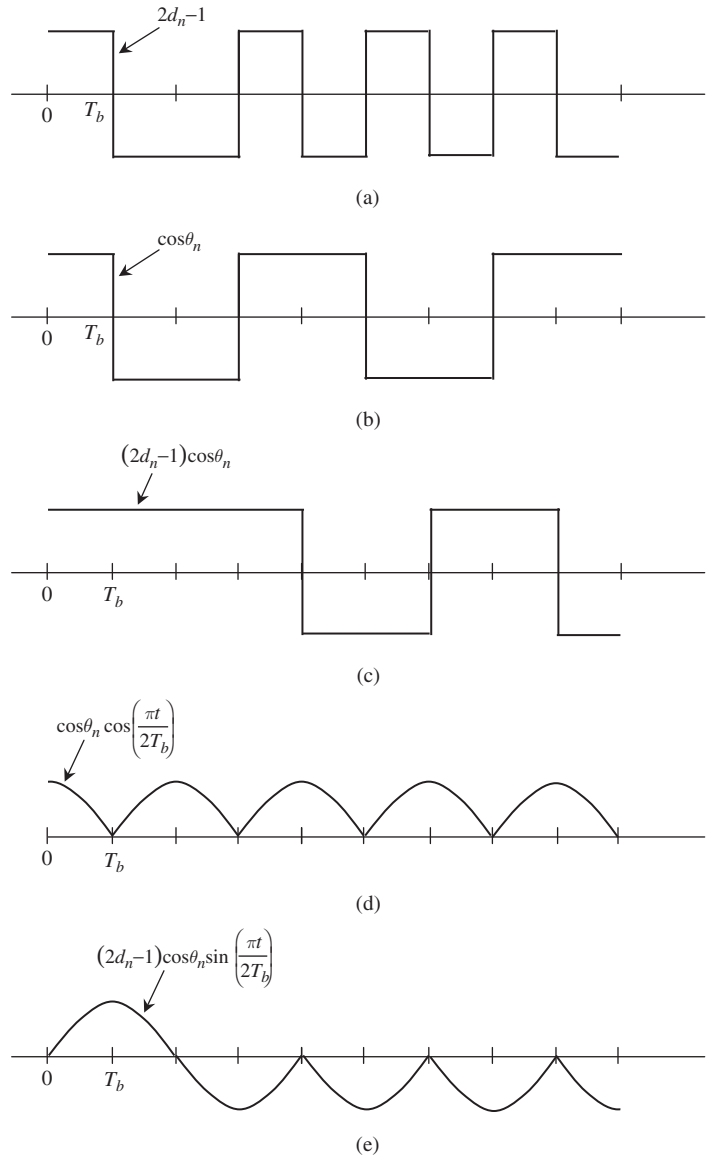

Figure 6.17 (a) Input data in antipodal format of period T_b; (b) in-phase antipodal data of period $2T_b$; (c) quadrature antipodal data of period $2T_b$; (d) in-phase antipodal signal of pulse shape $\cos(\pi t/2T_b)$; (e) quadrature antipodal signal of pulse shape $\sin(\pi t/2T_b)$.

other hand, the quadrature data stream $(2d_n - 1)\cos\theta_n$ is constant over a $2T_b$ interval starting with even $n = 0, 2, 4, 6, 8$. The two data streams are staggered by one bit interval. Figure 6.17 illustrates the in-phase and quadrature antipodal data streams $\cos\theta_n$ and $(2d_n - 1)\cos\theta_n$.

■

The above discussion also concludes that $\cos\theta_n \cos(\pi t/2T_b)$ is the in-phase antipodal signal of pulse shape $\cos(\pi t/2T_b)$ of $2T_b$ seconds. Also, $(2d_n - 1)\cos\theta_n \sin(\pi t/2T_b)$ is the quadrature antipodal signal of pulse shape $\sin(\pi t/2T_b)$ of $2T_b$ seconds. These two signals are staggered by T_b seconds. Note that $\sin(\pi t/2T_b)$ is simply $\cos(\pi t/2T_b)$ shifted by T_b seconds.

The power spectral density $S_L(f)$ of the complex envelope $s_L(t)$ in (6.62) is the sum of two identical power spectral densities $S_{L,I}(f)$ and $S_{L,Q}(f)$ of the in-phase and quadrature components, respectively. Following the analysis in Example 6.22, and noting that both in-phase and quadrature components have a period of $2T_b$ seconds, we have

$$S_{L,I}(f) = S_{L,Q}(f) = \frac{1}{2T_b}\left|F\left\{\cos\left(\frac{\pi t}{2T_b}\right)p_{2T_b}(t)\right\}\right|^2 \tag{6.66}$$

where $p_{2T_b}(t)$ is a squared pulse defined as follows:

$$p_{2T_b}(t) = \begin{cases} 1, & -T_b \le t < T_b \\ 0, & \text{otherwise} \end{cases} \tag{6.67}$$

From Table 2.2, we obtain

$$\begin{aligned}\left|F\left\{\cos\left(\frac{\pi t}{2T_b}\right)p_{2T_b}(t)\right\}\right|^2 &= \left|\frac{1}{2}\left[\delta\left(f-\frac{1}{4T_b}\right)+\delta\left(f+\frac{1}{4T_b}\right)\right] * 2T_b\frac{\sin 2\pi f T_b}{2\pi f T_b}\right|^2 \\ &= \left|T_b\left[\frac{\sin 2\pi T_b(f-1/4T_b)}{2\pi T_b(f-1/4T_b)}+\frac{\sin 2\pi T_b(f+1/4T_b)}{2\pi T_b(f+1/4T_b)}\right]\right|^2 \\ &= \left|\frac{4T_b}{\pi}\left[\frac{\cos 2\pi T_b f}{(4T_b f)^2-1}\right]\right|^2\end{aligned} \tag{6.68}$$

Substituting (6.68) into (6.66) and using the fact that $S_L(f) = 2S_{L,I}(f) = 2S_{L,Q}(f)$, we obtain

$$S_L(f) = \frac{16T_b}{\pi^2}\left[\frac{\cos 2\pi T_b f}{(4T_b f)^2-1}\right]^2 \tag{6.69}$$

Hence, the power spectral density of the MSK signal $s(t)$ in (6.61) can be evaluated as

$$S(f) = \frac{A^2}{4}[S_L(f-f_c) + S_L(f+f_c)] \tag{6.70}$$

Figure 6.18 shows the power spectral density of the *complex envelope* of an MSK signal. The first null bandwidth is $0.75/T_b$. The 99% power bandwidth of the complex envelope is about $1.2/T_b$. On the other hand, 90% of the signal power is contained in the bandwidth approximately equal to $0.78/T_b$. Thus, the spectral efficiency of MSK is between 0.8 and 1.3 bits/s/Hz, which is far superior than that of FSK. Also, for FSK, half the power is in the two harmonics of $f_c \pm 1/T_b$. This results in a tremendous waste of power since these two harmonics carry no information.

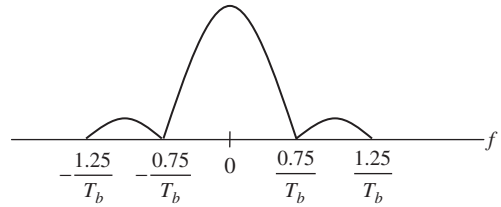

Figure 6.18 Power spectral density of the complex envelope of MSK.

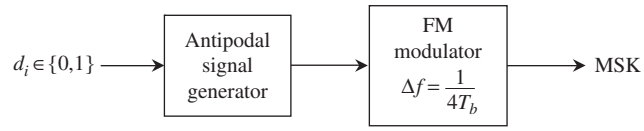

Figure 6.19 Analog implementation of MSK.

Modulator

The MSK signal in (6.57) can be implemented by an FM modulator with a peak frequency deviation $\Delta f = 1/4T_b$, as shown in Figure 6.19. This is referred to as the analog implementation of MSK.

The digital implementation of MSK can be carried out as follows. First, we observe that the in-phase data $\cos\theta_n$ and the quadrature data $(2d_n - 1)\cos\theta_n$ can be written as one data stream γ_n as

$$\gamma_n = \begin{cases} \cos\theta_n, & n: \text{ odd} \\ (2d_n - 1)\cos\theta_n, & n: \text{ even} \end{cases} \tag{6.71}$$

In other word, the in-phase and quadrature data are odd and even splits of the data $\{\gamma_n\}$. Example 6.24 illustrates the above observation.

Example 6.24 Combining in-phase and quadrature data

Using the same data in Example 6.23 and denoting c_n as the binary version of the antipodal data γ_n in (6.71), that is, $c_n = (\gamma_n + 1)/2$, we have:

n	d_n	$2d_n$–1	$\cos\theta_n$	$(2d_n$–1)$\cos\theta_n$	γ_n	c_n
0	1	1	1	1	1	1
1	0	−1	−1	1	−1	0
2	0	−1	−1	1	1	1
3	1	1	1	1	1	1
4	0	−1	1	−1	−1	0
5	1	1	−1	−1	−1	0
6	0	−1	−1	1	1	1
7	1	1	1	1	1	1
8	0	−1	1	−1	−1	0

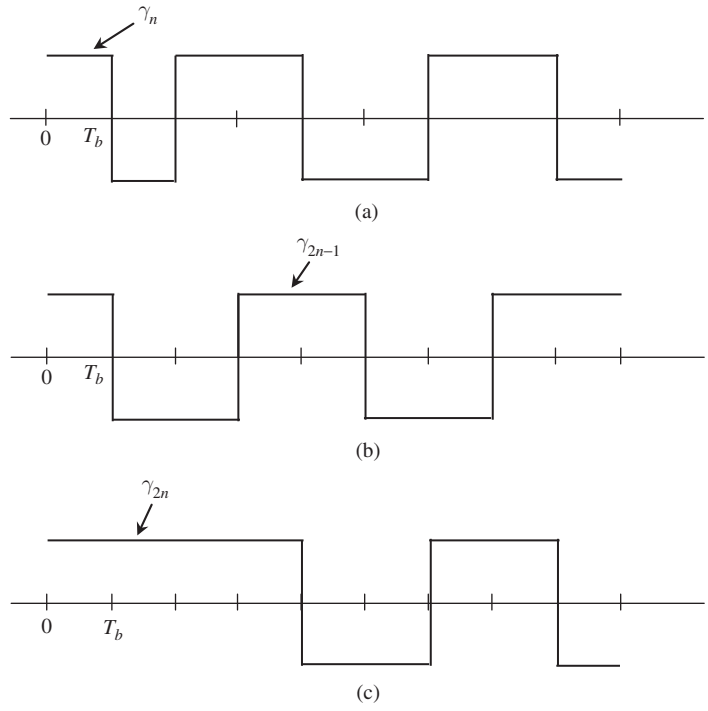

Figure 6.20 (a) Data γ_n; (b) odd split γ_{2n-1}; (c) even split γ_{2n}.

The antipodal data $\{\gamma_n\}$, and its even $\{\gamma_{2n}\}$ and odd $\{\gamma_{2n-1}\}$ splits are shown in Figure 6.20. Note that $\{\gamma_{2n}\}$ is identical to $\{(2d_n - 1)\cos\theta_n\}$ and $\{\gamma_{2n-1}\}$ is identical to $\{\cos\theta_n\}$ as seen in Figure 6.17.

■

We note that (6.71) can be rewritten in a more compact form, that is,

$$\gamma_n = (2d_n - 1)\gamma_{n-1} \tag{6.72}$$

as evident by Example 6.24. If we express the data in binary form, (6.72) becomes

$$c_n = \overline{d_n} \oplus c_{n-1} \tag{6.73}$$

Thus, the data c_n can be obtained from the original data d_n by differential encoding. A quadrature implementation of MSK is illustrated in Figure 6.21.

Note that the data d_n is clocked in at the bit rate of $1/T_b$ bits per second. On the other hand, the data c_{2n} and c_{2n-1} are clocked at the rate of $1/2T_b$ bits per second.

A variation of MSK is also employed, namely, precoded MSK, where the differential encoder from Figure 6.21 is omitted. This no longer guarantees that data bit $d_n = 1$ will be transmitted at $f_c + 1/4T_b$ and data bit $d_n = 0$ at $f_c - 1/4T_b$, hence noncoherent

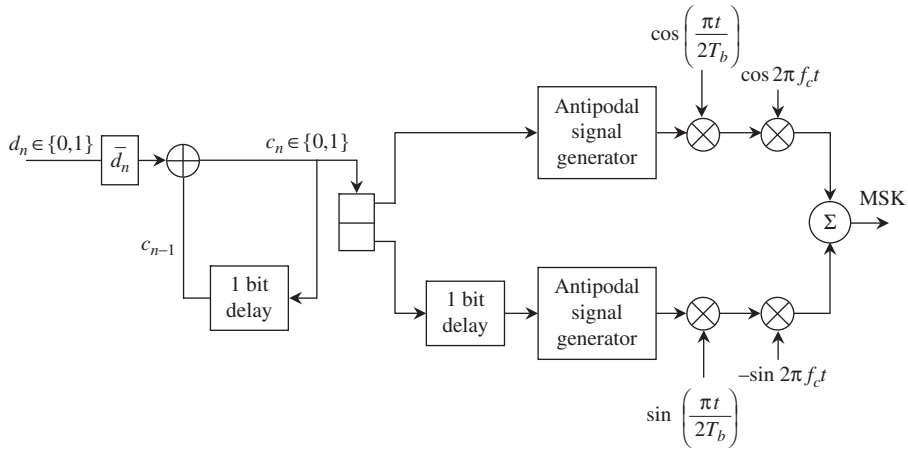

Figure 6.21 Quadrature implementation of the MSK modulator.

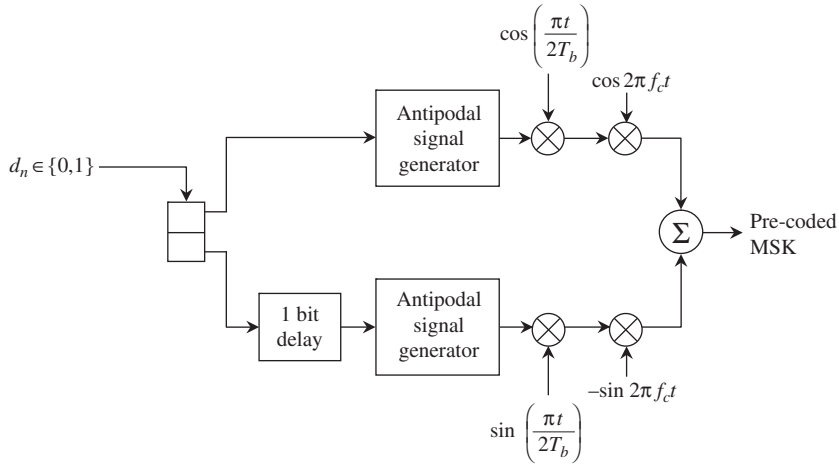

Figure 6.22 Precoded MSK modulator.

demodulation cannot be carried out. Figure 6.22 shows the modulator for precoded MSK. It is obvious that both MSK and precoded MSK should have the same power spectral densities. Note that MSK is also called *fast frequency shift keying* (FFSK). Both MSK and precoded MSK can be demodulated coherently, but MSK can also be demodulated noncoherently, and this is its advantage in applications where coherent demodulation is not possible.

6.8 Gaussian minimum shift keying (GMSK)

Gaussian minimum shift keying (GMSK) is a variation of MSK, and is employed in the European GSM cellular system to compact the power spectral density relative to that of

Table 6.1 Occupied bandwidth normalized to $1/T_b$ for a given percentage of power

	BT_b	90%	99%	99.9%
	0.2	0.52	0.79	0.99
GMSK	0.25	0.57	0.86	1.09
	0.5	0.69	1.04	1.33
MSK	∞	0.78	1.20	2.76

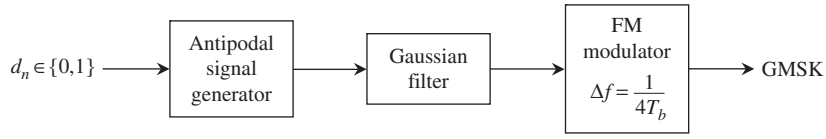

Figure 6.23 Analog implementation of GMSK.

MSK. This is achieved by employing a Gaussian filter for pulse shaping before modulation, as shown in Figure 6.23. The Gaussian filter has the following transfer function:

$$H(f) = \mathrm{e}^{-a^2 f^2} \tag{6.74}$$

where the parameter a is related to the 3 dB bandwidth B of $H(f)$ as follows:

$$a = \frac{1}{B}\sqrt{\frac{\ln 2}{2}} = \frac{0.59}{B} \tag{6.75}$$

Note that $|H(B)|^2 = \left|\exp(-0.59^2)\right|^2 = 0.5$, the half-power value, as expected. The impulse response of the Gaussian filter is

$$h(t) = \frac{\sqrt{\pi}}{a}\mathrm{e}^{-\left(\pi^2/a^2\right)t^2} \tag{6.76}$$

The signal $g(t)$ at the output of the Gaussian filter is frequency-modulated to produce the GMSK signal, which can be expressed as follows:

$$s(t) = A\cos\left[2\pi f_c t + 2\pi a_f \int_{-\infty}^{t} \sum_{i=-\infty}^{n} (2d_i - 1)\, g(\tau - iT_b)\mathrm{d}\tau\right] \tag{6.77}$$

where $a_f = \Delta f / \max|g(t)|$ with $\Delta f = 1/4T_b$ and the pulse shape $g(t) = p(t) * h(t)$. The squared pulse $p(t)$ with unit amplitude and duration T_b represents the pulse shape of the antipodal data signal. The Gaussian filter is employed to suppress the side lobe of the power spectral density function. This filter is commonly specified by the 3 dB bandwidth-bit time product BT_b . The Gaussian filter nonetheless introduces intersymbol interference, which increases the bit error rate of GMSK relative to MSK. The degradation in signal-to-noise ratio per bit E_b/N_0 is about 1.6 dB for $BT_b = 0.25$ as compared to MSK. Table 6.1 shows the occupied bandwidth normalized to $1/T_b$ for GMSK and MSK that contains a given percentage of power.

Example 6.25 GMSK in the GSM cellular standard [28]
This second generation (2G) European digital cellular system is the most widely used. The modulation is GMSK with $BT_b = 0.3$. The channel data rate is $1/T_b = 270.833$ kbps, hence, the 3 dB bandwidth of the Gaussian filter is $B = 81.25$ kHz. The data bit ones and zeros are represented by two frequencies, $f_c \pm 1/4T_b = f_c \pm 67.708$ kHz. The channel spacing is 200 kHz, which is equal to $0.7385/T_b$. The spectral efficiency for GMSK in GSM is about 270.833 kb/s/200 kHz = 1.35 bits/s/Hz. Note that the 90% power bandwidth of MSK is about $0.78/T_b$, which yields a spectral efficiency approximately equal to 1.3 bits/s/Hz. So GMSK is more spectrally efficient than MSK. A study of Table 6.1 also reveals that GMSK with $BT_b < 0.5$ produces much lower out-of-band power, and therefore reduces adjacent channel interference in a cellular environment.
■

6.9 The need for M-ary modulation

The study of binary modulation in the previous sections leads us to the conclusion that these techniques are not spectrally efficient. The highest spectral efficiency comes from GMSK, which has 1.35 bits/s/Hz in the GSM cellular standard. The bit energy-to-noise density ratio, E_b/N_0, for a practical operation in an AWGN channel is normally around 8–14 dB for binary modulation. A look back to the Shannon limit as shown in Figure 6.7 reveals that a much higher spectral efficiency can be achieved in this range of E_b/N_0. For example, from (6.10), a spectral efficiency of 6 bits/s/Hz can be achieved at $E_b/N_0 \approx 10$ dB. The premium bandwidth requirement in many real world applications dictates the necessity of modulation techniques other than binary modulation. This is where M-ary modulation comes into the picture. For example, data communication over the public switched telephone network (PSTN) is carried out at a bit rate of 56 kbps downstream (ISP server to client computer) and 33.6 kbps upstream (client computer to ISP server). The upstream data rate is achieved over a bandwidth of 4 kHz dictated by the channel filter at the Central Office. This yields a spectral efficiency of 8.4 bits/s/Hz. This cannot be achieved by any binary modulation technique. Of course, the required E_b/N_0 according to (6.10) could be much higher than 16 dB, as required by the Shannon capacity theorem.

Besides spectral efficiency, the premium power requirement of many real world applications dictates the use of power efficient M-ary modulation. Although a combination of error correction coding and binary modulation can, in many cases, achieve the goal of conserving the power of the transmitted signal, the use of M-ary modulation can further enhance the power saving, especially in power-saving applications. An example of the use of power efficient M-ary modulation is the reverse link (mobile to base station) in the second generation CDMA cellular standard IS-95, which employs 64-ary orthogonal modulation.

M-ary modulation employs a set of M distinct finite-energy signals to represent a set of $M = 2^k$ symbols. Each symbol can be viewed as a representation of k bits. The symbol time is denoted as T_s and the corresponding symbol rate is $1/T_s$. Since a symbol has k bits, it is obvious that $T_s = kT_b$, and $1/T_s = 1/kT_b$. Thus, the symbol rate is k times slower than the corresponding bit rate $1/T_b$. As in the case of binary modulation, we assume that the carrier frequency f_c is an integer multiple of the symbol rate.

6.10 M-ary amplitude shift keying (MASK)

This modulation is an extension of ASK, which employs a set of $M = 2^k$ finite-energy signals to represent M distinct symbols numbered as $n = 1, 2, \ldots, M$, with each symbol having k bits $d_0\, d_1 \cdots d_{k-1}$ as follows:

$$s_n(t) = A_n p(t) \cos 2\pi f_c t, \quad n = 1, 2, \ldots, M \tag{6.78}$$

where $p(t)$ is the pulse shape of a symbol and $\cos 2\pi f_c t$ is the carrier. A_n is the signal amplitude given by

$$A_n = (2n - M - 1)A \tag{6.79}$$

where A is the smallest signal amplitude. It is seen that $2A$ is the distance between adjacent signal amplitudes. The symbol rate is taken to be $1/T_s$, where T_s is the symbol time.

Signal space

From the analysis of Section 2.4, we observe that the basis function for the signal set $s_n(t)$ in (6.78) is given by

$$x_1(t) = \frac{A}{\sqrt{E}} p(t) \cos 2\pi f_c t \tag{6.80}$$

where E is the smallest symbol energy defined as

$$E = \int_{-\infty}^{\infty} [Ap(t) \cos 2\pi f_c t]^2 \mathrm{d}t \tag{6.81}$$

Thus, it is seen that the signal energy E_n of signal $s_n(t) = (2n - M - 1)\sqrt{E}x_1(t)$ can be expressed as follows:

$$E_n = \int_{-\infty}^{\infty} s_n^2(t)\, \mathrm{d}t = (2n - M - 1)^2 E \tag{6.82}$$

The MASK signal space is shown in Figure 6.24 for the cases $M = 4$ and $M = 8$.

Each symbol $d_0\, d_1 \cdots d_{k-1}$ is assigned a signal level via Gray code. Adjacent symbols differ by only one bit, thus a symbol error only results in one bit error. It is common to normalize the signal level with $\sqrt{E}$ so that the mapping can be represented as in Tables 6.2 and 6.3.

Table 6.2 4ASK symbol mapping

Symbol number n	Input bits $d_0\ d_1$	Signal level = $2n - \mathrm{M} - 1$
1	0 0	–3
2	0 1	–1
3	1 1	+1
4	1 0	+3

Table 6.3 8ASK symbol mapping

Symbol number n	Input bits $d_0\ d_1\ d_2$	Signal level = $2n - \mathrm{M} - 1$
1	0 0 0	–7
2	0 0 1	–5
3	0 1 1	–3
4	0 1 0	–1
5	1 1 0	+1
6	1 1 1	+3
7	1 0 1	+5
8	1 0 0	+7

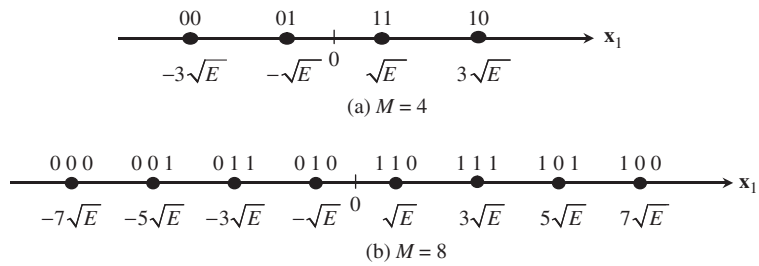

Figure 6.24 (a) 4ASK; (b) 8ASK.

Power spectral density

The MASK signal set in (6.78) can be combined into one for an infinite sequence of symbols as follows:

$$s(t) = \sum_{i=-\infty}^{\infty} (2D_i - M - 1)\, Ap(t - iT_s) \cos 2\pi f_c t \tag{6.83}$$

where $D_i \in \{1, 2, \ldots, M\}$ represents the ith symbol in the symbol stream. The complex envelope or equivalent lowpass signal of $s(t)$ is given by

$$m(t) = \sum_{i=-\infty}^{\infty} (2D_i - M - 1)\, p(t - iT_s) \tag{6.84}$$

which is commonly referred to as *M-ary pulse amplitude modulation* (MPAM). Thus, MASK is simply a DSB-AM signal with the MPAM message signal $m(t)$. The power spectral density of $m(t)$ is derived in the problem as follows:

$$S_m(f) = \frac{\sigma^2}{T_s}|P(f)|^2 + \left(\frac{\mu}{T_s}\right)^2 \sum_{k=-\infty}^{\infty} \left|P\left(\frac{k}{T_s}\right)\right|^2 \delta\left(f - \frac{k}{T_s}\right) \tag{6.85}$$

where $P(f)$ is the Fourier transform of the pulse shape $p(t)$ and μ and σ^2 are the mean value and variance of the signal levels $\{2D_i - M - 1\}$, respectively. Since the symbol levels are equally spaced and symmetrical around zero, the mean value $\mu = 0$. The variance σ^2 can be calculated as follows:

$$\begin{aligned}
\sigma^2 &= \mathbf{E}\left\{[2D_i - (M+1)]^2\right\} = \mathbf{E}\left\{4D_i^2 - 4D_i(M+1) + (M+1)^2\right\} \\
&= \left[4\mathbf{E}\{D_i^2\} - 4(M+1)\mathbf{E}\{D_i\} + (M+1)^2\right\} \\
&= \left[\frac{4}{M}\sum_{n=1}^{M} n^2 - \frac{4}{M}(M+1)\sum_{n=1}^{M} n + (M+1)^2\right\} \\
&= \left[\frac{2}{3}(M+1)(2M+1) - 2(M+1)^2 + (M+1)^2\right\} \\
&= \frac{1}{3}\left(M^2 - 1\right)
\end{aligned} \tag{6.86}$$

For example, we have $\sigma^2 = 5$ for 4ASK and $\sigma^2 = 21$ for 8ASK. Substituting (6.86) with $\mu = 0$ into (6.85) yields

$$S_m(f) = \frac{M^2 - 1}{3T_s}|P(f)|^2 \tag{6.87}$$

The MASK power spectral density is obtained by substituting (6.87) into (6.5). If a squared pulse shape $p(t)$ is employed, then the MASK power spectral density would look identical to that of PSK with an amplitude scaling factor of $M^2 - 1$, and with T_b replaced by T_s as illustrated in Figure 6.6 (recall that PSK is simply a DSB-AM signal with an anti-podal signaling message). For the raised-cosine pulse shape, the bandwidth is $B = (1+\beta)/T_s$, where β is the raised-cosine roll-off factor. Note that the symbol rate $1/T_s = 1/kT_b$, where $2^k = M$. Thus, in terms of the bit rate, $1/T_b$, the bandwidth in this case is $B = (1+\beta)/kT_b$. The spectral efficiency, which is the bit rate-to-bandwidth ratio, is $r = 1/BT_b = k/(1+\beta)$ bits/s/Hz, which is between $k/2$ and k bits/s/Hz. Therefore, the larger the number of bits per symbol $k = \log_2 M$, the smaller the bandwidth required, and the higher the spectral efficiency that can be achieved. We observe that an increase in power by a factor of $M^2 - 1$ accompanied a spectral efficiency gain of $k = \log_2 M < M^2 - 1$. Hence, it is obvious that MASK must use more transmitter power to achieve the same performance as PSK, given the fact that the minimum Euclidean distance for MASK is $2\sqrt{E}$, which is the same as that of PSK.

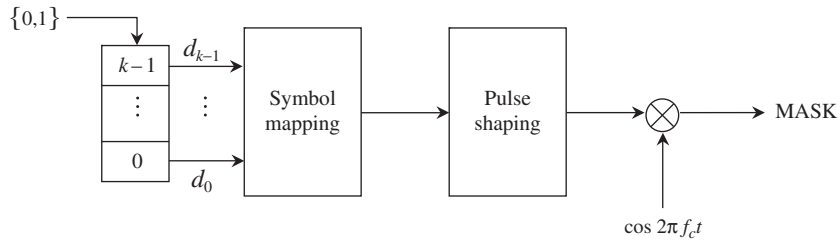

Figure 6.25 MASK modulator.

Modulator

The MASK modulator is illustrated in Figure 6.25. The binary data in bits are shifted with rate $1/T_b$ into a serial-to-parallel converter (demultiplexer) whose k outputs form a stream of k-bit symbols with rate $1/T_s = 1/kT_b$. Each symbol $d_0\, d_1 \cdots d_{k-1}$ is then mapped into its appropriate signal level. The pulse shape generator provides a pulse $p(t)$ with the appropriate signal level, which then modulates a carrier $\cos 2\pi f_c t$ to produce the MASK signal.

6.11 M-ary phase shift keying (MPSK)

As good as MASK is in providing high spectral efficiency (up to $k = \log_2 M$ b/s/Hz), its power efficiency is rather poor. In applications where high spectral efficiency and moderate to high power efficiency are desired, MPSK is the appropriate choice. In addition MPSK provides the constant amplitude requirement (similar to MSK) to work with a channel that has nonlinearity (power amplifier, satellite transponder). The most popular MPSK, namely 4PSK, commonly referred to as quadrature phase shift keying (QPSK), finds widespread use in practical applications. It can achieve twice the spectral efficiency of PSK and has the same power efficiency.

MPSK employs a set of $M = 2^k$ constant amplitude and finite energy signals to represent M distinct symbols, which we number as $n = 1, 2, \ldots, M$, with each symbol represented by $k = \log_2 M$ bits labeled as $d_0 d_1 \ldots d_{k-1}$, as follows:

$$s_n(t) = Ap(t)\cos\left(2\pi f_c t + (2n-1)\frac{\pi}{M}\right), \quad n = 1, 2, \ldots, M \tag{6.88}$$

where $p(t)$ is the pulse shape of a symbol, $\cos 2\pi f_c t$ is the carrier, and A is the constant amplitude. The symbol rate is taken to be $1/T_s$, where T_s is the symbol time, which is k times the bit interval T_b. The symbol rate is thus equal to $1/k$ times the bit rate $1/T_b$. The carrier frequency is assumed to be an integer multiple of the symbol rate.

Signal space

The MPSK signals in (6.88) can be expressed in the I-Q representation as

$$s_n(t) = \left[\cos\frac{(2n-1)\pi}{M}\right] Ap(t)\cos 2\pi f_c t - \left[\sin\frac{(2n-1)\pi}{M}\right] Ap(t)\sin 2\pi f_c t \tag{6.89}$$

Simply observing (6.89), we conclude that there are two basis functions for the signal set $s_n(t)$, $n = 1, 2, \ldots, M$, namely,

$$x_1(t) = \frac{A}{\sqrt{E_s}} p(t)\cos 2\pi f_c t \tag{6.90}$$

$$x_2(t) = -\frac{A}{\sqrt{E_s}} p(t)\sin 2\pi f_c t \tag{6.91}$$

where E_s is the symbol energy defined as

$$\begin{aligned} E_s &= \int_{-\infty}^{\infty} s_n^2(t)\mathrm{d}t = \int_{-\infty}^{\infty} \left[Ap(t)\cos\left(2\pi f_c t + (2n-1)\frac{\pi}{M}\right)\right]^2 \mathrm{d}t \\ &= \int_{-\infty}^{\infty} [Ap(t)\cos 2\pi f_c t]^2 \mathrm{d}t = \int_{-\infty}^{\infty} [-Ap(t)\sin 2\pi f_c t]^2 \mathrm{d}t \end{aligned} \tag{6.92}$$

In the cases where $p(t)$ is a unit amplitude pulse of duration T_s, the basis functions $x_1(t)$ and $x_2(t)$ form an orthonormal set per (2.87).

Example 6.26 Orthogonality with arbitrary pulse shape

In this example we examine the requirements for $x_1(t)$ and $x_2(t)$ to be orthogonal given a real pulse shape $p(t)$ with a Fourier transform $P(f)$. We have

$$\int_{-\infty}^{\infty} x_1(t)x_2(t)\,\mathrm{d}t = -\frac{A^2}{2E_s}\int_{-\infty}^{\infty} p(t)[p(t)\sin 4\pi f_c t]\,\mathrm{d}t \tag{6.93}$$

Applying the Parseval formula in Table 2.2 to the right-hand side of (6.93), we get

$$\begin{aligned} \int_{-\infty}^{\infty} x_1(t)x_2(t)\,\mathrm{d}t &= \frac{A^2}{\mathrm{j}4E_s}\int_{-\infty}^{\infty} P(f)[P^*(f-2f_c) - P^*(f+2f_c)]\,\mathrm{d}f \\ &= \frac{A^2}{\mathrm{j}4E_s}\int_{-\infty}^{\infty} P(f)[P(-f+2f_c) - P(-f-2f_c)]\,\mathrm{d}f \end{aligned} \tag{6.94}$$

If $P(f)$ is bandlimited to a spectrum W such that $W < f_c$, then $P(f)$ does not overlap with $P(-f+2f_c)$ or $P(-f-2f_c)$. Therefore, $P(f)P(-f+2f_c) = 0$ and $P(f)P(-f-2f_c) = 0$. Thus, the right-hand side of (6.94) is zero and $x_1(t)$ is orthogonal to $x_2(t)$. Note that this condition is sufficient only.

A stronger condition can be established by letting $P(f) = P(-f)$, that is, $P(f)$ is an even function, a condition that is normally met by practical pulse shapes. In this case,

Table 6.4 QPSK symbol mapping

Symbol number n	Input bits $d_0\ d_1$	I	Q
1	1 1	$+\sqrt{2}/2$	$+\sqrt{2}/2$
2	0 1	$-\sqrt{2}/2$	$+\sqrt{2}/2$
3	0 0	$-\sqrt{2}/2$	$-\sqrt{2}/2$
4	1 0	$+\sqrt{2}/2$	$-\sqrt{2}/2$

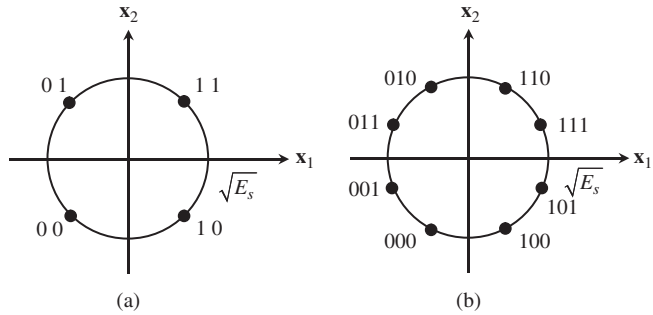

Figure 6.26 Signal space: (a) QPSK; (b) 8PSK. The I- and Q-channels are represented by $\mathbf{x}_1$ and $\mathbf{x}_2$, respectively.

$$\int_{-\infty}^{\infty} P(f)P(-f+2f_c)\,\mathrm{d}f = \int_{-\infty}^{\infty} P(f)P(-f-2f_c)\,\mathrm{d}f \tag{6.95}$$

and $x_1(t)$ is orthogonal to $x_2(t)$.

■

Using the basis functions $x_1(t)$ and $x_2(t)$ in (6.90) and (6.91), we can express the MPSK signal $s_n(t)$ in (6.89) as follows:

$$s_n(t) = \sqrt{E_s}\cos\frac{(2n-1)\pi}{M}x_1(t) + \sqrt{E_s}\sin\frac{(2n-1)\pi}{M}x_2(t) \tag{6.96}$$

Furthermore, in terms of vectors, we have

$$s_n = \begin{bmatrix} \sqrt{E_s}\cos\frac{(2n-1)\pi}{M} \\ \sqrt{E_s}\sin\frac{(2n-1)\pi}{M} \end{bmatrix} = \sqrt{E_s}\cos\frac{(2n-1)\pi}{M}\mathbf{x}_1 + \sqrt{E_s}\sin\frac{(2n-1)\pi}{M}\mathbf{x}_2 \tag{6.97}$$

where $\mathbf{x}_1$ and $\mathbf{x}_2$ are two-dimensional basis vectors given in (2.60).

The MPSK signal space is shown in Figure 6.26 for the cases $M = 4$ and $M = 8$. Customarily, the in-phase channel, represented by the basis vector $\mathbf{x}_1$, is denoted as the I-channel, and the quadrature channel, represented by $\mathbf{x}_2$, is denoted as the Q-channel. Symbols $d_0 d_1 \cdots d_{k-1}$ are assigned an I-value and a Q-value via Gray code, that is, adjacent symbols differ by only one bit. Signal levels are commonly normalized to $\sqrt{E_s}$. Tables 6.4 and 6.5 show the symbol mapping for QPSK and 8PSK

Table 6.5 8PSK symbol mapping

Symbol number n	Input bits $d_0\ d_1\ d_2$	I	Q
1	1 1 1	$+\cos\pi/8$	$+\sin\pi/8$
2	1 1 0	$+\sin\pi/8$	$+\cos\pi/8$
3	0 1 0	$-\sin\pi/8$	$+\cos\pi/8$
4	0 1 1	$-\cos\pi/8$	$+\sin\pi/8$
5	0 0 1	$-\cos\pi/8$	$-\sin\pi/8$
6	0 0 0	$-\sin\pi/8$	$-\cos\pi/8$
7	1 0 0	$+\sin\pi/8$	$-\cos\pi/8$
8	1 0 1	$+\cos\pi/8$	$-\sin\pi/8$

Power spectral density

Using the I-Q representation in (6.89), we can write the MPSK signal for an infinite sequence of symbols as follows:

$$s(t) = \sum_{i=-\infty}^{\infty} \cos\frac{(2D_i - 1)\pi}{M} Ap(t - iT_s)\cos 2\pi f_c t - \sum_{i=-\infty}^{\infty} \sin\frac{(2D_i - 1)\pi}{M} Ap(t - iT_s)\sin 2\pi f_c t \tag{6.98}$$

where $D_i \in \{1, 2, \ldots, M\}$ represents the ith symbol in the symbol stream. Let $s_L(t)$ be the complex envelope of $s(t)$, then

$$s(t) = A\,\mathrm{Re}\{s_L(t)\mathrm{e}^{\mathrm{j}2\pi f_c t}\} \tag{6.99}$$

where

$$s_L(t) = \sum_{i=-\infty}^{\infty} \cos\frac{(2D_i - 1)\pi}{M} p(t - iT_s) + \mathrm{j}\sum_{i=-\infty}^{\infty} \sin\frac{(2D_i - 1)\pi}{M} p(t - iT_s) \tag{6.100}$$

The power spectral density $S(f)$ of the MPSK signal $s(t)$ can be evaluated as

$$S(f) = \frac{A^2}{4}[S_L(f - f_c) + S_L(f + f_c)] \tag{6.101}$$

where $S_L(f)$ is the power spectral density of the complex envelope $s_L(t)$, which is the sum of the power spectral density $S_{L,I}(f)$ of the in-phase (real) component and the power spectral density $S_{L,Q}(f)$ of the quadrature (imaginary) component of $s_L(t)$. Both $S_{L,I}(f)$ and $S_{L,Q}(f)$ can be evaluated according to the expression (6.85), which is displayed here for clarity:

$$S_{L,I}(f) = \frac{\sigma_I^2}{T_s}|P(f)|^2 + \left(\frac{\mu_I}{T_s}\right)^2 \sum_{k=-\infty}^{\infty} \left|P\left(\frac{k}{T_s}\right)\right|^2 \delta\left(f - \frac{k}{T_s}\right) \tag{6.102}$$

$$S_{L,Q}(f) = \frac{\sigma_Q^2}{T_s}|P(f)|^2 + \left(\frac{\mu_Q}{T_s}\right)^2 \sum_{k=-\infty}^{\infty} \left|P\left(\frac{k}{T_s}\right)\right|^2 \delta\left(f - \frac{k}{T_s}\right) \tag{6.103}$$

where $P(f)$ is the Fourier transform of the pulse shape $p(t)$, μ_I and μ_Q are the mean values of the $M/2$ signal levels $\cos(2D_i - 1)\pi/M$ and $\sin(2D_i - 1)\pi/M$, respectively, and σ_I^2 and σ_Q^2 are the corresponding variances. Since the $M/2$ signal levels are symmetrical around zero, $\mu_I = \mu_Q = 0$. With each of the $M/2$ signal levels assumes a probability of $2/M$, the variances σ_I^2 and σ_Q^2 are

$$\sigma_I^2 = \frac{2}{M}\sum_{n=1}^{M/2} \cos^2 \frac{(2n-1)\pi}{M} = \frac{1}{2} \tag{6.104}$$

$$\sigma_Q^2 = \frac{2}{M}\sum_{n=1}^{M/2} \sin^2 \frac{(2n-1)\pi}{M} = \frac{1}{2} \tag{6.105}$$

Substituting $\mu_I = \mu_Q = 0$ and $\sigma_I^2 = \sigma_Q^2 = 1/2$ into (6.102) and (6.103), we get

$$S_{L,I}(f) = S_{L,Q}(f) = \frac{|P(f)|^2}{2T_s} \tag{6.106}$$

Therefore, the power spectral density $S_L(f)$ of the complex envelope is given by

$$S_L(f) = S_{L,I}(f) + S_{L,Q}(f) = \frac{|P(f)|^2}{T_s} \tag{6.107}$$

Consequently, the MPSK power spectral density is obtained by substituting (6.107) into (6.101). Figure 6.27 shows the power spectral density of an MPSK signal with unit

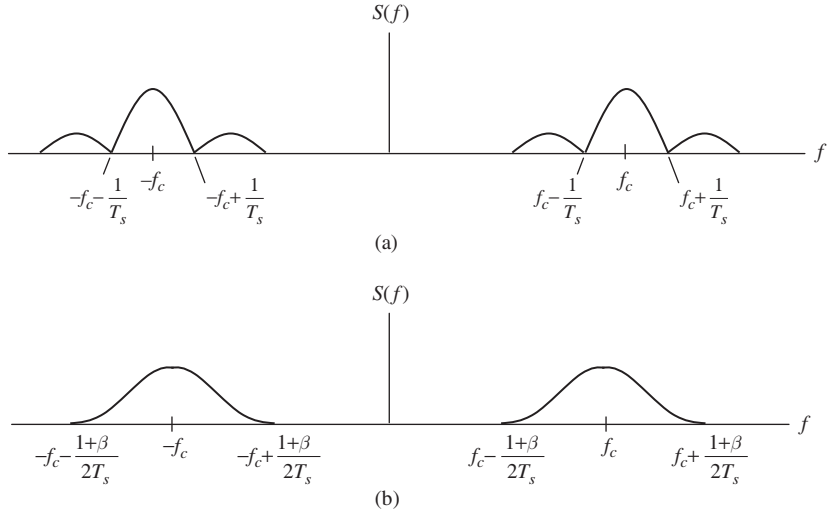

Figure 6.27 Power spectral density of MPSK: (a) squared pulse shape; (b) raised-cosine pulse shape.

amplitude squared pulse and with raised-cosine pulse. The latter has $P(f)$ given in (6.17) with T_s replacing T_b, and the former has $|P(f)| = |T_s \sin \pi f T_s / \pi f T_s|$ (see Table 2.2). It is clear from (6.87) and (6.107) that MPSK and MASK have the same spectral efficiency, namely, $r = k/(1+\beta)$ bits/s/Hz for a raised-cosine pulse shape, which is between $k/2$ and k bits/s/Hz.

From the power efficiency point of view we observe that the minimum Euclidean distance (or minimum signal separation) for MPSK is $2\sqrt{E_s} \sin \pi/M$ per (2.91), which gets smaller with increasing M. This in turn requires more power for a larger M. Obviously, MPSK is a modulation that trades power efficiency for bandwidth efficiency. Of particular interest is QPSK, the most widely used digital modulation. The minimum Euclidean distance for QPSK is $2\sqrt{E_s/2} = 2\sqrt{E_b}$, since $E_s = 2E_b$, where E_b is the bit energy. Thus, QPSK has the same minimum Euclidean distance as PSK, suggesting that QPSK is as power efficient as PSK. This is reinforced by the fact that a QPSK signal is a superposition of two orthogonal PSK signals as viewed by (6.96). Thus, if QPSK can be detected as two orthogonal PSK signals, the performance would be identical to PSK. On the other hand, the spectral efficiency of QPSK is twice that of PSK. This is certainly a rare combination.

Modulator

MPSK can be implemented by the I-Q modulator shown in Figure 6.28. The binary data in bits are shifted with rate $1/T_b$ into a serial-to-parallel converter (demultiplexer). The k outputs form a symbol with the symbol rate $1/T_s = 1/kT_b$. Each symbol $d_0 d_1 \cdots d_{k-1}$ is mapped into the I- and Q-levels that determine the amplitudes of the I- and Q-pulse shape $p(t)$. The I-pulse modulates the in-phase carrier $\cos 2\pi f_c t$, while the Q-pulse modulates the quadrature carrier $-\sin 2\pi f_c t$. The two signals are added to form the MPSK signal.

Offset quadrature phase shift keying (OQPSK)

This is a variation of QPSK where the quadrature component of QPSK is delayed by a bit time T_b with respect to the in-phase component. In QPSK, a phase change at the symbol transition can be 0°, ±90°, or 180°. For example, from Figure 6.26(a), a phase change of 90° occurs when symbol 01 succeeds 11, −90° when 10 succeeds 11, 180° when 00 succeeds 11, and 0° when another 11 succeeds 11. In some applications where a highly nonlinear power amplifier is employed, the large swing of phase (180°) can cause the sidelobes of the

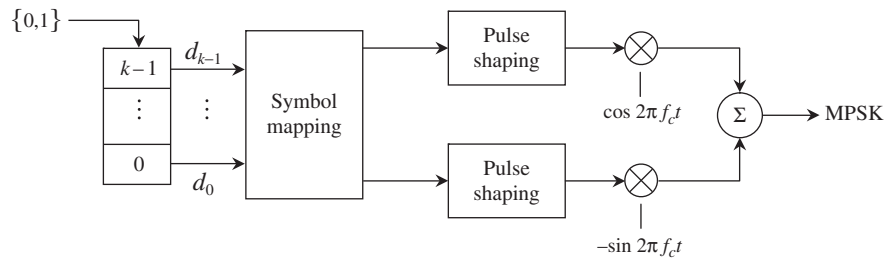

Figure 6.28 I-Q modulator for MPSK.

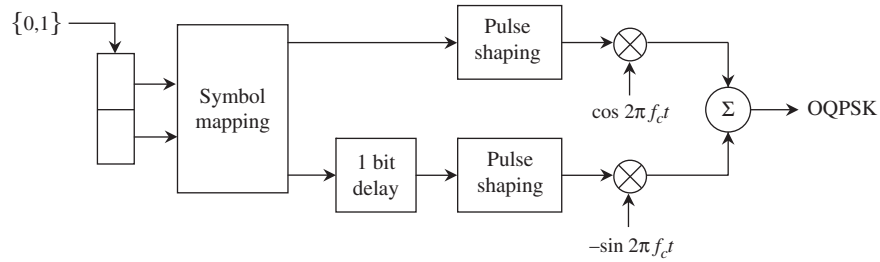

Figure 6.29 OQPSK modulator.

QPSK spectrum to regrow even if the signal is pre-filtered to suppress the sidelobes. This can cause interference to adjacent channels. Since post-filtering at the output of an RF power amplifier is not practical due to a high filter insertion loss (the filter bandwidth is normally very small compared to the carrier frequency), OQPSK might be employed to reduce sidelobe regrowth. The staggering of I and Q components implies that only one bit in a symbol can be succeeded by the next bit. If Gray code is used in symbol mapping, the phase changes can only occur with 0° and ±90°. Thus, the phase change of 180° is eliminated and the sidelobe regrowth can be reduced. The OQPSK modulator is shown in Figure 6.29. Note the similarity between OQPSK modulator and pre-coded MSK modulator in Figure 6.22. Pre-coded MSK can be viewed as OQPSK with sinusoidal weighted pulse shapes.

Example 6.27 Complex envelope of QPSK and OQPSK

In this example, we examine the real part (I-channel) and imaginary part (Q-channel) of the complex envelope of both QPSK and OQPSK and how the phase changes at the symbol transition. For comparison purposes, we index the time in bit interval T_b instead of the symbol time $T_s = 2T_b$ because the I-channel and the Q-channel of OQPSK are staggered by T_b. We also assume a unit amplitude squared pulse shape $p(t)$ of duration T_s. For clarity purposes, we normalize the I and Q outputs to unity. The delayed Q-output is denoted as Q_{OQPSK}, The input data bit at time index i, that is, $iT_b \le t < (i+1)T_b$, is denoted as d_i. Figure 6.30 shows the I- and Q-channel waveforms for both QPSK and OQPSK for the following data bits:

i	d_i	I	Q	Q_{OQPSK}	QPSK phase	OQPSK phase
0	1	+1	−1		$7\pi/4$	
1	0	+1	−1	−1		$7\pi/4$
2	1	+1	+1	−1	$\pi/4$	$7\pi/4$
3	1	+1	+1	+1		$\pi/4$
4	0	−1	−1	+1	$5\pi/4$	$3\pi/4$
5	0	−1	−1	−1		$5\pi/4$
6	0	−1	+1	−1	$3\pi/4$	$5\pi/4$
7	1	−1	+1	+1		$3\pi/4$
8	1	+1	+1	+1	$\pi/4$	$\pi/4$
9	1	+1	+1	+1		$\pi/4$
				+1		

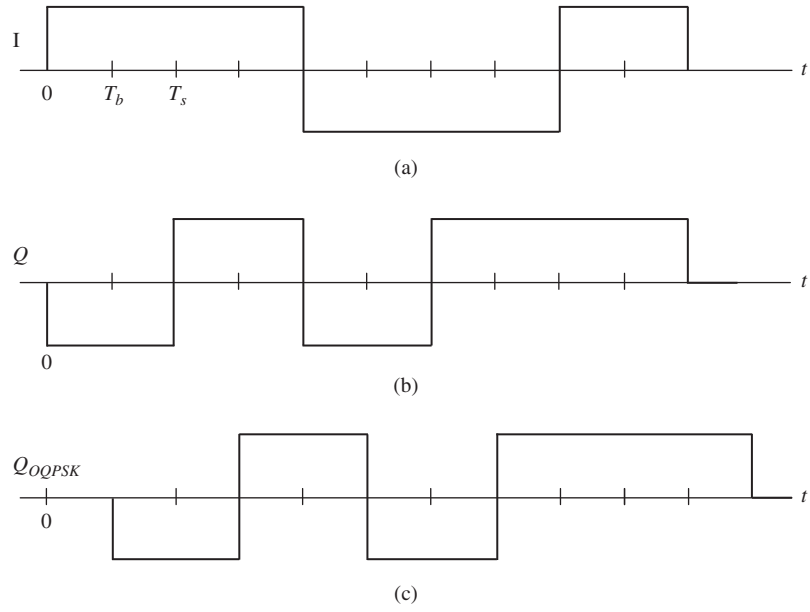

Figure 6.30 I- and Q-channel waveforms for QPSK and OQPSK.

Note that QPSK can change phase every symbol time, while OQPSK can only change phase every bit time (from the result of a change in either the I or Q bit, but not both). Despite switching phase every bit interval, OQPSK is still a superposition of two orthogonal PSK signals. Therefore, its power spectral density is still the same as that of QPSK.

■

6.12 Differential M-ary phase shift keying (DMPSK)

The use of absolute phase encoding in MPSK requires coherent demodulation at the receiver. The carrier phase must be extracted from the received MPSK signal by a carrier recovery circuit that inherently introduces M-fold phase ambiguity $2\pi i/M$ radians, $i = 1, 2, \ldots, M$. This results in a rotation of the signal points in the signal space by multiples of $2\pi/M$ radians and data symbols (hence, bits) will be demodulated incorrectly. Note that MPSK signal space has an M-fold symmetry, that is, the signal space remains unchanged with the rotation of $2\pi i/M$ radians for $i = 1, 2, \ldots, M$. Differential encoding of MPSK can resolve the phase ambiguity. Furthermore, it also allows noncoherent demodulation to be carried out in applications where coherent demodulation is not feasible.

The DMPSK signal $s(t)$ over a symbol time $T_s = kT_b = (\log_2 M)T_b$ and the recursive encoding rule are given by

Table 6.6 Differential encoding for DQPSK

Symbol D_i	Binary inputs $d_{I,i}\, d_{Q,i}$	$\theta_i - \theta_{i-1}$
1	0 0	0
2	1 0	$\pi/2$
3	1 1	π
4	0 1	$3\pi/2$

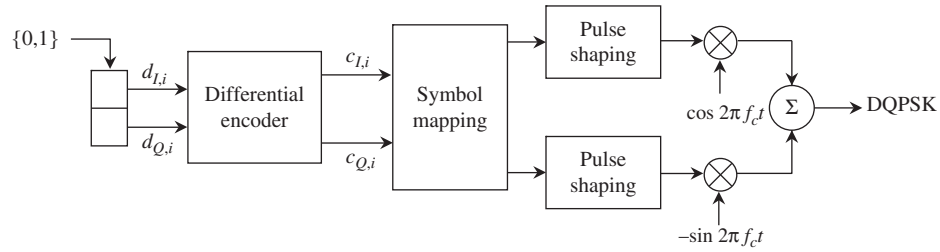

Figure 6.31 DQPSK modulator.

$$s(t) = Ap(t)\cos(2\pi f_c t + \theta_i) \tag{6.108}$$

$$\theta_i = \theta_{i-1} + (D_i - 1)\frac{2\pi}{M}, \qquad D_i \in \{1, 2, \ldots, M\} \tag{6.109}$$

where $p(t)$ is the pulse shape, D_i represents the ith symbol in the data stream, and θ_i and θ_{i-1} are the phases of the ith symbol and the previous $(i-1)$th symbol, respectively. Note that in the case of DPSK ($M = 2$) we have $D_i \in \{1, 2\}$, and $D_i - 1 = d_i \in \{0, 1\}$ is simply the ith data bit, per (6.25). Table 6.6 illustrates the differential encoding in (6.109) for DQPSK, which, in practice, can also be implemented via the following logical expressions:

$$c_{I,i} = \overline{(d_{I,i} \oplus d_{Q,i})}(c_{I,i-1} \oplus d_{Q,i}) \oplus (d_{I,i} \oplus d_{Q,i})(d_{I,i} \oplus c_{Q,i-1}) \tag{6.110}$$

$$c_{Q,i} = \overline{(d_{I,i} \oplus d_{Q,i})}(d_{I,i} \oplus c_{Q,i-1}) \oplus (d_{I,i} \oplus d_{Q,i})(c_{I,i-1} \oplus d_{Q,i}) \tag{6.111}$$

where the subscripts (I, i) and (Q, i) represent the ith bit in the in-phase and quadrature bit streams, respectively. Figure 6.31 shows a DQPSK modulator which consists of a differential encoder and a QPSK modulator.

Example 6.28 Differential encoding for DQPSK

In this example, we illustrate the differential encoding process for DQPSK by considering a data stream over five symbol times, which are indexed as $i = 0, 1, 2, 3, 4$. The mapping of $c_{I,i}$ and $c_{Q,i}$ into phase θ_i is carried out via Figure 6.26(a) and Table 6.6. The input symbol D_i with its binary representation $d_{I,i}d_{Q,i}$ produces the same $\theta_i - \theta_{i-1} \pmod{2\pi}$ via Table 6.6.

i	D_i	$d_{I,i}$	$d_{Q,i}$	$c_{I,i}$	$c_{Q,i}$	θ_i	$\theta_i - \theta_{i-1} \pmod{2\pi}$
0	1	0	0	0	0	$5\pi/4$	
1	4	0	1	0	1	$3\pi/4$	$3\pi/2$
2	2	1	0	0	0	$5\pi/4$	$\pi/2$
3	1	0	0	0	0	$5\pi/4$	0
4	3	1	1	1	1	$\pi/4$	π

■

Alternative differential encoding for DQPSK

Differential encoding rules are not unique. There are many ways of assigning binary inputs $d_{I,i}d_{Q,i}$ to a symbol D_i, which can lead to alternative encoding equations to (6.110) and (6.111). Table 6.7 shows an alternative rule which leads to the following logical implementation:

$$c_{I,i} = \overline{(d_{I,i} \oplus d_{Q,i})}(d_{I,i} \oplus c_{I,i-1}) \oplus (d_{I,i} \oplus d_{Q,i})(d_{Q,i} \oplus c_{Q,i-1}) \tag{6.112}$$

$$c_{Q,i} = \overline{(d_{I,i} \oplus d_{Q,i})}(d_{I,i} \oplus c_{Q,i-1}) \oplus (d_{I,i} \oplus d_{Q,i})(d_{I,i} \oplus c_{I,i-1}) \tag{6.113}$$

Example 6.29 Alternative differential encoding for DQPSK
Using (6.112) and (6.113), we perform the differential encoding using the mapping in Figure 6.26(a) and Table 6.7. It can be seen that the encoding rule in Table 6.7 is entirely equivalent to (6.112) and (6.113).

i	D_i	$d_{I,i}$	$d_{Q,i}$	$c_{I,i}$	$c_{Q,i}$	θ_i	$\theta_i - \theta_{i-1} \pmod{2\pi}$
0	4	1	1	1	1	$\pi/4$	
1	3	1	0	1	0	$7\pi/4$	$3\pi/2$
2	2	0	1	1	1	$\pi/4$	$\pi/2$
3	3	1	0	1	0	$7\pi/4$	$3\pi/2$
4	2	0	1	1	1	$\pi/4$	$\pi/2$
5	4	1	1	0	0	$5\pi/4$	π
6	3	1	0	0	1	$3\pi/4$	$3\pi/2$
7	1	0	0	0	1	$3\pi/4$	0

■

Table 6.7 Alternative differential encoding for DQPSK

Symbol D_i	Binary inputs $d_{I,i}\, d_{Q,i}$	$\theta_i - \theta_{i-1}$
1	0 0	0
2	0 1	$\pi/2$
3	1 0	$3\pi/2$
4	1 1	π

Direct symbol mapping

Instead of performing differential encoding and symbol mapping separately, the two operations can be combined into one, that is, the symbol $D_i \in \{1, 2, \ldots, M\}$ can be mapped directly into the I-level and Q-level. The DMPSK signal in (6.108) can be written in I-Q form as follows:

$$\begin{aligned} s(t) &= (\cos\theta_i)Ap(t)\cos 2\pi f_c t - (\sin\theta_i)Ap(t)\sin 2\pi f_c t \\ &= \left(\sqrt{E_s}\cos\theta_i\right)x_1(t) + \left(\sqrt{E_s}\sin\theta_i\right)x_2(t) \\ &= I_i x_1(t) + Q_i x_2(t) \end{aligned} \tag{6.114}$$

where E_s is the symbol energy, $x_1(t)$ and $x_2(t)$ are the two basis functions in (6.90) and (6.91), and I_i and Q_i are the ith symbol's I-level and Q-level, respectively, which are given by

$$I_i = \sqrt{E_s}\cos\theta_i \tag{6.115}$$

$$Q_i = \sqrt{E_s}\sin\theta_i \tag{6.116}$$

Substituting (6.109) into (6.115) and (6.116), we obtain the direct symbol mapping rule

$$I_i = I_{i-1}\cos\Delta\theta_i - Q_{i-1}\sin\Delta\theta_i \tag{6.117}$$

$$Q_i = I_{i-1}\sin\Delta\theta_i + Q_{i-1}\cos\Delta\theta_i \tag{6.118}$$

where $I_{i-1} = \sqrt{E_s}\cos\theta_{i-1}$ and $Q_{i-1} = \sqrt{E_s}\sin\theta_{i-1}, \Delta\theta_i = \theta_i - \theta_{i-1} = (D_i - 1)(2\pi/M)$.

Modulator

Figure 6.32 presents two implementations of DMPSK, one via differential encoding then symbol mapping, and one via direct symbol mapping.

DMPSK belongs to the family of MPSK; therefore, it has the same power spectral density as MPSK.

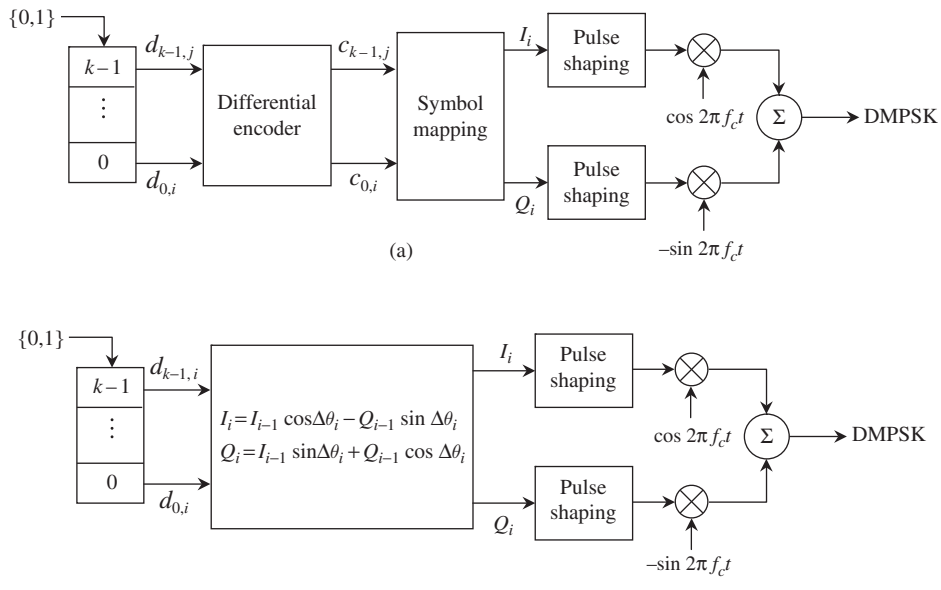

Figure 6.32 (a) DMPSK modulator via separate differential encoding and symbol mapping for $M = 4$. (b) DMPSK modulator via direct symbol mapping with $\Delta\theta_i = (D_i - 1)\, 2\pi/M$.

6.13 π/4-shifted differential quadrature phase shift keying (π/4-DQPSK)

In applications that require the control of adjacent channel interference, it is imperative to employ modulation techniques that are immune to the regrowth of the out-of-band (or sidelobes) portion of the power spectral density as the signal is amplified by a nonlinear power amplifier. Furthermore, in a fading channel, many applications may require noncoherent demodulation. DQPSK can be noncoherently demodulated, but cannot meet the first requirement because the maximum phase change between symbols is 180°. On the other hand, OQPSK has a maximum phase change of 90° and meets the first requirement but cannot be noncoherently demodulated. π/4-DQPSK offers a compromise between OQPSK and DQPSK. It can be noncoherently demodulated and has a maximum phase change of 135° between symbols, hence limiting spectral regrowth in a nonlinear channel.

The π/4-DQPSK signal over an arbitrary symbol time $T_s = 2T_b$ and the recursive encoding rule are given by

$$s(t) = Ap(t)\cos(2\pi f_c t + \theta_i) \tag{6.119}$$

$$\theta_i = \theta_{i-1} + (2D_i - 1)\frac{\pi}{4}, \quad D_i \in \{1, 2, 3, 4\} \tag{6.120}$$

Table 6.8 Differential encoding for $\pi/4$-DQPSK

Symbol D_i	Binary inputs $d_{I,i}\ d_{Q,i}$	$\Delta\theta_i = \theta_i - \theta_{i-1}$
1	0 0	$\pi/4$
2	0 1	$3\pi/4$
3	1 1	$5\pi/4$
4	1 0	$7\pi/4$

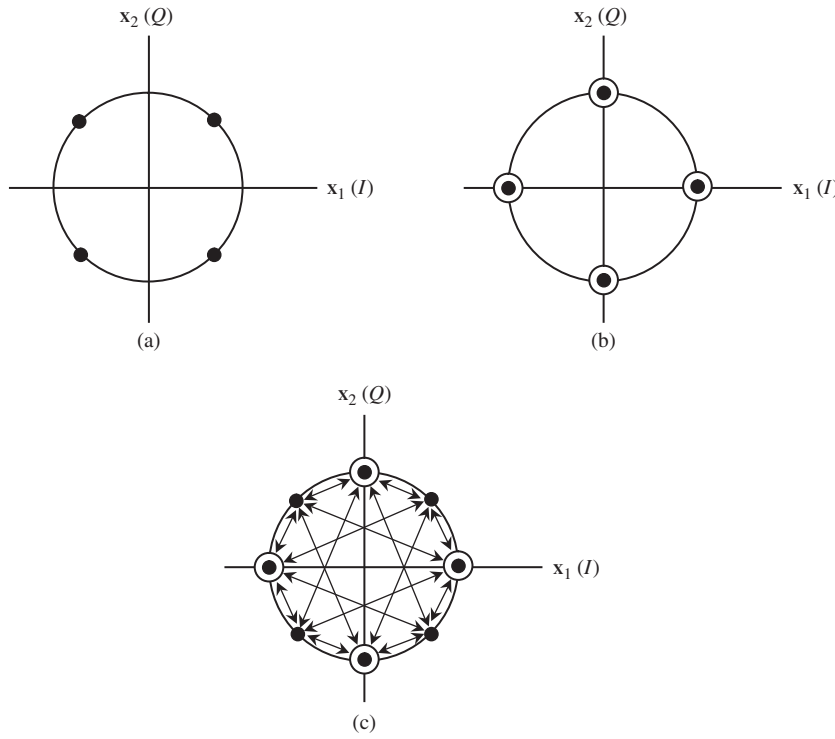

Figure 6.33 (a) Signal space for even symbol; (b) signal space for odd symbol; (c) signal space for two consecutive symbols.

where $p(t)$ is the pulse shape, D_i represents the ith symbol in the data stream, and θ_i and θ_{i-1} are the phases of the ith symbol and the previous $(i-1)th$ symbol, respectively. The differential encoding rule for $\pi/4$-DQPSK is shown in Table 6.8.

Signal space

The study of DQPSK indicates that a phase change in multiples of $\pi/2$ radians or 90° occurs between two consecutive symbols. Thus, the signal space for DQPSK is the same as that of QPSK (Figure 6.26(a)). On the other hand, a phase change in odd-multiples of $\pi/4$ radians or 45° occurs in consecutive symbols in $\pi/4$-DQPSK. This forces consecutive symbols to alternate between two signal spaces as shown in Figure 6.33(a) for the ith symbol in the

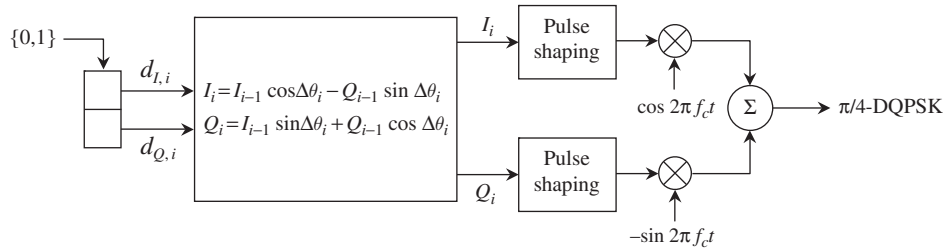

Figure 6.34 π/4-DQPSK modulator.

symbol stream where the time index i is even (even symbols) and Figure 6.33(b) for odd symbols. The superposition of the even and odd symbol signal spaces in Figure 6.33(c) provides a single signal space for any two consecutive symbols.

The signal levels for both I- and Q-channels can now take on five values, namely, 0, $\pm\sqrt{2}/2$, ± 1 (for QPSK and DQPSK, there are only two I- and Q-values, namely, $\pm\sqrt{2}/2$).

Direct symbol mapping

In this section we present the mapping of symbols $D_i \in \{1, 2, 3, 4\}$ (see Table 6.8) into the I-value and the Q-value. Following the analysis of DMPSK, the direct symbol mapping rule can be obtained from (6.117) and (6.118), with $\Delta\theta_i = (2D_i - 1)\pi/4$ replacing $\Delta\theta_i = (D_i - 1)2\pi/M$:

$$I_i = I_{i-1}\cos\left[(2D_i - 1)\frac{\pi}{4}\right] - Q_{i-1}\sin\left[(2D_i - 1)\frac{\pi}{4}\right] \tag{6.121}$$

$$Q_i = I_{i-1}\sin\left[(2D_i - 1)\frac{\pi}{4}\right] + Q_{i-1}\cos\left[(2D_i - 1)\frac{\pi}{4}\right] \tag{6.122}$$

The $\pi/4$-DQPSK modulator is shown in Figure 6.34.

Example 6.30 Direct symbol mapping

In this example we illustrate the differential encoding of π/4-DQPSK via Table 6.8 and the direct symbol mapping via the rule given in (6.121) and (6.122). The results are identical for both approaches. The sequence of symbols is selected to be $D_i = 3, 2, 4, 1, 3 \hat{=} 11, 01, 10, 00, 11$. The I-level and Q-level are both normalized to $\sqrt{E_s}$. The initial symbol $D_0 = 3 = 11$ serves as a reference symbol for the encoding process. We assign an initial phase $\theta_0 = 5\pi/4$ radians, and $I_0 = -\sqrt{2}/2$ and $Q_0 = -\sqrt{2}/2$. Using $s(t) = Ap(t)\cos(2\pi f_c t + \theta_i) = Ap(t)[\cos\theta_i]\cos 2\pi f_c t - Ap(t)[\sin\theta_i]\sin 2\pi f_c t$ in (6.114)–(6.116) we get

1. $I_0 = \cos\dfrac{5\pi}{4} = -\dfrac{\sqrt{2}}{2}, \quad Q_0 = \sin\dfrac{5\pi}{4} = -\dfrac{\sqrt{2}}{2}$

2. $I_1 = I_0 \cos\frac{3\pi}{4} - Q_0 \sin\frac{3\pi}{4} = \left(-\frac{\sqrt{2}}{2}\right)\left(-\frac{\sqrt{2}}{2}\right) - \left(-\frac{\sqrt{2}}{2}\right)\left(\frac{\sqrt{2}}{2}\right) = \frac{1}{2} + \frac{1}{2} = 1$

$Q_1 = I_0 \sin\frac{3\pi}{4} + Q_0 \cos\frac{3\pi}{4} = \left(-\frac{\sqrt{2}}{2}\right)\left(\frac{\sqrt{2}}{2}\right) + \left(-\frac{\sqrt{2}}{2}\right)\left(-\frac{\sqrt{2}}{2}\right) = \frac{1}{2} - \frac{1}{2} = 0$

3. $I_2 = I_1 \cos\frac{7\pi}{4} - Q_1 \sin\frac{7\pi}{4} = (1)\left(\frac{\sqrt{2}}{2}\right) - (0)\left(-\frac{\sqrt{2}}{2}\right) = \frac{\sqrt{2}}{2}$

$Q_2 = I_1 \sin\frac{7\pi}{4} + Q_1 \cos\frac{7\pi}{4} = (1)\left(-\frac{\sqrt{2}}{2}\right) + (0)\left(\frac{\sqrt{2}}{2}\right) = -\frac{\sqrt{2}}{2}$

4. $I_3 = I_2 \cos\frac{\pi}{4} - Q_2 \sin\frac{\pi}{4} = \left(\frac{\sqrt{2}}{2}\right)\left(\frac{\sqrt{2}}{2}\right) - \left(-\frac{\sqrt{2}}{2}\right)\left(\frac{\sqrt{2}}{2}\right) = \frac{1}{2} + \frac{1}{2} = 1$

$Q_3 = I_2 \sin\frac{\pi}{4} + Q_2 \cos\frac{\pi}{4} = \left(\frac{\sqrt{2}}{2}\right)\left(\frac{\sqrt{2}}{2}\right) + \left(-\frac{\sqrt{2}}{2}\right)\left(\frac{\sqrt{2}}{2}\right) = \frac{1}{2} - \frac{1}{2} = 0$

5. $I_4 = I_3 \cos\frac{5\pi}{4} - Q_3 \sin\frac{5\pi}{4} = (1)\left(-\frac{\sqrt{2}}{2}\right) - (0)\left(-\frac{\sqrt{2}}{2}\right) = -\frac{\sqrt{2}}{2}$

$Q_4 = I_3 \sin\frac{5\pi}{4} + Q_3 \cos\frac{5\pi}{4} = (1)\left(-\frac{\sqrt{2}}{2}\right) + (0)\left(-\frac{\sqrt{2}}{2}\right) = -\frac{\sqrt{2}}{2}$

					$\Delta\theta_i = \theta_i - \theta_{i-1} = (2D_i - 1)$		
i	D_i	$d_{I,i}$	$d_{Q,i}$	θ_i	$\pi/4 \pmod{2\pi}$	I_i	Q_i
0	3	1	1	$5\pi/4$	$5\pi/4$	$-\sqrt{2}/2$	$-\sqrt{2}/2$
1	2	0	1	0	$3\pi/4$	1	0
2	4	1	0	$7\pi/4$	$7\pi/4$	$\sqrt{2}/2$	$-\sqrt{2}/2$
3	1	0	0	0	$\pi/4$	1	0
4	3	1	1	$5\pi/4$	$5\pi/4$	$-\sqrt{2}/2$	$-\sqrt{2}/2$

■

Example 6.31 IS-136 cellular standard [28]

This North American digital cellular standard employs time division multiple access (TDMA) for channel allocation and is backward compatible with AMPS in terms of the carrier bandwidth (30 kHz) and frequency spectra (824–849 MHz for reverse channels and 869–894 MHz for forward channels). The modulation is $\pi/4$-DQPSK. The TDMA forward and reverse channel data rate is 48.6 kbps, which yields a spectral efficiency of 48.6 kbps/30 kHz = 1.62 bps/Hz. Each 30 MHz TDMA channel accommodates three full-rate users (encoded speech of 7.95 kbps) or six half-rate users (3.975 kbps).

■

6.14 M-ary quadrature amplitude modulation (MQAM)

Although MPSK can provide high spectral efficiency for many narrowband applications involving nonlinear power amplifiers that require constant amplitude modulation, MPSK is not power efficient for large M. The closely packed signal symbols on a circle of radius $\sqrt{E_s}$, where E_s is the symbol energy; lead to a small Euclidean distance between adjacent signal symbols and make them vulnerable to errors caused by noise. If the signal symbols can be placed throughout the two-dimensional signal space instead of being on a circle, power efficiency can be improved. Obviously, signal symbols must have different amplitudes and different phases. Such modulation techniques are called MQAM and are widely used in digital terrestrial microwave links, Internet communication via twisted-pair telephone wires, and in wireless local area networks (WLAN) such as IEEE 802.11a,g [7,8] and IEEE 802.16.

MQAM employs a set of $M = 2^k$ non-constant amplitude and finite energy signals to represent M distinct symbols numbered $n = 1, 2, \ldots, M$. A symbol is represented by $k = \log_2 M$ bits $d_0 d_1 \ldots d_{k-1}$ as follows:

$$s_n(t) = A_n p(t) \cos(2\pi f_c t + \theta_n), \qquad n = 1, 2, \ldots, M \tag{6.123}$$

where $p(t)$ is the pulse shape of a symbol, $\cos 2\pi f_c t$ is the carrier, and A_n and θ_n represent the amplitude and phase of the nth symbol, respectively. The symbol time is denoted as T_s, hence the symbol rate is $1/T_s$, which is $1/k$ times the bit rate $1/T_b$, where T_b is the bit time ($T_b = T_s/k$).

Signal space

The MQAM signal can be expressed in the I-Q representation as

$$\begin{aligned} s(t) &= (\cos\theta_n) A_n p(t) \cos 2\pi f_c t - (\sin\theta_n) A_n p(t) \sin 2\pi f_c t \\ &= (\alpha_n \cos\theta_n) A p(t) \cos 2\pi f_c t - (\alpha_n \sin\theta_n) A p(t) \sin 2\pi f_c t \end{aligned} \tag{6.124}$$

where $\alpha_n = A_n/A$ is the normalized signal amplitude, and A is the smallest signal amplitude. The two orthonormal basis functions $x_1(t)$ and $x_2(t)$ are given as

$$x_1(t) = \frac{A}{\sqrt{E}} p(t) \cos 2\pi f_c t \tag{6.125}$$

$$x_2(t) = -\frac{A}{\sqrt{E}} p(t) \sin 2\pi f_c t \tag{6.126}$$

where E is the smallest symbol energy, defined as

$$E = \int_{-\infty}^{\infty} [Ap(t) \cos 2\pi f_c t]^2 \mathrm{d}t = \int_{-\infty}^{\infty} [Ap(t) \sin 2\pi f_c t]^2 \mathrm{d}t \tag{6.127}$$

The orthogonality of $x_1(t)$ and $x_2(t)$ was given in (6.93)–(6.95). Thus, it is seen that the signal energy E_n of a particular signal $s_n(t) = \alpha_n Ap(t)\cos(2\pi f_c t + \theta_n)$ is

$$E_n = \int_{-\infty}^{\infty} s_n^2(t)\mathrm{d}t = \alpha_n^2 E \tag{6.128}$$

Using the basis functions $x_1(t)$ and $x_2(t)$ we can express $s_n(t)$ as follows:

$$s_n(t) = \sqrt{E}(\alpha_n \cos\theta_n)x_1(t) + \sqrt{E}(\alpha_n \sin\theta_n)x_2(t) \tag{6.129}$$

In terms of vectors, we have

$$s_n = \begin{bmatrix} \sqrt{E}(\alpha_n \cos\theta_n) \\ \sqrt{E}(\alpha_n \sin\theta_n) \end{bmatrix} = \sqrt{E}(\alpha_n \cos\theta_n)\mathbf{x}_1 + \sqrt{E}(\alpha_n \sin\theta_n)\mathbf{x}_2 \tag{6.130}$$

where $\mathbf{x}_1$ and $\mathbf{x}_2$ are the two-dimensional basis vectors given in (2.60). Equation (6.130) completely describes the signal space of MQAM. Figure 6.35 shows some popular signal spaces for MQAM. Both rectangular 16QAM and 64QAM are specified in the WLAN IEEE 802.11a,g standards [7,8] to be used as subcarrier modulation in orthogonal frequency division multiplexing (OFDM) (to be studied in Section 6.18).

Each symbol is assigned an I-level and a Q-level via Gray code, that is, adjacent symbols differ by only one bit. For a rectangular MQAM signal space, the signal levels are commonly normalized to $\sqrt{E}/\sqrt{2}$ so that the I-level is $I_n = \sqrt{2}\alpha_n \cos\theta_n$ and the Q-level is $Q_n = \sqrt{2}\alpha_n \sin\theta_n$ for the symbol represented by signal $\boldsymbol{s}_n$.

Tables 6.9 and 6.10 show the symbol mapping for rectangular 16QAM and 64QAM. For 16QAM, the first two bits d_0d_1 of the symbol $d_0d_1d_2d_3$ determine the I-value, and the last two bits d_2d_3 determine the Q-value. For 64QAM, the first three bits $d_0d_1d_2$ of the symbol $d_0d_1d_2d_3d_4d_5$ determine the I-value and the last three bits $d_3d_4d_5$ determine the Q-value.

Figure 6.36 illustrates the symbol mapping for 16QAM in Table 6.9. This procedure can be generalized to any rectangular MQAM with $M = 2^{2m}$.

Power spectral density

Using the I-Q representation, we can write the MQAM signal for an infinite sequence of symbols as follows:

$$s(t) = \sum_{i=-\infty}^{\infty} (\alpha_{D_i}\cos\theta_{D_i})Ap(t - iT_s)\cos 2\pi f_c t - \sum_{i=-\infty}^{\infty} (\alpha_{D_i}\sin\theta_{D_i})Ap(t - iT_s)\sin 2\pi f_c t \tag{6.131}$$

where $D_i \in \{1, 2, \ldots, M\}$ represents the ith symbol in the symbol stream. The I-Q representation in (6.131) can be transformed into the complex envelope representation as

$$s(t) = \frac{A}{\sqrt{2}}\mathrm{Re}\{s_L(t)\mathrm{e}^{\mathrm{j}2\pi f_c t}\} \tag{6.132}$$

where the complex envelope $s_L(t)$ is given by

Table 6.9 16QAM symbol mapping

Input bits $d_0\ d_1$	I	Input bits $d_2\ d_3$	Q
0 0	−3	0 0	−3
0 1	−1	0 1	−1
1 1	+1	1 1	+1
1 0	+3	1 0	+3

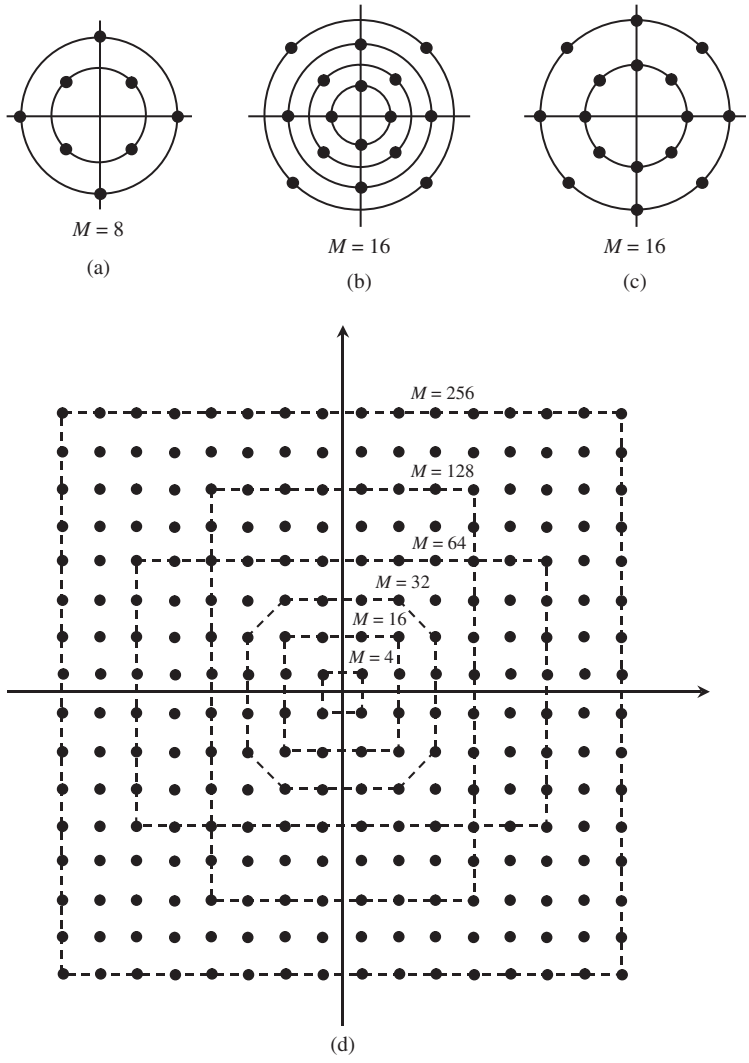

Figure 6.35 Various signal spaces for MQAM. The rectangular one is the most popular.

Table 6.10 64QAM symbol mapping

Input bits $d_0\ d_1\ d_2$	I	Input bits $d_3\ d_4\ d_5$	Q
0 0 0	−7	0 0 0	−7
0 0 1	−5	0 0 1	−5
0 1 1	−3	0 1 1	−3
0 1 0	−1	0 1 0	−1
1 1 0	+1	1 1 0	+1
1 1 1	+3	1 1 1	+3
1 0 1	+5	1 0 1	+5
1 0 0	+7	1 0 0	+7

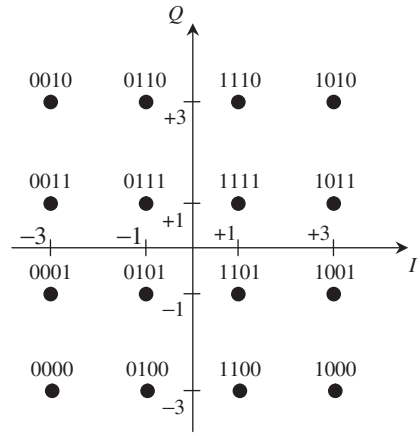

Figure 6.36 Gray encoding of 16QAM.

$$s_L(t) = \sum_{i=-\infty}^{\infty} \left(\sqrt{2}\alpha_{D_i} \cos\theta_{D_i}\right) p(t - iT_s) + \mathrm{j} \sum_{i=-\infty}^{\infty} \left(\sqrt{2}\alpha_{D_i} \sin\theta_{D_i}\right) p(t - iT_s) \quad (6.133)$$

The power spectral density of the MQAM signal $s(t)$ can be evaluated by (6.101). Following the procedure in Section 6.11, as indicated by (6.102) and (6.103), we need to evaluate μ_I, μ_Q, σ_I^2, and σ_Q^2. For symmetric signal spaces, we have $\mu_I = \mu_Q = 0$. The variances σ_I^2 and σ_Q^2 depend on particular signal spaces. For a rectangular MQAM with $M = 2^{2m}$ signal points, there are $\sqrt{M}$ normalized I-levels and $\sqrt{M}$ normalized Q-levels. These are $\pm 1, \pm 3, \ldots, \pm\left(\sqrt{M} - 1\right)$. Thus,

$$\begin{aligned} \sigma_I^2 &= \mathbf{E}\left\{I_{D_i}^2\right\} = \mathbf{E}\left\{2\alpha_{D_i}^2 \cos^2\theta_{D_i}\right\} \\ &= \frac{2}{\sqrt{M}}\left[1^2 + 3^2 + \cdots + \left(\sqrt{M} - 1\right)^2\right] \\ &= \frac{1}{3}(M - 1) \end{aligned} \quad (6.134)$$

Similarly,

$$\sigma_Q^2 = \frac{1}{3}(M-1) \tag{6.135}$$

Using (6.134) and (6.135) in (6.102) and (6.103), we obtain

$$S_{L,I}(f) = S_{L,Q}(f) = \frac{(M-1)|P(f)|^2}{3T_s} \tag{6.136}$$

Consequently, the power spectral density $S_L(f)$ of the complex envelope $s_L(t)$ is given by

$$S_L(f) = S_{L,I}(f) + S_{L,Q}(f) = \frac{2(M-1)|P(f)|^2}{3T_s} \tag{6.137}$$

The MQAM power spectral density can be obtained by substituting $S_L(f)$ into (6.101) and by noting that A is the smallest signal amplitude. By comparing (6.137) to (6.107) and (6.87), we conclude that MQAM, MPSK, and MASK have the same spectral efficiency. Their power spectral densities have the same shape but with different amplitudes. MQAM can be generated by the I-Q generator shown in Figure 6.28 for MPSK. The only difference is that the symbol mapping for MQAM generates non-constant symbol amplitudes.

Differential MQAM (DMQAM)

Recall from Section 6.12 that MPSK suffers an M-fold phase ambiguity. MQAM also has phase ambiguity, which depends on the shape of the signal space. The signal spaces in Figure 6.35 have 4-fold symmetry in (a), 4-fold symmetry in (b), 8-fold symmetry in (c), and 4-fold symmetry in (d). Any L-fold symmetrical signal space has L-fold phase ambiguity, which can be corrected by using differential encoding. The following rules can be employed for $L = 2^m$ [9,10]:

1. Partition the signal space into L symmetrical sectors. The first m bits $d_0 d_1 \ldots d_{m-1}$ of a k-bit symbol $d_0 d_1 \ldots d_{k-1}$ determine the change in sector.
2. The remaining $k-m$ bits $d_m d_{m+1} \ldots d_{k-1}$ determine the signal point in the sector. Note that each sector contains 2^{k-m} signal points which can be Gray encoded.

Differential encoding cannot preserve Gray code rule for the entire signal space. Therefore, it is obvious that DMQAM performance will not be as good as that of MQAM. On the other hand, data transmitted with MQAM must carry special codewords or pilot symbols to resolve L-fold ambiguity, hence increasing the overhead and reducing the system throughout.

Example 6.32 Differential encoding for D16QAM

Consider the 16QAM signal space shown in Figure 6.37. The four sectors are numbered I, II, III, and IV. The first two bits $d_0 d_1$ of a current 4-bit message symbol $d_0 d_1 d_2 d_3$ to be encoded for transmission (given the previous symbol as a reference) determine the sector. The last two bits $d_2 d_3$ of this current message symbol are employed to determine which of the four symbols in that sector the encoded symbol is. When $d_0 d_1$ is 00, the encoded symbol resides in the same

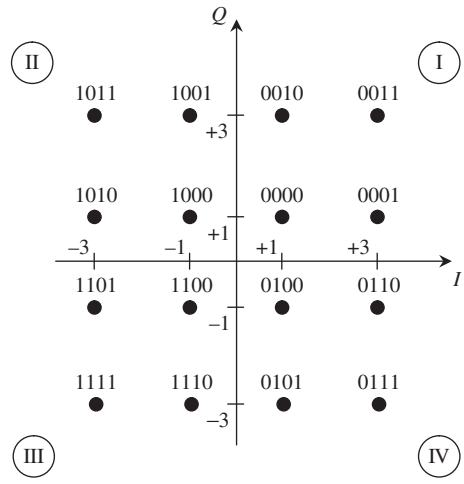

Figure 6.37 D16QAM signal space.

sector as the previously encoded symbol. When d_0d_1 is 10, the encoded symbol advances counterclockwise one sector. When d_0d_1 is 11, the encoded symbol advances counterclockwise two sectors. When d_0d_1 is 01, the encoded symbol advances counterclockwise three sectors. Using these rules, the message symbols 0000, 1101, 1001, 1100, 0011 are encoded as 0000, 1101, 0101, 1000, 1011. Note that 0000 is the reference symbol, and is selected arbitrarily. Also note that perfect Gray coding is not possible for all 16 signal points.

Time i	Message symbol	Sector	Encoded symbol	I	Q
0	0 0 0 0	I	0 0 0 0	1	1
1	1 1 0 1	III	1 1 0 1	−3	−1
2	1 0 0 1	IV	0 1 0 1	1	−3
3	1 1 0 0	II	1 0 0 0	−1	1
4	0 0 1 1	II	1 0 1 1	−3	3

■

6.15 Code shift keying (CSK)

From previous sections we have learned that modulation techniques with two-dimensional signal space, such as MPSK or MQAM, can boost their spectral efficiency tremendously at the expense of power efficiency. For applications where power is a premium resource, modulation techniques with M-dimensional signal space such as M-ary orthogonal modulation can be used. Two important such modulation techniques are *code shift keying*, which

will be presented in this section, and *M-ary frequency shift keying*, which will be addressed in Section 6.16.

CSK employs a set of $M = 2^k$ orthogonal sinusoidal *Walsh functions* to represent a set of M distinct k-bit symbols

$$s_n(t) = Aw_n(t)\cos 2\pi f_c t, \qquad n = 1, 2, \ldots, M \tag{6.138}$$

where $w_n(t)$ is the Walsh function in (2.52), A is the amplitude, and $\cos 2\pi f_c t$ is the carrier. The Walsh chip rate is $1/T_c$, where T_c is the Walsh chip time. Since there are M Walsh chips per symbol, $T_c = T_s/M$, where T_s is the symbol time. Furthermore, $T_s = kT_b$, where T_b is the bit time; therefore, the Walsh chip rate can be related to the bit rate as $1/T_c = (1/T_b)M/k$.

Power spectral density

Using (6.138), we can write a CSK waveform for an infinite sequence of symbols as follows:

$$s(t) = \sum_{i=-\infty}^{\infty} Aw_{D_i}(t)\,p(t - iT_s)\cos 2\pi f_c t \tag{6.139}$$

where $D_i \in \{1, 2, \ldots, M\}$ represent the ith symbol in the symbol stream and $p(t)$ is a squared pulse of unit amplitude and duration T_s. If we substitute (2.52) into (6.138), we obtain a stream of PSK waveforms clocking at the chip rate $1/T_c$. Therefore, the power spectral density of CSK is identical to that of PSK or DSB-AM given in (6.7), with T_c replacing T_b. Note that $1/T_c = (1/T_b)M/k$. Thus, CSK bandwidth is M/k times PSK bandwidth for a given bit rate.

Modulator

Generating CSK signals is quite straightforward from (6.139). The incoming bits are demultiplexed to form symbols, which are mapped to corresponding Walsh functions. The Walsh functions bi-phase modulate a carrier to form a CSK signal. The CSK modulator is shown in Figure 6.38.

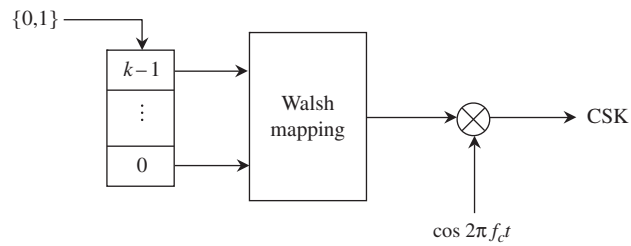

Figure 6.38 CSK modulator.

Example 6.33 IS-95 reverse channel [28]
The IS-95 reverse channel carries traffic from the mobile station to the base station in the 2G-CDMA cellular system. To provide noncoherent demodulation, CSK with 64 Walsh functions is employed. Data bits transmitted at rate 9.6 kbps (14.4 kbps) are encoded with a 1/3-rate (1/2-rate) convolutional code to provide a coded bit stream at 28.8 kbps for the CSK modulator, which forms a symbol with six bits. The CSK symbol rate is 28.8/6 = 4.8 ksps. The corresponding Walsh chip rate is $4.8 \times 64 = 307.2$ kcps. The chip stream is spread by multiplying it with a pseudo-noise (PN) sequence of chip rate 1.2288 Mcps. Thus, there are four PN chips per Walsh chip, or $64 \times 4 = 256$ PN chips per CSK symbol. The CSK signal occupies a bandwidth of 1.25 MHz. Since the symbol rate is only 4.8 ksps, while the CSK rate is 1.2288 Mcps, the spread factor is $1228.8/4.8 = 256$. This spread factor is responsible for the large processing gain of the CDMA cellular system. It enables the simultaneous transmission of many mobile stations over a 1.25 MHz channel.
■

6.16 M-ary frequency shift keying (MFSK)

MFSK belongs to the family of orthogonal modulation techniques. It employs a set of $M = 2^k$ orthogonal sinusoids to represent a set of M distinct k-bit symbols, $n = 1, 2, \ldots, M$, as follows:

$$s_n(t) = A\cos(2\pi f_n t + \theta_n), \qquad n = 1, 2, \ldots, M \tag{6.140}$$

where for a given positive integer $\ell \gg 1$, symbol rate $1/T_s$, and $f_c = \ell/T_s$,

$$f_n = f_c + (2n - M - 1)\frac{1}{2T_s} \tag{6.141}$$

The minimum frequency spacing is $1/T_s$ to preserve the orthogonality for the entire n sinusoids, as proved in (2.45). Note that the phase does not need to be continuous at the symbol transitions. For this case, the bandwidth of MFSK is approximately $(M + 1)/T_s$. The bandwidth can be made narrower if the phase is forced to be continuous at the symbol transitions. This implies that a continuous phase MFSK (CP-MFSK) signal must look like an FM signal with digital modulated data, and can take the following form for an Nth data symbol:

$$s(t) = A\cos\left[2\pi f_c t + 2\pi\left(\frac{1}{4T_s}\right)\int_{-\infty}^{t}\sum_{i=-\infty}^{N}(2D_i - M - 1)p(\tau - iT_s)\mathrm{d}\tau\right] \tag{6.142}$$

where $D_i \in \{1, 2, \ldots, M\}$ is the ith symbol in the symbol stream, and $p(t)$ is the squared pulse of unit amplitude and duration T_s. Following the derivation in (6.57), we can write $s(t)$ from (6.142) in a more compact form for the Nth data symbol:

$$s(t) = A\cos\left[2\pi f_c t + \frac{\pi}{2T_s}(2D_N - M - 1)(t - NT_s) + \phi_N\right] \tag{6.143}$$

where ϕ_N is defined as

$$\phi_N = \frac{\pi}{2}\sum_{i=-\infty}^{N-1}(2D_i - M - 1) \tag{6.144}$$

Let $h = 2T_s\Delta f$ be defined as the *digital modulation index*, where Δf is the *peak frequency deviation* of $s(t)$. Since $\Delta f = 1/4T_s$ per (6.142), it is seen that $h = 0.5$. Using h we can write $s(t)$ in the form

$$s(t) = A\cos[2\pi f_c t + \phi(t, \boldsymbol{D}_N)] \tag{6.145}$$

where $\boldsymbol{D}_N$ is a semi-infinite sequence from $-\infty$ to the Nth data symbol D_N:

$$\phi(t, \boldsymbol{D}_N) = 2\pi h(2D_N - M - 1)q(t - NT_s) + \phi_N \tag{6.146}$$

with the function $q(t)$ defined as

$$\begin{aligned} q(t) &= \frac{1}{2T_s}\int_0^t p(\tau)\,\mathrm{d}\tau \\ &= \frac{t}{2T_s} \end{aligned} \tag{6.147}$$

CP-MFSK is a special case of *continuous phase modulation* (CPM), which will be studied in Section 6.17.

By observing (6.142), we see that the message signal $m(t)$ for the CP-MFSK signal $s(t)$ is simply an MPAM with amplitudes in the set $\{\pm 1, \pm 3, \ldots, \pm(M-1)\}$ as seen from (6.84):

$$m(t) = \sum_{i=-\infty}^{N}(2D_i - M - 1)p(t - iT_s) \tag{6.148}$$

Power spectral density

The derivation of the power spectral density of CP-MFSK is quite complicated as compared to the case of binary CP-FSK ($M = 2$). This happens because the message signal is an MPAM signal instead of a simple antipodal signal. An analytical expression has been derived in [11] for CPM with rectangular pulse $p(t)$ as

$$S(f) = \frac{A^2 T}{2}\left[\frac{1}{M}\sum_{i=1}^{M}A_i^2(f) + \frac{2}{M^2}\sum_{i=1}^{M}\sum_{j=1}^{M}B_{ij}(f)\,A_i(f)A_j(f)\right] \tag{6.149}$$

where

$$A_i(f) = \frac{\sin\pi\left[fT_s - \frac{1}{2}(2i - M - 1)h\right]}{\pi\left[fT_s - \frac{1}{2}(2i - M - 1)h\right]} \tag{6.150}$$

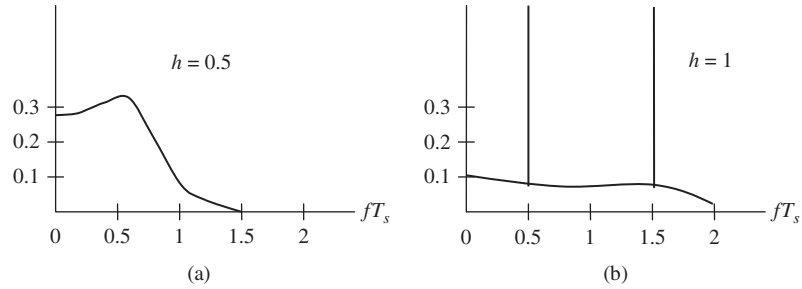

Figure 6.39 (a) CP-4FSK with $h = 0.5$; (b) CP-4FSK with $h = 1$.

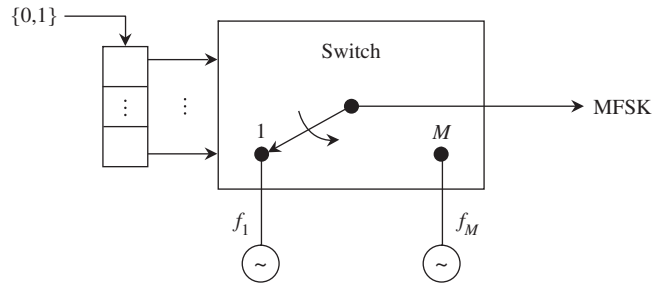

Figure 6.40 Modulator for discontinuous phase MFSK.

$$B_{ij}(f) = \frac{\cos\left(2\pi f T_s - v_{ij}\right) - u\cos v_{ij}}{1 + u^2 - 2u\cos 2\pi f T_s} \tag{6.151}$$

$$v_{ij} = \pi h(1 + j - M - 1) \tag{6.152}$$

$$u = \frac{\sin M\pi h}{M \sin \pi h} \tag{6.153}$$

By using $h = 0.5$, we can obtain the power spectral density for CP-MFSK. For $h = 1$, there are impulses occurring at M frequencies. Figure 6.39 shows the power spectral densities for $M = 4$ for the cases $h = 0.5$ and $h = 1$ as a function of the normalized frequency fT_s and normalized amplitude for $fT_s > 0$ only. The origin corresponds to the carrier frequency f_c. For $h = 0.5$, the bandwidth is approximately $M/2T_s = 2/T_s$, while for $h = 1$, it is about $M/T_s = 4/T_s$.

Modulator

The MFSK signal can be implemented with independent carriers as in Figure 6.40, or using an FM modulator to generate a continuous phase signal as in Figure 6.41.

Table 6.11 CPM pulse shapes [11]

Type	Waveform
L-REC	$p(t) = \begin{cases} \frac{1}{L}, & 0 \le t \le LT_s \\ 0, & \text{otherwise} \end{cases}$
L-RC	$p(t) = \begin{cases} \frac{1}{L}\left(1 - \cos\frac{2\pi t}{LT_s}\right), & 0 \le t \le LT_s \\ 0, & \text{otherwise} \end{cases}$
GMSK	$p(t) = Q\left[\frac{2\pi B}{\sqrt{\ln 2}}\left(t - \frac{T_s}{2}\right)\right] - Q\left[\frac{2\pi B}{\sqrt{\ln 2}}\left(t + \frac{T_s}{2}\right)\right], \quad 0 \le BT_s \le 1$
	$Q(x) = \int_x^\infty \frac{1}{\sqrt{2\pi}} e^{-x^2/2} dx$

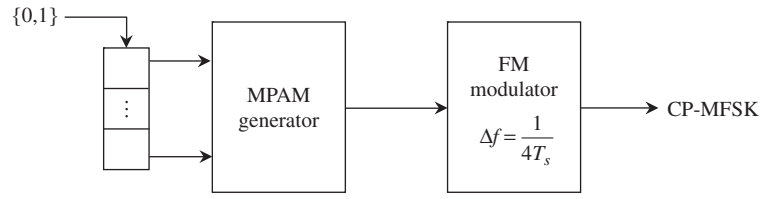

Figure 6.41 Modulator for CP-MFSK with a minimum frequency spacing equal to half the symbol rate or twice the peak frequency deviation Δf.

6.17 Continuous phase modulation (CPM)

CPM is a generalization of CP-MFSK in which the digital modulation index h can assume any value. For ease of decoding with finite phase states, h is chosen to be a rational number. If h varies in a cyclic manner from one symbol to another through a set of indices, the modulation is called *multi-h CPM*. The CPM waveform $s(t)$ is given by (6.145), where $\phi(t, \boldsymbol{D}_N) = 2\pi h \sum_{i=-\infty}^{N} (2D_i - M - 1)\, q(t - iT_s)$, and the pulse $q(t)$ is defined as

$$q(t) = \frac{1}{2T_s} \int_0^t p(\tau)\, d\tau \tag{6.154}$$

The symbol pulse shape $p(t)$ can take on various shapes, such as a rectangular pulse of duration L symbols, which is called L-REC, a raised cosine pulse shape of duration L symbols, which is called L-RC, and a Gaussian minimum shift keying pulse, which is called GMSK. Table 6.11 shows the equations that represent these common pulse shapes, which are also plotted in Figure 6.42. The CPM signal is commonly referred to as full response CPM when $p(t) = 0$ for $t > T_s$ and partial response CPM when $p(t) \neq 0$ for $t > T_s$. For GMSK pulse shapes, the parameter B in its equation represents the 3 dB bandwidth of the Gaussian pulse defined in (6.75).

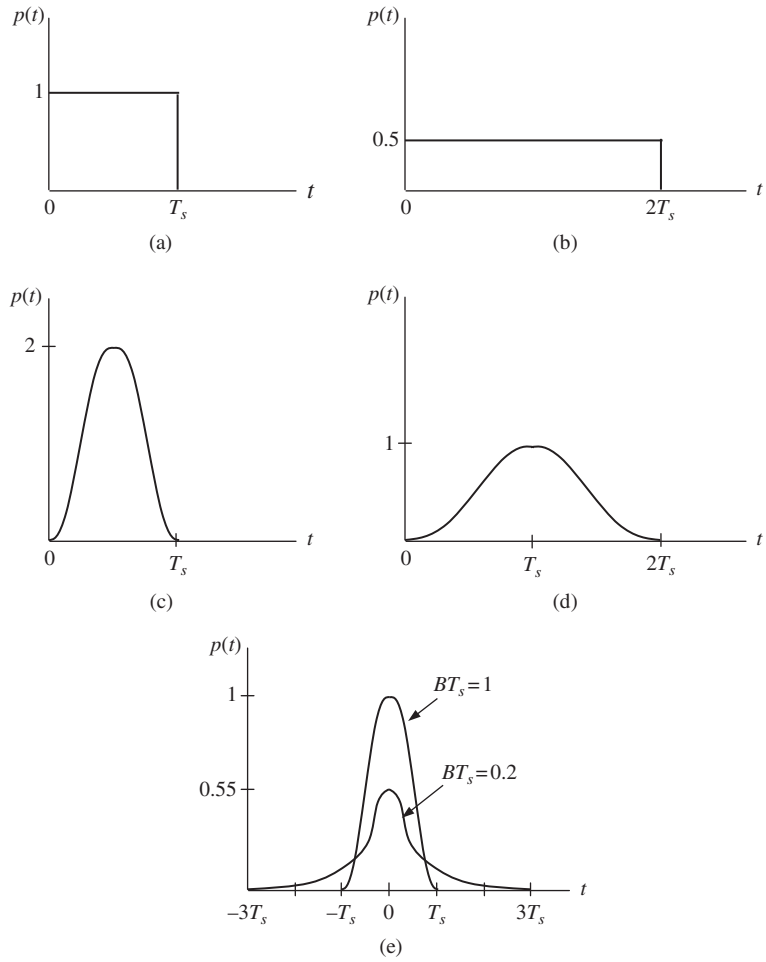

Figure 6.42 (a) 1-REC; (b) 2-REC; (c) 1-RC; (d) 2-RC; (e) GMSK with $BT_s = 0.2$ and $BT_s = 1$.

Power spectral density

The power spectral density of CPM with rectangular pulse shape is given in (6.149)–(6.153) and those of other pulse shapes can be found in [11] with 1-REC-4CPM and a set of $M = 4$ symbols. For $h < 0.3$, the occupied bandwidth approaches $2/T_s = 1/T_b$, which is less than that of MSK. With 3-RC-4CPM, again with $M = 4$ symbols, the bandwidth is almost halved with 3RC as compared to 1REC when using –40 dB as a measure of the bandwidth. Thus, the longer pulse shape $p(t)$ yields the smaller bandwidth. Also, L-RC results in better bandwidth efficiency than L-REC.

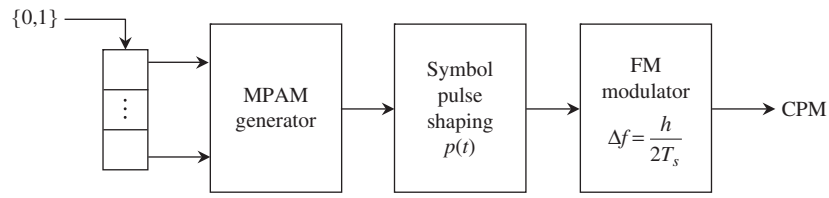

Figure 6.43 CPM modulator.

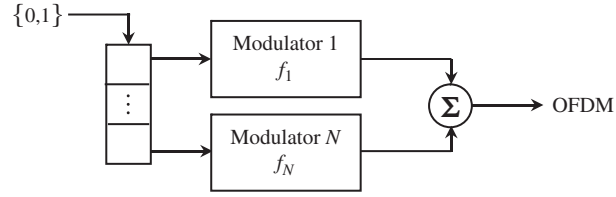

Figure 6.44 OFDM with N overlapping orthogonal subcarriers at frequencies $f_1, f_2, \ldots, f_N$.

Modulator

The CPM signal can be implemented with an FM modulator and a pulse shaping network as illustrated in Figure 6.43. Note that the smaller the digital modulation index h, the smaller the peak frequency deviation Δf, which results in a decrease in bandwidth.

6.18 Orthogonal frequency division multiplexing (OFDM)

A frequency division multiplexing (FDM) signal is the sum of N non-overlapping distinct carriers from N separate sources [2–6]. We now extend this concept to the sum of N overlapping but orthogonal subcarriers from a single source. This technique is referred to as *orthogonal frequency division multiplexing*, or OFDM, and is now widely used in many wireless systems including the popular IEEE 802.11a,g WLAN [7, 8]. Figure 6.44 shows the conceptual block diagram of an OFDM transmitter. The incoming data stream of rate $1/T$ bits/s is demultiplexed (serial-to-parallel conversion) into N parallel streams. Each parallel stream has a rate equal to $1/NT$ bits/s and independently modulates one of N orthogonal subcarriers. The modulation technique for each subcarrier can be different from each other theoretically, but is commonly chosen to be the same in practice. A portion of the data in a packet can be transmitted using a more power efficient modulation technique than other portions for reasons of reliability. For example, highly reliable data can be transmitted by PSK or QPSK, while others can be transmitted by 16QAM or 64QAM, which for the same *SNR per bit* yields a higher bit error rate. The OFDM subcarriers are chosen to be mutually

orthogonal with the minimum frequency spacing of $1/T_s$, which is the *subcarrier symbol rate*. For example, if PSK is the modulation technique for the subcarriers, then, $1/T_s = 1/NT$. On the other hand, if QPSK is used, then $1/T_s = 1/2NT$. For MQAM, we would have $1/T_s = 1/NT \log_2 M$. The OFDM signal in Figure 6.44 is simply the sum of N modulated subcarriers. When the number of subcarriers is large, the implementation in Figure 6.44 is not practical because of a large number of modulators. In the following discussion we investigate the implementation of OFDM at *baseband*, which is used in practical applications.

Practical baseband implementation

Consider the OFDM signal $s(t)$, which is the sum of N modulated subcarriers $s_k(t)$, $k = 0, 1, \ldots, N-1$. Using complex envelope notation for the subcarriers, we define

$$s_k(t) = \mathrm{Re}\left\{z_k(t)e^{j[2\pi(f_c+k\Delta f)t]}\right\}, \quad 0 \le t < T_s \tag{6.155}$$

where f_c is the nominal carrier frequency, $\Delta f = 1/T_s$ is the minimum frequency spacing, which is equal to the subcarrier symbol rate to provide orthogonality, and $z_k(t)$ is the complex envelope of the kth subcarrier or its equivalent lowpass signal, which is constant during a symbol interval and can be represented by

$$z_k(t) = Z(k) = I_k + jQ_k, \quad 0 \le t < T_s \tag{6.156}$$

where I_k and Q_k, the in-phase and quadrature components of $z_k(t)$, respectively, are the I- and Q-values of the kth subcarrier symbol.

For scaling purposes, we normalize the OFDM signal to N, the number of subcarriers, so that

$$s(t) = \frac{1}{N}\sum_{k=0}^{N-1} s_k(t), \quad 0 \le t < T_s \tag{6.157}$$

Substituting (6.155) into (6.157), we obtain

$$\begin{aligned} s(t) &= \frac{1}{N}\sum_{k=0}^{N-1} \mathrm{Re}\left\{Z(k)e^{j[2\pi(f_c+k\Delta f)t]}\right\} \\ &= \frac{1}{N}\sum_{k=0}^{N-1} \mathrm{Re}\left\{Z(k)e^{j2\pi k\Delta f t}e^{j2\pi f_c t}\right\} \\ &= \mathrm{Re}\left\{\left(\frac{1}{N}\sum_{k=0}^{N-1} Z(k)e^{j2\pi k\Delta f t}\right)e^{j2\pi f_c t}\right\}, \quad 0 \le t < T_s \end{aligned} \tag{6.158}$$

The complex envelope of the OFDM signal is therefore given by

$$s_L(t) = \frac{1}{N}\sum_{k=0}^{N-1} Z(k)e^{j2\pi k\Delta f t}, \quad 0 \le t < T_s \tag{6.159}$$

Consider a sampling rate equal to N times the subcarrier symbol rate, that is, the sampling time is simply T_s/N. Applying the sampling process to (6.159), we obtain the nth sample at time $t = nT_s/N$ as follows:

$$s_L\left(\frac{nT_s}{N}\right) = \frac{1}{N}\sum_{k=0}^{N-1} Z(k)\, \mathrm{e}^{\mathrm{j}2\pi k\Delta f n T_s/N},\ n = 0, 1, \ldots, N-1 \tag{6.160}$$

To preserve subcarrier orthogonality, we require that $\Delta f T_s = 1$. Furthermore, for ease of notation, we let $s_L(n) = s_L(nT_s/N)$, therefore

$$\begin{aligned} s_L(n) &= \frac{1}{N}\sum_{k=0}^{N-1} Z(k)\, \mathrm{e}^{\mathrm{j}2\pi kn/N}, \quad n = 0, 1, \ldots, N-1 \\ &= \mathrm{IDFT}\{Z(k)\} \end{aligned} \tag{6.161}$$

Equation (6.161) allows us to generate the sequence $s_L(n)$ from the *frequency samples* $Z(k) = I_k + \mathrm{j}Q_k,\ k = 0, 1, \ldots, N-1$, which consists of the I- and Q-values of N subcarrier symbols. This relation is referred to as the N-point *inverse discrete Fourier transform* (IDFT) of $Z(k)$ [12]. In turn, the inverse operation that allows the frequency samples $\{Z(k)\}$ to be obtained from the sequence $s_L(n)$ is called the N-point *discrete Fourier transform* (DFT) and is given by

$$\begin{aligned} Z(k) &= \sum_{n=0}^{N-1} s_L(n)\, \mathrm{e}^{-\mathrm{j}2\pi kn/N}, \quad k = 0, 1, \ldots, N-1 \\ &= \mathrm{DFT}\{s_L(n)\} \end{aligned} \tag{6.162}$$

Example 6.34 DFT of an OFDM signal

We wish to verify the DFT expression of (6.162) by using (6.161). We have

$$\begin{aligned} Z(k) &= \sum_{n=0}^{N-1} s_L(n)\, \mathrm{e}^{-\mathrm{j}2\pi kn/N} \\ &= \frac{1}{N}\sum_{n=0}^{N-1}\sum_{m=0}^{N-1} Z(m)\, \mathrm{e}^{\mathrm{j}2\pi n(m-k)/N} \\ &= \frac{1}{N}\sum_{m=0}^{N-1} Z(m)\left[\sum_{n=0}^{N-1} \mathrm{e}^{\mathrm{j}2\pi n(m-k)/N}\right] \\ &= Z(k) \end{aligned} \tag{6.163}$$

The right-hand side of the above equation reduces to $Z(k)$ by virtue of the following identity:

$$\sum_{n=0}^{N-1} \mathrm{e}^{\mathrm{j}2\pi n(m-k)/N} = \begin{cases} N, & m = k + rN,\ r \text{ is an integer} \\ 0, & \text{otherwise} \end{cases} \tag{6.164}$$

■

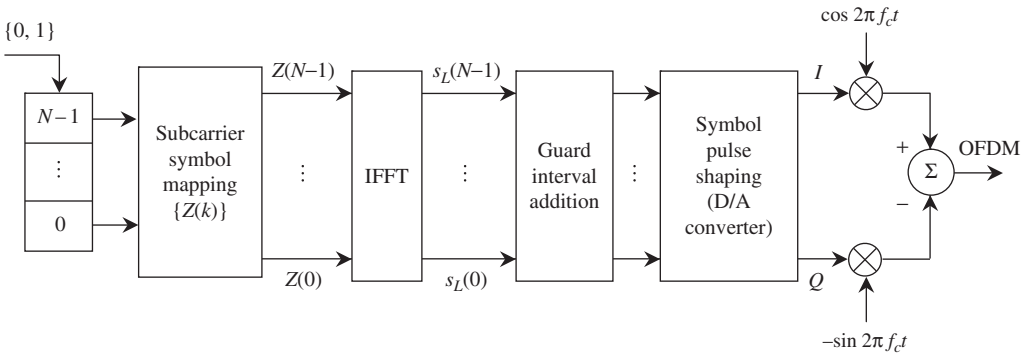

Figure 6.45 Block diagram of an OFDM modulator.

The frequency samples $\{Z(k)\}$ in (6.161) uniquely represent the sequence $s_L(n)$. The N samples $\{s_L(n)\}$ are sufficient for digital-to-analog conversion to $s_L(t)$. Both DFT and IDFT can be computed via computational algorithms called *fast Fourier transform* (FFT) and *inverse fast Fourier transform* (IFFT) [12]. The IDFT of the frequency samples $\{Z(k)\}$ in (6.161), which represent the I- and Q-values of the subcarrier symbols in (6.156) for a given symbol interval, allows us to implement an OFDM transmitter at baseband using the efficient IFFT algorithm. In practice, the number of subcarriers N is commonly chosen to be even. This allows the OFDM nominal carrier frequency f_c to be the average of the N subcarrier frequencies, and the IDFT in (6.161) and DFT in (6.162) can be carried out with the indices k and n running from $-N/2$ to $N/2$. The "0" subcarrier associated with the center frequency is omitted and filled with zero values. To implement IFFT/FFT, the size of N is chosen to be a power of 2.

Figure 6.45 illustrates the implementation of an OFDM modulator via the baseband approach. The incoming bit stream of 1s and 0s is demultiplexed into N parallel bit streams. For the kth bit stream, a group of $\log_2 M$ bits is mapped into a subcarrier symbol $Z(k) = I_k + \mathrm{j}Q_k,\ 0 \le t < T_s$. The sequence of N symbols $\{Z(k)\}_{k=0}^{N-1}$ is fed into the IFFT to obtain the sequence $\{s_L(n)\}_{n=0}^{N-1}$, which represents the samples of the OFDM complex envelope. The output of the D/A converter is a complex I-Q waveform

$$\hat{s}_L(t) = \sum_{n=0}^{N-1} s_L(n)p(t - nT_s/N) \tag{6.165}$$

where $p(t)$ is the *interpolation* pulse shape. The pulse shape $p(t)$ can have the form $\sin x/x$, which is used for reconstruction of a sampled signal (see Section 2.10). Note the similarity of (6.165) and the Nyquist–Shannon interpolation formula (2.247).

Example 6.35 A different view of OFDM

Let us again consider the interpolated I-Q complex signal generated by the D/A converter in (6.165). Using (6.161) we obtain

$$\begin{aligned}\hat{s}_L(t) &= \sum_{n=0}^{N-1} s_L(n)p(t - nT_s/N) \\ &= \frac{1}{N}\sum_{n=0}^{N-1}\sum_{k=0}^{N-1} Z(k)\, \mathrm{e}^{\mathrm{j}2\pi kn/N} p(t - nT_s/N) \\ &= \frac{1}{N}\sum_{k=0}^{N-1} Z(k) \sum_{n=0}^{N-1} \mathrm{e}^{\mathrm{j}2\pi kn/N} p(t - nT_s/N) \\ &= \frac{1}{\sqrt{N}}\sum_{k=0}^{N-1} Z(k) g_k(t)\end{aligned} \tag{6.166a}$$

We can choose $p(t)$ so that the N pulses $\{g_k(t)\}$ form a set of *orthonormal* pulses and they also satisfy the *Nyquist* criterion for zero ISI (Chapter 9). We have

$$g_k(t) = \frac{1}{\sqrt{N}}\sum_{n=0}^{N-1} \mathrm{e}^{\mathrm{j}2\pi kn/N} p(t - nT_s/N), \quad k = 0, 1, \ldots, N-1 \tag{6.166b}$$

$$p(t) = \sqrt{\frac{N}{T_s}}\frac{\sin(\pi Nt/T_s)}{\pi Nt/T_s} \tag{6.166c}$$

The above result shows that an OFDM symbol is indeed a normalized sum of N subcarrier symbols defined by the set of orthonormal pulse shapes $\{g_k(t)\}$.

■

In applications where intersymbol interference (ISI) is present (see Chapter 9), a guard time T_{GI} is added to the start of a symbol. The guard time will be deleted at the receiver before the FFT is performed to recover $\{Z_k\}$. This method can eliminate ISI if the maximum delay spread of the ISI can be reasonably predicted. The drawback is the loss in throughput because the symbol time is now $T_s + T_{GI}$. The guard time is created by prepending the IFFT sequence a circular extension or *cyclic prefix* of itself. For example, the cyclic prefix for $\{s_L(n)\}$, $n = 0, 1, \ldots, N-1$ is the last m samples $s_L(N-m)$, $s_L(N-m+1)$, $\ldots$, $s_L(N-1)$. These are added to the beginning of the sequence $s_L(0)$, $s_L(1)$, $\ldots$, $s_L(N-1)$. The new sequence now consists of $N + m$ samples. Naturally, the first m samples of the received version of $\{s_L(n)\}$ are discarded at the receiver before the FFT process. Due to the periodic nature of IFFT, the junction at the start of the original symbol will always be continuous. Note that discontinuities can exist at the junctions between adjacent symbols. Figure 6.46 shows how a guard time is created using cyclic prefix.

In wireless applications, the transmitted signal can arrive at the receiver via many propagation paths due to reflection from large objects (such as the ground, hills, or buildings), and diffraction which allows the signal to slide via rooftops or bend around objects,

Cyclic prefix	OFDM symbol	Cyclic Prefix	OFDM symbol

Figure 6.46 Copy and append cyclic prefix to create a guard interval.

and scattering from smaller objects (such as trees or lamp posts). Thus, the receiver can receive multiple attenuated and delayed copies of the transmitted signal. Often, a few dominant copies are present and the others are too weak to be significant. These dominant copies not only interfere with themselves, but the delayed ones also interfere with the next symbol. The former effect is called multipath fading resulting in a scaling and rotation of the symbol, which leads to performance degradation (higher symbol error rate). The latter effect is called ISI and can be eliminated by the guard time as discussed above.

Cyclic prefix

In this section we present a mathematical description of cyclic prefix and its role in removing ISI resulting from transmitting the OFDM signal through a multipath fading channel (see Chapter 10).

Example 6.36 Linear convolution and circular convolution

The *linear convolution* for two sequences $h(n)$ and $x(n)$ is given by

$$y(n) = h(n) * x(n) = \sum_k h(k)x(n-k) \tag{6.167}$$

The *discrete-time Fourier transform* (DTFT) of $y(n)$ is the product of DTFT $\{h(n)\}$ and DTFT $\{x(n)\}$

$$Y(\mathrm{e}^{\mathrm{j}2\pi f}) = H(\mathrm{e}^{\mathrm{j}2\pi f})X(\mathrm{e}^{\mathrm{j}2\pi f}) \tag{6.168}$$

where

$$\begin{aligned} H(\mathrm{e}^{\mathrm{j}2\pi f}) &= \mathrm{DTFT}\{h(n)\} = \sum_n h(n)\,\mathrm{e}^{-\mathrm{j}2\pi fn} \\ X(\mathrm{e}^{\mathrm{j}2\pi f}) &= \mathrm{DTFT}\{x(n)\} = \sum_n x(n)\,\mathrm{e}^{-\mathrm{j}2\pi fn} \end{aligned} \tag{6.169}$$

In OFDM the sequences $x(n)$ and $h(n)$ are of *finite length* N. Therefore, taking Fourier transform of $y(n)$ does not give the multiplication in the frequency domain unless we use cyclic prefix to convert linear convolution to *circular convolution*. Assume that the length of the sequences $x(n)$ and $h(n)$ is N (if their lengths are not the same, zeros can be used to pad the sequences to the same length). The length N_c needed so that linear convolution and circular convolution are the same from 0 to $N_c - 1$ is $2N - 1$. The circular convolution of two sequences $h(n)$ and $x(n)$ is given by

$$y(n) = h(n) \otimes x(n) = \sum_{k=0}^{N-1} h(k)x(n-k)_N \tag{6.170}$$

where $x(n-k)_N = x[(n-k) \bmod N]$ is the *circular shift* of the sequence $x(n)$, defined on 0 to $N-1$, to the right by k values. The circular shift can be viewed as wrapping the part of the sequence that falls outside the region of interest to the front of the sequence. Equivalently, this is the same as arranging the N-point sequence on the circumference of a

circle with a fixed reference. A counterclockwise rotation gives a new reference and a circularly shifted sequence. This is also equivalent to a *linear shift* of the periodic extension of $x(n)$. Consider the case of $k = 2$, we have the following circularly shifted sequence: $x(n-k)_N \sim \{x(N-2), x(N-1), x(0), x(1), \ldots, x(N-3)\}$.

The N-point DFT of $y(n)$ is given by

$$Y(k) = H(k)X(k), \quad k = 0, 1, \ldots, N-1 \tag{6.171a}$$

where $H(k)$ is the N-point DFT of $h(n)$ and $X(k)$ is the N-point DFT of $x(n)$.

$$\begin{aligned} H(k) &= \mathrm{DFT}\{h(n)\} = \sum_{n=0}^{N-1} h(n)\, \mathrm{e}^{-\mathrm{j}2\pi kn/N}, \quad k = 0, 1, \ldots, N-1 \\ X(k) &= \mathrm{DFT}\{x(n)\} = \sum_{n=0}^{N-1} x(n)\, \mathrm{e}^{-\mathrm{j}2\pi kn/N}, \quad k = 0, 1, \ldots, N-1 \end{aligned} \tag{6.171b}$$

Note that the DFT corresponds to samples of the DTFT taken every $1/N$. Thus, we have

$$\begin{aligned} H(k) &= H(\mathrm{e}^{\mathrm{j}2\pi f})_{f=k/N} = H(\mathrm{e}^{\mathrm{j}2\pi k/N}) \\ X(k) &= X(\mathrm{e}^{\mathrm{j}2\pi f})_{f=k/N} = X(\mathrm{e}^{\mathrm{j}2\pi k/N}) \end{aligned} \tag{6.172}$$

■

Example 6.37 DFT and circular convolution

We want to verify that the multiplication of the DFTs of two sequences results in a DFT of the circular convolution of the two sequences. Let us take the IFFT of $Y(k)$ in (6.171a). We have

$$\begin{aligned} y(n) &= \frac{1}{N} \sum_{k=0}^{N-1} Y(k)\, \mathrm{e}^{\mathrm{j}2\pi kn/N} \\ &= \frac{1}{N} \sum_{k=0}^{N-1} H(k)X(k)\, \mathrm{e}^{\mathrm{j}2\pi kn/N} \end{aligned} \tag{6.173}$$

Substituting (6.171b) into (6.173) we obtain the following expression:

$$\begin{aligned} y(n) &= \frac{1}{N} \sum_{k=0}^{N-1} \left[\sum_{l=0}^{N-1} h(l)\, \mathrm{e}^{-\mathrm{j}2\pi kl/N} \right] \left[\sum_{m=0}^{N-1} x(m)\, \mathrm{e}^{-\mathrm{j}2\pi km/N} \right] \mathrm{e}^{\mathrm{j}2\pi kn/N} \\ &= \frac{1}{N} \sum_{l=0}^{N-1} h(l) \sum_{m=0}^{N-1} x(m) \left[\sum_{k=0}^{N-1} \mathrm{e}^{\mathrm{j}2\pi k(n-l-m)/N} \right] \\ &= \sum_{l=0}^{N-1} h(l)x(n-l)_N \\ &= h(n) \otimes x(n), \quad n = 0, 1, \ldots, N-1 \end{aligned} \tag{6.174}$$

■

Now consider a transmitted OFDM symbol that is the sequence $s_L(n)$ of length N. This sequence serves as the input to a channel characterized by a *finite impulse response* (FIR) $h(n)$ of length $1 < L < N$. Let us form an *expanded* input sequence $\tilde{s}_L(n)$ of length $N+L-1$ by copying the last $L-1$ samples of $s_L(n)$, $-L+1 \le n \le N-1$, that is, the cyclic prefix of $s_L(n)$, and append them to the front of the sequence $s_L(n)$. Thus, the expanded sequence is $\tilde{s}_L(n) = s_L(n)_N,\ -L+1 \le n \le N-1$. Consequently, we have $\tilde{s}_L(n-k) = s_L(n-k)_N$, $-L+1 \le n-k \le N-1$. Also, we expand the sequence $h(n)$ to length $N+L-1$ with *zero padding*. The output of the FIR channel is the linear convolution of $h(n)$ and $\tilde{s}_L(n)$ as given by

$$\begin{aligned} y(n) = h(n) * \tilde{s}_L(n) &= \sum_{k=0}^{N+L-1} h(k)\tilde{s}_L(n-k) \\ &= \sum_{k=0}^{N+L-1} h(k)s_L(n-k)_N = \sum_{k=0}^{L-1} h(k)s_L(n-k)_N \\ &= h(n) \otimes s_L(n),\ n = -L+1, -L+2, \ldots, -1, 0, 1, \ldots, N-1 \end{aligned} \tag{6.175}$$

The first $L-1$ samples of $y(n)$, $n = -L+1, -L+2, \ldots, -1$, are *redundant* because they are associated with the cyclic prefix of $s_L(n)$. Furthermore, these samples also contain the ISI that results from passing the last $L-1$ samples of the previous OFDM symbol through the channel. These samples are discarded by the receiver prior to the DFT operation. If we take DFT of both sides of the above expression we obtain the frequency-domain samples as follows:

$$Y(k) = H(k)Z(k),\ k = 0, 1, \ldots, N-1 \tag{6.176}$$

Conversely, the time-domain sample $y(n)$ can be expressed in terms of $Y(k)$ via IDFT as

$$y(n) = \frac{1}{N}\sum_{k=0}^{N-1} H(k)Z(k)\, e^{j2\pi kn/N}, \quad n = 0, 1, \ldots, N-1 \tag{6.177}$$

The channel frequency response $H(k)$ can be measured by sending a *known* symbol $Z(k)$ and calculating the ratio of the received symbol $Y(k)$ to $Z(k)$, that is, $H(k) = Y(k)/Z(k)$. The length of cyclic prefix is a compromise between how much ISI one wishes to eliminate and how much reduction in system throughput one can accept.

The envelope of an OFDM signal is not constant. Occasionally, a large signal peak can occur when many subcarrier symbols are added in phase. This problem can result in the clipping of the signal amplitude in the D/A converter, causing errors in the transmitting of the symbols. Furthermore, it can saturate the transmitter power amplifier, causing intermodulation distortion. The latter problem can be solved by operating the amplifier in the linear region with enough power back-off. The former problem can be remedied by using error correction codes and interleaving as shown in Figure 6.47. Often a single metric called

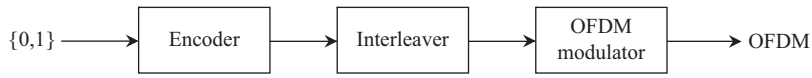

Figure 6.47 A practical OFDM modulator with error correction and interleaving.

peak-to-average power ratio (PAR) is used to describe the amount of back-off required for the power amplifier. Since the peak occurs infrequently, PAR does not seem to be very useful. For example, let the PAR of an OFDM signal be 8 dB. If a peak power exceeds a level of 4 dB above the average power level for only 1% of the time (that is, the probability of the signal being clipped is 0.01 if the amplifier is backed-off by 4 dB), then we might as well operate the amplifier with 4 dB back-off instead of 8 dB and design a code that can correct the error resulting from clipping.

The problem of signal clipping does not exist if OFDM is implemented at RF, as in Figure 6.44. The random phase shifts between subcarriers prevent the coherent addition of subcarriers. This suggests that pseudo-random phase shifts can be purposely introduced to the N subcarriers for baseband implementation. The information on the set of pseudo-random phase shifts for particular symbols can be transmitted on one of the N subcarriers for the receiver to remove during demodulation.

OFDM signal is the sum of N orthogonal subcarriers; therefore, its power spectral density is the sum of the power spectral densities of N subcarriers. If the subcarrier modulation is MPSK or MQAM, the spectral density of a subcarrier simply has a $(\sin x/x)^2$ shape, and hence, the OFDM signal has a spectrum that is fairly flat across the top. The bandwidth of an OFDM signal is approximately equal to $(N+1)/T_s$, that is, about $N+1$ times the subcarrier symbol rate $1/T_s$.

6.19 Trellis coded modulation (TCM)

M-ary modulation such as MPSK or MQAM is employed in applications that require high spectral efficiency. The IEEE 802.11a,g and 802.16 adopt PSK, QPSK, 16QAM, 64QAM, and 256QAM for wireless LAN and MAN. The spectral efficiency for these I-Q modulation techniques with $M = 2^k$ is k bits/s/Hz. Doubling the number of symbols in the symbol alphabet (doubling the signal vectors in the signal space) increases the spectral efficiency by a factor $(k+1)/k$. On the other hand, the power efficiency goes down by a factor $2k/(k+1)$, as presented in Chapter 7. Suppose an error-correction code of rate $r = k/(k+1)$ is used with $M = 2^{k+1}$ signal space, called the *expanded signal space*, then the spectral efficiency would be identical with that of the uncoded signal space with $M = 2^k$. Furthermore, the code is only useful if the coding gain is larger than the power loss. Binary convolutional codes are optimized for binary modulation. They can be used for M-ary modulation without loss of effectiveness if hard decoding is implemented. This happens because the demodulator supplies the hard decoder with bits. On the other hand, soft decoding requires the demodulator to supply either a quantized voltage or an analog voltage that represents the transmitted symbol. This may render the binary convolutional code less effective for soft decoding. M-ary convolutional codes optimized for MASK, MPSK, and MQAM have been found for some rates and constraints lengths, but users have very few options.

Ungerboeck TCM

In 1982 Ungerboeck [33] introduced trellis coded modulation (TCM), which is flexible and effective for *expanded* MPSK and MQAM with convolutional codes of arbitrary rate $r = k/(k+1)$. Conventional MPSK and MQAM employ Gray symbol mapping. With soft decision decoding, the *Euclidean free distance* of the code, which is the minimum Euclidean distance between any two code vectors, should be as large as possible for a given code rate and constraint length (the Euclidean free distance is not the *free distance* d_{free}, which is the smallest *Hamming distance* between any two distinct code sequences). Note that the Euclidean free distance has to be larger than the minimum Euclidean distance of the uncoded signal space of $M = 2^k$ to have any coding gain. Gray symbol mapping may fail to accomplish this goal with some codes and usually leads to low coding gain. To overcome this problem Ungerboeck proposed *symbol mapping by set partitioning* to obtain good coding gain for *expanded* MPSK and MQAM using simple convolutional codes. The essence of mapping by set portioning is to partition the expanded signal space into *subsets whose minimum Euclidean distances increase as the subsets become smaller.*

The next question is how to map code symbols (a code symbol has $k + 1$ bits) to signal vectors in the expanded signal space. The symbol mapping depends on the code structure. For example, one mother code of rate ½ is used to generate two output coded bits from one input information bit while the remaining input information bit serves as the third output coded bit. This results in a rate $2/3$ code. This code has a parallel transition between states because of the uncoded bit. Similarly, one can generate a higher rate code using more uncoded bits. For example, rate $3/4$ code is generated by using remaining input information bits as the third and fourth output coded bits. This code has two parallel transitions between states. Another example to obtain rate $3/4$ code is to use a rate $2/3$ mother code to generate three output coded bits from two input information bits while the remaining input information bit serves as the fourth output coded bit. This code has a parallel transition between states. The following rules are used for symbol mapping:

1. The output coded bits are used to select the subsets. This maximizes the Euclidean distance between transitions leaving or entering the same state.
2. The uncoded bits are used to select the signal points in the subsets. This maximizes the Euclidean distance between parallel transitions.

These rules are ad hoc methods for symbol mapping but they are effective in generating good coding gain for simple convolutional codes. The following examples illustrate the concept of symbol mapping by set partitioning.

Example 6.38 TCM-QPSK

The symbol mapping by set partitioning is illustrated in Figure 6.48 for QPSK using two output coded bits of a rate ½ convolutional code. The first partition has two subsets, each with two signal vectors and the minimum Euclidean distance is $2\sqrt{E_s}$ as compared to $\sqrt{2E_s}$ of QPSK. The subset on the left is selected by the first coded bit (bold face) when it is **0** and the subset on the right when it is **1**. The second coded bit selects the signal vector in the first

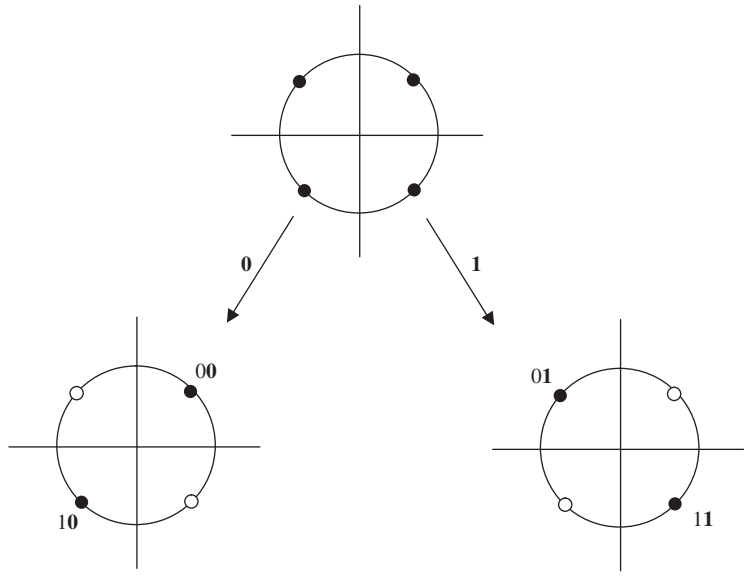

Figure 6.48 Symbol mapping by set partitioning for QPSK with rate ½ convolutional code. The bold face bit is the second coded bit and the other bit is the first coded bit.

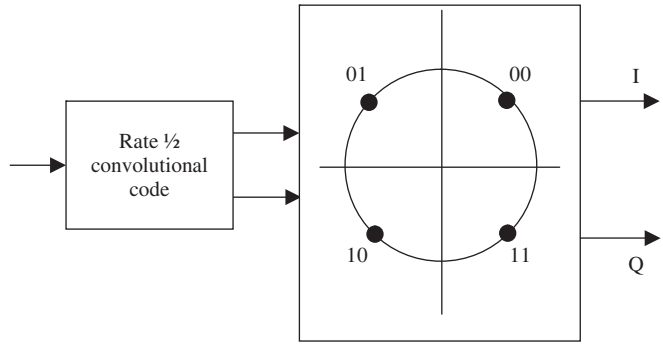

Figure 6.49 Implementation of TCM-QPSK.

quadrant (second quadrant) when it is 0 and the signal vector in the third quadrant (fourth quadrant) when it is 1. Note that the symbol mapping is clearly not Gray symbol mapping. We observe that two coded bits are transmitted in one QPSK symbol interval $T_s = 2T_b$, which is equivalent to transmitting one uncoded bit in one PSK bit interval T_b . This explains why TCM-QPSK has the same spectral efficiency as uncoded PSK. Figure 6.49 shows the implementation of TCM-QPSK.

■

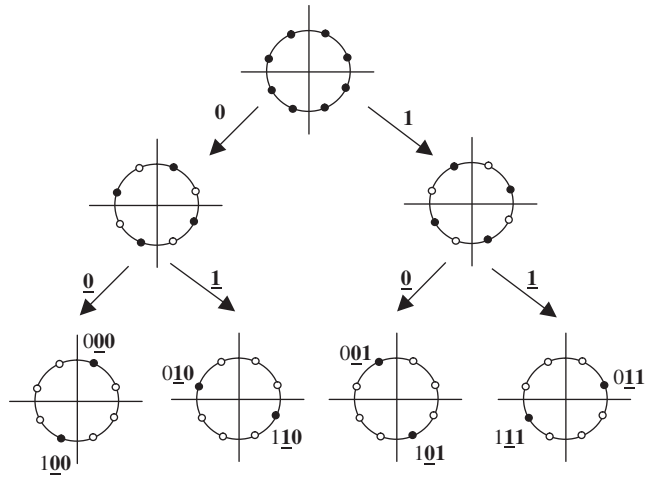

Figure 6.50 Symbol mapping by set partitioning for 8PSK with rate $^2/_3$ convolutional code. The first bit is the uncoded bit, the bold face and underlined bit is the second coded bit and the bold face bit is the first coded bit.

Example 6.39 TCM-8PSK

The symbol mapping by set partitioning is illustrated in Figure 6.50 for 8PSK using two output coded bits of a rate ½ convolutional code and an uncoded bit to form a rate ⅔ code. The first partition has two subsets, each with four signal vectors and the minimum Euclidean distance is $\sqrt{2E_s}$ as compared to $\sqrt{(2-\sqrt{2})E_s}$ of 8PSK. The subset on the left is selected by the first coded bit (bold face) when it is **0** and the subset on the right is selected when it is **1**. The second partition has four subsets, each with two signal vectors and the minimum Euclidean distance is $2\sqrt{E_s}$ as compared to $\sqrt{2E_s}$ of the previous partition. The second coded bit selects the subset on the left when it is $\underline{\mathbf{0}}$ and the subset on the right when it is $\underline{\mathbf{1}}$. The uncoded bit selects the signal vector in each quadrant. Note that the symbol mapping is clearly not Gray symbol mapping. We observe that three coded bits are transmitted in one 8PSK symbol interval $T_s = 3T_b$, which is equivalent to transmitting two uncoded bits in one QPSK symbol interval $T_s = 2T_b$. This explains why TCM-8PSK has the same spectral efficiency as uncoded QPSK. Figure 6.51 shows the implementation of TCM-8PSK.

■

Example 6.40 TCM-16QAM

The symbol mapping by set partitioning is illustrated in Figure 6.52 for 16QAM using three output coded bits of a rate $^2/_3$ convolutional code and an uncoded bit to form a rate $^3/_4$ code. The first partition has two subsets, each with eight signal vectors and the minimum Euclidean distance is $2\sqrt{2E_s}$ as compared to $2\sqrt{E_s}$ of 16QAM. The subset on the left is selected by the first coded bit (bold face) when it is **0** and the subset on the right is selected

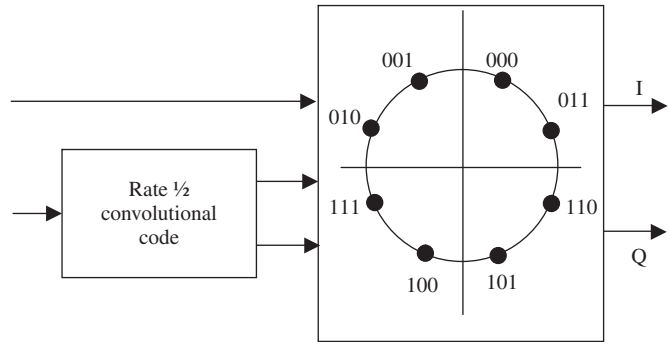

Figure 6.51 Implementation of TCM-8PSK

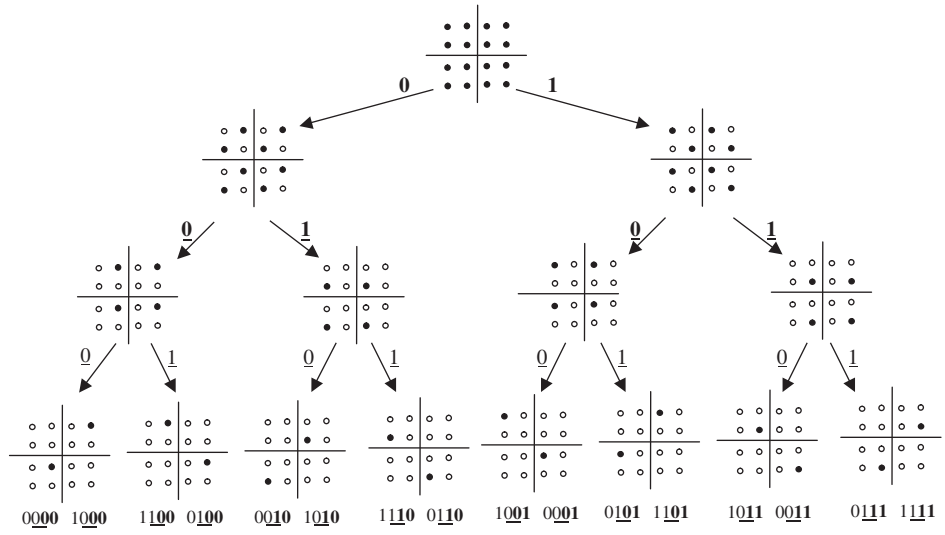

Figure 6.52 Symbol mapping by set partitioning for 16QAM with rate 3/4 convolutional code. The first bit is the uncoded bit, the underlined bit is the third coded bit, the bold face and underlined bit is the second coded bit, and the bold face bit is the first coded bit.

when it is **1**. The second partition has four subsets, each with four signal vectors and the minimum Euclidean distance is $4\sqrt{E_s}$ as compared to $2\sqrt{2E_s}$ of the first partition. The second coded bit selects the subset on the left when it is **0** and the subset on the right when it is **1**. The third partition has eight subsets, each with two signal vectors and the minimum Euclidean distance is $4\sqrt{2E_s}$ as compared to $4\sqrt{E_s}$ of the first partition. The third coded bit selects the subset on the left when it is 0 and the subset on the right when it is 1. The uncoded bit selects the signal vector in each quadrant. Note that the symbol mapping is clearly not Gray symbol mapping. We observe that four coded bits are transmitted in one 16QAM symbol interval $T_s = 4T_b$, which is equivalent to transmitting three uncoded bits in one

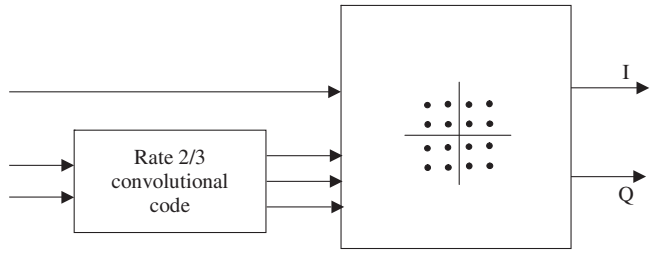

Figure 6.53 Implementation of TCM-16QAM.

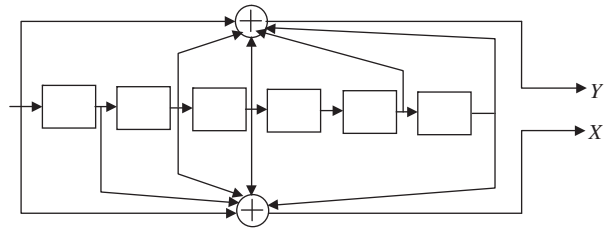

Figure 6.54 Industry standard rate ½ convolutional code.

8QAM symbol interval $T_s = 3T_b$. This explains why TCM-16QAM has the same spectral efficiency as uncoded 8QAM. Figure 6.53 shows the implementation of TCM-16QAM.

■

Pragmatic TCM

Ungerboeck TCM requires the use of a convolutional code with precise code rate $k/(k+1)$ for the expanded signal space. For example, rate $^2/_3$ must be used for 16QAM. *Pragmatic* TCM (adopted by the IEEE 802.16) employs various code rates such as ½ and $^2/_3$ for 16QAM, $^2/_3$ and $^3/_4$ for 64QAM, and $^3/_4$, $^5/_6$, and $^7/_8$ for 256QAM. Furthermore, one mother code of rate ½ is used for all modulation techniques with rates $^2/_3$ and $^3/_4$ codes derived from rate ½ code via *puncturing*. Rates $^5/_6$ and $^7/_8$ are derived from rate $^3/_4$ punctured code via the use of uncoded bits (two uncoded bits for rate $^5/_6$ and four uncoded bits for rate $^7/_8$). The use of a mother code of rate ½ for all required modulation techniques simplifies the encoder and the decoder. Figure 6.54 shows the *industry standard* rate ½ convolutional encoder with constraint length $K = 7$.

Example 6.41 Punctured codes in IEEE 802.16

A rate ½ convolutional code has two outputs X and Y. Rate $^2/_3$ code is obtained by puncturing the second bit of every pair of X-bits, namely X_1X_2. Thus, the sequence of transmitted coded bits is $X_1Y_1Y_2,\ X_3Y_3Y_4, \ldots$. Since it takes *two* information bits to generate *three* transmitted coded bits, the rate is $^2/_3$. Rate $^3/_4$ code is obtained by puncturing the second

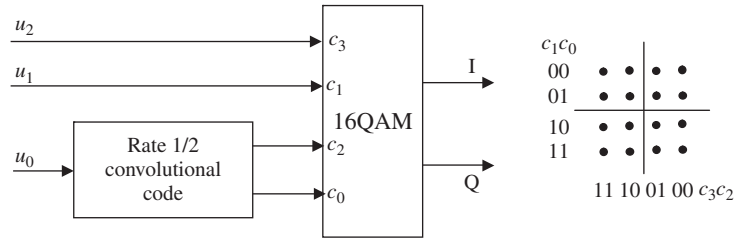

Figure 6.55 Pragmatic rate 3/4 TCM-16QAM. The I-value of a signal vector is generated by c_3c_2 and its Q-value is generated by c_1c_0 via set partitioning for 4ASK.

bit of every three X-bits, namely $X_1X_2X_3$, and by puncturing the third bit of every three Y-bits, namely $Y_1Y_2Y_3$. Thus, the sequence of transmitted coded bits is $X_1Y_1Y_2X_3,\ X_4Y_4Y_5X_6, \ldots$. Since it takes *three* information bits to generate *four* transmitted coded bits, the rate is 3/4.

■

Example 6.42 Pragmatic TCM-16QAM with rate 3/4 convolutional code

The industry standard rate ½ convolutional code in Figure 6.54 is used to generate various TCM configurations adopted by IEEE 802.16. Figure 6.55 shows the pragmatic TCM-16QAM with rate 3/4 code derived from rate ½ code. Two coded bits in addition to two uncoded bits are used for symbol mapping. Since the four I-values and four Q-values of 16QAM represent two orthogonal 4ASK, the symbol mapping is carried out via *set partitioning* independently for I-values and Q-values. This is not Ungerboeck symbol mapping by set partitioning as shown in Figure 6.52. The bits c_3c_2 generate the I-value of the signal vector and the bits c_1c_0 generate its Q-value. By convention the input bit u_2 arrives first, u_1 second, u_0 last. The *spectral efficiency* of this TCM is the same as that of *uncoded* 8QAM.

■

Example 6.43 Pragmatic TCM-16QAM with rate ½ convolutional code

As above, the industry standard rate ½ convolutional code in Figure 6.54 is used to generate the TCM configuration adopted by IEEE 802.16. Figure 6.56 shows the pragmatic TCM-16QAM with the rate ½ basic code. Four coded bits are used for symbol mapping. There are no parallel transitions in the trellis. *Gray mapping* is carried out independently for I-values and Q-values. This is not Ungerboeck symbol mapping by set partitioning as shown in Figure 6.52. Thus, given an input bit, a pair of coded bits c_3c_2 generates the I-value of the signal vector. The next input bit yields a pair of coded bits c_1c_0, which generates the Q-value of the signal vector. Note that two pairs of coded bits are generated for every pair of input bits; hence this is actually rate 2/4 TCM. The selection of Gray mapping is somewhat surprising but apparently it does well with this particular code. The *spectral efficiency* of this TCM is the same as that of *uncoded* QPSK.

■

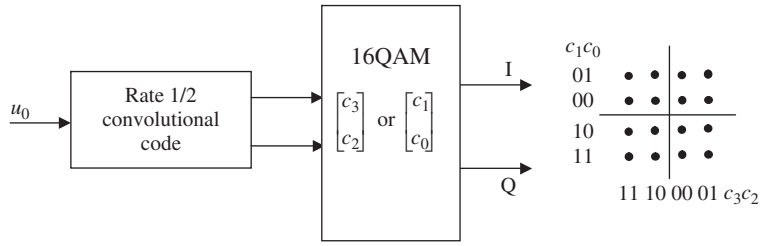

Figure 6.56 Pragmatic rate ½ TCM-16QAM. The I-value of a signal vector is generated by c_3c_2 and its Q-value is generated by c_1c_0 via Gray mapping.

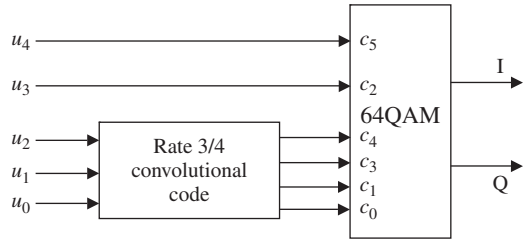

Figure 6.57 Pragmatic rate 5/6 TCM-64QAM.

Example 6.44 Pragmatic TCM-64QAM with rate 5/6 convolutional code

The TCM-64QAM shown in Figure 6.57 as adopted by IEEE 802.16 uses a rate 3/4 convolutional code derived from the punctured rate ½ code in Figure 6.54 as described in Example 6.41. Two uncoded bits with four coded bits are used for symbol mapping. There are two parallel transitions in the trellis. By convention the input bit u_4 arrives first, u_3 second, u_2 third, u_1 fourth, and u_0 last. The output coded bits are taken c_4 first, c_3 second, c_1 third, and c_0 last. The bits $c_5c_4c_3$ map the I-value of the signal vector. Bit c_5 selects the left-half plane with 1 and the right-half plane with 0, bits c_4c_3 select the four I-values according to Gray mapping. The bits $c_2c_1c_0$ map the Q-value of the signal vector. Bit c_3 selects the upper-half plane with 0 and the lower-half plane with 1, bits c_1c_0 select the four Q-values according to Gray mapping. Figure 6.58 shows the symbol mapping. The *spectral efficiency* of this TCM is the same as that of *uncoded* 32QAM.

■

Example 6.45 Pragmatic TCM-64QAM with rate 2/3 convolutional code

The industry standard rate ½ convolutional code in Figure 6.54 is used to generate this TCM configuration adopted by IEEE 802.16. Figure 6.59 shows the pragmatic TCM-64QAM. One uncoded bit and two coded bits are used for symbol mapping. There is a parallel transition in the trellis. Thus, given the first pair of input bits u_1u_0 with u_1 arriving first and u_0

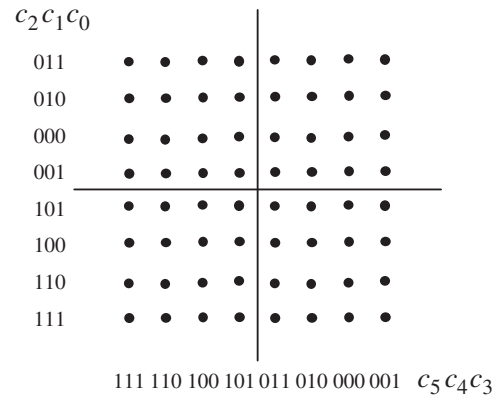

Figure 6.58 Symbol mapping for 64QAM.

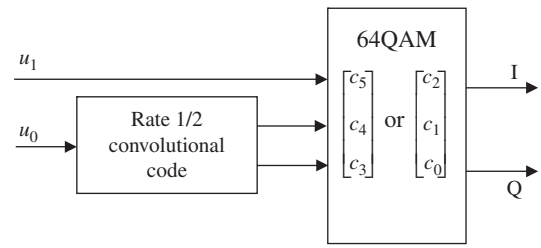

Figure 6.59 Pragmatic rate $4/6$ TCM-64QAM.

last, three coded bits $c_5c_4c_3$ are generated that map the I-value of the signal vector as in Figure 6.58. The next input bit pair generates three coded bits $c_2c_1c_0$ that map the Q-value of the signal vector as in Figure 6.58. Note that two three-bit code words are generated from two pairs of input bits; hence this is actually rate $4/6$ TCM. The *spectral efficiency* of this TCM is the same as that of *uncoded* 16QAM.

■

6.20 Summary

In this chapter we have provided a detailed study of major digital modulation techniques. We divided them into binary modulation and *M-ary* modulation. The binary modulation includes PSK, DPSK, ASK, FSK, MSK, and GMSK. PSK is a popular modulation that is employed widely in practice including signal in the wireless 802.11a and 802.11g standards. DPSK is employed to resolve the phase ambiguity and in applications that require noncoherent demodulation because phase tracking is not possible. DPSK is used in the wireless IEEE 802.11 standard. ASK is employed explicitly in fiber optic communication systems. GMSK is employed in the most

popular cellular standard, namely, GSM. The *M-ary* modulation techniques covered MASK, MPSK including OQPSK, DMPSK including $\pi/4$-DQPSK, MQAM, DMQAM, CSK, MFSK, CPM, and OFDM. We noted that 8ASK is employed in the HDTV standard in the United States. QPSK is perhaps the most popular modulation for satellite communication. QPSK and 16QAM, 64QAM, and 256QAM are used in the wireless 802.11a,g and 802.16 standards. $\pi/4$-DQPSK is used in the cellular IS-136 standard. CSK is employed in the reverse channel of the IS-95 cellular standard, and OFDM is the orthogonal multiplexing scheme for all the current wireless LAN and MAN standards cited above. The encoding of an I-Q signal with a convolutional code results in trellis coded modulation. Both Ungerboeck TCM and the pragmatic TCM used in 802.16 family are studied.

Problems

1. The ideal bandwidth of a PSK signal is $1/T_b$ if a $\sin x/x$ pulse shape is employed. What is the noiseless spectral efficiency of PSK? What is the noiseless spectral efficiency of PSK if a squared pulse shape is employed, assuming a null-to-null bandwidth? At $E_b/N_0 = 8$ dB compare the result of $\sin x/x$ pulse shape to the Shannon channel capacity using Figure 4.8 and Figure 6.7.
2. Consider a PSK signal with raised-cosine pulse shape with a roll-off factor $\beta = 0.5$. What is the noiseless spectral efficiency of PSK? For the same spectral efficiency what is the bit energy-to-noise density ratio E_b/N_0 to achieve a reliable transmission dictated by the Shannon channel capacity?
3. Generate the DPSK signal for the following data bit sequence 0100110.
4. Consider the use of two Walsh functions derived from the two rows of the Hadamard matrix

$$\mathbf{H}_2 = \begin{bmatrix} 1 & 1 \\ 1 & -1 \end{bmatrix}$$

   We have $w_1(t) = p(t) + p(t - T_b)$ and $w_2(t) = p(t) - p(t - T_b)$ where $p(t)$ is a squared pulse of unit amplitude and duration T_b. These two Walsh functions are orthogonal by inspection over $(0, 2T_b)$. Let us use these two functions for binary communication. Show that this modulation technique is actually DPSK.
5. What is the noiseless spectral efficiency of FSK if a squared pulse shape is employed, assuming a null-to-null bandwidth? At $E_b/N_0 = 8$ dB compare the above result to the Shannon channel capacity. For the same spectral efficiency as FSK, what is the required E_b/N_0 dictated by the Shannon channel capacity for reliable transmission?
6. What is the spectral efficiency of MSK, assuming a null-to-null bandwidth? At $E_b/N_0 = 8$ dB compare the above result to the Shannon channel capacity. For the same spectral efficiency as MSK, what is the required E_b/N_0 dictated by the Shannon channel capacity for reliable transmission?
7. What is the spectral efficiency of GMSK with $BT_b = 0.25$, assuming a 90%-power bandwidth? At $E_b/N_0 = 8$ dB compare the above results to the Shannon channel capacity. For the same spectral efficiency as GMSK, what is the required E_b/N_0 dictated by the Shannon channel capacity for reliable transmission?

8. Generate the in-phase and quadrature bit sequences for MSK given the input bit sequence 110011001.
9. What are the noiseless spectral efficiencies of 8PSK and 16QAM, assuming raised-cosine pulse shapes with roll-off factors $\beta = 0$? At $E_b/N_0 = 8$ dB compare the above results to the Shannon channel capacity using Figure 4.8 and Figure 6.7. For the same spectral efficiency, what is the required E_b/N_0 dictated by the Shannon channel capacity for reliable transmission?
10. Derive the power spectral density expression (6.85), assuming uncorrelated data symbols.
11. Find the corresponding I-Q-values and phases of OQPSK for the data sequence 0010110110.
12. Use Table 6.6 to provide the differential encoding for DQPSK for the following data sequences:
    (a) {3, 4, 2, 1, 3}, assuming the initial phase is $\pi/4$ radians.
    (b) {2, 3, 4, 1, 2}, assuming the initial phase is $7\pi/4$ radians.
13. Use direct symbol mapping to verify the result in Example 6.28.
14. Provide the direct symbol mapping for DQPSK for the data sequence {1, 2, 4, 1, 3}, assuming the initial phase is $5\pi/4$ radians.
15. Provide the direct symbol mapping for $\pi/4$-DQPSK for the data sequence {3, 2, 4, 1, 3}, assuming the initial phase is $\pi/2$ radians.
16. Provide the direct symbol mapping for $\pi/4$-DQPSK for the following data sequences:
    (a) {3, 2, 4, 1, 3}, assuming the initial phase is $\pi/4$ radians.
    (b) {4, 2, 4, 1, 3}, assuming the initial phase is $7\pi/4$ radians.
17. Design three signal spaces for 16QAM with Gray encoding.
18. Perform differential encoding for D16QAM using Figure 6.37 and the message symbols {0 1 1 1, 1 0 0 0, 0 0 0 1, 1 1 0 0, 0 0 10}.
19. Perform the differential encoding for D16QAM using Figure 6.37 and the message symbols {0 1 1 0, 1 0 0 1, 1 0 0 0, 1 1 0 0, 0 1 0 1}.
20. Find the minimum Euclidean distances and average symbol energies of the signal spaces in Figure 6.35(a)–(c). For $M = 16$, compare the results with rectangular 16QAM.
    (a) The radii of the inner and outer circles are $\sqrt{E}$ and $2\sqrt{E}$, respectively, for Figure 6.35(a).
    (b) The radii of the circles are $\sqrt{E}, 3\sqrt{E}/2, 2\sqrt{E}$, and $5\sqrt{E}/2$ for Figure 6.35(b).
    (c) The radii of the inner and outer circles are $\sqrt{E}$ and $2\sqrt{E}$, respectively, for Figure 6.35(c).
21. The Walsh functions satisfy the *closure property*, that is, they form a *group* under multiplication. This means for any $w_i(t)$, $w_j(t) \in W_N$, $w_i(t)w_j(t) = w_k(t) \in W_N$, where W_N is the set of N Walsh functions.
    (a) Demonstrate this property using W_4 as an example.
    (b) Convert the Walsh indices i, j, k to their corresponding Walsh binary indices $\boldsymbol{Q}_i$, $\boldsymbol{Q}_j$, $\boldsymbol{Q}_k$. Construct a set W_4 such that $w_i(t)w_j(t) = w_k(t) \in W_4$ implies $\boldsymbol{Q}_k = \boldsymbol{Q}_i \oplus \boldsymbol{Q}_j$ and vice versa.
22. Show that the Walsh sequences obtained from the rows of the Hadamard matrix via the mapping $1 \rightarrow 0, -1 \rightarrow 1$ satisfy the *closure property*, that is, they form a *group* under modulo-2 addition.

(a) Demonstrate this property using $\mathbf{H}_4$ as an example.
(b) Convert the Walsh indices i, j, k to their corresponding Walsh binary indices $\boldsymbol{Q}_i$, $\boldsymbol{Q}_j$, $\boldsymbol{Q}_k$. Does $\boldsymbol{w}_i \oplus \boldsymbol{w}_j = \boldsymbol{w}_k \in \boldsymbol{W}_4$ imply $\boldsymbol{Q}_k = \boldsymbol{Q}_i \oplus \boldsymbol{Q}_j$ and vice versa?

23. The Walsh functions of order N can be indexed according to the number of zero crossings or sign changes which are in the range of 0 to $N-1$. The ith index can be represented by a $\log_2 N$-binary index vector $\boldsymbol{Q}_i$.
(a) Find the set of index vectors for Walsh sequences of order 8.
(b) Show that the index vectors satisfy the *closure property*, that is, they form a *group* under modulo-2 addition.

24. The Walsh functions generated by the Hadamard matrix are not indexed according to the number of zero crossings or sign changes as denoted by $\log_2 N$-binary index $\boldsymbol{Q}_i$. Find $\log_2 N$-binary index $\boldsymbol{U}_i$ that can accomplish this task. What is the relationship between $\boldsymbol{Q}_i$ and $\boldsymbol{U}_i$? Find both binary indices for Walsh functions and Hadamard matrix of order 16.

25. Walsh sequences can be generated according to the equation $\boldsymbol{w}_i = \boldsymbol{Q}_i\mathbf{G}$, where $\mathbf{G}$ is the generator matrix and addition and multiplication are for the Galois field GF(2). The sequence $\boldsymbol{Q}_i$ is the $\log_2 N$-binary index vector. Find $\mathbf{G}$ for Walsh sequences (functions) of order 16. Note that $\mathbf{G}$ is not unique and the set of N Walsh sequences can be spanned by a set of $\log_2 N$ linearly independent basis sequences. Thus $\mathbf{G}$ is a $\log_2 N \times N$ generator matrix.

26. Design a linear feedback shift register circuit to generate Walsh sequences.

27. CSK with 128 Walsh functions is employed for a wireless link. Data bits transmitted at rate 64 kbps are encoded with a rate ½ convolutional code to provide a coded bit stream for the CSK modulator. What is the symbol rate? What is the Walsh chip rate? The chip stream is spread by multiplying with a pseudo-noise (PN) sequence of chip rate equal to twice the Walsh rate. Assuming a null-to-null bandwidth, what is the CSK signal bandwidth? What is the spread factor?

28. Consider M orthogonal signals $\{s_i(t)\}_{i=1}^{M}$ from which we construct a set of $2M$ *biorthogonal* signals $\{s_i(t), -s_i(t)\}_{i=1}^{M}$.
(a) What are the normalized correlations between any two signals in the set?
(b) What are the Euclidean distances of the signal set?
(c) If the two orthogonal signals are $\sin 2\pi f_c t$ and $\cos 2\pi f_c t$ what is the resultant set of biorthogonal signals?

29. Consider a set of M orthogonal signals $\{s_i(t)\}_{i=1}^{M}$ with signal energy E. This set can be fully represented by a corresponding set of orthogonal vectors $\{\boldsymbol{s}_i\}_{i=1}^{M}$. Let the mean of these vectors be $\bar{\boldsymbol{s}} = (1/M)\sum_{i=1}^{\boldsymbol{M}} \boldsymbol{s}_i$. Define a new set of signals $\boldsymbol{v}_i = \boldsymbol{s}_i - \bar{\boldsymbol{s}}$, $i = 1, 2, \ldots, M$. Calculate the signal energy of the new set. Find the crosscorrelation of any pair of signals in the new set. When $M = 2$ show that this simplex signaling reduces to PSK.

30. Consider four-dimensional signals which can be represented by a set of vectors. From one vector $\boldsymbol{s}_1 = (1, 1, 1, 1)$ the other vectors can be formed by replacing the components of s_1 by their negatives.
(a) How many bits does a symbol vector carry?
(b) What are the symbol and bit energies?
(c) What is the minimum Euclidean distance?
(d) What is the minimum correlation between signal pairs?

31. Consider four-dimensional signals which can be represented by a set of vectors. From one vector $\boldsymbol{s}_1 = (3, 1, 1, 1)$ the other vectors can be formed by replacing the components of $\boldsymbol{s}_1$ by their negatives and by permutation of the components.
    (a) How many bits does a symbol vector carry?
    (b) What are the symbol and bit energies?
    (c) What is the minimum Euclidean distance?
    (d) What is the minimum correlation between signal pairs?
32. Consider a CP-4FSK and assume that the symbol rate is 64 ksps. What are the modulated signal bandwidths for $h = 0.5$ and $h = 1$?
33. Consider 3-RC-4CPM with $h = 0.25$ and $h = 0.5$, and 40 dB bandwidth. What would be the bit rate for each case so that it has the same bandwidth as MSK? Use null-to-null bandwidth for MSK.
34. What is the noiseless spectral efficiency of OFDM with 48 16QAM subcarriers? What is the achievable spectral efficiency of OFDM at $E_b/N_0 = 10$ dB for reliable transmission? Use Figure 4.8 for 16QAM.
35. Show that the first $L - 1$ samples of $y(n)$ in (6.170) can be discarded because they contain samples from the cyclic prefix of the current sequence and the ISI samples from the preceding sequence.
36. The use of cyclic prefix increases the bandwidth and power.
    (a) Examine IEEE 802.11a,g and determine the increase in bandwidth.
    (b) Examine IEEE 802.11a,g and determine the loss in performance of various subcarrier modulation techniques given a fixed transmit power.
37. Provide a symbol mapping via set partitioning for a TCM-8PAM.
38. Design a pragmatic rate $3/4$ TCM-256QAM with the industry standard rate ½ convolutional code in Figure 6.56.
39. Design a pragmatic rate $7/8$ TCM-256QAM with the industry standard rate ½ convolutional code in Figure 6.56.

Further reading

For a thorough review of amplitude modulation and frequency modulation we refer the reader to the books by Couch [2], Haykin [3], Ziemer and Tranter [4], Proakis and Salehi [5], and Carlson *et al*. [6]. For further exploration of digital modulation the reader should consult [13–23]. For CPM in particular, the following books go into greater detail than our coverage: [10,11,13,15,21].

Bibliography

1. G. Keiser, *Optical Fiber Communications*, 4th edition, New York: McGraw-Hill, 2007.
2. L. W. Couch, II, *Digital and Analog Communication Systems*, 7th edition, Upper Saddle River, NJ: Prentice Hall, 2007.

3. S. Haykin, *Communication Systems*, 3rd edition, Chichester: John Wiley & Sons, 1994.
4. R. E. Ziemer and W. H. Tranter, *Principles of Communications*, 4th edition, Chichester: John Wiley & Sons, 1995.
5. J. G. Proakis and M. Salehi, *Fundamentals of Communication Systems*, Upper Saddle River, NJ: Pearson Prentice Hall, 2005.
6. A. Bruce Carlson, P. B. Crilly, and J. C. Rutledge, *Communication Systems*, 4th edition, New York: McGraw-Hill, 2002.
7. IEEE Standards 802.11a, 1999.
8. IEEE Standards 802.11g, 2003.
9. W. J. Weber, "Differential encoding for multiple amplitude and phase shift keying systems," *IEEE Trans. Communications*, Vol. **26**, No. 3, pp. 385–391, 1978.
10. F. Xiong, *Digital Modulation Techniques*, Boston, MA: Artech House, 2000.
11. J. G. Proakis and M. Salehi, *Digital Communications*, 5th edition, New York: McGraw-Hill, 2008.
12. J. G. Proakis and D. G. Manolakis, *Digital Signal Processing*, 4th edition, Upper Saddle River, NJ: Prentice Hall, 2007.
13. J. B. Anderson, T. Aulin, and C.-E. Sundberg, *Digital Phase Modulation*, New York: Plenum Press, 1986.
14. J. R. Barry, E. A. Lee, and D. G. Messerschmitt, *Digital Communication*, 3rd edition, Amsterdam: Kluwer Academic Publishers, 2004.
15. S. Benedetto, E. Biglieri, and V. Castellani, *Digital Transmission Theory*, Englewood Cliffs, NJ: Prentice-Hall, 1987.
16. R. E. Blahut, *Digital Transmission of Information*, Addison-Wesley, 1990.
17. R. G. Gallager, *Principles of Digital Communication*, Cambridge: Cambridge University Press, 2008.
18. R. D. Gitlin, J. F. Hayes, and S. B. Weinstein. *Data Communications Principles*, New York: Plenum Press, 1992.
19. U. Madhow, *Fundamentals of Digital Communication*, Cambridge: Cambridge University Press, 2008.
20. M. B. Pursley, *Introduction to Digital Communications*, Upper Saddle River, NJ: Pearson Prentice-Hall, 2005.
21. M. K. Simon, S. M. Hinedi, and W. C. Lindsey, *Digital Communication Techniques. Signal Design and Detection*, Englewood Cliffs, NJ: Prentice-Hall, 1995.
22. B. Sklar, *Digital Communications. Fundamentals and Applications*, 2nd edition, Upper Saddle River, NJ: Prentice-Hall, 2001.
23. R. E. Ziemer and R. L. Peterson, *Introduction to Digital Communication*, 2nd edition, Upper Saddle River, NJ: Prentice-Hall, 2001.
24. G. C. Clark, Jr. and J. B. Cain, *Error-Correction Coding for Digital Communications*, New York: Plenum Press, 1981.
25. A. Lapidoth, *A Foundation in Digital Communication*, Cambridge: Cambridge University Press, 2009.
26. S. Lin and D. J. Costello, Jr., *Error Control Coding*, 2nd edition, Upper Saddle River, NJ: Pearson Prentice-Hall, 2004.

27. K. Murota and K. Hirade, "GMSK modulation for digital mobile radio telephony," *IEEE Trans. Commun*., Vol. **COM-29**, No.7, pp. 1044–1050, 1981.
28. T. S. Rappaport, *Wireless Communications*, 2nd edition, Upper Saddle River, NJ: Prentice Hall, 2002.
29. C. E. Shannon, "A mathematical theory of communication," *Bell Syst. Tech. J*., Vol. **27**, pp. 379–423, 1948.
30. C. E. Shannon, "A mathematical theory of communication," *Bell Syst. Tech. J*., Vol. **27**, pp. 626–656, 1948.
31. S. G. Wilson, *Digital Modulation and Coding*, Englewood Cliffs, NJ: Prentice-Hall, 1996.
32. J. M. Wozencraft and I. M. Jacobs, *Principles of Communication Engineering*, New York: Wiley, 1965; Waveland Press, 1990.
33. G. Ungerboeck, "Channel coding with multilevel/phase signals," *IEEE Trans. Information Theory*, Vol. **IT-28**, No.1, pp. 55–67, 1982.

7 Demodulation

Introduction

The purpose of *digital demodulation* is to recover the information (bits, symbols) carried by the digitally modulated signals. This process can be achieved via *coherent* or *noncoherent* demodulation. The former requires a local reference carrier to be matched exactly in frequency and phase to the received signal. The latter requires only a match in frequency. Both types of demodulation involve *two* steps. In the first step, a *signal processor* is employed to convert the received signal that represents a bit (binary modulation) or a symbol (M-ary modulation) into a decision sample at maximum signal-to-noise ratio for the case of coherent demodulation. For noncoherent demodulation, the signal processor converts the received signal into a nonnegative decision sample independent of its unknown initial phase, which is cleverly discarded. Since the phase information is not employed, a loss in the signal-to-noise ratio for the decision sample results. The coherent signal processors are the *matched filter* and the *correlator*, both are equivalent at the time the decision sample is taken. The noncoherent signal processors are the *matched filter-envelope detector* (also known as *noncoherent matched filter*) and the *quadrature correlator-square law detector* (also known as *noncoherent correlator*), both are also equivalent at the time the decision sample is obtained. Binary demodulation employs one or two signal processors depending on the type of modulation. On the other hand, M-ary modulation requires a bank of L signal processors, $1 \leq L \leq M$.

In the *second* step, an *optimum detector* (*maximum likelihood detector*) is employed to determine the bit or the symbol represented by the decision sample. The optimum detector recovers the information with a minimum bit error probability for a given received signal-to-noise ratio. Figure 7.1 illustrates the digital demodulation concept. For binary demodulation, the optimum detector is the threshold detector or the maximum detector depending on the type of modulation. For M-ary demodulation, the optimum detector is the minimum Euclidean distance detector or the M-ary maximum detector, again, depending on the type of modulation.

Demodulation will be studied for the digital modulation techniques discussed in Chapter 6, which includes the family of I-Q modulation such as MASK, MPSK, and MQAM, the family of orthogonal signals such as CSK and MFSK, and the family of continuous phase modulation (CPM). We also provide a study of OFDM demodulation.

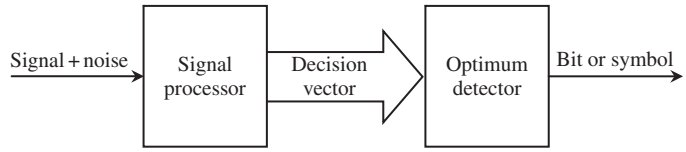

Figure 7.1 Generic digital demodulator. The decision vector may contain up to M decision samples.

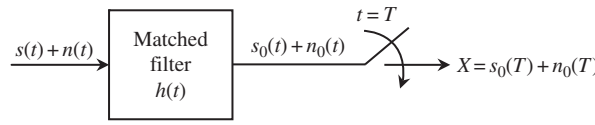

Figure 7.2 The matched filter.

7.1 The matched filter

The *matched filter* is the most important signal processor in signal detection. It is designed to *maximize* the *output signal-to-noise ratio* at the detection time. The requirement is that the received signal waveform must be known at the receiver. In communications, the waveform of a bit or symbol is known a priori. If the channel does not distort the signal, then the matched filter can be designed accordingly. Let us assume an AWGN channel with *input noise* $n(t)$ with power spectral density $N_0/2$ (W/Hz). The received *input signal* is denoted as $s(t)$ and is assumed to be *real* and *time-limited* to T seconds. The *impulse response* of the matched filter is denoted as $h(t)$. Furthermore, let $s_0(t)$ denote the *output signal* and $n_0(t)$ denote the *output noise*. We wish to design $h(t)$ in such a way to maximize the output signal-to-noise ratio at the detection time $t = T$, which is defined as

$$SNR_0 = \frac{s_0^2(T)}{n_0^2(T)} \tag{7.1}$$

The matched filter concept is illustrated in Figure 7.2. Note that SNR_0 is simply the ratio of the *square of the mean* to the *variance* of the *decision variable* $X = s_0(T) + n_0(T)$.

Time domain interpretation

First let us examine the output signal $s_0(t)$. Using convolution, we obtain

$$s_0(t) = \int_{-\infty}^{\infty} s(\tau)\, h(t-\tau)\mathrm{d}\tau \tag{7.2}$$

Similarly, the output noise $n_0(t)$ is given by

$$n_0(t) = \int_{-\infty}^{\infty} n(\tau)\, h(t-\tau)\mathrm{d}\tau \tag{7.3}$$

Using (7.3), we can evaluate the *mean-square value* of the noise sample $n_0(T)$:

$$\begin{aligned}\overline{n_0^2(T)} &= \mathbf{E}\left\{\int_{-\infty}^{\infty}\int_{-\infty}^{\infty} n(t)\,n(\tau)h(T-t)h(T-\tau)\mathrm{d}t\,\mathrm{d}\tau\right\}\\ &= \int_{-\infty}^{\infty}\int_{-\infty}^{\infty}\mathbf{E}\{\,n(t)n(\tau)\}\,h(T-t)h(T-\tau)\mathrm{d}t\,\mathrm{d}\tau\\ &= \frac{N_0}{2}\int_{-\infty}^{\infty}\int_{-\infty}^{\infty}\delta(t-\tau)\,h(T-t)h(T-\tau)\mathrm{d}t\,\mathrm{d}\tau\\ &= \frac{N_0}{2}\int_{-\infty}^{\infty}h^2(T-t)\mathrm{d}t\end{aligned} \tag{7.4}$$

We have used the fact that noise is *wide-sense stationary* so that $E\{n(t)n(\tau)\} = (N_0/2)\delta(t-\tau)$. Substituting (7.2) and (7.4) into (7.1), we have

$$\begin{aligned}SNR_0 &= \left(\frac{2}{N_0}\right)\frac{\left[\int_{-\infty}^{\infty}s(\tau)h(T-\tau)\mathrm{d}\tau\right]^2}{\int_{-\infty}^{\infty}h^2(T-t)\mathrm{d}t}\\ &= \left(\frac{2}{N_0}\right)\frac{\left[\int_{-\infty}^{\infty}s(t)h(T-t)\mathrm{d}t\right]^2}{\int_{-\infty}^{\infty}h^2(T-t)\mathrm{d}t}\end{aligned} \tag{7.5}$$

The right-hand side of (7.5) can be maximized with the help of the *Cauchy–Schwarz inequality*, which states that

$$\left|\int_{-\infty}^{\infty}a^*(t)\,b(t)\mathrm{d}t\right|^2 \le \int_{-\infty}^{\infty}|a(t)|^2\mathrm{d}t\;\int_{-\infty}^{\infty}|b(t)|^2\mathrm{d}t \tag{7.6}$$

where $a(t)$ and $b(t)$ are complex and finite energy functions. The equality holds *if and only if* within a scaling constant α

$$b(t) = \alpha\,a^*(t) \tag{7.7}$$

Without loss of generality, we assume $s(t)$ is real. Therefore, if we set $a(t) = s(t)$ and $b(t) = h(T-t)$, and apply (7.6) to (7.5), we get

$$\begin{aligned}SNR_0 &\le \left(\frac{2}{N_0}\right)\frac{\int_{-\infty}^{\infty}s^2(t)\,\mathrm{d}t\int_{-\infty}^{\infty}h^2(T-t)\,\mathrm{d}t}{\int_{-\infty}^{\infty}h^2(T-t)\mathrm{d}t}\\ &\le \left(\frac{2}{N_0}\right)\int_{-\infty}^{\infty}s^2(t)\mathrm{d}t \;\le\; \frac{2E}{N_0}\end{aligned} \tag{7.8}$$

where E is the energy of $s(t)$, defined as

$$E = \int_{-\infty}^{\infty}s^2(t)\,\mathrm{d}t \tag{7.9}$$

The maximum of SNR_0 is $2E/N_0$, which is achieved *if and only if*

$$h(T-t) = \alpha s^*(t) \tag{7.10}$$

or, equivalently,

$$h(t) = \alpha s^*(T-t) = \alpha s(T-t) \tag{7.11}$$

when $s(t)$ is real. This shows that $h(t)$ is simply a *time-reversed* and *T-translated* version of $s(t)$, hence the name matched filter. For simplicity we set $\alpha = 1$ in (7.11) and observe that at the detection time $t = T$, the matched filter collects the signal energy E, that is, the signal must have passed completely through the filter. It is then *sufficient* to assume that $s(t)$ is *time-limited* to T seconds to ensure that $SNR_0 = 2E/N_0$ at $t = T$, which is the maximum signal-to-noise ratio.

Example 7.1 Time-limited baseband pulse

Consider the signal $s(t) = Ap(t)$, where $p(t)$ is a *unit amplitude* pulse of *duration* T seconds as shown in Figure 7.3. The matched filter impulse response is simply a scaled version of the input signal, and the output signal $s_0(t)$ peaks at the detection time $t = T$ with amplitude $s_0(T) = \alpha A^2 T = \alpha E$. The output noise power, which can be evaluated from (7.4) and (7.10), is $\overline{n_0^2(T)} = \alpha^2 A^2 T N_0/2 = \alpha^2 E N_0/2$. The output signal-to-noise ratio at $t = T$ is $SNR_0 = s_0^2(T)/\overline{n_0^2(T)} = 2E/N_0$.

It is often convenient to analyze a bandpass signal via its complex envelope or equivalent lowpass signal. In this case, the equivalent lowpass noise of the original bandpass noise that accompanies the bandpass signal must be used. If the power spectral density of the bandpass noise is $N_0/2$, then, the power spectral density of the equivalent lowpass noise is N_0. Consider the bandpass signal $s(t) = Ap(t)\cos 2\pi f_c t$ with energy $E = A^2T/2$. The complex envelope or equivalent lowpass signal is $s_L(t) = Ap(t)$ with energy $E_L = A^2T = 2E$. The output of the matched filter that matches $s_L(t)$ is $s_{L,0}(T) = \alpha A^2 T = \alpha E_L$. The output noise power can be evaluated from (7.4) and (7.10) with N_0 replacing $N_0/2$ and $s_L(t)$ replacing

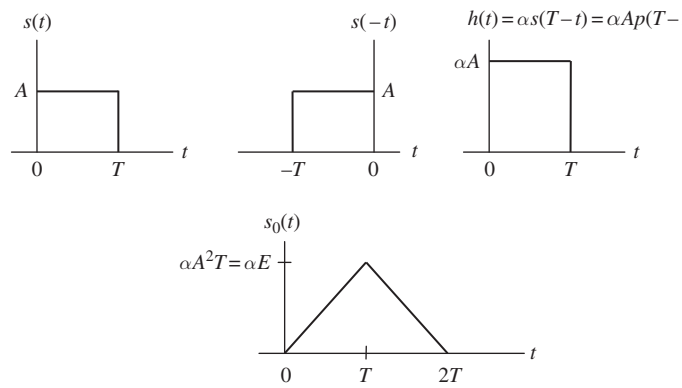

Figure 7.3 Matched filter impulse response and output.

$s(t)$ and is given by $\overline{n_{L,0}^2(T)} = \alpha^2 A^2 T N_0 = \alpha^2 E_L N_0$. Thus, the output signal-to-noise ratio is given as $SNR_{L,0} = s_{L,0}^2(T) \Big/ \overline{n_{L,0}^2(T)} = E_L/N_0 = 2E/N_0 = SNR_0$.

■

Example 7.2 Time-limited modulated pulse

Consider the signal $s(t) = Ap(t)\cos 2\pi f_c t$, where $p(t)$ is again a *unit amplitude* pulse of *duration* T seconds and f_c is the carrier frequency. The matched filter can be implemented after the voltage multiplier as shown in Figure 7.4.

The output $v(t)$ of the voltage multiplier is

$$\begin{aligned} v(t) &= s(t)\cos 2\pi f_c t = Ap(t)\cos^2 2\pi f_c t \\ &= \frac{A}{2}p(t) + \frac{A}{2}p(t)\cos 4\pi f_c t \end{aligned} \tag{7.12}$$

The high-frequency term $\frac{1}{2}Ap(t)\cos 4\pi f_c t$ is filtered out by the matched filter that matches the component $Ap(t)$. Alternatively, one can implement the matched filter that matches the signal $s(t)$ directly, as shown in Figure 7.5. Note that the output signal $s_0(t)$ is a modulated triangular pulse with a peak at the time $t = T$, where the maximum SNR_0 is achieved. The drawback of the implementation in Figure 7.5 is the requirement for more accurate sampling timing because of the sharp roll-off of the signal around the time $t = T$.

■

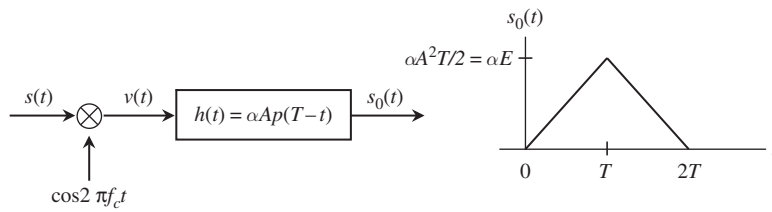

Figure 7.4 Matched filter for a modulated pulse.

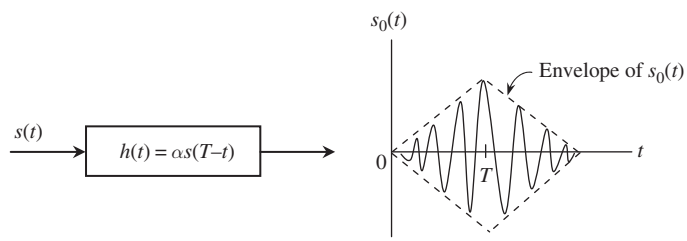

Figure 7.5 Alternative matched filter for a modulated pulse.

Frequency domain interpretation

The matched filter design can also be carried out in the frequency domain via the Fourier transform. Let $H(f)$ be the transfer function of the matched filter and $S(f)$ be the Fourier transform of the input signal $s(t)$. The Fourier transform of the output signal $s_0(t)$ is simply $H(f)S(f)$, and hence, $s_0(t)$ is given by the inverse Fourier transform

$$s_0(t) = \int_{-\infty}^{\infty} H(f)S(f)\,\mathrm{e}^{\mathrm{j}2\pi ft}\mathrm{d}f \tag{7.13}$$

Applying the Parseval formula to (7.4) we obtain the output noise power at $t = T$ as follows:

$$\overline{n_0^2(T)} = \frac{N_0}{2}\int_{-\infty}^{\infty} |H(f)|^2\mathrm{d}f \tag{7.14}$$

Substituting (7.13) and (7.14) into (7.1), we obtain

$$SNR_0 = \left(\frac{2}{N_0}\right)\frac{\left[\int_{-\infty}^{\infty} H(f)S(f)\mathrm{e}^{\mathrm{j}2\pi fT}\mathrm{d}f\right]^2}{\int_{-\infty}^{\infty}|H(f)|^2\mathrm{d}f} \tag{7.15}$$

$$\begin{aligned}
&\leq \left(\frac{2}{N_0}\right)\frac{\int_{-\infty}^{\infty}|H(f)|^2\mathrm{d}f\int_{-\infty}^{\infty}|S(f)|^2\mathrm{d}f}{\int_{-\infty}^{\infty}|H(f)|^2\mathrm{d}f}\\
&\leq \frac{2}{N_0}\int_{-\infty}^{\infty}|S(f)|^2\mathrm{d}f = \frac{2}{N_0}\int_{-\infty}^{\infty}s^2(t)\mathrm{d}t\\
&\leq \frac{2E}{N_0}
\end{aligned} \tag{7.16}$$

via the use of the Cauchy–Schwarz inequality and the Parseval formula, and the fact that $\left|S(f)\mathrm{e}^{\mathrm{j}2\pi fT}\right| = |S(f)|$. The maximum SNR_0 is obtained when

$$H(f) = \alpha S^*(f)\mathrm{e}^{-\mathrm{j}2\pi fT} \tag{7.17}$$

which yields (7.11) via the inverse Fourier transform

$$h(t) = \alpha s^*(T-t) = \alpha s(T-t) \tag{7.18}$$

when $s(t)$ is real.

Output signal and noise waveforms

Let us examine the waveform of the output signal $s_0(t)$. Directly substituting (7.11) or (7.18) into (7.2), and assuming a real signal $s(t)$, we have

$$\begin{aligned} s_0(t) &= \alpha \int_{-\infty}^{\infty} s(\tau)s(T-(t-\tau))\mathrm{d}\tau = \alpha \int_{-\infty}^{\infty} s(\tau)s(T-t+\tau)\mathrm{d}\tau \\ &= \alpha R_s(T-t) = \alpha R_s(t-T) \end{aligned} \tag{7.19}$$

where $R_s(\tau)$, by definition (2.191), is the autocorrelation of the input signal $s(t)$ with a time lag τ. Note that the autocorrelation is an even function by (2.194). At time $t = T$, we get

$$\begin{aligned} s_0(T) &= \alpha R_s(0) = \alpha \int_{-\infty}^{\infty} s^2(t)\mathrm{d}t \\ &= \alpha E \end{aligned} \tag{7.20}$$

Furthermore, the output noise in (7.3) is given by

$$n_0(t) = \alpha \int_{-\infty}^{\infty} n(\tau)s(T-t+\tau)\mathrm{d}\tau \tag{7.21}$$

and hence, at $t = T$,

$$n_0(T) = \alpha \int_{-\infty}^{\infty} n(t)s(t)\mathrm{d}t \tag{7.22}$$

Note that $\overline{n_0^2(T)} = \alpha^2 EN_0/2$ via (7.4) and (7.10).

Decision variable

In order to evaluate the matched filter performance in signal detection, we need to know that statistics of the decision variable $X = s_0(T) + n_0(T)$ at the output of the matched filter in Figure 7.2. First, we note that the matched filter is a linear filter; therefore, the output noise $n_0(t)$ is also Gaussian. Thus, X is a Gaussian random variable with the following statistics:

$$\overline{X} = s_0(T) = \alpha E \tag{7.23}$$

$$\sigma^2 = \overline{n_0^2(T)} = \alpha^2 EN_0/2 \tag{7.24}$$

$$f_X(x) = \frac{1}{\sqrt{2\pi}\sigma} \mathrm{e}^{-\left(x-\overline{X}\right)^2/2\sigma^2} \tag{7.25}$$

where $\overline{X}$, σ^2, and $f_X(x)$ are the mean, variance, and probability density function of X, respectively. Again α is a scaling factor which can always be set to unity if so desired.

The probability distribution function $F_X(x) = \Pr(X \le x)$ is given by

$$\begin{aligned} F_X(x) &= \Pr(X \le x) = \int_{-\infty}^{x} f_X(y)\mathrm{d}y \\ &= \frac{1}{\sqrt{2\pi}\sigma} \int_{-\infty}^{x} \mathrm{e}^{-\left(y-\overline{X}\right)^2/2\sigma^2}\mathrm{d}y = \frac{1}{\sqrt{2\pi}} \int_{\left(\overline{X}-x\right)/\sigma}^{\infty} \mathrm{e}^{-y^2/2}\mathrm{d}y \\ &= Q\left(\frac{\overline{X}-x}{\sigma}\right) \end{aligned} \tag{7.26}$$

where $Q(a)$ is the Gaussian integral with argument "a" defined as follows:

$$Q(a) = \frac{1}{\sqrt{2\pi}} \int_a^\infty \mathrm{e}^{-y^2/2} \mathrm{d}y \tag{7.27}$$

and

$$Q(-a) = 1 - Q(a) \tag{7.28}$$

Note that

$$\begin{aligned} \Pr(X > x) &= 1 - \Pr(X \leq x) \\ &= Q\left(\frac{x - \overline{X}}{\sigma}\right) \end{aligned} \tag{7.29}$$

Summary

The matched filter is a *coherent* signal processor because the signal waveform must be known exactly. Its impulse response is the *time-reversed* and *T-translated* waveform of the signal. It achieves the maximum output signal-to-noise ratio of $2E/N_0$ at the sampling time $t = T$. The output of the matched filter, expressed by $X = s_0(T) + n_0(T)$, completely represents the received signal $r(t) = s(t) + n(t)$. In other words, X represents sufficient statistics that summarize $r(t)$ for the purpose of detecting the input signal $s(t)$. Sufficient statistics allow viewing an infinite dimensional signal $x(t)$ as a scalar X well enough for the detection of $s(t)$. It can be shown via (7.20) that $e(t) = r(t) - Xx_1(t) = s(t) + n(t) - s_0(T)x_1(t) - n_0(T)x_1(t) = n(t) - n_0(T)x_1(t)$, where $x_1(t)$ is a unit energy function defined as $x_1(t) = s(t)/\sqrt{E}$ and α is selected to be $\alpha = 1/\sqrt{E}$, and is *uncorrelated* to X, that is, $\mathbf{E}\{e(t)X\} = 0$. Thus, $e(t)$ contains no information relevant to the detection of $s(t)$. Note that $s(t) = s_0(T)x_1(t)$, thus $s_0(T)$ is the projection of $s(t)$ into the basis function $x_1(t)$. Similarly, $n_0(T)$ is the projection of input noise $n(t)$ onto $x_1(t)$. Also note that the noise $e(t) = n(t) - n_0(T)x_1(t)$ is Gaussian, therefore, $\mathbf{E}\{e(t)X\} = 0$ also implies that $e(t)$ and X are *independent*. Therefore, $e(t)$ is irrelevant in the detection of $s(t)$. From the statistical point of view, the Gaussian random variable $X = s_0(T) + n_0(T)$ requires only two parameters to fully characterize it, namely, its mean and variance. Since the mean is $s_0(T)$ and the variance is the variance of $n_0(T)$, sufficient statistics are contained in X.

7.2 The correlator

When the input signal $s(t)$ to a matched filter is time-limited to T seconds, the matched filter output signal and noise at the sampling time $t = T$ in (7.20) and (7.22) can be written as

$$s_0(T) = \alpha \int_0^T s^2(t)\, \mathrm{d}t \tag{7.30}$$

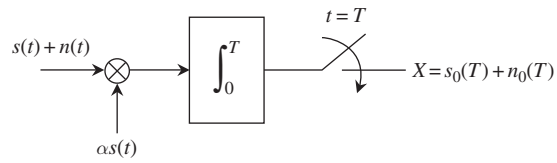

Figure 7.6 The correlator.

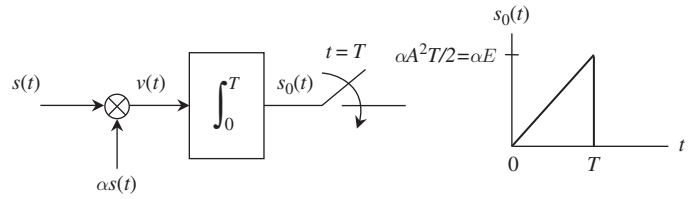

Figure 7.7 Correlator for a modulated pulse.

$$n_0(T) = \alpha \int_0^T n(t)s(t)\,\mathrm{d}t \tag{7.31}$$

The above two equations allow us to alternatively implement the matched filter by using a voltage multiplier and an integrator as illustrated in Figure 7.6. This equivalent version of the matched filter is called the *correlator*. Note that the equivalence is valid only at the sampling time $t = T$. This also implies that the output of the correlator represents sufficient statistics for the detection of $r(t) = s(t) + n(t)$.

Example 7.3 Time-limited modulated pulse

As in Example 7.2, we consider a modulated pulse $s(t) = Ap(t)\cos 2\pi f_c t$. The correlator for this signal is shown in Figure 7.7. The output $v(t)$ of the voltage multiplier is given by

$$\begin{aligned} v(t) &= \alpha s^2(t) \\ &= \alpha A^2 p^2(t)\cos^2 2\pi f_c t \\ &= \frac{1}{2}\alpha A^2 p(t) + \frac{1}{2}\alpha A^2 p(t)\cos 4\pi f_c t \end{aligned} \tag{7.32}$$

Note that $p^2(t) = p(t)$ and the high-frequency term $\frac{1}{2}\alpha A^2 p(t)\cos 4\pi f_c t$ is filtered out by the integrator, which acts as a lowpass filter. The output signal is $s_0(t) = \frac{1}{2}\alpha A^2 t\, p(t)$, which yields at $t = T$ the sample $s_0(T) = \alpha A^2 T/2 = \alpha E$. Thus, we obtain the same result as that of the matched filter approach in Example 7.2.

■

7.3 The matched filter–envelope detector (noncoherent matched filter)

Both the matched filter and correlator are coherent signal processors. They require the complete knowledge of the signal, that is, amplitude, frequency, and phase. In many

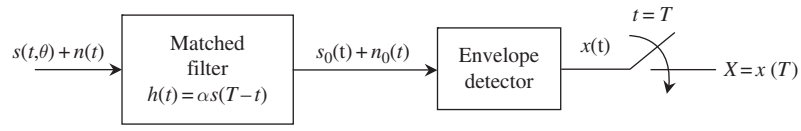

Figure 7.8 Matched filter–envelope detector for a signal $s(t)$ with an unknown phase θ.

applications, the phase of a modulated carrier cannot be tracked accurately. Therefore, the matched filter or the correlator will fail to work in these cases. Let us examine the case in Example 7.3. Suppose the signal $s(t)$ arrives at the receiver with an unknown phase θ, that is, $s(t) = Ap(t)\cos(2\pi f_c t + \theta)$. In this case, the output signal $v(t)$ is $v(t) = \frac{1}{2}\alpha A^2 p(t)\cos\theta + \frac{1}{2}\alpha A^2 p(t)\cos(4\pi f_c t + \theta)$. Thus, the output of the integrator is $s_0(t) = \frac{1}{2}\alpha A^2 t\, p(t)\cos\theta$, which yields $s_0(T) = \frac{1}{2}\alpha A^2 T\cos\theta$. It is obvious that $s_0(T) = 0$ when $\theta = 90^\circ$, which implies a zero output signal! To avoid the situation where coherent demodulation cannot be achieved with a matched filter or a correlator, we can employ a combination of matched filter–envelope detector (also referred to as noncoherent matched filter) or quadrature correlator–square-law detector (or noncoherent correlator). In this section we study the former while the latter will be examined in Section 7.4.

For a digital signal whose information is contained in its complex envelope (lowpass equivalent signal), an envelope detector can be employed at the output of the matched filter to extract the information bit. Obviously, we can just employ the envelope detector to extract the information bit without the use of a matched filter in some modulation techniques, such as standard AM (OOK or ASK, for example). On the other hand, the matched filter–envelope detector will give us better performance, as we will prove later. Figure 7.8 illustrates the matched filter–envelope detector.

We assume that the matched filter is matched to the transmitted signal $s(t)$, but when $s(t)$ arrives at the receiver, the channel introduces an unknown phase θ. Let us describe $s(t)$ by its envelope-phase representation as follows:

$$s(t) = R(t)\cos 2\pi f_c t \tag{7.33}$$

where $R(t)$ is the envelope of $s(t)$. The received signal $s(t, \theta)$ is therefore given by

$$s(t, \theta) = R(t)\cos(2\pi f_c t + \theta) \tag{7.34}$$

where θ is the unknown phase. The matched filter impulse response $h(t)$ is simply a time-reversed and T-translated version of $s(t)$ as given by (7.11) as follows:

$$\begin{aligned} h(t) &= \alpha s(T - t) \\ &= \alpha R(T - t)\cos[2\pi f_c(T - t)] \end{aligned} \tag{7.35}$$

The channel attenuation can be included in the parameter α in (7.35) if desired. The output signal $s_0(t)$ at the matched filter output is

$$\begin{aligned} s_0(t) &= \alpha \int_{-\infty}^{\infty} s(\tau,\theta)h(t-\tau)\,\mathrm{d}\tau = \alpha \int_{-\infty}^{\infty} \mathrm{s}(\tau,\theta)s(T-t+\tau)\,\mathrm{d}\tau \\ &= \alpha \int_{-\infty}^{\infty} R(\tau)\,\cos(2\pi f_c\tau+\theta)R(T-t+\tau)\cos[2\pi f_c(T-t+\tau)]\mathrm{d}\tau \\ &= \left[\alpha \int_{-\infty}^{\infty} R(\tau)R(T-t+\tau)\,\cos(2\pi f_c\tau+\theta)\,\cos 2\pi f_c\tau\,\,\mathrm{d}\tau\right]\cos[2\pi f_c(T-t)] \\ &\quad - \left[\alpha \int_{-\infty}^{\infty} R(\tau)R(T-t+\tau)\,\cos(2\pi f_c\tau+\theta)\sin 2\pi f_c\tau\,\,\mathrm{d}\tau\right]\sin[2\pi f_c(T-t)] \end{aligned} \tag{7.36}$$

Further simplification yields

$$s_0(t) = s_{0,I}(t)\cos[2\pi f_c(T-t)] - s_{0,Q}(t)\sin[2\pi f_c(T-t)] \tag{7.37}$$

where

$$\begin{aligned} s_{0,I}(t) &= \frac{\alpha}{2}\int_{-\infty}^{\infty} R(\tau)R(T-t+\tau)\cos\theta\,\,\mathrm{d}\tau \\ &\quad + \frac{\alpha}{2}\int_{-\infty}^{\infty} R(\tau)R(T-t+\tau)\cos(4\pi f_c\tau+\theta)\,\,\mathrm{d}\tau \end{aligned} \tag{7.38}$$

$$\begin{aligned} s_{0,Q}(t) &= -\frac{\alpha}{2}\int_{-\infty}^{\infty} R(\tau)R(T-t+\tau)\sin\theta\,\mathrm{d}\tau \\ &\quad + \frac{\alpha}{2}\int_{-\infty}^{\infty} R(\tau)R(T-t+\tau)\sin(4\pi f_c\tau+\theta)\,\mathrm{d}\tau \end{aligned} \tag{7.39}$$

are the *in-phase* and *quadrature* components of $s_0(t)$, respectively. Now consider the output noise $n_0(t)$. From (7.21), we get

$$\begin{aligned} n_0(t) &= \alpha \int_{-\infty}^{\infty} n(\tau)h(t-\tau)\,\mathrm{d}\tau = \alpha \int_{-\infty}^{\infty} n(\tau)s(T-t+\tau)\,\mathrm{d}\tau \\ &= \alpha \int_{-\infty}^{\infty} n(\tau)R(T-t+\tau)\,\cos[2\pi f_c(T-t+\tau)]\mathrm{d}\tau \\ &= \left[\alpha \int_{-\infty}^{\infty} n(\tau)R(T-t+\tau)\,\cos 2\pi f_c\tau\,\,\mathrm{d}\tau\right]\cos[2\pi f_c(T-t)] \\ &\quad - \left[\alpha \int_{-\infty}^{\infty} n(\tau)R(T-t+\tau)\,\sin 2\pi f_c\tau\,\,\mathrm{d}\tau\right]\sin[2\pi f_c(T-t)] \\ &= n_{0,I}(t)\cos[2\pi f_c(T-t)] - n_{0,Q}(t)\sin[2\pi f_c(T-t)] \end{aligned} \tag{7.40}$$

where

$$n_{0,I}(t) = \alpha \int_{-\infty}^{\infty} n(\tau)R(T-t+\tau)\cos 2\pi f_c\tau\,\,\mathrm{d}\tau \tag{7.41}$$

$$n_{0,Q}(t) = \alpha \int_{-\infty}^{\infty} n(\tau)R(T-t+\tau)\sin 2\pi f_c\tau\,\,\mathrm{d}\tau \tag{7.42}$$

are the in-phase and quadrature components of $n_0(t)$, respectively.

Combining (7.37) and (7.40), we obtain the output $s_0(t) + n_0(t)$ of the matched filter as follows:

$$\begin{aligned} s_0(t) + n_0(t) = &\left[s_{0,I}(t) + n_{0,I}(t)\right] \cos[2\pi f_c(T-t)] \\ &- \left[s_{0,Q}(t) + n_{0,Q}(t)\right] \sin[2\pi f_c(T-t)] \end{aligned} \tag{7.43}$$

Consequently, the output of the envelope detector is simply

$$x(t) = \sqrt{\left[s_{0,I}(t) + n_{0,I}(t)\right]^2 + \left[s_{0,Q}(t) + n_{0,Q}(t)\right]^2} \tag{7.44}$$

The decision variable X at the sampling time $t = T$ is given by $X = x(T)$ as

$$X = \sqrt{\left[s_{0,I}(T) + n_{0,I}(T)\right]^2 + \left[s_{0,Q}(T) + n_{0,Q}(T)\right]^2} \tag{7.45}$$

where

$$s_{0,I}(T) = \frac{\alpha}{2}\cos\theta \int_{-\infty}^{\infty} R^2(t)\,\mathrm{d}t + \frac{\alpha}{2}\int_{-\infty}^{\infty} R^2(t)\cos(4\pi f_c t + \theta)\,\mathrm{d}t \tag{7.46}$$

$$s_{0,Q}(T) = -\frac{\alpha}{2}\sin\theta \int_{-\infty}^{\infty} R^2(t)\,\mathrm{d}t + \frac{\alpha}{2}\int_{-\infty}^{\infty} R^2(t)\sin(4\pi f_c t + \theta)\,\mathrm{d}t \tag{7.47}$$

$$n_{0,I}(T) = \alpha \int_{-\infty}^{\infty} n(t)R(t)\cos 2\pi f_c t\ \mathrm{d}t \tag{7.48}$$

$$n_{0,Q}(T) = \alpha \int_{-\infty}^{\infty} n(t)R(t)\sin 2\pi f_c t\ \mathrm{d}t \tag{7.49}$$

Example 7.4 The evaluation of $s_{0,I}(T)$ and $s_{0,Q}(T)$

Let us examine (7.46) and (7.47). First let E be the energy of $s(t)$ as usual, that is

$$\begin{aligned} E &= \int_{-\infty}^{\infty} s^2(t)\,\mathrm{d}t = \int_{-\infty}^{\infty} R^2(t)\cos^2 2\pi f_c t\ \mathrm{d}t \\ &= \frac{1}{2}\int_{-\infty}^{\infty} R^2(t)\,\mathrm{d}t + \frac{1}{2}\int_{-\infty}^{\infty} R^2(t)\cos 4\pi f_c t\ \mathrm{d}t \end{aligned} \tag{7.50}$$

The second integral on the right is very small compared with the first integral on the right because of the oscillation due to the carrier at $2f_c$. For example, let $R(t) = Ap(t)$, where $p(t)$ is the *unit amplitude* pulse of T *seconds* duration. Then, the first integral on the right is $A^2T/2$, and the second integral is $(A^2T/2)[\sin 4\pi f_c T/4\pi f_c T]$, which is much smaller than $A^2T/2$ for $f_cT \gg 1$, a case we always encounter in practice. Thus, for all practical purposes $s_{0,I}(T)$ and $s_{0,Q}(T)$ in (7.46) and (7.47) can be reasonably approximated by

$$s_{0,I}(T) \approx \alpha E\cos\theta \tag{7.51}$$

$$s_{0,Q}(T) \approx -\alpha E\sin\theta \tag{7.52}$$

■

Example 7.5 Statistics of output noise components $n_{0,I}(T)$ and $n_{0,Q}(T)$

Using the fact that the input AWGN $n(t)$ has zero mean, we conclude that $\overline{n_{0,I}(T)} = \overline{n_{0,Q}(T)} = 0$. Thus, the variance of $n_{0,I}(T)$ or $n_{0,Q}(T)$ is the same as their mean-squared value. Using (7.48), we get

$$\overline{n_{0,I}^2(T)} = \alpha^2 \int_{-\infty}^{\infty} \int_{-\infty}^{\infty} \mathbf{E}\{n(t)n(\tau)\}\, R(t)R(\tau) \cos 2\pi f_c t \cos 2\pi f_c \tau \, \mathrm{d}t \, \mathrm{d}\tau \tag{7.53}$$

The autocorrelation of noise $n(t)$ is $\mathbf{E}\{n(t)n(\tau)\} = (N_0/2)\delta(t-\tau)$, and, therefore, using the same approximation that applies to (7.50), we have

$$\begin{aligned} \overline{n_{0,I}^2(T)} &= \frac{\alpha^2 N_0}{2} \int_{-\infty}^{\infty} R^2(t) \cos^2 2\pi f_c t \, \mathrm{d}t \\ &= \frac{\alpha^2 N_0}{4} \int_{-\infty}^{\infty} R^2(t) \, \mathrm{d}t + \frac{\alpha^2 N_0}{4} \int_{-\infty}^{\infty} R^2(t) \cos 4\pi f_c t \, \mathrm{d}t \\ &\approx \frac{\alpha^2 E N_0}{2} \end{aligned} \tag{7.54}$$

Similarly,

$$\overline{n_{0,Q}^2(T)} \approx \frac{\alpha^2 E N_0}{2} \tag{7.55}$$

We remark that the matched filter is a linear time-invariant systems; therefore, its output noise components are both Gaussian random variables with zero mean and variance $\alpha^2 E N_0/2$.

■

Output signal-to-noise ratio

We are now in a position to further explore the output signal-to-noise ratio SNR_0 at the matched filter–envelope detector output. Specifically, we first evaluate the total output power via (7.45), that is, the mean-square value of the decision variable X. Using (7.51)–(7.55), we obtain

$$\begin{aligned} \overline{X^2} &= s_{0,I}^2(T) + \overline{n_{0,I}^2(T)} + s_{0,Q}^2(T) + \overline{n_{0,Q}^2(T)} \\ &\approx \alpha^2 E^2 + \alpha^2 E N_0 \end{aligned} \tag{7.56}$$

The power of the signal component is $\alpha^2 E^2$ while that of noise is $\alpha^2 E N_0$. Thus, SNR_0 is given by

$$SNR_0 \approx \frac{\alpha^2 E^2}{\alpha^2 E N_0} = \frac{E}{N_0} \tag{7.57}$$

Comparing (7.57) to (7.8), we conclude that the matched filter–envelope detector produces half the output signal-to-noise ratio of the coherent matched filter, or 3 dB less.

Decision variable

In order to predict the performance of a digital communication receiver employing the matched filter–envelope detector, we need the statistics of the decision variable X in (7.45). First we observe that $s_{0,I}(T) + n_{0,I}(T)$ and $s_{0,Q}(T) + n_{0,Q}(T)$ are both Gaussian random variables with means $s_{0,I}(T) \approx \alpha E \cos\theta$ and $s_{0,Q}(T) \approx -\alpha E \sin\theta$, and common variance $\sigma^2 \approx \alpha^2 E N_0/2$. The decision variable X, being the square root of the sum of two squared Gaussian random variables, with non-zero mean, is therefore a *Rice* random variable. Its probability density function is given by

$$\begin{aligned} f_X(x) &= \frac{x}{\sigma^2} \mathrm{e}^{-\left(x^2+a^2\right)/2\sigma^2} I_0\left(\frac{ax}{\sigma^2}\right), \quad x \geq 0 \\ a^2 &= s_{0,I}^2(T) + s_{0,Q}^2(T) \approx \alpha^2 E^2 \\ \sigma^2 &= \frac{\alpha^2 E N_0}{2} \end{aligned} \tag{7.58}$$

Note that $a^2/2\sigma^2 = SNR_0 \approx E/N_0$. For the special case when the signal $s(t)$ is not present, then X is simply the square root of the sum of two squared zero mean Gaussian random variables with a common variance $\sigma^2 \approx \alpha^2 E N_0/2$. Thus, X is a *Rayleigh* random variable with a probability density function

$$f_X(x) = \frac{x}{\sigma^2} \mathrm{e}^{-x^2/2\sigma^2}, \quad x \geq 0 \tag{7.59}$$

Summary

The matched filter–envelope detector is a noncoherent signal processor that can be employed to detect the presence of a signal with an unknown phase. It achieves a maximum output signal-to-noise ratio of E/N_0 at the sampling time $t = T$. This is 3 dB less than that produced by a coherent matched filter. The decision variable X at the output of the matched filter–envelope detector completely represents the envelope of $r(t) = s(t, \theta) + n(t)$. In other words, X represents sufficient statistics that summarize $|r(t)|$ for the purpose of detecting $s(t)$ with an unknown phase θ. From the statistics point of view, the *Rice* random variable X requires only two parameters a and σ^2 to characterize it. Both parameters are contained in the in-phase and quadrature components of the matched filter output.

7.4 The quadrature correlator–square law detector (noncoherent correlator)

For the case where the received signal $s(t)$ is *time-limited* to T seconds, the matched filter–envelope detector output signal and noise at the sampling time $t = T$ in (7.46)–(7.49) can be written as

$$s_{0,I}(T) = \frac{\alpha}{2}\cos\theta \int_0^T R^2(t)\ \mathrm{d}t + \frac{\alpha}{2}\int_0^T R^2(t)\cos(4\pi f_c t + \theta)\,\mathrm{d}t \tag{7.60}$$

$$s_{0,Q}(T) = -\frac{\alpha}{2}\sin\theta \int_0^T R^2(t)\ \mathrm{d}t + \frac{\alpha}{2}\int_0^T R^2(t)\sin(4\pi f_c t + \theta)\,\mathrm{d}t \tag{7.61}$$

$$n_{0,I}(T) = \alpha \int_0^T n(t)R(t)\cos 2\pi f_c t\ \mathrm{d}t \tag{7.62}$$

$$n_{0,Q}(T) = \alpha \int_0^T n(t)R(t)\sin 2\pi f_c t\ \mathrm{d}t \tag{7.63}$$

Equations (7.60)–(7.63) can be implemented by the quadrature correlator–square law detector shown in Figure 7.9. It is completely equivalent to the matched filter–envelope detector at the sampling time $t = T$. The decision variable X is given in (7.45) together with its statistics in (7.58). In practice, the square root operation in Figure 7.9 is often omitted because the decision variable $Y = X^2$ is capable of producing the same decision as X. The decision variable Y, being the sum of two squared Gaussian random variables with non-zero means, is a non-central chi-squared random variable with two degrees of freedom, with the following probability density function:

$$f_Y(y) = \frac{1}{2\sigma^2}\mathrm{e}^{-\left(y+a^2\right)/2\sigma^2} I_0\left(\frac{\sqrt{y}a}{\sigma^2}\right), \quad y \geq 0 \tag{7.64}$$

where a^2 and σ^2 are given in (7.58). Again, when the signal $s(t)$ is not present, then Y is simply the sum of two squared zero-mean Gaussian random variables with a common variance σ^2. Thus, Y is a central chi-squared random variable with two degrees of freedom, with a probability density function

$$f_Y(y) = \frac{1}{2\sigma^2}\mathrm{e}^{-y/2\sigma^2}, \quad y \geq 0 \tag{7.65}$$

The output of the quadrature correlator–square law detector represents sufficient statistics that summarize $|r(t)| = |s(t,\theta) + n(t)|$ for the purpose of detecting $s(t)$ with an unknown phase θ.

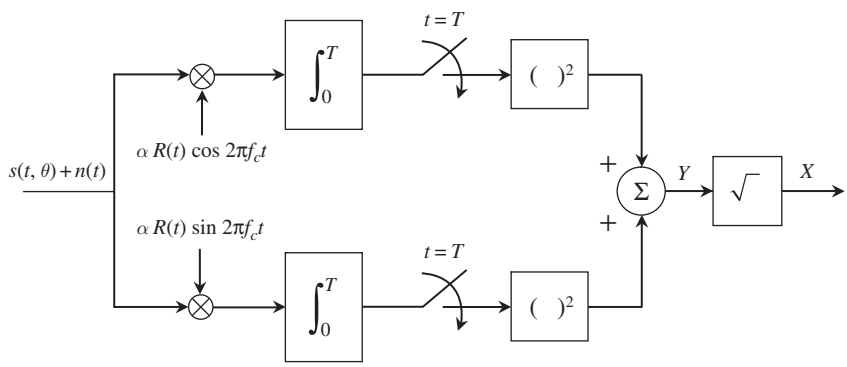

Figure 7.9 The quadrature correlator–square law detector for an input signal $s(t)$ with unknown phase θ.

7.5 The threshold detector

The threshold detector is a single input–single output bit detector. It accepts the decision variable X at the output of a signal processor such as the coherent matched filter or correlator and determines the presence of a binary signal based on whether X is above or below a preset threshold V_T. The threshold V_T is set in such a way to minimize the error probability or maximize the correct detection probability. The decision variable X takes on two possible values that represent two hypotheses H_1 and H_2. We could assign H_1 to the event when bit 1 was transmitted and H_2 to the event when bit 0 was transmitted. Associated with H_1 we have a Gaussian variable X with variance σ^2 and the probability density function

$$f_X(x|H_1) = \frac{1}{\sqrt{2\pi}\sigma} \mathrm{e}^{-(x-m_1)^2/2\sigma^2} \tag{7.66}$$

where $m_1 = \mathbf{E}(X|H_1)$ is the mean value of X given hypothesis H_1. Similarly, the probability density function of X given hypothesis H_2 is

$$f_X(x|H_2) = \frac{1}{\sqrt{2\pi}\sigma} \mathrm{e}^{-(x-m_2)^2/2\sigma^2} \tag{7.67}$$

where $m_2 = \mathbf{E}(X|H_2)$ is the mean value of X given by hypothesis H_2.

Optimum threshold

Without loss of generality, let $m_1 > V_T$ and $m_2 \leq V_T$. Therefore, given a value x of the decision variable X, hypothesis H_1 is chosen when $x > V_T$ and hypothesis H_2 is chosen when $x < V_T$. Obviously, an error occurs when $x < V_T$ given H_1. Similarly, an error occurs when $x > V_T$ given H_2. Thus, by using (7.26), we have

$$\Pr(X \leq V_T|H_1) = Q\left(\frac{m_1 - V_T}{\sigma}\right) \tag{7.68}$$

Also, by using (7.29), we get

$$\Pr(X > V_T|H_2) = Q\left(\frac{V_T - m_2}{\sigma}\right) \tag{7.69}$$

Applying the *total probability theorem* and using the fact that H_1 and H_2 are equally likely, that is, $\Pr(H_1) = \Pr(H_2) = 0.5$, we obtain the error probability for threshold detection as follows:

$$\begin{aligned} P_e &= \Pr(H_1)\Pr(X \leq V_T|H_1) + \Pr(H_2)\Pr(X > V_T|H_2) \\ &= \frac{1}{2}Q\left(\frac{m_1 - V_T}{\sigma}\right) + \frac{1}{2}Q\left(\frac{V_T - m_2}{\sigma}\right) \end{aligned} \tag{7.70}$$

We remark that P_e is a function of the threshold V_T; therefore, we can find the optimum threshold to minimize P_e by setting $\mathrm{d}P_e/\mathrm{d}V_T = 0$. Using the *Leibniz* differentiation rule on the right-hand side of (7.70), we obtain

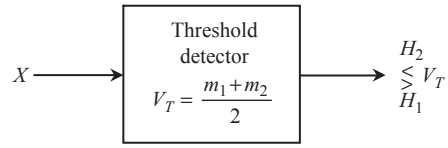

Figure 7.10 Threshold detection with optimum setting.

$$\frac{dP_e}{dV_T} = \frac{1}{2\sqrt{2\pi}\sigma} e^{-(V_T-m_1)^2/2\sigma^2} - \frac{1}{2\sqrt{2\pi}\sigma} e^{-(V_T-m_2)^2/2\sigma^2} = 0 \tag{7.71}$$

Solving the above equation, we get

$$(V_T - m_1)^2 = (V_T - m_2)^2 \tag{7.72}$$

This yields the optimum threshold V_T:

$$V_T = \frac{m_1 + m_2}{2} \tag{7.73}$$

Substituting (7.73) into (7.70), we obtain the minimum error probability

$$P_e = Q\left(\frac{m_1 - m_2}{2\sigma}\right) \tag{7.74}$$

Figure 7.10 illustrates the concept of threshold detection.

Maximum likelihood criterion

The above analysis shows that the optimum threshold yields the minimum error probability. Thus, by intuition, this criterion should be equivalent to the criterion in which the correct detection probability is maximized. In other words, we wish to design a detector that maximizes the *a-posteriori probability* $\Pr(H_i|x)$, $i = 1, 2$, given the decision value x of X. The decision that maximizes the a-posteriori probability $\Pr(H_i|x)$ is referred to as the *maximum a-posteriori* (MAP) *criterion*. When H_1 and H_2 are equally likely hypotheses, then the decision is called the *maximum likelihood* (ML) *criterion.* The strategy is to choose the hypothesis that has the higher probability given the particular value x of the decision variable X. Thus, we can state that

$$\Pr(H_1|x) \underset{H_1}{\overset{H_2}{\lessgtr}} \Pr(H_2|x) \tag{7.75}$$

Using the *Bayes theorem*, we can express $\Pr(H_i|x)$ as follows:

$$\Pr(H_i|x) = \frac{f_X(x|H_i)\Pr(H_i)}{f_X(x)}, \quad i = 1, 2 \tag{7.76}$$

where, by the total probability theorem, we have

$$f_X(x) = \sum_{i=1}^{2} f_X(x|H_i)\Pr(H_i) \tag{7.77}$$

We note that $f_X(x)$ is completely independent of H_i; therefore, after substituting (7.76) into (7.75), we obtain the *likelihood ratio*

$$\Lambda(x) = \frac{f_X(x|H_1)}{f_X(x|H_2)} \underset{H_1}{\overset{H_2}{\lessgtr}} \frac{\Pr(H_2)}{\Pr(H_1)} \tag{7.78}$$

Substituting (7.66) and (7.67) into (7.78) yields the following expression:

$$e^{[(x-m_2)^2-(x-m_1)^2]/2\sigma^2} \underset{H_1}{\overset{H_2}{\lessgtr}} \frac{\Pr(H_2)}{\Pr(H_1)} \tag{7.79}$$

The left-hand side is a monotonically increasing (or decreasing) function; therefore, the inequality is preserved if we take the natural logarithm of both sides of (7.79).

Also, since $\Pr(H_1) = \Pr(H_2) = 0.5$, $\ln[\Pr(H_2)/\Pr(H_1)] = 0$ and hence

$$(x - m_2)^2 - (x - m_1)^2 \underset{H_1}{\overset{H_2}{\lessgtr}} 0 \tag{7.80}$$

which leads to the value x as

$$x \underset{H_1}{\overset{H_2}{\lessgtr}} \frac{m_1 + m_2}{2} = V_T \tag{7.81}$$

Therefore, the maximum likelihood criterion establishes the same optimum threshold $V_T = (m_1 + m_2)/2$ that is required by the minimum error probability criterion. The threshold detector is thus a maximum likelihood detector.

7.6 The maximum detector

The *maximum detector* (also called a *comparator*) is a double input–single output bit detector. It accepts two decision variables X_1 and X_2 from the signal processors and chooses the one with the largest value. Let x_1 and x_2 be the values assumed by the decision variables X_1 and X_2, respectively. As usual, we assign hypothesis H_1 to the event that bit 1 was transmitted and hypothesis H_2 to bit 0. Then the decision is made as follows:

$$x_1 \underset{H_1}{\overset{H_2}{\lessgtr}} x_2 \tag{7.82}$$

Figure 7.11 illustrates the maximum detector. We can rewrite the decision rule in (7.82) using $x = x_1 - x_2$ as

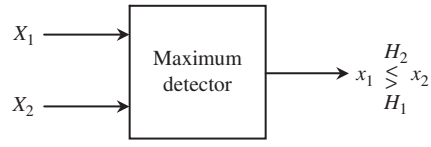

Figure 7.11 The maximum detector.

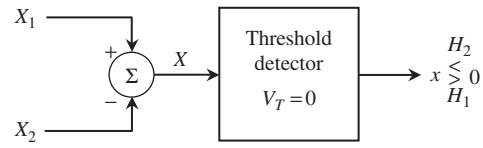

Figure 7.12 The equivalent realization of the maximum detector.

$$x = x_1 - x_2 \underset{H_1}{\overset{H_2}{\lessgtr}} 0 \tag{7.83}$$

The decision rule in (7.83) allows an equivalent implementation using a threshold detector as shown in Figure 7.12. This implies that the maximum likelihood detector can be used.

Gaussian decision variables

Let us consider two independent Gaussian decision variables X_1 and X_2 with a common variance σ^2. This is the case of binary communications with orthogonal signals. Define

$$\mu_1 = \mathbf{E}\{X_1|H_1\} \tag{7.84}$$

$$\mu_2 = \mathbf{E}\{X_2|H_2\} \tag{7.85}$$

In addition, we also assume that the following conditional means hold:

$$\mathbf{E}\{X_1|H_2\} = 0 \tag{7.86}$$

$$\mathbf{E}\{X_2|H_1\} = 0 \tag{7.87}$$

Then $X = X_1 - X_2$ is obviously a Gaussian random variable with variance $2\sigma^2$ and conditional means

$$m_1 = \mathbf{E}\{X|H_1\} = \mathbf{E}\{X_1|H_1\} - \mathbf{E}\{X_2|H_1\} = \mu_1 \tag{7.88}$$

$$m_2 = \mathbf{E}\{X|H_2\} = \mathbf{E}\{X_1|H_2\} - \mathbf{E}\{X_2|H_2\} = -\mu_2 \tag{7.89}$$

Therefore, applying the error probability expression for threshold detection of X in (7.74), we obtain the error probability for the maximum detector or its equivalent implementation using the threshold detector with Gaussian input decision variables as follows:

$$P_e = Q\left(\frac{\mu_1 + \mu_2}{2\sqrt{2}\sigma}\right) \tag{7.90}$$

Rice and Rayleigh decision variables

This case applies to noncoherent binary demodulation using a matched filter–envelope detector or quadrature correlator–square law detector. The maximum detector accepts two independent Rice and Rayleigh decision variables X_1 and X_2 with probability density functions given by (7.58) and (7.59), respectively. The error probability is given by symmetry as

$$\begin{aligned} P_e &= \Pr(H_1)\Pr(X_2 > x_1|H_1) + \Pr(H_2)\Pr(X_1 > x_2|H_2) \\ &= \frac{1}{2}\Pr(X_2 > x_1|H_1) + \frac{1}{2}\Pr(X_1 > x_2|H_2) \\ &= \Pr(X_2 > x_1|H_1) \end{aligned} \tag{7.91}$$

Using the probability density function of X_1 and X_2 in (7.58) and (7.59), we obtain

$$\begin{aligned} P_e &= \int_0^\infty f_{X_1}(x_1|H_1) \int_{x_1}^\infty f_{X_2}(x_2|H_1)\,\mathrm{d}x_2\,\mathrm{d}x_1 \\ &= \int_0^\infty \frac{x_1}{\sigma^2} \mathrm{e}^{-\left(x_1^2+a^2\right)/2\sigma^2} I_0\left(\frac{ax_1}{\sigma^2}\right) \int_{x_1}^\infty \frac{x_2}{\sigma^2} \mathrm{e}^{-x_2^2/2\sigma^2}\,\mathrm{d}x_2\,\mathrm{d}x_1 \end{aligned} \tag{7.92}$$

The inner integral with respect to x_2 is equal to $\mathrm{e}^{-x_1^2/2\sigma^2}$. Rearranging the terms on the right-hand side of (7.92), we have

$$P_e = \mathrm{e}^{-a^2/4\sigma^2} \int_0^\infty \frac{x_1}{\sigma^2} \mathrm{e}^{-\left(4x_1^2+a^2\right)/4\sigma^2} I_0\left(\frac{ax_1}{\sigma^2}\right)\mathrm{d}x_1 \tag{7.93}$$

Let $x = 2x_1$ be a new integral variable, and then P_e in (7.93) can be written as

$$\begin{aligned} P_e &= \mathrm{e}^{-a^2/4\sigma^2} \int_0^\infty \frac{x}{4\sigma^2} \mathrm{e}^{-\left(x^2+a^2\right)/4\sigma^2} I_0\left(\frac{ax}{2\sigma^2}\right)\mathrm{d}x \\ &= \frac{1}{2}\mathrm{e}^{-a^2/4\sigma^2} \int_0^\infty \frac{x}{\beta^2} \mathrm{e}^{-\left(x^2+a^2\right)/2\beta^2} I_0\left(\frac{ax}{\beta^2}\right)\mathrm{d}x \end{aligned} \tag{7.94}$$

Where $\beta^2 = 2\sigma^2$. The integral on the right-hand side of (7.94) is the integral of the *Rice* probability density function with parameter a^2 and β^2 over its entire range; hence, it is equal to 1. Thus,

$$P_e = \frac{1}{2}\mathrm{e}^{-a^2/4\sigma^2} \tag{7.95}$$

Substituting a^2 and σ^2 from (7.58) into (7.95) yields the *error probability* for the maximum detector with input *Rice* and *Rayleigh* decision variables as follows:

$$P_e = \frac{1}{2}\mathrm{e}^{-E/2N_0} \tag{7.96}$$

Example 7.6 Maximum likelihood criterion revisited

We have shown that a maximum detector can be implemented by an algebraic summer followed by a threshold detector. Thus, the maximum detector must be a maximum likelihood detector. In this example, we seek to verify this statement directly from the likelihood ratio. The maximum detector observes two decision variables X_1 and X_2, and bases its decision on the a-posteriori probabilities $\Pr(H_i|x_1, x_2) = f_{X_1X_2}(x_1, x_2|H_i)\Pr(H_i)/f_{X_1X_2}(x_1, x_2)$, $i = 1, 2$. Hence, the optimum decision is expressed similarly to (7.75) to yield

$$\frac{f_{X_1X_2}(x_1,x_2|H_1)}{f_{X_1X_2}(x_1,x_2|H_2)} \underset{H_1}{\overset{H_2}{\lessgtr}} \frac{\Pr(H_2)}{\Pr(H_1)} = 1 \tag{7.97}$$

Since X_1 and X_2 are independent, we get

$$f_{X_1X_2}(x_1,x_2|H_1) = f_{X_1}(x_1|H_1)f_{X_2}(x_2|H_1) \tag{7.98}$$

$$f_{X_1X_2}(x_1,x_2|H_2) = f_{X_1}(x_1|H_2)f_{X_2}(x_2|H_2) \tag{7.99}$$

Substituting (7.98) and (7.99) into (7.97), and making use of (7.58) and (7.59) for *Rice* and *Rayleigh* random variables, we arrive at the following result:

$$\frac{I_0\left(\frac{ax_1}{\sigma^2}\right)}{I_0\left(\frac{ax_2}{\sigma^2}\right)} \underset{H_1}{\overset{H_2}{\lessgtr}} 1 \tag{7.100}$$

which implies

$$I_0\left(\frac{ax_1}{\sigma^2}\right) \underset{H_1}{\overset{H_2}{\lessgtr}} I_0\left(\frac{ax_2}{\sigma^2}\right) \tag{7.101}$$

Since I_0 is a monotomically increasing function of its argument, (7.101) is equivalent to the following criterion:

$$x_1 \underset{H_1}{\overset{H_2}{\lessgtr}} x_2 \tag{7.102}$$

Thus, H_1 is chosen if $x_1 > x_2$, and H_2 is chosen if $x_1 \leq x_2$.

■

The above results should hold for the case when X_1 and X_2 are chi-squared random variables with probability density function given in (7.64) and (7.65). This is expected because squaring the two positive decision variables for comparison should not alter the outcome of the maximum detector. Thus, for non-central chi-squared and central chi-squared decision variables, the bit error probability of the maximum detector is also given by (7.96), that is,

$$P_e = \frac{1}{2}\mathrm{e}^{-E/2N_0} \tag{7.103}$$

7.7 Binary demodulation

Binary modulation employs two distinct signal waveforms to represent bits 1 and 0. Therefore, binary demodulation requires either the one-path demodulator shown in Figure 7.13 or the two-path demodulator shown in Figure 7.14.

The one-path demodulator handles binary signals that are linearly dependent, such as PSK and OOK, and performs coherent demodulation only. On the other hand, the two-path demodulator is applicable to orthogonal binary signals such as FSK, MSK, and DPSK. Both coherent and noncoherent demodulations can be performed by this demodulator using appropriate signal processors. Thus, for the one-path demodulator, the signal processor is

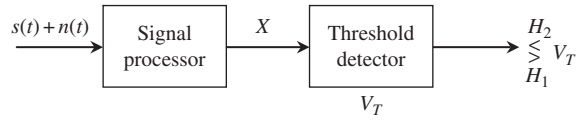

Figure 7.13 One-path binary demodulator.

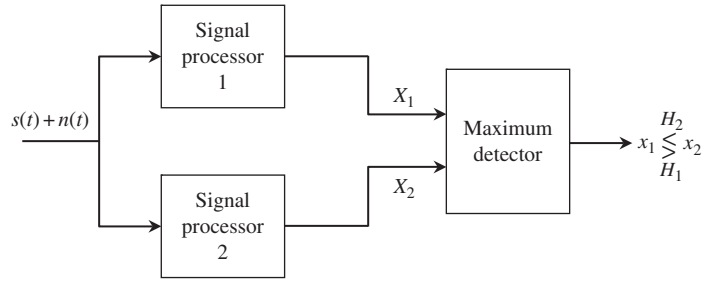

Figure 7.14 Two-path binary demodulator.

the matched filter or correlator. On the other hand, the signal processors for the two-path demodulator are either matched filters or correlators (coherent demodulation), or matched filter–envelope detectors or quadrature correlator–square law detectors (noncoherent demodulation). In the subsequent discussion we assume that hypothesis H_1 represents bit 1 and hypothesis H_2 represents bit 0 as usual.

Coherent PSK

As indicated by (6.13), PSK employs two signals $s_1(t) = s(t) : H_1$ and $s_2(t) = -s(t) : H_2$, where $s(t) = Ap(t)\cos 2\pi f_c t$. Therefore, the one-path coherent demodulator shown in Figure 7.15 can be used to recover the information bits. As usual, we denote T_b as the bit time. Also, without loss of generality we assume that the pulse shape $p(t)$ that represents a bit is a squared pulse of *unit amplitude* and *duration* T_b. The coherent carrier obtained from the carrier recovery circuit is denoted as $2\cos 2\pi f_c t$ if the matched filter is employed to be consistent with Figure 7.4. On the other hand, the recovered carrier is denoted as $2ap(t)\cos 2\pi f_c t$ when the integrator is used. Obviously, the integration time is T_b. The bit timing recovery circuit provides the clock signal with frequency $1/T_b$ to sample the output voltage of the matched filter or the integrator. The detection threshold is set to *zero* volts. Table 7.1 presents all the parameters related to Figure 7.15, where E_b is the bit energy.

Using these parameters in (7.74), we obtain the bit error probability P_b as follows:

$$\begin{aligned} P_b &= Q\left(\frac{m_1 - m_2}{2\sigma}\right) \\ &= Q\left(\sqrt{\frac{2E_b}{N_0}}\right) \end{aligned} \tag{7.104}$$

where E_b/N_0 is the bit energy-to-noise density ratio, commonly referred to as the signal-to-noise ratio per bit (SNR per bit). Figure 7.16 plots the bit error probability P_b versus E_b/N_0 (dB) for coherent PSK.

Table 7.1 Parameters for coherent PSK using (7.23) and (7.24)

Hypothesis	Signal	$m_1 = \mathbf{E}(X\|H_1)$	$m_2 = \mathbf{E}(X\|H_2)$	Noise variance, σ^2
H_1	$s_1(t) = s(t)$	αE_b		$\alpha^2 E_b N_0/2$
H_2	$s_2(t) = -s(t)$		$-\alpha E_b$	$\alpha^2 E_b N_0/2$

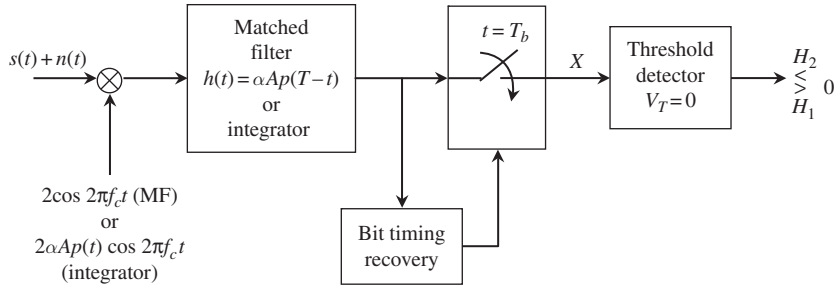

Figure 7.15 Coherent PSK demodulator. The scaling constant a is arbitrary.

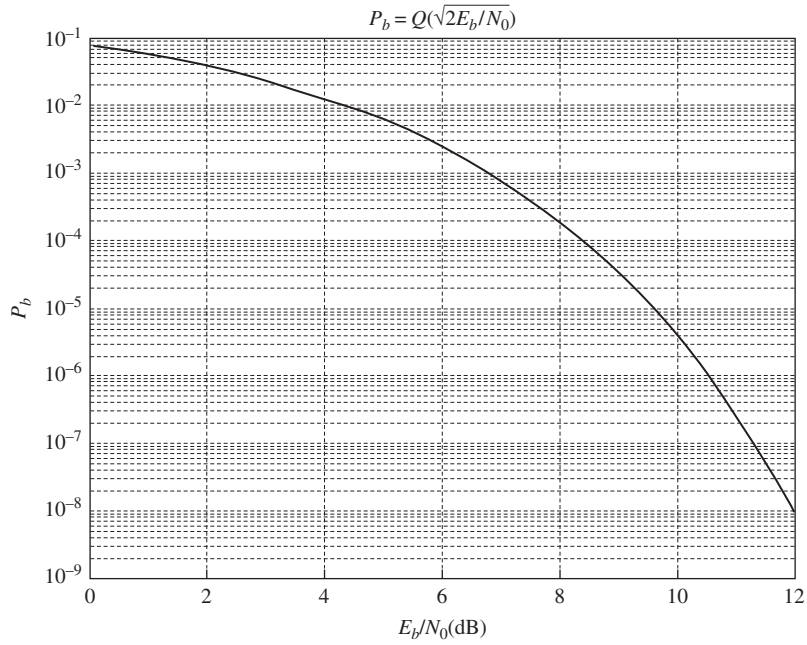

Figure 7.16 Bit error probability of coherent PSK. (Courtesy of Peter Harley.)

Coherent DPSK

DPSK can be coherently demodulated and differentially decoded as shown in Figure 7.17. The demodulated bit c_i is modulo-2 added to the previously demodulated bit c_{i-1} to provide the data bit d_i, that is,

$$d_i = c_i \oplus c_{i-1} \tag{7.105}$$

Since $c_i \oplus c_{i-1} = \overline{c_i} \oplus \overline{c_{i-1}}$, inverted data caused by phase ambiguity in the recovered carrier (i.e., the output of the carrier recovery circuit is $-\cos 2\pi f_c t$ instead of $\cos 2\pi f_c t$) is re-inverted and the phase ambiguity is resolved. Note that by substituting $c_i = d_i \oplus c_{i-1}$ of (6.26) into (7.105) one gets back that data bit d_i, since $d_i = d_i \oplus c_{i-1} \oplus c_{i-1}$.

Example 7.7 Phase ambiguity resolution

Let us consider again the differential encoding table from Example 6.20. We introduce a phase error of π radians in θ_i, the phase of the ith bit. Table 7.2 shows that differential decoding recovers the data bits d_i correctly except for the reference bit d_0, which is irrelevant.

Differential encoding tends to propagate errors, that is, bit errors tend to occur in pairs. Table 7.3 illustrates this phenomenon.

■

Table 7.2 Demodulation of DPSK signals

i	$\theta_i + \pi$	c_i	d_i
0	π	0	0
1	π	0	0
2	2π	1	1
3	3π	0	1
4	3π	0	0
5	4π	1	1
6	4π	1	0

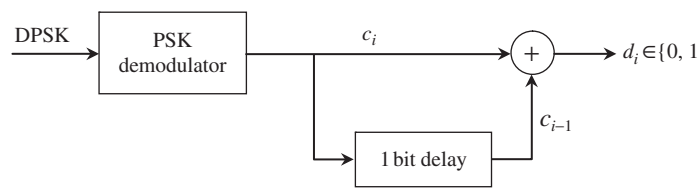

Figure 7.17 DPSK demodulator.

Table 7.3 Differential decoding errors

i	θ_i	c_i	d_i	
0	0	1	1	
1	π	0	1	} errors
2	π	0	0	
3	2π	1	1	
4	2π	1	0	
5	4π	1	0	} errors
6	3π	0	1	

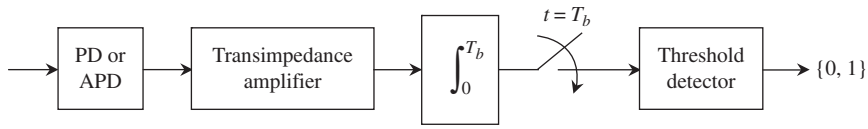

Figure 7.18 Direct detection of optical ASK.

The bit error probability of coherent DPSK [1] is given by

$$P_b = 2Q\left(\sqrt{\frac{2E_b}{N_0}}\right)\left[1 - Q\left(\sqrt{\frac{2E_b}{N_0}}\right)\right] \tag{7.106}$$

Apparently, at high bit energy-to-noise density ratio E_b/N_0, the bit error probability of coherent DPSK is approximately twice that of coherent PSK, as illustrated by Table 7.3.

Direct detection ASK

Lightwave ASK (or OOK) is directly detected via a photodiode such as *pin photodiode* (PD) or *avalanche photodiode* (APD) [2]. The performance of a photodiode is characterized by its *responsitivity* $\mathcal{R}$. The responsitivity specifies the photocurrent generated per unit optical power. Typical responsitivity is 0.7 A/W for wavelength of 1.3 μm and 1.5 μm. The *photocurrent* generated by a photodetector is $I = \mathcal{R}P$. Figure 7.18 shows the block diagram of an optical direct detection ASK receiver.

The lightwave ASK signal of (6.28) at the input of the pin or ADP photodetector produces a photocurrent $i(t)$ as follows:

$$i(t) = \begin{cases} i_1(t) = \dfrac{\mathcal{R}A^2}{2(1+r_e)}p(t) + i_s(t) \;:\; H_1 \\ i_2(t) = \dfrac{\mathcal{R}A^2}{2}\left(\dfrac{r_e}{1+r_e}\right)p(t) + i_s(t) \;:\; H_2 \end{cases} \tag{7.107}$$

where hypotheses H_1 and H_2 represent bits 1 and 0, respectively, and $i_s(t)$ is the shot noise current. The transimpedance amplifier converts the photocurrent into a voltage signal $x(t)$ at

its output. The amplifier transimpedance is Z_0 and its internal noise current is $i_a(t)$. We can write the output voltage signal $x(t)$ as

$$x(t) = Z_0[i(t) + i_a(t)] \tag{7.108}$$

Substituting (7.107) into (7.108) yields

$$x(t) = \begin{cases} x_1(t) = \dfrac{Z_0 \mathcal{R} A^2}{2(1+r_e)} p(t) + Z_0 i_n(t) \ : \ H_1 \\ x_2(t) = \dfrac{Z_0 \mathcal{R} A^2}{2} \left(\dfrac{r_e}{1+r_e} \right) p(t) + Z_0 i_n(t) \ : \ H_2 \end{cases} \tag{7.109}$$

where

$$i_n(t) = i_s(t) + i_a(t) \tag{7.110}$$

is the total shot noise plus amplifier noise current and $i_n(t)$ has a spectral density designated as $N_0\left(\mathrm{A}^2/\mathrm{Hz}\right)$. Note that the unit is ampere^2/hertz and not watt/hertz. The integrator integrates $x(t)$ for one bit time T_b and the sampler produces a decision variable X at the input of the threshold detector

$$X = \begin{cases} \dfrac{Z_0 \mathcal{R} A^2 T_b}{2(1+r_e)} + N \ : \ H_1 \\ \dfrac{Z_0 \mathcal{R} A^2 T_b}{2} \left(\dfrac{r_e}{1+r_e} \right) + N \ : \ H_2 \end{cases} \tag{7.111}$$

The conditional mean value of X and the noise sample N are given as

$$m_1 = E\{X|H_1\} = \frac{Z_0 \mathcal{R} A^2 T_b}{2(1+r_e)} \tag{7.112}$$

$$m_2 = E\{X|H_2\} = \frac{Z_0 \mathcal{R} A^2 T_b}{2} \left(\frac{r_e}{1+r_e} \right) \tag{7.113}$$

$$N = \int_0^{T_b} Z_0 i_n(t) \, \mathrm{d}t \tag{7.114}$$

The noise voltage $Z_0 i_n(t)$ can be modeled as AWGN with zero mean and power spectral density $Z_0^2 N_0$ (W/Hz). Thus, the variance σ^2 of the noise sample N in (7.114) is

$$\sigma^2 = Z_0^2 N_0 T_b \tag{7.115}$$

Substituting (7.112) and (7.113) into (7.73), we obtain the optimum threshold for the threshold detector as follows:

$$V_T = \frac{m_1 + m_2}{2} = \frac{Z_0 \mathcal{R} A^2 T_b}{4} \tag{7.116}$$

Note that the average received power P of the lightwave ASK signal is given by (6.28) as

$$\begin{aligned} P &= \frac{1}{2}\left[\frac{A^2}{2(1+r_e)}\right] + \frac{1}{2}\left[\frac{A^2 r_e}{2(1+r_e)}\right] \\ &= \frac{A^2}{4} \end{aligned} \tag{7.117}$$

Combining (7.116) and (7.117), we get the optimum threshold in terms of average power as

$$V_T = Z_0 \mathcal{R} P T_b \tag{7.118}$$

The minimum bit error probability is given by (7.74) with the help of (7.112), (7.113), (7.115), and (7.117) as follows:

$$P_b = Q\left(\frac{1 - r_e}{1 + r_e}\sqrt{\frac{T_b}{N_0}}\mathcal{R}P\right) \tag{7.119}$$

Example 7.8 Bit error probability of lightwave ASK

Consider a direct detection lightwave ASK receiver with total shot noise plus amplifier noise spectrum $N_0 = 10^{-22}\,\mathrm{A}^2/\mathrm{Hz}$. The photodiode detector has a responsitivity $\mathcal{R} = 0.7\,\mathrm{A/W}$ and the received optical power is $P = 10\,\mu\mathrm{W}$. The extinction ratio of the ASK signal is $r_e = 0.1$. It is desirable to have a bit error probability $P_b = 10^{-9}$. What is the bit rate?

We note that $Q(x) = 10^{-9}$ requires that $x = 6$. Thus, using (7.119) we obtain

$$\frac{1 - 0.1}{1 + 0.1}\sqrt{\frac{T_b}{10^{-22}}}(0.7)\left(10^{-5}\right) = 6$$

The bit rate $R_b = 1/T_b$ can be calculated as

$$R_b = \frac{1}{T_b} = 9.11\,\mathrm{Gb/s}$$

■

Coherent FSK

Coherent FSK can be conceptually demodulated by a two-path demodulator shown in Figure 7.19.

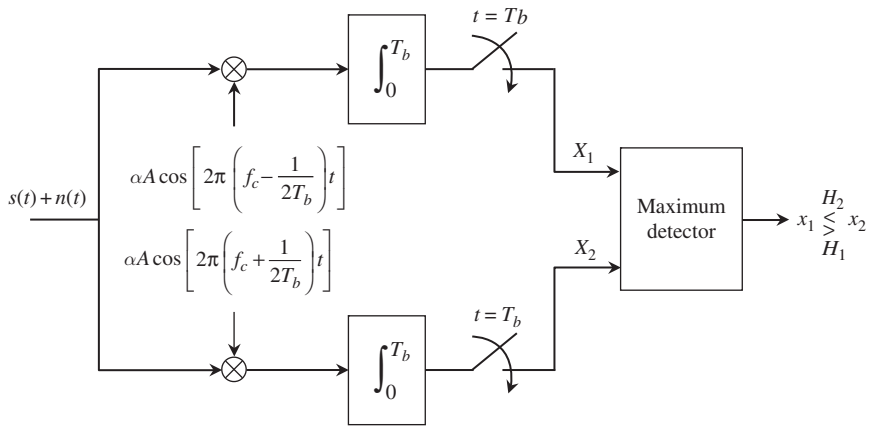

Figure 7.19 Coherent FSK demodulator.

Without loss of generality we assume that the carrier phase θ_n in (6.42) is zero radian, or equivalently, $\theta_1 = \theta_2 = 0$ radian for (6.36). Using the result for the maximum detector with Gaussian decision variables in Section 7.6, we obtain via (7.84) and (7.85)

$$\mu_1 = \mathbf{E}\{X_1|H_1\} = \alpha E_b \tag{7.120}$$

$$\mu_2 = \mathbf{E}\{X_2|H_2\} = \alpha E_b \tag{7.121}$$

where α is an arbitrary positive constant. Furthermore, the orthogonality of FSK also implies, via simple verification, that the following relations hold:

$$\mathbf{E}\{X_1|H_2\} = \mathbf{E}\{X_2|H_1\} = 0 \tag{7.122}$$

The conditional variance σ^2 of X_1 given H_1 or X_2 given H_2 is simply

$$\sigma^2 = \frac{1}{2}\alpha^2 E_b N_0 \tag{7.123}$$

The minimum bit error probability of coherent FSK can be obtained via (7.90) as follows:

$$P_b = Q\left(\sqrt{\frac{E_b}{N_0}}\right) \tag{7.124}$$

By comparing (7.124) with (7.104), we observe that coherent FSK requires 3 dB more in E_b/N_0 (a factor of 2) to achieve the same bit error probability as coherent PSK. This is the reason why coherent FSK is not employed in practice.

Coherent MSK and precoded MSK and GMSK

From Figures 6.21 and 6.22, we observe that MSK is precoded MSK preceded by a differential encoder. Note that differential encoding increases the bit error probability by a factor of two, approximately, as seen in the case of coherent DPSK versus coherent PSK. Thus, the bit error probability of coherent MSK has also a penalty of approximately a factor of two relative to that of coherent precoded MSK. Therefore, we only analyze the performance of coherent precoded MSK. Figure 7.20 shows the coherent demodulator for precoded MSK. Figure 7.21 shows the coherent demodulator for MSK, which is the precoded demodulator followed by a differential decoder to recover the data $\overline{d_n}$ according to the relation

$$\overline{d_n} = c_n \oplus c_{n-1} \tag{7.125}$$

Example 7.9 I-Q orthogonality

In this example we demonstrate the fundamental feature of an I-Q demodulator, namely, the orthogonality between the I-channel and the Q-channel. This can be established by proving the correlation between the local I-carrier $\cos(\pi t/2T_b)\cos 2\pi f_c t$ and Q-carrier $\sin(\pi t/2T_b)\sin 2\pi f_c t$ to be zero over the duration of $2T_b$, as dictated by Figures 6.17 and 6.20. Consider the correlation C, given by

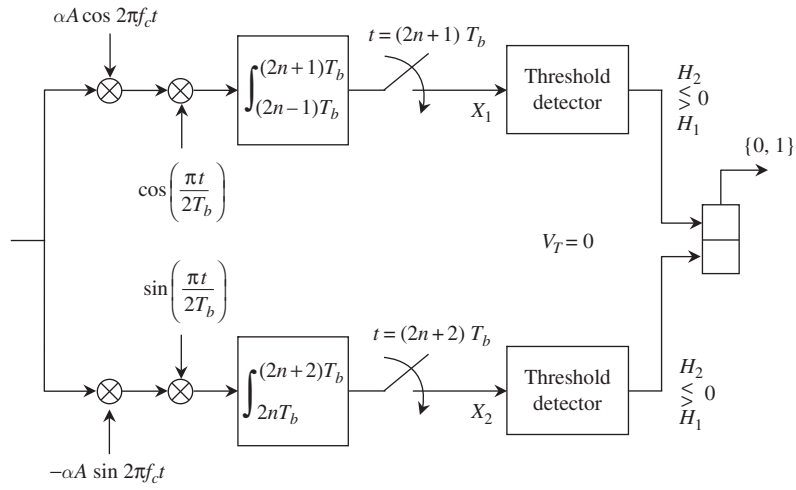

Figure 7.20 Coherent precoded MSK demodulator. The integration time is $2T_b$ reflecting the fact that an I-bit or a Q-bit spans an interval of $2T_b$ seconds, as seen in Figures 6.17 and 6.20.

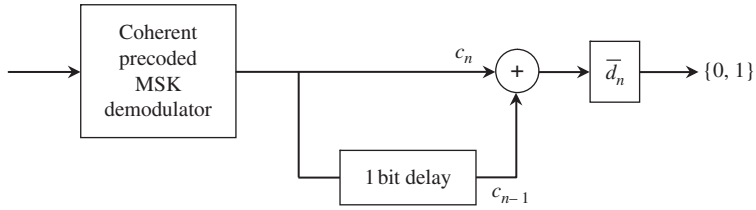

Figure 7.21 Coherent MSK demodulator.

$$
\begin{aligned}
C &= \int_0^{2T_b} \left[\cos\left(\frac{\pi t}{2T_b}\right)\cos 2\pi f_c t\right]\left[\sin\left(\frac{\pi t}{2T_b}\right)\sin 2\pi f_c t\right] \mathrm{d}t \\
&= \frac{1}{4}\int_0^{2T_b} \sin\left(\frac{\pi t}{T_b}\right)\sin 4\pi f_c t \,\mathrm{d}t \\
&= \frac{1}{8}\int_0^{2T_b} \left[\cos 2\pi\left(2f_c - \frac{1}{2T_b}\right)t - \cos 2\pi\left(2f_c + \frac{1}{2T_b}\right)t\right] \mathrm{d}t \\
&= 0
\end{aligned}
\tag{7.126}
$$

where f_c is assumed to be an integer multiple of $1/T_b$. If f_c is not an integer multiple of $1/T_b$ but $f_c \gg 1/T_b$, then the I-channel and Q-channel are *quasi-orthogonal*, which is approximately orthogonal for all practical purposes. Due to orthogonality, the I-noise and Q-noise are both uncorrelated, and since they are Gaussian, they are also statistically independent.

■

Example 7.10 I-noise and Q-noise

In this example, we verify the fact that the I-noise and Q-noise are statistically independent. Let $n(t)$ be the AWGN at the input of the demodulator in Figure 7.20. We assume that the power spectral density of $n(t)$ is $N_0/2$ (W/Hz) and therefore, its autocorrelation function is $\mathbf{E}\{n(t)n(\tau)\} = (N_0/2)\delta(t-\tau)$. Also, let N_1 be the noise sample at the input of the I-*threshold detector* and N_2 be the noise sample at the input of the Q-*threshold detector.* We have, by setting the sampling index $n = 0$ in Figure 7.20,

$$N_1 = \int_{-T_b}^{T_b} \alpha A \cos 2\pi f_c t \cos\left(\frac{\pi t}{2T_b}\right) n(t)\,\mathrm{d}t \tag{7.127}$$

$$N_2 = -\int_{0}^{2T_b} \alpha A \sin 2\pi f_c t \sin\left(\frac{\pi t}{2T_b}\right) n(t)\,\mathrm{d}t \tag{7.128}$$

Establish the correlation $\mathbf{E}\{N_1N_2\}$ as follows:

$$\begin{aligned}
\mathbf{E}\{N_1N_2\} &= -\alpha^2A^2 \int_{-T_b}^{T_b}\int_{0}^{2T_b} \mathbf{E}\{n(t)n(\tau)\}\left[\cos\left(\frac{\pi t}{2T_b}\right)\cos 2\pi f_c t\right]\left[\sin\left(\frac{\pi \tau}{2T_b}\right)\sin 2\pi f_c \tau\right]\mathrm{d}t\,\mathrm{d}\tau \\
&= -\alpha^2A^2 \int_{-T_b}^{T_b}\int_{0}^{2T_b} \frac{N_0}{2}\delta(t-\tau)\left[\cos\left(\frac{\pi t}{2T_b}\right)\cos 2\pi f_c t\right]\left[\sin\left(\frac{\pi \tau}{2T_b}\right)\sin 2\pi f_c \tau\right]\mathrm{d}t\,\mathrm{d}\tau \\
&= -\frac{1}{2}\alpha^2A^2N_0 \int_{0}^{2T_b}\left[\cos\left(\frac{\pi t}{2T_b}\right)\cos 2\pi f_c t\right]\left[\sin\left(\frac{\pi t}{2T_b}\right)\sin 2\pi f_c t\right]\mathrm{d}t \\
&= -\frac{1}{2}\alpha^2A^2N_0C \;=\; 0
\end{aligned} \tag{7.129}$$

by virtue of (7.126). Thus, N_1 and N_2 are uncorrelated and, since they are Gaussian random variables, they are independent. It is obvious from (7.127) and (7.128) that both N_1 and N_2 have zero mean since $n(t)$ has zero mean. Let us calculate the variances of N_1 and N_2. From (7.127), we get

$$\begin{aligned}
\sigma^2 = \mathbf{E}\{N_1^2\} &= \alpha^2A^2 \int_{-T_b}^{T_b}\int_{-T_b}^{T_b} \mathbf{E}\{n(t)n(\tau)\}\cos\left(\frac{\pi t}{2T_b}\right)\cos\left(\frac{\pi \tau}{2T_b}\right)\cos 2\pi f_c t\;\cos 2\pi f_c \tau\,\mathrm{d}t\,\mathrm{d}\tau \\
&= \alpha^2A^2 \int_{-T_b}^{T_b}\int_{-T_b}^{T_b} \frac{N_0}{2}\delta(t-\tau)\cos\left(\frac{\pi t}{2T_b}\right)\cos\left(\frac{\pi \tau}{2T_b}\right)\cos 2\pi f_c t\;\cos 2\pi f_c \tau\,\mathrm{d}t\,\mathrm{d}\tau \\
&= \frac{1}{2}\alpha^2A^2N_0 \int_{-T_b}^{T_b}\cos^2\left(\frac{\pi t}{2T_b}\right)\cos^2 2\pi f_c t\;\mathrm{d}t \\
&= \frac{1}{4}\alpha^2A^2N_0T_b
\end{aligned} \tag{7.130}$$

Similarly, it can be shown that the variance of N_2 is the same as that of N_1, that is,

$$\sigma^2 = \mathbf{E}\{N_2^2\} = \frac{1}{4}\alpha^2A^2N_0T_b \tag{7.131}$$

■

To evaluate the bit error probability of either coherent MSK or coherent pre-coded MSK, we need to know the statistic of the decision variables X_1 and X_2 at the input of the threshold detectors in Figure 7.20. Obviously, the variance of X_1 or X_2 is just the variance σ^2 of noise sample N_1 or N_2 as indicated in (7.130) or (7.131). It remains to find the mean value of X_1 and the mean value of X_2. The waveform of I-bits can be written with the help of Figure 6.20 as follows:

$$s_I(t) = A\gamma_{2n-1}\cos\left(\frac{\pi t}{2T_b}\right)\cos 2\pi f_c t, \qquad (2n-1)T_b \le t < (2n+1)T_b \tag{7.132}$$

$$s_Q(t) = A\gamma_{2n}\sin\left(\frac{\pi t}{2T_b}\right)\sin 2\pi f_c t, \qquad 2nT_b \le t < (2n+2)T_b \tag{7.133}$$

where γ_{2n-1} and γ_{2n} take on values of 1 given hypothesis H_1, or –1 given hypothesis H_2. The mean value of X_1 given H_1 is

$$\begin{aligned} m_1 = \mathbf{E}\{X_1|H_1\} &= \int_{(2n-1)T_b}^{(2n+1)T_b} s_I(t)\left[\alpha A\cos 2\pi f_c t\,\cos\left(\frac{\pi t}{2T_b}\right)\right]\mathrm{d}t \\ &= \int_{(2n-1)T_b}^{(2n+1)T_b} \alpha A^2\cos^2\left(\frac{\pi t}{2T_b}\right)\cos^2 2\pi f_c t\;\mathrm{d}t \\ &= \frac{1}{2}\alpha A^2 T_b \end{aligned} \tag{7.134}$$

The mean value of X_1 given H_2 is simply

$$m_2 = \mathbf{E}\{X_1|H_2\} = -\frac{1}{2}\alpha A^2 T_b \tag{7.135}$$

Similarly,

$$m_1 = \mathbf{E}\{X_2|H_1\} = \frac{1}{2}\alpha A^2 T_b \tag{7.136}$$

$$m_2 = \mathbf{E}\{X_2|H_2\} = -\frac{1}{2}\alpha A^2 T_b \tag{7.137}$$

Substituting (7.130), (7.134), and (7.135) into (7.74) yields the I-bit error probability

$$\begin{aligned} P_b(I) &= Q\left(\frac{m_1 - m_2}{2\sigma}\right) \\ &= Q\left(\sqrt{\frac{A^2 T_b}{N_0}}\right) \\ &= Q\left(\sqrt{\frac{2E_b}{N_0}}\right) \end{aligned} \tag{7.138}$$

where $E_b = A^2 T_b/2$ is the energy of the MSK bit. Note that both the I-bit and Q-bit have $2T_b$ duration, hence both have *twice* the energy of the MSK bit. Similarly, the Q-bit error probability can be obtained by substituting (7.131), (7.136), and (7.137) into (7.74)

$$P_b(Q) = Q\left(\sqrt{\frac{2E_b}{N_0}}\right) \tag{7.139}$$

Because the I-noise and Q-noise are statistically independent, and if we assume the I-bits and Q-bits are equally likely, then the bit error probability of coherent precoded MSK is

$$\begin{aligned} P_b &= \frac{1}{2}P_b(I) + \frac{1}{2}P_b(Q) \\ &= Q\left(\sqrt{\frac{2E_b}{N_0}}\right) \quad : \quad \text{coherent precoded MSK} \end{aligned} \tag{7.140}$$

Due to differential decoding, the bit error probability of coherent MSK suffers a penalty of approximately a factor of two and is given by

$$P_b \approx 2Q\left(\sqrt{\frac{2E_b}{N_0}}\right) \quad : \quad \text{coherent MSK} \tag{7.141}$$

Note that by observing Figures 6.21 and 7.20, we can remove the inverter $\overline{d_n}$ preceding the differential encoder in the MSK modulator, and the one that follows the differential decoder in the coherent MSK demodulator. Thus, the removal of $\overline{d_n}$ does not change the operation since inverting the data at the modulator and re-inverting it at the demodulator amounts to no change. If we map the binary data 0 into 1 and 1 into –1 via $d_n \rightarrow (1 - 2d_n)$ instead of $d_n \rightarrow (2d_n - 1)$, as in (6.57), we would not indeed have to add the inverter $\overline{d_n}$ to both modulator and demodulator for coherent MSK.

Coherent GMSK discussed in Section 6.8 employs Gaussian pulse shape $g(t) = p(t) * h(t)$, where $p(t)$ is the pulse of unit amplitude and duration T_b, and $h(t)$ is the impulse response of the Gaussian filter given in (6.76). Thus, GMSK can be coherently demodulated as suggested in [3,4] by the demodulator in Figure 7.22 employing a Costas loop.

The bit error probability for coherent GMSK [3,4] is given by

$$P_b = Q\left(\sqrt{\frac{2\alpha E_b}{N_0}}\right) \tag{7.142}$$

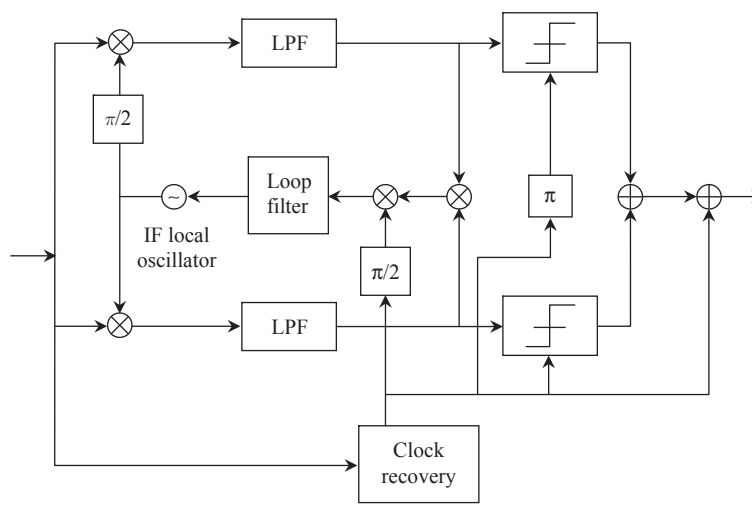

Figure 7.22 Costas loop demodulator for GMSK.

where $\alpha = 0.68$ for $BT_b = 0.25$ as described in Section 6.8. This yields a degradation of 1.6 dB relative to coherent precoded MSK due to intersymbol interference.

Noncoherent FSK and MSK

Noncoherent FSK can be demodulated using either the matched filter–envelope detector in Figure 7.8 for each frequency $f_1 = f_c - 1/2T_b$ (hypothesis H_1) or $f_2 = f_c + 1/2T_b$ (hypothesis H_2); or the quadrature correlator–square law detector in Figure 7.9 for each f_1 and f_2. Figures 7.23 and 7.24 illustrate the noncoherent demodulation of FSK. The matched filters have the impulse responses that match the FSK signals $s_1(t) = A \cos 2\pi f_1 t$ and $s_2(t) = A \cos 2\pi f_2 t$, respectively. Since envelope detectors are employed, it is irrelevant whether FSK has a continuous phase or not.

The bit error probability of noncoherent FSK is given in (7.96) as follows:

$$P_b = \frac{1}{2} e^{-E_b/2N_0} \tag{7.143}$$

where E_b is the bit energy and $N_0/2$ is the power spectral density of the input noise.

Since MSK is a special type of FSK, both demodulators in Figures 7.23 and 7.24 can be employed to noncoherently demodulate MSK. For MSK, the frequencies f_1 and f_2 are given by $f_1 = f_c + 1/4T_b$ and $f_2 = f_c - 1/4T_b$ per (6.60). The bit error probability in (7.143) also applies to noncoherent MSK.

Both FSK and MSK are digital FM signals, meaning that the modulating information signal is digital. Therefore, both FSK and MSK can be demodulated by a slope detector used in FM demodulation [5,6]. Figure 7.25 shows a generic demodulator using slope detector.

The IF filter bandwidth is chosen to avoid the distortion of the modulated signal. The bit error probability is given in [7] as follows:

$$P_b = e^{-E_b/N_0} \tag{7.144}$$

Comparing (7.144) with (7.143), we observe that the demodulation with a slope detector is superior to noncoherent demodulation with a matched filter–envelope detector or a

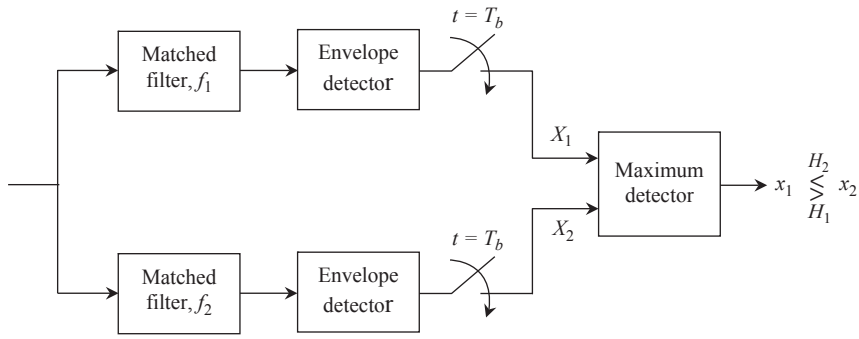

Figure 7.23 Noncoherent FSK demodulator employing the matched filter–envelope detector.

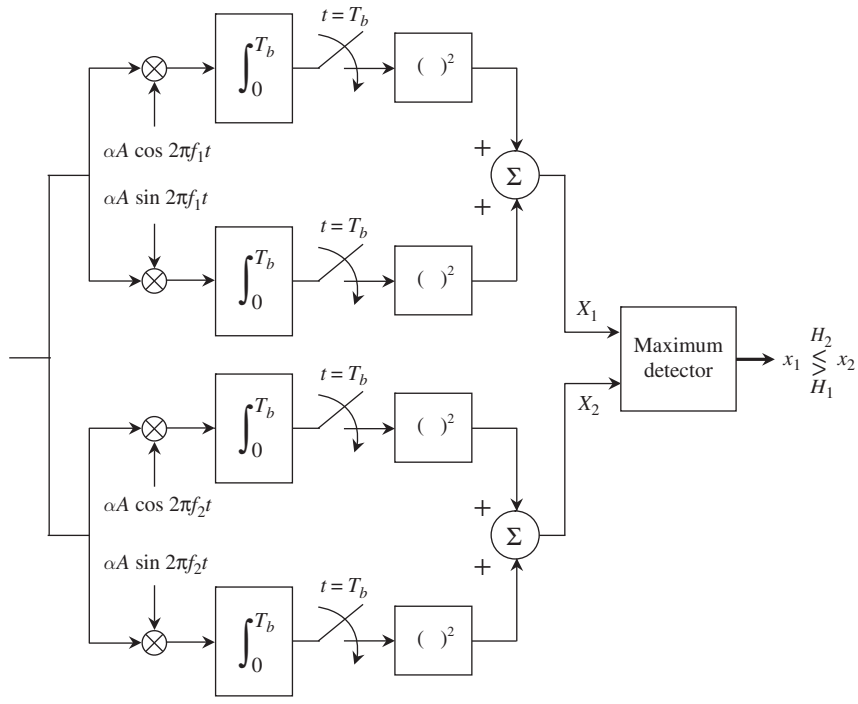

Figure 7.24 Noncoherent FSK demodulator employing the quadrature correlator–square law detector.

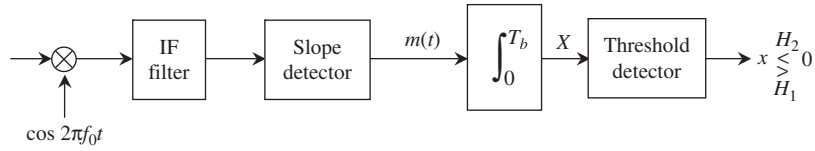

Figure 7.25 Continuous-phase FSK or MSK demodulator with slope detector. The signal $m(t)$ is the antipodal information signal.

quadrature correlation–square law detector by 3 dB in bit energy-to-noise density ratio (signal-to-noise ratio per bit). This improvement results from the fact that a slope detector is affected by quadrature noise only. Thus, the in-phase noise is not a factor, and the noise as seen by the threshold detector is 3 dB less in power.

For the case of continuous-phase FSK, coherent demodulation yields a bit error probability of $P_b = Q\left(\sqrt{E_b/N_0}\right)$, which is larger than the bit error probability of a demodulator with slope detector, $P_b = \exp(-E_b/N_0)$. For example, at $P_b = 10^{-4}$ the required E_b/N_0 for coherent demodulation is 11.4 dB. On the other hand, the required E_b/N_0 for demodulation with slope detector is 9.2 dB. This happens because the slope detector extracts the baseband signal $m(t)$, as seen in Figure 7.25, which is an antipodal signal. Then, $m(t)$ is optimally detected via a threshold detector. Note that an antipodal signal is the complex envelope of a PSK signal; therefore, threshold detection of an antipodal signal yields the same bit error probability as that of PSK. Since the slope detector output noise is no longer Gaussian, this

leads to a degradation in the bit error probability and compared to that of PSK, which is $Q\left(\sqrt{2E_b/N_0}\right)$. Thus, the bit error probability of the demodulator with slope detector falls between $Q\left(\sqrt{E_b/N_0}\right)$ and $Q\left(\sqrt{2E_b/N_0}\right)$.

Noncoherent DPSK

Recall from Section 6.4 that when the ith data bit $d_i = 0$ is transmitted, its differentially encoded bit c_i remains the same as the previously encoded bit c_{i-1}. In other words, the waveform for two consecutive encoded bits $c_{i-1}c_i$ can be written as

$$s_1(t) = s_{i-1}(t) + s_i(t), \qquad (i-1)T_b \le t < (i+1)T_b \tag{7.145}$$

where $s_{i-1}(t)$ and $s_i(t)$ are the transmitted PSK waveforms for the encoded bits c_{i-1} and c_i, respectively. Assume that the carrier phase θ varies slowly over any two consecutive bits, then we can express $s_{i-1}(t)$ and $s_i(t)$ as follows:

$$s_{i-1}(t) = \pm Ap(t-(i-1)T_b)\cos(2\pi f_c t + \theta) \tag{7.146}$$

$$s_i(t) = \pm Ap(t-iT_b)\cos(2\pi f_c t + \theta) \tag{7.147}$$

as seen in Example 6.20. On the other hand, when the ith data bit $d_i = 1$ is transmitted, its differentially encoded bit c_i is the complement of the previously encoded bit c_{i-1}, that is, $c_i = \overline{c_{i-1}}$. Thus, the waveform for two consecutive encoded bits $c_{i-1}c_i$ can be written as

$$s_2(t) = s_{i-1}(t) - s_i(t), \qquad (i-1)T_b \le t < (i+1)T_b \tag{7.148}$$

Clearly, $s_1(t)$ and $s_2(t)$ are orthogonal over the two-bit interval $2T_b$, that is

$$\int_{(i-1)T_b}^{(i+1)T_b} s_1(t)s_2(t)\,\mathrm{d}t = \int_{(i-1)T_b}^{(i+1)T_b} s_{i-1}^2(t)\,\mathrm{d}t - \int_{(i-1)T_b}^{(i+1)T_b} s_i^2(t)\,\mathrm{d}t = 0 \tag{7.149}$$

since both $s_{i-1}(t)$ and $s_i(t)$ have the same bit energy $E_b = A^2T_b/2$.

The above observations lead us to the following conclusion. *The data bit $d_i = 0$ is represented by the waveform $s_1(t)$, and $d_i = 1$ is represented by $s_2(t)$.* Thus, DPSK is truly an orthogonal modulation over any interval of $2T_b$. This enables DPSK to be demodulated noncoherently as shown in Figure 7.26. Note that the energy of $s_1(t)$ or $s_2(t)$ is $2E_b$ since they span an interval of $2T_b$. Thus, according to (7.56) and (7.57), the signal-to-noise ratio at the output of the matched filter is

$$SNR_0 = \frac{\alpha^2(2E_b)^2}{\alpha^2(2E_b)N_0} = \frac{2E_b}{N_0} \tag{7.150}$$

which is 3 dB higher than an FSK signal. Consequently, the bit error probability of noncoherent DPSK is given by

$$P_b = \frac{1}{2}\mathrm{e}^{-E_b/N_0} \tag{7.151}$$

as compared to (7.143) for FSK.

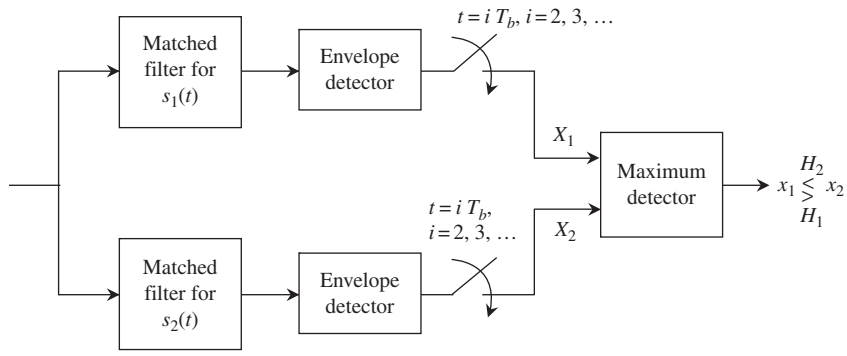

Figure 7.26 Noncoherent DPSK demodulator employing the matched filter–envelope detector.

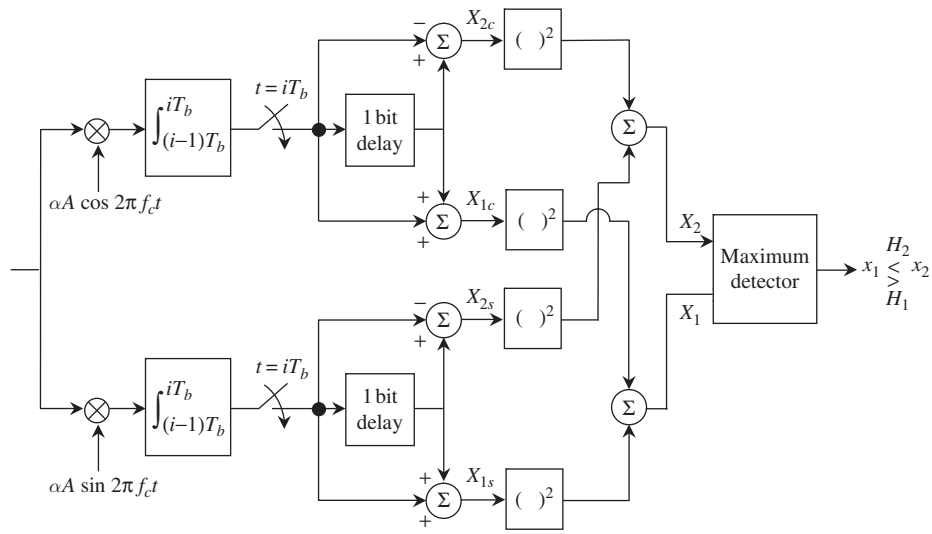

Figure 7.27 Noncoherent DPSK demodulator employing the quadrature correlator–square law detector.

Figure 7.27 shows a more practical implementation using a quadrature correlator–square law detector with appropriate delays to account for the two-bit interval orthogonal signals in (7.145) and (7.148).

Example 7.11 Operation of noncoherent DPSK in Figure 7.27

Consider again the sequence of received signals $s_i(t)$ in Example 6.20 of Section 6.4. We wish to demonstrate the process of noncoherent demodulation of this sequence of signals and to recover data, as shown in Table 7.4.

■

Table 7.4 Demodulation process

i	$s_i(t)$	X_{1c}	X_{1s}	X_{2c}	X_{2s}	X_1	X_2	d_i
0	$Ap(t)\cos(2\pi f_c t+\theta)$	$\alpha/2\ A^2T_b\cos\theta$	$-\alpha/2\ A^2T_b\sin\theta$	$-\alpha/2\ A^2T_b\cos\theta$	$\alpha/2\ A^2T_b\sin\theta$	$\alpha^2/4\ A^4T^2$	$\alpha^2/4A^4T_b^2$	
1	$Ap(t-T_b)\cos(2\pi f_c t+\theta)$	$\alpha\ A^2T\cos\theta$	$-\alpha A^2T_b\sin\theta$	0	0	$\alpha^2A^4T_b^2$	0	0
2	$-Ap(t-2T_b)\cos(2\pi f_c t+\theta)$	0	0	$\alpha A^2T_b\cos\theta$	$-\alpha A^2T_b\sin\theta$	0	$\alpha^2A^4T_b^2$	1
3	$Ap(t-3T_b)\cos(2\pi f_c t+\theta)$	0	0	$-\alpha A^2T_b\cos\theta$	$\alpha A^2T_b\sin\theta$	0	$\alpha^2A^4T_b^2$	1
4	$Ap(t-4T_b)\cos(2\pi f_c t+\theta)$	$\alpha A^2T_b\cos\theta$	$-\alpha A^2T_b\sin\theta$	0	0	$\alpha^2A^4T_b^2$	0	0
5	$-Ap(t-5T_b)\cos(2\pi f_c t+\theta)$	0	0	$\alpha A^2T_b\cos\theta$	$-\alpha A^2T_b\sin\theta$	0	$\alpha^2A^4T_b^2$	1
6	$-Ap(t-6T_b)\cos(2\pi f_c t+\theta)$	$-\alpha A^2T_b\cos\theta$	$\alpha A^2T_b\sin\theta$	0	0	$\alpha^2A^4T_b^2$	0	0

In the following discussion we will analyze the performance of the noncoherent demodulator in Figure 7.27 by considering the AWGN that accompanies the received signal. Let us assume that hypothesis H_1 represents the data bit 0, that is, we receive the signal $s_1(t)=s_{i-1}(t)+s_i(t),\ (i-1)T_b\le t<(i+1)T_b$ in (7.145). Then, given the bit energy $E_b=A^2T_b/2$, we have

$$\begin{aligned} X_{1c} &= \left(\pm\frac{\alpha}{2}A^2T_b\cos\theta+N'_{1c}\right)+\left(\pm\frac{\alpha}{2}A^2T_b\cos\theta+N''_{1c}\right)\\ &= \pm\alpha A^2T_b\cos\theta+N_{1c}=\pm 2\alpha E_b\cos\theta+N_{1c}\end{aligned} \tag{7.152}$$

$$\begin{aligned} X_{1s} &= \left(\mp\frac{\alpha}{2}A^2T_b\sin\theta+N'_{1s}\right)+\left(\mp\frac{\alpha}{2}A^2T_b\sin\theta+N''_{1s}\right)\\ &= \mp\frac{\alpha}{2}A^2T_b\sin\theta+N_{1s}=\mp 2\alpha E_b\sin\theta+N_{1s}\end{aligned} \tag{7.153}$$

where

$$N'_{1c}=\int_{(i-1)T_b}^{iT_b}n(t)[\alpha A\cos 2\pi f_c t]\,\mathrm{d}t,\qquad N''_{1c}=\int_{iT_b}^{(i+1)T_b}n(t)[\alpha A\cos 2\pi f_c t]\,\mathrm{d}t \tag{7.154}$$

$$N'_{1s}=\int_{(i-1)T_b}^{iT_b}n(t)[\alpha A\sin 2\pi f_c t]\,\mathrm{d}t,\qquad N''_{1s}=\int_{iT_b}^{(i+1)T_b}n(t)[\alpha A\sin 2\pi f_c t]\,\mathrm{d}t \tag{7.155}$$

and

$$N_{1c}=N'_{1c}+N''_{1c},\qquad N_{1s}=N'_{1s}+N''_{1s} \tag{7.156}$$

Given the input noise $n(t)$ with power spectral density $N_0/2\ (\mathrm{W/Hz})$ and, hence, autocorrelation $\mathbf{E}\{n(t)n(\tau)\}=(N_0/2)\delta(t-\tau)$, we can calculate the variance of N'_{1c}, N''_{1c}, N'_{1s}, and N''_{1s} to be $\alpha^2A^2T_bN_0/4$. This, in turn, yields the variance of N_{1c} and N_{1s} in (7.156) to be $\alpha^2A^2T_bN_0/2=\alpha^2E_bN_0$. Note that N'_{1c}, N''_{1c}, N'_{1s}, and N''_{1s} are statistically independent because they are uncorrelated zero mean Gaussian random variables. Similarly, we have

$$X_{2c}=N'_{1c}-N''_{1c} \tag{7.157}$$

$$X_{2s}=N'_{1s}-N''_{1s} \tag{7.158}$$

Thus, both X_{2c} and X_{2s} are independent Gaussian random variables with zero mean and variance $\alpha^2 A^2 T_b N_0/2 = \alpha^2 E_b N_0$.

The decision variables X_1 and X_2 are therefore given by

$$X_1 = X_{1c}^2 + X_{1s}^2 \tag{7.159}$$

$$X_2 = X_{2c}^2 + X_{2s}^2 \tag{7.160}$$

We observe that X_1 is the sum of two squared Gaussian random variables with means $\pm 2\alpha E_b \cos\theta$ and $\pm 2\alpha E_b \sin\theta$, and variance $\alpha^2 E_b N_0$. Thus, X_1 is a non-central chi-squared random variable with two degrees of freedom whose probability density function is given in (7.64) with X_1 replacing Y, and $a^2 = 4\alpha^2 E_b^2$ and $\sigma^2 = \alpha^2 E_b N_0$. On the other hand, the decision variable X_2 is the sum of two squared Gaussian random variables with zero mean and variance $\alpha^2 E_b N_0$. Thus, X_2 is a central chi-squared random variable whose probability density function is given in (7.65) with X_2 replacing Y, and $\sigma^2 = \alpha^2 E_b N_0$. The conditional bit error probability given H_1 can be derived in a similar fashion to (7.91)–(7.96). It is the same as the conditional bit error probability given hypothesis H_2 that corresponds to data bit 1 as dictated by symmetry. The bit error probability of noncoherent DPSK using the demodulator in Figure 7.27 is given by (7.103), which is the same as (7.96) with $E = 2E_b$ using the fact that $a^2/4\sigma^2$ in (7.95) is equal to E_b/N_0. Thus

$$P_b = \frac{1}{2} e^{-E_b/N_0} \tag{7.161}$$

In addition to the noncoherent demodulator in Figure 7.27, DPSK can also be noncoherently demodulated by another demodulator, such as the one shown in Figure 7.28, called a delay-and-multiply demodulator.

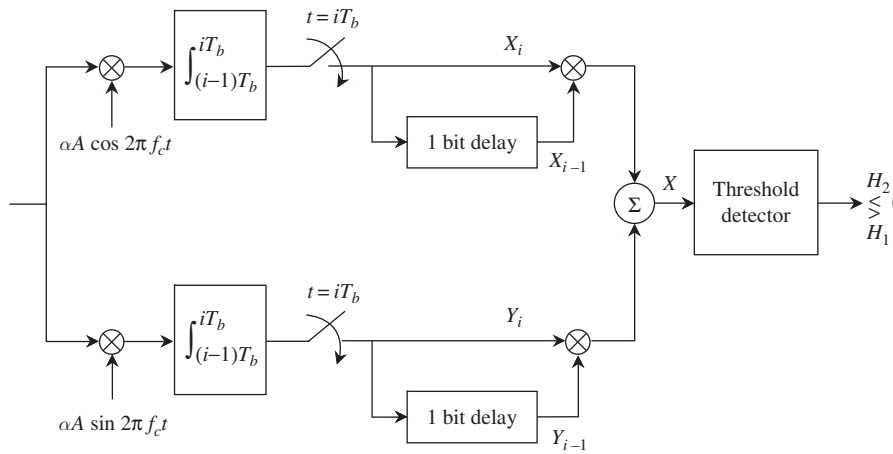

Figure 7.28 Alternative noncoherent DPSK demodulator employing the delay-and-multiply detector.

Table 7.5 Demodulation process

i	$s(t)$	X_i	X_{i-1}	Y_i	Y_{i-1}	X	d_i
0	$Ap(t)\cos(2\pi f_c t+\theta)$	$\alpha/2\ A^2T_b\cos\theta$	0	$-\alpha/2\ A^2T_b\sin\theta$	0	0	
1	$Ap(t-T_b)\cos(2\pi f_c t+\theta)$	$\alpha/2\ A^2T_b\cos\theta$	$\alpha/2\ A^2T_b\cos\theta$	$-\alpha/2\ A^2T_b\sin\theta$	$-\alpha/2\ A^2T_b\sin\theta$	$\alpha^2/4\ A^4T_b^2$	0
2	$-Ap(t-2T_b)\cos(2\pi f_c t+\theta)$	$-\alpha/2\ A^2T_b\cos\theta$	$\alpha/2\ A^2T_b\cos\theta$	$\alpha/2\ A^2T_b\sin\theta$	$-\alpha/2\ A^2T_b\sin\theta$	$-\alpha^2/4\ A^4T_b^2$	1
3	$Ap(t-3T_b)\cos(2\pi f_c t+\theta)$	$\alpha/2\ A^2T_b\cos\theta$	$-\alpha/2\ A^2T_b\cos\theta$	$-\alpha/2\ A^2T_b\sin\theta$	$\alpha/2\ A^2T_b\sin\theta$	$-\alpha^2/4\ A^4T_b^2$	1
4	$Ap(t-4T_b)\cos(2\pi f_c t+\theta)$	$\alpha/2\ A^2T_b\cos\theta$	$\alpha/2\ A^2T_b\cos\theta$	$-\alpha/2\ A^2T_b\sin\theta$	$-\alpha/2\ A^2T_b\sin\theta$	$\alpha^2/4\ A^4T_b^2$	0
5	$-Ap(t-5T_b)\cos(2\pi f_c t+\theta)$	$-\alpha/2\ A^2T_b\cos\theta$	$\alpha/2\ A^2T_b\cos\theta$	$\alpha/2\ A^2T_b\sin\theta$	$-\alpha/2\ A^2T_b\sin\theta$	$-\alpha^2/4\ A^4T_b^2$	1
6	$-Ap(t-6T_b)\cos(2\pi f_c t+\theta)$	$-\alpha/2\ A^2T_b\cos\theta$	$-\alpha/2\ A^2T_b\cos\theta$	$\alpha/2\ A^2T_b\sin\theta$	$\alpha/2\ A^2T_b\sin\theta$	$\alpha^2/4\ A^4T_b^2$	0

Example 7.12 Operation of noncoherent DPSK in Figure 7.28

Again we consider the sequence of received signals $s_i(t)$ in Example 7.11 and wish to recover the data, as shown in Table 7.5.

■

The performance of the delay-and-multiply demodulator can be analyzed by assuming hypothesis H_1 that represents $d_i = 0$:

$$X_i = \pm\frac{\alpha}{2}A^2T_b\cos\theta + N_{c,i} \tag{7.162}$$

$$X_{i-1} = \pm\frac{\alpha}{2}A^2T_b\cos\theta + N_{c,i-1} \tag{7.163}$$

$$Y_i = \mp\frac{\alpha}{2}A^2T_b\sin\theta + N_{s,i} \tag{7.164}$$

$$Y_{i-1} = \mp\frac{\alpha}{2}A^2T_b\sin\theta + N_{s,i-1} \tag{7.165}$$

where

$$N_{c,i} = \int_{iT_b}^{(i+1)T_b} n(t)[\alpha A\cos 2\pi f_c t]\,\mathrm{d}t, \qquad N_{c,i-1} = \int_{(i-1)T_b}^{iT_b} n(t)[\alpha A\cos 2\pi f_c t]\,\mathrm{d}t \tag{7.166}$$

$$N_{s,i} = \int_{iT_b}^{(i+1)T_b} n(t)[\alpha A\sin 2\pi f_c t]\,\mathrm{d}t, \qquad N_{s,i-1} = \int_{(i-1)T_b}^{iT_b} n(t)[\alpha A\sin 2\pi f_c t]\,\mathrm{d}t \tag{7.167}$$

Note that $N_{c,i}$, $N_{c,i-1}$, $N_{s,i}$, $N_{s,i-1}$ are independent Gaussian random variables with zero mean and variance $\alpha^2A^2T_bN_0/4 = \alpha^2E_bN_0/2$, where $E_b = A^2T_b/2$ is the bit energy. The decision variable X at the input of the threshold detector in Figure 7.28 is

$$X = X_{i-1}X_i + Y_{i-1}Y_i \tag{7.168}$$

Substituting (7.162)–(7.165) into (7.168), we get

$$\begin{aligned} X &= \left(\pm\frac{\alpha}{2}A^2T_b\cos\theta + N_{c,i-1}\right)\left(\pm\frac{\alpha}{2}A^2T_b\cos\theta + N_{c,i}\right) \\ &\quad + \left(\mp\frac{\alpha}{2}A^2T_b\sin\theta + N_{s,i-1}\right)\left(\mp\frac{\alpha}{2}A^2T_b\sin\theta + N_{s,i}\right) \\ &= \left(\pm\frac{\alpha}{2}A^2T_b\cos\theta + \frac{N_{c,i-1}}{2} + \frac{N_{c,i}}{2}\right)^2 - \left(\frac{N_{c,i-1}}{2} - \frac{N_{c,i}}{2}\right)^2 \\ &\quad + \left(\mp\frac{\alpha}{2}A^2T_b\sin\theta + \frac{N_{s,i-1}}{2} + \frac{N_{s,i}}{2}\right)^2 - \left(\frac{N_{s,i-1}}{2} - \frac{N_{s,i}}{2}\right)^2 \end{aligned} \tag{7.169}$$

Define the new Gaussian random variables as follows:

$$N_1 = \frac{N_{c,i-1}}{2} + \frac{N_{c,i}}{2} \tag{7.170}$$

$$N_2 = \frac{N_{s,i-1}}{2} + \frac{N_{s,i}}{2} \tag{7.171}$$

$$N_3 = \frac{N_{c,i-1}}{2} - \frac{N_{c,i}}{2} \tag{7.172}$$

$$N_4 = \frac{N_{s,i-1}}{2} - \frac{N_{s,i}}{2} \tag{7.173}$$

Thus, we can express the decision variable X in terms of the new noise variables N_1, N_2, N_3, and N_4 as follows:

$$X = \left(\pm\frac{\alpha}{2}A^2T_b\cos\theta + N_1\right)^2 + \left(\mp\frac{\alpha}{2}A^2T_b\sin\theta + N_2\right)^2 - N_3^2 - N_4^2 \tag{7.174}$$

Furthermore, let us define the non-central chi-squared and central chi-squared random variables X_1 and X_2 as follows:

$$X_1 = \left(\pm\frac{\alpha}{2}A^2T_b\cos\theta + N_1\right)^2 + \left(\mp\frac{\alpha}{2}A^2T_b\sin\theta + N_2\right)^2 \tag{7.175}$$

$$X_2 = N_3^2 + N_4^2 \tag{7.176}$$

Therefore, we can express X in terms of X_1 and X_2 as

$$X = X_1 - X_2 \tag{7.177}$$

The conditional bit error probability given H_1 is given by

$$\Pr(X < 0|H_1) = \Pr(X_2 > x_1|H_1) \tag{7.178}$$

The probability density function of the non-central chi-squared random variable X_1 in (7.175) is given by (7.64) with $a^2 = \alpha^2A^4T_b^2/4 = \alpha^2E_b^2$ and $\sigma^2 = \alpha^2E_bN_0/4$. Note that the variance of N_1 or N_2 is equal to one-half the variance of $N_{c,i}$ (or $N_{c,i-1}$ or $N_{s,i}$ or $N_{s,i-1}$) per (7.170) and (7.171). Thus, $a^2/4\sigma^2 = E_b/N_0$. Similarly, the probability density function of

Table 7.6 Performance of binary modulation techniques

Demodulation	Bit error probability	Bandwidth
Coherent PSK	$Q\left(\sqrt{2E_b/N_0}\right)$	$2/T_b$
Coherent DPSK	$\approx 2Q\left(\sqrt{2E_b/N_0}\right)$	$2/T_b$
Direct detection ASK	$Q\left(\frac{1-r_e}{1+r_e}\sqrt{T_b/N_0}\,\mathcal{R}P\right)$	$2/T_b$
Coherent FSK	$Q\left(\sqrt{E_b/N_0}\right)$	$3/T_b$
Coherent MSK	$\approx 2Q\left(\sqrt{2E_b/N_0}\right)$	$3/2T_b$
Coherent precoded MSK	$Q\left(\sqrt{2E_b/N_0}\right)$	$3/2T_b$
Coherent GMSK	$Q\left(\sqrt{2\alpha E_b/N_0}\right)$	$\approx 3/2T_b$
Noncoherent FSK	$\frac{1}{2}e^{-E_b/2N_0}$	$3/T_b$
Noncoherent MSK	$\frac{1}{2}e^{-E_b/2N_0}$	$3/2T_b$
Noncoherent MSK with slope detection	e^{-E_b/N_0}	$3/2T_b$
Noncoherent DPSK	$\frac{1}{2}e^{-E_b/N_0}$	$2/T_b$

the central chi-squared random variable X_2 in (7.176) is given by (7.59) with $\sigma^2 = \alpha^2 E_b N_0/4$ as dictated by (7.172) and (7.173). Therefore, the bit error probability in (7.178) can be evaluated in a similar fashion to (7.92)–(7.96) to yield

$$P_b = \frac{1}{2}e^{-E_b/N_0} \tag{7.179}$$

Performance summary of binary modulation techniques

Our study of binary demodulation reveals its simplicity and robustness in an AWGN channel. Coherent binary demodulation outperforms its noncoherent counterpart but requires a local carrier that matches the received signal in both phase and frequency. This requires a carrier recovery circuit that can extract the carrier from the received modulated signal. On the other hand, noncoherent binary demodulation only requires a local carrier that matches in frequency to the received signal. This requirement can be met easily with a local oscillator. Table 7.6 summarizes the bit error probability and bandwidth of each binary demodulation technique that corresponds to the binary modulation in Chapter 6. Since bandwidth is defined by the signal pulse shape, for the purpose of comparison between different demodulation techniques, we use the squared pulse shape and, consequently, null-to-null bandwidth. The bit error probability of each binary demodulation technique can be read directly from the two curves in Figure 7.29 with appropriate scaling.

7.8 Minimum Euclidean distance detector

The *minimum Euclidean distance* detector is a multiple input–single output detector employed specially for M-ary demodulation. In principle, it accepts an L-dimensional

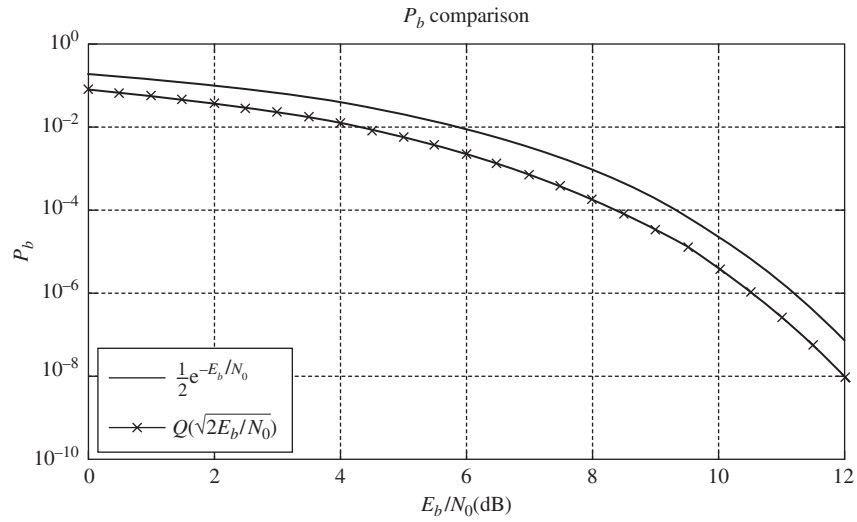

Figure 7.29 Bit error probability curves. (Courtesy of Peter Harley.)

decision column vector $\boldsymbol{X} = [X_k]$ at its input. This vector represents one of M possible hypotheses $H_1, H_2, \ldots, H_M$. Each hypothesis represents a symbol in the set of M-ary symbols. The decision vector $\boldsymbol{X}$ is a Gaussian vector with conditional mean $\boldsymbol{s}_i = [s_{ik}] = \mathbf{E}(\boldsymbol{X}|H_i),\ i = 1, 2, \ldots, M$, given hypothesis H_i. We have

$$\boldsymbol{X} = \boldsymbol{s_i} + \boldsymbol{N} \tag{7.180}$$

where $\boldsymbol{N}$ is the zero mean Gaussian noise vector with independent components whose variance is σ^2. Thus, the probability density function of $\boldsymbol{X}$ given H_i is

$$\begin{aligned} \boldsymbol{f_X}(\boldsymbol{x}|H_i) &= \prod_{k=1}^{L} f_{X_k}(x_k|H_i) = \prod_{k=1}^{L} \frac{1}{\sqrt{2\pi}\sigma} e^{-(x_k - s_{ik})^2/2\sigma^2} \\ &= \frac{1}{\left(\sqrt{2\pi}\sigma\right)^L} e^{-\frac{1}{2\sigma^2}\sum_{k=1}^{L}(x_k - s_{ik})^2} \end{aligned} \tag{7.181}$$

We wish to design a detector that selects a hypothesis H_i based on the minimum error probability criterion. This is equivalent to selecting H_i corresponding to the maximum of the set of a-posteriori probabilities $\Pr(H_i|x),\ i = 1, 2, \ldots, M$. This is called the *maximum a-posteriori probability criterion* (MAP), as first discussed in Section 7.5. When all symbols are equally likely, then the a-priori probabilities $\Pr(H_i), i = 1, 2, \ldots, M$, are equal to $1/M$ and the MAP criterion becomes the *maximum likelihood* (ML) *criterion*. Using the *Bayes rule*, we can express the a-posteriori probabilities $\Pr(H_i|x)$ as follows:

$$\Pr(H_i|\boldsymbol{x}) = \frac{f_{\boldsymbol{X}}(\boldsymbol{x}|H_i)\Pr(H_i)}{f_{\boldsymbol{X}}(\boldsymbol{x})}, \qquad i = 1, 2, \ldots, M \tag{7.182}$$

We note that $\Pr(H_i) = 1/M$, and $f_X(\boldsymbol{x}) = \sum_{i=1}^{M} \boldsymbol{f_X}(\boldsymbol{x}|H_i)\ \Pr(H_i)$ is completely independent of H_i, that is, $\boldsymbol{f_X}(\boldsymbol{x})$ is independent of which symbol is transmitted. Therefore, finding the

maximum of the set of $\Pr(H_i|x)$, $i = 1, 2, \ldots, M$, is equivalent to finding the maximum of the set of $\boldsymbol{f_X}(\boldsymbol{x}|H_i)$, $i = 1, 2, \ldots, M$. From (7.181) we note that $\boldsymbol{f_X}(\boldsymbol{x}|H_i)$ is a monotonically increasing function, thus, the maximum of the set of $\boldsymbol{f_X}(\boldsymbol{x}|H_i)$ corresponds to the maximum of the set of $\ln \boldsymbol{f_X}(\boldsymbol{x}|H_i)$, which is commonly referred to as the *ln-likelihood function*. The ln-likelihood function can be expressed as

$$\begin{aligned} \ln \boldsymbol{f_X}(\boldsymbol{x}|H_i) &= -L \ln\left(\sqrt{2\pi}\,\sigma\right) - \frac{1}{2\sigma^2} \sum_{k=1}^{L} (x_k - s_{ik})^2 \\ &= -L \ln\left(\sqrt{2\pi}\,\sigma\right) - \frac{1}{2\sigma^2} \|\boldsymbol{x} - \boldsymbol{s_i}\|^2 \end{aligned} \tag{7.183}$$

where the term $-L \ln\left(\sqrt{2\pi}\,\sigma\right)$ is common to all $\ln \boldsymbol{f_X}(\boldsymbol{x}|H_i)$. Hence, the *maximum* of the set $\ln \boldsymbol{f_X}(\boldsymbol{x}|H_i)$ corresponds to the *minimum* of the set of *Euclidean distances*

$$\boldsymbol{d}(\boldsymbol{x}, \boldsymbol{s_i}) = \|\boldsymbol{x} - \boldsymbol{s_i}\| = \sqrt{\sum_{k=1}^{L} (x_k - s_{ik})^2}, \qquad i = 1, 2, \ldots, M \tag{7.184}$$

The above analysis concludes that an optimum detector based on the *maximum likelihood criterion* selects the signal vector $\boldsymbol{s_i}$ that is closest in Euclidean distance to the sampled value $\boldsymbol{x}$ of the decision vector $\boldsymbol{X}$. Hence, the term *minimum Euclidean distance detector* is used.

Example 7.13 Threshold detector revisited

For the case of binary detection, the set of squared Euclidean distances in (7.184) consists of $d^2(x, s_1) = \|x - s_1\|^2 = (x - s_1)^2$ and $d(x, s_2) = \|x - s_2\|^2 = (x - s_2)^2$. Thus, the selection of either s_1 or s_2 based on the minimum Euclidean distance is equivalent to

$$(x - s_1)^2 \underset{H_2}{\overset{H_1}{\lessgtr}} (x - s_2)^2 \tag{7.185}$$

which is identical to (7.80). Hence, the threshold detector is *equivalent* to the minimum Euclidean distance detector for $M = 2$.

■

Figure 7.30 illustrates the minimum Euclidean distance detector. This type of detector is employed for *coherent M-ary demodulation* of signals, such as PSK, QPSK, MPSK, and

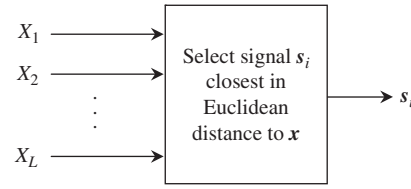

Figure 7.30 Minimum Euclidean distance detector.

MQAM. For these signals, $L = 2$, and this corresponds to a two-dimensional vector $\boldsymbol{x} = [x_1\, x_2]^t$, where x_1 and x_2 represent I and Q sampled values, respectively.

Symbol error probability

Recall that the decision vector $\boldsymbol{X}$ represents one of M possible hypotheses H_i, $i = 1, 2, \ldots, M$, with one hypothesis for each symbol of the set of M transmitted symbols. Thus, there are M detection regions in L-dimensional space, one for each symbol. Let R_i be the detection region for hypothesis H_i corresponding to the transmitted signal $\boldsymbol{s}_i$. The correct detection of $\boldsymbol{s_i}$ occurs when $\boldsymbol{X}$ falls inside R_i. Thus, the conditional correct detection probability given $\boldsymbol{s_i}$ was transmitted is

$$\Pr(\boldsymbol{X} \in R_i | H_i) = \int_{R_i} f_X(\boldsymbol{x}|H_i)\, \mathrm{d}\boldsymbol{x} \tag{7.186}$$

The symbol detection probability can be obtained via the total probability theorem as follows:

$$\begin{aligned} P_d &= \sum_{i=1}^{M} \Pr(\boldsymbol{X} \in R_i | H_i) \Pr(H_i) \\ &= \frac{1}{M} \sum_{i=1}^{M} \int_{R_i} f_X(\boldsymbol{x}|H_i)\, \mathrm{d}\boldsymbol{x} \end{aligned} \tag{7.187}$$

Hence, the symbol error probability is $1 - P_d$, or

$$P_e = 1 - \frac{1}{M} \sum_{i=1}^{M} \int_{R_i} f_X(\boldsymbol{x}|H_i)\, \mathrm{d}\boldsymbol{x} \tag{7.188}$$

It is not feasible to evaluate (7.188) for a large signal set such as MQAM. Fortunately, we can provide a tight upper bound for the symbol error probability by using the famous union bound. Let $A_i,\ i = 1, 2, \ldots, M$, be a set of M events, then the union bound states that

$$\Pr\left(\bigcup_{i=1}^{M} A_i\right) \leq \sum_{i=1}^{M} \Pr(A_i) \tag{7.189}$$

Returning to the *minimum Euclidean distance detector* and assume that we have hypothesis H_1, that is, $\boldsymbol{s}_1$ is transmitted. An error occurs if one of $\boldsymbol{s}_i,\ i = 2, 3, \ldots, M$, is closer to the sampled vector $\boldsymbol{X}$ than $\boldsymbol{s}_1$. Define the event A_i as the event that $\boldsymbol{s}_i$ is closer to $\boldsymbol{X}$ than $\boldsymbol{s}_1$ given that $\boldsymbol{s}_1$ was transmitted. The symbol error probability given H_1 is

$$P_{e|H_1} = \Pr\left(\bigcup_{i=2}^{M} A_i\right) \leq \sum_{i=2}^{M} \Pr(A_i) \tag{7.190}$$

Hence, we only need to evaluate $\Pr(A_i)$, which is the *pairwise error probability* in selecting between two signals $\boldsymbol{s}_i$ and $\boldsymbol{s}_1$, that is,

$$\Pr(A_i) = \Pr(\boldsymbol{s}_1 \to \boldsymbol{s}_i) = \Pr\left(\|\boldsymbol{X} - \boldsymbol{s}_i\|^2 < \|\boldsymbol{X} - \boldsymbol{s}_1\|^2 \middle| H_1\right) \tag{7.191}$$

Example 7.14 Pairwise error probability for a Gaussian channel

Let $\boldsymbol{s}_1 = \mathbf{E}\{\boldsymbol{X}|H_1\}$ and $\boldsymbol{s}_i = \mathbf{E}\{\boldsymbol{X}|H_i\}$ be two sampled L-dimensional vectors. Let $\boldsymbol{N} = [N_j]$ be the L-dimensional noise vector whose components are independent Gaussian random variables with zero mean and variance σ^2. Assume hypothesis H_1, that is, $\boldsymbol{s}_1$ was the transmitted vector, then $\boldsymbol{X} = \boldsymbol{s}_1 + \boldsymbol{N}$. We are interested in evaluating (7.191). Substituting $\boldsymbol{X}$ into (7.191), we get

$$\begin{aligned}\Pr(A_i) = \Pr(\boldsymbol{s}_1 \to \boldsymbol{s}_i) &= \Pr(\|\boldsymbol{s}_1 - \boldsymbol{s}_i + \boldsymbol{N}\|^2 < \|\boldsymbol{s}_1 - \boldsymbol{s}_1 + N\|^2 \big| H_1) \\ &= \Pr(\|\boldsymbol{s}_1 - \boldsymbol{s}_i + \boldsymbol{N}\|^2 < \|\boldsymbol{N}\|^2 \big| H_1)\end{aligned} \tag{7.192}$$

Since

$$\|\boldsymbol{s}_1 - \boldsymbol{s}_i + \boldsymbol{N}\|^2 = \|\boldsymbol{s}_1 - \boldsymbol{s}_i\|^2 + 2[\boldsymbol{s}_1 - \boldsymbol{s}_i]^t \boldsymbol{N} + \|\boldsymbol{N}\|^2 \tag{7.193}$$

Then

$$\Pr(A_i) = \Pr(\boldsymbol{s}_1 \to \boldsymbol{s}_i) = \Pr(\|\boldsymbol{s}_1 - \boldsymbol{s}_i\|^2 + 2[\boldsymbol{s}_1 - \boldsymbol{s}_i]^t \boldsymbol{N} + \|\boldsymbol{N}\|^2 < \|\boldsymbol{N}\|^2 | H_1) \tag{7.194}$$

Define

$$Z = \frac{[\boldsymbol{s}_i - \boldsymbol{s}_1]^t \boldsymbol{N}}{\|\boldsymbol{s}_i - \boldsymbol{s}_1\|} \tag{7.195}$$

Note that $[\boldsymbol{s}_i - \boldsymbol{s}_1]^t / \|\boldsymbol{s}_i - \boldsymbol{s}_1\|$ is a unit length vector, therefore, the random variable Z in (7.195) is a Gaussian random variable with zero mean and variance σ^2. Substituting (7.195) into (7.194) we get

$$\begin{aligned}\Pr(A_i) = \Pr(\boldsymbol{s}_1 \to \boldsymbol{s}_i) &= \Pr\left(Z > \frac{1}{2}\|\boldsymbol{s}_i - \boldsymbol{s}_1\| \middle| H_1\right) \\ &= Q\left(\frac{\|\boldsymbol{s}_i - \boldsymbol{s}_1\|}{2\sigma}\right)\end{aligned} \tag{7.196}$$

via (7.29). Define $d_{i,1}$ as the Euclidean distance between two vectors $\boldsymbol{s}_i$ and $\boldsymbol{s}_1$, that is,

$$d_{i,1} = \|\boldsymbol{s}_i - \boldsymbol{s}_1\| \tag{7.197}$$

Then

$$\Pr(A_i) = \Pr(\boldsymbol{s}_1 \to \boldsymbol{s}_i) = Q\left(\frac{d_{i,1}}{2\sigma}\right) \tag{7.198}$$

Hence, the pairwise error probability involving two vectors $\boldsymbol{s}_1$ and $\boldsymbol{s}_i$ in a Gaussian channel depends solely on their Euclidean distance and the variance of noise.

■

If we substitute $\Pr(A_i)$ in (7.198) into the union bound (7.190), we obtain the upper bound on the symbol error probability given H_1 as

$$P_{e|H_1} \leq \sum_{i=2}^{M} Q\left(\frac{d_{i,1}}{2\sigma}\right) \tag{7.199}$$

The $Q(\cdot)$ function decreases rapidly as its argument increases, thus, the left-hand side of (7.199) is dominated by the terms on the right-hand side with the smallest argument. Let us define $d_{min,1}$ as the smallest Euclidean distance of the set $d_{i,1}$, $i = 2, 3, \ldots, M$,

$$d_{min,1} = \min_i d_{i,1} \tag{7.200}$$

and N_1 as the number of signals that are $d_{min,1}$ distance from $\boldsymbol{s}_1$. Then, we can approximate (7.199) as follows:

$$P_{e|H_1} \approx N_1 Q\left(\frac{d_{min,1}}{2\sigma}\right) \tag{7.201}$$

Assuming all hypotheses are equally likely, then the average symbol error probability is

$$\begin{aligned} P_e &\approx \sum_{k=1}^{M} P_{e|H_k} \Pr(H_k) \\ &\approx \frac{1}{M} \sum_{k=1}^{M} N_k Q\left(\frac{d_{min,k}}{2\sigma}\right) \end{aligned} \tag{7.202}$$

Using the same argument as above, we define d_{min} as the minimum Euclidean distance between any signal pair and N_n as the average number of symbols at the minimum Euclidean distance d_{min}, that is, the average number of nearest neighbors

$$d_{min} = \min_k d_{min,k} \tag{7.203}$$

$$N_n = \frac{1}{M} \sum_{k=1}^{M} N_k \tag{7.204}$$

Then, the final approximation for the symbol error probability is given by

$$P_e \approx N_n Q\left(\frac{d_{min}}{2\sigma}\right) \tag{7.205}$$

7.9 M-ary maximum detector

This is a generalized version of the maximum detector discussed in Section 7.6 for binary demodulation. *The M-ary maximum detector* accepts M decision variables $X_1, X_2, \ldots, X_M$ and chooses one with the largest value. These M decision variables are elements of a decision M-dimensional column vector $\boldsymbol{X} = [X_j]$ that represents one of M possible hypotheses $H_1, H_2, \ldots, H_M$. The M-ary maximum detector is employed explicitly for M-ary orthogonal signals such as MFSK or CSK.

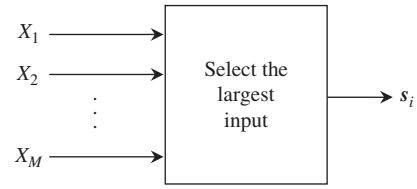

Figure 7.31 M-ary maximum detector.

Gaussian decision variables

Let us consider a decision M-dimensional column vector $\boldsymbol{X} = [X_j] = \boldsymbol{s}_i + \boldsymbol{N}$ assuming hypothesis H_i, that is, signal $\boldsymbol{s}_i$ was transmitted. Here, $\boldsymbol{N} = [N_j]$ is an M-dimensional Gaussian vector whose elements are independent zero mean Gaussian random variables with a common variance σ^2. The signal vector $\boldsymbol{s}_i$ belongs to the set of M orthogonal vectors where each vector $\boldsymbol{s}_j$ has $M-1$ zero elements except for the jth element, whose value is $\|\boldsymbol{s}_j\|$. It is quite obvious that a minimum Euclidean distance detector can detect vector $\boldsymbol{s}_i$ given $\boldsymbol{X}$. Such a detector would have $L = M$ inputs. We are interested in showing that, in the case of an orthogonal signal set, the minimum Euclidean distance detector reduces to a maximum detector. Indeed, from (7.184), given the sample value $\boldsymbol{x}$ of the decision vector $\boldsymbol{X}$, the minimum of the set of Euclidean distances $d(\boldsymbol{x}, \boldsymbol{s}_i) = \|\boldsymbol{x} - \boldsymbol{s}_i\|, i = 1, 2, \ldots, M$, corresponds to selecting the signal vector $\boldsymbol{s}_i$ that is closest in Euclidean distance to $\boldsymbol{x}$. But this happens if and only if the ith element of $\boldsymbol{s}_i$, which is $\|\boldsymbol{s}_i\|$, matches the mean value of the ith element of $\boldsymbol{x}$. In the case of no noise, it amounts to $d(\boldsymbol{x}, \boldsymbol{s}_i) = \|\boldsymbol{s}_i - \boldsymbol{s}_i\| = 0$ and $d(\boldsymbol{x}, \boldsymbol{s}_j) = \|\boldsymbol{s}_i - \boldsymbol{s}_j\| = \sqrt{\|\boldsymbol{s}_i\|^2 + \|\boldsymbol{s}_j\|^2} > d(\boldsymbol{x}, \boldsymbol{s}_i), j \neq i$. Hence, a maximum detector that selects the ith element of $\boldsymbol{x}$ to identify the transmitted vector $\boldsymbol{s}_i$ achieves the same goal. Figure 7.31 illustrates the above concept.

In practice, the orthogonal signal vectors $\boldsymbol{s}_i, i = 1, 2, \ldots, M$, commonly have the same length, that is, $\|\boldsymbol{s}_1\| = \|\boldsymbol{s}_2\| = \cdots = \|\boldsymbol{s}_M\| = \sqrt{E_s}$, where E_s is the common signal (symbol) energy. Furthermore, they have equal distance between them, hence

$$d_{min} = \sqrt{2}\,\|\boldsymbol{s}_i\| = \sqrt{2E_s} \tag{7.206}$$

Using the union bound in (7.190) and note $\Pr(A_i) = Q(d_{min}/2\sigma)$ for all events A_i due to (7.206), we arrive at the following upper bound for symbol error probability:

$$P_e \leq (M-1)Q\left(\frac{d_{min}}{2\sigma}\right) \tag{7.207}$$

Example 7.15 Exact symbol error probability

We are interested in evaluating symbol error probability of the M-ary maximum detector. Assuming hypothesis H_1, that is, signal vector $\boldsymbol{s}_1$ was transmitted, then $\boldsymbol{X} = \boldsymbol{s}_1 + \boldsymbol{N}$. In other words, the elements of $\boldsymbol{X} = [X_j]$ are given by

$$X_1 = \|\boldsymbol{s}_1\| + N_1 \tag{7.208}$$

$$X_j = N_j,\ \ j = 2,\ 3,\ \ldots,\ M \tag{7.209}$$

Note that X_j are independent Gaussian random variables with the following probability density functions:

$$f_{X_1}(x_1) = \frac{1}{\sqrt{2\pi}\,\sigma} \mathrm{e}^{-(x_1 - \|\boldsymbol{s}_1\|)^2/2\sigma^2} \tag{7.210}$$

$$f_{X_j}(x_j) = \frac{1}{\sqrt{2\pi}\,\sigma} \mathrm{e}^{-x_j^2/2\sigma^2}, \quad j = 2,\ 3,\ \ldots,\ M \tag{7.211}$$

It is seen that a correct detection occurs when every x_j is smaller than x_1, where x_1 is a sampled value of X_1. Such an event occurs with a conditional correct detection probability

$$\begin{aligned} P_{c|x_1} &= \Pr\{(X_2 < x_1) \cap (X_3 < x_1) \cap \cdots \cap (X_M < x_1) | H_1\} \\ &= [\Pr(X_2 < x_1 | H_1)]^{M-1} \end{aligned} \tag{7.212}$$

We have used the fact that X_j, $j = 2,\ 3,\ \ldots,\ M$, are independent and identically distributed random variables. Via (7.26) we get

$$\Pr(X_2 < x_1 | H_1) = \frac{1}{\sqrt{2\pi}\,\sigma} \int_{-\infty}^{x_1} \mathrm{e}^{-y^2/2\sigma^2} \mathrm{d}y = 1 - Q\left(\frac{x_1}{\sigma}\right) \tag{7.213}$$

Substituting (7.213) into (7.212) yields

$$P_{c|x_1} = \left[1 - Q\left(\frac{x_1}{\sigma}\right)\right]^{M-1} \tag{7.214}$$

By taking the expected value of $P_{c|x_1}$ with respect to x_1, using the probability density function in (7.210), we obtain the correct detection probability given hypothesis H_1:

$$\begin{aligned} P_c &= \int_{-\infty}^{\infty} \frac{1}{\sqrt{2\pi}\,\sigma} \mathrm{e}^{-(x_1 - \|\boldsymbol{s}_1\|)^2/2\sigma^2} \left[1 - Q\left(\frac{x_1}{\sigma}\right)\right]^{M-1} \mathrm{d}x_1 \\ &= \frac{1}{\sqrt{2\pi}} \int_{-\infty}^{\infty} \mathrm{e}^{-y^2/2} \left[1 - Q\left(y + \frac{\|\boldsymbol{s}_1\|}{\sigma}\right)\right]^{M-1} \mathrm{d}y \end{aligned} \tag{7.215}$$

Since all hypotheses are equiprobable, this is also the correct detection probability. The symbol error probability P_e is simply $1 - P_c$, and by using (7.206), we get

$$P_e = 1 - \frac{1}{\sqrt{2\pi}} \int_{-\infty}^{\infty} \mathrm{e}^{-y^2/2} \left[1 - Q\left(y + \frac{d_{min}}{\sqrt{2}\,\sigma}\right)\right]^{M-1} \mathrm{d}y \tag{7.216}$$

■

Example 7.16 Minimum Euclidean distance detector revisited

We are interested in the implementation of a minimum Euclidean distance detector using an M-ary maximum detector. Going back to (7.183) we note that given the sample value $\boldsymbol{x}$ of the decision vector $\boldsymbol{X}$, we have

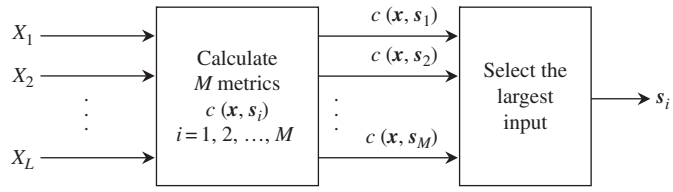

Figure 7.32 Alternative implementation of the minimum Euclidean distance detector.

$$\|\boldsymbol{x} - \boldsymbol{s}_i\|^2 = \|\boldsymbol{x}\|^2 + \|\boldsymbol{s}_i\|^2 - 2\boldsymbol{x}^t\boldsymbol{s}_i \tag{7.217}$$

Since $\|\boldsymbol{x}\|^2$ is common to all $\ln f_X(\boldsymbol{x}|H_i)$, the maximum of the set $\ln f_X(\boldsymbol{x}|H_i)$ corresponds to the maximum of the set

$$c(\boldsymbol{x}, \boldsymbol{s}_i) = 2\boldsymbol{x}^t\boldsymbol{s}_i - \|\boldsymbol{s}_i\|^2, \quad i = 1, 2, \ldots, M \tag{7.218}$$

The parameter $c(\boldsymbol{x}, \boldsymbol{s}_i)$ is often called the *correlation metric*. Thus, a minimum Euclidean distance detector actually computes the set of M metrics and selects the signal that corresponds to the largest metric. Figure 7.32 illustrates the alternative implementation of a minimum Euclidean distance detector.

■

Rice and Rayleigh decision variables

We are interested in generalizing the result in Section 7.6 for the binary maximum detector to the M-ary maximum detector. We now assume that the M-ary detector accepts M independent decision variables $X_1, X_2, \ldots, X_M$, with one being a Rice variable and the remaining $M - 1$ variables being Rayleigh variables. The M-dimensional vector $\boldsymbol{X} = [X_j]$ represents one of M possible hypotheses $H_1, H_2, \ldots, H_M$. We assume hypothesis H_i corresponds to the transmitted signal $\boldsymbol{s}_i$. Without loss of generality, we assume hypothesis H_1, that is, signal vector $\boldsymbol{s}_1$ was transmitted. The decision variable X_1 is then a Rice variable with the probability density function given by (7.58):

$$f_{X_1}(x_1) = \frac{x_1}{\sigma^2} e^{-\left(x_1^2 + a^2\right)/2\sigma^2} I_0\left(\frac{ax_1}{\sigma^2}\right), \quad x_1 \geq 0 \tag{7.219}$$

All other $M - 1$ decision variables X_k, $k = 2, 3, \ldots, M$, are Rayleigh variables with the probability density function given by (7.59):

$$f_{X_k}(x_k) = \frac{x_k}{\sigma^2} e^{-x_k^2/2\sigma^2}, \quad x_k \geq 0 \tag{7.220}$$

A correct detection occurs when every X_k is smaller than x_1, where x_1 is a sample value of X_1. Such event occurs with a conditional correct detection probability

$$\begin{aligned} P_{c|x_1} &= \Pr\{(X_2 < x_1) \cap (X_3 < x_1) \cap \cdots \cap (X_M < x_1) | H_1, x_1\} \\ &= [\Pr(X_2 < x_1 | H_1, x_1)]^{M-1} \end{aligned} \tag{7.221}$$

by virtue of independence between all X_k and the fact that they are identically distributed. By using (7.220) in (7.221) we obtain

$$\begin{aligned} P_{c|x_1} &= \left[\int_0^{x_1} f_{X_2}(x_2)\,\mathrm{d}x_2\right]^{M-1} \\ &= \left[\int_0^{x_1} \frac{x_2}{\sigma^2}\mathrm{e}^{-x_2^2/2\sigma^2}\,\mathrm{d}x_2\right]^{M-1} \\ &= \left[1-\mathrm{e}^{-x_1^2/2\sigma^2}\right]^{M-1} \end{aligned} \tag{7.222}$$

The condition on x_1 can be removed by averaging, with the help of (7.219),

$$\begin{aligned} P_c &= \int_0^{\infty} P_{c|x_1} f_{X_1}(x_1)\,\mathrm{d}x_1 \\ &= \int_0^{\infty} \left[1-\mathrm{e}^{-x_1^2/2\sigma^2}\right]^{M-1} \frac{x_1}{\sigma^2}\mathrm{e}^{-\left(x_1^2+a^2\right)/2\sigma^2} I_0\!\left(\frac{ax_1}{\sigma^2}\right)\mathrm{d}x_1 \\ &= \int_0^{\infty} \sum_{k=0}^{M-1} (-1)^k \binom{M-1}{k} \mathrm{e}^{-kx_1^2/2\sigma^2} \frac{x_1}{\sigma^2}\mathrm{e}^{-\left(x_1^2+a^2\right)/2\sigma^2} I_0\!\left(\frac{ax_1}{\sigma^2}\right)\mathrm{d}x_1 \end{aligned} \tag{7.223}$$

Using the identity

$$\int_0^{\infty} y\mathrm{e}^{-c^2y^2} I_0(y)\,\mathrm{d}y = \frac{1}{2c^2}\mathrm{e}^{1/4c^2} \tag{7.224}$$

in (7.223) we can obtain a closed-form expression for P_c:

$$P_c = \sum_{k=0}^{M-1} (-1)^k \binom{M-1}{k} \frac{1}{k+1}\mathrm{e}^{-\frac{k}{k+1}\left(\frac{a^2}{2\sigma^2}\right)} \tag{7.225}$$

Therefore, the probability of error is simply $P_e = 1 - P_c$, that is,

$$P_e = \sum_{k=1}^{M-1} (-1)^{k+1} \binom{M-1}{k} \frac{1}{k+1}\mathrm{e}^{-\frac{k}{k+1}\left(\frac{a^2}{2\sigma^2}\right)} \tag{7.226}$$

We would also like to find a union bound for P_e. Suppose $\boldsymbol{s}_1$ was transmitted, an error occurs when X_1 is smaller than all X_k, $k = 2, 3, \ldots, M$. Thus

$$\begin{aligned} P_{e|x_1} &= \Pr\{(X_2 > x_1) \cup (X_3 > x_1) \cup \cdots \cup (X_M > x_1) | H_1, x_1\} \\ &\le \sum_{j=2}^{M} \Pr\left(X_j > x_1 \middle| H_1, x_1\right) \end{aligned} \tag{7.227}$$

The conditional probability $\Pr\left(X_j > x_1 \middle| H_1, x_1\right)$ has been evaluated in (7.95). Furthermore, since all signals are equiprobable, the symbol error probability is simply the same for all signals $s_i(t)$. Thus, via (7.95) we get the union bound

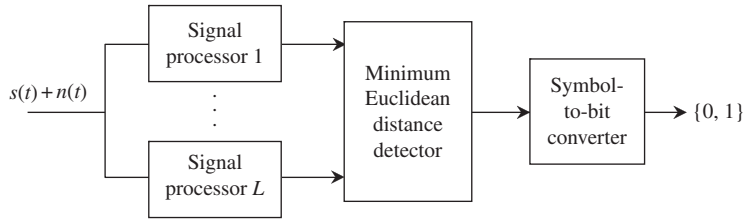

Figure 7.33 *L*-path demodulator. $L = 2$ for I-Q signals.

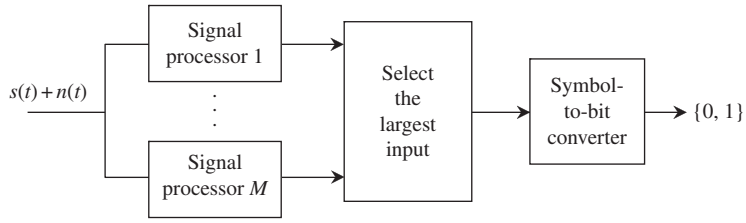

Figure 7.34 *M*-path demodulator.

$$P_e \leq \frac{1}{2}(M-1)\mathrm{e}^{-a^2/4\sigma^2} \tag{7.228}$$

which is the first term of the summation on the right-hand side of (7.226).

7.10 M-ary demodulation

M-ary modulation employs M distinct signal waveforms to represent M symbols. I-Q modulation such as MPSK or MQAM employs an L-path demodulator ($L = 2$) shown in Figure 7.33. On the other hand, orthogonal modulation such as MFSK or M-ary Walsh employs an M-path demodulator shown in Figure 7.34.

Both coherent and noncoherent demodulation can be performed by the M-path demodulator using the appropriate signal processors. The L-path demodulator is for coherent demodulation only. In the following discussion we provide the framework for the L-path demodulator followed by that of the M-path demodulator.

Coherent *L*-path demodulator: a signal space approach

I-Q modulated signals such as MPSK and MQAM are examples of linear modulation. In this case, a signal can be expressed as a linear combination of L orthonormal basis functions $x_k(t)$, $k = 1, 2, \ldots, L$, where $L \leq M$. For I-Q signals, $L = 2$, that is, only two orthonormal basis functions are necessary and sufficient. From (2.55), a signal $s_i(t)$, $i = 1, 2, \ldots, M$, that represents a symbol can be expressed as

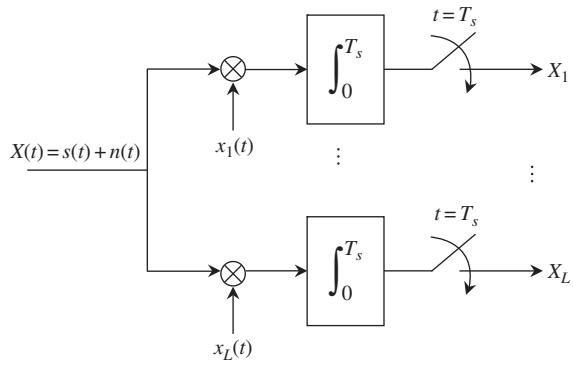

Figure 7.35 Signal processor for L-path demodulator. The received signal $s(t)$ represents one of the M signals $s_i(t)$, $i = 1, 2, \ldots, M$, and $n(t)$ is noise.

$$s_i(t) = \sum_{k=1}^{L} s_{ik} x_k(t), \qquad i = 1, 2, \ldots, M \tag{7.229}$$

where the coefficients of the series expansion s_{ik} are defined by

$$s_{ik} = \int_{-\infty}^{\infty} s_i(t) x_k(t)\, \mathrm{d}t, \qquad i = 1, 2, \ldots, M; \quad k = 1, 2, \ldots, L \tag{7.230}$$

The orthonormal basis functions $x_k(t)$, $k = 1, 2, \ldots, L$, can be obtained via the *Gram–Schmidt* procedure (the reader should not confuse $x_k(t)$ with $\boldsymbol{x} = [x_1\, x_2 \cdots\, x_L]^t$ used in (7.181)). The coefficients s_{ik}, $k = 1, 2, \ldots, L$, are the signal space coordinates of the symbol represented by $s_i(t)$. These L coordinates contain all the information about the symbol and can be used to recover the symbol in noise. Thus, (7.230) suggests the signal processor shown in Figure 7.35 for extracting s_{ik} from $s_i(t)$. We assume the signals s_i are time-limited to T_s seconds, where T_s is the symbol duration. The output decision variable of the sampler of the kth path is X_k, which is the sum of s_{ik} and the noise sample N_k.

The L-path signal processor thus consists of a bank of L correlators that digitize the transmitted signal $s_i(t)$ into an L-dimensional vector $\mathbf{s}_i = [s_{i1}\, s_{i2} \cdots\, s_{iL}]^t$. The input noise signal $n(t)$ is also digitized by the correlators into an L-dimensional vector $\boldsymbol{N} = [N_1\, N_2 \cdots\, N_L]^t$. The decision vector $\boldsymbol{X} = [X_1\, X_2 \cdots\, X_L]^t$ is therefore the sum of $\boldsymbol{s}_i$ and $\boldsymbol{N}$, that is,

$$\boldsymbol{X} = \boldsymbol{s}_i + \boldsymbol{N} \tag{7.231}$$

We are interested in the statistics of $\boldsymbol{N}$, and hence, the statistics of $\boldsymbol{X}$ given $\boldsymbol{s}_i$. As always, we assume that $n(t)$ is *wide-sense stationary* AWGN with zero mean and power spectral density $N_0/2$ (W/Hz). The noise autocorrelation function is $E\{n(t)n(\tau)\} = (N_0/2)\delta(t - \tau)$. The noise random variables N_k are given by

$$N_k = \int_0^{T_s} n(t) x_k(t)\, \mathrm{d}t, \qquad k = 1, 2, \ldots, L \tag{7.232}$$

It is evident that N_k is a zero mean Gaussian variable. The covariance of N_k is given by

$$\begin{aligned}\mathbf{E}\{N_k N_\ell\} &= \mathbf{E}\left\{\int_0^{T_s}\int_0^{T_s} n(t)n(\tau)x_k(t)x_\ell(\tau)\,\mathrm{d}t\,\mathrm{d}\tau\right\}\\ &= \int_0^{T_s}\int_0^{T_s} \mathbf{E}\{n(t)n(\tau)\}x_k(t)x_\ell(\tau)\,\mathrm{d}t\,\mathrm{d}\tau\\ &= \frac{N_0}{2}\int_0^{T_s} x_k(t)x_\ell(t)\,\mathrm{d}t\\ &= \frac{N_0}{2}\delta_{k\ell}\end{aligned} \tag{7.233}$$

where $\delta_{k\ell} = 0$, $k \neq \ell$, and $\delta_{k\ell} = 1$, $k = \ell$. It is quite obvious that the noise variables N_k are mutually uncorrelated. Since they are Gaussian, they are also statistically independent. Their variance is given by (7.233) by setting $k = \ell$, that is,

$$\sigma^2 = E\{N_k^2\} = \frac{N_0}{2} \tag{7.234}$$

Thus, the decision variables $X_k = s_{ik} + N_k$, $k = 1, 2, \ldots, L$, are also statistically independent Gaussian random variables with conditional mean s_{ik} and variance $\sigma^2 = N_0/2$. Figure 7.36 shows the complete block diagram of an L-path demodulator employing the minimum Euclidean distance detector. Figure 7.37 shows an alternative L-path demodulator employing the metric computer and maximum detector in Figure 7.32. Note that the received signal $X(t) = s_i(t) + n(t)$ is completely represented by the vector $\boldsymbol{X} = \boldsymbol{s}_i + \boldsymbol{N}$. In other words, the L components $X_k = s_{ik} + N_k$, $k = 1, 2, \ldots, L$, of the vector $\boldsymbol{X}$ are the only data based on $X(t)$ useful for detecting the symbol represented by the signal $s_i(t)$. They represent sufficient statistics that summarize $X(t)$ for the purposes of detection of $s_i(t)$. It can be shown that $e(t) = X(t) - \sum_k X_k x_k(t) = s_i(t) + n(t) - \sum_k s_{ik}x_k(t) - \sum_k N_k x_k(t) = n(t) - \sum_k N_k x_k(t)$ is uncorrelated to X_j, that is, $E\{e(t)X_j\} = 0, j = 1, 2, \ldots, N$. Furthermore, $e(t)$ and X_j are independent. Hence, $e(t)$ contains no relevant information concerning the detection of $s_i(t)$. This is expected since $e(t)$ depends only on the noise but not on the

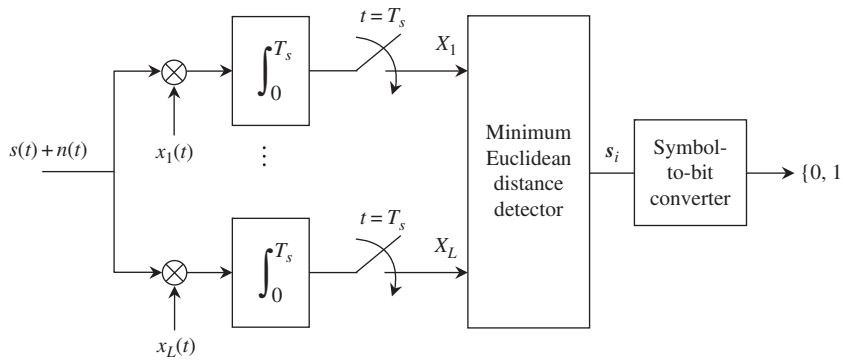

Figure 7.36 *L*-path demodulator employing the minimum Euclidean distance detector.

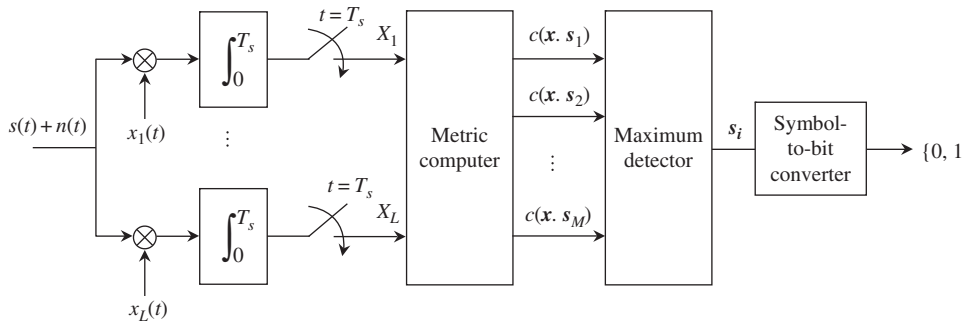

Figure 7.37 *L*-path demodulator employing the metric computer and maximum detector.

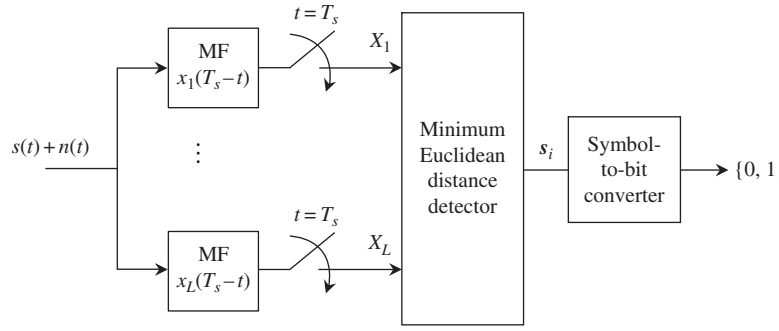

Figure 7.38 Matched filter implementation of the *L*-path demodulator with a minimum Euclidean distance detector.

signal. Sufficient statistics are important in digital communications because they allow the receiver to be practically built. They render a continuous-time signal $X(t)$ into a finite-dimensional vector $\boldsymbol{X}$ that is good enough for the detection of the transmitted signal.

The correlators in Figures 7.36 and 7.37 can also be replaced by the matched filters as indicated by Figures 7.38 and 7.39. The symbol error probability of the L-path demodulator is given by (7.205). Note that a symbol has $\log_2 M$ bits. Therefore, when M symbols are encoded with a Gray code, adjacent symbols differ by only one bit. Since adjacent symbols are closest in Euclidean distance, a symbol error due to noise results in the selection of one of the adjacent symbols for the true symbol. Thus a symbol error contains only one bit error. Gray code mapping thus results in the following approximate bit error probability:

$$P_b \approx \frac{P_e}{\log_2 M} = \frac{N_n}{\log_2 M} Q\left(\frac{d_{min}}{2\sigma}\right) \tag{7.235}$$

Coherent *M*-path demodulator

The coherent M-path demodulator is employed explicitly for orthogonal signals. A signal in an orthogonal signal set can be written in the form of (2.55) with $L = M$, that is,

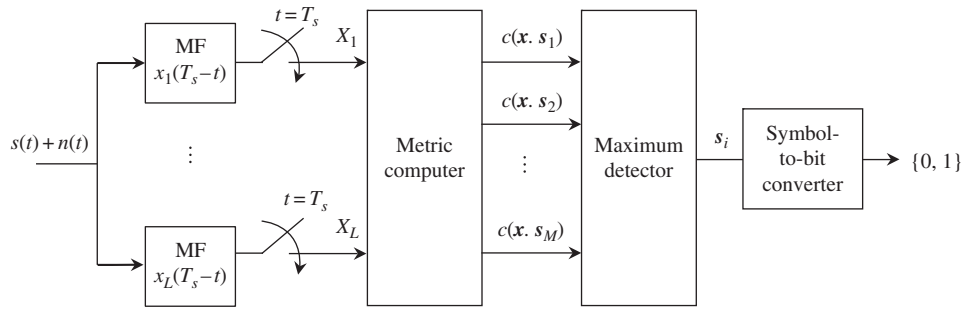

Figure 7.39 Matched filter implementation of the *L*-path demodulator with the metric computer and maximum detector.

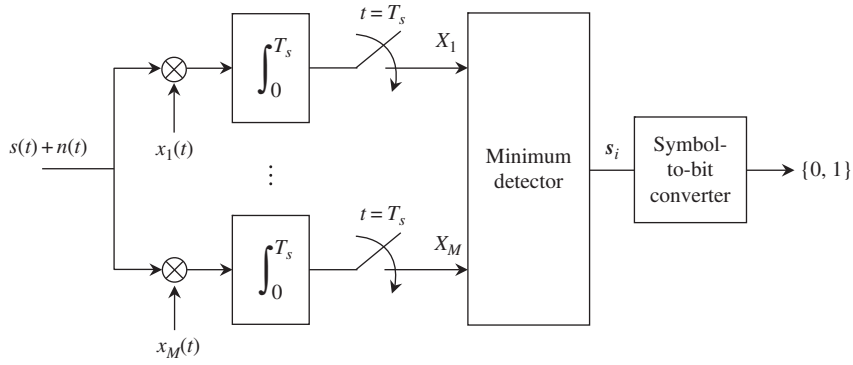

Figure 7.40 Coherent *M*-path demodulator.

$$\begin{aligned} s_i(t) &= \sum_{k=1}^{M} s_{ik} x_k(t) = s_{ii} x_i(t) \\ &= \sqrt{E_s}\, x_i(t), \qquad i = 1, 2, \ldots, M \end{aligned} \tag{7.236}$$

where E_s is the signal (symbol) energy. Since all $s_i(t)$ are mutually orthogonal, it is obvious that all $x_i(t)$ are mutually orthonormal. Equation (7.236) implies the following coherent demodulators shown in Figures 7.40 and 7.41.

Note that in the absence of noise, the output of the ith path sampler is $\sqrt{E_s}$ and the remaining outputs are all zero. Thus, the maximum detector just selects the signal vector $\boldsymbol{s}_i$. The symbol error probability of the M-path demodulator is given by the union bound (7.207) or by the exact expression in (7.216). To calculate the bit error probability, we note that when there is a symbol error, all $M - 1$ wrong symbols are equiprobable with probability $P_e/(M-1)$. Since each symbol has $k = \log_2 M$ bits, the probability distribution for i bit errors in a wrong symbol is $\binom{k}{i} P_e/(M-1)$. Thus, the average number of bit errors per wrong symbol is

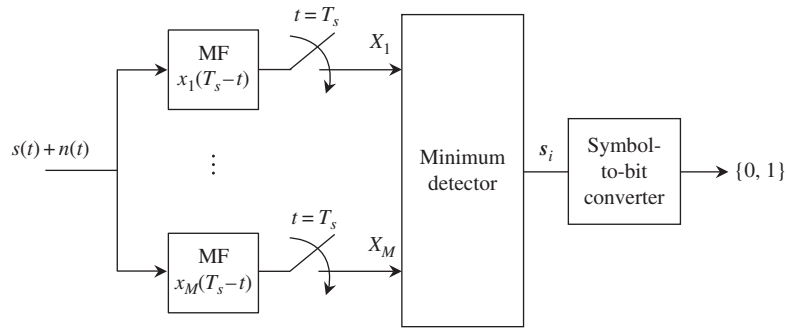

Figure 7.41 Matched filter implementation of the *M*-path demodulator.

$$\sum_{i=1}^{k} \binom{k}{i} \frac{P_e}{M-1} = k \frac{2^{k-1}}{M-1} P_e \tag{7.237}$$

There are k bits in a wrong symbol, thus the average bit error probability is simply the right-hand side of (7.237) divided by k:

$$P_b = \frac{M/2}{M-1} P_e \tag{7.238}$$

Substituting the union bound in (7.207) into (7.238) yields the *union bound* for P_b of the coherent M-path demodulator:

$$P_b \leq \frac{M}{2} Q\left(\frac{d_{min}}{2\sigma}\right) \tag{7.239}$$

The *exact bit error probability* is obtained via (7.216) and (7.238) as follows:

$$P_b = \frac{M/2}{M-1} \left[1 - \frac{1}{\sqrt{2\pi}} \int_{-\infty}^{\infty} \mathrm{e}^{-y^2/2} \left[1 - Q\left(y + \frac{d_{min}}{\sqrt{2}\,\sigma}\right)\right]^{M-1} \mathrm{d}y\right] \tag{7.240}$$

Noncoherent *M*-path demodulator

For noncoherent demodulation, the bank of M correlators in Figure 7.40 can be replaced by a bank of M quadrature correlators–square law detectors discussed in Section 7.4. Also, the bank of M matched filters in Figure 7.41 can be replaced by a bank of M matched filter–envelope detectors discussed in Section 7.3. Figures 7.42 and 7.43 show the two versions of the noncoherent M-path demodulator. We designate $x_i(t, \pi/2)$ as the unit energy quadrature version of $x_i(t)$, such that

$$\int_0^{T_s} x_i(t) x_i(t, \pi/2)\, \mathrm{d}t = 0, \qquad i = 1, 2, \ldots, M \tag{7.241}$$

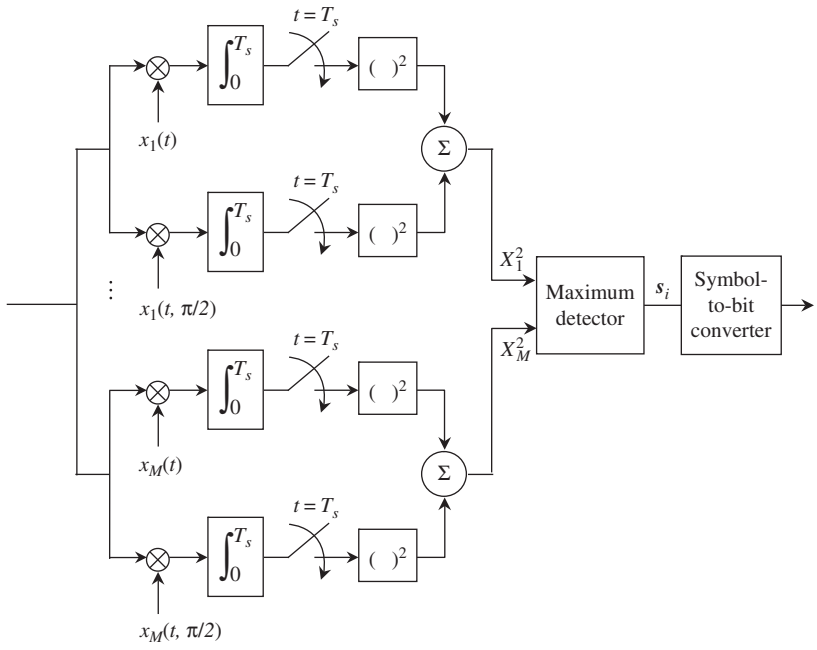

Figure 7.42 Noncoherent *M*-path demodulator employing the quadrature correlator–square law detector. The phase θ is the unknown carrier phase.

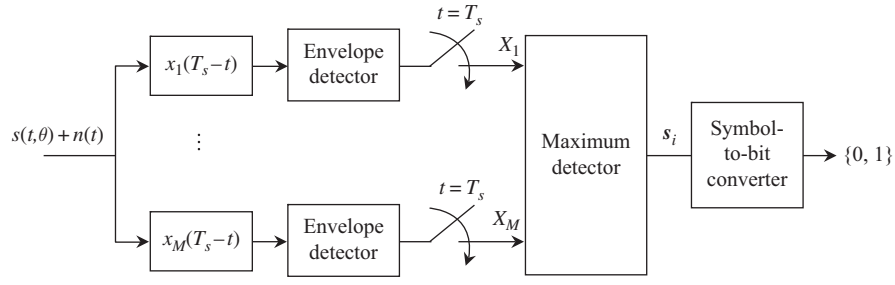

Figure 7.43 Noncoherent *M*-path demodulator employing the matched filter–envelope detector. The phase θ is the unknown carrier phase.

For example, if $x_1(t) = \sqrt{2/T_s}\cos 2\pi f_1 t$, then we have $x_1(t, \pi/2) = \sqrt{2/T_s}\sin 2\pi f_1 t$.

We also note that

$$\int_0^{T_s} x_i(t, \theta)x_i(t)\,\mathrm{d}t = \cos\theta \tag{7.242}$$

and

$$\int_0^{T_s} x_i(t, \theta)x_i(t, \pi/2)\,\mathrm{d}t = \sin\theta \tag{7.243}$$

where $x_i(t,\ \theta)$ is $x_i(t)$ with a phase shift of θ radians. From (7.236), it is seen that the output of the quadrature correlator–square law detector given that $s_i(t)$ was the transmitted signal is $X_i^2 = \left(\sqrt{E_s}\cos\theta + N_{I,i}\right)^2 + \left(\sqrt{E_s}\sin\theta + N_{Q,i}\right)^2$. The outputs of the remaining $M-1$ quadrature correlator–square law detectors are $X_j^2 = N_{I,j}^2 + N_{Q,j}^2$. The noise random variables $N_{I,i}$ and $N_{Q,i}$ are all independent Gaussian random variables with zero mean and variance $\sigma^2 = N_0/2$. From Section 7.4, we conclude that X_i^2 is a non-central chi-squared random variable and that X_j^2 is a central chi-squared random variable. On the other hand, the output of the ith matched filter–envelope detector X_i is a Rice random variable and X_j is a Rayleigh random variable as in Section 7.3. Both demodulators in Figures 7.42 and 7.43 yield identical symbol error probability as described in (7.226), where the parameters a^2 and σ^2 are given by $a^2 = E_s$ and $\sigma^2 = N_0/2$, that is,

$$P_e = \sum_{k=1}^{M-1} (-1)^{k+1} \binom{M-1}{k} \frac{1}{k+1} \mathrm{e}^{-\left(\frac{k}{k+1}\right)\left(\frac{E_s}{N_0}\right)} \tag{7.244}$$

The bit error probability is obtained via (7.238) as follows:

$$P_b = \frac{M/2}{M-1} \sum_{k=1}^{M-1} (-1)^{k+1} \binom{M-1}{k} \frac{1}{k+1} \mathrm{e}^{-\left(\frac{k}{k+1}\right)\left(\frac{E_b}{N_0}\right)\log_2 M} \tag{7.245}$$

As a comparison, the union bound for bit error probability can be evaluated via (7.228) and (7.238):

$$P_b \leq \frac{M}{4} \mathrm{e}^{-\left(\frac{E_b}{2N_0}\right)\log_2 M} \tag{7.246}$$

7.11 Coherent MASK

MASK is an M-ary modulation technique that requires only *one* orthonormal basis function. Therefore, a coherent one-path demodulator can be employed, that is, $L = 1$ in Figures 7.36–7.39. For simplicity purposes, we assume that the unit amplitude squared pulse shape is employed, hence, the *orthonormal* basis function $x_1(t)$ given in (6.80) becomes

$$x_1(t) = \sqrt{\frac{2}{T_s}} \cos 2\pi f_c t \tag{7.247}$$

with the aid of $E = A^2 T_s/2$, where E is the *smallest* signal (symbol) energy and T_s is the signal interval. Figure 7.44 shows the coherent demodulator for MASK.

The minimum Euclidean distance for MASK is $d_{min} = 2\sqrt{E}$; hence, according to (7.235), the approximate bit error probability is

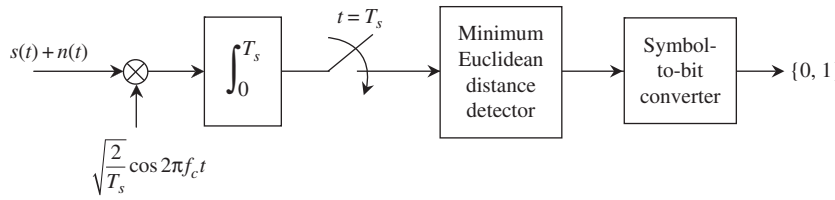

Figure 7.44 A coherent MASK demodulator.

$$P_b \approx \frac{N_n}{\log_2 M} Q\left(\sqrt{\frac{2E}{N_0}}\right) \tag{7.248}$$

To calculate the average number of nearest neighbors N_n, we observe from Figure 6.24 that the two outer symbols have one nearest neighbor. On the other hand, the inner symbols have two nearest neighbors. Thus,

$$\begin{aligned} N_n &= \frac{1}{M}[1 + 1 + 2(M-2)] \\ &= \frac{2(M-1)}{M} \end{aligned} \tag{7.249}$$

It is more relevant to express the bit error probability in terms of the *average* bit energy E_b than the *smallest* symbol energy E. Since $E_b = E_s/\log_2 M$, where E_s is the *average* symbol energy, we are interested in calculating E_s. From (6.82), we have

$$\begin{aligned} E_s &= \frac{1}{M}\sum_{n=1}^{M} E_n = \frac{1}{M}\sum_{n=1}^{M}[2n-(M+1)]^2 E \\ &= \frac{E}{M}\left[4\sum_{n=1}^{M} n^2 - 4(M+1)\sum_{n=1}^{M} n + M(M+1)^2\right] \\ &= \frac{E}{M}\left[\frac{2}{3}M(M+1)(2M+1) - 2M(M+1)^2 + M(M+1)^2\right] \\ &= \frac{1}{3}\left(M^2-1\right)E \end{aligned} \tag{7.250}$$

and hence

$$E_b = \frac{M^2-1}{3\ \log_2 M} E \tag{7.251}$$

Substituting (7.249) and (7.251) into (7.248), we obtain the approximate bit error probability

$$P_b \approx \frac{2(M-1)}{M\log_2 M} Q\left(\sqrt{\frac{6\log_2 M}{M^2-1}\left(\frac{E_b}{N_0}\right)}\right) \tag{7.252}$$

Example 7.17 Exact bit error probability of 4ASK

Consider the signal space of 4ASK shown in Figure 6.24(a) and repeated here for convenience.

Let H_1 be the hypothesis that signal $\boldsymbol{s}_1$ was transmitted. By symmetry, the conditional symbol error probabilities obey the relationships $P_{e|H_1} = P_{e|H_4}$ and $P_{e|H_2} = P_{e|H_3}$. Therefore, only $P_{e|H_1}$ and $P_{e|H_2}$ need to be evaluated. Let $\boldsymbol{X}$ be the received sample, which can be expressed as

$$\boldsymbol{X} = \boldsymbol{s}_1 + \boldsymbol{N} \tag{7.253}$$

where $\boldsymbol{N}$ is the AWGN sample with zero mean and variance $\sigma^2 = N_0/2$. We then have

$$\begin{aligned} P_{e|H_1} &= \Pr\{(\boldsymbol{X} \in R_2|H_1) \cup (\boldsymbol{X} \in R_3|H_1) \cup (\boldsymbol{X} \in R_4|H_1)\} \\ &= \Pr(\boldsymbol{X} \in R_2|H_1) + \Pr(\boldsymbol{X} \in R_3|H_1) + \Pr(\boldsymbol{X} \in R_4|H_1) \end{aligned} \tag{7.254}$$

using the fact that all regions R_i, $i = 1, 2, 3, 4$, do not overlap as indicated in Figure 7.45. We can establish the conditional bit error probability $P_{b|H_1}$ from $P_{e|H_1}$ by noting the following facts: when $\boldsymbol{X} \in R_2$, one bit error occurs since symbols 00 and 01 differ by only one bit; when $\boldsymbol{X} \in R_3$, two bit errors occur since symbols 00 and 11 differ by two bits; when $\boldsymbol{X} \in R_4$, only one bit error occurs since symbols 00 and 10 differ by one bit. Therefore, we obtain $P_{b|H_1}$ as follows:

$$P_{b|H_1} = \frac{1}{2}\Pr(\boldsymbol{X} \in R_2|H_1) + \Pr(\boldsymbol{X} \in R_3|H_1) + \frac{1}{2}\Pr(\boldsymbol{X} \in R_4|H_1) \tag{7.255}$$

Now let us evaluate the three terms on the right-hand side of (7.255):

$$\begin{aligned} \Pr(\boldsymbol{X} \in R_2|H_1) &= \Pr(-d_{min} < \boldsymbol{s}_1 + \boldsymbol{N} \le 0) = \Pr\left(-d_{min} < -\frac{3}{2}d_{min} + \boldsymbol{N} \le 0\right) \\ &= \Pr\left(\frac{1}{2}d_{min} < \boldsymbol{N} \le \frac{3}{2}d_{min}\right) = Q\left(\frac{d_{min}}{2\sigma}\right) - Q\left(\frac{3d_{min}}{2\sigma}\right) \end{aligned} \tag{7.256}$$

Similarly,

$$\begin{aligned} \Pr(\boldsymbol{X} \in R_3|H_1) &= \Pr(0 < \boldsymbol{s}_1 + \boldsymbol{N} \le d_{min}) = \Pr\left(0 < -\frac{3}{2}d_{min} + \boldsymbol{N} \le d_{min}\right) \\ &= \Pr\left(\frac{3}{2}d_{min} < \boldsymbol{N} \le \frac{5}{2}d_{min}\right) = Q\left(\frac{3d_{min}}{2\sigma}\right) - Q\left(\frac{5d_{min}}{2\sigma}\right) \end{aligned} \tag{7.257}$$

Finally,

$$\begin{aligned} \Pr(\boldsymbol{X} \in R_4|H_1) &= \Pr(\boldsymbol{s}_1 + \boldsymbol{N} > d_{min}) = \Pr\left(-\frac{3}{2}d_{min} + \boldsymbol{N} > d_{min}\right) \\ &= \Pr\left(\boldsymbol{N} > \frac{5}{2}d_{min}\right) = Q\left(\frac{5d_{min}}{2\sigma}\right) \end{aligned} \tag{7.258}$$

Substituting (7.256)–(7.258) into (7.255) yields the conditional bit error probability assuming hypothesis H_1:

$$P_{b|H_1} = \frac{1}{2}Q\left(\frac{d_{min}}{2\sigma}\right) + \frac{1}{2}Q\left(\frac{3d_{min}}{2\sigma}\right) - \frac{1}{2}Q\left(\frac{5d_{min}}{2\sigma}\right) \tag{7.259}$$

Next we evaluate the conditional symbol error probability $P_{e|H_2}$:

$$\begin{aligned} P_{e|H_2} &= \Pr\{(\boldsymbol{X} \in R_1|H_2) \cup (\boldsymbol{X} \in R_3|H_2) \cup (\boldsymbol{X} \in R_4|H_2)\} \\ &= \Pr(\boldsymbol{X} \in R_1|H_2) + \Pr(\boldsymbol{X} \in R_3|H_2) + \Pr(\boldsymbol{X} \in R_4|H_2) \end{aligned} \tag{7.260}$$

Following the argument that was used to evaluate $P_{b|H_1}$, we obtain the conditional bit error probability $P_{b|H_2}$ as follows:

$$P_{b|H_2} = \frac{1}{2}\Pr(\boldsymbol{X} \in R_1|H_2) + \frac{1}{2}\Pr(\boldsymbol{X} \in R_3|H_2) + \Pr(\boldsymbol{X} \in R_4|H_2) \tag{7.261}$$

The three terms on the right-hand side of (7.261) can be evaluated in the same fashion:

$$\begin{aligned} \Pr(\boldsymbol{X} \in R_1|H_2) &= \Pr(\boldsymbol{s}_2 + \boldsymbol{N} \le -d_{min}) = \Pr\left(-\frac{1}{2}d_{min} + \boldsymbol{N} \le -d_{min}\right) \\ &= \Pr\left(\boldsymbol{N} < -\frac{1}{2}d_{min}\right) = Q\left(\frac{d_{min}}{2\sigma}\right) \end{aligned} \tag{7.262}$$

Similarly,

$$\begin{aligned} \Pr(\boldsymbol{X} \in R_3|H_2) &= \Pr(0 < \boldsymbol{s}_2 + \boldsymbol{N} \le d_{min}) = \Pr\left(0 < -\frac{1}{2}d_{min} + \boldsymbol{N} \le d_{min}\right) \\ &= \Pr\left(\frac{1}{2}d_{min} < \boldsymbol{N} \le \frac{3}{2}d_{min}\right) = Q\left(\frac{d_{min}}{2\sigma}\right) - Q\left(\frac{3d_{min}}{2\sigma}\right) \end{aligned} \tag{7.263}$$

Also,

$$\begin{aligned} \Pr(\boldsymbol{X} \in R_4|H_2) &= \Pr(\boldsymbol{s}_2 + \boldsymbol{N} > d_{min}) = \Pr\left(-\frac{1}{2}d_{min} + \boldsymbol{N} > d_{min}\right) \\ &= \Pr\left(\boldsymbol{N} > \frac{3}{2}d_{min}\right) = Q\left(\frac{3d_{min}}{2\sigma}\right) \end{aligned} \tag{7.264}$$

By substituting (7.262)–(7.264) into (7.261), we obtain the conditional bit error probability given hypothesis H_2:

$$P_{b|H_2} = Q\left(\frac{d_{min}}{2\sigma}\right) + \frac{1}{2}Q\left(\frac{3d_{min}}{2\sigma}\right) \tag{7.265}$$

The average bit error probability P_b can be obtained via the *total probability theorem*, and the fact that $P_{e|H_1} = P_{e|H_4}$ and $P_{e|H_2} = P_{e|H_3}$:

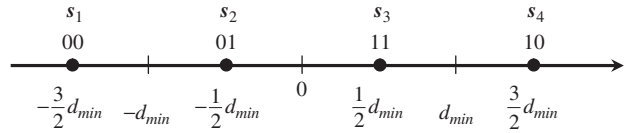

Figure 7.45 4ASK signal space with $d_{min} = 2\sqrt{E}$. There are four detection regions: $-\infty < R_1 \leq -d_{min}$; $-d_{min} < R_2 \leq 0$; $0 < R_3 \leq d_{min}$; and $d_{min} < R_4 \leq \infty$.

$$\begin{aligned} P_b &= \sum_{i=1}^{4} P_{b|H_i} \Pr(H_i) \\ &= \frac{3}{4} Q\left(\frac{d_{min}}{2\sigma}\right) + \frac{1}{2} Q\left(\frac{3d_{min}}{2\sigma}\right) - \frac{1}{4} Q\left(\frac{5d_{min}}{2\sigma}\right) \end{aligned} \tag{7.266}$$

Using the fact that $d_{min} = 2\sqrt{E} = 2\sqrt{E_b(3\log_2 M)/(M^2-1)}$ via (7.251) and $\sigma^2 = N_0/2$, we get the exact bit error probability of 4ASK as

$$P_b = \frac{3}{4} Q\left(\sqrt{\frac{4}{5}\left(\frac{E_b}{N_0}\right)}\right) + \frac{1}{2} Q\left(3\sqrt{\frac{4}{5}\left(\frac{E_b}{N_0}\right)}\right) - \frac{1}{4} Q\left(5\sqrt{\frac{4}{5}\left(\frac{E_b}{N_0}\right)}\right) \tag{7.267}$$

For a large bit energy-to-noise density ratio, that is, $E_b/N_0 \gg 1$, the second and third terms on the right-hand side of (7.267) are negligible compared to the first term, and P_b can be approximated by

$$P_b \approx \frac{3}{4} Q\left(\sqrt{\frac{4}{5}\left(\frac{E_b}{N_0}\right)}\right) \tag{7.268}$$

which is the same expression as (7.252) for $M = 4$.

■

7.12 Coherent MPSK

MPSK belongs to the class of I-Q modulation. As described in Sections 2.4 and 6.11, MPSK requires only two orthonormal basis functions. Thus, a coherent two-path demodulator can be employed for MPSK demodulation, that is, $L = 2$ in Figures 7.36–7.39. For simplicity, let us assume that a unit amplitude squared pulse shape is used, then, the two orthonormal basis functions $x_1(t)$ and $x_2(t)$ are given by (2.87) as

$$x_1(t) = \sqrt{\frac{2}{T_s}} \cos 2\pi f_c t \tag{7.269}$$

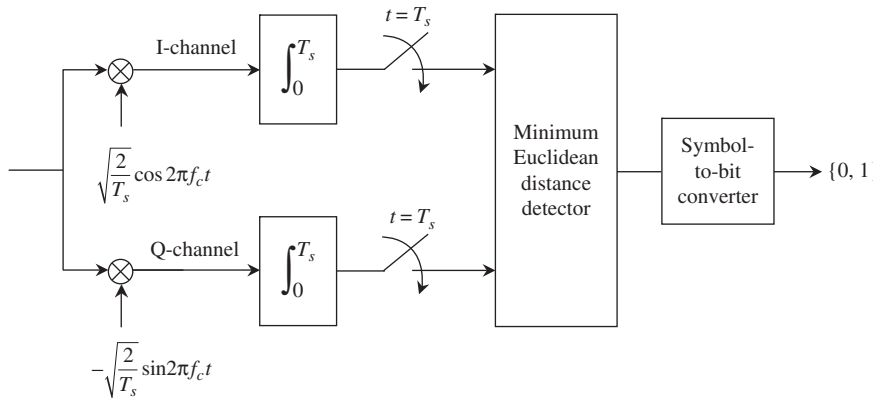

Figure 7.46 A coherent I-Q demodulator for MPSK.

$$x_2(t) = -\sqrt{\frac{2}{T_s}}\sin 2\pi f_c t \tag{7.270}$$

Figure 7.46 shows a coherent I-Q (two-path) demodulator for MPSK.

The minimum Euclidean distance for MPSK has been derived in (2.91) as $d_{min} = 2\sqrt{E_s}\sin(\pi/M)$. Substituting d_{min} into (7.235), we obtain the bit error probability of coherent MPSK with $M > 2$. Note that the average number of nearest neighbors for each signal point is $N_n = 2$ and the noise variance is $\sigma^2 = N_0/2$.

$$P_b \approx \frac{2}{\log_2 M} Q\left(\sqrt{\frac{2E_b}{N_0}\log_2 M}\,\sin\frac{\pi}{M}\right), \qquad M > 2 \tag{7.271}$$

Note that for PSK, that is, $M = 2$, we have $N_n = 1$, hence $P_b = Q(\sqrt{2E_b/N_0})$ as derived in (7.104).

Example 7.18 QPSK demodulator

QPSK is perhaps the most popular modulation of modern communications. It offers both power efficiency and bandwidth efficiency. For $M = 4$, the bit error probability of QPSK is given by (7.271) as

$$P_b \approx Q\left(\sqrt{\frac{2E_b}{N_0}}\right) \tag{7.272}$$

In (7.233), we showed that the I-noise and Q-noise are statistically independent. Therefore, in practice the I-bit X_1 and Q-bit X_2 at the sampler's output can be detected independently. In Example 7.13, we proved that the minimum Euclidean distance detector is equivalent to a threshold detector for a binary case such as PSK. Since QPSK is in effect the sum of two orthogonal PSK signals, we conclude that the I-bit X_1 can be detected by an I-threshold detector, and the Q-bit X_2 can be detected independently by a Q-threshold detector. The I-bit and Q-bit can then be multiplexed (parallel-to-serial conversion) into one output bit stream, as shown in Figure 7.47.

■

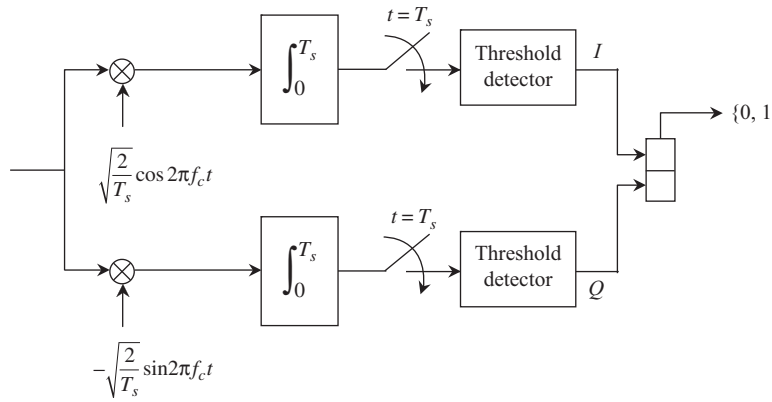

Figure 7.47 Coherent QPSK demodulator employing threshold detectors.

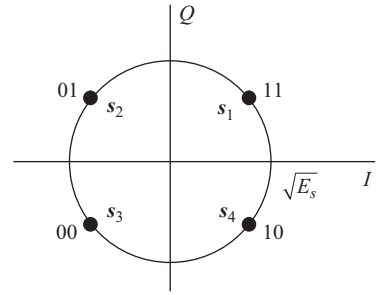

Figure 7.48 QPSK signal space with Gray encoding.

Example 7.19 Exact bit error probability of QPSK

We wish to show that the right-hand side of (7.272) is also the exact bit error probability of QPSK, not just an approximation. Let us consider the QPSK signal space in Figure 7.48. The symbols 11, 01, 00, and 10 are located in regions (quadrants) R_1, R_2, R_3, and R_4, respectively, and are represented by vectors $\boldsymbol{s}_1$, $\boldsymbol{s}_2$, $\boldsymbol{s}_3$, and $\boldsymbol{s}_4$, respectively. The conditional symbol error probability given hypothesis H_1 in which $\boldsymbol{s}_1$ was the transmitted vector is

$$P_{e|H_1} = \Pr\{(\boldsymbol{X} \in R_2|H_1) \cup (\boldsymbol{X} \in R_3|H_1) \cup (\boldsymbol{X} \in R_4|H_1)\} \tag{7.273}$$

Here, $\boldsymbol{X}$ is the received vector, that is, $\boldsymbol{X} = \boldsymbol{s}_1 + \boldsymbol{N}$, where $\boldsymbol{N}$ is the AWGN vector with statistically independent elements N_1 and N_2 and common variance $\sigma^2 = N_0/2$ via (7.233). The explanation for (7.273) is as follows: if $\boldsymbol{X} \in R_i$, $i = 2, 3, 4$, then $\boldsymbol{X}$ is closer to $\boldsymbol{s}_i$, $i = 2, 3, 4$, than $\boldsymbol{s}_1$, and hence an error would occur. Since R_2, R_3, R_4 do not overlap, we can express $P_{e|H_1}$ as

$$P_{e|H_1} = \Pr(\boldsymbol{X} \in R_2|H_1) + \Pr(\boldsymbol{X} \in R_3|H_1) + \Pr(\boldsymbol{X} \in R_4|H_1) \tag{7.274}$$

The conditional bit error probability can be established from the conditional symbol error probability $P_{e|H_1}$ by the following reasoning: as $\boldsymbol{X} \in R_2$, one bit error occurs since symbols 11 and 01 differ by only one bit; as $\boldsymbol{X} \in R_3$, two bit errors occur since the symbol 11 and 00 differ by two bits; as $\boldsymbol{X} \in R_4$, one bit error occurs since the symbol 11 and 10 differ by only one bit. Thus, with $\boldsymbol{X} \in R_2$ and $\boldsymbol{X} \in R_4$, a symbol of two bits was transmitted, but only one bit error occurs. On the other hand, if $\boldsymbol{X} \in R_3$, a symbol of two bits was transmitted, and both bits are in error. Therefore, the conditional bit error probability $P_{b|H_1}$ can be related to $P_{e|H_1}$ as

$$P_{b|H_1} = \frac{1}{2}\Pr(\boldsymbol{X} \in R_2|H_1) + \Pr(\boldsymbol{X} \in R_3|H_1) + \frac{1}{2}\Pr(\boldsymbol{X} \in R_4|H_1) \tag{7.275}$$

Let us express $\boldsymbol{X}$ in terms of its elements as follows:

$$\begin{aligned} \boldsymbol{X} &= \boldsymbol{s}_1 + \boldsymbol{N} \\ &= \begin{bmatrix} s_{11} + N_1 \\ s_{12} + N_2 \end{bmatrix} = \begin{bmatrix} \dfrac{d_{min}}{2} + N_1 \\ \dfrac{d_{min}}{2} + N_2 \end{bmatrix} \end{aligned} \tag{7.276}$$

where $s_{11} = s_{12} = d_{min}/2 = \sqrt{E_s/2}$ and $E_s = \|\boldsymbol{s}_i\|^2 = s_{i1}^2 + s_{i2}^2$, $i = 1, 2, 3, 4$, is the signal (symbol) energy. Using (7.276), we can calculate the three terms on the right-hand side of (7.275). Specifically, from Figure 7.47 we have

$$\begin{aligned} \Pr(\boldsymbol{X} \in R_2|H_1) &= \Pr\{(s_{11} + N_1 \le 0) \cap (s_{12} + N_2 > 0)\} \\ &= \Pr(s_{11} + N_1 \le 0)\Pr(s_{12} + N_2 > 0) \\ &= \Pr(N_1 \le -d_{min}/2)\Pr(N_2 > -d_{min}/2) \\ &= Q\left(\frac{d_{min}}{2\sigma}\right)\left[1 - Q\left(\frac{d_{min}}{2\sigma}\right)\right] \end{aligned} \tag{7.277}$$

By symmetry, we also have

$$\Pr(\boldsymbol{X} \in R_4|H_1) = Q\left(\frac{d_{min}}{2\sigma}\right)\left[1 - Q\left(\frac{d_{min}}{2\sigma}\right)\right] \tag{7.278}$$

It remains to evaluate $\Pr(\boldsymbol{X} \in \boldsymbol{R_3}|H_1)$. Again, using (7.276), we obtain

$$\begin{aligned} \Pr(\boldsymbol{X} \in R_3|H_1) &= \Pr\{(s_{11} + N_1 \le 0) \cap (s_{12} + N_2 \le 0)\} \\ &= \Pr(s_{11} + N_1 \le 0)\Pr(s_{12} + N_2 \le 0) \\ &= \Pr(N_1 \le -d_{min}/2)\Pr(N_2 \le -d_{min}/2) \\ &= Q^2\left(\frac{d_{min}}{2\sigma}\right) \end{aligned} \tag{7.279}$$

Substituting (7.277)–(7.279) into (7.275), we obtain the conditional bit error probability

$$\begin{aligned} P_{b|H_1} &= Q\left(\frac{d_{min}}{2\sigma}\right)\left[1 - Q\left(\frac{d_{min}}{2\sigma}\right)\right] + Q^2\left(\frac{d_{min}}{2\sigma}\right) \\ &= Q\left(\frac{d_{min}}{2\sigma}\right) \\ &= Q\left(\sqrt{\frac{E_s}{N_0}}\right) = Q\left(\sqrt{\frac{2E_b}{N_0}}\right) \end{aligned} \tag{7.280}$$

where $E_b = E_s/2$ is the bit energy and $\sigma^2 = N_0/2$. By symmetry and the fact that all symbols are equiprobable, we conclude that the bit error probability of QPSK is indeed the right-hand side of (7.272):

$$\begin{aligned} P_b &= \sum_{i=1}^{4} P_{b|H_1} \Pr(H_i) = \sum_{i=1}^{4} \frac{1}{4} Q\left(\sqrt{\frac{2E_b}{N_0}}\right) \\ &= Q\left(\sqrt{\frac{2E_b}{N_0}}\right) \end{aligned} \tag{7.281}$$

■

Example 7.20 Alternative coherent MPSK demodulator employing a phase detector

Since MPSK encodes the symbol in its phase, it is conceivable that a phase detector may be employed to detect the transmitted signal. From (6.97), we observe that the signal vector $\boldsymbol{s}_i$, $i = 1, 2, \ldots, M$, can be written as

$$\boldsymbol{s}_i = \begin{bmatrix} s_{i1} \\ s_{i2} \end{bmatrix} = \begin{bmatrix} \sqrt{E_s}\cos\theta_i \\ \sqrt{E_s}\sin\theta_i \end{bmatrix} \tag{7.282}$$

where $\theta_i = (2i-1)\pi/M$ is the encoding phase of a symbol. Note that $\theta_i = \tan^{-1}(s_{i2}/s_{i1})$, and $\|\boldsymbol{s}_i\|^2 = E_s$ for $i = 1, 2, \ldots, M$. From (7.218), the detection of a symbol is to select the largest correlation metric $c(\boldsymbol{x}, \boldsymbol{s}_i) = 2\boldsymbol{x}^t\boldsymbol{s}_i$ where $\|\boldsymbol{s}_i\|^2$ is ignored because it is the same for all signals $\boldsymbol{s}_i$, and $\boldsymbol{x}$ is the sampled value of $\boldsymbol{X} = \boldsymbol{s}_i + \boldsymbol{N}$. We have

$$\begin{aligned} c(\boldsymbol{x}, \boldsymbol{s}_i) &= 2[x_1 \;\; x_2]\begin{bmatrix} \sqrt{E_s}\cos\theta_i \\ \sqrt{E_s}\sin\theta_i \end{bmatrix} = 2\sqrt{E_s}(x_1\cos\theta_i + x_2\sin\theta_i) \\ &= 2\sqrt{E_s}\,R\cos(\theta_i - \theta) \end{aligned} \tag{7.283}$$

where

$$R = \sqrt{x_1^2 + x_2^2} \tag{7.284}$$

$$\theta = \tan^{-1}\left(\frac{x_2}{x_1}\right) \tag{7.285}$$

Note that in the absence of noise, we have $\theta = \tan^{-1}(s_{i2}/s_{i1}) = \theta_i$. Furthermore, R is independent of any transmitted signal $\boldsymbol{s}_i$. Therefore, in the alternative implementation of

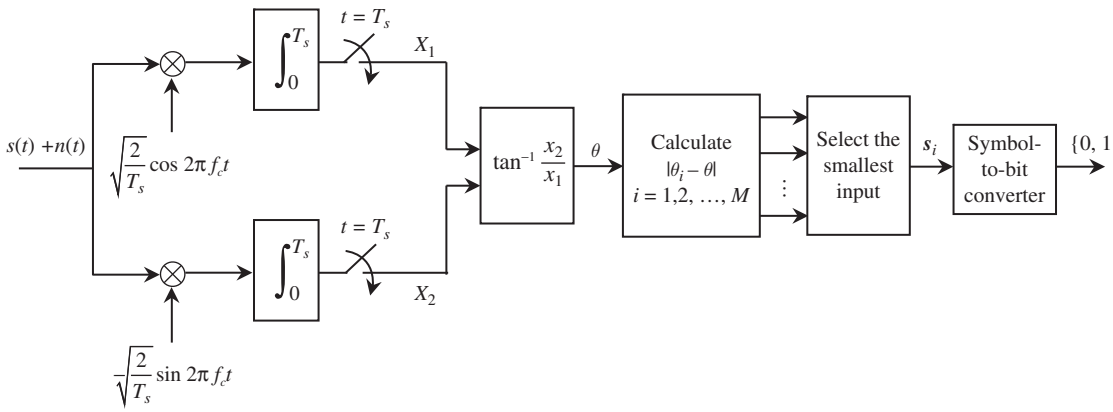

Figure 7.49 Coherent MPSK demodulator with a phase detector.

the minimum Euclidean distance detector (Figure 7.32), selecting the largest metric of M calculated metrics is equivalent to maximizing $\cos(\theta_i - \theta)$ in (7.283). For θ in the sector $\theta_i - \pi/M < \theta \leq \theta_i + \pi/M$ we always have $|\theta_i - \theta| < |\theta_j - \theta|$ for all $j \neq i$, and hence $\cos(\theta_i - \theta) > \cos(\theta_j - \theta)$, and consequently, $c(\boldsymbol{x}, \boldsymbol{s}_i) > c(\boldsymbol{x}, \boldsymbol{s}_j)$ for all $j \neq i$. Thus, for coherent MPSK, the two-path demodulator in Figure 7.46 can be alternatively implemented in Figure 7.49, which yields the same approximate bit error probability in (7.271).

■

Example 7.21 OQPSK demodulator

OQPSK is a variation of QPSK and has been described in Section 6.11. The configuration of the OQPSK modulator in Figure 6.29 suggests the coherent demodulator shown in Figure 7.50(a), which is basically the coherent two-path demodulator with a one-bit delay in the I-channel to compensate for the one-bit delay in the Q-channel of the modulator. Obviously, one could implement a coherent demodulator for OQPSK using the minimum Euclidean distance detector as shown in Figure 7.50(b). Both demodulators should give OQPSK an identical bit error probability to that of QPSK:

$$P_b = Q\left(\sqrt{\frac{2E_b}{N_0}}\right) \tag{7.286}$$

■

7.13 Coherent DMPSK

As mentioned in Section 6.12, differential encoding is used for two distinct purposes. First, differential encoding can resolve phase ambiguity in MPSK associated with the carrier

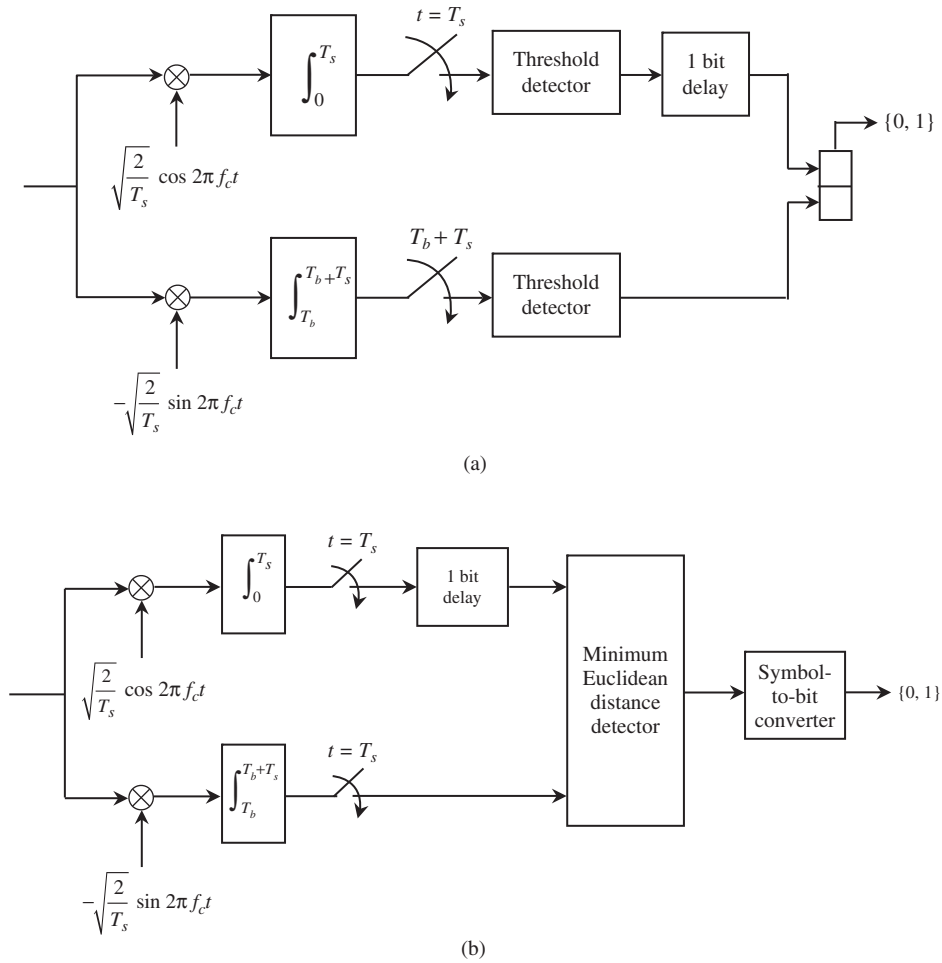

Figure 7.50 (a) Coherent OQPSK demodulator employing threshold detectors; (b) coherent OQPSK demodulator employing the minimum Euclidean distance detector.

recovery process. Second, differential encoding allows DMPSK to be demodulated noncoherently in applications where coherent demodulation is not feasible. In this section, we concentrate on the coherent demodulation of DMPSK with a differential decoding process to resolve phase ambiguity. The most important member of the DMPSK family is DQPSK, which we study first.

Example 7.22 Differential decoding for DQPSK

A coherent demodulator for DQPSK is illustrated in Figure 7.51. The differential decoder performs the inverse operation of the differential encoder, which is based on the following relations:

$$d_{I,i} = \overline{(c_{I,i} \oplus c_{Q,i})}(c_{Q,i} \oplus c_{Q,i-1}) \oplus (c_{I,i} \oplus c_{Q,i})(c_{I,i} \oplus c_{I,i-1}) \tag{7.287}$$

Table 7.7 Differential decoding for data in Example 6.28

i	$\theta_i + \pi/2$	$c_{I,i}$	$c_{Q,i}$	$d_{I,i}$	$d_{Q,i}$
0	$7\pi/4$	1	0	1	0
1	$5\pi/4$	0	0	0	1
2	$7\pi/4$	1	0	1	0
3	$7\pi/4$	1	0	0	0
4	$3\pi/4$	0	1	1	1

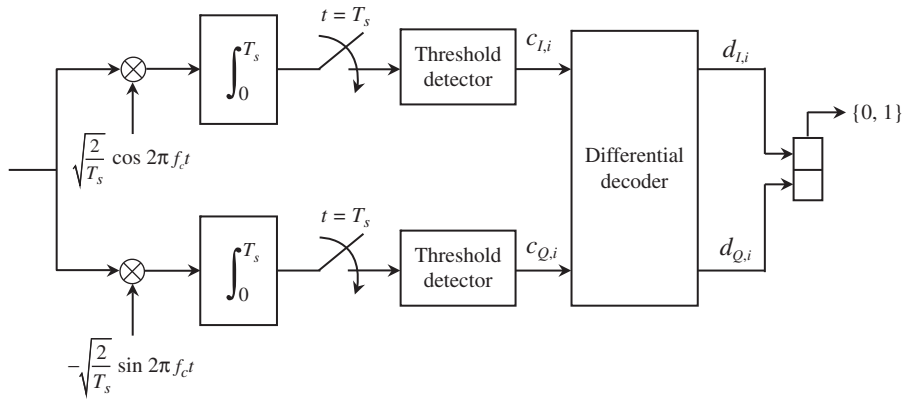

Figure 7.51 Coherent DQPSK demodulator.

$$d_{Q,i} = \overline{(c_{I,i} \oplus c_{Q,i})}(c_{I,i} \oplus c_{I,i-1}) \oplus (c_{I,i} \oplus c_{Q,i})(c_{Q,i} \oplus c_{Q,i-1}) \tag{7.288}$$

To illustrate the phase ambiguity resolution, we use the data in Example 6.28 and rotate the signal space by $\pi/2$ radians, that is, the phase θ_i of the received DQPSK signal is advanced by $\pi/2$ radians, to become $\theta_i + \pi/2$. Table 7.7 illustrates the differential decoding process to recover the correct transmitted data despite a phase error of $\pi/2$. The same result holds for a phase rotation of π, $3\pi/2$ or 2π radians.

■

Example 7.23 DQPSK with independent I–Q differential encoding/decoding

The I-channel and Q-channel of QPSK are independent PSK signals. Therefore, the I-bits and Q-bits can both be differentially encoded and decoded separately. This approach simplifies the differential encoder/decoder implementation. Figures 7.52 and 7.53 illustrate this concept.

■

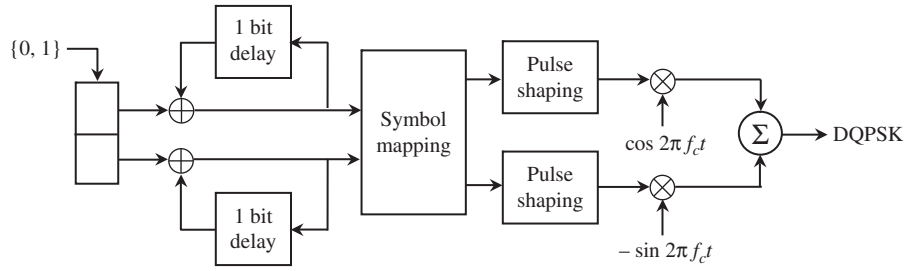

Figure 7.52 DQPSK modulator with separate I and Q differential encoders.

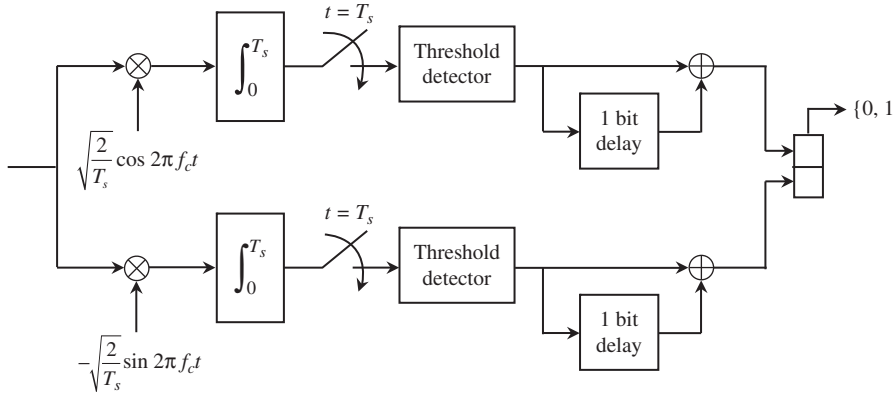

Figure 7.53 DQPSK demodulator with separate I and Q differential decoders.

The above two examples demonstrate the simplicity in implementing a coherent DQPSK demodulator. For higher-order DMPSK, differential decoding must be done via (6.109), which provides a recursive relation between the phases θ_{i-1} and θ_i of consecutive DMPSK symbols D_{i-1} and D_i, that is,

$$\theta_i = \theta_{i-1} + \Delta\theta_i \tag{7.289}$$

where

$$\Delta\theta_i = (D_i - 1)\frac{2\pi}{M}, \qquad D_i \in \{1, 2, \ldots, M\} \tag{7.290}$$

If $\Delta\theta_i$ can be recovered properly, then D_i would be detected, and hence the k-bit symbol represented by D_i, where $k = \log_2 M$. Figures 7.54 and 7.55 show two equivalent coherent DMPSK demodulators.

These coherent demodulators are simply coherent MPSK demodulators followed by differential decoders.

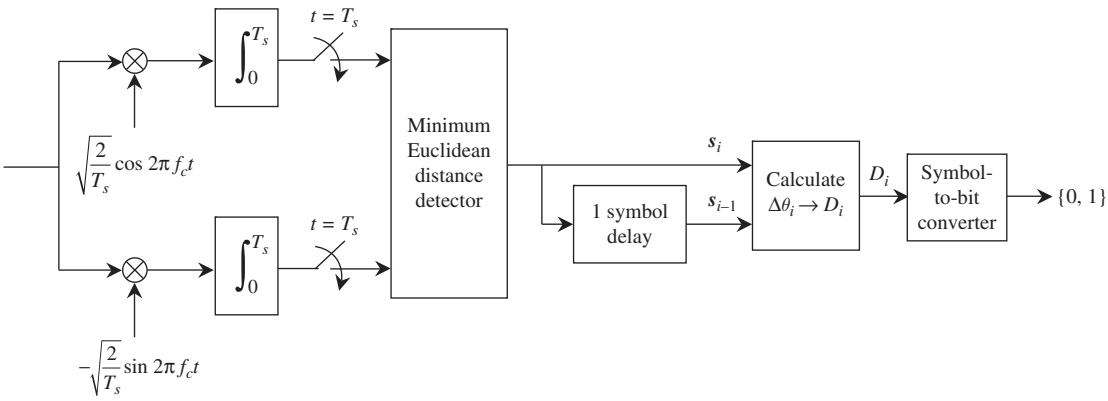

Figure 7.54 Coherent DMPSK demodulator. The phases of $\boldsymbol{s}_{i-1}$ and $\boldsymbol{s}_i$ are θ_{i-1} and θ_i, respectively, as indicated by the signal space (see (7.282)), and $\Delta\theta_i = \theta_i - \theta_{i-1}$.

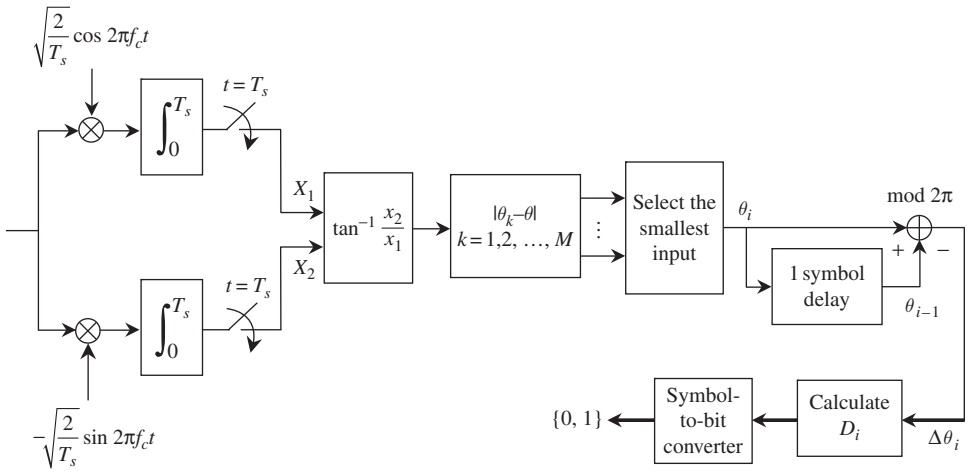

Figure 7.55 Alternative coherent DMPSK demodulator.

With the use of differential encoder/decoder, symbol errors tend to occur in pairs, as in the case of binary DPSK (see Table 7.3 in Example 7.7). Therefore, the bit error probability of coherent DMPSK is approximately twice that of coherent MPSK in (7.271):

$$P_b \approx \frac{4}{\log_2 M} Q\left(\sqrt{\frac{2E_b}{N_0}\log_2 M}\,\sin\frac{\pi}{M}\right) \tag{7.291}$$

7.14 Noncoherent DMPSK

DMPSK can be demodulated noncoherently based on the unique feature of differential encoding. As long as the carrier phase varies slowly and remains essentially invariant over

two consecutive symbol intervals, noncoherent demodulation is feasible and sometimes preferable in wireless communications over a fading channel. If this assumption holds, then any carrier phase θ unknown to the demodulator can be eliminated simply by establishing the phase difference between consecutive intervals. Let us add θ to the modulation phases θ_{i-1} and θ_i in (7.289):

$$\theta_i + \theta = \theta_{i-1} + \theta + \Delta\theta_i \tag{7.292}$$

Then the phase difference $\Delta\theta_i$ remains the same as in (7.290), that is,

$$\begin{aligned} \Delta\theta_i &= (\theta_i + \theta) - (\theta_{i-1} + \theta) = \theta_i - \theta_{i-1} \\ &= (D_i - 1)\frac{2\pi}{M}, \qquad D_i \in \{1, 2, \ldots, M\} \end{aligned} \tag{7.293}$$

Thus, the unknown carrier phase θ is eliminated and the data symbol can be recovered by deciding which one of the M equiangular decision regions $\Delta\theta_i$ belongs. This suggests the noncoherent demodulator illustrated in Figure 7.56. The detection regions are chosen in Figure 7.57 for the case of $M = 4$. These equiangular detection regions are defined by M phase angles $\phi_j = (j-1)2\pi/M, j = 1, 2, \ldots, M$. For example, if for a given $k \in \{1, 2, \ldots, M\}$, we have $|\Delta\theta_i - \phi_k| = \min_j |\Delta\theta_i - \phi_j|, j = 1, 2, \ldots, M$; then we choose $D_i = k$ as the output symbol. In general, we have M detection regions $R_j, j = 1, 2, \ldots, M$, where $\phi_j - \pi/M \le R_j < \phi_j + \pi/M$.

To evaluate the symbol error probability of the noncoherent DMPSK in Figure 7.56, let us assume that an unknown carrier phase θ is present as in (7.292). The received DMPSK signal for the ith symbol is

$$s(t) = Ap(t)\cos(2\pi f_c t + \theta_i + \theta) + n(t) \tag{7.294}$$

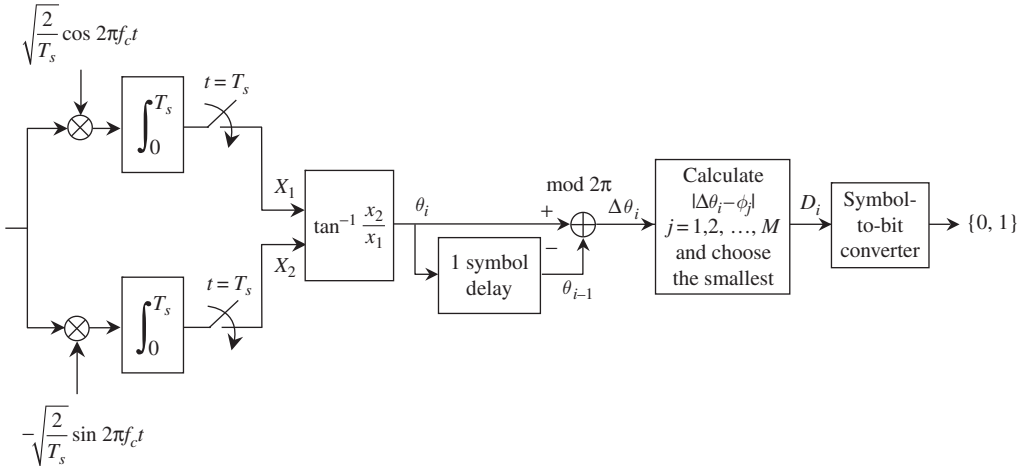

Figure 7.56 Noncoherent DMPSK demodulator, $\phi_j = (j-1)\,2\pi/M, j = 1, 2, \ldots, M$.

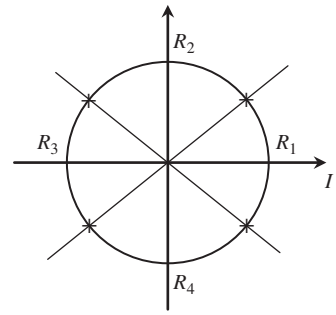

Figure 7.57 Four equiangular detection regions R_i, $i = 1, 2, 3, 4$, for $M = 4$; $-\pi/4 \leq R_1 < \pi/4$, $\pi/4 < R_2 \leq 3\pi/4$, $3\pi/4 < R_3 < 5\pi/4$, $5\pi/4 \leq R_4 < 7\pi/4$; $\phi_j = (j-1)\, 2\pi/M$, $j = 1, 2, \ldots, M$.

where $p(t)$ is assumed to be a unit-amplitude squared pulse of duration T_s, the symbol interval, and $n(t)$ is AWGN with power spectral density $N_0/2$ $(\mathrm{W/Hz})$. The decision vector $\boldsymbol{X}_i$ is given by

$$\boldsymbol{X}_i = \begin{bmatrix} X_{1,i} \\ X_{2,i} \end{bmatrix} = \begin{bmatrix} \sqrt{E_s}\cos(\theta_i + \theta) \\ \sqrt{E_s}\sin(\theta_i + \theta) \end{bmatrix} + \begin{bmatrix} N_{1,i} \\ N_{2,i} \end{bmatrix} \tag{7.295}$$

The noise samples $N_{1,i}$ and $N_{2,i}$ are independent Gaussian random variables with zero mean and variance $\sigma^2 = N_0/2$. The vector $\boldsymbol{X}_i$ can be written in phase notation as

$$\boldsymbol{X}_i = X_{1,i} + \mathrm{j}\, X_{2,i} = \|\boldsymbol{X}_i\| \mathrm{e}^{\mathrm{j}\rho_i} \tag{7.296}$$

Note that, without noise, the phase ρ_i of $\boldsymbol{X}_i$ is simply $\theta_i + \theta$. Similarly, the decision vector $\boldsymbol{X}_{i-1}$ for the previous $(i-1)$th symbol is

$$\boldsymbol{X}_{i-1} = \begin{bmatrix} X_{1,i-1} \\ X_{2,i-1} \end{bmatrix} = \begin{bmatrix} \sqrt{E_s}\cos(\theta_{i-1} + \theta) \\ \sqrt{E_s}\sin(\theta_{i-1} + \theta) \end{bmatrix} + \begin{bmatrix} N_{1,i} \\ N_{2,i} \end{bmatrix} \tag{7.297}$$

or, in phasor notation,

$$\boldsymbol{X}_{i-1} = X_{1,i-1} + \mathrm{j}\, X_{2,i-1} = \|\boldsymbol{X}_{i-1}\| \mathrm{e}^{\,\mathrm{j}\rho_{i-1}} \tag{7.298}$$

In the absence of noise, $\rho_{i-1} = \theta_{i-1} + \theta$. Define the phase difference $\beta = \rho_i - \rho_{i-1}$, which is equal to $\Delta\theta_i$ without noise. Since β is our decision variable, we are interested in its *probability distribution function* $F_\beta(\beta)$, which has been derived in [1]:

$$F_\beta(\beta) = -\frac{\sin\beta}{4\pi} \int_{-\pi/2}^{\pi/2} \frac{\mathrm{e}^{-(1-\cos\beta\cos x)E_s/N_0}}{1 - \cos\beta\cos x}\, \mathrm{d}x \tag{7.299}$$

From Figure 7.56, it is seen that a symbol is correctly detected if and only if $\beta - \phi_j$ falls into the angular detection region R_j given the differential phase $\Delta\theta_i = \phi_j$. Since the probability distribution function $F_\beta(\beta)$ is independent of ϕ_j, we can arbitrarily set $\phi_j = 0$ (which corresponds to $j = 1$ in $\phi_j = (j-1)2\pi/M$, $j = 1, 2, \ldots, M$) and hence the correct symbol detection probability is

$$P_c = \Pr\left\{-\frac{\pi}{M} \le \beta < \frac{\pi}{M}\right\} = \int_{-\pi/M}^{\pi/M} f_\beta(\beta)d\beta = F_\beta\left(\frac{\pi}{M}\right) - F_\beta\left(-\frac{\pi}{M}\right) \tag{7.300}$$

where $f_\beta(\beta)$ is the *probability density* of β. Therefore, the symbol error probability P_s is simply $1 - P_c$ and can be expressed as

$$\begin{aligned} P_s &= 1 - \int_{-\pi/M}^{\pi/M} f_\beta(\beta)\mathrm{d}\beta = \int_{-\pi}^{\pi} f_\beta(\beta)\mathrm{d}\beta - \int_{-\pi/M}^{\pi/M} f_\beta(\beta)\mathrm{d}\beta \\ &= 2\left[F_\beta(\pi) - F_\beta\left(\frac{\pi}{M}\right)\right] \end{aligned} \tag{7.301}$$

Substituting (7.299) into (7.301), we obtain

$$P_s = \frac{1}{2\pi}\left(\sin\frac{\pi}{M}\right)\int_{-\pi/2}^{\pi/2} \frac{\mathrm{e}^{-(1-\cos(\pi/M)\cos x)E_s/N_0}}{1-\cos(\pi/M)\cos x}\mathrm{d}x \tag{7.302}$$

For the case of $M = 2$, the above expression gives the bit error probability of noncoherent DPSK in (7.179). A simple approximation can be found in [1] for P_s in (7.302), as follows:

$$P_s \approx 2Q\left(\sqrt{\frac{2E_s}{N_0}}\sin\frac{\pi}{\sqrt{2}\,M}\right) \tag{7.303}$$

For Gray code bit-to-symbol mapping, the bit error probability for noncoherent DMPSK is given by

$$P_b \approx \frac{2}{\log_2 M}Q\left(\sqrt{\frac{2E_b}{N_0}\log_2 M}\,\sin\frac{\pi}{\sqrt{2}\,M}\right) \tag{7.304}$$

Compared with coherent MPSK in (7.271), noncoherent DMPSK requires approximately $\sin^2(\pi/M)/\sin^2\left(\pi/\sqrt{2}\,M\right)$ more in E_b/N_0 to achieve the same error rate. For large M, this is approximately $\sin^2(\pi/M)/\sin^2\left(\pi/\sqrt{2}\,M\right) \approx (\pi/M)^2/\left(\pi/\sqrt{2}\,M\right)^2 = 2$ or 3 dB.

Example 7.24 Noncoherent DPSK revisited

In this example, we wish to show that the noncoherent DPSK demodulator in Figure 7.28 and the one in Figure 7.56 for $M = 2$ are equivalent in performance. Let us start with the demodulator in Figure 7.56 that has two equiangular detection regions R_1 and R_2 as shown in Figure 7.58. The optimum detection selects the smallest of the two quantities $|\beta - \phi_1|$ and $|\beta - \phi_2|$, where $\beta = \rho_i - \rho_{i-1}$ with ρ_i and ρ_{i-1} defined in (7.296) and (7.298), respectively. This means that, given hypothesis H_1, that is, bit D_1 was transmitted with $\Delta\theta_i = \phi_1 = 0$, a correct detection implies $\beta \in R_1$ since $|\beta - 0| < |\beta - \pi|$. This is equivalent to $\cos\beta > 0$. On the other hand, given hypothesis H_2, that is, bit D_2 was transmitted with $\Delta\theta_i = \phi_2 = \pi$, a correct detection implies $\beta \in R_2$ since $|\beta - \pi| < |\beta - 0|$. This is equivalent to $\cos\beta < 0$. In summary,

$$\cos\beta > 0 \quad \Rightarrow \quad H_1 \quad \text{and} \quad \cos\beta \le 0 \Rightarrow \quad H_2 \tag{7.305}$$

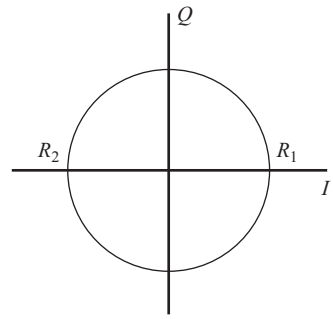

Figure 7.58 Two equiangular detection regions R_1 (right-half plane) and R_2 (left-half plane), with $\phi_1 = 0$ and $\phi_2 = \pi$ for $M = 2$.

Let us expand $\cos\beta = \cos(\rho_i - \rho_{i-1})$ into the following expression:

$$\cos\beta = \cos(\rho_i - \rho_{i-1}) = \cos\rho_i \cos\rho_{i-1} + \sin\rho_i \sin\rho_{i-1} \tag{7.306}$$

Using (7.296) and (7.298), we can scale $\cos\beta$ by a positive constant $\|\boldsymbol{X}_i\|\ \|\boldsymbol{X}_{i-1}\|$ without altering the decision rule in (7.306):

$$\begin{aligned}\|\boldsymbol{X}_i\|\,\|\boldsymbol{X}_{i-1}\|\cos\beta &= (\|\boldsymbol{X}_{i-1}\|\cos\rho_{i-1})(\|\boldsymbol{X}_i\|\cos\rho_i) + (\|\boldsymbol{X}_{i-1}\|\sin\rho_{i-1})(\|\boldsymbol{X}_i\|\sin\rho_i) \\ &= X_{1,i-1}X_{1,i} + X_{2,i-1}X_{2,i}\end{aligned} \tag{7.307}$$

where $X_{1,i}$, $X_{2,i}$ are given in (7.296) and $X_{1,i-1}$, $X_{2,i-1}$ are given in (7.298). Equation (7.307) is identical to (7.168); therefore, we conclude that the two demodulators in Figure 7.28 and 7.56 are equivalent.

■

7.15 Noncoherent π/4-DQPSK

There is virtually no difference in the demodulation of noncoherent π/4-DQPSK and DQPSK. Although π/4-DQPSK rotates its signal space by π/4 radians in successive symbols, it is the phase difference between the successive symbols that encodes the current symbol and not the absolute phase. Therefore, the noncoherent demodulator for DMPSK with $M = 4$ in Figure 7.56 applies for π/4-DQPSK with the four equiangular detection regions R_i, $i = 1, 2, 3, 4$, shown in Figure 7.59. The differential angle ϕ_j in Figure 7.56 is replaced by $\phi_j = (2j-1)\pi/4$, $j = 1, 2, 3, 4$.

The bit error probability of noncoherent π/4-DQPSK is identical to that of noncoherent DQPSK and is given by (7.304):

$$P_b \approx Q\left(\sqrt{1.11\frac{E_b}{N_0}}\right) \tag{7.308}$$

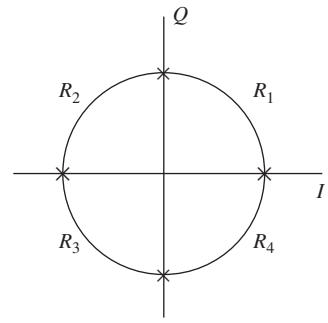

Figure 7.59 Detection regions for π/4-DQPSK: $0 \le R_1 \le \pi/2$, $\pi/2 \le R_2 < \pi$, $\pi \le R_3 \le 3\pi/2$, $3\pi/2 \le R_4 < 2\pi$; $\phi_j = (2j-1)\,\pi/4$, $j = 1, 2, 3, 4$.

In the following discussion, we present an alternative noncoherent demodulator that is equivalent to the one in Figure 7.56. Let hypothesis H_j represent symbol D_j, hence corresponding differential phase ϕ_j. The corresponding angular detection region for H_j is R_j. A correct detection given H_j occurs when the differential angle $\beta = \rho_i - \rho_{i-1}$ falls inside R_j. The detection rule can be expressed as follows:

$$\begin{aligned} &\cos\beta > 0 \quad \text{and} \quad \sin\beta > 0 \quad \Rightarrow \quad H_1 \\ &\cos\beta < 0 \quad \text{and} \quad \sin\beta > 0 \quad \Rightarrow \quad H_2 \\ &\cos\beta < 0 \quad \text{and} \quad \sin\beta < 0 \quad \Rightarrow \quad H_3 \\ &\cos\beta > 0 \quad \text{and} \quad \sin\beta < 0 \quad \Rightarrow \quad H_4 \end{aligned} \tag{7.309}$$

We note that $\cos\beta$ leads to the expression $X_1 = X_{1,i-1}X_{1,i} + X_{2,i-1}X_{2,i}$ as in (7.307). Similarly, $\sin\beta = \sin(\rho_i - \rho_{i-1}) = \sin\rho_i \cos\rho_{i-1} - \cos\rho_i \sin\rho_{i-1}$ leads to the expression $X_2 = X_{1,i-1}X_{2,i} - X_{2,i-1}X_{1,i}$. The detection rule in (7.309) can be expressed in terms of the decision variables X_1 and X_2 as

$$\begin{aligned} &X_1 > 0 \quad \text{and} \quad X_2 > 0 \quad \Rightarrow \quad H_1 \\ &X_1 < 0 \quad \text{and} \quad X_2 > 0 \quad \Rightarrow \quad H_2 \\ &X_1 < 0 \quad \text{and} \quad X_2 < 0 \quad \Rightarrow \quad H_3 \\ &X_1 > 0 \quad \text{and} \quad X_2 < 0 \quad \Rightarrow \quad H_4 \end{aligned} \tag{7.310}$$

The noncoherent demodulator that implements (7.310) is shown in Figure 7.60.

7.16 Coherent MQAM and DMQAM

MQAM belongs the class of I-Q modulation as MPSK, and hence it requires only two orthonormal basis functions to represent its signal as shown in (7.269) and (7.270). A coherent two-path demodulator for MQAM is illustrated in Figure 7.61.

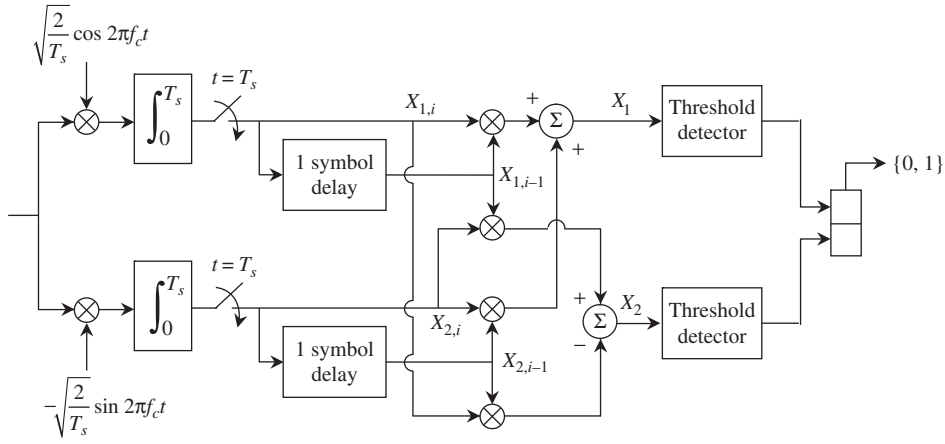

Figure 7.60 Alternative noncoherent π/4-DQPSK demodulator.

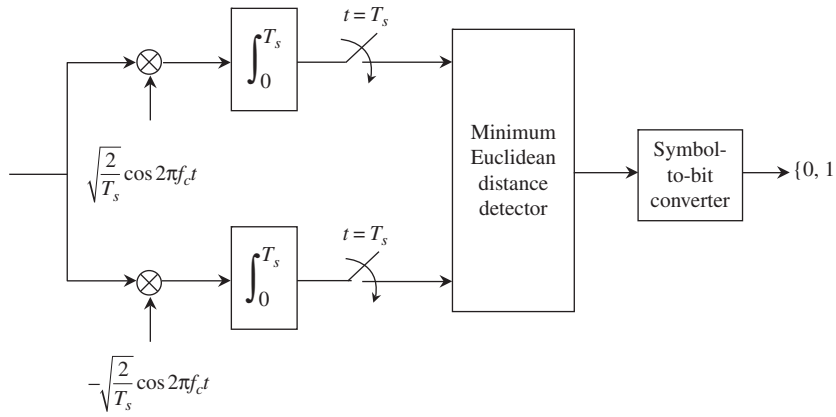

Figure 7.61 A coherent I-Q demodulator for MQAM.

Rectangular MQAM are commonly used in practice as in the WLAN Standards IEEE 802.11a, g with $M=16$ and $M=64$, and 802.16–16e with $M=16$, $M=64$, and $M=256$. In general, rectangular MQAM has $M = 2^k$, where k is an even positive integer. When k is odd, such as $M=32$ or $M=128$, the rectangular signal spaces can be modified to exclude the corner points as shown in Figure 6.35. The coordinates of signal vectors in rectangular MQAM are given by

$$[s_{ij}]_{M\times M} = \sqrt{\frac{E}{2}}\begin{bmatrix} (-\sqrt{M}+1,\ \sqrt{M}-1) & (-\sqrt{M}+3,\ \sqrt{M}-1) & \cdots & (\sqrt{M}-1,\ \sqrt{M}-1) \\ (-\sqrt{M}+1,\ \sqrt{M}-3) & (-\sqrt{M}+3,\ \sqrt{M}-3) & \cdots & (\sqrt{M}-1,\ \sqrt{M}-3) \\ \vdots & & \vdots & \\ (-\sqrt{M}+1,\ -\sqrt{M}+1) & (-\sqrt{M}+3,\ -\sqrt{M}+1) & \ldots & (\sqrt{M}-1,\ -\sqrt{M}+1) \end{bmatrix} \tag{7.311}$$

where E is the smallest symbol energy.

The average symbol energy for a rectangular MQAM can be shown to be

$$E_s = \frac{1}{M}\sum_{n=1}^{M} E_n = \frac{1}{3}(M-1)E \tag{7.312}$$

The average number of nearest neighbors can be calculated based upon the fact that there are four corner points, $4\left(\sqrt{M}-2\right)$ edge points, and $M - 4\left(\sqrt{M}-2\right) - 4 = M - 4\sqrt{M} + 4 = \left(\sqrt{M}-2\right)^2$ inner points. The corner point has two nearest neighbors, the edge point has three nearest neighbors, and the inner points have four nearest neighbors. Therefore, the average number of nearest neighbors is

$$\begin{aligned} N_n &= \frac{1}{M}\left[4\times 2 + 4\left(\sqrt{M}-2\right)\times 3 + \left(\sqrt{M}-2\right)^2 \times 4\right] \\ &= 4 - \frac{4}{\sqrt{M}} \end{aligned} \tag{7.313}$$

For example, $M = 16$ yields $N_n = 3$ and $M = 64$ yields $N_n = 3.5$. For very large M, N_n approaches 4.

The minimum Euclidean distance for rectangular MQAM is

$$d_{min} = \sqrt{2E} \tag{7.314}$$

Substituting E_s in (7.312) for E into (7.314), we get

$$d_{min} = \sqrt{\frac{6E_s}{M-1}} = \sqrt{\frac{6E_b \log_2 M}{M-1}} \tag{7.315}$$

Assuming that Gray code is employed for symbol-bit mapping, we can obtain the bit error probability for coherent MQAM using (7.235) and (7.313):

$$P_b \approx \frac{4\left(1-1/\sqrt{M}\right)}{\log_2 M} Q\left(\sqrt{\frac{3\ \log_2 M}{M-1}\left(\frac{E_b}{N_0}\right)}\right) \tag{7.316}$$

A glance at (7.271) and (7.316) shows that the two expressions are identical for $M = 4$. For $M > 4$, MQAM has a signal-to-noise ratio advantage equal to

$$g = \frac{3/(M-1)}{2\sin^2(\pi/M)} \tag{7.317}$$

This expression is shown numerically in Table 7.8.

To avoid phase ambiguity, DMQAM can be employed. With differential encoding, error propagation typically occurs and increases the bit error probability. The bit error probability of coherent DMQAM is given approximately as

Table 7.8 Signal-to-noise ratio advantage of MQAM over MPSK

M	g (dB)
8	1.65
16	4.20
32	7.02
64	9.95
128	12.92
256	15.92

$$P_b \approx \frac{8\left(1-1/\sqrt{M}\right)}{\log_2 M} Q\left(\sqrt{\frac{3\log_2 M}{M-1}\left(\frac{E_b}{N_0}\right)}\right) \tag{7.318}$$

This is twice the bit error probability of coherent MQAM, with a factor of 2 accounting for the error propagation of the differential encoding.

7.17 Coherent CSK and MFSK

CSK belongs to the family of orthogonal signaling, as does MFSK. The coherent M-path demodulator shown in Figure 7.40 therefore can be employed for coherent demodulation. The basis functions for CSK are

$$x_i(t) = \sqrt{\frac{2}{T_s}} w_i(t) \cos 2\pi f_c t, \qquad i = 1, 2, \ldots, M \tag{7.319}$$

where $w_i(t)$, $i = 1, 2, \ldots, M$, are the Walsh functions in (2.52). On the other hand, the basis functions for MFSK are

$$x_i(t) = \sqrt{\frac{2}{T_s}} \cos 2\pi f_i t, \qquad i = 1, 2, \ldots, M \tag{7.320}$$

$$f_i = f_c + (2i - M - 1)\frac{1}{2T_s} \tag{7.321}$$

Figures 7.62 and 7.63 show the coherent demodulators for CSK and MFSK, respectively. As usual, the basis functions must be obtained via carrier recovery.

The bit error probability of coherent CSK or MFSK can be evaluated via the exact expression in (7.240) or the union bound in (7.239). Specifically, the minimum Euclidean distance is given in (7.206) as $d_{min} = \sqrt{2E_s}$. Therefore, by substituting d_{min} into (7.239) and (7.240), and noting that $\sigma^2 = N_0/2$, we obtain the union bound

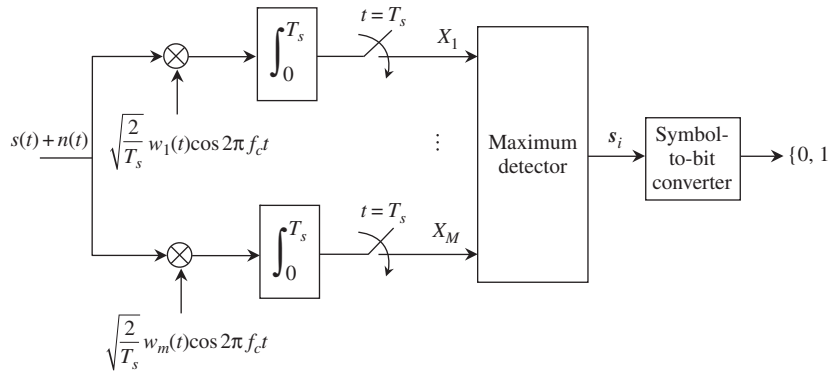

Figure 7.62 Coherent CSK demodulator.

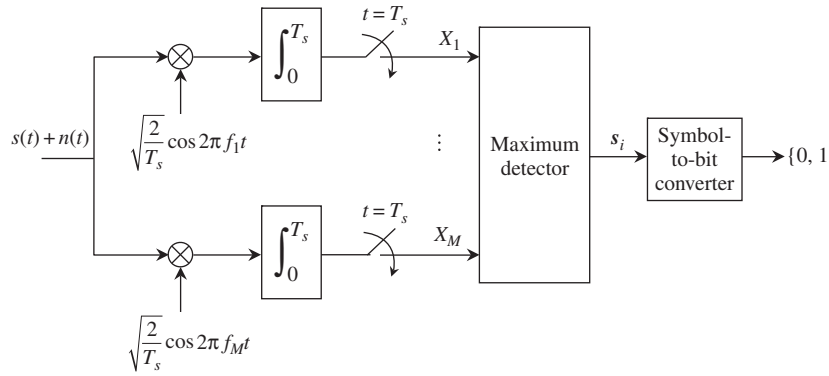

Figure 7.63 Coherent MFSK demodulator.

$$P_b \le \frac{M}{2} Q\left(\sqrt{\frac{E_s}{N_0}}\right) = \frac{M}{2} Q\left(\sqrt{\frac{E_b}{N_0}\log_2 M}\right) \tag{7.322}$$

and the exact expression

$$P_b = \frac{M/2}{M-1}\left[1 - \frac{1}{\sqrt{2\pi}}\int_{-\infty}^{\infty} \mathrm{e}^{-y^2/2}\left[1 - Q\left(y + \sqrt{\frac{2E_b}{N_0}\log_2 M}\right)\right]^{M-1} \mathrm{d}y\right] \tag{7.323}$$

For $P_b < 10^{-2}$, the union bound is very close to the exact expression.

7.18 Noncoherent CSK and MFSK

For noncoherent demodulation of CSK or MFSK, the noncoherent M-path demodulator in Figure 7.42 can be employed. As in the case of coherent demodulation, the basis functions and their corresponding quadrature counterparts for CSK are

$$x_i(t) = \sqrt{\frac{2}{T_s}} w_i(t) \cos 2\pi f_c t, \quad i = 1, 2, \ldots, M \tag{7.324}$$

$$x_i\left(t, \frac{\pi}{2}\right) = \sqrt{\frac{2}{T_s}} w_i(t) \sin 2\pi f_c t, \quad i = 1, 2, \ldots, M \tag{7.325}$$

For MFSK the basis functions and the corresponding quadrature functions are given by

$$x_i(t) = \sqrt{\frac{2}{T_s}} \cos 2\pi f_i t, \quad i = 1, 2, \ldots, M \tag{7.326}$$

$$x_i\left(t, \frac{\pi}{2}\right) = \sqrt{\frac{2}{T_s}} \sin 2\pi f_i t, \quad i = 1, 2, \ldots, M \tag{7.327}$$

$$f_i = f_c + (2i - M - 1)\frac{1}{2T_s} \tag{7.328}$$

Figures 7.64 and 7.65 show the noncoherent CSK and MFSK demodulators, respectively. The exact bit error probability and its union bound are given in (7.245) and (7.246), respectively, and are cited here again for convenience:

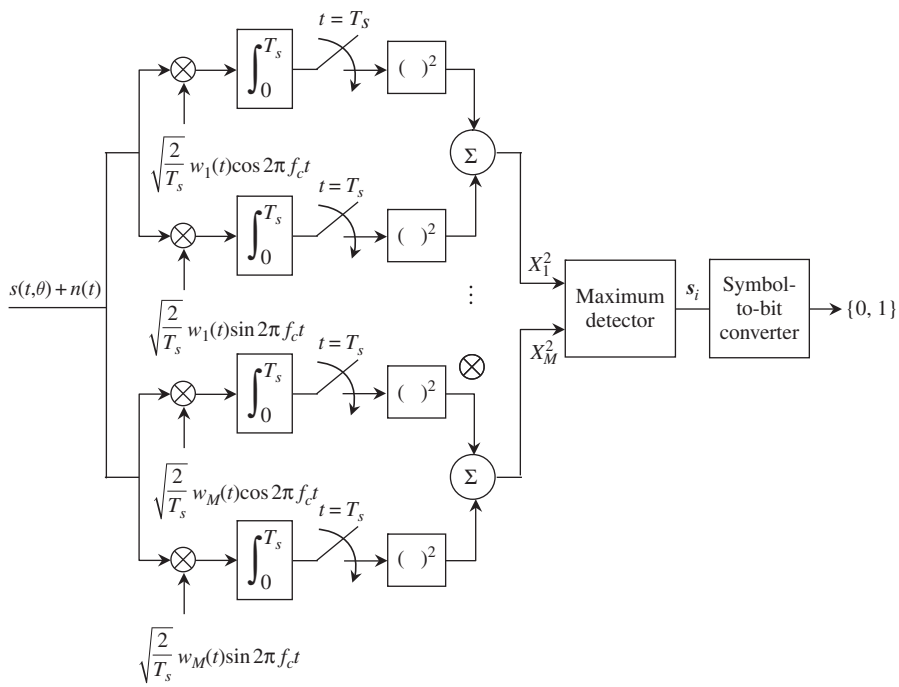

Figure 7.64 Noncoherent CSK demodulator.

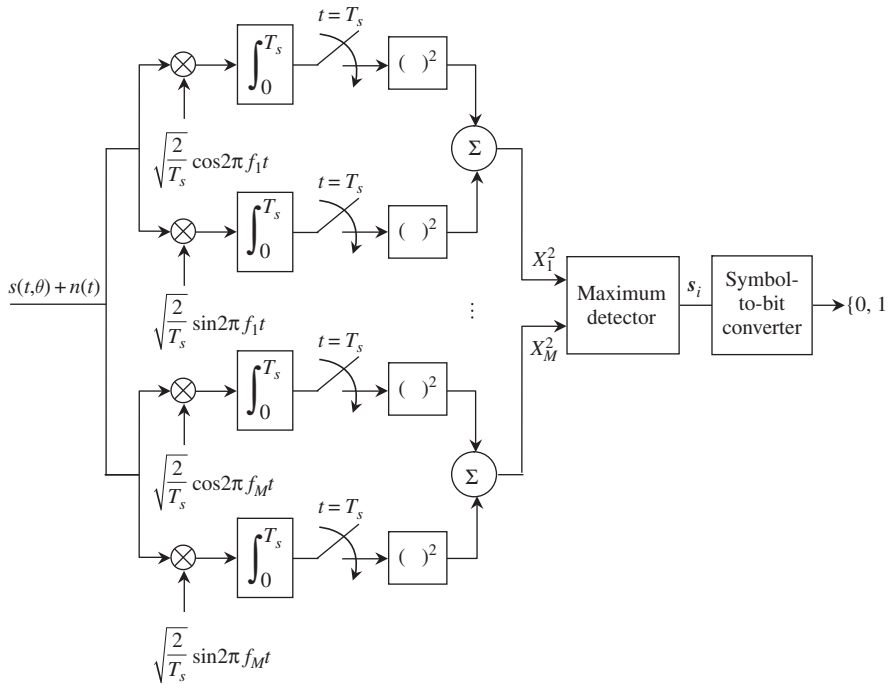

Figure 7.65 Noncoherent MFSK demodulator.

$$P_b = \frac{M/2}{M-1}\sum_{k=1}^{M-1}(-1)^{k+1}\binom{M-1}{k}\frac{1}{k+1}\mathrm{e}^{-\left(\frac{k}{k+1}\right)\left(\frac{E_b}{N_0}\right)\log_2 M} \tag{7.329}$$

$$P_b \leq \frac{M}{4}\mathrm{e}^{-\left(\frac{E_b}{2N_0}\right)\log_2 M} \tag{7.330}$$

For all practical purposes, the union bound approximates the exact expression well. For $P_b < 10^{-2}$ coherent demodulation enjoys an advantage of less than 1 dB in signal-to-noise ratio over noncoherent demodulation.

7.19 Coherent CPM with sequence detection

Coherent CPM includes both coherent MSK and precoded MSK, and CP-MFSK. The general waveform for CPM is given in (6.145) for the Nth data symbol D_N of the semi-infinite sequence $\boldsymbol{D}_N$:

$$s(t) = A\cos[2\pi f_c t + \phi(t, \boldsymbol{D}_N)] \tag{7.331}$$

where $\phi(t, \boldsymbol{D}_N)$ represents the phase of the carrier up to the end of the Nth symbol, that is, $NT_s \le t < (N+1)T_s$:

$$\phi(t, \boldsymbol{D}_N) = 2\pi h \sum_{i=-\infty}^{N} (2D_i - M - 1)\, q(t - iT_s), \quad NT_s \le t < (N+1)T_s \tag{7.332}$$

The digital modulation index h is assumed to be fixed for all symbols in our analysis and $D_i \in \{1, 2, \ldots, M\}$ is the ith symbol in the symbol stream. The pulse $q(t)$ is defined in (6.147) as the integral of the symbol pulse shape $p(t)$, which we assume to have duration L symbols. Thus, symbols with the indexes $i = N - L + 1, N - L + 2, \ldots, N$ influence the phase $\phi(t, \boldsymbol{D}_N)$ via its pulse shape, while symbols with indexes $i = -\infty, \ldots, N - L$ produce the phase accumulation in the past. Thus, we can represent $\phi(t, \boldsymbol{D}_N)$ as follows:

$$\begin{aligned} \phi(t, \boldsymbol{D}_N) &= \pi h \sum_{i=-\infty}^{N-L} (2D_i - M - 1) + 2\pi h \sum_{i=N-L+1}^{N} (2D_i - M - 1)\, q(t - iT_s) \\ &= \varphi_N + \varphi(t, \boldsymbol{D}_N), \quad NT_s \le t \le (N+1)T_s \end{aligned} \tag{7.333}$$

where φ_N represents the phase accumulation up to time $(N - L + 1)T_s$ and $\varphi(t, \boldsymbol{D}_N)$ represents the phase contribution between the time $(N - L + 1)T_s$ and $(N + 1)T_s$. To arrive at (7.333), we also assume that $q(t) = 0$ for $t < 0$ (causality) and $q(t) = 1/2$ for $t \ge LT_s$. This holds true for the symbol pulse shapes $p(t)$ in Table 6.11. When the digital modulation index h is rational, that is, $h = a/b$, where a and b are relative prime positive integers, then at $t = NT_s$ there are b terminal phase states when $L = 1$ for even a, and $2b$ terminal phase states for odd a. These terminal phase states are $\{0, \pi a/b, 2\pi a/b, \ldots, (b-1)\pi a/b\}$ and $\{0, \pi a/b, \ldots, (2b-1)\pi a/b\}$, respectively. For $L > 1$, the number of terminal states is bM^{L-1} for even a and $2bM^{L-1}$ for odd a.

Example 7.25 Phase states

Consider MSK, which is CP-FSK with $h = 1/2$ and rectangular symbol pulse shape with $L = 1$ (full response). The terminal phase states at $t = NT_s$ are $\{0, \pi/2, \pi, 3\pi/2\}$.

■

The above observations allow us to conclude that the phase function of CPM is a finite-state machine and can be represented by a state diagram or a state trellis. The state trellis is preferable because it allows us to view the state transitions in time. From (7.333) we can represent a state at time $t = NT_s$ as

$$\boldsymbol{S}_N = \begin{cases} \varphi_N, & L = 1 \\ \{\varphi_N, D_{N-1}, D_{N-2}, \ldots, D_{N-L+1}\}, & L > 1 \end{cases} \tag{7.334}$$

and a state at time $t = (N + 1)T_s$ can be updated from $\boldsymbol{S}_N$ as follows:

$$\boldsymbol{S}_{N+1} = \begin{cases} \varphi_{N+1}, & L = 1 \\ \{\varphi_{N+1}, D_N, D_{N-1}, \ldots, D_{N-L+2}\}, & L > 1 \end{cases} \tag{7.335}$$

where

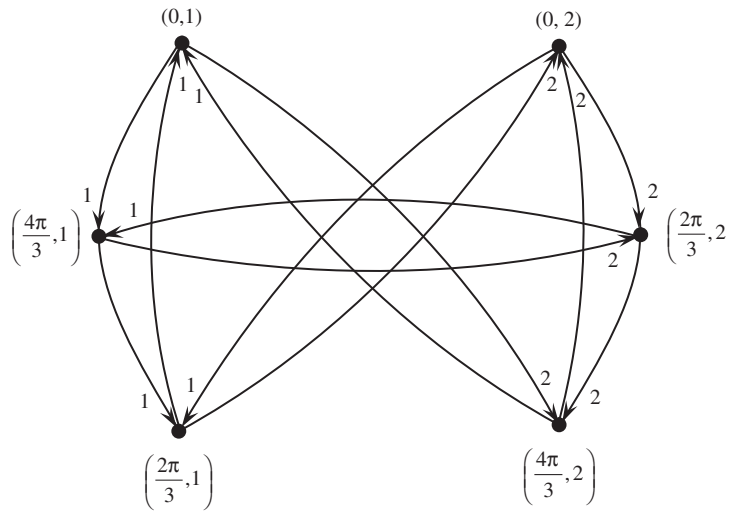

Figure 7.66 State diagram for CP-FSK with $h = 2/3$ and $L = 2$.

$$\varphi_{N+1} = \varphi_N + \pi h(2D_{N-L+1} - M - 1) \tag{7.336}$$

Example 7.26 Trellis for CP-FSK with $h = 2/3$ and $L = 2$

We consider the case of the rectangular symbol pulse shape only and note that the total number of states is $(3)(2)^{2-1} = 6$. Note that the three terminal phase states are $\{0, 2\pi/3, 4\pi/3\}$, and with $L = 2$ these three terminal phase states combine with two symbols in the set $D_i \in \{1, 2\}$ to form a total of six states $\{\varphi_N, D_{N-1}\}$, which are (0,1), (0,2), (2π/3, 1), (2π/3, 2), (4π/3, 1), and (4π/3, 2). Now, if the system is in terminal phase state $\varphi_N = 2\pi/3 \pmod{2\pi}$ and $D_{N-1} = 2$, then the next terminal phase state (mod 2π) for the next input symbol 2 is

$$\begin{aligned}\varphi_{N+1} &= \varphi_N + \pi h(2D_{N-1} - 2 - 1)\\ &= \frac{2\pi}{3} + \frac{2\pi}{3}(4 - 3) = \frac{4\pi}{3}\end{aligned} \tag{7.337}$$

and $D_N = 2$. The state diagram in Figure 7.66 shows the transition from state (φ_N, D_{N-1}) to state (φ_{N+1}, D_N). The trellis in Figure 7.67 shows the transition of state (φ_N, D_{N-1}) to state (φ_{N+6}, D_{N+5}) over six symbol periods. For example, the path (0,1), (4π/3,1), (2π/3,2), (4π/3, 2) through the trellis represents the detected symbol stream 1,1,2,2. On the other hand, the path (2π/3,1), (0,2), (2π/3,1), (0,1) represents the detected symbol stream 1,2,1,1.

■

The above example shows that the trellis can be used to detect a sequence of CPM symbols. The algorithm that performs sequence detection via a trellis is known as the *Viterbi algorithm*. To implement the Viterbi algorithm, one needs to evaluate the path metric at each

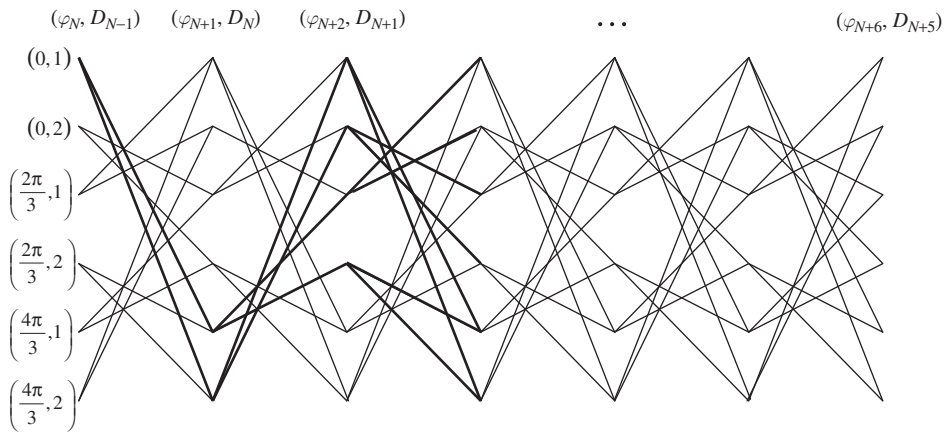

Figure 7.67 Trellis for CP-FSK with $h = 2/3$ and $L = 2$ for six symbol intervals. The starting state can be any one of the six states. The bold lines are the trellis for starting state (0,1), which reaches steady-state after three symbol periods.

node. For coherent demodulation, the most logical choice of metric is the correlation metric similar to (7.218) for symbol-by-symbol detection. Let us define the correlation metric for a received CPM signal plus noise $x(t)$ given the semi-infinite symbol sequence $\boldsymbol{D}_N$:

$$\begin{aligned} C_N &= \int_{-\infty}^{(N+1)T_s} x(t)\ \cos[2\pi f_c t + \phi(t, \boldsymbol{D}_N)]\mathrm{d}t \\ &= \int_{-\infty}^{(N+1)T_s} x(t)\ \cos 2\pi f_c t \cos\phi(t, \boldsymbol{D}_N)\,\mathrm{d}t - \int_{-\infty}^{(N+1)T_s} x(t)\ \sin 2\pi f_c t \sin\phi(t, \boldsymbol{D}_N)\,\mathrm{d}t \end{aligned} \tag{7.338}$$

Note that there are M^L distinct sequences of symbols $(D_N, D_{N-1}, \ldots, D_{N-L+1})$ and b or $2b$ possible terminal phase states φ_N. Therefore, there are bM^L or $2bM^L$ metrics in any symbol interval. The metric C_N can be expressed recursively as

$$\begin{aligned} C_N &= C_{N-1} + \int_{NT_s}^{(N+1)T_s} x(t)\ \cos[2\pi f_c t + \phi(t, \boldsymbol{D}_N)]\mathrm{d}t \\ &= C_{N-1} + \int_{NT_s}^{(N+1)T_s} x(t)\ \cos 2\pi f_c t \cos\phi(t, \boldsymbol{D}_N)\mathrm{d}t - \int_{NT_s}^{(N+1)T_s} x(t)\ \sin 2\pi f_c t \sin\phi(t, \boldsymbol{D}_N)\mathrm{d}t \\ &= C_{N-1} + \Delta_N \end{aligned} \tag{7.339}$$

We term C_N the path metric and Δ_N the branch metric. At each node in the trellis, a surviving path with the largest metric is retained. There are bM^{L-1} or $2bM^{L-1}$ surviving paths, one for each node. The path metrics are then updated by bM^L or $2bM^L$ branch metrics and new surviving paths are again retained for the next node. Thus, each surviving path has its metric updated by M new branch metrics. The coherent CPM demodulator is illustrated in Figure 7.68 based on (7.333) and (7.339).

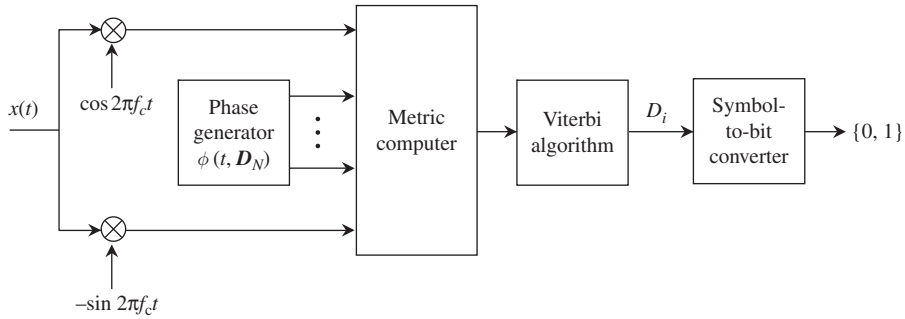

Figure 7.68 Coherent CPM demodulator.

Obviously, the initial signal phase must be known for coherent demodulation. In the following discussion we study the performance of the Viterbi algorithm which implements sequence detection. Therefore, we first establish the sequence error probability. If the observed sequence has a length of N symbols assuming the initial time is $t = 0$, then there are M^N different sequences. The Viterbi algorithm chooses the path of N symbols that is closest in Euclidean distance to the received sequence. Hence, the sequence error probability is upper bounded by the union bound

$$P_{se} \leq \sum_{i \neq j} Q\left(\frac{d_{ij}}{2\sigma}\right) \tag{7.340}$$

where $\sigma^2 = N_0/2$ is the noise variance, and d_{ij} is the Euclidean distance between two signals $s_i(t)$ and $s_j(t)$ that are unmerged from nT_s to $(n+N)T_s$, whose phase functions $\phi\left(t, \boldsymbol{D}_{N,i}\right)$ and $\phi\left(t, \boldsymbol{D}_{N,j}\right)$ contain two N-symbol sequences that must be different in their first symbol. Setting the index n to zero, we have

$$\begin{aligned} d_{ij}^2 &= \int_0^{NT_s} \left[s_i(t) - s_j(t)\right]^2 \mathrm{d}t \\ &= \int_0^{NT_s} s_i^2(t)\,\mathrm{d}t + \int_0^{NT_s} s_j^2(t)\,\mathrm{d}t - 2\int_0^{NT_s} s_i(t)s_j(t)\,\mathrm{d}t \end{aligned} \tag{7.341}$$

The first two terms on the right-hand side of (7.341) are the energy of the sequence of N symbols. Therefore, each term is equal to NE_s, where E_s is the symbol energy. Thus,

$$\begin{aligned} d_{ij}^2 &= 2NE_s - 2\int_0^{NT_s} A^2 \cos\left[2\pi f_c t + \phi\left(t, \boldsymbol{D}_{N,i}\right)\right] \cos\left[2\pi f_c t + \phi\left(t, \boldsymbol{D}_{N,j}\right)\right] \mathrm{d}t \\ &= 2NE_s - \frac{2E_s}{T_s}\int_0^{NT_s} \cos\left[\phi\left(t, \boldsymbol{D}_{N,i}\right) - \phi\left(t, \boldsymbol{D}_{N,j}\right)\right] \mathrm{d}t \end{aligned} \tag{7.342}$$

We have assumed that f_c is an integer multiple of $1/T_s$ so that the term containing the second harmonic is zero. Let us denote

$$\Delta\phi\left(t, \boldsymbol{D}_{N,i}, \boldsymbol{D}_{N,j}\right) = \phi\left(t, \boldsymbol{D}_{N,i}\right) - \phi\left(t, \boldsymbol{D}_{N,j}\right) \tag{7.343}$$

Substituting (7.332) into (7.343) yields the following expression

$$\Delta\phi\left(t, \boldsymbol{D}_{N,i}, \boldsymbol{D}_{N,j}\right) = 4\pi h \sum_{k=-\infty}^{N} \left(D_{k,i} - D_{k,j}\right) q(t - kT_s) \tag{7.344}$$

By using (7.343) and (7.344) in (7.342), we obtain the squared Euclidean distance as follows:

$$\begin{aligned} d_{ij}^2 &= \frac{2E_s}{T_s} \int_0^{NT_s} \left[1 - \cos \Delta\phi\left(t, \boldsymbol{D}_{N,i}, \boldsymbol{D}_{N,j}\right)\right] \mathrm{d}t \\ &= \frac{2E_s}{T_s} \int_0^{NT_s} \left\{1 - \cos\left[4\pi h \sum_{k=-\infty}^{N} \left(D_{k,i} - D_{k,j}\right) q(t - kT_s)\right]\right\} \mathrm{d}t \end{aligned} \tag{7.345}$$

The sequence error probability in (7.340) is dominated by the term corresponding to d_{min}, the minimum of all possible d_{ij}'s. Let A_d be the average number of paths of distance d from a given path (this concept is similar to the average number of nearest neighbors of a signal point), we can approximate the sequence error probability with the first few terms as follows:

$$P_{se} \leq \sum_{d=d_{min}}^{d_{min}+m} A_d \, Q\left(\frac{d}{2\sigma}\right) \tag{7.346}$$

where $3 \leq m \leq 5$ would suffice and

$$d_{min} = \lim_{N\to\infty} \min_{\substack{i,j \\ i\neq j}} d_{ij} \tag{7.347}$$

The value of d_{min}^2 of CP-MFSK of any digital modulation index $h = a/b$, where a and b are relative prime positive integers, is given for 1REC pulse shape (full response $L = 1$) as follows [7]:

$$d_{min}^2 = \begin{cases} 2E_s, & \text{integer } h \\ \min\limits_{\gamma}\{4E_s[1 - \mathrm{sinc}(\gamma h)], & b \geq M, \ \gamma = 2, 4, 6, \ldots, 2(M-1) \\ 4E_s[1 - \mathrm{sinc}(\gamma h)], & h < 0.3017, \ b < M \\ 2E_s, & h > 0.3017, \ b < M \end{cases} \tag{7.348}$$

where $\mathrm{sinc}(\gamma h) = \sin \pi\gamma h / \pi\gamma h$.

Example 7.27 Minimum Euclidean distance for coherent precoded MSK

MSK is CPM with $h = 1/2$; therefore, by using the second expression in (7.348), we obtain

$$d_{min}^2 = 4E_b[1 - \mathrm{sinc}(1)] = 4E_b\left(1 - \frac{\sin \pi}{\pi}\right) = 4E_b \tag{7.349}$$

This implies that $d_{min} = 2\sqrt{E_b}$, which is the same minimum Euclidean distance as PSK. This explains why coherent precoded MSK has the same bit error probability as coherent PSK.

■

When h is not rational, the minimum Euclidean distance varies with both h and N. For CP-FSK with 1REC pulse shape, it was shown that when $N = 3$, h reaches its maximum at 0.715 and $d_{min}^2 = 4.87E_b$ [8]. Compared with coherent precoded MSK, a gain of 0.85 dB in signal-to-noise ratio per bit is achieved. The value of h can be approximated by $h = 5/7$ and the Viterbi algorithm can be implemented using the phase trellis. Another observation from (7.348) shows that d_{min} increases with increasing M, since a larger M results in a larger symbol energy E_s. This also holds true for h that is not rational.

Example 7.28 CP-4FSK with $h = 5/7$ and 17/19

Let us examine the case of $M = 4$ to see how much improvement we can extract from a higher modulation order and higher modulation index. From the second expression in (7.348) for $h = a/b = 5/7$, we get

$$\begin{aligned} d_{min}^2 &= \min_{\gamma}\left\{4E_s\left[1 - \operatorname{sinc}\left(\frac{5\gamma}{7}\right)\right], \quad \gamma = 2,\ 4,\ 6\right. \\ &= \min_{\gamma}\left\{4E_s\left(1 - \frac{\sin 5\pi\gamma/7}{5\pi\gamma/7}\right)\right\} \\ &= \min\{4.87E_s,\ 3.81E_s,\ 3.77E_s\} \\ &= 3.77E_s = 7.54E_b \end{aligned} \tag{7.350}$$

Comparing (7.350) with (7.349) shows that CP-4FSK with $h = 5/7$ achieves a 2.75 dB gain over precoded MSK.

For $h = 17/19$, we obtain

$$\begin{aligned} d_{min}^2 &= \min_{\gamma}\left\{4E_s\left[1 - \operatorname{sinc}\left(\frac{17\gamma}{19}\right)\right], \quad \gamma = 2,\ 4,\ 6\right. \\ &= \min_{\gamma}\left\{4E_s\left(1 - \frac{\sin 17\pi\gamma/19}{17\pi\gamma/19}\right)\right\} \\ &= \min\{4.44E_s,\ 4.35E_s,\ 4.22E_s\} \\ &= 4.22E_s = 8.44E_b \end{aligned} \tag{7.351}$$

Thus, CP-4FSK with $h = 17/19$ achieves a 3.24 dB gain over precoded MSK.

■

This example shows that by increasing M one can achieve a better power efficiency, but only at the expense of bandwidth, since a higher digital modulation index is required.

Example 7.29 Viterbi algorithm

In this example, we illustrate the Viterbi algorithm for precoded MSK, which is CPM with $h = 1/2$ and 1-REC pulse shape. Since $h = a/b = 1/2$ and $L = 1$, there are four terminal phase states, namely, $\{0,\ \pi/2,\ \pi,\ 3\pi/2\}$, which are also the states for the trellis. The state diagram is shown in Figure 7.69 and the state trellis is shown in Figure 7.70.

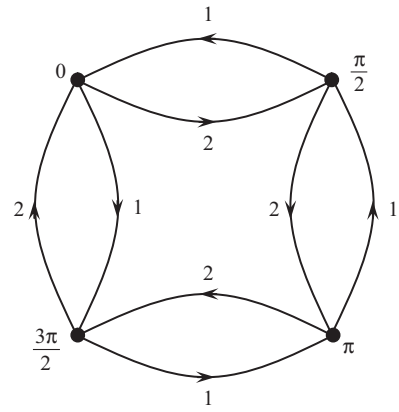

Figure 7.69 State diagram of precoded MSK.

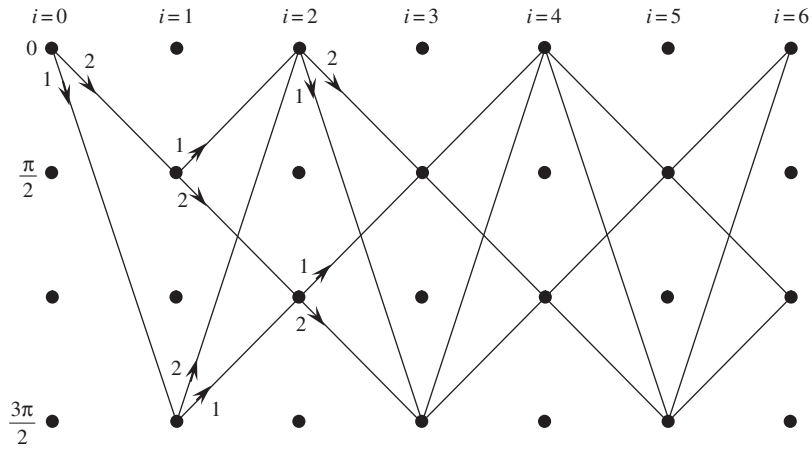

Figure 7.70 Trellis for precoded MSK over six bit intervals. The starting state is state 0.

Note that it takes a minimum of two bit intervals for a path to leave a state and re-enter the same state. Therefore, in the calculation of d^2_{min} for precoded MSK, the observed sequence has length $N = 2$ symbols. Let us assume that the algorithm starts at state 0 at time $t = 0$ and that the initial phase is zero. Consider the received bit sequence $\{1, 1\}$, which corresponds to the sequence of symbols $\{D_0 = 2, D_1 = 2\}$. We wish to use the Viterbi algorithm to recover this sequence of symbols. Assuming no noise, the received signal for each symbol interval is given in (7.331). The state $S_N \in \{0, \pi/2, \pi, 3\pi/2\}$ at each time index N will be denoted as $0_N, \pi/2_N, \pi_N, 3\pi/2_N$.

1. There are two paths leaving the initial sate 0_0 to enter state $\pi/2_1$ (when $D_0 = 2$) and state $3\pi/2_1$ (when $D_0 = 1$). The phases $\phi(t, D_0) = \varphi_0 + \varphi(t, D_0)$ are $\phi(t, 1) = 0 + \pi(2 - 2 - 1)q(t) = -\pi q(t)$ and $\phi(t, 2) = 0 + \pi(4 - 2 - 1)q(t) = \pi q(t)$. The metrics C_0 at each state $\pi/2_1$ and $3\pi/2_1$ are given by

$$C_0(\pi/2_1) = \int_0^{T_s} A\cos[2\pi f_c t + \phi(t,\,2)]\cos[2\pi f_c t + \phi(t,\,2)]\mathrm{d}t = \frac{AT_s}{2} \tag{7.352}$$

and

$$\begin{aligned} C_0(3\pi/2_1) &= \int_0^{T_s} A\cos[2\pi f_c t + \phi(t,\,2)]\cos[2\pi f_c t + \phi(t,\,1)]\mathrm{d}t \\ &= \frac{A}{2}\int_0^{T_s}\cos[\phi(t,\,2) - \phi(t,\,1)]\,\mathrm{d}t = \frac{A}{2}\int_0^{T_s}\cos[2\pi q(t)]\,\mathrm{d}t \\ &= \frac{A}{2}\int_0^{T_s}\cos\frac{2\pi t}{2T_s}\,\mathrm{d}t = 0 \end{aligned} \tag{7.353}$$

2. There are two paths leaving $\pi/2_1$ to enter state 0_2 (when $D_1 = 1$) and state π_2 (when $D_1 = 2$). There are also two paths leaving $3\pi/2_1$ to enter state 0_2 (when $D_1 = 2$) and state π_2 (when $D_1 = 1$). We calculate the two metrics for each state and retain only the survivor path with the largest metric. The phase $\phi(t,\,D_0,D_1) = \varphi_1 + \varphi(t,\,D_0,D_1) = \varphi_0 + \frac{\pi}{2}(2D_0 - 2 - 1) + \pi(2D_1 - 2 - 1)q(t - T_s)$ is given by

$$\phi(t,\,2,1) = \frac{\pi}{2}(4 - 2 - 1) + \pi(2 - 2 - 1)\frac{t - T_s}{2T_s} = -\frac{\pi t}{2T_s} + \pi \tag{7.354}$$

$$\phi(t,\,2,2) = \frac{\pi}{2}(4 - 2 - 1) + \pi(4 - 2 - 1)\frac{t - T_s}{2T_s} = \frac{\pi t}{2T_s} \tag{7.355}$$

$$\phi(t,\,1,2) = \frac{\pi}{2}(2 - 2 - 1) + \pi(4 - 2 - 1)\frac{t - T_s}{2T_s} = \frac{\pi t}{2T_s} - \pi \tag{7.356}$$

$$\phi(t,\,1,1) = \frac{\pi}{2}(2 - 2 - 1) + \pi(2 - 2 - 1)\frac{t - T_s}{2T_s} = -\frac{\pi t}{2T_s} \tag{7.357}$$

There are four new metrics to be computed and they are listed below with the first two for state 0_2 and the last two for state π_2:

$$\begin{aligned} C_1(0_2) &= C_0(\pi/2_1) + \int_{T_s}^{2T_s} A\cos[2\pi f_c t + \phi(t,\,2,\,1)]\cos[2\pi f_c t + \phi(t,\,2,\,2)]\mathrm{d}t \\ &= \frac{AT_s}{2} - \frac{A}{2}\int_{T_s}^{2T_s}\cos\frac{\pi t}{T_s}\mathrm{d}t = \frac{AT_s}{2} \quad : \quad \text{survivor} \end{aligned} \tag{7.358}$$

$$\begin{aligned} \hat{C}_1(0_2) &= C_0(3\pi/2_1) + \int_{T_s}^{2T_s} A\cos[2\pi f_c t + \phi(t,\,1,\,2)]\cos[2\pi f_c t + \phi(t,\,2,\,2)]\mathrm{d}t \\ &= -\frac{A}{2}\int_{T_s}^{2T_s}\mathrm{d}t = -\frac{AT_s}{2} < C_1(0_2) \quad : \quad \text{eliminated} \end{aligned} \tag{7.359}$$

$$C_1(\pi_2) = C_0(\pi/2_1) + \int_{T_s}^{2T_s} A\cos[2\pi f_c t + \phi(t,\,2,\,2)]\cos[2\pi f_c t + \phi(t,\,2,\,2)]\mathrm{d}t$$
$$= \frac{AT_s}{2} + \frac{A}{2}\int_{T_s}^{2T_s}\mathrm{d}t = AT_s \;:\quad \text{survivor} \tag{7.360}$$

$$\hat{C}_1(\pi_2) = C_0(3\pi/2_1) + \int_{T_s}^{2T_s} A\cos[2\pi f_c t + \phi(t,\,1,\,1)]\cos[2\pi f_c t + \phi(t,\,2,\,2)]\mathrm{d}t$$
$$= \frac{A}{2}\int_{T_s}^{2T_s}\cos\frac{\pi t}{T_s}\mathrm{d}t = 0 < C_1(\pi_2) \;:\quad \text{eliminated} \tag{7.361}$$

We now have *two surviving paths*: $\{0_0,\,\pi/2_1,\,\pi_2\}$ with metric $C_1(\pi_2) = AT_s$ and $\{0_0,\,\pi/2_1,\,0_2\}$ with metric $C_1(0_2) = AT_s/2$. Since $C_1(\pi_2) > C_1(0_2)$, we choose path $\{0_0,\,\pi/2_1,\,\pi_2\}$ as the *detected path*. The data symbols associated with this path is $\{D_0 = 2,\,D_1 = 2\}$ and the data bits can be calculated via $2D_i - M - 1$ with $M = 2$ as $\{1,\,1\}$, which is the correct data sequence.

■

The above example shows that the Viterbi algorithm can be used for sequence detection. Of course, in the case of precoded MSK, the demodulator in Figure 7.20 works well and is optimum for symbol-to-symbol detection. For partial response CPM ($L > 1$) with $M > 2$, the Viterbi algorithm is advantageous because the algorithm can be implemented easily as part of the digital baseband processor of the receiver. Furthermore, when the channel has memory, as in the case of intersymbol interference, symbol-by-symbol detection is no longer optimal and the Viterbi algorithm offers the best detection. In (7.346), we give the expression for sequence error probability. As an end user, we are more interested in the symbol error probability, which is given by

$$P_s \le \sum_{d=d_{min}}^{d_{min}+m} B_d\, Q\left(\frac{d}{2\sigma}\right) \tag{7.362}$$

where $3 \le m \le 5$ would suffice and B_d is the total number of symbol errors on all paths of distance d from a given path. The value of B_d can be obtained for each CPM with rational h by searching the trellis.

In summary, the Viterbi algorithm is a viable trellis detection scheme for coherent CP-MFSK with rational h. The Viterbi algorithm is indeed a maximum likelihood sequence detection scheme $(N \to \infty)$ that offers the best detection (as opposed to a symbol-by-symbol detection that has been the theme of the previous sections).

7.20 Coherent CPM with symbol-by-symbol detection

Using the memory embedded in CPM, we could design a coherent demodulator that can leverage the information contained in the phase to enhance the detection. The Viterbi

algorithm is one scheme that applies well to CP-MFSK with rational h. In this section, we study a method that does not rely on the trellis; therefore, it applies to any CPM in general. The method calculates the metrics of an observable sequence of N symbols, and then uses these metrics to make a decision on the first symbol only. Thus, the detection made on the kth symbol is based on the metrics of the observable sequence starting with the kth symbol and ending with the $(k+N-1)$th symbol. Since the decision is made on one symbol at a time, we could use the probability density function of the received signal $x(t) = s\left(t\middle|H_i, \boldsymbol{D}_{n,N-1}\right) +$ noise, given hypothesis H_i of M possible hypotheses (for M symbols) and $N-1$ observable symbols $\boldsymbol{D}_{n,N-1}$ that follow the kth symbol. There are $n = M^{N-1}$ equally likely combinations of observable sequences $\boldsymbol{D}_{n,N-1}$ of $N-1$ symbols. Noise is Gaussian with variance $\sigma^2 = N_0/2$. Using signals instead of vectors in (7.181), we get

$$f_X\left(x|H_i,\ \boldsymbol{D}_{n,N-1}\right) = \frac{1}{\sqrt{2\pi}\sigma} \mathrm{e}^{-\left(1/2\sigma^2\right)\int_0^{NT_s}\left[x(t)-s\left(t|H_i,\boldsymbol{D}_{n,N-1}\right)\right]^2 \mathrm{d}t} \tag{7.363}$$

Using (7.217) and noting that $\int x^2(t)\,\mathrm{d}t$ is common to all $\boldsymbol{D}_{n,N-1}$ and all signals $s\left(t\middle|H_i, \boldsymbol{D}_{n,N-1}\right)$ have the same energy NE_s, which is N times the symbol energy E_s, we can write the right-hand side of (7.363) as follows:

$$f_X\left(x|H_i,\ \boldsymbol{D}_{n,N-1}\right) = \frac{\alpha}{\sqrt{2\pi}\sigma} \mathrm{e}^{-\left(1/\sigma^2\right)\int_0^{NT_s} x(t)s\left(t|H_i,\boldsymbol{D}_{n,N-1}\right)\mathrm{d}t} \tag{7.364}$$

where the constant α is independent of $\boldsymbol{D}_{n,N-1}$ and is given by

$$\alpha = \mathrm{e}^{-\left(1/2\sigma^2\right)\left[\int_0^{NT_s} x^2(t)\mathrm{d}t + NT_sE_s\right]} \tag{7.365}$$

To remove the condition on $\boldsymbol{D}_{n,N-1}$, we need to average (7.364) over the probability density function of $\boldsymbol{D}_{n,N-1}$, which is discrete with a value of $1/M^{N-1}$ for each possible symbol D_i in the set $\{1, 2, \ldots, M\}$:

$$\begin{aligned} f_D\left(\boldsymbol{D}_{n,N-1}\right) &= \prod_{i=1}^{N-1} f_{D_i}(D_i) \\ &= \frac{1}{M^{N-1}} \prod_{i=1}^{N-1} \left[\delta(D_i-1) + \delta(D_i-2) + \cdots + \delta(D_i-M)\right] \end{aligned} \tag{7.366}$$

Thus the probability density function $f_X(x|H_i)$ is given by

$$f_X(x|H_i) = \frac{1}{M^{N-1}} \sum_{n=1}^{M^{N-1}} \frac{\alpha}{\sqrt{2\pi}\sigma} \mathrm{e}^{\left(1/\sigma^2\right)\int_0^{NT_s} x(t)s\left(t|H_i,\boldsymbol{D}_{n,N-1}\right)\mathrm{d}t} \tag{7.367}$$

Using (7.367), we construct the following M metrics:

$$c(x|H_i) = \sum_{n=1}^{M^{N-1}} \mathrm{e}^{\left(1/\sigma^2\right)\int_0^{NT_s} x(t)s\left(t|H_i,\boldsymbol{D}_{n,N-1}\right)\mathrm{d}t}, \qquad i = 1, 2, \ldots, M \tag{7.368}$$

The detector chooses a hypothesis that corresponds to the largest metric and outputs the first symbol of N observable symbols (first symbol plus $\boldsymbol{D}_{n,N-1}$ following symbols) that is

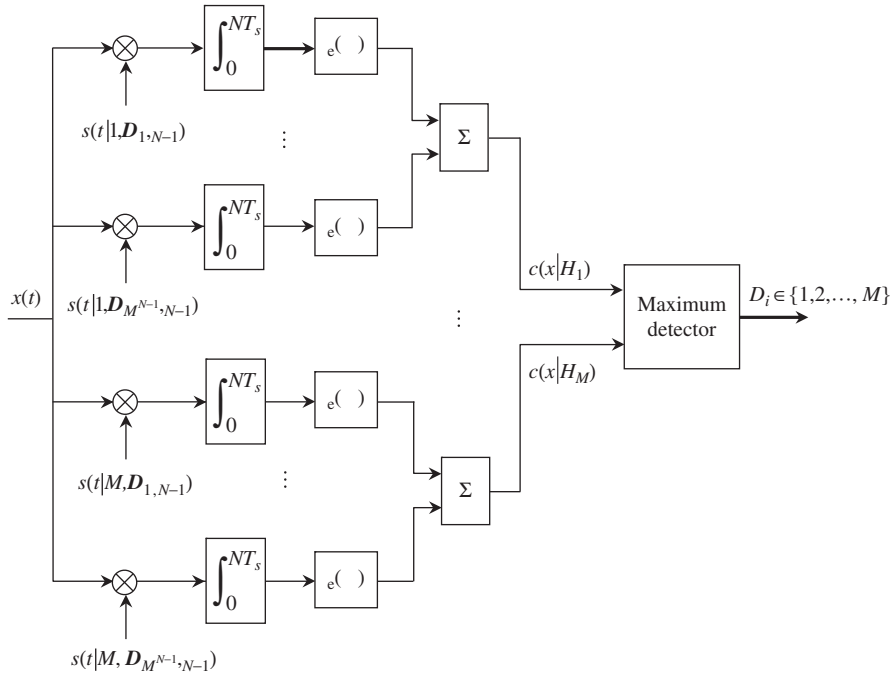

Figure 7.71 Coherent CPM with symbol-by-symbol detection using a sequence of N observable symbols.

represented by the hypothesis. The detector that follows the above rule is obviously a maximum likelihood detector $(N \to \infty)$. The symbol-by-symbol coherent CPM demodulator with N observable symbols is illustrated in Figure 7.71. Note that the signal $s\left(t|H_i,\ \boldsymbol{D}_{n,N-1}\right)$ is actually a sequence of N symbols with each symbol waveform given in (7.331). The performance of the symbol-by-symbol detection demodulator should be the same as the Viterbi demodulator in Figure 7.68 for $N \to \infty$. In practice, N is finite and limited to a few symbols, but at high signal-to-noise ratios the performance of both demodulators should be comparable.

7.21 Noncoherent CPM

When the initial phase of the received CPM signal is not known, coherent demodulation is not possible and noncoherent demodulation based on envelope detection must be employed. For symbol-by-symbol detection, we can modify the metric $c(x|H_i)$ in (7.368) to account for the unknown phase. Let us assume that the initial phase θ is uniformly distributed between 0 and 2π radians. The metric in (7.368) becomes

$$c(x|H_i,\ \theta) = \sum_{n=1}^{M^{N-1}} \mathrm{e}^{\left(1/\sigma^2\right)\int_0^{NT_s} x(t)s\left(t|H_i,\,\boldsymbol{D}_{n,N-1},\theta\right)\mathrm{d}t}, \qquad i = 1,\ 2,\ \ldots,\ M \tag{7.369}$$

where $x(t)$ is again the received CPM signal $s(t)$ plus noise over $0 \le t \le NT_s$ and

$$s\left(t|H_i,\ \boldsymbol{D}_{n,N-1},\ \theta\right) = A\cos\left[2\pi f_c t + \phi\left(t,\ \boldsymbol{D}_{n,N-1}\middle|H_i\right) + \theta\right] \qquad 0 \le t \le NT_s \tag{7.370}$$

We can express the right-hand side of (7.370) as follows:

$$s\left(t|H_i,\ \boldsymbol{D}_{n,N-1},\ \theta\right) = s\left(t|H_i,\ \boldsymbol{D}_{n,N-1}\right)\cos\theta - s\left(t,\ \frac{\pi}{2}\middle|H_i,\ \boldsymbol{D}_{n,N-1}\right)\sin\theta \tag{7.371}$$

where $s\left(t,\ \pi/2|H_i,\ \boldsymbol{D}_{n,N-1}\right)$ is the quadrature version of $s\left(t|H_i,\ \boldsymbol{D}_{n,N-1}\right)$ and both are given by

$$s\left(t|H_i,\ \boldsymbol{D}_{n,N-1}\right) = A\cos\left[2\pi f_c t + \phi\left(t,\ \boldsymbol{D}_{n,N-1}\middle|H_i\right)\right] \tag{7.372}$$

$$s\left(t,\ \frac{\pi}{2}\middle|H_i,\ \boldsymbol{D}_{n,N-1}\right) = A\sin\left[2\pi f_c t + \phi\left(t,\ \boldsymbol{D}_{n,N-1}\middle|H_i\right)\right] \tag{7.373}$$

Using the above result, we obtain the correlation between $x(t)$ and $s\left(t|H_i,\ \boldsymbol{D}_{n,N-1},\ \theta\right)$ as follows:

$$\begin{aligned}\int_0^{NT_s} x(t)\,s\left(t|H_i,\ \boldsymbol{D}_{n,N-1},\ \theta\right)\mathrm{d}t &= \cos\theta\int_0^{NT_s} x(t)\,s\left(t|H_i,\ \boldsymbol{D}_{n,N-1}\right)\mathrm{d}t \\ &\quad - \sin\theta\int_0^{NT_s} x(t)\,s\left(t,\ \frac{\pi}{2}\middle|H_i,\ \boldsymbol{D}_{n,N-1}\right)\mathrm{d}t \\ &= I_{n,i}\cos\theta - Q_{n,i}\sin\theta = Z_{n,i}\cos\left(\theta + \rho_{n,i}\right)\end{aligned} \tag{7.374}$$

where

$$I_{n,i} = \int_0^{NT_s} x(t)\,s\left(t|H_i,\ \boldsymbol{D}_{n,N-1}\right)\mathrm{d}t \tag{7.375}$$

$$Q_{n,i} = \int_0^{NT_s} x(t)\,s\left(t,\ \frac{\pi}{2}\middle|H_i,\ \boldsymbol{D}_{n,N-1}\right)\mathrm{d}t \tag{7.376}$$

$$Z_{n,i} = \sqrt{I_{n,i}^2 + Q_{n,i}^2}, \qquad \rho_{n,i} = \tan^{-1}\left(\frac{Q_{n,i}}{I_{n,i}}\right) \tag{7.377}$$

Substituting (7.374) into (7.369), we obtain the set of M conditional metrics

$$c(x|H_i,\ \theta) = \sum_{n=1}^{M^{N-1}} \mathrm{e}^{\left(1/\sigma^2\right)Z_{n,i}\cos\left(\theta+\rho_{n,i}\right)}, \qquad i = 1,\ 2,\ \ldots,\ M \tag{7.378}$$

The unconditional metrics can be obtained by averaging $c(x|H_i,\ \theta)$ using the probability density function $f_\theta(\theta) = 1/2\pi,\ 0 \le \theta \le 2\pi$:

$$
\begin{aligned}
c(x|H_i) &= \int_0^{2\pi} c(x|H_i,\,\theta) f_\theta(\theta)\mathrm{d}\theta \\
&= \sum_{n=1}^{M^{N-1}} \int_0^{2\pi} \frac{1}{2\pi} \mathrm{e}^{(1/\sigma^2) Z_{n,i} \cos(\theta+\rho_{n,i})}\mathrm{d}\theta \\
&= \sum_{n=1}^{M^{N-1}} I_0\left(\frac{Z_{n,i}}{\sigma^2}\right), \qquad i = 1,\,2,\,\ldots,\,M
\end{aligned}
\tag{7.379}
$$

where $I_0(\cdot)$ is the modified Bessel function of zeroth order.

Obviously, the demodulator that employs this set of metrics should choose the symbol that corresponds to the largest metric. Figure 7.72 shows the noncoherent CPM demodulator. Simon *et al*. [1] suggested that an odd number of observable symbols may be used ($N = 3,\,5,\,\ldots$). Noncoherent demodulation requires approximately 1 dB more in E_b/N_0 as compared to coherent demodulation [8]. A similar observation holds for noncoherent MFSK.

In the following discussion we focus on the use of the Viterbi algorithm for sequence detection of noncoherent CPM. The metric employed by the Viterbi algorithm must take into account the unknown initial phase θ of the received signal. Let us consider the correlation function of the Nth symbol interval between the received signal $x(t)$ and the local reference:

$$
\begin{aligned}
\int_{NT_s}^{(N+1)T_s} x(t)\,\cos[2\pi f_c t + \phi(t,\,\boldsymbol{D}_N) + \theta]\mathrm{d}t &= \cos\theta \int_{NT_s}^{(N+1)T_s} x(t)\,\cos[2\pi f_c t + \phi(t,\,\boldsymbol{D}_N)]\mathrm{d}t \\
&\quad - \sin\theta \int_{NT_s}^{(N+1)T_s} x(t)\,\sin[2\pi f_c t + \phi(t,\,\boldsymbol{D}_N)]\mathrm{d}t \\
&= I_N \cos\theta - Q_N \sin\,\theta = Z_N \cos(\theta + \rho_N)
\end{aligned}
\tag{7.380}
$$

where we define I_N, Q_N, Z_N, and ρ_N as follows:

$$
I_N = \int_{NT_s}^{(N+1)T_s} x(t)\,\cos[2\pi f_c t + \phi(t,\,\boldsymbol{D}_N)]\mathrm{d}t \tag{7.381}
$$

$$
Q_N = \int_{NT_s}^{(N+1)T_s} x(t)\,\sin[2\pi f_c t + \phi(t,\,\boldsymbol{D}_N)]\mathrm{d}t \tag{7.382}
$$

$$
Z_N = \sqrt{I_N^2 + Q_N^2}, \qquad \rho_N = \tan^{-1}\left(\frac{Q_N}{I_N}\right) \tag{7.383}
$$

It is obvious that the information about the Nth symbols is contained in the envelope Z_N of the correlation function. Therefore, the generic demodulator in Figure 7.68 also applies in this case but with a noncoherent path metric c_N defined for a path of N symbol as follows:

$$
c_N = \sum_{i=0}^{N} Z_i \tag{7.384}
$$

where Z_i is the noncoherent branch metric for the ith symbol defined in (7.383). The Viterbi algorithm can be carried out as described in Example 7.29.

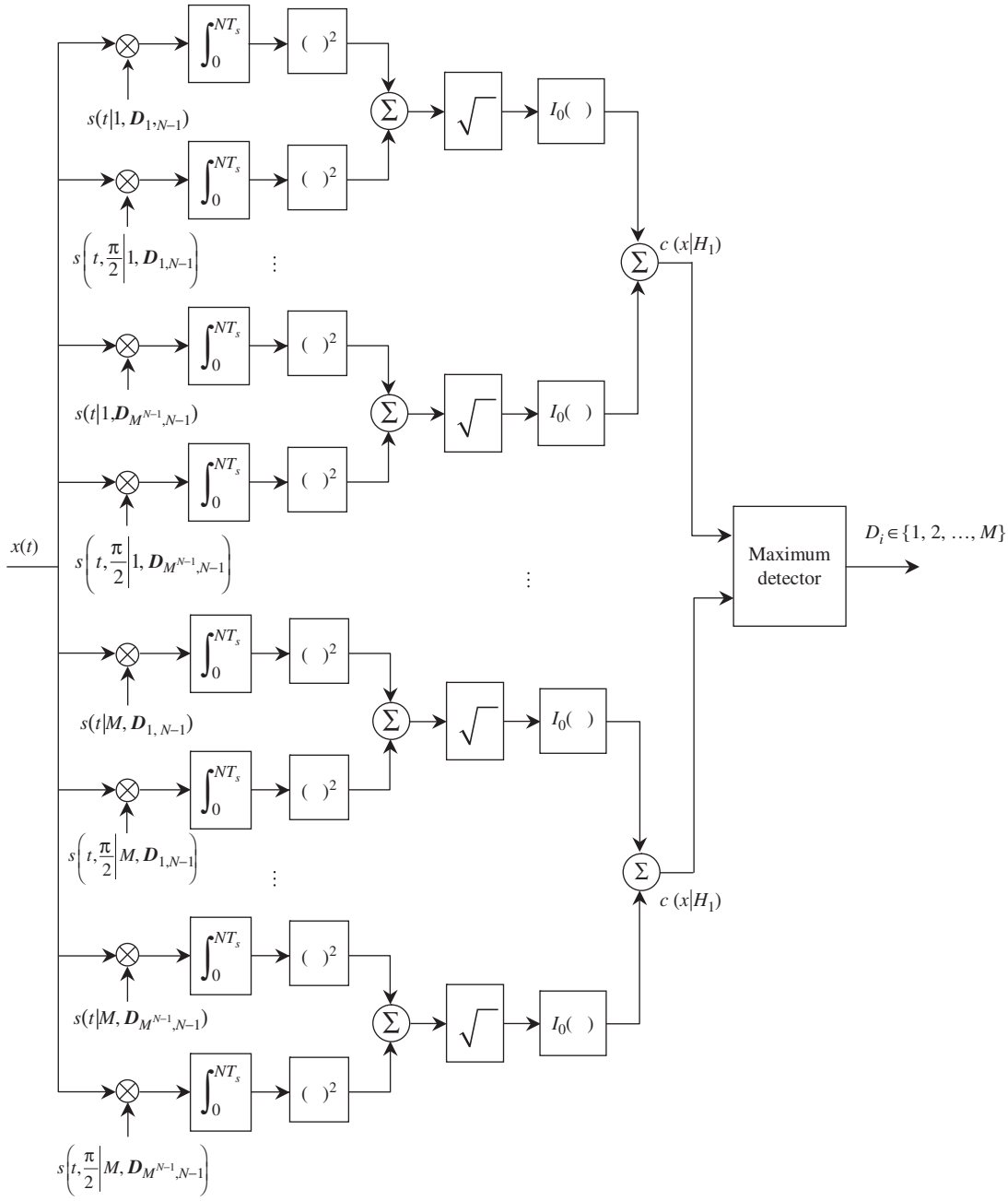

Figure 7.72 Noncoherent CPM with symbol-by-symbol detection using a sequence of N observable symbols.

7.22 Performance summary of M-ary modulation techniques

Our study shows the M-ary demodulation can be achieved coherently or noncoherently. As in the case of binary signals, coherent demodulation outperforms noncoherent demodulation. We consider three groups of M-ary signals, namely, the I-Q signals such as MASK, MPSK, and MQAM, and the orthogonal signals such as CSK and MFSK, and, finally, CPM. Coherent demodulation of the M-ary signals in these groups reveals that the I-Q signals are much less power-efficient than orthogonal signals, but much more bandwidth-efficient. On the other hand, CPM is a good compromise between power-efficiency and bandwidth-efficiency. Within the I-Q group, MQAM is more power-efficient than MPSK, which is, in turn, more power-efficient than MASK. One interesting fact emerges from this study, that is, noncoherent CSK and MFSK perform almost as well as their coherent counterparts for large M. Table 7.9 summarizes the performance of all M-ary modulation techniques.

Table 7.9 Performance of M-ary modulation techniques (the symbol duration is $T_s = T_b \log_2 M$)

Modulation	Bit error probability	Bandwidth
Coherent MASK	$\frac{2(M-1)}{M\log_2 M} Q\left(\sqrt{\frac{6\log_2 M}{M^2-1}\left(\frac{E_b}{N_0}\right)}\right)$	$\frac{2}{T_s}$
Coherent MPSK, $M > 2$	$\frac{2}{\log_2 M} Q\left(\sqrt{\frac{2E_b}{N_0}\log_2 M}\sin\frac{\pi}{M}\right)$	$\frac{2}{T_s}$
Coherent OQPSK	$Q\left(\sqrt{\frac{2E_b}{N_0}}\right)$	$\frac{2}{T_s}$
Coherent DMPSK, $M > 2$	$\frac{4}{\log_2 M} Q\left(\sqrt{\frac{2E_b}{N_0}\log_2 M}\sin\frac{\pi}{M}\right)$	$\frac{2}{T_s}$
Noncoherent DMPSK, $M > 2$	$\frac{2}{\log_2 M} Q\left(\sqrt{\frac{2E_b}{N_0}\log_2 M}\sin\frac{\pi}{\sqrt{2}M}\right)$	$\frac{2}{T_s}$
Noncoherent π/4-DQPSK	$Q\left(\sqrt{1.11\frac{E_b}{N_0}}\right)$	$\frac{2}{T_s}$
Coherent MQAM	$\frac{4\left(1-1/\sqrt{M}\right)}{\log_2 M} Q\left(\sqrt{\frac{3\log_2 M}{M-1}\left(\frac{E_b}{N_0}\right)}\right)$	$\frac{2}{T_s}$
Coherent DMQAM	$\frac{8\left(1-1/\sqrt{M}\right)}{\log_2 M} Q\left(\sqrt{\frac{3\log_2 M}{M-1}\left(\frac{E_b}{N_0}\right)}\right)$	$\frac{2}{T_s}$
Coherent CSK, MFSK	$< \frac{M}{2} Q\left(\sqrt{\frac{E_b}{N_0}\log_2 M}\right)$	$\frac{2M}{T_s}$ for CSK, $\frac{M}{T_s}$ for MFSK
Noncoherent CSK, MFSK	$< \frac{M}{4} e^{-(E_b/2N_0)\log_2 M}$	$\frac{2M}{T_s}$ for CSK, $\frac{M}{T_s}$ for MFSK
Coherent CPM	$P_s \le \sum_{d=d_{\min}}^{d_{\min}+5} B_d Q\left(\frac{d}{2\sigma}\right)$: Viterbi	[8]
Noncoherent CPM	About 1 dB less	[8]

7.23 OFDM demodulation

In Section 6.18, we provided a description of OFDM and its implementation. In this section, the demodulation process is discussed. The functional block diagram of the demodulation is depicted in Figure 7.73. The received OFDM signal is first demodulated into the I-Q baseband waveform, which contains the subcarrier symbols. The baseband waveform is passed through a filter $p(t)$ that represents the interpolation pulse employed by the D/A converter in the transmitter and then converted into time-domain samples $\{s_L(n)\}_{n=0}^{N-1}$ by the A/D converter at the sampling rate N/T_s. The guard interval created by the cyclic prefix is removed and the FFT processes the time-domain OFDM samples into the frequency-domain samples $\{Z(k)\}_{k=0}^{N-1}$, which represent the I-Q values of the subcarrier symbols. The subcarrier symbols are de-mapped into parallel bit streams. The parallel-to-serial converter (multiplexer) combines these parallel bit streams into one single serial bit stream at the output.

In practice, the demodulation of OFDM signals is not as straightforward as it was demonstrated in Figure 7.73, especially in a *multipath fading* channel. In the following discussion we use the WLAN standard IEEE 802.11a [9] which operates in the 5 GHz band for our study, although the discussion applies as well to the WLAN standard IEEE 802.11g [10], which operates in the 2.4 GHz band. OFDM is employed explicitly in IEEE 802.11a, while IEEE 802.11g employs both OFDM and direct sequence spread spectrum (DS-SS) to be backward compatible with WLAN standard IEEE 802.11b. In these standards, data symbols are transmitted in a packet, which is embedded in a frame whose format is given in Figure 7.74.

Table 7.10 shows the subcarrier modulation with associated data rate and the rate of convolutional codes employed for error correction. The timing-related parameters for IEEE

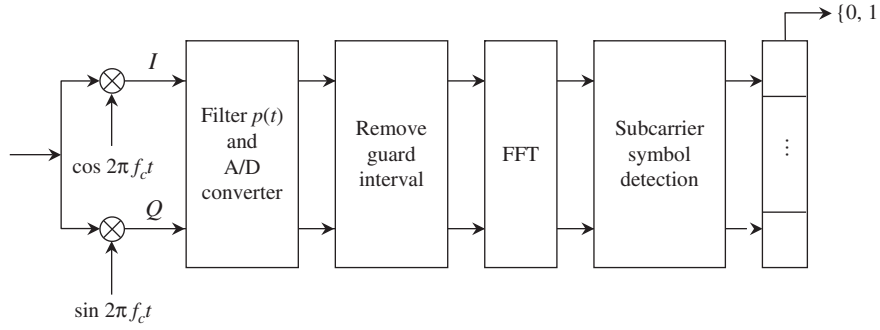

Figure 7.73 Block diagram of an OFDM demodulator.

Preamble: 12 symbols	Signal: One symbol	Data: Variable number of symbols

Figure 7.74 Frame format for IEEE 802.11a [9].

Table 7.10 Data rate and subcarrier modulation of IEEE 802.11a [9]

Data rate (Mbits/s)	Modulation	Coding rate (R)	Coded bits per subcarrier (N_{BPSC})	Coded bits per OFDM symbol (N_{CBPS})	Data bits per OFDM symbol (N_{DBPS})
6	BPSK	1/2	1	48	24
9	BPSK	3/4	1	48	36
12	QPSK	1/2	2	96	48
18	QPSK	3/4	2	96	72
24	16-QAM	1/2	4	192	96
36	16-QAM	3/4	4	192	144
48	64-QAM	2/3	6	288	192
54	64-QAM	3/4	6	288	216

Table 7.11 Timing-related parameters of IEEE 802.11a [9]

Parameter	Value
N_{SD}: number of data subcarriers	48
N_{SP}: number of pilot subcarriers	4
N_{ST}: number of subcarriers, total	52 ($N_{SD} + N_{SP}$)
Δ_F: subcarrier frequency spacing	0.3125 MHz (= 20 MHz/64)
T_{FFT}: IFFT/FFT period	3.2 μs ($1/\Delta_F$)
$T_{PREAMBLE}$: PLCP preamble duration	16 μs ($T_{SHORT} + T_{LONG}$)
T_{SIGNAL}: duration of the SIGNAL BPSK-OFDM symbol	4.0 μs ($T_{GI} + T_{FFT}$)
T_{GI}: GI duration	0.8 μs ($T_{FFT}/4$)
T_{GI2}: training symbol GI duration	1.6 μs ($T_{FFT}/2$)
T_{SYM}: symbol interval	4 μs ($T_{GI} + T_{FFT}$)
T_{SHORT}: short training sequence duration	8 μs ($10 \times T_{FFT}/4$)
T_{LONG}: long training sequence duration	8 μs ($T_{GI2} + 2 \times T_{FFT}$)

802.11a are shown in Table 7.11. The IEEE 802.11a standard specifies a 64-point IFFT (and hence 64-point FFT) as illustrated in Figure 7.75. The coefficients 1 to 26 are mapped into the same numbered IFFT inputs, while the coefficients −26 to −1 are copied into IFFT inputs 38 to 63. The rest of the inputs, 27 to 37, and the 0 (dc) input, are set to zero. After performing an IFFT, the output is cyclically extended to the desired length. The reverse process is carried out for an FFT.

Timing synchronization

In a packet-switched WLAN, timing synchronization must be acquired during the preamble in order to retrieve the data packet. The length and the content of the IEEE 802.11a preamble have been carefully designed to facilitate timing synchronization while keeping the frame overhead to a minimum. The preamble in Figure 7.76 consists of ten short OFDM symbols

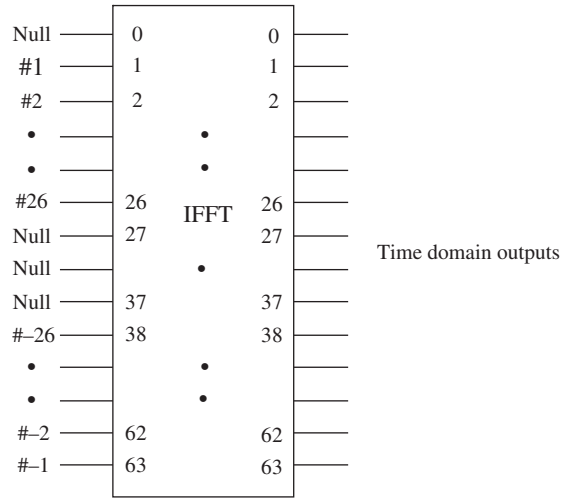

Figure 7.75 Inputs and outputs of IFFT [9].

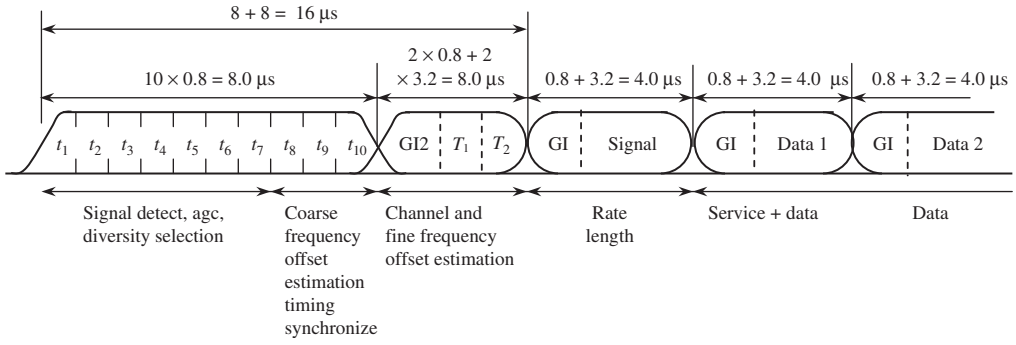

Figure 7.76 OFDM training structure [9].

and two long OFDM symbols. The parameters t_1 to t_{10} denote short training OFDM symbols, and T_1 and T_2 denote long training OFDM symbols. The total training length is 16 μs including two guard intervals (GI2) between the short symbol t_{10} and the long symbol T_1. The dashed boundaries in Figure 7.76 denote repetitions due to the periodicity of the IFFT. A short OFDM symbol consists of 12 subcarriers, which are modulated by the elements of the sequence S, given by

$$\begin{aligned} S_{-26,26} = \sqrt{\frac{13}{6}}\{&0, 0, 1+j, 0, 0, 0, -1-j, 0, 0, 0, 1+j, 0, 0, 0, \\ &-1-j, 0, 0, 0, -1-j, 0, 0, 0, 1+j, 0, 0, 0, 0, 0, 0, 0, -1-j, 0, 0, 0, \\ &-1-j, 0, 0, 0, 1+j, 0, 0, 0, 1+j, 0, 0, 0, 1+j, 0, 0, 0, 1+j, 0, 0\} \end{aligned} \tag{7.385}$$

The subscript $-26, 26$ of S represents 53 subcarriers (including a zero value at dc) numbering from -26 to 26. The multiplication factor $\sqrt{13/6}$ is employed to normalize the average power of the short training OFDM symbols, which employs only 12 subcarriers whose indexes are a multiple of 4. This results in a periodicity of $T_{\text{FFT}}/4 = 0.8\,\mu\text{s}$, which is the length of a short training OFDM symbol.

A long training OFDM symbol consists of 53 subcarriers, which are modulated by the elements of the sequence L, given by

$$\begin{aligned} L_{-26,26} = \{&1, 1, -1, -1, 1, 1, -1, 1, -1, 1, 1, 1, 1, 1, 1, -1, -1, 1, 1, -1, 1, -1, 1, 1, \\ &1, 1, 0, 1, -1, -1, 1, 1, -1, 1, -1, 1, -1, -1, -1, -1, -1, 1, 1, -1, -1, \\ &1, -1, 1, -1, 1, 1, 1, 1\} \end{aligned} \tag{7.386}$$

Thus, the length of a long training OFDM symbol is 3.2 μs, which is the same as the IFFT/FFT period. Timing synchronization requires at least two consecutive repeated OFDM symbols. The IEEE 802.11a preamble satisfies this requirement for both the short and long training sequences.

Symbol timing defines the FFT window, that is, the set of samples used to calculate the FFT window of each received OFDM symbol. In an ideal situation, symbol timing is fixed to the first sample of the FFT window. However, this is impossible since jitters in the symbol timing estimate around the mean value always exist. Each OFDM symbol has a guard interval, which is a cyclic prefix (CP) of its symbol. If the FFT window is set early, but within the guard interval, it contains samples from the cyclic prefix and the last samples of the symbol are not used at all. When the FFT window is late, then its start is after the first sample of the OFDM symbol, and the last samples are taken from the cyclic prefix of the next symbol. Therefore, *intersymbol interference* (ISI) can be introduced by the samples of the next symbol. Furthermore, the circular convolutional property required for subcarrier orthogonality is no longer satisfied. This results in *intercarrier interference* (ICI). Therefore, a late symbol timing estimate means a significant loss in performance. Figure 7.77 illustrates the FFT window timing.

In the following discussion, we present a timing synchronization method that employs a training sequence of two identical OFDM symbols. This method computes the metric m_n from the received complex baseband signal r_n as follows:

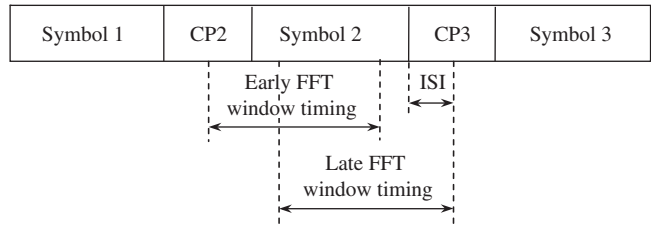

Figure 7.77 FFT window timing.

$$m_n = \frac{|c_n|^2}{P_n^2} \tag{7.387}$$

where the function c_n is the correlation and P_n is the received power of the second symbol and both are given by

$$c_n = \sum_{k=0}^{D-1} r_{n+k} r_{n+k+D}^* \tag{7.388}$$

$$P_n = \sum_{k=0}^{D-1} |r_{n+k+D}|^2 \tag{7.389}$$

The symbol timing estimate in an AWGN channel can be achieved using only the short training sequence that consists of a few identical OFDM symbols, with 16 samples in each symbol. Here, the delay D takes the values

$$D = 16\ell, \quad \ell = 1, 2, \ldots, 5 \tag{7.390}$$

In Figure 7.78 an 80-sample delay D was used. The simulation was run by setting the frequency offset ΔF between the transmitted and received signals to 100 kHz. The correct symbol timing occurs at the peak with $n = 401$ and the frequency offset is estimated to be $\Delta\hat{F} = 99.88$ kHz at $n = 401$.

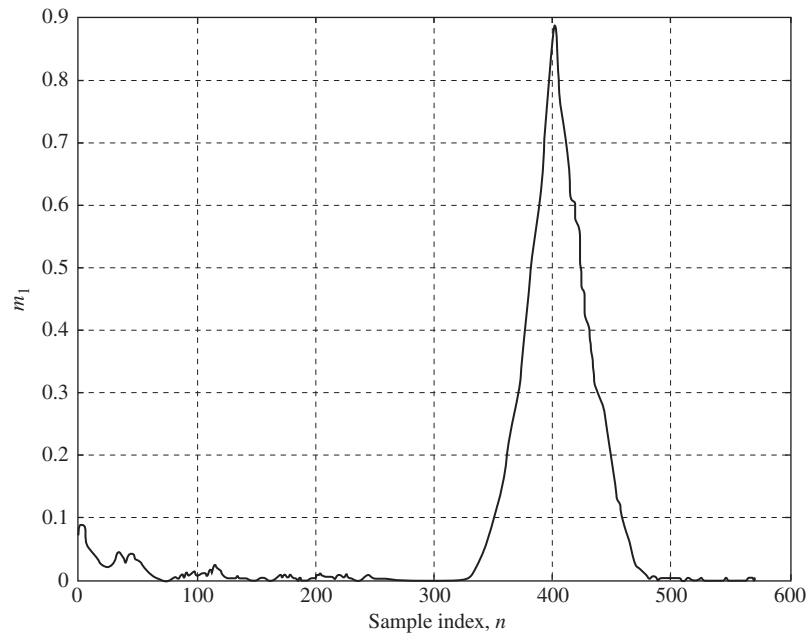

Figure 7.78 Symbol timing estimate in an AWGN channel with SNR = 10 dB [11].

Example 7.30 Frequency offset estimation

OFDM signals are more sensitive to carrier frequency offset than single carrier modulation signals. The performance degradation is caused by two main factors, namely, amplitude reduction of the desired subcarrier and *intercarrier interference*. The amplitude reduction occurs because the desired subcarrier is no longer sampled at the peak of the sinc-function of the FFT. Furthermore, orthogonality is no longer preserved between subcarriers resulting in ICI. The frequency offset can be estimated using the maximum likelihood principle (ML), which forms the correlation

$$c = \sum_{k=0}^{D-1} r_k r_{k+D}^* \tag{7.391}$$

between two consecutive symbols, where r_k is the received complex baseband signal. If there is a carrier frequency offset ΔF between the transmitted and received signals, we can write the correlation c as follows:

$$c = \sum_{k=0}^{D-1} s_k \, \mathrm{e}^{\mathrm{j}2\pi \Delta F \, k \, \tau_s} \left(s_{k+D} \mathrm{e}^{\mathrm{j}2\pi \Delta F (k+D) \tau_s} \right)^* \tag{7.392}$$

where $r_k = s_k \mathrm{e}^{\mathrm{j}2\pi \Delta F \, k \tau_s}$, and $1/\tau_s$ denotes the sampling rate, that is, $1/\tau_s = N/T_s$, where $1/T_s$ is the subcarrier symbol rate, which is also the subcarrier separation, and N is the number of subcarriers. Simplifying c we obtain

$$\begin{aligned} c &= \sum_{k=0}^{D-1} s_k s_{k+D}^* \, \mathrm{e}^{\mathrm{j}2\pi \Delta F \, k \, \tau_s} \mathrm{e}^{-\mathrm{j}2\pi \Delta F (k+D) \tau_s} \\ &= \mathrm{e}^{-\mathrm{j}2\pi \Delta F \, D \, \tau_s} \sum_{k=0}^{D-1} |s_k|^2 \end{aligned} \tag{7.393}$$

Thus the *estimated* carrier frequency offset is given by

$$\hat{\Delta F} = \frac{\theta_c}{2\pi D \tau_s} \tag{7.394}$$

where θ_c is the angle of c, that is, $\theta_c = \tan^{-1}[\mathrm{Im}(c)/\mathrm{Re(c)}]$. Note that θ_c is defined unambiguously only in $[-\pi, \pi]$, hence the absolute value of ΔF must obey

$$|\Delta F| < \frac{\pi}{2\pi D \tau_s} = \frac{1}{2D\tau_s} \tag{7.395}$$

Using IEEE 802.11a as an example for the short training OFDM symbol, the delay is $D = 16$, and for the long training OFDM symbol, the delay is $D = 64$. Furthermore, we use $1/\tau_s = N/T_s = 20\,\mathrm{MHz}$ as seen in Table 7.10. Thus,

$$|\Delta F_{short}| < \frac{20 \times 10^6}{2 \times 16} = 625\,\mathrm{kHz} \tag{7.396}$$

and

$$\left|\Delta F_{long}\right| < \frac{20 \times 10^6}{2 \times 64} = 156.25\,\text{kHz} \tag{7.397}$$

Thus the carrier frequency offset estimate would be more reliable with the short training sequence. For the IEEE 802.11a, the carrier frequency is about 5.3 GHz. The maximum clock error is 20×10^{-6}. Therefore, the maximum error between the transmitter and receiver clocks is 40×10^{-6}, and this results in a maximum frequency offset $\Delta F_{\max} = 5.3 \times 10^9 \times 40 \times 10^{-6} = 212\,\text{kHz}$. This frequency offset can only be estimated accurately with the short training sequence. If (7.388) is employed instead of (7.391) for frequency offset estimation, then (7.394) becomes

$$\Delta \hat{F} = \frac{\theta_{c_{\hat{n}}}}{2\pi D \tau_s} \tag{7.398}$$

where $\theta_{c_{\hat{n}}}$ is the angle of $c_{\hat{n}}$, the correlation value corresponding to the symbol timing estimate $\hat{n}$.

■

The carrier frequency offset can be estimated quite accurately. Figure 7.79 displays the probability distribution function (PDF) of the frequency offset estimate in an AWGN

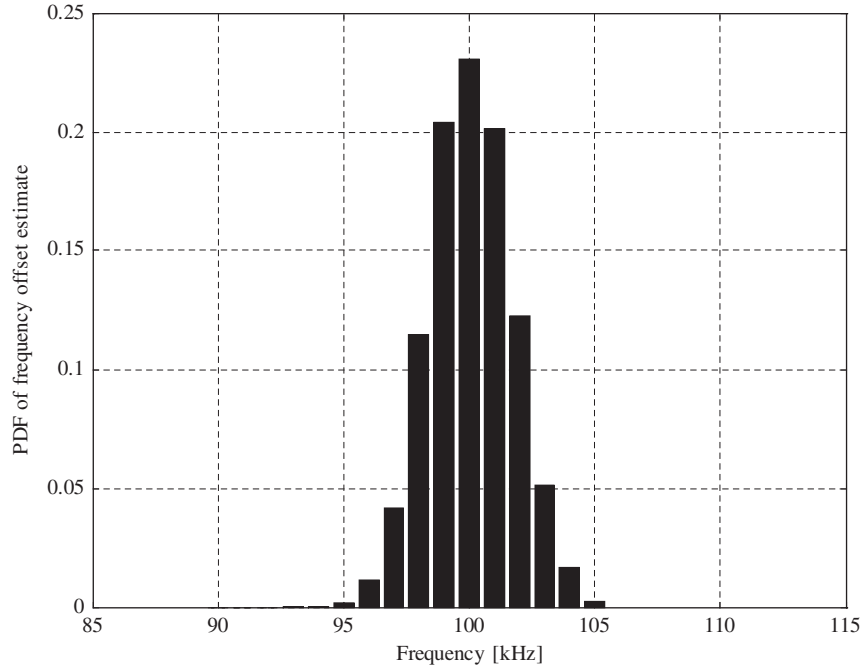

Figure 7.79 PDF of frequency-offset estimate in AWGN, SNR = 10 dB [11].

channel. The simulation was run with $\Delta F = 100$ kHz, $SNR = 10$ dB, and $D = 80$. The PDF is bell-shaped and centered at 100 kHz. The maximum frequency offset error can be taken to be 4 kHz.

Carrier phase synchronization

The error in the frequency offset estimate is small; therefore, the resulting loss in SNR due to ICI is negligible. The significant problem is the signal space rotation, which is the same for all subcarriers. Figure 7.80 shows the rotation of the QPSK signal points in the IEEE 802.11a during 11 OFDM symbols with a 3 kHz frequency error in an AWGN channel with $SNR = 20$ dB. For example, with the subcarrier spacing of 312.5 kHz as shown in Table 7.11, this frequency error amounts to only 1% of the subcarrier spacing. This results in negligible SNR loss. The significant problem is that after only 11 OFDM symbols, the signal points have crossed the decision boundaries. Therefore, correct demodulation is no longer possible even with very high SNR. Hence, carrier phase tracking must be implemented for demodulation of OFDM symbols. The IEEE 802.11a creates four pilot subcarriers to be transmitted along 48 data subcarriers. The pilot subcarriers enable the receiver to synchronize the carrier phase. Let the index k represent one of the four pilot subcarriers and the index ℓ represents the ℓth OFDM symbol after FFT. Thus, the received pilot symbol $R_{\ell,k}$ is equal to the known pilot symbol $P_{\ell,k}$ rotated by the relative frequency error f_Δ (the frequency error normalized to the subcarrier spacing) multiplied by the channel transfer function H_k, that is,

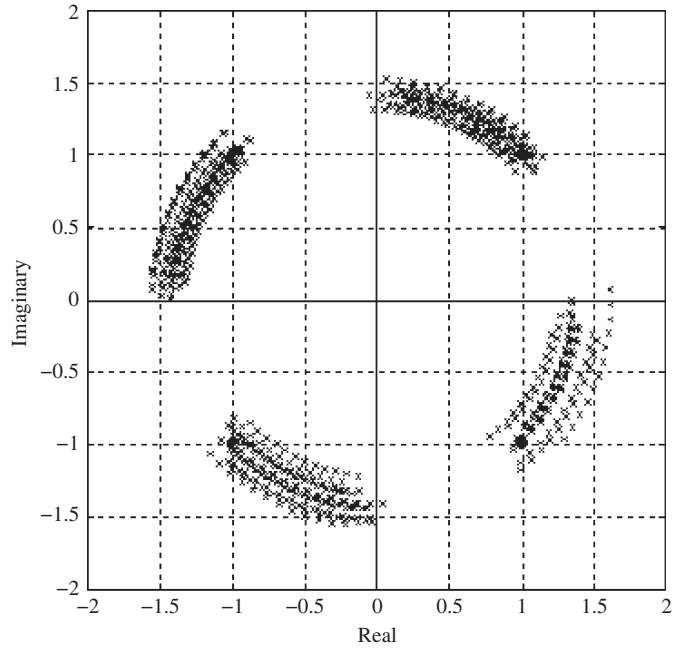

Figure 7.80 Rotation of IEEE 802.11a QPSK signal points due to 3 kHz frequency error [11].

$$R_{\ell,k} = H_k P_{\ell,k} e^{j2\pi \ell f_\Delta} \tag{7.399}$$

The phase estimate can be achieved based on the following correlation:

$$\begin{aligned} c_p &= \sum_{k=1}^{N_p} R_{\ell,k} \left(\hat{H}_k P_{\ell,k}\right)^* \\ &= e^{j2\pi \ell f_\Delta} \sum_{k=1}^{N_p} H_k \hat{H}_k^* \left|P_{\ell,k}\right|^2 \end{aligned} \tag{7.400}$$

where $\hat{H}_k$ is the estimate of the channel transfer function H_k and is assumed to be available, and N_p denotes the number of pilot subcarriers and is equal to 4 for IEEE 802.11a. The phase estimate θ_p is simply the angle of c_p, and is defined as

$$\theta_p = \tan^{-1} \frac{\mathrm{Im}(c_p)}{\mathrm{Re}(c_p)} \tag{7.401}$$

Since the pilot data are known, there is no ambiguity and the phase can be resolved correctly if the channel transfer function estimate $\hat{H}_k = H_k$. Hence, the channel estimation error results in phase estimation error.

The performance of the OFDM signal in an AWGN channel under ideal conditions is identical to the performance of its subcarrier modulation. If the subcarrier modulation is PSK or QPSK, the bit error probability is given by (7.104). If rectangular MQAM is employed, the bit error probability is given by (7.316). These are the modulation techniques employed by IEEE 802.11a as displayed in Table 7.9. For mobile WLAN systems, the performance of OFDM signals depends on many factors such as channel estimation, timing synchronization, carrier phase tracking, equalization, error correction coding, and the channel multipath fading effects.

7.24 Binary demodulation with convolutional codes

In this section we study the performance of coded binary modulation techniques when the channel coding is carried out with linear binary convolutional codes. Our investigation covers both hard decoding and unquantized soft decoding. Quantized soft decoding loses about 0.1–0.5 dB in signal-to-noise ratio relative to unquantized soft decoding. We assume the all-zero code vector $\boldsymbol{c}$ is the transmitted code vector, and if the code vector is decoded correctly, the Viterbi algorithm would choose the all-zero path of the decoding trellis. Any other path would correspond to a wrong code vector. The all-zero path of the decoding trellis has zero Hamming weight. An arbitrary path of the decoding trellis has a Hamming weight d that ranges from the minimum d_{free} to the maximum value d_M dictated by the length of the code vector (note that all paths merge with the all-zero path at the end because of the use of tail bits). When the Viterbi decoder selects a path of weight d there is an *event error*. The conditional event error probability is the *pair-wise error probability* of selecting the vector $\boldsymbol{c}'$ corresponding to the path of Hamming weight d over the all-zero code vector $\boldsymbol{c}$. We denote

this pair-wise error probability as $P(d) = \Pr(\boldsymbol{c} \rightarrow \boldsymbol{c}')$. The event error probability P_E is therefore the union bound of all $P(d)$. Letting A_d denote the *number of paths of Hamming weight d* that merge with the all-zero paths, we have

$$P_E < \sum_{d=d_{free}}^{d_M} A_d P(d) \tag{7.402}$$

From the event error probability we can obtain the union bound on the coded bit error probability by weighting the pair-wise error probability $P(d)$ with the *information weight* B_d (number of information bit errors) of all paths of Hamming weight d. Since there are k information bits per branch for a rate k/n code, the union bound is given by

$$P_b < \frac{1}{k} \sum_{d=d_{free}}^{d_M} B_d P(d) \tag{7.403}$$

Tables 7.12–7.14 display the weight structures of the best codes for rates 1/3, 1/2, and 2/3, respectively. The larger the constraint length the more powerful the code is.

Hard decoding

To evaluate the union bound for the bit error probability we need to calculate the pair-wise error probability $P(d)$. If the channel is a BSC then hard decoding is implemented. The *output of the detector* is the channel output 1s or 0s. These demodulated coded bits serve as

Table 7.12 Generator (octal) and information weights of the best rate 1/3 codes [12]

K	Generators	d_{free}	$B_{d_{free}}$	$B_{d_{free}+1}$	$B_{d_{free}+2}$	$B_{d_{free}+3}$	$B_{d_{free}+4}$
3	7,7,5	8	3	0	15	0	58
4	17,15,13	10	6	0	6	0	58
5	37,33,25	12	12	0	12	0	56
6	75,53,47	13	1	8	26	20	19
7	171,165,133	15	7	8	22	44	22
8	367,331,225	16	1	0	24	0	113

Table 7.13 Generator (octal) and information weights of the best rate 1/2 codes [12]

K	Generators	d_{free}	$B_{d_{free}}$	$B_{d_{free}+1}$	$B_{d_{free}+2}$	$B_{d_{free}+3}$	$B_{d_{free}+4}$
3	7,5	5	1	4	12	32	80
4	17,15	6	2	7	18	49	130
5	35,23	7	4	12	20	72	225
6	75,53	8	2	36	32	62	332
7	171,133	10	36	0	211	0	1404
8	371,247	10	2	22	60	148	340
9	753,561	12	33	0	281	0	2179

Table 7.14 Generator (octal) and information weights of the best rate 2/3 codes [12]

K	Generators	d_{free}	$B_{d_{free}}$	$B_{d_{free}+1}$	$B_{d_{free}+2}$	$B_{d_{free}+3}$	$B_{d_{free}+4}$
3	7,5,7	3	1	10	54	226	853
4	15,13,15	4	8	34	180	738	2 989
5	31,33,31	5	25	112	357	1858	8 406
6	73,41,73	6	75	0	1571	0	31 474
7	163,135,163	6	1	81	402	1487	6 793
8	337,251,337	8	395	0	6695	0	235 288
9	661,473,661	8	97	0	2863	0	56 633

the decoder input bits. Let p be the channel transition probability; the probability that the path of Hamming weight d is chosen over the all-zero path is given by

$$P(d) = \begin{cases} \sum_{i=(d+1)/2}^{d} \binom{d}{i} p^i (1-p)^{d-i}, & d \text{ odd} \\ \frac{1}{2}\binom{d}{d/2} p^{d/2}(1-p)^{d/2} + \sum_{i=d/2+1}^{d} \binom{d}{i} p^i (1-p)^{d-i}, & d \text{ even} \end{cases} \tag{7.404}$$

Example 7.31 PSK with hard decoding

The transition probability of a BSC that accommodates a PSK signal is $p = Q\left(\sqrt{2rE_b/N_0}\right)$, where r is the code rate (the *coded bit energy* is $E_c = rE_b$). For numerical illustration consider the case $E_b/N_0 = 4$ dB and the convolutional code of rate ½, $K = 9$. The channel transition probability is $p = 0.057$. The union bound yields the bit error probability $P_b = 2.2 \times 10^{-3}$. The uncoded bit error probability given the same transmitted power is $P_{b,uncoded} = 1.25 \times 10^{-2}$. To achieve the same bit error probability as the coded system, the uncoded system would need $E_b/N_0 = 6$ dB. Thus, coding provides 2 dB of coding gain.

■

Soft decoding–Gaussian input vector

When coherent demodulation is employed, the received vector $\boldsymbol{r} = \boldsymbol{s} + \boldsymbol{N}$ at the *output of the signal processor* (matched filter) serves as the input vector to the unquantized soft decoder (threshold detector is not needed). If a quantized soft decoder is employed, a quantizer is added between the signal processor and the decoder. The received vector $\boldsymbol{r}$ is a Gaussian vector, where $\boldsymbol{s}$ is the voltage vector that represents the transmitted code vector $\boldsymbol{c}$. The pair-wise error probability $P(d) = \Pr(\boldsymbol{c} \to \boldsymbol{c}')$ is given by (7.196):

$$P(d) = Q\left(\frac{\|\boldsymbol{s}' - \boldsymbol{s}\|}{2\sigma}\right) \tag{7.405}$$

where $\boldsymbol{s}'$ represents the code vector $\boldsymbol{c}'$ with Hamming weight d, and $\sigma^2 = N_0/2$ is the noise variance. The quantity $\|\boldsymbol{s}' - \boldsymbol{s}\|$ is simply the Euclidean distance between $\boldsymbol{s}$ and $\boldsymbol{s}'$.

Example 7.32 PSK with soft decoding

Consider the case of PSK and the convolutional code of rate 1/2, $K = 9$. The transmitted vector $\boldsymbol{s}$ that represents the all-zero code vector $\boldsymbol{c}$ is given by $\boldsymbol{s} = \left(\sqrt{rE_b}, \sqrt{rE_b}; \sqrt{rE_b}, \sqrt{rE_b}; \ldots; \sqrt{rE_b}, \sqrt{rE_b}\right)$. The code vector $\boldsymbol{c}'$ has d bit ones, and hence its corresponding vector $\boldsymbol{s}'$ has d components with value $-\sqrt{rE_b}$ and the remaining components have value $\sqrt{rE_b}$. Hence, the Euclidean distance between $\boldsymbol{s}$ and $\boldsymbol{s}'$ is $\|\boldsymbol{s}' - \boldsymbol{s}\| = 2\sqrt{drE_b}$. Thus we obtain the following expression for $P(d) = \Pr(\boldsymbol{c} \to \boldsymbol{c}')$:

$$P(d) = Q\left(\sqrt{\frac{2drE_b}{N_0}}\right) \tag{7.406}$$

For numerical illustration consider the case $E_b/N_0 = 4$ dB. The union bound yields the bit error probability $P_b = 1.4 \times 10^{-6}$. The uncoded bit error probability given the same transmitted power is $P_{b,uncoded} = 1.25 \times 10^{-2}$. To achieve the same bit error probability as the coded system, the uncoded system would need $E_b/N_0 = 10.4$ dB. Thus, coding provides a 6.4 dB coding gain. Figure 7.81 shows the bit error probability of PSK with convolutional codes of rate ½ and constraint lengths $K = 7, 8, 9$.

■

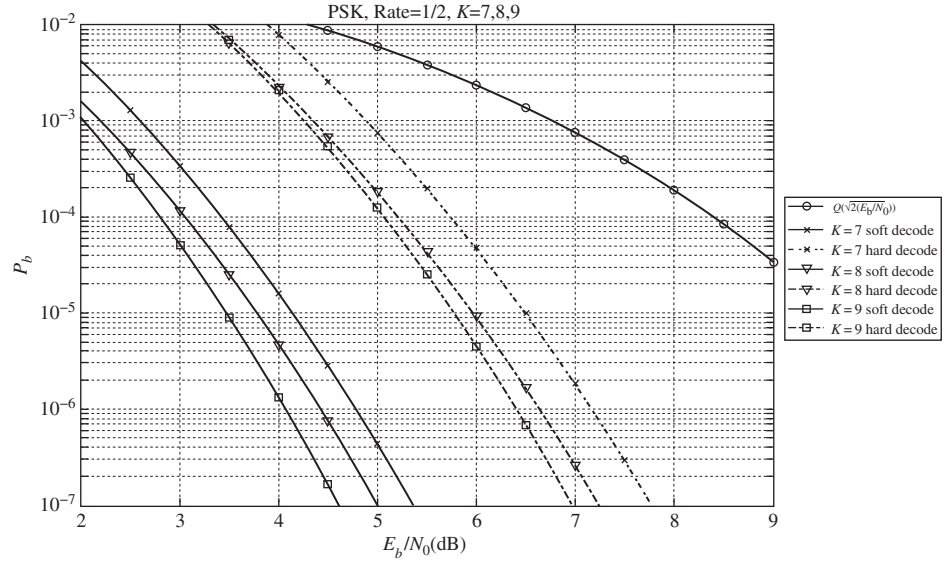

Figure 7.81 Bit error probability of PSK with convolutional codes of rate ½, $K = 7, 8, 9$. (Courtesy of Peter Harley.)

Example 7.33 QPSK and soft decoding

Although QPSK is an I-Q modulation, we can use binary convolutional codes as in the case of PSK. This is possible because the I-channel and the Q-channel are independent. For example, we can employ two identical encoders, one for the I-channel and one for the Q-channel. Two identical Viterbi soft decoders are needed for decoding. The performance of coded QPSK is identical to that of coded PSK but the required bandwidth is reduced by a factor of two. QPSK with rate ½, $K = 9$ convolutional codes achieves the same bandwidth as uncoded PSK.

■

Soft decoding–χ^2 input vector

When noncoherent demodulation is employed the $1 \times 2m$ received vector $r = (r_{1,1}\ r_{2,1}; r_{1,2}\ r_{2,2}; ...; r_{1,m}\ r_{2,m})$ at the output of the signal processor (noncoherent correlator) serves as the input vector to the unquantized soft decoder (maximum detector is not needed). If a quantized soft decoder is employed, a quantizer is added between the signal processor and the decoder. The received vector $\boldsymbol{r}$ is a χ^2-vector that represents the transmitted code vector $\boldsymbol{c}$, where $m = n(L + K - 1)$ is the code vector length representing L information bits. For each transmitted coded bit c_i, the decoder receives two observables $r_{1,i}$ and $r_{2,i}$ corresponding with two branches of the noncoherent correlator. Using the Bayes theorem we have

$$\Pr(\boldsymbol{c}|\boldsymbol{r}) = \frac{f_{\boldsymbol{R}}(\boldsymbol{r}|\boldsymbol{c})\Pr(\boldsymbol{c})}{f_{\boldsymbol{R}}(\boldsymbol{r})} \tag{7.407}$$

Since convolutional codes are linear, all code vectors of the same length are equally likely; therefore, $\Pr(\boldsymbol{c})$ is identical for all possible values of $\boldsymbol{c}$. Furthermore, $f_{\boldsymbol{R}}(\boldsymbol{r}) = \sum f_{\boldsymbol{R}}(\boldsymbol{r}|\boldsymbol{c})\Pr(\boldsymbol{c})$ is independent of whichever code vector was transmitted. The decoder that maximizes the a-posteriori probability $\Pr(\boldsymbol{c}|\boldsymbol{r})$, that is, maximizes the probability of selecting the transmitted code vector correctly given the received vector $\boldsymbol{r}$, is the ML decoder. Consequently, the ML decoder also maximizes the *likelihood* $f_{\boldsymbol{R}}(\boldsymbol{r}|\boldsymbol{c})$ of the transmitted code vector $\boldsymbol{c}$. Let us establish the *likelihood ratio*

$$\Lambda(\boldsymbol{r}) = \frac{f_{\boldsymbol{R}}(\boldsymbol{r}|\boldsymbol{c})}{f_{\boldsymbol{R}}(\boldsymbol{r}|\boldsymbol{c}')} = \frac{\prod_{i=1}^{2m} f_{R_{1,i}R_{2,i}}(r_{1,i}, r_{2,i}|c_i)}{\prod_{i=1}^{2m} f_{R_{1,i}R_{2,i}}(r_{1,i}, r_{2,i}|c'_i)} \tag{7.408}$$

As usual we assume that the all-zero-code vector $\boldsymbol{c}$ was transmitted. The code vector $\boldsymbol{c}'$ is represented by the path through the trellis that differs with the all-zero path in d bits. Thus, $f_{\boldsymbol{R}}(\boldsymbol{r}|\boldsymbol{c})$ and $f_{\boldsymbol{R}}(\boldsymbol{r}|\boldsymbol{c}')$ differ in only d products and therefore by rearranging these different products to be the first d products we have

$$\Lambda(\boldsymbol{r}) = \frac{\prod_{i=1}^{d} f_{R_{1,i}R_{2,i}}(r_{1,i}, r_{2,i}|c_i)}{\prod_{i=1}^{d} f_{R_{1,i}R_{2,i}}(r_{1,i}, r_{2,i}|c_i')} = \frac{\prod_{i=1}^{d} f_{R_{1,i}}(r_{1,i}|c_i) f_{R_{2,i}}(r_{2,i}|c_i)}{\prod_{i=1}^{d} f_{R_{1,i}}(r_{1,i}|c_i') f_{R_{2,i}}(r_{2,i}|c_i')} \tag{7.409}$$

By using (7.64) and (7.65) we have

$$\Lambda(\boldsymbol{r}) = \frac{\prod_{i=1}^{d} I_0\left(\frac{a\sqrt{r_{1,i}}}{\sigma^2}\right)}{\prod_{i=1}^{d} I_0\left(\frac{a\sqrt{r_{2,i}}}{\sigma^2}\right)} \tag{7.410}$$

The *ln-likelihood ratio* can be established as follows:

$$\ln \Lambda(\boldsymbol{r}) = \sum_{i=1}^{d} \ln I_0\left(\frac{a\sqrt{r_{1,i}}}{\sigma^2}\right) - \sum_{i=1}^{d} \ln I_0\left(\frac{a\sqrt{r_{2,i}}}{\sigma^2}\right) \tag{7.411}$$

An error event occurs, that is, $\boldsymbol{c}'$ is decoded instead of $\boldsymbol{c}$, when $\Lambda(\boldsymbol{r}) < 1$ or $\ln \Lambda(\boldsymbol{r}) < 0$. Since $I_0(\bullet)$ is a monotonically increasing function of its argument or squared argument, this is equivalent to

$$Y_1 = \sum_{i=1}^{d} r_{1,i} < Y_2 = \sum_{i=1}^{d} r_{2,i} \tag{7.412}$$

The two random variables Y_1 and Y_2 are χ^2-distributed. The pair-wise error probability $P(d) = \Pr(Y_1 < Y_2)$ is given by the following expression [8,12]:

$$P(d) = \frac{1}{2} \mathrm{e}^{-\gamma/2} \sum_{i=0}^{d-1} \frac{2^{-i}\gamma^i}{i!(d+i-1)!} \sum_{k=i}^{d-1} \frac{(k+d-1)!}{(k-i)!2^{k+d-1}} \tag{7.413}$$

where

$$\gamma = \frac{drE_b}{N_0} \tag{7.414}$$

Example 7.34 Noncoherent FSK with soft decoding

Consider the case of noncoherent FSK and the convolutional code of rate ½, $K = 9$. For numerical illustration consider the case $E_b/N_0 = 4$ dB. The union bound yields the bit error probability $P_b = 0.5$ (maximum error probability). The uncoded bit error probability given the same transmitted power is $P_{b,uncoded} = 0.14$. Thus, at low E_b/N_0, noncoherent FSK with soft decoding actually performs worse than uncoded noncoherent FSK or with hard decoding. This arises from the *combing loss* incurred by soft decoding. At low signal-to-noise ratios it is better to remove the noise prior to decoding to improve the performance, as is the case with hard decoding. Figure 7.82 shows the bit error probability of noncoherent FSK with convolutional codes of rate ½ and constraint lengths $K = 7, 8, 9$.

■

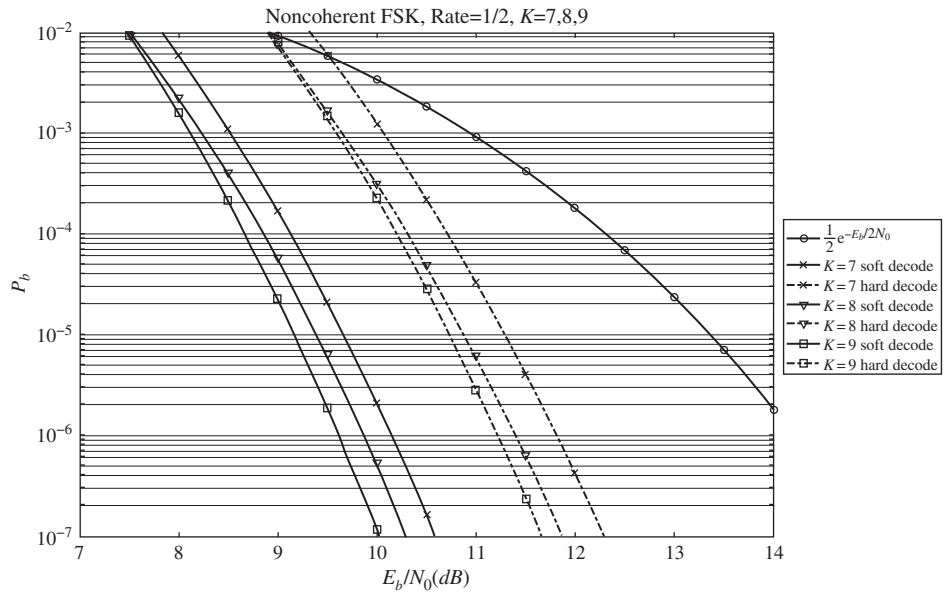

Figure 7.82 Bit error probability of noncoherent FSK with convolutional codes of rate ½, $K = 7, 8, 9$. (Courtesy of Peter Harley.)

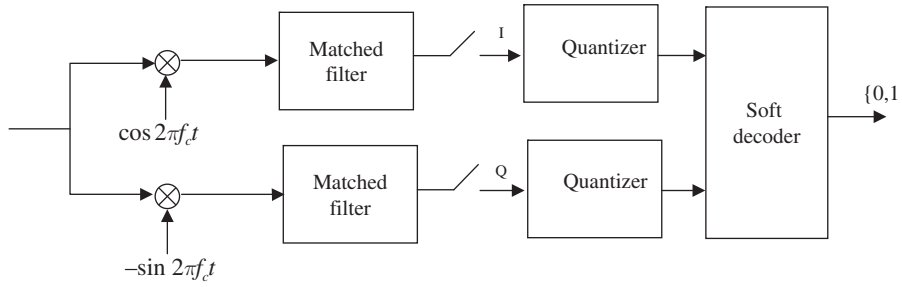

Figure 7.83 TCM demodulator and decoder.

7.25 TCM demodulation and decoding

A received TCM signal with the expanded signal space is first demodulated by an I-Q demodulator. The demodulated code word $\boldsymbol{r} = \boldsymbol{s} + \boldsymbol{N}$ at the *output of the I-Q signal processors* (matched filters) serves as the input code vector to the unquantized soft decoder (the minimum Euclidean distance detector is not needed). If a quantized soft decoder is employed, two quantizers are added between the signal processors and the decoder. Figure 7.83 shows the conceptual TCM demodulator and decoder.

The demodulated code word $\boldsymbol{r}$ is a Gaussian vector, where $\boldsymbol{s} = [\boldsymbol{s}_1\ \boldsymbol{s}_2 \cdots\ \boldsymbol{s}_k]$ is the voltage vector of k modulation symbols. Each symbol is represented by the I-Q vector $\boldsymbol{s}_l = [I_l\ \ Q_l]$

for the I-Q coordinates. The pair-wise error probability between two vector $\boldsymbol{s}$ and $\boldsymbol{s}'$ is $\Pr(\boldsymbol{s} \to \boldsymbol{s}')$ and is given by

$$\Pr(\boldsymbol{s} \to \boldsymbol{s}') = Q\left(\frac{\|\boldsymbol{s}' - \boldsymbol{s}\|}{2\sigma}\right) \tag{7.415}$$

where $\sigma^2 = N_0/2$ is the noise variance. The quantity $\|\boldsymbol{s}' - \boldsymbol{s}\|$ is simply the Euclidean distance between $\boldsymbol{s}$ and $\boldsymbol{s}'$. Let the *Euclidean free distance* of the code be the minimum Euclidean distance between different code words, that is,

$$\boldsymbol{d}_{free} = \min_{all\ i \neq j} d(\boldsymbol{s}^{(i)}, \boldsymbol{s}^{(j)}) \tag{7.416}$$

Then we have

$$\Pr(\boldsymbol{s} \to \boldsymbol{s}') \leq Q\left(\frac{\boldsymbol{d}_{free}}{2\sigma}\right) \tag{7.417}$$

On the other hand, the pair-wise error probability $\Pr(\boldsymbol{s}_i \to \boldsymbol{s}_j)$ between two symbols of the *uncoded signal space* is given by

$$\Pr(\boldsymbol{s}_i \to \boldsymbol{s}_j) \leq Q\left(\frac{d_{min}}{2\sigma}\right) \tag{7.418}$$

where d_{min} is the minimum Euclidean distance of the uncoded signal space.

The TCM *asymptotic coding gain* relative to the uncoded signal space with the same spectral efficiency and average power is conventionally defined as follows:

$$\boldsymbol{G} = \frac{\boldsymbol{d}_{free}^2}{d_{min}^2} \tag{7.419}$$

The goal in selecting codes for TCM is to maximize the asymptotic coding gain. Note that the bit error probability of TCM is given by $P_b \approx k^{-1}\boldsymbol{B}_{d_{free}} Q\left(\boldsymbol{d}_{free}/2\sigma\right)$ for code rate k/n, where $\boldsymbol{B}_{d_{free}}$ is the *information weight* (number of information bit errors) of all paths of Euclidean distance $\boldsymbol{d}_{free}$. On the other hand the bit error probability of the uncoded signal space is $P_b \approx N_n Q(d_{min}/2\sigma)/\log_2 M$. Therefore, the definition of asymptotic coding gain is indeed appropriate since it is based on the comparison of bit error probabilities while ignoring the constants. The asymptotic coding gain is somewhat larger than the true coding gain. The latter approaches the former at high signal-to-noise ratios per bit. It is not practical to evaluate the bit error probability by searching the code trellis to compute $\boldsymbol{B}_{d_{free}}$, especially when the code constraint length is large. It is much simpler to evaluate the bit error probability via simulation of the Viterbi algorithm. Tables 7.15–7.18 show the asymptotic coding gain for Ungerboeck TCMs.

Figure 7.84 shows the bit error probabilities versus E_b/N_0 for Ungerboeck TCM-16QAM and pragmatic TCM-16QAM. The coding gain at 10^{-6} bit error probability relative to uncoded 8QAM (Figure 6.35(a) is about 4.2–5 dB as compared to the optimistic asymptotic coding gain of 6 dB).

TCM decoding can be carried out via the Viterbi algorithm similar to the soft decoding of binary convolutional code in Example 4.27. The code symbol on each branch of the trellis is

Table 7.15 Asymptotic coding gain of TCM-8PSK

Constraint length K	$\boldsymbol{G}$ (dB)-8PSK
2	3
3	3.6
4	4.1
5	4.6
6	5
7	5.2
8	5.7

Table 7.16 Asymptotic coding gain of TCM-16PSK

Constraint length, K	$\boldsymbol{G}$ (dB)-16PSK
2	3.54
3	4
4	4.4
5	5.1
6	5.3
7	5.3
8	5.5

Table 7.17 Asymptotic coding gain of TCM-16QAM

Constraint length, K	$\boldsymbol{G}$ (dB)-16QAM
2	3
3	4
4	4.8
5	4.8
6	5.4
7	6
8	6

Table 7.18 Asymptotic coding gain of TCM-64QAM

Constraint length, K	$\boldsymbol{G}$ (dB)-64QAM
2	2.8
3	3.8
4	4.6
5	4.6
6	5.2
7	5.8
8	5.8

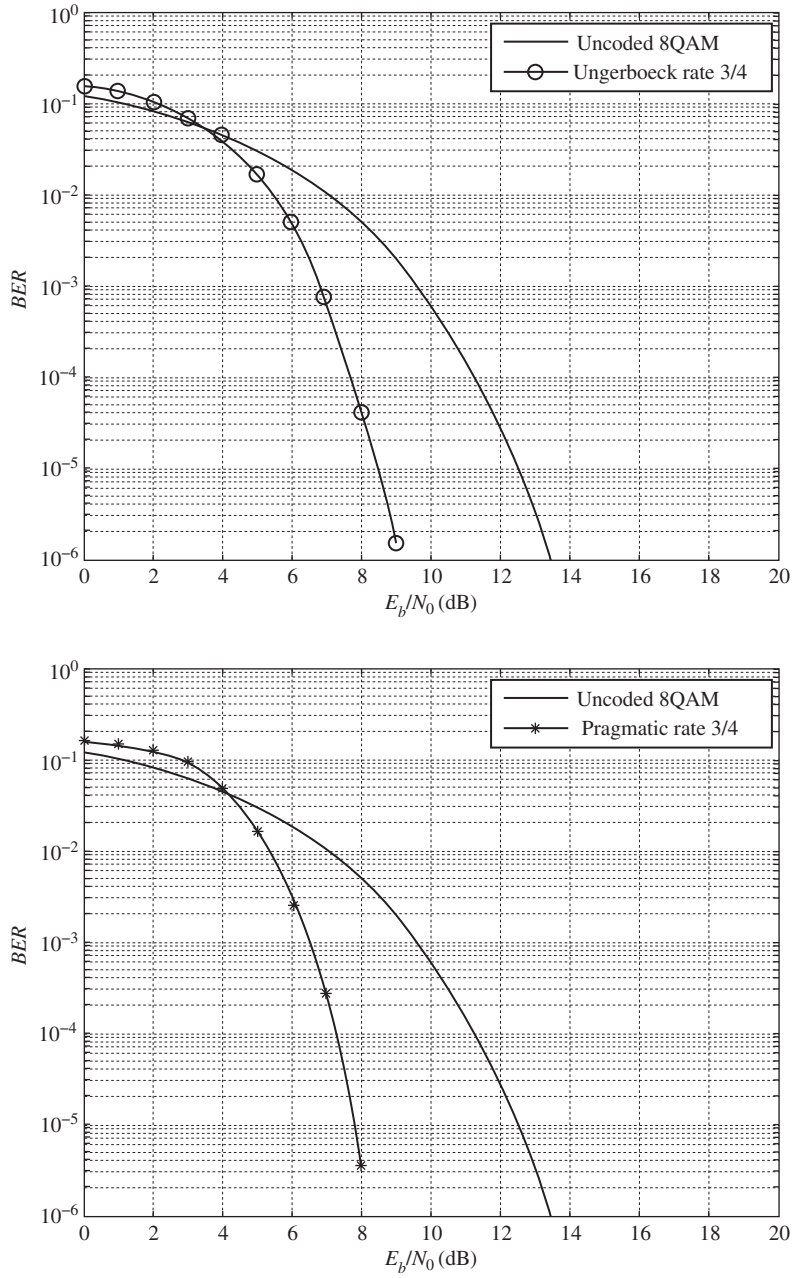

Figure 7.84 Bit error probability: (a) rate 3/4 Ungerboeck TCM-16QAM, (b) rate 3/4 pragmatic TCM-16QAM. (Courtesy of Lin Kiat Peh.)

mapped into an I-Q vector via symbol mapping by set partitioning for Ungerboeck TCM or via pragmatic symbol mapping for pragmatic TCM. The squared Euclidean distance between the code symbol of a branch and the corresponding received I-Q vector (at the outputs of the samplers) is calculated and added to the previous path squared Euclidean distance for each node. At each node in the trellis, the Viterbi algorithm chooses a branch that belongs to a path with the *smallest path squared Euclidean distance*. This retained path is called the *survivor path*. All other paths at each node with higher squared Euclidean distances are not retained. In the case of a tie, a survivor path might be chosen randomly. At the end of the decoding window, the survivor path with the smallest path squared Euclidean distance is selected and the associated code vector is chosen as the transmitted code vector.

Example 7.35 Viterbi algorithm for Ungerboeck TCM-QPSK

For illustration we use the same convolutional code as used in Example 4.27. The received vector $\boldsymbol{r} = (-1, 1; 0.5, 1; -0.5, 1; 1, 1; 1, 1)$ is normalized to $\sqrt{rE_s/2}$, where r is the code rate and E_s is the symbol energy. Each branch on the trellis is represented by one of the following voltage vectors: $00 \rightarrow (1, 1)$, $01 \rightarrow (-1, 1)$, $10 \rightarrow (-1, -1)$, $11 \rightarrow (1, -1)$ normalized to $\sqrt{rE_s/2}$ according to Figure 6.49. The path that associates with the code vector (00,00,00,00,00) has a normalized minimum squared Euclidean distance of 6.5 and hence is selected as the decoding path as shown in Figure 7.85. The two symbol errors that are caused by two underlined voltage errors are corrected.

■

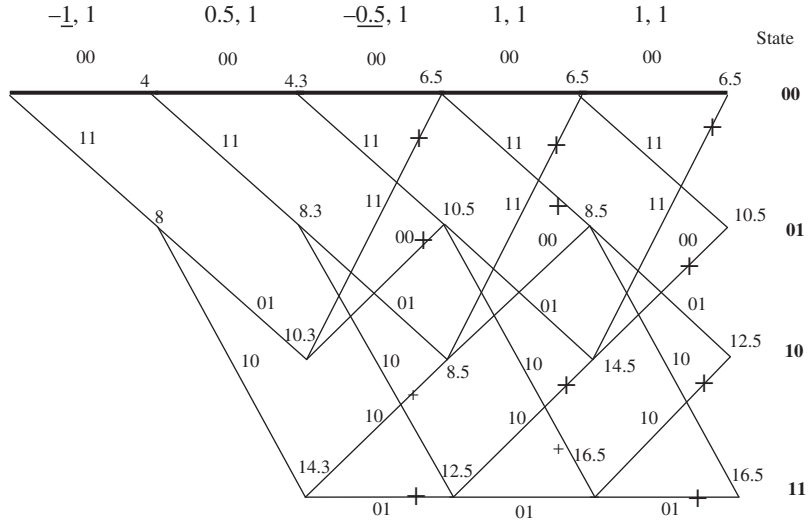

Figure 7.85 Unquantized soft Viterbi algorithm for Ungerboeck TCM-QPSK with rate ½, $K = 3$ convolutional code.

Example 7.36 Viterbi algorithm for Ungerboeck TCM-8PSK

The trellis of five time units in Figure 7.87 for the convolutional encoder in Figure 7.86 has parallel transitions that are encoded by the uncoded information bit with the upper branch (solid line) corresponding to 1 and the lower branch (dashed line) corresponding to 0. The upper (lower) code symbol is for the upper (lower) branch. The Viterbi algorithm for Ungerboeck TCM-8PSK is shown in Figure 7.87 for the received vector $r = (0.2, 0.7; -0.3, 0.5; 0.3, 0.5; 0.1, 0.8; 0.6, 0.3)$ normalized to $\sqrt{rE_s/2}$. The code symbols labeled on the branches are mapped to I-Q vectors according to Figure 6.55 as follows: $011 \rightarrow (0.92, 0.38)$, $000 \rightarrow (0.38, 0.92)$, $001 \rightarrow (-0.38, 0.92)$, $010 \rightarrow (-0.92, 0.38)$, $111 \rightarrow (-0.92, -0.38)$, $100 \rightarrow (-0.38, -0.92)$, $101 \rightarrow (0.38. - 0.92)$, $110 \rightarrow (0.92, -0.38)$. The decoded code symbol sequence is (000,010,011,001,011) as indicated by the heavy dashed line.

■

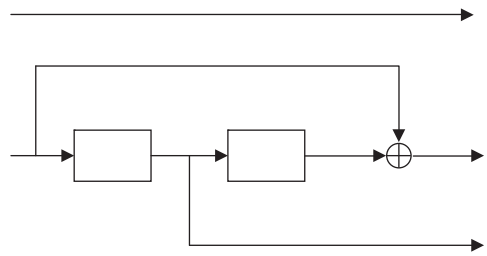

Figure 7.86 Rate 2/3 convolutional code with $K = 3$.

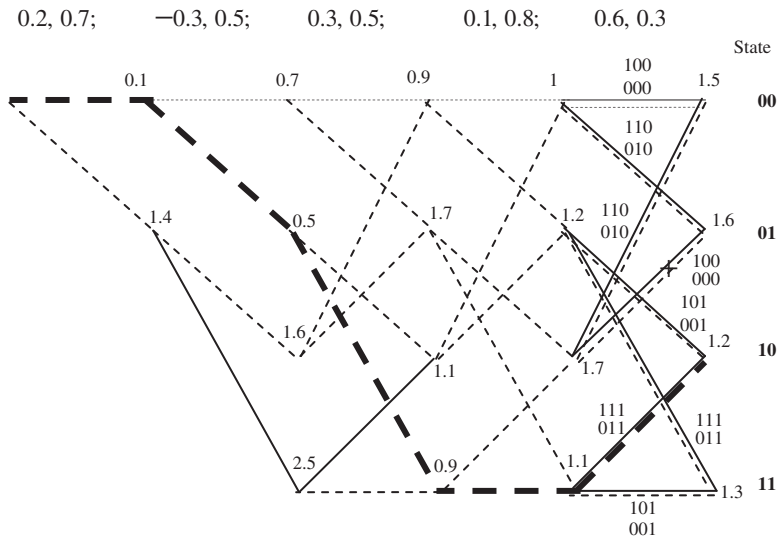

Figure 7.87 Unquantized soft Viterbi algorithm for Ungerboeck TCM-8PSK with rate 2/3, $K = 3$ convolutional code.

7.26 Summary

In this chapter we presented the principles of coherent demodulation and noncoherent demodulation. A digital demodulator basically consists of a signal processor and an optimum detector. The signal processor processes the received signal plus noise into a decision vector. The optimum detector uses the decision vector to recover the transmitted information with a minimum bit error probability. Four fundamental signal processors were studied. They are the coherent matched filter and correlator, which are equivalent at the sampling time, and the matched filter–envelope detector (noncoherent matched filter) and the quadrature correlator–square law detector (noncoherent correlator), which are also equivalent at the sampling time. Two optimum binary detectors were studied, namely, the *threshold detector* and the *maximum detector* (*comparator*). These optimum detectors are governed by the *maximum likelihood* criterion. The threshold detector is used with coherent binary demodulation, and the maximum detector can be employed for both coherent and noncoherent binary demodulations. We then proceeded to analyze the performance of binary demodulation such as coherent PSK, coherent DPSK, direct detection ASK for lightwave signals, coherent MSK and precoded MSK and GMSK, noncoherent FSK and MSK, and noncoherent DPSK.

Next, we studied the detector for M-ary signals, namely, the *minimum Euclidean distance detector* for coherent demodulation and the *M-ary maximum detector* for both coherent and noncoherent demodulation. Both detectors are governed by the maximum likelihood criterion. Afterward, we provided a detailed design of the coherent *L*-path demodulator based on the signal space approach. This optimum demodulator employs either *L* matched filters or *L* correlators for signal processing and either the *minimum Euclidean distance detector* or the *metric computer* and *maximum detector for detection*. The design of a coherent *M*-path demodulator was presented next. This type of demodulator employs either *M* matched filters or *M* correlators for signal processing and a maximum detector for detection. We then provided the design of a noncoherent *M*-path demodulator, which employs either *M* matched filter–envelope detectors or *M* quadrature correlator–square law detectors for signal processing, and a maximum detector for detection. Using the above designs we analyzed the performance of coherent MASK, coherent MPSK, coherent DMPSK, noncoherent DMPSK, noncoherent $\pi/4$-DQPSK, coherent MQAM and DMQAM, coherent CSK and MFSK, and noncoherent CSK and MFSK. We also considered two methods of detection for coherent CPM, namely, sequence detection via the Viterbi algorithm and symbol-by-symbol detection. Noncoherent CPM with symbol-by-symbol detection was also discussed. We concluded our study of M-ary demodulation techniques with a summary of their performance in an AWGN channel.

The study of OFDM demodulation was conducted in fair detail. We used the IEEE 802.11a standard as an example for our discussion, which included symbol timing estimation; frequency offset estimation; and carrier phase synchronization. The chapter ends with the performance analysis of TCM based on the asymptotic coding gain and simulation results.

Appendix 7A: The Q-function

The Q-function for $0 < x < 5$ is plotted in Figure 7.88.

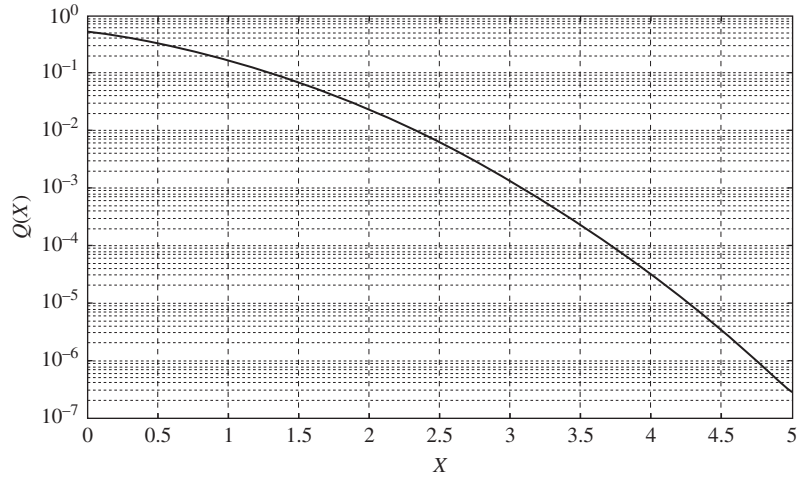

Figure 7.88 The Q-function. (Courtesy of Peter Harley.)

Problems

1. Determine the output of the matched filter of the pulse $p(t)$ when the input waveform is $s(t) = A[p(t) - p(t - T_b)]$ where $p(t)$ is the squared pulse of unit amplitude and duration T_b.
2. Given two complex vectors $\mathbf{u}$ and $\mathbf{v}$, show that $|\mathbf{u}^*\mathbf{v}| \leq \|\mathbf{u}\|\|\mathbf{v}\|$ with equality if and only if $\mathbf{u}$ and $\mathbf{v}$ are dependent, that is, $\mathbf{u} = \alpha\mathbf{v}$ for some arbitrary constant α (the Cauchy–Schwarz inequality). The notation $\mathbf{u}^*$ stands for the conjugate transpose of the vector $\mathbf{u}$.
3. Determine the output of the matched filter of the waveform $s(t) = 2B\frac{\sin 2\pi Bt}{2\pi Bt}$.
4. Consider the complex voltage signal $s(t) = A[p(t) + jp(t)]$, where $p(t)$ is the squared pulse of unit amplitude and duration T_b. Find the output voltage of the complex-valued matched filter at the sampling time $t = T_b$.
5. In Figure 7.3 assume that the sampling time has an error ε, that is, $T + \varepsilon$. Find the output signal-to-noise ratio of the matched filter.
6. Determine the output signal-to-noise ratio of the matched filter of the pulse $p(t)$ at the sampling time $T + \varepsilon$ $(0 \leq \varepsilon \leq T)$, where $p(t)$ is the squared pulse of unit amplitude and duration T, given the input signal $s(t) = A[p(t) - p(t - T)]$.
7. Find a pulse shape $p(t)$ with Fourier transform $P(f)$ whose matched filter works for both itself and its counterpart $q(t)$ with Fourier transform $Q(f) = \sqrt{P(f)}$.
8. Using the time-domain approach design a matched filter for signal $s(t)$ plus additive non-white noise $n(t)$ with real autocorrelation $R_n(\tau)$ whose Fourier transform $S_n(f)$ is a rational function. This can be achieved by first designing a noise whitening filter then the matched filter.
9. Using the frequency-domain approach, design a matched filter for the signal $s(t)$ with additive non-white noise $n(t)$ with rational power spectral density function $S_n(f)$.

10. Consider a bank of L matched filters that receive the same signal $s(t)$ but with different attenuation a_i, $i = 1, 2, \ldots, L$; that is, the ith matched filter input is $a_i s(t)$. The matched filter outputs are summed and sampled at time $t = T$ where T is the duration of the signal $s(t)$. The noise signals $n_1(t), n_2(t), \ldots, n_L(t)$ are independent and have identical power spectral density $N_0/2$. Find the output signal-to-noise ratio of the sum signal assuming the signal energy is E.
11. Consider a bank of L matched filters that receive the same signal $s(t)$ but with different attenuation a_i, $i = 1, 2, \ldots, L$; that is, the ith matched filter input is $a_i s(t)$. The matched filter outputs are summed and sampled at time $t = T$ where T is the duration of the signal $s(t)$. The noise signals $n_1(t), n_2(t), \ldots, n_L(t)$ are independent and have identical power spectral density $N_0/2$. Assume that the knowledge of the attenuation a_i is available, the sample of the ith matched filter is then weighted by a_i. Find the output signal-to-noise ratio of the sum signal assuming the signal energy is E.
12. Consider a PSK demodulator using a local reference carrier that is offset in phase with respect to the received signal by θ. Determine the bit error probability.
13. Consider a PSK demodulator with a sample timing error ε, that is, the sampling time for the ith bit is $t = iT_b + \varepsilon$. Determine the bit error probability.
14. Consider a PSK demodulator using a local reference carrier that is offset in phase with respect to the received signal by θ, and with a sample timing error ε, that is, the sampling time for the ith bit is $t = iT_b + \varepsilon$. Determine the bit error probability.
15. Consider the carrier recovery circuit in Figure 7.89. Show that the carrier of a PSK signal $s(t)$ can be reproduced at the output but it has a phase ambiguity of π radians. This means that the recovered carrier has a phase θ (modulo π). This might result in inverted data at the detector output. Suggest a method to correct this problem without using differential encoding.
16. A PSK signal with bit rate $1/T_b = 19.6$ kbps is demodulated to the baseband signal, which is a random sequence of antipodal signals. Use the circuit in Figure 7.90 to

Figure 7.89 PSK carrier recovery circuit.

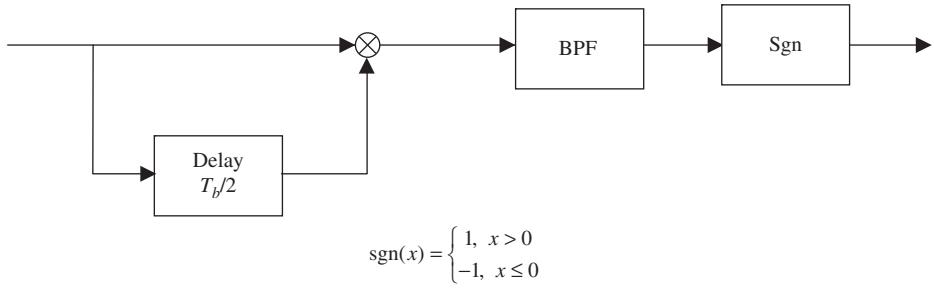

Figure 7.90 Half-bit delay timing recovery circuit for PSK signal.

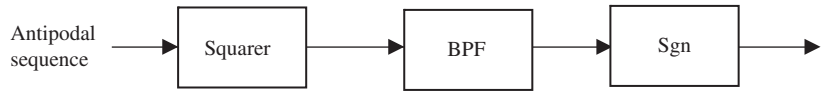

Figure 7.91 Squaring timing recovery circuit for PSK signal.

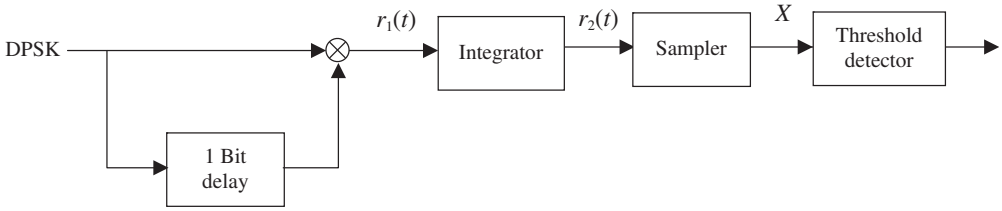

Figure 7.92 DPSK suboptimum demodulator.

recover the data clock signal from the antipodal signal sequence via simulation. It should be a periodic waveform with period T_b. The bandpass filter (BPF) should have a center frequency equal to $1/T_b$ and a bandwidth $B \ll 1/T_b$.

17. Consider a squaring timing recovery circuit for PSK signal shown in Figure 7.91. The PSK signal is first demodulated to baseband to produce an antipodal signal sequence. The data clock is recovered by using a squarer. Let the antipodal pulse shape be denoted as $p(t)$ and its Fourier transform be $P(f)$. Using the Poisson sum formula given by $\sum_k p(t - kT_b) = T_b^{-1} \sum_l P(l/T_b) \exp(j2\pi lt/T_b)$, show that a period signal with period T_b can be produced at the output. The sgn-function is given in Problem 16.
18. Consider the suboptimum demodulator of a DPSK signal shown in Figure 7.92.
    (a) Find the signal $r_1(t)$ and $r_2(t)$ when noise is absent.
    (b) Determine the detection threshold and decode the data bits for the following received differentially encoded bit sequence 0110001.
    (c) Assume the case of small noise, derive the approximate bit error probability.
19. A direct detection optical receiver operates at an input power level of -30 dBm. The noise spectral density is 10^{-16} mA^2/Hz. The photo detector's responsitivity is 0.5 and $\bar{r}_e = ⅓$. It is desired to achieve a bit error probability of at least 10^{-8}, determine the maximum bit rate.
20. Prove that if $s_1(t)$ and $s_2(t)$ are orthogonal baseband signals with identical absolute bandwidth B, then $s_1(t)\cos 2\pi f_c t$ and $s_2(t)\cos 2\pi f_c t$ are orthogonal signals as well, provided that $f_c > B$. Give an example for which the statement fails when $f_c < B$.
21. Consider an FSK signal employing a raised-cosine pulse shape with a roll-off factor β. The bit rate is $R_b = 1/T_b$. Determine the minimum frequency spacing for strict orthogonality.
22. Consider a noncoherent orthogonal FSK demodulator employing noncoherent correlators. The received signal is $s(t) = \sqrt{2/T_b}\cos[2\pi(f_1 + \Delta f)t + \theta]$. The frequency error is $\Delta f = 1/8T_b$ and the phase is $\theta = \pi/4$. Ignoring the high-frequency terms, find the output sample of the noncoherent correlator of the signal branch. Find the power loss relative to the case of no frequency error. Assume that f_i, i = 1, 2 are integer multiples of the bit rate and noise is negligible.

23. Consider the set of biorthogonal signals $\left\{\{s_i(t)\}_{i=1}^{M/2}, \{-s_i(t)\}_{i=1}^{M/2}\right\}$, where $\{s_i(t)\}_{i=1}^{M/2}$ is the set of $M/2$ orthogonal signals.
    (a) Design the demodulator using $M/2$ correlators, $M/2$ sign functions, and a maximum detector.
    (b) Derive the union bound for the symbol error probability.
24. The null-to-null bandwidth of PSK is $2/T_{b,PSK}$ and that of FSK is $3/T_{b,FSK}$ when the squared pulse shape is used. Consider two communication systems employing PSK and FSK with coherent detection. Both systems have identical bandwidth which is taken to be the null-to-null bandwidth of their signals. This implies that FSK would have to transmit at a lower rate than PSK.
    (a) If the bit rate of PSK is $R_{b,PSK}$ what would be the bit rate of FSK.
    (b) Assume that both systems receive signals with the same power P. What would be the bit error probability of each system in terms of P and $T_{b,PSK}$?
    (c) Both systems are required to have identical bit error probability, how much more (or less) power does FSK need?
25. The null-to-null bandwidth of PSK is $2/T_{b,PSK}$ and that of MSK is $1.5/T_{b,MSK}$ when the squared pulse shape is used. Consider two communication systems employing PSK and precoded MSK with coherent detection. Both systems have identical bandwidth which is taken to be the null-to-null bandwidth of their signals.
    (a) If the bit rate of PSK is $R_{b,PSK}$ what would be the bit rate of MSK.
    (b) Assume that both systems receive signals with the same power P. What would be the bit error probability of each system in terms of P and $T_{b,PSK}$?
    (c) Both systems are now required to have identical bit error probability, how much more (or less) power does MSK need?
26. Find the I-data and Q-data of MSK for the input bit sequence 110011001.
27. Consider a PSK receiver with the following parameters: system signal-to-noise ratio SNR = 7 dB, bit rate = 400 kbps, noise bandwidth = 500 kHz, system noise temperature = 500 K. What is the received power? Calculate the bit error probability.
28. Consider a PSK system where the a-priori probabilities of the transmitted bits are $\Pr(1) = q$ and $\Pr(0) = 1 - q$. Derive the bit error probability.
29. Perform the demodulation of DPSK given the phase sequence $(2\pi, 2\pi, \pi, 2\pi, 2\pi, 3\pi, 3\pi)$.
30. Consider a PSK signal with the squared pulse shape of unit amplitude and duration T_b, and carrier frequency $f_c - 1/4T_b$. This PSK signal is passed through a bandpass filter transfer function

$$H(f) = \sin[\pi(f - f_c)T_b - \pi/4]/[\pi(f - f_c)T_b - \pi/4] + \sin[\pi(f + f_c)T_b + \pi/4]/[\pi(f + f_c)T_b + \pi/4]$$

    Show that the output of the filter is indeed an MSK signal (serial MSK).
31. The two-path or IQ demodulator makes a decision on the two-dimensional vector $\boldsymbol{X} = \boldsymbol{s}_i + \boldsymbol{N}$. The symbol vector $\boldsymbol{s}_i = [s_{i1} \quad s_{i1}]^t$ can be mapped to the complex symbol $s_i = s_{i1} + js_{i2}$. The norm $\|\boldsymbol{s}_i\|$ is identical to the magnitude $|s_i|$. Design an equivalent complex demodulator using the complex reference carrier $e^{-j2\pi f_c t}$.

Figure 7.93 MPSK carrier recovery circuit.

32. Consider an I-Q demodulator with the received signal given by

$$s(t) = s_{i1}\sqrt{\frac{2}{T_s}}\cos 2\pi f_c t - s_{i2}\sqrt{\frac{2}{T_s}}\sin 2\pi f_c t, \quad 0 \le 0 \le T_s$$

$$x_1(t) = \sqrt{\frac{2}{T_s}}\cos(2\pi f_c t + \theta), \qquad x_2(t) = -\sqrt{\frac{2}{T_s}}\sin(2\pi f_c t + \theta)$$

The carrier frequency f_c is an integer multiple of the symbol rate $1/T_s$. The symbol vector is $\boldsymbol{s}_i = [s_{i1} \;\; s_{i2}]^t$. The angle θ is the phase error between the local carrier and the received signal. Write the expression for decision variable vector $\boldsymbol{X} = \mathbf{T}\mathbf{s}_i + \boldsymbol{N}$ by identifying the 2×2 matrix $\mathbf{T}$ and the noise vector $\boldsymbol{N}$ assuming the input noise is $n(t)$.

33. Derive the bit error probability of QPSK signal when the reference carrier has a phase error θ with respect to the received signal.
34. Perform the differential encoding and decoding for OQPSK.
35. To resolve the four-fold phase ambiguity in QPSK without resorting to differential encoding, a known unique word can be transmitted in the packet header and used to rotate the signal space. Design a logic circuit to accomplish this task based upon the detection of the unique word.
36. Consider the carrier recovery circuit for MPSK shown in Figure 7.93. Show that the recovered carrier has an M-fold phase ambiguity, that is, it cannot distinguish a rotation of the signal space by π/M radians.
37. Consider the noncoherent demodulation of a $\pi/4$-DQPSK signal. The received signal-to-noise ratio is $S/N = (E_b/N_0)(R_b/B)$, where B is the noise bandwidth and R_b is the bit rate. Given S/N (dB) = 13 dB and $B = 30$ kHz, what is the maximum bit rate that can be supported so that $P_b < 10^{-4}$?
38. Given the rectangular 16QAM find the error probability that signal vector representing symbol 1000 moves into regions occupied by symbols 1100 and 1101 in terms of the minimum Euclidean distance and noise variance σ^2. The I- and Q-values are normalized to $\sqrt{E/2}$, in Figure 7.94, where E is the smallest symbol energy. For example, we have $\boldsymbol{s_i} = [3\sqrt{E}/\sqrt{2} \; -3\sqrt{E}/\sqrt{2}]^t$ for symbol 1000. The minimum Euclidean distance of this signal space is $d_{min} = \sqrt{2E}$.
39. Consider two communication systems employing 16PSK and 16QAM with coherent detection. Assume that both systems have the same received power P. Both systems are required to have approximately the same bit error probability of 10^{-5}, what would be the bit rate of 16PSK relative to that of 16QAM?
40. Consider a 16QAM receiver with the following parameters: system signal-to-noise ratio SNR = 17 dB, bit rate = 24 Mbps, noise bandwidth = 30 MHz, system noise temperature = 500 K. What is the received power? Calculate the bit error probability.
41. Does the carrier recovery circuit in Figure 7.93 for MPSK with $M = 4$ apply to any rectangular QAM?

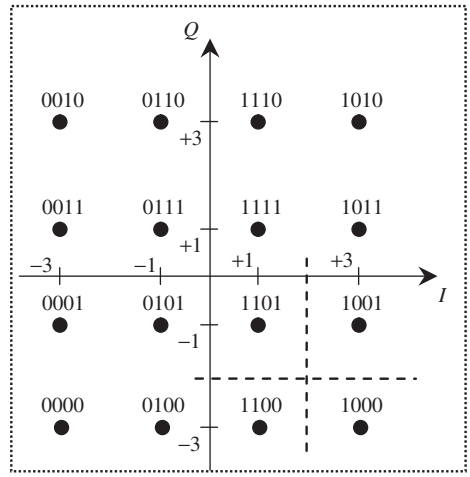

Figure 7.94 16QAM signal space.

42. Using (7.322) shows that $\lim_{M\to\infty} P_b = 0$ if $E_b/N_0 > 2\ln 2$ for orthogonal signals.
43. Consider coherent 64CSK and 64QAM. If the bit rate of 64CSK is R_b, what would be the bit rate of 64QAM, assuming that both systems receive the same power and are required to have identical bit error probability of 10^{-6}?
44. A channel produces a random received signal-to-noise ratio γ. It is desired to keep the received signal-to-noise ratio constant at the value *SNR*. Let the transmit power $P(\gamma)$ vary with γ subject to the average power constraint $\overline{P}$, that is, $\int_0^\infty P(\gamma) f_\Gamma(\gamma)\,\mathrm{d}\gamma \le \overline{P}$, where $f_\Gamma(\gamma)$ is the density of γ. The power adaptation strategy is given as $P(\gamma)/\bar{P} = SNR/\gamma$. Find a closed-form expression for *SNR*. If γ is uniformly distributed between 5 and 50, find the value of *SNR*. Based solely on the minimum Euclidean distances, if 64FSK is used at minimum γ, what modulation technique should be used for maximum γ with the least modification to the transmitter and receiver?
45. What are the noiseless spectral efficiencies of CSK assuming raised-cosine pulse shapes with roll-off factors $\beta = 0$ and 0.5? At these spectral efficiencies, what are the required E_b/N_0 dictated by the Shannon channel capacity for reliable transmission? Compare the result with DPSK and draw the conclusions.
46. Consider OFDM with 16 QPSK-subcarriers and a single carrier 256QAM.
    (a) For the same bit rate and assuming squared pulse shape, compare their bandwidths.
    (b) For the same received power, and assuming that the bit error probability of OFDM is twice that of 256QAM, compare the bit rates.
47. Consider OFDM-1 with 64 QPSK-subcarriers and OFDM-2 with 16 64QAM-subcarriers. Both have the same received power
    (a) Determine the subcarrier bit rate of OFDM-1 in terms of the subcarrier bit rate of OFDM-2 for the same subcarrier bit error probability of 10^{-4}.

(b) Determine the bit rate of OFDM-1in term of the bit rate of OFDM-2.
(c) Determine the bandwidth of OFDM-1in term of the bandwidth of OFDM-2.

48. Consider a CROSS-8QAM, which can be obtained from the rectangular 16QAM by retaining four inner signal points and four corner signal points and deleting eight edge signal points.
(a) Find the number of nearest neighbors for the inner signal point and the corner signal point and then the average number of nearest neighbors for the signal space.
(b) Derive the bit error probability using the union bound.
(c) For the same bit error probability of 10^{-5} find the required received power of CROSS-8QAM relative to that of 8PSK.

49. Derive the coding gains for convolutional encoded PSK with hard decoding and soft decoding at low bit error probability. Compare the coding gains. (Hint: use the first term of the union bound and the following Chernoff bound $Q(x) \leq e^{-x^2/2}$. These coding gains are referred to as *asymptotic coding gains*.)

50. Derive the bit error probability for a block code with hard decoding and soft decoding, assuming the block code minimum Hamming distance is d_{min} and the number of code words of weight d is A_d. Derive the coding gains for hard decoding and soft decoding at low bit error probability; assume that the modulation is PSK. Compare the coding gains. (Hint: use the first term of the union bound of the bit error probability and the following Chernoff bound $Q(x) \leq e^{-x^2/2}$. These coding gains are referred to as *asymptotic coding gains*.)

51. Consider a PSK signal encoded by a rate ⅓ convolutional code with constraint length $K = 4$. Assuming that soft decision decoding is employed, what is the required signal-to-noise ratio per bit at $P_b = 10^{-6}$? What is the coding gain at this bit error probability?

52. Consider a TCM-8PAM obtained via set partitioning. Assume that the asymptotic coding gain for this TCM is 4.6 dB; calculate the Euclidean free distance of the encoder.

53. Consider the TCM-8PSK shown in Figure 6.53. Assume that a convolutional code with rate ⅔ is employed and that the Euclidean free distance is $d_{free}^2 = d_0^2 + 2d_1^2$, where $d_0 = \sqrt{(2-\sqrt{2})E_s}$ and $d_1 = \sqrt{2E_s}$. Calculate the asymptotic coding gain for TCM-8PSK relative to uncoded QPSK.

54. Consider the TCM-16QAM shown in Figure 6.55. Assume that the asymptotic coding gain for the TCM-16QAM is 6 dB relative to uncoded 8PSK. Calculate the Euclidean free distance of the TCM.

55. Design a TCM-64QAM with separate I and Q encoding and decoding.

56. Perform the Viterbi algorithm for Ungerboeck TCM-QPSK using the trellis in Figure 4.13 for the received vector $\boldsymbol{r} = (0.7, -0.5, 0.8, -0.7, -0.8, 1, -0.9, 0.6, 1, -0.5)$ normalized to $\sqrt{rE_s/2}$, where r is the code rate.

57. Perform the Viterbi algorithm for Ungerboeck TCM-8PSK using the trellis in Figure 7.87 for the received vector $\boldsymbol{r} = (-0.6, 0.2, -0.3, -0.7, 0.9, 0.5, 0.3, 0.8, 0.4, 1)$ normalized to $\sqrt{rE_s}$, where r is the code rate.

Further reading

Simon *et al*. [1] is recommended for further study of additional modulation and demodulation techniques. For readers who are interested in optical communications we recommend [2]. References [9–11, 13–17] provide a detailed description of OFDM.

Bibliography

1. M. K. Simon, S. M. Hinedi, and W. C. Lindsey, *Digital Communication Techniques. Signal Design and Detection*, Englewood Cliffs, NJ: Prentice-Hall, 1995.
2. G. Keiser, *Optical Fiber Communications*, 4th edition, New York: McGraw-Hill, 2007.
3. K. Murota and K. Hirade, "GMSK modulation for digital mobile radio telephony," *IEEE Trans. Commun*., Vol. **29**, No.7, pp. 1044–1050, 1981.
4. T. S. Rappaport, *Wireless Communications*, 2nd edition, Upper Saddle River, NJ: Prentice-Hall, 2002.
5. R. E. Ziemer and R. L. Peterson, *Introduction to Digital Communication*, 2nd edition, Upper Saddle River, NJ: Prentice-Hall, 2001.
6. S. Haykin, *Communication Systems*, 3rd edition, Chichester: John Wiley & Sons, 1994.
7. F. Xiong, *Digital Modulation Techniques*, London: Artech House, 2000.
8. J. G. Proakis and M. Salehi, *Digital Communications*, 5th edition, New York: McGraw-Hill, 2008.
9. IEEE Standards 802.11a, 1999.
10. IEEE Standards 802.11g, 2003.
11. M. Segkos, "Advanced techniques to improve the performance of OFDM Wireless LAN," unpublished Masters thesis, Naval Postgraduate School, Monterey, CA, June 2004.
12. G. C. Clark, Jr. and J. B. Cain, *Error-Correction Coding for Digital Communications*, New York: Plenum Press, 1981.
13. T. Pollet, M. van Bladel and M. Moeneclaey, "BER sensitivity of OFDM systems to carrier frequency offset and Wiener phase noise," *IEEE Trans. Commun.*, Vol. **43**, No. 2, Part 3, pp. 191–193, 1995.
14. P. H. Moose, "A technique for orthogonal frequency division multiplexing frequency offset correction," *IEEE Trans. Commun.*, Vol. **42**, No. 10, pp. 2908–2914, 1994.
15. J.-J. Van de Beek, M. Sandell, and P. O. Börjesson, "ML estimation of time and frequency offset in OFDM systems," *IEEE Trans. Signal Processing*, Vol. **45**, No. 7, pp. 1800–1805, 1997.
16. M. Speth, D. Daecke, and H. Meyr, "Minimum overhead burst synchronization for OFDM based broadband transmission," *IEEE Global Telecommunications Conference*, Vol. **5**, pp. 2777–2782, 1998.

17. J.-J. van de Beek, O. Edfors, M. Sandell, S. K. Wilson, and O. Borjesson, "On channel estimation in OFDM systems," *IEEE Proc. VTC-1995*, Vol. **2**, pp. 815–819, 1995.
18. J. B. Anderson, T. Aulin, and C. E. Sundberg, *Digital Phase Modulation*, London: Plenum Press, 1986.
19. J. R. Barry, E. A. Lee, and D. G. Messerschmitt, *Digital Communication*, 3rd edition, Boston, MA: Kluwer Academic Publishers, 2004.
20. S. Benedetto, E. Biglieri, and V. Castellani, *Digital Transmission Theory*, Englewood Cliffs, NJ: Prentice-Hall, 1987.
21. R. E. Blahut, *Digital Transmission of Information*, London: Addison-Wesley, 1990.
22. R. G. Gallager, *Principles of Digital Communication*, Cambridge: Cambridge University Press, 2008.
23. R. D. Gitlin, J. F. Hayes, and S. B. Weinstein, *Data Communications Principles*, London: Plenum Press, 1992.
24. A. Lapidoth, *A Foundation in Digital Communication*, Cambridge: Cambridge University Press, 2009.
25. S. Lin and D. J. Costello, Jr., *Error Control Coding*, 2nd edition. Pearson Education, 2004.
26. U. Madhow, *Fundamentals of Digital Communication*, Cambridge: Cambridge University Press, 2008.
27. M. B. Pursley, *Introduction to Digital Communications*, Upper Saddle River, NJ: Pearson Prentice-Hall, 2005.
28. J. I. Marcum, "Statistical theory of target detection by pulsed radar," *IEEE Trans. Inf. Theory*, Vol. **6**, No. 2, pp. 59–67, 1960.
29. B. Sklar, *Digital Communications. Fundamentals and Applications*, 2nd edition, Upper Saddle River, NJ: Prentice-Hall, 2001.
30. A. J. Viterbi and J. K. Omura, *Principles of Digital Communication and Coding*, New York: McGraw-Hill, 1979.
31. S. G. Wilson, *Digital Modulation and Coding*, Englewood Cliffs, NJ: Prentice-Hall, 1996.
32. J. M. Wozencraft and I. M. Jacobs, *Principles of Communication Engineering*, New York: Wiley, 1965; Waveland Press, 1990.

8 Spread spectrum

Introduction

A *spread spectrum* modulated signal has a *bandwidth* much larger than the bandwidth of its *narrowband* counterpart for transmitting the message signal. For example, a spread spectrum PSK signal employed in the forward link of the 2G cellular standard IS-95 carrying a coded message signal of symbol rate 19.2 ksps has a bandwidth of 1.25 MHz. The narrowband PSK signal would only require a bandwidth of 19.53 kHz. This is an increase of bandwidth by a factor of 64. What is the reason behind the use of spread spectrum modulation? Historically, spread spectrum modulation originated from *military* applications. The purpose is to protect the received signal's integrity by reducing the effectiveness of a *jamming* signal. In order to jam a spread spectrum signal, the jamming signal must distribute its fixed transmitted power over a *larger* spread bandwidth. This would lower the magnitude of its *power spectral density* and correspondingly its jamming power in the *smaller* message bandwidth. There are basically two types of spread spectrum modulated signals: *direct sequence* (DS) and *frequency hop* (FH).

8.1 Direct sequence modulation

In direct sequence modulation the data 0s and 1s of *bit rate* $R_b = 1/T_b$ are used to modulate a *periodic pseudo-noise* (PN) *sequence* of N chip 0s and 1s. The *chip rate* is $R_c = 1/T_c = NR_b$, and the sequence period is the same as the bit time. Thus, when the data bit is 0 the PN sequence is transmitted, and when the data bit is 1 the *complement* PN sequence is transmitted. This operation can be implemented by repeating a data bit N times, then modulo-2 adding them to the N chips of the PN sequence. The output of the modulo-2 adder is fed to a PSK modulator to produce a *direct sequence–phase shift keying* (DS-PSK) spread spectrum signal. Since the chip rate is N times the bit rate, the DS-PSK bandwidth is N times the bandwidth of the corresponding narrowband PSK signal. The *spread factor* N is often called the *processing gain* of the spread spectrum signal. Since the processing gain is modulation and demodulation dependent and is also dependent on the type of jamming signal, it is usually a function of N. We will distinguish the two terminologies as we proceed. With respect to jamming, a direct sequence spread spectrum signal with a spread factor N can reduce the jamming variance (power) in its decision sample at the receiver by its processing gain. Figure 8.1 shows the block diagram of a DS-PSK modulator. In practice the PN

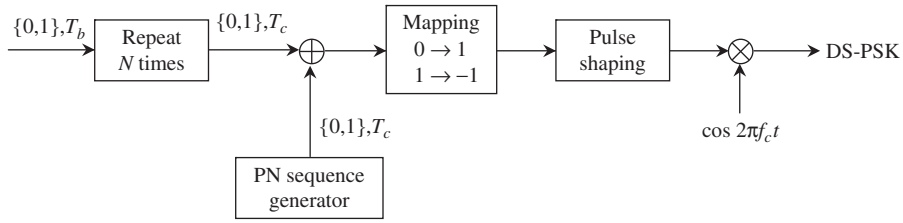

Figure 8.1 Direct sequence–phase shift keying.

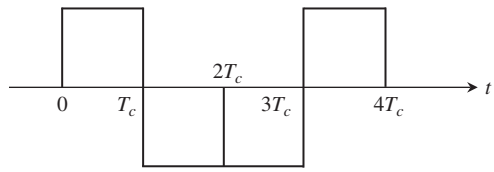

Figure 8.2 The complement PN sequence of four bits.

sequence period can be selected to be an *integer multiple* of the bit duration with the chip rate remaining as $R_c = 1/T_c = NR_b$. Thus, there are still N chips per bit and the spread factor remains N.

Example 8.1 Generating a DS-PSK signal

Consider the PN sequence $\boldsymbol{c} = (1001)$ and the data bit 1, which is repeated four times to provide the data sequence $\boldsymbol{d} = (1111)$. We write a sequence as a *vector* to facilitate the notation. The modulo-2 addition of these two sequences is $\boldsymbol{c} + \boldsymbol{d} = \bar{\boldsymbol{c}} = (0110)$. Applying the mapping of $0 \rightarrow 1$ *and* $1 \rightarrow -1$ to $\bar{\boldsymbol{c}}$ we obtain the sequence $\bar{\boldsymbol{c}} = (1 - 1 - 11)$. The baseband waveform of this sequence using the squared pulse shape is shown in Figure 8.2.

Equivalently, one can generate the sequence $\bar{\boldsymbol{c}}$ via multiplication instead of modulo-2 addition. Using the above mapping on the two sequences $\boldsymbol{c}$ and $\boldsymbol{d}$ we get the corresponding two sequences $\boldsymbol{c} = (-1\ 1\ 1 - 1)$ and $\bar{\boldsymbol{d}} = (-1 - 1 - 1 - 1)$. Multiplying the corresponding elements of the two sequences we get $\bar{\boldsymbol{c}}$. Figure 8.3 shows the alternative DS-PSK modulator.

■

The main feature of direct sequence spread spectrum is the PN sequence. There are many types of PN sequences that can be used in practice, but the most important one is the *maximal sequences* (also called *maximal-length sequences*) or for short, *m-sequences.* They can be generated by *linear feedback shift-registers* (LFSR). When the shift register has n stages the m-sequence has a period of $N = 2^n - 1$ chips. In practice a zero can be appended at the end of the m-sequence to produce an augmented PN sequence of period 2^n chips. An m-sequence can be generated by a *monic binary irreducible primitive polynomial* $h(x)$:

$$h(x) = 1 + h_1 x + h_2 x^2 + \cdots + h_{n-1} x^{n-1} + x^n, h_i \in \{0, 1\} \tag{8.1}$$

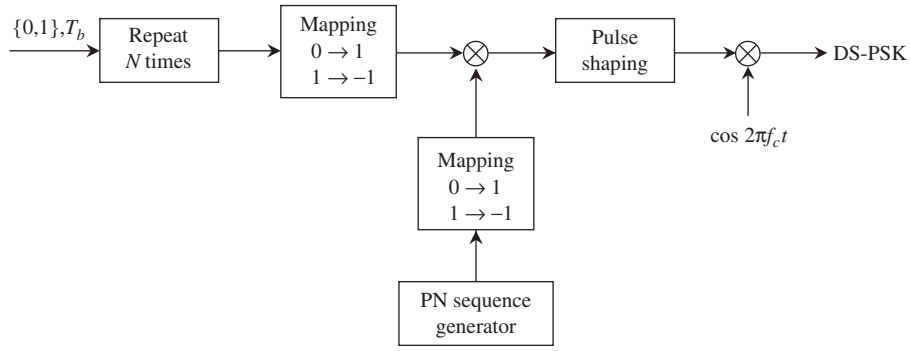

Figure 8.3 Alternative direct sequence–phase shift keying.

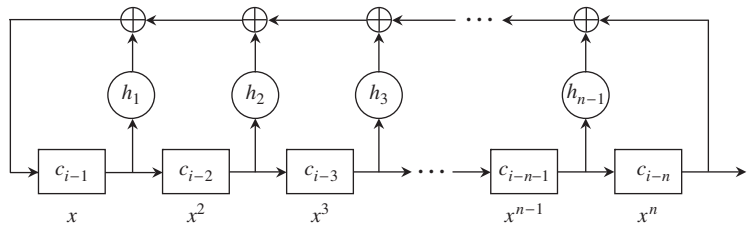

Figure 8.4 Linear feedback shift-register.

The polynomial coefficients, h_i, are the feedback *tap coefficients* of the LFSR shown in Figure 8.4. The m-sequence $\{c_i\}$ generated by this LFSR is given by the following equation via *modulo-2 addition*:

$$c_i = h_1 c_{i-1} + h_2 c_{i-2} + \cdots + h_{n-1} c_{i-n+1} + c_{i-n} \tag{8.2}$$

An m-sequence has 2^{n-1} ones and $2^{n-1} - 1$ zeros. The *discrete periodic autocorrelation* of an m-sequence is a *two-valued* function and is given by the *number of agreements* minus *disagreements* for the overall length of the sequence and a shifted replica of itself. These two values are $R_m(i) = 2^n - 1$ *for* $i = 0$ *and* $R_m(i) = -1$ *for* $i \neq 0$. The m-sequence has the smallest side lobe magnitude of any binary sequence with the same period. Applying the mapping of $0 \rightarrow 1$ *and* $1 \rightarrow -1$ to an m-sequence we obtain the same *discrete periodic autocorrelation*, that is,

$$R_m(i) = \sum_{k=0}^{2^n-1} c_k c_{k+i} = \begin{cases} 2^n - 1, & i = 0 \\ -1, & i \neq 0 \end{cases} \tag{8.3}$$

Figure 8.5 shows the autocorrelation function of a periodic m-sequence when a unit amplitude squared pulse of duration T_c is employed as the pulse shape of a chip.

Example 8.2 An m-sequence of period 7

Consider the m-sequence generated by the monic binary irreducible primitive polynomial $h(x) = 1 + x + x^3$ using a three-stage LFSR as shown in Figure 8.6. The period is 7. The

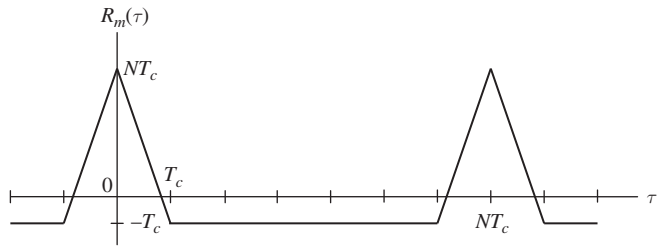

Figure 8.5 Autocorrelation function of an m-sequence, $N = 2^n - 1$.

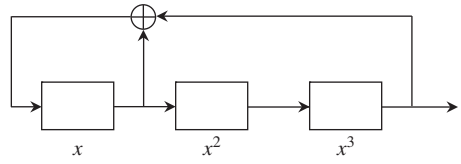

Figure 8.6 Generator of an m-sequence of period 7.

m-sequence is 1 1 1 0 1 0 0. It has been established that the number of agreements minus the number of disagreements for this m-sequence and any of the circular shifted replica of itself is -1.

■

Phase shift keying is not the only *carrier modulation* for direct sequence spread spectrum. The reverse link of IS-95 employs *code shift keying* (CSK) as a carrier modulation for direct sequence spread spectrum. In direct sequence–code shift keying (DS-CSK), $k = \log_2 M$ bits form a symbol. Each of the M symbols is assigned a distinct Walsh sequence from the set of M Walsh sequences that can be obtained from the rows of the Hadamard matrix in (2.50). The elements of the Walsh sequences are 1 or -1. To employ modulo-2 addition instead of multiplication, the mapping of $1 \rightarrow 0$ *and* $-1 \rightarrow 1$ can be applied to the M Walsh sequences to obtain the equivalent M Walsh sequences whose elements are in $\{0,1\}$. Let R_b be the bit rate, then the *symbol rate* R_s is R_b/k. Consequently, the Walsh chip rate R_w is MR_s. The PN sequence chip rate R_c is selected to be an integer multiple of the Walsh chip rate R_w, that is, $R_c = NR_w$, where N is an integer greater than or equal to 1. Thus, expressing the symbol rate in terms of the PN chip rate we have $R_c = NMR_s$. Hence, the *spreading factor* of DS-CSK is NM. The number of PN chips per Walsh chip is N. The PN sequence period can be an integer multiple of the Walsh period (the symbol period). To generate the DS-CSK signal, the Walsh chips of 0s or 1s are first repeated N times. Then, they are modulo-2 added to the PN chips of 0s or 1s. The mapping of $0 \rightarrow 1$ *and* $1 \rightarrow -1$ is then applied to the resulting spread Walsh symbol. A pulse shape assigned to the chip then modulates a carrier. Figure 8.7 illustrates the generation of a DS-CSK signal.

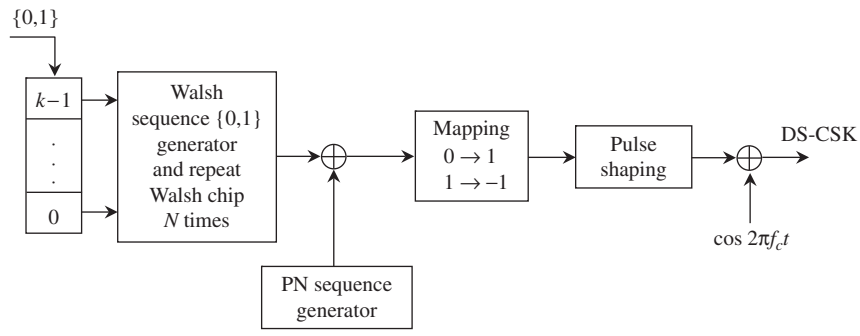

Figure 8.7 Direct sequence–code shift keying.

Orthogonal covering

Orthogonal covering or *code division multiplexing* (CDM) is a technique that employs orthogonal functions to multiplex different user bit streams onto one carrier without incurring interference between user data. Orthogonal Walsh functions are used in practice for this technique, such as in the forward link of IS-95. The concept is similar to the use of two orthogonal carriers $\cos 2\pi f_c t$ and $\sin 2\pi f_c t$ in I-Q modulation techniques. These two orthogonal carriers coexist in the same channel without mutual interference. Orthogonal covering is also employed by DS systems such as the 3G cellular systems, namely, WCDMA or CDMA 2000. Each user bit modulates an assigned Walsh sequence (symbol) of 0s and 1s and of chip rate $R_w = MR_b$, where R_b is the bit rate. This is done by repeating the data bit M times and then modulo-2 adding the repeated bits to the Walsh chips. A PN sequence of 0s and 1s of chip rate $R_c = N R_w$, where N is an integer greater than or equal to 1, is added (modulo-2) to the modulated Walsh chips, where each Walsh chip is repeated N times. The PN sequence is common to all users. The mapping of $0 \rightarrow 1$ *and* $1 \rightarrow -1$ is then applied to the resulting spread Walsh symbol. The multiplexing is then performed by algebraically adding the symbols of all users together. The set of M Walsh functions can accommodate up to M users. The sum of M user symbols serves as the baseband signal of a transmitted PSK signal with carrier $\cos 2\pi f_c t$. Figure 8.8 illustrates the basic concept of Walsh orthogonal covering.

To provide an effective method for *carrier phase synchronization* at the receiver, two different PN sequences can be employed for spreading in conjunction with I-Q or *quadrature modulation*. The I-channel employs a common spread PN_I sequence for all users and the Q-channel employs a common spread PN_Q sequence for all users as indicated in Figure 8.9. Note that the *same* sum of M user symbols is used in both I- and Q-channels. This technique is referred to as *quadrature spreading*.

Example 8.3 Orthogonal covering with 4-ary Walsh functions

Consider the 4-ary Walsh sequences which are rows of the Hadamard matrix obtained from the Hadamard matrix in (2.51) using the mapping $1 \rightarrow 0$ *and* $-1 \rightarrow 1$:

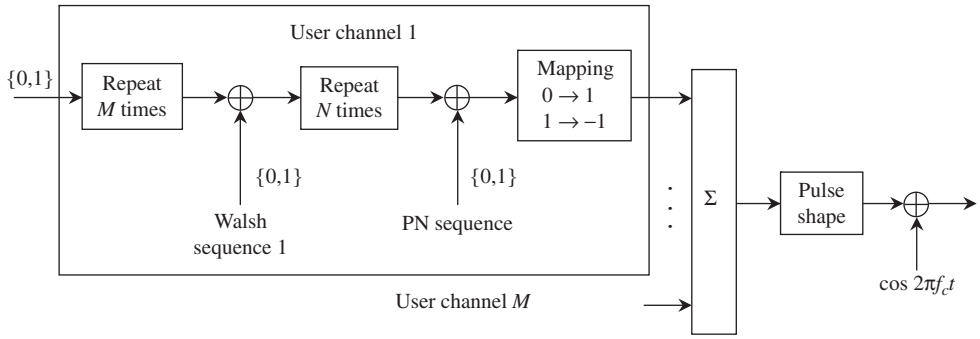

Figure 8.8 Walsh orthogonal covering.

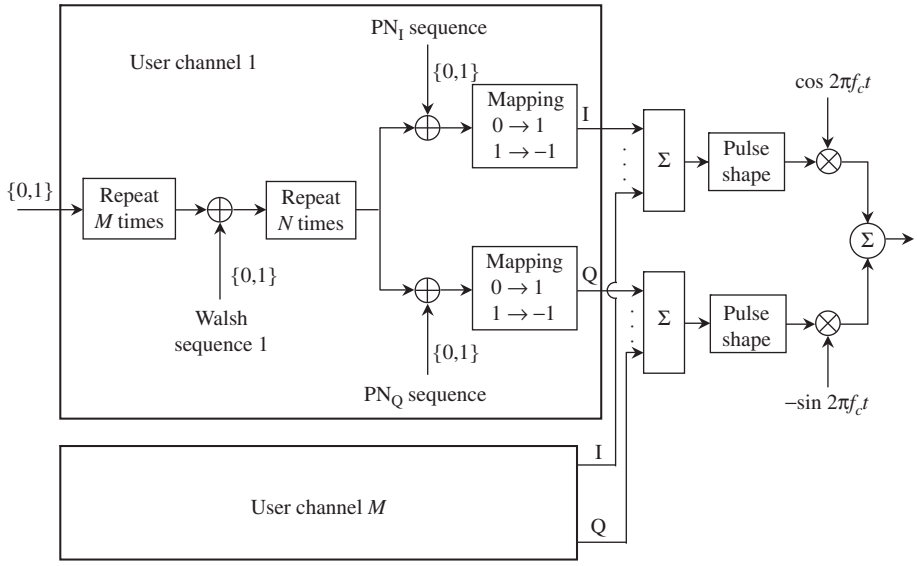

Figure 8.9 Quadrature orthogonal covering.

$$\mathbf{H}_4 = \begin{bmatrix} 0 & 0 & 0 & 0 \\ 0 & 1 & 0 & 1 \\ 0 & 0 & 1 & 1 \\ 0 & 1 & 1 & 0 \end{bmatrix} \tag{8.4}$$

They are given by

$$\boldsymbol{w}_1 = (0000), \boldsymbol{w}_2 = (0101), \boldsymbol{w}_3 = (0011), \boldsymbol{w}_4 = (0110) \tag{8.5}$$

These four Walsh sequences represent four orthogonal channels. Let the data sequences of these four channels be given by (each data bit is repeated four times)

$$\boldsymbol{d}_1 = (0000), \boldsymbol{d}_2 = (1111), \boldsymbol{d}_3 = (0000), \boldsymbol{d}_4 = (1111) \tag{8.6}$$

The resulting symbols in each channel are represented by the following sequences via *modulo-2 addition*:

$$\begin{aligned} \boldsymbol{s}_1 &= \boldsymbol{d}_1 + \boldsymbol{w}_1 = (0000), \boldsymbol{s}_2 = \boldsymbol{d}_2 + \boldsymbol{w}_2 = (1010), \\ \boldsymbol{s}_3 &= \boldsymbol{d}_3 + \boldsymbol{w}_3 = (0011), \boldsymbol{s}_4 = \boldsymbol{d}_4 + \boldsymbol{w}_4 = (1001) \end{aligned} \tag{8.7}$$

Orthogonal covering is achieved by applying the mapping $0 \rightarrow 1$ *and* $1 \rightarrow -1$ to the above symbols and then linearly combining them. We have, after the mapping,

$$\boldsymbol{s}_1 = (1\ 1\ 1\ 1), \boldsymbol{s}_2 = (-1\ \ 1 - 1\ \ 1), \boldsymbol{s}_3 = (1\ \ 1 - 1 - 1), \boldsymbol{s}_4 = (-1\ 1\ \ 1 - 1) \tag{8.8}$$

Note that scaling does not alter the orthogonality of the Walsh sequences (sequence and function are used interchangeably since a sequence becomes a function when a positive squared pulse shape of duration T_c is assigned to a +1 chip or binary 0 and a negative squared pulse shape of duration T_c is assigned to a -1 chip or binary 1), therefore, let us assume that we *scale* the symbol $\boldsymbol{s}_1$ by a *factor of two*, then, the orthogonal covering symbol is given by

$$\boldsymbol{s} = 2\boldsymbol{s}_1 + \boldsymbol{s}_2 + \boldsymbol{s}_3 + \boldsymbol{s}_4 = (1\ 5\ 1\ 1) \tag{8.9}$$

Figure 8.10 shows the waveform $s(t)$ of the orthogonal covering symbol $\boldsymbol{s}$ using the squared pulse shape.

Now let us consider a simple process to recover the data bit in each of the four channels. Let $w_1(t),\ w_2(t),\ w_3(t),$ *and* $w_4(t)$ represent the Walsh functions whose corresponding sequences are $\boldsymbol{w}_1,\ \boldsymbol{w}_2,\ \boldsymbol{w}_3,$ *and* $\boldsymbol{w}_4$, respectively. Define the *normalized inner product* of the two sequences $\boldsymbol{s}$ and $\boldsymbol{w_i}$ with elements in $\{1, -1\}$ as follows (the mapping $0 \rightarrow 1$ *and* $1 \rightarrow -1$ must be applied to the binary Walsh sequences before calculating the inner products):

$$\langle \boldsymbol{s}, \boldsymbol{w}_i \rangle / 4 \ = \ \boldsymbol{s}\boldsymbol{w}_i^t / 4 \ = \ \frac{1}{4T_c} \int_0^{4T_c} s(t) w_i(t) \mathrm{d}t, \ i = 1, 2, 3, 4 \tag{8.10}$$

We now have the following results:

$$\langle \boldsymbol{s}, \boldsymbol{w}_1 \rangle / 4 \ = \ 2, \ \langle \boldsymbol{s}, \boldsymbol{w}_2 \rangle / 4 \ = \ -1, \ \langle \boldsymbol{s}, \boldsymbol{w}_3 \rangle / 4 \ = \ 1, \ \langle \boldsymbol{s}, \boldsymbol{w}_4 \rangle / 4 \ = \ -1 \tag{8.11}$$

Suppose we employ a threshold detector with the threshold set to zero, and for any inner product with a positive value we detect bit 0, and negative value bit 1. Then, for channel 1 we detect bit 0, for channel 2 bit 1, for channel 3 bit 0, and for channel 4 bit 1.

■

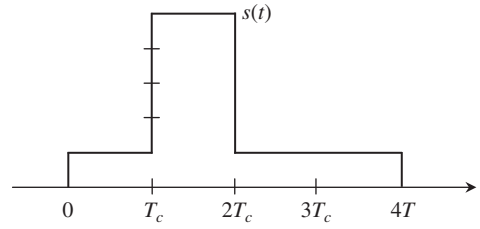

Figure 8.10 4-ary Walsh orthogonal covering waveform for four symbols in (8.6).

The above orthogonal covering technique applies to user channels with the same common rate, that is, a multiple of any user channel rate. Repetition of data bits must be used to bring the user channel rates to a common rate before orthogonal covering. Since the spread bandwidth is the same for all users as in WCDMA or CDMA 2000, *multi-rate* transmission from the base station requires different spread factors for different user channels. This necessitates the use of *variable-length orthogonal sequences* that can be constructed via a tree with Walsh sequences as its branches (rows of Hadamard matrix with binary elements):

1. Start at the root of the tree with binary 0.
2. Move to the next branch to create sequences with *twice* the length. The upper branch contains the *cascade of two parent node sequences*. The lower branch contains the *cascade of the parent node sequence and its complement.*
3. Variable-length orthogonal sequences *cannot come from the same branch of the tree*.

Figure 8.11 shows the tree for variable-length orthogonal sequences. All sequences that have the same length are in fact Walsh sequences but they do not appear in the order of the rows of the Hadamard matrix. For example, if we assign Walsh sequence (0101) for channel 1 (spread factor of 4), then Walsh sequences (01010101) and (01011010) cannot be used for any channel that requires a spread factor of 8. The remaining six Walsh sequences of length 8 are legitimate candidates for orthogonal covering.

Example 8.4 Orthogonal covering with 4-ary and 8-ary Walsh functions

Consider two user channels, one with bit rate $R_b = 1/T_b$, where T_b is the bit time (denoted as channel 1) and the other with bit rate $2R_b$ (denoted as channel 2). Note, *one bit of channel 1* covers the same duration as *two bits of channel 2*. Channel 1 employs a Walsh sequence $\boldsymbol{w}_1$ for spreading. This Walsh sequence has eight chips per bit; therefore, the chip rate is $8R_b$. Channel 2 employs a Walsh sequence $\boldsymbol{w}_2$ for spreading. This Walsh sequence has four chips per bit; therefore, the chip rate is also $8R_b$. Hence, the two channels meet the requirement of common chip rate and spread bandwidth. Let the data sequences of these two channels be given by (each data bit is repeated eight times for Channel 1 and four times for Channel 2)

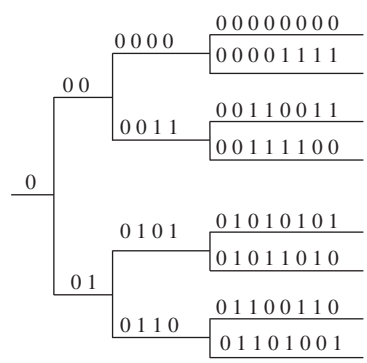

Figure 8.11 Variable length orthogonal sequences.

$$\boldsymbol{d}_1 = (11111111); \boldsymbol{d}_{2.0} = (0000) \text{ and } \boldsymbol{d}_{2,1} = (1111) \tag{8.12}$$

Furthermore, let the Walsh sequences be selected from Figure 8.11 as follows:

$$\boldsymbol{w}_1 = (00001111), \boldsymbol{w}_2 = (0101) \tag{8.13}$$

The resulting symbols in each channel are represented by the following sequences via *modulo-2 addition*:

$$\begin{aligned} &\boldsymbol{s}_1 = \boldsymbol{d}_1 + \boldsymbol{w}_1 = (11110000); \boldsymbol{s}_{2,0} = \boldsymbol{d}_{2,0} + \boldsymbol{w}_2 = (0101) \\ &\textit{and } \boldsymbol{s}_{2,1} = \boldsymbol{d}_{2,1} + \boldsymbol{w}_2 = (1010) \end{aligned} \tag{8.14}$$

Orthogonal covering is achieved by applying the mapping $0 \rightarrow 1$ *and* $1 \rightarrow -1$ to the above symbols and then linearly combining them. We have, after the mapping,

$$\boldsymbol{s}_1 = (-1-1-1-11111); \boldsymbol{s}_{2,0} = (1\ -1\ \ 1\ -1) \textit{ and } \boldsymbol{s}_{2,1} = (-1\ \ 1\ -1\ \ 1) \tag{8.15}$$

Let us assume that we scale the symbol $\boldsymbol{s}_1$ by a factor of two, then, the orthogonal covering symbol is given by

$$\boldsymbol{s} = 2\boldsymbol{s}_1 + (\boldsymbol{s}_{2,0}, \boldsymbol{s}_{2,1}) = (\boldsymbol{s}_{11}, \boldsymbol{s}_{12}) = (-1\ \ -3-1-3,\ 1\ \ 3\ \ 1\ \ 3) \tag{8.16}$$

We now calculate the following normalized inner products using the Walsh sequences $\boldsymbol{w}_1 = (1\ \ 1\ \ 1\ \ 1-1-1-1-1)$ and $\boldsymbol{w}_2 = (1-11-1)$:

$$\langle \boldsymbol{s}, \boldsymbol{w}_1 \rangle / 8 \ = \ -2; \ \langle \boldsymbol{s}_{11}, \boldsymbol{w}_2 \rangle / 4 \ = \ 1 \textit{ and } \ \langle \boldsymbol{s}_{12}, \boldsymbol{w}_2 \rangle / 4 \ = \ -1 \tag{8.17}$$

Suppose we again employ a threshold detector with the threshold set to zero, and for any inner product with a positive value we detect bit 0, and negative value bit 1. Then, for channel 1 we detect bit 1, and for channel 2 bits 0 and 1.

■

IS-95 forward link

The IS-95 forward link transmits user data and voice to the mobile station. The forward link has three types of channels: one *pilot* channel, one *sync* channel, seven *paging* channels, and 55 *traffic* channels. The transmitted symbol rate is held constant at 19.2 ksps, where *symbol* here refers to a *coded bit*. The *raw* bit rate before the application of overhead and error correction coding is no more than 14.4 kbps. The orthogonal covering is carried out by 64 Walsh sequences at a *chip rate* of 1.2288 Mcps. The *Walsh sequence period* is 64 chips. The *all-zeros Walsh sequence* is reserved explicitly for the pilot channel. The carrier modulation is the I-Q modulation, hence the spreading is carried out by two PN sequences. The I-channel and Q-channel PN sequences are two *m-sequences* specified by the following polynomials:

$$h_I(x) = 1 + x^5 + x^7 + x^8 + x^9 + x^{13} + x^{15} \tag{8.18}$$

$$h_Q(x) = 1 + x^3 + x^4 + x^5 + x^6 + x^{10} + x^{11} + x^{12} + x^{15} \tag{8.19}$$

These m-sequences can be generated by 15-stage LFSRs. Each sequence is lengthened by one chip added to a specific location in the sequence. Their period is $2^{15} = 32\,768$ chips. They are clocked at the same chip rate of 1.2288 Mcps as the Walsh sequence. The PN sequence period is 512 times the Walsh sequence period. Each base station is assigned a pair of PN sequences that is phase-offset from another base station's pair of PN sequences by exactly 64 chips. This yields a total 512 offsets of 64 chips, with one offset for each base station. The PN sequence spreading provides a processing gain against the co-channel forward links in adjacent cells.

The *pilot* channel is employed for *coherent demodulation* of all other channels at the mobile station. Since the *all-zeros Walsh sequence* (referred to as sequence 0; this is the first row of the 64 × 64 Hadamard matrix) does not alter the pilot bits (all zeros), the pilot bits can be recovered at the mobile station by *despreading* the PN sequences. Since no data modulation is present in the pilot channel, the acquisition of the quadrature PN sequences is fast. The pilot channel is shown in Figure 8.12.

The *sync* channel is employed by the mobile station in the cell of the base station to acquire initial time synchronization. The sync channel is spread by the *Walsh sequence 32* (this refers to the 33rd row of the 64 × 64 Hadamard matrix), which consists of 32 zeros followed by 32 ones. The acquisition of the pilot channel provides the PN despreading for the sync channel and hence all other channels. After that, this particular Walsh sequence then helps facilitate the sync channel acquisition. The information bit rate of the sync channel is 1.2 kbps. The information bits are encoded by a convolutional code of rate ½ and constraint length $K = 9$. The symbol coded rate is 2.4 ksps. Each coded symbol is then repeated twice before block interleaving to protect the symbols from possible burst errors occurring from deep fades in the mobile channel. Since the convolutional code can correct random errors but not burst errors, de-interleaving at the mobile station can break burst errors into random errors suitable for correction by the convolutional decoder. Each interleaved symbol is added (modulo-2) to the Walsh sequence 32 before being I-Q spread by the common I-channel and Q-channel PN sequences. The repetition of a symbol at a rate of 4.8 ksps for the modulo-2 addition to the Walsh sequence at a rate of 1.2288 Mcps is implicitly understood for paging and traffic channels as well. Figure 8.12 shows the generation of the sync channel without combining with other channels.

The *paging* channels carry all call set up information to the mobile station. The information bit rate is either 4.8 kbps or 9.6 kbps. The information bits are convolutional encoded as in the sync channel. The coded symbols are repeated to achieve a common coded symbol rate of 19.2 ksps. Block interleaving is employed to protect the data from channel burst errors. Data scrambling is applied to the output of the block interleaver for security. This is accomplished by adding (modulo-2) the interleaver output symbol with the binary value of the *long code* PN chip. This long code PN sequence is obtained from a long code operating at 1.2288 Mcps, where only the first chip of every 64 chips is used for data scrambling. In other words, the long code is decimated to 19.2 kcps by sampling every 64 chips. The long code is generated by the following polynomial:

$$\begin{aligned} h(x) = {} & 1 + x + x^2 + x^3 + x^5 + x^6 + x^7 + x^{10} + x^{16} + x^{17} \\ & + x^{18} + x^{19} + x^{21} + x^{22} + x^{25} + x^{26} + x^{27} + x^{31} + x^{33} + x^{35} + x^{42} \end{aligned} \tag{8.20}$$

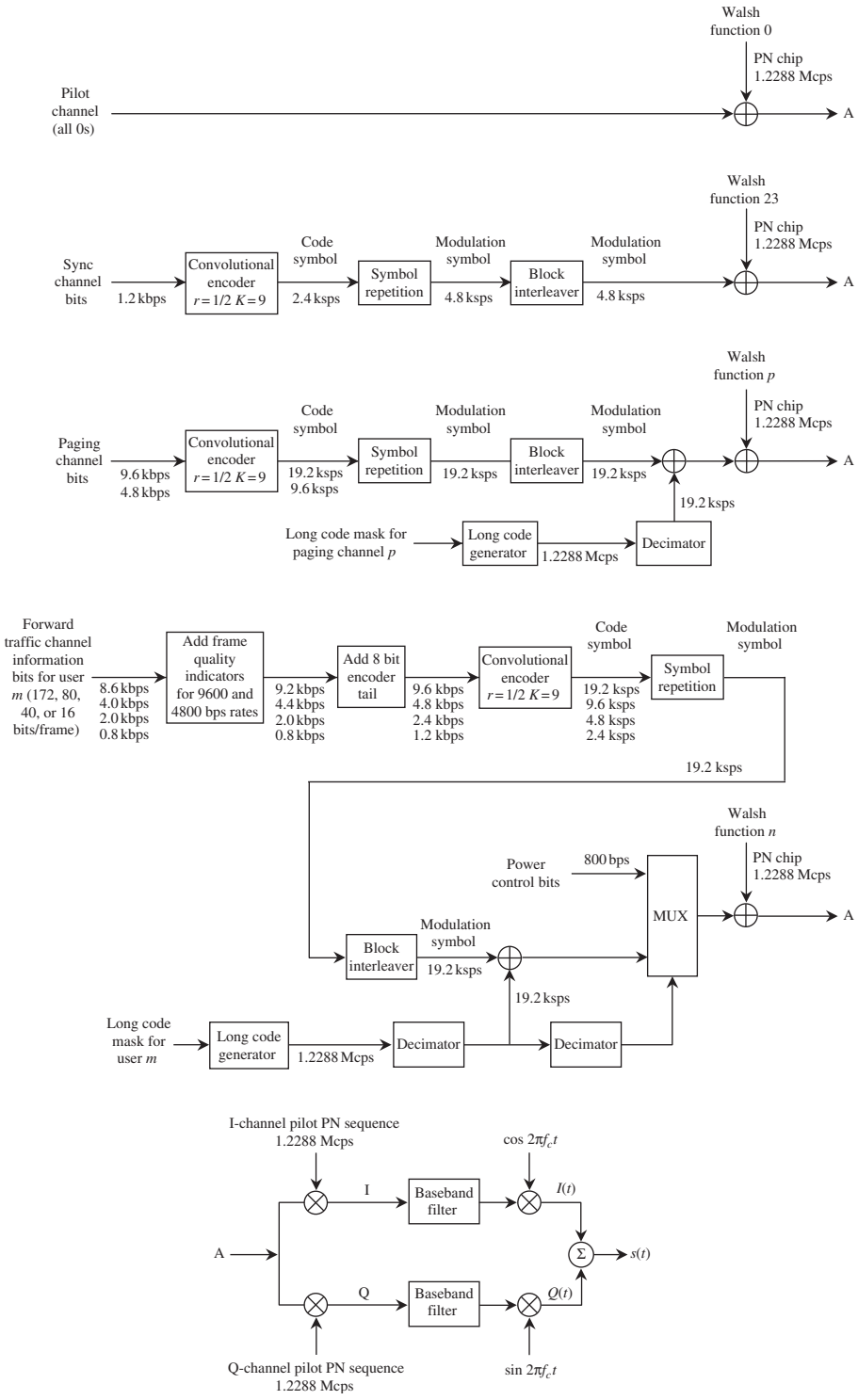

Figure 8.12 IS-95 forward link.

The long code is generated with a 42-stage LFSR. It has a period of $2^{42} - 1$ chips. The scrambled symbols are then spread by a designated Walsh sequence (the second to eighth rows of the 64×64 Hadamard matrix). Figure 8.12 shows the generation of the paging channel.

The *traffic* channel carries voice or data to the mobile user. Up to 55 traffic channels are available in each forward link. Some of the paging channels can be used for traffic channels. Figure 8.12 shows the generation of the traffic channel. Voice data are selected on a frame-by-frame (20 ms) basis. At 9.6 kbps (4.8 kbps) the frame contains 172 (80) *information bits* followed by 12 (8) *frame quality indicator bits* (*cyclic redundancy check* (CRC) error detection bits) and 8 encoder *tailing bits* used to reset the state of the convolutional encoder after each frame. At 2.4 kbps (1.2 kbps) the frame contains 40 (16) *information bits* followed by 8 encoder *tailing bits*. The information bits are convolutionally encoded and repeated to produce a common symbol rate at 19.2 kbps. Block interleaving is implemented for protection against burst errors. The interleaved code symbols are then scrambled by a long code PN sequence clocked at 19.2 kcps as in the paging channel to provide data privacy. The decimated long code PN sequence is further decimated to yield a clock signal at 800 Hz by sampling once every 24 chips. This clock is used by the *power control bits* at a rate of 800 bps to *puncture* the scrambled symbols. The power control bits are sent to the mobile station to control the mobile transmit power. This control process equalizes *the near-far effect*. The resulting symbol stream is spread by a designated Walsh sequence (the ninth to 32nd rows, and the 34th to 64th rows of the 64×64 Hadamard matrix). The above forward traffic channel is for Rate Set 1 (RS1), which is specified in the 2G standard IS-95A. A later version IS-95A specifies a Rate Set 2 (RS2) of 14.4, 7.2, 3.6, and 1.8 kbps. At 14.4 kbps (7.2 kbps) the frame contains 267 (125) *information bits* followed by 12 (10) *frame quality indicator bits* and 8 encoder *tailing bits*. At 3.6 kbps (1.8 kbps) the frame contains 55 (21) *information bits* followed by 8 (6) *frame quality indicator bits* and 8 encoder *tailing bits*. The convolutional code for RS2 is of rate ¾. It is obtained from the convolutional code of rate ½ in RS1 by puncturing (deleting) *two* output code symbols for every *six* output code symbols (which correspond to every *three* input code symbols). The 2.5G standard IS-95B can assign up to eight Walsh functions to a dedicated user for a maximum rate of 115.2 kbps (8×14.4 kbps), although in practice the rate is about half the maximum rate for constraints imposed on the *air interface*.

Code division multiple access (CDMA)

Code division multiple access (CDMA) is a spread spectrum multiple access technique commonly used in both commercial and military communication systems. For example, CDMA is employed on the *reverse links* of cellular systems such as IS-95, WCDMA, and CDMA 2000 to connect geographically dispersed mobile stations to their base station. Each mobile station has *its own spread PN sequence* and transmits its direct sequence spread spectrum signal on the *same carrier frequency* to the base station without any coordination. CDMA commonly employs a set of PN sequences that have *low crosscorrelation*, such as *Gold sequences*, *Kasami sequences*, and *phase-offset maximal sequences* (from the same mother maximal sequence). These PN sequences reduce the effect of *multi-user interference* of mobile signals in the same cell and on the same link as well as those in adjacent cells.

To avoid the *near-far effect*, mobile signals on the same reverse link must arrive at the base station with approximately the *same signal power*. Thus, CDMA requires near real-time *closed-loop power control* for all mobile stations in the same cell. The base station measures the mobile signal strength and sends an instruction on the forward link for the mobile station to adjust its transmitted power up or down by an incremental unit amount. Assume perfect power control, that is, all mobile signals in the same cell and on the same link arrive at their base station with exactly the same power P. Furthermore, assume that the reverse link has K mobile signals and each mobile signal has an identical spread factor equal to N. This means that the decision sample for each mobile signal at the base station has an interference variance (power) equal to $P(K-1)/N$. Also, the *output signal-to-interference ratio* is equal to $N/(K-1)$ (this is a conservative estimate since it does not take into account the modulation type and whether the demodulation is coherent or noncoherent. A more precise analysis can be found in a later section of this chapter). The *output signal-to-interference ratio* is the factor that limits the number of voice channels in a CDMA cellular system like IS-95. Note that the forward link of IS-95 has no multi-user interference because of the use of orthogonal covering. Thus, the IS-95 forward link can carry up to 62 voice channels if no paging channel is used. On the other hand, the IS-95 reverse link is constrained by multi-user interference and carries a smaller number of voice channels unless other efficient techniques are incorporated, such as *voice activation*, *diversity at the base station*, and *sectoring*. In fact, the capacity of IS-95 is *forward link-limited* rather than reverse link-limited once these efficient techniques are incorporated.

IS-95 reverse link

The IS-95 reverse link is composed of *access* channels and *traffic* channels from mobile stations in the same cell. These channels employ the *same carrier frequency*. Each access channel is spread by a distinct long code PN sequence; each traffic channel is also spread by a distinct long code PN sequence. These long code PN sequences allow the users on a reverse link to operate in a CDMA mode. Each user's long PN sequence is a phase-offset of the same 42-stage long code PN sequence of the forward link.

The access channel has 88 bits per 20 ms frame and is clocked at 4.4 kbps. Eight encoder tail bits are added to reset the encoder state to the all-zero state at the end of each frame. Therefore, the input bit rate of the convolutional encoder (rate ⅓ and constraint length 9) is 4.8 kbps. The encoder output coded symbol rate is three times the input bit rate which is equal to 14.4 ksps. Since the common bit rate for all channels is 9.6 kbps and the common coded symbol rate for all channels is 28.8 ksps, the access channel coded symbols are repeated to achieve 28.8 ksps before interleaving. This protects the data from channel burst errors. The coded symbols at the interleaver output are passed to a CSK modulator that employs 64 orthogonal Walsh functions, each with 64 chips, to represent a set of 64 distinct CSK symbols. A CSK symbol consists of *six* coded symbols. The CSK symbol rate is 28.8/6 = 4.8 ksps and the Walsh chip rate is $4.8 \times 64 = 307.2$ kcps. The Walsh chips are spread by a 42-stage long code PN sequence clocked at the rate of 1.2288 Mcps. Thus, a Walsh chip is spread by a factor of *four* and a CSK symbol is spread by a factor of 256. The *spread factor* is therefore equal to 256. Following the direct sequence spreading by the long code PN

sequence, the access channel is further scrambled in offset-quadrature by the I-channel PN sequence and the Q-channel PN sequence. The data in the Q-channel are delayed by half a PN chip time with respect to the data in the I-channel. The use of *offset-quadrature modulation* helps reduce the *sidelobe regrowth* in the signal spectrum when the signal is amplified by a nonlinear amplifier of the mobile transmitter. Hence, *offset-quadrature modulation* reduces adjacent channel interference (this is the same advantage obtained with OQPSK). Both I- and Q-channel PN sequences are clocked at the same rate of 1.2288 Mcps. Thus, the signal is not spread further by these two sequences. Nevertheless, the offset-quadrature spreading protects the reverse link against co-channel interference in adjacent cells. The access channel is used by the mobile station to initiate communication with the base station via a random access protocol. The protocol arranges a number of 20 ms slots into access slots. Each transmission in an access slot begins with a random delay to randomize the transmission times of mobile stations that may be transmitting in the same access slot. The purpose is to reduce packet collisions and improve the channel throughput. Figure 8.13 illustrates the generation of the access channel.

The reverse traffic channel carries data in 20 ms frames. The raw data rates are 0.8 kbps, 2 kbps, 4 kbps, and 8.6 kbps and are converted to data rates of 0.8 kbps, 2 kbps, 4.4 kbps, and 9.2 kbps when frame quality indicators are added to the frames for the two higher data rates (that is, the frame is encoded by cyclic redundancy check (CRC) code for error detection at the base station). Furthermore, an 8-bit encoder tail is added to the frame to reset the convolutional encoder to the all-zero state. The input rates to the encoder (rate ⅓, constraint length 9) vary from 1.2 kbps (12.5% duty cycle) to 9.6 kbps (100% duty cycle). Thus, the output rates of the encoder vary from 3.6 ksps to 28.8 ksps. To achieve a common transmission rate of 28.8 kbps the encoder symbols are repeated accordingly before interleaving to protect the data from channel burst errors. The coded symbols at the interleaver output are passed to a CSK modulator that employs 64 orthogonal Walsh functions, each with 64 chips, to represent a set of 64 distinct CSK symbols. A CSK symbol consists of *six* coded symbols. The CSK symbol rate is 28.8/6 = 4.8 ksps and the Walsh chip rate is $4.8 \times 64 = 307.2$ kcps. A frame of 20 ms contains 96 CSK symbols, which are divided into 16 slots of six CSK symbols. A data burst randomizer is employed to gate off the repeated symbols, which reduces the multi-user interference when the data rate is less than 9.6 ksps (that is, 4.8 kbps, 2.4 kbps, and 1.2 kbps). All slots are filled for a rate of 9.6 kbps, half-filled for 4.8 kbps, one quarter-filled for 2.4 kbps, and one eighth-filled for 1.2 kbps. Thus, all but one of the code symbol repetitions is deleted prior to transmission to achieve a variable transmission duty cycle. A user-distinct 42-stage long code PN sequence clocked at 1.2288 Mcps is used to spread the signal, achieving a spreading factor of 256. Finally, offset-quadrature spreading is employed (as in the access channel). Figure 8.13 shows the generation of the reverse traffic channel of the IS-95 reverse link.

The reverse traffic channel supports both RS1 and RS2. The convolutional code for RS2 is of rate ½. It is obtained from the convolutional code of rate ⅓ in RS1 by puncturing (deleting) *two* output code symbols for every *six* output code symbols (which correspond to every *two* input code symbols). The reverse traffic channel operates as a *fundamental code channel* shown in Figure 8.13 or as a *supplementary code channel* at the highest data rate without the data burst randomizer.

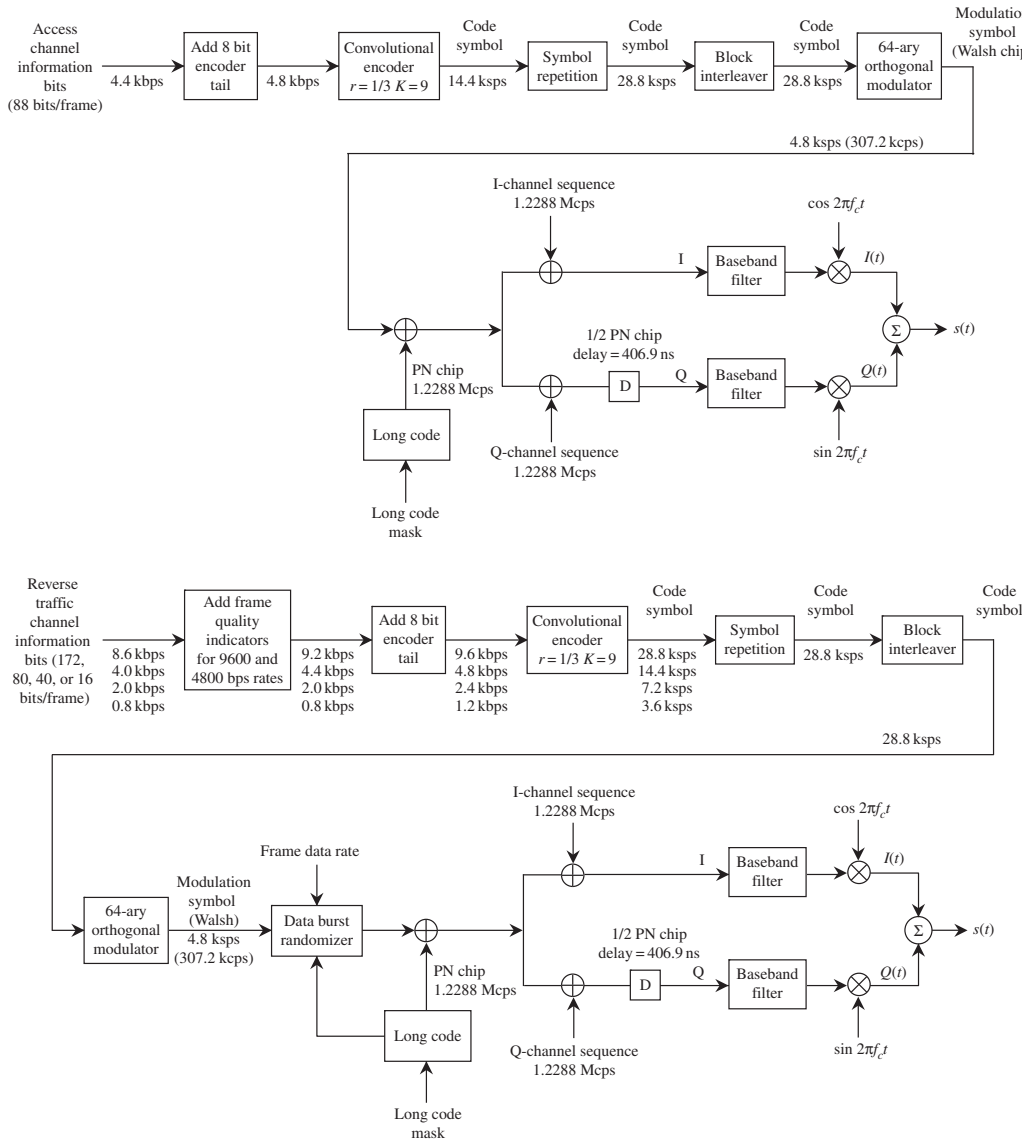

Figure 8.13 IS-95 reverse link.

8.2 Direct sequence demodulation

In the previous section we provided a detailed discussion of direct sequence spread spectrum modulation techniques. In the following discussion we will examine the demodulation process, and study the performance of direct sequence spread spectrum signals in the presence of a jamming signal. We also analyze the performance of CDMA signals.

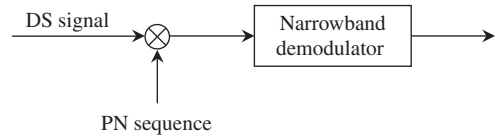

Figure 8.14 A direct sequence demodulator.

The demodulation process of a direct sequence spread spectrum signal can be illustrated by the general block diagram shown in Figure 8.14. The received DS signal is first despread by multiplying it by a *synchronized* replica of the PN sequence. This operation simultaneously spreads the jamming signal power over a bandwidth much larger than the data bandwidth. The despread signal is now a narrowband signal and can be demodulated by a conventional demodulator, depending on the modulation format. Note that the despreading process provides no advantage with respect to white noise due to the fact that the spectrum of white noise is theoretically infinite and can no longer be spread. Thus the performance of a DS signal in a white Gaussian noise channel is identical to the performance of its narrowband counterpart. Only when a jamming signal is present the benefit of spreading obtained.

Example 8.5 DS-PSK and tone jamming

Let us consider a DS-PSK signal $s(t)$ in an AWGN channel with the presence of a tone jamming signal $j(t)$ that has exactly the same carrier frequency. We assume that noise $n(t)$ has the power spectral density $N_0/2$ (W/Hz). Let $s(t)$ and $j(t)$ be represented as follows:

$$s(t) = Ad_i c(t)\cos 2\pi f_c t\,,\ iT_b < t \leq (i+1)T_b,\quad and\ j(t) = A_j\cos(2\pi f_c t + \theta) \quad (8.21)$$

where $d_i \in \{+1, -1\}$ is the ith data bit of duration T_b and $c(t)$ is the PN function of N chips. The period of $c(t)$ is T_b, and each chip is represented by a unit amplitude squared pulse shape of duration T_c. The spreading factor is $N = T_b/T_c$. The demodulator is shown in Figure 8.15. The decision sample at the detector input is given by

$$X = \frac{AT_b d_i}{2} + J + \mathcal{N} \quad (8.22)$$

where the random variables J and $\mathcal{N}$ represent the jamming and noise samples, respectively, and are expressed as follows:

$$J = \frac{1}{2}A_j\cos\theta\int_0^{T_b} c(t)\ \mathrm{d}t \text{ and } \mathcal{N} = \int_0^{T_b} n(t)c(t)\cos 2\pi f_c t\mathrm{d}t \quad (8.23)$$

Let L be the number of 1s minus the number of 0s in the PN sequence $c(t)$, and hence L can be positive or negative. Using the fact that the chips in the PN sequence have ± 1 amplitude, we have

$$J = \frac{1}{2}A_j T_c L\cos\theta \quad (8.24)$$

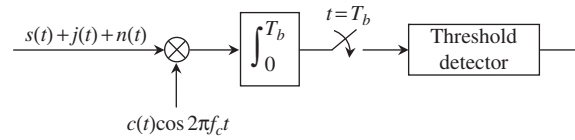

Figure 8.15 DS-PSK demodulator.

Assuming that the random phase θ is uniformly distributed, we calculate the jamming variance as

$$\sigma_j^2 = \frac{1}{8} A_j^2 T_c^2 L^2 \tag{8.25}$$

Using the fact that $c^2(t) = 1$, the noise variance can be calculated as follows:

$$\sigma^2 = \frac{N_0 T_b}{4} \tag{8.26}$$

Consequently, the *output signal-to-noise ratio* SNR_0 and the *output signal-to-jamming ratio* SJR_0 are given by

$$SNR_0 = \frac{(AT_b d_i/2)^2}{\sigma^2} = \frac{A^2 T_b}{N_0} = \frac{2E_b}{N_0} \tag{8.27a}$$

$$SJR_0 = \frac{(AT_b d_i/2)^2}{\sigma_j^2} = 2\left(\frac{N}{L}\right)^2 \left(\frac{A^2}{A_j^2}\right) = 2\left(\frac{N}{L}\right)^2 SJR_i \tag{8.27b}$$

where $SJR_i = A^2/A_j^2$ is the *input signal-to-jamming ratio*. Note that the output signal-to-noise ratio is identical to that of the narrowband PSK as expected since spreading the signal has no effect on noise. On the other hand the output signal-to-jamming ratio is enhanced by a *processing gain* equal to $2(N/L)^2$ relative to the input signal-to-jamming ratio. For example, if $c(t)$ represents a maximal sequence, then $L = 1$, and the *processing gain* is $2N^2$. Thus, tone jamming is not effective against a DS signal with a large *spread factor* N. Note the difference between *spread factor* and *processing gain*. The latter is modulation, demodulation, and jamming dependent while the former is not.

■

Example 8.6 DS-PSK and broadband jamming

Let us again consider the DS-PSK signal $s(t)$ in the above example. The channel is an AWGN channel with the presence of a broadband jamming signal $j(t)$ whose power spectral density is flat and is denoted as $J_0/2$ (W/Hz). We also assume that noise $n(t)$ has the power spectral density $N_0/2$ (W/Hz). Using the same approach as above we calculate the jamming variance and the *output signal-to-jamming ratio* SJR_0 as

$$\sigma_j^2 = \frac{J_0 T_b}{4} \tag{8.28}$$

$$SJR_0 = \frac{(AT_b d_i/2)^2}{\sigma_j^2} = \frac{A^2 T_b}{J_0} = \frac{2E_b}{J_0} \tag{8.29}$$

Let us now calculate the *input signal-to-jamming ratio* SJR_i. We have

$$SJR_i = \frac{A^2/2}{P_j} \tag{8.30}$$

where P_j is defined as the power of the jamming signal in the *equivalent noise bandwidth* of the DS-PSK signal, which is equal to the chip rate $1/T_c$:

$$P_j = \frac{J_0}{T_c} \tag{8.31}$$

Thus we have

$$SJR_i = \frac{A^2/2}{P_j} = \frac{A^2 T_c}{2J_0} = \frac{E_b}{NJ_0} \tag{8.32}$$

Combining (8.29) and (8.32) we obtain

$$SJR_0 = 2N(SJR_i) \tag{8.33}$$

The above result shows that a *processing gain* equal to $2N$ is achieved against broadband jamming. The *output signal-to-jamming-and-noise ratio* is given by $SJNR_0 = (SJR_0^{-1} + SNR_0^{-1})^{-1}$, where $SNR_0 = 2E_b/N_0$. The jamming sample at the integrator output is not Gaussian, but if N is large, the sample can be approximated as a Gaussian sample (based on the *central limit theorem*, any broadband signal that is passed through a narrowband filter whose bandwidth is much smaller than that of the broadband signal produces an output signal that is approximately Gaussian). Thus, the bit error probability of a DS-PSK signal in the presence of a broadband jamming signal can be approximated as $P_b \approx Q(\sqrt{SJNR_0})$

■

Example 8.7 DS-PSK and pulsed jamming

An effective jamming strategy that is commonly employed against a direct sequence spread spectrum signal is pulse jamming. In this strategy the jammer power is concentrated into pulses of duty cycle δ with peak power P_p. The jammer is on δ percent of the time and off $(1 - \delta)$ percent of the time. Thus, only δ percent of the transmitted symbols are jammed. We assume that the transmitter has no knowledge of the jammer's timing. Otherwise, the transmitter just ceases transmission when the jammer is on and resumes transmission when the jammer is off, thereby avoiding being jammed altogether. Again, assume that the jamming signal is broadband. The *output signal-to-pulse jamming ratio* is then given by $SJR_{0,p} = 2N(SJR_{i,p}) = 2\delta E_b/J_0$, where $SJR_{i,p}$ is the *input signal-to-pulse jamming ratio* $SJR_{i,p} = \delta(SJR_i) = \delta E_b/NJ_0$, where SJR_i is the *average input signal-to-jamming ratio* defined in the previous example for continuous broadband jamming. Thus, with pulse

jamming the *output signal-to-pulse jamming ratio* is decreased by a factor equal to δ. Using the *Gaussian approximation* and based on the *total probability theorem*, the bit error probability for the DS-PSK signal in pulse jamming is given by

$$P_b \approx \delta Q\left(\sqrt{(SJR_{0,p}^{-1} + SNR_0^{-1})^{-1}}\right) + (1-\delta)Q\left(\sqrt{SNR_0}\right) \tag{8.34}$$

If we consider the case when $SNR_0 \gg SJR_{0,p}$, then the bit error probability can be approximated as follows:

$$P_b \approx \delta Q\left(\sqrt{SJR_{0,p}}\right) = \delta Q\left(\sqrt{2N\delta(SJR_i)}\right) = \delta Q\left(\sqrt{2\delta E_b/J_0}\right) \tag{8.35}$$

For a fixed average jamming power, the jammer can select δ to maximize the bit error probability. The worst-case bit error probability and the optimum δ can be found numerically as

$$P_{b,max} \approx \frac{0.083}{N(SJR_i)} = \frac{0.083}{E_b/J_0}, \qquad \delta = \frac{0.71}{N(SJR_i)} = \frac{0.71}{E_b/J_0} \tag{8.36}$$

For illustration purpose, consider the case of $SJR_i = 1/20$ and $N = 128$, then $P_{b,max} \approx 0.013$ and $\delta = 0.11$. For comparison purposes consider the case of broadband jamming in the previous example. Assume that the effect of noise is negligible compared to that of the jamming signal. Then, the bit error probability for broadband jamming is given by $P_b \approx Q(\sqrt{SJNR_0}) = Q(\sqrt{2N(SJR_i)}) = Q(\sqrt{2E_b/J_0}) = Q(\sqrt{12.8}) = 1.7 \times 10^{-4}$. This shows that pulsed jamming is more effective than broadband jamming in general. The disadvantage is the requirement of a high peak power jammer. To combat pulsed jamming, error-correction coding may be employed.

■

Quadrature orthogonal covering demodulation

In this section we provide the demodulation of the quadrature orthogonal covering signal in Figure 8.9. The quadrature orthogonal covering signal can be represented in an arbitrary bit interval as follows:

$$\begin{aligned} s(t) \;=\; & \frac{A}{\sqrt{2}}\sum_{k=1}^{M} d_{i,k}c_I(t)w_k(t)\cos(2\pi f_c t + \theta) \\ & - \frac{A}{\sqrt{2}}\sum_{k=1}^{M} d_{i,k}c_Q(t)w_k(t)\sin(2\pi f_c t + \theta)\,,\; iT_b < t \leq\; (i+1)T_b \end{aligned} \tag{8.37}$$

where $d_{i,k} \in \{+1, -1\}$ is the ith bit in the kth channel. The I- and Q-channel PN functions are $c_I(t)$ and $c_Q(t)$, respectively. The arbitrary phase θ represents the phase difference between the received signal and the local carrier. The $\sqrt{2}$ factor means that half the power goes into the I-channel and the other half goes into the Q-channel. We assume that noise $n(t)$ has the power spectral density $N_0/2$ (W/Hz). The following operations are performed by the demodulator to extract the I-decision variable:

$$
\begin{aligned}
&s(t)[c_I(t)w_l(t)\cos 2\pi f_c t] \\
&\quad = \frac{A}{\sqrt{2}}\sum_{k=1}^{M} d_{i,k}c_I^2(t)w_k(t)w_l(t)\cos(2\pi f_c t+\theta)\cos 2\pi f_c t \\
&\qquad - \frac{A}{\sqrt{2}}\sum_{k=1}^{M} d_{i,k}c_I(t)c_Q(t)w_k(t)w_l(t)\sin(2\pi f_c t+\theta)\cos 2\pi f_c t \\
&\quad = \frac{A}{2\sqrt{2}}\sum_{k=1}^{M} d_{i,k}w_k(t)w_l(t)\cos\theta - \frac{A}{2\sqrt{2}}\sum_{k=1}^{M} d_{i,k}c_I(t)c_Q(t)w_k(t)w_l(t)\sin\theta
\end{aligned}
\tag{8.38}
$$

$$
\begin{aligned}
&s(t)[-c_Q(t)w_l(t)\sin 2\pi f_c t] \\
&\quad = -\frac{A}{\sqrt{2}}\sum_{k=1}^{M} d_{i,k}c_I(t)c_Q(t)w_k(t)w_l(t)\cos(2\pi f_c t+\theta)\sin 2\pi f_c t \\
&\qquad + \frac{A}{\sqrt{2}}\sum_{k=1}^{M} d_{i,k}c_Q^2(t)w_k(t)w_l(t)\sin(2\pi f_c t+\theta)\sin 2\pi f_c t \\
&\quad = \frac{A}{2\sqrt{2}}\sum_{k=1}^{M} d_{i,k}c_I(t)c_Q(t)w_k(t)w_l(t)\sin\theta + \frac{A}{2\sqrt{2}}\sum_{k=1}^{M} d_{i,k}w_k(t)w_l(t)\cos\theta
\end{aligned}
\tag{8.39}
$$

The high-frequency terms are ignored because they will be integrated to zero, since as usual we assume that the carrier frequency is an integer multiple of the symbol rate. Add (8.38) and (8.39) and include noise. We get the *signal and noise* of the I-channel:

$$
\begin{aligned}
s_I(t) &= s(t)[c_I(t)w_l(t)\cos 2\pi f_c t] + s(t)[-c_Q(t)w_l(t)\sin 2\pi f_c t] \\
&= \frac{A}{\sqrt{2}}\sum_{k=1}^{M} d_{i,k}w_k(t)w_l(t)\cos\theta
\end{aligned}
\tag{8.40}
$$

where the noise part is given by the following expression:

$$
n_I(t) = n(t)[c_I(t)w_l(t)\cos 2\pi f_c t] + n(t)[-c_Q(t)w_l(t)\sin 2\pi f_c t] \tag{8.41}
$$

Similarly, the following operations are performed by the demodulator to extract the Q-decision variable:

$$
\begin{aligned}
&s(t)[-c_I(t)w_l(t)\sin 2\pi f_c t] \\
&\quad = -\frac{A}{\sqrt{2}}\sum_{k=1}^{M} d_{i,k}c_I^2(t)w_k(t)w_l(t)\cos(2\pi f_c t+\theta)\sin 2\pi f_c t \\
&\qquad + \frac{A}{\sqrt{2}}\sum_{k=1}^{M} d_{i,k}c_I(t)c_Q(t)w_k(t)w_l(t)\sin(2\pi f_c t+\theta)\sin 2\pi f_c t \\
&\quad = \frac{A}{2\sqrt{2}}\sum_{k=1}^{M} d_{i,k}w_k(t)w_l(t)\sin\theta + \frac{A}{2\sqrt{2}}\sum_{k=1}^{M} d_{i,k}c_I(t)c_Q(t)w_k(t)w_l(t)\cos\theta
\end{aligned}
\tag{8.42}
$$

$$
\begin{aligned}
& s(t)[-c_Q(t)w_l(t)\cos 2\pi f_c t] \\
&= -\frac{A}{\sqrt{2}}\sum_{k=1}^{M} d_{i,k}c_I(t)c_Q(t)w_k(t)w_l(t)\cos(2\pi f_c t+\theta)\cos 2\pi f_c t \\
&\quad +\frac{A}{\sqrt{2}}\sum_{k=1}^{M} d_{i,k}c_Q^2(t)w_k(t)w_l(t)\sin(2\pi f_c t+\theta)\cos 2\pi f_c t \\
&= -\frac{A}{2\sqrt{2}}\sum_{k=1}^{M} d_{i,k}c_I(t)c_Q(t)w_k(t)w_l(t)\cos\theta+\frac{A}{2\sqrt{2}}\sum_{k=1}^{M} d_{i,k}w_k(t)w_l(t)\sin\theta
\end{aligned}
\tag{8.43}
$$

Add (8.42) and (8.43) and include noise. We get the *signal and noise* of the Q-channel:

$$
\begin{aligned}
s_Q(t) &= s(t)[-c_I(t)w_l(t)\sin 2\pi f_c t]+s(t)[-c_Q(t)w_l(t)\cos 2\pi f_c t] \\
&= \frac{A}{\sqrt{2}}\sum_{k=1}^{M} d_{i,k}w_k(t)w_l(t)\sin\theta
\end{aligned}
\tag{8.44}
$$

where the noise part is given by the following expression:

$$
n_Q(t) = n(t)[-c_I(t)w_l(t)\sin 2\pi f_c t]+n(t)[-c_Q(t)w_l(t)\cos 2\pi f_c t] \tag{8.45}
$$

To obtain the I- and Q-decision variables $X_{I,l}$ and $X_{Q,l}$ of the lth channel we integrate $s_I(t)+n_I(t)$ and $s_Q(t)+n_Q(t)$ with respect to t, where $iT_b < t \leq (i+1)T_b$. We have

$$
X_{I,l} = \frac{AT_b}{\sqrt{2}}d_{i,l}\cos\theta + N_{I,l} \tag{8.46}
$$

$$
X_{Q,l} = \frac{AT_b}{\sqrt{2}}d_{i,l}\sin\theta + N_{Q,l} \tag{8.47}
$$

Both decision variables are Gaussian variables with variance σ^2 given by

$$
\sigma^2 = \frac{N_0 T_b}{2} \tag{8.48}
$$

A *sinusoidal phase detector* can be employed on a designated lth channel to provide a correction voltage $e(t) = X_{I,l}X_{Q,l} \approx \frac{1}{4}A^2T_b^2\sin 2\hat{\theta}$ to drive a *voltage-controlled oscillator* (VCO) so that the noisy phase error $\hat{\theta}$ can be driven to zero in the case of small noise. A *phase-locked loop* (PLL) can accomplish this task. In the fading channel (see Chapter 10) of a cellular system the amplitude A is not constant. Therefore, it is not possible to use a PLL to track the phase. In practice, a pilot tone is transmitted using the first Walsh function (corresponding to the first row of the Hadamard matrix) with all *pilot bits* $d_{i,1}$ set to 1s, as in IS-95. The pilot channel 1 provides the noisy phase error $\hat{\theta}$ via the following operation:

$$
\hat{\theta} = \tan^{-1}\left(\frac{X_{Q,1}}{X_{I,1}}\right) \tag{8.49}
$$

This phase error can be converted to a dc voltage which can be used by a VCO to correct the phase error between the received signal and the local carrier. In both scenarios, the I-decision variable of the lth channel, namely $X_{I,l}$, is fed to a *threshold detector* to make a decision on which bit had been transmitted. Figure 8.16 illustrates the *coherent* demodulation of the I-Q orthogonal covering signal.

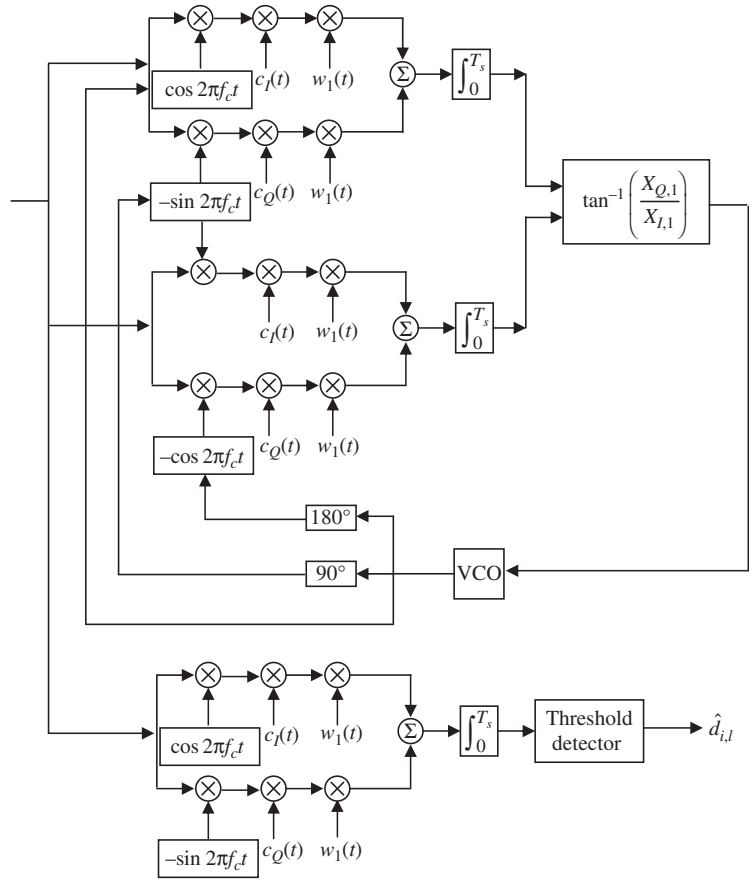

Figure 8.16 Coherent demodulator of the quadrature orthogonal covering signal.

The bit error probability of a Walsh channel is determined by the Gaussian decision variable $X_{I,l} = (1/\sqrt{2})AT_b d_{i,l} + N_{I,l}$ when synchronization is reached for which $\theta = 0^0$. The bit error probability for an AWGN channel is identical to PSK or QPSK and is given by

$$P_b = Q\left(\sqrt{\frac{A^2 T_b}{N_0}}\right) = Q\left(\sqrt{\frac{2E_b}{N_0}}\right) \tag{8.50}$$

For a fading channel the bit error probability is presented in Chapter 10.

Alternatively, the detection can be carried out by the following operation:

$$\begin{aligned} Y_l = X_{I,l}X_{I,1} + X_{Q,l}X_{Q,1} &= \left(\frac{AT_b}{\sqrt{2}} d_{i,l}\cos\theta + N_{I,l}\right)\left(\frac{AT_b}{\sqrt{2}} d_{i,1}\cos\theta + N_{I,1}\right) \\ &\quad + \left(\frac{AT_b}{\sqrt{2}} d_{i,l}\sin\theta + N_{Q,l}\right)\left(\frac{AT_b}{\sqrt{2}} d_{i,1}\sin\theta + N_{Q,1}\right) \\ &= \frac{A^2 T_b^2}{2} d_{i,l} d_{i,1} + N \end{aligned} \tag{8.51}$$

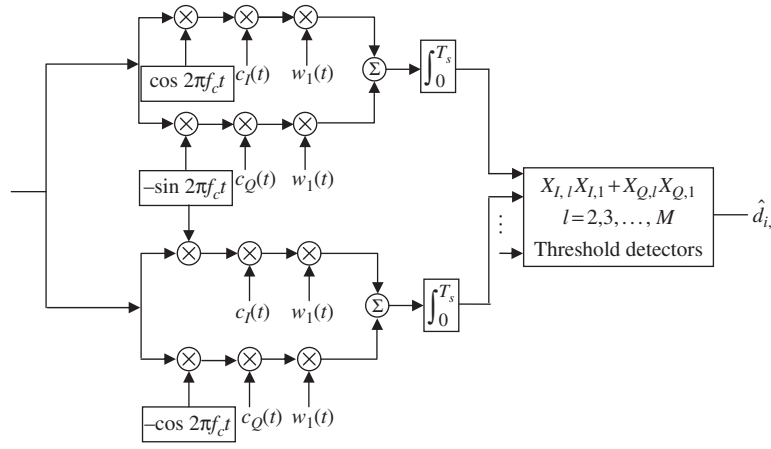

Figure 8.17 Pilot symbol-aided demodulator of the quadrature orthogonal covering signal.

where N is the noise variable defined as follows:

$$N = \left(\frac{AT_b}{\sqrt{2}}\cos\theta\right)\left(d_{i,l}N_{I,1} + d_{i,1}N_{I,l}\right) + \left(\frac{AT_b}{\sqrt{2}}\sin\theta\right)\left(d_{i,l}N_{Q,1} + d_{i,1}N_{Q,l}\right) + N_{I,1}N_{I,l} + N_{Q,1}N_{Q,l} \tag{8.52}$$

where the pilot bits $d_{i,1}$ are all 1. In the case of small noise we note that $Y_l \approx \frac{1}{2}A^2T_b^2 d_{i,l}$, for which the transmitted bit $d_{i,l}$ can be detected by a threshold detector. Figure 8.17 illustrates the *pilot symbol-aided* demodulation of the quadrature orthogonal covering signal. Note that the noise variable N is not a Gaussian variable. In practice the pilot tone is sent with a much higher power than those of the Walsh data signals (IS-95 and CDMA 2000), that is, $d_{i,1} \gg d_{i,l}$. In this case N is approximately Gaussian with variance $\frac{1}{2}A^2T_b^2 d_{i,1}^2\sigma^2$, where σ^2 is given in (8.48). Thus, (8.50) can be used to approximate the bit error probability for an AWGN channel or a fading channel (see Chapter 10).

Noncoherent demodulation of DS-CSK

Direct sequence–code shift keying is a power-efficient spread spectrum modulation. In practice it is implemented with quadrature spreading as in quadrature orthogonal covering technique. IS-95 employs DS-CSK with *offset quadrature spreading* in which the Q-channel is delayed by *half a chip*. The pilot tone is not transmitted along with the data signal. This happens because the pilot tone cannot be power-shared with other mobile signals as in the case of quadrature orthogonal covering signals at the base station. Since the cellular channel is a fading channel (Chapter 10), it is not possible to perform coherent demodulation of the quadrature DS-CSK signal without a pilot tone. Therefore noncoherent demodulation must be carried out. Let us consider a quadrature DS-CSK signal with Walsh function $w_k(t)$ that represents a transmitted kth symbol in the set of M symbols. The PN

spreading codes are $c_I(t)$ and $c_Q(t)$, and the carrier frequency is f_c, which is assumed to be an integer multiple of the symbol rate $1/T_s$.

$$s(t) = \frac{A}{\sqrt{2}} c_I(t) w_k(t) \cos(2\pi f_c t + \theta) - \frac{A}{\sqrt{2}} c_Q(t) w_k(t) \sin(2\pi f_c t + \theta), \quad 0 \le t \le T_s \tag{8.53}$$

The noncoherent demodulator has M branches corresponding to M distinct transmitted symbols. Each branch has two quadrature correlators that perform the following operations:

$$\begin{aligned} s(t)[c_I(t) w_l(t) \cos 2\pi f_c t] &= \frac{A}{\sqrt{2}} c_I^2(t) w_k(t) w_l(t) \cos(2\pi f_c t + \theta) \cos 2\pi f_c t \\ &\quad - \frac{A}{\sqrt{2}} c_I(t) c_Q(t) w_k(t) w_l(t) \sin(2\pi f_c t + \theta) \cos 2\pi f_c t \\ &= \frac{A}{2\sqrt{2}} w_k(t) w_l(t) \cos\theta - \frac{A}{2\sqrt{2}} c_I(t) c_Q(t) w_k(t) w_l(t) \sin\theta \end{aligned} \tag{8.54}$$

$$\begin{aligned} s(t)[-c_Q(t) w_l(t) \sin 2\pi f_c t] &= -\frac{A}{\sqrt{2}} c_I(t) c_Q(t) w_k(t) w_l(t) \cos(2\pi f_c t + \theta) \sin 2\pi f_c t \\ &\quad + \frac{A}{\sqrt{2}} c_Q^2(t) w_k(t) w_l(t) \sin(2\pi f_c t + \theta) \sin 2\pi f_c t \\ &= \frac{A}{2\sqrt{2}} c_I(t) c_Q(t) w_k(t) w_l(t) \sin\theta + \frac{A}{2\sqrt{2}} w_k(t) w_l(t) \cos\theta \end{aligned} \tag{8.55}$$

The high-frequency terms are ignored because they will be integrated to zero. Add (8.54) and (8.55) and include noise. We get the *signal and noise* of the I-correlator of the lth branch:

$$s_I(t) = s(t)[c_I(t) w_l(t) \cos 2\pi f_c t] + s(t)[-c_Q(t) w_l(t) \sin 2\pi f_c t] = \frac{A}{\sqrt{2}} w_k(t) w_l(t) \cos\theta \tag{8.56}$$

where the noise part is given by the following expression:

$$n_I(t) = n(t)[c_I(t) w_l(t) \cos 2\pi f_c t] + n(t)[-c_Q(t) w_l(t) \sin 2\pi f_c t] \tag{8.57}$$

Similarly, the following operations are performed by the demodulator to extract the signal of the Q-correlator of the lth branch:

$$\begin{aligned} s(t)[-c_I(t) w_l(t) \sin 2\pi f_c t] &= -\frac{A}{\sqrt{2}} c_I^2(t) w_k(t) w_l(t) \cos(2\pi f_c t + \theta) \sin 2\pi f_c t \\ &\quad + \frac{A}{\sqrt{2}} c_I(t) c_Q(t) w_k(t) w_l(t) \sin(2\pi f_c t + \theta) \sin 2\pi f_c t \\ &= \frac{A}{2\sqrt{2}} w_k(t) w_l(t) \sin\theta + \frac{A}{2\sqrt{2}} c_I(t) c_Q(t) w_k(t) w_l(t) \cos\theta \end{aligned} \tag{8.58}$$

$$\begin{aligned} s(t)[-c_Q(t)w_l(t)\cos 2\pi f_c t] &= -\frac{A}{\sqrt{2}}c_I(t)c_Q(t)w_k(t)w_l(t)\cos(2\pi f_c t+\theta)\cos 2\pi f_c t \\ &\quad +\frac{A}{\sqrt{2}}c_Q^2(t)w_k(t)w_l(t)\sin(2\pi f_c t+\theta)\cos 2\pi f_c t \\ &= -\frac{A}{2\sqrt{2}}c_I(t)c_Q(t)w_k(t)w_l(t)\cos\theta+\frac{A}{2\sqrt{2}}w_k(t)w_l(t)\sin\theta \end{aligned} \tag{8.59}$$

Add (8.58) and (8.59) and include noise. We get the *signal and noise* of the Q-correlator of the lth branch:

$$s_Q(t)=s(t)[-c_I(t)w_l(t)\sin 2\pi f_c t]+s(t)[-c_Q(t)w_l(t)\cos 2\pi f_c t]=\frac{A}{\sqrt{2}}w_k(t)w_l(t)\sin\theta \tag{8.60}$$

where the noise part is given by the following expression:

$$n_Q(t)=n(t)[-c_I(t)w_l(t)\sin 2\pi f_c t]+n(t)[-c_Q(t)w_l(t)\cos 2\pi f_c t] \tag{8.61}$$

To obtain the I- and Q-decision variables $X_{I,k}$ and $X_{Q,k}$ of the kth branch (signal branch) we integrate $s_I(t)+n_I(t)$ and $s_Q(t)+n_Q(t)$ with respect to t, where $0\le t\le T_s$. We have

$$X_{I,k}=\frac{AT_s}{\sqrt{2}}\cos\theta+N_{I,k} \tag{8.62}$$

$$X_{Q,k}=\frac{AT_s}{\sqrt{2}}\sin\theta+N_{Q,k} \tag{8.63}$$

Both decision variables are Gaussian variables with variance σ^2 given by

$$\sigma^2=\frac{N_0T_s}{2} \tag{8.64}$$

The $M-1$ noise branches provide the following noise variables for $l\neq k$:

$$X_{I,l}=N_{I,l} \tag{8.65}$$

$$X_{Q,l}=N_{Q,l} \tag{8.66}$$

The I- and Q-outputs of each branch are squared and added to provide M decision variables for the *maximum detector*:

$$X^2=X_{I,l}^2+X_{Q,l}^2,\quad l=1,2,\ldots,M \tag{8.67}$$

The bit error probability for an AWGN channel is given in Chapter 7 and for a fading channel in Chapter 10. Figure 8.18 shows the noncoherent demodulator for a quadrature DS-CSK signal.

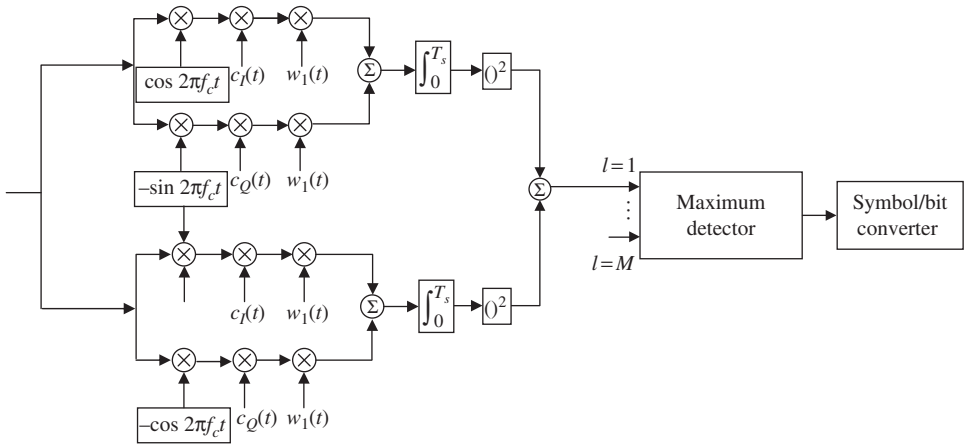

Figure 8.18 Noncoherent demodulator of the quadrature DS-CSK signal.

CDMA: performance evaluation

In this section we present the analysis of typical CDMA systems employed in practice. The three most well-known systems are the 3G cellular standards WCDMA and CDMA 2000, and the 2G cellular standard IS-95. The first two systems employ CDMA on the reverse link with coherent DS-QPSK and DS-IQ, including orthogonal covering. The third employs noncoherent DS-CSK. The analysis of DS-QPSK or DS-IQ is similar to DS-PSK, which we present in Chapter 10. We assume that the reverse link has K users, and with power control all user signals arrive at the base station with the same power. We designate user signal 1 as the signal of interest and user signals 2 to K are *multi-user interference* (MUI). We assume that noise $n(t)$ has the power spectral density $N_0/2$ (W/Hz). The composite signal received by the base station in an arbitrary bit interval is given by

$$\begin{aligned} s(t) &= Ad_{i,1}\, c_1(t)\, \cos\, 2\pi f_c t \;+\; A\sum_{k=2}^{K} d_{i,k} c_k(t-\tau_k) \cos\,[2\pi f_c(t-\tau_k)+\varphi_k\} \;+\; n(t) \\ &= Ad_{i,1}\, c_1(t)\, \cos\, 2\pi f_c t \;+\; A\sum_{k=2}^{K} d_{i,k} c_k(t-\tau_k) \cos(2\pi f_c t+\theta_k\} \;+\; n(t), \\ &\qquad iT_b < t \leq\; (i+1)T_b \end{aligned} \tag{8.68}$$

where τ_k is the kth path delay and θ_k is uniformly distributed in $(0, 2\pi)$ radians. The N-chip PN function $c_k(t)$ has period $NT_c = T_b$. The demodulator is the familiar one shown in Figure 8.14. The decision variable at the threshold detector input can be calculated as

$$X = \frac{AT_b d_{i,1}}{2} + \mathcal{I} + \mathcal{N} \tag{8.69}$$

where the noise variable $\mathcal{N}$ is a zero mean Gaussian random variable with the following variance:

$$\sigma^2 = \frac{N_0 T_b}{4} \tag{8.70}$$

The MUI variable $\mathcal{I}$ can be expressed as follows:

$$\begin{aligned}\mathcal{I} &= \frac{A}{2}\int_0^{T_b}\sum_{k=2}^{K} d_{i,k}\cos\theta_k\, c_1(t)\, c_k(t-\tau_k)\mathrm{d}t \\ &= \frac{A}{2}\sum_{k=2}^{K} d_{i,k}\cos\theta_k \int_0^{T_b} c_1(t)\, c_k(t-\tau_k)\,\mathrm{d}t \\ &= \frac{A}{2}\sum_{k=2}^{K} d_{i,k}\mathcal{I}_k\cos\theta_k\end{aligned} \tag{8.71}$$

where

$$\mathcal{I}_k = \int_0^{T_b} c_1(t)\, c_k(t-\tau_k)\,\mathrm{d}t \tag{8.72}$$

If the number of chips per period N of the PN sequences is large, the PN sequences can be approximated as independent zero mean random binary sequences. The autocorrelation of the random $\{+1,-1\}$-sequence is given by

$$R(\tau) = 1 - \frac{|\tau|}{T_c},\ |\tau| \le T_c \text{ and zero elsewhere} \tag{8.73}$$

We note that binary data has zero mean and unit variance, and that the variable $\cos\theta_k$ has zero mean and variance ½. Therefore, the variance of the MUI variable $\mathcal{I}$ is given by

$$\mathrm{Var}(\mathcal{I}) = \frac{A^2}{4}\sum_{k=2}^{K}[\mathrm{Var}(d_{i,k})\mathrm{Var}(\cos\theta_k)\mathrm{Var}(\mathcal{I}_k)] = \frac{A^2}{8}\sum_{k=2}^{K}\mathrm{Var}(\mathcal{I}_k) \tag{8.74}$$

We now proceed to evaluate the variance of the variable $\mathcal{I}_k$ in (8.72). Using the fact that all user PN sequences are independent we obtain

$$\mathrm{Var}(\mathcal{I}_k) = \int_0^{T_b}\int_0^{T_b} R^2(t-\tau)\,\mathrm{d}t\ \mathrm{d}\tau \tag{8.75}$$

Applying the following transformation $u = t-\tau,\ v = t+\tau$ we get the following result:

$$\mathrm{Var}(\mathcal{I}_k) = \frac{1}{2}\int_{-T_b}^{T_b} R^2(u)\,\mathrm{d}u \int_u^{2T_b-u}\mathrm{d}v = 2\int_0^{T_b} R^2(u)(T_b-u)\ \mathrm{d}u \tag{8.76}$$

Substituting (8.73) into (8.76) we have the variance given by

$$\mathrm{Var}(\mathcal{I}_k) = 2\int_0^{T_b/N}\left(1-\frac{Nu}{T_b}\right)^2(T_b-u)\ \mathrm{d}u = 2\left(\frac{T_b^2}{3N} - \frac{T_b^2}{12N^2}\right) \tag{8.77}$$

For large N, which is the case in practice, the variance can be approximated as

$$\mathrm{Var}(\mathcal{J}_k) \approx \frac{2T_b^2}{3N} \tag{8.78}$$

Substituting (8.78) into (8.74) we obtain the MUI variance necessary for further analysis:

$$\mathrm{Var}(\mathcal{J}) \approx \frac{(K-1)A^2T_b^2}{12N} \tag{8.79}$$

Returning to (8.69) we evaluate the *output signal-to-interference ratio* SIR_0 and the *output signal-to-noise ratio* SNR_0, as follows:

$$SNR_0 = \frac{(AT_b d_{i,1}/2)^2}{\sigma^2} = \frac{A^2T_b}{N_0} = \frac{2E_b}{N_0} \quad \text{and} \quad SIR_0 \approx \frac{(AT_b d_{i,1}/2)^2}{Var(\mathcal{J})} = \frac{3N}{K-1} \tag{8.80}$$

Combining SIR_0 and SNR_0 we obtain the *output signal-to-interference-and-noise ratio* $SINR_0$:

$$SINR_0 = (SIR_0^{-1} + SNR_0^{-1})^{-1} \approx \left(\frac{K-1}{3N} + \frac{N_0}{2E_b}\right)^{-1} \tag{8.81a}$$

Analysis that does not assume a random spreading sequence can be found in [1]. It is common in practice to approximate the *despread* ***input*** signal-to-interference ratio SIR_i and ***output*** SIR_0 by assuming the MUI power is distributed uniformly over the spread bandwidth. Thus, the MUI power spectral density is $J_0 = (K-1)E_b/N$ and we have

$$SIR_i = N/(K-1) \tag{8.81b}$$

$$SIR_0 = 2N/(K-1) \tag{8.81c}$$

This conservative approach compensates for the non-randomness of the PN sequence and it is up to the engineer to select which SIR_0 to use. We thus have an inequality for $SINR_0$, as follows:

$$\left(\frac{K-1}{2N} + \frac{N_0}{2E_b}\right)^{-1} \le SINR_0 \approx \left(\frac{K-1}{3N} + \frac{N_0}{2E_b}\right)^{-1} \tag{8.81d}$$

If N is large, the sample X in (8.69) can be approximated as a Gaussian sample (based on the *central limit theorem*, any broadband signal that is passed through a narrowband filter whose bandwidth is much smaller than that of the broadband signal produces an output signal that is approximately Gaussian). Thus, the bit error probability of a CDMA-PSK signal can be approximated as $P_b \approx Q(\sqrt{SINR_0})$. For the ideal case of random spread sequences we have

$$P_b \approx Q\left(\sqrt{\left(\frac{K-1}{3N} + \frac{N_0}{2E_b}\right)^{-1}}\right) < Q\left(\sqrt{\left(\frac{K-1}{2N} + \frac{N_0}{2E_b}\right)^{-1}}\right) \tag{8.82}$$

8.3 Frequency hop spread spectrum

A second type of spread spectrum modulation is the *frequency hop* (FH) spread spectrum. In this modulation technique, the narrowband modulated signal at the output of a modulator is sequentially hopped in a pseudorandom manner into the *frequency slots* or *bins* that form the entire *spread bandwidth*. The *hopping pattern* can be controlled by a PN sequence and the hopping rate can be performed several times per symbol (*fast hop*) or once per several symbols (*slow hop*). Figure 8.19 shows the block diagram of an FH modulator. The *frequency synthesizer* can generate a set of Q *local carriers* at frequencies $f_{L,1},\ f_{L,2}, \ldots, f_{L,Q}$. For each hop, a local carrier with instantaneous frequency $f_{L,i}$ selected from the set by the PN sequence is multiplied by the narrowband modulated signal at instantaneous carrier frequency f_j to produce a double-sideband signal at frequencies $f_{L,i} + f_j$ *and* $f_{L,i} - f_j$, assuming that $f_{L,i} \gg f_j$. A wideband bandpass filter can be used to reject the lower sideband and transmit only the upper sideband at the instantaneous hopping frequency $f_{L,i} + f_j$. The spread bandwidth W is defined by the set of Q local frequencies. For example, if the hop time is T_h and it is necessary to select the hopping frequencies to be orthogonal, then the separation between adjacent frequency slots or bins should be an integer multiple of $1/T_h$. Consequently, the spread bandwidth W is an integer multiple of $(Q+1)/T_h$. Both fast hop and slow hop spread spectrum techniques have found use in military and commercial systems but fast hop techniques are better than slow hop techniques in dealing with certain jamming signals.

A frequency hop (FH) signal can be demodulated with the aid of a synchronized local frequency synthesizer as shown in Figure 8.20. The FH signal is first de-hopped to a fixed intermediate frequency. The IF signal can then be demodulated with a conventional narrowband demodulator. In the following example we consider a jamming strategy that can be effective against a FH signal, namely *partial-band jamming*. We assume that the jammer moves the jamming signal frequency *randomly* to cover the fraction of the signal spectrum that it intends to jam. Otherwise, the transmitter merely hops its signal out of the *fixed* jammed spectrum and avoids being jammed altogether.

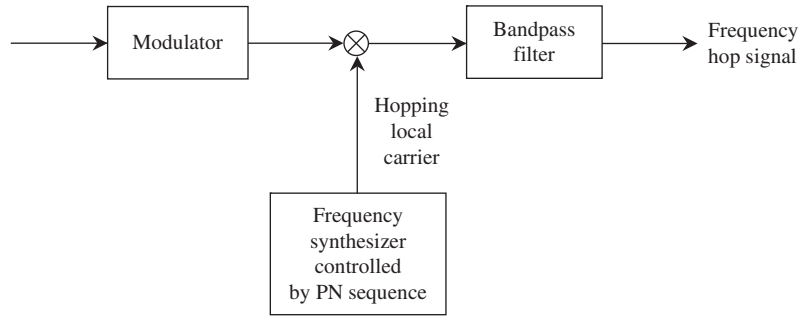

Figure 8.19 Frequency hop modulator.

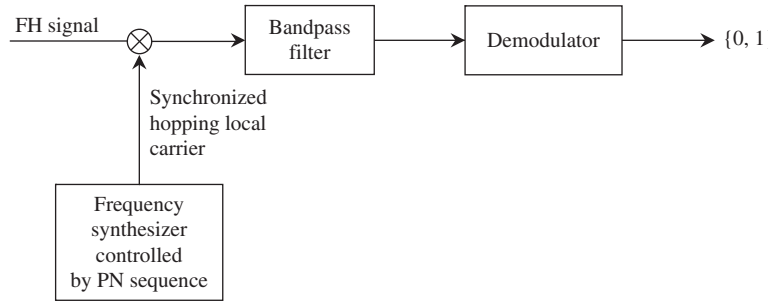

Figure 8.20 Frequency hop demodulator.

Partial-band jamming

Partial-band jamming of a FH signal is the counterpart of pulsed jamming of a DS signal. It allows the jammer to concentrate all power into a smaller bandwidth than the spread bandwidth in order to inflict greater damage.

Example 8.8 Noncoherent FH-FSK and partial-band jamming

Consider a slow frequency hop (SFH) noncoherent FSK signal with a spread bandwidth W and a partial-band Gaussian jamming signal that put all its power P_j in a band δW, where $\delta \leq 1$, to generate a *partial-band jamming power spectral density* $J_0/\delta = P_j/\delta W$, where $J_0 = P_j/W$ is the *average jamming power spectral density*. Let the FSK signal power be P and the bit rate be R_b, then the *bit energy-to-partial band jamming density ratio* is $\delta E_b/J_0 = \delta WP/P_jR_b$, where $E_b/J_0 = WP/P_jR_b$ is the *bit energy-to-average jamming density ratio*. If we assume that the effect of noise is negligible compared to that of the jamming signal, then the bit error probability is given by

$$P_b \approx \frac{\delta}{2}\mathrm{e}^{-\delta E_b/2J_0} = \frac{\delta}{2}\mathrm{e}^{-\delta WP/2P_jR_b} = \frac{\delta}{2}\mathrm{e}^{-\delta N(SJR_i)/2} \tag{8.83}$$

where $N = W/R_b$ is the *spread factor*, $SJR_i = P/P_j$ is the *input signal-to-jamming ratio*, and $N(SJR_i) = E_b/J_0$. The maximum bit error probability can be calculated as follows:

$$P_{b,max} = \frac{\mathrm{e}^{-1}}{N(SJR_i)} = \frac{0.368}{N(SJR_i)} = \frac{0.368}{E_b/J_0}, \qquad \delta = \frac{2}{N(SJR_i)} = \frac{2}{E_b/J_0} \tag{8.84}$$

Note the similarity between *pulse jamming* of DS-PSK signal in (8.36) and partial-band jamming of FH-FSK in (8.84). Both jamming strategies convert the bit error probability as an exponentially decayed function of $N(SJR_i) = E_b/J_0$ into an inversely proportional function of $N(SNR_i)$. To illustrate this, consider the case of $SJR_i = 1/20$ and $N = 128$, then $\delta = 0.3$ and $P_{b,max} = 0.058$. On the other hand, for a broadband jamming strategy the bit error probability is $P_b \approx 0.5\mathrm{e}^{-N(SJR_i)/2} = 0.02$. This shows that partial-band jamming is in general more effective than broadband jamming. Also a partial-band jammer does not need the *high peak* power transmitter required by a pulsed jammer.

■

Example 8.9 Noncoherent FH-MFSK and partial-band jamming

Consider a slow frequency hop noncoherent MFSK signal with a spread bandwidth W and a partial-band Gaussian jamming signal that has all its power P_j in a band δW, where $\delta \leq 1$, to generate a *partial-band jamming power spectral density* $J_0/\delta = P_j/\delta W$, where $J_0 = P_j/W$ is the *average jamming power spectral density.* The MFSK signal power is P and the bit rate is R_b, then the *bit energy-to-partial band jamming density ratio* is $\delta E_b/J_0 = \delta WP/P_jR_b$, where $E_b/J_0 = WP/P_jR_b$ is the *bit energy-to-average jamming density ratio*. If we assume that the effect of noise is negligible compared to that of the jamming signal, then the bit error probability is given by the union bound

$$P_b \leq \frac{\delta M}{4} e^{-(\delta E_b/2J_0)\log_2 M} \tag{8.85}$$

$$P_b \leq \frac{\delta M}{4} e^{-(\delta WP/2P_jR_b)\log_2 M} = \frac{\delta M}{4} e^{-\delta N \log_2 M (SJR_i)/2} \tag{8.86}$$

where $N = W/R_b$ is the *spread factor*, $SJR_i = P/P_j$ is the *input signal-to-jamming ratio* and $N(SJR_i) = E_b/J_0$. The maximum bit error probability can be calculated as follows:

$$\begin{aligned} P_{b,max} &\leq \frac{Me^{-1}/2}{N(SJR_i)\log_2 M} = \frac{0.184M}{N(SJR_i)\log_2 M} = \frac{0.184M/\log_2 M}{E_b/J_0} \\ \delta &= \frac{2}{N(SJR_i)\log_2 M} = \frac{2/\log_2 M}{E_b/J_0} \end{aligned} \tag{8.87}$$

Consider the case of M = 16, SJR_i = 1/20, and N = 128, then $\delta = 0.08$ and we have $P_{b,max} = 0.115$. On the other hand, for broadband jamming strategy the bit error probability is $P_b \approx 4e^{-4N(SJR_i)/2} = 10^{-5}$.

Let us consider the use of adaptive MFSK to improve the anti-jamming capability by starting with M = 2 and increasing M when partial-jamming is present. Assume that the jammer achieves optimum jamming for M = 2 with $\delta = 2/N(SJR_i)$. Substituting δ into (8.86) for $M > 2$ we have $P_b \leq Me^{-\log_2 M}/2N(SJR_i) = Me^{-\log_2 M}/2(E_b/J_0)$. For SJR_i = 1/20, and N = 128, then we have $P_b = 0.023$ (M = 16) and $P_b = 0.012$ (M = 64), as compared to $P_{b,max} = 0.058$ for M = 2.

■

Multi-tone jamming

With some knowledge of the FH signal structure, the jammer may further increase its effectiveness by randomly placing tones in the bandwidth of a MFSK signal.

Example 8.10 Noncoherent FH-MFSK and multi-tone jamming

Another jamming strategy is to randomly transmit q tones over the spread bandwidth, each with power P_j/q. When $P_j/q < P$, the MFSK demodulator still can detect the correct signal tone and the probability of error is determined by AWGN only. When $P_j/q > P$, a symbol

error is made if the jamming tone is within the FH bandwidth but not in the same noncoherent matched filter's bandwidth of the signal tone (because it enhances the detection of the signal by adding to the signal's energy). When $P_j/q = P$, a symbol error occurs with a probability 0.5 under the conditions described for $P_j/q > P$. The optimum number of jamming tones is approximately given by

$$q = \left\lfloor \frac{P_j}{P} \right\rfloor \tag{8.88}$$

where $\lfloor \bullet \rfloor$ denotes the largest integer less than or equal to P_j/P. Note that $1 \leq q \leq N_H$, where the number of hop bins is N_H. This value of q is optimum since a larger q results in $P_j/q < P$ and no error results; a smaller q results in fewer hop bins being jammed but no larger error probability for any one bin. The probability that any hop bin is jammed is given by

$$\Pr(\text{hop bin jammed}) = \frac{q}{N_H} \tag{8.89}$$

The probability that the hop is not jammed is

$$\Pr(\text{hop bin not jammed}) = 1 - \frac{q}{N_H} \tag{8.90}$$

Let us assume that *when a hop bin is jammed* only one jamming tone is present in the bandwidth of the MFSK signal. The symbol error probability is one minus the probability that the jamming tone and the signal are in the same noncoherent matched filter's bandwidth. This probability is $1 - (1/M)$ and the symbol error probability P_e is

$$P_e(q) = \begin{cases} \dfrac{M-1}{M}, & q > N_H \\ \dfrac{M-1}{M}\dfrac{q}{N_H} + \left(1 - \dfrac{q}{N_H}\right) P_e(0) \approx \dfrac{M-1}{M}\dfrac{q}{N_H}, & 1 \leq q \leq N_H \\ P_e(0), & q < 1 \end{cases} \tag{8.91}$$

where $P_e(0)$ represents the probability of symbol error when jamming is not present. The approximation in the second equation of (8.91) is valid when the effect of noise is negligible compared to that of the jamming signal. The bit error probability is given by

$$P_b = \frac{M/2}{M-1} P_e(q) \tag{8.92}$$

For numerical illustration consider the case of $SJR_i = P/P_j = 1/20$ and $N = W/R_b = 129$. Consider the case when the hop bins are contiguous and the hop bin bandwidth is equal to the MFSK bandwidth, which is $(M+1)R_s$. Hence, the number of hop bins is given as $N_H = W/[(M+1)R_b/\log_2 M] = N \log_2 M/(M+1)$. First consider $M = 2$; this yields $N_H = 43$. The number of jamming tones is $q = \lfloor P_j/P \rfloor = \lfloor 1/SJR_i \rfloor = 20$. The resulting bit error probability is $P_b = q/2N_H = 0.23$. There is no advantage for $M > 2$ in multi-tone jamming. It is not necessary to jam a hop bin with more than one jamming tone since one jamming tone can do as much damage as many.

■

Follower jamming

Another jamming strategy that can potentially nullify the effectiveness of frequency hopping is *follower jamming* or *repeater jamming*. This jamming strategy requires the jammer to be able to receive the hopped signal destined to the receiver either via the antenna main beam or via its side lobe. The jammer also needs a broadband receiver that can intercept the hopped signal. If the hop energy exceeds a preset threshold, then the jammer transmits a jamming signal at the same frequency as the hopped signal. In order to jam a hop, the jamming signal has to arrive at the receiver within a fraction of the dwell time of the hop (the duration of the hopped signal). The dwell time is smaller than or equal to the hop time. If the jamming energy in the fraction of the dwell time exceeds the hop energy, an error could occur. This procedure requires the sum of the jammer's processing time, the propagation delay between the transmitter and the jammer (intercept link), and the propagation delay between the jammer and the receiver (jamming link) to be smaller or equal to the fraction of the hop dwell time plus the propagation delay between the transmitter and the receiver. Thus the smaller the hop time and hence the dwell time, the closer to the receiver the jammer has to be in order to be effective. This increases the vulnerability of the jammer. In order to neutralize the effect of follower jamming, *fast frequency hopping* (FFH) is necessary. A FFH system employs *multiple hops* per bit to reduce the hop time. The demodulation can be done via *hard-decision* or *soft-decision* demodulation. A hard-decision demodulator detects L hops and outputs a sequence of L bits which is fed to a majority voter. If the number of 1s exceeds the number of 0s, the detected bit is bit 1; otherwise it is bit 0. If L is even, and there are the same number of 1s and 0s, choose either bit 1 or bit 0 with probability 0.5. A soft-decision binary noncoherent demodulator combines (sums) L hopped decision samples at the outputs of the I- and Q-channel noncoherent signal processors. The combined I-channel and the combined Q-channel decision variables are compared by a maximum detector to determine bit 1 or bit 0. Soft-decision demodulation may perform better than hard-decision demodulation. Both types of demodulation suffer performance loss for $L > 1$ compared to the case of $L = 1$ in an AWGN channel without any jamming. The *combining loss* [2–4] is a penalty to pay in exchange for an additional ability to neutralize a potent jammer.

Example 8.11 Noncoherent slow FH-MFSK and follower noise jamming

Consider a slow hop noncoherent MFSK signal with a hopping bandwidth W. The follower jammer must determine the frequency bin that contains the hop. Figure 8.21 shows a typical frequency bin determinator which consists of N_D branches. The nominal bandwidth of the bandpass filters is W/N_D. The center frequencies of the bandpass filters cover the entire spread bandwidth. The samples are taken at $T = N_D/W$ after the hop starts. The probability of correctly identifying the branch that contains a hop increases as N_D gets larger. Alternatively, the branch in Figure 8.21 can be replaced by an energy detector commonly referred to as *radiometer*. Each radiometer consists of a bandpass filter, a square-law detector, and an integrator followed by a sampler.

Let us denote d_{T-J}, d_{J-R}, and d_{T-R} as the transmitter–jammer, jammer–receiver, and transmitter–receiver distances, respectively. The jammer signal arrives at the receiver with

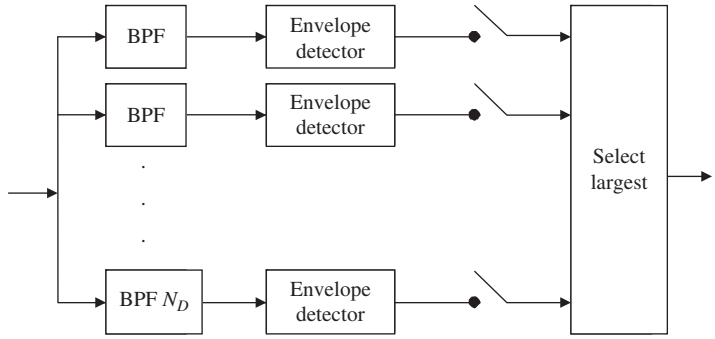

Figure 8.21 Frequency bin determinator.

a time delay $T_d + T$ relative to the start of a hop, where $T_d = (d_{T-J} + d_{J-R} - d_{T-R})/c$. Given the hop time $T_h > T_d + T$, the jammer can only jam a hop for duration $T_h - T_d - T$. Assume that the jamming signal is noise-like. The effective jamming power spectral density seen by the receiver during a hop is $J_0 = \delta P_j/(W/N_D)$, where the fraction of a hop being jammed is $\delta = [T_h - T_d - T]/T_h$. For numerical illustration, consider the case of one hop per symbol (slow hop) and let $P_{c,h}$ denote the *probability of correctly identifying the frequency bin by the jammer.* The probability of symbol error at the receiver is given by

$$P_e = P_{c,h}P_e(\text{jammed}) + (1 - P_{c,h})P_e(\text{not jammed}) \tag{8.93}$$

Note that P_e (not jammed) is the symbol error probability of MFSK with noise spectral density $N_0/2$, and $P_e(\text{jammed})$ is the symbol error probability of MFSK with noise spectral density $N_0/2$ replaced by the *jamming and noise power spectral density* $(J_0 + N_0)/2$. The bit error probability is $P_b = (M/2)P_e/(M-1)$. Let us assume that the jamming signal is strong enough to cause the maximum symbol error probability equal to $1 - 1/M$ for a jammed hop. Furthermore, assume that the probability of correctly identifying the frequency bin is 0.5. Then, the worst-case symbol error probability is $(M-1)/2M$, assuming the effect of noise is negligible compared to jamming. The corresponding worst-case bit error probability is $P_b = 1/4$.

Let us consider the case of $M = 2$, and again assume that the effect of noise is negligible compared to jamming. Using the ratio $E_b/J_0 = (W/\delta N_D R_b)SJR_i$, the bit error probability of slow FH-FSK is $P_b = P_{c,h}P_b(\text{jammed}) = 0.5P_{c,h}\exp[-(W/2\delta N_D R_b)SJR_i]$. For the case $W/\delta N_D R_b = 2$, $P_{c,h} = 0.5$, and $P_b = 0.058$, the required input signal-to-jamming ratio is given by $SJR_i = P/P_j = 1.47$. For the same bit error probability, the partial-band jamming strategy in Example 8.8 requires $SJR_i = 1/20$. Thus the follower noise jamming strategy may save the jammer 14.7 dB in power.

■

Example 8.12 Noncoherent fast FH-FSK and follower noise jamming

Let us consider the case where the FSK signal performs $L = 3$ hops per bit and again assume that the effect of noise is negligible compared to jamming. Using the ratio

$E_h/J_0 = (W/\delta N_D L R_b) SJR_i$, where $E_h = E_b/L$, the hop error probability of fast FH-FSK is $P_h = P_{c,h} P_h(\text{jammed}) = 0.5 P_{c,h} \exp[-(W/2\delta N_D L R_b) SJR_i]$. The fraction of a hop being jammed δ is now smaller than that of the case considered in Example 8.11. For numerical illustration, let $W/\delta N_D R_b = 6$, $P_{c,h} = 0.5$, and $SJR_i = P/P_j = 1.47$, then we have $P_h = 0.058$. By using (4.37) with L replacing n, P_h replacing p, and $t = 1$, we obtain the bit error probability $P_b = 0.01$ for hard decoding.

Now let us consider the case of soft decoding where L hops are combined for a decision. Using (7.413) with L replacing d, $r = 1/L$ we obtain the bit error probability $P_b = 0.004$, a slightly better performance than hard decoding.

■

8.4 Summary

The main theme of this chapter is the discussion of direct sequence spread spectrum, which is the cornerstone of commercial and military systems. We explored important techniques for direct sequence CDMA, such as fixed length and variable length orthogonal coverings. We also used IS-95 as an example to show the implementation of direct sequence spread spectrum in a major commercial system. We also presented various jamming scenarios applicable to both direct sequence and frequency hop spread spectrum systems. Pulsed (partial time) jamming is an effective jamming strategy against direct sequence spread spectrum systems, but this strategy also requires a high peak power transmitter. Partial band jamming is an effective jamming strategy against frequency hop spread spectrum systems and does not require a high peak power transmitter. Fast frequency hop systems can be deployed to combat the potent follower (repeater) jammers.

Problems

1. Consider a DS-PSK signal using the chip pulse shape $p(t)$. Express the waveform $s_i(t)$ for a data bit $d_i \in \{0, 1\}$ or $d_i \in \{-1, 1\}$. Express the waveform for an infinite number of bits.
2. Write the mathematical expression for the autocorrelation of a periodic m-sequence with squared chip pulse shape. Derive the corresponding power spectral density.
3. List the seven states and the outputs of the m-sequence generator $h(x) = 1 + x + x^3$.
4. Draw the generators for the polynomials $h(x) = 1 + x^2 + x^5$ and $h(x) = 1 + x^3 + x^5$.
5. The Gold sequences are generated by modulo-2 adding a pair of *preferred m-sequences* from two distinct generators of degree n. This results in $2^n + 1$ Gold sequences (which include the pair of preferred m-sequences) whose crosscorrelation has three values given by

$$R_{l,n} = \begin{cases} -t(n) \\ -1 \\ t(n)-2 \end{cases} \qquad t(n) = \begin{cases} 2^{(n+1)/2}+1, \text{odd } n \\ 2^{(n+2)/2}+1, \text{ even } n, \ n \neq 0 \pmod 4 \end{cases}$$

Generate the set of Gold sequences from the following preferred pair of m-sequence generators, $h(x) = x^3 + x + 1$ and $h(x) = x^3 + x^2 + 1$.

6. Consider three variable orthogonal covering channels 1, 2, and 3 that employ the Walsh sequences $\boldsymbol{w}_1 = (0110, 0110, 0110, 0110)$, $\boldsymbol{w}_2 = (0011, 1100)$, and $\boldsymbol{w}_3 = (0000)$. The data bits for the three channels are $d_1 = 1$; $d_{2,0} = 1$, $d_{2,1} = 1$; $d_{3,0} = 0$, $d_{3,1} = 0$, $d_{3,2} = 1$, $d_{3,3} = 1$.
   (a) Find the transmitted sequences $\boldsymbol{s}_1$; $\boldsymbol{s}_{2,0}, \boldsymbol{s}_{2,1}$; $\boldsymbol{s}_{3,0}, \boldsymbol{s}_{3,1}, \boldsymbol{s}_{3,2}, \boldsymbol{s}_{3,3}$ using the mapping $0 \rightarrow 1$ and $1 \rightarrow -1$.
   (b) Scale the sequence $\boldsymbol{s}_1$ by a factor of two. Find the orthogonal covering sequence $\boldsymbol{s}$.
   (c) Recover the data bits via inner products and threshold detection.
7. Consider three variable orthogonal covering channels 1, 2, and 3 that employ the Walsh sequences $\boldsymbol{w}_1 = (0000, 1111)$, $\boldsymbol{w}_2 = (0110, 1001)$, and $\boldsymbol{w}_3 = (0101)$. The data bits for the three channels are $d_1 = 0$; $d_2 = 1$; $d_{3,0} = 1$, $d_{3,1} = 1$.
   (a) Find the transmitted sequences $\boldsymbol{s}_1$; $\boldsymbol{s}_2$; $(\boldsymbol{s}_{3,0}, \boldsymbol{s}_{3,1})$ using the mapping $0 \rightarrow 1$ and $1 \rightarrow -1$.
   (b) Scale the sequence $\boldsymbol{s}_1$ by a factor of two. Find the orthogonal covering sequence $\boldsymbol{s}$.
   (c) Recover the data bits via inner products and threshold detection.
8. Consider a DS-PSK signal with a received signal power of 1 mW. The tone jamming signal has 500 mW of power. Assuming the PN spread sequence is an m-sequence and the output signal-to-jamming ratio is required to be at least 10 dB, find the necessary spread factor.
9. Design a DS-QPSK modulator and demodulator. Carry out the demodulation analysis to recover the I- and Q-channel bits.
10. Consider a DS-PSK signal with tone jamming.
   (a) The PN sequence employed by the DS-PSK signal is an m-sequence. Find the output signal-to-jamming ratio given the input signal-to-jamming ratio of -20 dB.
   (b) Given the output signal-to-noise ratio of 20 dB, find the output signal-to-noise and interference ratio.
11. Consider a DS-PSK signal with tone jamming:

$$s(t) = Ad_i c(t) \cos 2\pi f_c t, \ iT_b < t \leq (i+1)T_b, \quad \text{and}$$
$$j(t) = A_j \cos[2\pi(f_c + f)t + \theta]$$

where f is the offset frequency from the carrier frequency f_c. The spread factor is $N = T_b/T_c$. Assume coherent demodulation.
   (a) Write the decision variable $X = S + J + \mathcal{N}$ by identifying the signal component S, the jamming component J, and the noise component $\mathcal{N}$. Do not try to solve the integrals.
   (b) Consider a situation where the single-tone jamming signal is replaced by a multi-tone jamming signal $j(t) = \sum_{k=1}^{M} A_{j,k} \cos(2\pi f_c t + \theta_k)$. Calculate the jamming component and its variance assuming all M jamming tones have independent θ_k.

12. Consider a DS-PSK signal with a spread factor of 128 under pulsed jamming. The input signal-to-jamming ratio is -14 dB.
    (a) What is the worst-case output signal-to-pulse jamming ratio and the corresponding bit error probability?
    (b) What would be the power of a broadband jamming signal relative to the peak power of a pulsed jamming signal to achieve the same bit error probability at the jammed receiver?
13. Consider a DS-PSK signal that encounters a pulsed jamming signal with duty cycle $\delta = 0.1$. The average input signal power is 1 mW and the average jamming power is 10 mW. The received bit energy-to-noise density ratio is $E_b/N_0 = 7$ dB, and the spread factor is $N = 128$. Calculate the bit error probability. What is the bit error probability if the jammer optimizes δ? What is the corresponding pulse duty cycle?
14. Using the tight upper bound $Q(x) < e^{-x^2/2}/\sqrt{2\pi}x$, find the optimum pulse duty cycle and the worst-case bit error probability for pulsed jamming of a DS-PSK signal, assuming noise is negligible compared to the jamming signal.
15. The DS-PSK signal in Example 8.7 is encoded with a convolutional code of rate ½ and constraint length K. The Viterbi algorithm is carried out for each data frame as in IS-95, and the signal is jammed by a pulsed jammer. Jamming occurs for a complete data frame, that is, when a data frame is jammed, all bits in that frame are jammed and when the data frame is not jammed no bits are jammed.
    (a) Consider the case $K = 5$ (Table 7.13). Evaluate the bit error probability of the coded signal with soft decoding.
    (b) Consider the case $K = 9$ (Table 7.13). Evaluate the bit error probability of the coded signal with soft decoding. Compare the result with that of (a).
    (c) Repeat (a) for hard decoding. Compare the result with that of (a).
    (d) Evaluate the bit error probability with Golay code. Compare the result with that of (a).
16. Consider a DS-PSK-CDMA system that allows a total of K multiple access users.
    (a) The receiver of a user encounters a broadband Gaussian jamming signal with a power spectral density function $J_0/2$. The bit energy-to-jamming density ratio is $E_b/J_0 = 12$ dB. The bit energy-to-noise density ratio is $E_b/N_0 = 14$ dB. Find the minimum spread factor N that can accommodate at least $K = 25$ users at a bit error probability of 10^{-3}.
    (b) Now assume pulsed jamming with duty cycle $\delta = 0.1$, and evaluate the bit error probability.
17. Generalize (8.82) for K users with different powers P_i.
18. Consider a DS-PSK-CDMA system that allows a total of K multiple access users.
    (a) The bit energy-to-noise density ratio is $E_b/N_0 = 14$ dB. Find the minimum spread factor N that can accommodate at least $K = 25$ users at a bit error probability of 10^{-3}.
    (b) Now consider a convolutional code of rate ½, constraint length $K = 9$ (Table 7.13) and soft decoding. Using the parameters in (a) to determine the coded bit error probability. Compare the result to that of the uncoded signal with spread factor $2N$.

19. Provide the pulse shape that can uniformly distribute the MUI power over the spread bandwidth.
20. Consider a DS-QPSK signal under Gaussian broadband jamming with the I-channel jamming variance many times as large as the Q-channel jamming variance.

    Assume that the transmitter has the channel side information and is aware of the jamming strategy. What should the transmitter do to maximize the receiver performance?
21. Consider a coherent DS-CSK signal under pulsed jamming with duty cycle δ. Derive the bit error probability under the worse-case situation, assuming that the channel noise is negligible compared to the jamming signal.
22. Consider a noncoherent DS-CSK signal under pulsed jamming with duty cycle δ. Derive the bit error probability under the worse-case situation, assuming that the channel noise is negligible compared to the jamming signal.
23. Consider a coherent DS-CSK signal with $M = 16$ and a symbol rate spread factor $N = 128$ under pulsed jamming given the input signal-to-jamming ratio of -8 dB. Assuming that the channel noise is negligible compared to the jamming signal, what is the bit error probability? What would be the power of a broadband jamming signal relative to the peak power of a pulsed jamming signal in order to achieve the same bit error probability at the jammed receiver?
24. Consider a noncoherent DS-CSK signal with $M = 16$ and a symbol rate spread factor $N = 128$ under pulsed jamming given the input signal-to-jamming ratio of -8 dB. Assuming that the channel noise is negligible compared to the jamming signal, what is the bit error probability? What would be the power of a broadband jamming signal relative to the peak power of a pulsed jamming signal to achieve the same bit error probability at the jammed receiver?
25. Consider a coherent DS-CSK signal with $M = 16$ that encounters a pulsed jamming signal with duty cycle $\delta = 0.1$. The average input signal power is 4 mW and the average jamming power is 10 mW. The received bit energy-to-noise density ratio is $E_b/N_0 = 7$ dB, and the symbol rate spread factor is $N = 128$.
    (a) Calculate the bit error probability.
    (b) To achieve the same bit error probability as in (a) what would be the required symbol rate spread factor if the jammer optimizes δ?
26. The coherent DS-CSK signal is used with a convolutional code of rate ½ and constraint length $K = 5$ (Table 7.13). The Viterbi algorithm is carried out for each data frame as in IS-95. Jamming occurs for a complete data frame, that is, when a data frame is jammed, all bits in that frame are jammed and when the data frame is not jammed no bits are jammed. Assuming a symbol rate spread factor of 128 and the average input signal-to-jamming ratio of -8 dB, what is the coded bit error probability with hard decoding when the jamming duty cycle is 0.1? Assume that the channel noise is negligible compared to the jamming signal.
27. Consider a noncoherent DS-CSK-CDMA system that allows a total of K multiple access users.
    (a) The receiver of a user encounters a broadband Gaussian jamming signal with a power spectral density function $J_0/2$ uniform over the spread bandwidth. The bit

energy-to-jamming density ratio is $E_b/J_0 = 12$ dB. The bit energy-to-noise density ratio is $E_b/N_0 = 14$ dB. Find the minimum symbol rate spread factor N that can accommodate at least $K = 25$ users at a bit error probability of 10^{-3}, given $M = 64$.

(b) Now assume pulsed jamming with duty cycle $\delta = 0.1$, using the parameters in (a) to determine bit error probability.

28. Consider a noncoherent DS-CSK-CDMA system with $M = 64$ that allows a total of K multiple access users.
    (a) The bit energy-to-noise density ratio is $E_b/N_0 = 14$ dB. Find the minimum symbol rate spread factor N that can accommodate at least $K = 25$ users at a bit error probability of 10^{-3}.
    (b) If the symbol rate spread factor is doubled, how many multiple access users can the system accommodate for the same bit error probability?
29. What would be the power of a broadband jamming signal relative to the power of a partial-band jamming signal to achieve the same bit error probability at a slow noncoherent FH-FSK receiver? Give the numerical answer for a bit error probability of 10^{-2}.
30. Consider a slow noncoherent FH-DPSK signal with a spread factor of 128 under partial-band jamming given the input signal-to-jamming ratio of -14 dB. What are the optimum δ and the corresponding bit error probability? What would be the power of a broadband jamming signal relative to the power of a pulsed jamming signal to achieve the same bit error probability at the jammed receiver? Assume that channel the noise is negligible compared to the jamming signal.
31. Consider a slow noncoherent FH-FSK signal that encounters a partial-band jamming signal with $\delta = 0.1$. The average input signal power is 1 mW and the average jamming power is 10 mW. The received bit energy-to-noise density ratio is $E_b/N_0 = 10$ dB, and the spread factor is $N = 128$.
    (a) Calculate the bit error probability.
    (b) To achieve the same bit error probability what would be the required spread factor if the jammer optimizes δ?
32. Consider a slow noncoherent FH-MFSK signal that encounters a partial-band jamming signal with $\delta = 0.1$. The average input signal power is 1 mW and the average jamming power is 10 mW. The received bit energy-to-noise density ratio is $E_b/N_0 = 10$ dB, and the spread factor is $N = 128$.
    (a) Calculate the bit error probabilities for $M = 16, 64$.
    (b) To achieve the same bit error probabilities what would be the required spread factor if the jammer optimizes δ?
33. Compare the two cases of slow noncoherent FH-FSK in Examples 8.8 and 8.10 from the point of view of jamming power to achieve the same bit error probability at the jammed receiver.
34. Derive the bit error probability for slow noncoherent FH-DPSK under multi-tone jamming. Use the numerical values in Example 8.10 to evaluate the bit error probability.
35. Derive the bit error probability for slow noncoherent FH-MSK under multi-tone jamming.

36. Apply coding with a convolutional code of rate ½, constraint length $K = 5$ (see Table 7.13), and hard decoding to the slow noncoherent FH-FSK in Example 8.8 to see whether the performance can be improved. The spread bandwidth is the same as in the uncoded case.
37. Derive the bit error probability for a fast noncoherent FH-DPSK under follower jamming.
38. Consider a follower jamming strategy with $T_h = 1.5(T_d + T)$, $W/N_D R_b = 1$, $P_{c,h} = 0.3$, and $SJR_i = P/P_j = 2$. Calculate the bit error probability for a slow noncoherent FH-FSK signal.
39. What would be the power of a partial-band jamming signal relative to the power of a follower jamming signal to achieve the same bit error probability at a slow noncoherent FH-FSK receiver? Give the numerical answer for a bit error probability of 10^{-2} with the following known parameters: $N = W/R_b = N_D = 128$, $\delta = 0.5$, $P_{c,h} = 0.5$.
40. Consider a slow frequency hop multiple access system employing noncoherent MFSK (FHMA-MFSK). There are K active users in the system and the spread bandwidth is W.
    (a) Find the probability of a hit when two or more user signals collide in a hop bin.
    (b) Assuming random hopping, evaluate the bit error probability for a user.

Further reading

For advanced study on direct sequence spread spectrum we recommend Lee and Miller [5] and Viterbi [6]. For an introduction to CDMA 2000 and WCDMA references [7,8] may be consulted. Detailed discussion of frequency hop spread spectrum systems can be found in [9–12]. Sarwate and Pursley [13] provides a comprehensive discussion of PN sequences for CDMA applications.

Bibliography

1. M. B. Pursley, *Introduction to Digital Communications*, Upper Saddle River, NJ: Pearson Prentice Hall, 2005.
2. J. S. Lee, R. H. French, and L. E. Miller, "Probability of error analysis of a BFSK frequency-hopping system with diversity under partial-band interference – Part I: Performance of square-law linear combining soft decision receiver," *IEEE Trans. Commun.*, Vol. **32**, No. 6, pp. 645–653, 1984.
3. J. S. Lee, L. E. Miller, and Y. K. Kim, "Probability of error analysis of a BFSK frequency-hopping system with diversity under partial-band interference – Part II: Performance of square-law nonlinear combining soft decision receiver," *IEEE Trans. Commun.*, Vol. **32**, No. 6, pp. 1243–1250, 1984.

4. L. E. Miller, J. S. Lee, and A. P. Kadrichu, "Probability of error analysis of a BFSK frequency-hopping system with diversity under partial-band interference – Part III: Performance of square-law self-normalizing soft decision receiver," *IEEE Trans. Commun*., Vol. **34**, No. 7, pp. 669–675, 1986.
5. J. S. Lee and L. E. Miller, *CDMA Systems Engineering Handbook*, London: Artech House, 1998.
6. A. J. Viterbi, *CDMA: Principles of Spread Spectrum Communications*, Reading, MA: Addison-Wesley, 1995.
7. V. K. Garg, *Wireless Network Evolution. 2G to 3G*, Upper Saddle River, NJ: Prentice Hall, 2002.
8. A. Richardson, *WCDMA Design Handbook*, Cambridge: Cambridge University Press, 2005.
9. M. K. Simon, J. K. Omura, R. A. Scholtz, and B. K. Levitt, *Spread Spectrum Communications*, Rockville, MD: Computer Science Press, 1985.
10. R. C. Dixon, *Spread Spectrum Systems with Commercial Applications*, 3rd edition, Chichester: John Wiley & Sons, 1994.
11. R. L. Peterson, R. E. Ziemer, and D. E. Borth, *Introduction to Spread Spectrum Communications*, Englewood Cliffs, NJ: Prentice Hall, 1995.
12. D. J. Torrieri, *Principles of Secure Communications Systems*, London: Artech House, 1985.
13. D. V. Sarwate and M. B. Pursley, "Crosscorrelation properties of pseudorandom and related sequences," *Proc. IEEE*, Vol. **68**, No. 5 pp. 593–619, 1980.
14. S. W. Golomb, *Shift Register Sequences*, San Francisco, CA: Holden-Day, 1967.
15. R. A. Scholtz, "The origins of spread spectrum communications," *IEEE Trans. Commun.*, Vol. **30**, No. 5, pp. 822–852, May 1982.
16. TIA/EIA Interim Standard IS-54, "Cellular system dual mode mobile station–land station compatibility specifications," Electronic Industries Association, May 1990.
17. TIA/EIA Interim Standard IS-95, "Mobile station–base station compatibility standard for dual mode wideband spread spectrum cellular system," Electronic Industries Association, July 1993.
18. H. Urkowitz, "Energy detection of unknown deterministic signals," *IEEE Trans. Commun.*, Vol. **55**, pp. 523–531, 1967.

9 Intersymbol interference and equalization

Introduction

Intersymbol interference (ISI) is a phenomenon in which the energy of a symbol spills over into succeeding symbols causing interference. Tight filtering at the transmitter and receiver and/or channel distortion can cause the waveform that represents a symbol to spread out into succeeding symbol periods. In a terrestrial wireless channel, a signal can travel from the transmitter to the receiver via multiple delayed paths (echoes). If the delays between paths are large compared to a symbol period, the energy carried by these echoes can cause significant ISI to the succeeding symbols. In this chapter, we study the *Nyquist criterion* for zero ISI and provide the design of an optimum demodulator that can achieve *both maximum output signal-to-noise ratio* and *zero ISI*. We then study linear equalizers, such as the zero-forcing linear equalizer (ZF-LE), and the mean-square error linear equalizer (MSE-LE), and nonlinear equalizers, such as the zero-forcing decision-feedback equalizer (ZF-DFE) and the mean-square error decision-feedback equalizer (MSE-DFE). Both nonlinear equalizers perform better than their linear counterparts. We then study the *maximum likelihood sequence detection* (MLSD), which is the optimum nonlinear equalization technique. Finally, the fractionally spaced equalizer is introduced to solve the timing error problem in the previous equalizers.

9.1 Intersymbol interference

The use of a squared pulse shape to represent a bit or a symbol applies only to an AWGN channel whose bandwidth is theoretically infinite. In practice, if the channel bandwidth is much larger than the modulation bandwidth, the squared pulse shape can, for all practical purposes, be preserved at the input of the matched filter in the demodulator. Unfortunately, bandwidth is a precious resource, so for bandwidth conservation many practical communication systems are *bandlimited*. This is done via filtering at both transmitter and receiver. If the channel bandwidth is smaller than the signal bandwidth, pulse distortion occurs. The pulse distortion can be illustrated by the classic example of a squared pulse going through an *RC*-filter whose time constant *RC* is much less than the pulse width *T*. Figure 9.1 illustrates the pulse distortion. The decaying tail of the output pulse certainly interferes with the next pulse causing *pre-filtering intersymbol interference* (ISI) at the input of the matched filter designed for $p(t)$. For example, if PSK is the modulated signal and its equivalent lowpass

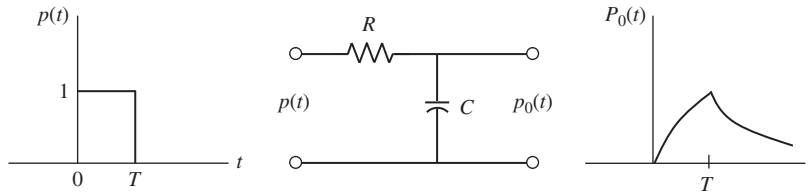

Figure 9.1 *RC*-filtering of a squared pulse. The output pulse is $p_0(t) = \left(1 - e^{-t/RC}\right)$ for $0 < t < T$ and $p_0(t) = \left(1 - e^{-T/RC}\right)e^{-(t-T)/RC}$ for $t > T$.

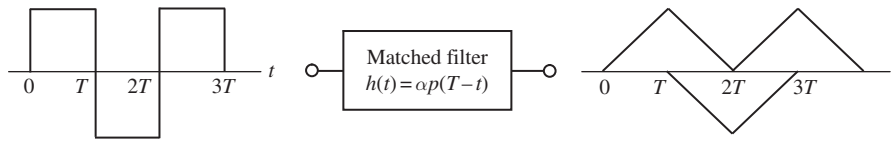

Figure 9.2 Zero ISI at sampling time T, $2T$, and $3T$ for squared pulses $\sum_{i=0}^{2} p(t - iT)$.

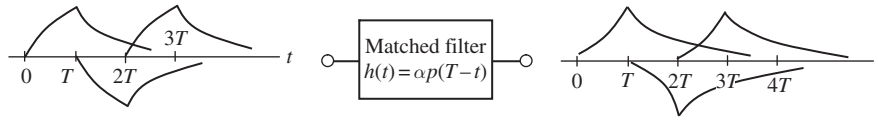

Figure 9.3 ISI at sampling time T, $2T$, and $3T$ for *RC*-filtered pulses $\sum_{i=0}^{2} p_0(t - iT)$.

channel can be modeled as an *RC*-filter, then $p_0(t)$ would appear at the input of the matched filter in Figure 7.15. Obviously, the pulse $p(t)$ is the complex envelope of a PSK bit and the pulse $p_0(t)$ is the distorted complex envelope of a PSK bit after going through an *RC*-filtering channel.

Let us now consider the output of a matched filter designed for the squared pulse and $p(t)$ and $p_0(t)$ at its input, respectively, as illustrated in Figures 9.2 and 9.3 for three consecutive bits 1, 0, 1.

We observe that the squared pulse shape presents no *post-filtering ISI* at the sampling time $t = T$, $2T$, $3T$. This happens because the output of the matched filter is a series of three triangular pulses whose positive or negative peak occurs right at the zero amplitude of other pulses. On the other hand, post-filtering ISI is clearly present for the series of *RC*-filtering pulses at the sampling time $t = T$, $2T$, $3T$. At the sampling time $t = 3T$, ISI due to $p_0(t)$ is constructive but ISI due to $p_0(t - T)$ is more destructive, so the net ISI effect is destructive. The same ISI effect occurs at $t = 2T$. The ISI effect on a particular bit can be either constructive or destructive, but the net effect is always destructive for a long series of bits or symbols as far as the bit or symbol error probability is concerned.

We note that the pre-filtering ISI is determined by the channel filtering. On the other hand, the post-filtering ISI is determined by both channel filtering and matched filtering. It is the latter that determines the performance degradation of a digitally modulated signal. Without

confusion, we simply use the word ISI to describe both pre-filtering ISI and post-filtering ISI unless otherwise stated. Note that pre-filtering ISI is irreversible since a matched filter designed for the *RC*-filtering pulse would not eliminate post-filtering ISI. In the following discussion, we seek to remedy ISI that arises from channel filtering by presenting the *Nyquist criterion for zero ISI*. The criterion provides the necessary and sufficient condition for a pulse shape to have zero ISI at the time a decision sample is taken. It makes no mention whether the sample is taken at maximum signal-to-noise ratio (SNR) or not. It is clear that a decision sample from an optimum demodulator designed for a bandlimited channel should meet both requirements, namely, *zero ISI* and *maximum SNR*. This is a subject that will be studied later in this section.

Nyquist criterion for zero ISI

The pulse $p(t)$ satisfies the zero ISI condition at the sampling time $t = kT$, that is,

$$p(kT) = \begin{cases} 1, & k = 0 \\ 0, & k \neq 0 \end{cases} \tag{9.1}$$

where k is an integer, *if and only if* the Fourier transform $P(f)$ of $p(t)$ satisfies the following condition:

$$\frac{1}{T}\sum_{m=-\infty}^{\infty} P\Big(f + \frac{m}{T}\Big) = 1 \tag{9.2}$$

Let us express the pulse $p(t)$ as the inverse Fourier transform of $P(f)$:

$$p(t) = \int_{-\infty}^{\infty} P(f)\, \mathrm{e}^{\mathrm{j}2\pi ft}\mathrm{d}f \tag{9.3}$$

Therefore, at the sampling time $t = kT$, we have

$$\begin{aligned} p(kT) &= \int_{-\infty}^{\infty} P(f)\, \mathrm{e}^{\mathrm{j}2\pi fkT}\mathrm{d}f = \sum_{m=-\infty}^{\infty}\int_{(2m-1)/2T}^{(2m+1)/2T} P(f)\mathrm{e}^{\mathrm{j}2\pi fkT}\mathrm{d}f \\ &= \sum_{m=-\infty}^{\infty}\int_{-1/2T}^{1/2T} P\Big(f + \frac{m}{T}\Big)\mathrm{e}^{\mathrm{j}2\pi fkT}\mathrm{d}f \\ &= \int_{-1/2T}^{1/2T}\sum_{m=-\infty}^{\infty} P\Big(f + \frac{m}{T}\Big)\mathrm{e}^{\mathrm{j}2\pi fkT}\mathrm{d}f \end{aligned} \tag{9.4}$$

If (9.2) holds true, then we have

$$\begin{aligned} p(kT) &= T\int_{-1/2T}^{1/2T} \mathrm{e}^{\mathrm{j}2\pi fkT}\mathrm{d}f \\ &= \frac{\sin k\pi}{k\pi} = \begin{cases} 1, & k = 0 \\ 0, & k \neq 0 \end{cases} \end{aligned} \tag{9.5}$$

To prove that (9.1) implies (9.2), let us express the periodic function in (9.2), whose period is $1/T$, as a Fourier series:

$$\sum_{m=-\infty}^{\infty} P\left(f+\frac{m}{T}\right) = \sum_{k=-\infty}^{\infty} c_k \mathrm{e}^{\mathrm{j}2\pi kfT} \tag{9.6}$$

where the coefficient c_k is given by

$$c_k = T\int_{-1/2T}^{1/2T} \sum_{m=-\infty}^{\infty} P\left(f+\frac{m}{T}\right)\mathrm{e}^{-\mathrm{j}2\pi fkT}\mathrm{d}f \tag{9.7}$$

Comparing (9.7) to (9.4), we obtain by virtue of (9.1)

$$c_k = Tp(-kT) = \begin{cases} T, & k=0 \\ 0, & k\neq 0 \end{cases} \tag{9.8}$$

Substituting (9.8) into (9.6) yields (9.2) and thus concludes the proof.

Note that when $P(f)$ is bandlimited to B, then the sampling rate $1/T$ must be less than or equal to $2B$. When $1/T > 2B$, there is no pulse shape that can produce zero ISI. Also note that the left-hand side of (9.2) is simply the Fourier transform of the sampled signal $p(t)\sum_m \delta(t+mT) = p(t)\sum_m \delta(t-mT)$ (by virtue of symmetry).

Example 9.1 The sin x/x pulse

Given the sampling interval T, there is only one pulse that satisfies the Nyquist criterion for zero ISI with minimum bandwidth. This pulse is the familiar type of sin x/x and is given by

$$p(t) = \frac{\sin(\pi t/T)}{\pi t/T} \tag{9.9}$$

The Fourier transform $P(f)$ of $p(t)$ is simply a constant T for $|f| \leq 1/2T$ and zero elsewhere, that is,

$$P(f) = \begin{cases} T, & |f| \leq \dfrac{1}{2T} \\ 0, & |f| > \dfrac{1}{2T} \end{cases} \tag{9.10}$$

Both $p(t)$ and $P(f)$ are shown in Figure 9.4. Note that the Nyquist sampling rate is twice the pulse bandwidth, which is $1/T$ and the Nyquist sampling time is T. Although the pulse is ideal, its energy spectrum poses difficulty for its generation. This is the same difficulty encountered in the realization of an ideal lowpass filter with an ideal brickwall transfer function. Therefore, the sin x/x pulse is more valuable for mathematical theory than practical applications.

■

Example 9.2 The raised-cosine pulse

The most popular zero-ISI pulse shape in practice is implemented via the raised-cosine pulse $p(t)$ given by

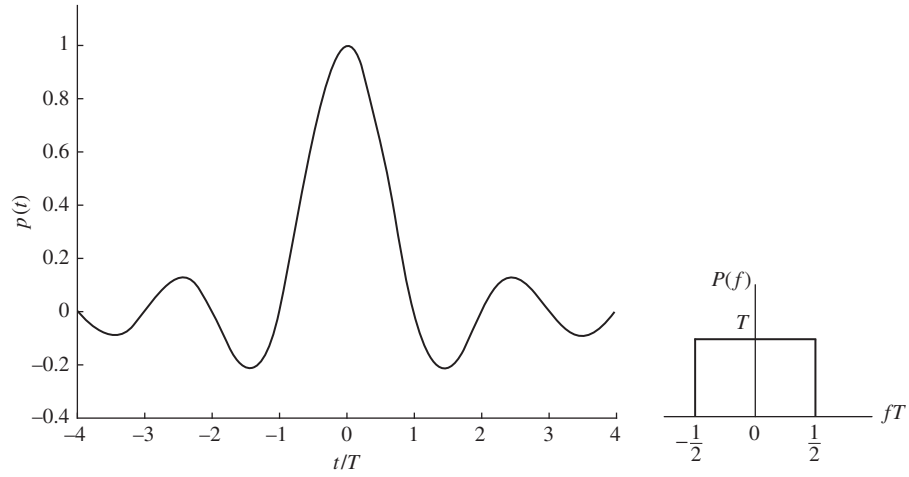

Figure 9.4 The ideal pulse for zero ISI and minimum bandwidth spectrum.

$$p(t) = \frac{\sin(\pi t/T)}{\pi t/T} \frac{\cos(\pi\beta t/T)}{1 - 4\beta^2 t^2/T^2} \tag{9.11}$$

The parameter β is commonly referred to as the *roll-off factor* and takes a value in the range $0 < \beta \leq 1$. Note that when $\beta = 0$, the raised-cosine pulse becomes the $\sin x/x$ pulse. The Fourier transform of the raised-cosine pulse is given as

$$P(f) = \begin{cases} T, & 0 \leq |f| \leq \frac{1-\beta}{2T} \\ \frac{T}{2}\left\{1 + \cos\left[\frac{\pi T}{\beta}\left(|f| - \frac{1-\beta}{2T}\right)\right]\right\}, & \frac{1-\beta}{2T} \leq |f| \leq \frac{1+\beta}{2T} \\ 0, & |f| > \frac{1+\beta}{2T} \end{cases} \tag{9.12}$$

Figure 9.5 shows both $p(t)$ and $P(f)$ for various values of β. The *energy spectrum* of $p(t)$ looks like the frequency response of a lowpass Butterworth filter with roll-off dictated by β. Therefore, it is easy to generate $p(t)$ in practice.

When the raised-cosine pulse shape is employed for data bits or symbols with rate $1/T$, the positive or negative peak of each bit or symbol coincides with the zero amplitude of other bits or symbols. Thus, there is no intersymbol interference.

■

9.2 Optimum demodulator for bandlimited channel

When the channel is bandlimited, a Nyquist pulse shape must be employed so that the decision sample contains zero ISI. Also, the decision sample must be obtained at maximum SNR. In this section, we study a demodulator that can accomplish the above tasks. We will use PSK as

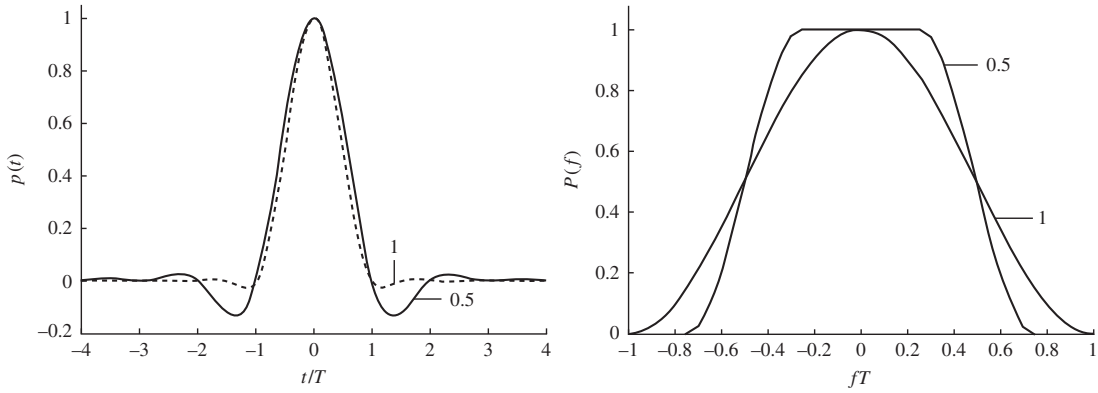

Figure 9.5 Raised-cosine pulse and its Fourier transform.

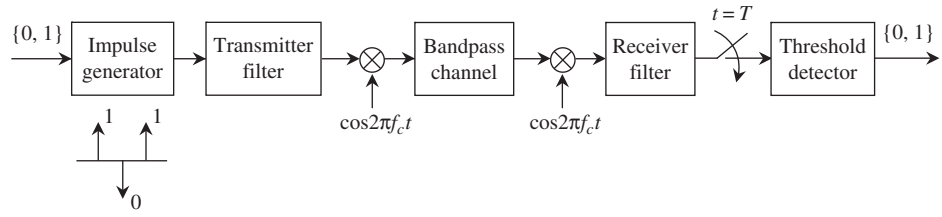

Figure 9.6 PSK modulator and demodulator for a bandlimited bandpass channel with a bandwidth of 2*B*.

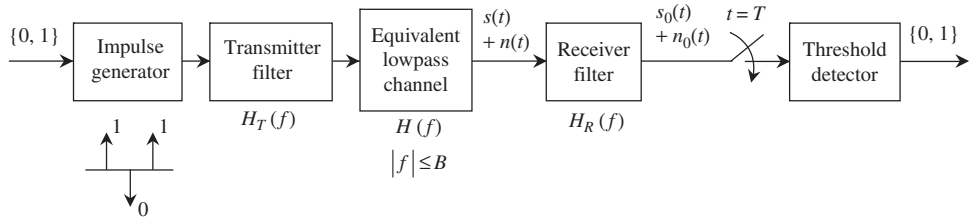

Figure 9.7. Equivalent lowpass model for a bandlimited PSK signal. The channel is bandlimited to *B*.

a case study but our analysis also applies to other modulation techniques. Figure 9.6 shows a generic PSK modulator and demodulator for a linear bandlimited bandpass channel.

It is more convenient to analyze the model in Figure 9.6 using its *equivalent lowpass* model. This model deals only with the *complex envelope* of the PSK signal and the corresponding *equivalent lowpass* channel of the *bandlimited bandpass* channel. Figure 9.7 illustrates the equivalent lowpass model. Let $H_T(f)$, $H_R(f)$, and $H(f)$ denote the *transfer functions* of the transmitter filter, receiver filter, and linear equivalent lowpass channel, respectively. Furthermore, let $s(t)$ and $n(t)$ denote the complex envelope of the received PSK signal and noise, respectively. For PSK, $s(t)$ is just an antipodal baseband signal. Furthermore, let $N(f)$ be the power spectral density of the *equivalent lowpass* noise $n(t)$, and for AWGN we take $N(f) = N_0(\text{W/Hz})$ by convention.

Obviously, the bandpass noise that accompanies the PSK signal at the input of the receiver in Figure 9.6 has a power spectral density $N(f-f_c)/2+ N(f+f_c)/2$, which is $N_0/2$ for AWGN. The output of the receiver filter is $s_0(t)+n_0(t)$, where $s_0(t)$ is the output signal and $n_0(t)$ is the output noise. At the sampling time $t = T$, we obtain the decision sample $s_0(T)+n_0(T)$. We want to design $H_T(f)$ and $H_R(f)$ to achieve maximum SNR_0 at the sampling time and also have zero ISI. We begin by noting that the Fourier transform $S_0(f)$ of $s_0(t)$ that represents a bit is

$$S_0(f) = S(f)H_R(f) = H_T(f)H(f)H_R(f) \tag{9.13}$$

where $S(f)$ is the Fourier transform of $s(t)$. Therefore, the output signal $s_0(t)$ can be expressed in terms of the inverse Fourier transform of $S_0(f)$ as

$$s_0(t) = \int_{-\infty}^{\infty} S_0(f)\,\mathrm{e}^{\,\mathrm{j}2\pi ft}\mathrm{d}f = \int_{-\infty}^{\infty} H_T(f)H(f)H_R(f)\,\mathrm{e}^{\,\mathrm{j}2\pi ft}\mathrm{d}f \tag{9.14}$$

At the sampling time $t = T$, we get

$$s_0(T) = \int_{-\infty}^{\infty} H_T(f)H(f)H_R(f)\,\mathrm{e}^{\,\mathrm{j}2\pi fT}\mathrm{d}f \tag{9.15}$$

It is obvious that the output signal power is $s_0^2(T)$, and the output noise power is given by

$$\overline{n_0^2(T)} = \int_{-\infty}^{\infty} N(f)\,|H_R(f)|^2\mathrm{d}f \tag{9.16}$$

The *output signal-to-noise ratio* at the output of the receiver filter at the sampling time $t = T$ is

$$\begin{aligned} SNR_0 &= \frac{|s_0(T)|^2}{\overline{n_0^2(T)}} \\ &= \frac{\left|\int_{-\infty}^{\infty} H_T(f)H(f)H_R(f)\,\mathrm{e}^{\,\mathrm{j}2\pi fT}\mathrm{d}f\right|^2}{\int_{-\infty}^{\infty} N(f)|H_R(f)|^2\mathrm{d}f} \\ &= \frac{\left|\int_{-\infty}^{\infty}\left[\frac{H_T(f)H(f)\mathrm{e}^{\,\mathrm{j}2\pi fT}}{\sqrt{N(f)}}\right]\left[\sqrt{N(f)}\,H_R(f)\right]\mathrm{d}f\right|^2}{\int_{-\infty}^{\infty} N(f)|H_R(f)|^2\mathrm{d}f} \end{aligned} \tag{9.17}$$

Applying the *Cauchy–Schwarz* inequality to the right-hand side of (9.17), we obtain the upper bound for SNR_0 as follows:

$$\begin{aligned} SNR_0 &\le \frac{\int_{-\infty}^{\infty}\frac{|H_T(f)|^2|H(f)|^2}{N(f)}\,\mathrm{d}f\int_{-\infty}^{\infty} N(f)|H_R(f)|^2\mathrm{d}f}{\int_{-\infty}^{\infty} N(f)|H_R(f)|^2\mathrm{d}f} \\ &\le \int_{-\infty}^{\infty}\frac{|H_T(f)|^2|H(f)|^2}{N(f)}\,\mathrm{d}f \end{aligned} \tag{9.18}$$

Condition for maximum SNR_0

The maximum output SNR_0, which is the right-hand side of (9.18), is attained if the following condition is satisfied:

$$\sqrt{N(f)}\,H_R(f) = \alpha \frac{H_T^*(f)H^*(f)\mathrm{e}^{-\mathrm{j}2\pi fT}}{\sqrt{N(f)}} \tag{9.19}$$

where α is an arbitrary constant. Therefore, we have

$$H_R(f) = \alpha \frac{H_T^*(f)H^*(f)\mathrm{e}^{-\mathrm{j}2\pi fT}}{N(f)} \tag{9.20}$$

In practice, filters are designed to have linear phase and, furthermore, we assume that the channel is linear; therefore, we can express $H_T(f)$, $H_R(f)$, and $H(f)$ as follows:

$$H_T(f) = |H_T(f)|\mathrm{e}^{-\mathrm{j}2\pi f t_T} \tag{9.21}$$

$$H_R(f) = |H_R(f)|\mathrm{e}^{-\mathrm{j}2\pi f t_R} \tag{9.22}$$

$$H(f) = \begin{cases} |H(f)|\mathrm{e}^{-\mathrm{j}2\pi f t_0}, & |f| \le B \\ 0, & |f| > B \end{cases} \tag{9.23}$$

where t_T, t_R, and t_0 are the time delays of the physically realizable transmitter and receiver filters and channel delay, respectively.

Substituting (9.21)–(9.23) into (9.20) yields, with $\alpha = |\alpha| \exp\{-\mathrm{j}2\pi f(t_T + t_R + t_0 - T)\}$,

$$H_R(f) = |\alpha| \frac{|H_T(f)|\,|H(f)|}{N(f)} \tag{9.24}$$

Condition for zero ISI

If we denote $P(f)$ as the energy spectrum of a Nyquist pulse, then the following condition must be met by $S_0(f)$ in (9.13):

$$H_T(f)H(f)H_R(f) = P(f)\mathrm{e}^{-\mathrm{j}2\pi f(t_T+t_R+t_0)}, \qquad |f| \le B \tag{9.25}$$

or, equivalently,

$$|H_T(f)|\,|H_R(f)|\,|H(f)| = P(f), \qquad |f| \le B \tag{9.26}$$

Solution for $|H_T(f)|$ and $|H_R(f)|$

Given $N(f)$ and $|H(f)|$, we can find a solution for $|H_T(f)|$ and $|H_R(f)|$ via (9.24) and (9.26). We have

$$|H_T(f)|^2 = \frac{1}{|\alpha|}\frac{N(f)P(f)}{|H(f)|^2}, \qquad |f| \le B \tag{9.27}$$

$$|H_R(f)|^2 = |\alpha|\frac{P(f)}{N(f)}, \qquad |f| \le B \tag{9.28}$$

Example 9.3 Optimum filters for AWGN channel

Let us consider the case of an AWGN channel with $N(f) = N_0$ (W/Hz). Selecting $|\alpha| = N_0$ in (9.27) and (9.28), we have

$$|H_T(f)| = \frac{\sqrt{P(f)}}{|H(f)|}, \qquad |f| \le B \tag{9.29}$$

$$|H_R(f)| = \sqrt{P(f)}, \qquad |f| \le B \tag{9.30}$$

For an ideal channel where $|H(f)| = 1$, $|f| \le B$, and $|H(f)| = 0$, $|f| > B$, we can design the transmit and receive filters as follows:

$$|H_T(f)| = |H_R(f)| = \sqrt{P(f)}, \qquad |f| \le B \tag{9.31}$$

As an illustration, if $P(f)$ is chosen to be the energy spectrum of a raised-cosine pulse in (9.12), then $|H_T(f)| = |H_R(f)| = \sqrt{P(f)}$, $|f| \le B$, implies that the transfer functions of both transmitter and receiver filters are square root raised-cosine. Note that in this case the bandwidth B of the equivalent lowpass channel is equal to $(1+\beta)/2T$, where $1/T$ is the bit rate and β is the roll-off factor of the raised-cosine pulse shape.

The transmitter filter can be considered as a cascade of two filters with transfer functions $\sqrt{P(f)}$ and $1/H(f)$, respectively. The combination of the filter $1/H(f)$ and the channel $H(f)$ creates a desired ideal channel with transfer functions $H_d(f) = 1$, $|f| \le B$ and $H_d(f) = 0$, $|f| > B$. The filter $1/H(f)$ is called the *equalizer*, and for the optimum demodulator it is located in the transmitter. In the next section, we will focus on the equalizer that is placed in the receiver, which is the case in practice. Figure 9.8 illustrates the channel model for an optimum demodulator.

■

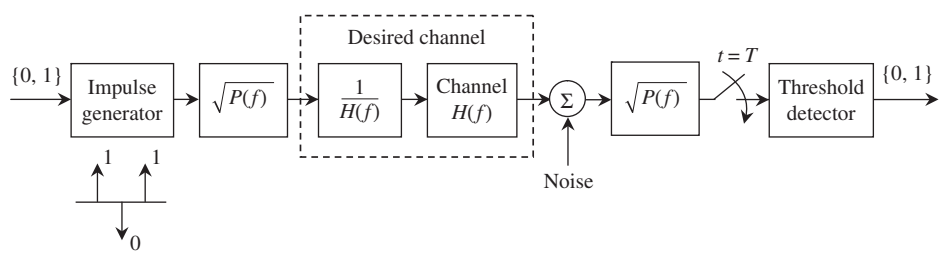

Figure 9.8 An ideal channel with zero ISI is created by equalization in the transmitter, which results in an optimum demodulator that achieves maximum output SNR_0 at the sampling time.

Example 9.4 Bit error probability of PSK in a bandlimited AWGN channel

The maximum output SNR_0 at the sampling time $t = T$ is given by the right-hand side of (9.18) as follows:

$$SNR_{0,max} = \int_{-\infty}^{\infty} \frac{|H_T(f)|^2 |H(f)|^2}{N_0} \mathrm{d}f \tag{9.32}$$

Note that $S(f) = H_T(f)H(f)$, therefore, using the Parseval relation, we get

$$\begin{aligned} SNR_{0,max} &= \frac{1}{N_0} \int_{-\infty}^{\infty} |S(f)|^2 \, \mathrm{d}f = \frac{1}{N_0} \int_{-\infty}^{\infty} s^2(t) \, \mathrm{d}t \\ &= \frac{2E_b}{N_0} \end{aligned} \tag{9.33}$$

where E_b is the bit energy. Note that $s(t)$ is the complex envelope of the PSK signal, therefore the energy of $s(t)$ is $2E_b$. The bit error probability is simply

$$P_b = Q\left(\sqrt{SNR_{0,max}}\right) = Q\left(\sqrt{\frac{2E_b}{N_0}}\right) \tag{9.34}$$

which is the same as the bit error probability for PSK with squared pulse shape. This result comes as no surprise, since the equalizer $1/|H(f)|$ in the transmitter totally compensates for the channel distortion and eliminates pre-filtering ISI before the noise enters the receiver.

■

9.3 Zero-forcing linear equalizer (ZF-LE)

The study of the optimum demodulator reveals that a decision sample can be obtained at *maximum signal-to-noise ratio* and with *zero ISI*. This can only happen *if and only if* equalization is implemented at the transmitter. The reason is simple: eliminate the pre-filtering ISI from the signal before it is received with noise, then design a filter matched to the signal to achieve the maximum output signal-to-noise ratio at the sampling time. In most real-world applications, this type of equalization is not practical simply because the channel frequency response is not known with sufficient precision by the transmitter. In addition, there is no way to vary the transmitter equalizer to respond to any changes in the channel. On the other hand, the channel estimation can easily be done at the receiver via a training sequence from the transmitter. Thus, the receiver equalizer can be made to vary in order to compensate for any changes in the channel. This situation arises in an application where the signal can travel an arbitrary path whenever a connection is established. The telephone network is a classic example where a new channel is encountered every time a call is made.

In a noisy bandlimited linear channel, the locations of the channel equalizer are not equivalent. When an equalizer is placed in the receiver, it can remove post-filtering ISI, but only at the expense of the output signal-to-noise ratio. This happens because the equalizer destroys the optimality of the matched filter, since the cascade of the matched filter and equalizer, whatever the order, is no longer a matched filter. Therefore, the receiver equalization cannot achieve optimum demodulation because it is an ad hoc method which tries to achieve a performance as close to that of an optimum demodulator as it can. Nevertheless, this type of equalization is more than adequate and widely used in practical applications.

Receiver equalization of the channel distortion is based on the knowledge of the channel contained in the received signal – a training sequence, for example. Any signal processor must process the received signal without loss of information and no signal processor can do it better than a matched filter matched to the received signal pulse. The decision sample at the matched filter output has the maximum signal-to-noise ratio, but it contains post-filtering ISI. Also, the noise samples are dependent since the noise power spectral density at the output of the matched filter is no longer white. To eliminate ISI, a linear equalizer is employed to force the post-filtering ISI to zero at the sampling time. Unfortunately, the equalizer also enhances noise and, therefore, destroys the optimality of the matched filter. Figure 9.9 illustrates the concept of linear equalization at the receiver using a *lowpass equivalent* model. It is obvious that the output of the equalizer must meet the Nyquist criterion in (9.1) or equivalently (9.2) to have zero ISI. This requirement implies that the frequency response of the equalizer must be the inverse of its input signal spectrum.

Let us consider a transmitted pulse $g(t)$ with Fourier transform $G(f)$ passing through a channel with impulse response $h(t)$ and corresponding transfer function $H(f)$. The received signal is $s(t) = g(t) * h(t)$ with the Fourier transform $S(f) = G(f)H(f)$. A matched filter with impulse response $s^*(-t)$ and corresponding frequency response $S^*(f)$ is employed. Note that the matched filter is non-causal for simplicity. A delay can always be introduced to make the matched filter causal without altering the result. The signal $s_0(t)$ at the matched filter output is sampled with rate $1/T \leq 2B$, where B is the bandwidth of the bandlimited channel. The sampled signal $x(t) = s_0(t)\sum_k \delta(t - kT) = s_0(t)\sum_k \delta(t + kT)$ is passed

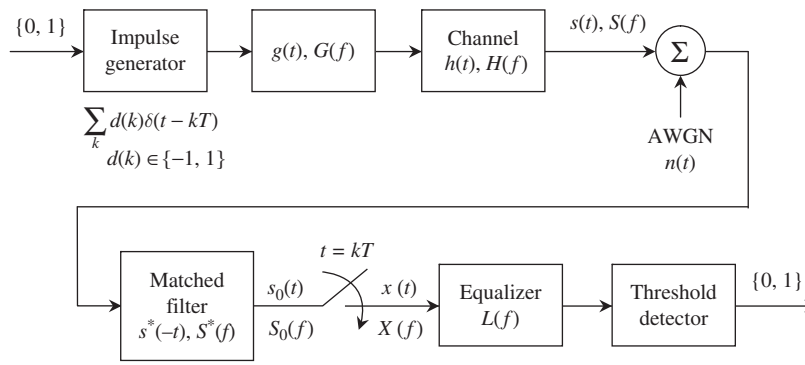

Figure 9.9 Continuous-time *lowpass equivalent* channel model with linear equalizer at the receiver.

through an equalizer to eliminate ISI. Let $S_0(f)$ be the Fourier transform of the matched filter output signal $s_0(t)$, then

$$S_0(f) = S(f)S^*(f) = |S(f)|^2 \tag{9.35}$$

Therefore, the Fourier transform $X(f)$ of the sampled signal $x(t)$ is given by (2.235) as

$$\begin{aligned} X(f) &= \frac{1}{T}\sum_{k=-\infty}^{\infty} S_0\left(f-\frac{k}{T}\right) = \frac{1}{T}\sum_{k=-\infty}^{\infty} S_0\left(f+\frac{k}{T}\right) \\ &= \frac{1}{T}\sum_{k=-\infty}^{\infty} \left|S\left(f-\frac{k}{T}\right)\right|^2 = \frac{1}{T}\sum_{k=-\infty}^{\infty} \left|S\left(f+\frac{k}{T}\right)\right|^2 \end{aligned} \tag{9.36}$$

Note that $X(f)$ is periodic with frequency $1/T$. Furthermore, the sampling rate must be in the range $B \le 1/T \le 2B$ for Nyquist criterion of zero ISI to hold. $X(f)$ is called the *folded spectrum* of the received signal $s(t)$.

In order for the sampled signal $x(t)$ to have zero ISI at the sampling time $t = 0$, its spectrum $X(f)$ must be equal to unity as dictated by the Nyquist criterion (9.2). This can only happen *if and only if* $s_0(t)$ is a Nyquist pulse. Since this is not possible, the only way to satisfy (9.2) is to force the sampled signal $x(t)$ through an equalizer whose transfer function $L(f)$ is equal to the inverse of $X(f)$, that is,

$$L(f) = \frac{1}{X(f)} \tag{9.37}$$

Now let us assume that the power spectral density of the *equivalent lowpass* AWGN $n(t)$ at the matched filter input is N_0. The matched filter output noise $n_0(t)$ has the power spectral density $N_0|S^*(f)|^2 = N_0|S(f)|^2$. Let $n_s(t) = n_0(t)\sum_k \delta(t-kT)$ be the sampled noise with the following autocorrelation:

$$\begin{aligned} R_{n_s}(\tau, n-k) &= \mathbf{E}[n_0(\tau)n_0(t+\tau)]\int \sum_k \sum_n \delta(t-kT)\delta(t+\tau-nT)\,\mathrm{d}t \\ &= R_{n_0}(\tau)\sum_k \sum_n \int \delta(t-kT)\delta(t+\tau-nT)\,\mathrm{d}t \\ &= R_{n_0}(\tau)\sum_k \sum_n \delta[\tau-(n-k)T] \end{aligned} \tag{9.38}$$

We are interested in the autocorrelation at the sampling time index $k = 0$, that is, $R_{n_s}(\tau) = R_{n_0}(\tau)\sum_n \delta(\tau - nT)$, whose Fourier transform is the power spectral density of the sampled noise

$$\begin{aligned} \Phi(f) &= \frac{N_0}{T}\sum_{k=-\infty}^{\infty} \left|S\left(f-\frac{k}{T}\right)\right|^2 = \frac{N_0}{T}\left|\sum_{k=-\infty}^{\infty} S\left(f+\frac{k}{T}\right)\right|^2 \\ &= N_0 X(f) \end{aligned} \tag{9.39}$$

Let $\Phi_0(f)$ be the power spectral density of the equalizer output noise, then we have

$$\Phi_0(f) = \Phi(f)|L(f)|^2 = \frac{N_0}{X(f)} = \frac{N_0}{\frac{1}{T}\sum\limits_{k=-\infty}^{\infty} \left|S\left(f + \frac{k}{T}\right)\right|^2} \tag{9.40}$$

It is apparent that if the spectrum $X(f)$ of the sampled signal $x(t)$ in (9.36) contains nulls or small values, then the output noise spectrum could become infinite or very large. Consequently, the variance of output noise tends to infinity or very large. Thus, the zero-forcing linear equalizer tries to obtain zero ISI at the expense of the output signal-to-noise ratio. Let us evaluate the noise power at the sampling time index $k = 0$. Denote $R_0(\tau)$ the autocorrelation of the equalizer output noise, which is the inverse Fourier transform of $\Phi_0(f)$. Note that the frequency response $L(f) = 1/X(f)$ of the equalizer is periodic with period $1/T$, therefore it can be expressed as a Fourier series. We have the following relationship:

$$\begin{aligned} \Phi_0(f) &= N_0 L(f) = N_0 \sum_{k=-\infty}^{\infty} \ell_k \, \mathrm{e}^{\mathrm{j}2\pi kfT}, \\ \ell_k &= T \int_{-1/2T}^{1/2T} L(f) \, \mathrm{e}^{-\mathrm{j}2\pi kfT} \mathrm{d}f = T \int_{-1/2T}^{1/2T} \frac{1}{X(f)} \mathrm{e}^{-\mathrm{j}2\pi kfT} \mathrm{d}f \\ R_0(\tau) &= N_0 \sum_{k=-\infty}^{\infty} \ell_k \, \delta(\tau + kT) \end{aligned} \tag{9.41}$$

Using (9.40), we obtain the noise power at the sampling time index $k = 0$ as follows:

$$\sigma^2 = R_0(0) = N_0 \ell_0 = N_0 T \int_{-1/2T}^{1/2T} L(f) \, \mathrm{d}f = N_0 T \int_{-1/2T}^{1/2T} \frac{1}{X(f)} \mathrm{d}f \tag{9.42}$$

Let $y(t) = p(t) \sum_k \delta(t - kT)$ be the sampled signal at the equalizer output and $Y(f)$ its Fourier transform. Since $Y(f) = L(f)X(f) = 1$, the pulse $p(t)$ obviously satisfies the Nyquist criterion (9.2), and hence at the sampling time index $k = 0$ we have $p(0) = 1$ per (9.1). Thus, the output signal power is $p^2(0) = 1$. Alternatively, we can view $y(t)$ as the inverse Fourier transform of $Y(f)$, and since $Y(f) = 1$ we have $y(t) = \delta(t)$. Hence, at the sampling index $k = 0$, $y(0)$ is simply the weight of $\delta(t)$, which is unity, and consequently the output signal power is $y^2(0) = p^2(0) = 1$. Therefore, the output signal-to-noise ratio is given by

$$SNR_{0,\,ZF\text{-}LE} = \frac{1}{\sigma^2} = \frac{1}{N_0 \ell_0} = \frac{1}{N_0 m_A(X^{-1})} \tag{9.43}$$

where $m_A(X^{-1}) = \ell_0$ denotes the *arithmetic mean* of $1/X(f)$ per (9.41). Note that SNR_0 cannot exceed the maximum output signal-to-noise ratio $SNR_{0,\,max}$ of the optimum filters given in (9.33), which is $2E_b/N_0$, that is, $1/N_0 m_A(X^{-1}) \le 2E_b/N_0$.

Example 9.5 Ideal channel with Nyquist pulse shape

Consider the case of an ideal channel with $H(f) = 1$, and a square root Nyquist transmitted pulse $g(t)$. In this case, the matched filter output signal $s_0(t)$ is a Nyquist pulse and its

sampled version $x(t)$ satisfies (9.1). The Fourier transform $X(f)$ of $x(t)$ also satisfies (9.2), that is, $X(f) = 1$. Therefore, no equalizer is needed in this case. Furthermore, $x(0) = 1$ via (9.1) and the noise power is simply $\sigma^2 = N_0 \int_{-\infty}^{\infty} s^2(t)\mathrm{d}t = N_0 \int_{-\infty}^{\infty} |S(f)|^2 \mathrm{d}f = N_0$ since the energy $2E_b$ of the Nyquist pulse is unity. Hence, $SNR_0 = x^2(0)/N_0 = 1/N_0$.

■

Example 9.6 Whitened matched filter

Let us return to the Fourier transform $X(f)$ of the sampled signal $x(t)$ in Figure 9.9. From (9.36), we observe that $X(f)$ is a nonnegative real function; therefore, it can be factored into the following product:

$$X(f) = F(f)F^*(f) \tag{9.44}$$

which also implies $X(f) = |F(f)|^2 = |F^*(f)|^2$. This suggests that the zero-forcing equalizer whose frequency response $L(f) = 1/X(f)$ can be decomposed into a cascade of two filters, one with response $1/F^*(f)$, and the other response $1/F(f)$. This concept is shown in Figure 9.10. Let us evaluate the noise spectrum at the output of the filter $1/F^*(f)$. The power spectral density of noise at the input of this filter is given in (9.39). Therefore, the output noise power spectral density is $\Phi(f)/\ |F^*(f)|^2 = N_0 X(f)/X(f) = N_0$, and this implies that the output noise is white.

■

The error probability for ZF-LE can be evaluated via the Q-function. For example, for PSK modulation or QPSK modulation, the bit error probability is simply $P_b = Q\left(\sqrt{SNR_{0,\,ZF\text{-}LE}}\right)$, where $SNR_{0,\,ZF\text{-}LE}$ is given in (9.43).

Up to this point, we have studied the concept of zero-forcing linear equalization (ZF-LE) at the receiver with the criterion of minimizing the effect of noise at the ZF-LE output subject to the constraint of zero ISI at the sampling time. As far as linear equalization is concerned, a demodulator that consists of a matched filter followed by a symbol-rate sampler and a ZF-LE provides the optimum performance in terms of minimizing the error probability. In practice, the use of a continuous-time matched filter, which is not easily adapted, poses some implementation problems if the channel response is not known with

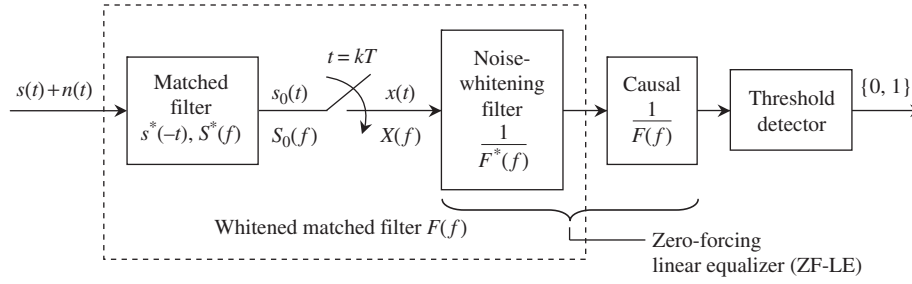

Figure 9.10 The whitened matched filter, which consists of a matched filter, a symbol-rate sampler, and a noise-whitening filter.

enough precision. In the following example, we present a suboptimum ZF-LE structure at the receiver that sacrifices some performance for practical consideration. The purpose is to eliminate ISI without the constraint of minimizing the effect of noise.

Example 9.7 Suboptimum ZF-LE

Instead of using the front-end matched filter, a wideband linear filter is employed in its place. This filter has a bandwidth larger than that of the received signal which passes through it undistorted. We can assume the transfer function of this front-end filter to be $H_{FE}(f) = 1$, $|f| \leq B_{FE}$, where $B_{FE} \geq 2B$. A symbol-rate sampler follows this front-end wideband filter. A ZF-LE with transfer function equal to the inverse of the sampled signal spectrum is employed to eliminate ISI. This concept is illustrated in Figure 9.11. Let $v_0(t)$ be the output of the front-end filter, and $V_0(f)$ its Fourier transform. We have

$$V_0(f) = S(f)H_{FE}(f) \tag{9.45}$$

Therefore, the Fourier transform $Q(f)$ of the sampled signal $q(t)$ is

$$\begin{aligned} Q(f) &= \frac{1}{T}\sum_{k=-\infty}^{\infty} V_0\left(f - \frac{k}{T}\right) = \frac{1}{T}\sum_{k=-\infty}^{\infty} V_0\left(f + \frac{k}{T}\right) \\ &= \frac{1}{T}\sum_{k=-\infty}^{\infty} S\left(f - \frac{k}{T}\right)H_{FE}\left(f - \frac{k}{T}\right) = \frac{1}{T}\sum_{k=-\infty}^{\infty} S\left(f + \frac{k}{T}\right)H_{FE}\left(f + \frac{k}{T}\right) \end{aligned} \tag{9.46}$$

To satisfy the Nyquist criterion (9.2) for zero ISI, the ZF-LE must have a frequency response equal to $1/Q(f)$. This yields an output signal $q_0(t)$ with a corresponding Fourier transform $Q_0(f) = Q(f)/Q(f) = 1$. Thus, at the sampling time $t = 0$, the output sample is unity via (9.1) and the sample power is also unity.

To evaluate the effect of noise, we again assume white noise $n(t)$ with power spectral density N_0. The front-end filter output noise has a power spectral density equal to $N_0|H_{FE}(f)|^2$. Therefore, the power spectral density of the sampled noise is given by

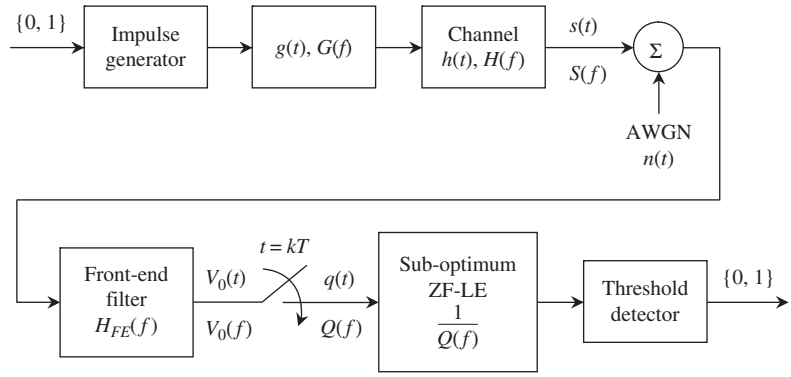

Figure 9.11 Channel model with suboptimum ZF-LE.

$$\Psi(f) = \frac{N_0}{T}\sum_{k=-\infty}^{\infty}\left|H_{FE}\left(f-\frac{k}{T}\right)\right|^2 = \frac{N_0}{T}\left|\sum_{k=-\infty}^{\infty}H_{FE}\left(f+\frac{k}{T}\right)\right|^2 \tag{9.47}$$

Consequently, the ZF-LE output noise possesses the following power spectral density:

$$\Psi_0(f) = \Psi(f)\frac{1}{|Q(f)|^2} = \frac{N_0\sum_{k=-\infty}^{\infty}\left|H_{FE}\left(f+\frac{k}{T}\right)\right|^2}{\frac{1}{T}\left|\sum_{k=-\infty}^{\infty}S\left(f+\frac{k}{T}\right)H_{FE}\left(f+\frac{k}{T}\right)\right|^2} \tag{9.48}$$

Let us consider Cauchy–Schwarz inequality for sums of the form

$$\left|\sum_{k=-\infty}^{\infty}a_k b_k\right|^2 \le \sum_{k=-\infty}^{\infty}|a_k|^2\sum_{k=-\infty}^{\infty}|b_k|^2 \tag{9.49}$$

By applying (9.49) to the denominator of (9.48), we have

$$\begin{aligned}\Psi_0(f) &\ge \frac{N_0\sum_{k=-\infty}^{\infty}\left|H_{FE}\left(f+\frac{k}{T}\right)\right|^2}{\frac{1}{T}\sum_{k=-\infty}^{\infty}\left|S\left(f+\frac{k}{T}\right)\right|^2\sum_{k=-\infty}^{\infty}\left|H_{FE}\left(f+\frac{k}{T}\right)\right|^2}\\ &\ge \frac{N_0}{\frac{1}{T}\sum_{k=-\infty}^{\infty}\left|S\left(f+\frac{k}{T}\right)\right|^2}\end{aligned} \tag{9.50}$$

Note that equality in (9.49) occurs if and only if $b_k = \alpha a_k^*$ where α is an arbitrary constant.

By comparing $\Psi_0(f)$ to the output noise power spectral density $\Phi_0(f)$ of the ZF-LE in (9.40), we conclude that $\Psi_0(f) \ge \Phi_0(f)$. Consequently, the output SNR_0 for the suboptimum ZF-LE is less than or equal to that of the ZF-LE given in (9.43). Note that $\Psi_0(f) = \Phi_0(f)$ if and only if $H_{FE}(f) = S^*(f)$, that is, the front-end filter is a matched filter!

■

So far, we have studied ZF-LE design via the analysis of the continuous-time sampled signal and its Fourier transform. Alternatively, we can also achieve the same goal by considering the discrete-time sequence of samples and its corresponding *discrete-time Fourier transform*. Let us consider the sampled signal $x(t)$ at the input of the equalizer in Figure 9.10. We note that $x(t) = \sum_k s_0(kT)\,\delta(t-kT)$, therefore the samples are $x(k) = s_0(kT)$. The sequence $x(k)$ and its discrete-time Fourier transform $X\left(\mathrm{e}^{\mathrm{j}2\pi f'}\right)$ are related by the following pair of equations:

$$\begin{aligned}x(k) &= \int_{-1/2}^{1/2}X\left(\mathrm{e}^{\mathrm{j}2\pi f'}\right)\mathrm{e}^{\mathrm{j}2\pi k f'}\mathrm{d}f'\\ X\left(\mathrm{e}^{\mathrm{j}2\pi f'}\right) &= \sum_{k=-\infty}^{\infty}x(k)\mathrm{e}^{-\mathrm{j}2\pi k f'}\end{aligned} \tag{9.51}$$

The relationship between $X\left(\mathrm{e}^{\,\mathrm{j}2\pi kf'}\right)$ and $X(f)$, the continuous-time Fourier transform of the sampled signal $x(t)$, can be established. First, $x(t) = \sum_k s_0(kT)\delta(t-kT) = \sum_k x(k)\delta(t-kT)$ and, since the Fourier transform of $\delta(t-kT)$ is $\mathrm{e}^{-\mathrm{j}2\pi kfT}$, it follows that

$$X(f) = \sum_{k=-\infty}^{\infty} x(k)\mathrm{e}^{-\mathrm{j}2\pi kfT} \tag{9.52}$$

Comparing (9.51) and (9.52), we see that $X\left(\mathrm{e}^{\,\mathrm{j}2\pi f'}\right)$ and $X(f)$ are related by

$$X\left(\mathrm{e}^{\,\mathrm{j}2\pi f'}\right) = X\left(\frac{f'}{T}\right), \quad |f'| \le 1/2 \tag{9.53}$$

Consequently, we obtain $X\left(\mathrm{e}^{\,\mathrm{j}2\pi f'}\right)$ in terms of $S(f)$ in (9.36) as follows:

$$X\left(\mathrm{e}^{\,\mathrm{j}2\pi f'}\right) = \frac{1}{T}\sum_{k=-\infty}^{\infty}\left|S\left(\frac{f'-k}{T}\right)\right|^2 == \frac{1}{T}\sum_{k=-\infty}^{\infty}\left|S\left(\frac{f'+k}{T}\right)\right|^2 \tag{9.54}$$

To deal with filter transfer functions, we employ the z-transform of the sequence $x(k)$, which is defined as

$$X(z) = \sum_{k=-\infty}^{\infty} x(k)z^{-k} \tag{9.55}$$

The z-transform reduces to the discrete-time Fourier transform when $z = \mathrm{e}^{\,\mathrm{j}2\pi f'}$, that is, on the unit circle in the complex z-plane. The sequence $x(k)$ can also be determined from $X(z)$ via the inverse z-transform using *contour integration* as follows:

$$x(k) = \frac{1}{2\pi\mathrm{j}}\int_C X(z)z^{k-1}\mathrm{d}z \tag{9.56}$$

Since the discrete-time Fourier transform $X\left(\mathrm{e}^{\,\mathrm{j}2\pi f'}\right)$ is nonnegative real, its corresponding z-transform $X(z)$ has a spectral factorization as follows:

$$X(z) = F(z)F^*\left(\frac{1}{z^*}\right) \tag{9.57}$$

where $F(z)$ is a minimum-phase transfer function, and $F^*(1/z^*)$ is a maximum-phase function. The function $F(z)$ accumulates all poles and zeroes of $X(z)$ within the unit circle, and one of each double-zero pair of $X(z)$ on the unit circle. Any zero α_k of $F(z)$ becomes zero at $1/\alpha_k^*$ of $F^*(1/z^*)$, and any pole β_k of $F(z)$ becomes a pole at $1/\beta_k^*$ of $F^*(1/z^*)$. If all the poles of $F(z)$ are inside the unit circle, then $F(z)$ is stable and causal. Since this implies that all poles of $F^*(1/z^*)$ are outside the unit circle, hence, $F^*(1/z^*)$ is stable and anti-causal. Figure 9.12 shows the optimum ZF-LE with discrete-time noise-whitening filter $1/F^*(1/z^*)$ and causal equalizer $1/F(z)$ instead of the sampled-data filters as in Figure 9.10.

It is quite obvious that the whitened matched filter can be described as a discrete-time minimum-phase filter with transfer function $F(z)$ when its input is the sequence of data symbols d_k transmitted by the modulator as indicated on Figure 9.12. The discrete-time

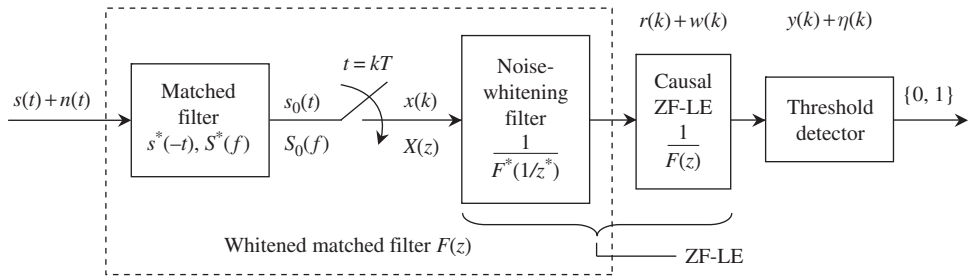

Figure 9.12 ZF-LE employing discrete-time filters.

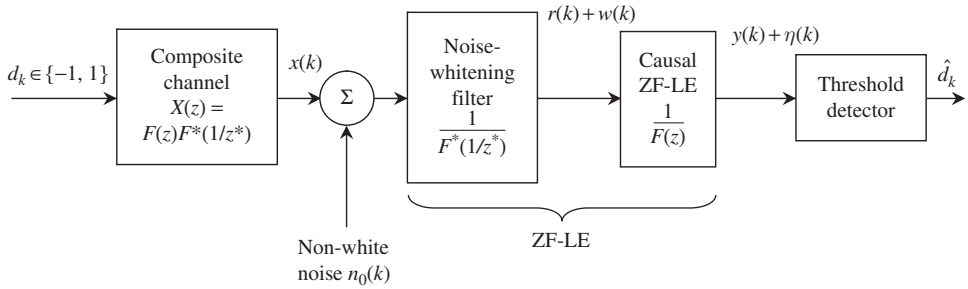

Figure 9.13 Discrete-time channel model for the ZF-LE sampled at the symbol rate. The equalizer input noise $w(k)$ has the spectrum $\Phi\left(e^{j2\pi f'}\right)/\left|F^*\left(e^{j2\pi f'}\right)\right|^2$, where $\Phi(f)$ is given in (9.39).

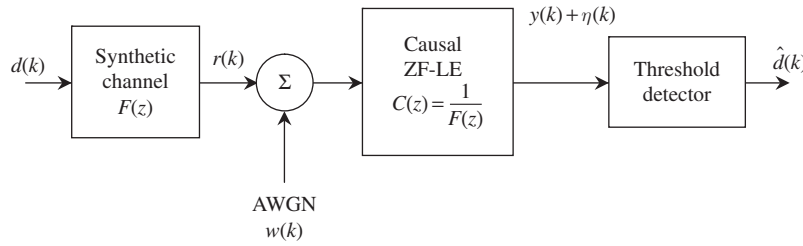

Figure 9.14 Simplified discrete-time channel model for the ZF-LE sampled at symbol rate.

channel model is illustrated by Figure 9.13. The sequence $x(k)$ is the sampled data at the output of the matched filter in Figure 9.12, and the noise sequence $n_0(k)$ is the non-white noise sample of the matched filter output noise $n_0(t)$. The output of the noise-whitening filter $1/F^*(1/z^*)$ is the signal sequence $r(k)$ plus the white noise sequence $w(k)$ whose spectrum is N_0. The simplified discrete-time channel model for the optimum ZF-LE is shown in Figure 9.14.

Let us denote the transfer function $1/F(z)$ of the equalizer in Figures 9.13 and 9.14 as

$$C(z) = \frac{1}{F(z)} = \sum_{k=0}^{\infty} c(k) z^{-k} \tag{9.58}$$

where $c(k)$ represents the filter coefficients (often called *tap weights*). Given the input signal sequence $r(k)$, the output signal sequence $y(k)$ is given by

$$y(k) = r(k) * c(k) = \sum_{i=0}^{\infty} r(i)c(k-i) = \sum_{i=0}^{\infty} c(i)r(k-i) \tag{9.59}$$

The output noise sequence $\eta(k)$ at the equalization output has the following power spectral density and variance:

$$\Phi_0\left(\mathrm{e}^{\mathrm{j}2\pi f'}\right) = \frac{N_0}{|F(\mathrm{e}^{\mathrm{j}2\pi f'})|^2} = \frac{N_0}{X(\mathrm{e}^{\mathrm{j}2\pi f'})} \tag{9.60}$$

$$\begin{aligned} \sigma^2 = \int_{-1/2}^{1/2} \Phi_0\left(\mathrm{e}^{\mathrm{j}2\pi f'}\right) \mathrm{d}f' = N_0 \int_{-1/2}^{1/2} \frac{\mathrm{d}f'}{X(\mathrm{e}^{\mathrm{j}2\pi f'})} = N_0 m_A\left(X^{-1}\right) \\ m_A\left(X^{-1}\right) = \int_{-1/2}^{1/2} \frac{\mathrm{d}f'}{X(\mathrm{e}^{\mathrm{j}2\pi f'})} \end{aligned} \tag{9.61}$$

where $m_A(X^{-1})$ is the *arithmetic mean* of $X^{-1}\left(\mathrm{e}^{\mathrm{j}2\pi f'}\right)$.

Example 9.8 Output signal-to-noise ratio of ZF-LE

Consider the *equivalent lowpass* pulse $s(t) = \sqrt{4Ea}\,\mathrm{e}^{-at}u(t)$ of the *modulated* pulse $s(t)\cos 2\pi f_c t$, where $u(t)$ is the unit step function and $a > 0$. Let E be the energy of the *modulated* pulse, then $2E$ is the energy of the pulse $s(t)$, that is,

$$2E = \int_{-\infty}^{\infty} s^2(t)\,\mathrm{d}t \tag{9.62}$$

The output $s_0(t)$ of the matched filter in Figure 9.12 is simply the autocorrelation of the pulse

$$\begin{aligned} s_0(t) = s_0(-t) &= \int_{-\infty}^{\infty} s(\tau)s(\tau - t)\,\mathrm{d}\tau \\ &= 2E\mathrm{e}^{-a|t|} \end{aligned} \tag{9.63}$$

Thus, the sequence $x(k) = s_0(kT)$ is simply given by

$$x(k) = 2E\mathrm{e}^{-aT|k|} = 2Eb^{|k|} \tag{9.64}$$

where $b = \mathrm{e}^{-aT}$. Using (9.55) the z-transform of the sequence $x(k)$ can be evaluated as follows:

$$X(z) = 2E\frac{b^2 - 1}{b} \cdot \frac{z}{(z-b)(z-b^{-1})} \tag{9.65}$$

Let us express $1/X(z)$ as a polynomial in z. We have

$$\frac{1}{X(z)} = \frac{1}{2E} \cdot \frac{b}{b^2-1} \cdot \frac{z^2 - (b+b^{-1})z + 1}{z} = \frac{1}{2E} \cdot \frac{b}{b^2-1}\left(z - b - b^{-1} + z^{-1}\right) \tag{9.66}$$

Consequently,

$$\frac{1}{X(\mathrm{e}^{\mathrm{j}2\pi f'})} = \frac{1}{2E} \cdot \frac{b}{b^2 - 1} \left(\mathrm{e}^{\mathrm{j}2\pi f'} - b - b^{-1} + \mathrm{e}^{-\mathrm{j}2\pi f'} \right) \tag{9.67}$$

Integrating $\Phi_0(f')$ in (9.61) using (9.67) for $|f'| \leq 1/2$ yields the output noise variance

$$\sigma^2 = \int_{-1/2}^{1/2} \frac{N_0}{X(\mathrm{e}^{\mathrm{j}2\pi f'})} \mathrm{d}f' = \frac{N_0}{2E} \cdot \frac{1 + b^2}{1 - b^2} \tag{9.68}$$

Note that $\sigma^2 = N_0 m_A(X^{-1})$, where $m_A(X^{-1})$ is the coefficient of the z^0-term in the series expansion of the ZF-LE transfer function $1/X(z)$, we have $\ell_0 = (1 + b^2)/[2E(1 - b^2)]$. Consequently, the equalizer output SNR_0 is given by (9.43) as

$$SNR_{0,\,ZF\text{-}LE} = \frac{1}{\sigma^2} = \frac{2E}{N_0} \cdot \frac{1 - b^2}{1 + b^2} \tag{9.69}$$

Note that $X(z)$ possesses poles at $z = b$ and $z = 1/b$. Therefore, as $b = \mathrm{e}^{-aT} \to 1$, that is, poles on the unit circle, $SNR_0 \to 0$, and the equalizer fails. Compared to the matched filter, the ZF-LE suffers a reduction in SNR_0 by a factor $(1 - b^2)/(1 + b^2)$.

■

Example 9.9 Transversal filter

In general, the linear equalizer is an *infinite impulse response* (IIR) filter. It can be approximated by a transversal filter, which is a classic name for a *finite impulse response* (FIR) filter with $2N + 1$ coefficients or *tap weights* $c(i)$. Specifically, we approximate the output of $y(k)$ of a linear equalizer with input $r(k)$ via (9.59) as follows:

$$y(k) = \sum_{i=-N}^{N} c(i) r(k - i) \tag{9.70}$$

The following constraints apply:

$$y(k) = \begin{cases} 1, & k = 0 \\ 0, & k = \pm 1, \pm 2, \ldots, \pm N \end{cases} \tag{9.71}$$

We can write (9.70) and (9.71) in matrix form as follows:

$$\begin{bmatrix} r(0) & r(-1) & \cdots & r(-2N) \\ r(-1) & r(0) & \cdots & r(-2N+1) \\ \vdots & \vdots & & \vdots \\ r(N) & r(N-1) & \cdots & r(-N) \\ \vdots & \vdots & & \vdots \\ r(2N) & r(2N-1) & \cdots & r(0) \end{bmatrix} \begin{bmatrix} c(N) \\ c(-N+1) \\ \vdots \\ c(0) \\ \vdots \\ c(N) \end{bmatrix} = \begin{bmatrix} 0 \\ 0 \\ \vdots \\ 1 \\ \vdots \\ 0 \end{bmatrix} \tag{9.72}$$

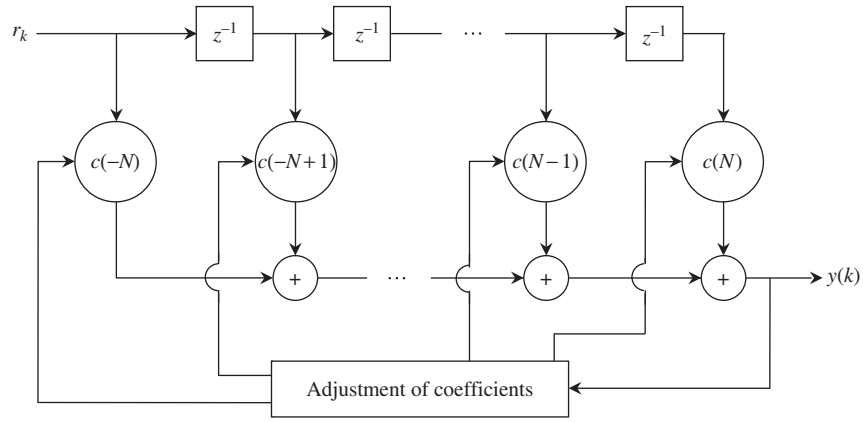

Figure 9.15 Transversal filter with $2N + 1$ coefficients.

or in compact form as

$$\boldsymbol{R}\boldsymbol{c} = \boldsymbol{y} \tag{9.73}$$

which yields the solution for $\boldsymbol{c}$ when $\boldsymbol{R}^{-1}$ exists as

$$\boldsymbol{c} = \boldsymbol{R}^{-1}\boldsymbol{y} \tag{9.74}$$

Figure 9.15 illustrates the transversal filter with $2N+1$ coefficients. If the input is causal, the number of coefficients reduces to $N+1$.

■

Summary

The ZF-LE equalizes the *folded spectrum* of the received signal via a filter with an inverse frequency response. It forces the ISI to be zero at the sampling time at the expense of the output signal-to-noise ratio. When the folded spectrum has nulls, the equalizer cannot equalize it since the output signal-to-noise ratio can go to zero. The output of the matched filter contains both anti-causal ISI (which affects preceding pulses) and causal ISI (which affects succeeding pulses) since it is symmetric at the sampling time. Nevertheless, the output of the whitened matched filter is causal because the whitened matched filter transfer function is $F(z)$, a minimum-phase function. In other words, the noise-whitening filter $1/F^*(1/z^*)$ totally eliminates anti-causal ISI (Figure 9.16). For the *suboptimum* ZF-LE, there is no spectral factorization for $Q(f)$ in (9.46) since it is not positive-real. The discrete-time channel model in Figure 9.14 still holds with $F(z)$ replaced by $Q(z)$. In this case, $Q(z)$ is not minimum-phase and the input to the ZF-LE $1/Q(z)$ is not guaranteed to be causal.

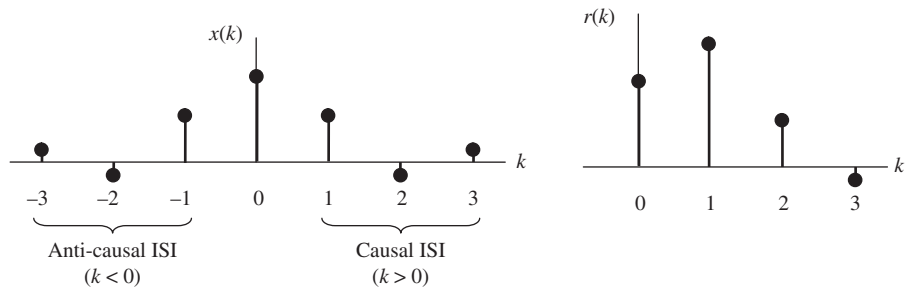

Figure 9.16 The output x_k of the sampled matched filter contains both anti-causal ISI and causal ISI. The output r_k of the whitened matched filter contains only causal ISI, which is eliminated by the equalizer $1/F(z)$.

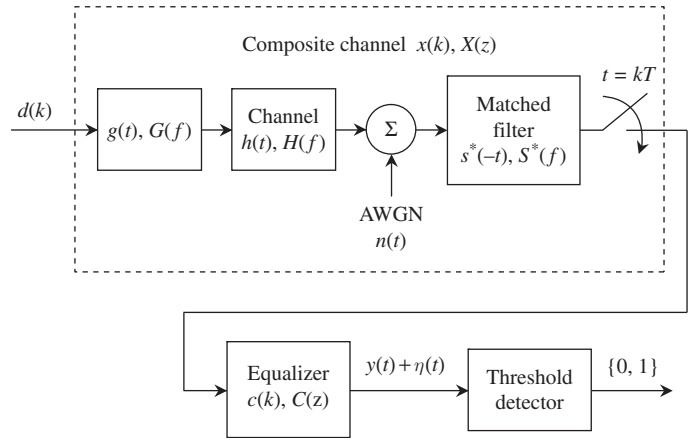

Figure 9.17 Discrete-time channel model for the MSE-LE sampled at the symbol rate.

9.4 Mean-square error linear equalizer (MSE-LE)

Unlike the ZF-LE, which forces ISI at the sampling time to zero, the MSE-LE allows some residual ISI at the equalizer output to improve the output SNR_0. By doing so, the MSE-LE can avoid infinite noise enhancement when the channel has nulls in its folded spectrum (poles on the unit circle). For continuity, we employ the discrete-time model counterpart of the continuous-time model as shown in Figure 9.17.

The input to the composite channel with transfer function $X(z)$ is the data process $d(k) \in \{-1,1\}$. We assume the data symbols $d(k)$ are uncorrelated and form a white wide-sense stationary process with constant power spectral density $S_d(f')$. The signal component $y(k)$ at the equalizer output is given by

$$y(k) = d(k) * x(k) * c(k) \tag{9.75}$$

Denote $\eta(k)$ the equalizer output noise. We wish to minimize the *mean-square error* (MSE) between $y(k) + \eta(k)$ and the transmitted data $d(k)$. Let the error $e(k)$ be defined as

$$e(k) = y(k) - d(k) + \eta(k) \tag{9.76}$$

Then the MSE is given by

$$\sigma_e^2 = \mathbf{E}\Big\{|e(k)|^2\Big\} = \mathbf{E}\Big\{|y(k) - d(k) + \eta(k)|^2\Big\} \tag{9.77}$$

The error $e(k)$ can be expressed as

$$e(k) = d(k) * [x(k) * c(k) - \delta(k)] + \eta(k) \tag{9.78}$$

Since MSE is simply the *variance* of $e(k)$, we can evaluate the power spectral density $S_e(f')$ of $e(k)$ and integrate it to get MSE. Assume that data and AWGN are uncorrelated, we can evaluate $S_e(f')$ directly from (9.78) as follows (for the sake of simplicity, we drop the argument f' in the filter response and power spectral densities):

$$S_e = S_d|XC - 1|^2 + S_\eta \tag{9.79}$$

where S_η is the power spectral density of the equalizer output noise. Note that the power spectral density of the equalizer input noise is given in (9.39) as N_0X, where N_0 is the power spectral density of the input AWGN. Thus,

$$S_\eta = N_0X|C|^2 \tag{9.80}$$

Substituting (9.80) into (9.79) yields the power spectral density of the equalizer output error as

$$S_e = S_d|XC - 1|^2 + N_0X|C|^2 \tag{9.81}$$

Note that S_e is positive-real, therefore to minimize the MSE, which is the integral of S_e, we only need to minimize S_e. We observe that when $C = 1/X$, S_e reduces to Φ_0 in (9.40) and σ_e^2 in (9.77) reduces to σ^2 in (9.42), which is the case of the ZF-LE for which $y(k) = d(k)$. Now, we wish to have some *residual* ISI at the equalizer output but minimize it together with noise and use the fact that the positive-real folded spectrum X can be factored into the following product:

$$X = FF^* = |F|^2 \tag{9.82}$$

Returning to (9.81) and completing the square term on the right-hand side, we obtain by using (9.82)

$$\begin{aligned} S_e &= S_d\Big(X^2|C|^2 + 1 - XC - X^*C^*\Big) + N_0X|C|^2 \\ &= (S_dX + N_0)X|C|^2 - S_d(XC + X^*C^* - 1) \\ &= S_i|F|^2|C|^2 - S_d|F|^2C - S_d|F|^2C^* + S_d \end{aligned} \tag{9.83}$$

where

$$S_i = S_dX + N_0 = S_d|F|^2 + N_0 \tag{9.84}$$

Continuing, we get

$$\begin{aligned} S_e &= \left(S_i|F|^2|C|^2 - S_d|F|^2C - S_d|F|^2C^* + S_d^2S_i^{-1}|F|^2\right) + \left(S_d - S_d^2S_i^{-1}|F|^2\right) \\ &= S_i\left|FC - S_dS_i^{-1}F\right|^2 + S_d\left(1 - S_dS_i^{-1}|F|^2\right) \end{aligned} \tag{9.85}$$

Note that $1 - S_dS_i^{-1}|F|^2 = N_0S_i^{-1}$ via (9.84), therefore

$$S_e = S_i\left|FC - S_dS_i^{-1}F\right|^2 + S_dN_0S_i^{-1} \tag{9.86}$$

We wish to minimize the first term on the right-hand side of (9.86) that contains the spectra of both ISI and noise at the equalizer input. This yields $FC - S_dS_i^{-1}F = 0$, and hence the following frequency response for the equalizer is obtained:

$$\begin{aligned} C &= S_dS_i^{-1} \\ &= \frac{S_d}{S_d|F|^2 + N_0} = \frac{S_d}{S_dX + N_0} \end{aligned} \tag{9.87}$$

The power spectral density of the MSE is given by

$$S_e = \frac{N_0S_d}{S_d|F|^2 + N_0} = \frac{N_0S_d}{S_dX + N_0} \tag{9.88}$$

For *white data* we can set $S_d(f) = 1$ to obtain the following *discrete-time transfer function* for the equalizer:

$$C(z) = \frac{1}{F(z)F^*(1/z^*) + N_0} \tag{9.89}$$

For white data the minimum MSE σ_e^2 in (9.88) is simply the integral of $S_e\left(\mathrm{e}^{\mathrm{j}2\pi f'}\right)$ from –1/2 to 1/2:

$$\sigma_e^2 = m_A(S_e) = \int_{-1/2}^{1/2} S_e\left(\mathrm{e}^{\mathrm{j}2\pi f'}\right)\mathrm{d}f' \tag{9.90}$$

Again, we use the notation $m_A(S_e)$ to denote the *arithmetic mean* of S_e. Comparing σ_e^2 with σ^2 of the ZF-LE in (9.61), we observe that $S_e = N_0/[X + N_0] < \Phi_0 = N_0/X$ due to the extra term N_0 in the denominator of S_e. Therefore, we always have $\sigma_e^2 \leq \sigma^2$. Furthermore, σ_e^2 does not approach infinity when X has spectral nulls. Thus, the MSE-LE avoids the infinite noise enlargement.

Figure 9.18 shows the discrete-time channel model for the MSE-LE, which incorporates a noise-whitening filter. Figure 9.19 shows an equivalent but simplified discrete-time channel model with a discrete-time pre-equalizing filter $F^*(1/z^*)$. This matched filter does not exist for the ZF-LE in Figure 9.14 since the ZF-LE already inverts the channel.

Example 9.10 Mean-square estimation approach to MSE-LE

We have derived the MSE-LE structure based upon an ad hoc approach. In this example, we use a more rigorous approach based on the *orthogonality principle* of mean-square estimation. From Figure 9.19, the error $e(k)$ at the equalizer output is

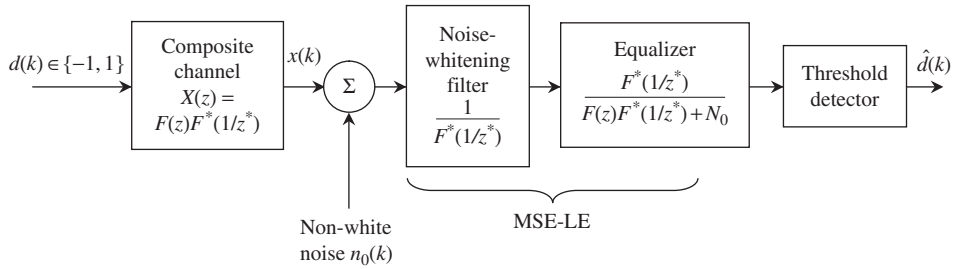

Figure 9.18 Discrete-time channel model for MSE-LE with a noise-whitening filter sampled at the symbol rate.

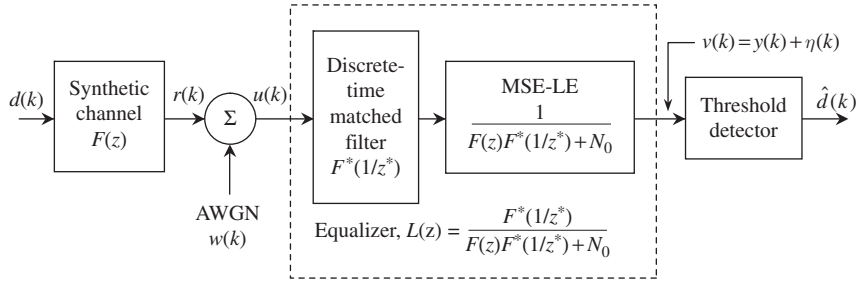

Figure 9.19 Simplified discrete-time channel model showing a pre-equalizing discrete-time matched filter sampled at the symbol rate.

$e(k) = y(k) + \eta(k) - d(k) = v(k) - d(k)$, and we wish to minimize the mean-square error $\sigma_e^2 = \mathbf{E}\left\{|e(k)|^2\right\}$. Let $F(z)$ be expressed as

$$F(z) = \sum_{k=-\infty}^{\infty} f(k)z^{-k} \tag{9.91}$$

Then the output $u(k)$ of the synthetic channel $F(z)$ is given by

$$u(k) = r(k) + w(k) = \sum_{m=-\infty}^{\infty} f(m)d(k-m) + w(k) \tag{9.92}$$

Let the transfer function of the equalizer be given by

$$L(z) = \sum_{k=-\infty}^{\infty} \ell(k)z^{-k} \tag{9.93}$$

The *orthogonality principle* of mean-square estimation states that $\sigma_e^2 = \mathbf{E}\left\{|e(k)|^2\right\}$ is minimum when the error $e(k)$ is orthogonal to the input $u^*(k-j)$, $-\infty < j < \infty$. That is,

$$\mathbf{E}\{e(k)u^*(k-j)\} = 0 \tag{9.94}$$

Note that the equalizer output $v(k)$ is equal to $u(k) * \ell(k)$, thus

$$v(k) = \sum_{i=-\infty}^{\infty} \ell(i)u(k-i) \tag{9.95}$$

Therefore, given $e(k) = v(k) - d(k)$, we obtain from (9.94) and (9.95)

$$\mathbf{E}\left\{ \left(\sum_{i=-\infty}^{\infty} \ell(i)u(k-i) - d(k) \right) u^*(k-j) \right\} = 0 \tag{9.96}$$

or, equivalently,

$$\sum_{i=-\infty}^{\infty} \ell(i)\mathbf{E}\{u(k-i)u^*(k-j)\} = \mathbf{E}\{d(k)u^*(k-j)\} \tag{9.97}$$

Assuming that $\mathbf{E}\{d(i)d^*(j)\} = 1$ for $i = j$ and $\mathbf{E}\{d(i)d^*(j)\} = 0$ for $i \neq j$, we have, via (9.92),

$$\begin{aligned} \mathbf{E}\{u(k-i)u^*(k-j)\} &= \sum_{m=-\infty}^{\infty} \sum_{\ell=-\infty}^{\infty} f(m)f^*(l)\mathbf{E}\{d(k-m-i)d^*(k-l-j)\} \\ &\quad + \mathbf{E}\{w(k-i)w^*(k-j)\} \\ &= \sum_{m=-\infty}^{\infty} f(m)f^*(m+i-j) + N_0\delta_{ij} \end{aligned} \tag{9.98}$$

Also, since white noise $w(k)$ and data $d(k)$ are uncorrelated, we have

$$\begin{aligned} \mathbf{E}\{d(k)u^*(k-j)\} &= \sum_{m=-\infty}^{\infty} f^*(m)\mathbf{E}\{d(k)d^*(k-m-j)\} \\ &= f^*(-j) \end{aligned} \tag{9.99}$$

Substituting (9.98) and (9.99) into (9.97), we get

$$\sum_{i=-\infty}^{\infty} \ell(i) \left[\sum_{m=-\infty}^{\infty} f(m)f^*(m+i-j) + N_0\delta_{ij} \right] = f^*(-j) \tag{9.100}$$

Taking the z-transform on both sides of (9.100) yields the following equation:

$$L(z)\left[F(z)F^*\left(\frac{1}{z^*}\right) + N_0\right] = F^*\left(\frac{1}{z^*}\right) \tag{9.101}$$

Thus,

$$L(z) = \frac{F^*(1/z^*)}{F(z)F^*(1/z^*) + N_0} \tag{9.102}$$

Therefore, $L(z)$ consists of a discrete-time matched filter $F^*(1/z^*)$, and the MSE-LE is given by

$$C(z) = \frac{1}{F(z)F^*(1/z^*) + N_0} \tag{9.103}$$

■

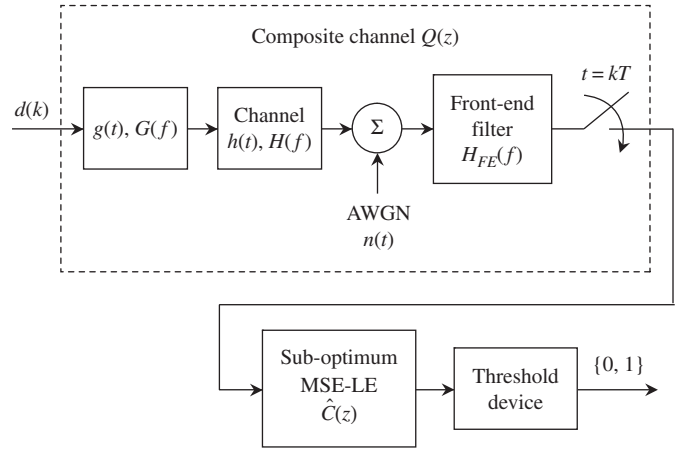

Figure 9.20 Discrete-time channel model for a suboptimum MSE-LE sampled at the symbol rate.

Example 9.11 Suboptimum MSE-LE

If the matched filter $S^*(f)$ in Figure 9.17 is difficult to realize, one can replace it with a front-end filter as in the case of the suboptimum ZF-LE shown in Figure 9.11. Figure 9.20 illustrates the concept of a suboptimum MSE-LE.

Following the previous analysis, we can evaluate the power spectral density $S_{\hat{e}}$ of the error $\hat{e}_k$ at the equalizer output as follows:

$$S_{\hat{e}} = S_d\left|Q\hat{C} - 1\right|^2 + S_{\hat{\eta}} \tag{9.104}$$

where $S_{\hat{\eta}}$ is the power spectral density of the equalizer output noise $\hat{\eta}_k$ and is given in terms of the input noise power spectral density Ψ as

$$S_{\hat{\eta}} = \Psi\left|\hat{C}\right|^2 \tag{9.105}$$

where the general expression of Ψ is given in (9.47). Combining (9.104) and (9.105), we obtain

$$S_{\hat{e}} = S_d\left|Q\hat{C} - 1\right|^2 + \Psi\left|\hat{C}\right|^2 \tag{9.106}$$

Let S_q denote the power spectral density of signal plus noise at the equalizer input, then

$$S_q = S_d|Q|^2 + \Psi \tag{9.107}$$

By using (9.107) in (9.106), we can write $S_{\hat{e}}$ as follows:

$$S_{\hat{e}} = S_q\left|\hat{C} - S_d S_q^{-1} Q^*\right|^2 + S_d \Psi S_q^{-1} \tag{9.108}$$

Obviously, $S_{\hat{e}}$ is minimized by choosing $\hat{C}$ to make the first term on the right-hand side of (9.108) equal to zero, which yields

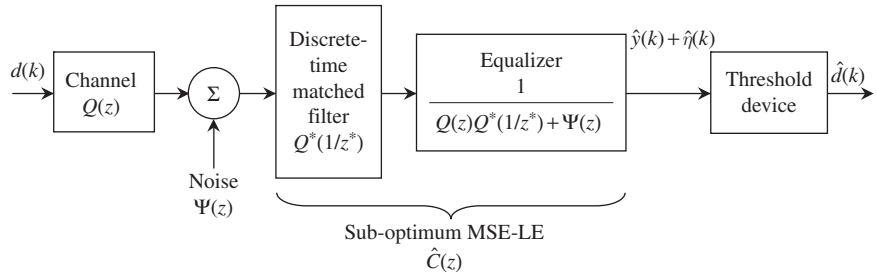

Figure 9.21 Discrete-time channel model for the suboptimum MSE-LE sampled at the symbol rate and white data with $S_d(z) = 1$.

$$\hat{C} = \frac{S_d Q^*}{S_d |Q|^2 + \Psi} \tag{9.109}$$

Consequently, the corresponding transfer function of the equalizer is

$$\hat{C}(z) = \frac{S_d(z) Q^*(1/z^*)}{S_d(z) Q(z) Q^*(1/z^*) + \Psi(z)} \tag{9.110}$$

Note that the role of the discrete-time matched filter reoccurs in the numerator of $\hat{C}(z)$ via its transfer function $Q^*(1/z^*)$, which we did not want in the first place! Figure 9.21 shows the discrete-time channel model for the suboptimum MSE-LE with white data input.

■

Let us attempt to compare the performance of the suboptimum MSE-LE to that of the minimum MSE-LE. For simplicity, we assume white data $S_d\left(\mathrm{e}^{\mathrm{j}2\pi f'}\right) = 1$ and from (9.108) we have, via the Cauchy–Schwarz inequality (9.49),

$$\begin{aligned} S_{\hat{e}}\left(\mathrm{e}^{\mathrm{j}2\pi f'}\right) &= \frac{\Psi\left(\mathrm{e}^{\mathrm{j}2\pi f'}\right)}{\left|Q\left(\mathrm{e}^{\mathrm{j}2\pi f'}\right)\right|^2 + \Psi\left(\mathrm{e}^{\mathrm{j}2\pi f'}\right)} \\ &= \frac{N_0 \sum_{k=-\infty}^{\infty} \left|H_{FE}\left(\frac{f'}{T} + \frac{k}{T}\right)\right|^2}{\frac{1}{T}\left|\sum_{k=-\infty}^{\infty} S\left(\frac{f'}{T} + \frac{k}{T}\right) H_{FE}\left(\frac{f'}{T} + \frac{k}{T}\right)\right|^2 + N_0 \sum_{k=-\infty}^{\infty} \left|H_{FE}\left(\frac{f'}{T} + \frac{k}{T}\right)\right|^2} \\ &\geq \frac{N_0}{\frac{1}{T}\sum_{k=-\infty}^{\infty} \left|S\left(\frac{f'}{T} + \frac{k}{T}\right)\right|^2 + N_0} = \frac{N_0}{X\left(\mathrm{e}^{\mathrm{j}2\pi f'}\right) + N_0} = S_e\left(\mathrm{e}^{\mathrm{j}2\pi f'}\right) \end{aligned} \tag{9.111}$$

Consequently, the MSE $\sigma_{\hat{e}}^2$ of the suboptimum MSE-LE is always greater than or equal to the MSE σ_e^2 of the minimum MSE-LE. Obviously, $\sigma_{\hat{e}}^2 = \sigma_e^2$ when $H_{FE}(f') = S^*(f')$, that is, the front-end filter is a matched filter.

To complete the comparison, we only need to examine the equalizer output $\hat{y}(k)$ for a symbol $d(k)$. We wish to show that $|\hat{y}(k)|^2 \leq |y(k)|^2$, that is, the suboptimum equalizer produces an output signal power that is less than or equal to that of the optimum equalizer. Without loss of generality, we can assume that data is white, that is, $S_d\left(\mathrm{e}^{\mathrm{j}2\pi f'}\right) = 1$. We only

need to compare the end-to-end transfer functions $\hat{Y}$ and Y of the two equalizers. This is possible since $\overline{|\hat{y}(k)|^2}$ and $\overline{|y(k)|^2}$ are just the arithmetic means of the frequency responses $|\hat{Y}|^2$ and $|Y|^2$, respectively, and both $\hat{Y}$ and Y are nonnegative-real. We have

$$\begin{aligned}\hat{Y} &= \frac{|Q|^2}{|Q|^2+\Psi} = \frac{1}{1+\left(\Psi/|Q|^2\right)} \\ &= \frac{1}{1+\left(N_0\sum_k |H_{FE}|^2\right)\Big/\left(\frac{1}{T}\left|\sum_k SH_{FE}\right|^2\right)} \\ &\le \frac{1}{1+N_0/\left(\frac{1}{T}\sum_k |S|^2\right)} = \frac{X}{X+N_0} \;=\; Y\end{aligned} \tag{9.112}$$

Integrating both sides of (9.112) over a full Nyquist period of unity yields $\overline{|\hat{y}(k)|^2} \le \overline{|y(k)|^2}$; the equality holds if and only if $H_{FE} = S^*$. In conclusion, any MSE-LE that does not employ a front-end matched filter has a smaller output signal-to-noise-and-ISI ratio than that of the minimum MSE-LE.

To assess the performance of the MSE-LE, we wish to find the equalizer output signal power so that we can establish a *figure-of-merit* such as the signal-to-MSE ratio. The output signal power $\overline{|y(k)|^2}$ of a symbol $d(k)$ is the arithmetic mean of the end-to-end frequency response $|Y|^2$, where $Y = X/(X+N_0)$ as seen in Figures 9.18 and 9.19. We can express Y in terms of $S_e = N_0/(X+N_0)$ as $Y = 1 - S_e$. Therefore, integrating over a full Nyquist period of unity we have $\overline{|y(k)|^2} = m_A\left[(1-S_e)^2\right]$. The output signal-to-MSE ratio $SNR_{0,MSE\text{-}LE} = \overline{|y(k)|^2}/\sigma_e^2 = m_A\left[(1-S_e)^2\right]/\, m_A(S_e)$ establishes a figure-of-merit for assessing the performance of the MSE-LE. Note that $(1-S_e)^2 \le 1 - S_e$, therefore we get $SNR_{0,MSE\text{-}LE} \le m_A(1-S_e)/m_A(S_e) = [1-m_A(S_e)]/m_A(S_e)$. Since ISI is not Gaussian, the Q-function cannot be employed to evaluate the error probability. Nevertheless, $SNR_{0,MSE\text{-}LE}$ is a useful quantity for comparing the performance of MSE-LE to that of MSE-DFE. We also note that it is not straightforward to compare the performances of MSE-LE and ZF-LE via $SNR_{0,MSE\text{-}LE}$ versus $SNR_{0,ZF\text{-}LE}$ in (9.43) unless we evaluate both $m_A(S_e)$ and $m_A(X^{-1})$. Although we have $\sigma_e^2 = m_A(S_e) \le \sigma^2 = N_0 m_A(X^{-1})$, we cannot deduce from this fact alone that the MSE-LE performs better than the ZF-LE.

9.5 Zero-forcing decision-feedback equalizer (ZF-DFE)

The study of linear equalizers reveals a weakness in the case of channels with spectral nulls or deep attenuation in the passband. The ZF-LE fails to equalize because of infinite or very large noise enhancement. The MSE-LE does not have the infinite noise enhancement but can have large noise enhancement. Nonlinear equalizers can overcome this weakness and improve the performance. We devote our effort to study two nonlinear equalizers, namely,

zero-forcing decision-feedback equalizer (ZF-DFE) in this section and mean-square error decision-feedback equalizer (MSE-DFE) in the next section.

The purpose of the ZF-DFE is to cancel out the causal ISI and completely avoid the infinite noise enhancement. With the use of the whitened matched-filter, only causal ISI appears at its output, as illustrated in Figure 9.14. Note that the synthetic channel transfer function $F(z)$ is a minimum phase function; hence, its output sequence $r(k)$ is always causal. On the other hand, the sequence $x(k)$ at the output of the composite channel $X(z)$ in Figure 9.13 is symmetric around zero, and therefore, contains both anti-causal ISI and causal ISI. The noise-whitening filter in Figure 9.13 in effect, removes the anti-causal ISI. Thus, we only need to design a filter that can remove the causal ISI. Assume that a symbol is detected correctly. Since we know the channel tap weighs $f(k)$ of $F(z)$, we can calculate the causal ISI produced by this symbol and subtract it from the next received symbol. In other words, the causal ISI effect from earlier symbols can be completely removed from any received symbol provided that all these earlier symbols were detected correctly. This process of removing ISI is known as zero-forcing decision-feedback equalization. Obviously, when the threshold detector makes an error, the ZF-DFE will calculate the wrong feedback and this could result in a long run of errors, termed *error propagation*.

Let us express the transfer function $F(z)$ in Figure 9.14 as follows:

$$F(z) = \sum_{k=0}^{\infty} f(k) z^{-k} \tag{9.113}$$

where $f(k)$ denotes the channel coefficients (tap weights). We can express the output sequence $r(k)$ of the synthetic channel as

$$\begin{aligned} r(k) &= d(k) * f(k) = \sum_{i=0}^{\infty} f(i) d(k-i) \\ &= f(0) d(k) + \sum_{i=1}^{\infty} f(i) d(k-i) \end{aligned} \tag{9.114}$$

where the first term is the desired symbol and the second term contains causal ISI produced by earlier (preceding) symbols $d(k-i)$. The ZF-DFE computes the second term based upon the estimated $\hat{d}(k-i)$ of $d(k-i)$, which is assumed to be correct. The estimated causal ISI is then subtracted from the received symbol $r(k)$ to yield

$$\begin{aligned} y(k) &= r(k) - \sum_{i=0}^{\infty} f(i) \hat{d}(k-i) \\ &= f(0) d(k) + \sum_{i=1}^{\infty} f(i) \left[d(k-i) - \hat{d}(k-i) \right] \\ &= f(0) d(k) \end{aligned} \tag{9.115}$$

assuming $\hat{d}(k-i) = d(k-i)$, that is, assuming *the previous symbols were detected correct* at the threshold detector output. The equalization is illustrated in Figure 9.22. Note that the output decision $\hat{d}(k)$ of the threshold detector contains no noise; therefore, noise does not

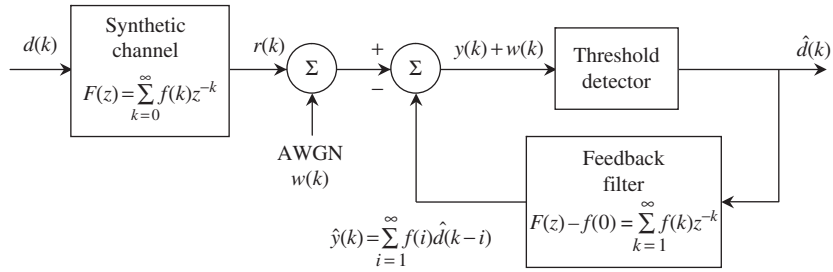

Figure 9.22 Simplified discrete-time channel model for ZF-DFE sampled at the symbol rate.

circulate back to the threshold detector input. The AWGN $w(k)$ whose power spectral density is N_0 (see Figure 9.14) is thus the threshold detector input noise.

Example 9.12 Minimum-phase transfer function revisited

Recall that the synthetic channel transfer function $F(z)$ is a spectral factor of $X(z)$ where $X\left(\mathrm{e}^{\mathrm{j}2\pi f'}\right)$ is the discrete-time Fourier transform of the output sequence $x(k)$ of the sampled matched filter in Figure 9.12. From (9.57) we obtain

$$\begin{aligned} X(z) &= F(z)F^*(1/z^*) \\ &= f^2(0)\left[f^{-1}(0)F(z)\right]\left[f^{-1}(0)F^*(1/z^*)\right] = f^2(0)\hat{F}(z)\hat{F}^*(1/z^*) \end{aligned} \tag{9.116}$$

Note that $f(0) = F(\infty)$, hence $f^{-1}(0)F(\infty) = 1$. The coefficient $f(0)$ is the constant term in the series expansion of $F(z)$ in (9.113). The transfer function $\hat{F}(z) = f^{-1}(0)F(z)$ is the *canonical factor* of $X(z)$, and it is a minimum-phase function as is $F(z)$. Since $\hat{F}(\infty) = 1$, $\hat{F}(z)$ can be expressed as follows:

$$\hat{F}(z) = f^{-1}(0)F(z) = \frac{\prod_{k=1}^{L}(1-\alpha_k z^{-1})}{\prod_{k=1}^{M}(1-\beta_k z^{-1})}, \qquad |\alpha_k| \le 1,\ |\beta| < 1 \tag{9.117}$$

where α_k and β_k are zeros and poles of $\hat{F}(z)$, respectively. The zeros α_k can be inside or on the unit circle, and the poles β_k must be inside the unit circle for stability. Substituting (9.117) into (9.116) and setting $z = \mathrm{e}^{\mathrm{j}2\pi f'}$, we obtain the discrete-time Fourier transform $X\left(\mathrm{e}^{\mathrm{j}2\pi f'}\right)$:

$$X\left(\mathrm{e}^{\mathrm{j}2\pi f'}\right) = f^2(0)\frac{\prod_{k=1}^{L}\left|1-\alpha_k \mathrm{e}^{-\mathrm{j}2\pi f'}\right|^2}{\prod_{k=1}^{M}\left|1-\beta_k \mathrm{e}^{-\mathrm{j}2\pi f'}\right|^2} \tag{9.118}$$

Taking the logarithm of X and integrating from –1/2 to 1/2, we get

$$\int_{-1/2}^{-1/2} \ln X(\mathrm{e}^{\mathrm{j}2\pi f'})\,\mathrm{d}f' = \ln f^2(0) + \sum_{k=1}^{L} \int_{-1/2}^{1/2} \ln\left|1 - \alpha_k \mathrm{e}^{-\mathrm{j}2\pi f'}\right|^2 \mathrm{d}f' - \sum_{k=1}^{M} \int_{-1/2}^{1/2} \ln\left|1 - \beta_k \mathrm{e}^{-\mathrm{j}2\pi f'}\right|^2 \mathrm{d}f' \tag{9.119}$$

Note that for a given complex number $\gamma_k = |\gamma_k|\mathrm{e}^{\mathrm{j}\theta}$, we have the following relationship, namely, $\ln\left|1 - \gamma_k \mathrm{e}^{-\mathrm{j}2\pi f'}\right|^2 = \ln\left|1 + |\gamma_k|^2 - 2|\gamma_k|\cos(2\pi f' - \theta)\right|$. The integral of this function over one period is zero for $|\gamma_k| \leq 1$. Therefore, we conclude that the two sum terms on the right-hand side of (9.119) are zero and we have

$$f^2(0) = \mathrm{e}^{\int_{-1/2}^{1/2} \ln X\left(\mathrm{e}^{\mathrm{j}2\pi f'}\right)\mathrm{d}f'} = m_G(X) \tag{9.120}$$

The term on the right-hand side of (9.120) is the *geometric mean* $m_G(X)$ of $X\left(\mathrm{e}^{\mathrm{j}2\pi f'}\right)$. In conclusion, given a nonnegative real function X, we can evaluate its geometric mean via (9.120) or via its spectral factorization (9.116).

■

Example 9.13 Geometric mean and arithmetic mean of nonnegative real functions $X\left(\mathrm{e}^{\mathrm{j}2\pi f'}\right)$ and $X^{-1}\left(\mathrm{e}^{\mathrm{j}2\pi f'}\right)$

From (9.120) we can express the geometric mean $m_G(X)$ of the nonnegative real function $X\left(\mathrm{e}^{\mathrm{j}2\pi f'}\right)$ via the *Jensen inequality*, as follows:

$$\ln m_G(X) = \int_{-1/2}^{1/2} \ln X\left(\mathrm{e}^{\mathrm{j}2\pi f'}\right)\mathrm{d}f' \leq \ln \int_{-1/2}^{1/2} X\left(\mathrm{e}^{\mathrm{j}2\pi f'}\right)\mathrm{d}f' = \ln m_A(X) \tag{9.121}$$

This implies

$$m_G(X) \leq m_A(X) \tag{9.122}$$

where $m_A(X)$, the average value of $X\left(\mathrm{e}^{\mathrm{j}2\pi f'}\right)$, is also the dc component in the Fourier series expansion of $X(f)$. If we replace X by X^{-1} in (9.122), we get

$$m_G\left(X^{-1}\right) \leq \int_{-1/2}^{1/2} \frac{1}{X\left(\mathrm{e}^{\mathrm{j}2\pi f'}\right)}\mathrm{d}f' = m_A\left(X^{-1}\right) \tag{9.123}$$

where $m_A(X^{-1})$, the average value of $1/X\left(\mathrm{e}^{\mathrm{j}2\pi f'}\right)$, is also the dc component in the Fourier series expansion of $1/X(f)$ as seen in (9.41). But we also have, via (9.118)–(9.120),

$$m_G\left(X^{-1}\right) = f^{-2}(0) = m_G^{-1}(X) \tag{9.124}$$

Therefore, substituting (9.124) into (9.123), we obtain

$$f^{-2}(0) \leq m_A\left(X^{-1}\right) \tag{9.125}$$

■

In order to compare the ZF-DFE to its closest cousin, the ZF-LE, we only need to evaluate the output signal-to-noise ratio for the received symbol $y(k) + w(k)$ at the input of the threshold detector. We already know that the noise sample $w(k)$ has the power spectral density N_0. Thus, its variance σ^2 is simply the integral of N_0 over the full Nyquist period of unity with respect to the discrete-time Fourier transform frequency f',

$$\sigma^2 = N_0 \tag{9.126}$$

The signal $y(k)$ given in (9.115) has a power given by

$$\overline{y^2(k)} = f^2(0) \tag{9.127}$$

since $\overline{d^2(k)} = 1$. Therefore, the output signal-to-noise ratio SNR_0 of the ZF-DFE is

$$SNR_{0,\,ZF\text{-}DFE} = \frac{\overline{y^2(k)}}{\sigma^2} = \frac{f^2(0)}{N_0} \tag{9.128}$$

Comparing the SNR_0 of the ZF-DFE to that of the ZF-LE in (9.43), with the help of (9.125), we get

$$SNR_{0,\,ZF\text{-}DFE} \geq SNR_{0,\,ZF\text{-}LE} \tag{9.129}$$

Hence, in the absence of error propagation, the ZF-DFE always performs better than or equal to the ZF-LE. For a channel with substantial ISI and a low signal-to-noise ratio, the performance of ZF-DFE could be worse than that of ZF-LE. The error probability of the ZF-DFE can be evaluated via the Q-function. For PSK or QPSK modulation, it is given by $P_b \approx Q\left(\sqrt{SNR_{0,\,ZF\text{-}DFE}}\right)$ at high signal-to-noise ratios.

Example 9.14 Output signal-to-noise ratio of ZF-DFE

Using the pulse $s(t) = \sqrt{4aE}\,\mathrm{e}^{-at}u(t)$ in Example 9.8, we obtain $X(z)$ via (9.65) as

$$\begin{aligned} X(z) &= 2E\left(1 - b^2\right)\frac{1}{1 - bz^{-1}}\,\frac{1}{1 - bz} \\ &= f^2(0)\hat{F}(z)\hat{F}^*(1/z^*) \end{aligned} \tag{9.130}$$

where the geometric mean of $X(z)$ is $m_G(X) = f^2(0) = 2E(1 - b^2)$. Thus the output signal-to-noise ratio is given by (9.128) as

$$SNR_{0,\,ZF\text{-}DFE} = \frac{f^2(0)}{N_0} = \frac{2E}{N_0}\left(1 - b^2\right) \tag{9.131}$$

Note that $SNR_0 \to 0$ as $b \to 1$, that is, the channel pole approaches the unit circle. Comparing (9.131) to (9.69) it can be seen that the ZF-DFE has an advantage of $1 + b^2$ in SNR_0 over the ZF-LE. Also note that the matched filter output signal-to-noise ratio is $2E/N_0$ in the case of zero ISI.

■

We have shown that in the absence of error propagation, which normally happens at high signal-to-noise ratios, the ZF-DFE is clearly superior to that of the ZF-LE. We explain this improvement by looking at Figures 9.14 and 9.22. The noise at the output of the ZF-LE is no longer white, therefore, they are correlated and depend on the channel transfer function. The ZF-DFE in effect adds a filter $F(z)$ at the output of the ZF-LE to whiten the output noise, that is, to make the noise sample uncorrelated and hence independent since it is Gaussian. The added filter reproduces the data sample $r(k)$, which contains causal ISI and hence can be removed by the feedback filter $F(z) - f(0)$ without enhancing noise. This added filter is called a *linear predictor*. Figure 9.23 shows the ZF-DFE obtained from the ZF-LE by adding a linear predictor. Note that the synthetic channel $F(z)$ is the discrete-time representation of the whitened matched filter and no filter can minimize noise better than it. This explains why $SNR_{0,ZF\text{-}DFE} \geq SNR_{0,ZF\text{-}LE}$.

In summary, in the absence of error propagation, the performance of the ZF-DFE is superior to that of the ZF-LE. There is no noise enhancement due to spectral nulls. At high output signal-to-noise ratios (more than 10 dB), the effect of error propagation is small, especially if the data is interleaved to make it look random. Error propagation tends to end after a few correct detections as the ZF-DFE clears itself of errors. The error probability for PSK, including error propagation, can be expressed as $P_b = N_p Q\left(\sqrt{SNR_{0,ZF\text{-}DFE}}\right)$, where N_p is a positive constant that accounts for the increase in the error rate due to error propagation.

9.6 Mean-square error decision-feedback equalizer (MSE-DFE)

The comparison of ZF-DFE with ZF-LE produces an insight into designing the MSE-DFE. From the point of view of ZF-DFE, it is necessary to whiten the noise at the output of the ZF-LE to improve performance. We can make the same conclusion regarding the MSE-DFE, that is, to improve its performance over the MSE-LE, we need to whiten the noise plus ISI at the output of the MSE-LE. This can be achieved by using a linear predictor $P(z)$ and a feedback filter $P(z) - 1$, where $P(\infty) = 1$ as shown in Figure 9.24, which is based on the concept depicted in Figure 9.23.

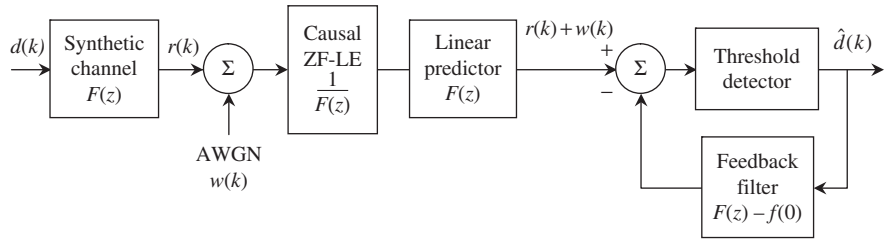

Figure 9.23 The ZF-DFE as the ZF-LE with a linear predictor and a feedback filter.

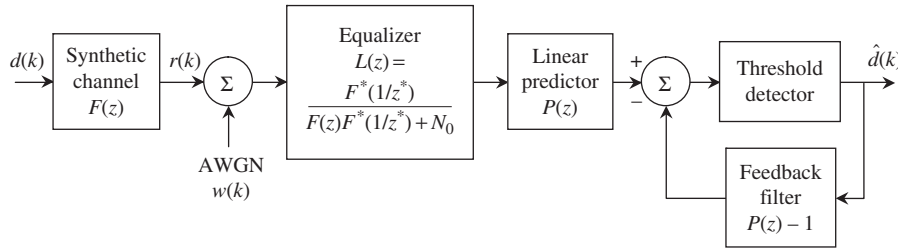

Figure 9.24 Simplified discrete-time channel model for the MSE-DFE sampled at the symbol rate.

The error spectrum of the MSE-DFE can be derived by assuming that *the previous symbols were correctly detected* at the threshold detector output. We have

$$\begin{aligned} e(k) &= \hat{y}(k) - d(k) + \hat{\eta}(k) \\ &= [d(k) * f(k) * l(k) * p(k) - d(k) * p(k) + d(k)] - d(k) + \hat{\eta}(k) \\ &= d(k) * p(k) * [f(k) * l(k) - \delta(k)] + \hat{\eta}(k) \end{aligned} \tag{9.132a}$$

$$\begin{aligned} \hat{S}_e &= S_d|XC-1|^2|P|^2 + N_0 X|C|^2|P|^2 \\ &= \left(S_d|XC-1|^2 + N_0 X|C|^2\right)|P|^2 \\ &= S_e|P|^2 \end{aligned} \tag{9.132b}$$

where $X = FF^*$, $C = 1/(X + N_0)$, and $S_e = S_d|XC-1|^2 + N_0 X|C|^2 = S_d N_0/[S_d X + N_0]$ is the error spectrum of the MSE-LE given in (9.81) and (9.86). To whiten S_e, we only need to choose $P(z)$ to be the inverse of the canonical minimum-phase spectral factor of $S_e(z)$, that is,

$$S_e(z) = m_G(S_e)\frac{1}{P(z)} \cdot \frac{1}{P^*(1/z^*)} \tag{9.133}$$

where $m_G(S_e)$ is the geometric mean of $S_e\left(\mathrm{e}^{\mathrm{j}2\pi f'}\right)$ and $P(\infty) = 1$ as in (9.116) and (9.120). By using (9.132b) and (9.133), we get

$$\begin{aligned} \hat{S}_e(z) &= S_e(z)P(z)P^*(1/z^*) \\ &= m_G(S_e) \end{aligned} \tag{9.134}$$

Thus, by using a linear predictor and a feedback filter, we can whiten the noise plus ISI error. Since $\hat{S}_e\left(\mathrm{e}^{\mathrm{j}2\pi f'}\right)$ is a constant, the MSE of the MSE-DFE is simply

$$\hat{\sigma}_e^2 = \int_{-1/2}^{1/2} \hat{S}_e\left(\mathrm{e}^{\mathrm{j}2\pi f'}\right) \mathrm{d}f' = m_G(S_e) \tag{9.135}$$

It is seen that $\hat{\sigma}_e^2 \le \sigma_e^2$, where σ_e^2 is the MSE of the MSE-LE given in (9.90). This occurs because the geometric mean $m_G(S_e)$ is less than or equal to the arithmetic mean $m_A(S_e)$. The combined equalizer–predictor transfer function is given by

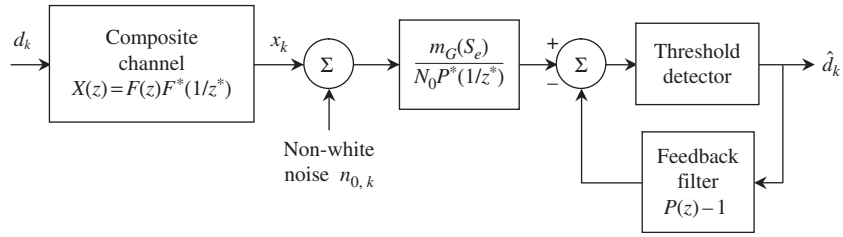

Figure 9.25 Discrete-time channel model for the MSE-DFE sampled at the symbol rate.

$$\begin{aligned} L(z)P(z) &= \frac{F^*(1/z^*)P(z)}{F(z)F^*(1/z^*)+N_0} \\ &= \frac{1}{N_0}F^*(1/z^*)P(z)S_e(z) \\ &= \frac{m_G(S_e)}{N_0}\cdot\frac{F^*(1/z^*)}{P^*(1/z^*)} \end{aligned} \tag{9.136}$$

Incorporating the above result into Figure 9.24 yields the discrete-time channel model for the MSE-DFE in Figure 9.25. The filter $1/P^*(1/z^*)$ is similar to the noise-whitening filter $1/F^*(1/z^*)$ in Figure 9.18. We can call it the *noise-ISI-whitening* filter. This filter also attempts to eliminate the anti-causal ISI in the sequence $x(k)$, which arises via filtering by $F^*(1/z^*)$ in (9.136). The feedback filter $P(z)-1$ attempts to cancel out the remaining causal ISI. Since we are dealing with MSE, some residual ISI remains at the threshold detector input. This is a compromise to reduce the effect of noise.

To assess the performance of the MSE-DFE, we wish to establish a *figure-of-merit* such as the *output signal-to-MSE ratio*. This implies that we need to evaluate the output signal power $\overline{|\hat{y}(k)|^2}$ for a symbol $d(k)$ at the threshold detector input. Note that $\overline{|\hat{y}(k)|^2}$ is just the arithmetic mean of the end-to-end frequency response $|\hat{Y}|^2$. Also we have $\hat{Y}=XP/(X+N_0)-P+1=1-N_0P/(X+N_0)=1-S_eP$, where $S_e=N_0/(X+N_0)$ is the error spectrum of the MSE-LE, assuming *no error* at the threshold detector output. Using (9.133), we get $\hat{Y}=1-m_G(S_e)/P^*$. Integrating $|\hat{Y}|^2$ over a full Nyquist period of unity yields the power of the signal component $\overline{|\hat{y}(k)|^2}=[1-m_G(S_e)]^2$. We have used the fact that $1/P^*$ is a maximum-phase function with $1/P^*(0)=1$; therefore, its average value is unity. Thus, the output signal-to-MSE ratio is

$$SNR_{0,MSE\text{-}DFE}=\overline{|\hat{y}(k)|^2}/\hat{\sigma}_e^2=[1-m_G(S_e)]^2/m_G(S_e)=\left(1-\hat{\sigma}_e^2\right)^2/\hat{\sigma}_e^2 \tag{9.137}$$

For comparison with MSE-LE, where $SNR_{0,MSE\text{-}LE}=m_A\left[(1-S_e)^2\right]/m_A(S_e)$, we have $SNR_{0,MSE\text{-}DFE}\geq SNR_{0,MSE\text{-}LE}$ when $m_A\left[(1-S_e)^2\right]\leq[1-m_G(S_e)]^2$. For a channel with substantial ISI and a low signal-to-noise ratio, the performance of MSE-DFE could be worse than that of MSE-LE.

Example 9.15 $SNR_{0,\ MSE\text{-}DFE}$

We use the same pulse $s(t) = \sqrt{4Ea}\,\mathrm{e}^{-at}u(t)$ as used in Example 9.8, where $X(z) = 2E(b^2 - 1)\ b^{-1}z(z-b)^{-1}(z-b^{-1})^{-1}$. For simplicity, we assume an input signal-to-noise ratio $E/N_0 = 7$ dB and $b = 0.5$. Thus,

$$\begin{aligned} S_e(z) &= \frac{N_0}{X(z)+N_0} = \frac{(z-0.5)(z-2)}{z^2 - 17.5z + 1} \\ &= \frac{(z-0.5)(z-2)}{(z-0.057)(z-17.44)} = 0.115\frac{(1-0.5z^{-1})(1-0.5z)}{(1-0.057z^{-1})(1-0.057z)} \end{aligned} \tag{9.138}$$

where $m_G(S_e) = 0.115$ and $1/P(z) = (1 - 0.5z^{-1})/\ (1 - 0.057z^{-1})$. Therefore, we obtain $SNR_{0,MSE\text{-}DFE} = [1 - m_G(S_e)]^2/m_G(S_e) = 6.8$ or 8.33 dB.

Note that, for the same specification, the ZF-DFE has an output signal-to-noise ratio of $SNR_{0,ZF\text{-}DFE} = 7.5$ or 8.75 dB. One should resist the temptation to draw the conclusion here that the ZF-DFE performs better than the MSE-DFE. Since ISI is not Gaussian, the Q-function cannot be employed to obtain the error probability for the MSE-DFE, therefore any comparison based solely on $SNR_{0,MSE\text{-}DFE}$ is not valid.

■

9.7 Maximum likelihood sequence detection

Equalizers that remove ISI completely (ZF) or reduce them to a large extent (MSE) are simple to implement with transversal filters. From the efficiency point of view, throwing away the symbol energy that resides in the ISI is not the best way to achieve a performance approaching that of the optimum demodulator in Section 9.2. But with symbol-by-symbol detection, this is the best method that one could use. In an AWGN channel with ISI, the energy of a symbol spans many symbol periods, so why not use the energy that resides in the ISI portion of the symbol to aid the detection? In other words, the entire symbol energy can be used and this can only be done via sequence detection. The best sequence detection is the *maximum likelihood sequence detection* (MLSD). In an AWGN channel with no ISI, the MLSD reduces to the maximum likelihood (symbol-by-symbol) detection studied in Chapter 8 because a sequence of symbols just contains isolated symbols. For a Nyquist channel, again there is no ISI, thus MLSD also reduces to the optimum demodulator in Section 9.2, where the detection is performed over a sequence of one symbol.

Let us consider a received sequence of K symbols at the output of the physical channel $h(t)$ in Figure 9.9. The corresponding received signal $r(t)$ is

$$r(t) = \sum_{k=0}^{K-1} d(k)s(t - kT) + n(t) \tag{9.139}$$

where $d(k)$ is the kth symbol, $s(t)$ is the received symbol waveform, and $n(t)$ is the AWGN.

For M-ary modulation, there are M^K possible transmitted sequences of length K symbols. Thus, we can readily apply the maximum likelihood principle for sequence detection developed in Chapter 4. Recall that maximum likelihood sequence detection states that minimizing the error probability is equivalent to selecting a sequence $s_i(t)$ in the sequence set that is closest in Euclidean distance to the received sequence $r(t)$. We can write the squared Euclidean distance $d^2(r, s_i)$ as follows:

$$d^2(r, s_i) = \int_{-\infty}^{\infty} |r(t) - s_i(t)|^2 \mathrm{d}t, \ i = 1, 2, \ldots, M^K \tag{9.140}$$

If we apply this maximum likelihood criterion to $r(t)$ in (9.139), we can derive a likelihood function for the MLSD. Thus, for $s_i(t) = \sum_{k=0}^{K-1} d(k)s(t - kT)$,

$$\begin{aligned} d^2(r, s_i) &= \int_{-\infty}^{\infty} |r(t)|^2 \mathrm{d}t - 2\mathrm{Re}\int_{-\infty}^{\infty} r(t)s_i^*(t)\,\mathrm{d}t + \int_{-\infty}^{\infty} |s_i(t)|^2 \mathrm{d}t \\ &= \int_{-\infty}^{\infty} |r(t)|^2 \mathrm{d}t - 2\mathrm{Re}\left[\sum_{k=0}^{K-1} d^*(k)\int_{-\infty}^{\infty} r(t)s^*(t - kT)\,\mathrm{d}t\right] \\ &\quad + \sum_{k=0}^{K-1}\sum_{m=0}^{K-1} d(k)d^*(m)\int_{-\infty}^{\infty} s(t - kT)s^*(t - mT)\,\mathrm{d}t \end{aligned} \tag{9.141}$$

Since the first term involving the integral of $|r(t)|^2$ is common to all $d^2(r, s_i)$, the minimum Euclidean distance corresponds to the maximum of the following *correlation metric*:

$$c(\boldsymbol{D}_K) = 2\mathrm{Re}\sum_{k=0}^{K-1} d^*(k)v(k) - \sum_{k=0}^{K-1}\sum_{m=0}^{K-1} d(k)d^*(m)x(m - k) \tag{9.142}$$

where $\boldsymbol{D}_K = (d(0), d(1), \ldots, d(K - 1))$ is the data sequence and

$$v(k) = \int_{-\infty}^{\infty} r(t)\, s^*(t - kT)\mathrm{d}t \tag{9.143}$$

$$x(m - k) = \int_{-\infty}^{\infty} s(t - kT)\, s^*(t - mT)\mathrm{d}t = x^*(k - m) \tag{9.144}$$

In summary, the MLSD chooses a symbol that corresponds to the smallest Euclidean distance $d(r, s_i),\ i = 1, 2, \ldots, M^K$, or one that has the largest correlation metric $c(\boldsymbol{D}_K)$. Such MLSD employs a front-end matched filter that matches the symbol waveform $s(t)$. The output of the matched filter is sampled at the symbol rate to produce a sequence of output samples v_k. These are decision variables that are used by the sequence detector to detect the sequence $\boldsymbol{D}_K$. The sequence $v(k)$ provides *sufficient statistics* for demodulation of $\boldsymbol{D}_K$. The sequence $x(k)$ is the discrete-time autocorrelation of the known symbol waveform $s(t)$.

Obviously one does not want to build a sequence detector that follows the sampled matched filter to evaluate M^K correlation metrics when K is large. Fortunately, one can use the *Viterbi detector*, which implements an efficient dynamic programming algorithm to

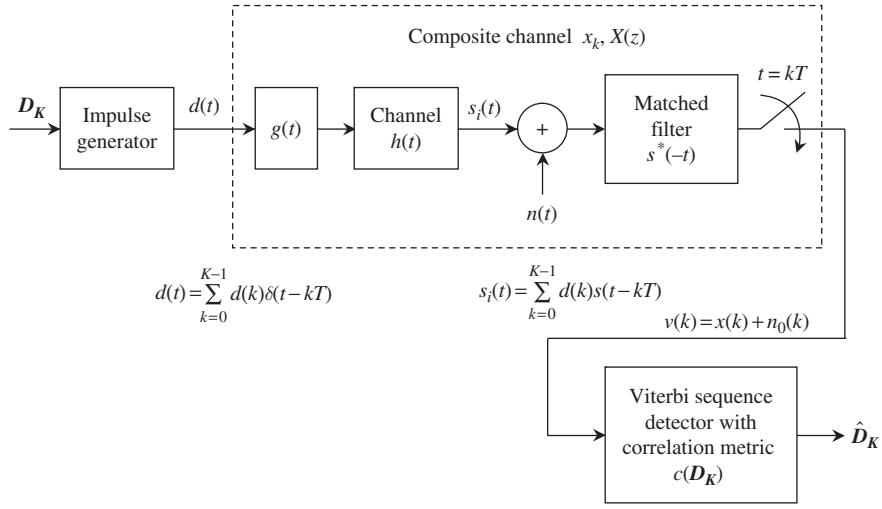

Figure 9.26 The MLSD with a front-end matched filter and a Viterbi sequence detector.

estimate the sequence of transmitted symbols. We have used the Viterbi algorithm in the decoding of convolutional codes in Chapter 4, and the detection of CPM signals in Chapter 7 based upon the minimum squared Euclidean distance. For MLSD, the correlation metric in (9.142) is used instead. This correlation metric can be computed recursively if we assume ISI affects only L past symbols and L future symbols, that is, $x(k) = 0$ for $|k| > L$. The recursive formula is given by [1,2]:

$$\begin{aligned} c(\boldsymbol{D}_k) &= c(\boldsymbol{D}_{k-1}) + 2\mathrm{Re}(d^*(k)v(k)) \\ &\quad - 2\mathrm{Re}\left(d^*(k)\sum_{m=k-L}^{k-1} d(m)x(k-m)\right) - |d(k)|^2 x(0) \end{aligned} \tag{9.145}$$

The Viterbi algorithm employs $c(\boldsymbol{D}_k)$ to compute paths through a trellis with M states. At each state only the path that has the largest correlation metric is retained, called the survivor path. All paths that enter this same state (commonly referred to as the node) with smaller correlation metrics are rejected. Thus, the complexity grows linearly with the sequence length K and not exponentially with M^K. Figure 9.26 shows the MLSD with the Viterbi sequence detector. For M-ary modulation, such as MPSK or MQAM, the data $d(k)$ is complex with $\mathrm{Re}(d(k))$ representing the I-channel data and $\mathrm{Im}(d(k))$ representing the Q-data channel. Figure 9.27 shows the equivalent discrete-time model for the MLSD.

Example 9.16 MLSD with whitened matched filter

The whitened matched filter consists of a sampled matched filter followed by a noise-whitening filter. Its importance cannot be understated. As we know, the sampled matched

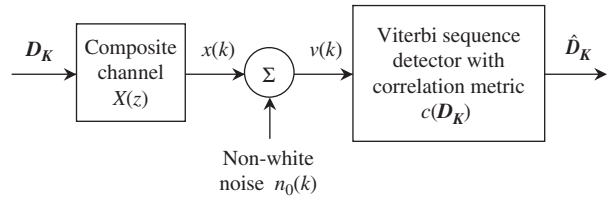

Figure 9.27 Discrete-time model for MLSD.

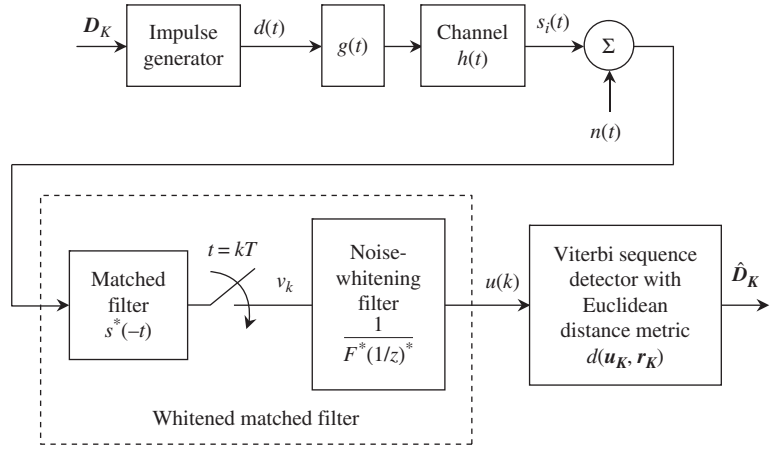

Figure 9.28 MLSD with a whitened matched filter.

filter output is symmetric about the sampling time. Hence, it contains both anti-causal ISI and causal ISI. Furthermore, the output noise samples are non-white and hence correlated but still Gaussian. On the other hand, the whitened matched filter output contains only causal ISI and the noise samples are white, hence, uncorrelated. Since they are Gaussian, they are also independent. We want to show that replacing the sampled matched filter in Figure 9.26 with a whitened matched filter does not change the optimality of the MLSD. Therefore, the demodulator shown in Figure 9.28 is entirely equivalent to that in Figure 9.26.

Let $X(z)$ denote the z-transform of the sequence $x(k)$ defined in (9.144), that is, the sequence of signal components at the sampled matched filter output. Performing a spectral factorization of $X(z)$ yields

$$X(z) = F(z)F^*\left(\frac{1}{z^*}\right) \tag{9.146}$$

where $F(z)$ is a minimum-phase function and $F^*(1/z^*)$ is a maximum-phase function as previously shown in (9.57). The noise-whitening filter in Figure 9.28 has the transfer function $1/F^*(1/z^*)$. The MLSD in Figure 9.28 can be represented by the simplified discrete-time model in Figure 9.29.

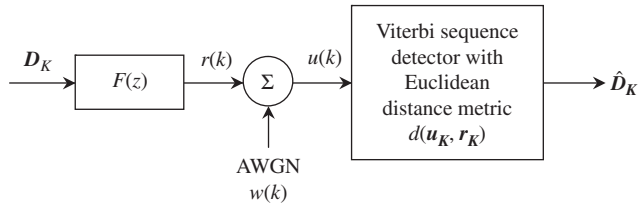

Figure 9.29 Simplified discrete-time model for MLSD with a whitened matched filter. The sequence r_K represents the filtered data sequence and $u_K = r_K + w_K$, where w_K is the AWGN sequence.

The sequence $u(k) = r(k) + w(k)$ provides *sufficient statistics* for the detection of the data sequence $d(k)$ since the noise samples $w(k)$ are independent. Indeed, we can write the probability density of the sequence $\boldsymbol{u}_K = (u(0), u(1), \ldots, u(K-1))$ given $\boldsymbol{D}_K = (d(0), d(1), \ldots, d(K-1))$ as follows:

$$\begin{aligned} f_{U_K}(\boldsymbol{u}_K|\boldsymbol{D}_K) &= \prod_{k=0}^{K-1} f_{U_K}(u(k)|\boldsymbol{D}_K) = \prod_{k=0}^{K-1} \frac{1}{\sqrt{2\pi}\,\sigma} \mathrm{e}^{-|u(k)-r(k)|^2/2\sigma^2} \\ &= \frac{1}{\left(\sqrt{2\pi}\,\sigma\right)^K} \mathrm{e}^{-\left(1/2\sigma^2\right)\sum_{k=0}^{K-1}|u(k)-r(k)|^2/2\sigma^2} \end{aligned} \tag{9.147}$$

where $\sigma^2 = N_0$ is the variance of the AWGN $w(k)$. Minimizing the ln-likelihood function $\ln f_{U_K}(\boldsymbol{u}_K|\boldsymbol{D}_K)$ results in minimizing the Euclidean distance

$$d(\boldsymbol{u}_K, \boldsymbol{D}_K) = \sqrt{\sum_{k=0}^{K-1} |u(k) - r(k)|^2} \tag{9.148}$$

over the set of M^K data sequences. The Euclidean distance metric is entirely equivalent to the correlation metric in (9.142) since both detectors apply the same maximum likelihood principle to the sequence of data $\boldsymbol{D}_K$.

■

Example 9.17 Equivalence of $d(\boldsymbol{u}_K, \boldsymbol{D}_K)$ and $c(\boldsymbol{D}_K)$

We wish to show that the Euclidean distance metric $d(\boldsymbol{u}_K, \boldsymbol{D}_K)$ in (9.148) and the correlation metric $c(\boldsymbol{D}_K)$ are equivalent. Let us expand $d^2(\boldsymbol{u}_K, \boldsymbol{D}_K)$ as follows:

$$\begin{aligned} d^2(\boldsymbol{u}_K, \boldsymbol{D}_K) &= \sum_{k=0}^{K-1} |u(k) - r(k)|^2 \\ &= \sum_{k=0}^{K-1} |u(k)|^2 - 2\mathrm{Re}\sum_{k=0}^{K-1} u(k)r^*(k) + \sum_{k=0}^{K-1} |r(k)|^2 \end{aligned} \tag{9.149}$$

The first term on the right-hand side of (9.149) is common to all $d^2(\boldsymbol{u}_K, \boldsymbol{D}_K)$; therefore, minimizing $d^2(\boldsymbol{u}_K, \boldsymbol{D}_K)$ corresponds to maximizing the following correlation metric:

$$\hat{c}(\boldsymbol{D}_K) = 2\mathrm{Re}\sum_{k=0}^{K-1} u(k)r^*(k) - \sum_{k=0}^{K-1} |r(k)|^2 \tag{9.150}$$

We can express the filtered data $r(k)$ from Figure 9.29 as

$$r(k) = d(k) * f(k) = \sum_{m=0}^{K-1} d(m)f(k-m) \tag{9.151}$$

where $f(k)$ denotes the coefficients of the transfer function $F(z)$ given by

$$F(z) = \sum_{k=0}^{L} f(k)z^{-k} \tag{9.152}$$

Substituting (9.151) into (9.150), we have

$$\begin{aligned}
\hat{c}(\boldsymbol{D}_K) &= 2\mathrm{Re}\sum_{m=0}^{K-1}\sum_{k=0}^{K-1} d^*(m)u(k)f^*(k-m) - \sum_{m=0}^{K-1}\sum_{n=0}^{K-1}\sum_{k=0}^{K-1} d(m)d^*(n)f(k-m)f^*(k-n) \\
&= 2\mathrm{Re}\sum_{m=0}^{K-1} d^*(m)\sum_{k=0}^{K-1} u(k)f^*(k-m) - \sum_{m=0}^{K-1}\sum_{n=0}^{K-1} d(m)d^*(n)\sum_{k=0}^{K-1} f(k-m)f^*(k-n) \\
&= 2\mathrm{Re}\sum_{m=0}^{K-1} d^*(m)v(m) - \sum_{m=0}^{K-1}\sum_{n=0}^{K-1} d(m)d^*(n)x(n-m) \\
&= c(\boldsymbol{D}_K)
\end{aligned} \tag{9.153}$$

The right-hand side of (9.153) is precisely (9.142) as expected. Note that the transfer function of the noise-whitening filter is $1/F^*(1/z^*)$. Therefore, $u(k)$, the output of this filter with input $v(k)$, is given in terms of the z-transform by $U(z) = V(z)/F^*(1/z^*)$, where $U(z)$ and $V(z)$ are the z-transforms of the sequences $u(k)$ and $v(k)$, respectively. Hence, $V(z) = F^*(1/z^*)U(z)$ is equivalent to $v(k)$, the output of $F^*(1/z^*)$ with input $u(k)$, that is, $v(k) = u(k) * f^*(-k)$ where $F^*(1/z^*)$ is the z-transform of the time-reversal sequence $f^*(-k)$.

■

Example 9.18 Viterbi algorithm

In this example we implement the Viterbi algorithm for searching a trellis that represents an AWGN channel with ISI. We consider binary modulation ($M = 2$) and use the simplified discrete-time model for MLSD in Figure 9.29 with $F(z) = f(0) + f(1)z^{-1}$, where $f(0)$ and $f(1)$ are normalized so that $f(0) = 1$ and $f(1) = 0.2$. Thus, there is only one memory $L = 1$ associated with $f(1)$. The trellis is shown in Figure 9.30 over four symbol times. The trellis in one symbol time is the state diagram of the ISI channel. With $M = 2$, the channel

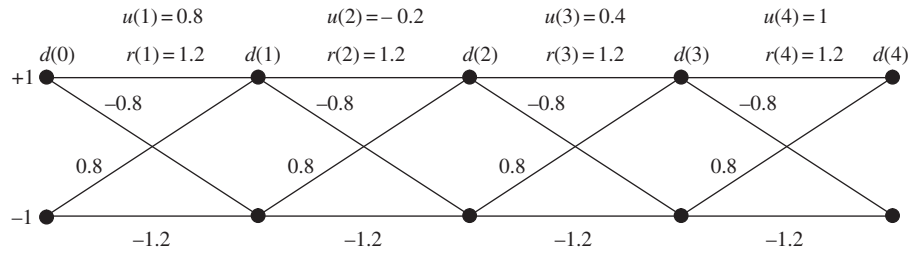

Figure 9.30 Trellis for MLSD with a whitened matched filter.

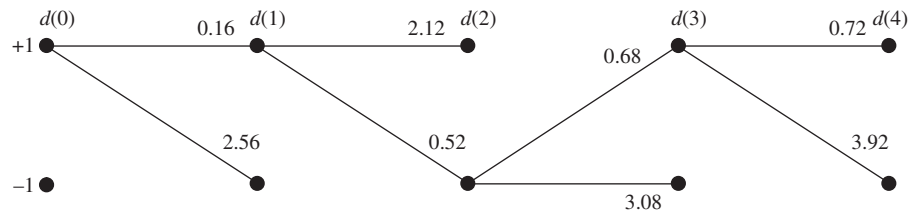

Figure 9.31 Metric of the survivor path.

can be one of $M^L = 2$ states. The states at time k are labeled with $d(k) = \pm 1$ and the corresponding channel outputs are $r(k) = f(0)d(k) + f(1)d(k-1) = d(k) + 0.2d(k-1)$. The channel outputs are labeled on the branches of the trellis. We assume the following received samples (channel outputs plus noise): $(u(1), u(2), u(3), u(4), \ldots) = (0.8, -0.2, 0.4, 1, \ldots)$.

Since the channel is a finite-state machine, we have a starting state and an ending state. We can achieve this condition by arbitrarily starting the sequence $\boldsymbol{D}_K = (d(0), d(1), \ldots, d(K))$ with $d(0) = 1$ (or $d(0) = -1$) and end the sequence with $d(K) = 1$ (or $d(K) = -1$). We then calculate the branch metric between time $k-1$ and k as given by $d^2(u(k), r(k)) = |u(k) - r(k)|^2$. This branch metric is added to the path metrics at time $k-1$, that is, $\sum_{m=0}^{K-1} |u(m) - r(m)|^2$. Afterwards, the path at time k that has the smallest path metric, called the survivor path, is retained and all other paths are discarded. Thus, at each node, only one path survives and its metric is stored for the next computation. For our example, we assume the starting state is $d(0) = 1$. In Figure 9.31 we show the metric of the survivor path at each node. At time $k = 4$, there are two survivor paths with metric 0.72 and 3.92. As these two paths merge at time $k = 3$, we can readily detect the information sequence up to this time, which is $1, 1, -1, 1$. If there is no merger, then the process must continue until the end of the sequence. If the sequence is too long, it may be truncated at the predetermined length K. If K is much larger than the channel memory L, there is little loss in performance.

■

9.8 Fractionally spaced equalizer (FSE)

All the previous equalizers were designed to operate at the symbol rate. They can modify the folded (aliased) spectrum $X(f)$ in (9.36) or equivalently $X\left(e^{j2\pi f'}\right)$ in (9.53), which is the *sum of aliased components* $|S(f+k/T)|^2$ or $|S(f'/T+k/T)|^2$. This requires a precise sampling timing, which might not be possible under some circumstance. For example, if the received pulse has a timing error t_0, that is, $s(t-kT-t_0)$ is processed as $s(t-kT)$, then a phase error $e^{-j2\pi f t_0}$ occurs in $|S(f+k/T)|^2$ in the form of modified aliased component $|S(f+k/T)|^2 e^{-j2\pi(f+k/T)t_0}$. The sampling timing error can cause the modified aliased components to have spectral nulls in the passband even though they are not present in $|S(f+k/T)|^2$. To solve the timing problem, we should design an equalizer that can modify the *aliased sum of equalized component* instead. That is, the equalization should be done on the modified aliased component $|S(f+k/T)|^2 e^{-j2\pi(f+k/T)t_0}$ before aliasing. This can only be done if the matched filter output is sampled faster than the Nyquist rate, that is, at least twice the channel bandwidth. A Nyquist channel with bandwidth $B=(1+\beta)/2T$ requires a sampling rate $1/T' > 2B = (1+\beta)/T$. Without loss of generality, we set the roll-off factor $\beta = 1$ to yield a sampling rate larger than twice the symbol rate. With the sampling rate $1/T'$, there is no aliasing in the spectrum $X'(f)$ at the output of the matched filter, where $X'(f)$ is given by

$$X'(f) = \frac{1}{T'}\sum_{k=-\infty}^{\infty}\left|S\left(f+\frac{k}{T'}\right)\right|^2 e^{-j2\pi(f+k/T')t_0} \tag{9.154}$$

Now consider a fractionally spaced equalizer (FSE) that immediately follows the Nyquist sampler as depicted in Figure 9.32.

The FSE has a periodic frequency response $C_{T'}(f)$. The output $Y'(f)$ of the FSE is periodic with period $1/T'$ and is given as

$$\begin{aligned} Y'(f) &= C_{T'}(f)X'(f) \\ &= C_{T'}(f)\left[\frac{1}{T'}|S(f)|^2 e^{-j2\pi f t_0}\right], \qquad |f| \le \frac{1}{2T'} \end{aligned} \tag{9.155}$$

where only the $k=0$ term is counted since $S(f) \neq 0$ only in $|f| \le 1/2T'$. Thus, $C_{T'}(f)$ can equalize any phase error $e^{-j\theta(f)}$ that is experienced by $S(f)$. The output of the FSE is then sampled again at the symbol rate $1/T$ to yield a spectrum $Y(f)$ of period T as follows:

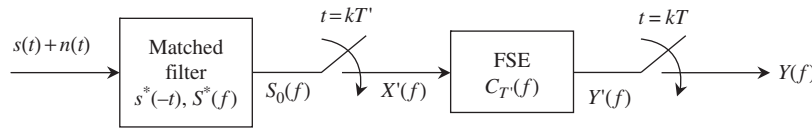

Figure 9.32 FSE with the sampling rate $1/T'$.

$$
\begin{aligned}
Y(f) &= \frac{1}{T}\sum_{k=-\infty}^{\infty} Y'\left(f+\frac{k}{T}\right) \\
&= \frac{1}{TT'}\sum_{k=-\infty}^{\infty} C_{T'}\left(f+\frac{k}{T}\right)\left|S\left(f+\frac{k}{T}\right)\right|^2 \mathrm{e}^{-\mathrm{j}2\pi(f+k/T)t_0}
\end{aligned}
\tag{9.156}
$$

Note that $Y(f)$ is the *aliased sum of equalized* $Y'(f+k/T)$, while $X'(f)$ is the *sum of aliased component* $|S(f+k/T')|^2$. The FSE, therefore, can be designed to assume the role of ZF-LE, MSE-LE, and the linear predictor of the DFE.

9.9 Summary

In this chapter we have provided a detailed study of *intersymbol interference* and fundamental *equalization* techniques. We introduced the concept of *zero ISI* via the *Nyquist criterion*. The *raised-cosine* pulse is the Nyquist pulse that is widely used in practice. The *optimum demodulator* was designed based on the criteria of zero ISI and maximum output signal-to-noise ratio. In other words, the pulse shape at the threshold detector input is a Nyquist pulse that achieves zero ISI at the sampling time. Furthermore, the sample presented to the threshold detector has a maximum signal-to-noise ratio. The optimum demodulator employs two filters in the transmitter. One filter has a frequency response equal to the *inverse* of the channel frequency response. In effect, the combination of this filter and the channel yield an ideal channel with no distortion. This process is called pre-equalization, where the channel distortion effect is pre-corrected at the transmitter. The receiver filter is designed to match the second filter in the transmitter to provide an output Nyquist pulse and to emulate the matched filter.

Pre-equalization in the transmitter is not practical because the transmitter often does not have the means to estimate the channel. Therefore, equalization is commonly carried out in the receiver where the channel response can be estimated. We presented two types of linear equalizers, namely, the *zero-forcing linear equalizer* (ZF-LE) and the *mean-square error linear equalizer* (MSE-LE). The ZF-LE forces the sample at the threshold detector input to have zero ISI. It does so at the expense of the output signal-to-noise ratio, which can go to zero if the channel response has *spectral nulls*. The MSE-LE compromises between ISI and the output signal-to-noise ratio.

The performance of linear equalizers can be improved by using feedback decision. We presented two nonlinear equalizers, namely, the *zero-forcing decision-feedback equalizer* (ZF-DFE) and the *mean-square error decision-feedback equalizer* (MSE-DFE). These nonlinear equalizers suffer *error propagation* but nevertheless may perform better than their linear counterparts. The best nonlinear equalizer is the *maximum likelihood sequence detector* (MLSD), which can be implemented by the *Viterbi algorithm*. Finally, we studied the *fractionally spaced* equalizer (FSE), which can correct the timing error problem in previously studied equalizers. The FSE works on the *aliased sum of equalized components* instead of the *sum of aliased components*, thereby solving the timing problem before it can be rendered uncorrectable by aliasing.

Problems

1. Show that the raised-cosine pulse shape and its Fourier transform satisfy the Nyquist criterion of zero ISI.
2. Show that $(1/T)\sum_m P(f + m/T)$ is the Fourier transform of $p(t)\sum_m \delta(t + mT) = p(t)\sum_m \delta(t - mT)$.
3. Show that when the sampling rate $1/T$ is greater than twice the absolute bandwidth B of the Fourier transform $P(f)$ of the pulse shape $p(t)$, then the Nyquist criterion of zero ISI cannot be satisfied.
4. Consider an antipodal signal with squared pulse shape $p(t)$ of unit amplitude and duration T. Sketch the waveform at the output of the matched filter when the input bit sequence is 10011. Specify the amplitudes at the sampling times. Is there any intersymbol interference?
5. Find the impulse response of the filter having the frequency response equal to the square root of $P(f) = T,\ -1/2T \le f \le 1/2T$ and zero otherwise.
6. Consider an antipodal signal with squared pulse shape $p(t)$ of unit amplitude and duration T. Derive the output waveform for one bit, say 1, at the output of an RC-filter (series resistance R and shunt capacitor C).
   (a) Sketch the output waveform when the input bit sequence is 10011and specify the amplitudes at the sampling times for the case $RC = T$. Is there any intersymbol interference?
   (b) Derive the output *SNR* for the *RC*-filter for a single bit at the sampling time T, assuming the noise spectrum is $N_0/2$. The antipodal signal amplitudes are $\pm A$.
   (c) Derive the one-shot output *SNR* for each bit in the sequence 10011 for the case above that includes intersymbol interference.
   (d) Derive the one-shot bit error probability for each bit in the sequence 10011 for the case (c) that includes intersymbol interference, assuming that noise is Gaussian.
7. Find the impulse response of the square root raised-cosine filter.
8. Verify (9.63).
9. Verify (9.65).
10. Consider a bandlimited QPSK signal whose bandwidth is B.
    (a) Draw the equivalent lowpass model for the transmitter, channel, and receiver.
    (b) Draw the block diagram of an optimum system that can achieve the maximum output SNR_0 at the sampling time.
11. Consider the following samples of the output pulse of a matched filter: $\ldots, 0, x(-1) = a,\ x(0) = 1 + a^2,\ x(1) = a,\ 0, \ldots$. Evaluate the composite channel transfer function, the synthetic channel transfer function, and the ZF-LE transfer function.
12. Consider a channel with impulse response $h(t) = a\delta(t) + b\delta(t - t_0)$. The input to this channel is the pulse $p(t)$.
    (a) Evaluate the channel output $s(t)$.
    (b) Consider a filter that is matched to $s(t)$ with a designated impulse response $\alpha s(T' - t)$, where α is a scaling constant and T' is a time delay. Evaluate the output $s_0(t)$ of the matched filter at the time $t = kT'$ when $T' = t_0$.

(c) Assuming that $p(t)$ is orthogonal to its t_0-translates, evaluate the output sequence $x(k) = s_0(kt_0)$. Evaluate the z-transform of $x(k)$.
(d) Find the synthetic channel transfer function of the sequence $x(k+1)$.

13. Consider the following sequence of pulses at the input of the matched filter: $v(t) = \sum_n d_n s(t - nT)$, where $d_n \in \{-1, 1\}$ represents the data bit at the time index n. Furthermore, let the *equivalent lowpass* pulse of the *modulated* pulse $s(t)\cos 2\pi f_c t$ be $s(t) = \sqrt{4Ea}\, e^{-at}u(t)$, $a > 0$ (see Example 9.8).
(a) Calculate the signal-to-noise ratio at the output of the sampler at the time index $k = 1$, assuming $d_0 = 1,\ d_1 = -1$.
(b) Calculate the signal-to-noise ratio at the output of the sampler at the time index $k = 2$, assuming $d_0 = 1,\ d_1 = 1,\ d_2 = -1$.
(c) Calculate the signal-to-noise ratio at the output of the sampler at the time index $k = 3$, assuming $d_0 = 1,\ d_1 = 1,\ d_2 = 1,\ d_3 = -1$.
(d) Compare the results in (a)–(c) to that of the ZF-LE.

14. Consider the following sequence of pulses at the input of the matched filter: $v(t) = \sum_n d_n s(t - nT)$, where $d_n \in \{-1, 1\}$ represents the data bit at the time index n. Furthermore, let the *equivalent lowpass* pulse of the *modulated* pulse $s(t)\cos 2\pi f_c t$ be $s(t) = \sqrt{2Ea}\, e^{-a|t|}$, $a > 0$ (see Example 9.8).
(a) Calculate the signal-to-noise ratio at the output of the sampler at the time index $k = 1$, assuming $d_0 = 1,\ d_1 = -1$.
(b) Calculate the signal-to-noise ratio at the output of the sampler at the time index $k = 2$, assuming $d_0 = 1,\ d_1 = 1,\ d_2 = -1$.
(c) Calculate the signal-to-noise ratio at the output of the sampler at the time index $k = 3$, assuming $d_0 = 1,\ d_1 = 1,\ d_2 = 1,\ d_3 = -1$.

15. Using Example 9.8, determine the sampling rate so that $SNR_{0,ZF\text{-}LE} = 1.5E/N_0$

16. Consider the composite channel $X(z) = 1 + 0.5z^{-1} + 0.5z$. Calculate the mean-square error of MSE-DFE via a spectral factorization.

17. Consider the channel specified by the FIR filter $F(z) = f(0) + f(1)z^{-1}$, where the channel tap weights are $f(0) = \sqrt{2E},\ f(1) = 0.4\sqrt{2E}$. The input to this channel is a sequence of two bits $\{d(k), d(k-1)\}$, where $d(i) \in \{-1, 1\}$. Calculate the power $|r(k)|^2$ of the output bit $r(k)$ for all four bit patterns. Find the one-shot bit error probability for each of the four bit patterns, assuming the modulation is PSK.

18. Consider the composite channel $X(z) = a^2 + bz + bz^{-1}$.
(a) Derive the condition on a and b so that $X(e^{j2\pi f'})$ is a positive-real function, that is, $X(z)$ can be expressed as $X(z) = F(z)F^*(1/z^*)$. Find $F(z)$ and $X(e^{j2\pi f'})$. Does $X(e^{j2\pi f'})$ have spectral nulls?
(b) Calculate $SNR_{0,ZF\text{-}LE}$.

19. Consider the synthetic channel $F(z) = f(0) + f(1)z^{-1}$.
(a) Calculate the mean-square errors of the MSE-LE and MSE-DFE.
(b) Calculate $SNR_{0,MSE\text{-}LE}$ and $SNR_{0,MSE\text{-}DFE}$.

20. Verify (9.121).

21. Consider a synthetic channel with transfer function $F(z) = f(0) + f(1)z^{-1}$.
(a) Derive the bit error probability for the received PSK signal.
(b) Derive the bit error probability for the received PSK signal with ZF-DFE.

22. Carry out the Viterbi algorithm using Figure 9.30 with the following data: $(u(1), u(2), u(3), u(4), \ldots) = (1, 0, 0.2, -1.1, \ldots)$, $F(z) = 1 + 0.1z^{-1}$.

Further reading

For further studies on ISI the reader is referred to the excellent text by Proakis [2], which also discusses controlled ISI. The effect of ISI can be found in the excellent book by Pursley [3]. More information on equalization techniques can be found in [2] or in the excellent books by Barry *et al*. [4] and Gitlin *et al*. [5]. The above books also cover *adaptive equalization*, in which the equalizer taps can be adjusted to accommodate a time-varying channel. More advanced topics on adaptive filters can also be found in Haykin [6]. A good discussion of sequence demodulation can be found in Blahut [1].

Bibliography

1. R. E. Blahut, *Digital Transmission of Information*, New York: Addison-Wesley, 1990.
2. J. G. Proakis, *Digital Communications*, 5th edition, New York: McGraw-Hill, 2008.
3. M. B. Pursley, *Introduction to Digital Communications*, Upper Saddle River, NJ: Pearson Prentice Hall, 2005.
4. J. R. Barry, E. A. Lee, and D. G. Messerschmitt, *Digital Communication*, 3rd edition, London: Kluwer Academic Publishers, 2004.
5. R. D. Gitlin, J. F. Hayes, and S. B. Weinstein, *Data Communications Principles*, London: Plenum Press, 1992.
6. S. Haykin, *Adaptive Filter Theory*, London: Prentice Hall, 1996.
7. S. A. Alteka and N. C. Beaulieu, "Upper bounds on the error probability of decision feedback equalization," *IEEE Trans. Inform. Theory*, Vol. **39**, pp. 145–156, 1993.
8. C. A. Belfiore and J. H. Park, "Decision feedback equalization," *Proc. IEEE*, Vol. **67**, No. 8, pp. 1143–1156, 1979.
9. G. D. Forney, Jr., "Maximum likelihood sequence estimation of digital sequences in the presence of intersymbol interference," *IEEE Trans. Inform. Theory*, Vol. **18**, pp. 363–378, 1972.
10. G. D. Forney, Jr., "The Viterbi algorithm," *Proc. IEEE*, Vol. **61**, No. 3, pp. 268–278, 1973.
11. R. W. Lucky, "Automatic equalization for digital communications," *Bell Syst. Tech. J.*, Vol. **44**, pp. 547–588, 1965.
12. R. W. Lucky, "Techniques for adaptive equalization of digital communication," *Bell Syst. Tech. J.*, Vol. **45**, pp. 255–286, 1966.
13. R. W. Lucky, J. Salz, and E. J. Weldon, Jr., *Principles of Data Communication*, New York: McGraw-Hill, 1968.
14. H. Nyquist, "Certain topics in telegraph transmission theory," *AIEE Trans.*, Vol. **47**, pp. 617–644, 1928.

15. A. Papoulis, *Probability, Random Variables, and Stochastic Processes*, 3rd edition, New York: McGraw-Hill, 1968.
16. S. Qureshi, "Adaptive equalization," *Proc. IEEE*, Vol. **53**, No. 9, pp. 1349–1387, 1985.
17. G. Ungerboeck, "Fractional tap-spacing equalizer and consequences for clock recovery in data modems," *IEEE Trans. Commun.*, Vol. **24**, No. 8, pp. 856–864, 1976.
18. S. Verdu, "Maximum likelihood sequence detection of intersymbol interference channels: a new upper bound on error probability," *IEEE Trans. Inform. Theory*, vol. **33**, pp. 62–68, 1987.

10 Fading channels

Introduction

Besides the intersymbol interference (ISI) that occurs via channel filtering, a digitally modulated signal can also have ISI when it is transmitted over a multipath fading channel. This type of channel is encountered in all forms of mobile wireless communication. In a multipath fading channel, the transmitted signal arrives at the receiver via multiple paths. These paths generally arise via signal reflection from the ground, hills, buildings, and any other large structures. They also arise from signal diffraction via bending around the corners of buildings or sliding across rooftops. They also can arise via signal scattering from small objects such as vehicles, lamp posts, trees, etc. Each signal path results in a randomly delayed, attenuated, and phase-shifted copy of the transmitted signal. These multipath copies combine at the receiver to give rise to a received signal whose *envelope* may be described by a Rayleigh fading process (no line-of-sight path), or a Rice fading process (one line-of-sight path), or a Nakagami fading process. Also, because the arrival times of the multipath copies are random, especially in a mobile environment, the multipath copies *might overlap* the next bit or symbol and hence cause intersymbol interference. This type of ISI cannot be eliminated by pulse shaping dictated by the Nyquist criterion for zero ISI, but can be alleviated by equalization (as discussed in Chapter 9). The above effects are collectively called *fading*. A fading channel that exhibits ISI is called a *frequency-selective fading* channel. A channel that exhibits negligible ISI is called a *flat fading* channel.

Figure 10.1 illustrates a frequency-selective fading channel in which a signal travels several propagation paths creating multiple received copies of it at the receiver.

Figures 10.2 and 10.3 illustrate the ISI process due to multipath fading effects for three bits 1, 0, 1 with a squared pulse shape at the input and output of the matched filter, respectively, in the case of two propagation paths. ISI occurs at the sampling time $t = 2T$, $3T$. Note that the amplitudes of these bits are not the same to reflect the channel fading effect. In this case, the complex envelope fading varies from bit to bit but remains essentially the same during a bit time. This phenomenon is commonly called *slow fading* to reflect the fact that the channel varies slowly within one or several bit times. When the channel varies substantially during a bit time, the channel is said to be a *fast fading* channel. Both slow and fast fading phenomena result from the movement of the transmitter and/or receiver, the so-called Doppler effect. In a bandlimited multipath fading channel, both filtering-induced ISI and multipath-induced ISI occur simultaneously and can cause serious performance degradation. Also, the time variation can induce carrier

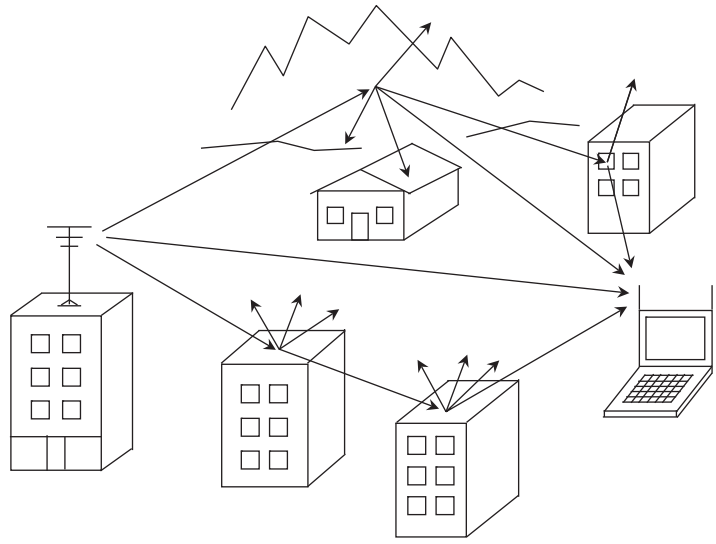

Figure 10.1 Multipath fading channel with multiple copies of the signal arriving at the receiver.

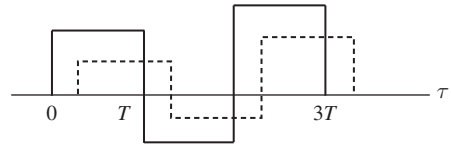

Figure 10.2 Pre-filtering ISI for a squared pulse shape. The solid line is for the first arrival and the dashed line is for the delayed second arrival.

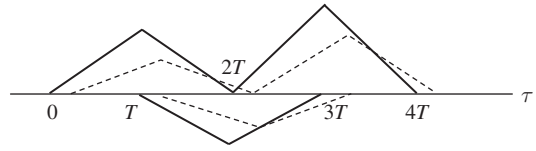

Figure 10.3 Post-filtering ISI at the output of the matched filter for two propagation paths.

phase error, which results in a loss of the signal-to-noise ratio at the coherent receiver. The combined time variation and multipath effect give rise to a *time-varying* and *space-varying* channel. This channel can be represented by an *impulse response* $h(\tau, t)$, where the time t represents the variations of the channel and the time τ represents the time arrivals of the multipath copies. When the channel is *time-invariant*, we have $h(\tau, t) = h(\tau)$. Wireless channels such as cellular channels, WLAN, WMAN, and underwater channels are common examples of *Rayleigh fading* channels, which have two non-conflicting attributes of the four attributes described above (slow fading, fast fading, flat fading, and frequency-selective fading).

10.1 Physical characterization of fading channels

The time variation and multipath effect of a channel must be quantitatively described to facilitate the design of the waveform and consequently its demodulation. In fact, these adverse conditions (relative to the AWGN channel) can be neutralized to a large extent or even taken advantage of if the designer is aware of their cause and effect.

Time-varying effect

We examine first the cause of time variation of the channel. It arises mainly from the *Doppler effect* due to the motion of the transmitter and/or receiver and the time variation of the structures of the medium. Let us consider a received *free space E-field* (V/m) at distance d greater than a *reference distance* d_0 from the transmitter. We have

$$E(d,t) = \frac{E_0 d_0}{d}\cos\left[2\pi f_c\left(t - \frac{d}{c}\right)\right] \tag{10.1}$$

where E_0 is the *free space* E-field at d_0. If we now assume that the receiver moves away from the transmitter with radial velocity v, the distance d increases in time by vt. The received E-field is given by

$$\begin{aligned} E(d,t) &= \frac{E_0 d_0}{d+vt}\cos\left[2\pi f_c\left(t - \frac{d}{c} - \frac{vt}{c}\right)\right] \\ &= \frac{E_0 d_0}{d+vt}\cos\left[2\pi f_c\left(\left(1 - \frac{v}{c}\right)t - \frac{d}{c}\right)\right] \end{aligned} \tag{10.2}$$

Thus the carrier frequency f_c becomes $f_c(1 - v/c)$. The received E-field encounters a *Doppler shift* of $f = -f_c v/c$. If the receiver moves toward the transmitter, the Doppler shift is $f = f_c v/c$. The Doppler shift induces two effects: the time-varying phase shift $\theta(t) = 2\pi f t$ and the time-varying amplitude $E_0 d_0/(d + vt)$. Let us consider the first example where the carrier frequency is $f_c = 1$ GHz and the receiver radial velocity is $v = 100$ km/hour (moving away). Then, the Doppler shift is -92.6 Hz. Consider a channel bit rate of 14.4 kbps, then the bit interval is 69.4 μs. Let us consider a bit which starts at time $t = 0$ and ends at time $t = 69.4$ μs. The phase shift at the end of the bit is -0.04 radians or $-2.3°$. If the criterion for *channel estimation* is no more than 45° ($\pi/4$ radians) phase error then the *delay requirement* for channel estimation cannot exceed $1/8f$ seconds or 20 bit times. Also, during 20 bit times the receiver moves a distance 0.039 m. This induces a *small variation* in the received E-field amplitude.

Now let us consider the second example of a transmitter and a receiver separated by a distance d. If we assume that the receiver moves straight toward the transmitter with radial velocity v, the distance d_1 decreases in time by vt. The Doppler shift of the LOS E-field is $f = f_c v/c$. In addition, suppose the receiver also receives a reflected E-field from a perfect reflector directly behind it. The distance traveled by this reflected E-field is d_2. Since the receiver is moving straight away from the reflector, the distance increases in time by vt.

The Doppler shift of the reflected E-field is $-f_c v/c$. The reflected signal is π radians out-of-phase with its incident E-field. Therefore, the total received E-field at the receiver is given as

$$\begin{aligned} E(d,t) &= \frac{E_0 d_0}{d_1 - vt}\cos\left[2\pi f_c\left(t - \frac{d_1}{c} + \frac{vt}{c}\right)\right] - \frac{E_0 d_0}{d_2 + vt}\cos\left[2\pi f_c\left(t - \frac{d_2}{c} - \frac{vt}{c}\right)\right] \\ &= \frac{E_0 d_0}{d_1 - vt}\cos\left[2\pi f_c\left(\left(1 + \frac{v}{c}\right)t - \frac{d_1}{c}\right)\right] - \frac{E_0 d_0}{d_2 + vt}\cos\left[2\pi f_c\left(\left(1 - \frac{v}{c}\right)t - \frac{d_2}{c}\right)\right] \end{aligned} \tag{10.3}$$

For simplicity let us consider the case where the receiver is close to the reflector so that the amplitudes of both LOS and reflected E-fields are approximately the same. Then the sum of the two E-fields can be approximated by the following expression:

$$E(d,t) \approx \frac{2E_0 d_0}{d_2 + vt}\sin[2\pi f_c(vt/c + (d_2 - d_1)/2c)]\sin[2\pi f_c(t - (d_2 + d_1)/2c)] \tag{10.4}$$

The received E-field now has a time-varying amplitude which varies according to the Doppler shift. The larger the Doppler shift, the faster the amplitude varies. This results in *deep fades* at intervals of $1/4f$ (or a quarter-wavelength) from the peak amplitudes. For the numerical values used in the first example, a deep fade occurs every 39 bits from the peak amplitudes. The difference between the Doppler shifts of the LOS and reflected E-fields is referred to as the *Doppler spread*, which we define below.

Definition 10.1 The *Doppler spread* of a fading channel is defined as follows:

$$f_D = \max_{i,j}|f_i - f_j| \tag{10.5}$$

where the maximum is taken over all positive Doppler shifts f_i and negative Doppler shifts f_j of the propagation paths.

For the above example the Doppler spread is $2f_c v/c$. In general, Doppler shift induces both time variation in signal amplitude and carrier phase error. These two phenomena cause a loss in the signal-to-noise ratio and degrade performance.

Definition 10.2 The *coherence time* of a fading channel is related to the *Doppler spread* as follows:

$$T_c = \frac{1}{4f_D} \tag{10.6}$$

According to this definition, the coherence time is an *empirical relation* that can be adjusted to fit the requirement. Obviously, the coherence time is infinite when there is no Doppler shift. This implies that the channel is time-invariant and no phase error occurs. There is still loss in signal amplitude due to the sum of the various signal rays at the receiver, but this loss can be compensated for with power control.

Space-varying effect

The fading wireless channel is also *space-varying*, that is, the multipath effect varies according to *different locations* of transmitter and receiver even when the transmitter and receiver are stationary and the structures of the medium do not change. Thus, a *multipath intensity profile* (MIP) which shows *power versus delay* or *magnitude versus delay* of each multipath copy is space-dependent, that is, it is a function of the transmitter and receiver coordinates. An example of a realization of MIP is shown in Figure 10.4. As previously discussed, the multipath effect might cause ISI in the received symbol stream. To characterize this effect we introduce two parameters called *multipath delay spread* and *coherence bandwidth*.

Definition 10.3 The *multipath delay spread* T_d of a fading channel is empirically defined as the maximum of the difference in propagation times between the first path with power P_1 and the *last significant path* of power P_l, such that P_1/P_l is *greater than but closest* to a given *threshold* γ. For example, the threshold can be taken to be $SNR = P_1/N$, the signal-to-noise ratio of the first path. The maximum is carried out over *all multipath intensity profiles*:

$$T_d = \max_{MIP}\left[\tau_l(t) - \tau_1(t)|\min_l\{P_1/P_l > \gamma\}\right] \tag{10.7}$$

This definition implies that the ISI effect of multipath copies should be kept small when one estimates the multipath delay spread for waveform design purposes. If the receiver locks onto the first path, then the spill-over symbol energy from delayed paths might cause ISI in the next symbol. Thus, one should include as many significant paths as possible so that the ISI effect is not underestimated. Equation (10.7) also implies that the transmission time of a symbol should far exceed the multipath delay spread to have a small ISI effect. Instead of designing for the worst case, real-time MIP can also be obtained from channel estimation to

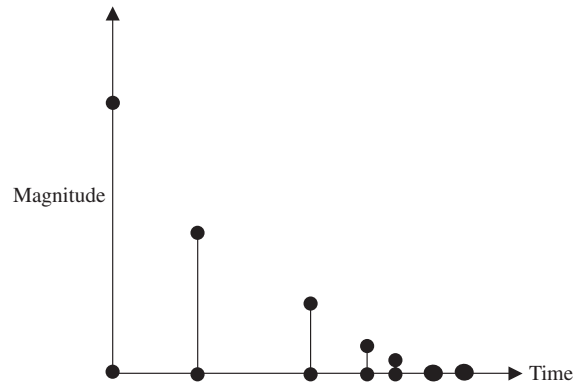

Figure 10.4 A multipath intensity profile.

vary the transmission rate to take advantage of the channel condition. This implies a higher symbol rate for small T_d and a lower symbol rate for a large T_d. For the MIP realization in Figure 10.4, the multipath delay spread can be taken to be the time spead between the first path and the fifth path, assuming $P_1/P_l \leq \gamma, l = 2, 3, 4$, and $P_1/P_5 > \gamma$.

Definition 10.4 The *coherence bandwidth* B_c of a fading channel is defined as the inverse of the *multipath delay spread*

$$B_c = \frac{1}{T_d} \tag{10.8}$$

This is the bandwidth necessary to accommodate the symbol time no smaller than the multipath delay spread and with $\sin x/x$ pulse shape.

Summary of fading characteristics

Slow fading: a channel experiences *slow fading* if the following condition is met:

$$\text{coherence time} > \text{channel estimation time}$$

Fast fading: a channel experiences *fast fading* if the following condition is met:

$$\text{coherence time} < \text{channel estimation time}$$

Flat fading: a channel experiences *flat fading* if the following condition is met:

$$\text{signal bandwidth} < \text{coherence bandwidth}$$
$$\text{or}$$
$$\text{multipath delay spread} < \text{symbol time}$$

Frequency-selective fading: a channel experiences *frequency-selective fading* if the following condition is met:

$$\text{signal bandwidth} > \text{coherence bandwidth}$$
$$\text{or}$$
$$\text{multipath delay spread} > \text{symbol time}$$

Table 10.1 presents the range of multipath delay spreads for typical outdoor and indoor environments.

Table 10.1 Multipath delay spread

Environment	Frequency (MHz)	Multipath delay spread
City	900	2–15 μs
Suburban	900	0.3–2 μs
Indoor	2400	20–300 ns

Example 10.1 OFDM for a fading channel

The multipath delay spread of a fading channel imposes the ISI limit on the symbol rate of a single-carrier system. For example, the at-home channel at 2400 MHz with a multipath delay spread of 25 ns limits the symbol rate to 40 Msps. If 64QAM is employed, the bit rate is limited to 240 Mbps. For the outdoor environment, the typical multipath delay spread is 1 μs. The limiting symbol rate is 1 Msps for 64QAM or 6 Mbps. To transmit at a rate of hundreds of Mbps, OFDM must be employed to combat the multipath effect. Let us examine the OFDM-based IEEE 802.11g with 48 data subcarriers. At the highest OFDM bit rate of 54 Mbps, the bit rate per 64QAM-subcarrier is 1.125 Mbps or 187.5 ksps. The tolerable multipath delay spread for 54 Mbps must be much smaller than the subcarrier symbol time, which is 5.3 μs. At the lowest OFDM bit rate of 6 Mbps, the bit rate per PSK-subcarrier is 125 kbps. The tolerable multipath delay spread must be much smaller than 8 μs. In practice, the tolerable multipath delay spread of 1 μs is much less than these symbol times, so the signal-to-noise-and-ISI ratio is high enough to accommodate a good bit error probability. Equalization and cyclic prefixes eliminate most ISI effect in the subcarriers.

■

10.2 Mathematical representation of fading channels

The mathematical representation of a *time-varying* and *space-varying* channel is beyond the scope of this book. For simplicity, we only discuss a time-varying channel for a *given set of coordinates* of both transmitter and receiver.

Channel impulse response

We use the complex envelope representation for a transmitted signal $s(t)$ with complex envelope (equivalent lowpass signal, baseband signal) $s_L(t)$ and carrier frequency f_c. The signal can be the E-field of a plane wave. We have

$$s(t) = \mathrm{Re}\{s_L(t)\mathrm{e}^{\mathrm{j}2\pi f_c t}\} \tag{10.9}$$

The received signal is the *sum* of *uncorrelated multipath copies* that pass through the fading channel with arbitrary path attenuations, phase-shifts, and delays (commonly referred to as *uncorrelated scattering* in the literature. Since fading involves reflection, diffraction, and scattering we prefer the term *uncorrelated fading* instead). These are called *resolvable paths*. Each multipath copy is itself the *sum of many uncorrelated signals of similar* (*or approximately the same*) *path delay* $\tau_i(t)$ but *different path attenuations* $a_{ik}(t)$ and *phase shifts* $\phi_{ik}(t)$, *which include the path Doppler effects*. These are called *non-resolvable* paths. We express the received signal as

$$\begin{aligned} x(t) &= \mathrm{Re}\left\{ \sum_i \sum_k a_{ik}(t) s_L(t-\tau_i(t))\, \mathrm{e}^{\,\mathrm{j}[2\pi f_c(t-\tau_i(t))+\phi_{ik}(t)]} \right\} \\ &= \mathrm{Re}\left\{ \left(\sum_i \sum_k a_{ik}(t) \mathrm{e}^{-\mathrm{j}[2\pi f_c \tau_i(t)-\phi_{ik}(t)]} s_L(t-\tau_i(t)) \right) \mathrm{e}^{\,\mathrm{j}2\pi f_c t} \right\} \end{aligned} \tag{10.10}$$

The complex envelope $x_L(t)$ of the received signal $x(t)$ is given by the following expression:

$$\begin{aligned} x_L(t) &= \sum_i \sum_k a_{ik}(t) \mathrm{e}^{-\mathrm{j}[2\pi f_c \tau_i(t)-\phi_{ik}(t)]} s_L(t-\tau_i(t)) \\ &= \sum_i h_i(t) s_L(t-\tau_i(t)) \end{aligned} \tag{10.11}$$

where the term $h_i(t)$ is the ith *complex path attenuation,* and is often referred to as the ith *channel tap*

$$h_i(t) = \sum_k a_{ik}(t) \mathrm{e}^{-\mathrm{j}[2\pi f_c \tau_i(t)-\phi_{ik}(t)]} \tag{10.12}$$

By the *central limit theorem* the channel tap $h_i(t)$ can be modeled as a *complex Gaussian random variable* whose in-phase and quadrature components have the same variance. Thus the magnitude $|h_i(t)|$ of the ith channel tap is a Rayleigh or Rice process (when a line-of-sight component is present). Alternatively, one can model the channel tap by a Nakagami process (see Chapter 3). From (10.11) we obtain the *complex envelope* of the *impulse response* (equivalent lowpass impulse response, baseband impulse response) of an uncorrelated fading channel as follows:

$$h(\tau, t) = \sum_i h_i(t) \delta(\tau - \tau_i(t)) \tag{10.13}$$

The corresponding *frequency response* of the fading channel at time t is given as

$$H(f, t) = \sum_i h_i(t) \mathrm{e}^{-\mathrm{j}2\pi f \tau_i(t)} \tag{10.14}$$

For the special case of the *time-invariant channel* the complex envelope and the frequency response are obtained from (10.13) and (10.14) as

$$h(\tau) = \sum_i h_i \delta(\tau - \tau_i), \qquad H(f) = \sum_i h_i \mathrm{e}^{-\mathrm{j}2\pi f \tau_i} \tag{10.15}$$

Example 10.2 Flat fading and frequency-selective fading channels
Let us consider the following two time-invariant channels with four channel taps and delays given in Table 10.2. The impulse and frequency responses are given as

$$h(\tau) = \sum_{i=1}^{4} h_i \delta(\tau - l_i T) \tag{10.16}$$

Table 10.2 Channel taps and delays

		Delay l_i	
i	Tap h_i	Channel 1	Channel 2
1	0.8	0	0
2	0.4	0.2	0.5
3	0.33	0.3	1.2
4	0.3	0.5	2

$$H(f) = \sum_{i=1}^{4} h_i \mathrm{e}^{-\mathrm{j}2\pi l_i f T} \tag{10.17}$$

The magnitude and phase versus the *frequency-time product fT* of the frequency responses are shown in Figure 10.5. The first channel is a flat fading channel when the *signal bandwidth-multipath delay spread product* is smaller than $fT = B_c T_s = 0.5$, where B_c is the channel coherence bandwidth and T_s is the symbol time. In this range, the magnitude spectrum is fairly flat and the phase is linear. For the same range of fT, the second channel has frequency-selective fading, since the magnitude spectrum shows considerable variation and the phase is not linear.

■

Multipath autocorrelation and Doppler profiles

With the channel impulse response available we can establish the channel autocorrelation:

$$R_h(\tau, \tau'; t_1, t_2) = \mathbf{E}[h(\tau, t_1) h^*(\tau', t_2)] \tag{10.18}$$

Substituting $h(\tau, t) = \sum_i h_i(t)\delta(\tau - \tau_i(t))$ into (10.18) we obtain

$$\begin{aligned} R_h(\tau, \tau'; t_1, t_2) &= \mathbf{E}\left[\sum_i h_i(t_1)\delta(\tau - \tau_i(t_1)) \sum_k h_k^*(t_2)\delta(\tau' - \tau_k(t_2))\right] \\ &= \sum_i \sum_k \mathbf{E}[h_i(t_1) h_k^*(t_2)]\, \delta(\tau - \tau_i(t_1))\, \delta(\tau' - \tau_k(t_2)) \end{aligned} \tag{10.19}$$

This means that the channel autocorrelation is non-zero only when all the delays are the same. Thus, the channel autocorrelation reduces to the following expression:

$$R_h(\tau; t_1, t_2) = \left[\sum_i \mathbf{E}[h_i(t_1) h_i^*(t_2)]\, \delta(\tau - \tau_i(t_1))\right] \tag{10.20}$$

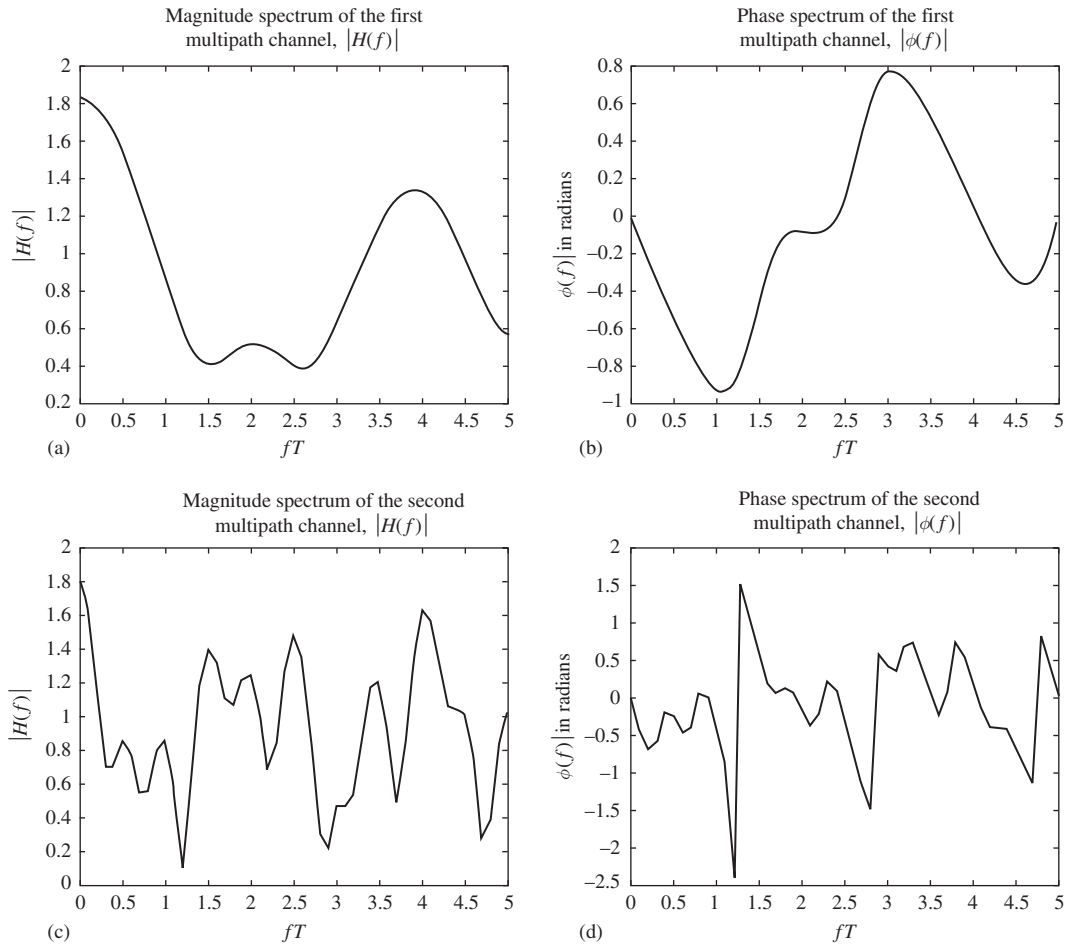

Figure 10.5 Frequency responses of (a),(b) the flat fading channel 1 and (c),(d) the frequency-selective fading channel 2.

If we assume that the fading process $\{h_i(t)\}$ is a *WSS random process* and also *ergodic* we can take the *ensemble average* of $R_h(\tau\,; t_1, t_2)$ to be its *time average*, which depends only on $\boldsymbol{t}' = t_2 - t_1$, and hence eliminate the time origin t_1. From now on we assume that the channel is *WSS and ergodic* and undergoes *uncorrelated fading*. Thus we have the *multipath autocorrelation profile*

$$R_h(\tau, \boldsymbol{t}') = \sum_i R_{h_i}(\boldsymbol{t}')\,\delta(\tau - \tau_i) \tag{10.21}$$

where the *i*th *path autocorrelation* is given by ($\boldsymbol{t}' = t_2 - t_1$)

$$R_{h_i}(\boldsymbol{t}') = \mathbf{E}[h_i(t_1)h_i^*(t_2)] \tag{10.22}$$

Taking the Fourier transform of the multipath autocorrelation profile $R_h(\tau, \boldsymbol{t}')$ in the $\boldsymbol{t}'$ variable we obtain the *multipath Doppler profile* $S_h(\tau, \boldsymbol{f}')$ of the fading channel

$$S_h(\tau, \boldsymbol{f}') = \sum_i S_{h_i}(\boldsymbol{f}')\delta(\tau - \tau_i) \tag{10.23}$$

where the *i*th *path Doppler power spectrum* $S_{h_i}(\boldsymbol{f}')$ is the Fourier transform of the path autocorrelation $R_{h_i}(\boldsymbol{t}')$. This means that all multipath copies of the transmitted signal are affected by the Doppler shift. The *Doppler spread* of the fading channel is approximately the *maximum* of the path Doppler spreads of significant paths (the path Doppler spread is twice the absolute bandwidth of the path Doppler spectrum.). The *coherence time* of the fading channel is defined as in (10.6).

Clarke–Doppler power spectrum

Let us consider a fading channel with *L uncorrelated non-resolvable* paths only, thus the channel is a *flat fading* channel. These paths arrive at the mobile receiver (moving with speed *v*) via scatterers around it with approximately the same delay but with different attenuations and phase shifts, and Doppler shifts $f_k = (f_c v/c)\cos\theta_k = f_m \cos\theta_k$, depending on the horizontal arrival angles θ_k. The maximum Doppler shift is $f_m = f_c v/c$. The impulse response of the channel is

$$h(\tau, t) = \left[\sum_k h_i \, \mathrm{e}^{-\mathrm{j}[2\pi(f_m \cos\theta_k)t]}\right]\delta(\tau) \tag{10.24}$$

Furthermore, we assume that the total received power is $P = L\mathbf{E}[|h_k|^2]$.

Discrete sum approach

The multipath autocorrelation profile for *fixed* horizontal arrival angles is given as follows:

$$R_h(\tau, \boldsymbol{t}') = \left[\sum_k \mathbf{E}[|h_k|^2] \, \mathrm{e}^{\mathrm{j}[2\pi(f_m \cos\theta_k)\boldsymbol{t}']}\right]\delta(\tau) \tag{10.25}$$

Assuming that the scatterers are *evenly spaced* around the mobile, we can express the arrival angle as $\theta_k = k(\Delta\theta)$ and $\Delta\theta = 2\pi/L$.

$$\begin{aligned} R_h(\tau, \boldsymbol{t}') &= \left[\frac{P}{L}\sum_k \mathrm{e}^{\mathrm{j}[2\pi(f_m \cos\ k\Delta\theta)\boldsymbol{t}']}\right]\delta(\tau) \\ &= \left[\frac{P}{2\pi}\sum_k \mathrm{e}^{\mathrm{j}[2\pi(f_m \cos\ k\Delta\theta)\boldsymbol{t}']}\Delta\theta\right]\delta(\tau) \end{aligned} \tag{10.26}$$

As the number of scatterers around the mobile approaches infinity, the summation becomes an integral and we have

$$\begin{aligned} R_h(\tau, \boldsymbol{t}') &= \left[\frac{P}{2\pi}\int_{-\pi}^{\pi} \mathrm{e}^{\mathrm{j}[2\pi(f_m \cos\ \theta)\boldsymbol{t}']}\,\mathrm{d}\theta\right]\delta(\tau) \\ &= [PJ_0(2\pi f_m \boldsymbol{t}')]\delta(\tau) \end{aligned} \tag{10.27}$$

Integral approach

The multipath autocorrelation profile for *random* horizontal arrival angles is given as follows:

$$\begin{aligned} R_h(\tau, t') &= \left[\sum_k \mathbf{E}[|h_k|^2]\, \mathbf{E}\left\{ \mathrm{e}^{\,\mathrm{j}[2\pi(f_m \cos\theta_k)t']} \right\}\right] \delta(\tau) \\ &= \left[\frac{P}{L}\sum_k \mathbf{E}\left\{ \mathrm{e}^{\,\mathrm{j}[2\pi(f_m \cos\theta_k)t']} \right\}\right] \delta(\tau) \\ &= \left[P\mathbf{E}\left\{ \mathrm{e}^{\,\mathrm{j}[2\pi(f_m \cos\theta_k)t']} \right\}\right] \delta(\tau) \end{aligned} \tag{10.28}$$

The horizontal arrival angle θ_k is assumed to be uniformly distributed in $(-\pi, \pi)$. Hence, we obtain

$$\begin{aligned} R_h(\tau, t') &= \left[\frac{P}{2\pi}\int_{-\pi}^{\pi} \mathrm{e}^{\,\mathrm{j}[2\pi(f_m \cos\,\theta)t']}\, \mathrm{d}\theta\right] \delta(\tau) \\ &= [PJ_0(2\pi f_m t')]\delta(\tau) \end{aligned} \tag{10.29}$$

The multipath Doppler profile is the Fourier transform of $R_h(\tau, t')$ in the t' variable, and is given by

$$S_h(\tau, f') = \begin{cases} \dfrac{P}{\pi\sqrt{f_m^2 - f'^2}}\delta(\tau), & |f'| \le f_m \\ 0, & \text{otherwise} \end{cases} \tag{10.30}$$

The *Clarke–Doppler power spectrum* is the value of $S_h(\tau, f')$ at $\tau = 0$, and is given by the following expression:

$$S_h(f') = \begin{cases} \dfrac{P}{\pi\sqrt{f_m^2 - f'^2}}, & |f'| \le f_m \\ 0, & \text{otherwise} \end{cases} \tag{10.31}$$

This power spectrum has singularities at $|f| = f_m$, which make it spike to infinity. This happens because the scattered waves are assumed to be on the horizontal plane only and uniformly distributed around the receiver. In practice, Doppler power spectra do resemble this theoretical one but do not have singularities at $\pm f_m$. The *Doppler spread* f_D of the Clarke fading channel is twice the maximum Doppler shift, that is,

$$f_D = f_m - (-f_m) = 2f_m \tag{10.32}$$

The *coherence time* is empirically given by (10.6) as

$$T_c = \frac{1}{4f_D} = \frac{1}{8f_m} \tag{10.33}$$

Let us examine the autocorrelation $R_h(\boldsymbol{t}') = PJ_0(2\pi f_m \boldsymbol{t}')$, which is the value of $R_h(\tau, \boldsymbol{t}')$ at $\tau = 0$, of the Clarke–Doppler power spectrum $S_h(\boldsymbol{f}')$. At the time difference $\boldsymbol{t}' = T_c = 1/8f_m$, the normalized autocorrelation value is $R_h(T_c)/P = J_0(0.79) = 0.85$. This shows that the correlation is still strong even after a time delay equal to the coherence time. Thus, the *empirical relation* between Doppler spread and coherence time is validated. The Clarke channel is a *slow fading channel* so long as the channel estimation time is smaller than the coherence time, which is one-eighth of the maximum Doppler shift.

Generalized Doppler power spectrum

The Clarke–Doppler power spectrum restricts all scattered waves to the horizontal plane. In practice the *uncorrelated* and *non-resolvable* waves arrive at the mobile with *polar angle* φ_k and *azimuth angle* θ_k, as depicted in the *xyz*-coordinates system shown in Figure 10.6. The mobile is on the horizontal *xy*-plane and moves with speed v in the direction established by the angle ψ with respect to the x-axis. Since we assume that the mobile receives L uncorrelated non-resolvable waves, the channel is a *flat fading* channel.

The complex envelope of the kth incident E-field is given by

$$E_k(d_k, t) = E_{0,k}(d_k)\, \mathrm{e}^{\mathrm{j}[k_0(x \sin \varphi_k \cos \theta_k + y \sin \varphi_k \sin \theta_k + z \cos \varphi_k) + \phi_k]} \tag{10.34}$$

where d_k is the distance traveled by the kth wave, $k_0 = 2\pi f_c/c$ is the free space wave number, and ϕ_k is the wave phase. The random variables $E_{0,k}(d_k)$, $\varphi_k, \theta_k, \phi_k$ are assumed to be *independent*. The total received E-field at the mobile is the sum of L incident waves:

$$E(\boldsymbol{d}, t) = \sum_k E_k(d_k, t) = \sum_k E_{0,k}(d_k)\, \mathrm{e}^{\mathrm{j}[k_0(x \sin \varphi_k \cos \theta_k + y \sin \varphi_k \sin \theta_k + z \cos \varphi_k) + \phi_k]} \tag{10.35}$$

where $\boldsymbol{d} = (d_1, d_2, \ldots, d_L)$ and the coordinates (x, y, z) are given in terms of the speed v and the initial mobile position (x_0, y_0, z_0) as

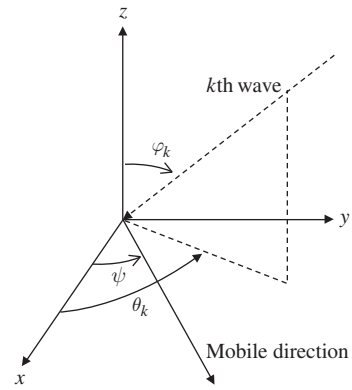

Figure 10.6 Wave angles and mobile direction.

$$\begin{aligned} x &= x_0 + (v\cos\psi)t \\ y &= y_0 + (v\sin\psi)t \\ z &= z_0 \end{aligned} \tag{10.36}$$

We consider the case of small-scale variations in E-field amplitudes and approximate the mean-square value of the E-fields as constant and independent of distance, that is, $\mathbf{E}[|E_{0,k}(d_k)|^2] = P/L$, where P is the total received power. The maximum Doppler shift is $f_m = f_c v/c$. The total received E-field is

$$\begin{aligned} E(\boldsymbol{d}, t) &= \sum_k E_k(d_k, t) \\ &= \sum_k E_{0,k}(d_k)\, \mathrm{e}^{\,\mathrm{j}[\xi + 2\pi f_m(\sin\,\varphi_k\cos\psi\cos\,\theta_k + \sin\,\varphi_k\sin\psi\sin\,\theta_k)t]} \\ &= \sum_k E_{0,k}(d_k)\, \mathrm{e}^{\,\mathrm{j}[\xi + 2\pi f_m(\sin\,\varphi_k\cos(\,\theta_k - \psi))t]} \end{aligned} \tag{10.37}$$

where $\xi = k_0(x_0 \sin\,\varphi_k \cos\,\theta_k + y_0 \sin\,\varphi_k \sin\,\theta_k + z_0 \cos\,\varphi_k) + \phi_k$. Define $h_k = E_{0,k}(d_k)\,\mathrm{e}^{\,\mathrm{j}\xi}$, then $\mathbf{E}[|h_k|^2] = \mathbf{E}[|E_{0,k}(d_k)|^2] = P/L$. The corresponding impulse response of the channel is

$$h(\tau, t) = \left[\sum_k h_k\, \mathrm{e}^{\,\mathrm{j}2\pi f_m(\sin\,\varphi_k\cos(\,\theta_k - \psi))t}\right]\delta(\tau) \tag{10.38}$$

and the multipath autocorrelation profile can be expressed as

$$\begin{aligned} R_h(\tau, \boldsymbol{t}') &= \left[\sum_k \mathbf{E}[|h_k|^2]\mathbf{E}\left[\,\mathrm{e}^{\,\mathrm{j}2\pi f_m(\sin\,\varphi_k\cos(\,\theta_k - \psi))\boldsymbol{t}'}\right]\right]\delta(\tau) \\ &= \frac{P}{L}\sum_k \mathbf{E}[\,\mathrm{e}^{\,\mathrm{j}2\pi f_m(\sin\,\varphi_k\cos(\,\theta_k - \psi))\boldsymbol{t}'}]\,\delta(\tau) \\ &= P\mathbf{E}[\,\mathrm{e}^{\,\mathrm{j}2\pi f_m(\sin\,\varphi\cos(\,\theta - \psi))\boldsymbol{t}'}]\,\delta(\tau) \end{aligned} \tag{10.39}$$

The autocorrelation is the value of $R_h(\tau, \boldsymbol{t}')$ at $\tau = 0$ and is given by

$$\begin{aligned} R_h(\boldsymbol{t}') &= P\mathbf{E}[\,\mathrm{e}^{\,\mathrm{j}2\pi f_m(\sin\,\varphi\cos(\,\theta - \psi))\boldsymbol{t}'}] \\ &= P\int_{\varphi=0}^{\pi}\int_{\theta=0}^{2\pi} \mathrm{e}^{\,\mathrm{j}2\pi f_m(\sin\,\varphi\cos(\,\theta - \psi))\boldsymbol{t}'} f_\varphi(\varphi) f_\theta(\theta)\,\mathrm{d}\varphi\,\mathrm{d}\theta \end{aligned} \tag{10.40}$$

The functions $f_\varphi(\varphi)$ and $f_\theta(\theta)$ are the probability density functions of the *polar angle* φ and *azimuth angle* θ, respectively. Since the mobile position is arbitrary on the horizontal plane, we can assume a *uniformly distributed* azimuth angle and hence we have $f_\theta(\theta) = 1/2\pi$. Therefore, the autocorrelation can be written as

$$R_h(\boldsymbol{t}') = P\int_{\varphi=0}^{\pi} J_0(2\pi f_m \boldsymbol{t}'\,\sin\varphi) f_\varphi(\varphi)\,\mathrm{d}\varphi \tag{10.41}$$

Taking the Fourier transform of the autocorrelation $R_h(\boldsymbol{t}')$ in the variable $\boldsymbol{t}'$ we obtain the *generalized Doppler power spectrum*

$$S_h(\boldsymbol{f}') = \begin{cases} \int_{\theta=\beta}^{\pi-\beta} \frac{P}{\pi f_m \sqrt{\sin^2\varphi - \sin^2\beta}} f_\varphi(\varphi)\, d\varphi, & |\boldsymbol{f}'| \le f_m \\ 0, & \text{otherwise} \end{cases}, \quad \sin\beta = \frac{\boldsymbol{f}'}{f_m} \tag{10.42}$$

For the special case of incident waves restricted to the horizontal plane, we have $f_\varphi(\varphi) = \sin\varphi\,\delta(\varphi - \pi/2)$ and the generalized Doppler power spectrum reduces to the Clarke–Doppler power spectrum. The generalized flat fading channel is also a *slow fading channel* so long as the channel estimation time is smaller than the coherence time, which is one-eighth of the maximum Doppler shift.

Example 10.3 Aulin–Doppler power spectrum
In this model the density function of the polar angle φ has the following expression:

$$f_\varphi(\varphi) = \frac{\sin\varphi}{2\sin\Delta\varphi}, \quad \pi/2 - \Delta\varphi \le \varphi \le \pi/2 + \Delta\varphi \tag{10.43}$$

Thus, the arrival angle of the incident waves is restricted to the angular region $\pi/2 - \Delta\varphi \le \varphi \le \pi/2 + \Delta\varphi$. Substituting $f_\varphi(\varphi)$ into (10.42) we obtain the *Aulin–Doppler power spectrum*, which does not have singularities at $\boldsymbol{f}' = \pm f_m$:

$$S_h(\boldsymbol{f}') = \begin{cases} \frac{P}{\pi f_m \sin\Delta\varphi} \sin^{-1}\left(\frac{\sin\Delta\varphi}{\sqrt{1-(\boldsymbol{f}'/f_m)^2}}\right), & 0 \le |\boldsymbol{f}'| \le f_m \cos\Delta\varphi \\ \frac{P}{2f_m \sin\Delta\varphi}, & f_m\cos\Delta\varphi \le |\boldsymbol{f}'| \le f_m \\ 0, & \text{otherwise} \end{cases} \tag{10.44}$$

■

10.3 Coherent demodulation

Coherent demodulation requires the knowledge of the channel taps $h_i(t)$. This can be achieved by transmitting a pilot tone with the signal, as in IS-95; by using pilot subcarriers, as in OFDM-based signals (IEEE 802.11a,g and 802.16,e); or by transmitting equally spaced pilot symbols, with the data symbols as in CDMA 2000 or WCDMA. The time between the pilot symbols is much smaller than the channel coherence time T_c to reduce channel estimation error (*slow fading*). In this case the channel taps can be considered *constant* during a symbol, that is, $h_i(t) \approx h_i,\ t \le T_s$. Since the channel taps are complex it is more convenient to work with an equivalent complex-valued demodulator than those discussed in Chapter 7. We will concentrate on I-Q (two-path) coherent demodulators.

Equivalent complex-valued demodulator

Let us consider the I-Q signal $s(t) = \sum_{k=1}^{2} s_{ik} x_k(t) = \mathrm{Re}\left[s_L(t)\, e^{j2\pi f_c t}\right]$, where $x_k(t)$ is the basis function (see Appendix 10A). For illustrative purposes let the *pulse shape* $p(t)$ be a

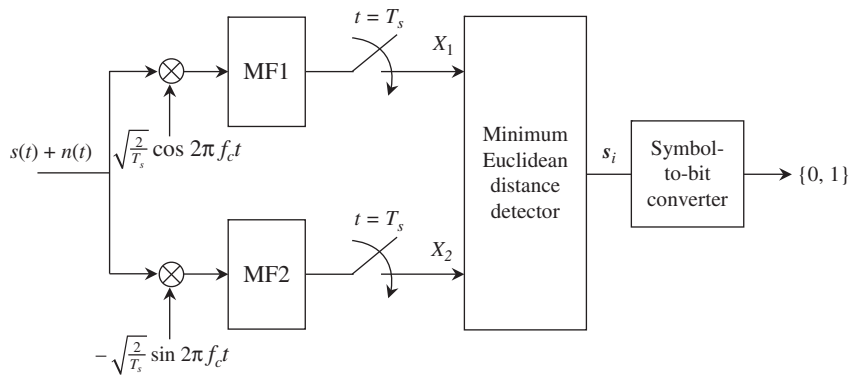

Figure 10.7 The I-Q demodulator.

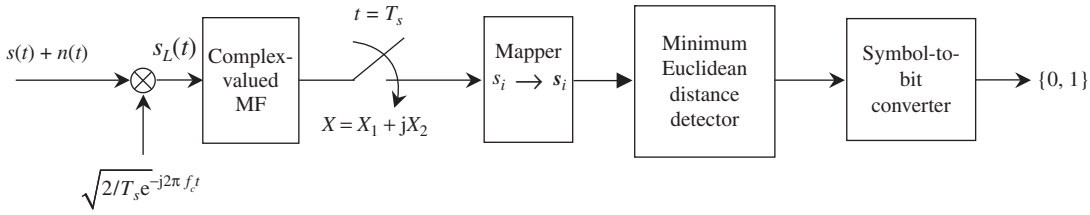

Figure 10.8 The equivalent complex-valued demodulator.

squared pulse of unit amplitude and duration T_s. The *complex envelope* $s_L(t)$ is $s_L(t) = s_{L,I}(t) + \mathrm{j}s_{L,Q}(t) = (s_{i1} + \mathrm{j}s_{i2})(\sqrt{2/T_s})\,p(t)$. The parameters s_{i1} and s_{i2} are the I- and Q-values, respectively, of an arbitrary symbol $s_i = s_{i1} + \mathrm{j}s_{i2}$ (in the set of M symbols represented in complex form). For an arbitrary pulse shape the matched filter impulse response is $\alpha p(t - T_s)$, where α is a normalization constant. The I-Q coherent demodulator for this signal is shown conceptually in Figure 10.7. The matched filters MF1 and MF2 are identical and matched to the signal pulse shape $p(t)$. Their impulse responses are $p(T_s - t)$. The decision vector $\boldsymbol{X}$ is the sum of the signal vector $s_i = [s_{i1}\ s_{i2}]^t$ and the Gaussian noise vector $\boldsymbol{N} = [N_1\ N_2]^t$. The I-noise N_1 and the Q-noise N_2 are independent and have the same variance σ^2. We have

$$\boldsymbol{X} = \boldsymbol{s}_i + \boldsymbol{N} \tag{10.45}$$

In Figure 10.8 the equivalent complex-valued coherent demodulator is shown (see Appendix 10A). The complex decision sample at the output of the complex-valued matched filter or complex-valued integrator is

$$\begin{aligned} X = X_1 + \mathrm{j}X_2 &= (s_{i1} + N_1) + \mathrm{j}(s_{i2} + N_2) \\ &= (s_{i1} + \mathrm{j}s_{i2}) + (N_1 + \mathrm{j}N_2) = s_i + N \end{aligned} \tag{10.46}$$

where $N = N_1 + \mathrm{j}N_2$ is the complex noise. As the signal passes through the channel, it is multiplied by the channel taps. Let us consider the case where the channel is a *flat fading*

channel. The received signal now has a complex envelope given by $hs_L(t)$, where the complex channel tap $h = |h|e^{j\theta}$ is assumed to be available via *perfect channel estimation*. To achieve the maximum signal-to-noise ratio (SNR) we require the use of the local complex carrier $\sqrt{2/T_s}(h^*/|h|)e^{-j2\pi f_c t}$, which is equal to $\sqrt{2/T_s}e^{-j\theta}e^{-j2\pi f_c t}$, such as the pilot tone in IS-95 or the pilot subcarriers in OFDM-based signals (IEEE 802.11a,g and 802.16,e). Consequently, the output of the complex-valued matched filter is the complex variable

$$\begin{aligned} X &= \frac{h^*}{|h|}(hs_i + N) \\ &= |h|s_i + \frac{h^*}{|h|}N \\ &= |h|(s_{i1} + js_{i2}) + \frac{h^*}{|h|}(N_1 + jN_2) \end{aligned} \tag{10.47}$$

Both I-noise $\mathcal{N}_1 = (h^*/|h|)N_1$ and Q-noise $\mathcal{N}_2 = (h^*/|h|)N_2$ have the same variance σ^2. The above complex decision variable can be written in vector form as follows:

$$\boldsymbol{X} = |h|\boldsymbol{s}_i + \boldsymbol{\mathcal{N}} \tag{10.48}$$

where $\boldsymbol{\mathcal{N}} = [\mathcal{N}_1 \ \mathcal{N}_2]^t$. Conditional on $|h|$, the decision variable vector for a slow-flat fading channel is identical to that of an AWGN channel, since the zero mean I-noise and Q-noise samples are statistically independent and have the same variance σ^2. For a slow-flat fading channel, the signal vector $\boldsymbol{s}_i$ is weighted by the channel tap magnitude $|h|$. The complex decision variable or its equivalent decision variable vector is a *sufficient statistic*. Given a realization $\boldsymbol{x}$ of $\boldsymbol{X}$ we wish to develop a *metric* for the *maximum likelihood detection*. The conditional probability density function of $\boldsymbol{X}$ given $|h|, H_i$ is

$$\begin{aligned} f_{\boldsymbol{X}}(\boldsymbol{x}|\ |h|, H_i) &= \prod_{k=1}^{2} f_{X_k}(x_k|\ |h|, H_i) = \prod_{k=1}^{2} \frac{1}{\sqrt{2\pi}\sigma} e^{-(x_k - |h|s_{ik})^2/2\sigma^2} \\ &= \frac{1}{\left(\sqrt{2\pi}\sigma\right)^2} e^{-\frac{1}{2\sigma^2}\sum_{k=1}^{2}(x_k - |h|s_{ik})^2} \\ &= \frac{1}{\left(\sqrt{2\pi}\sigma\right)^2} e^{-\frac{1}{2\sigma^2}\|\boldsymbol{x} - |h|\boldsymbol{s}_i\|^2} \end{aligned} \tag{10.49}$$

The *ln-likelihood function* can be expressed as

$$\ln f_{\boldsymbol{X}}(\boldsymbol{x}|\ |h|, H_i) = -2\ \ln\left(\sqrt{2\pi}\,\sigma\right) - \frac{1}{2\sigma^2}\|\boldsymbol{x} - |h|\boldsymbol{s}_i\|^2 \tag{10.50}$$

where the term $-2\ \ln\left(\sqrt{2\pi}\,\sigma\right)$ is common to all $\ln f_{\boldsymbol{X}}(\boldsymbol{x}|\ |h|, H_i)$. Hence, the *maximum* of the set $\ln f_{\boldsymbol{X}}(\boldsymbol{x}|\ |h|, H_i)$ corresponds to the *minimum* of the set of *Euclidean distances*

$$d(\boldsymbol{x},\ |h|\boldsymbol{s}_i) = \|\boldsymbol{x} - |h|\boldsymbol{s}_i\|,\ i = 1, 2, \ldots, M \tag{10.51}$$

This is the metric that the minimum Euclidean distance detector, with the *available channel tap h* from the pilot tone or pilot symbol, makes the decision on the transmitted signal. That is, it selects the signal vector $|h|\boldsymbol{s}_i$ that is closest in Euclidean distance to the sampled value

$\boldsymbol{x}$ of the decision vector $\boldsymbol{X}$. The conditional pair-wise error probability for a flat fading channel between two vectors $|h|\boldsymbol{s}_i$ and $|h|\boldsymbol{s}_j$ is

$$\Pr\left(|h|\boldsymbol{s}_i \to |h|\boldsymbol{s}_j\right) = Q\left(\frac{|h|\left\|\boldsymbol{s}_i - \boldsymbol{s}_j\right\|}{2\sigma}\right) \tag{10.52}$$

The conditional bit error probability for the Gray-coded signal set $\{\boldsymbol{s}_i\}_{i=1}^{M}$ is given by the following approximation:

$$P_b(|h|) \approx \frac{N_n}{\log_2 M} Q\left(\frac{|h| d_{min}}{2\sigma}\right) \tag{10.53}$$

where $d_{min} = \min_{i,j} ||\boldsymbol{s}_i - \boldsymbol{s}_j||$ is the *minimum Euclidean distance* of the signal set, $\sigma^2 = N_0/2$, and N_n is the average number of symbols at the minimum Euclidean distance d_{min} or the average number of nearest neighbors. Here $N_0/2$ is the power spectral density of noise. In (10.53) the equality holds for both PSK and QPSK. Knowing the statistics of the fading channel (Rayleigh, Rice, Nakagami) we can evaluate the bit error probability as follows:

$$\begin{aligned} P_b = \mathbf{E}[P_b(|h|)] &\approx \mathbf{E}\left[\frac{N_n}{\log_2 M} Q\left(\frac{|h| d_{min}}{2\sigma}\right)\right] \\ &\approx \mathbf{E}\left[\frac{N_n}{\log_2 M} Q\left(\sqrt{2|h|^2 \alpha\, SNR}\right)\right] \end{aligned} \tag{10.54}$$

where the *symbol signal-to-noise ratio SNR* and the positive constant α which depends on the modulation are given by

$$SNR = \frac{E_s}{N_0}, \quad \alpha SNR = \frac{1}{2}\left(\frac{d_{min}}{2\sigma}\right)^2 \tag{10.55}$$

The quantity $|h|^2 SNR$ is referred to as the *instantaneous SNR*, and does not exist in an AWGN channel.

Rayleigh

For convenience we normalize the channel tap such that $\mathbf{E}\left(|h|^2\right) = 1$. The channel tap $|h|$ is Rayleigh-distributed and $|h|^2$ is exponentially distributed with density functions

$$f_{|h|}(x) = 2x\mathrm{e}^{-x^2},\ f_{|h|^2}(y) = \mathrm{e}^{-y} \tag{10.56}$$

The corresponding bit error probability is given by the following closed-form expression (see Appendix 10B):

$$P_b = \frac{N_n}{2\log_2 M}\left(1 - \sqrt{\frac{\alpha\, SNR}{1 + \alpha\, SNR}}\right) \tag{10.57}$$

PSK: the minimum Euclidean distance is $d_{min} = 2\sqrt{E_b}$. With $\sigma^2 = N_0/2$, we obtain $\alpha SNR = E_b/N_0$. Furthermore, $N_n = 1$, $M = 2$, therefore the bit error probability for PSK is

$$P_b = \frac{1}{2}\left(1 - \sqrt{\frac{E_b/N_0}{1+E_b/N_0}}\right)(PSK) \tag{10.58}$$

QPSK: the minimum Euclidean distance is $d_{min} = \sqrt{2E_s}$. With $\sigma^2 = N_0/2$, we obtain $\alpha\, SNR = E_s/2N_0 = E_b/N_0$. Furthermore, $N_n = 2$, $M = 4$, therefore the bit error probability for QPSK is identical to that of PSK as expected

$$P_b = \frac{1}{2}\left(1 - \sqrt{\frac{E_b/N_0}{1+E_b/N_0}}\right)(QPSK) \tag{10.59}$$

MPSK: the minimum Euclidean distance is $d_{min} = 2\sqrt{E_s}\sin(\pi/M)$. Using $\sigma^2 = N_0/2$, we obtain $\alpha\, SNR = (E_s/N_0)\sin^2(\pi/M) = (\log_2 M)(E_b/N_0)\sin^2(\pi/M)$. Furthermore, $N_n = 2$, therefore the bit error probability for MPSK is given by

$$P_b \approx \frac{1}{\log_2 M}\left(1 - \sqrt{\frac{(\log_2 M)(E_b/N_0)\sin^2(\pi/M)}{1+(\log_2 M)(E_b/N_0)\sin^2(\pi/M)}}\right)(MPSK) \tag{10.60}$$

MQAM: the minimum Euclidean distance is $d_{min} = \sqrt{6E_b(\log_2 M)/(M-1)}$. Using $\sigma^2 = N_0/2$, we obtain $\alpha SNR = (3/2)[(\log_2 M)/(M-1)](E_b/N_0)$. Furthermore, $N_n = 4 - 4/\sqrt{M}$, therefore the bit error probability for MQAM is given by

$$P_b \approx \frac{2-2/\sqrt{M}}{\log_2 M}\left(1 - \sqrt{\frac{(3/2)[(\log_2 M)/(M-1)](E_b/N_0)}{1+(3/2)[(\log_2 M)/(M-1)](E_b/N_0)}}\right)(MQAM) \tag{10.61}$$

Rice

When there is a line-of-sight component among the non-direct (diffuse) components the channel tap $|h|$ is Rice-distributed:

$$f_{|h|}(x) = \frac{x}{\sigma_s^2}\mathrm{e}^{-(x^2+A^2)/2\sigma_s^2} I_0\left(\frac{Ax}{\sigma_s^2}\right) \tag{10.62}$$

The function $I_0(x)$ is a modified *Bessel function of the first kind of zero order*. When there is no signal, that is, $A = 0$ and $I_0(0) = 1$, the Rice density function reduces to the Rayleigh density function. We normalize the channel tap $|h|$ such that its mean-square value is $\mathbf{E}\left(|h|^2\right) = A^2 + 2\sigma_s^2 = 1$. The ratio $\kappa = A^2/2\sigma_s^2$ is called the *direct signal-to-diffuse signal ratio*. We have $A^2 = \kappa/(\kappa+1)$ and $2\sigma_s^2 = 1/(\kappa+1)$. Therefore, the Rice density function of $|h|$ and the *non-central* χ^2*-density function* of $|h|^2$ can be rewritten in term of the parameter κ as follows:

$$\begin{aligned} f_{|h|}(x) &= 2(\kappa+1)x\mathrm{e}^{-[(\kappa+1)x^2+\kappa]} I_0\left(2x\sqrt{\kappa(\kappa+1)}\right) \\ f_{|h|^2}(y) &= (\kappa+1)\mathrm{e}^{-[(\kappa+1)y+\kappa]} I_0\left(2\sqrt{\kappa(\kappa+1)y}\right) \end{aligned} \tag{10.63}$$

There is no closed-form expression for P_b with a Rice-distributed channel tap, and numerical integration has to be carried out to evaluate (10.54).

Nakagami-m

The Nakagami-m density function represents the most general fading statistics. The channel tap is Nakagami-distributed with the following density functions for $E\left(|h|^2\right) = 1$:

$$f_{|h|}(x) = \frac{2m^m}{\Gamma(m)} x^{2m-1} \mathrm{e}^{-mx^2}, \quad f_{|h|^2}(y) = \frac{m^m}{\Gamma(m)} y^{m-1} \mathrm{e}^{-my} \tag{10.64}$$

where $\Gamma(m)$ is the *Gamma function*. For $m = 1$, the Nakagami-m density function $f_{|h|}(x)$ reduces to the Rayleigh density function. The Rice density function can be approximated by the Nakagami-m density function by selecting $m = (\kappa+1)^2/(2\kappa+1)$. The bit error probability has the following closed-form expression (Appendix 10B):

$$P_b \approx \frac{N_n}{2\log_2 M}\left[1 - \sqrt{\frac{\alpha\, SNR/m}{1+\alpha\, SNR/m}} \sum_{k=0}^{m-1} \binom{2k}{k} \left(\frac{1}{4(1+\alpha\, SNR/m)}\right)^k\right], \ m: \text{integer}$$

$$P_b \approx \frac{N_n}{\log_2 M}\left[\frac{1}{2\sqrt{\pi}} \frac{\sqrt{\alpha\, SNR/m}}{(1+\alpha\, SNR/m)^{m+1/2}} \frac{\Gamma(m+\frac{1}{2})}{\Gamma(m+1)}\right] {}_2F_1\left(1, m+\tfrac{1}{2}; m+1; \frac{1}{1+\alpha\, SNR/m}\right),$$
$$m: \text{noninteger} \tag{10.65a}$$

where ${}_2F_1$ is the *Gauss hypergeometric function* given by the following infinite series:

$${}_2F_1(a,b;c;z) = \frac{\Gamma(c)}{\Gamma(a)\Gamma(b)} \sum_{n=0}^{\infty} \frac{\Gamma(a+n)\Gamma(b+n)}{\Gamma(c+n)} \frac{z^n}{n!} \tag{10.65b}$$

The equals sign holds for both PSK and QPSK. The bit error probabilities of PSK, QPSK, MPSK, and MQAM can be found by substituting the appropriate expressions for *SNR* into the above equation.

Example 10.4 Dismal performance of fading channels

The bit error probability of an AWGN channel decreases *exponentially* with the symbol signal-to-noise ratio *SNR*. This is the characteristic of the Q-function since it can be approximated as $Q(\sqrt{2SNR}) \approx \mathrm{e}^{-SNR}/\sqrt{4\pi SNR}$. On the other hand, the bit error probability of a slow-flat fading channel decreases *inversely* with *SNR*. This results in very poor performance, particularly for Rayleigh fading. If we consider the case of PSK at *SNR* = 10.5 dB, the bit error probability in an AWGN channel is about 10^{-6}. The same *SNR* yields a bit error probability of 0.02 in a slow-flat Rayleigh fading channel. What is the reason for such a poor performance? Let us look at the *instantaneous SNR* of a fading channel, that is, $|h|^2 SNR$. Since the channel tap $|h|$ is Rayleigh-distributed, it can take on any value from zero to infinity. Thus the probability that the instantaneous *SNR* can fall below a given value, no matter how small, is finite. Hence a deep fade can always occur with finite probability and

the result is a very high bit error probability on average. On the other hand, the AWGN channel has no instantaneous *SNR*, that is, no fades occur.

■

Example 10.5 SNR-outage probability

When deep fades occur in a fading channel the *instantaneous SNR* can be very low for the entire fade duration. Therefore, it makes sense to define a *SNR-outage probability* p_{out}, that is, the probability that the instantaneous *SNR* falls below a threshold value γ called the *outage signal-to-noise ratio*. We have

$$p_{out} = \Pr\left(|h|^2 SNR < \gamma\right) = \Pr\left(|h|^2 < \frac{\gamma}{SNR}\right) \tag{10.66}$$

For a slow-flat Rayleigh fading channel, $y = |h|^2$ is *exponentially distributed* with density function e^{-y}. Thus, the *SNR*-outage probability is given by

$$p_{out} = \int_0^{\gamma/SNR} e^{-y} dy = 1 - e^{-\gamma/SNR} \tag{10.67}$$

For numerical illustration, let the threshold be $\gamma = 1$ and $SNR = 10$. This yields a *SNR*-outage probability $p_{out} \approx 0.1$ and a bit error probability $P_b \approx 0.08$ for both PSK and QPSK. Either measure shows a very poor performance even for large *SNR*. There is almost a 10% chance that the instantaneous *SNR* is less than 1 (0 dB), and even the average *SNR* is 10 (10 dB)! Many communication devices cannot operate with a *SNR* below 0 dB, therefore it is possible that the link is cut off entirely during the outage. Hence, if one takes into account the dynamic range of the receiver, the bit error probability may be much larger than that predicted by the above analysis.

■

Example 10.6 MMSE channel tap estimation

Coherent demodulation requires the complex channel tap $h = |h|e^{j\theta}$ to be available via *perfect channel estimation*. In practice, h is made available from pilot symbols extracted from the pilot tone transmitting simultaneously with the signal (IS-95). Alternatively, the pilot symbols can be made available from pilot subcarriers in OFDM-based signals (IEEE 802.11a, g and 802.16,e). The pilot symbol is known but noisy and hence one wishes to have the best estimate. Let us consider the received pilot symbol in complex Gaussian noise N with zero mean and variance $2\sigma^2$ (both I- and Q-noise components of N have identical variance σ^2):

$$X = hs_p + N \tag{10.68}$$

Normalizing X to $s_p^*/|s_p|^2$ we obtain the equivalent sufficient statistic

$$Y = h + \mathcal{N} \tag{10.69}$$

where the complex noise $\mathcal{N} = (s_p^*/|s_p|^2)N$ has variance $2\sigma^2/|s_p|^2$.

We are interested in a linear estimate $\hat{h} = a^* X$ of h for some complex constant a given the known pilot symbol s_p. The criterion is to minimize $\mathbf{E}(|h - \hat{h}|^2)$, the *mean-square error*. The *orthogonality principle* states that $\mathbf{E}[(\hat{h} - h)Y^*)] = 0$, and this yields the constant a as follows:

$$a = \frac{\mathbf{E}\left(|h|^2\right)s_p}{\mathbf{E}\left(|h|^2\right)|s_p|^2 + 2\sigma^2} = \frac{SNR_p}{SNR_p + 1}\left(\frac{s_p}{|s_p|^2}\right) \tag{10.70}$$

where $SNR_p = |s_p|^2/2\sigma^2$ is the signal-to-noise ratio of the pilot symbol. Thus we have

$$\hat{h} = a^* X = \frac{\mathbf{E}\left(|h|^2\right)s_p^*}{\mathbf{E}\left(|h|^2\right)|s_p|^2 + 2\sigma^2}X = \frac{SNR_p}{SNR_p + 1}\left(\frac{s_p^*}{|s_p|^2}\right)X \tag{10.71}$$

The corresponding minimum mean-square error (MMSE) is given by

$$\text{MMSE} = \frac{2\sigma^2\mathbf{E}\left(|\text{h}|^2\right)}{\mathbf{E}\left(|h|^2\right)|s_p|^2 + 2\sigma^2} = \frac{\mathbf{E}\left(|h|^2\right)}{\mathbf{E}\left(|h|^2\right)SNR_p + 1} \tag{10.72}$$

and therefore we have $\text{MMSE} = 1/(SNR_p + 1)$ for $\mathbf{E}\left(|h|^2\right) = 1$. The estimate gets more accurate as the signal-to-noise ratio SNR_p of the pilot symbol increases.

■

Example 10.7 Direct channel tap estimation

The MMSE estimation requires knowledge of the pilot signal-to-noise ratio SNR_p, which may not be available. In this case a direct estimation of the channel tap can be performed as follows:

$$\hat{h} = \frac{s_p^*}{|s_p|^2}X \tag{10.73}$$

At high SNR_p both estimations give nearly identical results.

■

Effect of channel tap error

The noisy channel tap $\hat{h}$ leads to higher bit error probability. We wish to incorporate this effect in the above bit error probability analysis. To demodulate the signal we use the complex carrier $\sqrt{2/T_s}(\hat{h}^*/|\hat{h}|)\text{e}^{-\text{j}2\pi f_c t}$ and obtain the decision variable

$$\begin{aligned} X &= \frac{\hat{h}^*}{|\hat{h}|}(hs_i + N) \\ &= |h|\text{e}^{\text{j}\varepsilon}s_i + \frac{\hat{h}^*}{|\hat{h}|}N \end{aligned} \tag{10.74}$$

where $h = |h|e^{j\theta}$, $\hat{h} = |\hat{h}|e^{j\hat{\theta}}$, and $\varepsilon = \theta - \hat{\theta}$. Both I-noise $\mathcal{N}_1 = (\hat{h}^*/|\hat{h}|)N_1$ and Q-noise $\mathcal{N}_2 = (\hat{h}^*/|\hat{h}|)N_2$ have the same variance σ^2. The above complex decision variable can be written in vector form as follows:

$$\boldsymbol{X} = |h|\mathbf{T}\boldsymbol{s}_i + \boldsymbol{\mathcal{N}} \tag{10.75}$$

where $\boldsymbol{\mathcal{N}} = [\mathcal{N}_1 \ \mathcal{N}_2]^t$, and the transformation matrix $\mathbf{T}$ is the *phase error rotation matrix*

$$\mathbf{T} = \begin{pmatrix} \cos\varepsilon & -\sin\varepsilon \\ \sin\varepsilon & \cos\varepsilon \end{pmatrix} \tag{10.76}$$

The minimum Euclidean distance detector has the channel tap $\hat{h}$ available to it, but not h or the phase error ε. Therefore, the detector uses the faulty set of metrics $d\left(\boldsymbol{x}, |\hat{h}|\boldsymbol{s}_i\right) = \left\|\boldsymbol{x} - |\hat{h}|\boldsymbol{s}_i\right\|$, $i = 1, 2, \ldots, M$, for the detection of vector $\boldsymbol{s}_i$ instead of the correct set of metrics $d(\boldsymbol{x}, |h|\mathbf{T}\boldsymbol{s}_i) = \left\|\boldsymbol{x} - |h|\mathbf{T}\boldsymbol{s}_i\right\|$, $i = 1, 2, \ldots, M$, for maximum likelihood detection. This results in a higher bit error probability.

Example 10.8 Threshold detection for PSK

The threshold detector has been shown to be equivalent to the minimum Euclidean distance detector for an AWGN binary channel. In a fading channel, the Euclidean distance detector requires knowledge of the channel tap magnitude for maximum likelihood detection in the case of perfect channel estimation or the estimated channel tap magnitude otherwise. Let us consider the case of PSK where the threshold detector is used. Since the threshold is set at 0 volts irrespective of the channel tap magnitude, its knowledge is not required for threshold detection. Let us first consider the case of PSK; the Euclidean distance detector performs the following comparison:

$$\left(x - |\hat{h}|s_2\right)^2 - \left(x - |\hat{h}|s_1\right)^2 \underset{H_1}{\overset{H_2}{\lessgtr}} 0 \tag{10.77}$$

which leads to the decision of x for $s_1 = -s_2 = \sqrt{E_b}$ as

$$|\hat{h}|x \underset{H_1}{\overset{H_2}{\lessgtr}} 0 \tag{10.78}$$

This is threshold detection with the threshold set at 0 volts independently of $|\hat{h}|$. The conditional bit error probability of PSK with threshold detection is

$$P_b(|h|, \varepsilon) = Q\left(\sqrt{2|h|^2 SNR}\cos\varepsilon\right) \tag{10.79}$$

where $SNR = E_b/N_0$. The bit error probability of PSK is the expected value of $P_b(|h|, \varepsilon)$ with respect to both $|h|$ and ε. In practice, the phase of the estimated channel tap is used to drive a *voltage-controlled oscillator* (VCO) to correct the phase of the local carrier. The phase error ε between the received signal and the local carrier has the following *Tikhonov* density function:

$$f_\varepsilon(\varepsilon) = \begin{cases} \frac{\exp[(1/\sigma_\varepsilon^2)\cos\varepsilon]}{2\pi I_0(1/\sigma_\varepsilon^2)}, & |\varepsilon| \le \pi \\ 0, & \text{otherwise} \end{cases} \tag{10.80}$$

where σ_ε^2 is the variance of the phase error ε. The bit error probability of PSK in a Rayleigh fading channel is

$$P_b = \frac{1}{2}\int_{-\pi}^{\pi} \left(1 - \sqrt{\frac{SNR\cos^2\varepsilon}{1 + SNR\cos^2\varepsilon}}\right) f_\varepsilon(\varepsilon)\,\mathrm{d}\varepsilon \tag{10.81}$$

■

Example 10.9 Threshold detection for QPSK

From Figure 7.46, threshold detection can be performed independently on both I- and Q-channels. Since a QPSK signal is simply the sum of two independent and orthogonal PSK signals, the conditional bit error probability for the decision vector $\boldsymbol{X}$ is given from (10.75) and (10.76) as follows:

$$P_b(|h|,\varepsilon) = \frac{1}{2}Q\left(\sqrt{2|h|^2\alpha\,SNR}(\cos\varepsilon - \sin\varepsilon)\right) + \frac{1}{2}Q\left(\sqrt{2|h|^2\alpha\,SNR}(\cos\varepsilon + \sin\varepsilon)\right) \tag{10.82}$$

where $\alpha\,SNR = E_s/2N_0 = E_b/N_0$

The bit error probability of QPSK in a Rayleigh fading channel is given by

$$\begin{aligned} P_b = {} & \frac{1}{4}\int_{-\pi}^{\pi} \left(1 - \sqrt{\frac{\alpha\,SNR(\cos\varepsilon - \sin\varepsilon)^2}{1 + \alpha\,SNR(\cos\varepsilon - \sin\varepsilon)^2}}\right) f_\varepsilon(\varepsilon)\,\mathrm{d}\varepsilon \\ & + \frac{1}{4}\int_{-\pi}^{\pi} \left(1 - \sqrt{\frac{\alpha\,SNR(\cos\varepsilon + \sin\varepsilon)^2}{1 + \alpha\,SNR(\cos\varepsilon + \sin\varepsilon)^2}}\right) f_\varepsilon(\varepsilon)\,\mathrm{d}\varepsilon \end{aligned} \tag{10.83}$$

■

Example 10.10 Special case of I-Q signals with phase error in an AWGN channel

Let us consider the special case of an I-Q signal in a non-fading AWGN channel. The coherent demodulation is carried out by a local reference carrier that is phase-synchronized to the received signal via a carrier recovery circuit. Let ε be the phase error between the transmitted symbols and the local carrier symbol. The decision variable vector is obtained as follows:

$$\boldsymbol{X} = \mathbf{T}\boldsymbol{s}_i + \boldsymbol{\mathcal{N}} \tag{10.84}$$

where $\mathbf{T}$ is the phase error rotation unitary matrix given by (10.76). The bit error probability is a special case of that of a fading channel and is given by

$$P_b(\varepsilon) = \frac{N_n}{\log_2 M} Q\left(\frac{d_{min}(\varepsilon)}{2\sigma}\right) \tag{10.85}$$

where the *erroneous* minimum Euclidean distance $d_{min}(\varepsilon)$ (the detector has no knowledge of the phase error) is given by

$$d_{min}(\varepsilon) = \min_{i,j} d_{i,j}(\varepsilon) = \min_{i,j} \frac{\left\|\mathbf{T}\boldsymbol{s}_i - \boldsymbol{s}_j\right\|^2 - \left\|\mathbf{T}\boldsymbol{s}_i - \boldsymbol{s}_i\right\|^2}{\left\|\boldsymbol{s}_i - \boldsymbol{s}_j\right\|} \tag{10.86}$$

For PSK, we get $d_{min}(\varepsilon) = 2\sqrt{E_b}\cos\varepsilon$ and $\sigma^2 = N_0/2$; therefore, the bit error probability of PSK is given by

$$\begin{aligned} P_b(\varepsilon) &= Q\left(\frac{d_{min}(\varepsilon)}{2\sigma}\right) \\ &= Q\left(\sqrt{2\,SNR}\cos\varepsilon\right) \end{aligned} \tag{10.87}$$

where

$$SNR = \frac{E_b}{N_0} \tag{10.88}$$

For $\varepsilon = 22.5^\circ$ the loss of SNR is 0.7 dB, which shows that PSK is rather resistant to phase error.

■

Example 10.11 QPSK in a AWGN channel

Let us consider the Euclidean distance detector, which makes the decision based on the *erroneous* minimum Euclidean distance

$$d_{min}(\varepsilon) = \min_{i,j}\ d_{i,j}(\varepsilon) = \min_{i,j} \frac{\left[\left\|\mathbf{T}\boldsymbol{s}_i - \boldsymbol{s}_j\right\|^2 - \left\|\mathbf{T}\boldsymbol{s}_i - \boldsymbol{s}_i\right\|^2\right]}{\left\|\boldsymbol{s}_i - \boldsymbol{s}_j\right\|} \tag{10.89}$$

Now assume that vector $\boldsymbol{s}_1 = [\,1 \quad 1\,]^t\sqrt{E_s/2}$ was transmitted. The phase error is assumed to be $\varepsilon = 22.5^\circ$. Let us calculate the distance $d_{1,j}/\sqrt{E_s}$, j = 1, 2, 3, 4, with respect to the following signal vectors:

$$\boldsymbol{s}_2 = [\,-1 \quad 1\,]^t\sqrt{E_s/2},\ \boldsymbol{s}_3 = [\,-1 \quad -1\,]^t\sqrt{E_s/2}, \boldsymbol{s}_4 = [\,1 \quad -1\,]^t\sqrt{E_s/2} \tag{10.90}$$

The phase error rotation matrix $\mathbf{T}$ is given by

$$\mathbf{T} = \begin{bmatrix} 0.924 & -0.383 \\ 0.383 & 0.924 \end{bmatrix} \tag{10.91}$$

Furthermore,

$$\begin{aligned}&\|\mathbf{T}\boldsymbol{s}_1-\boldsymbol{s}_1\|^2=0.305(E_s/2),\quad \|\mathbf{T}\boldsymbol{s}_1-\boldsymbol{s}_2\|^2=2.47(E_s/2),\\&\|\mathbf{T}\boldsymbol{s}_1-\boldsymbol{s}_3\|^2=7.7(E_s/2),\quad \|\mathbf{T}\boldsymbol{s}_1-\boldsymbol{s}_4\|^2=5.53(E_s/2)\\&\|\boldsymbol{s}_1-\boldsymbol{s}_2\|=2\sqrt{E_s/2},\quad \|\boldsymbol{s}_1-\boldsymbol{s}_3\|=2\sqrt{2}\sqrt{E_s/2},\quad \|\boldsymbol{s}_1-\boldsymbol{s}_4\|=2\sqrt{E_s/2},\end{aligned}\tag{10.92}$$

Therefore,

$$d_{1,2}=1.08\sqrt{E_s/2},\quad d_{1,3}=d_{1,4}=2.6\sqrt{E_s/2}\tag{10.93}$$

By symmetry we conclude that the minimum of $d_{i,j}$ for all i, j is

$$d_{min}=1.08\sqrt{E_s/2}\tag{10.94}$$

When there is no phase error, that is, $\varepsilon=0^\circ$ we have $d_{min}(0^\circ)=2\sqrt{E_s/2}$, which is the minimum Euclidean distance of QPSK. Thus the phase error $\varepsilon=22.5^\circ$ reduces the minimum Euclidean distance by a factor of 1.85 relative to the case where there is no phase error. This results in a loss of *SNR* by a factor of 1.85^2 or 5.4 dB. This large loss of *SNR* is mostly due to the crosstalk between the I- and Q-channels. Thus, it is necessary to keep the phase error as small as feasible, particularly in MQAM, which is very sensitive to the phase error.

■

10.4 Pilot symbol-aided decision-feedback demodulation

To perform coherent demodulation the channel tap h must be made available at the receiver. In narrowband (non-spread spectrum) single-carrier systems, pilot symbols may be multiplexed (MUX, parallel-to-serial conversion) into the data symbol stream and sent with the same modulation or with different modulation. The demodulator demultiplexes (DEMUX, serial-to-parallel conversion) the data stream into the pilot stream and the data symbol stream. The pilot symbol rate is much smaller than the data symbol rate to keep the throughput high and much larger than the inverse of the channel coherence time (*coherence rate*) to keep the phase error small between updates. In OFDM systems, such as the IEEE 802.11a,g and 802.16e, the pilot symbols are transmitted continuously over the pilot subcarriers. In WCDMA they are transmitted periodically.

When dealing with a slow fading channel one should remember that slow fading does not mean zero Doppler shifts and hence zero Doppler phase errors. That just means the Doppler effect is small. But keeping the Doppler phase errors small can reduce throughput substantially. During fades, a wireless communication link may occasionally operate just above its outage threshold. A drop of 3 dB in *SNR* of the last symbol before update (one out of every few data symbols) may cause a substantial increase in the link error rate. The conclusion is that the Doppler effect should not be underestimated. In the following discussion we

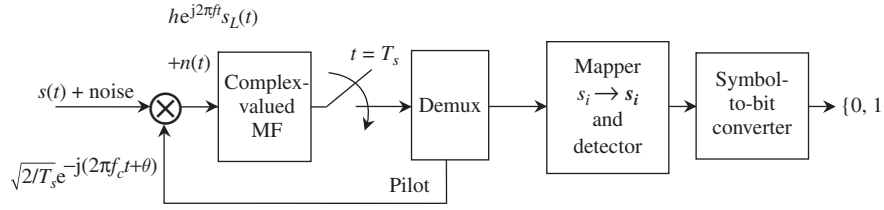

Figure 10.9 Demodulation with pilot symbols.

incorporate Doppler phase errors into an analysis of the pilot symbol-aided method. Figure 10.9 illustrates the implementation of pilot symbol-aided coherent demodulation.

Let us incorporate the Doppler phase errors. The received signal is first downconverted to baseband by a local carrier symbol. The matched filter impulse response is $p(T_s - t)$. To illustrate this, let the *pulse shape* $p(t)$ be a *squared pulse of unit amplitude and duration* T_s. Thus, the complex-valued matched filter can be replaced by a complex-valued integrator. The Doppler frequency is denoted by f. The *received pilot symbol* is $\mathbf{h}_p s_p = h_p \alpha_p s_p$, s_p is the pilot symbol, the *complex Doppler factor* $\alpha_p = |\alpha_p| e^{j\psi_p}$ is $\alpha_p = \frac{1}{T_s}\int_0^{T_s} e^{j2\pi ft} dt$, and the channel tap is $h_p = |h_p| e^{j\theta_p}$. The *Doppler channel tap* of the pilot symbol is $\mathbf{h}_p = h_p \alpha_p = |\mathbf{h}_p| e^{j\vartheta_p}$, where $|\mathbf{h}_p| = |h_p||\alpha_p|$ and $\vartheta_p = \theta_p + \psi_p$. The received lth data symbol $s_{i,l}$ after the pilot symbol (which corresponds to hypothesis H_i) is $\mathbf{h}_l s_{i,l} = h_l \alpha_l s_{i,l}$. The complex Doppler factor of the lth data symbol $s_{i,l}$ is $\alpha_l = |\alpha_l| e^{j\psi_l} = \frac{1}{T_s}\int_{lT_s}^{(l+1)T_s} e^{j2\pi ft} dt$, and the corresponding channel tap is $h_l = |h_l| e^{j\theta_l}$. The Doppler channel tap of the lth data symbol $s_{i,l}$ is $\mathbf{h}_l = h_l \alpha_l = |\mathbf{h}_l| e^{j\vartheta_l}$, where $|\mathbf{h}_l| = |h_l||\alpha_l|$ and $\vartheta_l = \theta_l + \psi_l$. The pilot symbol plus noise Y_p and the lth data symbol plus noise Y_l are respectively given as

$$\begin{aligned} Y_p &= \mathbf{h}_p s_p + N \\ Y_l &= \mathbf{h}_l s_{i,l} + N_l \end{aligned} \tag{10.95}$$

An estimation of the Doppler channel tap of the known pilot symbol from $Y_p = \mathbf{h}_p s_p + N$ yields the estimate $\hat{\mathbf{h}}_p$. Both magnitude $|\hat{\mathbf{h}}_p|$ and phase $\hat{\mathbf{h}}_p^* / |\hat{\mathbf{h}}_p| = e^{-j\hat{\vartheta}_p}$ of $\hat{\mathbf{h}}_p$ are available for detection of any data symbol until the next update. The detection is carried out by multiplying $\hat{\mathbf{h}}_p^* / |\hat{\mathbf{h}}_p| = e^{-j\hat{\vartheta}_p}$ by Y_l to obtain the following decision variable:

$$\begin{aligned} X_l &= \left(\hat{\mathbf{h}}_p^* / |\hat{\mathbf{h}}_p|\right) Y_l = e^{-j\hat{\vartheta}_p}(\mathbf{h}_l s_{i,l} + N_l) \\ &= |\mathbf{h}_l| e^{j\varepsilon_l} s_{i,l} + \mathfrak{N}_l \end{aligned} \tag{10.96}$$

where the phase $\varepsilon_l = \vartheta_l - \hat{\vartheta}_p$ is the *Doppler phase error* between the received data symbol and the received pilot symbol. The complex noise $\mathfrak{N}_l = \mathfrak{N}_{l,1} + j\mathfrak{N}_{l,2}$ is given as $\mathfrak{N}_l = e^{-j\hat{\vartheta}_p} N_l$ and its variance is the same as the variance $2\sigma^2$ of the complex noise N_l.

Example 10.12 Complex Doppler factor

Let us consider the complex Doppler factor $\alpha_l = |\alpha_l| e^{j\psi_l}$ of the lth data symbol, given as follows:

$$\alpha_l = \frac{1}{T_s}\int_{lT_s}^{(l+1)T_s} e^{j2\pi ft} dt = \left(\frac{\sin \pi f T_s}{\pi f T_s}\right) e^{j2\pi f T_s (l+1/2)} \tag{10.97}$$

The *Doppler loss* $|\alpha_l|$ and the *Doppler phase error* ψ_l are respectively given as

$$|\alpha_l| = \left|\frac{\sin \pi f T_s}{\pi f T_s}\right|, \psi_l = 2\pi f T_s(l + 1/2) \tag{10.98}$$

Using (10.98) with $l = 0$, the corresponding Doppler loss $|\alpha_p|$ and Doppler phase error ψ_p for the pilot symbol are

$$|\alpha_p| = \left|\frac{\sin \pi f T_s}{\pi f T_s}\right|, \psi_p = \pi f T_s \tag{10.99}$$

The differential Doppler phase error between the lth data symbol and the pilot symbol is $\psi_l - \psi_p = 2\pi f T_s l$, and *increases with time*. Thus the Doppler phase error is *compounded* and needs to be corrected.

To illustrate this, consider a symbol rate of 14.4 ksps, and a Doppler shift of 180 Hz. The Doppler loss is 0.999, which amounts to virtually no loss for the amplitude of the signal. The differential Doppler phase errors for the *fifth* and *tenth* symbols after the most recent channel update are 0.39 and 0.78 radians or 22.5°and 45°, respectively.

■

Differential and double-differential decision-feedback algorithms

To approach the performance of maximum likelihood detection the demodulator must have the most up-to-date Doppler channel tap instead of the Doppler channel tap of the pilot symbol, which is several symbols old. Depending on the severity of the Doppler shift, the most up-to-date Doppler channel tap can be as recent as the previously detected symbol. Therefore, this scenario requires the knowledge of the $(l-2)$th and $(l-1)$th Doppler channel taps to detect the lth data symbol (*the pilot symbol is designated as the* zeroth *symbol*). Note that the detection of the *first symbol* of the *first update* needs only the pilot channel tap. Assume that the $(l-1)$th symbol is detected *correctly* from the sample $X_{l-1} = \left(\hat{\mathbf{h}}_p^*/|\hat{\mathbf{h}}_p|\right) Y_{l-1} = \mathrm{e}^{-\mathrm{j}\hat{\vartheta}_p}(\mathbf{h}_{l-1}s_{i,l-1} + N_{l-1}) = |\mathbf{h}_{l-1}|\mathrm{e}^{\mathrm{j}\varepsilon_{l-1}}s_{i,l-1} + \mathfrak{N}_{l-1}$, then symbol $s_{i,l-1}$ is *known*. The $(l-1)$th Doppler channel tap magnitude $|\mathbf{h}_{l-1}|$ and error $\mathrm{e}^{\mathrm{j}\varepsilon_{l-1}}$ can now be *post-estimated* from the sample X_{l-1} to yield $|\hat{\mathbf{h}}_{l-1}|$ and $\mathrm{e}^{\mathrm{j}\hat{\varepsilon}_{l-1}}$ via $\left(\hat{\mathbf{h}}_p^*/|\hat{\mathbf{h}}_p|\right) X_{l-1} = X_{l-1}\mathrm{e}^{\mathrm{j}\hat{\vartheta}_p}$, for $l = -1, 1, 2, \ldots, L$, where L is the number of symbols in an update ($\hat{\mathbf{h}}_{-1}$ is needed for the detection of the first symbol following the pilot symbol, except for the first update). This *differential decision-feedback algorithm* (D-DF) continues with the next sample in following equation:

$$\begin{aligned}\hat{X}_l &= X_l\mathrm{e}^{-\mathrm{j}\hat{\varepsilon}_{l-1}} = \left(\hat{\mathbf{h}}_p^*/|\hat{\mathbf{h}}_p|\right) Y_l\mathrm{e}^{-\mathrm{j}\hat{\varepsilon}_{l-1}} \\ &= \left(|\mathbf{h}_l|\mathrm{e}^{\mathrm{j}\varepsilon_l}s_{i,l} + \mathfrak{N}_l\right)\mathrm{e}^{-\mathrm{j}\hat{\varepsilon}_{l-1}} = |\mathbf{h}_l|\mathrm{e}^{\mathrm{j}(\varepsilon_l - \hat{\varepsilon}_{l-1})}s_{i,l} + \hat{\mathfrak{N}}_l \\ &= |\mathbf{h}_l|\mathrm{e}^{\mathrm{j}\Delta\varepsilon_l}s_{i,l} + \hat{\mathfrak{N}}_l,\ l = -1, 1, 2, \ldots, L\end{aligned} \tag{10.100}$$

where the complex noise sample $\hat{\mathfrak{N}}_l = \mathfrak{N}_l\mathrm{e}^{-\mathrm{j}\hat{\varepsilon}_{l-1}}$ has variance $2\sigma^2$ and the parameter $\Delta\varepsilon_l = \varepsilon_l - \hat{\varepsilon}_{l-1}$ is the *differential Doppler phase error* between the lth symbol's Doppler

phase error and the $(l-1)$th symbol's *estimated* Doppler phase error. The bit error probability of *decision-feedback* demodulation is now dependent on $\Delta\varepsilon_l$ instead of ε_l. The former is much smaller than the latter hence yielding a smaller error probability. The *phase jitters* of $\hat{\varepsilon}_{l-1}$ and ε_l determine the accuracy of the tracking algorithm. The differential Doppler phase error should remain fairly constant over a few symbols. If the previous symbol $s_{i,l-1}$ was detected incorrectly there may be a spike in the post-estimated $\Delta\hat{\varepsilon}_l$ relative to the previous $\Delta\hat{\varepsilon}_{l-1}$. If this happens $\hat{\varepsilon}_{l-2}$ should be used in recalculating $\hat{X}_l$ in (10.100) instead of $\hat{\varepsilon}_{l-1}$. Also in the first equation of (10.100) one could use $\hat{\mathbf{h}}_{l-1}^*/|\hat{\mathbf{h}}_{l-1}|$ instead of $\hat{\mathbf{h}}_p^*/|\hat{\mathbf{h}}_p|$, but the pilot symbol is commonly transmitted with higher energy, hence its estimated phase is more accurate. Note that once $s_{i,l}$ is detected, the post-estimated $\Delta\hat{\varepsilon}_l$ can be calculated and used to evaluate the $\hat{\varepsilon}_l = \hat{\varepsilon}_{l-1} + \Delta\hat{\varepsilon}_l$ needed for the next sample, $\hat{X}_{l+1} = X_{l+1}\mathrm{e}^{-\mathrm{j}\hat{\varepsilon}_l}$.

If the differential Doppler phase error per symbol is greater than the tolerable limit, further correction may be implemented by using the following sample:

$$\begin{aligned}\hat{X}_l &= X_l\mathrm{e}^{-\mathrm{j}(2\hat{\varepsilon}_{l-1}-\hat{\varepsilon}_{l-2})} = \left(\hat{\mathbf{h}}_p^*/|\hat{\mathbf{h}}_p|\right)Y_l\mathrm{e}^{-\mathrm{j}(2\hat{\varepsilon}_{l-1}-\hat{\varepsilon}_{l-2})} \\ &= \left(|\mathbf{h}_l|\mathrm{e}^{\mathrm{j}\varepsilon_l}s_{i,l} + \mathfrak{N}_l\right)\mathrm{e}^{-\mathrm{j}(2\hat{\varepsilon}_{l-1}-\hat{\varepsilon}_l)} = |\mathbf{h}_l|\mathrm{e}^{\mathrm{j}(\varepsilon_l-\hat{\varepsilon}_{l-1}-[\hat{\varepsilon}_{l-1}-\hat{\varepsilon}_l])}s_{i,l} + \hat{\mathfrak{N}}_l \\ &= |\mathbf{h}_l|\mathrm{e}^{\mathrm{j}(\Delta\varepsilon_l-\Delta\hat{\varepsilon}_{l-1})}s_{i,l} + \hat{\mathfrak{N}}_l\end{aligned} \tag{10.101}$$

where $\Delta\hat{\varepsilon}_{l-1} = \hat{\varepsilon}_{l-1} - \hat{\varepsilon}_{l-2}$ is the *post-estimated* differential Doppler phase error of the $(l-1)$th symbol. This is the *double-differential decision-feedback algorithm* (DD-DF). The decision-feedback algorithm can be carried out in practice using a voltage proportional to the phase $\theta = \hat{\vartheta}_p + \hat{\varepsilon}_{l-1}$ (D-DF) or $\theta = \hat{\vartheta}_p + 2\hat{\varepsilon}_{l-1} - \hat{\varepsilon}_{l-2}$ (DD-DF) as input to a *voltage-controlled oscillator* (VCO) to correct the phase error between the received signal and the local carrier at the VCO output.

The complex decision variables in (10.96), (10.100), and (10.101) can be written in two-dimentional vector form as follows:

$$\boldsymbol{X}_l = |\mathbf{h}_l|\mathbf{T}_l\boldsymbol{s}_{i,l} + \boldsymbol{\mathcal{N}}_l \tag{10.102}$$

The transformation matrix $\mathbf{T}_l$ is the *phase error rotation matrix* given by

$$\mathbf{T}_l = \begin{pmatrix}\cos\boldsymbol{\varepsilon}_l & -\sin\boldsymbol{\varepsilon}_l \\ \sin\boldsymbol{\varepsilon}_l & \cos\boldsymbol{\varepsilon}_l\end{pmatrix} \tag{10.103}$$

where $\boldsymbol{\varepsilon}_l = \varepsilon_l$ for (10.96), $\boldsymbol{\varepsilon}_l = \Delta\varepsilon_l$ for (10.100), and $\boldsymbol{\varepsilon}_l = \Delta\varepsilon_l - \Delta\hat{\varepsilon}_{l-1}$ for (10.101). The *zero-mean I-noise and Q-noise variables* $\boldsymbol{\mathcal{N}}_{l,1}$ and $\boldsymbol{\mathcal{N}}_{l,2}$ of the noise vector $\boldsymbol{\mathcal{N}}_l$ are statistically independent and have the same variance σ^2.

For a flat fading channel, the signal vector $\boldsymbol{s}_{i,l}$ is weighted by the *unknown* Doppler channel tap magnitude $|\boldsymbol{h}_l|$, and the *unknown* phase error rotation matrix $\mathbf{T}_l$. Note that the minimum Euclidean distance detector has *no knowledge* of the phase error $\boldsymbol{\varepsilon}_l$, and the Doppler channel tap magnitude $|\mathbf{h}_l|$. Therefore, given a realization $\boldsymbol{x}_l$ of $\boldsymbol{X}_l$, the minimum Euclidean distance detector makes the decision *based solely* on the knowledge of the Doppler channel tap magnitude $|\hat{\mathbf{h}}_{l-1}|$, which it estimates from Y_{l-1} using the following erroneous metrics:

$$d\left(\boldsymbol{x}_l, |\hat{\mathbf{h}}_{l-1}|\boldsymbol{s}_{i,l}\right) = \left\|\boldsymbol{x}_l - |\hat{\mathbf{h}}_{l-1}|\boldsymbol{s}_{i,l}\right\|, i = 1, 2, \ldots, M \tag{10.104}$$

That is, it selects the signal vector $\left|\hat{\mathbf{h}}_{l-1}\right|\boldsymbol{s}_{i,l}$ that is closest in Euclidean distance to the sampled value $\boldsymbol{x}_l$ of the decision variable vector $\boldsymbol{X}_l$. Since the signal component of $\boldsymbol{X}_l$ is $\mathbf{T}_l\boldsymbol{s}_{i,l}$ instead of $\boldsymbol{s}_{i,l}$, the probability of error is going to be higher than in the case of no phase error because the detector is now using erroneous metrics that assume no phase error in the first place. The bit error probabilities of PSK and QPSK with threshold detection were given in (10.81) and (10.83) respectively. For MQAM the bit error probability can be evaluated with the help of the union bound using the pair-wise probability

The *pair-wise error probability* between two vectors $\boldsymbol{s}_{i,l}$ and $\boldsymbol{s}_{j,l}$ can be calculated based on the following expression:

$$\Pr\left(\boldsymbol{s}_{i,l} \to \boldsymbol{s}_{j,l}|H_i\right) = \Pr\left(\left\|\boldsymbol{x}_l - \left|\hat{\mathbf{h}}_{l-1}\right|\boldsymbol{s}_{j,l}\right\|^2 < \left\|\boldsymbol{x}_l - \left|\hat{\mathbf{h}}_{l-1}\right|\boldsymbol{s}_{i,l}\right\|^2 |H_i\right) \tag{10.105}$$

Substituting (10.102) into the above expression we obtain

$$\begin{aligned}\Pr\left(\boldsymbol{s}_{i,l} \to \boldsymbol{s}_{j,l}|H_i; \left|\hat{\mathbf{h}}_{l-1}\right|, |\mathbf{h}_l|, \boldsymbol{\varepsilon}_l\right) &= \Pr\left(\begin{array}{l}\left\|\,|\mathbf{h}_l|\mathbf{T}_l\boldsymbol{s}_{i,l} - \left|\hat{\mathbf{h}}_{l-1}\right|\boldsymbol{s}_{j,l} + \boldsymbol{\mathcal{N}}_l\right\|^2 \\ < \left\|\,|\mathbf{h}_l|\mathbf{T}_l\boldsymbol{s}_{i,l} - \left|\hat{\mathbf{h}}_{l-1}\right|\boldsymbol{s}_{i,l} + \boldsymbol{\mathcal{N}}_l\right\|^2 |H_i\end{array}\right) \\ &= \Pr\left(Z > \frac{1}{2}\boldsymbol{d}_{i,j}\left(\left|\hat{\mathbf{h}}_{l-1}\right|, |\mathbf{h}_l|, \boldsymbol{\varepsilon}_l\right)|\boldsymbol{H_i}\right)\end{aligned} \tag{10.106}$$

where $Z = ||\boldsymbol{s}_j - \boldsymbol{s}_i||^{-1}[\boldsymbol{s}_j - \boldsymbol{s}_i]^t$, $\boldsymbol{\mathcal{N}}_l$ is a zero mean Gaussian random variable with variance σ^2, and $\boldsymbol{d}_{i,j}\left(\left|\hat{\mathbf{h}}_{l-1}\right|, |\mathbf{h}_l|, \boldsymbol{\varepsilon}_l\right)$ is given by

$$\boldsymbol{d}_{i,j}\left(\left|\hat{\mathbf{h}}_{l-1}\right|, |\mathbf{h}_l|, \boldsymbol{\varepsilon}_l\right) = \frac{\left\|\,|\mathbf{h}_l|\mathbf{T}_l\boldsymbol{s}_{i,l} - \left|\hat{\mathbf{h}}_{l-1}\right|\boldsymbol{s}_{j,l}\right\|^2 - \left\|\,|\mathbf{h}_l|\mathbf{T}_l\boldsymbol{s}_{i,l} - \left|\hat{\mathbf{h}}_l\right|\boldsymbol{s}_{i,l}\right\|^2}{\left|\hat{\mathbf{h}}_{l-1}\right|\left\|\boldsymbol{s}_i - \boldsymbol{s}_j\right\|} \tag{10.107}$$

Therefore, we get

$$\Pr\left(\boldsymbol{s}_{i,l} \to \boldsymbol{s}_{j,l}|H_i; \left|\hat{\mathbf{h}}_{l-1}\right|, |\mathbf{h}_l|, \boldsymbol{\varepsilon}_l\right) = Q\left(\frac{\boldsymbol{d}_{i,j}\left(\left|\hat{\mathbf{h}}_{l-1}\right|, |\mathbf{h}_l|, \boldsymbol{\varepsilon}_l\right)}{2\sigma}\right) \tag{10.108}$$

The bit error probability of MQAM can be evaluated as follows:

$$\begin{aligned}P_b\left(\left|\hat{\mathbf{h}}_{l-1}\right|, |\mathbf{h}_l|, \boldsymbol{\varepsilon}_l\right) &= \frac{1}{\log_2 M}\sum_{i=1}^{M}\sum_{j=2}^{M}\Pr(H_i)\Pr\left(\boldsymbol{s}_{i,l} \to \boldsymbol{s}_{j,l}|H_i; \left|\hat{\mathbf{h}}_{l-1}\right|, |\mathbf{h}_l|, \boldsymbol{\varepsilon}_l\right) \\ &= \frac{1}{\log_2 M}\sum_{i=1}^{M}\sum_{j=2}^{M}\Pr(H_i)Q\left(\frac{\boldsymbol{d}_{i,j}\left(\left|\hat{\mathbf{h}}_{l-1}\right|, |\mathbf{h}_l|, \boldsymbol{\varepsilon}_l\right)}{2\sigma}\right)\end{aligned} \tag{10.109}$$

Knowing the statistics of the fading channel (Rayleigh, Ricean, Nakagami) and the Doppler error we can evaluate the bit error probability as follows:

$$P_b = \mathbf{E}\left[P_b\left(\left|\hat{\mathbf{h}}_{l-1}\right|, |\mathbf{h}_l|, \boldsymbol{\varepsilon}_l\right)\right] \tag{10.110}$$

For a slow fading channel where the channel taps remain constant over several symbol times, and in addition where the signal-to-noise ratio is high, we can set $\left|\hat{\mathbf{h}}_{l-1}\right| = |\mathbf{h}_l|$ in the bit error probability expression above and obtain a simpler expression.

Example 10.13 Throughput limit

The above study raises the following question: how often should channel estimation be carried out? Let us consider the scenario where a mobile traveling toward a base station at a speed of 100 km/hour receives a 1950 MHz signal from a base station. The Doppler spread is $f_D = 2f_c v/c = 361$ Hz. Consequently, the channel coherence time is estimated to be equal to $T_c = 1/4f_D = 6.9 \times 10^{-4}$ seconds. Therefore, the channel estimation rate must be much larger than the channel *coherence rate* $1/T_c = 1449$ bits/second. If the data rate is 14.4 kbps, which is about ten times the channel coherence rate, there is not much room for both frequent updates and high throughput. For example, if the channel estimation rate is five times the coherence rate to keep the Doppler phase error smaller than 22.5° at the end of the update, then the throughput is 50%. If the channel estimation rate is 2.5 times the coherence rate, then the throughput is 75%, but the Doppler phase error at the end of the update is 45°. If the Doppler spread is expected to remain fairly constant during the length of a transmitted packet, then frequent updates may not be required. In this case a differential Doppler phase error of $\psi_l - \psi_p = 2\pi f T_s l$ in (10.98) and (10.99) would be sufficient to correct the phase error for each symbol provided that the Doppler shift f can be accurately determined via frequency offset estimation using a training symbol sequence.

■

10.5 OFDM

In OFDM systems such as the IEEE 802.11a,g, 802.16, and 802.16e the pilot symbols are transmitted simultaneously with data symbols in the pilot subcarriers. For high mobility applications such as 802.16e the channel update is instantaneous and no Doppler *compounded effect* occurs. The Doppler effect of a data symbol in pilot-aided demodulation nevertheless does exist because the pilot subcarriers are at different frequencies to the data subcarriers. In addition, the Doppler shift may destroy the subcarrier orthogonality and hence creates *intercarrier interference* (ICI). Furthermore, although the subcarriers may be designed to experience slow fading, the entire OFDM channel is a frequency-selective fading channel. Thus, the phase shifts of subcarriers can be different and pilot symbol-aided demodulation still results in phase errors in the decision sample because of the phase rotation of the signal space of each subcarrier.

Example 10.14 Doppler shift in OFDM

In this example we illustrate the effect of Doppler shift on an OFDM signal that is used by high-mobility platforms. Consider the OFDM signal whose complex envelope is generated by the D/A converter as given in (6.166). We have

$$\begin{aligned} s(t) &= \mathrm{Re}\left(\hat{s}_L(t)\mathrm{e}^{\,\mathrm{j}2\pi f_c t}\right) \\ &= \mathrm{Re}\left\{\left[\sum_{l=0}^{N-1} s_L(l)p(t-lT_s/N)\right]\mathrm{e}^{\,\mathrm{j}2\pi f_c t}\right\} \end{aligned} \tag{10.111}$$

Now assume that the signal encounters a Doppler effect with Doppler frequency f. The carrier frequency is now $f_c + f$ and therefore the Doppler shifted OFDM signal is given by

$$\begin{aligned} s(t) &= \mathrm{Re}\left(\hat{s}_L(t)\mathrm{e}^{\,\mathrm{j}2\pi ft}\mathrm{e}^{\,\mathrm{j}2\pi f_c t}\right) \\ &= \mathrm{Re}\left\{\left[\sum_{l=0}^{N-1} s_L(l)\mathrm{e}^{\,\mathrm{j}2\pi ft}p(t-lT_s/N)\right]\mathrm{e}^{\,\mathrm{j}2\pi f_c t}\right\} \end{aligned} \tag{10.112}$$

The resulting complex envelope is

$$\hat{s}_L(t) = \sum_{l=0}^{N-1} s_L(l)\mathrm{e}^{\,\mathrm{j}2\pi ft}p(t-lT_s/N) \tag{10.113}$$

The A/D converter at the receiver samples this complex envelope with sample time nT_s/N to produce the set of N samples for the DFT. We have

$$\begin{aligned} \hat{s}_L(n) &= \sum_{l=0}^{N-1} s_L(l)\mathrm{e}^{\,\mathrm{j}2\pi nfT_s/N}p((n-l)T_s/N) \\ &= \sum_{l=0}^{N-1} s_L(l)\mathrm{e}^{\,\mathrm{j}2\pi nfT_s/N}\delta[n-l] \\ &= s_L(n)\mathrm{e}^{\,\mathrm{j}2\pi nfT_s/N},\ n = 0,1,\ldots,N-1 \end{aligned} \tag{10.114}$$

If the Doppler shift f is known via frequency offset estimation, the phase rotation due to the Doppler effect can be corrected via the multiplication of $\hat{s}_L(n)$ with $\mathrm{e}^{-\mathrm{j}2\pi nfT_s/N}$ to yield the distortionless sample $s_L(n)$. Substituting the original time-domain samples $s_L(n)$ generated by the transmitter as given in (6.161) we get

$$\hat{s}_L(n) = \frac{1}{N}\sum_{k=0}^{N-1} Z(k)\,\mathrm{e}^{\,\mathrm{j}2\pi n(k+fT_s)/N},\ n = 0,1,\ldots,N-1 \tag{10.115}$$

Taking the DFT of $\hat{s}_L(n)$ we obtain

$$\hat{Z}(k) = \sum_{n=0}^{N-1} \hat{s}_L(n)\mathrm{e}^{-\mathrm{j}2\pi kn/N}, k = 0,1,\ldots,N-1 \tag{10.116}$$

We can substitute $\hat{s}_L(n)$ into (10.116) to see the Doppler effect on a subcarrier symbol. We have

$$\hat{Z}(k) = \sum_{n=0}^{N-1}\left(\frac{1}{N}\sum_{m=0}^{N-1}\left[Z(m)\mathrm{e}^{\,\mathrm{j}2\pi nfT_s/N}\right]\mathrm{e}^{\,\mathrm{j}2\pi mn/N}\right)\mathrm{e}^{-\mathrm{j}2\pi kn/N}, k = 0,1,\ldots,N-1 \tag{10.117}$$

Exchanging the order of summation in (10.117) we get

$$\begin{aligned}\hat{Z}(k) &= \frac{1}{N}\sum_{m=0}^{N-1}\sum_{n=0}^{N-1} Z(m)\mathrm{e}^{\mathrm{j}2\pi n(m-k+fT_s)/N} \\ &= \frac{1}{N}\sum_{m=0}^{N-1} Z(m)\sum_{n=0}^{N-1}\mathrm{e}^{\mathrm{j}2\pi n(m-k+fT_s)/N} \\ &= \frac{1}{N}\left(\sum_{n=0}^{N-1}\mathrm{e}^{\mathrm{j}2\pi nfT_s/N}\right)Z(k) + \frac{1}{N}\sum_{\substack{m=0\\ m\neq k}}^{N-1} Z(m)\sum_{n=0}^{N-1}\mathrm{e}^{\mathrm{j}2\pi n(m-k+fT_s)/N} \\ &= \frac{1}{N}\frac{\mathrm{e}^{\mathrm{j}2\pi fT_s}-1}{\mathrm{e}^{\mathrm{j}2\pi fT_s/N}-1}Z(k) + \frac{1}{N}\sum_{\substack{m=0\\ m\neq k}}^{N-1}\frac{\mathrm{e}^{\mathrm{j}2\pi(m-k+fT_s)}-1}{\mathrm{e}^{\mathrm{j}2\pi(m-k+fT_s)/N}-1}Z(m) \\ &= \frac{1}{N}\frac{\sin(\pi fT_s)}{\sin(\pi fT_s/N)}\mathrm{e}^{\mathrm{j}\pi fT_s(N-1)/N}Z(k) \\ &\quad + \frac{1}{N}\sum_{\substack{m=0\\ m\neq k}}^{N-1}\frac{\sin[\pi(m-k+fT_s)]}{\sin[\pi(m-k+fT_s)/N]}\mathrm{e}^{\mathrm{j}\pi[m-k+fT_s](N-1)/N}Z(m), k=0,1,\ldots,N-1\end{aligned} \tag{10.118}$$

The right-hand side of the above equation is obtained via the following identity:

$$\sum_{n=0}^{N-1}\mathrm{e}^{\mathrm{j}n\phi} = \frac{\mathrm{e}^{\mathrm{j}N\phi}-1}{\mathrm{e}^{\mathrm{j}\phi}-1} = \frac{\sin(N\phi/2)}{\sin(\phi/2)}\mathrm{e}^{\mathrm{j}(N-1)/2} \tag{10.119}$$

The first term on the right-hand side of the above equation is the distorted subcarrier symbol and the second term is the *intercarrier interference* (ICI).

■

Now let us include the channel distortion effect. Denote the complex envelope of the channel impulse response as

$$h(t) = \sum\nolimits_{i=0}^{L-1} h(i)\delta(t-\tau_i) \tag{10.120}$$

where $\tau_0 = 0$. To be consistent with the notation in Section 6.18 we use the notation $h(i)$ to represent a channel tap for OFDM. The complex envelope of the received OFDM signal is given by

$$\begin{aligned}y(t) = h(t) * \hat{s}_L(t) &= \int_{-\infty}^{\infty} h(\tau)\hat{s}_L(t-\tau)\mathrm{d}\tau \\ &= \int_{-\infty}^{\infty}\sum_{i=0}^{L-1} h(i)\delta(\tau-\tau_i)\hat{s}_L(t-\tau)\mathrm{d}\tau \\ &= \sum_{i=0}^{L-1} h(i)\int_{-\infty}^{\infty}\delta(\tau-\tau_i)\hat{s}_L(t-\tau)\mathrm{d}\tau \\ &= \sum_{i=0}^{L-1} h(i)\hat{s}_L(t-\tau_i)\end{aligned} \tag{10.121}$$

where $\hat{s}_L(t)$ is given in (10.113). We assume the A/D converter contains the matched filter $p(t)$, which is a $\sin x/x$ pulse shape, therefore the output of the matched filter is just $p(t)$. The A/D converter samples the OFDM signal every T_s/N seconds to produce the set of N samples after discarding the cyclic prefix

$$\begin{aligned} y(n) &= \sum_{i=0}^{L-1} h(i)\hat{s}_L\left(\frac{nT_s}{N} - \tau_i\right) \\ &= \sum_{i=0}^{L-1} h(i) \sum_{l=0}^{N-1} s_L(l) \mathrm{e}^{\mathrm{j}2\pi f(nT_s/N - \tau_i)} p[(n-l)T_s/N - \tau_i] \\ &= \mathrm{e}^{\mathrm{j}2\pi nfT_s/N} \sum_{i=0}^{L-1} h(i) \mathrm{e}^{-\mathrm{j}2\pi f\tau_i} \sum_{l=0}^{N-1} s_L(l) p[(n-l)T_s/N - \tau_i] \\ &= \mathrm{e}^{\mathrm{j}2\pi nfT_s/N} \sum_{i=0}^{L-1} \tilde{h}(i)\tilde{s}_L(n,i), \;\; n = 0, 1, \ldots, N-1 \end{aligned} \tag{10.122}$$

where

$$\tilde{h}(i) = h(i)\mathrm{e}^{-\mathrm{j}2\pi f\tau_i} \tag{10.123}$$

$$\tilde{s}_L(n,i) = \sum_{l=0}^{N-1} s_L(l) p[(n-l)T_s/N - \tau_i] \tag{10.124}$$

Note that (10.121) reduces to (10.114) when there is no channel distortion, that is, when $h(t) = \delta(t)$. If we take the DFT of $y(n)$ we obtain the frequency domain samples which are distorted and contain ICI. We can eliminate ICI with Doppler correction before the DFT, that is, multiply $y(n)$ with $\mathrm{e}^{-\mathrm{j}2\pi nfT_s/N}$ to yield $\tilde{y}(n) = \sum_{i=0}^{L-1} \tilde{h}(i)\tilde{s}_L(n,i)$ and then take the DFT. The resulting frequency-domain samples still contain distortion because of the phase rotation of the channel taps $h(i)$ and the ISI in the time-domain samples $s_L(l)$ via the sum factors in (10.124). This type of distortion cannot be corrected and results in degradation.

Let us consider the case when the channel can be modeled as a FIR filter as discussed in Section 6.18. In this case we have L channel taps with delay $\tau_i = iT_s/N$. Again assuming that the Doppler shift has been corrected as described above, we obtain the following time-domain samples:

$$\begin{aligned} \tilde{y}(n) = y(n)\mathrm{e}^{-\mathrm{j}2\pi nfT_s/N} &= \sum_{i=0}^{L-1} \tilde{h}(i) \sum_{l=0}^{N-1} s_L(l) p[(n-l)T_s/N - \tau_i] \\ &= \sum_{i=0}^{L-1} \tilde{h}(i) \sum_{l=0}^{N-1} s_L(l) p[(n-l-i)T_s/N] = \sum_{i=0}^{L-1} \tilde{h}(i) \sum_{l=0}^{N-1} s_L(l)\delta[n-l-i] \\ &= \sum_{i=0}^{L-1} \tilde{h}(i) s_L(n-i)_N \\ &= \tilde{h}(n) \otimes s_L(n), \;\; n = 0, 1, \ldots, N-1 \end{aligned} \tag{10.125}$$

Taking the DFT of $\tilde{y}(n)$ we obtain the distorted frequency-domain samples given as

$$\tilde{Z}(k) = \tilde{H}(k)Z(k), \;\; k = 0, 1, \ldots \;\; N-1 \tag{10.126}$$

where $\tilde{H}(k)$ is the DFT of $\tilde{h}(n)$, that is,

$$\tilde{H}(k) = \sum_{n=0}^{L-1} \tilde{h}(n) \mathrm{e}^{-\mathrm{j}2\pi kn/N} = \sum_{n=0}^{L-1} h(n) \mathrm{e}^{-\mathrm{j}2\pi n(k+fT_s)/N} \tag{10.127}$$

In the case of no Doppler shift, that is, $f = 0$ we have $\tilde{H}(k) = H(k)$, where $H(k) = \sum_{n=0}^{L-1} h(n)\mathrm{e}^{-\mathrm{j}2\pi kn/N}$ is the DFT of $h(n)$, and we obtain the frequency-domain samples $\tilde{Z}(k) = H(k)Z(k), \; k = 0, 1, \ldots \; N-1$, which is the result derived in Section 6.18.

Returning to the general case in (10.122) and assuming that the Doppler shift has been corrected as described above we obtain the following time-domain samples:

$$\begin{aligned} \tilde{y}(n) &= y(n)\mathrm{e}^{-\mathrm{j}2\pi nfT_s/N} = \sum_{i=0}^{L-1} \tilde{h}(i) \sum_{l=0}^{N-1} s_L(l) p[(n-l)T_s/N - \tau_i] \\ &= \tilde{h}(0) s_L(n) + \sum_{i=1}^{L-1} \tilde{h}(i) \sum_{l=0}^{N-1} s_L(l) p[(n-l)T_s/N - \tau_i], n = 0, 1, \ldots, N-1 \end{aligned} \tag{10.128}$$

Taking the DFT of $\tilde{y}(n)$ we obtain the distorted frequency-domain samples as follows:

$$\begin{aligned} \tilde{Z}(k) &= \tilde{h}(0)Z(k) + DFT\left\{ \sum_{i=1}^{L-1} \tilde{h}(i) \sum_{l=0}^{N-1} s_L(l) p[(n-l)T_s/N - \tau_i] \right\}, \;\; k \\ &= 0, 1, \ldots, N-1 \end{aligned} \tag{10.129}$$

Even in the case of no Doppler shift we note that the second term on the right-hand side of (10.129) still exists (with $\tilde{h}(i)$ replaced by $h(i)$). This means that the cyclic prefix, which removes the ISI between consecutive OFDM symbols, cannot remove the *intersample interference* (ISI) within an OFDM symbol as in the case of L channel taps with delay $\tau_i = iT_s/N$. To remove the intersample interference when the channel tap delay τ_i is not an integer multiple of the sampling interval T_s/N, equalization must be employed after the removal of the cyclic prefix.

Low mobility

Wireless IEEE Standards such as 802.11a,g and 802.16 were designed for low mobility and hence their applications experience virtually no Doppler effects. In this scenario we add noise and have $\tilde{Z}(k) = H(k)Z(k) + \mathbf{N}_k, k = 0, 1, \ldots, N-1$ for the case of L channel taps with delay $\tau_i = iT_s/N$. Note that this expression is *identical* to its counterpart (10.95) in *single channel demodulation*. Therefore, the bit error probability of the mth subcarrier is given by (10.110) with appropriate replacement of variables:

$$P_{b,m} = \mathbf{E}\left[P_{b,m}\left(\left|\hat{H}_{l-1}(m)\right|, \left|\hat{H}_l(m)\right|, \boldsymbol{\varepsilon}_l(m)\right)\right] \tag{10.130}$$

where $\hat{H}_{l-1}(m)$, $\hat{H}_l(m)$, and $\boldsymbol{\varepsilon}_l(m)$ are the estimated DFTs of the subchannel taps of the $(l-1)$th symbol of the mth subcarrier, the subchannel taps of the lth symbol of the mth

subcarrier, and the differential phase error (10.100) or double-differential phase error (10.101) between these two DFTs, respectively. The bit error probability can be averaged over N subcarriers to yield

$$P_b = \frac{1}{N}\sum_{m=1}^{N-1} P_{b,m} \tag{10.131}$$

In evaluating the bit error probability we need to know, for example, the distribution of the differential phase errors $\boldsymbol{\varepsilon}_l(m)$ of the subcarriers. One possibility is to assume the differential phase error to be *uniformly distributed* in a given range $(-\Delta\boldsymbol{\varepsilon}, \Delta\boldsymbol{\varepsilon})$. At a high signal-to-noise ratio the estimation of subchannel taps can be quite accurate. Hence, the differential phase error can be insignificant, $\boldsymbol{\varepsilon}_l(m) \approx 0^0$, and the estimated subchannel taps $\left|\hat{H}_{l-1}(m)\right|$ can be closely approximated as $\left|\hat{H}_{l-1}(m)\right| \approx \left|\left|\hat{H}_l(m)\right|\right|$ by virtue of no Doppler shift. In this case, the bit error probability of low-mobility OFDM approaches (10.54).

High mobility

Incorporating noise and we have $\tilde{Z}(k) = \tilde{H}(k)Z(k) + \mathbf{N}_k$, $k = 0, 1, \ldots, N-1$ for the case of L channel taps with delay $\tau_i = iT_s/N$. As seen in the above discussion, Doppler-induced ICI and Doppler loss can have a pronounced effect on OFDM. Once the DFT is carried out to generate the subcarrier I-Q samples for detection, ICI is added directly to them like AWGN and cannot be undone. This phenomenon is similar to *aliasing* in undersampling. Therefore, ICI can only be cancelled out prior to DFT, namely, in the time domain samples $\tilde{s}_L(n)$. This requires knowledge of the Doppler shift. The remaining question is how to estimate the Doppler error. A training sequence can be transmitted in the packet header of each transmitted packet to allow for the estimation of the Doppler shift. Only one chosen subcarrier is used during this estimation time, that is, the OFDM signal is actually a single-carrier signal. Data symbols in all other subcarriers are set to zero to avoid ICI. The training sequence enhances the estimation of the subcarrier Doppler phase error via the *decision-feedback algorithm* since all training symbols are known a priori. If a training symbol is detected incorrectly, it can be corrected via the knowledge of its position in the sequence relative to the previously correctly detected symbol. Since only a single subcarrier is used, the channel phase shift is eliminated by the detection process in the previous section, assuming that it is constant for each symbol time. In practice, the training sequence is fairly short and it is likely that the channel phase shift remains constant during the entire sequence. The estimated *differential Doppler phase error* $\hat{\varepsilon}$ *for each training symbol* can be averaged out for the entire training sequence. Alternatively, the average differential Doppler phase error $\hat{\varepsilon}$ can be used to adjust the phase of the local in-phase and quadrature carriers to correct the Doppler effect before the DFT operation is carried out.

In the general case where the channel tap delay τ_i is not an integer multiple of the sampling interval T_s/N, equalization must be employed to remove the intra-subcarrier interference from the sequence $\tilde{y}(n)$ immediately after Doppler correction and cyclic prefix removal.

10.6 Noncoherent demodulation

For applications in which coherent demodulation is not possible (IS-95 reverse link, FH-MFSK), the demodulation of the received signal is performed noncoherently. The signal candidates for noncoherent demodulation include DMPSK, MFSK, and CSK. The conditional bit error probabilities are given as follows:

- **Noncoherent DMPSK, $\pi/4$-DQPSK:**

$$\begin{aligned} P_b\left(|h|^2\right) &\approx \frac{2}{\log_2 M} Q\left(\sqrt{2|h|^2 \alpha SNR}\right) \\ \alpha SNR &= \frac{E_b \log_2 M}{N_0} \sin^2 \frac{\pi}{\sqrt{2}\, M} \quad \text{(DMPSK)} \\ \alpha SNR &= 0.555 \frac{E_b}{N_0} \quad (\pi/4\text{-DQPSK}) \end{aligned} \tag{10.132}$$

- **Noncoherent CSK and MFSK:**

$$P_b\left(|h|^2\right) = \frac{M/2}{M-1} \sum_{k=1}^{M-1} (-1)^{k+1} \binom{M-1}{k} \frac{1}{k+1} \mathrm{e}^{-(k/(k+1))|h|^2 SNR} \tag{10.133}$$

where $SNR = E_s/N_0$.

Rayleigh

For convenience we normalize the channel tap such that $\mathbf{E}\left(|h|^2\right) = 1$. The channel tap $|h|$ is Rayleigh-distributed with density function given in (10.56). The corresponding bit error probabilities are given by the following closed-form expressions:

- **DMPSK, $\pi/4$-DQPSK:**

$$P_b \approx \frac{1}{\log_2 M} \left(1 - \sqrt{\frac{\alpha SNR}{1 + \alpha SNR}}\right) \tag{10.134}$$

- **CSK, MFSK:**

$$P_b = \frac{M/2}{M-1} \sum_{k=1}^{M-1} (-1)^{k+1} \binom{M-1}{k} \frac{1}{1 + k(1 + SNR)} \tag{10.135}$$

Rice

There is no closed-form expression for P_b of DMPSK and $\pi/4$-DQPSK with a Rice-distributed channel tap and numerical integration has to be carried out to evaluate (10.132) and (10.133). The closed-form expression for P_b of CSK and MFSK is given as

$$P_b = \frac{M/2}{M-1}\sum_{n=1}^{M-1}(-1)^{n+1}\binom{M-1}{n}\frac{\kappa+1}{\kappa+1+n(\kappa+1+SNR)}\exp\left(-\frac{n\kappa(SNR)}{\kappa+1+n(\kappa+1+SNR)}\right) \tag{10.136}$$

Nakagami-m

When m is an *integer*, the bit error probabilities have the following closed-form expressions:

- **DMPSK, π/4-DQPSK:**

$$P_b \approx \frac{2}{\log_2 M}\left[1-\sqrt{\frac{\alpha SNR/m}{1+\alpha SNR/m}}\sum_{k=0}^{m-1}\binom{2k}{k}\left(\frac{1}{4(1+\alpha SNR/m)}\right)^k\right], m: \text{integer} \tag{10.137}$$

- **CSK, MFSK:**

$$P_b = \frac{M/2}{M-1}\sum_{k=1}^{M-1}(-1)^{k+1}\binom{M-1}{k}\frac{(k+1)^{m-1}}{\left[1+k\left(1+\frac{SNR}{m}\right)\right]^m} \tag{10.138}$$

Doppler tracking of MFSK

Doppler shift affects noncoherent demodulation in a different fashion to coherent demodulation. Doppler shift causes the loss of orthogonality in orthogonal signals such as MFSK and CSK. For example, consider a received MFSK signal at a particular tone $f_k = k/T_s$ as $s(t) = |h_k|A\cos[2\pi(f_k+f)t+\theta_k]+n(t)$, $iT_s \le t < (i+1)T_s$, which experiences a Doppler shift f and fade h_k. Since adjacent tones are separated in frequency by $1/T_s$, there is a difference in Doppler shift for each tone, but the difference is negligible and is ignored for simplicity. The channel is assumed to experience *slow fading in a symbol time* so that the channel phase shift θ_k can be considered *constant* within a symbol time T_s. Let us demodulate this signal by first multiplying it by $\sqrt{2/T_s}\cos 2\pi f_l t$, $f_l = l/T_s$ and integrating the resulting signal from $t = iT_s$ to $t = (i+1)T_s$, in order to obtain the lth tone's *I-decision sample*:

$$\begin{aligned} X_{l,I} &= \int_{iT_s}^{(i+1)T_s}(|h_k|A\cos[2\pi(f_k+f)t+\theta_k])\sqrt{2/T_s}\cos 2\pi f_l t\,\mathrm{d}t + N_{l,I} \\ &\approx \frac{|h_k|A}{\sqrt{2T_s}}\int_{iT_s}^{(i+1)T_s}\cos(2\pi[(k-l)/T_s+f]t+\theta_k)\,\mathrm{d}t + N_{l,I} \\ &\approx |h_k|\sqrt{\frac{A^2T_s}{2}}\left(\frac{\sin(2\pi[(k-l)+fT_s](i+1)+\theta_k)-\sin(2\pi[(k-l)+fT_s]i+\theta_k)}{2\pi[(k-l)+fT_s]}\right) \\ &\quad + N_{l,I} \end{aligned} \tag{10.139}$$

Similarly, we demodulate this signal by multiplying it by $\sqrt{2/T_s}\sin 2\pi f_l t$ and integrating the resulting signal from $t = iT_s$ to $t = (i+1)T_s$ in order to obtain the lth tone's *Q-decision sample*:

$$
\begin{aligned}
X_{l,Q} &= \int_{iT_s}^{(i+1)T_s} (|h_k| A \cos[2\pi(f_k + f)t + \theta_k])\sqrt{2/T_s} \sin 2\pi f_l t \, \mathrm{d}t + N_{l,Q} \\
&\approx -\frac{|h_k|A}{\sqrt{2T_s}} \int_{iT_s}^{(i+1)T_s} \sin(2\pi[(k-l)/T_s + f]t + \theta_k) \, \mathrm{d}t + N_{l,Q} \\
&\approx |h_k| \sqrt{\frac{A^2 T_s}{2}} \left(\frac{\cos(2\pi[(k-l) + fT_s](i+1) + \theta_k) - \cos(2\pi[(k-l) + fT_s]i + \theta_k)}{2\pi[(k-l) + fT_s]} \right) \\
&\quad + N_{l,Q}
\end{aligned}
\tag{10.140}
$$

Both $N_{l,I}$ and $N_{l,Q}$ are independent Gaussian random variables with zero mean and variance $\sigma^2 = N_0/2$. The high-frequency term is insignificant compared to the first term and is dropped from the above expression. The decision variable of the lth tone is given by

$$
X_l = \sqrt{X_{l,I}^2 + X_{l,Q}^2} \tag{10.141}
$$

Thus, given $|h_k|$, X_l is *Rice* distributed and its density function is given as

$$
f_{X_l}(x_l) = \frac{x_l}{\sigma^2} \mathrm{e}^{-(x_l^2 + m_l^2)/2\sigma^2} I_0\left(\frac{m_l x_l}{\sigma^2}\right) \tag{10.142}
$$

where the parameter m_l^2 is the sum of the squares of the means of $X_{l,I}$ and $X_{l,Q}$ and is expressed as

$$
\begin{aligned}
m_l^2 &= \left(\overline{X}_{l,I}\right)^2 + \left(\overline{X}_{l,Q}\right)^2 \\
&= |h_k|^2 E_s \frac{\sin^2 \pi f T_s}{\left(\pi[(k-l) + fT_s]\right)^2}
\end{aligned}
\tag{10.143}
$$

where $E_s = A^2 T_s/2$ is the symbol energy. Note that $m_k^2 = |h_k|^2 E_s (\sin \pi f T_s / \pi f T_s)^2$. By using the results in Section 7.9 we can calculate the conditional symbol error probability of MFSK. We get

$$
\begin{aligned}
P_e(|h_k|, f) &= 1 - \int_0^\infty \left[\prod_{\substack{l=1 \\ l \neq k}}^{M} \int_0^{x_k} f_{X_l}(x_l) \, \mathrm{d}x_l \right] f_{X_k}(x_k) \, \mathrm{d}x_k \\
&= 1 - \int_0^\infty \left[\prod_{\substack{l=1 \\ l \neq k}}^{M} \left\{ 1 - \int_{x_k}^\infty f_{X_l}(x_l) \, \mathrm{d}x_l \right\} \right] f_{X_k}(x_k) \, \mathrm{d}x_k
\end{aligned}
\tag{10.144}
$$

The above integration can be expressed in term of the *Marcum* $\boldsymbol{Q}$*-function*, which is defined as follows:

$$
\begin{aligned}
\boldsymbol{Q}(a, b) &= \int_b^\infty x \mathrm{e}^{-(x^2 + a^2)/2} I_0(ax) \, \mathrm{d}x = 1 - \int_0^b x \mathrm{e}^{-(x^2 + a^2)/2} I_0(ax) \, \mathrm{d}x \\
&= \mathrm{e}^{-(a^2 + b^2)/2} \sum_{n=0}^{\infty} \left(\frac{a}{b}\right)^n I_n(ab) \\
&= 1 - \mathrm{e}^{-(a^2 + b^2)/2} \sum_{n=1}^{\infty} \left(\frac{b}{a}\right)^n I_n(ab), \quad b > a > 0.
\end{aligned}
\tag{10.145}
$$

where I_n is the modified Bessel function of the first kind of order n.

Therefore, we have

$$P_e(|h_k|,f) = 1 - \int_0^\infty \prod_{\substack{l=1 \\ l\neq k}}^{M} \left[1 - \boldsymbol{Q}\left(\frac{m_l}{\sigma}, \frac{x_k}{\sigma}\right)\right] f_{X_k}(x_k)\, \mathrm{d}x \tag{10.146}$$

The inequality in the above expression results from considering the worst-case scenario that is encountered by the middle tone at $k = M/2$. The bit error probability for MFSK is obtained via the following expression:

$$P_b(f) = \frac{M/2}{M-1}\left(\frac{1}{M}\sum_{k=1}^{M} \mathbf{E}[P_e(|h_k|,f)]\right) \tag{10.147}$$

Since the difference in Doppler shifts for adjacent tones is negligible, the Doppler shift f can be calculated from (10.143) in the case of *small noise* by establishing the ratio $r^2 = m_k^2/m_l^2$, called the *signal-to-intertone interference ratio*. For the worse-case scenario we consider two *adjacent* tones and let $l = k - 1$. For a given value of r^2 we obtain two Doppler shift values, one negative and one positive, as follows:

$$f_- = -\frac{1}{(r+1)T_s},\ f_+ = \frac{1}{(r-1)T_s},\ r^2 = \frac{m_k^2}{m_{k-1}^2} \tag{10.148}$$

The *sign ambiguity* of the Doppler shifts can be resolved if the movement of both transmitter and receiver is known (moving toward or moving away from each other). The global positioning system (GPS) can supplement the receiver with the sign information. The Doppler shift can be employed by a tracking phase-locked loop (PLL) to demodulate the signal and cancel out the Doppler effect. In practice, the *noisy* ratio r^2 is obtained as $r^2 = X_k^2/X_{k-1}^2$. The frequency jitter due to noise determines the accuracy of the estimate of the Doppler shift.

The sign ambiguity of the Doppler shifts can also be resolved via the use of dual demodulators with a PLL tracking Doppler shift f_- and another PLL tracking f_+ using the following *decision-feedback selection* algorithm (DFS). Suppose the ith symbol in the symbol stream represented by tone f_k was correctly detected. The Doppler shifts f_- and f_+ are then estimated as described in (10.148). The dual demodulators demodulate the next $(i+1)$th symbols (two of them) represented by tone f_n. The values of $X_n^2(f_-)$ and $X_n^2(f_+)$ are compared and the $(i+1)$th symbol corresponding to the *larger value* is selected. Suppose the correct Doppler shift is $f_- \approx f$ and assume that the signal-to-noise ratio is high, then the decision variables for the dual demodulators are

$$X_n^2(f_-) \approx m_n^2(f_-) = |h_n|^2 E_s \left(\sin^2[\pi(f - f_-)T_s]/[\pi(f - f_-)T_s]^2\right) \approx |h_n|^2 E_s$$

and

$$X_n^2(f_+) \approx m_n^2(f_+) = |h_n|^2 E_s \left(\sin^2[\pi(f - f_+)T_s]/(\pi(f - f_+)T_s)^2\right) < |h_n|^2 E_s.$$

The decision is to select the symbol corresponding to $X_n^2(f_-)$.

The above analysis for MFSK applies equally well to all orthogonal signals, such as CSK employed in the reverse link of IS-95, MSK, and DPSK, although (10.148) differs for different modulation techniques.

Table 10.3 Decision-feedback selection for 64FSK

Carrier frequency (GHz)	Speed (km/h)	Doppler shift f (Hz)	$\frac{m_{k-1}^2}{\lvert h_k\rvert^2 E_s}$	$\frac{m_k^2}{\lvert h_k\rvert^2 E_s}$	r	f_- (Hz)	f_+ (Hz)	$\frac{m_n^2(f_-)}{\lvert h_n\rvert^2 E_s}$	$\frac{m_n^2(f_+)}{\lvert h_n\rvert^2 E_s}$
1	500	463	0.023	0.883	6.18	–334	463	0.69	1
2	500	926	0.046	0.597	3.59	–523	926	0.25	1

Example 10.15 Doppler tracking in 64FSK at 14.4 kbps (Table 10.3)
Consider a 64FSK link with a bit rate of 14.4 kbps and signal-to-noise ratio $E_s/N_0 = 30$ dB. The symbol rate is $1/T_s = 2400$ sps. The signal-to-noise ratio is high enough to make the measurement of m_{k-1}^2 reliable. From (10.143) calculate $m_k^2/|h_k|^2E_s$ and $m_{k-1}^2/|h_k|^2E_s$. The signal-to-noise ratio in the $(k-1)$th tone for 1 GHz is $\mathbf{E}(m_{k-1}^2)/N_0 = (E_s/N_0)[(\sin^2 \pi f T_s)/(\pi[1+fT_s])^2] = 1000\ (0.023) = 23$ or about 14 dB. The signal-to-noise ratio in the $(k-1)$th tone for 2 GHz is $\mathbf{E}(m_{k-1}^2)/N_0 = (E_s/N_0)[(\sin^2 \pi f T_s)/(\pi[1+fT_s])^2] = 1000\ (0.046) = 46$ or about 17 dB. The signal-to-intertone interference ratio for 1 GHz is $m_k^2/m_{k-1}^2 = 0.883/0.023 = 38.4$ or 16 dB and that for 2 GHz is $m_k^2/m_{k-1}^2 = 0.597/0.046 = 13$ or 11 dB as compared to infinity for zero Doppler shift. For 2 GHz, the Doppler effect dominates the effect of the channel noise.
■

Doppler tracking of CSK

CSK is a modulation technique employed on the reverse link of IS-95. The set of M orthogonal Walsh functions represents M distinct symbols. Let us consider a CSK signal for the ith symbol at carrier frequency f_c with Walsh function $w_k(t)$ as $s(t) = |h_k|Aw_k(t)\cos[2\pi(f_c+f)t+\theta_k] + n(t)$, $iT_s \le t < (i+1)T_s$. The signal is assumed to experience a Doppler shift f and fade h_k. *Slow fading in a symbol time* is also assumed so that the channel phase shift θ_k can be considered *constant* within a symbol time T_s. The Walsh chip time is $T_c = T_s/M$. Let us demodulate this signal by first multiplying it with $\sqrt{2/T_s}w_k(t)\cos 2\pi f_c t$ and integrating the resulting signal from $t = iT_s$ to $t = (i+1)T_s$ in order to obtain the kth Walsh's *I-decision sample*:

$$\begin{aligned} X_{k,I} &= \int_{iT_s}^{(i+1)T_s} (|h_k|Aw_k(t)\cos[2\pi(f_c+f)t+\theta_k])\sqrt{2/T_s}w_k(t)\cos 2\pi f_c t\,\mathrm{d}t + N_{k,I} \\ &\approx \frac{|h_k|A}{\sqrt{2T_s}}\int_{iT_s}^{(i+1)T_s}\cos(2\pi f t+\theta_k)\,\mathrm{d}t + N_{k,I} \\ &\approx |h_k|\sqrt{\frac{A^2T_s}{2}}\left(\frac{\sin(2\pi f T_s(i+1)+\theta_k)-\sin(2\pi f T_s i+\theta_k)}{2\pi f T_s}\right) + N_{k,I} \end{aligned} \tag{10.149}$$

Similarly we demodulate this signal by multiplying it with $\sqrt{2/T_s}w_k(t)\sin 2\pi f_c t$ and integrating the resulting signal from $t = iT_s$ to $t = (i+1)T_s$ in order to obtain the kth Walsh's *I-decision sample*:

$$\begin{aligned} X_{k,Q} &= \int_{iT_s}^{(i+1)T_s} (|h_k|Aw_k(t)\cos[2\pi(f_c+f)t+\theta_k])\sqrt{2/T_s}w_k(t)\sin 2\pi f_c \mathrm{t}\,\mathrm{d}t + N_{l,Q} \\ &\approx -\frac{|h_k|A}{\sqrt{2T_s}}\int_{iT_s}^{(i+1)T_s}\sin(2\pi ft+\theta_k)\,\mathrm{d}t + N_{l,Q} \\ &\approx |h_k|\sqrt{\frac{A^2T_s}{2}}\left(\frac{\cos(2\pi fT_s(i+1)+\theta_k)-\cos(2\pi fT_s i+\theta_k)}{2\pi fT_s}\right) + N_{l,Q} \end{aligned} \tag{10.150}$$

Both $N_{l,I}$ and $N_{l,Q}$ are independent Gaussian random variables with zero mean and variance $\sigma^2 = N_0/2$. The high-frequency term is insignificant compared to the first term and is dropped from the above expression. The decision variable of the kth Walsh function is given by

$$X_k = \sqrt{X_{k,I}^2 + X_{k,Q}^2} \tag{10.151}$$

Thus, X_k is *Rice* distributed and its density function is given as

$$f_{X_k}(x_k) = \frac{x_k}{\sigma^2}\mathrm{e}^{-(x_k^2+m_k^2)/2\sigma^2}I_0\left(\frac{m_k x_k}{\sigma^2}\right) \tag{10.152}$$

where the parameter m_k^2 is the sum of the squares of the means of $X_{k,I}$ and $X_{k,Q}$ and is expressed as

$$\begin{aligned} m_k^2 &= \left(\overline{X}_{k,I}\right)^2 + \left(\overline{X}_{k,Q}\right)^2 \\ &= |h_k|^2 E_s \frac{\sin^2 \pi fT_s}{(\pi fT_s)^2} \end{aligned} \tag{10.153}$$

where $\sqrt{A^2T_s/2}$ is the symbol energy.

Let us now establish the decision variable of the lth Walsh function $w_l(t)$. In the case of *zero Doppler shift*, this decision variable represents the envelope of Gaussian noise and is Rayleigh distributed. We have

$$\begin{aligned} X_{l,I} &= \int_{iT_s}^{(i+1)T_s} (|h_k|Aw_k(t)\cos[2\pi(f_c+f)t+\theta_k])\sqrt{2/T_s}w_l(t)\cos 2\pi f_c t\,\mathrm{d}t + N_{l,I} \\ &\approx \frac{|h_k|A}{\sqrt{2T_s}}\int_{iT_s}^{(i+1)T_s} w_k(t)w_l(t)\cos(2\pi ft+\theta_k)\,\mathrm{d}t + N_{l,I} \\ &\approx \frac{|h_k|A}{\sqrt{2T_s}}\int_{iT_s}^{(i+1)T_s} w_j(t)\cos(2\pi ft+\theta_k)\,\mathrm{d}t + N_{l,I} \end{aligned} \tag{10.154}$$

Note that the *product of two Walsh functions* in the same set is another Walsh function in the same set (*closure property*). Without loss of generality we choose the Walsh function that represents the sequence of $M/2$ zeros followed by $M/2$ one or, in term of ± 1 amplitudes, the sequence of $M/2$ *plus one amplitudes* followed by $M/2$ *minus one amplitudes*, namely,

$$\boldsymbol{w}_l = (\underbrace{11,\ldots 1}_{M/2}, \underbrace{-1-1,\ldots -1}_{M/2})$$

This is the $(M/2+1)$th row of the Hadamard matrix. Thus we get

$$\begin{aligned} X_{l,I} &\approx \frac{|h_k|A}{\sqrt{2T_s}} \int_{iT_s}^{(i+1)T_s} w_j(t)\cos(2\pi ft+\theta_k)\,\mathrm{d}t + N_{l,I} \\ &\approx \frac{|h_k|A}{\sqrt{2T_s}} \left[\int_{iT_s}^{(i+1/2)T_s} \cos(2\pi ft+\theta_k)\,\mathrm{d}t - \int_{(i+1/2)T_s}^{(i+1)T_s} \cos(2\pi ft+\theta_k)\,\mathrm{d}t \right] + N_{l,I} \\ &\approx |h_k|\sqrt{\frac{A^2T_s}{2}} \left[\begin{array}{c} \frac{\sin(2\pi fT_s(i+1/2)+\theta_k)-\sin(2\pi fT_si+\theta_k)}{2\pi fT_s} \\ -\frac{\sin(2\pi fT_s(i+1)+\theta_k)-\sin(2\pi fT_s(i+1/2)+\theta_k)}{2\pi fT_s} \end{array} \right] + N_{l,I} \\ &\approx |h_k|\sqrt{\frac{A^2T_s}{2}} \left[\frac{2\,\sin(2\pi fT_s(i+1/2)+\theta_k) - \sin(2\pi fT_si+\theta_k) - \sin(2\pi fT_s(i+1)+\theta_k)}{2\pi fT_s} \right] \\ &\quad + N_{l,I} \end{aligned} \tag{10.155}$$

Similarly we demodulate this signal by multiplying it with $\sqrt{2/T_s}w_l(t)\sin 2\pi f_c t$ and integrating the resulting signal from $t = iT_s$ to $t = (i+1)T_s$ in order to obtain the lth Walsh's *Q-decision sample*:

$$\begin{aligned} X_{l,Q} &= \int_{iT_s}^{(i+1)T_s} (|h_k|Aw_k(t)\cos[2\pi(f_c+f)t+\theta_k])\sqrt{2/T_s}w_l(t)\sin 2\pi f_c t\,\mathrm{d}t + N_{l,Q} \\ &\approx -\frac{|h_k|A}{\sqrt{2T_s}} \int_{iT_s}^{(i+1)T_s} w_j(t)\sin(2\pi ft+\theta_k)\,\mathrm{d}t + N_{l,I} \\ &\approx |h_k|\sqrt{\frac{A^2T_s}{2}} \left[\frac{2\,\cos(2\pi fT_s(i+1/2)+\theta_k) - \cos(2\pi fT_si+\theta_k) - \cos(2\pi fT_s(i+1)+\theta_k)}{2\pi fT_s} \right] \\ &\quad + N_{l,Q} \end{aligned} \tag{10.156}$$

Consequently, we obtain

$$\begin{aligned} m_l^2 &= \left(\overline{X}_{l,I}\right)^2 + \left(\overline{X}_{l,Q}\right)^2 \\ &= |h_k|^2 E_s \frac{16\sin^2(\pi fT_s/2) - 4\sin^2\pi fT_s}{(2\pi fT_s)^2} \end{aligned} \tag{10.157}$$

The bit error probability of CSK is identical to that of MFSK discussed in the previous section.

The Doppler shift f can be calculated in the case of *small noise* by establishing the ratio $r^2 = m_k^2/m_l^2$, which is called the *signal-to-interchannel interference ratio*. For a given value of r we obtain two Doppler shift values, one negative and one positive, as follows:

$$\begin{aligned} &f_- = -\frac{2}{\pi T_s}\cos^{-1}\left(\frac{1}{\sqrt{1+1/r^2}}\right),\ f_+ = \frac{2}{\pi T_s}\cos^{-1}\left(\frac{1}{\sqrt{1+1/r^2}}\right), \\ &r^2 = \frac{m_k^2}{m_l^2}, \quad \boldsymbol{w}_l = (\underbrace{11,\ldots 1}_{M/2}, \underbrace{-1-1,\ldots -1}_{M/2}) \end{aligned} \tag{10.158}$$

Table 10.4 Decision-feedback selection for 64CSK

Carrier frequency (GHz)	Speed (km/h)	Doppler shift f (Hz)	$\frac{m_l^2}{\lvert h_k\rvert^2 E_s}$	$\frac{m_k^2}{\lvert h_k\rvert^2 E_s}$	r	f_- (Hz)	f_+ (Hz)	$\frac{m_n^2(f_-)}{\lvert h_n\rvert^2 E_s}$	$\frac{m_n^2(f_+)}{\lvert h_n\rvert^2 E_s}$
1	500	463	0.086	0.883	3.2	–463	463	0.596	1
2	500	926	0.287	0.597	1.44	–926	926	0.073	1

The *sign ambiguity* of the Doppler shifts can be resolved if the movement of both transmitter and receiver is known (moving toward or moving away from each other). The global positioning system (GPS) can supplement the receiver with the sign information. The Doppler shift can be employed by a tracking phase-locked loop (PLL) to demodulate the signal and cancel out the Doppler effect. In practice, the *noisy* ratio r^2 is obtained as $r^2 = X_k^2/X_l^2$. The frequency jitter due to noise determines the accuracy of the estimate of the Doppler shift.

The sign ambiguity of the Doppler shifts can also be resolved via the use of dual demodulators with a PLL tracking Doppler shift f_- and another PLL tracking f_+ using the following *decision-feedback selection* algorithm. Suppose the ith symbol in the symbol stream represented by Walsh function $w_k(t)$ was correctly detected. The Doppler shifts f_- and f_+ are then estimated as described in (10.158). The dual demodulators demodulate the next $(i + 1)$th symbols (two of them) represented by Walsh function $w_n(t)$. The values of $X_n^2(f_-)$ and $X_n^2(f_+)$ are compared and the $(i + 1)$th symbol corresponding to the *larger value* is selected. Suppose the correct Doppler shift is $f_- \approx f$ and assume that the signal-to-noise ratio is high, then the decision variables for the dual demodulators are

$$X_n^2(f_-) \approx m_n^2(f_-) = |h_n|^2 E_s \left(\sin^2[\pi(f - f_-)T_s]/(\pi(f - f_-)T_s)^2 \right) \approx |h_n|^2 E_s$$

and

$$X_n^2(f_+) \approx m_n^2(f_+) = |h_n|^2 E_s \left(\sin^2[\pi(f - f_+)T_s]/(\pi(f - f_+)T_s)^2 \right) < |h_n|^2 E_s.$$

The decision is to select the symbol corresponding to $X_n^2(f_-)$.

Example 10.16 Doppler tracking in 64CSK at 14.4 kbps (Table 10.4)

Consider a 64CSK link with a bit rate of 14.4 kbps and signal-to-noise ratio $E_s/N_0 = 30$ dB. The symbol rate is $1/T_s = 2400$ sps. The signal-to-noise ratio is high enough to make the measurement of m_l^2 reliable. From (10.153) and from (10.157) calculate $m_k^2/|h_k|^2 E_s$ and $m_l^2/|h_k|^2 E_s$. The signal-to-noise ratio in the lth channel for 1 GHz is $\mathbf{E}(m_l^2)/N_0 = (E_s/N_0)[(16\sin^2 \pi f T_s/2 - 4\sin^2 \pi f T_s)/(2\pi f T_s)^2] = 1000(0.086) = 86$ or about 19 dB. The signal-to-noise ratio in the lth channel for 2 GHz is $\mathbf{E}(m_l^2)/N_0 = (E_s/N_0)[(16\sin^2 \pi f T_s/2 - 4\sin^2 \pi f T_s)/(2\pi f T_s)^2] = 1000(0.287) = 287$ or about 25 dB. The signal-to-intertone interference ratio for 1 GHz is $m_k^2/m_l^2 = 0.883/0.086 = 10.3$ or 10 dB and that for 2 GHz is $m_k^2/m_l^2 = 0.597/0.287 = 2.1$ or 3 dB as compared to infinity for zero Doppler shift. For both cases, the Doppler effects dominate the effect of the channel noise. Comparing the results in Tables 10.3 and 10.4 we observe that Doppler effect is more pronounced in CSK than in MFSK given the same Doppler shift. With CSK, the orthogonality is achieved via *orthogonal time functions*. On the other hand, MFSK achieves orthogonality via *orthogonal sinusoidal tones*. The sinusoidal tones do not change phases during

a symbol time while Walsh functions may change phases every chip time. This effect causes a larger leakage of signal energy onto other Walsh channels when Doppler shift is present and leads to larger signal-to-interchannel interferences.

■

10.7 Pilot tone-aided demodulation of orthogonal covering signal

In this section we provide the modulation and demodulation of generalized quadrature orthogonal covering signals where IS-95, CDMA 2000, and WCDMA forward links are a special case. We introduce the concept of *complex spreading and despreading* to eliminate the *I-Q crosstalk interference* in real spreading and despreading first introduced in Chapter 8.

Complex spreading and despreading

In complex spreading an arbitrary input I-bit d_k and an input Q-bit $\hat{d}_k$ normalized to the smallest symbol energy $E = A^2 T_s/2$, such as those in MPSK or MQAM, are first modulo-2 added to a Walsh sequence unique for a user k. The spread I-bit is then modulo-2 added to the I-PN sequence c_I, and the spread Q-bit is added to the Q-PN sequence c_Q. These I- and Q-bits of 0s and 1s are mapped into 1s and −1s. Their difference is the *transmitted I-bit*. Similarly, the same spread Q-bit is modulo-2 added to the I-PN sequence and the same spread I-bit is modulo-2 added to the Q-PN sequence. These I- and Q-bits of 0s and 1s are mapped into 1s and −1s and their sum is the resulting *transmitted Q-bit*. The transmitted I-bits of all M users are added together and the transmitted Q-bits of all M users are also added together. The *sum I- and sum Q-bits* are pulse-shaped and then used to modulate the I-Q carriers. The *complex spreading* is summarized in the following *I- and Q-baseband* signals:

$$s_{L,I}(t) = \sum_{k=1}^{M} \left[d_k c_I(t) - \hat{d}_k c_Q(t) \right] w_k(t) \tag{10.159}$$

$$s_{L,Q}(t) = \sum_{k=1}^{M} \left[\hat{d}_k c_I(t) + d_k c_Q(t) \right] w_k(t) \tag{10.160}$$

The complex baseband signal $s_L(t) = s_{L,I}(t) + \mathrm{j}s_{L,Q}(t)$ is the envelope of the orthogonal covering signal $s(t) = \mathrm{Re}\left[s_L(t) \mathrm{e}^{\mathrm{j}2\pi f_c t} \right]$, and is given by

$$s_L(t) = s_{L,I}(t) + \mathrm{j}s_{L,Q}(t) = \sum_{k=1}^{M} \boldsymbol{d}_k \boldsymbol{c}(t) w_k(t) \tag{10.161}$$

where $\boldsymbol{d}_k = d_k + \mathrm{j}\hat{d}_k$ is the *complex symbol* and $\boldsymbol{c}(t) = c_I(t) + \mathrm{j}c_Q(t)$ is the *complex PN function*, hence the name complex spreading.

Complex despreading is achieved by the following operation:

$$\begin{aligned} 2s(t)\left[\boldsymbol{c}^*(t)\mathrm{e}^{-\mathrm{j}2\pi f_c t}\right] &= 2\mathrm{Re}\left[s_L(t)\mathrm{e}^{\,\mathrm{j}2\pi f_c t}\right]\boldsymbol{c}^*(t)\mathrm{e}^{-\mathrm{j}2\pi f_c t} \\ &= \left[s_L(t)\mathrm{e}^{\,\mathrm{j}2\pi f_c t} + s_L^*(t)\mathrm{e}^{-\mathrm{j}2\pi f_c t}\right]\boldsymbol{c}^*(t)\mathrm{e}^{-\mathrm{j}2\pi f_c t} \\ &= s_L(t)\boldsymbol{c}^*(t) + s_L^*(t)\boldsymbol{c}^*(t)\mathrm{e}^{-\mathrm{j}4\pi f_c t} \end{aligned} \tag{10.162a}$$

The high-frequency term is filtered out, and the following operation results:

$$\begin{aligned} s_L(t)\boldsymbol{c}^*(t) &= s_L(t)[c_I(t) - \mathrm{j}c_Q(t)] = [s_{L,I}(t) + \mathrm{j}s_{L,Q}(t)][c_I(t) - \mathrm{j}c_Q(t)] \\ &= [s_{L,I}(t)c_I(t) + s_{L,Q}(t)c_Q(t)] + \mathrm{j}[s_{L,Q}(t)c_I(t) - s_{L,I}(t)c_Q(t)] \end{aligned} \tag{10.162b}$$

The I-value is given by

$$\begin{aligned} s_{L,I}(t)c_I(t) + s_{L,Q}(t)c_Q(t) &= \sum_{k=1}^{M}\left[d_k c_I^2(t) - \hat{d}_k c_I(t)c_Q(t)\right]w_k(t) \\ &\quad + \sum_{k=1}^{M}\left[\hat{d}_k c_I(t)c_Q(t) + d_k c_Q^2(t)\right]w_k(t) \\ &= \sum_{k=1}^{M} d_k w_k(t) + \sum_{k=1}^{M} d_k w_k(t) \\ &= 2\sum_{k=1}^{M} d_k w_k(t) \end{aligned} \tag{10.163}$$

and the Q-value is

$$\begin{aligned} s_{L,Q}(t)c_I(t) - s_{L,I}(t)c_Q(t) &= \sum_{k=1}^{M}\left[\hat{d}_k c_I^2(t) + d_k c_I(t)c_Q(t)\right]w_k(t) \\ &\quad - \sum_{k=1}^{M}\left[d_k c_I(t)c_Q(t) - \hat{d}_k c_Q^2(t)\right]w_k(t) \\ &= \sum_{k=1}^{M} \hat{d}_k w_k(t) + \sum_{k=1}^{M} \hat{d}_k w_k(t) \\ &= 2\sum_{k=1}^{M} \hat{d}_k w_k(t) \end{aligned} \tag{10.164}$$

The I- and Q-bits contain no I-Q crosstalk interference with complex spreading and despreading. Figure 10.10 shows the modulator for the complex spreading orthogonal covering signal. Figure 10.11 shows the mathematically equivalent complex modulator where the lines are used for complex operations.

Doppler analysis

The received quadrature orthogonal covering signal can be represented in an arbitrary symbol interval $lT_s < t \leq (l+1)T_s$ as follows:

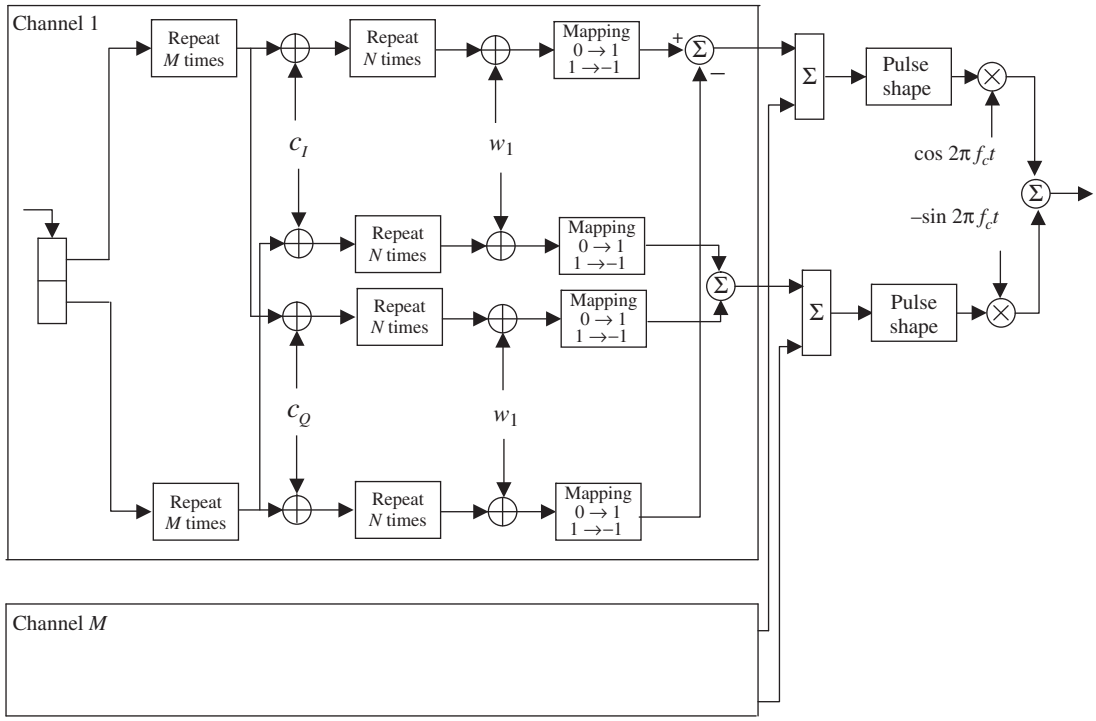

Figure 10.10 Complex spreading orthogonal covering modulator.

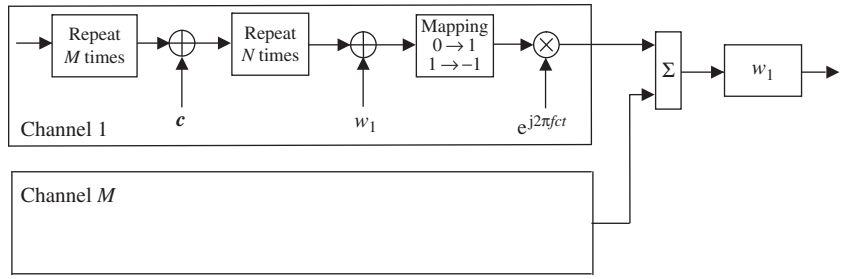

Figure 10.11 Equivalent complex-valued modulator.

$$r(t) = |h|A\sum_{k=1}^{M}\left[d_k c_I(t) - \hat{d}_k c_Q(t)\right] w_k(t)\cos\left[2\pi(f_c + f)t + \theta\right]$$
$$- |h|A\sum_{k=1}^{M}\left[\hat{d}_k c_I(t) + d_k c_Q(t)\right] w_k(t)\sin\left[2\pi(f_c + f)t + \theta\right] + n(t)\,, \qquad (10.165)$$
$$lT_s < t \leq (l+1)T_s$$

where d_k and $\hat{d}_k$ are the lth in-phase and quadrature bits in the kth channel normalized to the smallest symbol energy $E = A^2 T_s/2$, respectively. The I- and Q-channel PN functions are $c_I(t)$ and $c_Q(t)$, respectively. The phase θ represents the channel phase shift (the phase of the

channel tap $h = |h|\mathrm{e}^{\mathrm{j}\theta}$) and the arbitrary phase of the carrier. We assume the channel tap is time-invariant in a symbol time, that is, the channel fading rate is much smaller than the symbol rate. The phase θ represents the phase error between $s(t)$ and the local carrier that translates it to baseband. We assume that noise $n(t)$ has the power spectral density $N_0/2$ (W/Hz). In terms of the complex envelope representation we have

$$r(t) = \mathrm{Re}\left[r_L(t)\,\mathrm{e}^{\mathrm{j}2\pi f_c t}\right] + n(t) \tag{10.166}$$

where the complex envelope $r_L(t)$ is given by the following expression:

$$r_L(t) = Ah\mathrm{e}^{\mathrm{j}2\pi ft}\sum_{k=1}^{M}\boldsymbol{d}_k\boldsymbol{c}(t)w_k(t) \tag{10.167}$$

The complex PN sequence $\boldsymbol{c}(t)$ and the complex symbol $\boldsymbol{d}_k$ are given by

$$\boldsymbol{c}(t) = c_I(t) + \mathrm{j}c_Q(t), \boldsymbol{d}_k = d_k + \mathrm{j}\hat{d}_k \tag{10.168}$$

With the aid of the pilot symbol, the channel tap h is available and is used to demodulate the signal $r(t)$ to *complex baseband* via a complex local carrier $\sqrt{2/T_s}(h^*/|h|)\mathrm{e}^{-\mathrm{j}2\pi f_c t}$. Next, the *complex despreading* process is carried out by multiplying the complex baseband signal by $\boldsymbol{c}^*(t)/2$, where $|\boldsymbol{c}(t)|^2 = 2$. Then, the *dechannelization* process is carried out to separate individual channels via the multiplication of the despreading baseband signal with $w_m(t)$, where $w_m^2(t) = 1$. The signal processing part is completed via the integration of the complex dechannelized signal over a symbol time to obtain the predetection *complex sample* X_m. We have

$$\begin{aligned} X_m &= \int_{lT_s}^{(l+1)T_s} A\sqrt{\frac{1}{2T_s}}|h|\mathrm{e}^{\mathrm{j}2\pi ft}\sum_{k=1}^{M}\boldsymbol{d}_k w_k(t)w_m(t)\,\mathrm{d}t + N_m \\ &= |h|\sum_{k=1}^{M}\left[A\sqrt{\frac{1}{2T_s}}\boldsymbol{d}_k\right]\int_{lT_s}^{(l+1)T_s} w_k(t)w_m(t)\mathrm{e}^{\mathrm{j}2\pi ft}\,\mathrm{d}t + N_m \\ &= |h|\sum_{k=1}^{M}\gamma_{k,m}s_{i,k} + N_m \end{aligned} \tag{10.169}$$

where $s_{i,k}$ (hypothesis H_i) with energy $E_{i,k} = \left|s_{i,k}\right|^2$ and *complex Doppler factor* $\gamma_{k,m}$ are given by

$$\begin{aligned} &s_{i,k} = \sqrt{\frac{A^2T_s}{2}}\boldsymbol{d}_k = \sqrt{E}\boldsymbol{d}_k, \quad E_{i,k} = \left|s_{i,k}\right|^2 = E|\boldsymbol{d}_k|^2, \quad E = \text{smallest symbol energy} \\ &\gamma_{k,m} = \frac{1}{T_s}\int_{lT_s}^{(l+1)T_s} w_k(t)w_m(t)\mathrm{e}^{\mathrm{j}2\pi ft}\,\mathrm{d}t \end{aligned} \tag{10.170}$$

Note that, with zero Doppler shift, the term $\gamma_{k,m}$ is 1 for $k = m$ and 0 for $k \neq m$, since the product of two different complex Walsh functions is another complex Walsh function in the same set (*closure property*) and the integration over its period is always zero except for the first Walsh function (Walsh sequences have the same number of zeros and ones except for the first Walsh sequence). The Gaussian noise variable N_m has zero mean and variance $N_0/2$.

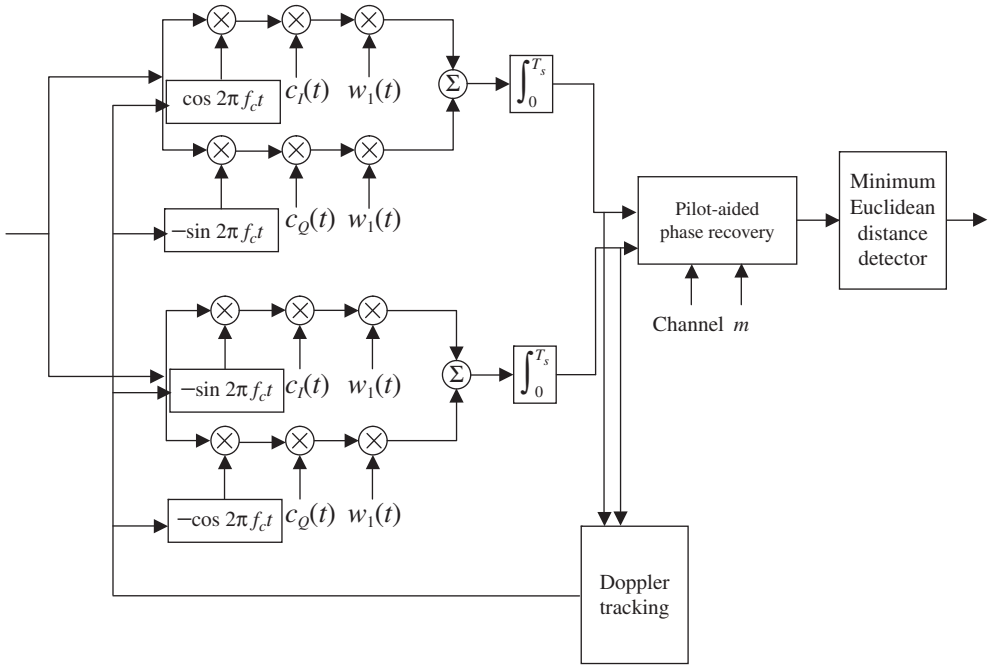

Figure 10.12 Pilot-aided demodulation of complex spreading orthogonal covering signal with Doppler tracking of local in-phase and quadrature carriers.

The lth symbol sample in *Walsh channel m* can alternatively be expressed as

$$\begin{aligned} X_m &= |h|\gamma_{m,m}s_{i,m} + I_m + N_m = \mathbf{h}_{m,m}s_{i,m} + \mathbf{N}_m \\ I_m &= \sum_{\substack{k=1 \\ k\neq m}}^{M} \mathbf{h}_{k,m}s_{i,k}, \mathbf{N}_m = I_m + N_m \end{aligned} \tag{10.171}$$

where $\mathbf{h}_{k,m} = |h|\gamma_{k,m}$, and the term I_m is the *interchannel interference* (ICI) caused by the Doppler shift that destroys the orthogonality of the orthogonal covering signal. Note that $|\gamma_{m,m}| \leq 1$ and, therefore, both pilot and data symbols experience losses in their magnitudes which translate into losses in the signal power. We have seen this phenomenon before in OFDM and CSK with noncoherent demodulation. The *interchannel interference* in an orthogonal covering signal is an analogy of the *intercarrier interference* (ICI) in OFDM. Since the pilot tone is transmitted on the same carrier as the data signals, there is no *differential Doppler phase error* between the received pilot and data symbols. The bit error probability of a Walsh channel is evaluated in a similar manner to OFDM, with appropriate replacement of variables. Figures 10.12 and 10.13 show the demodulators for the complex spreading orthogonal covering signal with Doppler tracking.

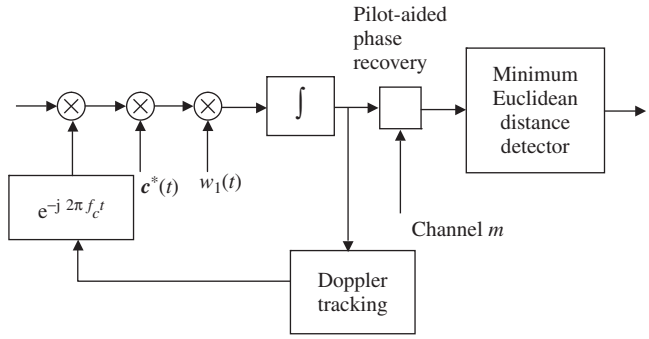

Figure 10.13 Equivalent complex-valued demodulator.

Example 10.17 Variance of interchannel interference

The variance of interchannel interference (ICI) in each Walsh channel indicates the degree of non-orthogonality experienced by a quadrature orthogonal covering signal due to Doppler shift. For I-Q signals such as MPSK and rectangular MQAM, the symbols are independent and have zero mean. Furthermore, we have $\mathbf{E}\left(|h_i|^2\right) = 1$ by convention. Thus, from (10.171) the ICI variance can be simplified as follows:

$$\begin{aligned}\sigma_{I_m}^2 &= \mathbf{E}\left(|I_m|^2\right) = \sum_{\substack{k=1\\k\neq m}}^{M}\sum_{\substack{l=1\\l\neq m}}^{M}\mathbf{E}\left(|h|^2\right)\mathbf{E}\left(s_{i,k}s_{i,l}^*\right)\gamma_{k,m}\gamma_{l,m}^* \\ &= \sum_{\substack{k=1\\k\neq m}}^{M}\mathbf{E}\left(|s_{i,k}|^2\right)|\gamma_{k,m}|^2\end{aligned} \tag{10.172}$$

The parameter $|\gamma_{k,m}|^2$ has been calculated in (10.157) using the Walsh function that represents the $(M/2+1)$th row of the Hadamard matrix as follows:

$$|\gamma_{k,m}|^2 = \frac{16\sin^2(\pi f T_s/2) - 4\sin^2\pi f T_s}{(2\pi f T_s)^2} \tag{10.173}$$

■

The remaining question is how to estimate the Doppler frequency. A training pilot sequence can be transmitted in the packet header of each transmitted packet to allow for the estimation of the Doppler shift. Only the pilot Walsh channel is used during this estimation time, that is, the orthogonal covering signal is actually a single-carrier signal. Data symbols in all other Walsh channels are set to zero to avoid ICI. The training sequence enhances the estimation of the Doppler shift via the *decision-feedback algorithm* since all training pilot symbols are known a priori. If a training pilot symbol is detected incorrectly, it can be corrected via the knowledge of its position in the sequence relative to the previously correctly detected pilot symbol. Since only a single Walsh channel is used the channel phase shift is eliminated by

the detection process in (10.100), assuming that it is constant for each symbol time. In practice the training pilot sequence is short and the channel phase shift remains constant with high probability during the entire sequence. The *differential Doppler phase error for each training symbol* can be estimated and averaged out for the entire training sequence. The Doppler shift f can be corrected by using the average differential Doppler phase error $\hat{\varepsilon}$ of the training sequence to drive a VCO to correct the phase of the local in-phase and quadrature carriers. This is equivalent to multiplying the right-hand side of (10.167) by $e^{-j2\pi ft}$ to obtain the Doppler-corrected received envelope:

$$r_L(t) = Ah \sum_{k=1}^{M} \boldsymbol{d}_k \boldsymbol{c}(t) w_k(t) \tag{10.174}$$

This is also the complex baseband signal for the low-mobility case without interchannel interference. Thus, the complex spreading orthogonal covering signal has the same performance as the single channel discussed previously. Mathematically, the decision variable X_p in (10.169) for a training pilot sequence with the all-zero Walsh function is given as follows:

$$\begin{aligned} X_p &= \int_{lT_s}^{(l+1)T_s} A\sqrt{\frac{1}{2T_s}} |h| e^{j2\pi ft} \boldsymbol{d}_p dt + N_p \\ &= |h||\alpha| e^{j2\pi f(l+1/2)T_s} \left[\sqrt{\frac{A^2 T_s}{2}} \boldsymbol{d}_p \right] + N_p \\ &= \mathbf{h} s_p + N_p \end{aligned} \tag{10.175}$$

where $|\alpha|$ is given in (10.98). The *Doppler phase error* $(\mathbf{h}/|\mathbf{h}|)$ can be estimated from the knowledge of the pilot symbol s_p and used to correct the Doppler effect.

10.8 Noncoherent demodulation of offset quadrature DS-CSK

IS-95 employs noncoherent *offset* quadrature DS-CSK. Let us consider such a received DS-CSK signal $r(t)$ at carrier frequency f_c with Walsh function $w_k(t)$ and PN functions $c_I(t)$ and $c_Q(t)$ during the ith symbol interval as

$$\begin{aligned} r(t) = &\frac{|h_k|A}{\sqrt{2}} c_I(t) w_k(t) \cos[2\pi(f_c + f)t + \theta_k] \\ &- \frac{|h_k|A}{\sqrt{2}} c_Q(t - T_c/2) w_k(t - T_c/2) \sin[2\pi(f_c + f)t + \theta_k] + n(t), \\ &\qquad\qquad iT_s < t \le (i+1)T_s \end{aligned} \tag{10.176}$$

The I- and Q-channel PN functions are $c_I(t)$ and $c_Q(t)$, respectively. The phase θ_k represents the phase of the channel tap h_k. We assume that the channel tap is time-invariant in a symbol time, that is, the channel fading rate is much smaller than the symbol rate. We assume that

noise $n(t)$ has the power spectral density $N_0/2$ (W/Hz). In terms of complex envelope representation we have

$$r(t) = \mathrm{Re}\left[r_L(t)\,\mathrm{e}^{\mathrm{j}2\pi f_c t}\right] + n(t) \tag{10.177}$$

where the complex envelope $r_L(t)$ is given by the following expression:

$$r_L(t) = \frac{A|h_k|}{\sqrt{2}}\mathrm{e}^{\mathrm{j}\theta_k}\mathrm{e}^{\mathrm{j}2\pi ft}\boldsymbol{c}(t) \tag{10.178}$$

The complex function $\boldsymbol{c}(t)$ is given by

$$\boldsymbol{c}(t) = c_I(t)w_k(t) + \mathrm{j}c_Q(t - T_c/2)w_k(t - T_c/2) \tag{10.179}$$

The signal $r(t)$ is first translated to *complex baseband* by a complex local carrier $\sqrt{2/T_s}\mathrm{e}^{-\mathrm{j}2\pi f_c t}$, which is offset by the unknown phase θ_k with respect to $r(t)$. Next, the *complex despreading* process is carried out by multiplying the complex baseband signal with $\boldsymbol{c}^*(t)$, where $|\boldsymbol{c}(t)|^2 = 2$. The signal processing part is completed via the integration of the complex despreading signal over a symbol time to obtain the M predetection *complex samples* X_m. We have

$$\begin{aligned} X_m &= \int_{iT_s}^{(i+1)T_s} A\sqrt{\frac{1}{2T_s}}|h_k|\mathrm{e}^{\mathrm{j}\theta_k}\mathrm{e}^{\mathrm{j}2\pi ft}\boldsymbol{c}_k(t)\boldsymbol{c}_m^*(t)\,\mathrm{d}t + N_m \\ &= |h_k|\mathrm{e}^{\mathrm{j}\theta_k}A\sqrt{\frac{1}{2T_s}}\int_{iT_s}^{(i+1)T_s}\boldsymbol{c}_k(t)\boldsymbol{c}_m^*(t)\mathrm{e}^{\mathrm{j}2\pi ft}\,\mathrm{d}t + N_m \\ &= \sqrt{E_s}\,|h_k|\mathrm{e}^{\mathrm{j}\theta_k}\sum_{k=1}^{M}\gamma_{k,m} + N_m \end{aligned} \tag{10.180}$$

where the symbol energy E_s and *complex Doppler factor* $\gamma_{k,m}$ are given by

$$\begin{aligned} E_s &= \frac{A^2T_s}{2} \\ \gamma_{k,m} &= \frac{1}{T_s}\int_{iT_s}^{(i+1)T_s}\boldsymbol{c}_k(t)\boldsymbol{c}_m^*(t)(t)e^{\mathrm{j}2\pi ft}\,\mathrm{d}t \end{aligned} \tag{10.181}$$

Let us consider the case of *zero Doppler shift*, where the term $\gamma_{k,m}$ is 2 for $k = m$. For $k \neq m$, $\gamma_{k,m}$ is not zero as expected because the *I-Q crosstalk* is present due to a half-chip delay in the Q-channel. This *I-Q crosstalk* is much smaller than 2 and can be ignored. Without the half-chip delay there would be no I-Q crosstalk and $\gamma_{k,m}$ would be zero for $k \neq m$. The complex Gaussian noise variable N_m has independent I-noise and Q-noise, each with zero mean and variance N_0. The M decision variables at the input of the maximum detector are $|X_m|^2, m = 1, 2, \ldots, M$. The bit error probability of noncoherent offset quadrature DS-CSK is identical to that of noncoherent MFSK and CSK, which were presented in Section 10.7. The Doppler tracking method is also identical to that of noncoherent CSK. Figure 10.14 shows the block diagram of the noncoherent demodulator for offset quadrature DS-CSK.

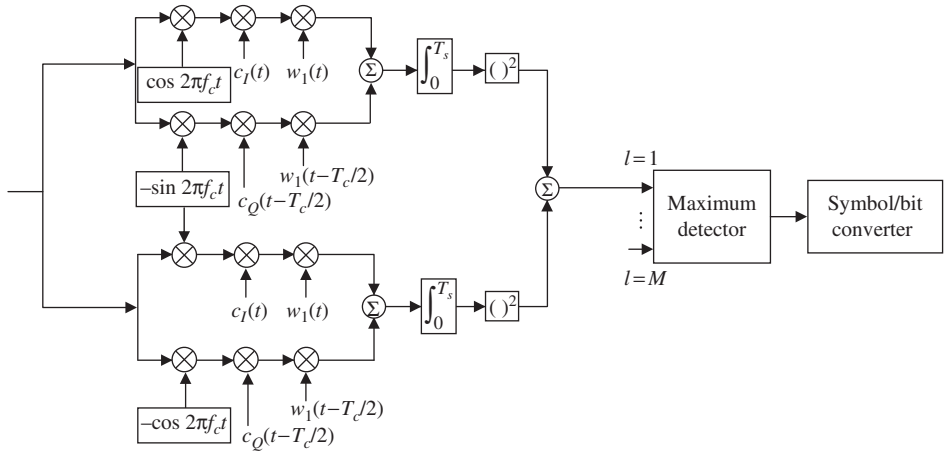

Figure 10.14 Noncoherent demodulator for offset quadrature DS-CSK.

10.9 Time diversity

In a fading channel a deep fade can force the *signal-to-noise ratio* to fall below an operational threshold. Consequently, an outage of the communication link occurs with the loss of many symbols. There are two techniques to counter the effect of deep fades, namely, *error-correction coding* (Chapter 4) and *diversity*. In fact, diversity is a modified form of the *repetition code* with rate $1/n$. In practice, diversity is physically implemented in a variety of ways such as *time diversity*, *frequency diversity*, and *antenna diversity*. The purpose of diversity is to provide the receiver copies of the same symbol transmitted via L subchannels that experience *independent* fades (*L-fold* diversity). The plan is to rely on the low probability of simultaneous outages on all L subchannels to increase the survivability of symbols transmitted in deep fades occurring on a subset of L subchannels. We first discuss time diversity and move on to frequency diversity and antenna diversity in later sections.

Time diversity is a *controlled* diversity method implemented by repeating a transmitted symbol L times. The repeated symbols are then *interleaved* over a *time frame* that is much longer than an *average fade duration* (fade duration is defined as the time the signal envelope or signal power stays below a detection threshold). Thus, copies of the same symbol are placed in various symbol slots in the frame. The separation of consecutive symbol slots is longer than an average deep fade. This procedure in effect creates L independent subchannels to counter deep fades on a subset of subchannels. The interleaved symbols will be *deinterleaved* at the receiver into L *consecutive* copies for detection. The interleaving operation can be carried out by *block interleaving*, which is popular in wireless communication systems such as cellular and wireless LANs. A block interleaver is an array with n rows and m columns ($n \times m$ cells). The number of rows n is chosen to be an integer multiple of L. Repeated symbols are written into the interleaver by columns filling all cells. The time frame therefore consists of $n \times m$ symbol slots. The symbols are read out

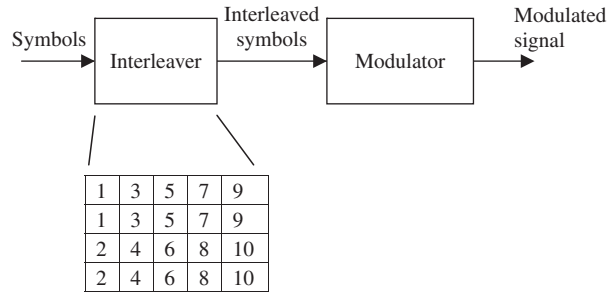

Figure 10.15 Interleaving for time diversity.

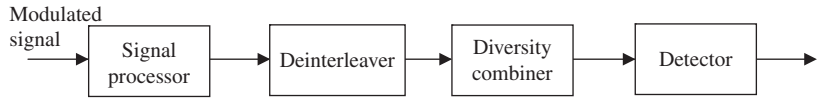

Figure 10.16 Deinterleaving and diversity combining for time diversity.

from the interleaver row by row. Consecutive copies of a symbol are separated by copies of $m - 1$ other symbols. Thus, for the interleaving to be effective the average deep fade should be shorter than m symbol times. Figure 10.15 shows a time diversity ($L = 2$) modulator with a 4×5 interleaver. Figure 10.16 shows a time diversity demodulator with a deinterleaver and a *diversity combiner* to combine the L deinterleaved decision vectors for detection. The decision vectors are sample voltage vectors at the output of the signal processor. Therefore, the deinterleaver works either with *analog* components or with digitally encoded *quantized* components of the vectors. To preserve the same throughput, time diversity increases the symbol rate L times (the transmission bandwidth therefore also increases L times). For a fixed transmitted power, this effectively reduces the symbol energy by a factor of L, which means a higher *channel transition probability*. To be useful, a *diversity combiner* must overcome this problem with a *gain* in the average signal-to-noise ratio at its output so that the detected symbols can have an overall lower error probability.

Level crossing rate

The *average fade duration* given a *threshold voltage level* V determines the separation in time of consecutive copies of a transmitted symbol after interleaving. This quantity, denoted as τ, is defined as the ratio of the sum of fade durations to their number, in a sufficiently large time interval T. We have

$$\tau = \frac{1}{\mathcal{R}_V T} \sum_{i=1}^{\mathcal{R}_V T} \tau_i \tag{10.182}$$

where $\mathcal{R}_V$ is the *level crossing rate*, which is defined as the average rate at which the signal envelope crosses the threshold V in the positive direction, as indicated in Figure 10.17.

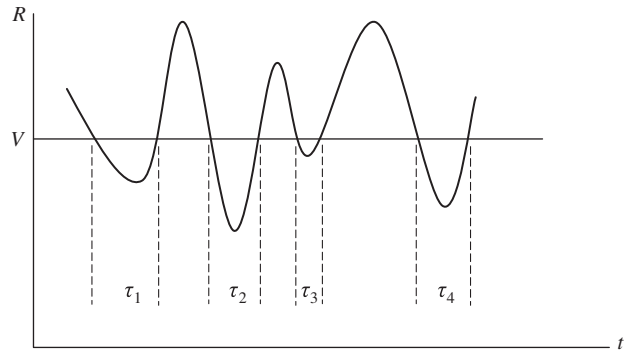

Figure 10.17 Level crossings and fade durations given the signal threshold V.

Thus $\mathcal{N}_V = \mathcal{R}_V T$ is the *average number of level crossings* the signal envelope experiences in the time interval T. We wish to evaluate $\mathcal{R}_V$ in order to calculate τ. Let us denote r as the signal envelope and $\dot{r}$ is its derivative, that is, the slope of the signal envelope. Let us consider the differential quantities $\mathrm{d}t$, $\mathrm{d}r$, and $\mathrm{d}\dot{r}$. We observe that $\mathrm{d}r/\dot{r}$ is the time it takes the signal envelope to go from V to $V + \mathrm{d}r$ once in the positive direction. The average time the signal envelope spends in the range $(V, V + \mathrm{d}r)$ with its slope in the range $(\dot{r}, \dot{r} + \mathrm{d}\dot{r})$ given the time duration $\mathrm{d}t$ is $f(V, \dot{r})\mathrm{d}r\,\mathrm{d}\dot{r}\,\mathrm{d}t$, where $f(r, \dot{r})$ is the *joint density function* of r and $\dot{r}$. The corresponding number of level crossings in $\mathrm{d}t$ is given by $f(V, \dot{r})\mathrm{d}r\,\mathrm{d}\dot{r}\,\mathrm{d}t/(\mathrm{d}r/\dot{r}) = \dot{r}f(V, \dot{r})\,\mathrm{d}\dot{r}\,\mathrm{d}t$. Hence, the average number of level crossings in the time interval T is

$$\mathcal{N}_V = \int_0^T \int_0^\infty \dot{r} f(V, \dot{r})\,\mathrm{d}\dot{r}\,\mathrm{d}t = T \int_0^\infty \dot{r} f(V, \dot{r})\,\mathrm{d}\dot{r} \tag{10.183}$$

Consequently, the level crossing rate is obtained as follows:

$$\mathcal{R}_V = \frac{\mathcal{N}_V}{T} = \int_0^\infty \dot{r} f(V, \dot{r})\,\mathrm{d}\dot{r} \tag{10.184}$$

Rice has shown that the random variables r and $\dot{r}$ are independent and their joint density function for *Rayleigh fading* is given by

$$f(r, \dot{r}) = \left(\frac{r}{\sigma_s^2} \mathrm{e}^{-r^2/2\sigma_s^2}\right)\left(\frac{1}{4\pi^3 \sigma_s^2 f_m^2} \mathrm{e}^{-\dot{r}^2/4\pi^2\sigma_s^2 f_m^2}\right) \tag{10.185}$$

The first term on the right-hand side of (10.185) is the familiar Rayleigh density function of the signal envelope, where $\mathbf{E}(r^2) = 2\sigma_s^2$. The second term contains the parameter f_m, which denotes the *maximum Doppler shift* experienced by the signal. Therefore, the level crossing rate is obtained via direct integration as

$$\mathcal{R}_V = \sqrt{2\pi} f_m \rho \mathrm{e}^{-\rho^2} \tag{10.186}$$

where

$$\rho^2 = \frac{V^2}{2\sigma_s^2} = \left(\frac{V}{V_{rms}}\right)^2 \tag{10.187}$$

The parameter ρ^2 is given in term of the *rms signal voltage level* $V_{rms} = \sqrt{\mathbf{E}(r^2)}$.

Average fade duration

The average fade duration in (10.182) can be alternatively expressed in terms of the probability $\Pr(r \leq V)$ that the signal envelope r falls below the threshold level V. Given a sufficiently long interval T we have

$$\Pr(r \leq V) = \frac{1}{T}\sum_{i=1}^{\mathcal{R}_V T} \tau_i \tag{10.188}$$

Thus, for $\mathcal{R}_V \neq 0$, the average fade duration is given by

$$\begin{aligned} \tau &= \frac{1}{\mathcal{R}_V}\Pr(r \leq V) = \frac{1}{\mathcal{R}_V}\int_0^V \frac{r}{\sigma_s^2} e^{-r^2/2\sigma_s^2} dr \\ &= \frac{e^{\rho^2} - 1}{\sqrt{2\pi} f_m \rho} \end{aligned} \tag{10.189}$$

We note that when there is no Doppler shift, that is, $f_m = 0$, then the level crossing rate is zero (no level crossings). Consequently, the average fade duration is also zero (not infinite as in (10.189), which is valid only for $\mathcal{R}_V \neq 0$). This implies that the channel is time-invariant (the coherence time is infinite) and interleaving would not be effective. Thus, *time diversity may not be effective in time intervals where the channel experiences no fading*.

Example 10.18 Average fade duration

Let us consider the scenario where a mobile traveling toward a base station at a speed of 100 km/hour receives a 1950 MHz signal from a base station. The maximum Doppler shift is $f_m = f_c v/c = 180$ Hz. Let us assume that the *threshold signal-to-noise ratio* is $V^2/2\sigma^2 = 3$ dB, where the noise variance is σ^2, and the signal-to-noise ratio is $V_{rms}^2/\sigma^2 = 10$ dB. The parameter ρ^2 is calculated to be 0.4. This yields the average fade duration $\tau = 1.7$ ms. If the symbol time is much smaller than 1.7 ms (the symbol rate is much larger than 580 symbols/s) many symbols could be affected by a deep fade and a burst of errors may result. Interleaving can randomize bursts of errors and enables time diversity to work effectively. It also enables random error-correction codes to correct bursts of errors. The channel coherence time, which is one-eighth of the inverse of the maximum Doppler shift, is 0.7 ms. Thus, at a symbol rate of 14.4 ksps the symbol time is 0.07 ms, which is ten times smaller than the channel coherence time. Therefore, the channel can be said to be slow fading if the channel estimation time is less than the channel coherence time. The average fade duration is 2.4 times the channel coherence time, hence the interleaving time must be larger than 2.4 times the channel coherence time or, equivalently, about 24 symbols.

■

10.10 Maximal ratio combining (MRC)

In an L-fold diversity system with fixed throughput and fixed transmitted power, the energy of a transmitted copy is only $1/L$ the symbol energy. Thus, an *optimum coherent combiner* in the receiver must obtain a *combining decision sample* whose signal-to-noise ratio is the sum of signal-to-noise ratios of L received copies. Functionally, this means that the combiner must rotate the phases of the decision sample of L copies to align their phases (*co-phasing*) and weight each copy with their respective subchannel tap before summing (*weighting*). Thus, strong subchannels are given more weight than weak subchannels; this is similar to the *water-filling strategy* in an AWGN channel. This optimum coherent combining technique is referred to as *maximal ratio combining* (MRC). Let us consider the pre-combining samples of L copies of an arbitrary transmitted symbol s_i at the output of the matched filter. Each copy has a corresponding complex subchannel tap h_l. We have

$$Y_l = h_l s_i + N_l, \quad l = 1, 2, \ldots, L \tag{10.190}$$

The complex Gaussian random variable N_l has a variance $2\sigma^2$. We can express L in vector form as follows:

$$\boldsymbol{Y} = \boldsymbol{h} s_i + \boldsymbol{N} \tag{10.191}$$

where $\boldsymbol{Y} = [Y_1 \ Y_2 \ldots \ Y_L]^t, \boldsymbol{h} = [h_1 \ h_2 \ldots \ h_L]^t$, and $\boldsymbol{N} = [N_1 \ N_2 \ldots \ N_L]^t$.

Now assume *perfect channel estimation*, then the *sufficient statistic* for coherent demodulation is $(\boldsymbol{h}^*/\|\boldsymbol{h}\|)\boldsymbol{Y}$. We use the notation $\boldsymbol{h}^*$ for the *conjugate and transpose* of vector $\boldsymbol{h}$. We have the following MRC decision variable:

$$\begin{aligned} X &= \frac{\boldsymbol{h}^*}{\|\boldsymbol{h}\|}(\boldsymbol{h} s_i + \boldsymbol{N}) \\ &= \|\boldsymbol{h}\| s_i + \frac{\boldsymbol{h}^*}{\|\boldsymbol{h}\|}\boldsymbol{N} \end{aligned} \tag{10.192}$$

The complex Gaussian noise $(\boldsymbol{h}^*/\|\boldsymbol{h}\|)\boldsymbol{N}$ has variance $2\sigma^2$. Note that the above operation is equivalent to $\|\boldsymbol{h}\|X = \sum_{l=1}^{L} h_l^* Y_l = \sum_{l=1}^{L} |h_l|^2 s_i + \sum_{l=1}^{L} h_l^* N_l$ as mentioned above (co-phasing and weighting). The normalization with $\|\boldsymbol{h}\| = \sqrt{\sum_{l=1}^{L} |h_l|^2}$ still preserves the sufficient statistic.

The *instantaneous MRC output signal-to-noise ratio* $\boldsymbol{SNR}_{0,i}$, given the symbol s_i, is $\boldsymbol{SNR}_{0,i} = \|\boldsymbol{h}\|^2 |s_i|^2/2\sigma^2 = \sum_l |h_l|^2 |s_i|^2/2\sigma^2 = \sum_l \boldsymbol{SNR}_{l,i}$, where $\boldsymbol{SNR}_{l,i} = |h_l|^2 |s_i|^2/2\sigma^2$ is the *instantaneous signal-to-noise ratio* of the pre-combining lth copy of symbol s_i. Thus, MRC achieves the *maximum output signal-to-noise ratio*, which is the sum of L input signal-to-noise ratios (a fact that can also be verified by *Cauchy–Schwarz inequality*). The name maximal ratio combining is the truncated version of *maximal signal-to-noise ratio combining*.

Assume *perfect channel estimation*, and use the mapping $s_i \rightarrow \boldsymbol{s}_i$ for a complex variable to a two-dimensional vector, then the conditional pair-wise error probability between two vectors $\|\boldsymbol{h}\|\boldsymbol{s}_i$ and $\|\boldsymbol{h}\|\boldsymbol{s}_j$ is

$$\Pr\left(\|\boldsymbol{h}\|\boldsymbol{s}_i \to \|\boldsymbol{h}\|\boldsymbol{s}_j\right) = Q\left(\frac{\|\boldsymbol{h}\|\left\|\boldsymbol{s}_i - \boldsymbol{s}_j\right\|}{2\sigma}\right) \tag{10.193}$$

The conditional bit error probability for the Gray-coded signal set $\{\boldsymbol{s}_i\}_{i=1}^{M}$ is given by the following approximation:

$$P_b(\|\boldsymbol{h}\|) \approx \frac{N_n}{\log_2 M} Q\left(\frac{\|\boldsymbol{h}\| d_{min}}{2\sigma}\right) \tag{10.194}$$

where $d_{min} = \min_{i,j} ||\boldsymbol{s}_i - \boldsymbol{s}_j||$ is the *minimum Euclidean distance* of the signal set, $\sigma^2 = N_0/2$, and N_n is average number of symbols at the minimum Euclidean distance d_{min} or the average number of nearest neighbors. Here $N_0/2$ is the power spectral density of noise. Knowing the statistics of the fading channel (Rayleigh, Rice, Nakagami) we can evaluate the bit error probability as follows:

$$\begin{aligned} P_b &= \mathbf{E}[P_b(\|\boldsymbol{h}\|)] \approx \mathbf{E}\left[\frac{N_n}{\log_2 M} Q\left(\frac{\|\boldsymbol{h}\| d_{min}}{2\sigma}\right)\right] \\ &= \mathbf{E}\left[\frac{N_n}{\log_2 M} Q\left(\sqrt{2\|\boldsymbol{h}\|^2 \alpha \boldsymbol{SNR}}\right)\right] \end{aligned} \tag{10.195}$$

where the *diversity symbol signal-to-noise ratio* $\boldsymbol{SNR}$ and the positive constant α, which depends on the modulation, are given by

$$\boldsymbol{SNR} = \frac{\boldsymbol{\mathcal{E}}_s}{N_0} = \frac{E_s}{LN_0}, \ \alpha \boldsymbol{SNR} = \frac{1}{2}\left(\frac{d_{min}}{2\sigma}\right)^2 \tag{10.196}$$

The *diversity symbol energy* $\boldsymbol{\mathcal{E}}_s$ is given by $\boldsymbol{\mathcal{E}}_s = E_s/L$.

Rayleigh

When the iid subchannel tap magnitudes $|h_i|$ are Rayleigh distributed with normalized mean-square value $\mathbf{E}\left(|h_i|^2\right) = 1$, the combining channel tap magnitude $\|\boldsymbol{h}\|^2 = \sum_{l=1}^{L} |h_l|^2$ has a χ^2-*density function with 2L degrees of freedom*. We have

$$f_{\|\boldsymbol{h}\|^2}(y) = \frac{y^{L-1}\mathrm{e}^{-y}}{(L-1)!} \tag{10.197}$$

The corresponding bit error probability is given by the following two equivalent closed-form expressions from Appendix 10B:

$$P_b \approx \frac{N_n}{2\log_2 M}\left[1 - \mu \sum_{k=0}^{L-1} \binom{2k}{k} \left(\frac{1-\mu^2}{4}\right)^k\right] \tag{10.198a}$$

$$P_b \approx \frac{N_n}{\log_2 M}\left(\frac{1-\mu}{2}\right)^L \sum_{l=0}^{L-1} \binom{L-1+l}{l} \left(\frac{1+\mu}{2}\right)^l \tag{10.198b}$$

where

$$\mu = \sqrt{\frac{\alpha \boldsymbol{SNR}}{1 + \alpha \boldsymbol{SNR}}} \tag{10.199}$$

- **PSK**: the minimum Euclidean distance is $d_{min} = 2\sqrt{\mathcal{E}_b}$, where the *diversity bit energy* is $\mathcal{E}_b$. With the noise variance $\sigma^2 = N_0/2$, we obtain $\alpha\boldsymbol{SNR} = \mathcal{E}_b/N_0 = E_b/LN_0$. Furthermore, $N_n = 1$, $M = 2$, therefore the bit error probability for PSK is

$$P_b \approx \frac{1}{2}\left[1 - \mu \sum_{k=0}^{L-1} \binom{2k}{k} \left(\frac{1-\mu^2}{4}\right)^k\right] \text{(PSK)} \tag{10.200a}$$

$$P_b = \left(\frac{1-\mu}{2}\right)^L \sum_{l=0}^{L-1} \binom{L-1+l}{l} \left(\frac{1+\mu}{2}\right)^l \text{(PSK)} \tag{10.200b}$$

- **QPSK**: the minimum Euclidean distance is $d_{min} = \sqrt{2\mathcal{E}_s}$, where the *diversity symbol energy* is $\mathcal{E}_s$. With $\sigma^2 = N_0/2$, we obtain $\alpha\,\boldsymbol{SNR} = \mathcal{E}_s/2N_0 = E_s/2LN_0$. Furthermore, $N_n = 2$, $M = 4$, therefore the bit error probability for QPSK is identical to that of PSK as expected

$$P_b \approx \frac{1}{2}\left[1 - \mu \sum_{k=0}^{L-1} \binom{2k}{k} \left(\frac{1-\mu^2}{4}\right)^k\right] \text{(QPSK)} \tag{10.201a}$$

$$P_b = \left(\frac{1-\mu}{2}\right)^L \sum_{l=0}^{L-1} \binom{L-1+l}{l} \left(\frac{1+\mu}{2}\right)^l \text{(QPSK)} \tag{10.201b}$$

- **MPSK**: the minimum Euclidean distance is $d_{min} = 2\sqrt{\mathcal{E}_s}\sin(\pi/M)$, where the *diversity symbol energy* is $\mathcal{E}_s$. Using the noise variance $\sigma^2 = N_0/2$, we obtain $\alpha\,\boldsymbol{SNR} = \alpha(\boldsymbol{\mathcal{E}_s}/\boldsymbol{N_0})\sin^2(\pi/\boldsymbol{M}) = \alpha(\boldsymbol{E_s}/\boldsymbol{LN_0})\sin^2(\pi/\boldsymbol{M})$. Furthermore, $N_n = 2$, therefore the bit error probability for MPSK is given by

$$P_b \approx \frac{1}{\log_2 M}\left[1 - \mu \sum_{k=0}^{L-1} \binom{2k}{k} \left(\frac{1-\mu^2}{4}\right)^k\right] (\text{MPSK},\ M > 2) \tag{10.202a}$$

$$P_b \approx \frac{2}{\log_2 M}\left(\frac{1-\mu}{2}\right)^L \sum_{l=0}^{L-1} \binom{L-1+l}{l} \left(\frac{1+\mu}{2}\right)^l (\text{MPSK},\ M > 2) \tag{10.202b}$$

- **MQAM**: the minimum Euclidean distance is $d_{min} = \sqrt{6\mathcal{E}_s/(M-1)}$. Using $\sigma^2 = N_0/2$, we obtain $\alpha\boldsymbol{SNR} = 3(\mathcal{E}_s/N_0)/2(M-1) = 3(E_s/LN_0)/2(M-1)$. Furthermore, $N_n = 4 - 4/\sqrt{M}$, therefore the bit error probability for MQAM is given by

$$P_b \approx \frac{2 - 2/\sqrt{M}}{\log_2 M}\left[1 - \mu \sum_{k=0}^{L-1} \binom{2k}{k} \left(\frac{1-\mu^2}{4}\right)^k\right] \text{(MQAM)} \tag{10.203a}$$

$$P_b \approx \frac{4 - 4/\sqrt{M}}{\log_2 M}\left(\frac{1-\mu}{2}\right)^L \sum_{l=0}^{L-1} \binom{L-1+l}{l} \left(\frac{1+\mu}{2}\right)^l \text{(MQAM)} \tag{10.203b}$$

Rice

When the independent subchannel tap magnitudes $|h_i|$ are Rice distributed with normalized mean-square value $\boldsymbol{E}\left(|h_i|^2\right) = 1$, the combining channel tap magnitude $\|\boldsymbol{h}\|^2 = \sum_{l=1}^{L} |h_l|^2$ has a *non-central χ^2–density function with 2L degrees of freedom* given by

$$f_{\|\boldsymbol{h}\|^2}(y) = (\kappa+1)y^{(L-1)/2}\mathrm{e}^{-[(\kappa+1)y+\kappa]}I_0\left(2\sqrt{\kappa(\kappa+1)y}\right) \tag{10.204}$$

where κ was first identified in (10.63). The bit error probability can be evaluated via direct integration.

Nakagami-m

When the independent subchannel tap magnitudes $|h_i|$ are Nakagami-m distributed with normalized mean-square value $\mathbf{E}\left(|h_i|^2\right) = 1$, the combining channel tap squared magnitude $\|\boldsymbol{h}\|^2 = \sum_{l=1}^{L} |h_l|^2$ has a density function given by

$$f_{\|\boldsymbol{h}\|^2}(y) = \frac{m^{mL}}{\Gamma(mL)}y^{mL-1}\mathrm{e}^{-my} \tag{10.205}$$

The bit error probability is given in Appendix 10B as

$$\begin{aligned} P_b &\approx \frac{N_n}{2\log_2 M}\left[1 - \sqrt{\frac{\alpha\boldsymbol{SNR}/m}{1+\alpha\boldsymbol{SNR}/m}}\sum_{k=0}^{mL-1}\binom{2k}{k}\left(\frac{1}{4(1+\alpha\boldsymbol{SNR}/m)}\right)^k\right],\ m:\text{integer} \\ P_b &\approx \frac{N_n}{\log_2 M}\left[\frac{1}{2\sqrt{\pi}}\frac{\sqrt{\alpha\boldsymbol{SNR}/m}}{(1+\alpha\boldsymbol{SNR}/m)^{mL+1/2}}\frac{\Gamma(mL+\frac{1}{2})}{\Gamma(mL+1)}\right]{}_2F_1\left(1, mL+\tfrac{1}{2}; mL+1; \frac{1}{1+\alpha\boldsymbol{SNR}/m}\right), \\ &\quad m:\text{noninteger} \end{aligned} \tag{10.206}$$

Example 10.19 Diversity gain

Let us consider a Rayleigh fading channel and compare the performance of an L-fold time diversity I-Q signal to the performance of its counterpart without diversity, assuming that both signals have the same transmitted power and input bit rate. Using (10.57) and assuming high *SNR* (*SNR* $\gg$ 1) we have for the non-diversity signal

$$\begin{aligned} P_b &= \frac{N_n}{2\log_2 M}\left(1 - \sqrt{\frac{\alpha SNR}{1+\alpha SNR}}\right) \approx \frac{N_n}{2\log_2 M}\left(1 - \left[1 - \frac{1}{2\alpha SNR}\right]\right) \\ &\approx \frac{N_n}{\log_2 M}\left(\frac{1}{4\alpha SNR}\right) \end{aligned} \tag{10.207}$$

For the diversity signal we make the following approximations for the parameters involving μ in (10.198):

$$\frac{1+\mu}{2} \approx 1, \text{and } \frac{1-\mu}{2} \approx \frac{1}{4\alpha \boldsymbol{SNR}} \tag{10.208}$$

Furthermore,

$$\sum_{l=0}^{L-1} \binom{L-1+l}{l} = \binom{2L-1}{L} \tag{10.209}$$

Note that the time diversity signal has the transmission symbol rate equal to L times that of the signal without diversity. Thus the diversity symbol energy is only $1/L$ times the non-diversity symbol energy or equivalently, $\boldsymbol{SNR} = SNR/L$. Thus, the bit error probability of an I-Q signal with diversity at high $\boldsymbol{SNR}$ is given by

$$\begin{aligned} P_b &\approx \frac{N_n}{\log_2 M} \binom{2L-1}{L} \left(\frac{1}{4\alpha \boldsymbol{SNR}}\right)^L \\ &\approx \frac{N_n}{\log_2 M} L^L \binom{2L-1}{L} \left(\frac{1}{4\alpha\, SNR}\right)^L \end{aligned} \tag{10.210}$$

Thus, with diversity, the bit error probability decreases inversely with the Lth power of the input signal-to-noise ratio. On the other hand, without diversity, the bit error probability decreases inversely with the input signal-to-noise ratio.

For illustration consider the case when $\alpha SNR = 100$ (20 dB), $L = 3$, $N_n = 2$, $M = 4$ (QPSK). We have $P_b \approx 2.5 \times 10^{-3}$ for no diversity as compared to $P_b \approx 3.9 \times 10^{-6}$ for a three-fold diversity with MRC. In other words, to achieve the same bit error probability the signal without diversity must have an SNR of about 48 dB instead of 20 dB. The *diversity gain* is approximately 28 dB.

■

Example 10.20 Outage probability of a diversity link with MRC

We define the outage probability p_{out} of a diversity link, that is, the probability that the instantaneous $\boldsymbol{SNR}$ falls bellow a threshold value γ as follows:

$$p_{out} = \Pr\left(\|\boldsymbol{h}\|^2 \boldsymbol{SNR} < \gamma\right) = \Pr\left(\|\boldsymbol{h}\|^2 < \frac{\gamma}{\boldsymbol{SNR}}\right) \tag{10.211}$$

For a slow-flat Rayleigh fading channel we can use the χ^2-*density function with 2L degrees of freedom*. Thus, the outage probability is given by

$$\begin{aligned} p_{out} &= \int_0^{\gamma/\boldsymbol{SNR}} \frac{y^{L-1} \mathrm{e}^{-y}}{(L-1)!} \mathrm{d}y \\ &= 1 - \mathrm{e}^{-\gamma/\boldsymbol{SNR}} \sum_{k=0}^{L-1} \frac{1}{k!} \left(\frac{\gamma}{\boldsymbol{SNR}}\right)^k \end{aligned} \tag{10.212}$$

For numerical illustration, we compare the performance of an L-fold time diversity I-Q signal with $\boldsymbol{SNR}$ to the performance of its non-diversity counterpart with SNR, assuming that both signals have the same transmitted power and input bit rate. Thus, we have $\boldsymbol{SNR} = SNR/L$. Let the threshold be $\gamma = 1$ and SNR = 11.2 (10.5 dB), and $L = 3$. This yields an outage probability $p_{out} \approx 2.5 \times 10^{-3}$ as compared to 0.09 for the case where there is no diversity (see Example 10.5).

■

10.11 Selection combining (SC)

Selection combining (SC) is a *suboptimum* combining technique that is commonly employed in receive antenna diversity. To provide diversity the subchannel with the *largest* tap squared magnitude is selected for each transmitted symbol. Let us consider the pre-combining samples of L copies of an arbitrary transmitted symbol s_i at the output of the matched filter. Each copy has a corresponding iid complex subchannel tap h_l. We have

$$Y_l = h_l s_i + N_l, \quad l = 1, 2, \ldots, L \tag{10.213}$$

Now assume *perfect channel estimation*, then the *sufficient statistic* for coherent demodulation is $\left(h_l^*/|h_l|\right) Y_l$. We have the following pre-combining decision variables:

$$\begin{aligned} X_l &= \frac{h_l^*}{|h_l|}(h_l s_i + N_l) \\ &= |h_l| s_i + \frac{h_l^*}{|h_l|} N_l, \quad l = 1, 2, \ldots, L \end{aligned} \tag{10.214}$$

Both the I- and Q-noise components of $\left(h_l^*/|h_l|\right) N_l$ have the same variance σ^2. The selection combiner chooses the decision variable with the largest subchannel tap squared magnitude:

$$|h|^2 = \max_l \left(|h_1|^2, |h_2|^2, \ldots, |h_L|^2 \right) \tag{10.215}$$

The probability density function of $|h|^2$ is given by the following expression:

$$f_{|h|^2}\left(|h|^2\right) = L f_{|h_l|^2}\left(|h|^2\right) \left[F_{|h_l|^2}\left(|h|^2\right) \right]^{L-1} \tag{10.216}$$

where $F_{|h_l|^2}\left(|h_l|^2\right)$ is the probability distribution function of $|h_l|^2$. The probability of bit error for an I-Q signal is given by

$$\begin{aligned} P_b &= \mathbf{E}[P_b(|h|)] \approx \mathbf{E}\left[\frac{N_n}{\log_2 M} Q\left(\frac{|h| d_{min}}{2\sigma} \right) \right] \\ &\approx \mathbf{E}\left[\frac{N_n}{\log_2 M} Q\left(\sqrt{2|h|^2 \alpha \boldsymbol{SNR}} \right) \right] \end{aligned} \tag{10.217}$$

where the *diversity symbol signal-to-noise ratio* ***SNR*** is given by

$$\alpha\,\boldsymbol{SNR} = \frac{1}{2}\left(\frac{d_{min}}{2\sigma}\right)^2 \tag{10.218}$$

Example 10.21 Coherent selection combining in a Rayleigh fading channel

For iid Rayleigh-distributed subchannel tap magnitudes, the density and distribution functions of $|h_l|^2$ are respectively given as

$$f_{|h_l|^2}(y) = \mathrm{e}^{-y}, \quad F_{|h_l|^2}(y) = 1 - \mathrm{e}^{-y} \tag{10.219}$$

Therefore, the density function of $|h|^2$ can be calculated as follows:

$$\begin{aligned} f_{|h|^2}(z) &= L\mathrm{e}^{-z}(1-\mathrm{e}^{-z})^{L-1} \\ &= \sum_{l=1}^{L}(-1)^{l-1}\binom{L}{l} L\,\mathrm{e}^{-lz} \end{aligned} \tag{10.220}$$

Finally, the bit error probability in a Rayleigh fading channel can be evaluated using the above density function. We get

$$P_b \approx \frac{N_n}{2\log_2 M}\sum_{l=1}^{L}(-1)^{l-1}\binom{L}{l}\left(1-\sqrt{\frac{\alpha\,\boldsymbol{SNR}}{l+\alpha\,\boldsymbol{SNR}}}\right) \tag{10.221}$$

For illustration we compare the performance of an L-fold time diversity I-Q signal with ***SNR*** to the performance of its non-diversity counterpart with *SNR*, assuming that both signals have the same transmitted power and input bit rate. Thus, we have $\boldsymbol{SNR} = SNR/L$. Consider the case when $SNR = 100$ (20 dB), $L = 3$, $N_n = 2$, $M = 4$ (QPSK), hence $\boldsymbol{SNR} = SNR/L = 100/3$. We have $P_b \approx 2.5 \times 10^{-3}$ for no diversity as compared to $P_b \approx 2.2 \times 10^{-5}$ for a three-fold diversity with SC. In other words, to achieve the same bit error probability the signal without diversity must have an *SNR* of about 41 dB instead of 20 dB. The *diversity gain* is approximately 21 dB as compared to 28 dB for MRC in Example 10.19.

■

Example 10.22 Noncoherent selection combining in a Rayleigh fading channel

Selection combining can be applied to signals that require noncoherent demodulation, such as DPSK, MFSK, and CSK. Let us consider noncoherent FSK in a Rayleigh fading channel. The conditional bit error probability, given the largest subchannel tap magnitude $|h|$, is given by

$$P_b(|h|) = \frac{1}{2}\mathrm{e}^{-|h|^2\boldsymbol{SNR}/2} \tag{10.222}$$

Taking the expectation of $P_b(|h|)$ with respect to $|h|^2$ by using the density function of $|h|^2$ in the above example we obtain the bit error probability as follows:

$$P_b = \sum_{l=1}^{L} (-1)^{l-1} \binom{L}{l} \frac{l}{2l + \boldsymbol{SNR}} = L \sum_{l=0}^{L-1} \binom{L-1}{l} (-1)^l \frac{1}{2(l+1) + \boldsymbol{SNR}} \quad (10.223)$$

For illustration consider the case of FSK with time diversity $L = 3$. The nondiversity signal-to-noise ratio is $SNR = 100$ (20 dB). Thus, the diversity signal-to-noise ratio is $\boldsymbol{SNR} = SNR/L = 100/3$. We have $P_b = 1/(2 + SNR) \approx 10^{-2}$ for no diversity as compared to $P_b \approx 4.6 \times 10^{-4}$ for a three-fold diversity with SC. In other words, to achieve the same bit error probability the signal without diversity must have an *SNR* of about 33 dB instead of 20 dB. The *diversity gain* is approximately 13 dB.

■

10.12 Equal gain combining (EGC)

Equal gain combining (EGC) is another *suboptimum* combining technique that works with both coherent and noncoherent signals. In coherent demodulation only the *co-phasing* process is carried out without the *weighting* process. Functionally, this means that the combiner only needs to rotate the phases of the decision sample of L copies to align their phases and then add them to form the combining decision sample.

Coherent EGC

Let us consider the pre-combining samples of L copies of an arbitrary transmitted symbol s_i of a *coherent I-Q signal* at the output of the matched filter. Each copy has a corresponding iid complex subchannel tap h_l. We have

$$Y_l = h_l s_i + N_l, \quad l = 1, 2, \ldots, L \quad (10.224)$$

Now assume *perfect channel estimation*, then the *sufficient statistic* for coherent demodulation is $\left(h_l^*/|h_l|\right) Y_l$. We have the following pre-combining decision variables:

$$\begin{aligned} X_l &= \frac{h_l^*}{|h_l|}(h_l s_i + N_l) \\ &= |h_l| s_i + \frac{h_l^*}{|h_l|} N_l, \quad l = 1, 2, \ldots, L \end{aligned} \quad (10.225)$$

Both the I- and Q-noise components of $\left(h_l^*/|h_l|\right) N_l$ have the same variance σ^2. The EGC decision variable is given by

$$X = \sum_{l=1}^{L} X_l = |h| s_i + N \quad (10.226)$$

where $|h| = |h_1| + \cdots + |h_L|$ and N is a complex Gaussian variable with variance $2L\sigma^2$. The bit error probability is given in (10.194) if the density function of $|h|$ is known. Since $|h|$ is

the sum of L iid random variables, its density function is the L-fold convolution of L identical density functions. There is no closed-form expression for Rayleigh, Rice, or Nakagami-m cases. We note that coherent EGC does not equal the performance of MRC because it weights all subchannels equally. Furthermore, there is no reduction in complexity with respect to MRC because the channel estimation is carried out in the same manner as MRC. In fact, the sufficient statistic for MRC is $X_l = h_l^* Y_l$, as compared to $X_l = \left(h_l^*/|h_l|\right) Y_l$ for coherent EGC.

Noncoherent EGC

In this section we consider the application of noncoherent EGC to orthogonal signals such as MFSK and CSK in a Rayleigh fading channel. From (7.236), the output of the first quadrature correlator–square law detector given $s_{1,l}(t)$ was the lth copy of the transmitted signal is $X_{1,l}^2 = \left(|h_l|\sqrt{\mathcal{E}_s}\cos\theta_l + N_{I,1,l}\right)^2 + \left(|h_l|\sqrt{\mathcal{E}_s}\sin\theta_l + N_{Q,1,l}\right)^2$. The *diversity symbol energy* $\mathcal{E}_s$ is $1/L$ times the symbol energy E_s, that is, $\mathcal{E}_s = E_s/L$. The outputs of the remaining $M-1$ quadrature correlator–square law detectors are $X_{j,l}^2 = N_{I,j,l}^2 + N_{Q,j,l}^2,\ j = 2, 3, \ldots, M$. The noise random variables $N_{I,i,l}$ and $N_{Q,i,l}$ are all independent Gaussian random variables with zero mean and variance $\sigma^2 = N_0/2$. Note that both $|h_l|\cos\theta_l$ and $|h_l|\sin\theta_l$ are zero-mean Gaussian random variables, therefore we conclude that $X_{1,l}^2$ and $X_{j,l}^2$ are central chi-squared random variables given the subchannel tap magnitudes $|h_l|,\ l = 1, 2, \ldots, L$. The independent outputs of all L noncoherent EGC combiners are

$$U_1 = \sum_{l=1}^{L} X_{1,l}^2,\ U_j = \sum_{l=1}^{L} X_{j,l}^2 \tag{10.227}$$

The density functions of $U_j, j = 1, 2, \ldots, M$, are the *central χ^2–density function with 2L degrees of freedom* given by

$$f_{U_j}(u_j) = \frac{1}{(2\sigma_j^2)^L (L-1)!} u_j^{L-1} \mathrm{e}^{-u_j/2\sigma_j^2},\quad u_j \geq 0 \tag{10.228}$$

where the parameter σ_j^2 is the mean-square value of each component of $X_{j,l}^2$ and is given as

$$\sigma_1^2 = \mathcal{E}_s/2 + \sigma^2 = \mathcal{E}_s/2 + N_0/2,\ \sigma_j^2 = \sigma^2 = N_0/2, j = 2, 3, \ldots, M \tag{10.229}$$

For convenience we normalize the mean-square value of the subchannel tap magnitude to unity: $\mathbf{E}\left(|h_l|^2\right) = 1$. The conditional symbol error probability given u_1 is *one minus the probability that all $M-1$ variables U_j are less than u_1*. Furthermore, the probability that a variable U_j is less than u_1 is

$$\begin{aligned} \Pr(U_j < u_1) &= \int_0^{u_1} f_{U_j}(u_j)\,\mathrm{d}u_j \\ &= 1 - \mathrm{e}^{-u_1/2\sigma_j^2} \sum_{l=0}^{L-1} \frac{1}{l!}\left(\frac{u_1}{2\sigma_j^2}\right)^l \end{aligned} \tag{10.230}$$

Therefore, we get the bit error probability as follows:

$$\begin{aligned} P_b &= \frac{M/2}{M-1}\left(1-\int_0^\infty \left[\Pr(U_j<u_1)\right]^{M-1} f_{U_1}(u_1)\,\mathrm{d}u_1\right) \\ &= \frac{M/2}{M-1}\left(1-\int_0^\infty \left[1-\mathrm{e}^{-u_1/2\sigma_j^2}\sum_{l=0}^{L-1}\frac{1}{l!}\left(\frac{u_1}{2\sigma_j^2}\right)^l\right]^{M-1} \frac{1}{(2\sigma_1^2)^L(L-1)!}u_1^{L-1}\mathrm{e}^{-u_1/2\sigma_1^2}\,\mathrm{d}u_1\right) \\ &= \frac{M/2}{M-1}\left(1-\int_0^\infty \left[1-\mathrm{e}^{-u_1}\sum_{l=0}^{L-1}\frac{u_1^l}{l!}\right]^{M-1} \frac{1}{(1+\boldsymbol{SNR})^L(L-1)!}u_1^{L-1}\mathrm{e}^{-u_1/(1+\boldsymbol{SNR})}\,\mathrm{d}u_1\right) \end{aligned} \tag{10.231}$$

where $\boldsymbol{SNR} = \mathcal{E}_s/N_0 = E_s/LN_0$.

Example 10.23 Noncoherent EGC in a Rayleigh fading channel

Let us consider noncoherent FSK ($M = 2$) in a Rayleigh fading channel. The bit error probability has a closed-form expression given as

$$P_b = \sum_{l=0}^{L-1}\binom{L-1+l}{l}\frac{[1+\boldsymbol{SNR}]^l}{[2+\boldsymbol{SNR}]^{L+l}} \tag{10.232}$$

For illustration consider the case of FSK and time diversity $L = 3$. The nondiversity signal-to-noise ratio is $SNR = 100$ (20 dB). Thus, the diversity signal-to-noise ratio is $\boldsymbol{SNR} = SNR/L = 100/3$. We have $P_b = 1/(2+SNR) \approx 10^{-2}$ for no diversity as compared to $P_b \approx 2.2\times 10^{-4}$ for a three-fold diversity with EGC. In other words, to achieve the same bit error probability the signal without diversity must have an *SNR* of about 36.6 dB instead of 20 dB. The *diversity gain* is approximately 16.6 dB as compared to 13 dB for noncoherent SC.

■

10.13 Frequency diversity

Frequency diversity can be implemented either as *controlled* diversity methods in *fast frequency hop* systems (FFH) and OFDM, or as a *frequency-selective* diversity method for a multipath fading channel. The latter method is also referred to as *multipath-delay* diversity. No control is exercised in frequency-selective diversity and the receiver is designed to combine copies of the transmitted symbol arriving via delayed paths. For frequency diversity to be effective, copies of the transmitted symbol must experience independent fades. This happens naturally in a multipath fading channel. The drawback is the presence of ISI in a multi-tap channel which must be equalized for frequency-selective diversity to work. Equalization does not provide diversity gain and at best it approaches the performance of a

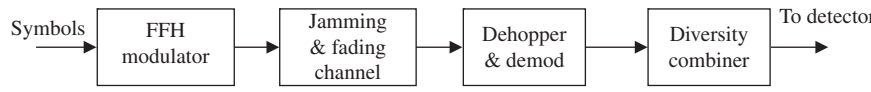

Figure 10.18 Diversity combining for FFH.

single-tap channel. Direct sequence spread spectrum signals provide both multipath-delay diversity and ISI equalization at the expense of lower throughput unless CDMA is used.

Fast frequency hop (FFH)

Fast frequency hop (FFH) is employed primarily in military communication systems to combat partial-band jamming. A symbol is pseudo-randomly hopped many times during its transmission to ensure some copies survive the jamming. In a jamming and fading channel the copies, after dehopping, can be noncoherently combined via EGC or SC to achieve diversity. As far as fading is concerned, the smallest frequency separation between hopping bins must be larger than the channel coherence bandwidth to ensure uncorrelated fading for the copies of the transmitted symbol. To avoid ISI each copy must experience flat fading, that is, the hop bandwidth must be smaller than the channel coherence bandwidth. In addition, for the channel to be slow fading the hop time must be smaller than the channel coherence time. Figure 10.18 shows the block diagram of a FFH system.

To alleviate the effects of partial-band jamming that weight more on jammed hops, some sort of *automatic gain control* (AGC) is necessary. In one type of AGC, called *noise-normalization*, the noise power in a given hop of a transmitted symbol is measured and its reciprocal is used to normalize (multiply) the outputs of the matched filter–envelope detectors of a noncoherent demodulator. This is similar to weighting the subchannel tap magnitudes in MRC, and the purpose is to deemphasize the effect of jammed hops in the combining process. Another type of AGC is the *self-normalization* process, where the reciprocal of the sum of the outputs of the matched filter–envelope detectors is used to normalize (multiply) the output of each detector before combining. As a result, the output of each detector when a hop contains a large amount of interference will be smaller than the output when interference is not present. Thus, the hops without interference will have a greater weight on the decision statistics than hops containing interference.

OFDM subcarrier combining

Controlled diversity for a frequency selective channel can be implemented via OFDM. Let us consider the decision variables of N subcarrier symbols for the case of low-mobility OFDM:

$$\hat{Z}(k) = H_k Z(k) + \mathbf{N}_k, \quad k = 0, 1, \ldots, N-1 \tag{10.233}$$

For diversity to work the subchannel taps H_k must be uncorrelated. This puts constraints on the number of subcarriers, the separation between diversity groups, and the length of the *cyclic prefix* that is employed to remove subcarrier ISI. Consider a frequency selective

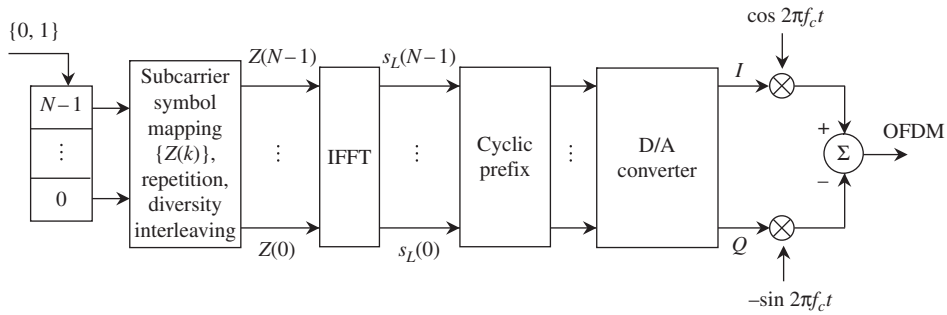

Figure 10.19 OFDM diversity modulator.

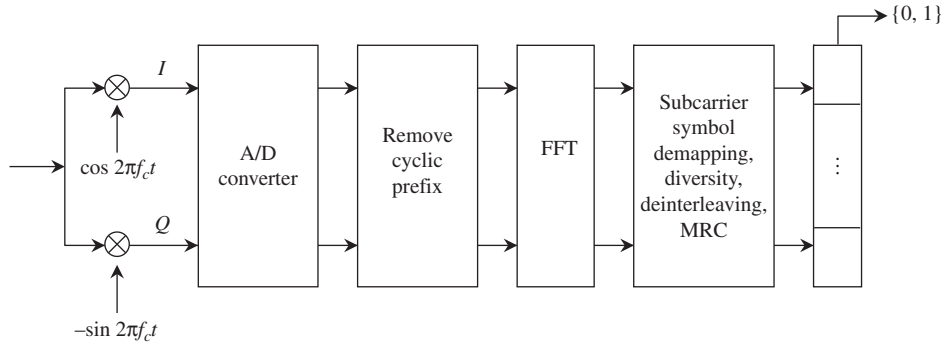

Figure 10.20 OFDM diversity demodulator.

channel with L channel taps representing L uncorrelated paths. Let T_d be the multipath delay spread, then the channel bandwidth is approximately $B = L/T_d$. The coherence bandwidth is $B_c = 1/T_d$, therefore the channel bandwidth consists of L *uncorrelated diversity-subchannels* with each diversity-subchannel bandwidth the same as the coherence bandwidth, that is, $B = LB_c$. Each of these L diversity-subchannels can house N/L *contiguous correlated subcarriers* with subcarrier bandwidth equal to B/N. The OFDM signal with bandwidth B can therefore achieve L-fold diversity since OFDM in effect subdivides the channel bandwidth B into L uncorrelated diversity-subchannels. To remove ISI between adjacent OFDM symbols a cyclic prefix of L IFFT samples is added to an OFDM symbol of N IFFT samples. To ensure that the channel is also a slow fading channel, the subcarrier bandwidth B/N must greatly exceed the Doppler spread f_D, that is, $B/N \gg f_D$. Since the channel coherence time T_c is $T_c = 1/4f_D$, this also implies that $N \ll 4BT_c$. For good efficiency, the cyclic prefix must be much smaller than the OFDM block length, that is, $L \ll N$. Hence, a good OFDM diversity system must satisfy the design contraint $BT_d \ll N \ll 4BT_c$. Figures 10.19 and 10.20 show the implementation of an OFDM diversity system. For illustration purposes consider a frequency-selective fading channel of L taps. We assume that the channel is *underspread* ($T_d \ll T_c$) and select the number of subcarriers N as a power of two that satisfies the above design constraint. Each diversity subchannel consists of $\lfloor N/L \rfloor$ correlated subcarriers ($\lfloor x \rfloor$ = integer part of x). The Lth diversity

subchannel can be filled with $N - L\lfloor N/L \rfloor$ unused subcarriers, which can be discarded before combining takes place at the demodulator. After diversity deinterleaving the pre-combining variables of L *diversity subcarriers* for the case of low-mobility OFDM are

$$\hat{Z}(k) = H_{l,k}Z(k) + \mathbf{N}_{l,k}, \quad l = 1, 2, \ldots, L; \quad k = 0, 1, \ldots, \lfloor N/L \rfloor \tag{10.234}$$

Applying MRC to the above L pre-combining variables for each diversity subcarrier symbol, the bit error probability of the L-fold diversity system is given by (10.194). The performance of an L-fold diversity OFDM signal with diversity ***SNR*** as compared to the performance of its non-diversity counterpart with non-diversity *SNR* is the same as that for time diversity discussed previously, assuming that both signals have the same transmitted power and input bit rate.

Rake receiver

Multipath-delay diversity that occurs naturally in a *frequency-selective fading* channel can be implemented via a special receiver called a *Rake receiver*. This type of receiver is particularly suited to a direct sequence spread spectrum signal with a wide bandwidth covering many coherence bandwidths. Such a wideband channel is modeled as an L-tap channel with the following impulse response:

$$h(\tau, t) = \sum_{l=0}^{L-1} h_i(t)\delta(\tau - \tau_i(t)) \tag{10.235}$$

where $\tau_0(t) < \tau_1(t) < \cdots < \tau_{L-1}(t)$. We assume that the channel varies slowly so that the channel taps remain constant over many symbols (the channel coherence time is several symbols long). Furthermore, the multipath delay spread is assumed to be less than a symbol time (the channel is underspread) so that ISI affects only the next symbol. These assumptions are valid for most practical wireless systems. Thus, the L-tap channel model is time-invariant and can be expressed as follows:

$$h(\tau) = \sum_{l=0}^{L-1} h_l\delta(\tau - \tau_l) \tag{10.236}$$

With the time-varying component t eliminated we can replace the delay-time τ with t to work with the received signal conventionally expressed in time t. Hence, we have

$$h(t) = \sum_{l=0}^{L-1} h_l\delta(t - \tau_l) \tag{10.237}$$

Let us consider the transmitted symbol $\boldsymbol{d}_k = d_k + \mathrm{j}\hat{d}_k, kT_s \leq t < (k+1)T_s$ of a complex speading I-Q signal, where d_k and $\hat{d}_k$ are the kth in-phase and quadrature bits normalized to the smallest symbol energy $E = A^2T_s/2$, respectively. The transmitted signal is given by

$$s(t) = \mathrm{Re}\left[s_L(t)\,\mathrm{e}^{\,\mathrm{j}2\pi f_c t}\right] \tag{10.238}$$

where the carrier frequency f_c is assumed to be an integer multiple of $1/T_s$ and the complex envelope $s_L(t)$ is given by the following expression:

$$s_L(t) = \boldsymbol{d}_k \boldsymbol{c}(t - kT_s) \tag{10.239}$$

The complex spreading PN sequence $\boldsymbol{c}(t)$ with unit amplitude squared pulse shape and chip time T_c and period NT_c (selected to be an integer multiple of T_s) is expressed in terms of both in-phase and quadrature PN sequences $\boldsymbol{c}_I(t)$ and $c_Q(t)$ as

$$c(t) = c_I(t) + \mathrm{j}c_Q(t), 0 < t \leq NT_c \tag{10.240}$$

For the paths to be resolvable it is necessary for the chip time to be smaller than the smallest delay between paths. The convolution of $s_L(t)$ and $h(t)$ results in the received complex envelope $r_L(t)$, which contains L copies of each transmitted symbol and its associated ISI from the preceding and succeeding symbols. We have

$$r_L(t) = A \sum_{l=0}^{L-1} h_l \boldsymbol{d}_k \, \mathrm{e}^{-\mathrm{j}2\pi f_c \tau_l} \boldsymbol{c}(t - kT_s - \tau_l) + I_{k-1}(t) + I_{k+1}(t) + n(t) \tag{10.241}$$

where noise $n(t)$ has the power spectral density $N_0/2$ (W/Hz). The term $I_{k-1}(t)$ represents $L-1$ ISI signals from the preceding $(k-1)$th symbol and the term $I_{k+1}(t)$ represents $L-1$ ISI signals from the succeeding symbol $(k+1)$th, respectively. We have

$$I_{k-1}(t) = A \sum_{l=1}^{L-1} h_l \boldsymbol{d}_{k-1} \, \mathrm{e}^{-\mathrm{j}2\pi f_c \tau_l} c(t - (k-1)T_s - \tau_l) \tag{10.242}$$

$$I_{k+1}(t) = A \sum_{l=1}^{L-1} h_l \boldsymbol{d}_{k+1} \, \mathrm{e}^{-\mathrm{j}2\pi f_c \tau_l} c(t - (k+1)T_s - \tau_l) \tag{10.243}$$

Any arbitrary mth path of the kth symbol experiences $L-m$ ISI signals from the preceding $(k-1)$th symbol and $m-1$ ISI signals from the $(k+1)$th symbol. Assume that the channel taps h_l and path delays τ_l are available via *perfect channel estimation*. They are then used to demodulate the received signal $r(t) = \mathrm{Re}\left[r_L(t)\,\mathrm{e}^{\mathrm{j}2\pi f_c t}\right]$ to L *complex baseband signals* (corresponding to L paths) via L complex local carriers $\sqrt{2/T_s}\mathrm{e}^{-\mathrm{j}2\pi f_c(t-\tau_l)}$, $l = 1, 2, \ldots, L$. Next, the *complex despreading* process is carried out for the interested symbol by multiplying the complex baseband signals with $\boldsymbol{c}^*(t - kT_s - \tau_l)/2$, $l = 1, 2, \ldots, L$, where $|c(t)|^2 = 2$. This is followed by integrating the demodulated baseband signals for one symbol time to obtain L pre-combining decision variables. This demodulation process creates L *Rake fingers*. The output of the lth Rake finger for the kth symbol is given as

$$\begin{aligned} Y_l &= \int_{kT_s - \tau_l}^{(k+1)T_s - \tau_l} A\sqrt{\frac{1}{2T_s}} h_l \boldsymbol{d}_k \, \mathrm{d}t + I_l + I_l^- + I_l^+ + N_l \\ &= h_l s_k + I_l + I_l^- + I_l^+ + N_l \end{aligned} \tag{10.244}$$

where s_k is the unnormalized kth symbol with energy $E_k = |s_k|^2$ given by

$$\begin{aligned} &s_k = \sqrt{\frac{A^2 T_s}{2}} \boldsymbol{d}_k = \sqrt{E}\boldsymbol{d}_k, \quad E_k = |s_k|^2 = E|\boldsymbol{d}_k|^2, \\ &E = A^2 T_s/2 = \text{smallest symbol energy} \end{aligned} \tag{10.245}$$

The complex Gaussian noise variable N_l has zero mean and variance $2\sigma^2 = N_0$, where $\sigma^2 = N_0/2$ is the variance of the in-phase noise or quadrature noise. The *self-interference* I_l is referred to as *intrapath interference* (IPI), and I_l^- and I_l^+ are ISI. Given the unnormalized $(k-1)$th and $(k+1)$th symbols, the expressions for these three parameters are

$$\begin{aligned} I_l &= \frac{1}{2}\int_{kT_s-\tau_l}^{(k+1)T_s-\tau_l} \sum_{\substack{m=0\\ m\neq l}}^{L-1} A\sqrt{\frac{1}{2T_s}} h_m \boldsymbol{d}_k \mathrm{e}^{-\mathrm{j}2\pi f_c(\tau_m-\tau_l)} \boldsymbol{c}(t-kT_s-\tau_m)\boldsymbol{c}^*(t-kT_s-\tau_l)\,\mathrm{d}t \\ &= \frac{1}{2T_s}\sum_{\substack{m=0\\ m\neq l}}^{L-1} h_m s_k \mathrm{e}^{-\mathrm{j}2\pi f_c(\tau_m-\tau_l)} \int_{kT_s-\tau_l}^{(k+1)T_s-\tau_l} \boldsymbol{c}(t-kT_s-\tau_m)\boldsymbol{c}^*(t-kT_s-\tau_l)\,\mathrm{d}t \end{aligned} \tag{10.246}$$

$$\begin{aligned} I_l^- &= \frac{1}{2}\int_{kT_s-\tau_l}^{kT_s-\tau_l+\tau_m} \sum_{\substack{m=2\\ m>l}}^{L-l} A\sqrt{\frac{1}{2T_s}} h_m \boldsymbol{d}_{k-1} \mathrm{e}^{-\mathrm{j}2\pi f_c(\tau_m-\tau_l)} \boldsymbol{c}(t-(k-1)T_s-\tau_m) \\ &\quad \times \boldsymbol{c}^*(t-kT_s-\tau_l)\,\mathrm{d}t \\ &= \frac{1}{2T_s}\sum_{\substack{m=1\\ m>l}}^{L-l-1} h_m s_{k-1} \mathrm{e}^{-\mathrm{j}2\pi f_c(\tau_m-\tau_l)} \int_{kT_s-\tau_l}^{kT_s-\tau_l+\tau_m} \boldsymbol{c}(t-(k-1)T_s-\tau_m)\boldsymbol{c}^*(t-kT_s-\tau_l)\,\mathrm{d}t \end{aligned} \tag{10.247}$$

$$\begin{aligned} I_l^+ &= \frac{1}{2}\int_{(k+1)T_s-\tau_l}^{(k+1)T_s-\tau_l+\tau_m} \sum_{\substack{m=0\\ m<l}}^{l-2} A\sqrt{\frac{1}{2T_s}} h_m \boldsymbol{d}_{k+1} \mathrm{e}^{-\mathrm{j}2\pi f_c(\tau_m-\tau_l)} \boldsymbol{c}(t-(k+1)T_s-\tau_m)\boldsymbol{c}^*(t-kT_s-\tau_l)\,\mathrm{d}t \\ &= \frac{1}{2T_s}\sum_{\substack{m=0\\ m<l}}^{l-2} h_m s_{k+1} \mathrm{e}^{-\mathrm{j}2\pi f_c(\tau_m-\tau_l)} \int_{(k+1)T_s-\tau_l}^{(k+1)T_s-\tau_l+\tau_m} \boldsymbol{c}(t-(k+1)T_s-\tau_m)\boldsymbol{c}^*(t-kT_s-\tau_l)\,\mathrm{d}t \end{aligned} \tag{10.248}$$

In the above integrals the product of two complex PN sequences is defined over their overlapping interval only. The independent IPI and ISI variables can be approximated as zero mean complex Gaussian variables with variances $2\sigma_I^2$, $2\sigma_{I^-}^2$, and $2\sigma_{I^+}^2$, respectively, where σ_I^2, $\sigma_{I^-}^2$, and $\sigma_{I^+}^2$ are the variances of the corresponding in-phase interference or quadrature interference. Combining the three interferences with Gaussian noise and denoting it as $\boldsymbol{\mathcal{N}}_l = I_l + I_l^- + I_l^+ + N_l$, with the total variance as the sum of variances $2\sigma^2 = 2\sigma_I^2 + 2\sigma_{I^-}^2 + 2\sigma_{I^+}^2 + 2\sigma^2$, we obtain L Rake finger outputs for the kth symbol as follows:

$$Y_l = h_l s_k + \boldsymbol{\mathcal{N}}_l, \quad l = 1, 2, \ldots, L \tag{10.249}$$

Defining the vector $\boldsymbol{h}$ as $\boldsymbol{h} = [h_1\ h_2 \ldots h_L]^t$ and applying *maximal ratio combining* to the above L Rake finger outputs we obtain the bit error probability for the Rake receiver of an I-Q signal as

$$P_b = \mathbf{E}\left[\frac{N_n}{\log_2 M} Q\left(\sqrt{2\|\boldsymbol{h}\|^2 \alpha \boldsymbol{SINR}}\right)\right] \tag{10.250}$$

where the *path signal-to-interference-and-noise ratio* ***SINR*** and the positive constant α, are given by

$$\alpha \boldsymbol{SINR} = \frac{1}{2}\left(\frac{d_{min}}{2\sigma}\right)^2 \tag{10.251}$$

where $d_{min} = \min_{i,j} ||\boldsymbol{s}_i - \boldsymbol{s}_j||$ is the *minimum Euclidean distance* of the I-Q signal set (as usual we use the mapping $s_i \to \boldsymbol{s}_i$ to convert complex-valued symbols to two-dimentional vector symbols). Note that the *path* ***SINR*** of the Rake receiver is similar to the *diversity* ***SNR*** discussed previously for controlled time diversity and frequency diversity such as OFDM. In a controlled diversity method with L copies of a transmitted symbol, the energy going into each diversity symbol is $1/L$ times the non-diversity symbol energy. On the other hand, the DS-SS transmitter transmits only one copy of the transmitted symbol (no diversity), and the channel provides diversity for the receiver in the form of L resolvable paths. Given a transmitted power P, the lth path has an average power $P_l < P$ and, hence, the symbol in a path has only a fraction of the energy of the transmitted symbol. If we assume that all paths have a *normalized unit mean-square value*, that is, $E(|h_l|^2) = 1,\ l = 1, 2, \ldots, L$, then each path symbol has $1/L$ times the energy of the transmitted symbol. Thus, without the Rake receiver, one would have a power loss of $10\log L$ (dB). The bit error probability of the Rake receiver is the same as that of MRC, with ***SINR*** replacing ***SNR*** in the appropriate bit error probability expressions. To evaluate the bit error probability of the Rake receiver it is necessary to find the variances of IPI and ISI variables. These variances can be found using the results developed for CDMA in Chapter 8, assuming that the PN sequence can be modeled as a random binary sequence (when the period of the PN sequence, in chips, is much larger than the number of chips per symbol). In practice, the multipath delay spread is much smaller than the symbol time of a direct sequence spread spectrum signal in the cellular and PCS bands. Hence, IPI is much larger than ISI and consequently we have $\sigma_I^2 \gg \sigma_{I^-}^2 + \sigma_{I^+}^2$. For this case, we can approximate the total variance of interference and noise as $\sigma^2 \approx \sigma_I^2 + \sigma^2 = (L-1)E_s/N + N_0/2$, where $E_s = \mathbf{E}(|s_k|^2)$ is the *average symbol energy* and N is the spread factor. Note that in time and OFDM diversities with diversity ***SNR***, the performance comparision with a non-diversity receiver with *SNR* is carried out with $\boldsymbol{SNR} = SNR/L$. In the case of the Rake receiver, the performance comparision with a *non-Rake* receiver is carried out with both receivers having the same ***SINR***, since the non-Rake receiver just *locks onto only one path*. Thus, when channel noise dominates IPI, the performance of the Rake receiver with ***SINR*** approaches the performance of the maximal ratio combiner as compared to a non-Rake receiver with the same ***SINR***. The bit error probability of a non-Rake receiver is given by (10.195) with the magnitude of the path channel tap $|h|$ replacing $\|\boldsymbol{h}\|$, and this is identical to (10.54) with ***SINR*** replacing *SNR*. Thus, an additional power gain of $10\log L$ (dB) besides diversity gain is achieved for a Rake receiver when compared to a non-Rake receiver. This is not the case for controlled diversity. Figure 10.21 shows the conceptual complex-valued Rake receiver.

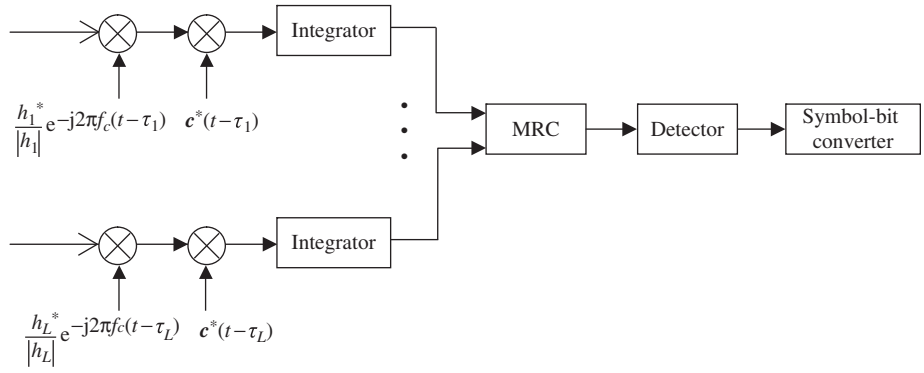

Figure 10.21 The complex-valued Rake receiver.

Example 10.24 Channel estimation for a Rake receiver

The channel estimation consists of estimating the channel taps h_l and the tap delays τ_l. This could be done by using the pilot tone or pilot symbols that are known a priori by the receiver. Once PN sequence synchronization is accomplished, the Rake fingers are synchronized and the tap delays are immediately known. The outputs of the Rake fingers for a given known symbol s_k are of the form

$$Y_l = h_l s_k + N_l, \quad l = 1, 2, \ldots, L \tag{10.252}$$

The channel taps can be estimated via MMSE estimation (Example 10.6) or direct estimation (Example 10.7).

■

Example 10.25 Performance of a Rake receiver

Let us consider a three-tap channel with $L = 3$, $\boldsymbol{SINR} = 100$ (20 dB), $N_n = 1$, $M = 2$ (PSK). Using (10.57) or (10.207) with $\alpha\boldsymbol{SINR}$ replacing αSNR we have $P_b \approx 2.5 \times 10^{-3}$ for a *non-Rake* receiver that locks onto one path. For a Rake receiver, the bit error probability is calculated from (10.210) with $\alpha\boldsymbol{SINR}$ replacing $\alpha\boldsymbol{SNR}$ to yield $P_b \approx 1.6 \times 10^{-7}$. In other words, to achieve this bit error probability the non-Rake receiver must have a $\alpha\boldsymbol{SINR}$ about 62 dB instead of 20 dB. The *diversity gain* is approximately 42 dB.

Now let us consider the case where the spread factor of the PN sequence is $N = 256$. The minimum Euclidean distance for PSK is $d_{min} = \sqrt{2E_b}$. The path signal-to-interference-and-noise ratio is given by the expression (8.81) $\alpha\boldsymbol{SINR} = \frac{1}{2}(d_{min}/2\sigma)^2 = [(L-1)/N + N_0/E_b]^{-1} = 100$ if $E_b/N_0 = 457$. Note that $\alpha SNR = E_b/N_0$ is the channel signal-to-noise ratio. In this case the interference dominates the channel noise.

■

10.14 Receive antenna diversity (SIMO)

Antenna diversity is most popular with cellular systems and wireless LANs. It can be implemented as *receive antenna diversity* with one transmit antenna and multiple receive antennas (Figure 10.22). This is also referred to as the *single-input multiple-output* (SIMO) system. On the other hand, receive antenna diversity puts some constraints on the receiver, such as antenna separation, in order to be effective.

For receive antenna diversity to work the channel taps of the received paths must be uncorrelated. This would provide spatial diversity in the case of deep fading at one or more receive antennas. The hope is that the received signal at other antennas might still be strong enough for reliable detection. Consider the case of base station-to-mobile transmission (forward channel) in a cellular system. The mobile station is commonly close to the ground surrounded by numerous local scatterers. Therefore, the waves arrive equally likely from all azimuth angles and the paths decorrelate over small spatial distance. This requires a small separation between receive antennas, commonly less than *one signal wavelength*. On the other hand, in the mobile-to-base station transmission (reverse channel), the base station antennas are normally located high above the ground and local scatterers participate weakly in the received signals. Most waves arriving at the base station come from a limited angular region surrounding the mobile station. This implies that the paths decorrelate over a larger spatial distance as compared to the forward channel. The antenna separation at the base station is normally more than *ten signal wavelengths*.

Consider an antenna array of two *isotropic* elements in the x–z plane with *element* 1 at the origin of the coordinate system. Let d be the element separation and ψ be the angle between the array and the x-axis. The plane wave arrives with elevation angle φ and azimuth angle θ, as shown in Figure 10.23.

The E-field phasors for the waves incident on *elements* 1 and 2 are given by

$$\begin{aligned} \boldsymbol{V}_1(\varphi,\theta) &= \boldsymbol{V}_0(\varphi,\theta) \\ \boldsymbol{V}_2(\varphi,\theta) &= \boldsymbol{V}_0(\varphi,\theta)\, \mathrm{e}^{\,\mathrm{j}k_0 d(\cos\psi\cos\theta\sin\varphi+\sin\psi\cos\varphi)} \end{aligned} \tag{10.253}$$

where $\boldsymbol{V}_0(\varphi,\theta)$ is *unity* for isotropic antenna elements and $k_0 = 2\pi f_c/c = 2\pi/\lambda$ is the free space wave number. To determine the degree of correlatedness between the two waves we examine the spatial correlation coefficient ρ, which is defined as the *cosine of the angle* between the two phasors. We have

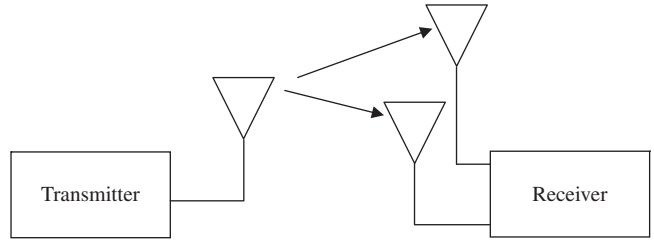

Figure 10.22 The conceptual receive antenna diversity.

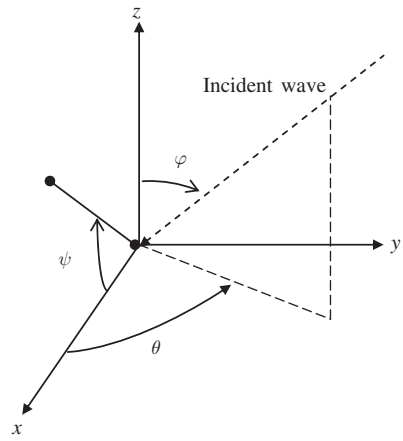

Figure 10.23 Two-antenna array with incident plane waves.

$$\rho = \frac{\mathbf{E}\left(\boldsymbol{V}_1 \boldsymbol{V}_2^*\right)}{\sqrt{\mathbf{E}\left(|\boldsymbol{V}_1|^2\right)\mathbf{E}\left(|\boldsymbol{V}_2|^2\right)}} \tag{10.254}$$

Substituting the phasor expressions into the above equation we obtain

$$\begin{aligned}\rho &= \frac{\int_{\varphi=0}^{\pi}\int_{\theta=0}^{2\pi} \boldsymbol{V}_1(\varphi,\theta)\boldsymbol{V}_2^*(\varphi,\theta) f_{\varphi\theta}(\varphi,\theta)\,\mathrm{d}\varphi\mathrm{d}\theta}{\sqrt{\int_{\varphi=0}^{\pi}\int_{\theta=0}^{2\pi}|\boldsymbol{V}_1(\varphi,\theta)|^2 f_{\varphi\theta}(\varphi,\theta)\,\mathrm{d}\varphi\mathrm{d}\theta \int_{\varphi=0}^{\pi}\int_{\theta=0}^{2\pi}|\boldsymbol{V}_2(\varphi,\theta)|^2 f_{\varphi\theta}(\varphi,\theta)\,\mathrm{d}\varphi\mathrm{d}\theta}} \\ &= \int_{\varphi=0}^{\pi}\int_{\theta=0}^{2\pi} \mathrm{e}^{-\mathrm{j}k_0 d(\cos\psi\cos\theta\sin\varphi+\sin\psi\cos\varphi)} f_{\varphi\theta}(\varphi,\theta)\,\mathrm{d}\varphi\mathrm{d}\theta\end{aligned} \tag{10.255}$$

The function $f_{\varphi\theta}(\varphi,\theta)$ is the joint probability density function of the *polar angle* φ and *azimuth angle* θ, respectively. In our analysis we assume that φ and θ are independent and hence $f_{\varphi\theta}(\varphi,\theta) = f_\varphi(\varphi) f_\theta(\theta)$. Note that $0 \le |\rho|^2 \le 1$. A larger value of $|\rho|^2$ indicates a stronger correlation between the two incident plane waves. On the other hand, when $|\rho|^2 = 0$ the two incident plane waves are uncorrelated.

Mobile station antennas

The mobile station is close to the ground with rich scatterers around it. Therefore, it is reasonable to assume that the waves arrive at the mobile station with equal probability from all angles in the azimuth plane (the Clarke model). Hence, the azimuth angle θ is uniformly distributed in $(0, 2\pi)$ and $f_\theta(\theta) = 1/2\pi$. We have

$$\begin{aligned}\rho &= \int_{\varphi=0}^{\pi}\left[\frac{1}{2\pi}\int_{\theta=0}^{2\pi} \mathrm{e}^{-\mathrm{j}k_0 d\cos\psi\cos\theta\sin\varphi} d\theta\right] \mathrm{e}^{-\mathrm{j}k_0 d\sin\psi\cos\varphi} f_\varphi(\varphi)\,\mathrm{d}\varphi \\ &= \int_{\varphi=0}^{\pi} J_0(k_0 d\,\cos\psi\sin\varphi)\,\mathrm{e}^{-\mathrm{j}k_0 d\sin\psi\cos\varphi} f_\varphi(\varphi)\,\mathrm{d}\varphi\end{aligned} \tag{10.256}$$

For the horizontal array ($\psi = 0$) we get

$$\rho = \int_{\varphi=0}^{\pi} J_0(k_0 d \sin\varphi) f_\varphi(\varphi) \mathrm{d}\varphi \tag{10.257}$$

For a vertical array ($\psi = \pi/2$ radians) we get

$$\rho = \int_{\varphi=0}^{\pi} \mathrm{e}^{-\mathrm{j}k_0 d\cos\varphi} f_\varphi(\varphi)\, \mathrm{d}\varphi \tag{10.258}$$

Furthermore, $f_\varphi(\varphi) = \sin\varphi\, \delta(\varphi - \pi/2)$ is the density function for the elevation angle. Therefore, for a *horizontal array* the spatial correlation coefficient is

$$\rho = J_0(k_0 d) \ \ (\textit{Clarke model} - \textit{horizontal array}) \tag{10.259}$$

On the other hand, $\rho = 1$ for a vertical array since the waves traveling in the horizontal plane to arrive at the two vertically separated antennas are identical.

We can also use the Aulin model to assume that the arrival angle of the incident waves is restricted to the angular region $\pi/2 - \Delta\varphi \le \varphi \le \pi/2 + \Delta\varphi$. In this model the density function of the polar angle φ is given in (10.43) and the spatial correlation coefficient for a *vertical array* is

$$\rho = \frac{\sin(k_0 d \sin\Delta\varphi)}{k_0 d \sin\Delta\varphi} \quad (\textit{Aulin model} - \textit{vertical array}) \tag{10.260}$$

Example 10.26 Separation of antenna elements

Consider the application of receive antenna diversity to cellular communication at 1.9 GHz. The corresponding wavelength is $\lambda = 15.8$ cm and the wave number is $k_0 = 39.8$. For a horizontal array Clarke model, the degree of correlatedness can be assessed via $|\rho|^2 = |J_0(k_0 d)|^2$. For numerical illustration let $k_0 d = 2.2$, which requires the inter-element spacing to be $d = 5.5$ cm (about 0.35λ). This inter-element spacing corresponds to $|\rho|^2 = 0.012$ or -19 dB. Hence, the received paths from the transmitter to the receive antenna elements are virtually uncorrelated.

For a vertical array Aulin model and the same requirement $|\rho|^2 = 0.012$ or -19 dB, we get $k_0 d \sin\Delta\varphi = 5.6$ radians. This implies that $d = 5.6/k_0 \sin\Delta\varphi$. For numerical illustration let $\Delta\varphi = \pi/4$ radians, then $d = 20$ cm (about 1.27λ).

■

Base station antennas

The base station antenna array is commonly located high above the ground and has only a few local scatterers around it. Most of the waves arriving at the array come from scatterers surrounding the mobile station instead. For cellular communications, the mobile station can be a few kilometers from the base station. Even with a high antenna tower, the elevation angles of the arriving waves from scatterers around the mobile station are very small – a few

degrees at most. To ensure that all mobile stations at the edge of the cell (with the weakest signals) can benefit from diversity, the inter-element spacing must be large enough for diversity paths to be uncorrelated. Let us consider a vertical array Aulin model with the requirement $|\rho|^2 = 0.012$ or -19 dB. We get $k_0 d \sin\Delta\varphi = 5.6$ radians. This implies that $d = 5.6/k_0 \sin\Delta\varphi$. For numerical illustration let $\Delta\varphi = 5^0$, then d = 2m (about 12.8 λ). Thus, the inter-element spacing at the base station antenna array is much larger than inter-element spacing at the mobile station antenna array.

Performance

The following examples illustrate the performance of communication systems employing receive antenna diversity alone or with other controlled diversity techniques.

Example 10.27 Receive antenna diversity gain

We wish to evaluate the diversity gain over a single-antenna receiver. We assume that all paths are uncorrelated and non-resolvable and the channel is a slow fading Rayleigh channel. The modulation is QPSK. The multiple-antenna receiver achieves a power gain of $10\log L$ (dB) over a single antenna receiver, where L is the number of the antenna elements in the array. We note that there are practical constraints on the number of antenna elements an array can have, such as size and cost. Each antenna element output must be separately processed by a dedicated receiver before the combining process. For a large L, this would lead to a huge and exorbitantly expensive antenna receiver. To compare the performance between the diversity receiver and the single-antenna receiver we observe that the diversity $\alpha\boldsymbol{SNR}$ is identical to the αSNR of the single-antenna receiver. Consider the case of MRC with $L = 3$ antenna elements and $\alpha\boldsymbol{SNR} = 100$ (20 dB). Using (10.210) we get $P_b \approx 1.6 \times 10^{-9}$ for a diversity receiver. Using (10.57) or (10.219) with $\alpha SNR = \alpha\boldsymbol{SNR}$ we have $P_b \approx 2.5 \times 10^{-3}$ for a single-antenna receiver. In other words, to achieve the bit error probability of the diversity receiver, the single-antenna receiver must have an αSNR of about 62 dB instead of 20 dB. The *diversity gain* is approximately 42 dB. Note that with receive antenna diversity there is no self-interference caused by multipaths (IPI) as experienced by the Rake receiver. Therefore, the required input signal-to-noise ratio αSNR for a Rake receiver must be well above 20 dB to assure a total input signal-to-interference-and-noise ratio of 20 dB.

■

Example 10.28 Receive antenna diversity/controlled diversity

In power-limited applications the combining of a controlled diversity technique such as time diversity or OFDM diversity with receive antenna diversity can significantly lower the bit error probability. Given a controlled L_1-fold diversity and an L_2-fold receive antenna diversity (that is, L_2 distinct L_1-fold diversity receivers) we have a total of $L = L_1 L_2$ pre-combining variables that form the input to the combiner.

For numerical illustration, let us consider a Rayleigh fading channel and compare the performance of a three-fold receive antenna diversity/three-fold controlled diversity QPSK

signal with MRC to the performance of its counterpart without diversity assuming both signals have the same transmitted power and input bit rate. We have $L_1 = L_2 = 3$ and $L = 9$. Assume that the required bit error probability for the diversity system is $P_b \approx 4.2 \times 10^{-6}$. Using (10.210) with $N_n = 2,\ M = 4$ for QPSK and $L = 9$, the L_1-fold diversity signal-to-noise ratio is $\alpha\boldsymbol{SNR} = 3$ or 4.8 dB. A non-diversity system with $\alpha SNR = L_1\alpha\boldsymbol{SNR} = 9$ or 9.5 dB would have a bit error probability of 2.6×10^{-2}. A three-fold controlled diversity would require $\alpha\boldsymbol{SNR} = 33.4$ or 15.2 dB, and a non-diversity system must have $\alpha SNR = 48$ dB to have $P_b \approx 4.2 \times 10^{-6}$. The L-fold *diversity gain* is approximately $48 - 9.5 = 38.5$ dB as compared to 28 dB for the L_1-fold diversity system (Example 10.19).

■

Example 10.29 Receive antenna diversity/Rake diversity

The difference between Rake diversity and controlled diversity is the fact that a Rake receiver enjoys a power gain advantage of $10 \log L$ (dB) over a controlled diversity receiver. Ideally, each finger of the Rake receiver receives the full energy of the symbol. On the other hand, the controlled diversity receiver receives $1/L$ times the energy of a symbol, assuming the same bit rate and equal transmitted power for each system. Given L_1-fold Rake and L_2-fold receive antenna diversity (that is, L_2 distinct L_1-fold Rake receivers) we have a total of $L = L_1L_2$ pre-combining variables from L Rake fingers that form the input to the combiner.

For numerical illustration, let us consider a Rayleigh fading channel and compare the performance of a three-fold receive antenna diversity/three-fold Rake diversity DS-PSK signal with MRC to the performance of its counterpart without diversity assuming both signals have the same transmitted power and input bit rate. We have $L_1 = L_2 = 3$ and $L = 9$. Assume that the required bit error probability for the diversity system is $P_b \approx 4.2 \times 10^{-6}$. Using (10.210) with $\alpha\boldsymbol{SINR}$ replacing $\alpha\boldsymbol{SNR}$, and $N_n = 1,\ M = 2$ for PSK, and $L = 9$, the *path signal-to-interference-and-noise ratio* is $\alpha\boldsymbol{SINR} \approx 3$ or 4.8 dB. A non-receive antenna diversity/non-Rake receiver with $\alpha\ \boldsymbol{SINR} = 3$ or 4.8 dB would have a bit error probability of 2.6×10^{-2}. A three-fold Rake receiver would require $\alpha\boldsymbol{SINR} = 15.2$ dB and a non-receive antenna diversity/non-Rake receiver must have $\alpha\boldsymbol{SINR}$ of 48 dB to have $P_b \approx 4.2 \times 10^{-6}$, which is not possible because IPI limits $\alpha\ \boldsymbol{SINR}$ to no more than 20 dB (Example 10.25).

Now let us consider the case where the spread factor of the PN sequence is $N = 256$. The minimum Euclidean distance for PSK is $d_{min} = \sqrt{2E_b}$. The path signal-to-interference-and-noise ratio is $\alpha\boldsymbol{SINR} = {}^1\!/_2(d_{min}/2\sigma)^2 = [(L_1 - 1)/N + N_0/E_b]^{-1} = 3$ from above. This requires a channel signal-to-noise ratio equal to $\alpha SNR = E_b/N_0 \approx 3$ or 4.8 dB. In this case the channel noise dominates interference. On the other hand, for a non-receive antenna diversity/non-Rake DS-PSK receiver to have $P_b \approx 2.5 \times 10^{-3}$ at $\alpha\boldsymbol{SINR} = 20$ dB (as mentioned above, this receiver cannot do better than this) we must have $\alpha SNR = E_b/N_0 = 457$ or 26.6 dB. Then, the diversity gain defined as the difference between αSNR required for the diversity receiver to achieve $P_b \approx 4.2 \times 10^{-6}$ and αSNR required for the non-diversity DS-PSK receiver to achieve $P_b \approx 2.5 \times 10^{-3}$ is 26.6 dB minus 4.8 dB, which is 21.8 dB.

■

10.15 Transmit antenna diversity (MISO)

Antenna diversity can also be implemented as *transmit antenna diversity* with multiple transmit antennas and one receive antenna (Figure 10.24). This is also referred to as a *multiple-input single-output* (MISO) system. The general case of multiple transmit and receive antennas is treated in the next section. Transmit antenna diversity is a *controlled diversity* technique that provides *spatial* repetition of a transmitted symbol via different antennas. The concept is similar to time diversity, which provides time repetition of a transmitted symbol via different symbol times. Time diversity is a repetition code where the code word consists of L copies of the transmitted symbol. These channel tap weighted copies are made available at the input of the combiner after deinterleaving. Spatial repetition via different transmit antennas alone cannot provide separate copies of the symbol at the receiver because the single-antenna receiver receives the *sum* of these channel tap weighted copies without the ability to separate them for combining. A combination of these two diversity techniques should provide the receiver with *sufficient statistics* to separate copies of a transmitted symbol for combining. This is dictated by (10.190) for *maximal ratio combining*. Therefore, transmit antenna diversity is also referred to as *orthogonal space-time coding*. As in the case of receive antenna diversity we assume that the transmit antennas have sufficient inter-element spacing to ensure all paths from the transmitter to the receiver are uncorrelated.

Space-time coding

For L_s symbol times and L_t-fold transmit antenna diversity we obtain a space-time block code represented by a complex $L_s \times L_t$ matrix $\mathbf{G}$, which consists of L_t parallel code words (the columns of the matrix) whose elements are the transmitted symbols. The repetition code is a special case of the space-time block code with $L_t = 1$, and the code word contains L_s copies of one transmitted symbol, thus providing a diversity order of L_s. This indicates that the rate of the repetition code is $1/L_s$, which is quite inefficient. A space-time block code allows the transmission of m symbol copies in each code word of L_s symbols, thereby increasing the code rate to m/L_s. The diversity order of the space-time code is L_t, the number

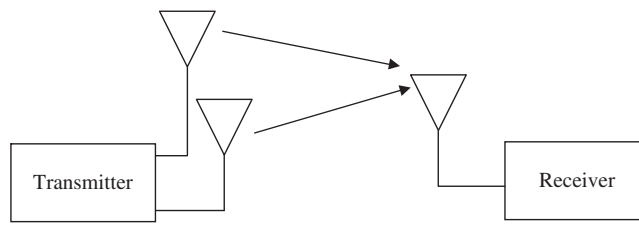

Figure 10.24 The conceptual transmit antenna diversity.

of transmit antennas. To separate the symbol copies for combining it is necessary that the columns of the code matrix $\mathbf{G}$ be (*complex*) *orthogonal* since the transmitter sends all L_t code words concurrently over L_s symbol times. Also, the channel is assumed to remain *constant* for m symbol times. If we assume *perfect channel estimation*, then, for a given transmitted space-time block code matrix $\mathbf{G}$, the *sufficient statistics* for *maximal ratio combining* is dictated by the ability to obtain a matrix $\mathbf{H}$ from the vector $\mathbf{G}\boldsymbol{h}$ as follows:

$$\begin{aligned} \mathbf{G}\boldsymbol{h} &\rightarrow \mathbf{H}\boldsymbol{s} \\ \mathbf{H}^*\mathbf{H} &= \|\boldsymbol{h}\|^2\mathbf{I}_m \end{aligned} \tag{10.261}$$

where $\boldsymbol{h} = [h_1\ h_2 \cdots h_{L_t}]^t$ is the channel tap vector representing L_t paths; $\boldsymbol{s}$ is the symbol vector whose m components are the transmitted symbols on their complex conjugates; $\mathbf{H}$ is referred to as the *channel tap matrix*, an $L_s \times m$ matrix whose elements are the channel taps and its complex conjugates and whose structure depends on $\mathbf{G}$; and $\mathbf{I}_m$ is the $m \times m$ identity matrix. The columns of $\mathbf{H}$ are *orthogonal*, a necessary condition for the detection of $\boldsymbol{s}$ to be decomposed into m separate complex variables. This implies that the columns of $\mathbf{G}$ must also be orthogonal such that $\mathbf{G}^*\mathbf{G} = \|\boldsymbol{s}\|^2\mathbf{I}_{L_t}$. The matrix $\mathbf{H}$ is known by the receiver via channel estimation and the known structure of $\mathbf{G}$. We use the notation $\boldsymbol{A}^*$ for the *conjugate and transpose* of a matrix $\mathbf{A}$. Note that the vector $\mathbf{G}\boldsymbol{h}$ is the sum of L_t channel tap weighted code words. Let $\mathfrak{N} = [\mathfrak{N}_1\mathfrak{N}_2 \cdots \mathfrak{N}_{L_s}]^t$ be the Gaussian noise vector whose elements are independent zero mean complex Gaussian variables with identical variance $2\sigma^2$. The *pre-mapped* vector at the input of the combiner is

$$\boldsymbol{Z} = \mathbf{G}\boldsymbol{h} + \mathfrak{N} \tag{10.262}$$

The vector $\boldsymbol{Z}$ is *mapped* into vector $\boldsymbol{Y}$ by changing some of its elements into their complex conjugates as dictated by the structure of $\mathbf{G}$ such that

$$\boldsymbol{Y} = \mathbf{H}\boldsymbol{s} + \boldsymbol{N} \tag{10.263}$$

The noise vector $\boldsymbol{N} = [N_1\ N_2\ N_{L_s}]^t$ has independent zero mean complex Gaussian components with identical variance $2\sigma^2$. The maximum ratio combiner performs the operation $\mathbf{H}^*\boldsymbol{Y}/\|\boldsymbol{h}\|$ to obtain the decision vector $\boldsymbol{X}$:

$$\begin{aligned} \boldsymbol{X} &= \frac{1}{\|\boldsymbol{h}\|}\mathbf{H}^*\mathbf{H}\boldsymbol{s} + \frac{1}{\|\boldsymbol{h}\|}\mathbf{H}^*\boldsymbol{N} \\ &= \|\boldsymbol{h}\|\boldsymbol{s} + \frac{1}{\|\boldsymbol{h}\|}\mathbf{H}^*\boldsymbol{N} \end{aligned} \tag{10.264}$$

The complex jointly Gaussian noise vector $(\mathbf{H}^*/\|\boldsymbol{h}\|)\boldsymbol{N}$ has a diagonal covariance matrix $\mathbf{E}\left(\mathbf{H}^*\boldsymbol{N}\boldsymbol{N}^*\mathbf{H}/\|\boldsymbol{h}\|^2\right) = \mathbf{H}^*\mathbf{E}(\boldsymbol{N}\boldsymbol{N}^*)\mathbf{H}/\|\boldsymbol{h}\|^2 = 2\sigma^2\mathbf{H}^*\mathbf{H}/\|\boldsymbol{h}\|^2 = 2\sigma^2\mathbf{I}_m$. This implies that the components of this noise vector are *white* and have identical variance $2\sigma^2$, and hence are independent. Thus, the decision vector $\boldsymbol{X}$ consists of m *independent* complex decision variables $X_k, k = 1, 2, \ldots, m$, that can be detected by m parallel minimum Euclidean distance detectors.

Example 10.30 Diversity gain with space-time coding
We wish to evaluate the diversity gain over a single-antenna receiver. We assume that all paths are uncorrelated and non-resolvable and the channel is a slow fading Rayleigh channel such that it can be viewed as constant over m symbol times. The L_t-antenna transmitter divides a fixed transmitted power over L_t antennas. Therefore, the transmitted symbol energy has only $1/L_t$ times the energy of a symbol transmitted by a single-antenna transmitter. To compare the performance between the transmit diversity receiver and the non-transmit diversity receiver we observe that the diversity ***SNR*** is equal to SNR/L_t, where SNR is the signal-to-noise ratio of the non-transmit diversity receiver. The transmit diversity gain with space-time coding is identical to that of a L_t-fold time diversity system with single-antenna transmitter and single-antenna receiver. Compared to a single-antenna transmitter and L_t-antenna receiver system, the space-time coding system suffers a $10\log L_t$ (dB) power penalty.
■

Alamouti code

The Alamouti space-time block code is recommended in the IEEE 802.16 standard for WMAN. The code is specified by the matrix $\mathbf{G}$ whose code words $[s_1 \quad -s_2^*]^t$ and $[s_2 \quad s_1^*]^t$ are the columns of $\mathbf{G}$:

$$\begin{array}{c} \text{Antenna 1} \quad \text{Antenna 2} \\ \uparrow \qquad\quad \uparrow \\ \mathbf{G} = \begin{bmatrix} s_1 & s_2 \\ -s_2^* & s_1^* \end{bmatrix} \begin{array}{l} \rightarrow \text{ Symbol time 1} \\ \rightarrow \text{ Symbol time 2} \end{array} \end{array} \tag{10.265}$$

Note that the columns of $\mathbf{G}$ are orthogonal and so are the rows, that is, $\mathbf{G}^*\mathbf{G} = \mathbf{G}\mathbf{G}^* = \|\boldsymbol{s}\|^2\mathbf{I}_2$, where $\boldsymbol{s} = [s_1 \quad s_2]^t$. The Alamouti code allows the transmission of two symbols over two antennas in two consecutive symbol times. Thus, the *code rate* is *unity* since $m/L_s = 2/2 = 1$. Hence, the Alamouti code requires no bandwidth expansion and is the *perfect* space-time block code. The sum of the channel-tap weighted code words plus noise is

$$\begin{aligned} \boldsymbol{Z} &= h_1\begin{bmatrix} s_1 \\ -s_2^* \end{bmatrix} + h_2\begin{bmatrix} s_2 \\ s_1^* \end{bmatrix} + \begin{bmatrix} \mathfrak{N}_1 \\ \mathfrak{N}_2 \end{bmatrix} \\ &= \begin{bmatrix} h_1 s_1 + h_2 s_2 \\ h_2 s_1^* - h_1 s_2^* \end{bmatrix} + \begin{bmatrix} \mathfrak{N}_1 \\ \mathfrak{N}_2 \end{bmatrix} = \mathbf{G}\boldsymbol{h} + \mathfrak{N} \end{aligned} \tag{10.266}$$

The vector $\boldsymbol{Z} = \mathbf{G}\boldsymbol{h} + \mathfrak{N}$ can be mapped into $\boldsymbol{Y} = \mathbf{H}\boldsymbol{s} + \boldsymbol{N}$ by changing the second element of $\boldsymbol{Z} = [Z_1 \quad Z_2]^t$, which is $Z_2 = h_2 s_1^* - h_1 s_2^* + \mathfrak{N}_2$, into its complex conjugate $Z_2^* = h_2^* s_1 - h_1^* s_2 + \mathfrak{N}_2^*$. Thus we have

$$\begin{aligned}\boldsymbol{Y} = \mathbf{H}\boldsymbol{s} + \boldsymbol{N} = \begin{bmatrix} Z_1 \\ Z_2^* \end{bmatrix} &= \begin{bmatrix} h_1 s_1 + h_2 s_2 \\ h_2^* s_1 - h_1^* s_2 \end{bmatrix} + \begin{bmatrix} N_1 \\ N_2 \end{bmatrix} \\ &= \begin{bmatrix} h_1 & h_2 \\ h_2^* & -h_1^* \end{bmatrix} \begin{bmatrix} s_1 \\ s_2 \end{bmatrix} + \begin{bmatrix} N_1 \\ N_2 \end{bmatrix}\end{aligned} \tag{10.267}$$

where $\boldsymbol{N} = [N_1 \;\; N_2]^t = [\mathfrak{N}_1 \;\; \mathfrak{N}_2^*]^t$, and the corresponding channel tap matrix $\mathbf{H}$ of the code matrix $\mathbf{G}$ is given by

$$\mathbf{H} = \begin{bmatrix} h_1 & h_2 \\ h_2^* & -h_1^* \end{bmatrix} \tag{10.268}$$

Assume that the channel taps h_1 and h_2 are obtained from *perfect channel estimation*. The receiver uses the matrix $\mathbf{H}$ to perform *maximal ratio combining* via the operation $\mathbf{H}^* \boldsymbol{Y}/\|\boldsymbol{h}\| = \mathbf{H}^*(\mathbf{H}\boldsymbol{s} + \boldsymbol{N})/\|\boldsymbol{h}\| = \|\boldsymbol{h}\|\boldsymbol{s} + \mathbf{H}^*\boldsymbol{N}/\|\boldsymbol{h}\|$, where $\boldsymbol{h} = [h_1 \;\; h_2]^t$. Let us examine the noise vector $\mathbf{H}^*\boldsymbol{N}/\|\boldsymbol{h}\|$, we have

$$\frac{1}{\|\boldsymbol{h}\|}\mathbf{H}^*\boldsymbol{N} = \frac{1}{\|\boldsymbol{h}\|}\begin{bmatrix} h_1^* N_1 + h_2 N_2 \\ h_2^* N_1 - h_1 N_2 \end{bmatrix} \tag{10.269}$$

The jointly Gaussian components have zero mean and identical variance $2\sigma^2$. Furthermore, they are uncorrelated since $\mathbf{E}\left[\left(h_1^* N_1 + h_2 N_2\right)\left(h_2^* N_1 - h_1 N_2\right)^*\right] = 0$. Thus, the noise components are independent.

Rate ½ space-time code

Alamouti code is a perfect space-time block code of unity rate for *complex* symbols. It provides two-fold diversity. There are no perfect space-time block codes with complex symbols for diversity order greater than two. To achieve sufficient statistics as described in (10.261) for such cases, the code rate has to be smaller than unity. In this section we discuss rate ½ space-time code with four-fold diversity whose code matrix $\mathbf{G}$ is given below:

$$\begin{array}{l} \text{Antenna 1} \qquad\qquad \text{Antenna 4} \\ \uparrow \qquad \cdots\cdots\cdots \qquad \uparrow \\ \mathbf{G} = \end{array} \begin{bmatrix} s_1 & s_2 & s_3 & s_4 \\ -s_2 & s_1 & -s_4 & s_3 \\ -s_3 & s_4 & s_1 & -s_2 \\ -s_4 & -s_3 & s_2 & s_1 \\ s_1^* & s_2^* & s_3^* & s_4^* \\ -s_2^* & s_1^* & -s_4^* & s_3^* \\ -s_3^* & s_4^* & s_1^* & -s_2^* \\ -s_4^* & -s_3^* & s_2^* & s_1^* \end{bmatrix} \begin{array}{l} \rightarrow \text{Symbol time 1} \\ \rightarrow \text{Symbol time 2} \\ \rightarrow \text{Symbol time 3} \\ \rightarrow \text{Symbol time 4} \\ \rightarrow \text{Symbol time 5} \\ \rightarrow \text{Symbol time 6} \\ \rightarrow \text{Symbol time 7} \\ \rightarrow \text{Symbol time 8} \end{array} \tag{10.270}$$

There are four symbols transmitting over eight symbol times (rate ½) via four antennas (four-fold diversity). The mapping of vector $\boldsymbol{Z} = \mathbf{G}\boldsymbol{h} + \mathfrak{N}$ into $\boldsymbol{Y} = \mathbf{H}\boldsymbol{s} + \boldsymbol{N}$ is accomplished via the matrix $\mathbf{H}$ given by

$$\mathbf{H} = \frac{1}{\sqrt{2}} \begin{bmatrix} h_1 & h_2 & h_3 & h_4 \\ h_2 & -h_1 & h_4 & -h_3 \\ h_3 & -h_4 & -h_1 & h_2 \\ h_4 & h_3 & -h_2 & -h_1 \\ h_1^* & h_2^* & h_3^* & h_4^* \\ h_2^* & -h_1^* & h_4^* & -h_3^* \\ h_3^* & -h_4^* & -h_1^* & h_2^* \\ h_4^* & h_3^* & -h_2^* & -h_1^* \end{bmatrix} \tag{10.271}$$

Note that $\mathbf{H}^*\mathbf{H} = \|\boldsymbol{h}\|^2\mathbf{I}_4$, where $\boldsymbol{h} = [\,h_1 \quad h_2 \quad h_3 \quad h_4\,]^t$. Therefore, the sufficient statistics (10.261) are satisfied and *maximal ratio combining* can be performed via the operation $\boldsymbol{X} = \mathbf{H}^*(\mathbf{H}\boldsymbol{s} + \boldsymbol{N})/\|\boldsymbol{h}\| = \|\boldsymbol{h}\|\boldsymbol{s} + \mathbf{H}^*\boldsymbol{N}/\|\boldsymbol{h}\|$, where $\boldsymbol{s} = [\,s_1 \quad s_2 \quad s_3 \quad s_4\,]^t$ can be detected separately by four parallel minimum Euclidean distance detectors.

Sufficient statistics

The sufficient statistics in (10.261) do not apply to some space-time block codes. In this section we present other sufficient statistics, and that they apply to space-time block codes of smaller rate, such as rate ¾. If we assume *perfect channel estimation* then, for a given orthogonal space-time block code matrix $\mathbf{G}$, where $\mathbf{G}^*\mathbf{G} = \|\boldsymbol{s}\|^2\mathbf{I}_{L_t}$, *maximal ratio combining* is achieved for any received vector $\boldsymbol{Z} = \mathbf{G}\boldsymbol{h} + \mathfrak{N}$, if there exist m vectors $\boldsymbol{h}_i^*$, $i = 1,2, \ldots, m$, with identical norm $\left\|\boldsymbol{h}_i^*\right\|^2 = \|\boldsymbol{h}\|^2$ such that

$$\begin{aligned} &\frac{1}{\|\boldsymbol{h}\|}\boldsymbol{h}_i^*\boldsymbol{Y}_i = \|\boldsymbol{h}\|s_i + N_i, \quad i = 1, 2, \ldots, m \\ &\boldsymbol{h}_i^*\boldsymbol{h}_i = \|\boldsymbol{h}\|^2 \end{aligned} \tag{10.272}$$

where m is the number of transmitted symbols in the code vector; $\mathfrak{N} = [\mathfrak{N}_1 \ \mathfrak{N}_2 \ \ldots \ \mathfrak{N}_{L_s}]^t$ is the Gaussian noise vector whose elements are independent zero mean complex Gaussian variables with identical variance $2\sigma^2$; $\boldsymbol{h} = [h_1 \ h_2 \ \cdots \ h_{L_t}]^t$ is the channel tap vector representing L_t paths; $\boldsymbol{Y}_i = \left[Y_{i,1} \ Y_{i,2} \ \cdots \ Y_{i,L_s}\right]^t$ is the *allowable* received vector, where $Y_{i,k} \in \{Z_k, -Z_k, Z_k^*, -Z_k^*\}$; and $\boldsymbol{h}_i$ is referred to as the ith *channel tap vector*. The jointly complex Gaussian noise vector $\boldsymbol{N} = [N_1 \ N_2 \cdots N_m] = \left[\boldsymbol{h}_1^*\hat{\mathfrak{N}}_1/\|\boldsymbol{h}\| \quad \boldsymbol{h}_2^*\hat{\mathfrak{N}}_2/\|\boldsymbol{h}\| \quad \ldots, \boldsymbol{h}_m^*\hat{\mathfrak{N}}_m/\|\boldsymbol{h}\|\right]$ contains independent components where $\hat{\mathfrak{N}}_i = \left[\hat{\mathfrak{N}}_{i,1}\hat{\mathfrak{N}}_{i,2}\cdots\hat{\mathfrak{N}}_{i,L_s}\right]$, $\hat{\mathfrak{N}}_{i,k} \in \{\mathfrak{N}_k, -\mathfrak{N}_k, \mathfrak{N}_k^*, -\mathfrak{N}_k^*\}$.

Rate ¾ space-time code

In this section we discuss rate ¾ space-time code whose code matrix $\mathbf{G}$ is given below:

$$\mathbf{G} = \begin{bmatrix} s_1 & s_2 & s_3 & 0 \\ -s_2^* & s_1^* & 0 & -s_3 \\ -s_3^* & 0 & s_1^* & s_2 \\ 0 & s_3^* & -s_2^* & s_1 \end{bmatrix} \tag{10.273}$$

Note that the columns of $\mathbf{G}$ are orthogonal, that is, $\mathbf{G}^*\mathbf{G} = \|\boldsymbol{s}\|^2\mathbf{I}_4$, where $\boldsymbol{s} = [s_1 \ s_2 \ s_3]^t$. Four code words (four columns of **G)** contain three symbols each, and are transmitted over four symbol times (rate ¾) and via four antennas (four-fold diversity). The statistics in (10.261) are not sufficient for this code. Instead we use the sufficient statistics (10.272). We have

$$\boldsymbol{h}_1^* = \begin{bmatrix} h_1^* & h_2 & h_3 & h_4^* \end{bmatrix}, \ \boldsymbol{h}_2^* = \begin{bmatrix} h_2^* & -h_1 & h_4^* & -h_3 \end{bmatrix}, \ \boldsymbol{h}_3^* = \begin{bmatrix} h_3^* & -h_4^* & -h_1 & h_2 \end{bmatrix} \tag{10.274}$$

$$\boldsymbol{Z} = \mathbf{G}\boldsymbol{h} + \mathfrak{N}, \quad \boldsymbol{Z} = \begin{bmatrix} Z_1 \\ Z_2 \\ Z_3 \\ Z_4 \end{bmatrix} = \begin{bmatrix} h_1 s_1 + h_2 s_2 + h_3 s_3 \\ h_2 s_1^* - h_1 s_2^* - h_4 s_3 \\ h_3 s_1^* + h_4 s_2 - h_1 s_3^* \\ h_4 s_1 - h_3 s_2^* + h_2 s_3^* \end{bmatrix} + \begin{bmatrix} \mathfrak{N}_1 \\ \mathfrak{N}_2 \\ \mathfrak{N}_3 \\ \mathfrak{N}_4 \end{bmatrix} \tag{10.275}$$

$$\begin{aligned} &\boldsymbol{Y}_1 = \begin{bmatrix} Z_1 & Z_2^* & Z_3^* & Z_4 \end{bmatrix}^t, \ \boldsymbol{Y}_2 = \begin{bmatrix} Z_1 & Z_2^* & Z_3 & Z_4^* \end{bmatrix}^t, \ \boldsymbol{Y}_3 = \begin{bmatrix} Z_1 & Z_2 & Z_3^* & Z_4^* \end{bmatrix}^t \\ &\hat{\mathfrak{N}}_1 = \begin{bmatrix} \mathfrak{N}_1 & \mathfrak{N}_2^* & \mathfrak{N}_3^* & \mathfrak{N}_4 \end{bmatrix}^t, \ \hat{\mathfrak{N}}_2 = \begin{bmatrix} \mathfrak{N}_1 & \mathfrak{N}_2^* & \mathfrak{N}_3 & \mathfrak{N}_4^* \end{bmatrix}^t, \ \hat{\mathfrak{N}}_3 = \begin{bmatrix} \mathfrak{N}_1 & \mathfrak{N}_2 & \mathfrak{N}_3^* & \mathfrak{N}_4^* \end{bmatrix}^t \end{aligned} \tag{10.276}$$

Example 10.31 Channel estimation

To estimate the channel tap vector $\boldsymbol{h}$ of a transmit diversity channel let us consider the received vector $\boldsymbol{Z} = \mathbf{G}\boldsymbol{h} + \mathfrak{N}$. Since $\mathbf{G}^*\mathbf{G} = \|\boldsymbol{s}\|^2\mathbf{I}_{L_t}$, the channel estimation can be carried out with known pilot symbol vector $\boldsymbol{s}$, that is, $\mathbf{G}$ is known to the receiver. The following sufficient statistics provide the MMSE of the vector $\boldsymbol{h}$:

$$\begin{aligned} \hat{\boldsymbol{h}} &= \frac{1}{\|\boldsymbol{s}\|^2}\mathbf{G}^*\mathbf{G}\boldsymbol{h} + \frac{1}{\|\boldsymbol{s}\|^2}\mathbf{G}^*\mathfrak{N} \\ &= \boldsymbol{h} + \hat{\mathfrak{N}} \end{aligned} \tag{10.277}$$

The jointly complex Gaussian noise vector $\left(\mathbf{G}^*/\|\boldsymbol{s}\|^2\right)\mathfrak{N}$ has the diagonal covariance matrix $\mathbf{E}\left(\mathbf{G}^*\mathfrak{N}\mathfrak{N}^*\mathbf{G}/\|\boldsymbol{s}\|^4\right) = \mathbf{G}^*\mathbf{E}(\mathfrak{N}\mathfrak{N}^*)\mathbf{G}/\|\boldsymbol{s}\|^4 = 2\sigma^2\mathbf{G}^*\mathbf{G}/\|\boldsymbol{s}\|^4 = (2\sigma^2/\|\boldsymbol{s}\|^2)\mathbf{I}_m$. This implies that the components of this noise vector are *white* and have identical variance $2\sigma^2/\|\boldsymbol{s}\|^2$. The components of $\boldsymbol{h}$ can be estimated in the mean-square error sense as described in Example 10.6. In fact, at high signal-to-noise ratio $\hat{\boldsymbol{h}}$ can serve as the estimate of $\boldsymbol{h}$.

■

10.16 Transmit–receive antenna diversity (MIMO)

In the above two sections we show how powerful diversity can be whether it is implemented as receive antenna diversity or transmit antenna diversity. If we combine both implementations to form a *multiple-input multiple-output* (MIMO) system we obtain the full diversity benefit. Let us assume that we implement transmit diversity via space-time

coding with a complex $L_s \times L_t$ code matrix $\mathbf{G}$, which provides L_t-fold diversity via L_t transmit antennas for m complex symbols transmitting over L_s symbol times (code rate is m/L_s). On the receive side we implement diversity via L_r receive antennas. We wish to show that with proper *maximal ratio combining* we can achieve the full diversity of order $L = L_t L_r$.

Let us consider *space-time codes that possess the sufficient statistics* (10.261). For each lth receive antenna, there corresponds an orthogonal channel tap matrix $\boldsymbol{H_l}$ obtained from the mapping $\mathbf{G}\boldsymbol{h}_l \rightarrow \mathbf{H}_l\boldsymbol{s}$, where $\boldsymbol{h}_l = [h_{l,1}\ h_{l,2}\ \cdots\ h_{l,L_t}]^t$ is the lth channel tap vector representing L_t paths from L_t transmit antennas to the lth receive antenna. The receivers compute the following pre-combining vectors:

$$\boldsymbol{X}_l = \mathbf{H}_l^*(\mathbf{H}_l\boldsymbol{s} + \boldsymbol{N}_l) = \|\boldsymbol{h}_l\|^2\boldsymbol{s} + \mathbf{H}_l^*\boldsymbol{N}_l,\ \ l = 1, 2, \ldots,\ L_r \tag{10.278}$$

Define the channel tap vector $\boldsymbol{h}$ as follows:

$$\boldsymbol{h} = [\boldsymbol{h}_1\ \boldsymbol{h}_2 \cdots \boldsymbol{h}_{L_r}]^t \tag{10.279}$$

The normalized sum of the pre-combining vectors, $\boldsymbol{X}$, exhibits the maximal ratio combining for all $L = L_t L_r$ paths and is given by

$$\begin{aligned} \boldsymbol{X} &= \frac{1}{\|\boldsymbol{h}\|}\sum_{l=1}^{L_r}\boldsymbol{X}_l = \frac{1}{\|\boldsymbol{h}\|}\sum_{l=1}^{L_r}\|\boldsymbol{h}_l\|^2\boldsymbol{s} + \frac{1}{\|\boldsymbol{h}\|}\sum_{l=1}^{L_r}\mathbf{H}_l^*\boldsymbol{N}_l \\ &= \|\boldsymbol{h}\|\boldsymbol{s} + \frac{1}{\|\boldsymbol{h}\|}\sum_{l=1}^{L_r}\mathbf{H}_l^*\boldsymbol{N}_l \end{aligned} \tag{10.280}$$

The decision vector $\boldsymbol{X}$ can be detected by m parallel minimum Euclidean distance detectors. The noise vector has the covariance $2\sigma^2\mathbf{I}_m$.

Let us now consider *space-time codes that possess the sufficient statistics* (10.272). For each lth receive antenna, there correspond m channel tap vectors $\boldsymbol{h}_{i,l}^*$, $i = 1, 2, \ldots, m$. The receiver computes $X_{i,l} = \boldsymbol{h}_{i,l}^*\boldsymbol{Y}_{i,l} = \|\boldsymbol{h}_l\|^2 s_i + \|\boldsymbol{h}_l\|N_{i,l},\ \ i = 1, 2, \ldots, m;\ l = 1, 2, \ldots, L_r$, where $\boldsymbol{h}_l = [h_{l,1}\ h_{l,2} \cdots h_{l,L_t}]^t$ is the lth channel tap vector representing L_t paths from L_t transmit antennas to the lth receive antenna. The receivers compute the following combining variables based on the channel tap vector $\boldsymbol{h} = [\boldsymbol{h}_1\ \boldsymbol{h}_2 \cdots \boldsymbol{h}_{L_r}]^t$:

$$\begin{aligned} X_i &= \frac{1}{\|\boldsymbol{h}\|}\sum_{l=1}^{L_r}X_{i,l} = \frac{1}{\|\boldsymbol{h}\|}\sum_{l=1}^{L_r}\|\boldsymbol{h}_l\|^2 s_i + \frac{1}{\|\boldsymbol{h}\|}\sum_{l=1}^{L_r}\|\boldsymbol{h}_l\|N_{i,l} \\ &= \|\boldsymbol{h}\|s_i + \frac{1}{\|\boldsymbol{h}\|}\sum_{l=1}^{L_r}\|\boldsymbol{h}_l\|N_{i,l},\ \ i = 1, 2, \ldots, m \end{aligned} \tag{10.281}$$

The m decision variables X_i can be detected by m parallel minimum Euclidean distance detectors. The noise variable has the variance $2\sigma^2$.

To conclude the study of diversity we make the following observations. With regard to transmit antenna diversity via space-time coding, the transmit diversity gain is identical to that of a L_t-fold time diversity system with single-antenna transmitter and single-antenna receiver (note that space-time coding utilizes bandwidth more efficiently than time diversity). Compared to a single-antenna transmitter and L_t-antenna receiver system, a space-time

coding system suffers $10 \log L_t$ (dB) power penalty. On the other hand, there is no power penalty for receive antenna diversity; however, physical constraints often prevent the implementation of many antennas on a receiver such as a cell phone, personal digital assistant, or notebook computer, for example. Thus, transmit–receive antenna diversity offers a compromise solution by reducing the number of both transmit and receive antennas to satisfy both physical contraints and power requirements.

Example 10.32 2×2 MIMO system

Consider a MIMO system with two transmit antennas utilizing the Alamouti code and two receive antennas. Let h_{lj} be the channel tap between the jth ($j = 1, 2$) transmit antenna and the lth ($l = 1, 2$) receive antenna. The sum of the channel tap weighted code word at the first receive antenna ($l = 1$) is

$$\begin{aligned} \boldsymbol{Z}_1 &= h_{11}\begin{bmatrix} s_1 \\ -s_2^* \end{bmatrix} + h_{12}\begin{bmatrix} s_2 \\ s_1^* \end{bmatrix} + \begin{bmatrix} \mathfrak{N}_{11} \\ \mathfrak{N}_{12} \end{bmatrix} \\ &= \begin{bmatrix} h_{11}s_1 + h_{12}s_2 \\ h_{12}s_1^* - h_{11}s_2^* \end{bmatrix} + \begin{bmatrix} \mathfrak{N}_{11} \\ \mathfrak{N}_{12} \end{bmatrix} = \mathbf{G}\boldsymbol{h}_1 + \mathfrak{N}_1 \end{aligned} \tag{10.282}$$

where $\boldsymbol{h}_1 = [h_{11}\ h_{12}]^t$. Similarly, for the second receive antenna ($l = 2$) we have

$$\begin{aligned} \boldsymbol{Z}_2 &= h_{21}\begin{bmatrix} s_1 \\ -s_2^* \end{bmatrix} + h_{22}\begin{bmatrix} s_2 \\ s_1^* \end{bmatrix} + \begin{bmatrix} \mathfrak{N}_{21} \\ \mathfrak{N}_{22} \end{bmatrix} \\ &= \begin{bmatrix} h_{21}s_1 + h_{22}s_2 \\ h_{22}s_1^* - h_{21}s_2^* \end{bmatrix} + \begin{bmatrix} \mathfrak{N}_{21} \\ \mathfrak{N}_{22} \end{bmatrix} = \mathbf{G}\boldsymbol{h}_2 + \mathfrak{N}_2 \end{aligned} \tag{10.283}$$

where $\boldsymbol{h}_2 = [h_{21}\ h_{22}]^t$. The vector $\boldsymbol{Z}_l$ can be mapped into the vector $\boldsymbol{Y}_l = \mathbf{H}_l\boldsymbol{s} + \boldsymbol{N}_l$ by changing the second element Z_{l2} of $\boldsymbol{Z}_l = [Z_{l1}\ Z_{l2}]^t$ into its complex conjugate. Thus, for $s = [s_1\ s_2]^t$ we have

$$\boldsymbol{Y}_l = \mathbf{H}_l\boldsymbol{s} + \boldsymbol{N}_l = \begin{bmatrix} Z_{l1} \\ Z_{l2}^* \end{bmatrix}, \quad l = 1, 2 \tag{10.284}$$

Specifically, we obtain

$$\begin{aligned} \boldsymbol{Y}_1 &= \begin{bmatrix} h_{11}s_1 + h_{12}s_2 \\ h_{12}^*s_1 - h_{11}^*s_2 \end{bmatrix} + \begin{bmatrix} \mathfrak{N}_{11} \\ \mathfrak{N}_{12} \end{bmatrix} \\ &= \begin{bmatrix} h_{11} & h_{12} \\ h_{12}^* & -h_{11}^* \end{bmatrix}\begin{bmatrix} s_1 \\ s_2 \end{bmatrix} + \begin{bmatrix} \mathfrak{N}_{11} \\ \mathfrak{N}_{12}^* \end{bmatrix} \\ &= \mathbf{H}_1\boldsymbol{s} + \boldsymbol{N}_1 \end{aligned} \tag{10.285}$$

where

$$\mathbf{H}_1 = \begin{bmatrix} h_{11} & h_{12} \\ h_{12}^* & -h_{11}^* \end{bmatrix}, \quad \mathbf{H}_1^*\mathbf{H}_1 = \|\boldsymbol{h}_1\|^2\mathrm{I}_2 \tag{10.286}$$

Also,

$$\begin{aligned}\boldsymbol{Y}_2 &= \begin{bmatrix} h_{21}s_1 + h_{22}s_2 \\ h_{22}^* s_1 - h_{21}^* s_2 \end{bmatrix} + \begin{bmatrix} \mathfrak{N}_{21} \\ \mathfrak{N}_{22}^* \end{bmatrix} \\ &= \begin{bmatrix} h_{21} & h_{22} \\ h_{22}^* & -h_{21}^* \end{bmatrix} \begin{bmatrix} s_1 \\ s_2 \end{bmatrix} + \begin{bmatrix} \mathfrak{N}_{21} \\ \mathfrak{N}_{22}^* \end{bmatrix} \\ &= \mathbf{H}_2 \boldsymbol{s} + \boldsymbol{N}_2 \end{aligned} \tag{10.287}$$

where

$$\mathbf{H}_2 = \begin{bmatrix} h_{21} & h_{22} \\ h_{22}^* & -h_{21}^* \end{bmatrix}, \quad \mathbf{H}_2^* \mathbf{H}_2 = \|\boldsymbol{h}_2\|^2 \mathbf{I}_2 \tag{10.288}$$

Therefore, the decision variable $\boldsymbol{X}_l$ at the lth antenna is $\boldsymbol{X}_l = \mathbf{H}_l^*(\mathbf{H}_l \boldsymbol{s} + \boldsymbol{N}_l) = \|\boldsymbol{h}_l\|^2 \boldsymbol{s} + \mathbf{H}_l^* \boldsymbol{N}_l$, $l = 1, 2$. Specifically, we have

$$\begin{aligned} \boldsymbol{X}_1 &= \|\boldsymbol{h}_1\|^2 \boldsymbol{s} + \mathbf{H}_1^* \boldsymbol{N}_1 \\ \boldsymbol{X}_2 &= \|\boldsymbol{h}_2\|^2 \boldsymbol{s} + \mathbf{H}_2^* \boldsymbol{N}_2 \end{aligned} \tag{10.289}$$

The MRC decision variable is the normalized sum of $\boldsymbol{X}_1$ and $\boldsymbol{X}_2$. For the channel tap vector $\boldsymbol{h} = [h_{11}\ h_{12}\, h_{21}\ h_{22}]^t$ we have

$$\boldsymbol{X} = \frac{1}{\|\boldsymbol{h}\|}(\boldsymbol{X}_1 + \boldsymbol{X}_2) = \frac{\|\boldsymbol{h}_1\|^2 + \|\boldsymbol{h}_2\|^2}{\|\boldsymbol{h}\|} \boldsymbol{s} + \frac{1}{\|\boldsymbol{h}\|}(\mathbf{H}_1^* \boldsymbol{N}_1 + \mathbf{H}_2^* \boldsymbol{N}_2) \tag{10.290}$$

Since $\|\boldsymbol{h}_1\|^2 + \|\boldsymbol{h}_2\|^2 = |h_{11}|^2 + |h_{12}|^2 + |h_{21}|^2 + |h_{22}|^2 = \|\boldsymbol{h}\|^2$, we obtain the following MRC decision vector:

$$\boldsymbol{X} = \|\boldsymbol{h}\| \boldsymbol{s} + \boldsymbol{N} \tag{10.291}$$

where the noise vector is $\boldsymbol{N} = (\mathbf{H}_1^* \boldsymbol{N}_1 + \mathbf{H}_2^* \boldsymbol{N}_2)/\|\boldsymbol{h}\|$. The covariance of noise $\boldsymbol{N}$ is given by $\mathbf{E}(\boldsymbol{N}\boldsymbol{N}^*) = \mathbf{H}_1^* \mathbf{E}(\boldsymbol{N}_1 \boldsymbol{N}_1^*) \mathbf{H}_1 + \mathbf{H}_2^* \mathbf{E}(\boldsymbol{N}_2 \boldsymbol{N}_2^*) \mathbf{H}_2$. Since $\mathbf{E}(\boldsymbol{N}_l \boldsymbol{N}_l^*) = 2\sigma^2 \mathbf{I}_2$, $l = 1, 2$, we obtain $\mathbf{E}(\boldsymbol{N}\boldsymbol{N}^*) = 2\sigma^2 \left(\|\boldsymbol{h}_1\|^2 + \|\boldsymbol{h}_2\|^2 \right) \mathbf{I}_2 / \|\boldsymbol{h}\|^2 = 2\sigma^2 \mathbf{I}_2$.

■

10.17 Channel capacity

The capacity of a *complex* AWGN channel was established by Shannon as $C = \log_2(1 + SNR)$ bits/ symbol (bits/transmission) where $SNR = E_s/N_0$. For a rate less than C, there exists a coding system such that the code words can be transmitted over the channel with an arbitrarily small frequency of errors. For a fading channel such capacity cannot be established because of outages which do not exist in an AWGN channel. The instantaneous signal-to-noise ratio at the receiver is a random variable which is a function of the squared magnitude of the channel tap. Since the instantaneous *SNR* can be zero, the

instantaneous channel capacity can also be theoretically zero during a deep fade. Hence, a positive transmission rate is always greater than C during a deep fade, and no coding systems exist that allow the code words to be transmitted during an outage with an arbitrarily small frequency of errors. Thus, the average channel capacity does not exist in most practical fading channels. However, we can still define channel capacity in the outage sense, which we will explore for the various channels studied in the previous sections.

Slow fading

In a slow fading single-tap (flat fading) channel, the channel estimation time is smaller than the channel coherence time. With perfect channel estimation where the Doppler effect is nullified completely, the instantaneous signal-to-noise ratio is simply $|h|^2 SNR$, where h is the channel tap. Thus, the instantaneous channel capacity can be defined as

$$C = \log_2\left(1 + |h|^2 SNR\right) \text{ bits/symbol} \tag{10.292}$$

When the instantaneous channel capacity falls below the transmission rate R due to fading the error probability cannot be made arbitrarily small and an outage occurs. We define the *capacity-outage probability* as follows:

$$\Pr(C < R) = \Pr\left[\log_2\left(1 + |h|^2 SNR\right) < R\right] \tag{10.293}$$

For a specified p_o, there exists an outage capacity C_o which is the *maximum* transmission rate for which the capacity-outage probability is less than p_o. Setting $\Pr(C < R) = p_o$ and solving for $R = C_o$ we have

$$\begin{aligned} p_o &= \Pr\left[\log_2\left(1 + |h|^2 SNR\right) < C_o\right] \\ &= \Pr\left[|h|^2 < \frac{2^{C_o} - 1}{SNR}\right] \\ &= F_{|h|^2}\left(\frac{2^{C_o} - 1}{SNR}\right) \end{aligned} \tag{10.294}$$

where $F_{|h|^2}(y)$ is the distribution function of $|h|^2$. Let $F^{(-1)}_{|h|^2}(y)$ be the *inverse function* of $F_{|h|^2}(y)$, that is, $F_{|h|^2}\left[F^{(-1)}_{|h|^2}(p_o)\right] = p_o$, we can evaluate C_o as follows:

$$C_o = \log_2\left[1 + F^{(-1)}_{|h|^2}(p_o) SNR\right] \text{ bits/symbol} \tag{10.295}$$

The quantity $F^{(-1)}_{|h|^2}(p_o) SNR$ is referred to as the *outage signal-to-noise ratio*.

Example 10.33 Outage capacity of a slow fading Rayleigh channel

The distribution function of the squared magnitude of the channel tap $|h|^2$ of a Rayleigh channel is

$$F_{|h|^2}(y) = 1 - \mathrm{e}^{-y} \tag{10.296}$$

The corresponding inverse function $F^{(-1)}_{|h|^2}(p_o)$ is therefore given by

$$F^{(-1)}_{|h|^2}(p_o) = \ln \frac{1}{1-p_o} \tag{10.297}$$

Hence, we obtain the outage capacity of a slow fading Rayleigh channel as

$$C_o = \log_2[1 - \{\ln(1-p_o)\}SNR] \text{ bits/symbol} \tag{10.298}$$

For an outage probability $p_o = 0.01$, the outage signal-to-noise ratio is $0.01\,SNR$. This is almost 100 times smaller than that of an AWGN channel. Using the identity $\log_2 x = \ln x / \ln 2$ and $SNR = 10$, the outage capacity is approximately 4% of the AWGN channel capacity, which is $C = \log_2(1 + SNR)$.

■

Slow fading–receive antenna diversity

The instantaneous channel capacity for a slow fading single-tap channel with L-fold receive antenna diversity and maximal ratio combining is given by

$$C = \log_2\left(1 + \|\boldsymbol{h}\|^2 SNR\right) \text{ bits/symbol} \tag{10.299}$$

where $\boldsymbol{h} = [h_1\ h_2 \cdots h_L]^t$ is the channel tap vector whose components are the channel taps of the receive paths. The outage capacity for a specified outage probability p_o is

$$C_o = \log_2\left[1 + F^{(-1)}_{\|\boldsymbol{h}\|^2}(p_o)SNR\right] \text{ bits/symbol} \tag{10.300}$$

where

$$\begin{aligned} p_o &= \Pr\left[\log_2\left(1 + \|\boldsymbol{h}\|^2 SNR\right) < C_o\right] \\ &= \Pr\left[\|\boldsymbol{h}\|^2 < \frac{2^{C_o} - 1}{SNR}\right] \\ &= F_{\|\boldsymbol{h}\|^2}\left(\frac{2^{C_o} - 1}{SNR}\right) \end{aligned} \tag{10.301}$$

For a slow-flat Rayleigh fading channel we can use the *χ^2-density function with 2L degrees of freedom*. Thus, the distribution function for L-fold diversity is given by

$$F_{\|\boldsymbol{h}\|^2}(y) = 1 - \mathrm{e}^{-y} \sum_{k=0}^{L-1} \frac{y^k}{k!} \tag{10.302}$$

There is no closed-form solution for $F^{(-1)}_{\|\boldsymbol{h}\|^2}(p_o)$, and hence C_o, so the result has to be obtained numerically.

Example 10.34 Outage capacity of a slow fading–receive antenna diversity Rayleigh channel

Consider an outage probability $p_o = 0.01$ and $L = 2$. For $SNR = 10$, the outage capacity is approximately 38% of the AWGN channel capacity, which is $C = \log_2(1 + SNR)$.

■

Slow fading–transmit antenna diversity

Let us now consider the case of transmit antenna diversity using space-time coding with a $L_s \times L_t$ code matrix $\mathbf{G}$ that provides L_t-fold transmit antenna diversity at a code rate $r = m/L_s$, where m symbols are transmitted in L_s symbol times. For a fixed transmitted power P, each antenna radiates a signal with power P/L_t. This implies that the instantaneous signal-to-noise ratio at the receiver is $\|\boldsymbol{h}\|^2 SNR/L_t$. The instantaneous capacity of a transmit diversity channel employing space-time coding is given by

$$C = \log_2\left(1 + \|\boldsymbol{h}\|^2 \frac{SNR}{L_t}\right) \text{ bits/symbol} \tag{10.303}$$

An outage occurs if the instantaneous capacity falls below the target rate R. Thus

$$\Pr(C < R) = \Pr\left[\log_2\left(1 + \|\boldsymbol{h}\|^2 \frac{SNR}{L_t}\right) < R\right] \tag{10.304}$$

Given an outage probability p_o, the outage capacity is given as

$$C_o = \log_2\left[1 + F^{(-1)}_{\|\boldsymbol{h}\|^2}(p_o)\frac{SNR}{L_t}\right] \text{ bits/symbol} \tag{10.305}$$

where $p_o = F_{\|\boldsymbol{h}\|^2}\left(L_t[2^{C_o} - 1]/SNR\right)$ and $F^{(-1)}_{\|\boldsymbol{h}\|^2}(p_o)$ can be calculated from (10.302).

Example 10.35 Outage capacity of a slow fading–transmit antenna diversity Rayleigh channel

Consider an outage probability $p_o = 0.01$ and Alamouti code ($m = 2$, $L_s = 2$, $L_t = 2$). For $SNR = 10$, the outage capacity is approximately 24% of the AWGN channel capacity, which is $C = \log_2(1 + SNR)$. As a comparison, the outage capacity of a non-diversity channel is 4% of the AWGN channel capacity, and the outage capacity of a two-fold receive antenna diversity channel is 38% of the AWGN channel capacity. The outage capacity for a space-time code with rate $r < 1$ is multiplied by the code rate r when compared to the capacity of the non-diversity system or the receive antenna diversity system.

■

Slow fading–transmit and receive antenna diversity

When transmit antenna diversity is combined with receive antenna diversity then full diversity is achieved. Consider transmit antenna diversity using space-time coding with a $L_s \times L_t$ code matrix $\mathbf{G}$ that provides L_t-fold transmit antenna diversity at a code rate $r = m/L_s$, where m symbols are transmitted in L_s symbol times. Furthermore, consider receive antenna diversity with L_r antennas. For a fixed transmitted power P, each transmit antenna radiates a signal with power P/L_t. This implies that the instantaneous signal-to-noise ratio at the receiver is $\|\boldsymbol{h}\|^2 SNR/L_t$, where $\boldsymbol{h} = [\boldsymbol{h}_1\ \boldsymbol{h}_2 \cdots \boldsymbol{h}_{L_r}]^t$ is the channel tap vector and $\boldsymbol{h}_l = [h_{l,1}\ h_{l,2} \cdots h_{l,L_t}]^t$, $l = 1, 2, \ldots, L_r$, is the lth channel tap vector representing L_t paths from the transmit antennas to the lth receive antenna. Given an outage probability p_o, the outage capacity for L-fold diversity ($L = L_t L_r$) is given as

$$C_o = \log_2\left[1 + F^{(-1)}_{\|\boldsymbol{h}\|^2}(p_o)\frac{SNR}{L_t}\right] \text{ bits/symbol} \tag{10.306}$$

where $p_o = F_{\|\boldsymbol{h}\|^2}\left(L_t[2^{C_o} - 1]/SNR\right)$ and $F^{(-1)}_{\|\boldsymbol{h}\|^2}(p_o)$ can be calculated from (10.302) for $L = L_t L_r$.

Example 10.36 Outage capacity of a slow fading–transmit and receive antenna diversity Rayleigh channel

Consider an outage probability $p_o = 0.01$ and Alamouti code (m = 2, L_s = 2, $L_t = 2$) working with two-fold receive diversity for a total of four-fold diversity, for SNR = 10, the outage capacity is approximately 68% of the AWGN channel capacity, which is $C = \log_2(1 + SNR)$. As a comparison, the outage capacity of a non-diversity channel is 4% of the AWGN channel capacity, the outage capacity of a two-fold transmit antenna diversity channel is 24% of the AWGN channel capacity, and the outage capacity of a two-fold receive antenna diversity channel is 38% of the AWGN channel capacity.

■

Slow fading–OFDM

OFDM is designed to work in an *underspread frequency-selective* channel. With N subcarriers, OFDM provides N parallel slow fading subchannels with no ISI (flat fading) in the ideal case. The use of a cyclic prefix to reduce ISI could only lower the channel capacity but is necessary in practice. For a fixed transmitted power P, each subchannel power is P/N. This implies that the instantaneous signal-to-noise ratio of the lth subchannel at the receiver is $\|H_l\|^2 SNR/N$. The instantaneous channel capacity is

$$C = \sum_{l=1}^{N} \log_2\left(1 + |H_l|^2\frac{SNR}{N}\right) \text{ bits/symbol} \tag{10.307}$$

If the OFDM target rate is $R = NR_s$, where R_s is the subcarrier symbol rate, then an outage occurs if $C < R$, and the outage probability is

$$\Pr(C<R) = \Pr\left[\sum_{l=1}^{N} \log_2\left(1 + |H_l|^2 \frac{SNR}{N}\right) < R\right] \tag{10.308}$$

The above expression shows that as long as the OFDM capacity is *above* R, there exists a coding system such that the code words can be transmitted over the channel with an arbitrarily small frequency of errors. This happens irrespective of the fades experienced by the subchannels, which could make some subchannel rates drop below R/N. This implies that coding should be carried out *across* all subcarriers (this also means across many coherence bandwidths) instead of over individual subcarriers. This ensures that if errors occur in some subcarriers during a deep fade, they could still be corrected if the remaining subcarriers have high signal-to-noise ratios. On the other hand, if coding is carried out for each individual subcarrier, then a deep fade may wipe out a subcarrier entirely with no chance of correcting the errors even if the remaining subcarriers have no error. Therefore, coding for each individual subcarrier provides poor diversity, and coding across all subcarriers provides full diversity. The advantage of coding for each individual subcarrier is that the decoding can be carried out at a lower subcarrier rate and parallel processing of all subcarriers shortens the code latency. Furthermore, there are codes such as *trellis coded modulation* that can provide excellent performance when implemented with MQAM subcarriers. On the other hand, codes such as *low-density parity-check* codes are excellent for coding across all subcarriers.

Example 10.37 Time-invariant and frequency-selective channel

Let us consider a frequency-selective channel that experiences very slow fading and can be modeled as a time-invariant channel. By using OFDM one can effectively convert this channel into N parallel subchannels that experience small ISI via the use of cyclic prefixes. The maximum rate of reliable communication for N parallel subchannels with noise variance $\sigma^2 = N_0$ is given by

$$C(N) = \max_{P_1 \ldots P_N} \sum_{k=1}^{N} \log_2\left(1 + |H_k|^2 SNR_k\right) \text{ bits/OFDM symbol} \tag{10.309}$$

where $SNR_k = P_k/\sigma^2 = P_k/N_0$, $\sum_{k=1}^{N} P_k = \mathcal{P}$, and H_k is the DFT of the L-tap channel $\boldsymbol{h} = [h_0\ h_1\ \cdots\ h_{L-1}\ 0\ \cdots\ 0]^t$ multiplied by $\sqrt{N}$, that is, $H_k = \sum_{l=0}^{L-1} h_l e^{-j2\pi kl/N}$. Hence, the power constraint optimization problem is the *water filling* strategy, which yields the following power allocation:

$$P_k = \max\left(0, \frac{1}{\lambda} - \frac{N_0}{|H_k|^2}\right) \tag{10.310}$$

where the Lagrange multiplier λ is selected such that $\sum_{k=1}^{n} P_k = \mathcal{P}$. Let us specify the L-tap channel model as follows:

$$h(t) = \sum_{l=0}^{L-1} h_l \delta(t - \tau_l) \tag{10.311}$$

The corresponding frequency response is the *Fourier transform* of the channel impulse response $h(t)$. We have

$$H(f) = \sum_{l=0}^{L-1} h_l \mathrm{e}^{-\mathrm{j}2\pi f \tau_l} \tag{10.312}$$

For simplicity let the path delay be $\tau_l = lT$, where T is the delay between two adjacent paths. We have

$$H(f) = \sum_{l=0}^{L=1} h_l \mathrm{e}^{-\mathrm{j}2\pi flT} \tag{10.313}$$

Thus, the subchannel tap $H_k = \sum_{l=0}^{L-1} h_l \mathrm{e}^{-\mathrm{j}2\pi kl/N}$ is the value of $H(f)$ sampled at frequency $f = k/NT$, $k = 0, 1, \ldots, N-1$, namely, $H_k = H(k/NT)$. Note that H_k is also the *discrete-time Fourier transform* of the finite sequence $[h_l]$, sampled at $f = k/N$, namely, $H_k = H\left(\mathrm{e}^{\mathrm{j}2\pi kl/N}\right)$. Let us consider the case when the number of subcarriers N is large as it tends to infinity. This implies that the optimal power allocation converges to the *water filling* power allocation over the channel frequency response as follows:

$$P(f) = \max\left(0, \frac{1}{\lambda} - \frac{N_0}{|H(f)|^2}\right) \tag{10.314}$$

where the Lagrange multiplier λ is selected such that

$$\int_0^{1/T} P(f)\,\mathrm{d}f = \mathscr{P} \tag{10.315}$$

The water filling channel capacity converges to the following expression:

$$C = \int_0^{1/T} \log_2\left(1 + \frac{|H(f)|^2 P(f)}{N_0}\right) \mathrm{d}f \quad \text{bits/s} \tag{10.316}$$

The water filling power allocation achieves the maximum reliable rate of communication over independent subchannels. This is simpler and more effective than coding across all subcarriers. It can be carried out by independent subcarrier coding with adaptive rate and by using adaptive modulation to meet the power requirement. The water filling power allocation requires the transmitter to know the state of the channel, namely, the transmitter has the *channel side information* (CSI). If the channel state is known only at the receiver, that is, only the *channel side information at the receiver* (CSIR) is available, than coding across all subcarriers is the appropriate strategy.

■

Fast fading

Fast fading occurs when the channel estimation time is larger than the channel coherence time. In previous material we have shown that Doppler tracking and correction can be done down to the symbol time. This means that the Doppler phase error can be effective reduced to no more than the phase error that accumulates over one symbol time. If the Doppler shift is too large, as is the case with high-speed platforms such as high-speed trains, aircraft, and low-Earth-orbit satellites, the Doppler phase error over a symbol time may incur a large loss in the symbol signal-to-noise ratio of MQAM. This results in fast fading where the channel coherence time is less than a symbol time. In such a fast fading channel, the average fade duration is short and the symbols fade independently. For a quadrature (complex) channel this means that symbol errors can occur randomly and there exists a coding system that ensures the maximum reliable rate, which is the ensemble average rate given by

$$C = \mathbf{E}\left[\log_2\left(1 + |h|^2 SNR\right)\right] \text{ bits/symbol} \tag{10.317}$$

If we assume Rayleigh fading, at *low SNR* the capacity can be approximated as

$$\begin{aligned} C &= \mathbf{E}\left[\log_2\left(1 + |h|^2 SNR\right)\right] \approx \frac{\boldsymbol{E}\left[\left(|h|^2 SNR\right)\right]}{\ln 2} \\ &\approx \frac{SNR}{\ln 2} \end{aligned} \tag{10.318}$$

where $\mathbf{E}\left(|h|^2\right) = 1$. The right-hand side of the above equation is also the capacity of an AWGN channel at low SNR. At *high SNR* we have

$$C = \mathbf{E}\left[\log_2\left(|h|^2 SNR\right)\right] \approx \log_2 SNR + E\left[\log_2\left(|h|^2\right)\right] \tag{10.319}$$

At high *SNR* the capacity of an AWGN channel is $\log_2 SNR$. For a fast Rayleigh fading channel $\mathbf{E}\left[\log_2\left(|h|^2\right)\right] = -0.83$ and $C \approx \log_2 SNR - 0.83 = \log_2(0.56\, SNR)$. Thus, a fast Rayleigh fading channel needs an additional 2.5 dB in *SNR* to achieve the same capacity as that of an AWGN channel. For $SNR = 10$, the capacity of a fast Rayleigh fading channel is 72% of the capacity of an AWGN channel. This is much better than a slow Rayleigh fading channel where the outage capacity is about 30% the capacity of an AWGN channel for an outage probability of 0.1. From the capacity point of view, slow fading is more *detrimental* than fast fading. From the bit error probability point of view, a more complex coding system is needed for a fast fading channel to achieve the same bit error probability as compared with an AWGN channel. This is necessary because in a fast fading channel one must deal with both *envelope* fading (such as Rayleigh fading) and Doppler *phase error*. On the other hand, a slow fading channel only requires the coding system to deal with envelope fading since the effect of Doppler shift is virtually nullified by Doppler tracking and correction. Furthermore, since fast fading commonly occurs at low bit rates and with high-speed platforms, most wireless applications for high data rates and low mobility are not affected.

10.18 Summary

A fading channel is characterized by a time-varying effect and a space-varying effect. The former results from the Doppler effect due to the movement of the transmitter and receiver. The latter results from the signal envelope variation due to multipath echoes; these multipath components also vary according to the location of the transmitter and receiver. The time-varying effect can be empirically described by the channel coherence time or its counterpart the Doppler spread. If the channel coherence time is greater than the channel estimation time we have a slow fading channel. If the channel coherence time is smaller than the channel estimation time we have a fast fading channel. The space-varying effect can be empirically described by the multipath delay spread or its counterpart the channel coherence bandwidth. If the multipath delay spread is smaller than the symbol time we have a flat fading channel. If the multipath delay spread is greater than the symbol time we have a frequency-selective fading channel. The Doppler spectrum (Clarke or Aulin) allows one to calculate the Doppler spread or channel coherence time.

The performance of ideal coherent demodulation in a Rayleigh or Nakagami-m fading channel was evaluated using known closed-form expressions. Bit error probability for IQ signals with known phase errors were also derived. To correct the phase error due to Doppler shift we proposed the pilot symbol-aided decision-feedback demodulation. This demodulation method employs *differential decision-feedback* (D-DF) and *double-differential decision-feedback* (DD-DF) algorithms. The latter can correct the Doppler phase error down to the symbol time.

The performance of OFDM in the presence of Doppler shift was analyzed to show the effect of intercarrier interference, which can be removed prior to DFT. The cyclic prefix can remove ISI between OFDM symbols but the intrasubcarrier interference can only be alleviated via equalization.

The performance of ideal noncoherent demodulation in a Rayleigh or Nakagami-m fading channel was evaluated using known closed-form expressions. Doppler tracking of both MFSK and CSK were studied. Pilot-tone aided demodulation of complex spreading orthogonal covering signals used in IS-95, CDMA 2000, and WCDMA was investigated as well as noncoherent demodulation of offset quadrature DS-CSK signals.

Diversity is employed in practice to combat fading based on the fact that multiple receptions of the same symbol are affected differently in a fading channel. Some receptions might survive and others might be wiped out. The survivors may be of help in detecting the symbol. There are primarily four types of diversity, namely, time diversity, frequency diversity, path diversity, and antenna diversity. Time diversity effectiveness requires symbols to be interleaved over a time frame larger than the average fade duration. Frequency diversity is commonly employed in fast frequency hopping and possibly in OFDM. Path diversity is exploited by the Rake receiver operating in a resolvable multipath fading environment. Antenna diversity is the most powerful diversity technique that can be implemented either at the receiver, at the transmitter, or at both transmitter and receiver. Antenna diversity is also referred to as MIMO. Diversity signal is detected via maximal ratio combining, selection combining, and equal gain combining. Transmit diversity in many practical systems is implemented via an orthogonal space-time code such as the well-known Alamouti block code. The maximum rate is unity.

The capacity of a slow fading channel is best defined as the outage capacity since the ensemble average capacity does not exist. On the other hand, the ensemble average capacity of a fast fading channel does exist. Slow fading is more detrimental to the channel capacity than fast fading. However, fast fading requires a more complex coding scheme to compensate for both envelope fading and Doppler error.

Appendix 10A: Complex-valued demodulators

The IQ-demodulator can be equivalently represented by the complex-valued demodulator shown in Figure 10.8. Let $s_i(t)$ be the waveform of an arbitrary IQ symbol as follows:

$$s_i(t) = \sum_{k=1}^{2} s_{ik} x_k(t) = s_{i1} x_1(t) + s_{i2} x_2(t) \tag{10A.1}$$

where the basis functions $x_1(t)$ and $x_2(t)$ are given by

$$x_1(t) = \frac{1}{\sqrt{E_x}} p(t) \cos 2\pi f_c t, \quad x_2(t) = -\frac{1}{\sqrt{E_x}} p(t) \sin 2\pi f_c t \tag{10A.2}$$

The function $p(t)$ is the pulse shape, and E_x is defined as

$$E_x = \int_{-\infty}^{\infty} [p(t) \cos 2\pi f_c t]^2 \mathrm{d}t = \int_{-\infty}^{\infty} [-p(t) \sin 2\pi f_c t]^2 \mathrm{d}t \tag{10A.3}$$

The sufficient condition for orthogonality of the basis functions is demonstrated in (6.94) of Example 6.26. Using complex envelope representation we can express the waveform $s_i(t)$ as follows:

$$s_i(t) = \mathrm{Re}\left[s_L(t) \mathrm{e}^{\mathrm{j}2\pi f_c t}\right] = \frac{1}{2}\left[s_L(t) \mathrm{e}^{\mathrm{j}2\pi f_c t} + s_L^*(t) \mathrm{e}^{-\mathrm{j}2\pi f_c t}\right] \tag{10A.4}$$

where the complex envelope $s_L(t)$ is

$$s_L(t) = \frac{1}{\sqrt{E_x}} p(t) s_{i1} + \mathrm{j} \frac{1}{\sqrt{E_x}} p(t) s_{i2} \tag{10A.5}$$

To demodulate the IQ symbol $s_i = s_{i1} + \mathrm{j}s_{i2}$ we multiply the received signal $s_i(t)$ by a local complex carrier $\sqrt{2/T_s}\mathrm{e}^{-\mathrm{j}2\pi f_c t}$ to obtain

$$\sqrt{\frac{2}{T_s}} \mathrm{e}^{-\mathrm{j}2\pi f_c t} s_i(t) = \frac{1}{\sqrt{2T_s}} s_L(t) + \frac{1}{\sqrt{2T_s}} s_L^*(t) \mathrm{e}^{-\mathrm{j}4\pi f_c t} \tag{10A.6}$$

The high-frequency term is rejected by the complex-valued matched filter $h(t) = \alpha p(t - T_s)$, where α is a normalization constant. The output of the complex-valued matched filter is $s_i = s_{i1} + \mathrm{j}s_{i2}$. The mapper maps $s_i = s_{i1} + \mathrm{j}s_{i2}$ to the symbol vector $\boldsymbol{s}_i = [s_{i1}\ s_{i2}]^t$ by taking the real part and imaginary part of s_i.

Appendix 10B: Bit error probabilities

The bit error probability of an IQ signal in a Rayleigh or Nakagami-m fading channel can be derived using available closed-form expressions. The general bit error probability is given by

$$P_b = \mathbf{E}[P_b(|h|)] \approx \mathbf{E}\left[\frac{N_n}{\log_2 M} Q\left(\sqrt{2|h|^2 \alpha\, SNR}\right)\right] \tag{10B.1}$$

Rayleigh

The density function of $|h|$ is $f_{|h|}(x) = 2x\mathrm{e}^{-x^2}$ and the following expression can be employed to evaluate P_b [7]:

$$\int_0^\infty Q(ax)\mathrm{e}^{b^2x^2} x\mathrm{d}x = \frac{1}{4b^2}\left[\frac{a}{\sqrt{a^2 - 2b^2}} - 1\right], \quad \mathrm{Re}(a^2) > 2\mathrm{Re}(b^2) \tag{10B.2}$$

Setting $b^2 = -1$, $a = \sqrt{2\alpha SNR}$, we obtain the bit error probability

$$P_b = \frac{N_n}{2\log_2 M}\left(1 - \sqrt{\frac{\alpha\, SNR}{1 + \alpha\, SNR}}\right) \tag{10B.3}$$

Nakagami-m

The density function of $|h|^2$ is $f_{|h|^2}(y) = \frac{m^m}{\Gamma(m)} y^{m-1}\mathrm{e}^{-my}$ and the following expression can be employed to evaluate P_b [8]:

$$\begin{aligned}\int_0^\infty Q(\sqrt{cy})y^{b-1}\mathrm{e}^{-ay}\mathrm{d}y = {} & \frac{1}{2\sqrt{\pi}}\frac{\sqrt{c/2a}}{(1 + c/2a)^{b+1/2}}\frac{\Gamma(b)}{a^b}\frac{\Gamma(b+\frac{1}{2})}{\Gamma(b+1)} \\ & \times {}_2F_1\left(1, b+\frac{1}{2}; b+1; (1+c/2a)^{-1}\right)\end{aligned} \tag{10B.4}$$

Setting $a = m$, $b = m$, $c = 2\alpha SNR$, and $c/2a = \alpha SNR/m$, we obtain the bit error probability:

$$P_b \approx \frac{N_n}{\log_2 M}\left[\frac{1}{2\sqrt{\pi}}\frac{\sqrt{\alpha\, SNR/m}}{(1 + \alpha\, SNR/m)^{m+1/2}}\frac{\Gamma(m+\frac{1}{2})}{\Gamma(m+1)}\right]{}_2F_1\left(1, m+\tfrac{1}{2}; m+1; \frac{1}{1+\alpha\, SNR/m}\right) \tag{10B.5}$$

When b is an integer the following expression can be used to obtain a simpler closed-form bit error probability

$$\int_0^\infty Q(\sqrt{cy})y^{b-1}\mathrm{e}^{-ay}\mathrm{d}y = \frac{\Gamma(b)}{2a^b}\left[1 - \sqrt{\frac{c/2a}{1+c/2a}}\sum_{k=0}^{b-1}\binom{2k}{k}\left(\frac{1}{4(1+c/2a)}\right)^k\right], \quad b: \text{integer} \tag{10B.6}$$

where $\Gamma(b) = (b-1)!$ Setting $a = m$, $b = m$, and $c/2a = \alpha SNR/m$, we obtain

$$P_b \approx \frac{N_n}{2\log_2 M}\left[1-\sqrt{\frac{\alpha SNR/m}{1+\alpha SNR/m}}\sum_{k=0}^{m-1}\binom{2k}{k}\left(\frac{1}{4(1+\alpha SNR/m)}\right)^k\right],\ m:\text{integer} \tag{10B.7}$$

Alternatively we can use the following closed-form expression to evaluate the bit error probability [9]:

$$\begin{aligned}&\int_0^\infty Q(\sqrt{cy})y^{b-1}\mathrm{e}^{-ay}\mathrm{d}y\\&=\frac{\Gamma(b)}{a^b}\left(\frac{\sqrt{1+2a/c}-1}{2\sqrt{1+2a/c}}\right)^b\left[\sum_{k=0}^{b-1}\binom{b-1+k}{k}\left(\frac{\sqrt{1+2a/c}+1}{2\sqrt{1+2a/c}}\right)^k\right],\\&b:\text{integer}\end{aligned} \tag{10B.8}$$

Setting $a=m$, $b=m$, and $c/2a=\alpha SNR/m$, we obtain

$$P_b \approx \frac{N_n}{\log_2 M}\left(\frac{\sqrt{1+m/\alpha SNR}-1}{2\sqrt{1+m/\alpha SNR}}\right)^m\left[\sum_{k=0}^{m-1}\binom{m-1+k}{k}\left(\frac{\sqrt{1+m/\alpha SNR}+1}{2\sqrt{1+m/\alpha SNR}}\right)^k\right],$$
m : integer

(10B.9)

Rayleigh–diversity: χ^2-density function with $2L$ degrees of freedom

The density function of $\|\boldsymbol{h}\|^2$ is $f_{\|\boldsymbol{h}\|^2}(y)=y^{L-1}\mathrm{e}^{-y}/(L-1)!$ and the expression in (10B.6) can be employed to obtain the general bit error probability of a diversity system given by

$$P_b = \boldsymbol{E}\left[\frac{N_n}{\log_2 M}Q\left(\sqrt{2\|\boldsymbol{h}\|^2\alpha\,\boldsymbol{SNR}}\right)\right] \tag{10B.10}$$

Setting $a=1$, $b=L$, and $c/2a=\alpha\,\boldsymbol{SNR}$, and noting that $\Gamma(L)=(L-1)!$, we obtain

$$P_b \approx \frac{N_n}{2\log_2 M}\left[1-\sqrt{\frac{\alpha\boldsymbol{SNR}}{1+\alpha\boldsymbol{SNR}}}\sum_{k=0}^{L-1}\binom{2k}{k}\left(\frac{1}{4(1+\alpha\boldsymbol{SNR})}\right)^k\right] \tag{10B.11}$$

Alternatively, using (10B.8) we have

$$P_b \approx \frac{N_n}{\log_2 M}\left(\frac{\sqrt{1+1/\alpha\boldsymbol{SNR}}-1}{2\sqrt{1+1/\alpha\boldsymbol{SNR}}}\right)^L\left[\sum_{k=0}^{L-1}\binom{L-1+k}{k}\left(\frac{\sqrt{1+1/\alpha\boldsymbol{SNR}}+1}{2\sqrt{1+1/\alpha\boldsymbol{SNR}}}\right)^k\right],$$
L : integer

(10B.12)

or, equivalently,

$$P_b \approx \frac{N_n}{\log_2 M}\left(\frac{1-\mu}{2}\right)^L \left[\sum_{k=0}^{L-1}\binom{L-1+k}{k}\left(\frac{1+\mu}{2}\right)^k\right],\ L:\text{integer} \tag{10B.13}$$

where the parameter μ is given by

$$\mu = \sqrt{\frac{\alpha \boldsymbol{SNR}}{1+\alpha \boldsymbol{SNR}}} \tag{10B.14}$$

Problems

1. A mobile approaches a base station at 100 km/hour. The mobile transmits a packet of 200 bits at a rate of 100 kbps. The carrier frequency is 1.9 GHz. The multipath delay spread is $T_d = 0.25\,\mu s$. The signal-to-ISI ratio is approximated by $SIR = 0.9T_b/T_d$. The signal-to-noise ratio is $SNR = 100\cos^2\theta$, where the carrier phase error due to Doppler shift is θ. Calculate the signal-to-noise-and-ISI of the last bit of the packet.
2. Let us consider the scenario when a mobile traveling at speed of 100 km/hour receives a 1950 MHz signal from a base station. The data rate is 14.4 kbps.
   (a) Find the Doppler spread.
   (b) Find the channel coherence time.
   (c) If the channel estimation time is ¼ of the channel coherence time, what is the channel throughput, assuming each channel estimation update is achieved via a transmitted pilot symbol that replaces a data symbol?
3. Using (10.17) plot the magnitude and phase spectra for the following channel:

Channel taps and delays		
i	Tap, h_i	Delay, l_i
1	0.75	0
2	0.35	0.9
3	0.2	1.7
4	0.01	3

4. Using (10.17) plot the magnitude and phase spectra for the following channel:

Channel taps and delays		
i	Tap, h_i	Delay, l_i
1	0.75	0.8
2	0.55	0.85
3	0.40	0.9

5. Plot the Clarke–Doppler power spectrum in (10.31) and the Aulin–Doppler power spectrum in (10.44).

6. Using polar coordinate transformation, evaluate the bit error probability of a coherent I-Q signal in a Rayleigh fading channel.
7. Determine the *SNR*-outage probability of a slow-flat Nakagami-m fading channel. Let $m = 3$, the threshold is $\gamma = 1$, and $SNR = 10$.
8. Determine the *SNR*-outage probability of a slow-flat Ricean fading channel. Let $\kappa = 4.5$, the threshold is $\gamma = 1$, and $SNR = 10$.
9. Plot the bit error probability of PSK in an AWGN channel with phase error $\varepsilon = 0°, 10°, 22.5°, 30°, 45°, 60°$.
10. Plot the bit error probability of QPSK in an AWGN channel with phase error $\varepsilon = 0°, 10°, 22.5°, 30°, 45°$.
11. Plot the bit error probability of 16QAM in an AWGN channel with phase error $\varepsilon = 0°, 10°, 22.5°, 30°, 45°$.
12. Plot the bit error probability of 64QAM in an AWGN channel with phase error $\varepsilon = 0°, 10°, 22.5°, 30°, 45°$.
13. Verify (10.82).
14. Plot the bit error probability of 16QAM in a Rayleigh fading channel with phase error $\varepsilon = 5°, 10°, 22.5°$.
15. Plot the bit error probability of 64QAM in a Rayleigh fading channel with phase error $\varepsilon = 5°, 10°, 22.5°$.
16. Show that the bit error probabilities of MPSK and MQAM in a Rayleigh fading channel are inversely proportional to the signal-to-noise ratio.
17. Evaluate the bit error probability of PSK with convolutional code $K = 7$, rate ½, and soft decision in a Rayleigh fading channel at 10 dB signal-to-noise ratio per bit.
18. Consider the reception of a DS-PSK signal in a Rayleigh fading channel with pulsed jamming.
    (a) Derive the bit error probability in term E_b/N_0, assuming AWGN is neglible compared to the jamming signal.
    (b) Assume a pulse duty cycle equal to $\delta = 0.1$ and $E_b/N_0 = 20$ dB. Calculate the bit error probability.
19. A packet of length L is sent over a Rayleigh fading channel via PSK. Assuming that bit errors occur randomly and that the required packet error probability is 10^{-2}, calculate the corresponding signal-to-noise ratio per bit for $L = 200$ bits.
20. Consider a mobile traveling toward a base station at a speed of 100 km/hour that receives a 5400 MHz PSK signal from a base station. It is required that the throughput be at least 80% and that the loss in *SNR* relative to the ideal case is no more than 2 dB. Calculate the minimum bit rate assuming Rayleigh fading.
21. Consider a fading channel with Doppler spread $f_D = 200\,Hz$. A PSK signal operating with a bit rate of 128 kbps employs pilot bits for channel estimation.
    (a) Specify the condition for slow fading. Estimate the maximum channel estimation time in bits.
    (b) Calculate the phase error for the above maximum estimation time.
    (c) Revise the estimation time to get a reasonable phase error of no more than $\pi/8$ radians.

22. Consider a mobile moving toward a base station at radial velocity $v = 110$ km/hour. The mobile transmits a PSK signal at 28.8 kbps to the base station. The data frame is 300 bits including 20 overhead bits. The channel estimation is achieved by inserting pilot bits periodically. The carrier frequency is 1.9 GHz.
    (a) Calculate the channel estimation time in bits so that the Doppler phase error cannot exceed 30°.
    (b) Calculate the number of pilot bits per frame.
    (c) Calculate the frame efficiency.
23. Consider a perfect reflector model in Equation (10.4). Assume that the receiver radial velocity is 80 km/hour, and the received signal has a carrier frequency of 1.9 GHz.
    (a) Calculate the deep fade frequency.
    (b) Calculate the deep fade period.
    (c) Suggest a method to eliminate the deep fades.
    (d) Suggest a method to improve the reception via signal combining.
24. Consider a QPSK signal with phase error $\varepsilon = 22.5°$ in a Rayleigh fading channel. The bit error probability is given by

$$P_b = \frac{1}{4}\left(1 - \sqrt{\frac{\alpha\, SNR(\cos\varepsilon - \sin\varepsilon)^2}{1 + \alpha\, SNR(\cos\varepsilon - \sin\varepsilon)^2}}\right) + \frac{1}{4}\left(1 - \sqrt{\frac{\alpha\, SNR(\cos\varepsilon + \sin\varepsilon)^2}{1 + \alpha\, SNR(\cos\varepsilon + \sin\varepsilon)^2}}\right)$$

    For $\alpha SNR = E_b/N_0 = 30$ dB evaluate the loss of signal-to-noise ratio.
25. Consider two independent Rayleigh random variables X and Y.
    (a) Find the probability density function of $Z = X/Y$
    (b) Find the probability distribution function of Z.
    (c) Find the probability density function of $V = Z^2$.
26. Consider two independent Rice random variables X and Y. Find the probability density function of $Z = X/Y$.
27. Derive the bit error probability of DS-PSK under broadband jamming, assuming that both signal and jammer undergo independent Rayleigh fading and the AWGN effect is negligible relative to the jamming effect.
28. Derive the bit error probability of DS-PSK under pulsed jamming, assuming that both signal and jammer undergo independent Rayleigh fading and the AWGN effect is negligible relative to the jamming effect.
29. Consider a Rayleigh channel and a DS-CDMA/PSK signal with power control so that all user signals arriving at the base station have the same mean power P.
    (a) Derive the probability density function of the user output signal power.
    (b) Derive the probability density function of the MUI, assuming the MUI power is distributed uniformly over the spread bandwidth.
    (b) Derive the probability density function of the output signal-to-interference ratio when AWGN is negligible compared to MUI.
30. Consider a DS-PSK signal under broadband jamming, assuming that both signal and jammer undergo independent Rayleigh fading and the AWGN effect is negligible relative to the jamming effect. Derive the $N(SJR_i)$-outage probability, that is, the

probability that the instantaneous despread input signal-to-jamming ratio falls below a threshold value γ. N is the spread factor.

31. Consider a DS-PSK signal under pulse jamming, assuming that both signal and jammer undergo independent Rayleigh fading and the AWGN effect is negligible relative to the jamming effect. Derive the $N\delta(SJR_i)$-outage probability, that is, the probability that the instantaneous despread input signal-to-pulsed jamming ratio falls below a threshold value γ. N is the spread factor and δ is the pulsed jamming duty cycle.
32. For a Rayleigh fading channel derive the bit error probability of noncoherent FH-MFSK under partial-band jamming, assuming that the AWGN effect is negligible relative to the jamming effect.
33. Derive the bit error probability of noncoherent FH-MFSK under partial-band jamming, assuming that both signal and jammer undergo independent Rayleigh fading and the AWGN effect is negligible relative to the jamming effect.
34. For a Rayleigh fading channel derive the bit error probability of noncoherent slow FH-FSK under follower jamming, assuming that the AWGN effect is negligible relative to the jamming effect.
35. It is required that the first symbol after the most recent channel update suffers no more than 10° of differential Doppler phase error when the Doppler shift is 180 Hz. Estimate the maximum bit rate for 64QAM. Calculate the Doppler loss at this bit rate for a Rayleigh channel.
36. Consider a mobile traveling toward a base station at a speed of 100 km/hour that receives a 5400 MHz QPSK signal from a base station. It is required that the throughput be at least 80% and that the loss in *SNR* relative to the ideal case is no more than 3 dB at a bit error probability of 5×10^{-3}. Calculate the minimum bit rate assuming Rayleigh fading.
37. Consider a mobile traveling toward a base station at a speed of 100 km/hour that receives a 5400 MHz 16QAM signal from a base station. It is required that the throughput be at least 50% and that the loss in *SNR* relative to the ideal case is no more than 6 dB.
    (a) Calculate the pilot symbol rate.
    (b) Calculate the minimum bit rate assuming Rayleigh fading.
38. Derive (10.136).
39. Derive (10.138).
40. Rework Table 10.3 for 128FSK.
41. Rework Table 10.4 for 128CSK.
42. Establish the signal-to-interchannel interference ratio for pilot tone-aided demodulation of an orthogonal covering signal in the presence of Doppler shift f=180 Hz for the following cases:
    (a) QPSK with bit rate of 28.8 kbps.
    (b) 64QAM with bit rate of 86.4 kbps.
43. Approximate interchannel interference as AWGN and assume a bit error probability of 10^{-3} for orthogonal covering QPSK with normalized Doppler shift $fT_s = 0.01$. Calculate the required E_b/N_0.

44. Approximate interchannel interference as AWGN and assume a bit error probability of 10^{-3} for orthogonal covering 64QAM with normalized Doppler shift $fT_s = 0.01$. Calculate the required average E_b/N_0.
45. Show that Figure 10.12 implements the despreading operation (10.162).
46. Consider a mobile traveling toward a base station at a speed of 100 km/hour that receives a 5400 MHz signal from a base station. Assume that the threshold signal-to-noise ratio is $V^2/2\sigma^2 = 6$ dB, where the noise variance is σ^2. Also assume that the signal-to-noise ratio is $V_{rms}^2/\sigma^2 = 15$ dB. The symbol rate is 9.6 ksps.
    (a) Calculate the average fade duration.
    (b) Find the interleaving interval in symbols.
47. Use the Cauchy–Schwarz inequality to show that MRC achieves a maximum output signal-to-noise ratio which is the sum of L input signal-to-noise ratios.
48. Verify (10.221).
49. Verify (10.223).
50. Verify (10.232)
51. Using the Chernoff bound $Q(x) \leq \mathrm{e}^{-x^2/2}$ show that the bit error probability of an I-Q signal in a Rayleigh fading channel is upper bounded by

$$P_b = \mathbf{E}\left[\frac{N_n}{\log_2 M} Q\left(\sqrt{2\|\boldsymbol{h}\|^2 \alpha \boldsymbol{SNR}}\right)\right] \leq \frac{N_n}{\log_2 M} \frac{1}{(1+\alpha \boldsymbol{SNR})^L}$$

52. Repeat Problem 51 for both Nakagami-m and Ricean fading channels.
    (a) Derive the result via direct integration.
    (b) Derive the result using the Laplace transform (or moment generating function).
53. The function $Q(x)$ can also be expressed by the following integral [10]:

$$Q(x) = \frac{1}{\pi}\int_0^{\pi/2} \mathrm{e}^{-x^2/2\sin^2\theta}\mathrm{d}\theta, \quad x>0$$

    Use the above integral to express the bit error probability of the I-Q signal as follows:

$$P_b = \mathbf{E}\left[\frac{N_n}{\log_2 M} Q\left(\sqrt{2\|\boldsymbol{h}\|^2 \alpha\, \boldsymbol{SNR}}\right)\right] = \frac{N_n}{\log_2 M}\frac{1}{\pi}\int_0^{\pi/2} \Phi\left(\frac{\alpha SNR}{\sin^2\theta}\right)\, \mathrm{d}\theta$$

    where $\Phi(s)$ is the Laplace transform of the density function of $\|\boldsymbol{h}\|^2$.
    (a) Find $\Phi(s)$ for the Rayleigh density function.
    (b) Find $\Phi(s)$ for the Nakagami-m density function.
54. Find the outage probability of coherent selection combining for a given signal-to-noise ratio threshold.
55. Find the bit error probability of noncoherent DPSK with selection combining.
56. For a Rayleigh fading channel, compare the performance of a three-fold receive antenna diversity 64QAM signal with MRC and $\alpha SNR = 1000$ (30 dB) to the performance of its counterpart without diversity, assuming that both signals have the same transmitted power and input bit rate. Calculate the diversity gain.
57. Compare the performance of an I-Q signal with three-fold receive antenna diversity to the performance of its non-diversity counterpart, assuming that both signals have the

same transmitted power and input bit rate. Consider the case of 64QAM with $\alpha SNR = 1000$ (30 dB) and Rayleigh fading. Calculate the diversity gain with selection combining.

58. Derive the bit error probability of an L-fold diversity noncoherent DPSK signal with EGC in a Nakagami-m fading channel. (Hint: Use (11.1-13)–(11.1-14) from [11].)
59. Consider a Rayleigh channel and an L-fold diversity combining technique where the two largest of L decision samples of a coherent I-Q signal are combined (second-order SC). The density function of the largest random variable of L random variables is derived in (10.216).
    (a) Derive the density function of the kth largest random variable of L random variables.
    (b) Derive the joint density funtion of the two largest random variables of L random variables.
    (c) Derive the density function of the sum of the two largest random variables of L random variables and the bit error probability for receive antenna diversity.
60. Derive the bit error probability for an L-fold diversity convolutionally coded PSK signal with MRC in a slow Rayleigh fading channel.
61. Derive the bit error probability for an L-fold diversity TCM-MQAM signal with MRC in a slow Rayleigh fading channel.
62. Consider a three-tap channel with $L = 3$, $\boldsymbol{SINR} = 200$, and 16QAM.
    (a) Calculate the bit error probability for a non-Rake receiver.
    (b) Calculate the bit error probability for a Rake receiver.
    (c) For a spread factor of 256, calculate $\alpha\boldsymbol{SINR} = \frac{1}{2}(d_{min}/\mathbf{2}\boldsymbol{\sigma})^2$ and specify the signal-to-noise ratio per bit E_b/N_0 to achieve $\alpha\boldsymbol{SINR} = 200$.
63. Verify that $\boldsymbol{Z} = \mathbf{G}\boldsymbol{h} + \mathfrak{N}$ maps to $\boldsymbol{Y} = \mathbf{H}\boldsymbol{s} + \boldsymbol{N}$ via (10.270) and (10.271).
64. Show that (10.272) is satisfied using (10.274)–(10.276) as an example.
65. For a real signal space, the space-time block code of unity rate does not have the limit of two transmit antennas as in the Alamouti code. In fact, a space-time block code with unity rate for any real signal space can have any number of transmit antennas. Consider the following real code matrix:

$$\mathbf{G} = \begin{bmatrix} \mathbf{G}_1 & -\mathbf{G}_2^t \\ \mathbf{G}_2 & \mathbf{G}_1^t \end{bmatrix}$$

    (a) Find the necessary and sufficient condition for $\mathbf{G}$ to be orthogonal.
    (b) Use the following two matrices to construct $\mathbf{G}$ and perform the MRC operation for a four-fold transmit diversity, assuming that the signal is PSK:

$$\mathbf{G}_1 = \begin{bmatrix} s_1 & s_2 \\ -s_2 & s_1 \end{bmatrix}, \quad \mathbf{G}_2 = \begin{bmatrix} s_3 & -s_4 \\ s_4 & s_3 \end{bmatrix}$$

66. Investigate the possibility of using the following matrix as orthogonal space-time block code. If not, can it be used as nonorthogonal space-time block code? What will be the consequence(s) of doing so?

$$\mathbf{G} = \begin{bmatrix} s_1 & 0 & -s_2^* \\ 0 & s_1 & -s_3 \\ s_2 & s_3^* & s_1^* \\ -s_3 & s_2^* & 0 \end{bmatrix}$$

67. Investigate the possibility of using the following matrix as orthogonal space-time block code:

$$\mathbf{G} = \begin{bmatrix} s_1 & s_2 & s_3 \\ -s_2^* & s_1^* & 0 \\ -s_3^* & 0 & s_1^* \\ 0 & -s_3^* & s_2^* \end{bmatrix}$$

68. Investigate the possibility of using the following matrix as orthogonal space-time block code:

$$\mathbf{G} = \begin{bmatrix} s_1 & 0 & s_2 & -s_3 \\ 0 & s_1 & s_3^* & s_2^* \\ -s_2^* & -s_3 & s_1^* & 0 \\ s_3^* & -s_2 & 0 & s_1^* \end{bmatrix}$$

69. Investigate the possibility of using the following real matrix as orthogonal space-time block code for a real signal space:

$$\mathbf{G} = \begin{bmatrix} s_1 & s_2 & s_3 & s_4 \\ -s_2 & s_1 & -s_4 & s_3 \\ -s_3 & s_4 & s_1 & -s_2 \\ -s_4 & -s_3 & s_2 & s_1 \end{bmatrix}$$

70. Find the outage capacity of a slow fading Rayleigh channel for $p_o = 0.01$ for the following cases:
    (a) no diversity;
    (b) receive antenna diversity with $L = 2$;
    (c) transmit antenna diversity with Alamouti code;
    (d) transmit antenna diversity with a rate ¾ space-time code and four antennas;
    (e) transmit and receive antenna diversity with Alamouti code and two receive antennas.
71. Find the outage capacity of a fading channel characterized by the channel tap with the following density function: $f_{|h|}(x) = 2x/(x^2+1)^2, x > 0$.
72. Consider a MIMO system characterized by the $L_r \times L_t$ channel tap matrix $H = [h_{ij}]$, where h_{ij} represents the channel tap from the jth transmit antenna ($j = 1, 2, \ldots, L_t$) to the ith receive antenna ($i = 1, 2, \ldots, L_r$). Given the transmit signal vector $\boldsymbol{s}$, the received signal vector $\boldsymbol{y}$ is given by

$$\boldsymbol{y} = \mathbf{H}\boldsymbol{s} + \boldsymbol{N}$$

where $\boldsymbol{N}$ is the zero mean complex Gaussian noise vector whose iid components have identical variance (circular symmetric). Assuming that $(\mathbf{H}^*\mathbf{H})^{-1}$ exists, that is, $\mathbf{H}$ is of full column rank, design a zero-forcing (ZF) detector to recover the transmit vector $\boldsymbol{s}$. Is the output noise white? Find its covariance matrix.

73. Consider a MIMO system characterized by the $L_r \times L_t$ channel tap matrix $\mathbf{H} = [h_{ij}]$, where h_{ij} represents the channel tap from the jth transmit antenna ($j = 1, 2, \ldots, L_t$) to the ith receive antenna ($i = 1, 2, \ldots, L_r$). Given the transmit signal vector $\boldsymbol{s}$, the received signal vector $\boldsymbol{y}$ is given by

$$\boldsymbol{y} = \mathbf{H}\boldsymbol{s} + \boldsymbol{N}$$

where $\boldsymbol{N}$ is the zero mean complex Gaussian noise vector whose iid components have identical variance (circular symmetric). Consider a minimum mean-square error (MMSE) detector that minimizes the MSE given by $\mathbf{E}\left[\|\mathbf{C}\boldsymbol{y} - \boldsymbol{s}\|^2\right]$. Find $\mathbf{C}$.

74. Consider a MIMO system characterized by the $L_r \times L_t$ channel tap matrix $\mathbf{H} = [h_{ij}]$, where h_{ij} represents the channel tap from the jth transmit antenna ($j = 1, 2, \ldots, L_t$) to the ith receive antenna ($i = 1, 2, \ldots, L_r$). Given the transmit code matrix $\mathbf{G}$, the received signal vector $\mathbf{Y}$ is given by

$$\mathbf{Y} = \mathbf{HG} + \mathbf{N}$$

where $\mathbf{N}$ is the complex Gaussian noise matrix whose iid components have zero mean and identical variance (circular symmetric). Consider a maximum likelihood (ML) detector that minimizes the squared Frobenius norm $\|\mathbf{Y} - \mathbf{HG}\|^2$. The squared Frobenius norm of a matrix $\mathbf{A}$ is defined as $||\mathbf{A}||^2 = Tr(\mathbf{AA}^*) = \sum_i \sum_j |a_{ij}|^2 = \sum_k \lambda_k$, where λ_k are the eigenvalues of $\mathbf{AA}^*$. Derive the pairwise error probability $\Pr(\mathbf{HG}_i \rightarrow \mathbf{HG}_j)$. (Hint: use the Chernoff bound for the Q-function and find the density function of $\left\|\mathbf{HG}_i - \mathbf{HG}_j\right\|^2$.)

Further reading

For a comprehensive study of propagation models we recommend [1,2]. Excellent treatment of capacity of a fading channel for various wireless systems such as CDMA, OFDM, and MIMO can be found in [3]. For the readers who wish to explore MIMO in depth, references [4–6] should be consulted.

Bibliography

1. W. C. Jakes, *Microwave Mobile Communications*, IEEE Press, 1974.
2. R. Janaswamy, *Radiowave Propagation and Smart Antennaa for Wireless Communications*, London: Kluwer, 2001.
3. D. Tse and P. Viswanath, *Fundamentals of Wireless Communication*, Cambridge: Cambridge University Press, 2005.
4. E. Biglieri and G. Taricco, *Transmission and Reception with Multiple Antennas: Theoretical Foundations*, Now Publishers, 2004.
5. E. G. Larsson and P. Stoica, *Space-Time Block Coding for Wireless Communications*, Cambridge: Cambridge University Press, 2003.

6. A. Paulraj, R. Nabar, and D. Gore, *Introduction to Space-Time Wireless Communications*, Cambridge: Cambridge University Press, 2003.
7. E. W. Ng and M. Geller, "A table of integrals of the error functions," *J. Res. Nat. Bureau Standards – B. Math. Sci.*, Vol. **73B**, No. 1, pp. 1–20, 1969.
8. T. Eng and L. B. Milstein, "Coherent DS-CDMA performance in Nakagami multipath fading," *IEEE Trans. Commun.*, Vol. **43**, No. 2–4, pp. 1134–1143, 1995.
9. P. A. Bello and B. D. Nelin, "Predetection diversity combining with selectivity fading channels," *IRE Trans. Commun. Syst.*, Vol. **10**, pp. 32–42, 1962.
10. J. Craig, "New, simple and exact result for calculationg the probability of error for two-dimensional signal constellation," *Proceedings of the Military Communication Conference*, Boston, MA, pp. 25.51–25.55, 1991.
11. J. G. Proakis, *Digital Communications*, 5th edition, New York: McGraw-Hill, 2008.
12. J. R. Barry, E. A. Lee, and D. G. Messerschmitt, *Digital Communication*, 3rd edition, London: Kluwer, 2004.
13. E. Biglieri *et al*., *MIMO Wireless Communications*, Cambridge: Cambridge University Press, 2007.
14. A. Goldsmith, *Wireless Communications*, Cambridge: Cambridge University Press, 2005.
15. S. Haykin and M. Moher, *Modern Wireless Communications*, Upper Saddle River, NJ: Pearson Prentice-Hall, 2005.
16. M. K. Simon and M.-S. Alouini, *Digital Communication over Fading Channels. A Unified Approach to Performance Analysis*, Chichester: John Wiley & Sons, 2000.
17. S. M. Alamouti, "A simple transmit diversity technique for wireless communication," *IEEE J. Selected Areas Commun.*, Vol. **16**, No. 8, pp. 1451–1458, 1998.

Index